frontiers | Research Topics

Natural products and immune inflammation: mechanistic understanding based on systems biology

Edited by
Xianyu Li, Boyang Ji, Weicheng Hu, Sang-Han Lee and Guang Wang

Published in
Frontiers in Pharmacology

ISSN 1664-8714
ISBN 978-2-8325-6588-9
DOI 10.3389/978-2-8325-6588-9

Generative AI statement
Any alternative text (Alt text) provided alongside figures in the articles in this ebook has been generated by Frontiers with the support of artificial intelligence and reasonable efforts have been made to ensure accuracy, including review by the authors wherever possible. If you identify any issues, please contact us.

About Frontiers

Frontiers is more than just an open access publisher of scholarly articles: it is a pioneering approach to the world of academia, radically improving the way scholarly research is managed. The grand vision of Frontiers is a world where all people have an equal opportunity to seek, share and generate knowledge. Frontiers provides immediate and permanent online open access to all its publications, but this alone is not enough to realize our grand goals.

Frontiers journal series

The Frontiers journal series is a multi-tier and interdisciplinary set of open-access, online journals, promising a paradigm shift from the current review, selection and dissemination processes in academic publishing. All Frontiers journals are driven by researchers for researchers; therefore, they constitute a service to the scholarly community. At the same time, the *Frontiers journal series* operates on a revolutionary invention, the tiered publishing system, initially addressing specific communities of scholars, and gradually climbing up to broader public understanding, thus serving the interests of the lay society, too.

Dedication to quality

Each Frontiers article is a landmark of the highest quality, thanks to genuinely collaborative interactions between authors and review editors, who include some of the world's best academicians. Research must be certified by peers before entering a stream of knowledge that may eventually reach the public - and shape society; therefore, Frontiers only applies the most rigorous and unbiased reviews. Frontiers revolutionizes research publishing by freely delivering the most outstanding research, evaluated with no bias from both the academic and social point of view. By applying the most advanced information technologies, Frontiers is catapulting scholarly publishing into a new generation.

What are Frontiers Research Topics?

Frontiers Research Topics are very popular trademarks of the *Frontiers journals series*: they are collections of at least ten articles, all centered on a particular subject. With their unique mix of varied contributions from Original Research to Review Articles, Frontiers Research Topics unify the most influential researchers, the latest key findings and historical advances in a hot research area.

Find out more on how to host your own Frontiers Research Topic or contribute to one as an author by contacting the Frontiers editorial office: frontiersin.org/about/contact

Natural products and immune inflammation: mechanistic understanding based on systems biology

Topic editors

Xianyu Li — China Academy of Chinese Medical Sciences, China
Boyang Ji — BioInnovation Institute (BII), Denmark
Weicheng Hu — Yangzhou University, China
Sang-Han Lee — Kyungpook National University, Republic of Korea
Guang Wang — Jinan University, China

Citation

Li, X., Ji, B., Hu, W., Lee, S.-H., Wang, G., eds. (2025). *Natural products and immune inflammation: mechanistic understanding based on systems biology*. Lausanne: Frontiers Media SA. doi: 10.3389/978-2-8325-6588-9

Table of contents

frontiers | Frontiers in Pharmacology

TYPE Editorial
PUBLISHED 24 June 2025
DOI 10.3389/fphar.2025.1642311

OPEN ACCESS

EDITED BY
Javier Echeverria,
University of Santiago, Chile

REVIEWED BY
Dâmaris Silveira,
University of Brasilia, Brazil

*CORRESPONDENCE
Xianyu Li,
phd_xianyuli@foxmail.com

RECEIVED 06 June 2025
ACCEPTED 17 June 2025
PUBLISHED 24 June 2025

CITATION
Ma Z and Li X (2025) Editorial: Natural products and immune inflammation: mechanistic understanding based on systems biology. *Front. Pharmacol.* 16:1642311. doi: 10.3389/fphar.2025.1642311

Editorial: Natural products and immune inflammation: mechanistic understanding based on systems biology

Zhen Ma[1] and Xianyu Li[2]*

[1]Institute of Materia Medica, China Academy of Chinese Medical Sciences, Beijing, China, [2]Experiment Research Center, China Academy of Chinese Medical Sciences, Beijing, China

KEYWORDS

immune inflammation, herbal medicine, artificial intelligence, natural compounds, omics

Editorial on the Research Topic
Natural products and immune inflammation: mechanistic understanding based on systems biology

Immune inflammatory response is the core of the body's defense and repair, but its imbalance is the common underlying mechanism factor for major chronic diseases such as cancer, autoimmune diseases, neurodegenerative diseases, and metabolic syndrome. Faced with these complex diseases, modern drug discovery and development often encounters bottlenecks such as single target, drug resistance, and side effects. Natural products, with their structural diversity and multi-target effects, have been empirically validated through millennia of human use and are becoming valuable therapeutic resources for combating immune inflammation related diseases. However, the complex composition and unclear mechanism of action of natural products are like a "black box", which seriously hinders their scientific evaluation and clinical translation. The theory of systems biology can provide a new perspective, and we have analyzed 21 excellent articles to explain this viewpoint. The rise of systems biology provides a revolutionary key to unlocking this "black box" and gaining a deeper understanding of the precise network of natural products regulating immune inflammation (Zhang et al., 2019; Li and Zhang, 2013).

The traditional linear research paradigm of "one gene, one protein, one drug" is inadequate for analyzing the typical complex system of "multi-component, multi-target, multi-pathway" in natural products. Systems biology adopts a holistic perspective, integrating multidimensional data such as genomics, transcriptomics, proteomics, metabolomics, and microbiology, and employing bioinformatics and computational models for integrated analysis (Kitano, 2002; Hopkins, 2008). It allows us to go beyond the limitations of single molecular events and provide a holistic view of how natural products disrupt the entire biological network, and ultimately reshape immune homeostasis (Li and Zhang, 2013).

Research driven by systems biology has profoundly revealed the immune regulatory mechanisms of numerous traditional Chinese medicine products and prominent natural product compounds. In the articles included in this Research Topic, it is revealed that ephedra sinica polysaccharides (from *Ephedra sinica*can) modulate the intestinal microbiota and anti-inflammatory immunity of bacterial metabolites in rheumatoid

arthritis, increase the levels of IL-1 β and IL-6 in restored mouse serum, and inhibit the entry of inflammatory factors from the intestine into the joints. The elevation of HDAC1 and HDAC2 levels induced by intestinal inflammation leads to NF-κ B phosphorylation and activation of TLR4 and MyD88 in synovial tissue of rheumatoid arthritis, which is a key factor contributing to immune imbalance in rheumatoid arthritis. Through integrated genomic and metabolomic analyses, it was found that the potential mechanism of action of ephedra sinica polysaccharides is enriched in taurine and hypotaurine metabolism, porphyrin metabolism, and the enrichment of short-chain fatty acid (SCFA)-producing bacteria. At the same time, metabolites involved in metabolic pathways may help ephedra sinica polysaccharides inhibit intestinal and synovial inflammation to alleviate rheumatoid arthritis. For natural product monomers, gene transcription testing found that Tanshinone IIA's (from *Salvia miltiorrhiza*) of the ATM/GADD45/ORC pathway alleviates myocardial ischemia-reperfusion injury, while Tanshinone IIA's of ATM significantly increases the protein expression levels of ATM, GADD45, and ORC1. By integrating transcriptome and protein interaction network analysis, researchers found that curcumin not only directly inhibits the expression of pro-inflammatory factors TNF - α and IL - 6, but also exerts broad-spectrum anti-inflammatory effects by regulating key JAK - STAT, NF - κ B, and MAPK signaling pathways (Aggarwal and Harikumar, 2009; He et al., 2015). The polyphenol EGCG in green tea demonstrates another advantage of systems biology - revealing host microbe interactions. Integrated metagenomic and metabolomic analyses demonstrated that EGCG significantly remodels the structure of intestinal microbiota, enrich beneficial bacteria producing short chain fatty acids, and enhance the expression of proteins critical for intestinal barrier integrity, thereby reducing systemic low-grade inflammation (Yang et al., 2016). The therapeutic evolution of artemisinin (derived from *Artemisia annua*) from antimalarial agents to immunomodulatory agents also benefited from systematic analysis. Research has found that its derivatives can activate the transcription factor Nrf2 pathway, induce the expression of a series of antioxidant enzymes, and inhibit the excessive activation of NLRP3 inflammasomes, demonstrating significant immunomodulatory and joint-protective effects in rheumatoid arthritis models (Wang et al., 2015; Krishna et al., 2008).

However, the journey of systems biology in natural product research still faces multiple challenges. The complexity of Chinese herbal medicine is the primary obstacle. The identification of active ingredients, interactions among each component, and their contributions to *in vivo* metabolic transformation products constitute an extremely complex network system, which has long hindered scientific interpretation and precise application (Gertsch, 2011; Efferth and Koch, 2011). The heterogeneity and dynamics of biological systems are equally crucial. The significant genetic background, epigenetic status, baseline immune status, and gut microbiota differences among individuals result in highly variable responses to the same natural product (Bashiardes et al., 2017; Zmora et al., 2019). The gap between system level insights and clinically effective interventions urgently needs to be bridged. How to transform complex network model predictions into actionable and precise therapeutic strategies, such as patient stratification, dose optimization, and combination therapies, and designing a experimental frameworks capable of capturing these network effects, remains a major challenge in current research (Barabási et al., 2011; He et al., 2023).

The rise of high-throughput omics technology has provided revolutionary tools to solve this problem (Wang et al., 2015). Proteomics can comprehensively depict the dynamic changes in inflammation-related protein expression profiles, post-translational modifications, and signaling pathways following traditional Chinese medicine intervention, accurately targeting key effector proteins and targets (Chen et al., 2020). Combining metabolomics analysis of small molecule metabolite disturbances can reveal the impact of traditional Chinese medicine on inflammation related metabolic reprogramming. Transcriptomics elucidates upstream regulatory mechanisms at the gene expression level. The collaborative application of these omics technologies not only enables the systematic analysis of the mechanism of action network of classical formulas, surpassing the limitations of single-target research (Wu et al., 2024), but also enables the discovery of potential specific combinations of biomarkers such as cytokines, acute phase proteins, metabolites, etc. For efficacy evaluation and disease classification (Chen et al., 2020). This has laid a solid foundation for modernizing traditional Chinese medicine formulas, guiding clinical precision medication, and developing innovative Chinese medicine formulations based on clear targets. In the future, the integration of multi omics data in systems biology and artificial intelligence analysis (Wu et al., 2024) will further promote the research on traditional Chinese medicine immune inflammation regulation from a "black box" to a more transparent and more precise stage, and accelerate its integration into international scientific and medical practice.

Author contributions

ZM: Writing – original draft. XL: Writing – review and editing.

Funding

The author(s) declare that financial support was received for the research and/or publication of this article. This work was supported by Beijing Natural Science Foundation General Project (7242254).

Conflict of interest

The authors declare that the research was conducted in the absence of any commercial or financial relationships that could be construed as a potential conflict of interest.

Generative AI statement

The author(s) declare that no Generative AI was used in the creation of this manuscript.

Publisher's note

References

Aggarwal, B. B., and Harikumar, K. B. (2009). Potential therapeutic effects of curcumin, the anti-inflammatory agent, against neurodegenerative, cardiovascular, pulmonary, metabolic, autoimmune and neoplastic diseases. *Int. J. Biochem. and cell Biol.* 41 (1), 40–59. doi:10.1016/j.biocel.2008.06.010

Barabási, A. L., Gulbahce, N., and Loscalzo, J. (2011). Network medicine: a network-based approach to human disease. *Nat. Rev. Genet.* 12 (1), 56–68. doi:10.1038/nrg2918

Bashiardes, S., Tuganbaev, T., Federici, S., and Elinav, E. (2017). The microbiome in anti-cancer therapy. *Seminars Immunol.* 32, 74–81. doi:10.1016/j.smim.2017.04.001

Chen, H., He, Y., Chen, S., Qi, S., and Shen, J. (2020). Therapeutic targets of oxidative/nitrosative stress and neuroinflammation in ischemic stroke: applications for natural product efficacy with omics and systemic biology. *Pharmacol. Res.* 158, 104877. doi:10.1016/j.phrs.2020.104877

Efferth, T., and Koch, E. (2011). Complex interactions between phytochemicals. The multi-target therapeutic concept of phytotherapy. *Curr. drug targets* 12 (1), 122–132. doi:10.2174/138945011793591626

Gertsch, J. (2011). Botanical drugs, synergy, and network pharmacology: forth and back to intelligent mixtures. *Planta medica.* 77 (11), 1086–1098. doi:10.1055/s-0030-1270904

He, X., Liu, X., Zuo, F., Shi, H., and Jing, J. (2023). Artificial intelligence-based multi-omics analysis fuels cancer precision medicine. *Seminars cancer Biol.* 88, 187–200. doi:10.1016/j.semcancer.2022.12.009

He, Y., Yue, Y., Zheng, X., Zhang, K., Chen, S., and Du, Z. (2015). Curcumin, inflammation, and chronic diseases: how are they linked? *Mol. Basel, Switz.* 20 (5), 9183–9213. doi:10.3390/molecules20059183

Hopkins, A. L. (2008). Network pharmacology: the next paradigm in drug discovery. *Nat. Chem. Biol.* 4 (11), 682–690. doi:10.1038/nchembio.118

Kitano, H. (2002). Systems biology: a brief overview. *Sci. (New York, N.Y.)* 295 (5560), 1662–1664. doi:10.1126/science.1069492

Krishna, S., Bustamante, L., Haynes, R. K., and Staines, H. M. (2008). Artemisinins: their growing importance in medicine. *Trends Pharmacol. Sci.* 29 (10), 520–527. doi:10.1016/j.tips.2008.07.004

Li, S., and Zhang, B. (2013). Traditional Chinese medicine network pharmacology: theory, methodology and application. *Chin. J. Nat. Med.* 11 (2), 110–120. doi:10.1016/S1875-5364(13)60037-0

Wang, J., Zhang, C. J., Chia, W. N., Loh, C. C., Li, Z., Lee, Y. M., et al. (2015). Haem-activated promiscuous targeting of artemisinin in Plasmodium falciparum. *Nat. Commun.* 6, 10111. doi:10.1038/ncomms10111

Wu, C., Wu, C., Peng, L., Wu, M., Li, Z., and Chen, J. (2024). Multi-omics approaches for the understanding of therapeutic mechanism for huang-qi-long-dan granule against ischemic stroke. *Pharmacol. Res.* 205, 107229. doi:10.1016/j.phrs.2024.107229

Yang, C. S., Zhang, J., Zhang, L., Huang, J., and Wang, Y. (2016). Mechanisms of body weight reduction and metabolic syndrome alleviation by tea. *Mol. Nutr. and food Res.* 60 (1), 160–174. doi:10.1002/mnfr.201500428

Zhang, W., Huai, Y., Miao, Z., Qian, A., and Wang, Y. (2019). Systems pharmacology for investigation of the mechanisms of action of traditional Chinese medicine in drug discovery. *Front. Pharmacol.* 10, 743. doi:10.3389/fphar.2019.00743

Zmora, N., Suez, J., and Elinav, E. (2019). You are what you eat: diet, health and the gut microbiota. *Nat. Rev. Gastroenterology and hepatology* 16 (1), 35–56. doi:10.1038/s41575-018-0061-2

frontiers | Frontiers in Pharmacology

TYPE Original Research
PUBLISHED 10 October 2023
DOI 10.3389/fphar.2023.1268641

OPEN ACCESS

EDITED BY
Guang Wang,
Jinan University, China

REVIEWED BY
Xiaofeng Yang,
Chongqing Medical University, China
Linfu Li,
Gannan Medical University, China

*CORRESPONDENCE
Shiyuan Wang,
60020005@sdutcm.edu.cn
Qingyang Zhao,
60060062@sdutcm.edu.cn

RECEIVED 28 July 2023
ACCEPTED 21 September 2023
PUBLISHED 10 October 2023

CITATION
Wang Y, Xu Y, Tan J, Ye J, Cui W, Hou J, Liu P, Li J, Wang S and Zhao Q (2023), Anti-inflammation is an important way that Qingre-Huazhuo-Jiangsuan recipe treats acute gouty arthritis.
Front. Pharmacol. 14:1268641.
doi: 10.3389/fphar.2023.1268641

Anti-inflammation is an important way that Qingre-Huazhuo-Jiangsuan recipe treats acute gouty arthritis

Yazhuo Wang[1], Yang Xu[1], Jingrui Tan[1], Jiaxue Ye[1], Weizhen Cui[1], Jie Hou[1], Peiyu Liu[1], Jianwei Li[1], Shiyuan Wang[2]* and Qingyang Zhao[2]*

[1]Institute of Traditional Chinese Medicine, Shandong University of Traditional Chinese Medicine, Jinan, China, [2]Institute of Nursing, Shandong University of Traditional Chinese Medicine, Jinan, China

Background: Acute gouty arthritis (AGA) significantly impairs patients' quality of life. Currently, existing therapeutic agents exhibit definite efficacy but also lead to serious adverse reactions. Therefore, it is essential to develop highly efficient therapeutic agents with minimal adverse reactions, especially within traditional Chinese medicine (TCM). Additionally, food polyphenols have shown potential in treating various inflammatory diseases. The Qingre-Huazhuo-Jiangsuan-Recipe (QHJR), a modification of Si-Miao-San (SMS), has emerged as a TCM remedy for AGA with no reported side effects. Recent research has also highlighted a strong genetic link to gout.

Methods: The TCM System Pharmacology (TCMSP) database was used to collect the main chemical components of QHJR and AGA-related targets for predicting the metabolites in QHJR. HPLC-Q-Orbitrap-MS was employed to identify the ingredients of QHJR. The collected metabolites were then used to construct a Drugs-Targets Network in Cytoscape software, ranked based on their "Degree" of significance. Differentially expressed genes (DEGs) were screened in the Gene Expression Omnibus (GEO) database using GEO2R online analysis. Subsequently, Gene Ontology (GO) and Kyoto Encyclopedia of Genes and Genomes (KEGG) enrichment analyses were performed. The DEGs were utilized to construct a Protein-Protein Interaction (PPI) Network via the STRING database. *In vivo* experimental validation was conducted using colchicine, QHJR, rapamycin (RAPA), and 3-methyladenine (3-MA) as controls to observe QHJR's efficacy in AGA. Synovial tissues from rats were collected, and qRT-PCR and Western blot assays were employed to investigate Ampk-related factors (Ampk, mTOR, ULK1), autophagy-related factors (Atg5, Atg7, LC3, p62), and inflammatory-related factors (NLRP3). ELISA assays were performed to measure inflammatory-related factor levels (IL-6, IL-1β, TNF-α), and H&E staining was used to examine tissue histology.

Abbreviations: QHJR, Qingre-Huazhuo-Jiangsuan Recipe; RAPA, rapamycin; 3-MA, 3-Methyladenine; LC3, Light Chain 3; TCMSP, The TCM system pharmacology database; DEGs, differentially expressed genes; TCM, Traditional Chinese medicine; GO, Gene ontology; KEGG, Kyoto Encyclopedia of Genes and Genomes; GEO, Gene expression omnibus; PPI network, Protein-Protein Interaction network; HE, Hematoxylin-eosin staining assay; ELISA, Enzyme-linked immunosorbent assay; qRT-PCR, Quantitative Real-Time PCR; WB, Western blot.

Results: Network analysis screened out a total of 94 metabolites in QHJR for AGA. HPLC-Q-Orbitrap-MS analysis identified 27 of these metabolites. Notably, five metabolites (Neochlorogenic acid, Caffeic acid, Berberine, Isoliquiritigenin, Formononetin) were not associated with any individual herbal component of QHJR in TCMSP database, while six metabolites (quercetin, luteolin, formononetin, naringenin, taxifolin, diosgenin) overlapped with the predicted results from the previous network analysis. Further network analysis highlighted key components, such as Caffeic acid, cis-resveratrol, Apigenin, and Isoliquiritigenin. Other studies have found that their treatment of AGA is achieved through reducing inflammation, consistent with this study, laying the foundation for the mechanism study of QHJR against AGA. PPI analysis identified TNF, IL-6, and IL-1β as hub genes. GO and KEGG analyses indicated that anti-inflammation was a key mechanism in AGA treatment. All methods demonstrated that inflammatory expression increased in the Model group but was reversed by QHJR. Additionally, autophagy-related expression increased following QHJR treatment. The study suggested that AMPKα and p-AMPKα1 proteins were insensitive to 3 MA and RAPA, implying that AMPK may not activate autophagy directly but through ULK1 and mTOR.

Conclusion: In conclusion, this study confirms the effectiveness of QHJR, a modified formulation of SMS (a classic traditional Chinese medicine prescription for treating gout), against AGA. QHJR, as a TCM formula, offers advantages such as minimal safety concerns and potential long-term use. The study suggests that the mechanism by which QHJR treats AGA may involve the activation of the AMPK/mTOR/ULK1 pathway, thereby regulating autophagy levels, reducing inflammation, and alleviating AGA. These findings provide new therapeutic approaches and ideas for the clinical treatment of AGA.

KEYWORDS

QHJR, AGA, apoptosis, autophagy, inflammation, gene

1 Introduction

Acute gouty arthritis (AGA) represents a major and increasingly serious public health issue, whose incidence is increasing year by year and seriously impacting people's health and lives (Zhu et al., 2011; Khanna et al., 2015; Terkeltaub, 2017). AGA is a common inflammatory disease, mainly manifested by a potent inflammatory response resulting from monosodium urate (MSU) crystal deposition in tissues including joints (Fischer et al., 2018; Gu et al., 2021). MSU crystals accumulate in periarticular tissues, which can stimulate joint synovium and produce pathological reactions including leucocyte exudate, synovial vasodilation, and enhanced permeability (Lyu et al., 2021). The existing anti-inflammatory drugs adopted for treating and preventing gouty arthritis (GA) have been limited (Gu et al., 2021). However, just 1/2 of AGA cases can respond to the existing therapeutics (Yuan et al., 2019; Gu et al., 2021). Therefore, it is essential to investigate the efficacy of Traditional Chinese Medicine (TCM).

Traditional Chinese Medicine (TCM) has been used to treat gouty arthritis (GA) for centuries. The most widely used TCM treatments for GA are acupuncture and the Chinese herbal medicine Si-Miao-San (Chi et al., 2020; Pu et al., 2021). Acupuncture is based on the theory of meridians, while SMS is a combination of four herbs that have been used to treat GA for over 1,000 years (Chi et al., 2020; Pu et al., 2021), SMS can significantly improve the symptoms of acute arthritis in gout patients, and its curative effect is not lower than colchicine, with small side effects (Chi et al., 2020; Pu et al., 2021). SMS is effective in the treatment of GA through anti-inflammation and lowering urate (Chi et al., 2020; Pu et al., 2021). Acupuncture treatment for GA involves the ing spleen, to the unifying kidney, dissipating dampness, resolving blood stasis, clearing away heat, and removing toxins (Chi et al., 2020; Pu et al., 2021). Qingre-Huazhuo-Jiangsuan Recipe (QHJR), one of the TCM prescriptions, is prepared based on the classic TCM prescription Si-Miao-San that can be empirically adopted for treating GA during the clinical practice of TCM (Fan et al., 2010). In traditional Chinese medicine, the pathological mechanism of GA is primarily believed to involve "damp-heat descending, leading to obstructing the meridians and the sluggish circulation of qi and blood." However, AGA has a sudden onset, and its pathological mechanism is mainly characterized by "internal accumulation of damp-heat turbidity, which flows and affects the viscera and joints." Therefore, based on SMS (a previous treatment method), modifications were made by retaining and increasing the dosage of Coix lacryma-jobi var. ma-yuen (Rom.Caill.) Stapf (Poaceae; Coicis semen) and Atractylodes Lancea (Thunb.) DC (Asteraceae; Atractylodis rhizoma), and incorporating other heat-clearing, detoxifying, and turbidity-resolving herbs to consolidate the treatment. QHJR is composed of 11 botanical drugs, including Reynoutria japonica Houtt (Polygonaceae; Polygoni cuspidati rhizoma et radix), Spatholobus suberectus Dunn (Fabaceae; Spatholobi caulis), Dioscorea septemloba Thunb (Dioscoreaceae; Dioscoreae spongiosae rhizoma), Atractylodes Lancea (Thunb.) DC (Asteraceae; Atractylodis rhizoma), Plantago depressa Willd

(Plantaginaceae; Plantaginis semen), Clematis chinensis Osbeck (Ranunculaceae; Clematidis radix et rhizoma), Smilax glabra Roxb (Smilacaceae; Smilacis glabrae rhizoma), Poria cocos (Schw.) Wolf (Polyporaceae; Poria), Curcuma longa L (Zingiberaceae; Curcumae longae rhizoma), Perilla frutescens L.) Britton (Lamiaceae; Perillae folium) and Coix lacryma-jobi var. ma-yuen (Rom.Caill.) Stapf (Poaceae; Coicis semen). Please refer to Supplementary Table S1 for details. The drugs of first choice for acute gouty arthritis are nonsteroidal anti-inflammatory drugs (NSAID), corticosteroids, and colchicine (Engel et al., 2017). Colchicine is a well-established and affordable anti-inflammatory agent with a long history of use for treating various diseases, primarily rheumatic and cardiac conditions, as well as gout attacks (Thompson and Nidorf, 2018; El Hasbani et al., 2021). However, it is important to note that it has potential side effects, such as liver failure (Abbott et al., 2017), diarrhea (Tardif et al., 2019), and vomiting (Angelidis et al., 2018). Colchicine has been shown to have several mechanisms of action in the treatment of gout, including inhibiting the activation of the NLRP3 inflammasome, blocking the release of IL-1β (Cronstein and Terkeltaub, 2006; Nuki, 2008; Dalbeth et al., 2014). Its primary mode of treatment is anti-inflammatory, which is consistent with this study (Thompson and Nidorf, 2018). In this study, QHJR was compared to colchicine as a control group to investigate whether it could reduce inflammation consistently or not and to explore the mechanism of QHJR on AGA.

The molecules identified in gout are involved in a multitude of critical processes, including the degradation of the extracellular matrix in cartilage cells, transduction of inflammatory signals, and regulation of fibroblast-like synoviocyte invasion pathways (Liu et al., 2014; Chew et al., 2018; Shu et al., 2022). In addition, miRNAs and lncRNAs have been shown to play indispensable roles in the initiation of inflammation in acute gout as constituents of MSU-induced inflammatory pathways (Papanagnou et al., 2016; Xu B. Y. et al., 2020; Galozzi et al., 2021; Shu et al., 2022). The results underscore the potential of these molecules as targets for the prediction and management of AGA, thereby warranting further study and exploration.

Autophagy represents the basic intracellular decomposition event, and has different effects on immunity, thereby maintaining cell homeostasis while also determining their fate (Hao and Liu, 2021). Autophagy is a finely regulated cellular program in which multiple pathways play vital roles. During the last decade, human genetic research suggests that autophagy is tightly associated with autoimmune/inflammatory disorders and cancers (Lyu et al., 2021). Recent research shows that autophagy is related to arthritis progression. For example, based on Yun Yu et al. (Yu S. et al., 2020), autophagy expression has effects on arthritis. According to Piras et al. (Piras et al., 2017; Yang et al., 2021), autophagy suppression decreased bone erosion severity and osteoclast (OC) number, suggesting that the critical function of autophagy is protecting bone tissues. Studies have shown that autophagy plays a key role in the pathogenesis of GA (Han et al., 2021). MSU crystals, which are associated with gouty arthritis, have been shown to induce autophagy in macrophages and synovial tissues from patients with gouty arthritis (Xiao et al., 2023; Yuan et al., 2023). Autophagy-lysosomal pathway (ALP) perturbations have been observed in synovial macrophages from patients with gouty arthritis (Chen et al., 2023). Autophagy is involved in decreasing inflammation. It has been suggested that autophagy induced by *P*P121 can alleviate MSU crystal-induced acute gouty arthritis via inhibition of the NLRP3 inflammasome (Yuan et al., 2023). Autophagy inhibits inflammatory signaling complexes (Deretic and 2021). Autophagy may directly regulate inflammation by removing or down-regulating pro-inflammatory cytokines and degrading inflammasome components (Pang et al., 2022). Modulation of autophagy, which plays a critical role in inflammation by influencing the development, homeostasis, and survival of inflammatory cells, might lead to therapeutic interventions for diseases associated with inflammation (Qian et al., 2017). The aforementioned literature research highlights the critical role of autophagy in AGA. To validate the role of autophagy in inflammation, this study employed rapamycin (RAPA, an autophagy inducer) and 3-methyladenine (3-MA, an autophagy inhibitor) as control groups to observe changes in autophagy levels and their impact on AGA. This approach aimed to elucidate the mechanism of action of QHJR in AGA.

AMP-activated protein kinase (AMPK), the highly conserved serine/threonine-protein kinase, serves as an intracellular energy sensor with significant effects on catabolism and anabolism regulation (Li and Chen, 2019). Referred to as the metabolic master switch, AMPK plays a pivotal role in controlling cellular energy supply and is synthesized in various organs, including the liver, brain, fat cells, and muscle cells (Li and Chen, 2019). Functioning as a regulator of autophagy, AMPK promotes autophagy and facilitates the autophagic degradation of mitochondria (mitophagy) by inducing the fragmentation of damaged mitochondria and promoting the translocation of the autophagy machinery to these damaged organelles (Li and Chen, 2019). AMPK plays a significant role in the maintenance of cellular energy homeostasis, which is closely related to autophagy (Wang S. et al., 2022). AMPK-mediated pathways are involved in autophagy and aging processes (Ge et al., 2022). AMPK can accelerate autophagy through its different actions at diverse autophagy regulatory levels, which are obtained by the specific phosphorylation of autophagy-related protein complexes (Li and Chen, 2019). In summary, AMPK and autophagy are closely related, and AMPK plays a significant role in the regulation of autophagy.

Gout is commonly associated with excesses in soluble urate and in nutrition, both of which involve AMPK activity (Wang et al., 2016; Terkeltaub, 2017). AMPK activation has been found to alleviate high uric acid-induced Na^+-K^+-ATPase signaling impairment and cell injury in renal tubules (Xiao et al., 2019). Charles McWherter et al. (McWherter et al., 2018) found that Arhalofenate acid inhibits monosodium urate crystal-induced inflammatory responses through activation of AMPK signaling, which likely contributes to a reduction of gout flares (McWherter et al., 2018). These findings suggest that AMPK may play a role in the development and treatment of gouty arthritis. Further research is needed to fully understand the implications of AMPK in gout and to develop effective treatments targeting AMPK. The activation of AMPK is found to cause autophagy through two distinct mechanisms, namely, the direct phosphorylation of ULK1 (Unc-51-Like Kinase 1, a mammalian orthologue of Atg1) and the inhibition of the mammalian target of rapamycin (mTOR) protein kinase complex (Li and Chen, 2019). This signal pathway has been confirmed, also providing a strong theoretical foundation for QHJR treatment of AGA. In this study, to explore the mechanism of QHJR on AGA, we validated whether the Ampkα1/ulk1/mTOR pathway could be activated by QHJR to regulate autophagy, reduce inflammation, and effectively alleviate AGA.

2 Methods

2.1 QHJR metabolites screening

We employed the TCMSP database (https://old.tcmsp-e.com/tcmsp.php) (Ru et al., 2014) to explore the metabolite composition of QHJR. This database provides comprehensive information on various molecular aspects, such as composition number, molecular name, molecular weight, fat-water partition coefficient, hydrogen bond donor-acceptor count, oral bioavailability (OB), intestinal epithelium permeability, blood-brain barrier (BBB) permeability, drug similarity (DL), and drug half-life (HL). The OB represents the percentage of unchanged drug that reaches the systemic circulation after oral administration. DL indexes can be used to optimize pharmacokinetic and pharmaceutical properties, such as solubility and chemical stability (Zhou et al., 2020; Liu et al., 2023). The criteria of OB ≥ 30% and DL ≥ 0.18 have been set to screen for active compounds because they indicate that the compound has good oral bioavailability and drug-like properties, which are important for a compound to be effective as a drug (https://www.tcmsp-e.com/load_intro.php?id=29) (Yu Y. et al., 2020; Ruan et al., 2020; Ye et al., 2023).

2.2 Network construction

The UniProt database (https://www.uniprot.org/) and Search Tool for the Retrieval of Interacting Genes database (https://string-db.org) were utilized to convert protein gene names and obtain drug component targets. For comprehensive information on human genes, encompassing genome, proteome, transcription, heredity, and function, we turned to the GeneCards Database (https://www.genecards.org/) (Safran et al., 2010). AGA-related targets were gathered from the GeneCards Database. The cross-targets were obtained by merging the disease-related targets with the drug-component targets. After the data were imported into Cytoscape 3.9.1 software (Shannon et al., 2003), a "Botanical drug-metabolite-target" network model was constructed, in which the nodes represent herbs, ingredients, and targets, while the edges represent the relationship role among the three nodes. We calculated the 'degree' value according to the number of associations between each node (Liu et al., 2023; Ye et al., 2023).

2.3 Data sources and screen out DEGs

The initial step of our study involved performing a keyword search using "acute gouty arthritis" and "*Homo sapiens*" in the search field of the GEO database (https://www.ncbi.nlm.nih.gov/geo/). These keywords were selected to retrieve relevant data. Through this search, we identified gene chip data with the accession number GSE160170. The GSE160170 dataset was based on the GPL21827 platform, specifically the Agilent-079487 Arraystar Human LncRNA microarray V4 (Probe Name version). This dataset comprised a total of 6 specimens from individuals with gout and 6 specimens from individuals serving as normal controls.

2.4 PPI network

To construct a protein-protein interaction (PPI) network, we employed the STRING database (https://string-db.org/) (Szklarczyk et al., 2021). Subsequently, the Cytoscape 3.9.1 software's "cytoHubba" plugin (Doncheva et al., 2023) was utilized to compute the top ten hub genes from both upregulated and downregulated hub genes.

2.5 GO and KEGG analysis

To investigate the functional annotations of DEGs, we performed GO analysis (Liu et al., 2018)and KEGG (Kanehisa et al., 2017) analysis using the online tool DAVID (https://david.ncifcrf.gov/). To identify significantly enriched genes, we set the critical value at $p < 0.05$ and $|\log2(FC)| > 1$. In this study, the "clusterprofiler" package in the R software was employed to analyze the primary functions of the DEGs.

2.6 Preparation of drugs

11 botanical drugs of QHJR (Supplementary Table S1) were purchased from Shandong Provincial Hospital of TCM pharmacy (Jinan, China), and prepared using the water decoction and alcohol precipitation method at the Experimental Center of Shandong University of TCM (Jinan, China). Colchicine (MedChemExpress, Lot No: HY-16569), 200 mg per unit. Rapamycin (MedChemExpress, Lot No: HY-10219), 10 mg per unit. 3-Methyladenine (MedChemExpress, Lot No: HY-19312), 50 mg per unit.

First, fry the Atractylodis rhizoma and Coicis semen until they turn slightly yellow, and prepare the Plantaginis semen by wrapping it with gauze. Soak all the botanical drugs (except Plantaginis semen) in purified water for 2 h, then remove them and prepare for decoction. Next, place all the botanical drugs (Polygoni cuspidati rhizoma et radix, Spatholobi caulis, Dioscoreae spongiosae rhizoma, Atractylodis rhizoma, Plantaginis semen, Clematidis radix et rhizoma, Smilacis glabrae rhizoma, Poria, Curcumae longae rhizoma, Perillae folium, Coicis semen) in a pot filled with 2 L of water and boil for 0.5 h. Concentrate the decoction to concentrations of 5.15 g/mL (botanical drug/water), 2.56 g/mL (botanical drug/water), and 1.3 g/mL (botanical drug/water) respectively according to the concentration requirements of the QHJR-High, QHJR-Medium, and QHJR-Low groups. The "g/mL" means "drug—solvent ratio", which is all the botanical drugs of QHJR to pure water. Filter the botanical drugs using gauze to collect the herbal liquid. The decoction was then entrusted to a temperature-controlled refuge within a refrigerator, maintained at a frosty 4 °C.

2.7 QHJR extract and HPLC-Q-Orbitrap-MS analysis

Prepare the drug solution (QHJR) (Supplementary Table S1) with a concentration of 2.56 g/mL (botanical drug/water) following the method described above and store it in a refrigerator at −18 °C. After thawing, the samples were vigorously treated by vortexing for 30 s and centrifugation at 12,000 rpm and 4°C for 10 min. A 200 μL

portion from each sample was transferred to an Eppendorf tube and combined with 1,000 μL of a 4:1 (v/v) methanol-water extraction solution. This mixture underwent another round of vortexing and centrifugation at 12,000 rpm and 4°C for 10 min. The resulting supernatant was meticulously filtered through a 0.22-μm filter and placed in an autosampler vial for subsequent analysis. The liquid chromatography (LC) separation utilized an HPLC AQ-C18 column (1.8 μm × 150 mm × 2.1 mm, Welch, China) with mobile phases of 0.1% formic acid A) and methanol B). The LC system operated at a flow rate of 300 μL/min, an injection volume of 5 μL, and the following gradient: 0–5 min (2%–20% B), 5–10 min (20%–50% B), 10–15 min (50%–80% B), 15–20 min (80%–95% B), and 20–27 min (95% B) (Supplementary Table S2). An LC system integrated with a Q-Orbitrap mass spectrometer (Thermo Fisher Scientific, United States) played a pivotal role in analyzing the chemical composition of QHJR. The system employed carefully selected parameters including a sheath gas flow rate of 40 Arb, an auxiliary gas flow rate of 15 Arb, a full MS resolution of 70,000, a capillary temperature of 300°C, an MS/MS resolution of 17,500, a spray voltage of 3.2 kV (positive), and a collision energy of 30 in NCE mode. This setup effectively unraveled the intricate molecular constituents. The task of determining the chemical composition of QHJR was entrusted to Wuhan Xavier Biotechnology Co., Ltd., who followed established protocols and methodologies with meticulous care. The detailed information is available in Supplementary Table S2.

2.8 Drug-target network

The key metabolites predicted and identified were searched in the PubChem database (https://pubchem.ncbi.nlm.nih.gov/) to obtain their structural information. The obtained structures were then imported into Swiss Target Prediction (http://www.swisstargetprediction.ch/) to predict their target proteins. Disease-related target proteins were retrieved from the GeneCards database (https://www.genecards.org/) (Safran et al., 2010)and filtered for those related to the disease among the identified metabolite targets. The disease-related metabolites and their corresponding targets were imported into Cytoscape (Shannon et al., 2003)3.9.1 for constructing a metabolite-target network and analysis.

2.9 Animals and establishment of AGA models

A total of 88 male Sprague-Dawley rats with SPF-grade, weighing 180 ± 20 g, were sourced from Beijing Weitong Lihua Laboratory Animal Technology Co., Ltd (License number: Beijing Baishan SCXK 2016–0006). The rats were categorized into 8 groups (n = 11) for further experimentation, including the Normal group, Model group, QHJR-H group, QHJR-M group, QHJR-L group, Colchicine group, RAPA g, group, and 3-MA group. The rate in the Normal group injected normal saline (NS) was used as the control. The others were injected with normal MSU to the sestablishAGA model (according to Fischer, Brusco et al. (Fischer et al., 2018) method) on day 5. Normal group and Model group with pure water by gavage, colchicine group with colchicine by gavage. QHJR groups were given QHJR-H, QHJR-M, and QHJR-L, respectively. The 3-MA and RAPA groups were intraperitoneally injected with 3-MA and RAPA, respectively.

2.10 H&E assay

The knee joints of rats were dissected to obtain synovial tissues, which were subsequently fixed in 4% paraformaldehyde for a duration exceeding 24 h. The fixed tissues were then embedded in paraffin. Additional synovial tissues were preserved in liquid nitrogen at −80 °C for subsequent Quantitative Real-Time PCR and Western blot assays. Following this, 4-μm thick sections of paraffin-embedded tissue were deparaffinized, stained with hematoxylin and eosin (HE), subjected to dehydration using fractional xylene and ethanol, and ultimately sealed with neutral gums.

2.11 ELISA assay

Blood samples were collected from the abdominal aorta of rats, and the freshly obtained blood was allowed to stand before being centrifuged at 3500 rpm for a duration of 10 min. The serum was extracted at −80 °C for preservation. The levels of TNF-α, IL-1β, and IL-6 were determined using an ELISA kit, following the manufacturer's instructions.

2.12 qRT-PCR assay

Ex Taq-enzyme Kit (Solarbio PC1100) was employed to extract total synovial RNA, while PrimeScript RTregent Kit (Takara, Japan) was used to prepare cDNA through reverse transcription. qRT-PCR machine CFX96 (Excell Bio IT041-0002, China) was used for qRT-PCR, and the reaction system included respective primers (1 μL each), Power SYBR® Green Master Mix (2*, 12.5 μL), DEPC water (9.5 μL) and cDNA (1 μL). The reaction procedure was presented as follows activation under 95°C; 20-s amplification under 95°C; 30-s un3058°C and 20-s under 72°C for a total of 40 cycles. The $2^{-\Delta\Delta CT}$ method was performed to quantify PCR analysis. Supplementary Table S3 displays the sequences of all primers utilized in this study (Sangon Biotech, Shanghai, China).

2.13 Western blot

The mixture containing RIPA lysates and protease/phosphatase inhibitors was adopted for extracting total synovial proteins. Protein content was quantified by a BCA kit (Solarbio PC0020). Protein aliquots were separated through SDS-PAGE, followed by transfer onto PVDF membranes (Millipore). Then, membranes were blocked using 5% defatted milk for 2 h, followed by overnight primary antibody incubation under 4°C (as shown in Supplementary Table S4). Next, the ECL Kit (Solarbio, no. PE0010) was used for visualizing protein bands, using β-actin as the endogenous control. Images were analyzed with ImageJ (Table 4).

2.14 Statistical analysis

There are 3 samples for each set of data. Data were represented by means ± SD. Tukey's multiple comparison test was conducted by one-way ANOVA by GraphPad Prism version 8.0. *$p < 0.05$,**$p < 0.01$, ***$p < 0.001$ represented obviously difference.

3 Results

3.1 QHJR's target prediction for AGA

A comprehensive search for 1,620 metabolites in QHJR was performed using the TCMSP database, including 315 from Polygoni Cuspidati Rhizoma Et Radix, 405 from Spatholobus Suberectus Dunn, 14 from Dioscoreae Septemlo Bae Rhizoma, 67 from Atractylodes lancea (Thunb.)Dc., 189 from Plantaginis Semen, 67 from Radix Clematidis, 315 from Smilacis Glabrae Rhixoma, 21 from Poria Cocos (Schw.) Wolf., 38 from Curcumaelongae Rhizoma, 145 from Perilla Frutescens, and 44 from Coicis Semen. Screening based on OB ≥ 30% and DL ≥ 0.18 yielded 117 metabolites, with 10 from Polygoni Cuspidati Rhizoma Et Radix, 24 from Spatholobus Suberectus Dunn, 2 from Dioscoreae Septemlo Bae Rhizoma, 9 from Atractylodes Lancea (Thunb.)Dc., 9 from Plantaginis Semen, 7 from Radix Clematidis, 15 from Smilacis Glabrae Rhixoma, 15 from Poria Cocos (Schw.) Wolf., 3 from Curcumaelongae Rhizoma, 14 from Perilla Frutescens, and 9 from Coicis Semen. After removing duplicates, 94 metabolites were identified. Table 1 displays these metabolites found in QHJR.

Protein gene names were converted using the STRING and UniProt databases, and AGA targets were subsequently identified in GeneCards. The intersection of these targets was then employed to construct the "Botanical drug-Metabolite-Target" network, as depicted in Figure 1. Our predictions suggested that these metabolites predicted in QHJR may have the potential to impact the target, as detailed in Table 2.

3.2 Chemical composition of QHJR extract

The main components in extracts of QHJR were analyzed qualitatively based on HPLC-Q-Orbitrap-MS. The analysis results are shown in Figure 2 and Table 3, including the total ion chromatogram of HPLC-Q-Orbitrap-MS, as well as the structural formula of the main chemical components in QHJR. According to the above analysis, as well as the comparison of TCMSP database and literature, 27 main metabolites were detected, identified and speculated within 30 min by the mass spectrum behavior and fragment ion characteristics (Figure 2) (Table 3), as follow: Citric acid, Chlorogenic acid, Geniposidic acid, Neochlorogenic acid, 3,4-Dihydroxybenzaldehyde, Catechin, Caffeic acid, cis-Resveratrol, Berberine, Ferulic acid, Safrole, Astilbin, Taxifolin, 7-Hydroxycoumarine, Apigenin, Quercetin, Isoliquiritigenin, Naringenin, Genistein, Luteolin, Curcumin, Biochanin A, Dibutyl phthalate, 2-Hydroxymyristic acid, Palmitic acid, Formononetin, Diosgenin. Of these metabolites, six were found to agree with prior predictions by Network Analysis (quercetin, luteolin, formononetin, naringenin, taxifolin, and diosgenin), while five metabolites (Neochlorogenic acid, Caffeic acid, Berberine, Isoliquiritigenin, Formononetin) of them that are shown in the TCMSP database to not belong to any single herbal component of QHJR. From this, we infer that these metabolites may be the result of interactions between different botanical drugs within QHJR, generating new metabolites. These findings suggest that QHJR may not only work through the individual actions of its constituent herbs but also potentially through the synergistic production of new metabolites, contributing to its therapeutic effect on AGA.

3.3 Identification of related genes in AGA

To identify novel targets for treating AGA, we conducted a genetic analysis of this condition. Using the GEO database, we obtained the GSE160170 dataset and performed online analysis using GEO2R. DEGs were screened out as $p < 0.05$ and $|\log2(FC)| > 1$, and it was shown as the volcano (Figure 3A) and heatmap (Figure 3B) by RStudio (Version 4.2.1). By comparing the gout group to the control group, we identified 2,369 DEGs in GSE160170, comprising 1,390 upregulated and 979 downregulated genes. Normalization of the original data was achieved using the R packages ggplot2 (version 3.4.1) and pheatmap (version 1.0.12), enabling visualization of the volcano and hotspot maps depicting the relevant gene expression (Figures 3A,B).

Following the removal of redundant genes, we subjected the remaining 1,412 DEGs from GSE160170 to PPI analysis using the STRING database (Fig. A–C). Then, the top 10 hub genes were identified based on their node degree and included TNF, IL6, IL1B, IL10, IFNG, CD80, CXCL8, CCL3, STAT1, and IL1A (Figure 4D).

3.4 KEGG and GO enrichment analysis

DEGs in GSE160170 exhibit associations with leukocyte chemotaxis, cell chemotaxis, leukocyte migration, reproductive system development, reproductive structure development, regulation of vasculature development, positive regulation of leukocyte migration, *etc.*, based on GO analysis (as depicted in Figure 5A). Furthermore, the DEGs are relevant to various pathways including Viral protein interaction with cytokine and cytokine receptor, Toll-like receptor signaling pathway, TNF signaling pathway, TGF-beta signaling pathway, Rheumatoid arthritis, p53 signaling pathway, Osteoclast differentiation, Non-alcoholic fatty liver disease, NOD-like receptor signaling pathway, NF-kappa B signaling pathway, Neutrophil extracellular trap formation, MAPK signaling pathway, Lipid and atherosclerosis, Inflammatory bowel disease, IL-17 signaling pathway, Hepatitis C, Gap junction, FoxO signaling pathway, Cytokine-cytokine receptor interaction, Chemokine signaling pathway, C-type lectin receptor signaling pathway, Apoptosis-multiple species, Apoptosis, *etc.*, based on KEGG analysis (Figure 5B).

Our current study results, in combination with previous protein-protein interaction (PPI) analysis, indicate that QHJR may reduce inflammation through the involvement of TNF, IL6, IL1B, and other factors. Therefore, we further investigated and evaluated the role of QHJR in the treatment of AGA by establishing a rat model of AGA *in vivo* to explore if it was related to inflammation.

TABLE 1 Metabolites were predicted of QHJR in the TCMSP database.

Botanical drug	Code	Metabolites	OB(%)	DL
Polygoni Cuspidati Rhizoma Et Radix	MOL013281	6,8-Dihydroxy-7-methoxyxanthone	35.83	0.21
Polygoni Cuspidati Rhizoma Et Radix	MOL013287	Physovenine	106.21	0.19
Polygoni Cuspidati Rhizoma Et Radix	MOL013288	Picralinal	58.01	0.75
Polygoni Cuspidati Rhizoma Et Radix	MOL002259	Physciondiglucoside	41.65	0.63
Polygoni Cuspidati Rhizoma Et Radix	MOL002268	rhein	47.07	0.28
Polygoni Cuspidati Rhizoma Et Radix	MOL002280	Torachrysone-8-O-beta-D-(6'-oxayl)-glucoside	43.02	0.74
Polygoni Cuspidati Rhizoma Et Radix	MOL000358	beta-sitosterol	36.91	0.75
Polygoni Cuspidati Rhizoma Et Radix	MOL000492	(+)-catechin	54.83	0.24
Polygoni Cuspidati Rhizoma Et Radix	MOL000006	luteolin	36.16	0.25
Polygoni Cuspidati Rhizoma Et Radix	MOL000098	quercetin	46.43	0.28
Spatholobus Suberectus Dunn	MOL000296	hederagenin	36.91	0.75
Spatholobus Suberectus Dunn	MOL000033	(3S,8S,9S,10R,13R,14S,17R)-10,13-dimethyl-17-[(2R,5S)-5-propan-2-yloctan-2-yl]-2,3,4,7,8,9,11,12,14,15,16,17-dodecahydro-1H-cyclopenta [a]phenanthren-3-ol	36.23	0.78
Spatholobus Suberectus Dunn	MOL000392	formononetin	69.67	0.21
Spatholobus Suberectus Dunn	MOL000417	Calycosin	47.75	0.24
Spatholobus Suberectus Dunn	MOL000449	Stigmasterol	43.83	0.76
Spatholobus Suberectus Dunn	MOL000461	3,7-dihydroxy-6-methoxy-dihydroflavonol	43.8	0.26
Spatholobus Suberectus Dunn	MOL000468	8-o-Methylreyusi	70.32	0.27
Spatholobus Suberectus Dunn	MOL000469	3-Hydroxystigmast-5-en-7-one	40.93	0.78
Spatholobus Suberectus Dunn	MOL000470	8-C-α-L-arabinosylluteolin	35.54	0.66
Spatholobus Suberectus Dunn	MOL000471	aloe-emodin	83.38	0.24
Spatholobus Suberectus Dunn	MOL000483	(Z)-3-(4-hydroxy-3-methoxy-phenyl)-N-[2-(4-hydroxyphenyl)ethyl]acrylamide	118.35	0.26
Spatholobus Suberectus Dunn	MOL000490	petunidin	30.05	0.31
Spatholobus Suberectus Dunn	MOL000491	Augelicin	37.5	0.66
Spatholobus Suberectus Dunn	MOL000493	campesterol	37.58	0.71
Spatholobus Suberectus Dunn	MOL000497	licochalcone a	40.79	0.29

(Continued on following page)

TABLE 1 (*Continued*) Metabolites were predicted of QHJR in the TCMSP database.

Botanical drug	Code	Metabolites	OB(%)	DL
Spatholobus Suberectus Dunn	MOL000500	Vestitol	74.66	0.21
Spatholobus Suberectus Dunn	MOL000501	Consume close grain	68.12	0.27
Spatholobus Suberectus Dunn	MOL000502	Cajinin	68.8	0.27
Spatholobus Suberectus Dunn	MOL000503	Medicagol	57.49	0.6
Spatholobus Suberectus Dunn	MOL000506	Lupinidine	61.89	0.21
Spatholobus Suberectus Dunn	MOL000507	Psi-Baptigenin	70.12	0.31
Dioscoreae Septemlo Bae Rhizoma	MOL013233	EINECS 213–897–0	71.96	0.72
Dioscoreae Septemlo Bae Rhizoma	MOL000546	diosgenin	80.88	0.81
Atractylodes Lancea (Thunb.)Dc.	MOL000173	wogonin	30.68	0.23
Atractylodes Lancea (Thunb.)Dc.	MOL000179	2-Hydroxyisoxypropyl-3-hydroxy-7-isopentene-2,3-dihydrobenzofuran-5-carboxylic	45.2	0.2
Atractylodes Lancea (Thunb.)Dc.	MOL000184	NSC63551	39.25	0.76
Atractylodes Lancea (Thunb.)Dc.	MOL000186	Stigmasterol 3-O-beta-D-glucopyranoside_qt	43.83	0.76
Atractylodes Lancea (Thunb.)Dc.	MOL000188	3β-acetoxyatractylone	40.57	0.22
Atractylodes Lancea (Thunb.)Dc.	MOL000085	beta-daucosterol_qt	36.91	0.75
Atractylodes Lancea (Thunb.)Dc.	MOL000088	beta-sitosterol 3-O-glucoside_qt	36.91	0.75
Atractylodes Lancea (Thunb.)Dc.	MOL000092	daucosterin_qt	36.91	0.76
Atractylodes Lancea (Thunb.)Dc.	MOL000094	daucosterol qt	36.91	0.76
Plantaginis Semen	MOL001663	(4aS,6aR,6aS,6bR,8aR,10R,12aR,14bS)-10-hydroxy-2,2,6a,6b,9,9,12a-heptamethyl-1,3,4,5,6,6a,7,8,8a,10,11,12,13,14b-tetradecahydropicene-4a-carboxylic acid	32.03	0.76
Plantaginis Semen	MOL001735	Dinatin	30.97	0.27
Plantaginis Semen	MOL000359	sitosterol	36.91	0.75
Plantaginis Semen	MOL005869	daucostero_qt	36.91	0.75
Plantaginis Semen	MOL007813	Dihydrotricetin	58.12	0.28
Plantaginis Semen	MOL007819	Hypolaetin	33.24	0.28
Plantaginis Semen	MOL007835	orobanchoside_qt	55.99	0.82
Plantaginis Semen	MOL007836	plantaginin_qt	54.04	0.24
Radix Clematidis	MOL002372	(6Z,10E,14E,18E)-2,6,10,15,19,23-hexamethyltetracosa-2,6,10,14,18,22-hexaene	33.55	0.42
Radix Clematidis	MOL005594	ClematosideA'_qt	37.51	0.76
Radix Clematidis	MOL005598	Embinin	33.91	0.73
Radix Clematidis	MOL005603	Heptyl phthalate	42.26	0.31

(Continued on following page)

TABLE 1 (*Continued*) Metabolites were predicted of QHJR in the TCMSP database.

Botanical drug	Code	Metabolites	OB(%)	DL
Smilacis Glabrae Rhixoma	MOL013117	4,7-Dihydroxy-5-methoxyl-6-methyl-8-formyl-flavan	37.03	0.28
Smilacis Glabrae Rhixoma	MOL013118	Neoastilbin	40.54	0.74
Smilacis Glabrae Rhixoma	MOL013119	Enhydrin	40.56	0.74
Smilacis Glabrae Rhixoma	MOL013129	(2R,3R)-2-(3,5-dihydroxyphenyl)-3,5,7-trihydroxychroman-4-one	63.17	0.27
Smilacis Glabrae Rhixoma	MOL001736	(-)-taxifolin	60.51	0.27
Smilacis Glabrae Rhixoma	MOL004328	naringenin	59.29	0.21
Smilacis Glabrae Rhixoma	MOL004567	isoengelitin	34.65	0.7
Smilacis Glabrae Rhixoma	MOL004575	astilbin	36.46	0.74
Smilacis Glabrae Rhixoma	MOL004576	taxifolin	57.84	0.27
Smilacis Glabrae Rhixoma	MOL004580	cis-Dihydroquercetin	66.44	0.27
Smilacis Glabrae Rhixoma	MOL000273	(2R)-2-[(3S,5R,10S,13R,14R,16R,17R)-3,16-dihydroxy-4,4,10,13,14-pentamethyl-2,3,5,6,12,15,16,17-octahydro-1H-cyclopenta [a]phenanthren-17-yl]-6-methylhept-5-enoic acid	46.43	0.28
Poria Cocos (Schw.) Wolf.	MOL000275	trametenolic acid	30.93	0.81
Poria Cocos (Schw.) Wolf.	MOL000276	7,9 (11)-dehydropachymic acid	38.71	0.8
Poria Cocos (Schw.) Wolf.	MOL000279	Cerevisterol	35.11	0.81
Poria Cocos (Schw.) Wolf.	MOL000280	(2R)-2-[(3S,5R,10S,13R,14R,16R,17R)-3,16-dihydroxy-4,4,10,13,14-pentamethyl-2,3,5,6,12,15,16,17-octahydro-1H-cyclopenta [a]phenanthren-17-yl]-5-isopropyl-hex-5-enoic acid	37.96	0.77
Poria Cocos (Schw.) Wolf.	MOL000282	ergosta-7,22E-dien-3beta-ol	31.07	0.82
Poria Cocos (Schw.) Wolf.	MOL000283	Ergosterol peroxide	43.51	0.72
Poria Cocos (Schw.) Wolf.	MOL000285	(2R)-2-[(5R,10S,13R,14R,16R,17R)-16-hydroxy-3-keto-4,4,10,13,14-pentamethyl-1,2,5,6,12,15,16,17-octahydrocyclopenta [a]phenanthren-17-yl]-5-isopropyl-hex-5-enoic acid	40.36	0.81
Poria Cocos (Schw.) Wolf.	MOL000287	3beta-Hydroxy-24-methylene-8-lanostene-21-oic acid	38.26	0.82
Poria Cocos (Schw.) Wolf.	MOL000289	pachymic acid	38.7	0.81
Poria Cocos (Schw.) Wolf.	MOL000290	Poricoic acid A	33.63	0.81
Poria Cocos (Schw.) Wolf.	MOL000291	Poricoic acid B	30.61	0.76
Poria Cocos (Schw.) Wolf.	MOL000292	poricoic acid C	30.52	0.75
Poria Cocos (Schw.) Wolf.	MOL000300	dehydroeburicoic acid	38.15	0.75
Poria Cocos (Schw.) Wolf.	MOL000953	CLR	44.17	0.83
Curcumaelongae Rhizoma	MOL005030	gondoic acid	37.87	0.68
Perilla Frutescens	MOL006202	LAX	30.7	0.2
Perilla Frutescens	MOL002773	beta-carotene	44.11	0.2
Perilla Frutescens	MOL006209	cyanin	37.18	0.58
Perilla Frutescens	MOL006210	eugenyl-β-D-glucopyranoside (cirtrusinc)	47.42	0.76
Perilla Frutescens	MOL001506	Supraene	40.52	0.23
Perilla Frutescens	MOL001749	ZINC03860434	33.55	0.42
Perilla Frutescens	MOL001771	poriferast-5-en-3beta-ol	43.59	0.35
Perilla Frutescens	MOL007179	Linolenic acid ethyl ester	36.91	0.75
Perilla Frutescens	MOL007514	methyl icosa-11,14-dienoate	46.1	0.2
Perilla Frutescens	MOL001323	Sitosterol alpha1	39.67	0.23
Coicis Semen	MOL001494	Mandenol	43.28	0.78

(Continued on following page)

TABLE 1 (*Continued*) Metabolites were predicted of QHJR in the TCMSP database.

Botanical drug	Code	Metabolites	OB(%)	DL
Coicis Semen	MOL002882	[(2R)-2,3-dihydroxypropyl] (Z)-octadec-9-enoate	42	0.19
Coicis Semen	MOL008118	Coixenolide	34.13	0.3
Coicis Semen	MOL008121	2-Monoolein	32.4	0.43

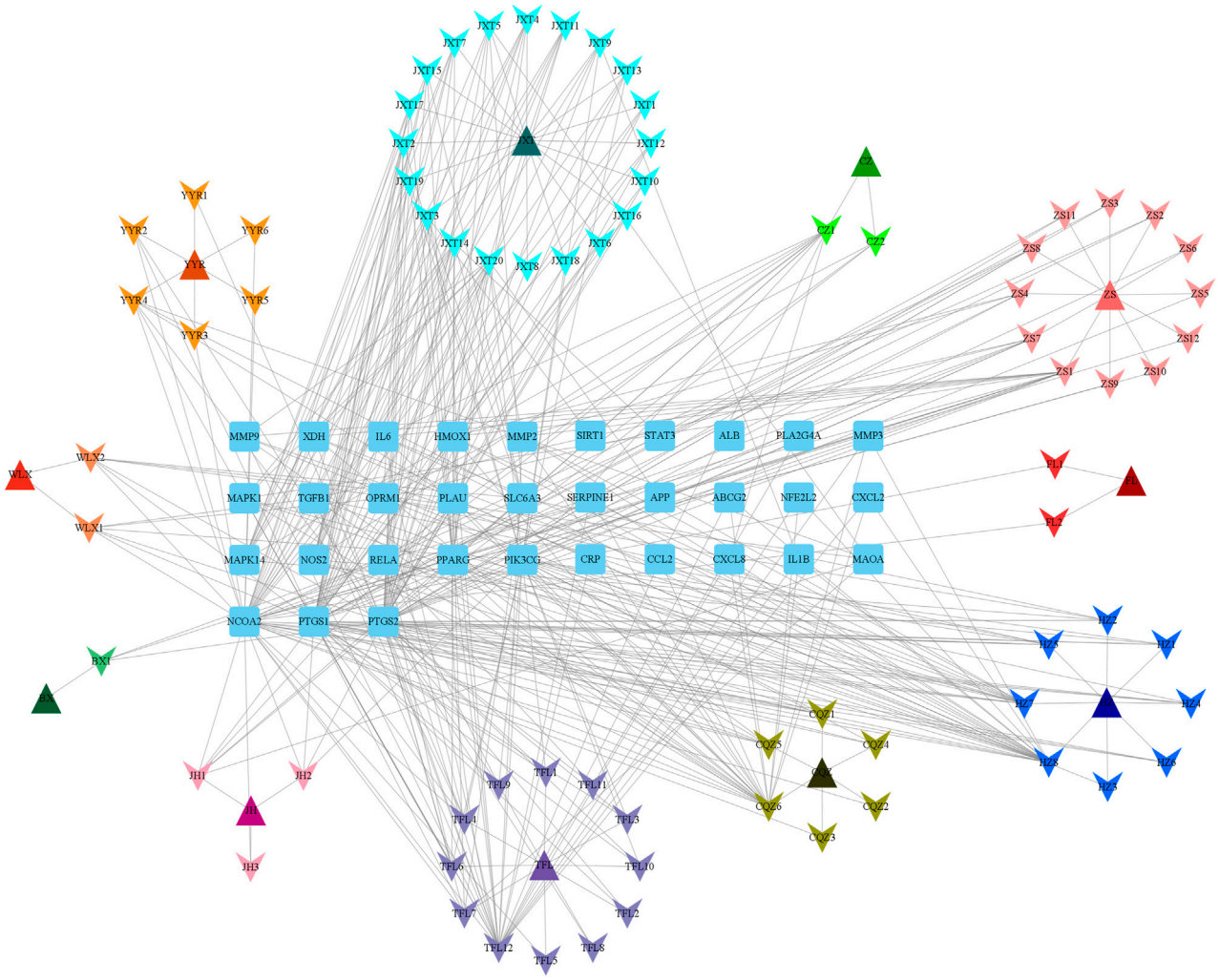

FIGURE 1
Network of QHJR's active-metabolite-target. The square represents the target. The triangle represents the traditional Chinese medicine in QHJR. The arrow represents the active metabolite.

3.5 QHJR affects AGA

Firstly, We established the AGA model. Rats in the Normal group were injected with NS, and in other groups were injected with MSU. The previous studies (Fischer et al., 2018; Zhao J. et al., 2022; Wang X. et al., 2022; Zhao L. et al., 2022) have demonstrated that 8 h after the MSU injection is the key point for AGA Model. We observed the swelling of rat knees, with few changes in the Normal control group, while it had obvious redness and swelling in the Model group (Figure 6A), suggesting that the AGA model was established successfully by MSU injection. H&E assay revealed that the lining cells of the synovial membrane were regularly arranged in a single layer, and the surface of the synovial membrane was smooth and orderly without inflammatory infiltration in Normal group (Figure 6B). As displayed in the Model group, it was characterized by several inflammatory cells infiltration (including lymphocytes, plasma cells, neutrophils, and eosinophils.) (Figure 6B). The observed results are in line with the successful outcome of the model construction. Notably, both the QHJR and colchicine groups exhibited varying degrees of alleviation in

TABLE 2 The Metabolites of botanical drugs in QHJR for AGA by predicting.

Metabolites	ID	Degree	AverageShortestPathLength	BetweennessCentrality	ClosenessCentrality
quercetin	MOL000098	25	1.965811966	0.07219322	0.508695652
luteolin	MOL000006	14	2.136752137	0.026107878	0.468
wogonin	MOL000173	11	2.427350427	0.023736504	0.411971831
licochalcone a	MOL000497	11	2.205128205	0.030326409	0.453488372
formononetin	MOL000392	9	2.478632479	0.021283568	0.403448276
naringenin	MOL004328	7	2.478632479	0.003962642	0.403448276
Hypolaetin	MOL007819	7	2.273504274	0.008043303	0.439849624
Psi-Baptigenin	MOL000507	7	2.495726496	0.003644405	0.400684932
Cajinin	MOL000502	7	2.273504274	0.006374379	0.439849624
Vestitol	MOL000500	7	2.495726496	0.004189551	0.400684932
8-o-Methylreyusi	MOL000468	7	2.273504274	0.006374379	0.439849624
Stigmasterol	MOL000449	7	2.273504274	0.009350993	0.439849624
Calycosin	MOL000417	7	2.273504274	0.006374379	0.439849624
beta-sitosterol	MOL000358	7	2.256410256	0.009819465	0.443181818
Dinatin	MOL001735	6	2.290598291	0.006881825	0.436567164
petunidin	MOL000490	6	2.290598291	0.005380608	0.436567164
aloe-emodin	MOL000471	6	2.290598291	0.006377143	0.436567164
Physovenine	MOL013287	6	2.512820513	0.006369406	0.397959184
beta-carotene	MOL002773	5	2.495726496	0.019538023	0.400684932
taxifolin	MOL004576	5	2.512820513	0.002066119	0.397959184
campesterol	MOL000493	5	2.307692308	0.003231239	0.433333333
rhein	MOL002268	5	2.290598291	0.004853717	0.436567164
6,8-Dihydroxy-7-methoxyxanthone	MOL013281	5	2.512820513	0.003512472	0.397959184
Mandenol	MOL001494	4	2.341880342	0.006668133	0.427007299
cis-Dihydroquercetin	MOL004580	4	2.52991453	0.001265361	0.39527027
(-)-taxifolin	MOL001736	4	2.52991453	0.001265361	0.39527027
4,7-Dihydroxy-5-methoxyl-6-methyl-8-formyl-flavan	MOL013117	4	2.52991453	0.001265361	0.39527027
Dihydrotricetin	MOL007813	4	2.512820513	0.002609127	0.397959184
3β-acetoxyatractylone	MOL000188	4	2.564102564	0.006458836	0.39
diosgenin	MOL000546	4	2.581196581	0.025255951	0.387417219
hederagenin	MOL000296	4	2.324786325	0.002425875	0.430147059
(+)-catechin	MOL000492	4	2.324786325	0.003898026	0.430147059
Linolenic acid ethyl ester	MOL007179	3	2.52991453	0.001435086	0.39527027
LAX	MOL006202	3	2.52991453	0.001435086	0.39527027
gondoic acid	MOL005030	3	2.495726496	0.001747611	0.400684932
(2R,3R)-2-(3,5-dihydroxyphenyl)-3,5,7-trihydroxychroman-4-one	MOL013129	3	2.564102564	0.000825	0.39
Consume close grain	MOL000501	3	2.564102564	0.000467	0.39

(Continued on following page)

TABLE 2 (*Continued*) The Metabolites of botanical drugs in QHJR for AGA by predicting.

Metabolites	ID	Degree	AverageShortestPathLength	BetweennessCentrality	ClosenessCentrality
(Z)-3-(4-hydroxy-3-methoxy-phenyl)-N-[2-(4-hydroxyphenyl)ethyl] acrylamide	MOL000483	3	2.564102564	0.000467	0.39
3,7-dihydroxy-6-methoxy-dihydroflavonol	MOL000461	3	2.564102564	0.000467	0.39
2-Monoolein	MOL008121	2	2.905982906	0.00122972	0.344117647
Sitosterol alpha1	MOL001323	2	2.564102564	0.002295637	0.39
methyl icosa-11,14-dienoate	MOL007514	2	2.820512821	0.000706	0.354545455
poriferast-5-en-3beta-ol	MOL001771	2	2.820512821	0.000706	0.354545455
eugenyl-β-D-glucopyranoside (cirtrusinc)	MOL006210	2	2.547008547	0.000805	0.39261745
cyanin	MOL006209	2	2.547008547	0.000805	0.39261745
CLR	MOL000953	2	2.923076923	0.001725953	0.342105263
(2R)-2-[(3S,5R,10S,13R,14R,16R,17R)-3,16-dihydroxy-4,4,10,13,14-pentamethyl-2,3,5,6,12,15,16,17-octahydro-1H-cyclopenta [a] phenanthren-17-yl]-6-methylhept-5-enoic acid	MOL000273	2	2.923076923	0.008473327	0.342105263
isoengelitin	MOL004567	2	2.598290598	0.000448	0.384868421
daucostero_qt	MOL005869	2	2.905982906	0.000753	0.344117647
sitosterol	MOL000359	2	2.905982906	0.000753	0.344117647
Medicagol	MOL000503	2	2.991452991	0.00014	0.334285714
8-C-α-L-arabinosylluteolin	MOL000470	2	2.598290598	0.000263	0.384868421
Picralinal	MOL013288	2	3.555555556	0.000151	0.28125

symptoms associated with AGA, such as inflammatory cell infiltration. These findings suggest that QHJR could effectively mitigate AGA in a manner comparable to that of colchicine.

3.6 The main potential targets of QHJR

As depicted in Figure 7, the multi-component traditional Chinese medicine QHJR exhibits therapeutic effects on AGA through a multi-target mechanism, as evidenced by the ability of 27 chemical components to act on diverse targets. Through comprehensive network analysis, the top 6 metabolites, namely, QHJR-10 (Caffeic acid), QHJR-17 (cis-Resveratrol), QHJR-7 (Ferulic acid), QHJR-8 (Apigenin), QHJR-15 (Quercetin), and QHJR-16 (Isoliquiritigenin), were identified with degrees of 16, 16, 15, 13, 13, and 13, respectively, implying they may be the key potential metabolites of QHJR for anti-AGA (Table 4). It was shown that 2 metabolites of them, which is QHJR-10 (Caffeic acid) and QHJR-16 (Isoliquiritigenin), as shown in the TCMSP database, do not belong to any single herbal component of QHJR. This suggests that QHJR may not be replaceable by any single botanical drug. However, further validation is still required to prove the research's accuracy.

3.7 Anti-inflammation is the vital way to anti-AGA for QHJR

The results of the Biological function analysis suggested that AGA was closely related to inflammation, such as leukocyte chemotaxis, leukocyte migration, NOD-like receptor signaling pathway, and TNF signaling pathway. etc. Especially in the predicted hub genes of AGA, TNF, IL-6, and IL-1β were identified as joint targets of QHJR, suggesting that the primary mechanism underlying the treatment of QHJR for anti-AGA may reduce inflammation. To investigate this further, we analyzed the effects of QHJR on the level of inflammation markers TNF-α, IL-6, and IL-1β using the ELISA method. Our results demonstrate that QHJR treatment significantly inhibited the level of TNF-α, IL-6, and IL-1β induced by MSU (Figures 8A–C). In addition, qRT-PCR analysis revealed that NLRP3 levels significantly elevated depending on MSU-induced (Figure 8D). Compared with the Model group, QHJR treatment significantly downregulated the level, and its trend was consistent with colchicine (Figure 8D). These findings indicate that QHJR inhibits the inflammatory response and may represent an effective treatment for AGA. In summary, our study highlights the importance of targeting the inflammatory response as a key therapeutic approach for AGA.

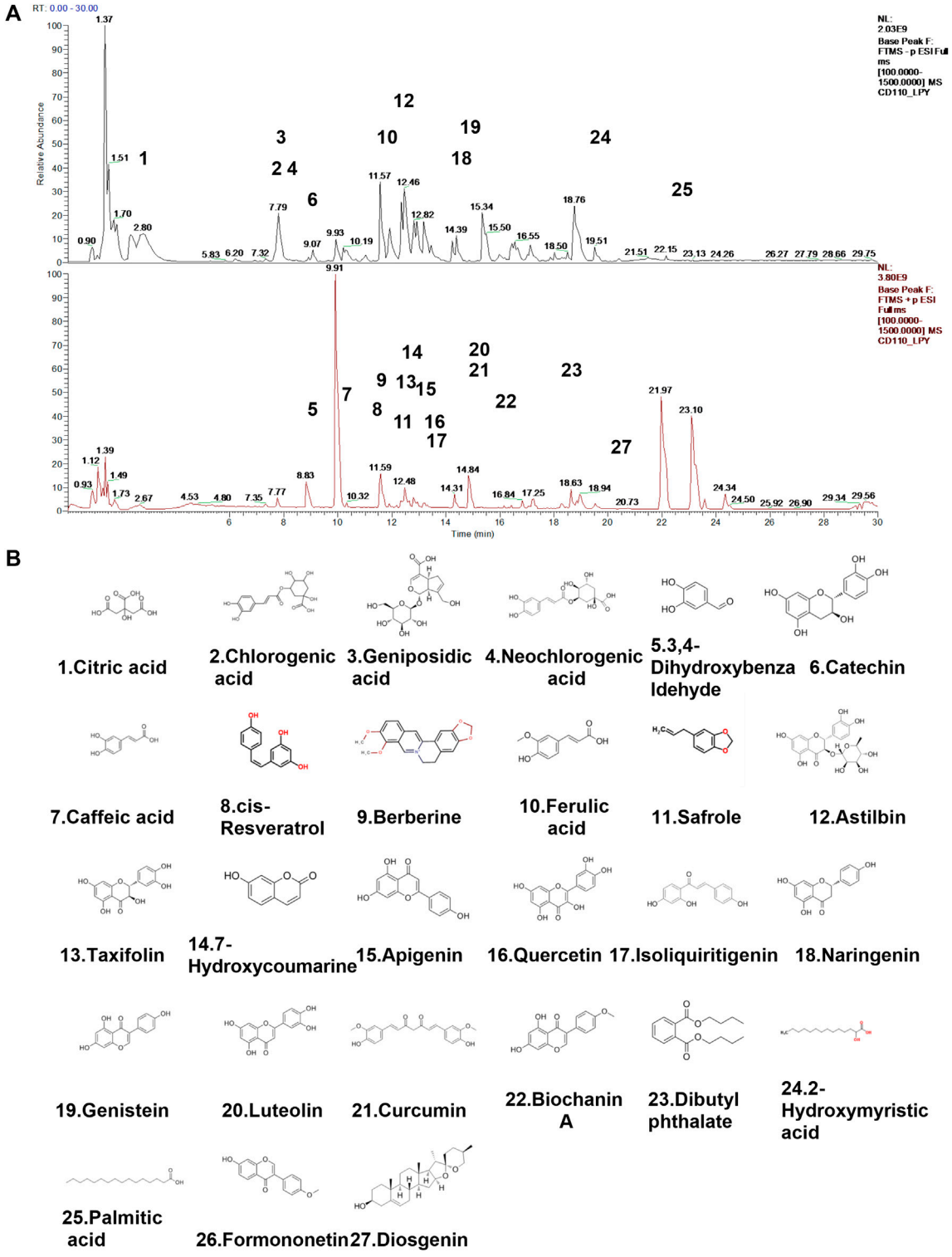

FIGURE 2
Identification of chemical constituents of QHJR. **(A)** Total ion chromatographic analysis. **(B)** Main metabolite structural formula. The structural formulas of the main metabolites shown in **(B)** are sourced from the websites (https://hmdb.ca/metabolites/HMDB0000002) and (https://www.chemsrc.com/).

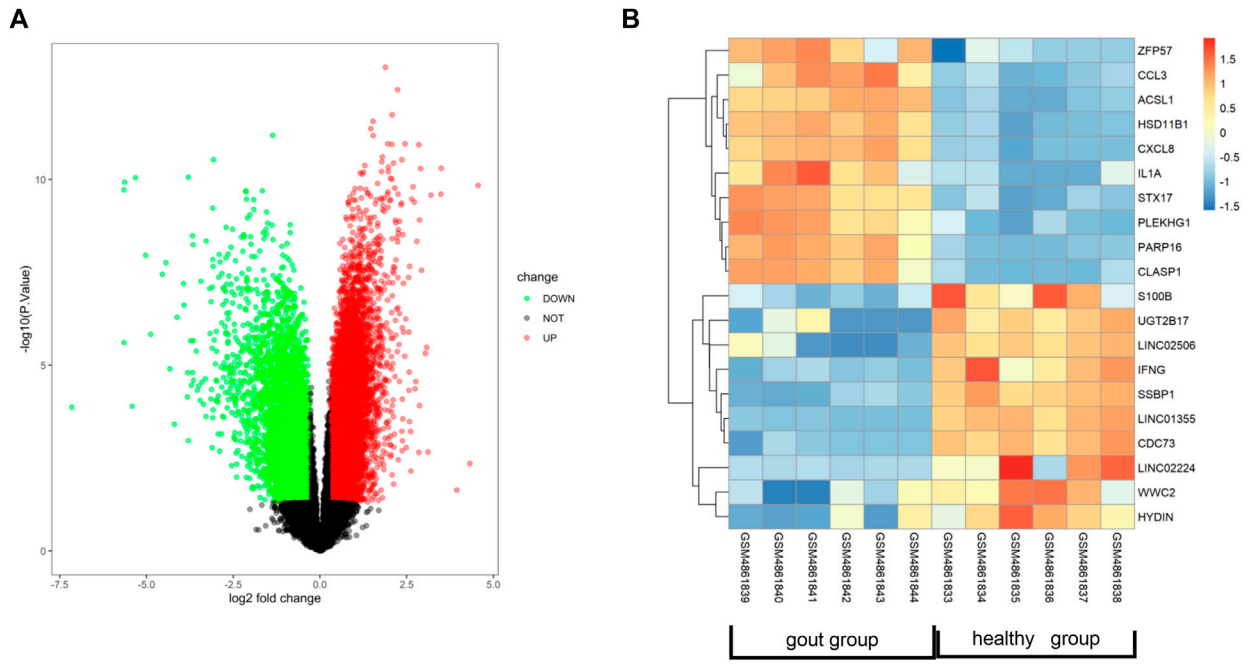

FIGURE 3
Identification of related genes of AGA. **(A)** Volcano map showing differentially expressed genes in dataset GSE160170. **(B)** Heat map showing gout-related genes in data set GSE160170.

3.8 QHJR anti-AGA by activating autophagy

Autophagy has been reported to lower the inflammation. To investigate how autophagy influenced the treatment of AGA, autophagy level was first measured in inflammation. We added 3-MA which is an autophagy inhibitor, and RAPA which is an autophagy promoter as the controls. Many ATG proteins have vital effects on autophagy. Atg5 plays an essential part in canonical autophagy and autophagy-related processes (Masud et al., 2019). Interaction between p62/SQSTM1(p62) and light chain 3 (LC3) has an important impact on autophagosome generation and aggregated protein degradation in autophagosomes and lysosomes (Lyu et al., 2021). Compared with the Model group, the findings showed that Atg5 and Atg7 mRNA (Figures 9D,E) and LC3II/I protein (Figures 9H,I) levels dramatically increased in the RAPA group, and Atg5 mRNA (Figures 9D,E) and LC3II/I protein (Figures 9H,I) level significantly declined in 3-MA group. It was shown that the level of p62 was obviously inhibited in the RAPA group in comparison with the Model group and that the level of p62 was significantly enhanced in the 3-MA group relative to the RAPA group (Figures 9G,H). This was coincident with the role of 3-MA and RAPA.

Next, we examined the expression of autophagy in inflammatory-related factors. H&E assay displayed that the RAPA group had declined inflammatory cell infiltration relative to the Model group (Figure 9A). In addition, the RAPA group showed significantly declined inflammation relative to the Model group (Figure 9A). NLRP3 and IL-6 levels of the Model group were significantly increased relative to Normal group; IL-6 and NLRP3 levels were weakened in RAPA group compared with Model group (Figures 9B,C). Moreover, it was confirmed that promoting autophagy could reduce inflammation.

Moreover, the expressions of Atg5 and Atg7 (Figures 9D,E), Beclin-1, LC3II/β-actin, and LC3II/I (Figures 9F,H–J) were increased in QHJR groups compared with Model group. The findings displayed that the level of p62 was lowered in QHJR groups compared with the Model group (Figures 9G,H). It suggested that QHJR might activate autophagy. We demonstrated that QHJR could reduce inflammation before, and QHJR activated autophagy, suggesting that QHJR could attenuate inflammation by activating autophagy.

3.9 QHJR activated autophagy via phosphorylating AMPK

Considering that AMPKα is an energy sensor exerting a positive regulatory effect on autophagy by inhibiting mTOR to remove the phosphorylation inhibition of ULK1 at Ser757 and induce the binding of ULK1 to AMPK (Li and Chen, 2019), we aimed to confirm whether AMPK pathway has impacts on autophagy. WB and qRT-PCR assays were performed to examine AMPK-pathway-related levels in the RAPA and 3-MA groups. Compared with Model group, AMPKα and p-AMPKα1 (Thr 172) protein exhibited few significant changes in RAPA and 3-MA groups (Figures 10A,B), AMPK mRNA level (Figure 10C) was elevated in RAPA group, while levels of mTOR and p-mTOR (Ser2448) mRNA and protein

TABLE 3 QHJR was analyzed qualitatively by HPLC-Q-Orbitrap-MS.

Name	Metabolites	Formula	RT [min]	+	-	Calc.MW	m/z
QHJR-1	Citric acid	C6 H8 O7	2.788		[M-H]-1	192.0262	191.0188
QHJR-2	Chlorogenic acid	C16 H18 O9	7.726		[M-H + HAc]-1	294.0736	353.0875
QHJR-3	Geniposidic acid	C16 H22 O10	7.801		[M-H]-1	374.1209	373.1135
QHJR-4	Neochlorogenic acid	C16 H18 O9	8.254		[M-H-H2O]-1	372.1055	353.0877
QHJR-5	3,4-Dihydroxybenzaldehyde	C7 H6 O3	9.059	[M + H]+1		138.0316	139.0388
QHJR-6	Catechin	C15 H14 O6	9.068		[M-H]-1	290.0788	289.0718
QHJR-7	Caffeic acid	C9 H8 O4	10.323	[M + H]+1		180.0421	181.0494
QHJR-8	cis-Resveratrol	C14 H12 O3	11.585	[M + H]+1		228.0781	229.0854
QHJR-9	Berberine	C20 H18 N O4	11.672	[M + H]+1		335.1153	336.1226
QHJR-10	Ferulic acid	C10 H10 O4	11.85		[M-H]-1	194.0572	193.0498
QHJR-11	Safrole	C10 H10 O2	12.444	[M + H]+1		162.0679	163.0751
QHJR-12	Astilbin	C21 H22 O11	12.475		[M-H]-1	450.1156	449.1083
QHJR-13	Taxifolin	C15 H12 O7	12.487	[M + H]+1		304.0576	305.0648
QHJR-14	7-Hydroxycoumarine	C9 H6 O3	12.611	[M + H]+1		162.0315	163.0387
QHJR-15	Apigenin	C15 H10 O5	13.226	[M + H]+1		270.0524	271.0597
QHJR-16	Quercetin	C15 H10 O7	13.624	[M + H]+1		302.0421	303.0494
QHJR-17	Isoliquiritigenin	C15 H12 O4	13.689	[M + H]+1		256.0731	257.0804
QHJR-18	Naringenin	C15 H12 O5	14.562		[M-H]-1	272.0684	271.0613
QHJR-19	Genistein	C15 H10 O5	15.02		[M-H]-1	270.0529	269.0457
QHJR-20	Luteolin	C15 H10 O6	15.158	[M + H]+1		286.0476	287.0546
QHJR-21	Curcumin	C21 H20 O6	15.166	[M + H]+1		368.1253	369.1325
QHJR-22	Biochanin A	C16 H12 O5	16.147	[M + H]+1		284.0681	285.0752
QHJR-23	Dibutyl phthalate	C16 H22 O4	18.638	[M + H]+1		278.1512	279.1585
QHJR-24	2-Hydroxymyristic acid	C14 H28 O3	19.733		[M-H]-1	244.2036	243.1963
QHJR-25	Palmitic acid	C16 H32 O2	22.71		[M-H]-1	256.24	255.2327
QHJR-26	Formononetin	C16 H12 O4	15.905	[M + H]+1		268.0731	269.0804
QHJR-27	Diosgenin	C27 H42 O3	20.419	[M + H]+1		396.3021	397.3093

(Figures 10F–H) and p-ULK1 (Ser 757) protein (Figures 10D–F) were descended in RAPA group; besides, ULK1 protein levels were elevated in RAPA group (Figures 10D–F). It displayed that the protein levels of mTOR, p-mTOR, and p-ULK1 (Figures 10D–I) and the mRNA level of mTOR (Figure 10H) were enhanced in the Model group compared with the Normal group. It suggested that AMPK might activate autophagy by suppressing p-ULK1 and p-mTOR.

AMPK phosphorylation at Thr172 exerts a vital role in activating AMPK, which usually acts as the activity indicator (Li and Chen, 2019). To verify whether AMPK was activated by QHJR, it was discovered that the p-AMPKα1 (Thr 172) protein level of the QHJR group increased relative to the Model group (Figures 10A,B). Compared with the Model group, it was shown that p-ULK1(Ser 757) and p-mTOR (Ser-2448) protein levels of the QHJR group decreased (Figures 10D,F–H). The activation of mTOR represents the well-recognized factor negatively regulating autophagy activation, and mTOR (Ser-2448) phosphorylation can serve as the activity marker. The obtained findings demonstrated that the AMPKα/mTOR/ULK1 pathway was activated after being subjected to the treatment of QHJR. All the findings demonstrated that QHJR could delay inflammation which was MSU-induced by enhancing autophagy using AMPKα/mTOR/ULK1 pathway.

4 Discussion

Acute gouty arthritis, is a common ailment, particularly among the middle-aged and elderly demographics (Grazio, 2012; Guo et al., 2023). The pathophysiology of this condition originates from the

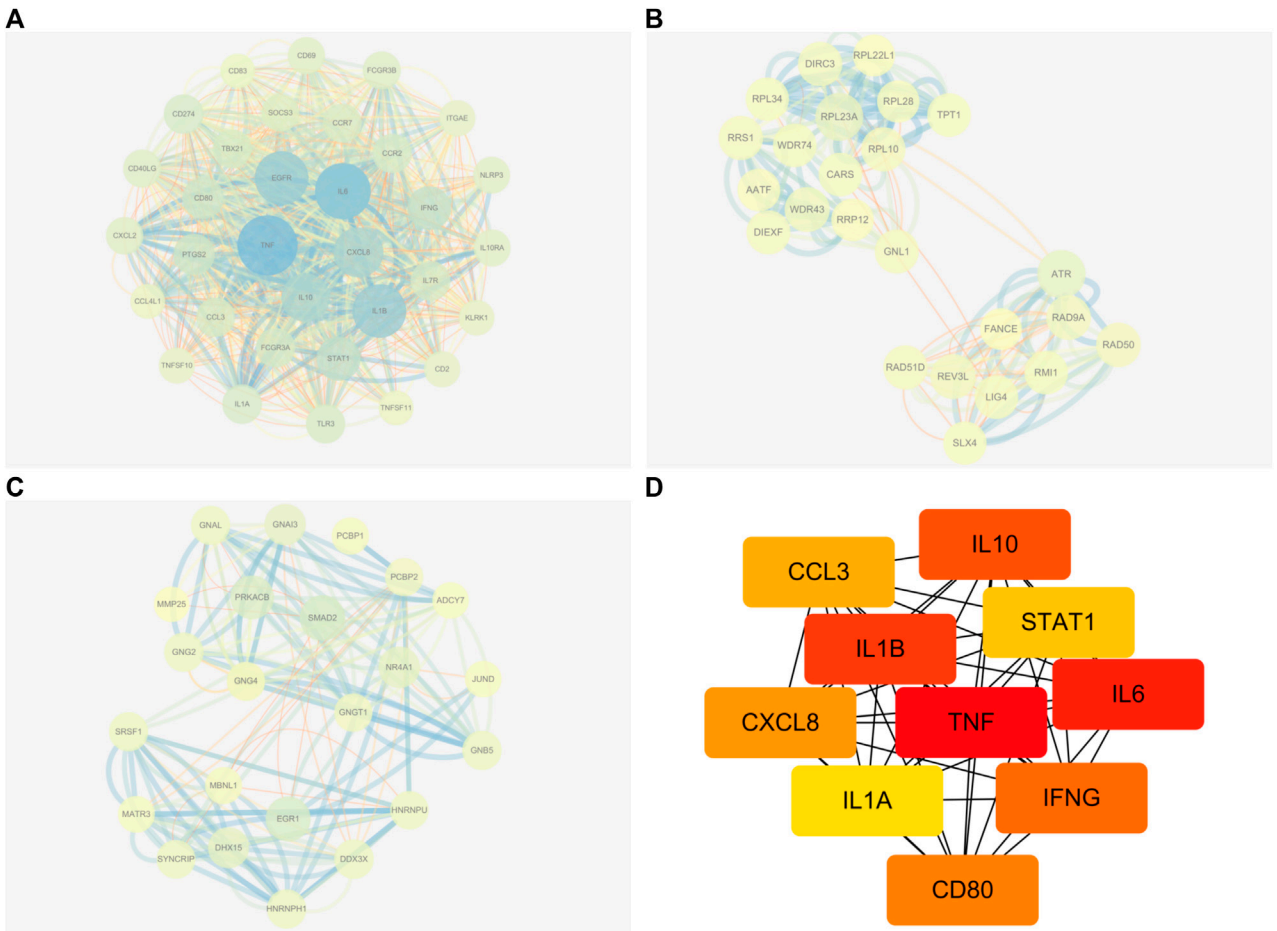

FIGURE 4
Results of PPI networks analysis of DEGs. **(A-C)** DEGs of PPI network analysis. **(D)** Hub genes of DEGs.

excessive build-up of uric acid, a metabolic byproduct of purine in the human system, and subsequent crystallization within the joints, triggering an acute arthritic response (Grazio, 2012; Guo et al., 2023). Ordinarily, hepatic and renal metabolism disposes of uric acid (Guo et al., 2023). However, dysfunction in its production or elimination causes its retention, facilitating the formation of urate crystal deposits, provoking inflammation, and pain, and significantly impacting the patient's quality of life (Grazio, 2012). The disease's onset may cause debilitating symptoms such as severe pain, joint dysfunction, redness, and fever (Grazio, 2012). The condition's chronicity leads to soft tissue and joint injury, ultimately resulting in deformities and compromised function (Xu Y. T. et al., 2020). Additionally, gout triggers urate nephropathy, cardiovascular disease, metabolic syndrome, and other medical complications, further worsening the patient's health (Li et al., 2019; Cohen-Rosenblum et al., 2022).

Currently, due to the increasing incidence rates and limitations of Western medicine (such as toxic side effects) (Nuki, 2008), the development of TCM has offered hope to patients. However, a limitation of TCM is that most CHM products do not possess up-to-date data regarding their safety and modern scientific evidence for their claimed clinical uses (Zhou J. et al., 2019). As a result, more research is needed to confirm the efficacy of TCM treatments for gouty arthritis. TCM has played a role in arthritis. For example, according to Lei Zhang et al. (Zhang W. et al., 2019), Total glucosides of paeony (TGP) and Paeoniflorin (Pae) generated immunomodulation and anti-inflammation by inhibiting the activation of synoviocytes and immunocytes, reducing inflammatory factor generation while reversing the aberrant signaling in synoviocytes. Menglin He et al. (He et al., 2022) considered Gentiopicroside (GPS) as treating AGA by reducing inflammation and pain. Xvwu Qian et al. (Qian et al., 2023) found that Atractylodes macrocephala played a good role in reducing hyperuricemia and inflammation. This is consistent with our study, as our research demonstrates that MSU-induced inflammation is upregulated in AGA, but expression levels decrease after QHJR treatment. Furthermore, the trend is consistent with the effects of colchicine treatment, suggesting the effectiveness of QHJR in AGA. To explore the specific mechanisms by which QHJR acts on AGA, we conducted further investigations.

Chinese herbal compounds exhibit remarkable therapeutic efficacy against various diseases. Their intricate composition, multifaceted therapeutic targets, and intricate treatment modalities present formidable challenges to the comprehensive

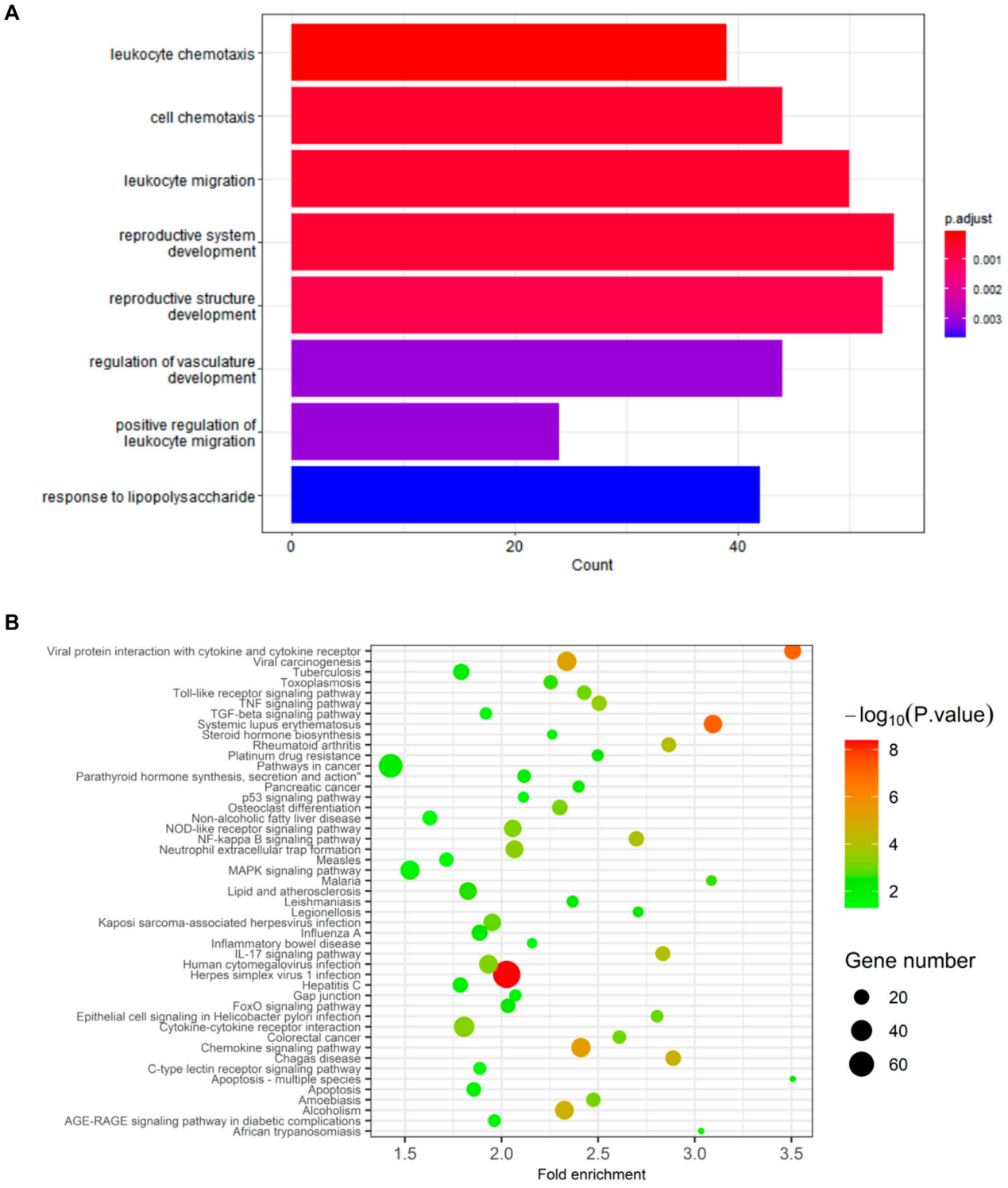

FIGURE 5
Results of GO and KEGG analysis. **(A)** GO analysis. **(B)** KEGG analysis.

elucidation of their underlying mechanisms. In recent times, network pharmacology has risen to prominence as a favored methodology for dissecting the intricate mechanisms of action inherent to complex Traditional Chinese Medicine (TCM) formulations (Wang et al., 2020b; Liu et al., 2023). OB and DL values are based on general rules and assumptions about compound properties, such as molecular weight, lipophilicity, and solubility. However, these values may not always accurately predict a compound's behavior in the body or its potential as a drug (Zhu et al., 2013; Lage et al., 2018; Hoare, 2021). Chinese herbal

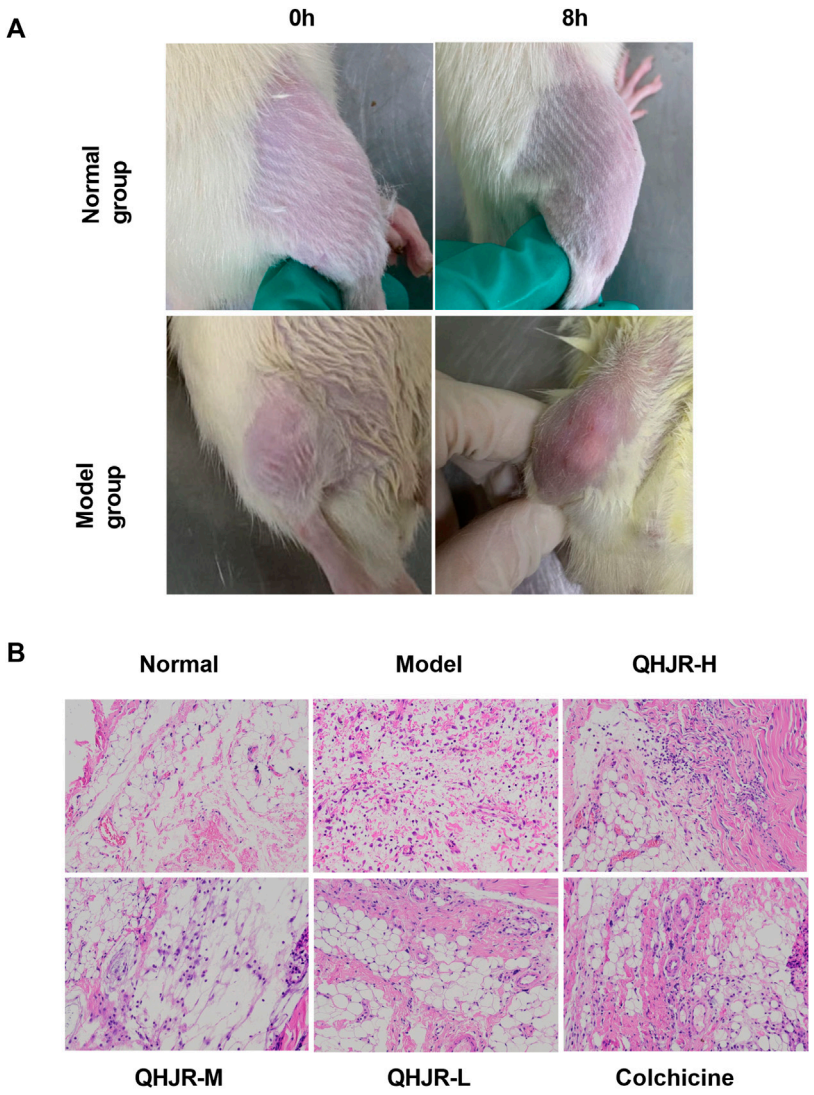

FIGURE 6
AGA was induced by MSU. **(A)** The swelling of rat knees at 0 and 8 h by MSU injection in Normal and Model groups. **(B)** Synovial tissues were examined by H&E staining.

compounds lacking proper pharmacokinetic properties would fail to reach their target organs and thereby hinder the expression of their biological effects (Mao et al., 2017; Liu et al., 2023). It has been empirically demonstrated that compounds with an oral bioavailability (OB) of ≥30% and a drug-likeness (DL) index ≥0.18 can be absorbed and distributed within the human body, thus earning the designation of pharmacokinetically active (Xu et al., 2012; Tao et al., 2013; Liu et al., 2023). The considerable therapeutic effects of QHJR on AGA within the compound-key targets network may be attributed to the presence of compounds with high degrees (Liu et al., 2023). Using network analysis, we initially predicted the metabolites in QHJR that could potentially target AGA. Subsequently, after performing chemical composition identification of QHJR using HPLC-Q-Orbitrap-MS, we found 27 metabolites, which revealed that 6 metabolites (quercetin, luteolin, formononetin, naringenin, taxifolin, diosgenin) were consistent with the predicted results which by Network Analysis. Additionally, we have identified five compounds (Neochlorogenic acid, Caffeic acid, Berberine, Isoliquiritigenin, and Formononetin) that, according to the TCMSP database, do not belong to any single herbal component of QHJR. Therefore, we infer that they result from interactions among the individual constituents of QHJR. Neochlorogenic acid has been studied for its potential effects on inflammation and is helpful in the treatment of rheumatoid arthritis (Gao et al., 2020). Caffeic acid, another caffeoylquinic acid derivative, has been studied for its effects on pain and inflammation in a murine model of gouty arthritis (Matosinhos et al., 2022). Recent studies have shown that berberine can inhibit the inflammatory response induced by monosodium urate (MSU) crystals and improve gouty arthritis symptoms (Liu et al., 2016). Berberine has also been shown to alleviate gouty arthritis in mice through the inhibition of xanthine oxidase activity (Xu et al., 2021). It was found that isoliquiritigenin inhibited rheumatoid arthritis, which is an inflammatory disease (Zhou and Wink, 2019). Another

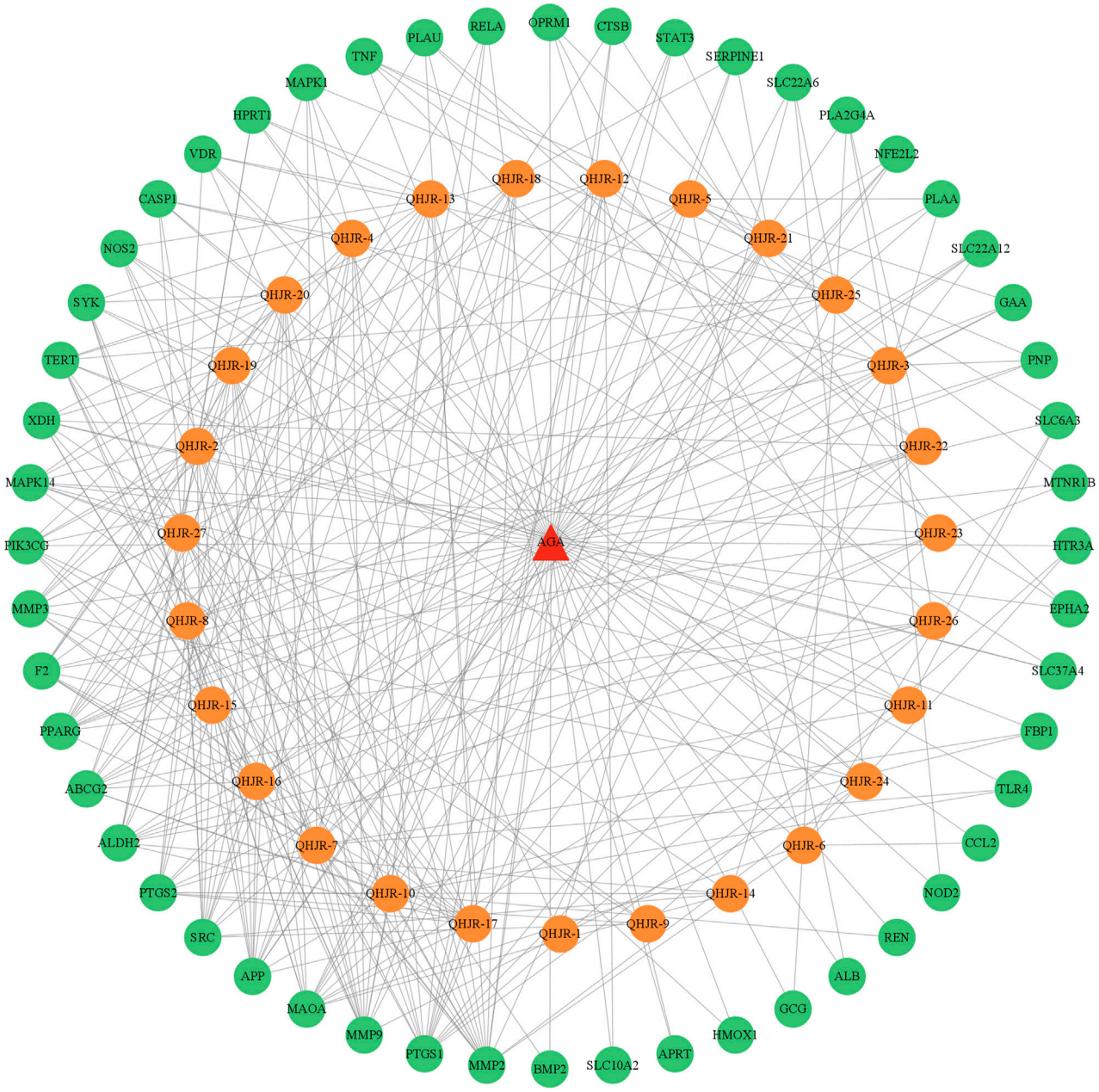

FIGURE 7
Network of drug targets.

study reported that isoliquiritigenin is a potent inhibitor of NLRP3 inflammasome activation, which is implicated in the etiology of gouty arthritis (Lin et al., 2020). Formononetin has been shown to have significant effects on inflammation *in vitro* and animal models of many diseases, including rheumatoid arthritis and gouty arthritis (Zhang L. et al., 2019; Liu et al., 2022). TCMSP is still a valuable resource for drug discovery as it provides drug targets and diseases of each active compound, which can automatically establish the compound-target and target-disease networks that let users view and analyze the drug action mechanisms (Ru et al., 2014). However, the limitation of TCMSP is that it lacks some medicinal and pharmacological data, the dose-effect relationship of ingredients, and the drug diversity of components in each formula (Zhang W. et al., 2019). Thus, the generation of new metabolites by QHJR is merely a hypothesis, and further pharmacological experiments are required to validate this finding. Nevertheless, these metabolites do exist in QHJR, and numerous studies have confirmed that they possess varying degrees of decreasing inflammation, and have effects on AGA. This lays a foundation for the mechanism study of QHJR against AGA.

PharmMapper and SwissTarget, along with other target prediction databases, are essential tools for unraveling molecular interactions governing drug targets. These resources

TABLE 4 Network topology parameters of metabolites in QHJR.

Name	Degree	AverageShortestPathLength	BetweennessCentrality	ClosenessCentrality
QHJR-10	16	2.303797468	0.025338657	0.434065934
QHJR-17	16	2.278481013	0.022804202	0.438888889
QHJR-7	15	2.329113924	0.020040591	0.429347826
QHJR-8	13	2.35443038	0.017043398	0.424731183
QHJR-15	13	2.35443038	0.010956889	0.424731183
QHJR-16	13	2.35443038	0.011578714	0.424731183

enable researchers to explore complex mechanisms and elucidate drug efficacy. With advanced algorithms and data integration, these platforms empower comprehensive investigation of the intricate drug-target relationship. Leveraging these databases, researchers gain insights into candidate drug therapeutics, driving novel pharmaceutical discovery. SwissTarget Prediction utilizes reverse screening to predict possible protein targets for drug candidates (Kanehisa et al., 2017; Wang et al., 2017). We conducted a Network analysis of the 27 metabolites identified through HPLC-Q-Orbitrap-MS. The results revealed that among these 27 metabolites, QHJR-10 (Caffeic acid), QHJR-16 (Isoliquiritigenin), QHJR-17 (cis-resveratrol), QHJR-7 (Ferulic acid), QHJR-8 (Apigenin), and QHJR-15 (Quercetin) exhibited the most prominent levels. We hypothesize that they may potentially be the key metabolites of QHJR in the treatment of AGA. Among them, QHJR-10 (Caffeic acid) and QHJR-16 (Isoliquiritigenin) mentioned earlier are the newly generated metabolites that may result from the interactions between the individual herbal components of QHJR. There is research that found that cis-resveratrol could reduce inflammation by inhibiting canonical and non-canonical inflammasomes in macrophages (Huang et al., 2014). Apigenin alleviates

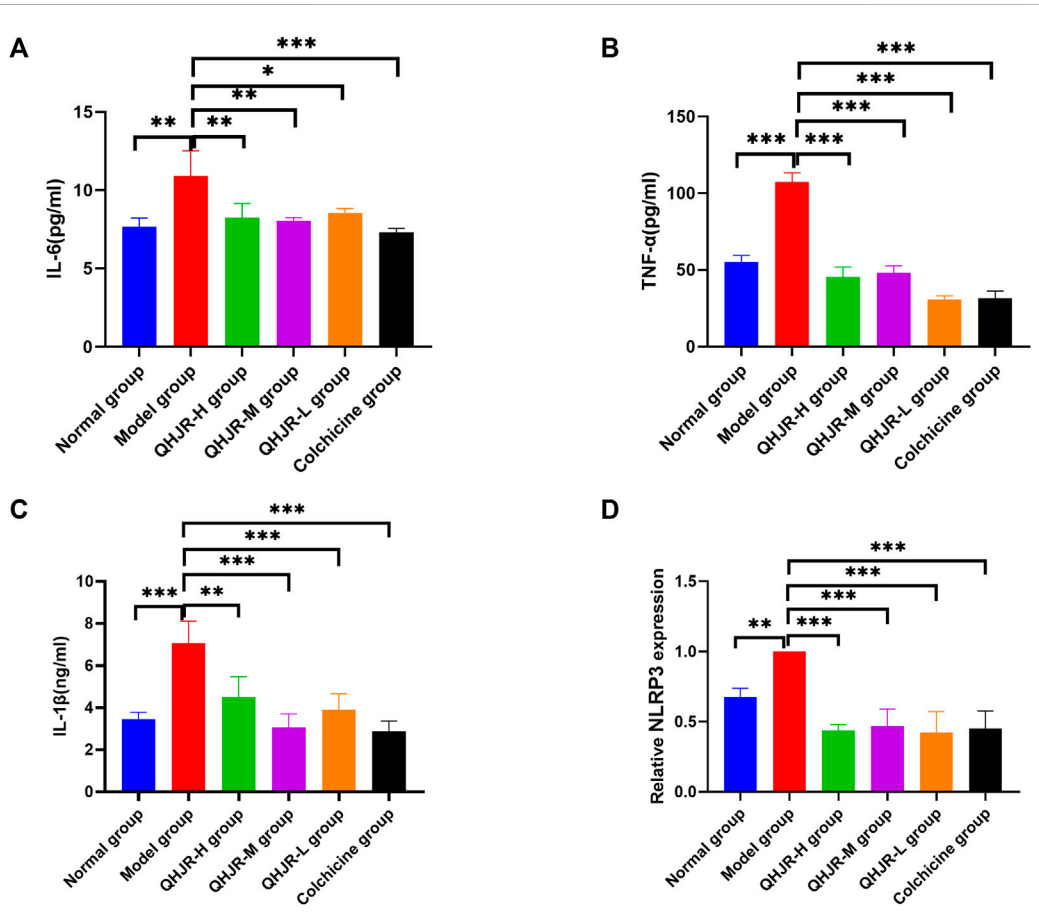

FIGURE 8
QHJR reduced the MSU-induced inflammation. **(A–C)** Inflammatory-related factor IL-6, TNF-α, and IL-1β levels through ELISA. **(D)** NLRP3 mRNA level was examined by qRT-PCR. (*$p < 0.05$, **$p < 0.01$, ***$p < 0.001$).

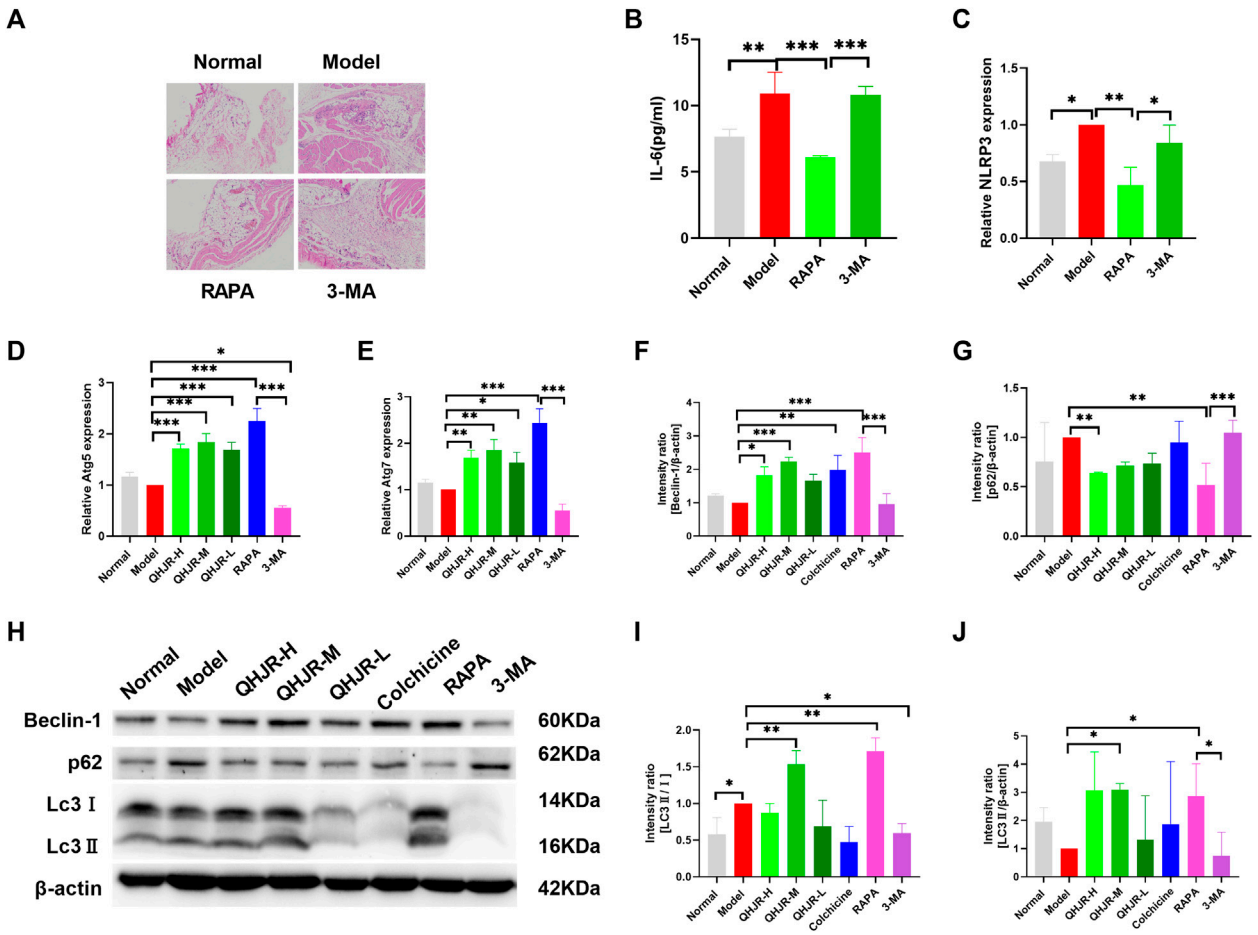

FIGURE 9
QHJR was involved in autophagy to regulate inflammation. **(A)** H&E method was adopted for detecting the expression of inflammation and autophagy. **(B)** Results of IL-6 expressions by Elisa. **(C–E)** The expressions of NLRP3, Atg5, and Atg7 were examined by RT-qPCR. **(F,H)** Results of Beclin-1/β-actin expressions by WB. **(G,H)** Results of p62/β-actin expressions by WB. **(I,J,H)** Results of LC3II/I and LC3II/β-actin expressions by WB. (*$p < 0.05$, **$p < 0.01$, ***$p < 0.001$).

macrophage-polarization-induced inflammatory response (Ji et al., 2023). Apigenin has been shown to exert anti-inflammatory activity (Ouyang et al., 2021). Multiple studies have indeed demonstrated the effectiveness of ferulic acid (Doss et al., 2016; Ganesan and Rasool, 2019) and quercetin (Huang et al., 2012; Ruiz-Miyazawa et al., 2017) in treating AGA. However, due to their widespread distribution in the plant kingdom and their involvement in various disease processes, their therapeutic potential for multiple diseases has been extensively investigated through network analysis (Qi et al., 2020; Yang et al., 2020; Zhang et al., 2022). Further discussion on this topic will not be pursued extensively here. Furthermore, consistent with previous studies, these metabolites can alleviate AGA by reducing inflammation. However, computational models used in virtual screening may not always ensure that all predictions are correct (Sadybekov and Katritch, 2023). These key potential metabolites are currently only predictions, and their actual efficacy requires further experimental validation. This study aims to comprehensively investigate the mechanism of QHJR through an integrated approach of bioinformatic analysis and experimental validation.

The publicly available GEO platform was utilized to identify DEGs between healthy individuals and patients. The DEGs present promising therapeutic targets for combating the disease. Leveraging the GEO platform, researchers can gain critical insights into the molecular changes underlying the pathological condition, facilitating the development of targeted therapeutic interventions (Liao et al., 2018). Thus, the microarray data from GSE160170 in GEO were used to generate DEGs, forming the AGA target library. KEGG and GO tools were employed to analyze the molecular mechanisms and signaling pathways associated with QHJR drug therapies. This integrative approach aimed to unveil the complex molecular foundations and understand the therapeutic potential of QHJR (Kanehisa et al., 2017; Liu et al., 2018). Our findings indicated that the majority of enriched pathways with QHJR's potential targets were associated with inflammation, suggesting that the suppression of inflammation might be a crucial aspect of QHJR's treatment of AGA. Furthermore, through our comprehensive analysis of the PPI

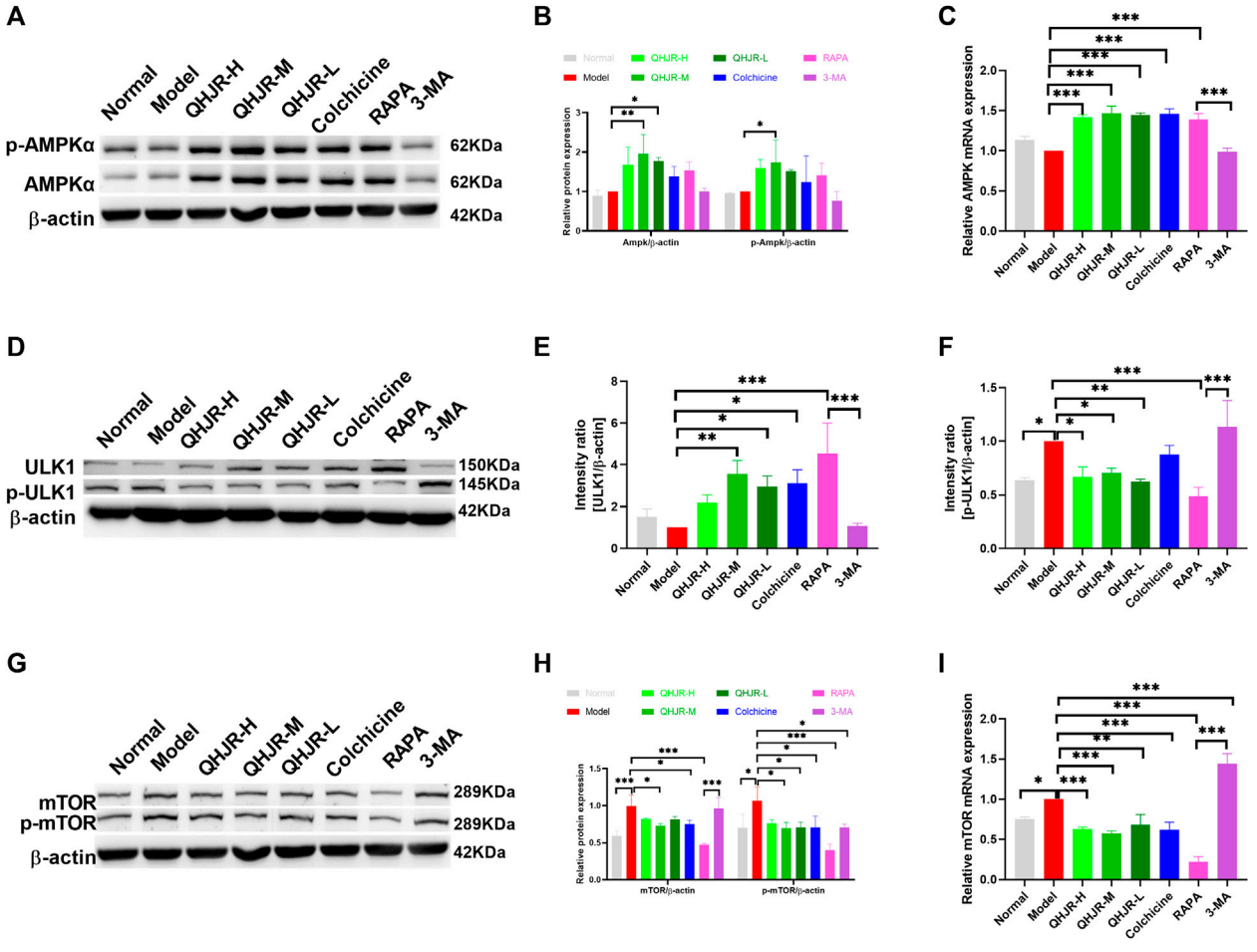

FIGURE 10
AMPK pathway was activated. **(A,B)** Results of AMPKα, p-AMPKα expression by WB. **(C)** Results of AMPK expression by qRT-PCR. **(D–F)** Results of ULK1, p-ULK1 expression by WB. **(G,H)** Results of mTOR, p-mTOR expression by WB. **(I)** Results of mTOR expression by qRT-PCR. (*$p < 0.05$, **$p < 0.01$, ***$p < 0.001$).

Network, we successfully identified key hub genes with high node degrees, namely, TNF, IL-1β, and IL-6. These hub genes not only hold significant relevance to inflammation but also emerged as the top candidates based on their centrality within the network. This finding further strengthens the hypothesis that these genes play crucial roles in the regulation and modulation of inflammatory processes. This is consistent with previous research. Previous studies have reported, Acute gouty arthritis is an inflammatory condition that is characterized by the deposition of monosodium urate (MSU) crystals in the joints (Busso and So, 2010; Zhang Q. B. et al., 2021). A study on human blood monocytes and synovial cells found that urate crystals stimulate the production of TNF-α, which is involved in the inflammatory process of gouty arthritis (Di Giovine, 1991). Amaral et al.found that TNF-α drives the expression of pro-IL-1β mRNA and IL-1β protein in experimental gout and that its transmembrane form is sufficient to trigger MSU-induced inflammation in mice (Amaral et al., 2016). Pro-inflammatory factors, esp. IL-1β; plays a vital role in gouty arthritis (Chang et al., 2017). When MSU crystals are absorbed by macrophages, they expedite IL-1β release. Recent clinical trials have shown that IL-1β blockade can reduce recurrent attacks of gouty arthritis (So et al., 2007; Dinarello, 2010). The upregulation of IL-1β, IL-6, and TNFα has been observed in patients with acute gouty arthritis (Busso and So, 2010; Zhang T. et al., 2021). NLRP3 inflammasome produces IL-1β in gout, composed of NLRP3, ASC, and pro-caspase-1 (Chang et al., 2017). W. Chang et al. (Wang et al., 2021) found that the expression of NLRP3 was upregulated in AGA. MicroRNA-223 has been found to suppress IL-1β and TNF-α production in gouty inflammation by targeting the NLRP3 inflammasome (Zhang T. et al., 2021). Our data displayed that inflammation level was significantly increased by the HE method. In addition, the level of NLRP3, TNF-α, IL-1β, and IL-6 was significantly increased after MSU induction, but QHJR and colchicine reversed this trend. This indicates that QHJR alleviates AGA by reducing inflammation. This is also consistent with the previous findings.

KEGG analysis indicates that apoptosis may be a key mechanism. Previous studies have shown that anti-inflammatory effects mediated by cell apoptosis are closely related to autophagy (Zhu and He, 2015), and a special factor called Beclin-1 is closely related to both cell apoptosis and autophagy (Zhu and He, 2015; Tang et al., 2022; Xu et al., 2022). Beclin-1 is the first mammalian autophagy gene (Xu

et al., 2022). In addition to its involvement in autophagy, endocytosis, and phagocytosis (Zhu and He, 2015), Beclin-1 is also involved in the regulation of cell apoptosis and is expressed in various diseases, such as lung cancer (Zheng et al., 2020), colon cancer (Zhang et al., 2014), ovarian cancer (Cai et al., 2014), *etc.* Moreover, Beclin 1 is required for apoptotic cell engulfment and to coordinate actin dynamics and membrane phospholipid synthesis to promote efficient apoptotic cell engulfment (Konishi et al., 2012). Autophagy represents the self-defense mechanism in eukaryotes upon different survival pressures, and it is under precise modulation via different pathways, especially the AKT/mTOR pathway which is demonstrated to negatively regulate autophagy (Yang et al., 2021). Previous studies have reported that autophagy is closely related to GA which is MSU-induced (Piao et al., 2022). Altered ATG expression suggests that autophagy is involved in the pathogenesis of gouty arthritis (GA) and participates in regulating inflammation and metabolism (Dalbeth et al., 2019). However, conflicting evidence exists about the role of autophagy in GA. The autophagy-lysosomal pathway was found to be associated with gouty knee arthritis (Fu et al., 2023; Yuan et al., 2023). MSU crystal-induced acute gouty arthritis can be alleviated by autophagy induced by *p*P121 via inhibition of the NLRP3 inflammasome (Yuan et al., 2023). Autophagy contributes to the pathogenesis of gout through crosstalk with pyroptosis (Zhao L. et al., 2022). Uric acid suppresses autophagy and diminishes the anti-inflammatory capacity of the cell (Crisan et al., 2017). However, it is not specific whether autophagy expression is low or not in acute gouty arthritis. Our study displayed that p-mTOR and p-ULK1 were increased by AGA, suggesting that autophagy expression may be lowly expressed in AGA. This also confirms that autophagy is a fine regulatory mechanism. Autophagy plays a role in the regulation of inflammation and metabolism. Recent research has shown that autophagy negatively regulates proinflammatory responses and downregulates the production of cytokines such as IL-1β, IL-6, and TNF-α(Bussi et al., 2017). Autophagy modulates the transcription, processing, and secretion of IL-1β, acting as an important negative feedback mechanism for the regulation of inflammation (Harris, 2013). In our study, H&E staining analysis indicated that lymphoplasmacytic and other inflammatory levels were decreased by RAPA treatment. Inflammation-related factors (NLRP3, IL-6) confirmed that autophagy could decline inflammation which was MSU-induced. The findings suggested that autophagy could attenuate inflammation, consistent with previous studies. Our study suggested that autophagy-related factors (Atg5, Atg7, Beclin-1, LC3, p62) were activated after QHJR treatment, and QHJR upregulated autophagy expression. From this, we infer that QHJR may reduce inflammation and treat AGA by activating autophagy.

AMPK could regulate autophagy through phosphorylating autophagy-related factors, coordinately regulating ULK1 to induce autophagy with mTORC1 (Li and Chen, 2019). The previous studies demonstrated that medicine could treat arthritis by upregulating AMPK. Jing Zhou et al. (Zhou X. et al., 2019) found that BBR played the role of treating arthritis by upregulating the expression of phosphorylation AMPK. Yan Zhou et al. (Zhou et al., 2015) demonstrated that it suppressed SNP-mediated chondrocyte apoptosis while ameliorating cartilage degeneration by the activation of AMPK pathways and the inhibition of p38 MAPK activity. This study found that AMPKα and p-AMPKα1(Thr 172) had no obvious changes by RAPA and 3-MA treating, while p-ULK1 (Ser757) and p-mTOR (Ser2448) had obvious changes, confirming that AMPK might not directly adjust autophagy and AMPK might regulate autophagy through phosphorylating ULK1 and mTOR. This is slightly different from previous research. The data showed that the expressions of p-AMPKα1, p-ULK1, and p-mTOR expression were significantly activated after QHJR treatment. This suggests that QHJR may potentially alleviate inflammation and treat AGA by regulating the AMPKα/mTOR/ULK1 pathway to activate autophagy.

5 Conclusion

To sum up, all the findings confirmed that QHJR played an important role in AGA, and anti-inflammation is the main mechanism of QHJR for AGA. In our study, it was confirmed the high expression of the predicted key genes in AGA, and their expression was reduced after QHJR treatment, laying the foundation for the mechanism study of QHJR in the treatment of AGA. Following identification, we found the presence of 27 metabolites in QHJR, and the TCMSP database indicates that five of these metabolites do not belong to any single herbal component of QHJR. It is hypothesized that these metabolites may arise from interactions among the individual herbal components of QHJR, suggesting that QHJR cannot be substituted by any single herbal constituent. We found that AMPK may not directly activate autophagy. Furthermore, QHJR regulates autophagy by activating the AMPKα/mTOR/ULK1 pathway, thus reducing MSU-induced inflammation and contributing to the treatment of AGA. This provides novel insights and approaches for the clinical treatment of AGA.

However, this study still has limitations. For example, we found that there is no direct relationship between Ampk and autophagy, but further verification is needed. Furthermore, due to the limitations of network analysis, the predicted key potential metabolites still need further experimental validation for the accuracy of the research.

Data availability statement

The datasets presented in this study can be found in online repositories. The names of the repository/repositories and accession number(s) can be found below: https://www.ncbi.nlm.nih.gov/, 2020.

Ethics statement

The animal study was approved by Laboratory Animal Center of Shandong University of Traditional Chinese Medicine (Approval No. SDUTCM20220102001). The study was conducted in accordance with the local legislation and institutional

requirements and was performed following the principles of care and protection of laboratory animals.

Author contributions

YW: Conceptualization, Data curation, Formal Analysis, Visualization, Writing–original draft, Writing–review and editing. YX: Investigation, Writing–review and editing. JT: Resources, Writing–review and editing. JY: Data curation, Writing–review and editing. SW: Conceptualization, Funding acquisition, Resources, Supervision, Writing–review and editing. QZ: Conceptualization, Project administration, Supervision, Writing–review and editing.

Funding

The author(s) declare financial support was received for the research, authorship, and/or publication of this article. This work was supported by the Natural Science of Shandong Province (Grant No. ZR2020MH352) and Shandong Province Medical and Health Science and Technology Development Plan Project (Grant No. 202102080579).

Conflict of interest

The authors declare that the research was conducted in the absence of any commercial or financial relationships that could be construed as a potential conflict of interest.

Publisher's note

All claims expressed in this article are solely those of the authors and do not necessarily represent those of their affiliated organizations, or those of the publisher, the editors and the reviewers. Any product that may be evaluated in this article, or claim that may be made by its manufacturer, is not guaranteed or endorsed by the publisher.

Supplementary material

The Supplementary Material for this article can be found online at: https://www.frontiersin.org/articles/10.3389/fphar.2023.1268641/full#supplementary-material

References

Abbott, C. E., Xu, R., and Sigal, S. H. (2017). Colchicine-induced hepatotoxicity. *ACG Case Rep. J.* 4, e120. doi:10.14309/crj.2017.120

Amaral, F. A., Bastos, L. F. S., Oliveira, T. H. C., Dias, A. C. F., Oliveira, V. L. S., Tavares, L. D., et al. (2016). Transmembrane TNF-alpha is sufficient for articular inflammation and hypernociception in a mouse model of gout. *Eur. J. Immunol.* 46 (1), 204–211. doi:10.1002/eji.201545798

Angelidis, C., Kotsialou, Z., Kossyvakis, C., Vrettou, A. R., Zacharoulis, A., Kolokathis, F., et al. (2018). Colchicine pharmacokinetics and mechanism of action. *Curr. Pharm. Des.* 24 (6), 659–663. doi:10.2174/1381612824666180123110042

Bussi, C., Peralta Ramos, J. M., Arroyo, D. S., Gaviglio, E. A., Gallea, J. I., Wang, J. M., et al. (2017). Autophagy down regulates pro-inflammatory mediators in BV2 microglial cells and rescues both LPS and alpha-synuclein induced neuronal cell death. *Sci. Rep.* 7, 43153. doi:10.1038/srep43153

Busso, N., and So, A. (2010). Mechanisms of inflammation in gout. *Arthritis Res. Ther.* 12 (2), 206. doi:10.1186/ar2952

Cai, M., Hu, Z., Liu, J., Gao, J., Liu, C., Liu, D., et al. (2014). Beclin 1 expression in ovarian tissues and its effects on ovarian cancer prognosis. *Int. J. Mol. Sci.* 15 (4), 5292–5303. doi:10.3390/ijms15045292

Chang, W. C., Jan Wu, Y. J., Chung, W. H., Lee, Y. S., Chin, S. W., Chen, T. J., et al. (2017). Genetic variants of PPAR-gamma coactivator 1B augment NLRP3-mediated inflammation in gouty arthritis. *Rheumatol. Oxf.* 56 (3), 457–466. doi:10.1093/rheumatology/kew337

Chen, Y. H., Chen, W. Y., Yu, C. L., Tsai, C. Y., and Hsieh, S. C. (2023). Gouty arthritis involves impairment of autophagic degradation via cathepsin D inactivation-mediated lysosomal dysfunction that promotes apoptosis in macrophages. *Biochim. Biophys. Acta Mol. Basis Dis.* 1869 (6), 166703. doi:10.1016/j.bbadis.2023.166703

Chew, C. L., Conos, S. A., Unal, B., and Tergaonkar, V. (2018). Noncoding RNAs: Master regulators of inflammatory signaling. *Trends Mol. Med.* 24 (1), 66–84. doi:10.1016/j.molmed.2017.11.003

Chi, X., Zhang, H., Zhang, S., and Ma, K. (2020). Chinese herbal medicine for gout: a review of the clinical evidence and pharmacological mechanisms. *Chin. Med.* 15, 17. doi:10.1186/s13020-020-0297-y

Cohen-Rosenblum, A. R., Somogyi, J. R., Hynes, K. K., and Guevara, M. E. (2022). Orthopaedic management of gout. *J. Am. Acad. Orthop. Surg. Glob. Res. Rev.* 6 (11), e22.00216. doi:10.5435/JAAOSGlobal-D-22-00216

Crisan, T. O., Cleophas, M. C. P., Novakovic, B., Erler, K., van de Veerdonk, F. L., Stunnenberg, H. G., et al. (2017). Uric acid priming in human monocytes is driven by the AKT-PRAS40 autophagy pathway. *Proc. Natl. Acad. Sci. U. S. A.* 114 (21), 5485–5490. doi:10.1073/pnas.1620910114

Cronstein, B. N., and Terkeltaub, R. (2006). The inflammatory process of gout and its treatment. *Arthritis Res. Ther.* 8 (1), S3. doi:10.1186/ar1908

Dalbeth, N., Choi, H. K., Joosten, L. A. B., Khanna, P. P., Matsuo, H., Perez-Ruiz, F., et al. (2019). Gout. *Nat. Rev. Dis. Prim.* 5 (1), 69. doi:10.1038/s41572-019-0115-y

Dalbeth, N., Lauterio, T. J., and Wolfe, H. R. (2014). Mechanism of action of colchicine in the treatment of gout. *Clin. Ther.* 36 (10), 1465–1479. doi:10.1016/j.clinthera.2014.07.017

Deretic, V. (2021). Autophagy in inflammation, infection, and immunometabolism. *Immunity* 54 (3), 437–453. doi:10.1016/j.immuni.2021.01.018

Di Giovine, F. S., Malawista, S. E., Thornton, E., and Duff, G. W. (1991). Urate crystals stimulate production of tumor necrosis factor alpha from human blood monocytes and synovial cells. Cytokine mRNA and protein kinetics, and cellular distribution. *J. Clin. Invest.* 87 (4), 1375–1381. doi:10.1172/JCI115142

Dinarello, C. A. (2010). How interleukin-1β induces gouty arthritis. *Arthritis Rheum.* 62 (11), 3140–3144. doi:10.1002/art.27663

Doncheva, N. T., Morris, J. H., Holze, H., Kirsch, R., Nastou, K. C., Cuesta-Astroz, Y., et al. (2023). Cytoscape stringApp 2.0: Analysis and visualization of heterogeneous biological networks. *J. Proteome Res.* 22 (2), 637–646. doi:10.1021/acs.jproteome.2c00651

Doss, H. M., Dey, C., Sudandiradoss, C., and Rasool, M. K. (2016). Targeting inflammatory mediators with ferulic acid, a dietary polyphenol, for the suppression of monosodium urate crystal-induced inflammation in rats. *Life Sci.* 148, 201–210. doi:10.1016/j.lfs.2016.02.004

El Hasbani, G., Jawad, A., and Uthman, I. (2021). Colchicine: An ancient drug with multiple benefits. *Curr. Pharm. Des.* 27 (26), 2917–2924. doi:10.2174/1381612826666201023144320

Engel, B., Just, J., Bleckwenn, M., and Weckbecker, K. (2017). Treatment options for gout. *Dtsch. Arztebl Int.* 114 (13), 215–222. doi:10.3238/arztebl.2017.0215

Fan, J., Liu, K., Zhang, Z., Luo, T., Xi, Z., Song, J., et al. (2010). Modified Si-Miao-San extract inhibits the release of inflammatory mediators from lipopolysaccharide-stimulated mouse macrophages. *J. Ethnopharmacol.* 129 (1), 5–9. doi:10.1016/j.jep.2010.02.002

Fischer, S. P. M., Brusco, I., Camponogara, C., Piana, M., Faccin, H., Gobo, L. A., et al. (2018). Arctium minus crude extract presents antinociceptive effect in a mice acute gout attack model. *Inflammopharmacology* 26 (2), 505–519. doi:10.1007/s10787-017-0384-6

Fu, W., Ge, M., and Li, J. (2023). Phospholipase A2 regulates autophagy in gouty arthritis: Proteomic and metabolomic studies. *J. Transl. Med.* 21 (1), 261. doi:10.1186/s12967-023-04114-6

Galozzi, P., Bindoli, S., Doria, A., Oliviero, F., and Sfriso, P. (2021). Autoinflammatory features in gouty arthritis. *J. Clin. Med.* 10 (9), 1880. doi:10.3390/jcm10091880

Ganesan, R., and Rasool, M. (2019). Ferulic acid inhibits interleukin 17-dependent expression of nodal pathogenic mediators in fibroblast-like synoviocytes of rheumatoid arthritis. *J. Cell Biochem.* 120 (2), 1878–1893. doi:10.1002/jcb.27502

Gao, X. H., Zhang, S. D., Wang, L. T., Yu, L., Zhao, X. L., Ni, H. Y., et al. (2020). Anti-inflammatory effects of neochlorogenic acid extract from mulberry leaf (morus alba L.) against LPS-stimulated inflammatory response through mediating the AMPK/Nrf2 signaling pathway in A549 cells. *Molecules* 25 (6), 1385. doi:10.3390/molecules25061385

Ge, Y., Zhou, M., Chen, C., Wu, X., and Wang, X. (2022). Role of AMPK mediated pathways in autophagy and aging. *Biochimie* 195, 100–113. doi:10.1016/j.biochi.2021.11.008

Grazio, S. (2012). New and emerging drugs for uric arthritis. *Reumatizam* 59 (2), 110–118.

Gu, Y., Zhu, Y., Deng, G., Liu, S., Sun, Y., and Lv, W. (2021). Curcumin analogue AI-44 alleviates MSU-induced gouty arthritis in mice via inhibiting cathepsin B-mediated NLRP3 inflammasome activation. *Int. Immunopharmacol.* 93, 107375. doi:10.1016/j.intimp.2021.107375

Guo, J., Sun, D., Xu, X., Liu, P., and Sun, H. (2023). Relief effects of Laoshan cherry extracts as a dietary supplement against the symptoms of acute gouty arthritis in rats induced by urate crystals. *J. Food Sci.* 88 (3), 1188–1196. doi:10.1111/1750-3841.16462

Han, J., Shi, G., Li, W., Wang, S., Bai, J., Sun, X., et al. (2021). Zisheng shenqi decoction ameliorates monosodium urate-mediated gouty arthritis in rats via promotion of autophagy through the AMPK/mTOR signaling pathway. *Evid. Based Complement. Altern. Med.* 2021, 6918026. doi:10.1155/2021/6918026

Hao, Z., and Liu, Y. (2021). IL-38 and IL-36 target autophagy for regulating synoviocyte proliferation, migration, and invasion in rheumatoid arthritis. *Dis. Markers* 2021, 7933453. doi:10.1155/2021/7933453

Harris, J. (2013). Autophagy and IL-1 family cytokines. *Front. Immunol.* 4, 83. doi:10.3389/fimmu.2013.00083

He, M., Hu, C., Chen, M., Gao, Q., Li, L., and Tian, W. (2022). Effects of Gentiopicroside on activation of NLRP3 inflammasome in acute gouty arthritis mice induced by MSU. *J. Nat. Med.* 76 (1), 178–187. doi:10.1007/s11418-021-01571-5

Hoare, S. R. J. (2021). The problems of applying classical pharmacology analysis to modern *in vitro* drug discovery assays: Slow binding kinetics and high target concentration. *SLAS Discov.* 26 (7), 835–850. doi:10.1177/24725552211019653

Huang, J., Zhu, M., Tao, Y., Wang, S., Chen, J., Sun, W., et al. (2012). Therapeutic properties of quercetin on monosodium urate crystal-induced inflammation in rat. *J. Pharm. Pharmacol.* 64 (8), 1119–1127. doi:10.1111/j.2042-7158.2012.01504.x

Huang, T. T., Lai, H. C., Chen, Y. B., Chen, L. G., Wu, Y. H., Ko, Y. F., et al. (2014). cis-Resveratrol produces anti-inflammatory effects by inhibiting canonical and non-canonical inflammasomes in macrophages. *Innate Immun.* 20 (7), 735–750. doi:10.1177/1753425913507096

Ji, X., Du, W., Che, W., Wang, L., and Zhao, L. (2023). Apigenin inhibits the progression of osteoarthritis by mediating macrophage polarization. *Molecules* 28 (7), 2915. doi:10.3390/molecules28072915

Kanehisa, M., Furumichi, M., Tanabe, M., Sato, Y., and Morishima, K. (2017). Kegg: New perspectives on genomes, pathways, diseases and drugs. *Nucleic Acids Res.* 45 (D1), D353–D361. doi:10.1093/nar/gkw1092

Khanna, P. P., Shiozawa, A., Walker, V., Bancroft, T., Essoi, B., Akhras, K. S., et al. (2015). Health-related quality of life and treatment satisfaction in patients with gout: results from a cross-sectional study in a managed care setting. *Patient Prefer Adherence* 9, 971–981. doi:10.2147/PPA.S83700

Konishi, A., Arakawa, S., Yue, Z., and Shimizu, S. (2012). Involvement of Beclin 1 in engulfment of apoptotic cells. *J. Biol. Chem.* 287 (17), 13919–13929. doi:10.1074/jbc.M112.348375

Lage, O. M., Ramos, M. C., Calisto, R., Almeida, E., Vasconcelos, V., and Vicente, F. (2018). Current screening methodologies in drug discovery for selected human diseases. *Mar. Drugs* 16 (8), 279. doi:10.3390/md16080279

Li, Y., and Chen, Y. (2019). AMPK and autophagy. *Adv. Exp. Med. Biol.* 1206, 85–108. doi:10.1007/978-981-15-0602-4_4

Li, Y., Piranavan, P., Sundaresan, D., and Yood, R. (2019). Clinical characteristics of early-onset gout in outpatient setting. *ACR Open Rheumatol.* 1 (7), 397–402. doi:10.1002/acr2.11057

Liao, M., Shang, H., Li, Y., Li, T., Wang, M., Zheng, Y., et al. (2018). An integrated approach to uncover quality marker underlying the effects of Alisma orientale on lipid metabolism, using chemical analysis and network pharmacology. *Phytomedicine* 45, 93–104. doi:10.1016/j.phymed.2018.04.006

Lin, Y., Luo, T., Weng, A., Huang, X., Yao, Y., Fu, Z., et al. (2020). Gallic acid alleviates gouty arthritis by inhibiting NLRP3 inflammasome activation and pyroptosis through enhancing Nrf2 signaling. *Front. Immunol.* 11, 580593. doi:10.3389/fimmu.2020.580593

Liu, H., Cao, M., Jin, Y., Jia, B., Wang, L., Dong, M., et al. (2023). Network pharmacology and experimental validation to elucidate the pharmacological mechanisms of Bushen Huashi decoction against kidney stones. *Front. Endocrinol. (Lausanne)* 14, 1031895. doi:10.3389/fendo.2023.1031895

Liu, Q., Zhang, X., Dai, L., Hu, X., Zhu, J., Li, L., et al. (2014). Long noncoding RNA related to cartilage injury promotes chondrocyte extracellular matrix degradation in osteoarthritis. *Arthritis Rheumatol.* 66 (4), 969–978. doi:10.1002/art.38309

Liu, W., Liu, J., and Rajapakse, J. C. (2018). Gene Ontology enrichment improves performances of functional similarity of genes. *Sci. Rep.* 8 (1), 12100. doi:10.1038/s41598-018-30455-0

Liu, Y. F., Wen, C. Y. Z., Chen, Z., Wang, Y., Huang, Y., and Tu, S. H. (2016). Effects of berberine on NLRP3 and IL-1β expressions in monocytic THP-1 cells with monosodium urate crystals-induced inflammation. *Biomed. Res. Int.* 2016, 2503703. doi:10.1155/2016/2503703

Liu, Y., Luo, D., and Xu, B. (2022). The combination of molecular docking and network pharmacology reveals the molecular mechanism of Danggui Niantong decoction in treating gout. *Med. Baltim.* 101 (47), e31535. doi:10.1097/MD.0000000000031535

Lyu, W., Li, Q., Wang, Y., Du, C., Feng, F., Chi, H., et al. (2021). Computational design of binder as the LC3-p62 protein-protein interaction. *Bioorg Chem.* 115, 105241. doi:10.1016/j.bioorg.2021.105241

Mao, Y., Peng, L., Kang, A., Xie, T., Xu, J., Shen, C., et al. (2017). Influence of jiegeng on pharmacokinetic properties of flavonoids and saponins in gancao. *Molecules* 22 (10), 1587. doi:10.3390/molecules22101587

Masud, S., Prajsnar, T. K., Torraca, V., Lamers, G. E. M., Benning, M., Van Der Vaart, M., et al. (2019). Macrophages target Salmonella by Lc3-associated phagocytosis in a systemic infection model. *Autophagy* 15 (5), 796–812. doi:10.1080/15548627.2019.1569297

Matosinhos, R. C., Bezerra, J. P., Barros, C. H., Fernandes Pereira Ferreira Bernardes, A. C., Coelho, G. B., Carolina de Paula Michel Araújo, M., et al. (2022). Coffea arabica extracts and their chemical constituents in a murine model of gouty arthritis: How they modulate pain and inflammation. *J. Ethnopharmacol.* 284, 114778. doi:10.1016/j.jep.2021.114778

McWherter, C., Choi, Y. J., Serrano, R. L., Mahata, S. K., Terkeltaub, R., and Liu-Bryan, R. (2018). Arhalofenate acid inhibits monosodium urate crystal-induced inflammatory responses through activation of AMP-activated protein kinase (AMPK) signaling. *Arthritis Res. Ther.* 20 (1), 204. doi:10.1186/s13075-018-1699-4

Nuki, G. (2008). Colchicine: its mechanism of action and efficacy in crystal-induced inflammation. *Curr. Rheumatol. Rep.* 10 (3), 218–227. doi:10.1007/s11926-008-0036-3

Ouyang, X., Li, N. Z., Guo, M. X., Zhang, M. M., Cheng, J., Yi, L. T., et al. (2021). Active flavonoids from *Lagotis brachystachya* attenuate monosodium urate-induced gouty arthritis *via* inhibiting TLR4/MyD88/NF-κB pathway and NLRP3 expression. *Front. Pharmacol.* 12, 760331. doi:10.3389/fphar.2021.760331

Pang, Y., Wu, L., Tang, C., Wang, H., and Wei, Y. (2022). Autophagy-inflammation interplay during infection: Balancing pathogen clearance and host inflammation. *Front. Pharmacol.* 13, 832750. doi:10.3389/fphar.2022.832750

Papanagnou, P., Stivarou, T., and Tsironi, M. (2016). The role of miRNAs in common inflammatory arthropathies: Osteoarthritis and gouty arthritis. *Biomolecules* 6 (4), 44. doi:10.3390/biom6040044

Piao, M. H., Wang, H., Jiang, Y. J., Wu, Y. L., Nan, J. X., and Lian, L. H. (2022). Taxifolin blocks monosodium urate crystal-induced gouty inflammation by regulating phagocytosis and autophagy. *Inflammopharmacology* 30 (4), 1335–1349. doi:10.1007/s10787-022-01014-x

Piras, S., Furfaro, A. L., Brondolo, L., Passalacqua, M., Marinari, U. M., Pronzato, M. A., et al. (2017). Differentiation impairs Bach1 dependent HO-1 activation and increases sensitivity to oxidative stress in SH-SY5Y neuroblastoma cells. *Sci. Rep.* 7 (1), 7568. doi:10.1038/s41598-017-08095-7

Pu, M. J., Yao, C. J., Liu, L. M., Ren, L. J., Li, Y. L., and Xie, Y. (2021). Traditional Chinese medicine for gouty arthritis: A protocol for meta-analysis. *Med. Baltim.* 100 (3), e23699. doi:10.1097/MD.0000000000023699

Qi, P., Li, J., Gao, S., Yuan, Y., Sun, Y., Liu, N., et al. (2020). Network pharmacology-based and experimental identification of the effects of quercetin on alzheimer's disease. *Front. Aging Neurosci.* 12, 589588. doi:10.3389/fnagi.2020.589588

Qian, M., Fang, X., and Wang, X. (2017). Autophagy and inflammation. *Clin. Transl. Med.* 6 (1), 24. doi:10.1186/s40169-017-0154-5

Qian, X., Jiang, Y., Luo, Y., and Jiang, Y. (2023). The anti-hyperuricemia and anti-inflammatory effects of Atractylodes macrocephala in hyperuricemia and gouty arthritis rat models. *Comb. Chem. High. Throughput Screen* 26 (5), 950–964. doi:10.2174/1386207325666220603101540

Ru, J., Li, P., Wang, J., Zhou, W., Li, B., Huang, C., et al. (2014). Tcmsp: a database of systems pharmacology for drug discovery from herbal medicines. *J. Cheminform* 6, 13. doi:10.1186/1758-2946-6-13

Ruan, X., Du, P., Zhao, K., Huang, J., Xia, H., Dai, D., et al. (2020). Mechanism of Dayuanyin in the treatment of coronavirus disease 2019 based on network pharmacology and molecular docking. *Chin. Med.* 15, 62. doi:10.1186/s13020-020-00346-6

Ruiz-Miyazawa, K. W., Staurengo-Ferrari, L., Mizokami, S. S., Domiciano, T. P., Vicentini, F. T. M. C., Camilios-Neto, D., et al. (2017). Quercetin inhibits gout arthritis in mice: induction of an opioid-dependent regulation of inflammasome. *Inflammopharmacology* 25, 555–570. doi:10.1007/s10787-017-0356-x

Sadybekov, A. V., and Katritch, V. (2023). Computational approaches streamlining drug discovery. *Nature* 616 (7958), 673–685. doi:10.1038/s41586-023-05905-z

Safran, M., Dalah, I., Alexander, J., Rosen, N., Iny Stein, T., Shmoish, M., et al. (2010). *GeneCards version 3: the human gene integrator*. Oxford: Database, baq020.

Shannon, P., Markiel, A., Ozier, O., Baliga, N. S., Wang, J. T., Ramage, D., et al. (2003). Cytoscape: a software environment for integrated models of biomolecular interaction networks. *Genome Res.* 13 (11), 2498–2504. doi:10.1101/gr.1239303

Shu, J., Chen, M., Ya, C., Yang, R., and Li, F. (2022). Regulatory role of miRNAs and lncRNAs in gout. *Comput. Math. Methods Med.* 2022, 6513565. doi:10.1155/2022/6513565

So, A., De Smedt, T., Revaz, S., and Tschopp, J. (2007). A pilot study of IL-1 inhibition by anakinra in acute gout. *Arthritis Res. Ther.* 9 (2), R28. doi:10.1186/ar2143

Szklarczyk, D., Gable, A. L., Nastou, K. C., Lyon, D., Kirsch, R., Pyysalo, S., et al. (2021). Correction to 'the STRING database in 2021: customizable protein-protein networks, and functional characterization of user-uploaded gene/measurement sets. *Nucleic Acids Res.* 49 (18), 10800. doi:10.1093/nar/gkab835

Tang, J., Hu, P., Zhou, S., Zhou, T., Li, X., and Zhang, L. (2022). Lymphoma cell-derived extracellular vesicles inhibit autophagy and apoptosis to promote lymphoma cell growth via the microRNA-106a/Beclin1 axis. *Cell Cycle* 21 (12), 1280–1293. doi:10.1080/15384101.2022.2047335

Tao, W., Xu, X., Wang, X., Li, B., Wang, Y., Li, Y., et al. (2013). Network pharmacology-based prediction of the active ingredients and potential targets of Chinese herbal Radix Curcumae formula for application to cardiovascular disease. *J. Ethnopharmacol.* 145 (1), 1–10. doi:10.1016/j.jep.2012.09.051

Tardif, J. C., Kouz, S., Waters, D. D., Bertrand, O. F., Diaz, R., Maggioni, A. P., et al. (2019). Efficacy and safety of low-dose colchicine after myocardial infarction. *N. Engl. J. Med.* 381 (26), 2497–2505. doi:10.1056/NEJMoa1912388

Terkeltaub, R. (2017). What makes gouty inflammation so variable? *BMC Med.* 15 (1), 158. doi:10.1186/s12916-017-0922-5

Thompson, P. L., and Nidorf, S. M. (2018). Colchicine: an affordable anti-inflammatory agent for atherosclerosis. *Curr. Opin. Lipidol.* 29 (6), 467–473. doi:10.1097/MOL.0000000000000552

Wang, S., Li, H., Yuan, M., Fan, H., and Cai, Z. (2022a). Role of AMPK in autophagy. *Front. Physiol.* 13, 1015500. doi:10.3389/fphys.2022.1015500

Wang, X., Long, H., Chen, M., Zhou, Z., Wu, Q., Xu, S., et al. (2022b). Modified Baihu decoction therapeutically remodels gut microbiota to inhibit acute gouty arthritis. *Front. Physiol.* 13, 1023453. doi:10.3389/fphys.2022.1023453

Wang, X., Shen, Y., Wang, S., Li, S., Zhang, W., Liu, X., et al. (2017). PharmMapper 2017 update: a web server for potential drug target identification with a comprehensive target pharmacophore database. *Nucleic Acids Res.* 45 (W1), W356–W360. doi:10.1093/nar/gkx374

Wang, Y., Shi, Y., Zou, J., Zhang, X., Liang, Y., Tai, J., et al. (2020). Network pharmacology exploration reveals a common mechanism in the treatment of cardio-cerebrovascular disease with Salvia miltiorrhiza Burge. and Carthamus tinctorius L. *BMC Complement. Med. Ther.* 20 (1), 351. doi:10.1186/s12906-020-03026-y

Wang, Y., Viollet, B., Terkeltaub, R., and Liu-Bryan, R. (2016). AMP-activated protein kinase suppresses urate crystal-induced inflammation and transduces colchicine effects in macrophages. *Ann. Rheum. Dis.* 75 (1), 286–294. doi:10.1136/annrheumdis-2014-206074

Wang, Y., Zhu, W., Lu, D., and Zhang, C. (2021). Tetrahydropalmatine attenuates MSU crystal-induced gouty arthritis by inhibiting ROS-mediated NLRP3 inflammasome activation. *Int. Immunopharmacol.* 100, 108107. doi:10.1016/j.intimp.2021.108107

Xiao, J., Zhu, S., Guan, H., Zheng, Y., Li, F., Zhang, X., et al. (2019). AMPK alleviates high uric acid-induced Na(+)-K(+)-ATPase signaling impairment and cell injury in renal tubules. *Exp. Mol. Med.* 51 (5), 1–14. doi:10.1038/s12276-019-0254-y

Xiao, L., Lin, S., Xu, W., and Sun, E. (2023). Downregulation of Sox8 mediates monosodium urate crystal-induced autophagic impairment of cartilage in gout arthritis. *Cell Death Discov.* 9 (1), 95. doi:10.1038/s41420-023-01388-z

Xu, B. Y., Huang, Y. J., Sun, B. G., Gu, D., Zhang, Y. L., Zhang, X. Q., et al. (2020a). Skin-patch of xin huang pian on relieving joint symptoms in patients with acute gouty arthritis: A randomized, double-blind, active-controlled trial. *J. Adv. Nurs.* 76 (6), 1416–1424. doi:10.1111/jan.14338

Xu, H., Qin, Z. H., Wei, Y., and Wu, J. (2022). Editorial: Beclin 1 and autophagy---in memory of beth levine (1960-2020). *Front. Cell Dev. Biol.* 10, 1058861. doi:10.3389/fcell.2022.1058861

Xu, L., Lin, G., Yu, Q., Li, Q., Mai, L., Cheng, J., et al. (2021). Anti-hyperuricemic and nephroprotective effects of dihydroberberine in potassium oxonate- and hypoxanthine-induced hyperuricemic mice. *Front. Pharmacol.* 12, 645879. doi:10.3389/fphar.2021.645879

Xu, X., Zhang, W., Huang, C., Li, Y., Yu, H., Wang, Y., et al. (2012). A novel chemometric method for the prediction of human oral bioavailability. *Int. J. Mol. Sci.* 13 (6), 6964–6982. doi:10.3390/ijms13066964

Xu, Y. T., Leng, Y. R., Liu, M. M., Dong, R. F., Bian, J., Yuan, L. L., et al. (2020b). MicroRNA and long noncoding RNA involvement in gout and prospects for treatment. *Int. Immunopharmacol.* 87, 106842. doi:10.1016/j.intimp.2020.106842

Yang, G., Xia, X., Zhong, H., Shen, J., and Li, S. (2021). Protective effect of tangeretin and 5-hydroxy-6,7,8,3',4'-pentamethoxyflavone on collagen-induced arthritis by inhibiting autophagy via activation of the ROS-AKT/mTOR signaling pathway. *J. Agric. Food Chem.* 69 (1), 259–266. doi:10.1021/acs.jafc.0c06801

Yang, L., Hu, Z., Zhu, J., Liang, Q., Zhou, H., Li, J., et al. (2020). Systematic elucidation of the mechanism of quercetin against gastric cancer via network pharmacology approach. *Biomed. Res. Int.* 2020, 3860213. doi:10.1155/2020/3860213

Ye, B., Chen, P., Lin, C., Zhang, C., and Li, L. (2023). Study on the material basis and action mechanisms of sophora davidii (Franch.) skeels flower extract in the treatment of non-small cell lung cancer. *J. Ethnopharmacol.* 317, 116815. doi:10.1016/j.jep.2023.116815

Yu, S., Wang, J., and Shen, H. (2020a). Network pharmacology-based analysis of the role of traditional Chinese herbal medicines in the treatment of COVID-19. *Ann. Palliat. Med.* 9 (2), 437–446. doi:10.21037/apm.2020.03.27

Yu, Y., Cai, W., Zhou, J., Lu, H., Wang, Y., Song, Y., et al. (2020b). Anti-arthritis effect of berberine associated with regulating energy metabolism of macrophages through AMPK/HIF-1α pathway. *Int. Immunopharmacol.* 87, 106830. doi:10.1016/j.intimp.2020.106830

Yuan, W., Liu, T., Wang, Y. Y., He, S., Zhang, F., Wang, X. B., et al. (2023). Autophagy induced by PP121 alleviates MSU crystal-induced acute gouty arthritis via inhibition of the NLRP3 inflammasome. *Int. Immunopharmacol.* 123, 110756. doi:10.1016/j.intimp.2023.110756

Yuan, X., Fan, Y. S., Xu, L., Xie, G. Q., Feng, X. H., and Qian, K. (2019). Jia-Wei-Si-Miao-Wan alleviates acute gouty arthritis by targeting NLRP3 inflammasome. *J. Biol. Regul. Homeost. Agents* 33 (1), 63–71.

Zhang, J., Li, H., Wang, W., and Li, H. (2022). Assessing the anti-inflammatory effects of quercetin using network pharmacology and *in vitro* experiments. *Exp. Ther. Med.* 23 (4), 301. doi:10.3892/etm.2022.11230

Zhang, L., Yu, J., Wang, C., and Wei, W. (2019a). The effects of total glucosides of paeony (TGP) and paeoniflorin (Pae) on inflammatory-immune responses in rheumatoid arthritis (RA). *Funct. Plant Biol.* 46 (2), 107–117. doi:10.1071/FP18080

Zhang, M. Y., Gou, W. F., Zhao, S., Mao, X. Y., Zheng, Z. H., Takano, Y., et al. (2014). Beclin 1 expression is closely linked to colorectal carcinogenesis and distant metastasis of colorectal carcinoma. *Int. J. Mol. Sci.* 15 (8), 14372–14385. doi:10.3390/ijms150814372

Zhang, Q. B., Zhu, D., Dai, F., Huang, Y. Q., Zheng, J. X., Tang, Y. P., et al. (2021a). MicroRNA-223 suppresses IL-1β and TNF-α production in gouty inflammation by targeting the NLRP3 inflammasome. *Front. Pharmacol.* 12, 637415. doi:10.3389/fphar.2021.637415

Zhang, T., Wang, G., Zheng, J., Li, S., and Xu, J. (2021b). Profile of serum cytokine concentrations in patients with gouty arthritis. *J. Int. Med. Res.* 49 (11), 3000605211055618. doi:10.1177/03000605211055618

Zhang, W., Huai, Y., Miao, Z., Qian, A., and Wang, Y. (2019b). Systems pharmacology for investigation of the mechanisms of action of traditional Chinese medicine in drug discovery. *Front. Pharmacol.* 10, 743. doi:10.3389/fphar.2019.00743

Zhao, J., Wei, K., Jiang, P., Chang, C., Xu, L., Xu, L., et al. (2022a). Inflammatory response to regulated cell death in gout and its functional implications. *Front. Immunol.* 13, 888306. doi:10.3389/fimmu.2022.888306

Zhao, L., Ye, W., Zhu, Y., Chen, F., Wang, Q., Lv, X., et al. (2022b). Distinct macrophage polarization in acute and chronic gout. *Lab. Invest.* 102 (10), 1054–1063. doi:10.1038/s41374-022-00798-4

Zheng, H. C., Zhao, S., Xue, H., Zhao, E. H., Jiang, H. M., and Hao, C. L. (2020). The roles of Beclin 1 expression in gastric cancer: A marker for carcinogenesis, aggressive behaviors and favorable prognosis, and a target of gene therapy. *Front. Oncol.* 10, 613679. doi:10.3389/fonc.2020.613679

Zhou, J. X., and Wink, M. (2019). Evidence for anti-inflammatory activity of isoliquiritigenin, 18β glycyrrhetinic acid, ursolic acid, and the traditional Chinese medicine plants Glycyrrhiza glabra and eriobotrya japonica, at the molecular level. *Med. (Basel)* 6 (2), 55. doi:10.3390/medicines6020055

Zhou, J., Yu, Y., Yang, X., Wang, Y., Song, Y., Wang, Q., et al. (2019a). Berberine attenuates arthritis in adjuvant-induced arthritic rats associated with regulating polarization of macrophages through AMPK/NF-κB pathway. *Eur. J. Pharmacol.* 852, 179–188. doi:10.1016/j.ejphar.2019.02.036

Zhou, S., Ai, Z., Li, W., You, P., Wu, C., Li, L., et al. (2020). Deciphering the pharmacological mechanisms of taohe-chengqi decoction extract against renal fibrosis through integrating network pharmacology and experimental validation *in vitro* and *in vivo*. *Front. Pharmacol.* 11, 425. doi:10.3389/fphar.2020.00425

Zhou, X., Li, C. G., Chang, D., and Bensoussan, A. (2019b). Current status and major challenges to the safety and efficacy presented by Chinese herbal medicine. *Med. (Basel)* 6 (1), 14. doi:10.3390/medicines6010014

Zhou, Y., Liu, S. Q., Yu, L., He, B., Wu, S. H., Zhao, Q., et al. (2015). Berberine prevents nitric oxide-induced rat chondrocyte apoptosis and cartilage degeneration in a rat osteoarthritis model via AMPK and p38 MAPK signaling. *Apoptosis* 20 (9), 1187–1199. doi:10.1007/s10495-015-1152-y

Zhu, H., and He, L. (2015). Beclin 1 biology and its role in heart disease. *Curr. Cardiol. Rev.* 11 (3), 229–237. doi:10.2174/1573403x10666141106104606

Zhu, T., Cao, S., Su, P. C., Patel, R., Shah, D., Chokshi, H. B., et al. (2013). Hit identification and optimization in virtual screening: Practical recommendations based on a critical literature analysis. *J. Med. Chem.* 56 (17), 6560–6572. doi:10.1021/jm301916b

Zhu, Y., Pandya, B. J., and Choi, H. K. (2011). Prevalence of gout and hyperuricemia in the US general population: the national health and nutrition examination survey 2007-2008. *Arthritis Rheum.* 63 (10), 3136–3141. doi:10.1002/art.30520

frontiers | Frontiers in Pharmacology

TYPE Original Research
PUBLISHED 13 October 2023
DOI 10.3389/fphar.2023.1279215

OPEN ACCESS

EDITED BY
Xianyu Li,
China Academy of Chinese Medical Sciences, China

REVIEWED BY
Ali Sharif,
Lahore College for Women University, Pakistan
Liufeng Mao,
Guangdong Pharmaceutical University, China

*CORRESPONDENCE
Arham Shabbir,
arham.shabbir@lcwu.edu.pk
Musaab Dauelbait,
musaabelnaim@gmail.com

RECEIVED 17 August 2023
ACCEPTED 29 September 2023
PUBLISHED 13 October 2023

CITATION
Sattar S, Shabbir A, Shahzad M, Akhtar T, Anjum SM, Bourhia M, Nafidi H-A, Bin Jardan YA, Dauelbait M and Mobashar A (2023), Evaluation of anti-inflammatory and immunomodulatory potential of Lawsone (2-hydroxy-1,4-naphthoquinone) using pre-clinical rodent model of rheumatoid arthritis. *Front. Pharmacol.* 14:1279215. doi: 10.3389/fphar.2023.1279215

Evaluation of anti-inflammatory and immunomodulatory potential of Lawsone (2-hydroxy-1,4-naphthoquinone) using pre-clinical rodent model of rheumatoid arthritis

Sara Sattar[1], Arham Shabbir[1,2]*, Muhammad Shahzad[3], Tasleem Akhtar[3], Syed Muneeb Anjum[4], Mohammed Bourhia[5], Hiba-Allah Nafidi[6], Yousef A. Bin Jardan[7], Musaab Dauelbait[8]* and Aisha Mobashar[1]

[1]Department of Pharmacology, Faculty of Pharmacy, The University of Lahore, Lahore Campus, Lahore, Pakistan, [2]Department of Pharmacology, Institute of Pharmacy, Faculty of Pharmaceutical and Allied Health Sciences, Lahore College for Women University, Lahore, Pakistan, [3]Department of Pharmacology, University of Health Sciences, Lahore, Pakistan, [4]Institute of Pharmaceutical Sciences, University of Veterinary and Animal Sciences, Lahore, Pakistan, [5]Department of Chemistry and Biochemistry, Faculty of Medicine and Pharmacy, Ibn Zohr University, Laayoune, Morocco, [6]Department of Food Science, Faculty of Agricultural and Food Sciences, Laval University, Quebec, QC, Canada, [7]Department of Pharmaceutics, College of Pharmacy, King Saud University, Riyadh, Saudi Arabia, [8]Department of Scientific Translation, Faculty of Translation, University of Bahri, Khartoum, Sudan

Background: Lawsone (2-hydroxy-1,4-naphthoquinone) is naturally present in *Lawsonia Inermis* and flowers of *Eicchornia crassipes*. This study assessed the anti-arthritic potential of Lawsone, using FCA-induced Sprague-Dawley rats.

Methods: Arthritic progress was analyzed through a macroscopic scoring scale, measurement of paw edema, and histopathological changes. Effects of Lawsone on mRNA expression levels of inflammatory markers were examined using the reverse transcription PCR technique. ELISA technique was used to evaluate the PGE2 levels. Moreover, levels of biochemical and hematological parameters were also analyzed.

Results: The research elucidated that Lawsone showed an inhibitory potential towards arthritic progress and ameliorated the paw edema. The histopathological analysis also validated the inhibition in arthritic development. Treatment with Lawosne reduced the expression levels of inflammatory markers in rats i.e., VEGF, TNF-α, MMP-2, MMP-3, NF-κB, IL-1β, and IL-6. PGE2 levels (all $p < 0.001$) were also found reduced in treatment groups. Lab investigations showed improved results of hematological and hepatic parameters in the treated groups as compared to the positive control. This study found no hepatotoxic or nephrotoxic effects of Lawsone in the test doses.

Abbreviations: RA, Rheumatoid Arthritis; FCA, Freund's Complete Adjuvant; H&E, Hematoxylin and Eosin; PGE2, Prostaglandin E2; ELISA, Enzyme-linked Immunosorbent Assay; ALT, Alanine Transaminase; AST, Aspartate Aminotransferase; Hb, Hemoglobin; CBC, Complete Blood Count; VEGF, Vascular Endothelial Growth Factor; TNF-α, Tumor Necrosis Factor- α; MMP-2 and MMP-3, matrix metalloproteinase; NF-κB, Nuclear Factor-Kappa B; IL-1β and IL-6, Interleukins.

Conclusion: Lawsone possesses an anti-arthritic property which could be ascribed to its immunomodulatory and anti-inflammatory effects.

KEYWORDS

arthritis, inflammation, cytokines, rheumatism, phytochemical

1 Introduction

RA is defined as an autoimmune multisystem disease, having primary symptoms like pain, inflammation of synovial membrane & peripheral joints, deterioration of articular tissues, morning stiffness, and constrained joint mobility (Scherer, Haupl, and Burmester, 2020).

It involves multiple systems and has a complex pathology (Kaur and Sultana, 2012). RA involves both immune cells, i.e., B-cells, T-cells, macrophages, and soluble inflammatory mediators of our defense system (Yap et al., 2018). RA development is the consequence of the imbalance between the expressed values of pro-inflammatory and anti-inflammatory cytokines, resulting in the proliferation of cells in the synovial layer and infiltration of cytokines, chemokines, growth factors, and hormones in the joints RA (Bugatti et al., 2014). RA can also result in severe disabilities, hence compromising the quality of life in both physical and mental spheres (Matcham et al., 2014).

In the case of RA, the average mortality ratio varies from 1.28 to 2.89. The overall data from the population of developed countries shows the RA occurrence rate to be 0.5%–1% (Uroos et al., 2017; Li and Zhang, 2020). As per World Health Organization (WHO) report, RA causes 0.8% of total global years of life lost due to disability (YLD). According to the Global Burden of Disease (GBD) 2017 report, the prevalence of RA is higher in developed countries, such as North America, Western Europe, and the Caribbean, followed by India and South America (Finckh et al., 2022). The risk of RA seems to be greater in women than men and also enhances with age (Shabbir et al., 2014). The prominent risk factors for RA are female gender, age, tobacco use, silica exposure, and obesity (Yap et al., 2018).

Inflammatory and edematous conditions like RA are usually treated by corticosteroids, non-steroidal anti-inflammatory drugs (NSAIDs), disease-modifying anti-rheumatic drugs (DMARDs), opiates and anti-TNFs. NSAIDs, like piroxicam, are preferred to be the "first-line" therapeutic drugs for the treatment of RA, as they restrict the upregulation of IL-6, IL-1, TNF-α, and pro-inflammatory prostaglandins by blocking the cyclooxygenase pathway of the arachidonic acid cascade. DMARDs, e.g., methotrexate, are immune-modulators that regulate a disturbed immune system (Uroos et al., 2017). American College of Rheumatology guidelines for the treatment of RA (2021) strongly recommends the use of methotrexate as monotherapy with moderate-to-high RA disease activity for DMARD naïve patients. These recommendations are over the use of sulfasalazine or hydroxychloroquine. The guidelines also acknowledge that short term glucocorticoids are often important to reduce the symptoms of RA before the beginning of onset of action of DMARDs. However, the duration of glucocorticoid therapy should be as short as possible and the lowest effective dose should be used. Along with this acknowledgment, the guidelines conditionally recommend the use of conventional synthetic DMARDs without short term glucocorticoids (Fraenkel et al., 2021).

DMARDs cause mild alopecia, rash, nausea, loss of appetite, raised rheumatoid nodules, oral ulcers and other neurological complications (Guo et al., 2018). Anti-TNFs drugs inhibit the expression of TNF and block the inflammatory response. But they cause headache, abdominal pain, vomiting, diarrhea, itching, bruising, bleeding, rash, cellulitis, and lower respiratory tract complications. Corticosteroids such as prednisone hormones, effectively reduce synovitis. However, long-term usage of corticosteroids also includes increase risk of osteoporosis, diabetes mellitus, peptic ulcer, gastrointestinal bleeding, cataracts, and infections. Short-term opiates, such as fentanyl and oxycodone, help in pain management in RA but the long-term ones are linked with side effects such as respiratory depression, dependence, and tolerance (Mobashar et al., 2020a).

All of this demands the development of a novel but safe anti-arthritic regimen (Uroos et al., 2017). There have been discovered many plant-based products that showed significant effects in the reduction of chronic joint inflammation, such as rheumatoid arthritis (Bang et al., 2009; Mubashir et al., 2014).

Lawsone (Lawsonia, 2-hydroxy-1,4 napthaquinone), has the orange-red colour artifact and is naturally present in *Lawsonia Inermis* and flowers of *Eicchornia crassipes* (Kapadia et al., 2013). It has anti-inflammatory, hepatoprotective, anti-bacterial, anti-fungal, molluscicidal, anti-parasitic, and antiplatelet and anti-cancer activities (Cape, Bowman, and Kramer, 2006; Adeli-Sardou et al., 2019). Its wound-healing activity was reported by using ethanolic extract of Lawsone which depicted a visible wound-healing effect in incision and excision models of rat. Lawsone increased the pentobarbitone-induced sleeping time in an anti-inflammatory model of rats. It is also used in folk medicine for treatment of inflammatory diseases (Badoni Semwal et al., 2014). The *in vitro* anti-inflammatory potential of the Lawsone complexes depicted the modulation in the activity of NF-κB and TNF-α with results similar to prednisolone (Vanco et al., 2017). It also proved to be effective the in amelioration of interleukins levels, resulting in the reduction of inflammation and edema (Biradar and Veeresh, 2013). A study has previously reported cytotoxic effects of lawsone which are probably mediated through the release of O_2^-, H_2O_2, and OH^-. The study indicated that Lawsone is non-mutagenic (Sauriasari et al., 2007). This research assessed the anti-arthritic potential of Lawsone, using FCA-induced Sprague-Dawley rats.

2 Methodology

2.1 Test animals

Sprague-Dawley rats of both sexes, with a weight range of 150–250 g, were subjected to investigate the anti-arthritic property of Lawsone. Sprague-Dawley rats were obtained from the University of Veterinary & Animal Sciences, Lahore. Rats were fed with a standard pellet diet and water *ad libitum*. They were kept under 12 h dark/light cycles and average conditions of humidity (60%–70%) and temperature of (28°C ± 2°C) at the

University of Veterinary & Animal Sciences, Lahore. They were familiarized with the surroundings 1 week earlier than the trial (Kyei, Koffuor, and Boampong, 2012).

2.2 Assessment of anti-arthritic effect

30 Sprague-Dawley rats were dispersed into 5 groups. Except for the negative control (group 1), arthritis was induced in the rest of the 4 groups by injecting FCA (0.1 mL) into the sub-plantar area, starting from day 0. Group 1 and arthritic control, i.e., group 2 were fed with normal saline (NS) per oral (Akhtar and Arham Shabbir, 2019), from day 8–22. The reference group (group 3) was dosed with piroxicam (10 mg/kg b.w., i.p.) (Shabbir et al., 2014). Group 4 was given Lawsone (100 mg/kg b.w., p.o.) and group 5 was given Lawsone (200 mg/kg b.w., p.o.) from day 8–22. The anti-inflammatory doses of Lawsone were selected from the literature review. Previously Lawsone has shown anti-inflammatory and anti-oxidant activity in in vivo rat models of inflammation at the doses of 100 and 200 mg/kg b.w. (Biradar and Veeresh, 2013). Lawsone was obtained from Alfa Aesar (LOT: 10192582).

2.3 Measurement of the arthritic score and paw edema

Morphological features of arthritis were analyzed macroscopically for all the rats on the 8th, 13th, 18th, and 23rd days (Akhtar and Arham Shabbir, 2019). A score of 0 was used for the normal paw. Scores 1 to 2 were for mild to moderate inflammation and erythema of digits. Score 3 was given to severe inflammation and erythema of digits. Score 4 was given to significant deformity and incapability of movement of limbs. The paw volume was also recorded on the same days using a digital vernier caliper.

2.4 Histopathological evaluation

The ankle joints of all groups, injected with FCA, were separated and fixed with 10% formalin, and afterward decalcified by a decalcifying agent (10% formic acid with 10% formalin). Then, samples were fixed with paraffin and stained by the H&E method, after cutting into slices of 5 μm thickness. Arthritic parameters such as bone eruption, formation of pannus, and intrusion of inflammatory cells were analyzed. Results were predicted through a scale having 0, 1, 2, 3, and 4 ranges for normal, mild, moderate, and gross variations respectively.

2.5 Analysis of mRNA expression levels of pro-inflammatory cytokines: TNF-α, IL-1β, IL-6, NF-κB, MMP-2, MMP-3, and VEGF

Blood samples of rats were collected and RNA is extracted using the Total RNA Isolation (TRIzol) method. A Nanodrop spectrophotometer (major science mini-300) was used to quantify the total RNA extracted. Then, cDNA was generated by following the RevertAid First Strand cDNA synthesis kit's protocol (Thermo Scientific LOT 00960732). GAPDH was taken as a housekeeping gene. Primers of IL-1β, MMP-2, and MMP-3 were designed manually. Sequences of other primers, i.e., IL-6, TNF-α, NF-κB, and VEGF were followed from previously published papers, as exhibited in Table 1. cDNA (1 μL) was centrifuged with forward-reverse primer mix (1 μL), nuclease-free water, and PCR Master Mix (5 μL). The thermal cycler was operated for 35 cycles of the following 3 phases: denaturation (95°C for 10 s), annealing (according to temperatures displayed in Table 4) for 20 s, and subsequently extension (72°C for 30 s) cycles.

2.6 Determination PGE2 levels

Rat Prostaglandin E2 ELISA kit (Bioassay Technology Laboratory Cat No. E-0504Ra) was used to determine serum levels of PGE2. Results were obtained by measuring Optical Density (OD) using ELISA reader (BIORAD, PR 4100) at 450 nm wavelength.

2.7 Assessment of hematological parameters

An automated hemocytometer was used to calculate the hemoglobin (Hb) content as well as WBCs, RBCs, and platelet counts.

2.8 Biochemical parameters

Serum samples were processed to calculate the values of AST, ALT, urea and creatinine, through an automated chemistry analyzer.

2.9 Statistical analysis

Data were given as Mean ± SD, using one-way analysis of variance (ANOVA) and *post hoc* Tukey's test, to arbitrate the significant difference among groups. Here, $p < 0.05$ was reflected as statistically significant.

3 Results

3.1 Lawsone repressed arthritic progress

Arthritic development, manifesting swelling and erythema, was observed macroscopically after sub-planter induction of FCA. Treatment with Lawsone was initiated from day 8th till the 23rd day. The arthritic control group indicated a significant ($p < 0.001$) escalation in arthritic development than the vehicle control group since the 8th day. Lawsone treated groups displayed significant diminution in arthritis in contrast to group 2 on the 13th, 18th, and 23rd day respectively. On the 18th and 23rd days, macroscopic observation depicted a significant decrease in arthritis-related swelling and erythema in groups treated with Lawsone as shown in Figure 1.

3.2 Lawsone decreased paw edema

After FCA induction, paw edema was measured in all groups of Sprague Dawley rats using a digital vernier caliper on the 8th, 13th, and

TABLE 1 Primer sequences.

Genes	Forward primer	Reverse primer	Annealing temperature (°C)	Product size	Reference
IL-1β	5′-CCTGCTAGTGTGTGATGTTC-3′	5′-GAGGTGCTGATGTACCAGTT-3′	58	390	ENSRNOG0000004649
IL-6	5′-AGACTTCCAGCCAGTTGCCT-3′	5′-CTGACAGTGCATCATCGCTG-3′	60	233	(Uttra et al., 2018)
TNF-α	5′-CCTCTTCTCATTCCTGCTCGT-3″	5′-TGAGATCCATGCCATTGGCC-3′	60	266	(Shabbir et al., 2016)
NF-κB	5′-CAAGGAAGAGGATGTGGGGTT-3	5′-AGCTGAGCATGAAGGTGGATG-3′	60	207	(Shabbir et al., 2016)
VEGF	5′-GTTCAGAGCGGAGAAAGCATT-3	5′-CTTGCAACGCGAGTCTGTGT-3′	60	80	(Zhu et al., 2019)
MMP-2	5′-CGAACAAGTATGAGAGCTGC-3′	5′-CGGTCATCATCGTAGTTGGT-3′	57	85	ENSRNOG00000016695
MMP-3	5′-CCTTTTGATGGGCCTGGAAT-3′	5′-GTGACATCATCTGTCCATCG-3′	58	107	ENSRNOG00000032626
GAPDH	5′-GTCATCAACGGGAAACCCAT-3′	5′-CTTGCCGTGGGTAGAGTCAT-3	60	229	(Shabbir et al., 2016)

23rd days. Paw volumes observed on the 8th day exhibited a significant rise in paw edema than the vehicle control group. On the other hand, Lawsone treated groups displayed a significant decline in paw edema on the 13th day than the positive control group. On, the 23rd day, all treated groups exhibited significantly reduced levels of paw edema ($p < 0.001$) in contrast to the positive control group as presented in Figure 2.

3.3 Lawsone modulated histopathological parameters

Histopathological evaluation showed a significant reduction in arthritic score in the arthritic control group than the vehicle control group. All treated groups demonstrated attenuation of arthritic score at day 23 as shown in Figure 3 and Figure 4.

3.4 Lawsone declined the mRNA expression values of TNF-α, IL-1β, IL-6 & NF-κB

Blood samples treated with Lawsone were collected and processed. Significant downregulation of pro-inflammatory cytokines and matrix metalloproteinase enzymes was found, as shown in Figure 5. Arthritic control showed significant upregulation of TNF-α, IL-1β, and IL-6 in comparison to the vehicle control group. Expression levels of all these markers were significantly suppressed by the phytochemical as compared to the arthritic control group.

The positive control group displayed a significant ($p < 0.001$) escalation of NF-κB than the vehicle control group. Significantly ($p < 0.001$) reduced expressed values of NF-κB were found in Lawsone-treated groups than the arthritic control group.

3.5 Lawsone attenuated MMP-2, MMP-3 and VEGF expression levels

Significant ($p < 0.001$) upregulation of MMP-3, MMP-2 & VEGF in the arthritic control group was observed as opposed to the vehicle control group. However, suppression of MMP-3, MMP-2, and VEGF levels was found statistically significant after treatment with Lawsone than the positive control group as shown in Figure 6.

3.6 Lawsone significantly reduced PGE2 levels

A substantial ($p < 0.001$) raise of PGE2 was depicted in the positive control group as compared to the negative control group. However, when groups treated with Lawsone showed a significant ($p < 0.001$) decline of PGE2 levels than the arthritic control group as shown in Table 2.

3.7 Lawsone modulated hematological markers

A significant decline ($p < 0.001$) in RBC and Hb content was detected in the arthritic control group than in the vehicle control group. Lawsone treated groups showed an increase in RBC and Hb content to the positive control group. The data showed non-significant difference among all groups for TLC count.

However, the arthritic control group presented a significant elevation ($p < 0.001$) in PLT count than the vehicle control group. Lawsone treated groups showed lessened values ($p < 0.05$) of PLT count than the arthritic control group. Modulation in hematological markers is shown in Table 3.

3.8 Lawsone improved markers of liver function test

Significantly increased ALT ($p < 0.001$) and AST ($p < 0.01$) values were found in the arthritic control group than the vehicle control group. Hepatic parameters were found significantly improved in treated groups (Table 4).

3.9 No nephrotoxic effect of lawsone

The values of urea and creatinine, in all groups, were not statistically significantly different as compared to each other. This depicts that Lawsone is safe in terms of renal parameters (Table 4).

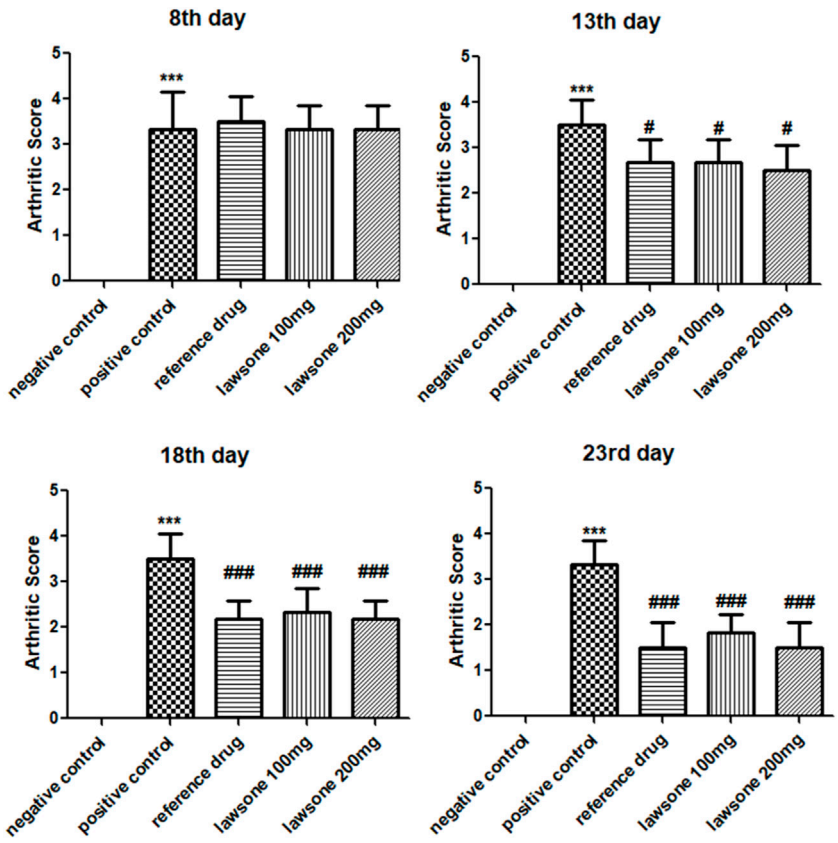

FIGURE 1
showing arthritic score in all groups after arthritic induction by FCA on 8th, 13th, 18th & 23rd day. Data is calculated as mean ± SD (n = 06). ***p < 0.001 in comparison to vehicle control group and #p < 0.05; ##p < 0.01; ###p < 0.001 in correlation to arthritic control group. Values of negative control group are zero, therefore are non-visible.

4 Discussion

In our current research, the anti-arthritic effect of Lawsone was analyzed, by using an FCA-induced rat arthritic model (Mobashar et al., 2022). FCA was chosen to induce arthritis in the Sprague-Dawley rat model because the clinical and pathological changes induced by FCA are considered similar to those that appear in human RA, which includes increased paw-edema volumes and thickening of the soft-tissue at the site of injection (Patil et al., 2011). It is the autoimmune disorder of connective tissues, especially the joints, cartilage, and bones, causing their disability and other systemic disorders, influenced by both genetic (MHC genes) and environmental factors (smoking, diet, obesity, infections, and microbiota (Croia et al., 2019). The major cause of RA development is the imbalance between the expression levels of pro-inflammatory and anti-inflammatory cytokines. Upregulation of pro-inflammatory cytokines or downregulation of anti-inflammatory cytokines results in the development of RA (Mobashar et al., 2020b). Characteristic features of RA involve the conversion of the synovial membrane into pannus, destroying the surrounding cartilage and bone with the presence of activated macrophages and synovial fibroblasts that form matrix metalloproteinase (Gautam, Singh, and Nainwani, 2013). Common complications in RA involve neurological disorders, tendon rupture, and joint damage (Yap et al., 2018). Its symptoms also involve fever, fatigue, and weight loss (Mobashar et al., 2020a). Chronic RA can also affect some major organs like the lung, heart, skin, eyes, kidneys, and digestive system (Radu and Bungau, 2021; Maity and Wairkar, 2022). Arthritis can cause severe disability, thus compromising health, and may even cause premature death (Murugananthan et al., 2013; Choudhary et al., 2014).

Lawsone has been shown to possess anti-inflammatory and anti-oxidant properties. These properties were accredited with ameliorative effect of lawsone in acute pancreatitis (Biradar and Veeresh, 2013). Lawsone is also known to inhibit paw edema in rat model by suppressing the inflammatory markers like, TNF-α and NF-κB (Vanco et al., 2017). In a recent study, we found Lawsone as the major active ingredient of *Eichhornia crassipes* and validated the plant for anti-arthritic property. It was suggested to evaluate the phytochemical for its potential against arthritis in future (Sattar et al., 2023). Therefore, we designed the current study to evaluate the anti-arthritic property of Lawsone using similar inflammatory markers and protocols as mentioned in our previous publication. Current research showed that the Lawsone downregulated the inflammatory markers, both *in vitro* and *in vivo*, and inhibited the development of RA in the treated groups. The anti-arthritic potential was evident by attenuation of histopathological parameters, arthritic score, paw edema, and hematological markers.

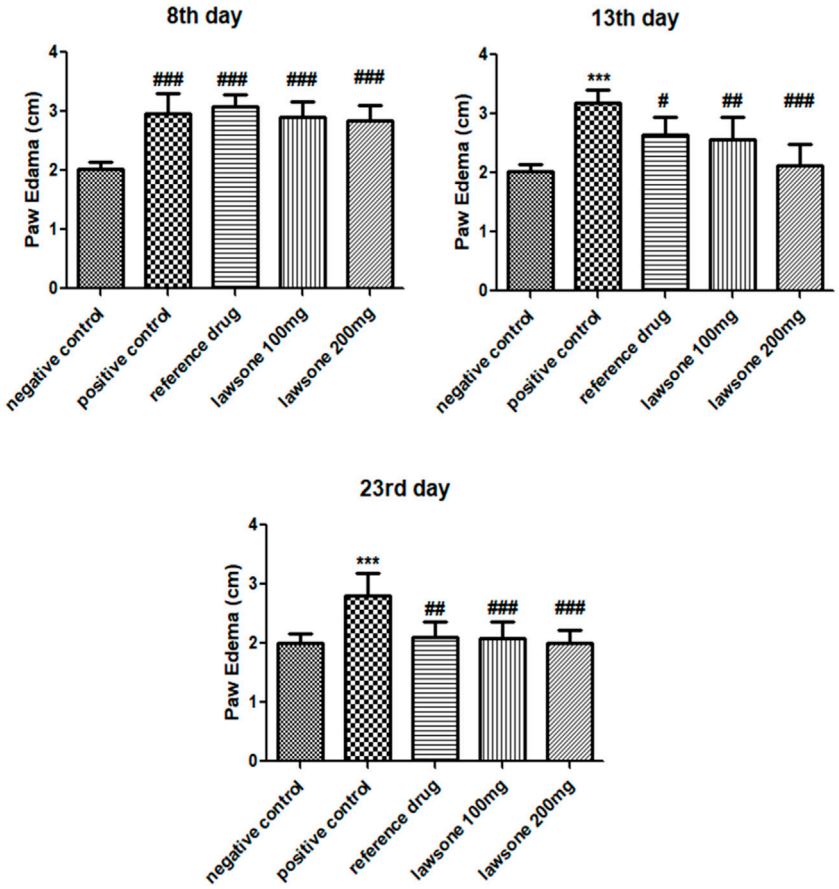

FIGURE 2
On 8th day, treatment groups were compared with negative control group, while on other days, they were compared with positive control. Data is calculated as mean ± SD (n = 06). ***p < 0.001 in correlation to vehicle control group and #p < 0.05; ##p < 0.01; ###p < 0.001 in correlation to arthritic control group.

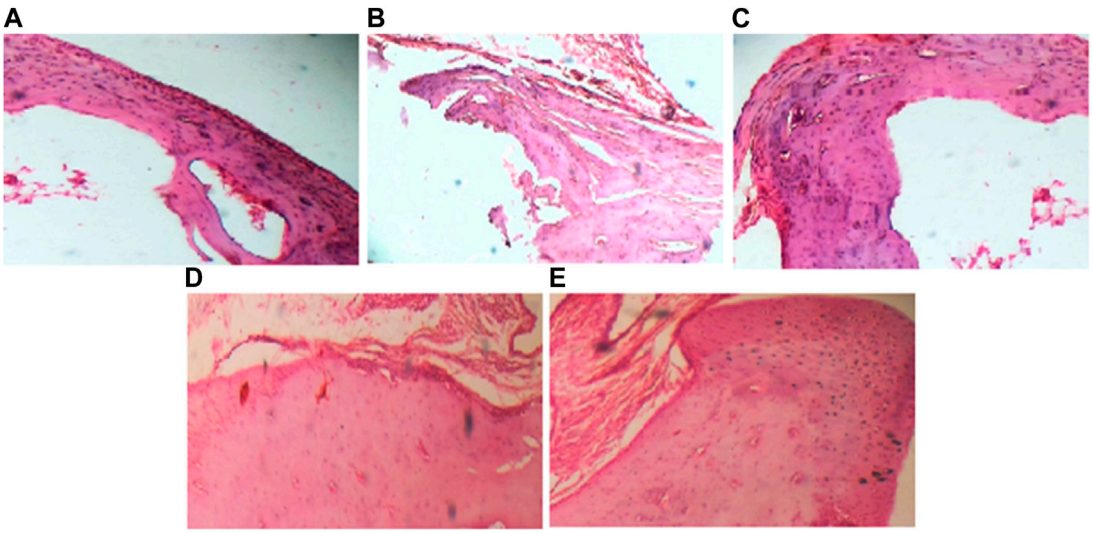

FIGURE 3
(40x) Histopathological evaluation of Sprague Dawley rats after FCA induction and treatment. **(A)** depicts negative control group; **(B)** depicts positive control group; **(C)** depicts reference drug group; **(D)** depicts group treated with Lawsone 100 mg; **(E)** depicts group treated with Lawsone 200 mg.

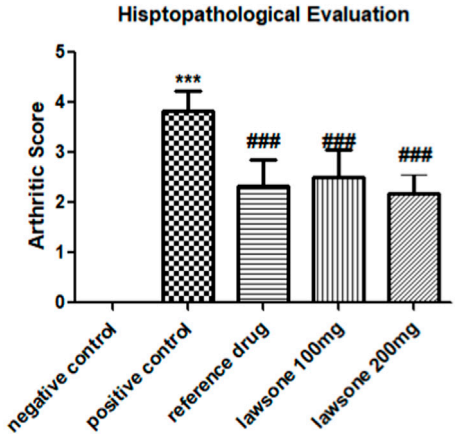

FIGURE 4
Histopathological evaluation of Sprague Dawley rats after FCA induction and treatment. Data is calculated as mean ± SD (n = 06). ***p < 0.001 as compared to vehicle control group and ###p < 0.001 in contrast to arthritic control group.

Cytokines play a crucial role in triggering the auto-immune system, leading to severe synovitis and the destruction of articular tissues (Alunno et al., 2017; Helli et al., 2019). The inhibitory effect of Lawsone on the expression of pro-inflammatory markers (TNF-α, IL-1β, IL-6, NF-κB, and VEGF) and matrix metalloproteinase enzymes (MMP-2 and MMP-3) was determined in current study.

Increased values of TNF-α result in inflammation and articular damage by stimulating the expression of cytokines and encouraging the immune cells such as, B-lymphocytes, T-lymphocytes, and NK cells, to proliferate and differentiate (Farrugia and Baron, 2016). It also acts synergistically with IL-1 in the degradation of proteoglycans, resulting in joint damage (Schiff, 2000). Inhibition of TNF-α results in the downregulation of the expression of other inflammatory cytokines (Wiens et al., 2010). IL-1β is responsible for bone erosion and pannus formation in RA, by binding to IL-1 receptor, mostly expressed in cartilage pannus (Harrison et al., 2008). It can stimulate pro-inflammatory cytokines in the cell lines significantly, especially the transcription and translation of MMPs, IL-6, and TNF-α (Chen et al., 2019).

IL-6 exerts its pleiotropic activity after binding to its receptor and triggering events via JAK-mediated events in target cells. It targets the plasmablasts and causes the proliferation of autoantibodies. Moreover, IL-6 actively promotes the maturation of T follicular helper cells, which then release IL-21, which is also a factor for the differentiation of B cells. Overall dysregulation of IL-6 is an important factor that leads to a decrease in inflammation.

NF-κB is found in inactive form in cytoplasm, where an inhibitory protein IκB is attached with it. Various cytokines such as, TNF-α, IL-1β, and chemokines phosphorylate IκB resulting in activaton of NF-κB (Roman-Blas and Jimenez, 2016). Activated NF-

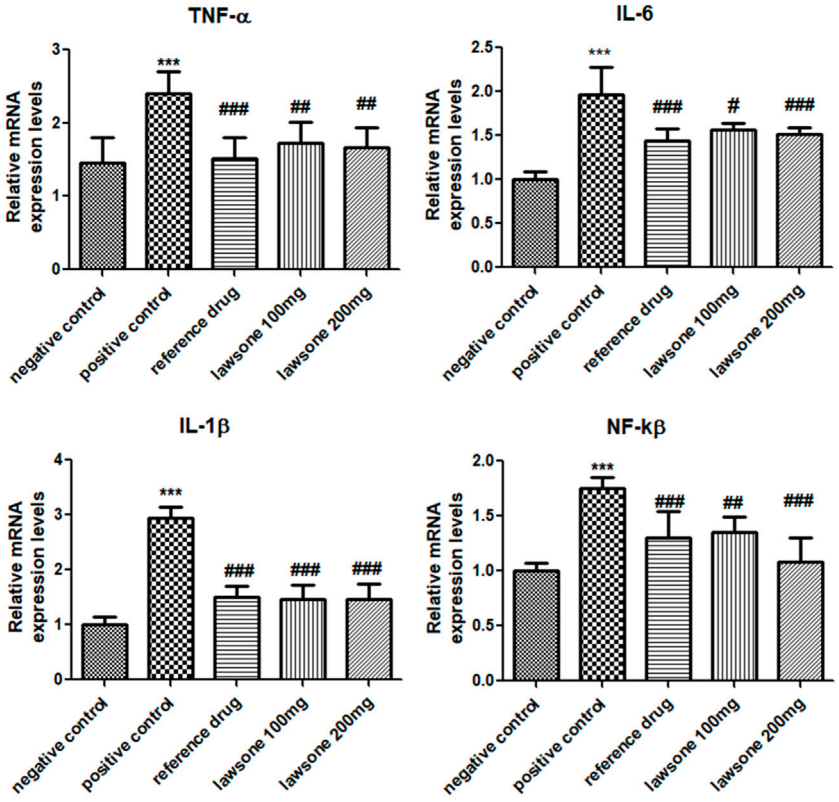

FIGURE 5
Lawsone reduced the mRNA expression values of TNF-α, IL-1β, IL-6 and NF-κB. Values are stated as mean ± SD (n = 06). ***p < 0.001 in contrast to vehicle control group and #p < 0.05; ###p < 0.001 in correlation to arthritic control group.

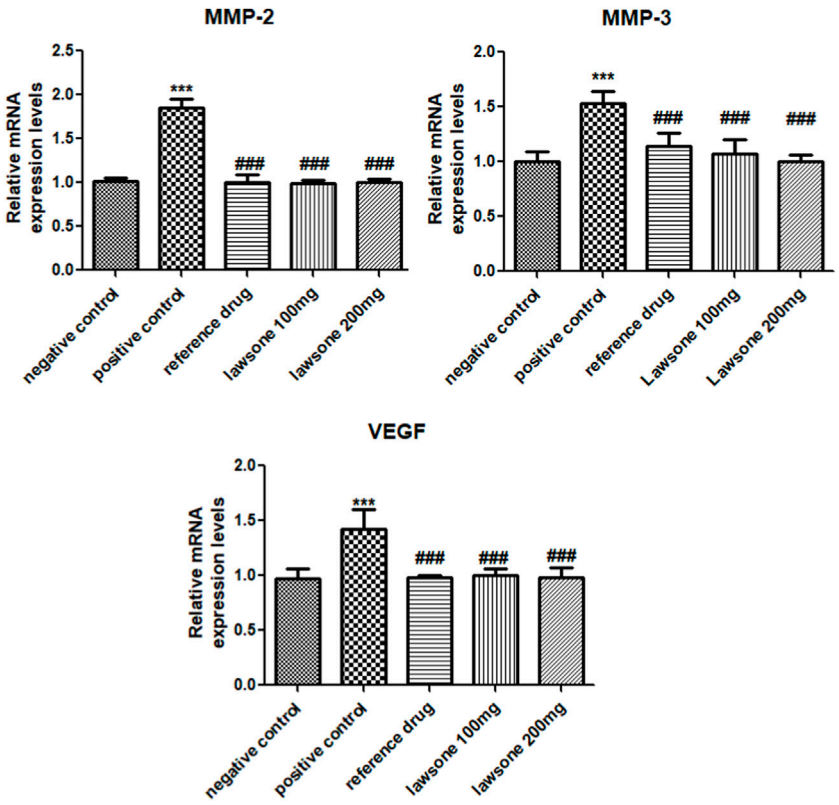

FIGURE 6
Lawsone declined the mRNA expression values of MMP-2, MMP-3 & VEGF. Values are calculated as mean ± SD (n = 06). ***p < 0.001 in contrast to vehicle control group and #p < 0.05; ##p < 0.001; ###p < 0.001 in contrast to arthritic control group.

TABLE 2 Lawsone significantly declined PGE2 Levels as compared to arthritic control group. Data is stated as mean ± SD (n = 06). ***p < 0.001 in contrast to vehicle control and ###p < 0.001 as compared to arthritic control group.

Groups	PGE2 (pg/mL)
Vehicle control	0.445 ± 0.023
Arthritic control	4.598 ± 0.65***
Reference drug	1.061 ± 0.161###
Lawsone 100 mg	1.052 ± 0.192###
Lawsone 200 mg	0.874 ± 0.061###

κB is notorious for mediating synovial inflammatory processes by proliferation of fibroblast-like synoviocytes, triggering transcription and expression of pro-inflammatory cytokines, causing the production of osteoclasts which leads to bone erosion, unwanted apoptosis, initiation of Th1 activation, and upregulation of synovial cells (Mobashar et al., 2020b; Ding et al., 2023).

VEGF is responsible for synovial inflammation, hyperplasia, and angiogenesis in the affected joints. It is produced by rheumatoid synoviocytes and upregulated by pro-inflammatory cytokines, such as TNF-α, IL-1, and IL-8, and hypoxia. It initiates a self-perpetuating cycle of the inflammatory response by attaching to Flt-1 receptors on macrophages, leading to synovial hyperplasia through various signaling intermediates such as, MAPK, Phosphoinositide 3-kinase (PI3K), protein kinase B (AKT), phospholipase C-γ (PlC-γ) and small GTPases (Yoo et al., 2008). Elevated serum levels of VEGF are detected in RA patients more than healthy controls or patients with osteoarthritis, thus VEGF is now taken as one of the first indicators in the investigation of RA (Malemud, 2007).

MMPs are also notorious for the bone remodeling, differentiation, recruitment and migration of osteoblasts and osteocytes, and solubilization of osteoid. TNF-α, IL-6, and IL-1β activate MMP genes in RA synovial fibroblasts through the binding of several different transcription factors (Araki and Mimura, 2017).

It is well known that cytokines, e.g., IL-1 and TNF-α, and cytokine inducers increase the levels of PGE2 during immune response (Davidson et al., 2001). PGE2 is a lipid-mediator and is responsible for bone erosion, destruction of articular cartilage, vasodilation, extravasation of fluid, and acute pain (Fattahi and Mirshafiey, 2012) in RA. It evokes cAMP/PKA signaling pathway through four different prostanoid E (EP) receptors on synovium, chondrocytes, liver, and monocytic phagocytes (McCoy, Wicks, and Audoly, 2002).

In current study, treatment with Lawsone downregulated the relative mRNA expressions levels of inflammatory markers, which are mostly known to be amplified in immunomodulatory diseases (Seibl et al., 2003; Huang et al., 2007; Kim et al., 2007; Gheorghe et al., 2009). The downregulation of these pro-inflammatory markers by Lawsone indicated that the amelioration of RA could

TABLE 3 Lawsone modulated Hematological Markers: Data is stated as mean ± SD (n = 06). $^{**}p < 0.01$; $^{***}p < 0.001$ in contrast to negative control group and $^{\#}p < 0.05$; $^{\#\#}p < 0.01$; $^{\#\#\#}p < 0.001$ in correlation to positive control group.

Hematological parameters	Vehicle control group	Arthritic control group	Reference drug group	Lawsone 100 mg	Lawsone 200 mg
RBC (million/mm^3)	9.865 ± 1.118	5.51 ± 0.846*	8.805 ± 1.061$^{\#\#\#}$	10.4 ± 1.2$^{\#\#\#}$	10.28 ± 0.667$^{\#\#\#}$
TLC (cells/μl)	7.067 ± 0.65	7.217 ± 0.595	6.933 ± 0.265	7.15 ± 0.689	7.267 ± 0.683
PLT count (10^9/L)	782 ± 0.533	928.7 ± 40.06**	754.2 ± 50.9$^{\#\#\#}$	764.58 ± 0.818$^{\#\#\#}$	759.5 ± 57.89$^{\#\#\#}$
Hb (g/dL)	11.37 ± 1.133	8.89 ± 0.357***	11.12 ± 0.741$^{\#\#\#}$	11.57 ± 0.941$^{\#\#\#}$	11.68 ± 0.823$^{\#\#\#}$

TABLE 4 Lawsone improved markers of liver function test and showed no nephrotoxic effect: Values are stated as mean ± SD (n = 06). $^{**}p < 0.01$; $^{***}p < 0.001$ in contrast to vehicle control and $^{\#}p < 0.05$; $^{\#\#}p < 0.01$ in contrast to arthritic control group.

Biochemical parameters	Vehicle control group	Arthritic control group	Reference drug group	Lawsone 100 mg	Lawsone 200 mg
ALT (IU/L)	42 ± 3.098	54.83 ± 2.401***	43.5 ± 1.643$^{\#\#\#}$	43.17 ± 2.927$^{\#\#\#}$	43.67 ± 2.338$^{\#\#\#}$
AST (IU/L)	300.8 ± 39.0	400.8 ± 31.63***	332 ± 37.95$^{\#}$	315.7 ± 35.02$^{\#\#}$	335.5 ± 30.96$^{\#}$
Urea (mmol/L)	23.17 ± 4.491	24.5 ± 6.317	28 ± 6.261	30.5 ± 3.886	28.50 ± 3.782
Creatinine (mg/dL)	0.666 ± 0.051	0.666 ± 0.103	0.616 ± 0.116	0.633 ± 0.136	0.616 ± 0.04

be ascribed to the phytochemical's potential immunomodulatory and anti-inflammatory properties (Izhar et al., 2021).

The most important function in the activation of proinflammatory cytokines and prognosis of RA is played by the Janus kinase/signal transducers and activators of transcription (JAK/STAT) signal transduction pathway. Normally, JAK/STAT negative regulators and active STAT protein inhibitors restrict cytokine activation. However, both regulators are malfunctioned in RA, resulting in constant positive signaling of JAK/STAT pathway and consequently increased expression levels of MMPs (Malemud, 2023). MMPs degrade the collagen matrix and promotes the inavasion of synovial panuus into the articular cartilage through various cell signaling pathways, including MAPK, NF-κB, and AMP-activated protein kinase (AMPK) pathwyas (Araki and Mimura, 2017). It is well known that imbalance between Th1 and Th2 cells is a key factor in the pathogenesis of RA, where Th1 mediated cell variants predominantly differentiate the others. This predominance is achieved by p38 MAPK pathway and inhitbion of p38 activity can prevent the differentiation of Th1 cells (Ding et al., 2023). The anti-inflammatory effect of Lawsone could possibly be mediated by mentioned pathways, however, further studies are required to evaluate the effects of Lawsone on signaling pathways involved in pathogenesis of RA.

In the current study, lab investigations showed reduced values of RBC count and Hb content in the positive control group, which indicates the anemic condition of rats (Song et al., 2013). It may be due to the deficiency in the generation of cells as a result of declined bone marrow functioning and/or reduced iron storage in the reticuloendothelial system. Anemia in RA is mainly due to the alteration in the production and functioning of hepcidin and ferroportin, due to pro-inflammatory cytokines, especially 1L-6. It can lead to other diseases as well such as arteriosclerosis (Atwa et al., 2022). Moreover, the rise in PLT counts in the positive control group indicates the immunomodulatory as a defense response to attacking pathogens (Naz et al., 2020). Treatment with Lawsone normalized the levels of evaluated hematological parameters (RBC, PLT, and Hb content), Likewise, evaluation of hepatic and renal markers also proved the safety of Lawsone in terms of hepatotoxicity or nephrotoxicity.

4 Conclusion

The current research proved that Lawsone possesses significant anti-inflammatory and anti-arthritic properties against FCA-induced RA in animal models. Treatment with Lawsone reduced arthritic progress and paw edema along with histopathological parameters. Diminution of RA may be attributed to the decline in the expression levels of inflammatory parameters like TNF- α, IL-1β, IL-6, NF-κB, MMP-2, MMP-3, and VEGF by the phytochemical. Lawsone also reduced the levels of PGE2 and results were found comparable to piroxicam in amelioration of RA. Current study presented the data on mRNA expression levels of inflammatory markers. For further validation of the data, it is suggested to analyse protein levels of tested inflammatory markers in future studies using Western Blot technique.

Data availability statement

The data used to support the findings of this study are available from the corresponding author upon reasonable request.

Ethics statement

The animal study was approved by The current research is approved by the Institutional Research Ethics Committee, University of Lahore under IREC-2019-90. Notably, all animal experimentation was conducted in accordance with applicable laws, regulations, and guidelines, prioritizing animal welfare and

minimizing any potential harm. The study was conducted in accordance with the local legislation and institutional requirements.

Author contributions

SS: Conceptualization, Data curation, Investigation, Writing–original draft. AS: Conceptualization, Methodology, Supervision, Writing–review and editing. MS: Formal analysis, Validation, Resources. TA: Formal analysis, Data curation, Visualization. SMA: Resources, Investigation, Validation. MB: Project administration, Resources, Writing–review and editing. H-AN: Funding acquisition, Visulalization, Software. YABJ: Funding acquisition, validation, Software. MD: Investigation, Resources, Project administration. AM: Validation, software, Writing–review and editing.

Funding

The author(s) declare financial support was received for the research, authorship, and/or publication of this article. This research work was partially supported by Higher Education Commission Indigenous 5000 fellowship program (Phase 2, Batch IV) awarded to Ms. Sara Sattar. The authors would like to extend their sincere appreciation to the Researchers Supporting Project, King Saud University, Riyadh, Saudi Arabia for funding this work through the project number (RSP 2023R457).

Conflict of interest

The authors declare that the research was conducted in the absence of any commercial or financial relationships that could be construed as a potential conflict of interest.

Publisher's note

All claims expressed in this article are solely those of the authors and do not necessarily represent those of their affiliated organizations, or those of the publisher, the editors and the reviewers. Any product that may be evaluated in this article, or claim that may be made by its manufacturer, is not guaranteed or endorsed by the publisher.

References

Adeli-Sardou, M., Yaghoobi, M. M., Torkzadeh-Mahani, M., and Dodel, M. (2019). Controlled release of lawsone from polycaprolactone/gelatin electrospun nano fibers for skin tissue regeneration. *Int. J. Biol. Macromol.* 124, 478–491. doi:10.1016/j.ijbiomac.2018.11.237

Akhtar, G., and Arham Shabbir, (2019). Urginea indica attenuated rheumatoid arthritis and inflammatory paw edema in diverse animal models of acute and chronic inflammation. *J. Ethnopharmacol.* 238, 111864. doi:10.1016/j.jep.2019.111864

Alunno, A., Carubbi, F., Giacomelli, R., and Gerli, R. (2017). Cytokines in the pathogenesis of rheumatoid arthritis: new players and therapeutic targets. *BMC Rheumatol.* 1, 3. doi:10.1186/s41927-017-0001-8

Araki, Y., and Mimura, T. (2017). Matrix Metalloproteinase Gene Activation Resulting from Disordred Epigenetic Mechanisms in Rheumatoid Arthritis. *Int. J. Mol. Sci.* 18 (5), 905. doi:10.3390/ijms18050905

Atwa, E. T., Omar, H. M., Amin, A., and Hammad, M. (2022). Red cell distribution width and mean platelet volume in rheumatoid arthritis patients: Its association with disease activity. *Reumatol. Clin. Engl. Ed.* 18 (7), 399–405. doi:10.1016/j.reumae.2021.04.011

Badoni Semwal, R., Semwal, D. K., Combrinck, S., Cartwright-Jones, C., and Viljoen, A. (2014). Lawsonia inermis L. (henna): ethnobotanical, phytochemical and pharmacological aspects. *J. Ethnopharmacol.* 155 (1), 80–103. doi:10.1016/j.jep.2014.05.042

Bang, J. S., Oh, D. H., Choi, H. M., Sur, B. J., Lim, S. J., Kim, J. Y., et al. (2009). Anti-inflammatory and antiarthritic effects of piperine in human interleukin 1beta-stimulated fibroblast-like synoviocytes and in rat arthritis models. *Arthritis Res. Ther.* 11 (2), R49. doi:10.1186/ar2662

Biradar, S., and Veeresh, B. (2013). Protective effect of lawsone on L-Arginine induced acute pancreatitis in rats. *Indian J. Exp. Biol.* 51 (3), 256–261.

Bugatti, S., Vitolo, B., Caporali, R., Montecucco, C., and Manzo, A. (2014). B cells in rheumatoid arthritis: From pathogenic players to disease biomarkers. *Biomed. Res. Int.* 2014, 681678. doi:10.1155/2014/681678

Cape, J. L., Bowman, M. K., and Kramer, D. M. (2006). Computation of the redox and protonation properties of quinones: towards the prediction of redox cycling natural products. *Phytochemistry* 67 (16), 1781–1788. doi:10.1016/j.phytochem.2006.06.015

Chen, J., Wu, W., Zhang, M., and Chen, C. (2019). Taraxasterol suppresses inflammation in IL-1β-induced rheumatoid arthritis fibroblast-like synoviocytes and rheumatoid arthritis progression in mice. *Int. Immunopharmacol.* 70, 274–283. doi:10.1016/j.intimp.2019.02.029

Choudhary, M., Kumar, V., Gupta, P. K., and Singh, S. (2014). Anti-arthritic activity of Barleria prionitis Linn. leaves in acute and chronic models in Sprague Dawley rats. *Bull. Fac. Pharm. Cairo Univ.* 52 (2), 199–209. doi:10.1016/j.bfopcu.2014.07.002

Croia, C., Bursi, R., Sutera, D., Petrelli, F., Alunno, A., and Puxeddu, I. (2019). One year in review 2019: pathogenesis of rheumatoid arthritis. *Clin. Exp. Rheumatol.* 37 (3), 347–357.

Davidson, J., Abul, H. T., Milton, A. S., and Rotondo, D. (2001). Cytokines and cytokine inducers stimulate prostaglandin E2 entry into the brain. *Pflugers Arch.* 442 (4), 526–533. doi:10.1007/s004240100572

Ding, Q., Hu, W., Wang, R., Yang, Q., Zhu, M., Li, M., et al. (2023). Signaling pathways in rheumatoid arthritis: implications for targeted therapy. *Signal Transduct. Target Ther.* 8 (1), 68. doi:10.1038/s41392-023-01331-9

Farrugia, M., and Baron, B. (2016). The role of TNF-α in rheumatoid arthritis: a focus on regulatory T cells. *J. Clin. Transl. Res.* 2 (3), 84–90.

Fattahi, M. J., and Mirshafiey, A. (2012). Prostaglandins and rheumatoid arthritis. *Arthritis* 2012, 239310. doi:10.1155/2012/239310

Finckh, A., Gilbert, B., Hodkinson, B., Bae, S. C., Thomas, R., Deane, K. D., et al. (2022). Global epidemiology of rheumatoid arthritis. *Nat. Rev. Rheumatol.* 18 (10), 591–602. doi:10.1038/s41584-022-00827-y

Fraenkel, L., Bathon, J. M., England, B. R., St Clair, E. W., Arayssi, T., Carandang, K., et al. (2021). 2021 American College of Rheumatology Guideline for the Treatment of Rheumatoid Arthritis. *Arthritis Care Res. Hob.* 73 (7), 924–939. doi:10.1002/acr.24596

Gautam, R. K., Singh, D., and Nainwani, R. (2013). Medicinal plants having anti-arthritic potential: A review. *Int. J. Pharm. Sci. Rev. Res.* 19 (1), 96–102.

Gheorghe, K. R., Korotkova, M., Catrina, A. I., Backman, L., Af Klint, E., Claesson, H.-E., et al. (2009). Expression of 5-lipoxygenase and 15-lipoxygenase in rheumatoid arthritis synovium and effects of intraarticular glucocorticoids. *Arthritis Res. Ther.* 11 (3), R83–R11. doi:10.1186/ar2717

Guo, Q., Wang, Y., Xu, D., Nossent, J., Pavlos, N. J., and Xu, J. (2018). Rheumatoid arthritis: pathological mechanisms and modern pharmacologic therapies. *Bone Res.* 6, 15. doi:10.1038/s41413-018-0016-9

Harrison, P., Pointon, J. J., Chapman, K., Roddam, A., and Wordsworth, B. P. (2008). Interleukin-1 promoter region polymorphism role in rheumatoid arthritis: a meta-analysis of IL-1B-511A/G variant reveals association with rheumatoid arthritis. *Rheumatol. Oxf.* 47 (12), 1768–1770. doi:10.1093/rheumatology/ken374

Helli, B., Shahi, M. M., Mowla, K., Jalali, M. T., and Haghighian, H. K. (2019). A randomized, triple-blind, placebo-controlled clinical trial, evaluating the sesamin supplement effects on proteolytic enzymes, inflammatory markers, and clinical indices in women with rheumatoid arthritis. *Phytother. Res.* 33 (9), 2421–2428. doi:10.1002/ptr.6433

Huang, Q. Q., Ma, Y., Adebayo, A., and Pope, R. M. (2007). Increased macrophage activation mediated through toll-like receptors in rheumatoid arthritis. *Arthritis & Rheumatism Official J. Am. Coll. Rheumatology* 56 (7), 2192–2201. doi:10.1002/art.22707

Izhar, H., Shabbir, A., Shahzad, M., Mobashar, A., and Ahmed, S. S. (2021). *Phyllanthus reticulatus* Prevents Ethanol-Induced Gastric Ulcer via Downregulation of IL-8 and TNF-α Levels. *Evid. Based Complement. Altern. Med.* 2021, 1734752. doi:10.1155/2021/1734752

Kapadia, G. J., Rao, G. S., Sridhar, R., Ichiishi, E., Takasaki, M., Suzuki, N., et al. (2013). Chemoprevention of skin cancer: effect of Lawsonia inermis L. (Henna) leaf powder and its pigment artifact, lawsone in the Epstein- Barr virus early antigen activation assay and in two-stage mouse skin carcinogenesis models. *Anticancer Agents Med. Chem.* 13 (10), 1500–1507. doi:10.2174/18715206113139990096

Kaur, G., and Sultana, S. (2012). Evaluation of antiarthritic activity of isoeugenol in adjuvant induced arthritis in murine model. *Food Chem. Toxicol.* 50 (8), 2689–2695. doi:10.1016/j.fct.2012.05.016

Kim, H.-R., Cho, M.-L., Kim, K.-W., Juhn, J.-Y., Hwang, S.-Y., Yoon, C.-H., et al. (2007). Up-regulation of IL-23p19 expression in rheumatoid arthritis synovial fibroblasts by IL-17 through PI3-kinase-NF-kappaB- and p38 MAPK-dependent signalling pathways. *Rheumatology* 46 (1), 57–64. doi:10.1093/rheumatology/kel159

Kyei, S., Koffuor, G. A., and Boampong, J. N. (2012). Antiarthritic effect of aqueous and ethanolic leaf extracts of *Pistia stratiotes* in adjuvant-induced arthritis in Sprague-Dawley rats. *J. Exp. Pharmacol.* 4, 41–51. doi:10.2147/JEP.S29792

Li, X. Z., and Zhang, S. N. (2020). Herbal compounds for rheumatoid arthritis: Literatures review and cheminformatics prediction. *Phytother. Res.* 34 (1), 51–66. doi:10.1002/ptr.6509

Maity, S., and Wairkar, S. (2022). Dietary polyphenols for management of rheumatoid arthritis: Pharmacotherapy and novel delivery systems. *Phytother. Res.* 36 (6), 2324–2341. doi:10.1002/ptr.7444

Malemud, C. J. (2007). Growth hormone, VEGF and FGF: involvement in rheumatoid arthritis. *Clin. Chim. Acta* 375 (1-2), 10–19. doi:10.1016/j.cca.2006.06.033

Malemud, C. J. (2023). The role of the JAK/STAT signal pathway in rheumatoid arthritis. *Ther. Adv. Musculoskelet. Dis.* 10 (5-6), 117–127. doi:10.1177/1759720X18776224

Matcham, F., Scott, I. C., Rayner, L., Hotopf, M., Kingsley, G. H., Norton, S., et al. (2014). The impact of rheumatoid arthritis on quality-of-life assessed using the SF-36: a systematic review and meta-analysis. *Semin. Arthritis Rheum.* 44 (2), 123–130. doi:10.1016/j.semarthrit.2014.05.001

McCoy, J. M., Wicks, J. R., and Audoly, L. P. (2002). The role of prostaglandin E2 receptors in the pathogenesis of rheumatoid arthritis. *J. Clin. Invest.* 110 (5), 651–658. doi:10.1172/JCI15528

Mobashar, A., Shabbir, A., Shahzad, M., and ul Hassan, S. (2020a). Evaluation of Immunomodulatory and Antiarthritic Potential of Trigonella gharuensis Extracts. *Evid. Based Complement. Altern. Med.* 2020, 8836080. doi:10.1155/2020/8836080

Mobashar, A., Shabbir, A., Shahzad, M., and Gobe, G. (2022). Preclinical Rodent Models of Arthritis and Acute Inflammation Indicate Immunomodulatory and Anti-Inflammatory Properties of Juglans regia Extracts. *Evid. Based Complement. Altern. Med.* 2022, 1695701. doi:10.1155/2022/1695701

Mobashar, A., Shabbir, A., Shahzad, M., and Hassan, S.Ul. (2020b). Evaluation of Immunomodulatory and Antiarthritic Potential of Trigonella gharuensis Extracts. *Evid. Based Complement. Altern. Med.* 2020, 8836080. doi:10.1155/2020/8836080

Mubashir, K., Ganai, B. A., Ghazanfar, K., and Akbar, S. (2014). Evaluation of Antiarthritic Potential of Methanolic Extract of Gentiana kurroo Royle. *Arthritis* 2014, 810615. doi:10.1155/2014/810615

Murugananthan, G., Kumar, G. S., Chethan, P. S., and Mohan, S. (2013). Anti-Arthritic and Anti-Inflammatory Constituents from Medicinal Plants. *J. Appl. Pharm. Sci.* 3.

Naz, R., Ahmed, Z., Shahzad, M., Shabbir, A., and Kamal, F. (2020). Amelioration of Rheumatoid Arthritis by Anacardium occidentale via Inhibition of Collagenase and Lysosomal Enzymes. *Evid. Based Complement. Altern. Med.* 2020, 8869484. doi:10.1155/2020/8869484

Patil, K. R., Patil, C. R., Jadhav, R. B., Mahajan, V. K., Patil, P. R., and Gaikwad, P. S. (2011). Anti-Arthritic Activity of Bartogenic Acid Isolated from Fruits of Barringtonia racemosa Roxb. (Lecythidaceae). *Evid. Based Complement. Altern. Med.* 2011, 785245. doi:10.1093/ecam/nep148

Radu, A. F., and Bungau, S. G. (2021). Management of Rheumatoid Arthritis: An Overview. *Cells* 10 (11), 2857. doi:10.3390/cells10112857

Roman-Blas, J. A., and Jimenez, S. A. (2016). NF-kappaB as a potential therapeutic target in osteoarthritis and rheumatoid arthritis. *Osteoarthr. Cartil.* 14 (9), 839–848. doi:10.1016/j.joca.2006.04.008

Seibl, R., Birchler, T., Loeliger, S., Hossle, J. P., E Gay, R., Saurenmann, T., et al. (2003). Expression and regulation of Toll-like receptor 2 in rheumatoid arthritis synovium. *Am. J. pathology* 162 (4), 1221–1227. doi:10.1016/S0002-9440(10)63918-1

Sattar, S., Shabbir, A., Shahzad, M., Akhtar, T., Ahmad, A., Alnasser, S. M., et al. (2023). *Eichhornia crassipes* Ameliorated Rheumatoid Arthritis by Modulating Inflammatory Cytokines and Metalloproteinase Enzymes in a Rat Model. *Medicina* 59 (9), 1594. doi:10.3390/medicina59091594

Sauriasari, R., Wang, D. H., Takemura, Y., Tsutsui, K., Masuoka, N., Sano, K., et al. (2007). Cytotoxicity of lawsone and cytoprotective activity of antioxidants in catalase mutant *Escherichia coli*. *Toxicology* 235 (1-2), 103–111. doi:10.1016/j.tox.2007.03.019

Scherer, H. U., Haupl, T., and Burmester, G. R. (2020). The etiology of rheumatoid arthritis. *J. Autoimmun.* 110, 102400. doi:10.1016/j.jaut.2019.102400

Schiff, M. H. (2000). Role of interleukin 1 and interleukin 1 receptor antagonist in the mediation of rheumatoid arthritis. *Ann. Rheum. Dis.* 59 (1), i103–i108. doi:10.1136/ard.59.suppl_1.i103

Shabbir, A., Shahzad, M., Ali, A., and Zia-ur-Rehman, M. (2014). Anti-arthritic activity of N'-[(2,4-dihydroxyphenyl)methylidene]-2-(3,4-dimethyl-5,5-dioxidopyrazolo[4,3-c] [1,2] benzothiazin-1(4H)-yl)acetohydrazide. *Eur. J. Pharmacol.* 738, 263–272. doi:10.1016/j.ejphar.2014.05.045

Shabbir, A., Shahzad, M., Ali, A., and Zia-ur-Rehman, M. (2016). Discovery of New Benzothiazine Derivative as Modulator of Pro- and Anti-inflammatory Cytokines in Rheumatoid Arthritis. *Inflammation* 39 (6), 1918–1929. doi:10.1007/s10753-016-0427-y

Song, S. N., Iwahashi, M., Tomosugi, N., Uno, K., Yamana, J., Yamana, S., et al. (2013). Comparative evaluation of the effects of treatment with tocilizumab and TNF-alpha inhibitors on serum hepcidin, anemia response and disease activity in rheumatoid arthritis patients. *Arthritis Res. Ther.* 15 (5), R141. doi:10.1186/ar4323

Uroos, M., Abbas, Z., Sattar, S., Umer, N., Shabbir, A., Rehman Shafiq Ur, , et al. (2017). Nyctanthes arbor-tristis Ameliorated FCA-Induced Experimental Arthritis: A Comparative Study among Different Extracts. *Evid. Based Complement. Altern. Med.* 2017, 4634853. doi:10.1155/2017/4634853

Uttra, A. M., Alamgeer, M. S., Shabbir, A., and Jahan, S. (2018). Ephedra gerardiana aqueous ethanolic extract and fractions attenuate Freund Complete Adjuvant induced arthritis in Sprague Dawley rats by downregulating PGE2, COX2, IL-1β, IL-6, TNF-α, NF-kB and upregulating IL-4 and IL-10. *J. Ethnopharmacol.* 224, 482–496. doi:10.1016/j.jep.2018.06.018

Vanco, J., Travnicek, Z., Hosek, J., and Suchy, P. (2017). *In vitro* and *in vivo* anti-inflammatory active copper(II)-lawsone complexes. *PLoS One* 12 (7), e0181822. doi:10.1371/journal.pone.0181822

Wiens, A., Venson, R., Correr, C. J., Otuki, M. F., and Pontarolo, R. (2010). Meta-analysis of the efficacy and safety of adalimumab, etanercept, and infliximab for the treatment of rheumatoid arthritis. *Pharmacotherapy* 30 (4), 339–353. doi:10.1592/phco.30.4.339

Yap, H. Y., Tee, S. Z., Wong, M. M., Chow, S. K., Peh, S. C., and Teow, S. Y. (2018). Pathogenic Role of Immune Cells in Rheumatoid Arthritis: Implications in Clinical Treatment and Biomarker Development. *Cells* 7 (10), 161. doi:10.3390/cells7100161

Yoo, S., Kwok, S., and Kim, an W. (2008). Proinflammatory Role of Vascular Endothelial Growth Factor in the Pathogenesis of Rheumatoid Arthritis: Prospects for Therapeutic Intervention. *Mediat. Inflamm.* 2008, 129873. doi:10.1155/2008/129873

Zhu, J., Su, C., Chen, Y., Hao, X., and Jiang, J. (2019). Electroacupuncture on ST36 and GB39 Acupoints Inhibits Synovial Angiogenesis via Downregulating HIF-1α/VEGF Expression in a Rat Model of Adjuvant Arthritis. *Evidence-Based Complementary Altern. Med.* 2019, 5741931. doi:10.1155/2019/5741931

frontiers | Frontiers in Pharmacology

TYPE Clinical Trial
PUBLISHED 23 November 2023
DOI 10.3389/fphar.2023.1279519

OPEN ACCESS

EDITED BY
Guang Wang,
Jinan University, China

REVIEWED BY
Ying Zhang,
Beijing University of Chinese Medicine, China
Shengxian Wu,
Beijing University of Chinese Medicine, China

*CORRESPONDENCE
Fengmei Lian,
lfm565@sohu.com
Rong Ma,
mr1974@163.com
Xiaolin Tong,
tongxiaolin66@sina.com

†These authors have contributed equally to this work and share first authorship

RECEIVED 18 August 2023
ACCEPTED 10 November 2023
PUBLISHED 23 November 2023

CITATION
An X, Shi C, Han Y, Li X, Dong L, Li Y, Chen H, Wang Y, Li J, Liu G, Lian F, Ma R and Tong X (2023), The rational dose for MaXingShiGan decoction is crucial for its clinical effectiveness in treating bronchial pneumonia: three randomized, double-blind, dose-parallel controlled clinical studies.
Front. Pharmacol. 14:1279519.
doi: 10.3389/fphar.2023.1279519

The rational dose for MaXingShiGan decoction is crucial for its clinical effectiveness in treating bronchial pneumonia: three randomized, double-blind, dose-parallel controlled clinical studies

Xuedong An[1†], Changren Shi[2†], Yaowei Han[2], Xinmin Li[2], Lijing Dong[3], Yan Li[3], Hui Chen[4], Yushui Wang[5], Jinsong Li[6], Geli Liu[7], Fengmei Lian[1*], Rong Ma[2*] and Xiaolin Tong[1*]

[1]Guang'anmen Hospital of China Academy of Chinese Medical Sciences, Beijing, China, [2]The First Affiliated Hospital of Tianjin University of Traditional Chinese Medicine, Tianjin, China, [3]Tianjin Hangu District Traditional Chinese Medicine Hospital, Tianjin, China, [4]The Second Affiliated Hospital of Tianjin University of Traditional Chinese Medicine, Tianjin, China, [5]Tianjin Nankai Hospital, Tianjin, China, [6]Tianjin Municipal People's Hospital, Tianjin, China, [7]General Hospital of Tianjin Medical University, Tianjin, China

Objective: Evaluate the impact of adjusting the overall dose, Gypsum Fibrosum [Mineral; Gypsum] (ShiGao, SG) dose, and *Prunus armeniaca* L. [Rosaceae; Semen Armeniacae Amarum] (KuXingRen, KXR) dose on the efficacy of MaXingShiGan Decoction (MXSG) in treating children with bronchial pneumonia (Wind-heat Blocking the Lung), in order to provide strategy supported by high-quality evidence for the selection of rational clinical doses of MXSG.

Methods: Based on the basic dose of MXSG, we conducted three randomized, double-blind, dose parallel controlled, multicenter clinical trials, involving adjustments to the overall dose, SG dose, and KXR dose, and included 120 children with bronchial pneumonia (Wind-heat Blocking the Lung) respectively. And the patients were divided into low, medium, and high dose groups in a 1:1:1 ratio, with 40 cases in each group. The intervention period lasted for 10 days. The primary outcome was the clinical cured rate, while the secondary outcomes included the effectiveness in alleviating major symptoms of bronchial pneumonia (including fever, cough, dyspnea, and phlegm congestion). And the occurrence of adverse events was recorded.

Results: We first recorded and analyzed the baseline characteristics of the three studies, including age, gender, height, and so on. The results indicated that there were no significant differences among the dose groups within each study. For the study adjusting the overall dose of MXSG, the results showed that both the medium-dose group and high-dose group had significantly higher clinical cured rates compared to the low-dose group (Chi-square value 9.01, p = 0.0111). However, there was no significant benefit between the high-dose group and the medium-dose group (81.58% vs. 81.08%). Regarding phlegm congestion, excluding fever, cough, and dyspnea, both the medium-dose group and high-dose group had significantly higher clinical cured rates than

the low-dose group (Chi-square value 6.31, p = 0.0426), and there was no significant benefit between the high-dose group and the medium-dose group (69.23% vs. 75.00%). A total of 5 adverse events were observed, of which only 1 case in the medium-dose group was possibly related to the experimental medication. For the study adjusted the SG dose in MXSG, the results showed that the high-dose group had the highest clinical cured rate, but the inter-group difference was not statistically significant (Chi-square value 3.36, p = 0.1864). The area under the curve (AUC) for cough in the medium-dose group was significantly lower than in the low-dose group and high-dose group (F-test value 3.14, p = 0.0471). Although no significant differences were observed in fever and dyspnea among the groups, the AUC in the high-dose group was lower than in the medium-dose and low-dose groups. In comparing the complete defervescence time, both the high-dose group (p < 0.0001) and the medium-dose group (p = 0.0015) achieved faster than the low-dose group. The high-dose group slightly outperformed the medium-dose group (0.50 (0.50, 0.80) vs. 0.80 (0.40, 1.40)), although the difference was not significant. In the medium-dose group, 1 adverse event was observed, but it was not related to the experimental medication. For the study adjusted the KXR dose in MXSG, the results showed that both the medium-dose group and high-dose group had significantly higher cured rates compared to the low-dose group (Chi-square value 47.05, p < 0.0001). However, there was no significant benefit comparing the high-dose group to the medium-dose group (90.00% vs. 92.50%). Regarding clinical symptoms, the results indicated that for cough (F-test value 3.16, p = 0.0460) and phlegm congestion (F-test value 3.84, p = 0.0243), the AUC for both the medium-dose group and high-dose group were significantly lower than in the low-dose group. Although there was benefit in the high-dose group compared to the medium-dose group, it was not statistically significant. No adverse events were observed during the study period.

Conclusion: The synthesis of the three conducted clinical studies collectively indicates that for children with bronchial pneumonia (Wind-heat Blocking the Lung), the basic clinical dose of MXSG may represents an optimal intervention dose based on the accumulated clinical experience of doctors. If the dose is insufficient, the clinical effects might be compromised, but using a higher dose does not significantly enhance benefits. Concerning different symptoms, increasing the overall formula's dose has a favorable impact on improving phlegm congestion, increasing the SG is effective in improving symptoms such as fever, cough, and dyspnea, while higher dose of KXR is effective in alleviating cough and phlegm congestion. These findings suggest that for MXSG, achieving the optimal intervention dose is crucial to achieve better clinical efficacy. For the SG and KXR, if certain symptoms are more severe, increasing the dose can be considered within safe limits, can lead to significant clinical benefits in symptom improvement. This also explains why the dose of MXSG might vary among clinical doctors, while maintaining a balance between safety and effectiveness. Of course, our study is still exploratory clinical trials, and further studies are needed to confirm our findings.

Clinical Trial Registration: https://www.chictr.org.cn/index.html; Identifier: ChiCTR-TRC-13003093, ChiCTR-TRC-13003099.

KEYWORDS

MaXingShiGan decoction, bronchial pneumonia, dose-effect, traditional Chinese medicine, clinical study

1 Introduction

In 2019, the Global Burden of Disease (GBD) study indicated that lower respiratory infections, including pneumonia and bronchitis, affected nearly 500 million people worldwide (Walker et al., 2013; GBD, 2019 Diseases and Injuries Collaborators, 2020). Among them, bronchopneumonia, one of the leading causes of death in children under 5 years old, characterized by acute inflammation of the bronchial mucosa caused by biological or non-biological factors, is a common ailment in children and

infants, which characterized by symptoms such as fever, cough, phlegm obstruction, and breathing difficulties (Berlucchi et al., 2014; Chang et al., 2014; Zhang et al., 2018; Ye et al., 2021), which imposes a significant economic burden on families and healthcare systems (Nair et al., 2013). Factors contributing to bronchopneumonia include poor air quality, underdeveloped respiratory systems in children, compromised immune function, and malnutrition (Bradley et al., 2011; Zec et al., 2016; Liu et al., 2020). Among the primary causative agents of bronchopneumonia, *mycoplasma* pneumoniae, bacteria, and viruses play significant roles (Zhang et al., 2007). Treatment strategies for pneumonia mainly involve symptomatic relief, anti-infective therapy, and prevention of complications. Despite the widespread use of infant vaccines that have substantially reduced hospitalization rates due to childhood pneumonia, it remains a major contributor to child mortality (Williams et al., 2002; Black et al., 2010). Notably, glucocorticoids and antibiotics are common therapeutic agents for pneumonia; however, long-term use of these drugs has led to drug resistance and adverse reactions (Ling et al., 2020).

Originating from the "Shang Han Lun," MaXingShiGan Decoction (MSXG) is a traditional Chinese formula composed mainly of *Ephedra sinica* Stapf [Ephedraceae; HERBA EPHEDRAE] (MaHaung, MH), *Prunus armeniaca* L. [Rosaceae; Semen Armeniacae Amarum] (KuXingRen, KXR), Gypsum Fibrosum [Mineral; Gypsum] (ShiGao, SG), and *Glycyrrhiza glabra* L. [Fabaceae; RADIX GLYCYRRHIZAE] (GanCao, GC). It itself and the derivative formulas such as Lianhua Qingwen Capsules, Han Shi Yi Formula, QingFeiPaiDu Decoction, are commonly employed to treat upper respiratory infections, acute bronchitis, pneumonia, bronchial asthma, and played a pivotal role in the management of the COVID-19 pandemic in China (Zhu and Liu, 2004; Liao et al., 2017; Wang et al., 2020a; Wang et al., 2020b; Tian et al., 2020; Xiao et al., 2020). Additionally, a prior randomized, double-blind, placebo-controlled, multicenter clinical study that we conducted demonstrated the efficacy of MSXG in effectively treating community-acquired childhood pneumonia and significantly improving fever and other clinical symptoms (Zheng et al., 2022).

For traditional Chinese formulas, in addition to the composition of the ingredients, dose is a crucial factor influencing their therapeutic effects, for dose affects the blood concentration of the herbal medicine and can impact the absorption of other components. For instance, KXR and SG can influence the content of ephedrine, a main active component of MH (Liang et al., 2007). GC and KXR can enhance the solubility of SG in water (Guo et al., 2010). Due to variations in individual constitution, metabolism, and illness severity, the question arises: how should the dose of MSXG be adjusted to achieve optimal efficacy while ensuring safety? Should the dose of the entire formula be increased, or is it sufficient to adjust the dose of a single ingredient? Traditional Chinese medicine (TCM) doses often derive from the clinical experience of doctors, which can be subjective and lack high-quality evidence supporting the scientific basis for dose adjustments. This underscores the critical importance of rational clinical application of MSXG.

To address these issues, we conducted three clinical studies. The first directly divided MSXG into low, medium, and high dose groups to observe the varying efficacy among these groups. This was done to evaluate the clinical significance of adjusting the entire formula's dose. Subsequently, considering the distinct effects of different ingredients in MSXG—such as the use of KXR mainly for treating cough and SG primarily for temperature reduction—we designed two separate clinical studies. These studies aimed to adjust the dose of KXR and SG respectively and assess the impact of adjusting individual ingredients on clinical efficacy.

2 Materials and methods

The studies were carried in Guang'anmen Hospital of China Academy of Chinese Medical Sciences, the First Affiliated Hospital of Tianjin University of Traditional Chinese Medicine, the second Affiliated Hospital of Tianjin University of Traditional Chinese Medicine, Tianjin Nankai Hospital, Tianjin Hangu District Traditional Chinese Medicine Hospital, Tianjin People's Hospital, Tianjin Medical University General Hospital. The studies had obtained approval from the ethics committee of Guanganmen Hospital, Chinese Academy of Chinese Medical Sciences (Ethics approval number: 2010–35), and has been registered on Chinese Clinical Trial Registry (https://www.chictr.org.cn/index.html, ChiCTR-TRC-13003093, ChiCTR-TRC-13003099).

2.1 Quality control and safety experiments of MSXG

We have established the detailed decoction process for the MSXG, which involves taking traditional Chinese herbs, adding 8 times their weight in water, soaking for 30 min, bringing to a boil, and then simmering on low heat for 40 min. Afterward, it is allowed to cool, filtered through gauze, and the resulting liquid is collected. Initially, we determined the content of the purchased herbs according to the standards set by the Chinese Pharmacopoeia to decide which herbal materials to use in the clinical study.

We employed both HPLC (High-Performance Liquid Chromatography) and titration methods to determine the content of MSXG. The results showed that the similarity of fingerprint profiles for 10 batches of samples was all greater than 0.95, indicating the stability of the preparation process for MSXG. Specific fingerprint peaks were identified, including ephedrine, pseudoephedrine, amygdalin, glycyrrhizin, and glycyrrhetinic acid. Our data on the fingerprint spectrum of Mahuang Xingren Gan Tang has been published. (*Wei Huizhen, Wang Xin, Wang Yuesheng, et al. Study on Multi-Wavelength Switching Fingerprint Spectrum of Mahuang Xingren Gan Tang. Journal of Traditional Chinese Medicine and Traditional Chinese Medicine Materials, 2012, 23(01): 60–62.*)

Before conducting clinical research, we conducted two animal experiments. The first experiment detected the components absorbed into the bloodstream, including ephedrine or pseudoephedrine, methyl ephedrine, glycyrrhizin, glycyrrhetinic acid, and isoglycyrrhizin. The second experiment evaluated the toxicity of MSXG, and the results showed that there were no significant toxic reactions observed at a maximum single oral dose equivalent to 87.5 human daily doses (Supplementary Appendix).

2.2 Study design

All 3 clinical studies conducted randomized, double-blind, dose-controlled, multi-center design. Regarding the sample size of the studies, we employed adaptive design. Each study aimed to recruit a total of 120 eligible patients according to the inclusion criteria, with 40 cases in each group. Depending on the statistical results, the number of cases could be increased by 30–60 cases as deemed appropriate.

In study 1, a total of 120 patients were enrolled and randomly divided into three different dose groups for MSXG: low, medium, and high, with 40 patients in each group.

In study 2, a total of 120 patients were enrolled, and only the dose of SG in MSXG was adjusted. They were divided into three different dose groups: low, medium, and high, with 40 patients in each group.

In Study 3, a total of 120 patients were enrolled, and only the dose of KXR in MSXG was adjusted. They were divided into three different dose groups: low, medium, and high, with 40 patients in each group.

2.3 Patients

2.3.1 Inclusion criteria

The patient meets the diagnostic criteria for bronchial pneumonia (Wind-heat Blocking the Lung) in the "Prevention and Treatment of Children's Four Diseases, Prevention and Treatment of Pediatric Pneumonia" and "Zhu Futang Practical Pediatrics" (seventh edition). The diagnostic criteria for TCM syndromes were referenced from "Diagnostic Criteria for Traditional Chinese Medicine Diseases and Syndromes and Efficacy Standards: Pediatric Diseases" (Supplementary Appendix).

1) The course of pneumonia should not exceed 48 h.
2) Within 24 h before enrollment maximum body temperature ≥38.5°C.
3) Age 3–6 years old.
4) Weight ≥14 kg.
5) White blood cell count ≤10×10^9/L, neutrophil ratio less than 70%.
6) Normal C-reactive protein.
7) Hospitalized patients.
8) Legal guardian of the child Informed and signed informed consent.

2.3.2 Exclusion criteria

1) Patients with heart failure, respiratory failure, toxic encephalopathy, exudative pleurisy and other comorbidities.
2) Clearly complicated bacterial infection.
3) Complicated with serious primary diseases such as heart, liver, kidney and hematopoietic system, mentally ill patients, if clinically significant arrhythmia, alanine aminotransferase more than double the upper limit of normal, serum creatinine >150 μmol/L, urea >10 mmol/L, or/and proteinuria >+, or/and erythrocyte urine >+.
4) According to the judgment of the investigator, there are other diseases that reduce the possibility of enrolling or complicate enrollment.
5) Those who could not cooperate or are participating in clinical trials of other drugs.
6) Allergic constitution (allergic to more than two types of substances) or known those who were allergic to the components of this preparation.
7) According to the judgment of the doctor, those who were likely to be lost to follow-up.

2.4 Interventions

All patients, in addition to receiving azithromycin (Zithromax, Pfizer Pharmaceuticals, 0.5 mg per dose, 5–10 mg/kg·d, once daily) as the foundational treatment, were administered different doses of MXSG based on their respective assigned groups. (Supplementary Tables SA1–SA3).

The MXSG was composed of 4 herbs: *Ephedra sinica* Stapf (MaHaung, MH), *Prunus armeniaca* L. (KuXingRen, KXR), Gypsum fibrosum (ShiGao, SG), and *Glycyrrhiza uralensis* Fisch. (GanCao, GC). And the basic dose of MXSG was MH 6g, KXR 9g, SG 24g, GC 6g, which were supplied by Yanjing Herb Pharmaceutical Co., Ltd., (Beijing, China), decocted and distributed uniformly by the First Affiliated Hospital of Tianjin University of Traditional Chinese Medicine, and conform to the Chinese Pharmacopoeia (2010 edition).

For Study 1, the doses for each group were as follows:

- Low-dose group: MH 3g, KXR 3g, SG 12g, GC 3g.
- Medium-dose group: MH 6g, KXR 6g, SG 24g, GC 6g.
- High-dose group: MH 9g, KXR 9g, SG 36g, GC 9g.

For Study 2, the doses for each group were:

- low-dose group: MH 6g, KXR 6g, SG 16g, GC 6g.
- Medium-dose group: MH 6g, KXR 6g, SG 24g, GC 6g.
- high-dose group: MH 6g, KXR 6g, SG 36g, GC 6g.

For Study 3, the doses for each group were:

- low-dose group: MH 6g, KXR 3g, SG 16g, GC 6g.
- Medium-dose group: MH 6g, KXR 6g, SG 24g, GC 6g.
- high-dose group: MH 6g, KXR 9g, SG 24g, GC 6g.

Uniform labelling format for the study drugs, including contents: name of clinical trial drug (for clinical research only), medication method, specification, storage conditions, drug number, expiry date, drug supply unit, matters needing attention. The observing physician should distribute the drugs according to the order of visit and the drug number of each patient. The drug number should not be selected, and the drug number would remain unchanged throughout the trial. Each patient would be provided with enough study drugs of the same drug number for 10 days. Strict management and use of test drugs and control drugs, each participating unit to establish a strict test department of specially assigned custody, distribution system. The First Affiliated Hospital of Tianjin University of Traditional Chinese Medicine delivered each group of TCM decoction directly to the special custodian of each hospital department, and establish a perfect drug reception

procedure. The drug should not be heated or exposed to direct sunlight during delivery, and freezing is prohibited. Unused test drugs should be stored in the refrigerator at 2 ~ 8°C. The study drugs are the responsibility of the investigator, and the investigator should not transfer the investigational drugs to any non-clinical trial participants. The investigator must ensure that the drug is used only in the subjects of the clinical trial, that the dose and administration are in accordance with the trial protocol, and that any remaining drug is withdrawn.

3 Outcomes

3.1 Baseline characteristics

The gender, age, height, weight, medical history, symptoms of the patients were recorded.

3.2 Effect outcomes

3.2.1 Primary outcome

The clinical cured rate (number of clinical cured patients/total number of patients * 100%) as the primary outcome, the evaluation criteria of disease efficacy as follows:

1) Clinical cured: ①the fine moist rales disappeared in the lung auscultation; ②the fever was completely relieved; ③ the dyspnea disappeared.
2) Not cured: Those who did not reach the clinical cured standard.
3) Invalid: ① the daily maximum body temperature dropped by less than 0.5°C; ② the symptoms and signs have no obvious change or aggravation. Both conditions are met at the same time.

3.2.2 Second outcomes

We first evaluate the main clinical symptoms of bronchitis, including fever, cough, dyspnea, and phlegm congestion.

For study 1, we used the symptom disappearance rate, and the evaluation criteria were: Clinical cured: Symptoms disappear after treatment. Significant effect: After treatment, the severity of symptoms decreased by 2 levels, from severe to mild. Effective: After treatment, the severity of symptoms decreases by 1 level, from severe to moderate, or from moderate to mild. Invalid: There is no change before and after treatment. (Supplementary Table SA4).

For Study 2 and Study 3, we considered that adjusting for a single drug may result in relatively small differences in efficacy between groups. Therefore, the improvement in symptom (fever, cough, phlegm obstruction, dyspnea) was evaluated with the area under the curve (AUC) between the symptom and time.

We observed during study that some patients had resolved their fever symptoms before the study's completion. Aimed to comprehensively assess the efficacy of SG in Study 2 regarding fever management, we evaluated the complete defervescence time among the groups. This refers to the time required for the body temperature to return to normal (≤37.2°C) and remain so for more than 24 h after the administration of the drug.

3.3 Safety outcomes

Safety outcomes included detection of chest X-ray, white blood cell count and classification, C-reactive protein, *mycoplasma* pneumoniae antibody, and routine stool, urine, electrocardiogram, liver and kidney function.

1) Vital signs: including body temperature, resting heart rate, resting breathing, blood pressure.
2) Laboratory tests: including blood routine (erythrocytes, hemoglobin, leukocytes, neutrophils, lymphocytes, platelets), urine routine (erythrocytes, leukocytes, urine protein, urine sugar), stool routine (leukocytes, erythrocytes), liver and kidney function, including alanine aminotransferase (ALT), aspartate aminotransferase (AST), blood urea nitrogen (BUN), Serum creatinine (Cr).
3) Electrocardiogram.
4) Chest radiograph.
5) Adverse event.

3.4 Statistical analysis

All analyses were performed using SAS 9.2. All statistical tests adopt two-sided test. If the *p*-value was less than or equal to 0.05, it would be considered that the tested difference was statistically significant (unless otherwise specified). The description of quantitative indicators would calculate the number of cases, missing number, mean, standard deviation, minimum value, maximum value, median and interquartile spacing. F test/ Wilcoxon rank sum test was used to compare the quantitative indexes between groups; For qualitative indexes, chi square test/ Fisher exact test was used for comparison between groups.

Full analysis set (FAS): All subjects who had been randomized into groups, taken the test drug at least once, and have post-dose evaluation data constitute the FAS of this trial. Missing data in the efficacy-related portion of the FAS would be supplemented using the last previous observation carried forward (LOCF). FAS was used for the analysis of primary and secondary efficacy measures and was the main dataset for efficacy evaluation in this trial.

Per-protocol analysis (PPS): Subjects who met the inclusion criteria specified by the trial protocol; completed the 6-day planned visit; no drugs or treatments were used during the trial that might affect the evaluation of efficacy; adherence was good (80%–120%).

Safety Set (SS): All subjects who have been randomized into different groups, received the investigational drug at least once, and possess safety evaluation data after drug administration constitute the SS of this trial.

4 Results

4.1 Baseline characteristics

3 studies each enrolled 120 patients with bronchial pneumonia (Wind-heat Blocking the Lung). For Study 1, a total of 112 patients completed the study, with 39 in the low-dose group, 37 in the medium-dose group, and 36 in the high-dose group. For Study 2, a

total of 110 patients completed the study, including 35 in the low-dose group, 37 in the medium-dose group, and 38 in the high-dose group. For Study 3, a total of 100 patients completed the study, with 26 in the low-dose group, 37 in the medium-dose group, and 37 in the high-dose group. The baseline characteristics of the subjects were presented in the Supplementary Tables SA5–SA7, and there were no differences between the groups in each study, including age, gender, height, and so on. Flowcharts for each study are provided in the Supplementary Figures SA1–SA3.

4.2 Primary outcome

We first analyzed the effects of MXSG in the treatment of bronchial pneumonia in 3 studies. The results showed that for the FAS, the cured rate was 75.71% (268/354), and for the PPS, the cured rate was 83.13% (266/320). For Study 1, the FAS results revealed that among the patients in the low-dose group, 22 individuals (55.00%) achieved clinical cured, while in the medium-dose group, 31 patients (81.58%) achieved clinical cured, and in the high-dose group, 30 patients (81.08%) achieved clinical cured. There was a significant difference in the comparison between the groups (Chi-square value: 9.01, p = 0.0111), indicating that both the medium-dose and high-dose groups had significantly higher clinical cured rates than the low-dose group. The PPS results showed that among the patients in the low-dose group, 22 individuals (56.41%) achieved clinical cured, while in the medium-dose group, 31 patients (86.11%) achieved clinical cured, and in the high-dose group, 30 patients (85.71%) achieved clinical cured. There was a significant difference in the comparison between the groups (Chi-square value: 11.83, p = 0.0027), indicating that both the medium-dose and high-dose groups had significantly higher clinical cured rates than the low-dose group.

For Study 2, the FAS results showed that among the patients in the low-dose group, 30 individuals (75.00%) achieved clinical cured, in the medium-dose group, 34 patients (85.00%) achieved clinical cured, and in the high-dose group, 36 patients (90.00%) achieved clinical cured. There was no significant difference in the comparison between the groups (Chi-square value: 3.36, p = 0.1864), indicating that there were no significant differences in clinical cured rates among the groups. The PPS results showed that among the patients in the low-dose group, 30 individuals (85.71%) achieved clinical cured, in the medium-dose group, 34 patients (91.89%) achieved clinical cured, and in the high-dose group, 36 patients (94.74%) achieved clinical cured. There was no significant difference in the comparison between the groups (two-sided exact probability, p = 0.3760), indicating that there were no significant differences in clinical cured rates among the groups.

For Study 3, the FAS results showed that among the patients in the low-dose group, 12 individuals (30.77%) achieved clinical cured, in the medium-dose group, 36 patients (90.00%) achieved clinical cured, and in the high-dose group, 32 patients (92.50%) achieved clinical cured. There was a significant difference in the comparison between the groups (Chi-square value: 47.05, p < 0.0001), indicating that both the medium-dose and high-dose groups had significantly higher clinical cured rates than the low-dose group. The PPS results showed that among the patients in the low-dose group, 11 individuals (42.31%) achieved clinical cured, in the medium-dose group, 36 patients (97.30%) achieved clinical cured, and in the high-dose group, 36 patients (97.30%) achieved clinical cured. There was a significant difference in the comparison between the groups (two-sided exact probability, p < 0.0001), indicating that both the medium-dose and high-dose groups had significantly higher clinical cured rates than the low-dose group (Figure 1).

4.3 Second outcomes

For the FAS in Study 1, the fever results showed that, 36 patients (100.00%) in the low-dose group achieved clinical cured, 33 patients (94.29%) in the medium-dose group, and 34 patients (97.14%) in the high-dose group. There was no significant difference between the groups (two-sided exact probability, p = 0.3208). For cough, 19 patients (48.72%) in the low-dose group achieved clinical cured, 28 patients (71.79%) in the medium-dose group, and 24 patients (64.86%) in the high-dose group. There was no significant difference between the groups (Chi-square value: 4.62, p = 0.0992). For dyspnea, 14 patients (77.78%) in the low-dose group achieved clinical cured, 10 patients (62.50%) in the medium-dose group, and 18 patients (75.00%) in the high-dose group. There was no significant difference between the groups (two-sided exact probability, p = 0.5713). For phlegm obstruction, 19 patients (48.72%) in the low-dose group achieved clinical cured, 27 patients (69.23%) in the medium-dose group, and 27 patients (75.00%) in the high-dose group. There was a significant difference between the groups (Chi-square value: 6.31, p = 0.0426).

For the PPS in Study 1, the fever results showed, 36 patients (100.00%) in the low-dose group achieved clinical cured, 32 patients (100.00%) in the medium-dose group, and 33 patients (100.00%) in the high-dose group. There was no significant difference between the groups (p = 1.000). For cough, 19 patients (48.72%) in the low-dose group achieved clinical cured, 28 patients (77.78%) in the medium-dose group, and 23 patients (65.71%) in the high-dose group. There was a significant difference between the groups (Chi-square value: 6.93, p = 0.0313). For dyspnea, 14 patients (77.78%) in the low-dose group achieved clinical cured, 9 patients (64.29%) in the medium-dose group, and 17 patients (73.91%) in the high-dose group. There was no significant difference between the groups (two-sided exact probability, p = 0.6900). For phlegm obstruction, 19 patients (48.72%) in the low-dose group achieved clinical cured, 27 patients (75.00%) in the medium-dose group, and 27 patients (77.14%) in the high-dose group. There was a significant difference between the groups (Chi-square value: 8.46, p = 0.0145). (Figure 2).

For the FAS in Study 2, the fever AUC results showed, the low-dose group was 7.60 ± 5.09, the medium-dose group was 7.78 ± 5.72, and the high-dose group was 5.93 ± 4.16. There was no significant difference between the groups (F-test value: 1.65, p = 0.1970). For cough, the low-dose group was 20.73 ± 7.20, the medium-dose group was 18.25 ± 4.93, and the high-dose group was 21.53 ± 5.95. There was a significant difference between the groups (F-test value: 3.14, p = 0.0471). For dyspnea, the low-dose group was 3.15 ± 4.19, the medium-dose group was 2.98 ± 3.42, and the high-dose group was 1.58 ± 2.55. There was no significant difference between the groups (F-test value: 2.50, p = 0.0863). For phlegm obstruction, the low-dose

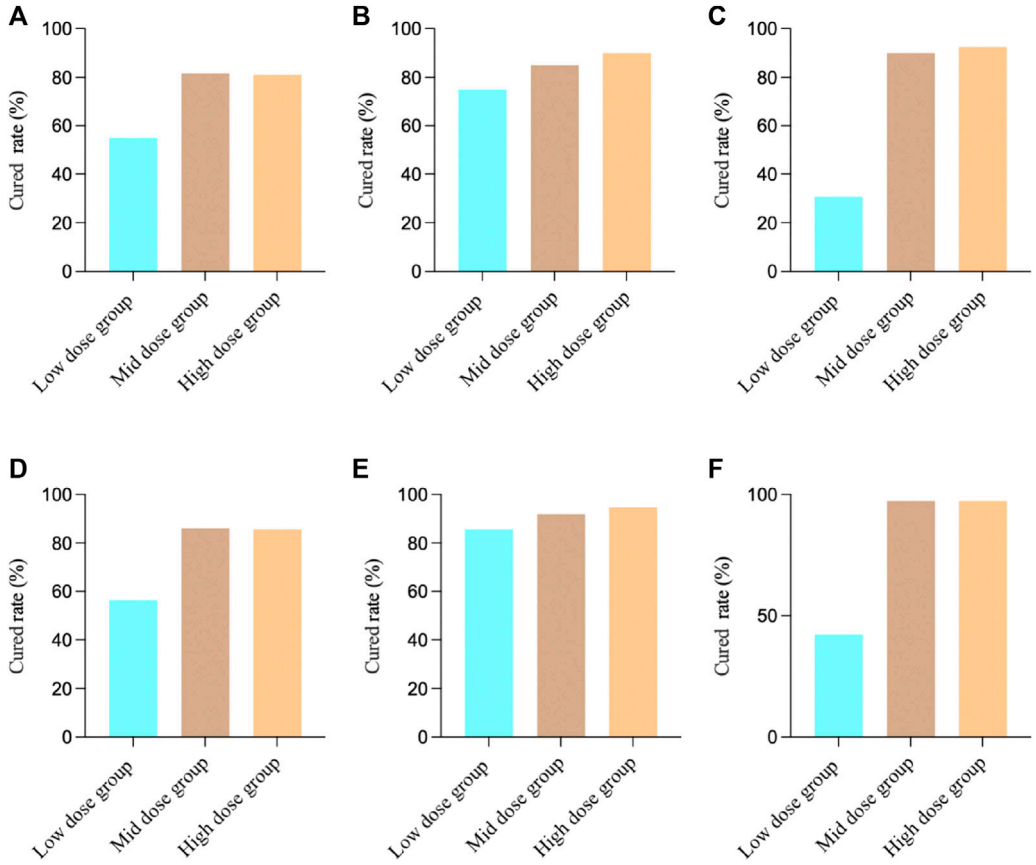

FIGURE 1
Clinical cured results in different studies. **(A)** Study 1 FAS Results; **(B)** Study 2 FAS Results; **(C)** Study 3 FAS Results; **(D)** Study 1 PPS Results; **(E)** Study 2 PPS Results; **(F)** Study 3 PPS Results.

group was 19.70 ± 8.04, the medium-dose group was 17.85 ± 6.65, and the high-dose group was 19.88 ± 6.04. There was no significant difference between the groups (F-test value: 1.04, $p = 0.3567$).

For the PPS in Study 2, the fever AUC results showed, the low-dose group was 7.86 ± 5.35, the medium-dose group was 7.43 ± 5.44, and the high-dose group was 5.39 ± 3.33. There was no significant difference between the groups (F-test value: 2.81, $p = 0.0649$). For cough, the low-dose group was 21.74 ± 6.55, the medium-dose group was 18.86 ± 4.56, and the high-dose group was 21.87 ± 5.74. There was a significant difference between the groups (F-test value: 3.32, $p = 0.0398$). For dyspnea, the low-dose group was 3.29 ± 4.35, the medium-dose group was 3.16 ± 3.48, and the high-dose group was 1.66 ± 2.59. There was no significant difference between the groups (F-test value: 2.47, $p = 0.0898$). For phlegm obstruction, the low-dose group was 20.86 ± 7.71, the medium-dose group was 18.46 ± 6.53, and the high-dose group was 20.18 ± 5.88. There was no significant difference between the groups (F-test value: 1.23, $p = 0.2962$).

During the study, we observed that many patients experienced complete relief from fever symptoms around 3 days of intervention. Therefore, we compared the time of complete fever resolution among different groups to assess the onset of action of the intervention medication. For FAS, the complete antipyretic time in high dose group (Log-Rank test, statistic 25.38, $p < 0.0001$) and medium-dose group (Log-Rank test, statistic 10.07, $p = 0.0015$) showed statistical differences compared to low-dose group after treatment, and there was no statistical difference between the high and middle dose groups (Log-Rank test, statistic 2.48, $p = 0.1152$). For PPS, the complete antipyretic time in high dose group (Log-Rank test, statistic 30.13, $p < 0.0001$) and medium-dose group (Log-Rank test, statistic 11.17, $p = 0.0008$) showed statistical differences compared to low-dose group after treatment, and there was no statistical difference between the high and middle dose groups (Log-Rank test, statistic 3.34, $p = 0.07$). (Figure 3).

For the FAS in Study 3, the fever AUC results showed, the low-dose group was 1.62 ± 2.65, the medium-dose group was 1.60 ± 2.73, and the high-dose group was 2.10 ± 3.80. There were no significant differences between the groups (F-test value: 0.33, $p = 0.7171$). For cough, the low-dose group was 23.87 ± 8.02, the medium-dose group was 20.75 ± 7.17, and the high-dose group was 20.25 ± 5.33. There was a significant difference among the groups (F-test value: 3.16, $p = 0.0460$). For dyspnea, the low-dose group was 0.08 ± 0.48, the medium-dose group was 0.68 ± 2.25, and the high-dose group was 0.73 ± 2.76. There were no significant differences between the groups (F-test value: 1.18, $p = 0.3115$). For phlegm obstruction, the low-dose group was 23.08 ± 8.64, the medium-dose group was 19.73 ± 7.64, and the high-dose group was 18.68 ± 5.47. There were no significant differences between the groups (F-test value: 3.84, $p = 0.0243$).

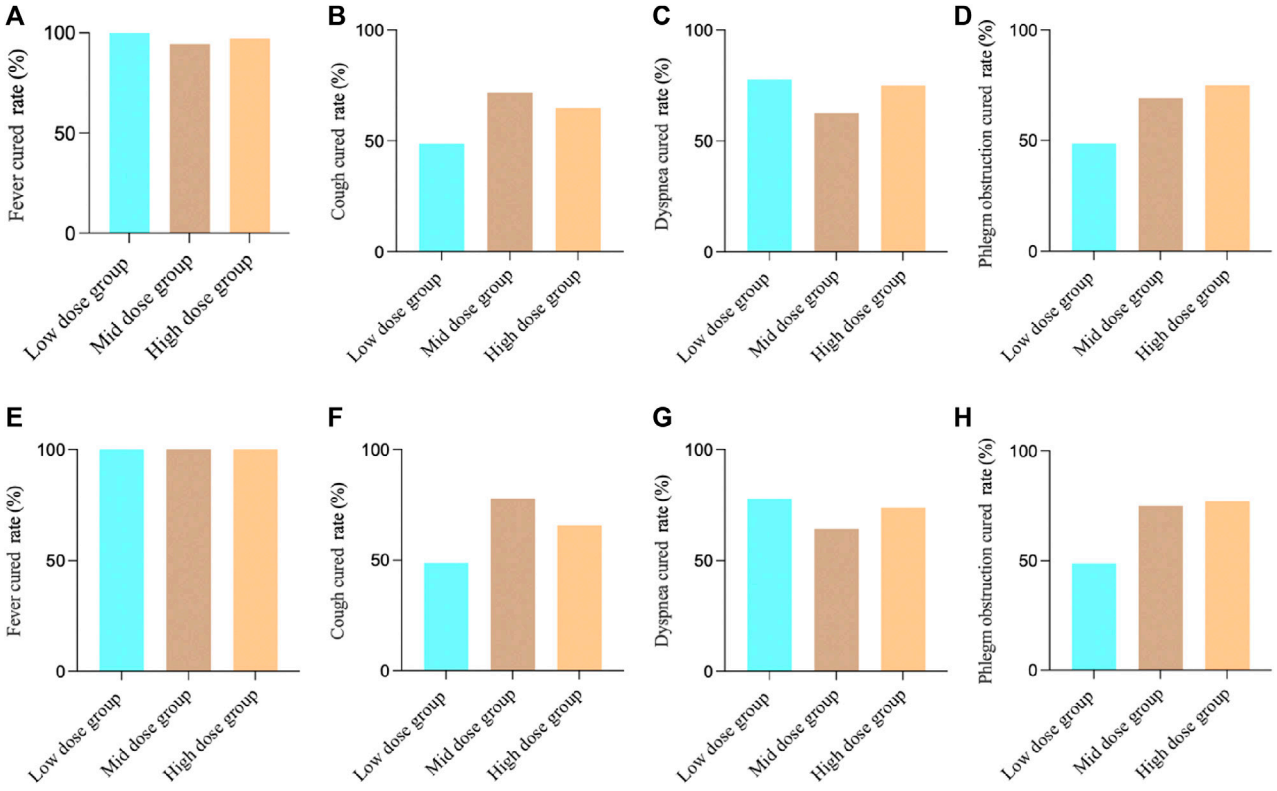

FIGURE 2
Study 1 results of different symptoms. **(A)** FAS results of fever; **(B)** FAS results of cough; **(C)** FAS results of dyspnea; **(D)** FAS results of phlegm obstruction; **(E)** PPS results of fever; **(F)** PPS results of cough; **(G)** PPS results of dyspnea; **(H)** PPS results of phlegm obstruction.

For the PPS in Study 3, the fever AUC results showed, the low-dose group was 1.65 ± 2.62, the medium-dose group was 1.24 ± 2.36, and the high-dose group was 2.19 ± 3.92. There were no significant differences between the groups (F-test value: 0.87, $p = 0.4219$). For cough, the low-dose group was 27.04 ± 6.61, the medium-dose group was 21.68 ± 6.59, and the high-dose group was 20.38 ± 5.16. There was a significant difference among the groups (F-test value: 9.74, $p = 0.0001$). For dyspnea, the low-dose group was 0.12 ± 0.59, the medium-dose group was 0.73 ± 2.33, and the high-dose group was 0.78 ± 2.87. There were no significant differences between the groups (F-test value: 0.77, $p = 0.4646$). For phlegm obstruction, the low-dose group was 26.77 ± 7.18, the medium-dose group was 20.46 ± 7.39, and the high-dose group was 18.81 ± 5.29. There was a significant difference among the groups (F-test value: 11.71, $p < 0.001$). (Figure 4).

4.4 Adverse events

In Study 1, a total of 5 adverse events were reported. Among them, there were 2 adverse events in the medium-dose group, with 1 of them possibly related to the investigational drug. In the high-dose group, there were 3 adverse events, but none of them were likely related to the investigational drug. In Study 2, there was a total of 1 adverse event observed, occurring in the high-dose group. However, this adverse event was not likely related to the investigational drug. In Study 3, no adverse events were observed. (Supplementary Table SA8).

5 Discussion

Safety and efficacy are two fundamental attributes of therapeutic drugs, including TCMs. As the understanding of treatment outcomes and adverse reactions in TCMs deepens, the dose-response relationship—selecting the appropriate dosage to maximize therapeutic effectiveness while minimizing adverse reactions—is becoming a crucial concern in the modernization of TCM. Consequently, a comprehensive understanding of the accuracy of herbal dose selection is of paramount importance in the daily practice of TCM, ensuring optimal treatment for patients with various ailments (Zha et al., 2015). In clinical practice, for different TCMs and formulations composed of these, clinical applications in TCM have accumulated a considerable amount of experience. However, much of this experience is based on individual expertise and has yet to be validated through high-quality evidence. This is precisely one of the significant aims of conducting this study—to establish a basis for this through rigorous evidence-based research.

In summary, we conducted 3 clinical studies focusing on the commonly used clinical formula MXSG in treating bronchial pneumonia. First, in terms of clinical efficacy, the clinical cured rate of the low-dose group was the lowest among the 3studies. Although there was a slight increase in the clinical cured rate in the high-dose group compared to the medium-dose group, it was not statistically significant. Taking into consideration the clinical components and safety concerns, the medium dose appears to be the optimal dosage

10.3389/fphar.2023.1279519

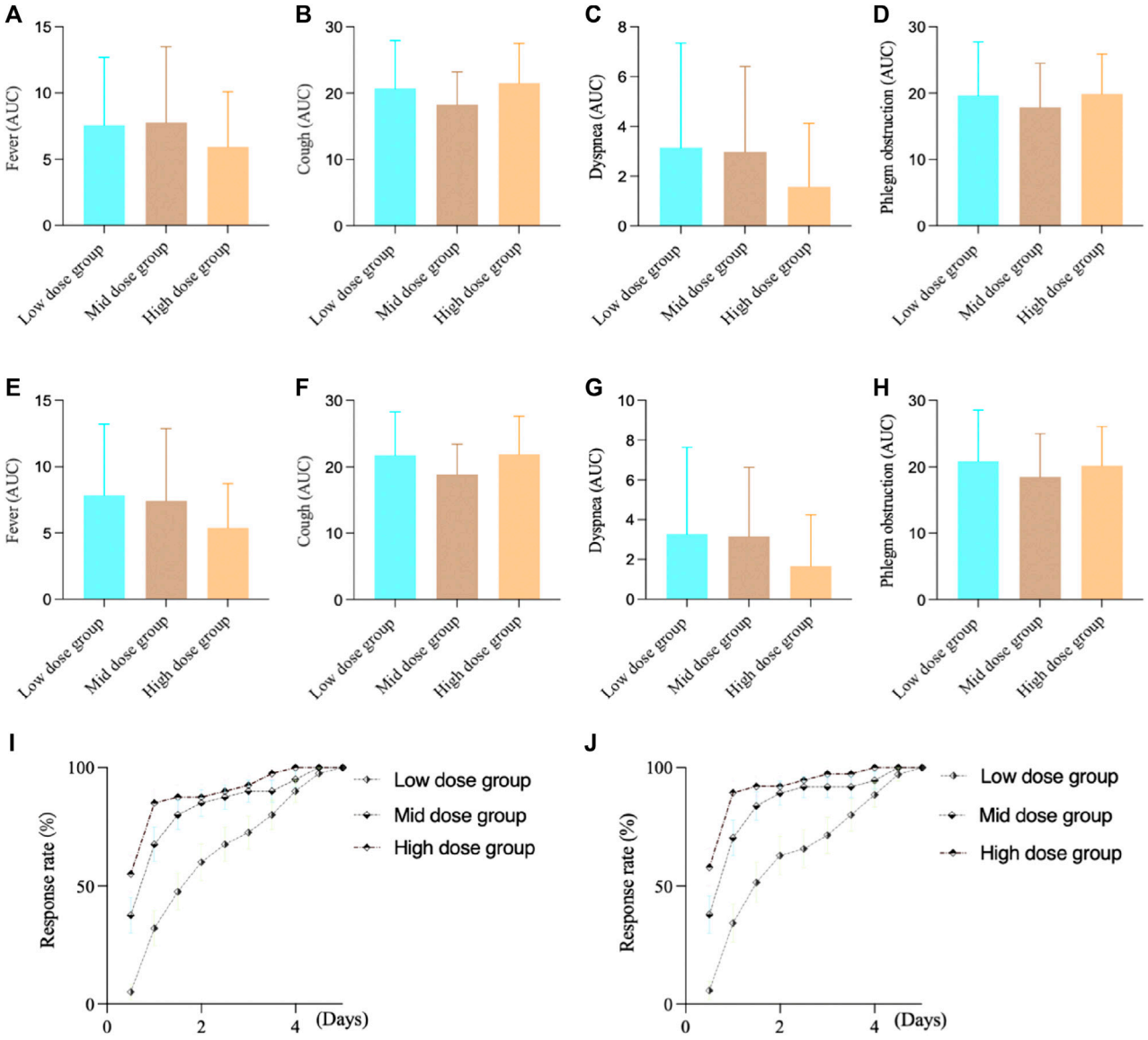

FIGURE 3
Study 2 results of different symptoms. **(A)** FAS results of fever; **(B)** FAS results of cough; **(C)** FAS results of dyspnea; **(D)** FAS results of phlegm obstruction; **(E)** PPS results of fever; **(F)** PPS results of cough; **(G)** PPS results of dyspnea; **(H)** PPS results of phlegm obstruction; **(I)** FAS results of complete antipyretic time; **(J)** PPS results of complete antipyretic time.

for clinical treatment of bronchitis. However, when assessing individual symptoms, in Study 1, the clinical cured rates for cough and phlegm obstruction were higher in both the medium and high-dose groups compared to the low-dose group. Meanwhile, there was no significant clinical benefit observed in the high-dose group compared to the low-dose group. This emphasizes the importance of clinical effectiveness, and increasing the overall dosage might not result in significant clinical benefits. For Study 2 and Study 3, the results indicated that the clinical efficacy of the medium and high-dose groups was significantly better than that of the low-dose group. However, while the high-dose group exhibited some improvement compared to the medium-dose group, the difference was not statistically significant. In terms of clinical symptoms, the AUC results for fever and dyspnea indicated that the high-dose group had the most significant therapeutic effect. When combined with the results of the complete defervescence rate, patients in the high-dose group were more likely to have fever symptoms subside in a shorter time frame. Additionally, no significant drug-related adverse events were observed, suggesting that the rational increase of SG on top of the commonly used dosage can lead to more significant fever-reducing effects. This includes clinical recovery from fever as well as a shorter duration until the disappearance of fever symptoms. In Study 3, the results were consistent with Study 1 and Study 2. Both the medium and high-dose groups had significantly higher clinical cured rates compared to the low-dose group. However, there was no significant clinical benefit observed in the high-dose group compared to the medium-dose group. In terms of clinical symptoms, the results showed that the high-dose group had the most significant therapeutic effect in terms of cough and phlegm obstruction. Both the high and medium-dose groups

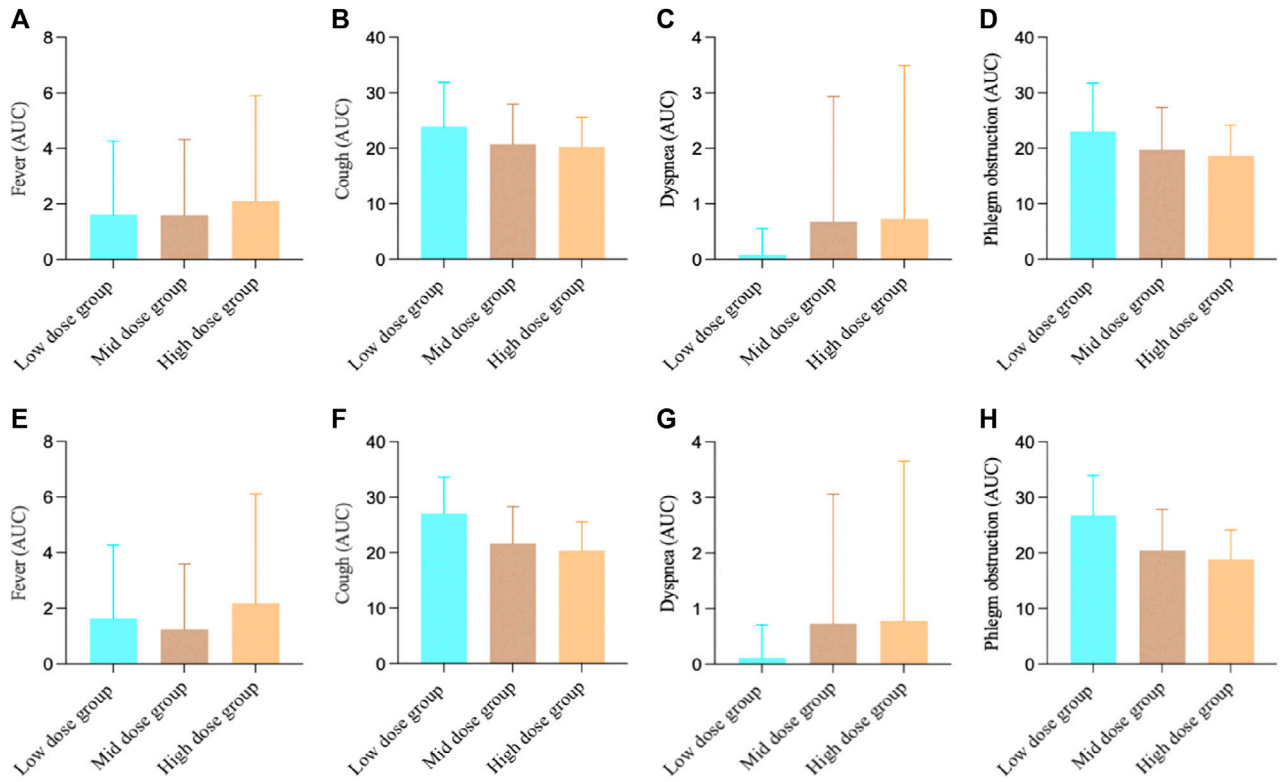

FIGURE 4
Study 3 results of different symptoms **(A)** FAS results of fever; **(B)** FAS results of cough; **(C)** FAS results of dyspnea; **(D)** FAS results of phlegm obstruction; **(E)** PPS results of fever; **(F)** PPS results of cough; **(G)** PPS results of dyspnea; **(H)** PPS results of phlegm obstruction.

were superior to the low-dose group. In conclusion, we conducted 3 clinical studies centered around MXSG and primarily investigated how to adjust its dosage during clinical applications. Our findings suggest that the commonly used clinical dosage is the optimal one for the entire formula. If the dosage is not enough, the desired clinical efficacy may not be achieved, and increasing the dosage further may not result in significant clinical benefits. For different herbs within the formula, adjusting the dosage of SG, a cooling agent, does not significantly improve the overall efficacy but does show notable changes in fever symptoms. As for KXR, its adjustment produces more significant improvements in cough symptoms.

As mentioned above, MXSG is used to treat respiratory tract infections, acute bronchitis, pneumonia, bronchial asthma and other lung diseases, as well as H1N1, Corona Virus Disease 2019 (COVID-19) and other pulmonary infectious diseases (Wang et al., 2011), with mechanism of stimulation of beta 2-adrenergic receptors on bronchial smooth muscle, inhibition of neutrophil entry into the airways, and reduction of airway inflammation (Kao et al., 2001), and exerts broad-spectrum antiviral effects by inhibiting viral RNA and protein synthesis (Hsieh et al., 2012). The pharmacodynamic mechanism mainly involves antiviral, alleviating lung inflammation and reducing lung cell apoptosis. *In vivo* animal experiments have shown that MXSG could reduce lung inflammation induced by lipopolysaccharide in a rat model of pneumonia, possibly by regulating the coagulation system (Yang et al., 2020). MXSG colud also inhibit the activation of the high mobility group protein 1/Toll-like receptor 4/nuclear factor kappa-B (NF-κB) signaling pathway and reduce the levels of inflammatory cytokines, thereby alleviating inflammatory damage (Fei et al., 2019). Clinical studies have confirmed that MXSG in combination with other drugs could significantly improve the antipyretic effect, such as Oseltamivir and MXSG + Yinqiaosan alone or in combination could shorten the time of fever in patients with H1N1 influenza virus infection. These data suggest that MXSG + Yinqiaosan could be used as an alternative treatment for H1N1 influenza virus infection (Wang et al., 2011). The main active components of ephedra are ephedrine and pseudoephedrine, which could exert anti-inflammatory effects by reducing the degradation of NF-κB in the cytoplasm and the production of tumor necrosis factor-α (TNF-α) (Wu et al., 2014). Among them, ephedrine has a more significant bronchial dilating effect (Laitinen et al., 1982). And pseudoephedrine, as a sympathomimetic drug, combined with emodin could regulate the polarization of macrophages to improve Lipopolysaccharide (LPS)-induced acute lung injury (Wang et al., 2022).

For the SG in MXSG, the main component is CaSO4·2H2O, also including manganese (Mn), nickel (Ni) and other trace elements. SG is mainly used in TCM to clear heat and related cough, with antipyretic and cooling effects (Lin and Gao, 1994). Studies have shown that SG has anti-inflammatory and antipyretic effects, which may be related to the reduction of hypothalamic prostaglandin E2 content, while CaSO4.2H2O has no obvious anti-inflammatory and antipyretic effects, which also explains that other trace elements may play a key role (Zhou et al., 2012). The action mechanism of SG also includes affecting the firing activity of temperature-sensitive neurons in the preoptic area of the anterior hypothalamus (PO/AH) under the action

of pyrogen, and playing an antipyretic role at the level of central neurons (Fan et al., 1997; Wang et al., 2008). Animal experiments showed that the healthy and harmless rabbits with fever caused by intravenous injection of typhoid vaccine were given SG decoction orally, and the control group was given antipyrine. The results show that it does have a significant cooling effect, with a rapid cooling rate similar to antipyrine (Zhou, 2015). SG combined with MH has antipyretic and anti-asthmatic effects (Mei et al., 2016), and SG combined with Anemarrhena could exert anti-allergic effects (Makino et al., 2014). Glycyrrhizic acid, the main active ingredient in GC, has broad-spectrum antiviral activity, and glycyrrhizin could inhibit SARS-related virus replication (Cinatl et al., 2003). Glycyrrhizin could reduce viral infection of cells, mainly by reducing endocytosis of the cell membrane and reducing viral uptake (Wolkerstorfer et al., 2009). Liquiritigenin exerts anti-inflammatory effects due to inhibition of NF-κB activation in macrophages, thereby reducing Inductible Nitric Oxide Synthase and pro-inflammatory cytokine production (Kim et al., 2008). KXR is protective during epithelial-mesenchymal transition in chronic obstructive pulmonary disease mice (Wang et al., 2019). Other studies have shown that amygdalin, one of the main pharmacologically active ingredients of KXR, could inhibits NF-κB and NOD-like receptor protein 3 (NLRP3) signaling pathways, thereby reducing the expression of pro-inflammatory cytokines (such as pro-IL-1b), resulting in anti-inflammatory effects (Zhang et al., 2017).

However, our studies also have certain limitations. Could the lack of significant benefits after further adjustments in MXSG dosage be attributed to the fact that patients' blood drug concentrations have already reached their maximum? Additionally, can the clinically established baseline dosage of MXSG be applicable to every individual patient? These questions cannot be addressed through our studies alone and may need to be answered through subsequent PK/PD experiments. Of course, MXSG is a compound composed of various plants and minerals. Although our clinical studies, including previously published research, have confirmed its significant clinical efficacy, the active ingredients and mechanism of action are yet to be determined. Furthermore, in our studies, the subjects were all Chinese. The efficacy of MXSG in other ethnic groups and the optimal effective dosage require further evaluation.

In conclusion, the results from these 3 clinical studies indicate that, for the clinical application of MXSG, the commonly used clinical dosage is optimal. Increasing the dosage of the drug may not yield significant benefits. Adjusting the dosage of SG or KXR could lead to a certain degree of improvement in fever and cough symptoms, all within the boundaries of safety. Our research provides high-quality evidence-based support for the rational clinical application and dosage selection of MXSG. Moreover, it offers insights and methods that can be referenced for determining dosages of other TCM formulas and for related research endeavors. Of course, our research is still exploratory clinical trials, and further studies are needed to confirm our findings.

Data availability statement

The original contributions presented in the study are included in the article/Supplementary Material, further inquiries can be directed to the corresponding authors.

Ethics statement

The studies involving humans were approved by ethics Committee of Guang'anmen Hospital, Chinese Academy of Chinese Medical Sciences. The studies were conducted in accordance with the local legislation and institutional requirements. Written informed consent for participation in this study was provided by the participants' legal guardians/next of kin.

Author contributions

XA: Writing–original draft, Writing–review and editing. CS: Writing–review and editing. YH: Project administration, Writing–review and editing. XL: Writing–review and editing. LD: Project administration, Writing–review and editing. YL: Project administration, Writing–review and editing. HC: Project administration, Writing–review and editing. YW: Project administration, Writing–review and editing. JL: Project administration, Writing–review and editing. GL: Writing–review and editing. FL: Writing–review and editing. RM: Writing–review and editing. XT: Writing–review and editing.

Funding

The author(s) declare financial support was received for the research, authorship, and/or publication of this article. This study was supported by the National key basic research development plan (973) project (2010CB530601).

Conflict of interest

The authors declare that the research was conducted in the absence of any commercial or financial relationships that could be construed as a potential conflict of interest.

Publisher's note

Supplementary material

The Supplementary Material for this article can be found online at: https://www.frontiersin.org/articles/10.3389/fphar.2023.1279519/full#supplementary-material

References

Berlucchi, M., Pelucchi, F., Timpano, S., Zorzi, A., and Padoan, R. (2014). A conservative treatment for plastic bronchitis in pediatric age. *Am. J. Otolaryngol.* 35 (2), 204–206. doi:10.1016/j.amjoto.2013.11.003

Black, R. E., Cousens, S., Johnson, H. L., Lawn, J. E., Rudan, I., Bassani, D. G., et al. (2010). Global, regional, and national causes of child mortality in 2008: a systematic analysis. *Lancet* 375 (9730), 1969–1987. doi:10.1016/S0140-6736(10)60549-1

Bradley, J. S., Byington, C. L., Shah, S. S., Alverson, B., Carter, E. R., Harrison, C., et al. (2011). The management of community-acquired pneumonia in infants and children older than 3 months of age: clinical practice guidelines by the Pediatric Infectious Diseases Society and the Infectious Diseases Society of America. *Clin. Infect. Dis.* 53 (7), e25–e76. doi:10.1093/cid/cir531

Chang, C. C., Cheng, A. C., and Chang, A. B. (2014). Over-the-counter (OTC) medications to reduce cough as an adjunct to antibiotics for acute pneumonia in children and adults. *Cochrane Database Syst. Rev.* 3, Cd006088. doi:10.1002/14651858.CD006088.pub4

Cinatl, J., Morgenstern, B., Bauer, G., Chandra, P., Rabenau, H., and Doerr, H. W. (2003). Glycyrrhizin, an active component of liquorice roots, and replication of SARS-associated coronavirus. *Lancet* 361 (9374), 2045–2046. doi:10.1016/s0140-6736(03)13615-x

Fan, S., Sun, L., Wu, Y., and Zhao, H. (1997). Effect of the compatibility of puerarin and gypsum on the firing of cat POAH thermosensitive neurons under the action of pyrogen. *Chin. J. Appl. Physiology* (01), 72–75.

Fei, Y. X., Zhao, B., Yin, Q. Y., Qiu, Y. Y., Ren, G. H., Wang, B. W., et al. (2019). Ma xing shi Gan decoction attenuates PM2.5 induced lung injury via inhibiting HMGB1/TLR4/nfκb signal pathway in rat. *Front. Pharmacol.* 10, 1361. doi:10.3389/fphar.2019.01361

GBD 2019 Diseases and Injuries Collaborators (2020). Global burden of 369 diseases and injuries in 204 countries and territories, 1990-2019: a systematic analysis for the Global Burden of Disease Study 2019. *Lancet* 396 (10258), 1204–1222. doi:10.1016/S0140-6736(20)30925-9

Guo, H., Wen, Q., Ran, R., and Wang, M. (2010). Influence of different compatibility on contents of calcium and magnesium dissolution in maxing shigan decoction. *Zhongguo Zhong Yao Za Zhi* 35 (22), 2985–2989. doi:10.4268/cjcmm20102211

Hsieh, C. F., Lo, C. W., Liu, C. H., Lin, S., Yen, H. R., Lin, T. Y., et al. (2012). Mechanism by which ma-xing-shi-gan-tang inhibits the entry of influenza virus. *J. Ethnopharmacol.* 143 (1), 57–67. doi:10.1016/j.jep.2012.05.061

Kao, S. T., Yeh, T. J., Hsieh, C. C., Shiau, H. B., Yeh, F. T., and Lin, J. G. (2001). The effects of Ma-Xing-Gan-Shi-Tang on respiratory resistance and airway leukocyte infiltration in asthmatic Guinea pigs. *Immunopharmacol. Immunotoxicol.* 23 (3), 445–458. doi:10.1081/iph-100107343

Kim, Y. W., Zhao, R. J., Park, S. J., Lee, J. R., Cho, I. J., Yang, C. H., et al. (2008). Anti-inflammatory effects of liquiritigenin as a consequence of the inhibition of NF-kappaB-dependent iNOS and proinflammatory cytokines production. *Br. J. Pharmacol.* 154 (1), 165–173. doi:10.1038/bjp.2008.79

Laitinen, L. A., Empey, D. W., Bye, C., Britton, M. G., McDonnell, K., and Hughes, D. T. (1982). A comparison of the bronchodilator action of pseudoephedrine and ephedrine in patients with reversible airway obstruction. *Eur. J. Clin. Pharmacol.* 23 (2), 107–109. doi:10.1007/BF00545963

Liang, G. Y., He, Z. Y., Wu, K. Y., Jin, F. Y., Li, X., and Feng, H. (2007). Studies on factors influencing on ephedrine contents in Maxing Shigan decoction. *Zhongguo Zhong Yao Za Zhi* 32 (24), 2600–2603.

Liao, Y. N., Hu, W. L., Chen, H. J., and Hung, Y. C. (2017). The use of Chinese herbal medicine in the treatment of chronic obstructive pulmonary disease (COPD). *Am. J. Chin. Med.* 45 (2), 225–238. doi:10.1142/S0192415X17500148

Lin, Na, and Gao, X. (1994). Experimental observation on antipyretic effect of rhubarb combined with gypsum on rabbits with fever. *Chin. J. Traditional Chin. Med.* (07), 436–437.

Ling, Y., Zhang, T., Guo, W., Zhu, Z., Tian, J., Cai, C., et al. (2020). Identify clinical factors related to Mycoplasma pneumoniae pneumonia with hypoxia in children. *BMC Infect. Dis.* 20 (1), 534. doi:10.1186/s12879-020-05270-6

Liu, H., Wang, W., and Gao, X. (2020). Comparison of the efficacy of ambroxol hydrochloride and N -acetylcysteine in the treatment of children with bronchopneumonia and their influence on prognosis. *Exp. Ther. Med.* 20 (6), 130. doi:10.3892/etm.2020.9260

Makino, T., Shiraki, Y., and Mizukami, H. (2014). Interaction of gypsum and the rhizome of Anemarrhena asphodeloides plays an important role in anti-allergic effects of byakkokakeishito in mice. *J. Nat. Med.* 68 (3), 505–512. doi:10.1007/s11418-014-0827-y

Mei, F., Xing, X. F., Tang, Q. F., Chen, F. L., Guo, Y., Song, S., et al. (2016). Antipyretic and anti-asthmatic activities of traditional Chinese herb-pairs, Ephedra and Gypsum. *Chin. J. Integr. Med.* 22 (6), 445–450. doi:10.1007/s11655-014-1952-x

Nair, H., Simões, E. A., Rudan, I., Gessner, B. D., Azziz-Baumgartner, E., Zhang, J. S. F., et al. (2013). Global and regional burden of hospital admissions for severe acute lower respiratory infections in young children in 2010: a systematic analysis. *Lancet* 381 (9875), 1380–1390. doi:10.1016/S0140-6736(12)61901-1

Tian, J., Yan, S., Wang, H., Zhang, Y., Zheng, Y., Wu, H., et al. (2020). Hanshiyi Formula, a medicine for Sars-CoV2 infection in China, reduced the proportion of mild and moderate COVID-19 patients turning to severe status: a cohort study. *Pharmacol. Res.* 161, 105127. doi:10.1016/j.phrs.2020.105127

Walker, C. L. F., Rudan, I., Liu, L., Nair, H., Theodoratou, E., Bhutta, Z. A., et al. (2013). Global burden of childhood pneumonia and diarrhoea. *Lancet* 381 (9875), 1405–1416. doi:10.1016/S0140-6736(13)60222-6

Wang, C., Cao, B., Liu, Q. Q., Zou, Z. Q., Liang, Z. A., Gu, L., et al. (2011). Oseltamivir compared with the Chinese traditional therapy maxingshigan-yinqiaosan in the treatment of H1N1 influenza: a randomized trial. *Ann. Intern Med.* 155 (4), 217–225. doi:10.7326/0003-4819-155-4-201108160-00005

Wang, W. B., Li, J. T., Hui, Y., Shi, J., Wang, X. Y., and Yan, S. G. (2022). Combination of pseudoephedrine and emodin ameliorates LPS-induced acute lung injury by regulating macrophage M1/M2 polarization through the VIP/cAMP/PKA pathway. *Chin. Med.* 17 (1), 19. doi:10.1186/s13020-021-00562-8

Wang, Y., Yang, Yu, Xia, B., Sun, L., Wu, Y., and Yang, C. (2008). Effects of gypsum on the firing of pyrogen-treated thermosensitive neurons in PO/AH of cats. *Chin. J. Appl. Physiology* 24 (03), 320–323.

Wang, Y., Zhao, B., Fei, Y., Yin, Q., Zhu, J., Ren, G., et al. (2020b). Ma xing shi gan decoction eliminates PM2.5-induced lung injury by reducing pulmonary cell apoptosis through Akt/mTOR/p70S6K pathway in rats. *Biosci. Rep.* 40 (7). doi:10.1042/BSR20193738

Wang, Y. F., Fei, Y. X., Zhao, B., Yin, Q. Y., Zhu, J. P., Ren, G. H., et al. (2020a). Ma xing shi Gan decoction protects against pm2.5-induced lung injury through suppression of epithelial-to-mesenchymal transition (EMT) and epithelial barrier disruption. *Evid. Based Complement. Altern. Med.* 2020, 7176589. doi:10.1155/2020/7176589

Wang, Z., Fang, K., Wang, G., Guan, X., Pang, Z., Guo, Y., et al. (2019). Protective effect of amygdalin on epithelial-mesenchymal transformation in experimental chronic obstructive pulmonary disease mice. *Phytother. Res.* 33 (3), 808–817. doi:10.1002/ptr.6274

Williams, B. G., Gouws, E., Boschi-Pinto, C., Bryce, J., and Dye, C. (2002). Estimates of world-wide distribution of child deaths from acute respiratory infections. *Lancet Infect. Dis.* 2 (1), 25–32. doi:10.1016/s1473-3099(01)00170-0

Wolkerstorfer, A., Kurz, H., Bachhofner, N., and Szolar, O. H. (2009). Glycyrrhizin inhibits influenza A virus uptake into the cell. *Antivir. Res.* 83 (2), 171–178. doi:10.1016/j.antiviral.2009.04.012

Wu, Z., Kong, X., Zhang, T., Ye, J., Fang, Z., and Yang, X. (2014). Pseudoephedrine/ephedrine shows potent anti-inflammatory activity against TNF-α-mediated acute liver failure induced by lipopolysaccharide/D-galactosamine. *Eur. J. Pharmacol.* 724, 112–121. doi:10.1016/j.ejphar.2013.11.032

Xiao, M., Tian, J., Zhou, Y., Xu, X., Min, X., Lv, Y., et al. (2020). Efficacy of Huoxiang Zhengqi dropping pills and Lianhua Qingwen granules in treatment of COVID-19: a randomized controlled trial. *Pharmacol. Res.* 161, 105126. doi:10.1016/j.phrs.2020.105126

Yang, R., Liu, H., Bai, C., Wang, Y., Zhang, X., Guo, R., et al. (2020). Chemical composition and pharmacological mechanism of qingfei paidu decoction and ma xing shi Gan decoction against coronavirus disease 2019 (COVID-19): *in silico* and experimental study. *Pharmacol. Res.* 157, 104820. doi:10.1016/j.phrs.2020.104820

Ye, J., Ye, H., Wang, M., and Zhao, Y. (2021). Total serum IL-6 and TNF-C levels in children with bronchopneumonia following treatment with methylprednisolone in combination with azithromycin. *Am. J. Transl. Res.* 13 (8), 9458–9464.

Zec, S. L., Selmanovic, K., Andrijic, N. L., Kadic, A., Zecevic, L., and Zunic, L. (2016). Evaluation of drug treatment of bronchopneumonia at the pediatric clinic in sarajevo. *Med. Arch.* 70 (3), 177–181. doi:10.5455/medarh.2016.70.177-181

Zha, L. H., He, L. S., Lian, F. M., Zhen, Z., Ji, H. Y., Xu, L. P., et al. (2015). Clinical strategy for optimal traditional Chinese medicine (TCM) herbal dose selection in disease therapeutics: expert consensus on classic TCM herbal formula dose conversion. *Am. J. Chin. Med.* 43 (8), 1515–1524. doi:10.1142/S0192415X1550086X

Zhang, A., Pan, W., Lv, J., and Wu, H. (2017). Protective effect of amygdalin on LPS-induced acute lung injury by inhibiting NF-κB and NLRP3 signaling pathways. *Inflammation* 40 (3), 745–751. doi:10.1007/s10753-017-0518-4

Zhang, X. L., Ji, W., Ji, Z. H., Ding, Y. F., Zhu, H., Yan, Y. D., et al. (2007). Epidemiological study on respiratory syncytial virus and its bronchopneumonia among children in Suzhou. *Zhonghua Yu Fang. Yi Xue Za Zhi* 41 (5), 371–374.

Zhang, X. M., Lu, A. Z., Yang, H. W., Qian, L. L., Wang, L. B., and Zhang, X. B. (2018). Clinical features of postinfectious bronchiolitis obliterans in children undergoing long-term nebulization treatment. *World J. Pediatr.* 14 (5), 498–503. doi:10.1007/s12519-018-0193-z

Zheng, Y., Shi, C., Han, Y., Li, X., Dong, L., Li, Y., et al. (2022). Efficacy and safety of a Chinese herbal formula Maxing Ganshi Decoction in children with community-acquired pneumonia: a randomized, double-blind, placebo-controlled, multicenter trial. *Front. Pharmacol.* 13, 948831. doi:10.3389/fphar.2022.948831

Zhou, H. (2015). Material basis and mechanism of heat clearing effect of gypsum. *J. traditional Chin. Med.* 30 (06), 860–862.

Zhou, Y., Li, M., Tang, Z., Wang, B., and Zhang, B. (2012). Study on antipyretic and anti-inflammatory effects and mechanisms of traditional Chinese medicine gypsum and its main components. *J. Shaanxi Coll. Traditional Chin. Med.* 35 (05), 74–76.

Zhu, Y., and Liu, X. (2004). Treatment of chronic bronchitis with modified ma xing shi gan tang and er chen tang. *J. Tradit. Chin. Med.* 24 (1), 12–13.

frontiers | Frontiers in Pharmacology

TYPE Original Research
PUBLISHED 03 January 2024
DOI 10.3389/fphar.2023.1309582

OPEN ACCESS

EDITED BY
Boyang Ji,
BioInnovation Institute (BII), Denmark

REVIEWED BY
Xiang Liu,
TriArm Therapeutics Limited, China
Guang Chen,
The University of Hong Kong, Hong Kong SAR, China

*CORRESPONDENCE
Yi-Chun Chen,
alineycc@gmail.com
Ching-Mao Chang,
magicbjp@gmail.com

†These authors have contributed equally to this work and share first authorship

RECEIVED 08 October 2023
ACCEPTED 05 December 2023
PUBLISHED 03 January 2024

CITATION
Chen H-T, Tung C-H, Yu B-H, Chang C-M and Chen Y-C (2024), Renal and survival benefits of seventeen prescribed Chinese herbal medicines against oxidative-inflammatory stress in systemic lupus erythematosus patients with chronic kidney disease: a real-world longitudinal study.
Front. Pharmacol. 14:1309582.
doi: 10.3389/fphar.2023.1309582

Renal and survival benefits of seventeen prescribed Chinese herbal medicines against oxidative-inflammatory stress in systemic lupus erythematosus patients with chronic kidney disease: a real-world longitudinal study

Hsiao-Tien Chen[1†], Chien-Hsueh Tung[2,3†], Ben-Hui Yu[4], Ching-Mao Chang[5,6,7*] and Yi-Chun Chen[3,8*]

[1]Department of Chinese Medicine, Chi Mei Medical Center, Tainan City, Taiwan, [2]Division of Allergy, Immunology and Rheumatology, Department of Internal Medicine, Dalin Tzu Chi Hospital, Buddhist Tzu Chi Medical Foundation, Chiayi, Taiwan, [3]School of Medicine, Tzu Chi University, Hualien, Taiwan, [4]Department of Radiation Oncology, Dalin Tzu Chi Hospital, Buddhist Tzu Chi Medical Foundation, Chiayi, Taiwan, [5]Center for Traditional Medicine, Taipei Veterans General Hospital, Taipei, Taiwan, [6]Institute of Traditional Medicine, National Yang Ming Chiao Tung University, Taipei, Taiwan, [7]School of Medicine, College of Medicine, National Yang Ming Chiao Tung University, Taipei, Taiwan, [8]Division of Nephrology, Department of Internal Medicine, Dalin Tzu Chi Hospital, Buddhist Tzu Chi Medical Foundation, Chiayi, Taiwan

Background: Systemic lupus erythematosus (SLE) significantly links to LN, a type of CKD with high mortality despite modern Western treatments. About 70% of SLE patients develop LN, and 30% advance to end-stage renal disease (ESRD). Concerns about glucocorticoid side effects and LN worsening due to oxidative stress prompt alternative treatment searches. In Taiwan, over 85% of SLE patients opt for complementary methods, especially Chinese herbal medicine (CHM). We pinpointed seventeen CHMs for SLE (PRCHMSLE) with antioxidative and anti-inflammatory properties from national health insurance data (2000–2017). Our primary aim was to assess their impact on renal and survival outcomes in SLE patients progressing to CKD (SLE-CKD), with a secondary focus on the risks of hospitalization and hyperkalemia.

Methods: We established a propensity-matched cohort of 1,188 patients with SLE-CKD, comprising 594 PRCHMSLE users and 594 nonusers. We employed Cox proportional hazards models and restricted mean survival time (RMST) analyses to assess the renal and survival outcomes of PRCHMSLE users. Moreover, we performed pooling and network analyses, specifically focusing on the renal effects linked to PRCHMSLE.

Abbreviations: SLE, systemic lupus erythematosus; LN, lupus nephritis; ESRD, end-stage renal disease; CKD, chronic kidney disease; CHM, Chinese herbal medicine; NHI, National Health Insurance; PRCHMSLE, potentially renoprotective CHMs for systemic lupus erythematosus; LGTD2005; Longitudinal Generation Tracking Database; RMST, restricted mean survival time.

Results: PRCHMSLE use was associated with decreased adjusted hazard ratios for ESRD (0.45; 95% confidence interval, 0.25–0.79, $p = 0.006$), all-cause mortality (0.56; 0.43–0.75, $p < 0.0001$), non-cardiovascular mortality (0.56; 0.42–0.75, $p < 0.0001$), and hospitalization (0.72; 0.52–0.96, $p = 0.009$). Hyperkalemia risk did not increase. Significant differences in RMST were observed: 0.57 years (95% confidence interval, 0.19–0.95, $p = 0.004$) for ESRD, 1.22 years (0.63–1.82, $p < 0.0001$) for all-cause mortality, and 1.21 years (0.62–1.80, $p < 0.0001$) for non-cardiovascular mortality, favoring PRCHMSLE use. Notably renoprotective PRCHMSLE included Gan-Lu-Ying, *Anemarrhena asphodeloides* Bunge [Asparagaceae; Rhizoma Anemarrhenae] (Zhi-Mu), *Rehmannia glutinosa* (Gaertn.) DC. [Orobanchaceae; Radix Rehmanniae] (Sheng-Di-Huang), Jia-Wei-Xiao-Yao-San, and *Paeonia suffruticosa* Andr. [Paeoniaceae; Cortex Moutan] (Mu-Dan-Pi). Network analysis highlighted primary treatment strategies with central components like Liu-Wei-Di-Huang-Wan, *Paeonia suffruticosa* Andr. [Paeoniaceae; Cortex Moutan] (Mu-Dan-Pi), *Anemarrhena asphodeloides* Bunge [Asparagaceae; Rhizoma Anemarrhenae] (Zhi-Mu), *Rehmannia glutinosa* (Gaertn.) DC. [Orobanchaceae; Radix Rehmanniae] (Sheng-Di-Huang), and Zhi-Bai-Di-Huang-Wan.

Conclusion: This work underscores the pronounced renal and survival benefits associated with the seventeen PRCHMSLE in the treatment of SLE-CKD, concurrently mitigating the risks of hospitalization and hyperkalemia. This highlights their potential as alternative treatment options for individuals with this condition.

KEYWORDS

renoprotective Chinese herbal medicines, systemic lupus erythematosus, lupus nephritis, CKD, oxidative-inflammatory stress, ESRD, all-cause mortality, network analysis

1 Introduction

Systemic lupus erythematosus (SLE) is an autoimmune disease characterized by multiorgan inflammation and is a significant cause of lupus nephritis (LN) (Davidson, 2016). An alarming 70% of individuals with SLE suffer from lupus nephritis, and up to 30% of lupus patients progress to ESRD, making it the most severe and frequent manifestation of the disease (Maroz and Segal, 2013). This impact is characterized by the glomerular deposition of immune complexes, which subsequently triggers an inflammatory response (Davidson, 2016). Despite advancements in immunosuppressive therapies, there has not been a significant decline in the progression to ESRD or in mortality rates in recent decades. The prognosis for these patients is grim; those who progress to ESRD have a staggering 26-fold increased risk of mortality (Yap et al., 2012).

Oxidative stress and inflammation are critical factors in the pathogenesis of SLE, notably aggravating LN by initiating immune complex deposition in the glomeruli, promoting inflammatory cell recruitment, and causing progressive fibrosis (Bona et al., 2020; Justiz Vaillant et al., 2023). Glucocorticoids inhibit many of the initial events in the inflammatory response, significantly improving the prognosis for those with LN (Coutinho and Chapman, 2011). However, both short-term high doses and cumulative exposure to glucocorticoids can lead to undesirable side effects, including cardiovascular events, peptic ulcers, sleep disorders, weight gain, and osteoporosis (Mejia-Vilet and Ayoub, 2021). As a result, a recent cross-sectional study revealed that over 85% of Taiwanese patients with SLE regularly employ complementary therapies (Lu et al., 2022).

Chinese herbal medicine (CHM) is a prominent complementary medicinal system worldwide, with its clinical practices dating back thousands of years (Liu et al., 2022). Previous research has shown reduced risks of ESRD and overall mortality in patients with advanced chronic kidney disease (CKD) (Chen et al., 2022) and advanced diabetic kidney disease (Guo et al., 2021). There are also reports of decreased risks of overall mortality (Ma et al., 2016), LN (Chang et al., 2017), and cardiovascular disease (Yu and Hsieh, 2021) in SLE patients using CHM. Evidence suggests that seventeen potentially renoprotective CHMs for SLE (PRCHMSLE), which counteract oxidative-inflammatory stress collectively, are acknowledged as complementary treatment options for SLE (Huang et al., 2016; Jiang et al., 2020; Wang et al., 2021). These 17 PRCHMSLE are *Rehmannia glutinosa* (Gaertn.) DC. [Orobanchaceae; Radix Rehmanniae] (Sheng-Di-Huang), *Anemarrhena asphodeloides* Bunge [Asparagaceae; Rhizoma Anemarrhenae (Zhi-Mu), *Paeonia lactiflora* Pall. [Paeoniaceae; Radix Paeoniae Alba] (Bai Shao), *Paeonia suffruticosa* Andr. [Paeoniaceae; Cortex Moutan (Mu-Dan-Pi), *Salvia miltiorrhiza* Bge. [Lamiaceae; Radix Salviae Miltiorrhizae (Dan-Shan), *Paeonia lactiflora* Pall. var. rubra [Paeoniaceae; Radix Paeoniae Rubra] (Chi-Shao), *Lithospermum erythrorhizon* Siebold & Zucc. [Boraginaceae; Radix Lithospermi] (Zi-Cao), *Artemisia annua* L. [Asteraceae; Herba Artemisiae Annuae (Qing-Hao), *Hedyotis diffusa* Willd. [Rubiaceae; Herba Hedyotis] (Bai-Hua-She-She-Cao), *Scutellaria barbata* D. Don [Lamiaceae; Herba Scutellariae Barbatae (Ban-Zhi-Lian), Zhi-Bai-Di-Huang-Wan, Liu-Wei-Di-Huang-Wan, Gan-Lu-Ying, Qin-Jiao-Bie-Jia-Tang, Jia-Wei-Xiao-Yao-San, Yin-Qiao-San, and Gui-Zhi-Shao-Yao-ZhiMu-Tang (Supplementary Table S1). However, there exists a gap in large-scale evidence assessing the effects of these 17 PRCHMSLE on ESRD and mortality outcomes, as well as their pooling effect and a network core pattern analysis on ESRD outcomes in SLE patients progressing to CKD. Given that Taiwan's National Health Insurance

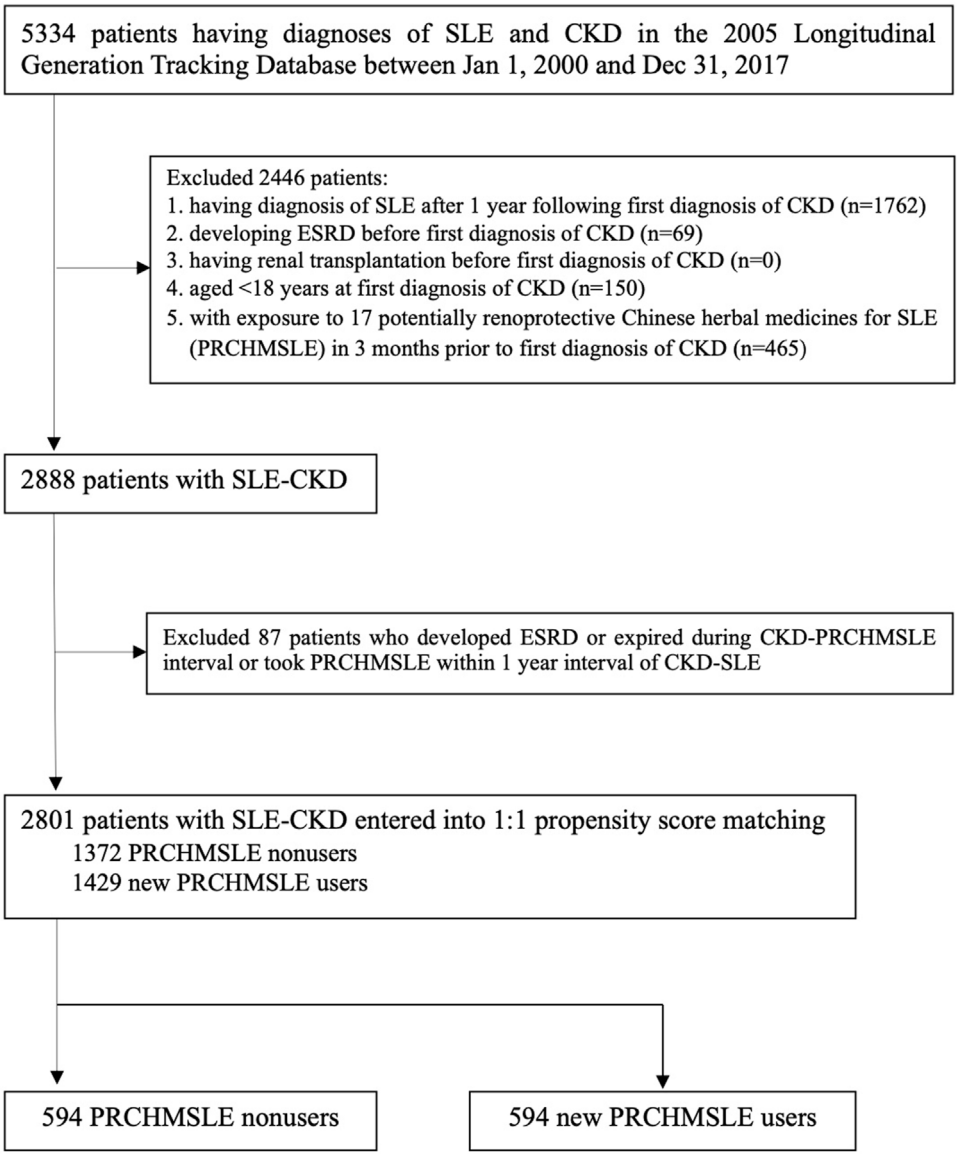

FIGURE 1
Flowchart for selecting *systemic lupus erythematosus* (SLE) patients progressing to chronic kidney disease (CKD).

(NHI) covers prescribed CHMs that are free from aristolochic acid (Chen et al., 2022), we utilized NHI longitudinal claims data from 2000 to 2017 to bridge this knowledge gap.

2 Materials and methods

2.1 Study design and data source

The retrospective cohort study examined 2 million de-identified claims from Taiwan's 2005 Longitudinal Generation Tracking Database (LGTD 2005) spanning the years 2000–2017. Given the nature of the data, informed consent was not required, and the study received an exemption from a full review by the Institutional Review Board of the Dalin Tzu Chi Hospital (B10804001). The LGTD2005 was randomly selected from the entirety of beneficiaries under Taiwan's NHI program. Further details about Taiwan's LGTD2005 and the NHI program are discussed in our previous research (Chen et al., 2015a; Chen et al., 2022; Chen et al., 2023). The LGTD2005 employs the ICD-9-CM and, starting in 2016, the ICD-10-CM diagnostic codes for disease identification. While it provides extensive data on medication and herbal treatments, it does not include information on laboratory results or lifestyle factors.

2.2 Study population (SLE patients progressing to CKD [patients with SLE-CKD])

The study cohort comprised 5,334 patients diagnosed with both SLE and CKD from 1 January 2000, to 31 December 2017 (Figure 1). We excluded patients under 18 years at the time of their initial CKD diagnosis, patients diagnosed with SLE (based on ICD 9/10-CM

codes) more than a year after their first CKD diagnosis, patients who developed ESRD or underwent renal transplantation before their initial CKD diagnosis, and patients who were exposed to the 17 PRCHMSLE within 3 months prior to their first CKD diagnosis. After these exclusions, 2888 SLE patients progressing to CKD (SLE-CKD) were enrolled from 2000 to 2017.

2.3 Exposure to seventeen potentially renoprotective CHMs for SLE (PRCHMSLE)

SLE patients who received at least one of any 17 PRCHMSLE (Supplementary Table S1) after CKD diagnosis during the study period were categorized as PRCHMSLE users, aligning with the user definition employed in previous studies (Chang et al., 2017; Chen et al., 2022). The remaining SLE patients who never used any 17 PRCHMSLE after CKD diagnosis during the study period were defined as nonusers. Considering the exposure to the 17 PRCHMSLE post the first CKD diagnosis, and excluding patients who developed ESRD, those who passed away during the CKD-PRCHMSLE interval, and those who began using PRCHMSLE within a year of the CKD-SLE diagnosis, we identified 2,801 patients with SLE-CKD from 2000 to 2017. Of this cohort, 1,429 (51%) were new PRCHMSLE users, and 1,372 (49%) were nonusers.

2.4 Covariates

We assessed several variables, including age, sex, Charlson comorbidity index (an indicator of overall disease burden), and frequency of medical visits (to address potential detection bias). Baseline comorbidities considered were diabetes (defined by ICD-9/10- CM codes or the use of antihyperglycemic drugs), hypertension (defined by ICD-9/10-CM codes or antihypertensives), hyperlipidemia (defined by ICD-9/10-CM codes or antilipidemic drugs) (Chen et al., 2022), rheumatoid arthritis, Sjögren's syndrome, and Raynaud's disease (all defined by ICD-9/10-CM codes) (Chang et al., 2017). Additionally, we evaluated the use of three potentially confounding medications—non-steroidal anti-inflammatory drugs, steroids (including prednisolone and methylprednisolone), and other medications apart from steroids (such as cyclophosphamide, azathioprine, hydroxychloroquine, and mycophenolate mofetil) (Chang et al., 2017)—within the year prior to the index date.

2.5 Propensity score matching

Propensity score method was employed to mitigate confounding related to the indication of PRCHMSLE utilization. The propensity score, indicating the likelihood of using PRCHMSLE, was calculated using the logistic regression that was built on all covariates (age per year, sex, comorbidities, Charlson comorbidity index, number of medical visits, and confounding drugs) to adjust for the baseline differences between PRCHMSLE users and nonusers. Propensity score matching was performed using the nearest-neighbor approach without replacement and employed a caliper value of 0.0001 to ensure precision throughout the matching process (Chen et al., 2022). For each PRCHMSLE user, a propensity score-matched nonuser was chosen. To mitigate immortal bias (Chen et al., 2022; Chen et al., 2023), it was verified that each matched nonuser was alive when PRCHMSLE usage began. The index date for PRCHMSLE users was marked as the exact day when PRCHMSLE therapy was initiated, confirming that PRCHMSLE users had lived from the start of CKD up to this index date. For nonusers, the index date was aligned to coincide with the exact day of PRCHMSLE initiation by the user.

2.6 Study outcomes and follow-up

The primary outcomes of this study were ESRD, all-cause mortality, cardiovascular mortality, and non-cardiovascular mortality. Participants were tracked from their index date until the event of ESRD or other censoring occurrences, such as death or the study's conclusion on 31 December 2017, whichever was earlier. ESRD was identified based on the acquisition of a catastrophic illness certificate for long-term dialysis (Chen et al., 2015a; Chen et al., 2022; Chen et al., 2023). Mortality was ascertained by a patient's withdrawal from the NHI program (Chen et al., 2015a; Chen et al., 2022; Chen et al., 2023). In the mortality outcome analysis, patients were consistently observed up to their time of death. Cardiovascular mortality included deaths attributed to primary diagnoses such as coronary heart disease, stroke, peripheral vascular disease, and heart failure, as classified by ICD 9/10-CM codes (Yu et al., 2022). If ESRD events occurred earlier during the follow-up, they were not treated as censoring points (Huang et al., 2022). The secondary outcomes investigated in this study were concentrated on assessing the risks of hospitalization and hyperkalemia. Hospitalization rates were considered as a proxy for glucocorticoid side effects (Peterson et al., 2021), while the presence of both SLE (Lee et al., 1988) and CKD (Chen et al., 2022) heightened the risk of hyperkalemia. Incidents of hospitalization and hyperkalemia were monitored throughout the study period, with the latter being identified through the presence of ICD-9/10-CM codes for hyperkalemia or the utilization of potassium-lowering agents (Chen et al., 2022).

2.7 Pooling effects of 17 PRCHMSLE

We evaluated the pooling effects of the 17 PRCHMSLE on ESRD occurrence and identified the top five agents demonstrating the most robust renoprotective effects.

2.8 Network analysis

To identify the primary patterns of CHM use in treating SLE, we utilized the open-source tool NodeXL (http://nodexl.codeplex.com/), as detailed in our previous research (Chang et al., 2015). Every selected CHM combination was incorporated into this network analysis. Within the network diagram, relationships between a CHM and its associated prescription were illustrated using lines of varying thickness, from 1 to 5, with thicker lines representing more common prescription patterns. This method effectively emphasized the dominant trends in the prescription of these renoprotective CHMs throughout our study.

TABLE 1 Baseline characteristics of study cohorts by use of 17 potentially renoprotective Chinese herbal medicines for SLE (PRCHMSLE) in patients with SLE-CKD.

Variable	Propensity-matched patients with SLE-CKD		
	Users (n = 594)	Nonusers (n = 594)	SMD
Sex, *n* (%)			0.018
Men	102 (17.2)	106 (17.9)	
Women	492 (82.8)	488 (82.2)	
Age (year), *n* (%)			0.021
≤35	155 (26.1)	154 (25.9)	
35–50	176 (29.6)	177 (29.8)	
50–65	154 (25.9)	151 (25.4)	
>65	109 (18.4)	112 (18.9)	
Mean (SD)	48.3 (16.9)	48.7 (17.7)	
Comorbidities, *n* (%)			
Diabetes	67 (11.3)	61 (10.3)	0.033
Hypertension	295 (49.7)	288 (48.5)	0.024
Hyperlipidemia	93 (15.7)	86 (14.5)	0.033
Rheumatoid arthritis	26 (4.4)	21 (3.5)	0.043
Sjögren's syndrome	19 (3.2)	25 (4.2)	0.053
Raynaud's disease	6 (1.0)	5 (0.8)	0.018
Charlson comorbidity index, *n* (%)			0.017
≤1	398 (67.0))	405 (68.1)	
1–2	110 (18.5)	108 (18.2)	
2–4	58 (9.8)	54 (9.1)	
≥4	28 (4.7)	27 (4.6)	
Mean (±SD)	1.23 (1.2)	1.21 (1.2)	
No. of medical visits, *n* (%)			0.115
≤12	190 (32.0)	201 (33.8)	
12–24	181 (30.5)	185 (31.2)	
>24	223 (37.5)	208 (35.0)	
Mean (SD)	23.3 (18.6)	21.3 (16.6)	
Confounding drugs, *n* (%)			
NSAID	484 (81.5)	481 (81.0)	0.013
Steroids[†]	43 (7.2)	39 (6.6)	0.026
Drugs other than steroids[††]	15 (2.5)	13 (2.2)	0.022

Abbreviations: SLE, systemic lupus erythematosus; CKD, chronic kidney disease; SD, standard deviation; NSAID, non-steroidal anti-inflammatory drug; SMD, standardized mean difference.
[†]Include prednisolone and methylprednisolone.
[††]Include cyclophosphamide, azathioprine, hydroxycholorquine, and mycopenolate mofetil.

2.9 Statistical analyses

Disparities in baseline characteristics between PRCHMSLE users and nonusers were assessed using the standardized mean difference approach. A value of <0.1 signified minimal distinction between the two groups after propensity score matching (Chen et al., 2022). Death prior to ESRD occurrence was considered a competing risk event (Chen et al., 2015a). For the cumulative incidence of ESRD, the calculation and comparison in data with competing risk were conducted using modified Kaplan-Meier and Gray's methods (Chen et al., 2015a). In analyzing all-cause mortality, the Kaplan-Meier method was employed. We assessed differences in the complete time-to-event distributions

TABLE 2 15-year-restricted mean survival time (RMST) and Cox proportional hazards model analyses on study outcomes among propensity score–matched PRCHMSLE users and PRCHMSLE nonusers.

Outcomes	Events (%)		Estimated event rate (events/ 1,000 person-years)		RMST (95% CI), tau = 15 years					
	Users	Nonusers	Users	Nonusers	Users	Nonusers	Difference, year (95% CI)	*p-value*	Estimated aHR (95% CI)	*p-value*
ESRD	17 (2.9)	33 (5.6)	3.9	10.6	14.57 (14.39, 14.78)	13.99 (13.69, 14.34)	0.57 (0.19, 0.95)	0.004	0.45 (0.25, 0.79)	0.006
All-cause mortality	92 (15.5)	115 (19.4)	20.7	34.1	12.99 (12.65, 13.38)	11.8 (11.37, 12.31)	1.22 (0.63, 1.82)	<0.0001	0.56 (0.43, 0.75)	<0.0001
Cardiovascular mortality	2 (0.34)	3 (0.51)	0.45	0.89	14.9 (14.8, 15.1)	14.9 (14.8, 15.0)	0.02 (−0.10, 0.14)	0.74	0.69 (0.11, 4.27)	0.69
Non-cardiovascular mortality	90 (15.2)	112 (18.9)	20.3	33.2	13.0 (12.6, 13.4)	11.9 (11.4, 12.4)	1.21 (0.62, 1.80)	<0.0001	0.56 (0.42, 0.75)	<0.0001

Abbreviations: PRCHMSLE, potentially renoprotective Chinese herbal medicines for systemic lupus erythematosus; ESRD, end-stage renal disease; aHR, adjusted hazard ratio; CI, confidence interval.
Adjusted for all covariates (age per year, sex, comorbidities, number of medical visits, Charlson comorbidity index, confounding drugs), and competing risk for ESRD.

between the study groups by utilizing a modified log-rank test for ESRD and a log-rank test for all-cause mortality.

We computed the incidence rates per 1,000 person-years for the study outcomes in both groups. The assumption of proportional hazards was confirmed using a log (-log (survival)) plot against the log of survival time, which demonstrated no violations. The primary and secondary study outcomes were assessed using the Cox proportional hazard model. By comparing PRCHMSLE users with nonusers, we estimated adjusted hazard ratios (aHRs) with their associated 95% confidence intervals (CIs). These estimates considered all covariates mentioned in Table 1 and considered competing mortality when evaluating the risk of ESRD (Chen et al., 2015a).

Complementary restricted mean survival time (RMST) analysis was utilized specifically to evaluate the primary study outcomes. RMST, defining the area beneath the survival curve up to a given (restricted) time, was employed as an alternative to the conventional Cox analysis (Perego et al., 2020). The difference in RMST quantified the delay in achieving a specific outcome during a given interval and depicted the disparity between the areas under the survival curves for the intervention and control groups. Hence, the RMST difference was instrumental in assessing the clinical significance of an advantage, separate from the relative treatment effects highlighted by HRs. We gauged the RMST differences by contrasting the areas under the survival curves between PRCHMSLE users and nonusers. A positive RMST difference was in favor of PRCHMSLE treatment, indicating an average delay in achieving the study outcomes among the two groups. Additionally, we reviewed the 15-year RMST difference, along with its associated 95% CI, for the study outcomes between the two groups. This juxtaposition enriched the insights beyond the aHR evaluations and facilitated a holistic comprehension of the results.

We also employed Poisson regression to estimate the adjusted incident rate ratio of hyperkalemia associated with PRCHMSLE use. Recurrent episodes of hyperkalemia were classified as a single prolonged event when they transpired within 28 days of each other, whereas episodes occurring at least 28 days apart were treated as distinct events (Chen et al., 2022).

Statistical analyses were conducted using SAS software (version 9.4; SAS Institute, Inc., Cary, N.C., USA). A statistical significance was determined if the 95% CI for aHRs did not encompass 1, or when the 95% CI for the difference in RMST did not contain 0. A two-tailed *p*-value less than 0.05 was considered statistically significant.

2.10 Sensitivity analyses

To enhance the reliability of our primary findings, we carried out three sensitivity analyses. First, the PRCHMSLE-usage group was redefined based on cumulative usage exceeding 30 and 60 days. Second, the risk assessment for study outcomes was reassessed by excluding CKD patients who either passed away or advanced to ESRD within 30, 60, or 90 days post the index date. Lastly, subgroup analyses were conducted considering baseline characteristics.

3 Results

3.1 Baseline characteristics

After propensity score matching, a balanced distribution of all baseline characteristics was observed between 594 PRCHMSLE users and 594 nonusers in the SLE-CKD patient group (Table 1; Supplementary Figure S1). This resulted in a discernible differentiation between the matched cohorts, evidenced by a c-index of 0.65 and a Hosmer–Lemeshow test *p*-value of 0.39, suggesting a satisfactory model fit.

3.2 Association between 17 PRCHMSLE and the primary study outcomes

Among patients with SLE-CKD, 50 individuals (4.2%) progressed to ESRD, while 207 (17.4%) experienced all-cause deaths, with 5 attributed to cardiovascular mortality and 202 to non-cardiovascular mortality (Table 2). The 15-year cumulative incidences of ESRD (p = 0.0032) in the presence of competing mortality and all-cause mortality (p = 0.0005) were markedly lower for PRCHMSLE users compared to nonusers (Figure 2). After adjusting for all covariates, PRCHMSLE use in patients with SLE-CKD was significantly correlated with decreased risks of ESRD (aHR: 0.45; 95% CI: 0.25–0.79, p = 0.006), all-cause mortality (aHR: 0.56; 95% CI: 0.43–0.75, p < 0.0001), cardiovascular mortality (aHR: 0.69; 95% CI: 0.11–4.27, p = 0.69), and non-cardiovascular mortality (aHR: 0.56; 95% CI: 0.42–0.75, p < 0.0001). Over a 15-year span, compared to nonuse, PRCHMSLE use was linked to a delay of 0.57 (95% CI: 0.19–0.95, p = 0.004), 1.22 years (95% CI: 0.63–1.82, p < 0.0001), 0.02 years (95% CI: 0.10–0.14, p = 0.74), and 1.21 years (95% CI: 0.62–1.80, p < 0.0001) in the onset of ESRD, all-cause mortality, cardiovascular mortality, and non-cardiovascular mortality, respectively. Considering a type I error α of 0.05, an event rate of 0.034 per year for the nonuser group, a median follow-up of 5.4 years, a censoring rate of 0.96, and a user-to-nonuser ratio of 1:1, we would need 490 participants in both user and non-user groups to achieve a power (1-β) of 0.9, sufficient to detect a 50% shift in the hazard ratio. Given our sample of 594 individuals in each category and an aHR of 0.45, our study displays a test power exceeding 0.9.

3.3 Association between 17 PRCHMSLE and the secondary study outcomes

PRCHMSLE use was associated with lower risks of hospitalization (aHR: 0.72; 95% CI: 0.56–1.92, p = 0.009) (Supplementary Table S5). Moreover, PRCHMSLE use was not associated with an elevated risk of hyperkalemia (adjusted incidence rate ratio: 0.74; 95% CI: 0.49–1.10, p = 0.13) (Supplementary Table S6).

3.4 Top five renoprotective effects among the 17 PRCHMSLE

Utilizing both the Cox model (Figure 3A) and RMST (Figure 3B) analyses, the top five PRCHMSLE formulas that exhibited the most pronounced renoprotective effects through pooling were Gan-Lu-Ying, *Anemarrhena asphodeloides* Bunge [Asparagaceae; Rhizoma Anemarrhenae] (Zhi-Mu), *Rehmannia glutinosa* (Gaertn.) DC. [Orobanchaceae; Radix Rehmanniae] (Sheng-Di-Huang), Jia-Wei-Xiao-Yao-San, and *Paeonia suffruticosa* Andr. [Paeoniaceae; Cortex Moutan] (Mu-Dan-Pi).

3.5 Network analysis

The network analysis (Figure 4) revealed the dominant patterns of both formulas and individual herbs used in the treatment of SLE.

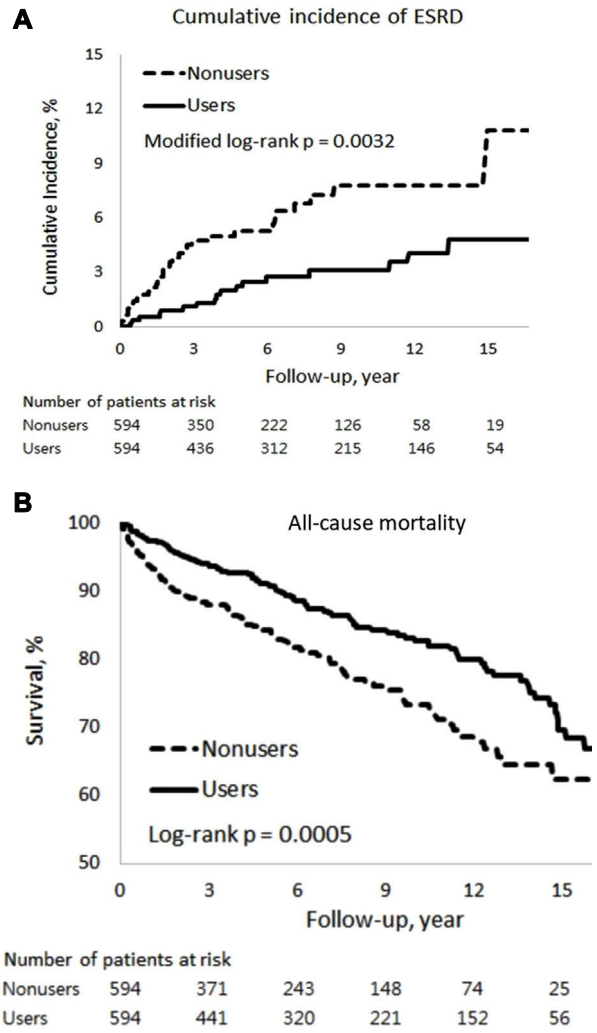

FIGURE 2
Cumulative incidences of **(A)** end-stage renal disease (ESRD) and **(B)** all-cause mortality among PRCHMSLE users and nonusers.

The core patterns comprised Liu-Wei-Di-Huang-Wan, *Paeonia suffruticosa* Andr. [Paeoniaceae; Cortex Moutan] (Mu-Dan-Pi), *Anemarrhena asphodeloides* Bunge [Asparagaceae; Rhizoma Anemarrhenae] (Zhi-Mu), *Rehmannia glutinosa* (Gaertn.) DC. [Orobanchaceae; Radix Rehmanniae] (Sheng-Di-Huang), and Zhi-Bai-Di-Huang-Wan.

3.6 Sensitivity analyses

We conducted three sensitivity analyses to verify the robustness of our results. In the subgroup analyses of patients with SLE-CKD, the outcomes for ESRD and all-cause mortality were predominantly favorable, and this trend persisted across most subgroups in both the Cox and RMST analyses, with a preference towards PRCHMSLE use over nonuse (Supplementary Table S2). When excluding patients with SLE-CKD who either died or developed ESRD within 30, 60, or 90 days post the index date, these associations remained consistent (Supplementary Table S3).

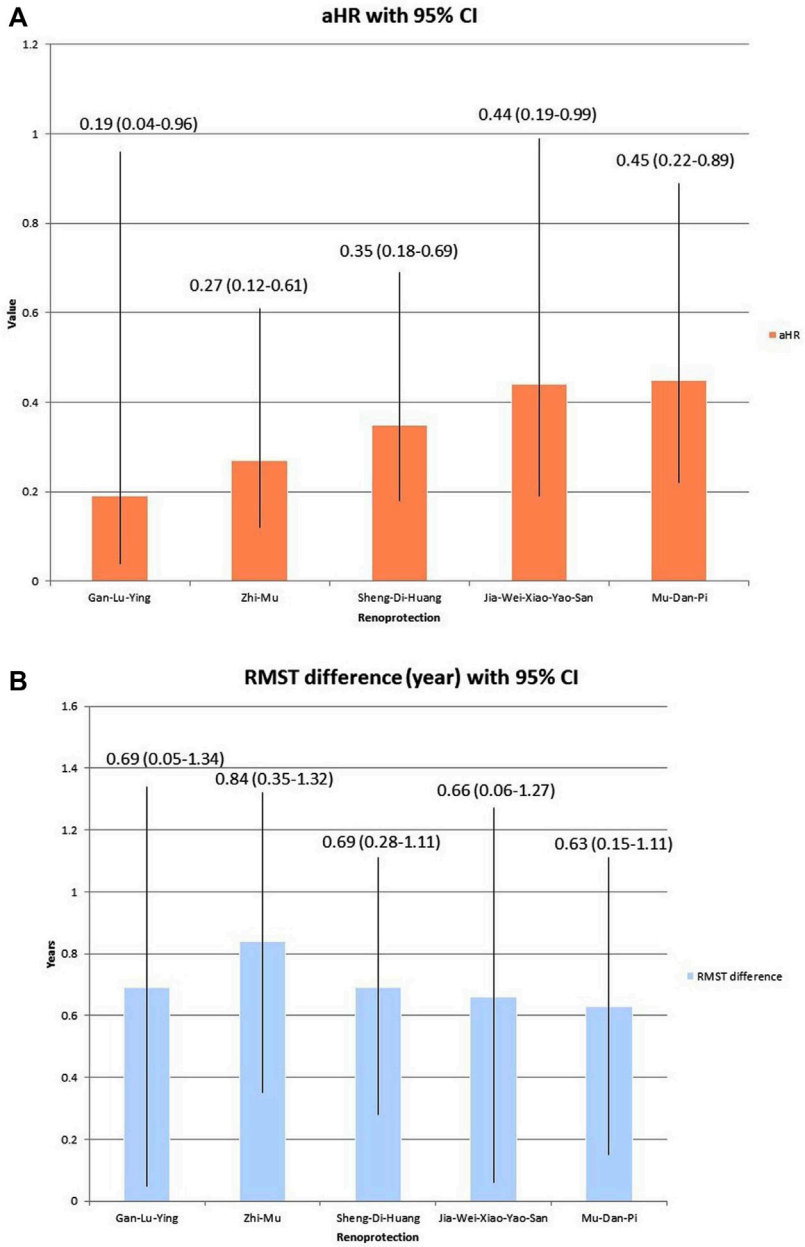

FIGURE 3
Top five renoprotection in the pooling effect of 17 potentially renoprotective Chinese herbal medicines for SLE (PRCHMSLE), analyzed through **(A)** adjusted hazard ratios (aHRs) of end-stage renal disease and **(B)** restricted mean survival time (RMST) differences in end-stage renal disease. Abbreviation: CI, confidence interval.

The relationship between PRCHMSLE use and the decreased risks of ESRD and all-cause mortality persisted regardless of the varying definitions of PRCHMSLE use among patients with SLE-CKD (Supplementary Table S4).

4 Discussion

This study is the first to highlight the main renal and survival (especially, non-cardiovascular survival) benefits of using 17 PRCHMSLE in patients with SLE-CKD. Moreover, PRCHMSLE use not only resulted in the reduction of hospitalization risk but also demonstrated no elevated likelihood of hyperkalemia. These results build on prior research indicating renal and survival advantages (Chang et al., 2017) and remain consistent across multiple subgroups, further solidifying their validity through extensive sensitivity analyses. The findings suggest the targeting of various pathways associated with inflammation and oxidative stress for immune modulation in SLE. Notably, the top five treatments offering the most renal protection were Gan-Lu-Ying, *Anemarrhena asphodeloides* Bunge [Asparagaceae; Rhizoma Anemarrhenae] (Zhi-Mu), *Rehmannia*

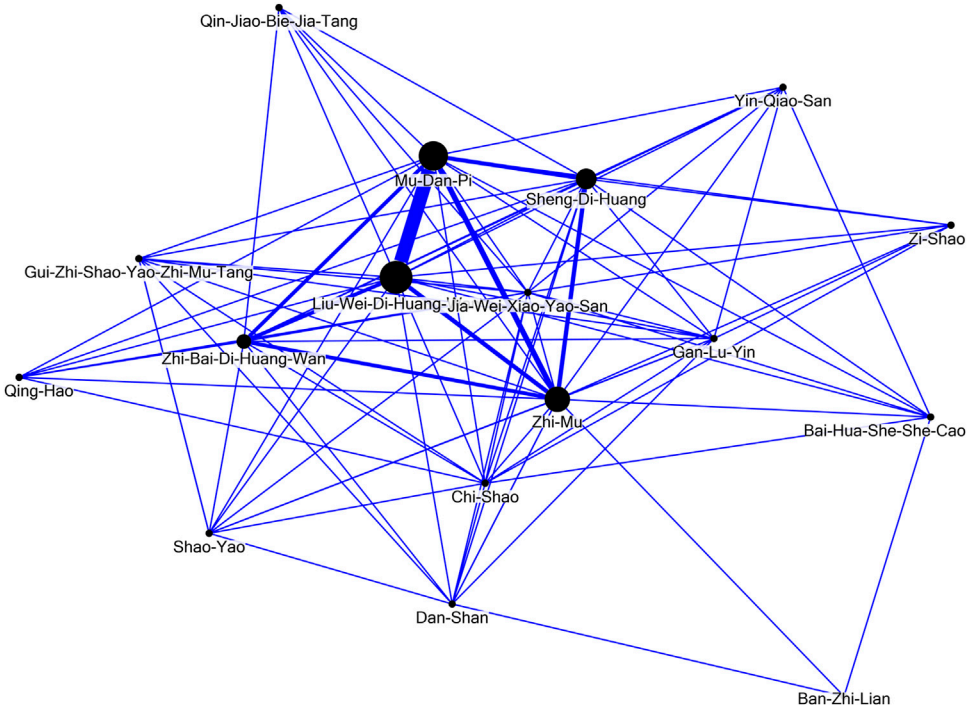

FIGURE 4
Network analysis of the seventeen potentially renoprotective Chinese herbal medicines for *systemic lupus erythematosus* (PRCHMSLE).

glutinosa (Gaertn.) DC. [Orobanchaceae; Radix Rehmanniae] (Sheng-Di-Huang), Jia-Wei-Xiao-Yao-San, and *Paeonia suffruticosa* Andr. [Paeoniaceae; Cortex Moutan] (Mu-Dan-Pi). Furthermore, this research introduces a groundbreaking discovery: a core prescription pattern, identified through network analysis that features Liu-Wei-Di-Huang-Wan, *Paeonia suffruticosa* Andr. [Paeoniaceae; Cortex Moutan] (Mu-Dan-Pi), *Anemarrhena asphodeloides* Bunge [Asparagaceae; Rhizoma Anemarrhenae] (Zhi-Mu), *Rehmannia glutinosa* (Gaertn.) DC. [Orobanchaceae; Radix Rehmanniae] (Sheng-Di-Huang), and Zhi-Bai-Di-Huang-Wan.

SLE is a complex disease affecting multiple bodily systems, including renal, cardiovascular, and pulmonary functions (Vymetal et al., 2016). Recent cohort studies using Taiwan's NHI claims data have spotlighted potential benefits of CHMs in SLE management, indicating decreased risks of LN (Chang et al., 2017), mortality (Ma et al., 2016), cardiovascular disease (Yu and Hsieh, 2021), pneumonia (Wang et al., 2023), and hospitalization (Ma et al., 2023). Significantly, LN is a chief factor in SLE-related deaths (Sciascia et al., 2017). A notable study by Chang et al. (Chang et al., 2017) emphasized that combining conventional and herbal medicine therapies reduced the risk of LN among Taiwanese SLE patients. Ma et al. (Ma et al., 2016) pinpointed various CHM formulas, such as Zhi-Bo-Di-Huang-Wan, Jia-Wei-Xiao-Yao-San, and Liu-Wei-Di-Huang-Wan, which markedly improved patient survival. However, our research opinions distinguish themselves from prior studies in several key aspects. Firstly, earlier investigations utilizing NHI claims data typically juxtaposed overall CHM users with non-users, rather than specifically delving into the 17 PRCHMSLE identified as suitable for SLE treatment. Secondly, all preceding studies extracted the top ten medications used post CHM application from the NHI claims data and subsequently examined each drug's mechanism within the context of SLE. Notably, they did not independently analyze CHMs known to provide protection against renal implications and SLE, marking a significant point of departure. Thirdly, no previous studies undertook a pooling effect or network analysis on the 17 PRCHMSLE deemed appropriate for SLE, underscoring a unique aspect of our research approach. Fourthly, this study represents a pioneering effort in evaluating the safety, particularly the risk of hyperkalemia, in patients with SLE-CKD undergoing treatment with CHMs, with a specific focus on PRCHMSLE. Fifthly, this study represents the inaugural application of RMST analysis in research involving CHM and SLE, offering valuable insights and more interpretable results than hazard ratios for assessing the clinical efficacy of PRCHMSLE. Our findings indicated that PRCHMSLE use was associated with a postponement of ESRD by 0.57 years, a delay in mortality by 1.22 years, and a deferment of non-cardiovascular events by 1.21 years over a 15-year period.

In line with previous research (Ma et al., 2016; Chen et al., 2022; Chen et al., 2023; Ma et al., 2023), our findings indicated that patients receiving the 17 PRCHMSLE may experience a reduction in all-cause mortality, a lower incidence of ESRD, fewer hospital admissions, and no potential for an increase in the risk of hyperkalemia. We also identified a lower risk of non-cardiovascular mortality in patients with SLE-CKD using PRCHMSLE compared to nonusers, mirroring findings from a previous NHI-based cohort study that indicated a reduced risk of pneumonia in patients with SLE using CHMs compared to nonusers (Wang et al., 2023). However, our results did not demonstrate a significant reduction in the risk of

cardiovascular mortality in patients with SLE-CKD using PRCHMSLE. This contrasted with a previous NHI-based cohort study (Yu and Hsieh, 2021) that suggested a lower cardiovascular disease risk in patients with SLE who were on CHM. The differences in event rates observed in distinct study populations, such as those with SLE (Yu and Hsieh, 2021) *versus* SLE-CKD in our study, might contribute to the observed disparity.

Historically, research utilizing Taiwan's NHI claims data primarily addressed prescription frequencies for a range of medical conditions. Yet, this data might not truly mirror underlying prescription patterns or therapeutic objectives, potentially causing misconceptions in future research and clinical trials. Using network analysis alongside data mining offers a deeper understanding of the clinical reasoning and prevalent agreement among traditional Chinese medicine experts. This underlines the need to weave evidence-based methods into upcoming CHM research. Our prior study (Chang et al., 2017) employed network analysis to identify main CHM prescription patterns for SLE, aligning with frequently prescribed medicines. In the present study, network analysis was employed to unravel the predominant prescription patterns for the treatment of patients with SLE. This methodology was tailored to evaluate the selected dual-drug combinations. In this context, connections between CHM and their co-prescribed counterparts were symbolized, with a denser line width denoting more frequent prescription affiliations. Within the 17 PRCHMSLE, network core pattern analysis identified the top five with renoprotective qualities as Gan-Lu-Ying, *Anemarrhena asphodeloides* Bunge [Asparagaceae; Rhizoma Anemarrhenae] (Zhi-Mu), *Rehmannia glutinosa* (Gaertn.) DC. [Orobanchaceae; Radix Rehmanniae] (Sheng-Di-Huang), Jia-Wei-Xiao-Yao-San, and *Paeonia suffruticosa* Andr. [Paeoniaceae; Cortex Moutan] (Mu-Dan-Pi). These quintessential formulae and individual herbs, recurrently prescribed in our study, exhibit antioxidant, anti-inflammatory, and immune-modulatory properties (Ma et al., 2016; Zhao et al., 2016; Zhuang et al., 2022).

Managing SLE and CKD necessitates a holistic approach targeting autoimmune responses, oxidative stress, inflammation, and fibrosis (Davidson, 2016; Bona et al., 2020). These 17 PRCHMSLE collectively display antioxidant, anti-inflammatory, and antifibrotic characteristics that combat renal failure (Huang et al., 2016; Jiang et al., 2020; Wang et al., 2021). Gan-Lu-Yin, historically revered in ancient Asia, is recognized for treating oral inflammations such as periodontitis, stomatitis, and glossodynia (Inagaki et al., 2021). In terms of autoimmunity, Gan-Lu-Yin has shown notable protective effects on SLE patient survival (Ma et al., 2016). It acts as an intervention, curbing T cell activation and reducing TH responses, as seen in Sjögren's syndrome (Lee et al., 2021). Furthermore, it deters TNF-α expression in human oral cancer cells through the ERK and NF-κB pathways (Yang et al., 2016). These insights infer that Gan-Lu-Yin extracts bear anti-inflammatory qualities and act as inhibitors of tissue degradation. Studies indicate that *Anemarrhena asphodeloides* Bunge [Asparagaceae; Rhizoma Anemarrhenae] (Zhi-Mu) derivatives exhibit a plethora of pharmacological activities, encompassing antioxidation (Zhao et al., 2016), anti-inflammatory responses (Liu et al., 2023), antidiabetic properties (Yuan et al., 2015), and immune modulation (Zhang et al., 2020). *Rehmannia glutinosa* (Gaertn.) DC. [Orobanchaceae; Radix Rehmannia (Sheng-Di-Huang), esteemed for its capacity to purge pathogenic heat from blood and enrich Yin per Chinese medical doctrine (Zhang et al., 2008), is prevalent in many SLE prescriptions like Liu-Wei-Di-Huang-Wan and Zhi-Bai-Di-Huang-Wan (Ma et al., 2016; Chang et al., 2017). Its primary active element has proven to activate the Nrf2/Keap1 route and suppress pro-inflammatory factor expression, thus assuming dual roles as anti-inflammatory and antioxidant agents (Ren et al., 2023). Sheng-Di-Huang's (*Rehmannia glutinosa* (Gaertn.) DC. [Orobanchaceae; Radix Rehmannia) therapeutic facets may be rooted in its anti-inflammatory and immunomodulatory effects, likely derived from its multifaceted composition engaging various targets and channels (Wang et al., 2022; Zhuang et al., 2022). *Paeonia suffruticosa* Andr. [Paeoniaceae; Cortex Mouta (Mu-Dan-Pi) extracts have demonstrated inhibitory influences on NF-κB and IRF reporters, along with curtailing downstream cytokine production, behaving as dose-regulated immunomodulators (Chen et al., 2020). Moreover, they offer antioxidant potency and present anti-inflammatory properties (Li et al., 2018). *Paeonia suffruticosa* Andr. [Paeoniaceae; Cortex Mouta (Mu-Dan-Pi) is integral to Jia-Wei-Xiao-Yao-San, a commonly prescribed formula in Taiwan. It is notable that Jia-Wei-Xiao-Yao-San also features prominently in Taiwan's NHI claims data, largely because of its broad therapeutic applications for ailments like sleep disorders and depression (Chen et al., 2015b)—ailments frequently concurrent with SLE. This concoction, classified under harmonizing formula prescription patterns, is acknowledged for its renoprotective traits in kidney diseases (Lin et al., 2021). Additionally, it showcases antifibrotic and antioxidative qualities, including the suppression of xanthine oxidase activity in hepatic fibrosis rats (Chien et al., 2014).

The study boasts significant strengths. It utilized a nationally representative sample, guaranteeing strong statistical power and dependability. Comprehensive tracking of study events and prescriptions reduced information and recall bias. Several statistical methods were adopted, including propensity score matching to counteract confounding, competing risk analysis to avert ESRD overestimation, RMST analysis for straightforward estimates, and sensitivity analyses to ensure result dependability and accuracy. Additionally, in-depth assessments of the pooling effect and network analysis concerning renal and survival outcomes were conducted for the seventeen PRCHMSLE.

However, the study also presents certain limitations. First, it did not assess adherence to prescribed PRCHMSLE or potential interactions between herbal and Western medicines. Moreover, it overlooked pulse and syndromic diagnoses present in administrative claims. Second, care should be taken when generalizing these findings to Western healthcare settings since the PRCHMSLE formulas are sanctioned by Taiwan's Committee of Chinese Medicine and Pharmacy. Third, even after employing propensity score matching and adjusting variables in the Cox proportional hazard regression, certain confounders absent from LGTD 2005, like lifestyle, health behaviors, environmental factors, and specific laboratory data, restrict the all-encompassing evaluation of ESRD and mortality risks. Fourth, as our analysis was solely centered on CHM, we did not present or delve into other alternative modalities such as acupuncture, tuina, massage, or those documented in the LGTD 2005. Lastly, being an observational study, it does not ascertain causation, and unaccounted-for confounding factors might affect the results.

5 Conclusion

Our real-world results show significant renal and survival advantages without an associated increase in hospitalization and hyperkalemia risks linked to the use of seventeen PRCHMSLE in treating patients with SLE-CKD. These herbal medicines have demonstrated marked renoprotective effects for SLE-CKD patients by modulating various targets within oxidative stress and inflammation pathways. Additionally, our network analysis has unveiled the core prescription pattern, underscoring the potential for diverse therapeutic strategies and alternative/complementary approaches in SLE-CKD management, thus broadening the scope for disease management.

Data availability statement

The raw data supporting the conclusion of this article will be made available by the authors, without undue reservation.

Ethics statement

The studies involving humans were approved by THE Institutional Review Board of the Dalin Tzu Chi Hospital (B10804001). The studies were conducted in accordance with the local legislation and institutional requirements. The ethics committee/institutional review board waived the requirement of written informed consent for participation from the participants or the participants' legal guardians/next of kin because Patient consent was waived by both the National Health Insurance Administration and the Institutional Review Board of Buddhist Dalin Tzu Chi Hospital due to the de-identified database. Written informed consent was not obtained from the individual(s) for the publication of any potentially identifiable images or data included in this article because Patient consent was waived by both the National Health Insurance Administration and the Institutional Review Board of Buddhist Dalin Tzu Chi Hospital due to the de-identified database.

Author contributions

H-CT: Conceptualization, Formal Analysis, Writing–original draft, Writing–review and editing. B-HY: Data curation, Formal Analysis, Investigation, Methodology, Validation, Writing–review and editing. C-MC: Data curation, Formal Analysis, Investigation, Methodology, Writing–original draft, Writing–review and editing. Y-CC: Conceptualization, Data curation, Formal Analysis, Funding acquisition, Investigation, Methodology, Project administration, Supervision, Validation, Visualization, Writing–original draft, Writing–review and editing.

Funding

The author(s) declare financial support was received for the research, authorship, and/or publication of this article. This study was funded by the Buddhist Dalin Tzu Chi Hospital (DTCRD109-I-24).

Conflict of interest

The authors declare that the research was conducted in the absence of any commercial or financial relationships that could be construed as a potential conflict of interest.

The author(s) declared that they were an editorial board member of Frontiers, at the time of submission. This had no impact on the peer review process and the final decision.

Publisher's note

Supplementary material

The Supplementary Material for this article can be found online at: https://www.frontiersin.org/articles/10.3389/fphar.2023.1309582/full#supplementary-material

References

Bona, N., Pezzarini, E., Balbi, B., Daniele, S. M., Rossi, M. F., Monje, A. L., et al. (2020). Oxidative stress, inflammation and disease activity biomarkers in lupus nephropathy. *Lupus* 29, 311–323. doi:10.1177/0961203320904784

Chang, C. M., Chu, H. T., Wei, Y. H., Chen, F. P., Wang, S., Wu, P. C., et al. (2015). The core pattern analysis on Chinese herbal medicine for sjogren's syndrome: a nationwide population-based study. *Sci. Rep.* 5, 9541. doi:10.1038/srep09541

Chang, C. M., Wu, P. C., Chiang, J. H., Wei, Y. H., Chen, F. P., Chen, T. J., et al. (2017). Integrative therapy decreases the risk of lupus nephritis in patients with systemic lupus erythematosus: a population-based retrospective cohort study. *J. Ethnopharmacol.* 196, 201–212. doi:10.1016/j.jep.2016.12.016

Chen, H. T., Yu, B. H., Yeh, M. H., Hung, S. K., and Chen, Y. C. (2023). Dose- and time-dependent renoprotection of Angelica sinensis in patients with chronic kidney disease: a longitudinal cohort study. *Front. Pharmacol.* 14, 1153583. doi:10.3389/fphar.2023.1153583

Chen, T. F., Hsu, J. T., Wu, K. C., Hsiao, C. F., Lin, J. A., Cheng, Y. H., et al. (2020). A systematic identification of anti-inflammatory active components derived from Mu Dan Pi and their applications in inflammatory bowel disease. *Sci. Rep.* 10, 17238. doi:10.1038/s41598-020-74201-x

Chen, Y. C., Chen, H. T., Yeh, C. C., Hung, S. K., and Yu, B. H. (2022). Four prescribed Chinese herbal medicines provide renoprotection and survival benefit without hyperkalemia risk in patients with advanced chronic kidney disease: a nationwide cohort study. *Phytomedicine* 95, 153873. doi:10.1016/j.phymed.2021.153873

Chen, Y. C., Su, Y. C., Li, C. Y., Wu, C. P., and Lee, M. S. (2015a). A nationwide cohort study suggests chronic hepatitis B virus infection increases the risk of end-stage renal disease among patients in Taiwan. *Kidney. Int.* 87, 1030–1038. doi:10.1038/ki.2014.363

Chen, Y. L., Lee, C. Y., Huang, K. H., Kuan, Y. H., and Chen, M. (2015b). Prescription patterns of Chinese herbal products for patients with sleep disorder and major depressive disorder in Taiwan. *J. Ethnopharmacol.* 171, 307–316. doi:10.1016/j.jep.2015.05.045

Chien, S. C., Chang, W. C., Lin, P. H., Chang, W. P., Hsu, S. C., Chang, J. C., et al. (2014). A Chinese herbal medicine, jia-wei-xiao-yao-san, prevents dimethylnitrosamine-induced hepatic fibrosis in rats. *ScientificWorldJournal* 2014, 217525. doi:10.1155/2014/217525

Coutinho, A. E., and Chapman, K. E. (2011). The anti-inflammatory and immunosuppressive effects of glucocorticoids, recent developments and mechanistic insights. *Mol. Cell. Endocrinol.* 335, 2–13. doi:10.1016/j.mce.2010.04.005

Davidson, A. (2016). What is damaging the kidney in lupus nephritis? *Nat. Rev. Rheumatol.* 12, 143–153. doi:10.1038/nrrheum.2015.159

Guo, J. C., Pan, H. C., Yeh, B. Y., Lu, Y. C., Chen, J. L., Yang, C. W., et al. (2021). Associations between using Chinese herbal medicine and long-term outcome among pre-dialysis diabetic nephropathy patients: a retrospective population-based cohort study. *Front. Pharmacol.* 12, 616522. doi:10.3389/fphar.2021.616522

Huang, H. K., Liu, P. P., Lin, S. M., Hsu, J. Y., Yeh, J. I., Lai, E. C., et al. (2022). Diabetes-related complications and mortality in patients with atrial fibrillation receiving different oral anticoagulants: a nationwide analysis. *Ann. Intern. Med.* 175, 490–498. doi:10.7326/M21-3498

Huang, K. P., Zhang, Z. H., Li, R. M., and Chen, X. (2016). The therapeutic effects of the Chinese herbal medicine, lang chuang fang granule, on lupus-prone MRL/lpr mice. *Evid. Based. Complement. Altern. Med.* 2016, 8562528. doi:10.1155/2016/8562528

Inagaki, Y., Kido, J. I., Nishikawa, Y., Kido, R., Sakamoto, E., Bando, M., et al. (2021). Gan-Lu-Yin (kanroin), traditional Chinese herbal extracts, reduces osteoclast differentiation *in vitro* and prevents alveolar bone resorption in rat experimental periodontitis. *J. Clin. Med.* 10, 386. doi:10.3390/jcm10030386

Jiang, Y., Zhang, Q., Wang, H., Tang, D., Zhang, Y., Zhang, Y., et al. (2020). Expressions of IFN-gamma and IL-4 before and after treatment of lupus nephritis with traditional Chinese medicine combined with cyclophosphamide and their values for efficacy prediction and evaluation. *Iran. J. Public. Health.* 49, 886–895. PMID: 32953676. doi:10.18502/ijph.v49i5.3205

Justiz Vaillant, A. A., Goyal, A., and Varacallo, M. (2023). *Systemic lupus erythematosus; StatPearls*. Florida, USA: Treasure Island.

Lee, F. O., Quismorio, F. P., Jr., Troum, O. M., Anderson, P. W., Do, Y. S., and Hsueh, W. A. (1988). Mechanisms of hyperkalemia in systemic lupus erythematosus. *Arch. Intern Med.* 148, 397–401. doi:10.1001/archinte.1988.00380020141019

Lee, G. A., Chang, C. M., Wu, Y. C., Ma, R. Y., Chen, C. Y., Hsue, Y. T., et al. (2021). Chinese herbal medicine SS-1 inhibits T cell activation and abrogates T(H) responses in Sjogren's syndrome. *J. Formos. Med. Assoc.* 120, 651–659. doi:10.1016/j.jfma.2020.07.024

Li, S. S., Wu, Q., Yin, D. D., Feng, C. Y., Liu, Z. A., and Wang, L. S. (2018). Phytochemical variation among the traditional Chinese medicine Mu Dan Pi from Paeonia suffruticosa (tree peony). *Phytochemistry* 146, 16–24. doi:10.1016/j.phytochem.2017.11.008

Lin, H. L., Lin, M. Y., Tsai, C. H., Wang, Y. H., Chen, C. J., Hwang, S. J., et al. (2021). Harmonizing formula prescription patterns in patients with chronic kidney disease: a population-based cross-sectional study. *Front. Pharmacol.* 12, 573145. doi:10.3389/fphar.2021.573145

Liu, C., Cong, Z., Wang, S., Zhang, X., Song, H., Xu, T., et al. (2023). A review of the botany, ethnopharmacology, phytochemistry, pharmacology, toxicology and quality of Anemarrhena asphodeloides Bunge. *J. Ethnopharmacol.* 302, 115857. doi:10.1016/j.jep.2022.115857

Liu, L., Zhang, L., and Li, M. (2022). Application of herbal traditional Chinese medicine in the treatment of lupus nephritis. *Front. Pharmacol.* 13, 981063. doi:10.3389/fphar.2022.981063

Lu, M. C., Hsu, C. W., Lo, H. C., Chang, H. H., and Koo, M. (2022). Association of clinical manifestations of systemic lupus erythematosus and complementary therapy use in Taiwanese female patients: a cross-sectional study. *Med. Kaunas.* 58, 944. doi:10.3390/medicina58070944

Ma, Y. C., Lin, C. C., Li, C. I., Chiang, J. H., Li, T. C., and Lin, J. G. (2016). Traditional Chinese medicine therapy improves the survival of systemic lupus erythematosus patients. *Semin. Arthritis. Rheum.* 45, 596–603. doi:10.1016/j.semarthrit.2015.09.006

Ma, Y. C., Lin, J. G., Lin, C. C., Li, C. I., Cheng, H. M., and Li, T. C. (2023). Traditional Chinese formulas reduce hospitalization for infection among patients with systemic lupus erythematosus in Taiwan. *J. Herb. Med.* 41, 100704–100708. doi:10.1016/j.hermed.2023.100704

Maroz, N., and Segal, M. S. (2013). Lupus nephritis and end-stage kidney disease. *Am. J. Med. Sci.* 346, 319–323. doi:10.1097/MAJ.0b013e31827f4ee3

Mejia-Vilet, J. M., and Ayoub, I. (2021). The use of glucocorticoids in lupus nephritis: new pathways for an old drug. *Front. Med. (Lausanne).* 8, 622225. doi:10.3389/fmed.2021.622225

Perego, C., Sbolli, M., Specchia, C., Fiuzat, M., Mccaw, Z. R., Metra, M., et al. (2020). Utility of restricted mean survival time analysis for heart failure clinical trial evaluation and interpretation. *JACC. Heart. Fail.* 8, 973–983. doi:10.1016/j.jchf.2020.07.005

Peterson, R. G., Xiao, R., Katcoff, H., Fisher, B. T., and Weiss, P. F. (2021). Effect of first-line biologic initiation on glucocorticoid exposure in children hospitalized with new-onset systemic juvenile idiopathic arthritis: emulation of a pragmatic trial using observational data. *Pediatr. Rheumatol. Online J.* 19, 109. doi:10.1186/s12969-021-00597-z

Ren, H., Li, K., Min, Y., Qiu, B., Huang, X., Luo, J., et al. (2023). Rehmannia glutinosa polysaccharides: optimization of the decolorization process and antioxidant and anti-inflammatory effects in LPS-stimulated porcine intestinal epithelial cells. *Antioxidants (Basel)* 12, 914. doi:10.3390/antiox12040914

Sciascia, S., Radin, M., Yazdany, J., Levy, R. A., Roccatello, D., Dall'era, M., et al. (2017). Efficacy of belimumab on renal outcomes in patients with systemic lupus erythematosus: a systematic review. *Autoimmun. Rev.* 16, 287–293. doi:10.1016/j.autrev.2017.01.010

Vymetal, J., Skacelova, M., Smrzova, A., Klicova, A., Schubertova, M., Horak, P., et al. (2016). Emergency situations in rheumatology with a focus on systemic autoimmune diseases. *Biomed. Pap. Med. Fac. Univ. Palacky. Olomouc. Czech. Repub.* 160, 20–29. doi:10.5507/bp.2016.002

Wang, W., Wang, Y. H., Yang, K., Ye, X., Wang, X., and Wei, J. C. (2023). Traditional Chinese medicine use is associated with lower risk of pneumonia in patients with systemic lupus erythematosus: a population-based retrospective cohort study. *Front. Pharmacol.* 14, 1185809. doi:10.3389/fphar.2023.1185809

Wang, Y., Han, M., Pedigo, C. E., Xie, Z. M., Wang, W. J., and Liu, J. P. (2021). Chinese herbal medicine for systemic lupus erythematosus: a systematic review and meta-analysis of randomized, placebo-controlled trials. *Chin. J. Integr. Med.* 27, 778–787. doi:10.1007/s11655-021-3497-0

Wang, Y. J., Li, Y. X., Li, S., He, W., Wang, Z. R., Zhan, T. P., et al. (2022). Progress in traditional Chinese medicine and natural extracts for the treatment of lupus nephritis. *Biomed. Pharmacother.* 149, 112799. doi:10.1016/j.biopha.2022.112799

Yang, J. S., Wu, C. C., Lee, H. Z., Hsieh, W. T., Tang, F. Y., Bau, D. T., et al. (2016). Suppression of the TNF-alpha level is mediated by Gan-Lu-Yin (traditional Chinese medicine) in human oral cancer cells through the NF-kappa B, AKT, and ERK-dependent pathways. *Environ. Toxicol.* 31, 1196–1205. doi:10.1002/tox.22127

Yap, D. Y., Tang, C. S., Ma, M. K., Lam, M. F., and Chan, T. M. (2012). Survival analysis and causes of mortality in patients with lupus nephritis. *Nephrol. Dial. Transpl.* 27, 3248–3254. doi:10.1093/ndt/gfs073

Yu, B. H., Chen, Y. C., Li, Y. D., Chiou, W. Y., and Chen, Y. C. (2022). No dose-response relationship of clarithromycin utilization on cardiovascular outcomes in patients with stable coronary heart disease: analysis of Taiwan's national health insurance claims data. *Front. Cardiovasc. Med.* 9, 1018194. doi:10.3389/fcvm.2022.1018194

Yu, H. H., and Hsieh, C. J. (2021). Integrative therapy combining Chinese herbal medicines with conventional treatment reduces the risk of cardiovascular disease among patients with systemic lupus erythematosus: a retrospective population-based cohort study. *Front. Pharmacol.* 12, 737105. doi:10.3389/fphar.2021.737105

Yuan, Y. L., Guo, C. R., Cui, L. L., Ruan, S. X., Zhang, C. F., Ji, D., et al. (2015). Timosaponin B-II ameliorates diabetic nephropathy via TXNIP, mTOR, and NF-κB signaling pathways in alloxan-induced mice. *Drug. Des. devel. Ther.* 9, 6247–6258. doi:10.2147/DDDT.S96435

Zhang, R. X., Li, M. X., and Jia, Z. P. (2008). Rehmannia glutinosa: review of botany, chemistry and pharmacology. *J. Ethnopharmacol.* 117, 199–214. doi:10.1016/j.jep.2008.02.018

Zhang, S., Zhang, Q., An, L., Zhang, J., Li, Z., Zhang, J., et al. (2020). A fructan from Anemarrhena asphodeloides Bunge showing neuroprotective and immunoregulatory effects. *Carbohydr. Polym.* 229, 115477. doi:10.1016/j.carbpol.2019.115477

Zhao, X., Liu, C., Qi, Y., Fang, L., Luo, J., Bi, K., et al. (2016). Timosaponin B-II ameliorates scopolamine-induced cognition deficits by attenuating acetylcholinesterase activity and brain oxidative damage in mice. *Metab. Brain. Dis.* 31, 1455–1461. doi:10.1007/s11011-016-9877-z

Zhuang, Y., Zhang, X., Luo, S., Wei, F., Song, Y., Lin, G., et al. (2022). Exploring the molecular mechanism of Zhi Bai di huang wan in the treatment of systemic lupus erythematosus based on network pharmacology and molecular docking techniques. *Processes* 10, 1914. doi:10.3390/pr10101914

frontiers | Frontiers in Pharmacology

TYPE Review
PUBLISHED 08 January 2024
DOI 10.3389/fphar.2023.1323377

OPEN ACCESS

EDITED BY
Weicheng Hu,
Yangzhou University, China

REVIEWED BY
Xinyu Wang,
Philadelphia College of Osteopathic Medicine–Georgia Campus, United States
Ying-Jan Wang,
National Cheng Kung University, Taiwan

*CORRESPONDENCE
Kali Xiang,
kakaenshi@126.com
Guangcai Li,
44830705@qq.com

†These authors have contributed equally to this work

RECEIVED 17 October 2023
ACCEPTED 20 December 2023
PUBLISHED 08 January 2024

CITATION
Liu P, Tang W, Xiang K and Li G (2024), Pterostilbene in the treatment of inflammatory and oncological diseases.
Front. Pharmacol. 14:1323377.
doi: 10.3389/fphar.2023.1323377

Pterostilbene in the treatment of inflammatory and oncological diseases

Peijun Liu[1†], Weihua Tang[2†], Kali Xiang[1*] and Guangcai Li[1*]

[1]Department of Respiratory and Critical Care Medicine, The Central Hospital of Enshi Tujia and Miao Autonomous Prefecture, Enshi, China, [2]Department of Radiology, The Central Hospital of Enshi Tujia and Miao Autonomous Prefecture, Enshi, China

Pterostilbene (PTS), a naturally occurring analog of resveratrol (RSV), has garnered significant attention due to its potential therapeutic effects in treating inflammatory and oncological diseases. This comprehensive review elucidates the pharmacological properties, mechanisms of action, and therapeutic potential of PTS. Various studies indicate that PTS exhibits anti-inflammatory, antioxidant, and antitumour properties, potentially making it a promising candidate for clinical applications. Its influence on regulatory pathways like NF-κB and PI3K/Akt underscores its diverse strategies in addressing diseases. Additionally, PTS showcases a favorable pharmacokinetic profile with better oral bioavailability compared to other stilbenoids, thus enhancing its therapeutic potential. Given these findings, there is an increased interest in incorporating PTS into treatment regimens for inflammatory and cancer-related conditions. However, more extensive clinical trials are imperative to establish its safety and efficacy in diverse patient populations.

KEYWORDS

pterostilbene, anti-inflammatory, antioxidant, antitumour, oral bioavailability

Introduction

Pterostilbene (PTS), identified as trans-3,5-dimethoxy-4-hydroxystilbene, is a natural substance mainly discovered in blueberries and the wood of pterocarpus marsupium (Rimando et al., 2004). Stilbenes, including resveratrol (RSV), PTS, and pinostilbene, are plant compounds known for their potential health benefits, but the low bioavailability of RSV can limit its effectiveness (Salehi et al., 2018). RSV exhibits environmental instability, particularly its sensitivity to ultraviolet radiation, oxygen, alkaline pH, and elevated temperatures, leading to diminished bioavailability and biological activity. Consequently, numerous RSV derivatives, especially methylated compounds, are under investigation for enhanced stability and efficacy (Liu et al., 2011; Mamalis and Jagdeo, 2017). Compared to other stilbene compounds, pterostilbene boasts higher bioavailability, potentially amplifying its nutritional advantages and leading to noteworthy clinical outcomes (Kapetanovic et al., 2011). Stilbenoids are naturally occurring phenolic chemicals found in various plant species, among which resveratrol is a well-known derivative. RSV belongs to the group of phytoalexins, which are antimicrobial substances produced by plants to combat infections (Akinwumi et al., 2018). In the metabolism of stilbenoid compounds, RSV undergoes methylation to produce PTS. This biotransformation adds methyl groups to the hydroxyl moieties of RSV. PTS, once formed, can be further metabolized *in vivo*. The combined action of phase II metabolic enzymes and gut microbiota leads to the demethylation of PTS, creating pinostilbene with a

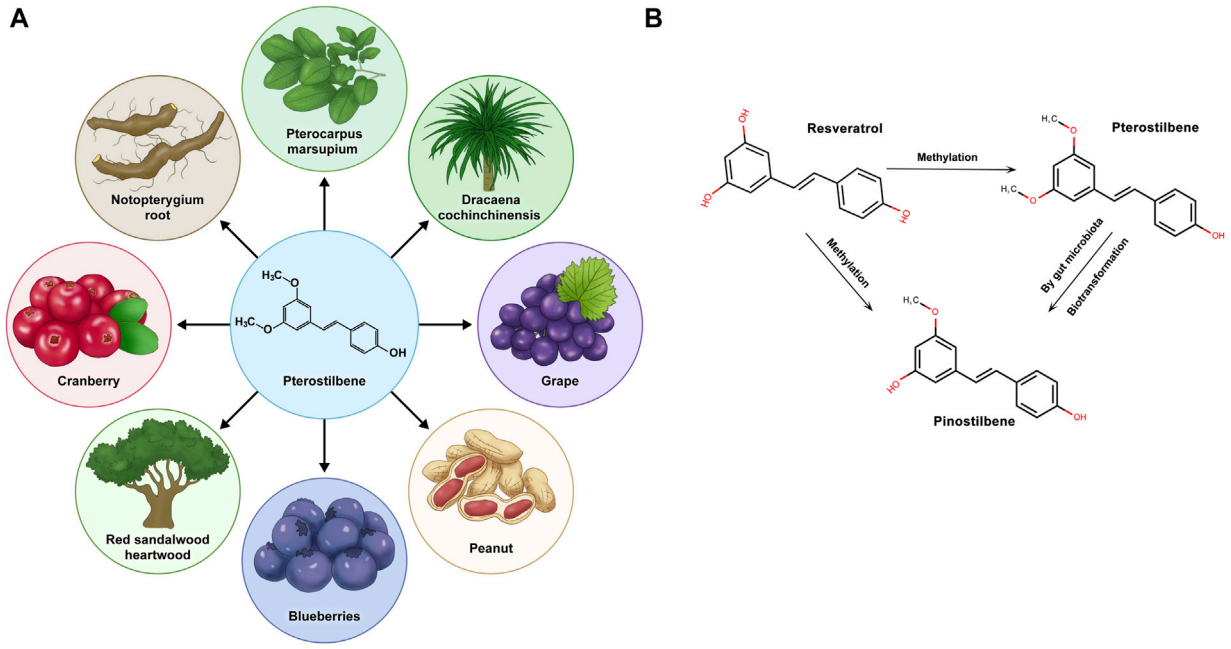

FIGURE 1
Pterostilbene is derived from natural plants and transforms within the organism. **(A)** Pterostilbene is sourced from various natural plants. **(B)** Pterostilbene, along with resveratrol and pinostilbene, undergoes specific methylation processes within the physiological environment of the organism, leading to potential metabolic changes.

singly methylated hydroxyl group. Pinostilbene, PTS, and RSV all possess the foundational framework of a stilbene configuration (C6-C2-C6), highlighting a commonality in their chemical frameworks. These phytoalexins are antimicrobial substances synthesized by plants when they come under attack by pathogens, thereby playing a significant role in the plant's defense mechanism (Ahuja et al., 2012; Jeandet et al., 2013).

PTS is a prominent nonflavonoid polyphenolic compound naturally found in various plants. Characterized by its lipophilicity, PTS appears in cis and trans isomeric structures, with the trans isomer being more dominant. Although first discovered in the heartwood of sandalwood, later research has discerned its occurrence in blueberries and grapes (Kosuru et al., 2016) (Figure 1A). While both share structural similarities, adding two methyl groups to PTS grants it unique pharmacological properties distinct from RSV (Estrela et al., 2013). A notable characteristic of PTS distinguishing it from other phytoalexins is its broad spectrum of pharmacological traits, including anti-inflammatory, antioxidant, and anticancer effects (Mccormack and Mcfadden, 2013; Akinwumi et al., 2018). Moreover, scientific studies have demonstrated that, compared to its parent compound, RSV, PTS exhibits superior bioavailability and metabolic stability, thus showing potential for further therapeutic applications (Yun et al., 2014; Peng et al., 2018). Throughout time, PTS has demonstrated advantages across multiple areas, including neuroprotection, antioxidation, and anti-inflammatory and anticancer properties, positioning it as a promising subject for continued studies in health prevention. (Hougee et al., 2005; Chen et al., 2017; Abd-Elmawla et al., 2023).

Inflammation acts as a core reaction of the immune system to harm or infections. This defensive response incorporates immune cells, blood vessels, and cellular agents to address the primary source of cellular damage, remove harmed cells and tissues, and start the process of cellular and tissue recovery (Antonelli and Kushner, 2017; Roy et al., 2022). Research indicates that PTS exhibits anti-inflammatory attributes via various pathways. Experiments with animal subjects and cellular models have highlighted the inflammation-reducing capabilities of PTS, pointing to its prospective utility in addressing inflammation-related conditions (Lim et al., 2020; Lin et al., 2020; Nagarajan et al., 2022). The use of PTS in cancer treatment is just starting, but it represents a potentially sensitizing therapy that could improve the outcome of numerous oncology treatments (Obrador et al., 2021). PTS has exhibited potential benefits in hindering and treating multiple cancer forms, such as those of the breast, prostate, colon, lung, liver, and skin (Dhar et al., 2016; Kumar et al., 2017; Ma et al., 2019). Its action pathways include controlling cell cycle dynamics, triggering programmed cell death, impeding the creation of new blood vessels, and curbing the spread of cancer cells (Estrela et al., 2013; Tzeng et al., 2021). This review aims to provide a comprehensive overview of the current knowledge and applications of PTS in inflammatory and oncological diseases.

Pharmacokinetics

PTS, a compound sourced naturally from the diet, has garnered attention because of its expansive medicinal properties (Nagarajan et al., 2022). Compared to RSV, PTS has a more stable metabolism and enhanced pharmacological activity (Wang and Sang, 2018), owing to the presence of two methoxy groups, which are absent in RSV (Kapetanovic et al., 2011) (Figure 1B). The systemic clearance

rate of PTS, reflected by its half-life, is consistent across different administration methods, indicating a swift process of absorption, distribution, metabolism, and excretion (Wang and Sang, 2018). The pharmacokinetic comparison between PTS and RSV in rats, as conducted by Kapetanovic, demonstrated that PTS's peak plasma level was significantly higher than that of RSV, also exhibiting a notably increased oral bioavailability (Kapetanovic et al., 2011). ADME, an acronym for absorption, distribution, metabolism, and excretion, serves as a crucial framework in pharmacology to assess how drugs interact within the body. This model is particularly useful in understanding the behavior of compounds such as PTS.

Absorption of pterostilbene

After ingestion, PTS is rapidly absorbed, contributing to its superior oral bioavailability of approximately 80%–95% (Lin et al., 2020). This rapid absorption facilitates its availability for systemic circulation. The compound's low molecular weight and two methoxy groups enhance its lipophilic nature, aiding its penetration through the blood-brain barrier and offering potential benefits to the central nervous system (Deng et al., 2015). The ability of PTS to cross the blood-brain barrier efficiently not only broadens its therapeutic scope but also makes it a promising candidate for treating a range of neurological conditions, where effective drug delivery across this barrier is often a significant challenge.

Distribution of pterostilbene

Following absorption, PTS exhibits a distinct distribution across various tissues in C57BL/6 mice. Within 20 min of oral intake, PTS primarily concentrates in the stomach, liver, and testes, indicating significant absorption and metabolic activity. It also appears notably in the kidneys, intestines, and lungs, suggesting potential effects on excretion, digestion, and respiratory functions. Additionally, PTS is present in the brain, spleen, skeletal muscles, and heart, highlighting its systemic reach and possible impacts on neurological, immune, muscular, and cardiovascular health. This pattern reveals PTS's diverse interactions across various organs in a descending concentration order (Wang et al., 2022). The brain's unique metabolic response to PTS highlights its potential in neurotherapeutic applications. This compound is selectively utilized by brain tissue, suggesting efficacy in treating neurological conditions. Its ability to cross the blood-brain barrier and engage in brain metabolism underscores its suitability for targeting brain-related disorders. This selective uptake suggests Pterostilbene's promise in developing more focused and effective neurological treatments (Azzolini et al., 2014).

Metabolism of pterostilbene

PTS undergoes significant first-pass metabolism in the liver, which is vital for its systemic clearance. This metabolism primarily involves phase II detoxification reactions, predominantly glucuronidation, and sulfation, transforming PTS into more water-soluble forms suitable for excretion (Kapetanovic et al., 2011; Gómez-Zorita et al., 2021; Li et al., 2023). Compared to RSV, PTS has a much lower glucuronidation efficiency in the liver, affecting its human metabolism (Dellinger et al., 2014). In comparison to RSV, its structural counterpart, PTS exhibits a considerably lower efficiency in glucuronidation within the liver. This difference in glucuronidation efficiency plays a significant role in the metabolic fate of PTS in human bodies, influencing its overall metabolism and bioavailability. The lower glucuronidation rate of PTS, as opposed to RSV, potentially allows for a longer systemic presence and a prolonged therapeutic window. This characteristic of PTS metabolism is pivotal in understanding its pharmacokinetics and pharmacodynamics, providing insights into its potential advantages over RSV in clinical applications.

Excretion of pterostilbene

The majority of Pterostilbene's glucuronide-conjugated metabolites are excreted within 12 h post-administration, indicating rapid renal and total serum clearance (Remsberg et al., 2008). This swift elimination reduces the chances of PTS accumulation, enhancing its suitability as a therapeutic agent. The rapid clearance is particularly beneficial for treatments requiring regular dosing, ensuring stable therapeutic levels without the risk of toxicity from accumulation. This attribute allows precise control over the drug's pharmacokinetics, enabling adjustments in dosage or frequency to suit individual patient needs while maintaining safety and efficacy. The extent of Pterostilbene's binding to plasma proteins can significantly impact its free concentration in the bloodstream and its subsequent distribution to tissues, affecting both its efficacy and clearance rate. Overall, Pterostilbene's pharmacokinetic profile makes it a promising candidate for safe and effective therapies, especially in cases requiring frequent administration.

Antioxidant activity

Oxidative stress is a condition characterized by an imbalance between the generation of reactive oxygen species (ROS) and the body's capacity to counteract or eliminate these detrimental molecules (Schieber and Chandel, 2014). This imbalance can lead to oxidative damage to cells and tissues, triggering various health issues, including inflammation, aging, and chronic diseases. To maintain physiological balance, the human body relies on antioxidant systems to neutralize ROS, such as antioxidant enzymes and antioxidants like vitamin C and vitamin E. Major ROS include hydrogen peroxide (H_2O_2), superoxide anion (O_2^-), and hydroxyl radicals (Baskaran et al., 2021). These highly reactive molecules can be produced through endogenous metabolic processes or as a result of exposure to environmental stressors. Antioxidant therapy aims to counteract oxidative stress by either neutralizing ROS or enhancing the body's antioxidant defense mechanisms (Rahman et al., 2020). PTS, a derivative of RSV, exhibits antioxidant activity through direct and indirect mechanisms. It acts as a ROS scavenger, neutralizing harmful free radicals and preventing cellular damage linked to chronic

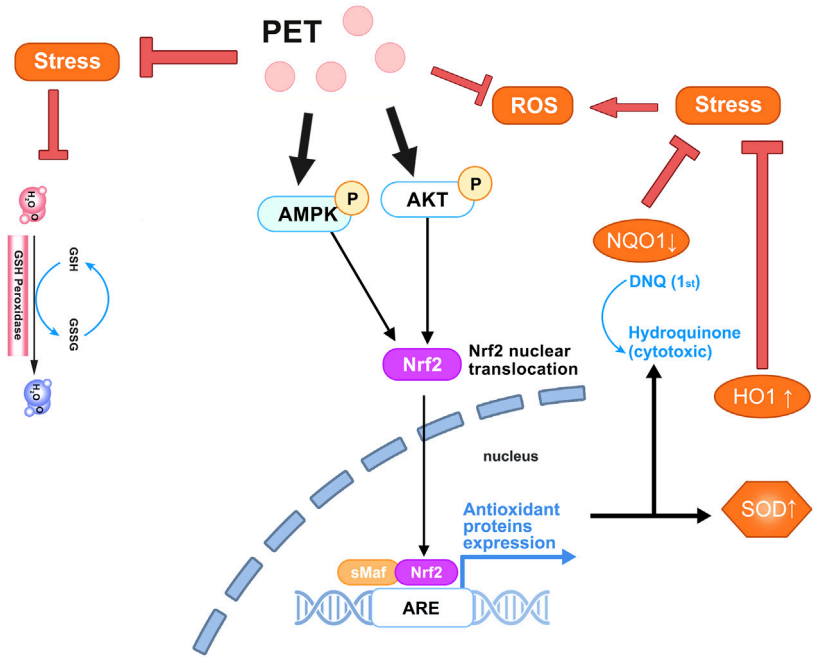

FIGURE 2
The antioxidative mechanism of pterostilbene in the physiological environment. Pterostilbene promotes the phosphorylation of AMPK and AKT, facilitates the nuclear translocation of Nrf2, and mitigates ROS, thereby alleviating oxidative stress.

diseases. Additionally, PTS indirectly enhances the body's antioxidant defenses by upregulating enzymes, providing comprehensive protection against oxidative stress. This dual action of directly combating free radicals and boosting internal defense mechanisms underscores PTS's potential as an effective compound in antioxidant therapies and chronic disease management.

PTS can reduce oxidative stress and counteract ROS like H_2O_2 and O_2^-(Mccormack and Mcfadden, 2013). PTS has been found to proficiently diminish the production of ROS in human retinal endothelial cells (HREC), particularly under high-glucose environments. PTS exerts its indirect antioxidant effects by modulating cellular pathways and enhancing the expression of crucial antioxidant enzymes. Zhou et al. showed that PTS activates the phosphorylation of AMPK and AKT, prompting the shift of Nrf2 from the cytoplasm into the nucleus. This action then heightens the expression of Nrf2-regulated genes, NQO1 and HO-1, underscoring pterostilbene's robust antioxidant capabilities (Zhou et al., 2019). Additionally, it aids in boosting the expression of several peroxidase enzymes in diverse cellular systems, especially total glutathione, glutathione peroxidase, glutathione reductase, and superoxide dismutase (Mccormack and Mcfadden, 2013). Furthermore, as an antioxidant, PTS can neutralize harmful free radicals in the body, thereby preventing cellular damage that can lead to chronic inflammation and potential cancer (Jayakumar et al., 2021). Following the administration of PTS at a dosage of 40 mg/kg over 6 weeks, it exhibited a pronounced capability to neutralize free radicals within the system of diabetic rats, resulting in a marked decrease in oxidative stress (Amarnath Satheesh and Pari, 2006). In an *in vitro* investigation utilizing the H_2O_2-induced intestinal porcine enterocyte cell line (IPEC-J2), it was found that both RSV and PTS significantly ameliorated oxidative stress-induced intestinal damage. This therapeutic effect was achieved by regulating mitochondrial redox balance and functionality through the SIRT1 signaling pathway. Notably, PTS exhibited a markedly enhanced efficacy in affording this protective action in comparison to RSV (Chen et al., 2021). The antioxidant mechanism of PTS is shown in Figure 2.

Anti-inflammatory effects of pterostilbene

Inflammation is a complex and highly orchestrated biological response that serves as a fundamental component of the body's defense mechanism. When the body encounters harmful stimuli, including pathogens, injured cells, or irritants, a sophisticated cascade of events is triggered to protect and restore tissue integrity (Arulselvan et al., 2016). At its core, inflammation is a protective response aimed at eliminating the source of injury or infection and initiating the healing process. This multifaceted process involves the activation of immune cells, the release of signaling molecules, and the recruitment of various cellular components to the site of inflammation (Henao-Mejia et al., 2012). It is an essential part of the immune response that facilitates the healing process and repairs injured tissues. While these processes are vital for healing and defense against further damage, prolonged or widespread inflammation can be a driving force behind the emergence and advancement of many diseases (Libby et al., 2018; Sochocka et al., 2019). PTS has garnered significant attention in multiple preclinical researches for its potent anti-inflammatory properties. By targeting various stages

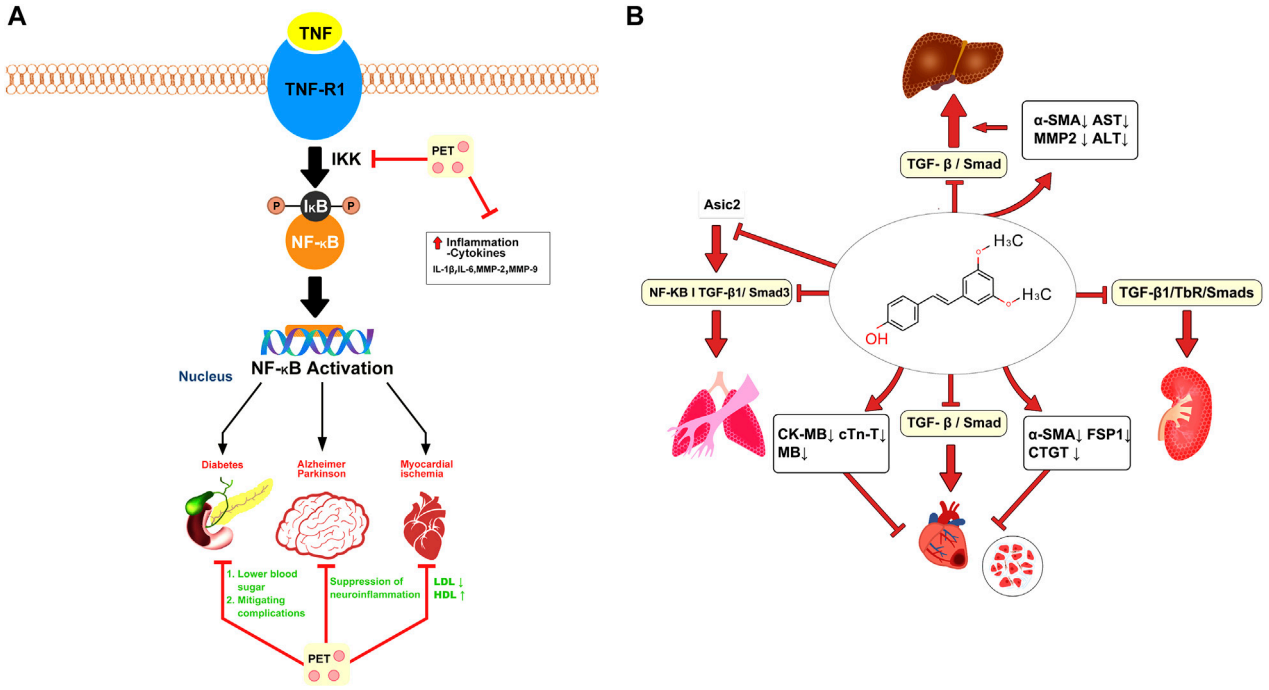

FIGURE 3
Pterostilbene attenuates inflammatory and fibrotic processes. **(A)** Pterostilbene mitigates inflammation by inhibiting the NF-κB pathway, thereby alleviating conditions such as diabetes, myocardial ischemia, and Parkinson's disease. **(B)** Pterostilbene alleviates systemic fibrosis (heart, liver, lungs, and kidneys) by inhibiting the TGF/Smad pathway and several other mechanisms.

of the inflammatory cascade, PTS effectively reduces the immediate symptoms and concurrently plays a role in averting the long-term complications typically linked with chronic inflammation. These studies suggest that the principal mechanism behind PTS's effectiveness lies in its ability to modulate various signaling pathways intricately associated with inflammation (Kosuru et al., 2016; Wu et al., 2019).

PTS mitigates inflammation by decreasing inflammatory indicators, notably tumor necrosis factor-alpha (TNF-α), and obstructing NF-κB activation, a primary orchestrator of inflammation (Lin et al., 2016; Liu et al., 2019). By suppressing the production of TNF-α, PTS can effectively reduce the extent of the inflammatory response (Yi et al., 2022). By inhibiting the activation of NF-κB, PTS prevents this sequence of events and reduces the inflammatory response (Zhang et al., 2023). *In vitro* studies have indicated that PTS inhibits the activation of NF-κB, leading to the downregulation of proinflammatory cytokines, including TNF-α, interleukin-1beta (IL-1β), and interleukin-6 (IL-6) (Zeng et al., 2020). Utilizing its antioxidative mechanisms, PTS curbs the emergence of inflammatory markers like TNF-α, IL-1β, IL-6, MMP-2, and MMP-9 in corneal epithelial cells under hyperosmotic stress, thus shielding them from inflammation (Li et al., 2016). Overproduction of these cytokines, essential for immune reactions to pathogens and damage, often instigates excessive inflammatory responses.

In animal models of inflammation, PTS has been shown to reduce edema, inflammatory cell infiltration, and cytokine production (Park et al., 2010). Edema, or swelling caused by excess fluid trapped in body tissues, is a common symptom of inflammation (Liu et al., 2019). The anti-edematous characteristics of PTS can assist in reducing swelling and, as a result, lessen the physical discomfort brought on by inflammation (Yan et al., 2021). Another pivotal aspect of inflammation is the infiltration of inflammatory cells into the affected area, leading to tissue damage and furthering the inflammatory response (Mack, 2018). Evidence from animal studies suggests that PTS can attenuate this cell infiltration, thus helping to limit tissue damage and the propagation of the inflammatory response (Liu et al., 2016). The potential anti-inflammatory mechanism of PTS is depicted in Figure 3A.

Pterostilbene surpasses resveratrol in alleviating inflammation

Compared to RSV, PTS exhibits stronger anti-inflammatory activities. Rats were divided into five groups to investigate the impact of PTS (15 or 30 mg/kg/d) and RSV (30 mg/kg/d) on the progression of non-alcoholic fatty liver disease (NAFLD). One group was fed a standard diet, while the other four were given a high-fat, high-fructose diet supplemented with either PTS or RSV for 8 weeks. The study focused on the effects of these compounds on oxidative stress, inflammation, fibrosis, and pre-carcinogenic stages. The results demonstrated that PTS, particularly at a dose of 30 mg/kg/d, effectively alleviated liver oxidative stress and inflammation caused by the high-fat, high-fructose diet (Gómez-Zorita et al., 2020). Following lipopolysaccharide (LPS) injection, weaned piglets exhibited activated inflammatory responses and severe

oxidative stress, as well as enhanced nuclear translocation of NF-κB and increased protein expression of NLRP3 and cleaved caspase. PTS is more effective than RSV in reducing liver damage by targeting the NF-κB/NLRP3 signaling pathway and mitigating inflammation and oxidative stress (Li et al., 2022).

Anti-inflammatory effect of pterostilbene in diabetes

Inflammation is a crucial factor in the progression of numerous diseases, particularly diabetes, where it serves not only as a hallmark of the disease but also as a driving force for its development and complications (Rohm et al., 2022). In diabetes, sustained high blood glucose levels can induce oxidative stress and inflammatory responses, thereby exacerbating insulin resistance and impacting pancreatic function, further deteriorating the condition (Hurrle and Hsu, 2017). Research has validated the role of PTS in managing diabetic inflammation. Obesity is closely related to diabetes; ómez-Morita found that PTS, at a dosage of 15 mg/kg, was more effective than RSV in reducing weight in rats fed a high-fat diet (Gómez-Zorita et al., 2014). The enhanced performance of PTS is linked to its increased liposolubility, stemming from the substitution of a hydroxyl group with a methoxy group, which boosts its absorption. PTS modulates blood sugar levels, improves insulin response and lipid profiles, and reduces inflammation and oxidative damage in rats with diet-driven obesity and STZ-triggered diabetes by utilizing the PI3K/Akt signaling route (Sun et al., 2019). In addition to effectively controlling high blood sugar, PTS offers potential protective benefits against the complications often associated with diabetes. These complications can range from cardiovascular disease, due to the persistent strain on the heart and blood vessels, to kidney disease, resulting from the body's struggle to filter blood without sufficient insulin (Millán et al., 2019; Dodda et al., 2020).

Anti-inflammatory effect of pterostilbene in nervous system disorders

In neurodegenerative diseases, inflammation is a critical factor in disease progression and symptom severity. Neuroinflammation, characterized by the activation of microglial cells and the release of inflammatory cytokines, contributes significantly to neuronal damage and death (Muzio et al., 2021). This inflammatory process is a common pathological feature in conditions such as Alzheimer's and Parkinson's disease (King et al., 2019). PTS exhibits neuroprotective effects, as evidenced by its capacity to improve neurological function, lower neurological scoring, and enhance neuronal survival *in vivo*. It has also been shown to boost the number of mature neurons, augment cell vitality, and limit neuronal apoptosis. Pterostilbene's protective function further extends to the reduction of infarct volume in the brain, the alleviation of cerebral edema, a decrease in the number of activated microglial cells, and the suppression of eNOS and IL-1β expression (Liu et al., 2020). Through attenuating the levels of oxidative stress markers such as 4-hydroxynonenal and 8-hydroxyguanosine, reducing lactate dehydrogenase leakage, reversing elevated MDA concentrations in the ischemic brain hemisphere, and restoring depleted SOD activity, PTS effectively neutralizes oxidative stress, highlighting its influential role as an antioxidant agent (Zhou et al., 2015). PTS has demonstrated neuroprotective effects in preclinical models of Alzheimer's disease and Parkinson's disease, potentially due to its anti-inflammatory, antioxidant, and anti-apoptotic properties (Millán et al., 2019; Liu et al., 2020). PTS effectively suppresses neuroinflammation, one of the key pathological features of neurodegenerative diseases, by inhibiting the activation of microglial cells (Zhou et al., 2015). Elevated cholesterol and triglyceride levels heighten the risk of heart-related ailments, such as heart attacks and strokes. Pterostilbene's potential to enhance lipid markers might serve as a preventive measure against these conditions. Specifically, it's believed to reduce LDL cholesterol, commonly deemed as harmful, while boosting the levels of the beneficial HDL cholesterol (Brenner and Boileau, 2019).

Antifibrotic effect of pterostilbene

Fibrosis involves an overaccumulation of fibrous connective tissue, stemming mainly from abnormal extracellular matrix buildup. This leads to the creation of scar tissue, potentially causing organ malfunctions and affecting various organs throughout the body (Wynn, 2007). Lee et al. explored the potential of PTS in counteracting inflammation and cell overgrowth effects from dimethylnitrosamine (DMN) in liver fibrosis using male SD rats. Rats were categorized into a control DMN model and two groups receiving different PTS doses. Following a month of DMN injections and PTS treatment, the DMN model group displayed elevated liver enzyme levels and noticeable liver tissue harm. On the other hand, rats treated with 20 mg/kg of PTS showed a decline in these liver enzyme levels and lessened liver damage. This suggests that PTS could potentially enhance liver health, mitigate DMN-triggered liver harm, and decelerate liver fibrosis by targeting hepatic stellate cells (Lee et al., 2013). Gu et al. discovered that PTS and pirfenidone could significantly inhibit the TGF-β1/TbR/Smads signaling pathway in the rat renal cortex. This intervention suppressed fructose-induced epithelial-mesenchymal transition (EMT) in rat proximal tubular epithelial cells, contributing to a reduction in renal tubulointerstitial fibrosis. Moreover, PTS was shown to elevate the expression of pIR, pIRS-1, and pAkt within the rat renal cortex (Gu et al., 2019).

TGF-β1 triggers EMT and ECM buildup, reducing autophagy and cell apoptosis in A549 and AECs cells. Remarkably, PTS at 30 μmol/L lessened the impact of TGF-β1 on pulmonary fibrosis. PTS effectively counteracts EMT and ECM buildup and bolsters cell apoptosis and autophagy in comparison to TGF-β1. Transcriptome sequencing demonstrates a marked decline in ASIC2 protein levels due to PTS. Enhancing ASIC2 expression through plasmid introduction reverses pterostilbene's effects, accelerating EMT and ECM buildup while suppressing cell apoptosis and autophagy. It is inferred that pterostilbene's role in alleviating pulmonary fibrosis is linked to ASIC2 downregulation (Peng et al., 2021). KANG et al. explored the effects of PTS on fructose-induced myocardial fibrosis in rats and discovered that it reduced serum markers of cardiac damage, including CK-MB, cTn-T, and M.B. The study implies that PTS may alleviate fructose-

induced myocardial injury by inhibiting the TGF-β1/Smad signaling pathway, thereby potentially protecting the heart (Kang et al., 2019). The potential antifibrotic mechanism of PTS is illustrated in Figure 3B.

Pterostilbene in tumor therapy

Cancer is a complex disease caused by genetic and environmental factors, commonly including genetic mutations, chronic inflammation, lifestyle aspects like smoking and diet, and environmental exposures such as radiation and chemicals (Jin et al., 2019). At its core, the disease often involves genetic mutations, which can be either inherited or acquired over a person's lifetime. These mutations disrupt the normal cell cycle, leading to uncontrolled cell growth and tumor formation (Nussinov et al., 2022). Chronic inflammation is another key factor, serving as both a cause and a consequence of cancerous growth, creating a vicious cycle that exacerbates the disease. Lifestyle choices play a crucial role as well; habits such as smoking and unhealthy dietary patterns have been strongly linked to increased cancer risk. These lifestyle factors can act as catalysts, accelerating the onset and progression of the disease. Moreover, environmental exposures, notably to radiation and harmful chemicals, can directly damage DNA or create conditions conducive to cancer development. These elements collectively contribute to the complexity of cancer, making it a challenging disease to understand and treat (Jardim et al., 2023). Current treatment modalities primarily consist of surgery, radiotherapy, chemotherapy, and immunotherapy, each with limitations like side effects and drug resistance (Miller et al., 2019). In oncology, traditional chemotherapy agents, while effective, often come with a hefty price tag and a host of adverse effects. PTS emerges as a beacon, both economically viable and associated with reduced side effects. PTS demonstrates superior bioactivity when compared to RSV. Highlighting its potency, PTS, with an impressive IC50 value of 22.4 μmol/L, has shown a remarkably more robust inhibitory impact on the HT-29 colon cancer cell line than RSV, which displays an IC50 value of 43.8 μmol/L (Paul et al., 2009). Such merits have not gone unnoticed, attracting a burgeoning community of researchers eager to unlock its potential further. Empirical studies have highlighted pterostilbene's impressive anticancer properties prowess, with efficacy demonstrated across a spectrum of malignant neoplasms (Ma et al., 2019). There is growing interest in the prospect of utilizing PTS as a stand-alone therapeutic agent or synergistically alongside existing FDA-approved anti-cancer treatments. Such novel therapeutic strategies underscore a promising horizon for its clinical integration. Delving into its mode of action, it becomes evident that pterostilbene's antitumor mechanisms are intricate and operate on multiple cellular and molecular fronts. PTS inhibits cancer cell migration and invasion, critical steps in cancer metastasis. PTS may regulate specific enzymes associated with aging and lifespan, which could impact its anticancer properties (Li et al., 2018). This effect has been noted in studies involving breast, lung, and colorectal cancer cells. The tumor-fighting capabilities of PTS can mainly be traced back to several key factors.

DNA methylation and histone modification

Cancer develops from a complex mix of genetic and environmental influences, involving aberrations in DNA methylation, histone modifications, and the expression of microRNAs (miRNAs) (Saleh et al., 2020). DNA methylation, a key epigenetic mechanism, involves the addition of a methyl group to the DNA molecule, typically at cytosine bases in CpG dinucleotides, which can lead to the silencing of tumor suppressor genes (Haghani et al., 2023). Histone modifications, including acetylation and methylation, change the structure of chromatin, influencing gene expression. PTS and RSV, other dietary phytochemicals with chemopreventive properties, can achieve anticancer effects by altering DNA methylation, modulating histone modifications, or regulating miRNA expression (Lee et al., 2018). Stilbenoid compounds like PTS and RSV can modify the DNA methylation patterns in breast cancer cells through epigenetic mechanisms. This alteration reduces the activity of cancer-boosting NOTCH signaling, limiting the growth and spread of breast cancer cells (Lubecka et al., 2016). When used together, RSV and PTS gradually restore the expression of estrogen receptor-alpha (ERα) in ERα-negative breast cancer cells. This restoration arises from the adjustment of DNA methylation and histone acetylation in these cells, profoundly influencing the functions of DNMT, HDAC, and HAT(Kala and Tollefsbol, 2016). In ovarian carcinoma, PTS potently modulates the phosphorylation of STAT3, subsequently impeding cell cycle advancement and initiating apoptosis, thereby manifesting its pronounced antineoplastic effects (Wen et al., 2018).

Suppression of cell growth and enhancement of cell apoptosis

PTS impacts several mechanisms linked to cancer advancement. Both *in vitro* and *in vivo* examinations have shown that PTS can restrain tumor cell expansion and trigger apoptosis by influencing different signaling routes, including the PI3K/Akt, MAPK, and NF-κB pathways (Mak et al., 2013; Hsiao et al., 2014; Tong et al., 2021). Perecko et al. found that PTS induced apoptosis in leukemia cells through the MAPK pathway (Hsiao et al., 2014). Increased activity of cyclooxygenase-2 (COX-2) has been noted in lung cancer, and PTE has been identified to regulate the growth and apoptosis of NSCLC cells by focusing on COX-2 (Wang et al., 2023). In conjunction with the HDAC inhibitor vorinostat, PTS proficiently modulates the MTA1/HIF-1α pathway, curbing both cellular proliferation and angiogenesis. This combined action notably hinders the advancement of prostate tumors in murine models, all while showcasing a more favorable toxicity profile. Distinctively, PTS attenuates MTA1 expression within hepatocellular carcinoma cells and concurrently reduces the enzymatic activities of HDAC1 and HDAC2. Such interference destabilizes the intricate MTA1/HDAC molecular assembly, culminating in the heightened acetylation of phosphatase and tensin homolog (PTEN) and the tumor suppressor P53. As a result, a cascade of cellular responses ensues, characterized by inhibited cellular proliferation, amplified apoptotic initiation, cell

cycle stagnation, and a marked reduction in cellular migratory and invasive capabilities (Butt et al., 2017; Qian et al., 2017; Qian et al., 2018a). Several studies have shed light on these mechanisms. PTS inhibited the proliferation of prostate cancer cells by modulating the PTEN/Akt pathway (Dhar et al., 2015; Qian et al., 2018b). PTS acts through a unique biochemical process, enhancing the acetylation and reactivation of the tumor suppressor gene PTEN. This effect is achieved by suppressing the MTA1/HDAC complex, which usually deacetylates proteins, thus altering their function. By inhibiting this complex, PTS ensures PTEN remains active, playing a key role in regulating the Akt pathway. The Akt pathway is involved in cell growth and survival, and its overactivity can lead to cancer. Therefore, Pterostilbene's ability to reactivate PTEN and regulate the Akt pathway highlights its potential as a therapeutic agent in cancer treatment. This mechanism offers a new perspective on targeting cellular pathways for disease therapy, particularly in cancer, where cell growth and survival pathways are often dysregulated.

Pterostilbene modulates miRNA in tumors

Cancer development is deeply influenced by microRNAs (miRNAs), which are crucial in regulating gene expression post-transcription. They can function as oncogenes, promoting cancer by downregulating tumor suppressors, or as tumor suppressors themselves, inhibiting cancer by targeting oncogenes. This duality in cancer biology makes miRNAs significant for both understanding cancer mechanisms and developing targeted therapies. Their regulation of key cellular processes like cell growth and apoptosis underscores their potential as biomarkers for cancer diagnosis and targets for innovative treatments (Peng and Croce, 2016). PTS exhibits a dose-dependent inhibitory effect on the vitality of endometrial cancer cells, notably inducing apoptosis *in vitro* through the downregulation of miR-663b (Wang et al., 2017). Regarding prostate cancer, the anticancer effects of PTS are manifested through the reduction of miR-17 family members, a phenomenon observed in both experimental and biological settings (Kumar et al., 2017). PTS enhances PTEN expression in liver cancer cells by directly inhibiting miR-19a, which leads to reduced cell growth, cell cycle halt at the S phase, increased apoptosis, and decreased cell invasion (Qian et al., 2018b). Given the importance of miRNAs in cancer diagnosis and outcome prediction, influencing these molecules might be a pivotal feature of pterostilbene's cancer-fighting capabilities.

Pterostilbene modulates endoplasmic reticulum stress in tumor

Endoplasmic reticulum stress (ERS) and the subsequent unfolded protein response (UPR) are crucial in the evolution and advancement of cancer. They act as a protective mechanism against physiological stress and can initiate apoptosis if the stress continues (Wang et al., 2012). Consequently, modulation of E.R. stress and manipulation of the UPR present promising methods for novel anticancer therapies. PTS induces the ROS-mitochondria-dependent apoptosis mechanism mediated by ERS, contributing to its anti-cancer activity in human esophageal cancer cells and inhibiting cell proliferation, invasion, and adhesion (Feng et al., 2016). PTS administration can activate ERS and elevate levels of ERS-associated molecules like p-PERK, ATF4, and CHOP. This action facilitates the transfer of Ca^{2+} from the endoplasmic reticulum to the cytoplasm, boosts reactive oxygen species (ROS) signaling, fosters cell apoptosis, and curtails the movement and adhesion of non-small cell lung cancer cells (Ma et al., 2017). Recent studies indicate that PTS enhances the vulnerability of triple-negative breast cancer cells to TRAIL-driven apoptosis by triggering the ROS/ERS signaling route and amplifying DR4 and DR5 expression (Hung et al., 2017). The ability of PTS to modulate ERS could have profound implications for cancer therapy, representing a promising avenue for future research.

Pterostilbene promotes the autophagy in tumors

Autophagy is a cellular self-digestion process in which a cell recycles portions of its components to maintain homeostasis and adapt to metabolic stress. In terms of cancer, autophagy can play a dual role by promoting cancer cell survival under pressure and preventing tumor progression by maintaining cellular integrity and reducing inflammation and genome instability (Amaravadi et al., 2019). Following exposure to PTS, cell contraction, membrane disruption, and autophagic vesicle genesis are conspicuous in cisplatin-resistant oral cancer cells. Concurrently, an augmentation in the expression of proteins integral to autophagy is observed, thus alluding to the potent autophagy-inducing efficacy of PTS. Importantly, PTS exerts inhibitory control over cell vitality and fusion, a characteristic that is both time and concentration-dependent (Chang et al., 2018). PTS demonstrates its antitumor efficacy through the induction of autophagy, and intriguingly, it does not exert apparent toxic effects on the heart, liver, and kidneys of tumor model mice. This safety profile underscores its potential as a promising antitumor agent (Mei et al., 2018). PTS exhibits its anticancer effects by inducing autophagy, presenting high therapeutic efficacy with minimal side effects. Its effectiveness and safety profile suggest a promising potential for development into an effective anticancer drug and its application in clinical settings.

Pterostilbene inhibits epithelial-mesenchymal transition and apoptosis in tumors

EMT is a pivotal mechanism facilitating cell migration and invasion, enabling the spread of tumor cells from their origin. PTS interacts with this mechanism, potentially thwarting or dampening EMT (Song et al., 2019). In triple-negative breast cancer cells, PTS hinders their migratory and invasive traits, characterized by a rise in the EMT marker E-cadherin and a decline in Snail, Slug, Vimentin, and ZEB1 (Su et al., 2015). Furthermore, PTS triggers apoptosis in vascular endothelial cells, a crucial strategy to combat cancer spread. Its action is linked to

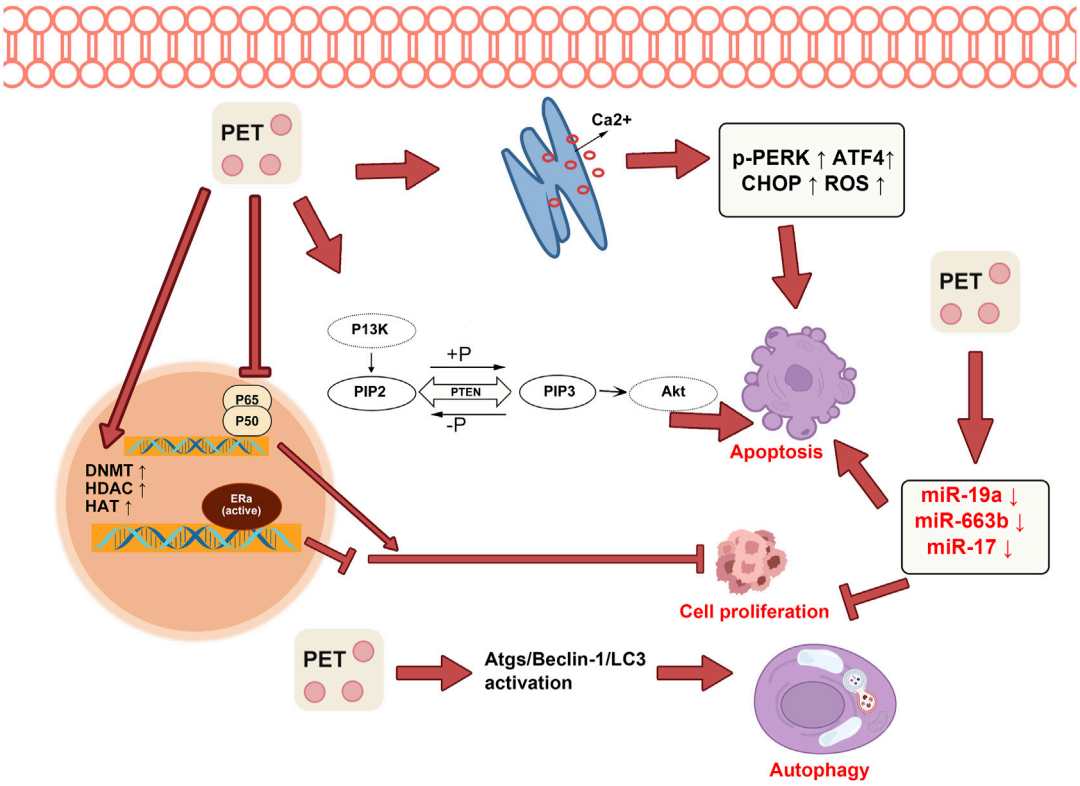

FIGURE 4
Pterostilbene inhibits tumor cell proliferation and promotes both cell apoptosis and autophagy. Pterostilbene effectively enhances endoplasmic reticulum Ca^{2+} efflux, leading to stimulation of the endoplasmic reticulum stress response and subsequent activation of the PI3K-AKT pathway, which effectively inhibits cell apoptosis. Moreover, it exerts suppressive effects on cell proliferation by inhibiting the NF-κB pathway and modulating the expression of specific microRNAs, including miR-17, miR-19a, and miR-663b. Additionally, pterostilbene promotes tumor cell autophagy by activating the Atgs/Beclin-1/lc3 pathways.

fostering autophagy *via* a surge in intracellular calcium concentration, leading to the activation of AMPKα1 (Zhang et al., 2013). A research piece from 2018 by Chen and others highlighted pterostilbene's capacity to curtail lung cancer cell metastasis by stimulating autophagy (Chen et al., 2012). In their study, varying PTS dosages reduced tumor size and burden in mice by notable percentages. Pterostilbene's interaction with the EMT process offers promising avenues in cancer therapies. Specifically, it downregulates NFκB, Twist1, and Vimentin and amplifies E-cadherin expression, markedly reducing tumorigenesis and metastasis in MDA-MB-231 cells when co-cultured with M2 TAMs (Mak et al., 2013).

Pterostilbene exerts a regulatory role in tumor stem cells

Cancer stem cells (CSCs) form a unique subset within the broader population of cancer cells, characterized primarily by their remarkable ability to self-renew and differentiate into various cell types. These cells are pivotal in the hierarchy of tumor cells due to their distinct characteristics. CSCs are known to be the primary contributors to the resilience of tumors, playing a significant role in drug resistance, recurrence, and metastasis of cancers. Their ability to evade traditional treatments and regenerate the tumor population makes them critical targets in cancer therapy (Zhao et al., 2018). PTS exhibits dose-dependent inhibition of self-renewal capacities and the gene expression of cancer stem cells in lung cancer cells cocultured with M2-TAMs (M2 phenotype tumor-associated macrophages). This effect appears to be mediated through the downregulation of the cancer-promoting gene, MUC1, which suppresses polarization towards M2 and reduces the accumulation of cancer stem cells (Huang et al., 2016). Through an array of signaling pathways, RSV and PTS can target CSCs in various malignancies, including but not limited to breast cancer, colorectal cancer, leukemia, glioblastoma, and lung cancer (Zhang et al., 2018).

Pterostilbene improves tumor drug resistance

The intricate nature of cancer often gives rise to the emergence of drug resistance, greatly impeding the effectiveness of numerous chemotherapy agents. This resistance can be attributed to diverse mechanisms, such as modifications in drug targets, heightened drug efflux, enhanced DNA repair, and evasion of drug-induced apoptosis (Cree and Charlton, 2017). PTS also reverses multidrug

resistance in cancer cells, suggesting its potential role in overcoming chemotherapy resistance (Wang et al., 2023). PTS amplifies cisplatin resistance by elevating LC3-II and Atg12 mRNA levels and boosting Atgs/Beclin-1/lc3-associated signals. This increased autophagy activity hinders the anti-cancer efficacy against human oral cancer CAR cells (Chang et al., 2018). The combined use of PTS and autophagy inhibitors has been shown to improve the therapeutic efficacy of chemotherapy drugs against both chemotherapy-sensitive and chemotherapy-resistant cancer cells. This beneficial effect likely stems from pterostilbene's capability to trigger autophagy, a cellular recycling process that cancer cells often exploit for survival, especially under stress conditions such as chemotherapy (Hsieh et al., 2014). The possible mechanisms of antitumor pterostilbene are shown in Figure 4.

Comparative efficacy of resveratrol and pterostilbene in tumor treatment

RSV and PTS, both exhibiting low IC50 values, have been found to downregulate the viral oncogene E6 and tumor protein VEGF levels. In mice treated with pterostilbene, a reduction in tumor size was observed, which was associated with apoptosis. This apoptotic process was indicated by the upregulation of activated caspase-3. On the other hand, resveratrol treatment in mice resulted in cell cycle arrest as evidenced by the downregulation of PCNA. These findings suggest that both resveratrol and pterostilbene have the potential to act as antineoplastic agents in treating HPV E6-positive tumors. They may suppress tumor growth through two distinct mechanisms: pterostilbene inducing apoptosis and resveratrol causing cell cycle arrest (Chatterjee et al., 2019). PTS demonstrated superior efficacy over RSV in suppressing HeLa cell growth, colony survival, and metastasis, and notably inhibiting tumorphere formation and migration in cancer stem-like cells. Its superior inhibitory effect is attributed to enhanced activation through multiple mechanisms, including cell cycle arrest at S and G2/M phases, induction of ROS-mediated caspase-dependent apoptosis, and inhibition of matrix metalloproteinase (MMP)-2/-9 expression (Shin et al., 2020).

Specific functions of pterostilbene and resveratrol

Obstructive sleep apnea (OSA) is typified by frequent episodes where the upper air passage experiences complete or partial blockage, lasting at least 10 seconds during sleep (Stöwhas et al., 2019). This disorder is widespread among sleep-related health issues. These occurrences trigger a cycle of chronic intermittent hypoxia (CIH), a rise in oxidative stress, and an increase in the levels of cytokines that promote inflammation (Kheirandish-Gozal and Gozal, 2019). The study explored the impact of RSV on lung damage due to CIH, a condition commonly associated with OSA. Following 12 weeks of CIH exposure, rats displayed heightened levels of inflammatory cytokines and increased apoptosis in lung tissues. Treatment with RSV led to reduced inflammation and cell death, as well as enhanced levels of Nrf2 and HO-1 proteins, suggesting that RSV could alleviate lung inflammation and apoptosis related to CIH by triggering the Nrf2/ARE pathway (Lian et al., 2020). Sun et al. demonstrated that resveratrol effectively mitigates myocardial damage associated with CIH by reducing oxidative and endoplasmic reticulum stress and suppressing the NLRP3 inflammasome (Sun et al., 2020).

This study explored the role of PTS, structurally similar to and more active than RSV. In exploring the effects of PTS on brain oxidative stress induced by CIH, a key factor in sleep disorders, the study revealed significant neurological improvements in a CIH mouse model. PTS was found to boost neuronal health, enhance antioxidant levels, and diminish both apoptosis and inflammation within the brain (Liu et al., 2023). Furthermore, it effectively modulated immune responses, increasing anti-inflammatory cells and cytokines, while reducing pro-inflammatory agents. The study highlights Pte's role in alleviating oxidative stress and correcting immune imbalances in neural cells, achieved through the activation of the p-ERK signaling pathway. Pterostilbene's effectiveness in tackling the intricate combination of oxidative stress and immune imbalances in OSA showcases its potential as a highly targeted and efficient therapeutic approach. This promising natural compound's ability to address multiple facets of OSA—from reducing oxidative damage in brain cells to balancing immune responses—signifies a substantial leap forward in developing effective treatments for this widely prevalent sleep disorder. Such multifaceted therapeutic action positions PTS as a noteworthy candidate in the future landscape of OSA management, potentially revolutionizing treatment protocols with its unique and powerful properties.

Safety and tolerability

The safety of PTS has been extensively studied in preclinical trials. Remarkably, even at a high dose of 3,000 mg/(kg·d), no observable toxic side effects were detected in animal subjects (Ruiz et al., 2009). Furthermore, the current human trials conducted to evaluate the safety of PTS have also yielded positive results. These trials suggest that when administered at therapeutic doses, PTS is safe for human consumption. This is particularly important as it indicates that PTS could be administered to patients without causing severe side effects that could potentially outweigh its benefits (Yang et al., 2017; Sun et al., 2023). However, long-term safety data are lacking, and some studies have raised concerns about potential liver toxicity at high doses (Lacerda et al., 2018). Therefore, further research is needed to determine the optimal dosing and duration of PTS treatment.

Conclusion

Growing evidence points to pterostilbene's strong anti-inflammatory and anti-cancer capabilities, highlighting its potential as a treatment for inflammatory and cancer-related conditions. Its antioxidant and neuroprotective attributes further amplify its therapeutic promise. While preliminary clinical studies are encouraging, comprehensive and rigorous trials are imperative to thoroughly assess its therapeutic benefits and safety. As studies progress, delineating the mechanisms of pterostilbene's actions and

determining the best dosage and delivery techniques for various medical uses will be essential.

Author contributions

PL: Data curation, Methodology, Resources, Writing–original draft. WT: Formal Analysis, Resources, Writing–original draft. KX: Conceptualization, Investigation, Writing–review and editing. GL: Conceptualization, Methodology, Writing–review and editing.

Funding

The author(s) declare that no financial support was received for the research, authorship, and/or publication of this article.

Conflict of interest

The authors declare that the research was conducted in the absence of any commercial or financial relationships that could be construed as a potential conflict of interest.

Publisher's note

All claims expressed in this article are solely those of the authors and do not necessarily represent those of their affiliated organizations, or those of the publisher, the editors and the reviewers. Any product that may be evaluated in this article, or claim that may be made by its manufacturer, is not guaranteed or endorsed by the publisher.

References

Abd-Elmawla, M. A., Abdelalim, E., Ahmed, K. A., and Rizk, S. M. (2023). The neuroprotective effect of pterostilbene on oxaliplatin-induced peripheral neuropathy via its anti-inflammatory, anti-oxidative and anti-apoptotic effects: comparative study with celecoxib. *Life Sci.* 315, 121364. doi:10.1016/j.lfs.2022.121364

Ahuja, I., Kissen, R., and Bones, A. M. (2012). Phytoalexins in defense against pathogens. *Trends Plant Sci.* 17, 73–90. doi:10.1016/j.tplants.2011.11.002

Akinwumi, B. C., Bordun, K. M., and Anderson, H. D. (2018). Biological activities of stilbenoids. *Int. J. Mol. Sci.* 19, 792. doi:10.3390/ijms19030792

Amaravadi, R. K., Kimmelman, A. C., and Debnath, J. (2019). Targeting autophagy in cancer: recent advances and future directions. *Cancer Discov.* 9, 1167–1181. doi:10.1158/2159-8290.Cd-19-0292

Amarnath Satheesh, M., and Pari, L. (2006). The antioxidant role of pterostilbene in streptozotocin-nicotinamide-induced type 2 diabetes mellitus in wistar rats. *J. Pharm. Pharmacol.* 58, 1483–1490. doi:10.1211/jpp.58.11.0009

Antonelli, M., and Kushner, I. (2017). It's time to redefine inflammation. *Faseb J.* 31, 1787–1791. doi:10.1096/fj.201601326R

Arulselvan, P., Fard, M. T., Tan, W. S., Gothai, S., Fakurazi, S., Norhaizan, M. E., et al. (2016). Role of antioxidants and natural products in inflammation. *Oxid. Med. Cell Longev.* 2016, 5276130. doi:10.1155/2016/5276130

Azzolini, M., La Spina, M., Mattarei, A., Paradisi, C., Zoratti, M., and Biasutto, L. (2014). Pharmacokinetics and tissue distribution of pterostilbene in the rat. *Mol. Nutr. Food Res.* 58, 2122–2132. doi:10.1002/mnfr.201400244

Baskaran, S., Finelli, R., Agarwal, A., and Henkel, R. (2021). Reactive oxygen species in male reproduction: a boon or a bane? *Andrologia* 53, e13577. doi:10.1111/and.13577

Brenner, C., and Boileau, A. C. (2019). Pterostilbene raises low density lipoprotein cholesterol in people. *Clin. Nutr.* 38, 480–481. doi:10.1016/j.clnu.2018.10.007

Butt, N. A., Kumar, A., Dhar, S., Rimando, A. M., Akhtar, I., Hancock, J. C., et al. (2017). Targeting MTA1/HIF-1α signaling by pterostilbene in combination with histone deacetylase inhibitor attenuates prostate cancer progression. *Cancer Med.* 6, 2673–2685. doi:10.1002/cam4.1209

Chang, H. P., Lu, C. C., Chiang, J. H., Tsai, F. J., Juan, Y. N., Tsao, J. W., et al. (2018). Pterostilbene modulates the suppression of multidrug resistance protein 1 and triggers autophagic and apoptotic mechanisms in cisplatin-resistant human oral cancer car cells via Akt signaling. *Int. J. Oncol.* 52, 1504–1514. doi:10.3892/ijo.2018.4298

Chatterjee, K., Mukherjee, S., Vanmanen, J., Banerjee, P., and Fata, J. E. (2019). Dietary polyphenols, resveratrol and pterostilbene exhibit antitumor activity on an hpv E6-positive cervical cancer model: an *in vitro* and *in vivo* Analysis. *Front. Oncol.* 9, 352. doi:10.3389/fonc.2019.00352

Chen, R. J., Lee, Y. H., Yeh, Y. L., Wu, W. S., Ho, C. T., Li, C. Y., et al. (2017). Autophagy-inducing effect of pterostilbene: a prospective therapeutic/preventive option for skin diseases. *J. Food Drug Anal.* 25, 125–133. doi:10.1016/j.jfda.2016.10.022

Chen, R. J., Tsai, S. J., Ho, C. T., Pan, M. H., Ho, Y. S., Wu, C. H., et al. (2012). Chemopreventive effects of pterostilbene on urethane-induced lung carcinogenesis in mice via the inhibition of egfr-mediated pathways and the induction of apoptosis and autophagy. *J. Agric. Food Chem.* 60, 11533–11541. doi:10.1021/jf302778a

Chen, Y., Zhang, H., Ji, S., Jia, P., Chen, Y., Li, Y., et al. (2021). Resveratrol and its derivative pterostilbene attenuate oxidative stress-induced intestinal injury by improving mitochondrial redox homeostasis and function via Sirt1 signaling. *Free Radic. Biol. Med.* 177, 1–14. doi:10.1016/j.freeradbiomed.2021.10.011

Cree, I. A., and Charlton, P. (2017). Molecular chess? Hallmarks of anti-cancer drug resistance. *BMC Cancer* 17, 10. doi:10.1186/s12885-016-2999-1

Dellinger, R. W., Garcia, A. M., and Meyskens, F. L., Jr. (2014). Differences in the glucuronidation of resveratrol and pterostilbene: altered enzyme specificity and potential gender differences. *Drug Metab. Pharmacokinet.* 29, 112–119. doi:10.2133/dmpk.dmpk-13-rg-012

Deng, L., Li, Y., Zhang, X., Chen, B., Deng, Y., and Li, Y. (2015). Uplc-ms method for quantification of pterostilbene and its application to comparative study of bioavailability and tissue distribution in normal and lewis lung carcinoma bearing mice. *J. Pharm. Biomed. Anal.* 114, 200–207. doi:10.1016/j.jpba.2015.04.045

Dhar, S., Kumar, A., Li, K., Tzivion, G., and Levenson, A. S. (2015). Resveratrol regulates pten/akt pathway through inhibition of mta1/hdac unit of the nurd complex in prostate cancer. *Biochim. Biophys. Acta* 1853, 265–275. doi:10.1016/j.bbamcr.2014.11.004

Dhar, S., Kumar, A., Zhang, L., Rimando, A. M., Lage, J. M., Lewin, J. R., et al. (2016). Dietary pterostilbene is a novel mta1-targeted chemopreventive and therapeutic agent in prostate cancer. *Oncotarget* 7, 18469–18484. doi:10.18632/oncotarget.7841

Dodda, D., Rama Rao, A., and Veeresham, C. (2020). *In vitro* and *in vivo* evaluation of pterostilbene for the management of diabetic complications. *J. Ayurveda Integr. Med.* 11, 369–375. doi:10.1016/j.jaim.2018.01.003

Estrela, J. M., Ortega, A., Mena, S., Rodriguez, M. L., and Asensi, M. (2013). Pterostilbene: biomedical applications. *Crit. Rev. Clin. Lab. Sci.* 50, 65–78. doi:10.3109/10408363.2013.805182

Feng, Y., Yang, Y., Fan, C., Di, S., Hu, W., Jiang, S., et al. (2016). Pterostilbene inhibits the growth of human esophageal cancer cells by regulating endoplasmic reticulum stress. *Cell Physiol. Biochem.* 38, 1226–1244. doi:10.1159/000443071

Gómez-Zorita, S., Fernández-Quintela, A., Lasa, A., Aguirre, L., Rimando, A. M., and Portillo, M. P. (2014). Pterostilbene, a dimethyl ether derivative of resveratrol, reduces fat accumulation in rats fed an obesogenic diet. *J. Agric. Food Chem.* 62, 8371–8378. doi:10.1021/jf501318b

Gómez-Zorita, S., González-Arceo, M., Trepiana, J., Aguirre, L., Crujeiras, A. B., Irles, E., et al. (2020). Comparative effects of pterostilbene and its parent compound resveratrol on oxidative stress and inflammation in steatohepatitis induced by high-fat high-fructose feeding. *Antioxidants (Basel)* 9, 1042. doi:10.3390/antiox9111042

Gómez-Zorita, S., Milton-Laskíbar, I., Aguirre, L., Fernández-Quintela, A., Xiao, J., and Portillo, M. P. (2021). Effects of pterostilbene on diabetes, liver steatosis and serum lipids. *Curr. Med. Chem.* 28, 238–252. doi:10.2174/0929867326666191029112626

Gu, T. T., Chen, T. Y., Yang, Y. Z., Zhao, X. J., Sun, Y., Li, T. S., et al. (2019). Pterostilbene alleviates fructose-induced renal fibrosis by suppressing tgf-β1/tgf-B type I receptor/smads signaling in proximal tubular epithelial cells. *Eur. J. Pharmacol.* 842, 70–78. doi:10.1016/j.ejphar.2018.10.008

Haghani, A., Li, C. Z., Robeck, T. R., Zhang, J., Lu, A. T., Ablaeva, J., et al. (2023). DNA methylation networks underlying mammalian traits. *Science* 381, eabq5693. doi:10.1126/science.abq5693

Henao-Mejia, J., Elinav, E., Strowig, T., and Flavell, R. A. (2012). Inflammasomes: far beyond inflammation. *Nat. Immunol.* 13, 321–324. doi:10.1038/ni.2257

Hougee, S., Faber, J., Sanders, A., De Jong, R. B., Van Den Berg, W. B., Garssen, J., et al. (2005). Selective cox-2 inhibition by a pterocarpus marsupium extract characterized by pterostilbene, and its activity in healthy human volunteers. *Planta Med.* 71, 387–392. doi:10.1055/s-2005-864130

Hsiao, P. C., Chou, Y. E., Tan, P., Lee, W. J., Yang, S. F., Chow, J. M., et al. (2014). Pterostilbene simultaneously induced G0/G1-phase arrest and map-mediated mitochondrial-derived apoptosis in human acute myeloid leukemia cell lines. *PLoS One* 9, e105342. doi:10.1371/journal.pone.0105342

Hsieh, M. J., Lin, C. W., Yang, S. F., Sheu, G. T., Yu, Y. Y., Chen, M. K., et al. (2014). A combination of pterostilbene with autophagy inhibitors exerts efficient apoptotic characteristics in both chemosensitive and chemoresistant lung cancer cells. *Toxicol. Sci.* 137, 65–75. doi:10.1093/toxsci/kft238

Huang, W. C., Chan, M. L., Chen, M. J., Tsai, T. H., and Chen, Y. J. (2016). Modulation of macrophage polarization and lung cancer cell stemness by Muc1 and development of a related small-molecule inhibitor pterostilbene. *Oncotarget* 7, 39363–39375. doi:10.18632/oncotarget.8101

Hung, C. M., Liu, L. C., Ho, C. T., Lin, Y. C., and Way, T. D. (2017). Pterostilbene enhances trail-induced apoptosis through the induction of death receptors and downregulation of cell survival proteins in trail-resistance triple negative breast cancer cells. *J. Agric. Food Chem.* 65, 11179–11191. doi:10.1021/acs.jafc.7b02358

Hurrle, S., and Hsu, W. H. (2017). The etiology of oxidative stress in insulin resistance. *Biomed. J.* 40, 257–262. doi:10.1016/j.bj.2017.06.007

Jardim, S. R., De Souza, L. M. P., and De Souza, H. S. P. (2023). The rise of gastrointestinal cancers as a global phenomenon: unhealthy behavior or progress? *Int. J. Environ. Res. Public Health* 20, 3640. doi:10.3390/ijerph20043640

Jayakumar, T., Wu, M.-P., Sheu, J.-R., Hsia, C.-W., Bhavan, P. S., Manubolu, M., et al. (2021). Involvement of antioxidant defenses and nf-κb/erk signaling in anti-inflammatory effects of pterostilbene, a natural analogue of resveratrol. *Appl. Sci.* 11, 4666. doi:10.3390/app11104666

Jeandet, P., Clément, C., Courot, E., and Cordelier, S. (2013). Modulation of phytoalexin biosynthesis in engineered plants for disease resistance. *Int. J. Mol. Sci.* 14, 14136–14170. doi:10.3390/ijms140714136

Jin, J., Wu, X., Yin, J., Li, M., Shen, J., Li, J., et al. (2019). Identification of genetic mutations in cancer: challenge and opportunity in the new era of targeted therapy. *Front. Oncol.* 9, 263. doi:10.3389/fonc.2019.00263

Kala, R., and Tollefsbol, T. O. (2016). A novel combinatorial epigenetic therapy using resveratrol and pterostilbene for restoring estrogen receptor-α (ERα) expression in erα-negative breast cancer cells. *PLoS One* 11, e0155057. doi:10.1371/journal.pone.0155057

Kang, L. L., Zhang, D. M., Jiao, R. Q., Pan, S. M., Zhao, X. J., Zheng, Y. J., et al. (2019). Pterostilbene attenuates fructose-induced myocardial fibrosis by inhibiting ros-driven pitx2c/mir-15b pathway. *Oxid. Med. Cell Longev.* 2019, 1243215. doi:10.1155/2019/1243215

Kapetanovic, I. M., Muzzio, M., Huang, Z., Thompson, T. N., and Mccormick, D. L. (2011). Pharmacokinetics, oral bioavailability, and metabolic profile of resveratrol and its dimethylether analog, pterostilbene, in rats. *Cancer Chemother. Pharmacol.* 68, 593–601. doi:10.1007/s00280-010-1525-4

Kheirandish-Gozal, L., and Gozal, D. (2019). Obstructive sleep apnea and inflammation: proof of concept based on two illustrative cytokines. *Int. J. Mol. Sci.* 20, 459. doi:10.3390/ijms20030459

King, E., O'brien, J., Donaghy, P., Williams-Gray, C. H., Lawson, R. A., Morris, C. M., et al. (2019). Inflammation in mild cognitive impairment due to Parkinson's disease, lewy body disease, and Alzheimer's disease. *Int. J. Geriatr. Psychiatry* 34, 1244–1250. doi:10.1002/gps.5124

Kosuru, R., Rai, U., Prakash, S., Singh, A., and Singh, S. (2016). Promising therapeutic potential of pterostilbene and its mechanistic insight based on preclinical evidence. *Eur. J. Pharmacol.* 789, 229–243. doi:10.1016/j.ejphar.2016.07.046

Kumar, A., Rimando, A. M., and Levenson, A. S. (2017). Resveratrol and pterostilbene as a microrna-mediated chemopreventive and therapeutic strategy in prostate cancer. *Ann. N. Y. Acad. Sci.* 1403, 15–26. doi:10.1111/nyas.13372

Lacerda, D. S., Bianchi, S. E., Pinós, W. L., Campos-Carraro, C., Türck, P., Hickmann, A. R., et al. (2018). Effect of pterostilbene complexed with cyclodextrin on rat liver: potential reduction of oxidative damage and modulation redox-sensitive proteins. *Med. Chem. Res.* 27, 2265–2278. doi:10.1007/s00044-018-2233-6

Lee, M. F., Liu, M. L., Cheng, A. C., Tsai, M. L., Ho, C. T., Liou, W. S., et al. (2013). Pterostilbene inhibits dimethylnitrosamine-induced liver fibrosis in rats. *Food Chem.* 138, 802–807. doi:10.1016/j.foodchem.2012.11.094

Lee, P. S., Chiou, Y. S., Ho, C. T., and Pan, M. H. (2018). Chemoprevention by resveratrol and pterostilbene: targeting on epigenetic regulation. *Biofactors* 44, 26–35. doi:10.1002/biof.1401

Li, J., Ruzhi, D., Hua, X., Zhang, L., Lu, F., Coursey, T. G., et al. (2016). Blueberry component pterostilbene protects corneal epithelial cells from inflammation via anti-oxidative pathway. *Sci. Rep.* 6, 19408. doi:10.1038/srep19408

Li, Y., Sun, C., Zhang, Y., Chen, X., Huang, H., Han, L., et al. (2023). Phase I metabolism of pterostilbene, a dietary resveratrol derivative: metabolite identification, species differences, isozyme contribution, and further bioactivation. *J. Agric. Food Chem.* 71, 331–346. doi:10.1021/acs.jafc.2c05334

Li, Y., Zhang, H., Tu, F., Cao, J., Hou, X., Chen, Y., et al. (2022). Effects of resveratrol and its derivative pterostilbene on hepatic injury and immunological stress of weaned piglets challenged with lipopolysaccharide. *J. Anim. Sci.* 100, skac339. doi:10.1093/jas/skac339

Li, Y. R., Li, S., and Lin, C. C. (2018). Effect of resveratrol and pterostilbene on aging and longevity. *Biofactors* 44, 69–82. doi:10.1002/biof.1400

Lian, N., Zhang, S., Huang, J., Lin, T., and Lin, Q. (2020). Resveratrol attenuates intermittent hypoxia-induced lung injury by activating the nrf2/are pathway. *Lung* 198, 323–331. doi:10.1007/s00408-020-00321-w

Libby, P., Loscalzo, J., Ridker, P. M., Farkouh, M. E., Hsue, P. Y., Fuster, V., et al. (2018). Inflammation, immunity, and infection in atherothrombosis: jacc review topic of the week. *J. Am. Coll. Cardiol.* 72, 2071–2081. doi:10.1016/j.jacc.2018.08.1043

Lim, Y. R. I., Preshaw, P. M., Lim, L. P., Ong, M. M. A., Lin, H. S., and Tan, K. S. (2020). Pterostilbene complexed with cyclodextrin exerts antimicrobial and anti-inflammatory effects. *Sci. Rep.* 10, 9072. doi:10.1038/s41598-020-66031-8

Lin, W. S., Leland, J. V., Ho, C. T., and Pan, M. H. (2020). Occurrence, bioavailability, anti-inflammatory, and anticancer effects of pterostilbene. *J. Agric. Food Chem.* 68, 12788–12799. doi:10.1021/acs.jafc.9b07860

Lin, Y. J., Ding, Y., Wu, J., and Ning, B. T. (2016). Pterostilbene as treatment for severe acute pancreatitis. *Genet. Mol. Res.* 15. doi:10.4238/gmr.15038330

Liu, H., Wu, X., Luo, J., Wang, X., Guo, H., Feng, D., et al. (2019). Pterostilbene attenuates astrocytic inflammation and neuronal oxidative injury after ischemia-reperfusion by inhibiting nf-κb phosphorylation. *Front. Immunol.* 10, 2408. doi:10.3389/fimmu.2019.02408

Liu, J., Fan, C., Yu, L., Yang, Y., Jiang, S., Ma, Z., et al. (2016). Pterostilbene exerts an anti-inflammatory effect via regulating endoplasmic reticulum stress in endothelial cells. *Cytokine* 77, 88–97. doi:10.1016/j.cyto.2015.11.006

Liu, J., Xu, J., Mi, Y., Yang, Y., Li, Q., Zhou, D., et al. (2020). Pterostilbene alleviates cerebral ischemia and reperfusion injury in rats by modulating microglial activation. *Food Funct.* 11, 5432–5445. doi:10.1039/d0fo00084a

Liu, P., Zhou, P., Zhang, X., Zhao, D., Chen, H., and Hu, K. (2023). Pterostilbene mediates glial and immune responses to alleviate chronic intermittent hypoxia-induced oxidative stress in nerve cells. *PLoS One* 18, e0286686. doi:10.1371/journal.pone.0286686

Liu, Y., Chan, F., Sun, H., Yan, J., Fan, D., Zhao, D., et al. (2011). Resveratrol protects human keratinocytes hacat cells from uva-induced oxidative stress damage by downregulating Keap1 expression. *Eur. J. Pharmacol.* 650, 130–137. doi:10.1016/j.ejphar.2010.10.009

Lubecka, K., Kurzava, L., Flower, K., Buvala, H., Zhang, H., Teegarden, D., et al. (2016). Stilbenoids remodel the DNA methylation patterns in breast cancer cells and inhibit oncogenic notch signaling through epigenetic regulation of Maml2 transcriptional activity. *Carcinogenesis* 37, 656–668. doi:10.1093/carcin/bgw048

Ma, Z., Yang, Y., Di, S., Feng, X., Liu, D., Jiang, S., et al. (2017). Pterostilbene exerts anticancer activity on non-small-cell lung cancer via activating endoplasmic reticulum stress. *Sci. Rep.* 7, 8091. doi:10.1038/s41598-017-08547-0

Ma, Z., Zhang, X., Xu, L., Liu, D., Di, S., Li, W., et al. (2019). Pterostilbene: mechanisms of its action as oncostatic agent in cell models and *in vivo* studies. *Pharmacol. Res.* 145, 104265. doi:10.1016/j.phrs.2019.104265

Mack, M. (2018). Inflammation and fibrosis. *Matrix Biol.* 68, 106–121. doi:10.1016/j.matbio.2017.11.010

Mak, K. K., Wu, A. T., Lee, W. H., Chang, T. C., Chiou, J. F., Wang, L. S., et al. (2013). Pterostilbene, a bioactive component of blueberries, suppresses the generation of breast cancer stem cells within tumor microenvironment and metastasis via modulating nf-κb/microrna 448 circuit. *Mol. Nutr. Food Res.* 57, 1123–1134. doi:10.1002/mnfr.201200549

Mamalis, A., and Jagdeo, J. (2017). The combination of resveratrol and high-fluence light emitting diode-red light produces synergistic photobotanical inhibition of fibroblast proliferation and collagen synthesis: a novel treatment for skin fibrosis. *Dermatol Surg.* 43, 81–86. doi:10.1097/dss.0000000000000921

Mccormack, D., and Mcfadden, D. (2013). A review of pterostilbene antioxidant activity and disease modification. *Oxid. Med. Cell Longev.* 2013, 575482. doi:10.1155/2013/575482

Mei, H., Xiang, Y., Mei, H., Fang, B., Wang, Q., Cao, D., et al. (2018). Pterostilbene inhibits nutrient metabolism and induces apoptosis through ampk activation in multiple myeloma cells. *Int. J. Mol. Med.* 42, 2676–2688. doi:10.3892/ijmm.2018.3857

Millán, I., Desco, M. D. C., Torres-Cuevas, I., Pérez, S., Pulido, I., Mena-Mollá, S., et al. (2019). Pterostilbene prevents early diabetic retinopathy alterations in a rabbit experimental model. *Nutrients* 12, 82. doi:10.3390/nu12010082

Miller, K. D., Nogueira, L., Mariotto, A. B., Rowland, J. H., Yabroff, K. R., Alfano, C. M., et al. (2019). Cancer treatment and survivorship statistics, 2019. *CA Cancer J. Clin.* 69, 363–385. doi:10.3322/caac.21565

Muzio, L., Viotti, A., and Martino, G. (2021). Microglia in neuroinflammation and neurodegeneration: from understanding to therapy. *Front. Neurosci.* 15, 742065. doi:10.3389/fnins.2021.742065

Nagarajan, S., Mohandas, S., Ganesan, K., Xu, B., and Ramkumar, K. M. (2022). New insights into dietary pterostilbene: sources, metabolism, and health promotion effects. *Molecules* 27, 6316. doi:10.3390/molecules27196316

Nussinov, R., Tsai, C. J., and Jang, H. (2022). How can same-gene mutations promote both cancer and developmental disorders? *Sci. Adv.* 8, eabm2059. doi:10.1126/sciadv.abm2059

Obrador, E., Salvador-Palmer, R., Jihad-Jebbar, A., López-Blanch, R., Dellinger, T. H., Dellinger, R. W., et al. (2021). Pterostilbene in cancer therapy. *Antioxidants (Basel)* 10, 492. doi:10.3390/antiox10030492

Park, E. S., Lim, Y., Hong, J. T., Yoo, H. S., Lee, C. K., Pyo, M. Y., et al. (2010). Pterostilbene, a natural dimethylated analog of resveratrol, inhibits rat aortic vascular smooth muscle cell proliferation by blocking akt-dependent pathway. *Vasc. Pharmacol.* 53, 61–67. doi:10.1016/j.vph.2010.04.001

Paul, S., Rimando, A. M., Lee, H. J., Ji, Y., Reddy, B. S., and Suh, N. (2009). Anti-inflammatory action of pterostilbene is mediated through the P38 mitogen-activated protein kinase pathway in colon cancer cells. *Cancer Prev. Res. (Phila)* 2, 650–657. doi:10.1158/1940-6207.Capr-08-0224

Peng, R. M., Lin, G. R., Ting, Y., and Hu, J. Y. (2018). Oral delivery system enhanced the bioavailability of stilbenes: resveratrol and pterostilbene. *Biofactors* 44, 5–15. doi:10.1002/biof.1405

Peng, Y., and Croce, C. M. (2016). The role of micrornas in human cancer. *Signal Transduct. Target Ther.* 1, 15004. doi:10.1038/sigtrans.2015.4

Peng, Y., Zhang, Y., Zhang, Y., Wang, X., and Xia, Y. (2021). Pterostilbene alleviates pulmonary fibrosis by regulating Asic2. *Chin. Med.* 16, 66. doi:10.1186/s13020-021-00474-7

Qian, Y. Y., Liu, Z. S., Pan, D. Y., and Li, K. (2017). Tumoricidal activities of pterostilbene depend upon destabilizing the mta1-nurd complex and enhancing P53 acetylation in hepatocellular carcinoma. *Exp. Ther. Med.* 14, 3098–3104. doi:10.3892/etm.2017.4923

Qian, Y. Y., Liu, Z. S., Yan, H. J., Yuan, Y. F., Levenson, A. S., and Li, K. (2018a). Pterostilbene inhibits mta1/hdac1 complex leading to pten acetylation in hepatocellular carcinoma. *Biomed. Pharmacother.* 101, 852–859. doi:10.1016/j.biopha.2018.03.022

Qian, Y. Y., Liu, Z. S., Zhang, Z., Levenson, A. S., and Li, K. (2018b). Pterostilbene increases pten expression through the targeted downregulation of microrna-19a in hepatocellular carcinoma. *Mol. Med. Rep.* 17, 5193–5201. doi:10.3892/mmr.2018.8515

Rahman, M. H., Akter, R., Bhattacharya, T., Abdel-Daim, M. M., Alkahtani, S., Arafah, M. W., et al. (2020). Resveratrol and neuroprotection: impact and its therapeutic potential in Alzheimer's disease. *Front. Pharmacol.* 11, 619024. doi:10.3389/fphar.2020.619024

Remsberg, C. M., Yáñez, J. A., Ohgami, Y., Vega-Villa, K. R., Rimando, A. M., and Davies, N. M. (2008). Pharmacometrics of pterostilbene: preclinical pharmacokinetics and metabolism, anticancer, antiinflammatory, antioxidant and analgesic activity. *Phytother. Res.* 22, 169–179. doi:10.1002/ptr.2277

Rimando, A. M., Kalt, W., Magee, J. B., Dewey, J., and Ballington, J. R. (2004). Resveratrol, pterostilbene, and piceatannol in vaccinium berries. *J. Agric. Food Chem.* 52, 4713–4719. doi:10.1021/jf040095e

Rohm, T. V., Meier, D. T., Olefsky, J. M., and Donath, M. Y. (2022). Inflammation in obesity, diabetes, and related disorders. *Immunity* 55, 31–55. doi:10.1016/j.immuni.2021.12.013

Roy, P., Orecchioni, M., and Ley, K. (2022). How the immune system shapes atherosclerosis: roles of innate and adaptive immunity. *Nat. Rev. Immunol.* 22, 251–265. doi:10.1038/s41577-021-00584-1

Ruiz, M. J., Fernández, M., Picó, Y., Mañes, J., Asensi, M., Carda, C., et al. (2009). Dietary administration of high doses of pterostilbene and quercetin to mice is not toxic. *J. Agric. Food Chem.* 57, 3180–3186. doi:10.1021/jf803579e

Saleh, R., Toor, S. M., Sasidharan Nair, V., and Elkord, E. (2020). Role of epigenetic modifications in inhibitory immune checkpoints in cancer development and progression. *Front. Immunol.* 11, 1469. doi:10.3389/fimmu.2020.01469

Salehi, B., Mishra, A. P., Nigam, M., Sener, B., Kilic, M., Sharifi-Rad, M., et al. (2018). Resveratrol: a double-edged sword in health benefits. *Biomedicines* 6, 91. doi:10.3390/biomedicines6030091

Schieber, M., and Chandel, N. S. (2014). Ros function in redox signaling and oxidative stress. *Curr. Biol.* 24, R453–R462. doi:10.1016/j.cub.2014.03.034

Shin, H. J., Han, J. M., Choi, Y. S., and Jung, H. J. (2020). Pterostilbene suppresses both cancer cells and cancer stem-like cells in cervical cancer with superior bioavailability to resveratrol. *Molecules* 25, 228. doi:10.3390/molecules25010228

Sochocka, M., Donskow-Łysoniewska, K., Diniz, B. S., Kurpas, D., Brzozowska, E., and Leszek, J. (2019). The gut microbiome alterations and inflammation-driven pathogenesis of Alzheimer's disease-a critical review. *Mol. Neurobiol.* 56, 1841–1851. doi:10.1007/s12035-018-1188-4

Song, L., Chen, T. Y., Zhao, X. J., Xu, Q., Jiao, R. Q., Li, J. M., et al. (2019). Pterostilbene prevents hepatocyte epithelial-mesenchymal transition in fructose-induced liver fibrosis through suppressing mir-34a/sirt1/P53 and tgf-β1/smads signalling. *Br. J. Pharmacol.* 176, 1619–1634. doi:10.1111/bph.14573

Stöwhas, A. C., Lichtblau, M., and Bloch, K. E. (2019). Obstructive sleep apnea syndrome. *Prax. (Bern 1994)* 108, 111–117. doi:10.1024/1661-8157/a003198

Su, C. M., Lee, W. H., Wu, A. T., Lin, Y. K., Wang, L. S., Wu, C. H., et al. (2015). Pterostilbene inhibits triple-negative breast cancer metastasis via inducing microrna-205 expression and negatively modulates epithelial-to-mesenchymal transition. *J. Nutr. Biochem.* 26, 675–685. doi:10.1016/j.jnutbio.2015.01.005

Sun, C., Li, Y., Zhang, Y., Huang, H., Chen, H., Chen, J., et al. (2023). Subacute oral toxicology and toxicokinetics of pterostilbene, a novel top1/tdp1 inhibiting anti-tumor reagent. *Drug Chem. Toxicol.* 46, 392–399. doi:10.1080/01480545.2022.2042014

Sun, H., Liu, X., Long, S. R., Teng, W., Ge, H., Wang, Y., et al. (2019). Antidiabetic effects of pterostilbene through pi3k/akt signal pathway in high fat diet and stz-induced diabetic rats. *Eur. J. Pharmacol.* 859, 172526. doi:10.1016/j.ejphar.2019.172526

Sun, Z. M., Guan, P., Luo, L. F., Qin, L. Y., Wang, N., Zhao, Y. S., et al. (2020). Resveratrol protects against cih-induced myocardial injury by targeting Nrf2 and blocking Nlrp3 inflammasome activation. *Life Sci.* 245, 117362. doi:10.1016/j.lfs.2020.117362

Tong, C., Wang, Y., Li, J., Cen, W., Zhang, W., Zhu, Z., et al. (2021). Pterostilbene inhibits gallbladder cancer progression by suppressing the pi3k/akt pathway. *Sci. Rep.* 11, 4391. doi:10.1038/s41598-021-83924-4

Tzeng, W. S., Teng, W. L., Huang, P. H., Lin, T. C., Yen, F. L., and Shiue, Y. L. (2021). Pterostilbene nanoparticles downregulate hypoxia-inducible factors in hepatoma cells under hypoxic conditions. *Int. J. Nanomedicine* 16, 867–879. doi:10.2147/ijn.S282172

Wang, H., Xu, J., Dong, P., Li, Y., Cui, Y., Li, H., et al. (2022). Comprehensive Analysis of pterostilbene metabolites *in vivo* and *in vitro* using a uhplc-Q-exactive plus mass spectrometer with multiple data-mining methods. *ACS Omega* 7, 38561–38575. doi:10.1021/acsomega.2c03924

Wang, J., Fang, X., and Liang, W. (2012). Pegylated phospholipid micelles induce endoplasmic reticulum-dependent apoptosis of cancer cells but not normal cells. *ACS Nano* 6, 5018–5030. doi:10.1021/nn300571c

Wang, P., and Sang, S. (2018). Metabolism and pharmacokinetics of resveratrol and pterostilbene. *Biofactors* 44, 16–25. doi:10.1002/biof.1410

Wang, Y. L., Shen, Y., Xu, J. P., Han, K., Zhou, Y., Yang, S., et al. (2017). Pterostilbene suppresses human endometrial cancer cells *in vitro* by down-regulating mir-663b. *Acta Pharmacol. Sin.* 38, 1394–1400. doi:10.1038/aps.2017.60

Wang, Z., Wang, T., Chen, X., Cheng, J., and Wang, L. (2023). Pterostilbene regulates cell proliferation and apoptosis in non-small-cell lung cancer via targeting cox-2. *Biotechnol. Appl. Biochem.* 70, 106–119. doi:10.1002/bab.2332

Wen, W., Lowe, G., Roberts, C. M., Finlay, J., Han, E. S., Glackin, C. A., et al. (2018). Pterostilbene suppresses ovarian cancer growth via induction of apoptosis and blockade of cell cycle progression involving inhibition of the Stat3 pathway. *Int. J. Mol. Sci.* 19, 1983. doi:10.3390/ijms19071983

Wu, J., Li, M., He, J., Lv, K., Wang, M., Guan, W., et al. (2019). Protective effect of pterostilbene on concanavalin a-induced acute liver injury. *Food Funct.* 10, 7308–7314. doi:10.1039/c9fo01405e

Wynn, T. A. (2007). Common and unique mechanisms regulate fibrosis in various fibroproliferative diseases. *J. Clin. Invest.* 117, 524–529. doi:10.1172/jci31487

Yan, W., Ren, D., Feng, X., Huang, J., Wang, D., Li, T., et al. (2021). Neuroprotective and anti-inflammatory effect of pterostilbene against cerebral ischemia/reperfusion injury via suppression of cox-2. *Front. Pharmacol.* 12, 770329. doi:10.3389/fphar.2021.770329

Yang, S. C., Tseng, C. H., Wang, P. W., Lu, P. L., Weng, Y. H., Yen, F. L., et al. (2017). Pterostilbene, a methoxylated resveratrol derivative, efficiently eradicates planktonic, biofilm, and intracellular mrsa by topical application. *Front. Microbiol.* 8, 1103. doi:10.3389/fmicb.2017.01103

Yi, M., Wang, G., Niu, J., Peng, M., and Liu, Y. (2022). Pterostilbene attenuates the proliferation and differentiation of TNF-α-treated human periodontal ligament stem cells. *Exp. Ther. Med.* 23, 304. doi:10.3892/etm.2022.11233

Yun, H., Park, S., Kim, M. J., Yang, W. K., Im, D. U., Yang, K. R., et al. (2014). Amp-activated protein kinase mediates the antioxidant effects of resveratrol through regulation of the transcription factor Foxo1. *Febs J.* 281, 4421–4438. doi:10.1111/febs.12949

Zeng, Q., Lian, W., Wang, G., Qiu, M., Lin, L., and Zeng, R. (2020). Pterostilbene induces Nrf2/Ho-1 and potentially regulates nf-κb and jnk-akt/mtor signaling in ischemic brain injury in neonatal rats. *3 Biotech.* 10, 192. doi:10.1007/s13205-020-02167-8

Zhang, L., Cui, L., Zhou, G., Jing, H., Guo, Y., and Sun, W. (2013). Pterostilbene, a natural small-molecular compound, promotes cytoprotective macroautophagy in vascular endothelial cells. *J. Nutr. Biochem.* 24, 903–911. doi:10.1016/j.jnutbio.2012.06.008

Zhang, L., Wen, X., Li, M., Li, S., and Zhao, H. (2018). Targeting cancer stem cells and signaling pathways by resveratrol and pterostilbene. *Biofactors* 44, 61–68. doi:10.1002/biof.1398

Zhang, Z. T., Deng, S. M., Chen, C., He, Q. H., Peng, X. W., Liang, Q. F., et al. (2023). Pterostilbene could alleviate diabetic cognitive impairment by suppressing TLR4/NF-κB pathway through microbiota-gut-brain axis. *Phytother. Res.* 37, 3522–3542. doi:10.1002/ptr.7827

Zhao, Y., Dong, Q., Li, J., Zhang, K., Qin, J., Zhao, J., et al. (2018). Targeting cancer stem cells and their niche: perspectives for future therapeutic targets and strategies. *Semin. Cancer Biol.* 53, 139–155. doi:10.1016/j.semcancer.2018.08.002

Zhou, J., Ci, X., Ma, X., Yu, Q., Cui, Y., Zhen, Y., et al. (2019). Pterostilbene activates the nrf2-dependent antioxidant response to ameliorate arsenic-induced intracellular damage and apoptosis in human keratinocytes. *Front. Pharmacol.* 10, 497. doi:10.3389/fphar.2019.00497

Zhou, Y., Zhang, X. M., Ma, A., Zhang, Y. L., Chen, Y. Y., Zhou, H., et al. (2015). Orally administrated pterostilbene attenuates acute cerebral ischemia-reperfusion injury in a dose- and time-dependent manner in mice. *Pharmacol. Biochem. Behav.* 135, 199–209. doi:10.1016/j.pbb.2015.06.009

frontiers | Frontiers in Pharmacology

TYPE Original Research
PUBLISHED 06 February 2024
DOI 10.3389/fphar.2024.1343936

OPEN ACCESS

EDITED BY
Boyang Ji,
BioInnovation Institute (BII), Denmark

REVIEWED BY
Xianyu Li,
China Academy of Chinese Medical Sciences, China
Rhitajit Sarkar,
National Institute of Diabetes and Digestive and Kidney Diseases (NIH), United States

*CORRESPONDENCE
Putri Cahaya Situmorang,
putri.cahaya@usu.ac.id

RECEIVED 27 November 2023
ACCEPTED 25 January 2024
PUBLISHED 06 February 2024

CITATION
Situmorang PC, Ilyas S, Syahputra RA, Nugraha AP, Putri MSS and Rumahorbo CGP (2024), *Rhodomyrtus tomentosa (Aiton) Hassk.* (haramonting) protects against allethrin-exposed pulmo damage in rats: mechanistic interleukins.
Front. Pharmacol. 15:1343936.
doi: 10.3389/fphar.2024.1343936

Rhodomyrtus tomentosa (Aiton) Hassk. (haramonting) protects against allethrin-exposed pulmo damage in rats: mechanistic interleukins

Putri Cahaya Situmorang[1]*, Syafruddin Ilyas[1], Rony Abdi Syahputra[2], Alexander Patera Nugraha[3], Mimmy Sari Syah Putri[1] and Cheryl Grace Pratiwi Rumahorbo[1]

[1]Study Program of Biology, Faculty of Mathematics and Natural Sciences, Universitas Sumatera Utara, Medan, Indonesia, [2]Department of Pharmacology, Faculty of Pharmacy, Universitas Sumatera Utara, Medan, Indonesia, [3]Department of Orthodontics, Faculty of Dental Medicine, Universitas Airlangga, Surabaya, Indonesia, [4]Study Program of Mathematics, Faculty of Mathematics and Natural Sciences, Universitas Sumatera Utara, Medan, Indonesia

Inhaling Allethrin (C19H26O3) may induce oxidative stress in lung cells by causing the formation of free radi-cals. Interleukins (IL) are a group of secreted cytokines or proteins and signaling molecules initially produced as an immune response by leukocytes. *Rhodomyrtus tomentosa (Aiton) Hassk.* (haramonting) contains antioxidants that may prevent lung damage induced by allethrin-containing electric mosquito repellents. In this study, six groups of rats were exposed to allethrin via an electric mosquito repellent, including positive, negative, and comparison control groups and three groups were administered Rhodomyrtus tomentosa (Aiton) Hassk at 100 mg/kg BW, 200 mg/kg BW, and 300 mg/kg BW. After 30 days, the pulmonary tissue and the blood were taken for immunohisto-chemical and ELISA analysis. The accumulation of inflammatory cells causes the thickening of the alveolar wall structures. Injuries were more prevalent in the A+ group than in the other groups. The connection between the alveoli and blood capillaries, which can interfere with alveolar gas exchange, is not regulated, and the lu-minal morphology is aberrant, causing damage to the alveolar epithelial cells. Exposure to electric mosquito coils containing allethrin can increase the expression of interleukin-1, interleukin-8, interleukin-9, and interleu-kin-18 in blood serum and tissues while decreasing the expression of interleukin-6 and interleukin-10. Like the Vitamin C group, Rhodomyrtus tomentosa can increase alveolar histological alterations by decreasing the ex-pression of IL-1β, IL-8, IL-9, and IL-18 while increasing IL-6 and IL-10. So that this plant can be developed in the future as a drug to prevent lung harm from exposure.

KEYWORDS

IL-1β, IL-6, IL-8, IL-9, IL-10, IL-18

1 Introduction

Technological advancements are advancing rapidly with the evolution of mosquito-repellent products. One of them is an electric form that does not produce smoke, such as mosquito coils, which has piqued the interest of many people, or people believe electric mosquito repellents are safer and more effective (Enayati et al., 2007). In Indonesia, mosquitoes are viewed as a vector for various diseases; consequently, many Indonesians use mosquito repellents, including electric mosquito repellent, to prevent mosquito bites (Ipa et al., 2020). First, however, we must be aware that Allethrin (C19H26O3) is a compound derived from pyrethroids that are used in electric mosquito repellents to eradicate mosquitoes and other insects that risk human health (Gargouri et al., 2018). The accumulation of allethrin in the body can form free radicals that induce oxidative stress in cells, a precursor to cancer (Arif et al., 2021). Through the production of free radicals, allethrin induces toxicity via oxidative stress. Hydrogen peroxide is a type of dangerous free radical (Gargouri et al., 2018). The toxic metabolism of the organism produces hydrogen peroxide. Hydrogen peroxide can generate harmful hydroxyl radicals through the Fenton and Haber-Weiss reactions (Phaniendra et al., 2015). Due to exposure to various free radicals, living organisms develop various defense mechanisms, including catalase, an enzymatic antioxidant defense (Phaniendra et al., 2015). If the insect repellent is inhaled or ingested for an extended period, serious side effects may occur (Naz et al., 2019). When used routinely, the active ingredients in electric mosquito repellents can gradually affect and cause abnormalities in the lungs and other organs of the human body (Naz et al., 2019).

The lungs are susceptible to interference as an organ of the body interacting with the outside world. As a consequence of exposure to hazardous particles, the structure of the lungs is disturbed and damaged (Neves et al., 2019). After exposure to mosquito repellents, alterations in the weight and color of the lungs of rats provide evidence of this disturbance (Hazarika et al., 2022). According to research, long-term use of mosquito repellents containing allethrin may increase the potential of developing ARI (Hazarika et al., 2022). Aside from a high temperature, dizziness, and shortness of breath, this illness can cause a cough, a runny nose, nasal congestion, a sore throat, lethargy, and vertigo (Neves et al., 2019). In addition, molecular studies show that allethrin activates the PI3K/AKT/mTOR messaging pathway, leading to oxidative damage, apoptosis, and autophagy (Jalouli et al., 2022).

Leukocytes produce a cytokine class called interleukins (IL) (Kany et al., 2019). Interleukins regulate cell growth, differentiation, and activation across immune and inflammatory responses (Kany et al., 2019). Interleukins are a protein superfamily that can cause a variety of responses in tissue and cell by binding to specific high-affinity cell surface receptors (Dinarello, 2018). Physical activity is one of the most effective mechanisms for lowering pro-inflammatory interleukin production because it strengthens the immune system (Taherkhani et al., 2020). Other processes that may affect the fat tissue include tissue inflammation decrease and, ultimately, the correction of hypoxia (Taherkhani et al., 2020).

The cytokine family IL-1 comprises 11 members; the lung is one of many essential tissues mediating fibrosis and inflammatory conditions (Borthwick, 2016). Seven of these members serve as agonists, the remaining three act as receptor antagonists, and the remaining member is an anti-inflammatory cytokine (Taherkhani et al., 2020). IL-1 is a vital inflammatory mediator (Borthwick, 2016). While it is essential to the body's ability to fight off infection, chronic sickness and acute injury contribute to tissue damage. IL-6 contributes vital functions in inflammatory conditions, immunology, and hematopoiesis and promotes fibrosis formation (Borthwick, 2016). IL-6 is widely acknowledged as a crucial actor in host defense due to its several roles in the immunological and hematopoietic function and causing an acute phase response (Tanaka et al., 2014). One of the most critical functions of IL-8 is inflammation, which helps bring more immune cells, like neutrophils, to infected areas (Cesta et al., 2022). Epithelial cells, which are smooth muscle cells in the respiratory system, also emit IL-8 in addition to macrophages (Cesta et al., 2022). Some of the impacts of IL-8 signaling include increased cancer cell, endothelial cell, and myeloid-derived suppressor cell motility (Pease and Sabroe, 2002). Inflammation with eosinophils, Hyperplasia, and hypertrophy of the mucosal vessels, as well as hyperresponsiveness of the bronchial tubes, are just some of the physiological changes within the respiratory tract that have been related to the pleiotropic cytokine IL-9 (Li et al., 2022). IL-10 is a cytokine that functions as an anti-inflammatory that aids in regulating the body's defenses to diseases, thereby protecting the organism from infection and maintaining tissue homeostasis (Iyer and Cheng, 2012). IFN production is another inflammatory cytokine that IL-18 greatly stimulates. Macrophages, dendritic cells, lymphocytes, and even specific nonimmune cells may produce IL-18 (Ihim et al., 2022).

Rhodomyrtus tomentosa (Aiton) Hassk., or haramonting, is a typical North Sumatera herbal plant containing acyl phloroglucinol, flavonoids, tannins, Rhodomyrtone, and acyl phloroglucinol (Zhang et al., 2018; Situmorang et al., 2022). This plant has been shown to enhance the histology of the testicles, liver, and cervical cancer (Irianti et al., 2020; Situmorang et al., 2023). This investigation examines the expression of the interleukin family in rat lung tissue and blood serum following exposure to allethrin via electric mosquito repellent. It is anticipated that the high antioxidant content of R. tomentosa can eventually be turned into herbal medicine, particularly for preventing lung damage caused by allethrin-containing electric mosquito repellents.

2 Materials and methods

2.1 Chemical and reagents

The antibodies used for the ELISA kit were ELISA Kit IL-1β PitokineR (Catalog number: EKO393-CAP), ELISA Kit Rat IL-6 (Catalog#E-E1-R0015, Elabscience), Rat IL-8 CXCL8 Elisa Kit (Catalog#Abx576575, Abbexa). Rat IL-9 ELISA Kit (Catalog#ERA34RB, ThermoFisher, United States), Rat IL-10 ELISA Kit (Catalog#ab214566, Abcam, United States) and Rat IL-18 ELISA Kit (Catalog#ab213909, Abcam, United States). The antibodies used for Immunohistochemistry were Invitrogen IL-1β Polyclonal Antibody (Catalog #PA5-119221,ThermoFisher Scientific, United States), Invitrogen IL-6 Monoclonal Antibody (Catalog #AHC0762, ThermoFisher Scientific, United States),

Invitrogen IL-8 (CXCL8) Polyclonal Antibody (Catalog # PA5-79113, ThermoFisher Scientific, United States), Bios IL-9 Polyclonal Antibody (Catalog#BS-2428R,ThermoFisher, United States), Invitrogen IL-10 Polyclonal Antibody (Catalog# PA5-94918, ThermoFisher Scientific, United States), Invitrogen IL-18 Polyclonal antibody (Catalog#PA5-79481, ThermoFisher Scientific, United States). Storage buffer solution (Catalogue # BS-0812R) was phosphate buffer solution (PBS) containing 50% glycerol and 1% bovine serum albumin (BSA).

2.2 Preparation of the *Rhodomyrtus tomentosa*

Rhodomyrtus tomentosa (Aiton) Hassk (Myrtaceae family) Leaves are mostly cultivated in the Berastasi region of Sumatera Utara Province, Indonesia. Registration number 012/MEDA/2022 at the Medanense Botanical Herbarium indicates that Dr. Nursahara Pasaribu, MSc of Universitas Sumatera Utara identified and approved the voucher in Medan, Indonesia. Afterwards, the object is subjected to a purification procedure that includes washing and subsequent natural drying. A quantity of 1.02 kg of *R. tomentosa (Aiton) Hassk* leaf powder was extracted by maceration in technical ethanol (70%) until fully submerged. The solvent used for extraction was replaced every 24 h. Upon acquiring an ethanol extract, it was subjected to evaporation in order to produce a concentrated ethanol extract. The formulation of this recipe was optimized for the oil phase, surfactants, and co-surfactants. A 0.5 mg dosage of *R. tomentosa (Aiton) Hassk* extract was added to the Tween 20 solution for sonification. Prior to the addition of capriol 90 and homogenization, PEG 400 was introduced and subjected to sonication. The resulting product is diluted at a ratio of 1 part product to 100 parts distilled water, and then thoroughly mixed using an ultrasonic equipment to ensure uniformity (Ilyas et al., 2021).

2.3 Animal handling

This investigation utilized 36 male of *Rattus norvegicus*. Male rats are 180–200 g in weight and 10–14 weeks old. Each group of six male rats contained six male rats was divided into six groups. Two weeks were used to acclimate male rats to the laboratory environment before they were placed in an enclosure with a constant room temperature (25.0.3°C) and humidity level (35%–60%). The cage was illuminated for 12 h, followed by 12 h of darkness. Male Rats were fed corn and pellets *ad libitum* and had unrestricted access to water. Rats were placed in a 40 cm × 30 cm plastic container. The rodents were placed in a 40-by-30-cm plastic case. The research was conducted with sanction from the USU FMIPA Medan Health Research Ethics Committee (No. 0896/KEPH-FMIPA/2022).

2.4 Research design

These investigations were conducted using a Randomized Complete Design (RCD). This form of study is referred to as an experimental study. One month was spent exposing rats to an electric mosquito repellent containing allethrin. In this investigation, six treatment groups were investigated. A-are negative control, A+ are rat exposed to allethrin, A1 are rat administered 0.2 mg/kg BW of vitamin C and then exposed to allethrin, A2 are rat administered 100 mg/kg BW of *R. tomentosa* and then exposed to allethrin, and A3 are rat administered 200 mg/kg BW of vitamin C and then exposed to allethrin. *Rhodomyrtus tomentosa* was then exposed to allethrin, and A4 were rat that was administered 300 mg/kg BW of *R. tomentosa* that was then exposed to allethrin. Within 30 days, administration of *Rhodomyrtus tomentosus* and exposure to an allethrin-containing mosquito repellent for 3 hours. After 30 days, a ketamine injection was administered for surgery, and the lungs and blood were removed for immunohistochemical and ELISA analysis, respectively.

2.5 Measurement of haematology parameters

A sterile pipette was used to obtain blood samples from the heart. To prevent hemolysis, water exposure was avoided. Within a microcentrifuge tube containing 0.5 mL, an anticoagulant solution consisting of 10 mL/1 mL EDTA was added. The City of Medan Health Laboratory ran the hematology tests. According to the guidelines provided by the manufacturer, each sample was analyzed three times.

2.6 Measurement of MDA, NGAL, and SOD

Measurements of MDA, NGAL, and SOD were obtained from blood samples collected from the heart. The duplicate reagent was poured to 50 mL wells, and blood samples were added to the rest. Each well received 50 mL biotinylated detection ab working solution. After covering the plate, 45 min were spent in an incubator at 37°C. After incubation, each well was refilled with 350 mL of wash buffer. The buffer was allowed to sit for a couple of minutes. After drying with absorbent paper, the solution was removed from each well. After three washing, each well received 100 L of HRP conjugate working solution. The dish was covered again and incubated at 37°C for 30 min. Each well received 90 mL substrate reagent following incubation. After that, a new cover plate was placed over everything and incubated at 37°C for 15 min. After the final incubation, each well received 50 mL of stop solution and the plate was covered to prevent light exposure for MDA Analysis. Regarding the measurement of NGAL, Subjected to centrifugation at a speed of 4,230 revolutions per minute for a duration of 5 minutes. After removing the supernatant, the samples were partitioned into three 0.5 cc containers. Prior to the evaluation, the samples were subjected to freezing and stored at a temperature of −200°C. The measurements were conducted using a commercial NGAL. Regarding the measurement of SOD, The standard solution was transferred into microplate wells using Eppendorf tubes. The microplate's empty wells received 0.1 mL of sample diluent buffer and rat blood serum as controls. The lid was a 90-min

microplate replica heated at 37°. The cover was removed and the wells emptied and transferred to tissue paper to remove any liquid from the microplate. Each well received 0.1 mL biotin SOD antibody solution. Reader. After sealing, the microplate was incubated at 37°C for 60 min. Each well received 0.1 mL of streptavidin-biotin complex (SABC) solution after incubation. After that, we covered the microplate and incubated it at 37°C for 30 min 90 L of TMB were pumped into each well after five wash buffer rinses. The microplate was sealed and incubated at 37°C for 25–30 min to turn blue. An ELISA reader at 450 nm measured OD absorbance.

2.7 Enzyme-linked immunosorbent assay (ELISA)

The initial blood sample was extracted from the rat's cardiac organ. To avoid coagulation, the blood should be placed in a tube containing an anticoagulant such as EDTA or citrate. The vials were incubated at ambient temperature for a duration of 10–20 min, followed by centrifugation at a speed of 2000–3,000 revolutions per minute for a period of 20 min. Subsequently, the gathered liquid portion might be utilized for examination. Subsequently, ten-well microplates were employed to create the standards. Dispense 100 µL of standard diluent into well 1 and 50 µL into well 2. Wells 3 and 4 each hold 50 µL of liquid, which is a portion of the total liquid found in wells 1 and 2. Similarly, wells 5 and 6 augment the solution volume by an additional 50 ul compared to the previous well, and this pattern continues until wells 9 and 10, when there is an additional 50 ul compared to the preceding wells. Subsequently, the mixture was incubated for a duration of 30 min at a temperature of 37°C, continuing throughout the night. The washing solution was made by dissolving 1 mL in 29 mL of distilled water. Subsequently, following the depletion of the well, proceed to cleanse it on five occasions using the washing solution prepared in Step 3. To facilitate the attachment of the antigen in the sample to the plate, introduce blocking buffer onto the plate and allow it to incubate for a duration of 60 min at a temperature of either 37°C or 40°C for a period of 24 h. Each well was filled with a 10:40 ratio of sample to diluent, with 10 ul of sample and 40 ul of diluent. Place the piece directly at the lowest point of the well. Next, it is necessary to meticulously blend the sample and sample diluent. Place the plate in a heated incubator and maintain it at a warm temperature for a duration of 120 min. Add 100 µM of biotinylated antibody to each well. The incubation period should last 24 h at a temperature of 37°C, with a duration of 60 min. The well should be emptied and the cleaning solution prepared in Step 3 should be used to cleanse the well on five separate occasions. Add 100 µL of ABC solution into each well. Place in a storage area with a temperature of 370°C for a duration of 30 min. Subsequently, drain the well and vigorously clean it with the washing solution prepared in Step 3 on five occasions. Subsequently, each well was subjected to treatment with 90 ul of HRP conjugate and 90 ul of TMB. Allow the plate to remain at a temperature of 370°C for a duration of 30 min. We introduced 100 µL of stop solution into each well, resulting in a transition from a blue color to a yellow tint. The determination of optical density (OD) values should be conducted using an ELISA reader set at a wavelength of 450 nm, with each sample being replicated three times (Simanullang et al., 2022a; Simanullang et al., 2022b).

2.8 Immunohistochemistry

IL-1β, IL-6, IL-8, IL-9, IL-10, and IL-18 were analyzed by immunohistochemistry to determine the histological effects of Rhodomyrtus tomentosa administration on the expression of several cytokines. The thickness of the paraffin-embedded lung tissue was between 4–5 microns. The tissue was pretreated by being heated at pH 6.0 and 350W in a citrate buffer. Antibodies against IL-1β, IL-6, IL-8, IL-9, IL-10, and IL-18 were incubated with the tissue after a PBS wash. Analysis of IL-1 in paraffin-embedded lung tissue. Polyclonal antibody (Product # PA5-119221) was used at 20 g/mL, and HRP-Linked Caprine Anti-Rabbit IgG was used at 2 g/mL, both in separate incubations with the samples. Overnight incubation at 4°C and 95% humidity with 1:20 dilution of IL-6 monoclonal antibody (Product # AHC0762) in 3% BSA-PBS. Storage buffer PBS containing 5 mg BSA was used to incubate IL-8 (CXCL8) with polyclonal antibody against IL-8 (CXCL8). Peroxidase-conjugated goat anti-rabbit IgG was employed as the secondary antibody, and the incubation temperature was set to 37°C for 30 min. DAB was used as the chromogen in conjunction with the HRP Conjugated Rabbit IgG Super Vision Assay Kit to create an image of the tissue segment. Anti-IL-9 Polyclonal Antibody, Unconjugated (bs-2428R) was used to label formalin-fixed, paraffin-embedded rat lungs at a dilution of 1:200, with a secondary antibody conjugate and DAB staining following. Next, 1 g/mL rabbit anti-IL10 antibody (Product # PA5-94918) was incubated with the tissue segment at 4°C for 24 h. Peroxidase-conjugated goat anti-rabbit IgG was employed as the secondary antibody, and the incubation temperature was set to 37°C for 30 min. Use a 1 g/mL dilution of the polyclonal antibody (Product # PA5-79481) against IL-18 (overnight at 4°C), followed by 30 min at 37°C with biotinylated goat anti-rabbit IgG. Staining with haematoxylin Mayer followed a chromogenic visualisation process with 3,3-diaminobenzidine (DAB) hydrochloride (Ilyas et al., 2022).

2.9 Statistical analysis of data

Average and standard deviation figures are provided for the data. The data was analyzed using SPSS 24's ANOVA and Kruskal–Wallis tests (for non-parametric data).

3 Results

3.1 Effect of *Rhodomyrtus tomentosa* on hematology parameters of allethrin-exposed rats

Hematological parameters were altered in Rats after treatment of 100–300 mg/kg BW of haramonting, as reported in Table 1. Hematological parameters were substantially different between groups A+ and B after administration of 100 mg/kg BW of haramonting. Hemoglobin, SGOT, and SGPT were substantially different in the Rhodomyrtus tomentosa 200 mg/kg BW group compared to the A+ group. Hemoglobin, leukocytes, lymphocytes, eosinophils, monocytes, SGOT, SGPT, and creatinine were substantially different in the 300 mg/kg BW group compared to

TABLE 1 *Effect of Rhodomyrtus tomentosa on Hematology parameters of* allethrin-exposed rats.

Hematology	Unit	Treatments (Mean ± SD)					
		A-	A+	A1	A2	A3	A4
Hemoglobin	g/dL	13.72 ± 0.41	28.07 ± 3.02$^{\#}$	15.44 ± 1.02*	27.08 ± 2.24	20.11 ± 2.07	16.44 ± 2.92*
Erythrocytes	x10^6/μL	8.51 ± 0.22	9.07 ± 0.06$^{\#}$	8.59 ± 0.04	8.69 ± 2.03	8.65 ± 1.04	8.60 ± 0.01
Leukocytes	x 10^3/μL	8.59 ± 0.23	13.03 ± 0.82$^{\#}$	9.02 ± 0.92*	12.76 ± 2.22	11.02 ± 1.02	9.32 ± 0.07*
Haematocrit	%	43.79 ± 1.03	47.08 ± 2.07	43.70 ± 2.01	46.09 ± 9.13	42.41 ± 4.20	42.70 ± 5.03
Neutrophils	x 10^3/μL	1.44 ± 0.09	3.04 ± 0.07$^{\#}$	1.48 ± 0.02*	3.02 ± 0.04	2.91 ± 0.01	1.48 ± 0.02
Lymphocytes	x 10^3/μL	5.86 ± 0.07	8.81 ± 1.07$^{\#}$	5.91 ± 0.34*	8.04 ± 1.97	7.22 ± 1.13	5.82 ± 0.04
Eosinophils	x 10^3/μL	0.048 ± 0.01	0.099 ± 0.01$^{\#}$	0.050 ± 0.01*	0.082 ± 0.01	0.067 ± 0.01	0.055 ± 0.01*
Monocytes	x 10^3/μL	0.471 ± 0.03	0.872 ± 0.01$^{\#}$	0.501 ± 0.01*	0.774 ± 0.02	0.603 ± 0.01	0.582 ± 0.01*
SGOT	u/L	114. 21 ± 4.81	231.92 ± 8.55$^{\#}$	115.07 ± 9.11*	200.95 ± 9.78	188.07 ± 9.81*	117.06 ± 9.21**
SGPT	u/L	50.16 ± 3.22	162.07 ± 12.09$^{\#\#}$	52.19 ± 10.02*	153.25 ± 9.56	86.91 ± 8.77*	55.39 ± 9.92**
Creatinine	mg/dL	0.44 ± 0.01	0.78 ± 0.01$^{\#}$	0.49 ± 0.02*	0.70 ± 0.02	0.61 ± 0.02	0.55 ± 0.01*
Ureum	mg/dL	21.09 ± 1.11	38.01 ± 3.22$^{\#}$	22.11 ± 3.15*	36.24 ± 1.29	32.42 ± 0.96	23.11 ± 2.95*

A-: control, A+: allethrin-exposed rats, A1: allethrin-exposed rats +0.02 mg Vitamin C, A2: allethrin-exposed rats +100 mg/Kg BW, of *Rhodomyrtus tomentosa*, A3: allethrin-exposed rats +200 mg/Kg BW, of *Rhodomyrtus tomentosa*, A4: allethrin-exposed rats +300 mg/Kg BW, of *Rhodomyrtus tomentosa*, ($^{\#}p < 0.05$ vs A-. $^{\#\#}p < 0.01$ vs A-, $^{*}p < 0.05$ compared A+, $^{**}p < 0.01$ vs A+).

TABLE 2 Effect of *Rhodomyrtus tomentosa of* allethrin-exposed rats on level of SOD, MDA and NGAL.

Parameters	Unit	Groups (Mean ± SD)					
		A-	A+	A1	A2	A3	A4
SOD	pg/mL	23.88 ± 2.41	14.62 ± 1.69$^{\#}$	23.21 ± 3.02*	18.12 ± 2.04	20.88 ± 0.09*	23.91 ± 3.04*
MDA	μM/L	8.45 ± 0.03	12.87 ± 2.88$^{\#}$	8.40 ± 1.09*	10.34 ± 2.21	9.87 ± 1.03*	8.81 ± 1.03*
NGAL	Ng/mL	0.215 ± 0.01	0.667 ± 0.01$^{\#}$	0.212 ± 0.01*	0.581 ± 0.01	0.435 ± 0.01*	0.235 ± 0.01*

A-: control, A+: allethrin-exposed rats, A1: allethrin-exposed rats +0.02 mg Vitamin C, A2: allethrin-exposed rats +100 mg/Kg BW, of *Rhodomyrtus tomentosa*, A3: allethrin-exposed rats +200 mg/Kg BW, of *Rhodomyrtus tomentosa*, A4: allethrin-exposed rats +300 mg/Kg BW, of *Rhodomyrtus tomentosa*, ($^{\#}p < 0.05$ vs C-, $^{*}p < 0.05$ vs C+).

the A+ group, but were comparable in the vitamin C or control groups (A1). Neither neutrophils, hematocrit, nor urea differed across groups ($p > 0.05$). The hematological data in Table 1 indicate that administration of 100–300 mg/kg BW of Rhodomyrtus tomentosa has an effect on the hematological parameters of rats, excluding neutrophil, hematocrit, and urea levels. In all categories, neutrophil, hematocrit, and urea levels are considered normal.

3.2 Effect of *Rhodomyrtus tomentosa* of allethrin-exposed rats on level of SOD, MDA and NGAL

When compared to groups A- and A1, there were significant differences found in the levels of SOD, MDA, and NGAL in rodents that had been exposed to allethrin ($p < 0.05$ or $p = 0.030$). The SOD levels of rats given 100 or 200 mg/kg BW of *R. tomentosa* were significantly different from those of rats in the A+ group, with the difference decreasing with higher dosages of these botanicals. *Rhodomyrtus tomentosa* reduced MDA levels compared to the A+ group at a dosage of 300 mg/kg BW (Table 2). *Rhodomyrtus tomentosa* reduced levels of MDA and NGAL in a dose-dependent manner. Antioxidants found in *R. tomentosa* have been shown to increase SOD activity and decrease serum levels of MDA and NGAL. *Rhodomyrtus tomentosa* has been shown to increase SOD activity, which in turn protects cells against oxidant disturbances and oxidative stress, both of which can lead to a number of lung disorders and injuries. Increased MDA and NGAL levels, along with reduced SOD activity, are indicators of increased lipid peroxide caused by an antioxidant deficiency.

3.3 Morphological and histological analysis of the lungs of allethrin-exposed rats after administration of *Rhodomyrtus tomentosa*

The color of the lungs differed between the control group (A-) and the allethrin exposure group (A+), with A-exhibiting a rich red hue and A+ exhibiting a pale hue with spots around the organs. Spots were also observed following administration of haramonting, but they diminished as the dose was increased (Figure 1). Rats exposed to an electric mosquito repellent containing allethrin developed lung injury. Based on histological findings (Figure 2), both Group A-

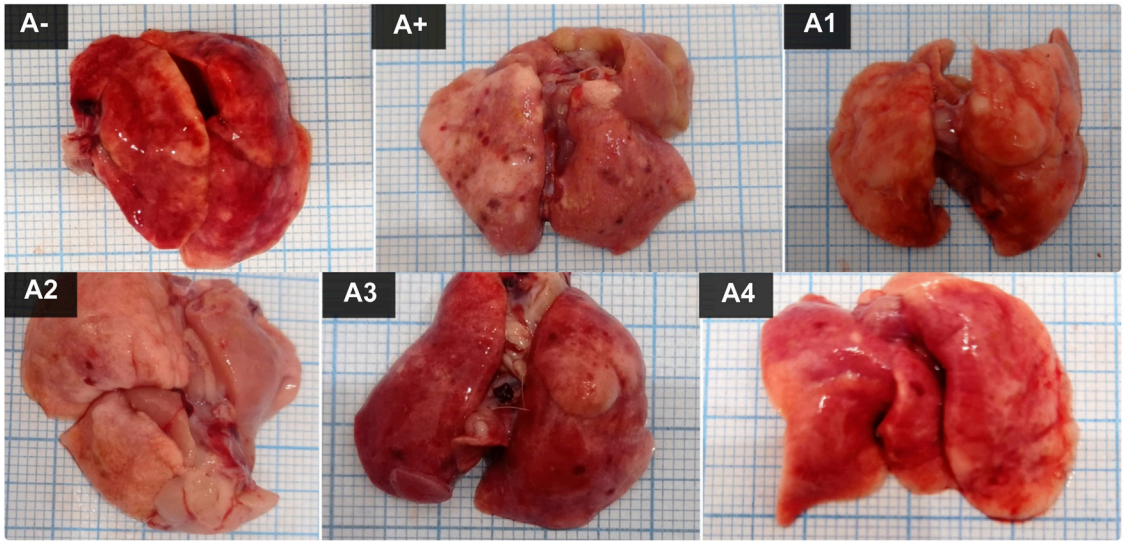

FIGURE 1
The lung Morphological of allethrin-exposed rats after administration of *Rhodomyrtus tomentosa*. **(A-)**: Control, **(A+)**: allethrin-exposed rats, **(A1)**: allethrin-exposed rats +0.02 mg Vitamin C, **(A2)**: allethrin-exposed rats +100 mg/Kg BW of *Rhodomyrtus tomentosa*, **(A3)**: allethrin-exposed rats +200 mg/Kg BW of *Rhodomyrtus tomentosa*, **(A4)**: allethrin-exposed rats +300 mg/Kg BW of *Rhodomyrtus tomentosa*.

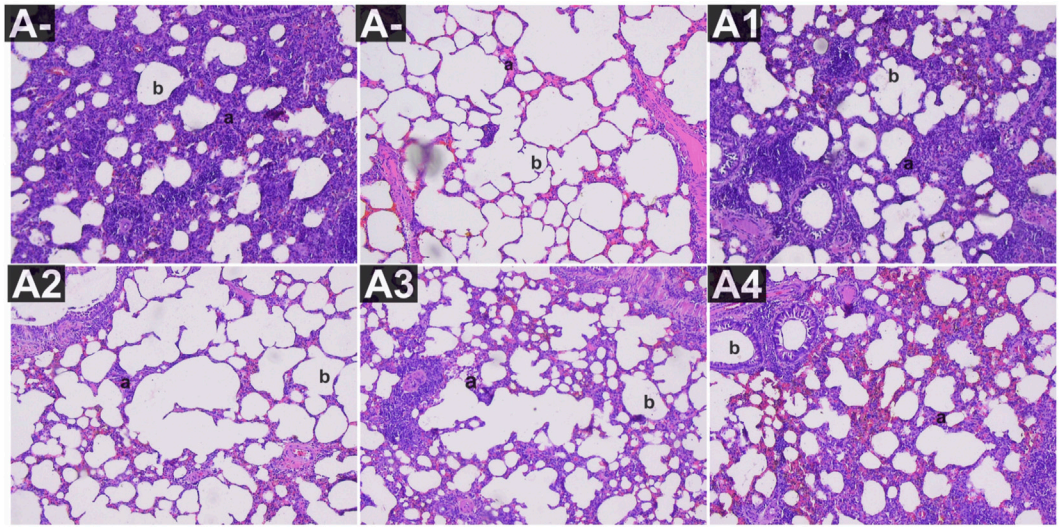

FIGURE 2
Histological analysis of the lungs of allethrin-exposed rats after administration of *Rhodomyrtus tomentosa*. **(A-)**: Control, **(A+)**: allethrin-exposed rats, **(A1)**: allethrin-exposed rats +0.02 mg Vitamin C, **(A2)**: allethrin-exposed rats +100 mg/Kg BW of *Rhodomyrtus tomentosa*, **(A3)**: allethrin-exposed rats +200 mg/Kg BW of *Rhodomyrtus tomentosa*, **(A4)**: allethrin-exposed rats +300 mg/Kg BW of *Rhodomyrtus tomentosa*. **(a)**. Membrane, **(b)**. Lumen (40x).

(control) and Group A1 had thickened alveolar membranes, but lumen size and alveolar density varied. However, herbal administration (A2 to A4) elongated the alveolar connections, diminished the cell nucleus, and weakened the cell membrane. The accumulation of inflammatory cells in the alveolar wall structures led to their thickening. The incidence of injury was greater in the A+ group than in the other groups. Damage is also observed in the alveolar epithelial cells as a result of the connection between the alveoli and blood capillaries, in which the alveolar gas exchange is not tightly regulated and the lumen morphology is irregular.

3.4 Expression of IL-1β on lung histological changes and serum after administration of *Rhodomyrtus tomentosa* in allethrin-exposed rats

Blood serum from rats was analyzed to determine IL-1β expression. Following the administration of haramonting (*R. tomentosa*) at the lowest dose, rat blood that had been exposed to allethrin via an electric mosquito repellent exhibited a high level of IL-1β expression. *Rhodomyrtus tomentosa* inhibited IL-1 *β*

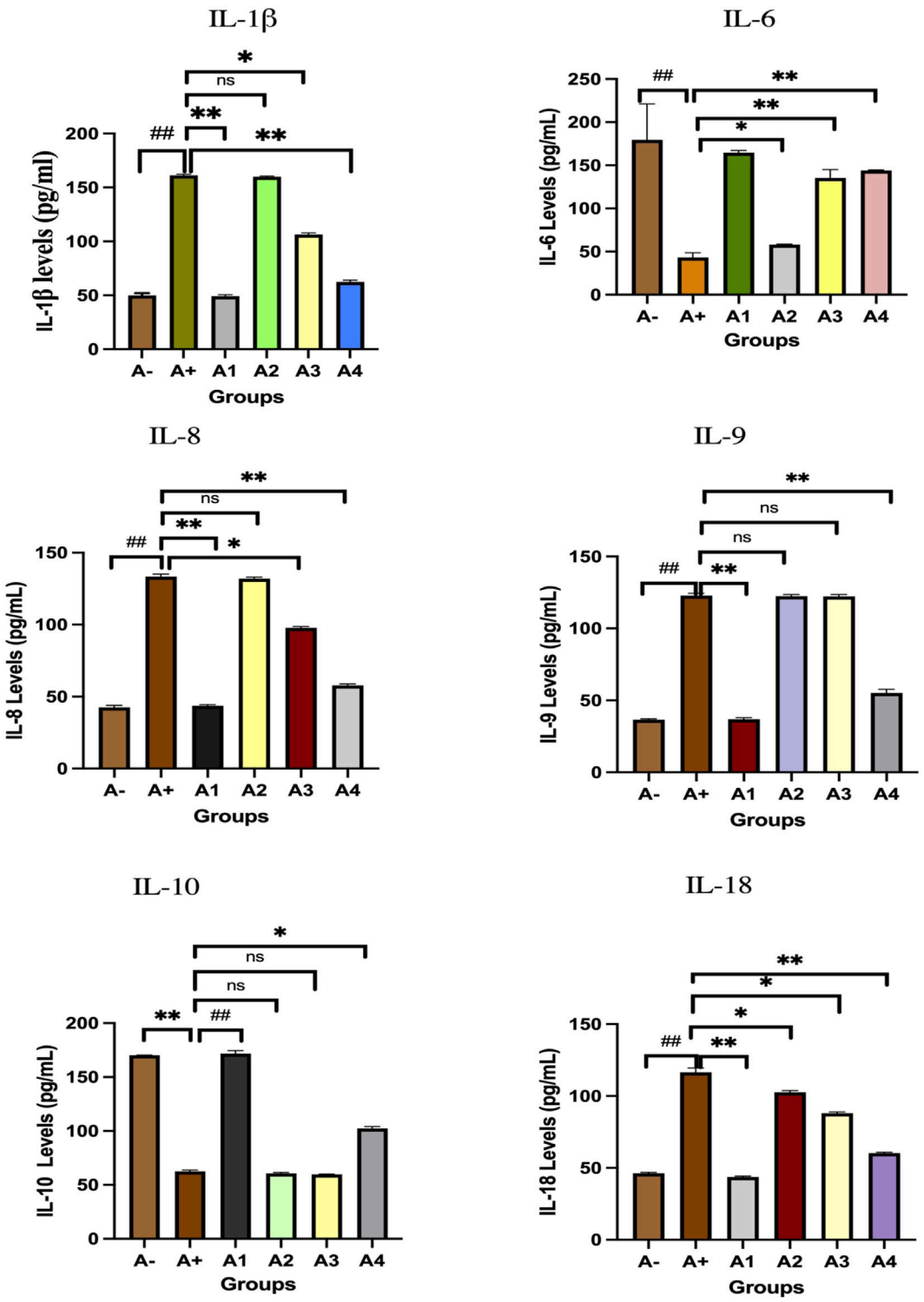

FIGURE 3
Expression of interleukins family after administration of *Rhodomyrtus tomentosa* in allethrin-exposed rats. A-: Control, A+: allethrin-exposed rats, A1: allethrin-exposed rats +0.02 mg Vitamin C, A2: allethrin-exposed rats +100 mg/Kg BW of *Rhodomyrtus tomentosa*, A3: allethrin-exposed rats +200 mg/Kg BW of *Rhodomyrtus tomentosa*, A4: allethrin-exposed rats +300 mg/Kg BW of *Rhodomyrtus tomentosa* ($^{ns}p > 0.05$, $^{\#\#}p < 0.01$ vs A-, $^{*}p < 0.05$ vs A+, $^{**}p < 0.01$ vs A+).

expression noticeably at 200 and 300 mg/kgBW. There is evidence that the highest dose of this plant can inhibit IL-1β production (Figure 3). Kruskal–Wallis tests performed on the nonparametric data showed that there were significant variations in IL-1β expression between the groups (Supplementary Table S3). The Mann-Whitney test showed that there was a statistically significant difference between the A+ group and IL-1β expression ($p < 0.01$, $p = 0.001$). *Rhodomyrtus tomentosa* (100 mg/kg BW) and

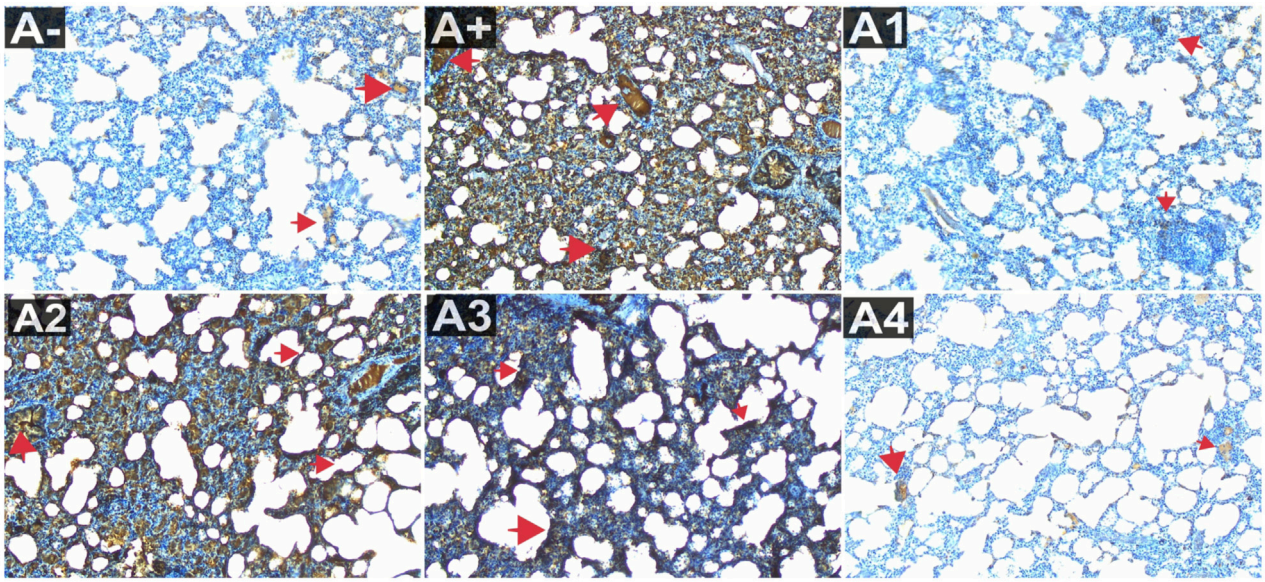

FIGURE 4
Expression of IL-1β on lung histological changes after administration of *Rhodomyrtus tomentosa* in allethrin-exposed rats. **(A-)**: Control, **(A+)**: allethrin-exposed rats, **(A1)**: allethrin-exposed rats +0.02 mg Vitamin C, **(A2)**: allethrin-exposed rats +100 mg/Kg BW of *Rhodomyrtus tomentosa*, **(A3)**: allethrin-exposed rats +200 mg/Kg BW of *Rhodomyrtus tomentosa*, **(A4)**: allethrin-exposed rats +300 mg/Kg BW of *Rhodomyrtus tomentosa* ($^{ns}p > 0.05$, $^{\#\#}p < 0.01$ vs A-, $^{*}p < 0.05$ vs A+, $^{**}p < 0.01$ vs A+).

A2 (100 mg/kg BW) were both below the threshold for statistical significance required to detect a difference. There were no statistically significant changes ($p > 0.01$) between the A+ and control groups at 100 mg/kg BW, but there were at 200 and 300 mg/kg BW. The analysis results in the table are supported by histological changes in the lung tissue due to IL-1β expression. The expression of IL-1 was highest in Group A+ and lowest in Group A- and *Rhodomyrtus* tomentosa at 300 mg/kg BW (Figure 4).

3.5 Expression of IL-6 on lung histological changes and serum after administration *of Rhodomyrtus tomentosa* in allethrin-exposed rats

The comparison group (A1) expressed the most IL-6, followed by the Vitamin C-treated group (A1) and the control group (A-). Allethrin exposure via electric mosquito repellent can reduce IL-6 (A+) expression. Even at the lowest dose, *R. tomentosa* suppressed the production of this protein (A1). The expression of IL-6 was upregulated at 200 and 300 mg/kgBW, although the mean value was the same as in the vitamin C group (Figure 3). The IL-6 expression levels were substantially different between the groups ($p < 0.01$). Expression levels of IL-6 were found to be significantly different between the A group and the A+ group using the Mann-Whitney test ($p < 0.00$, $p = 0.002$). While there was no statistically significant difference between 100 and 300 mg/kg BW of *R. tomentosa,* histological analysis of alterations in this protein (Figure 5) showed that there was an overall decrease. Expression of IL-6 was highest in the A- and A1 groups (control and vitamin C, respectively), and lowest in the A4 group.

3.6 Expression of IL-8 on lung histological changes and serum after administration of *Rhodomyrtus tomentosa* in allethrin-exposed rats

Figure 3 depicts the expression of IL-8 in the blood serum of rats exposed to electric mosquito repellents. When this plant was given at a dose of 100 mg/kg BW, there was no discernible change in IL-8 expression. There was a statistically significant reduction in IL-8 expression at dosages of 200 mg/kg BW ($p < 0.05$) and 300 mg/kg BW (A3). According to the results of the Kruskal–Wallis test presented, there is a statistically significant distinction in IL-8 expression between the groups. According to the Mann-Whitney test, there was a statistically significant difference between the A+ group and the IL-8 expression group ($p < 0.01$, $p = 0.002$). There was insufficient data to determine whether or not *R. tomentosa* (100 mg/kg BW) or A2 (100 mg/kg BW) had any effect. At lower doses (200 and 300 mg/kg BW), there were no statistically significant differences ($p > 0.05$) between the A+ group and the comparator groups (A1 and A-). This can be seen in (Figure 6) The *R. tomentosa* at 300 mg/kg BW (A4) group had the lowest levels of IL-8 expression, followed by group A+ and group A-.

3.7 Expression of IL-9 on lung histological changes and serum after administration of *Rhodomyrtus tomentosa* in allethrin-exposed rats

Expression of IL-9 in the blood serum of rats exposed to electric mosquito repellents revealed an increase in IL-9 expression that was

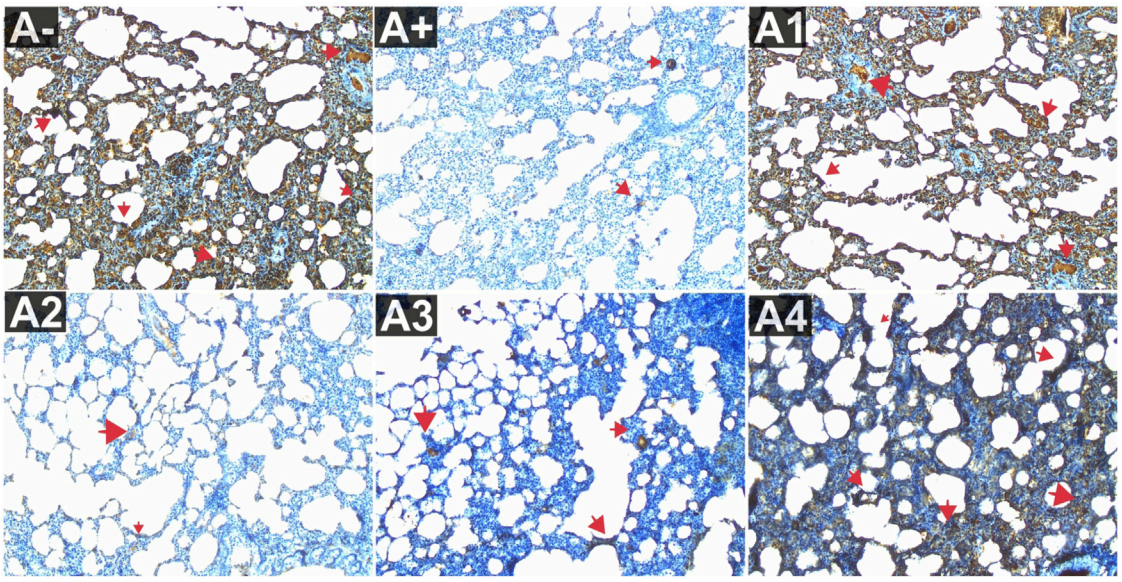

FIGURE 5
Expression of IL-6 on lung histological changes after administration of *Rhodomyrtus tomentosa* in allethrin-exposed rats. **(A-)**: Control, **(A+)**: allethrin-exposed rats, **(A1)**: allethrin-exposed rats +0.02 mg Vitamin C, **(A2)**: allethrin-exposed rats +100 mg/Kg BW of *Rhodomyrtus tomentosa*, **(A3)**: allethrin-exposed rats +200 mg/Kg BW of *Rhodomyrtus tomentosa*, **(A4)**: allethrin-exposed rats +300 mg/Kg BW of *Rhodomyrtus tomentosa*.

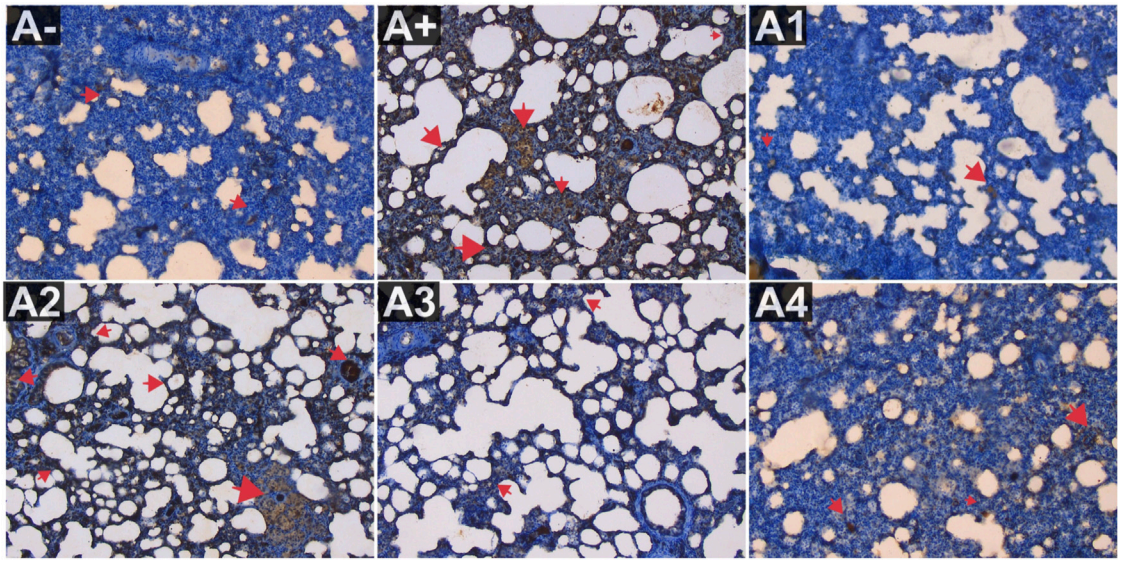

FIGURE 6
Expression of IL-8 on lung histological changes after administration of *Rhodomyrtus tomentosa* in allethrin-exposed rats. **(A-)**: Control, **(A+)**: allethrin-exposed rats, **(A1)**: allethrin-exposed rats +0.02 mg Vitamin C, **(A2)**: allethrin-exposed rats +100 mg/Kg BW of *Rhodomyrtus tomentosa*, **(A3)**: allethrin-exposed rats +200 mg/Kg BW of *Rhodomyrtus tomentosa*, **(A4)**: allethrin-exposed rats +300 mg/Kg BW of *Rhodomyrtus tomentosa* ($^{ns}p > 0.05$, $^{\#\#}p < 0.01$ vs A-, $^{*}p < 0.05$ vs A+, $^{**}p < 0.01$ vs A+).

not significantly different at 100 mg/kg BW (A2) and 200 mg/kg BW (A3). At the greatest dose, 300 mg/kgBW (A3), there was a significant reduction in IL-8 expression. According to the results of the Kruskal–Wallis test presented in Supplementary Table S1, there is a statistically significant difference in IL-9 expression between the groups. The Mann-Whitney test revealed a statistically significant disparity between the A+ group and the IL-9 expression group ($p < 0.01$, $p = 0.003$). *Rhodomyrtus tomentosa* doses between 100 and 200 mg/kg body weight showed no statistically significant difference ($p > 0.05$) between groups A+. However, when compared to the A+ group, substantial differences emerged at 300 mg/kg BW. The expression of IL-9 was highest in group A+ and lowest in group A- and Vitamin C (A1) (Figure 7). Nevertheless, the administration of this plant yields

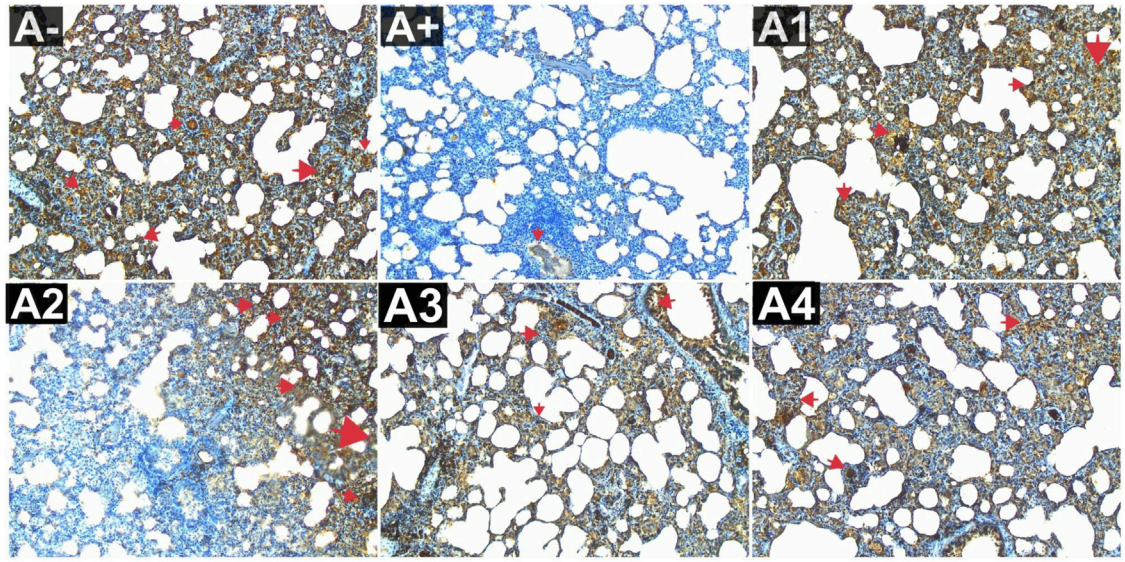

FIGURE 7
Expression of IL-9 on lung histological changes after administration of *Rhodomyrtus tomentosa* in allethrin-exposed rats. **(A-)**: Control, **(A+)**: allethrin-exposed rats, **(A1)**: allethrin-exposed rats +0.02 mg Vitamin C, **(A2)**: allethrin-exposed rats +100 mg/Kg BW of *Rhodomyrtus tomentosa*, **(A3)**: allethrin-exposed rats +200 mg/Kg BW of *Rhodomyrtus tomentosa*, **(A4)**: allethrin-exposed rats +300 mg/Kg BW of *Rhodomyrtus tomentosa* ($^{ns}p > 0.05$, $^{\#\#}p < 0.01$ vs A-, $^{*}p < 0.05$ vs A+, $^{**}p < 0.01$ vs A+).

identical outcomes to those of Vitamin C, so enhancing lung histology, but the histological architecture of the lungs in the untreated group of rats exhibited damage characterized by the initial loss of the alveolar septum, together with the presence of inflammatory cell infiltration and edema, as a result of chemical exposure.

3.8 Expression of IL-10 on lung histological changes and serum after administration of *Rhodomyrtus tomentosa* in allethrin-exposed rats

The expression of IL-10 was also evaluated in the blood serum of rats allethrin exposed to electric mosquitoes, which revealed a decrease in IL-10 expression that was not substantially different at 100 mg/kg BW (A2) and 200 mg/kg BW (A3). Figure 3 displayed considerable increase in IL-10 expression at the highest doses of vitamin C (A1) and 300 mg/kgBW (A3). IL-10 expression differed significantly ($p < 0.01$, Supplementary Table S1) between the groups. The Mann-Whitney *U* test revealed a statistically significant difference in IL-10 expression between the A+ group and the other groups ($p < 0.00$, $p = 0.001$). At 100 mg/kg BW of *R. tomentosa*, this difference was not statistically significant. There was a big discrepancy between the A+ dose and the standard dose of 200–300 mg/kgBW. Figure 8 shows that IL-10 expression was highest in the control (A-) and vitamin C (A1) groups and lowest in the A+ group. Histologically, In the untreated group of rats, the alveoli were coated with macrophages. An increase in the number of alveoli can be observed, along with an increase in the number of macrophages or dust cells around the alveoli. The alveoli exhibit a granular texture and seem smooth on the alveolar macrophages. The cytoplasm, which has an oval form, is visible across the whole field of vision. Moreover, alterations in the structure of the membrane. The alveoli become apparent due to the loss of endothelial cells that line the blood vessels around them. This leads to the enlargement of the blood vessels, allowing the blood cells to exit and disseminate. Pulmonary edema is characterized by the swelling of the alveolar surface and widening of the lumen of the alveoli, which can be observed visually. This leads to pulmonary harm and impairs the functioning of the respiratory system. Nevertheless, the administration of this plant yields identical outcomes to those of Vitamin C, so enhancing lung histology.

3.9 Expression of IL-18 on lung histological changes and serum after administration of *Rhodomyrtus tomentosa in* allethrin-exposed rats

IL-18 expression was also evaluated in the blood serum of rats exposed to alltehrin from electric mosquitoes, which showed a decrease in expression at each dose level where IL-18 expression was lowest at A-, A1 and followed by the highest dose of *R. tomentosa*, namely, 300 mg/kg BW (A3). Kruskal–Wallis test results (Supplementary Table S1) reveal that there is a statistically significant difference in IL-18 expression across groups. Using the Mann-Whitney *U* test, we found that A+ and B+ groups substantially differed from one another in IL-18 expression ($p < 0.01$, $p = 0.002$). There was no statistically significant difference between *R. tomentosa* (100 mg/kg) and A2 ($p > 0.02$). Histologically Nonetheless, alterations appeared at 200 and 300 mg/kg BW ($p < 0.05$) in Figure 9 when compared to the A+ group. Group A+ showed the highest IL-18 expression, whereas groups A- and *R. tomentosa* 300 mg/kg BW (A4) showed the lowest.

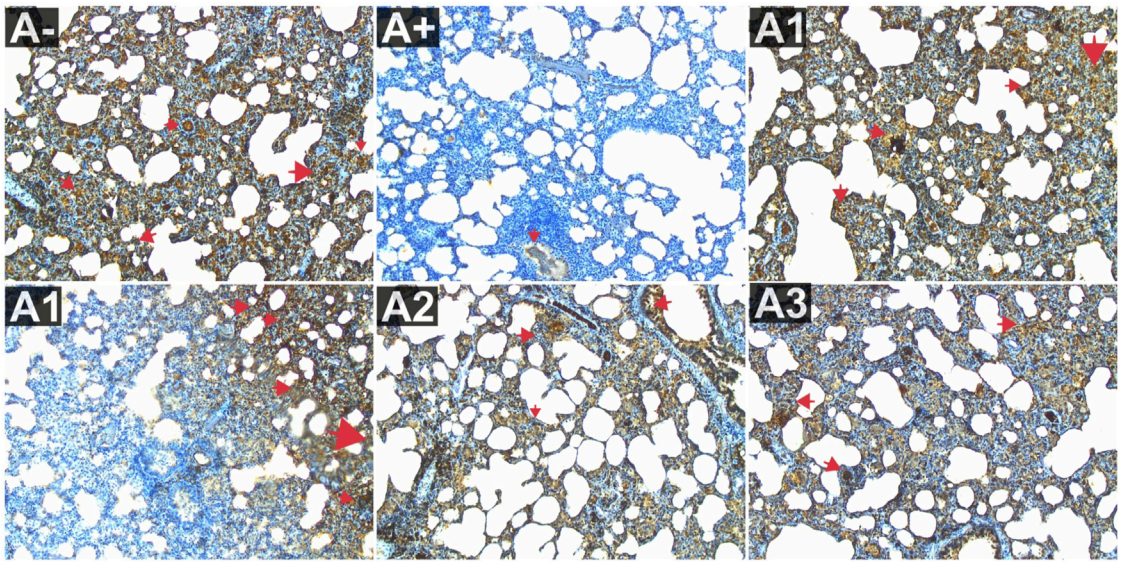

FIGURE 8
Expression of IL-9 on lung histological changes after administration of *Rhodomyrtus tomentosa* in allethrin-exposed rats. **(A-)**: Control, **(A+)**: allethrin-exposed rats, **(A1)**: allethrin-exposed rats +0.02 mg Vitamin C, **(A2)**: allethrin-exposed rats +100 mg/Kg BW of *Rhodomyrtus tomentosa*, **(A3)**: allethrin-exposed rats +200 mg/Kg BW of *Rhodomyrtus tomentosa*, **(A4)**: allethrin-exposed rats +300 mg/Kg BW of *Rhodomyrtus tomentosa* ($^{ns}p > 0.05$, $^{\#\#}p < 0.01$ vs A-, $^{*}p < 0.05$ vs A+, $^{**}p < 0.01$ vs A+).

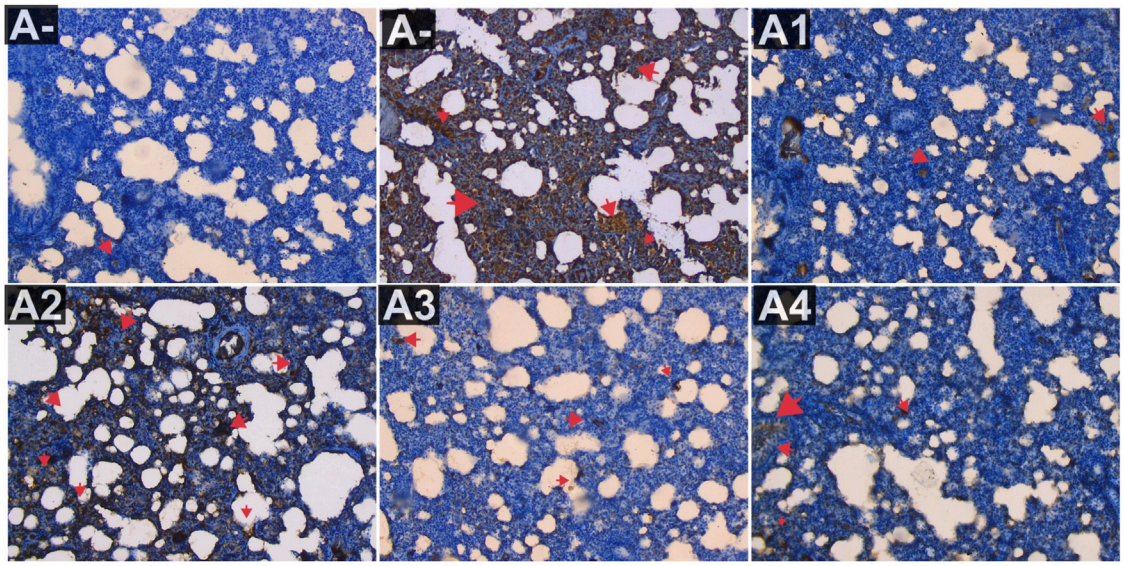

FIGURE 9
Expression of IL-18 on lung histological changes after administration of *Rhodomyrtus tomentosa* in allethrin-exposed rats. **(A-)**: Control, **(A+)**: allethrin-exposed rats, **(A1)**: allethrin-exposed rats +0.02 mg Vitamin C, **(A2)**: allethrin-exposed rats +100 mg/Kg BW of *Rhodomyrtus tomentosa*, **(A3)**: allethrin-exposed rats +200 mg/Kg BW of *Rhodomyrtus tomentosa*, **(A4)**: allethrin-exposed rats +300 mg/Kg BW of *Rhodomyrtus tomentosa* ($^{ns}p > 0.05$, $^{\#\#}p < 0.01$ vs A-, $^{*}p < 0.05$ vs A+, $^{**}p < 0.01$ vs A+).

3 Discussion

In rat models subjected to allectrin-containing electric mosquito repellents, 100–300 mg/kg BW *R. tomentosa* impacted hematological parameters. Neutrophils, hematocrit, and urea were similar. Electric mosquito repellents with allectrins cause oxidative stress in model rats' lung tissue. These modifications include more hemoglobin, leukocytes, lymphocytes, eosinophils, and monocytes (Situmorang et al., 2021a). The average diameter distribution of Haramonting is 600.1 nm ± 135.8. The LC50 and LD50 values for Haramonting are 2,961.535 ppm and 10.4 ± 0.135 mg/kg BW, respectively. Therefore, it has a low level of

toxicity (Situmorang et al., 2021b). The histological examination of the heart, kidneys, lungs, and brain was conducted to assess toxicity (Situmorang et al., 2021b). The investigation revealed that a dosage of 400 mg/kgBW resulted in histological damage to these organs, So the dosage used in this trial did not exceed 300 mg per kilogram of body weight (Situmorang et al., 2021b). *Rhodomyrtus tomentosa* can control these cells because it contains antioxidants that fight free radicals (Lai et al., 2015; Zhang et al., 2018). *Rhodomyrtus tomentosa regulated* SOD, MDA, and NGAL expression at 200–300 mg/Kg BW, but the comparison group, A1 (Vitamin C), and A4 groups did not differ. Lack of antioxidants increases lipid peroxide activity, which enhances MDA and NGAL and lowers SOD. SOD deficiency increases MDA in injured tissues (Buyukokuroglu et al., 2008). If superoxide anions remain high, undetected tissue damage can ensue. Radical superoxide anions are very reactive (Phaniendra et al., 2015). Haramonting's antioxidants reduce blood MDA and NGAL, increasing SOD activity. *Rhodomyrtus tomentosa* increases SOD activity, protecting cells against oxidant disturbances and oxidative stress, which can cause disease and lung tissue injury (Lavanya et al., 2012).

The A+ (allethrin-exposed) group had the highest IL-1β expression, while the A- and *R. tomentosa* 300 mg/kg BW groups had the lowest. Allethrin can cause bronchitis and lung damage in asthmatics (Hernández et al., 2011). The potential hazards of alltehrin on respiratory health in mosquito coils arise due to suspicions that producers of these coils do not fully disclose all the components in their chemical analysis reports (Kasumba et al., 2016). An analysis of the organic chemistry and elemental makeup of mosquito coil ash is necessary to determine the specific compounds present in the matrix (Abdulla Al-Mamun et al., 2017). Indoor usage of mosquito repellant can result in the accumulation of substantial quantities of ash particles and toxins. Allethrin is the sole organic ingredient in mosquito repellent that has environmental and human concerns (Vorselaars et al., 2021). IL-1β is a powerful pro-inflammatory cytokine secreted after infections and traumas (Hernández et al., 2011). Allethrin, an iNOS-containing drug, reduced IL-1β levels in lung tissue using immunohistochemical examination (Indalao et al., 2017). IL-1β promotes the development of active B lymphocytes into plasma cells by promoting monocytes to become conventional dendritic cells (DCs) and macrophages (Indalao et al., 2017). Flow cytometry was used to detect cytokines at the protein level on IL-1β, a secreted isoform of IL-1β. Recent mouse studies suggest that IL-1β stimulation drives smoke-induced inflammation without inflammation (Jiang et al., 2023). *Rhodomyrtus tomentosa* antioxidants directly react with free radicals, minimizing oxidative damage. They indirectly reduce oxidative damage by lowering free radical-generating enzymes or enhancing antioxidant enzymes in cells (Zhang et al., 2018). The DPPH assay gave the methanol extract an IC50 of 107 g/mL, the FRAP assay gave it 0.162 nm at 500 g/mL, and the Metal Chelating Assay gave it 36% at 100 g/mL. HPLC showed gallic acid, tannic acid, and quercetin (Sukweenadhi et al., 2020). *Rhodomyrtus tomentosa* is utilized as an antioxidant in food to prevent oxidation (Lavanya et al., 2012; Lai et al., 2015). It is used in pharmaceuticals as an alternative antioxidant to protect biomolecules from free radical damage in a variety of human illnesses (Lavanya et al., 2012).

Control (A-) and vitamin C (A1) groups expressed the greatest IL-6, whereas A4 expressed the least. Lung vitamins like vitamin C are antioxidants. It helps overcome chronic respiratory disorders. Oxidative stress from toxins and free radicals damages lung tissue, especially in chronic lung disease patients (Lei et al., 2022). Vitamin C protects alveoli and reduces COPD risk (Lei et al., 2022). We employed Vitamin C as a control due to its previous utilization in lung health research as a preventive measure and an anti-inflammatory agent (Hemilä and Douglas, 1999; Chambial et al., 2013; Holford et al., 2020). Allethrin induces IL-6 expression by stimulating the infiltration of myeloid-derived suppressor cells, neutrophils, and inflammatory stem-like cells via Janus-activated signal transducers/kinases and transcription pathway 3 activators (Ibrahim et al., 2020). These cytokines reduce inflammation (Ibrahim et al., 2020). *Rhodomyrtus tomentosa* leaf extract is antioxidant-rich. Antioxidants prevent oxidation by transforming reactive free radicals into stable ones. Mouse studies show that mitochondrial antioxidants prevent inflammation and organ failure (Zhang et al., 2018). IL-6 receptor signaling reduces oxidative stress and allethrin-induced damage (Qing et al., 2020). IL-8 expression was highest in allethrin-exposed groups and lowest in *R. tomentosa* 300 mg/kg BW (A4) groups. Allethrin attacks neutrophils and other immune cells at the infection site, causing inflammation and IL-8 production. Epithelial, airway smooth muscle, and endothelial cells generate IL-8 (Pease and Sabroe, 2002). Even at low doses, IL-8 chemotaxis stimulates neutrophils to release lysosomal enzymes, upregulate adhesion molecules, increase intracellular calcium, and increase oxidative stress, which maintains *R. tomentosa* expression. Certain leukocytes and endothelial cells emit IL-8. Hypoxia and chemotherapeutic medications can also cause fibroblasts and cancer cells to release IL-8 (Gonzalez-Aparicio and Alfaro, 2020). When given to treat chronic pulmonary diseases, vitamin C reduced its expression as an antioxidant. In chronic lung disease patients, toxins and free radicals cause oxidative stress and lung tissue destruction. A quantitative UV-Vis spectrophotometer study found that the methanol fraction of *Rhodomyrtus toementosa* leaf methanol extract had the strongest antioxidant activity with an IC50 value of 51.95 g/mL (Idris et al., 2022). Inflammation-induced oxidative stress may be caused by high IL-8 and insufficient glutathione. In other words, reactive oxygen species boost interleukin-8 and decrease glutathione (Cesta et al., 2022). Thus, interleukin-8 and the oxidant-antioxidant system are linked (Cesta et al., 2022). In contrast, the control and Vitamin C (A1) groups expressed the least IL-9. Due to its immunopathological connection with T helper 2 (TH2), allethrin increased IL-9 expression in rats (Li et al., 2017). Th9 cells, which express IL-9, are overrepresented in blood and $CD4^+$ T cells. Both mast cells and eosinophils, IL-9's targets, contribute to allergic disease by releasing pro-inflammatory chemicals at inflammation sites (Li et al., 2017). IL-9, a pleiotropic cytokine, can cause allergic inflammation and cause eosinophilic inflammation, mucosal gland hyperplasia and hypertrophy, and bronchial hyperreactivity in asthmatics (Li et al., 2022). Vitamin C's anti-inflammatory, immune-supportive, and cofactor role for mono- and dioxygenases may have reduced IL-9 expression after supplementation (Ellulu et al., 2015). Water-soluble vitamin C protects cells inside and out from free radical damage. Vitamin C helps free radicals stabilize by providing electrons (Lobo et al., 2010). The antioxidant-rich herb haramonting neutralizes free radicals that damage lung tissue. Free radical damage can cause lung cancer and other issues. Our bodies produce some antioxidants, but Haramonting must be obtained from diet or herbal supplements.

IL-10 expression was highest in the control (A-) and vitamin C (A1) groups and lowest in the A+ group. Allethrin-exposed rats have low levels of IL-10, which selectively blocks the CD28 co-stimulatory pathway in T cells to inhibit and develop antigen-specific immunity (Dennis et al., 2013). IL-10 only suppresses T cells triggered by a few activated T cell receptors, hence CD28 costimulation is needed (Dennis et al., 2013). IL-10 controls innate and cell-mediated immunity and homeostasis (Iyer and Cheng, 2012). IL-10 inhibits cell cytokine, activated antigen, and mitogen production. Free radical damage from allethrin, mutagens, and stimulants like neutrophils and monocytes is prevented by vitamin C (Rojas et al., 2017). Super Oxide Dismutase (SOD) converts oxygen to hydrogen peroxide. Zinc enhances the hydroxyl radical (OH)-removing chemical metallothionein (Marreiro et al., 2017). Vitamin C increases natural killer cell activity and lymphocyte expansion (Carr and Maggini, 2017). Terpenoids and steroids in *R. tomentosa* have significant antioxidant properties, with IC50 values of 6–50 ppm (Hamid et al., 2017). Rhodomyrtus tomentosa 300 mg/kg BW (A4) and A-expressed the least IL-18, while A+ expressed the most. A+ cells produce more IL-18 because it activates Th1 cells and increases FasL, which promotes $CD8^+$ T and NK cell cytotoxicity (Widowati et al., 2020). IFN- production is another inflammatory cytokine boosted by IL-18. IL-18, like IL-1, is produced by macrophages, dendritic cells, possibly lymphocytes, and nonimmune cells. Its function is regulated by the expression of its receptors by a variety of targets, proteinase cleavage, and blocking proteins. Since monocytes, macrophages, keratinocytes, and mesenchymal cells produce IL-18, a dose of 100 mg/kgBW is appropriate. *Rhodomyrtus tomentosa's* IL-18 suppression is insufficient. The superiority of A1 over A3 is not always apparent, suggesting that this plant may have advantages over Vitamin C. Perhaps, it could become an antioxidant-rich medicinal ingredient in the future. This is strengthened by its phytochemicals and antioxidants. Rhodomyrtone, a primary plant-derived component from *R. tomentosa* (Myrtaceae) leaf extract, may be a natural antioxidant (Wunnoo et al., 2021). The plant's herbal component reduced IL-18 expression at 200–300 mg/kg body weight. LPS decreased RAW cell NO production with IC50 values of 3.8–74.3 M (Vo and Ngo, 2019). The phloroglucinol derivative from *R. tomentosa* leaves had anti-inflammatory properties (Vo and Ngo, 2019). Another intriguing study found that *R. tomentosa* controls immune system gene expression to reduce inflammation. Kidney head macrophages showed elevated IL-1β, IL-8, and TNF□β levels, while IL-10 and TGFβ expression was boosted (Kany et al., 2019). Rhodomyrtone inhibits the NF-B, ERK, JNK, and p38 signaling pathways to promote cutaneous organ cultures by decreasing TNF- and IL-17A transcription and expression (Wunnoo et al., 2021). Rhodomyrtone also inhibits keratinocyte hyperproliferation, treating various inflammatory cytokine-mediated diseases (Wunnoo et al., 2021).

4 Conclusion

In Conclusion, the concentrations of pro-inflammatory cytokines IL-1β, IL-8, IL-9, and IL-18 are elevated in both the bloodstream and tissues after being exposed to an electric mosquito repellent that contains allethrin. Nevertheless, the concentrations of anti-inflammatory cytokines IL-6 and IL-10 are reduced. Allethrin stimulates the production of reactive oxygen species (ROS), which leads to the alteration of the antioxidant response in this plant through the involvement of IL-6, IL-10 in Haramonting administration, and Vitamin C. The connection between autophagy and the antioxidant response will be established by IL-6 and IL-10, resulting in a reduction of reactive oxygen species (ROS) in the lungs. This reduction will result in an elevation of the crucial antioxidant factor NRF2, which will rapidly migrate to the mitochondria to suppress mitochondrial function and stimulate mitophagy. Moreover, it is probable that cellular levels of cyclic adenosine monophosphate (cAMP) play a role in promoting mitophagy, which is the process of removing damaged mitochondria, in order to decrease the production of reactive oxygen species (ROS). *Rhodomyrtus tomentosa* has the potential to enhance alveolar histological changes. Similar to the Vitamin C group, it reduces the expression of IL-1β, IL-8, IL-9, and IL-18, while increasing the expression of IL-6 and IL-10. The administration of Haramonting results in a substantial increase in the levels of IL-6 and IL-10. This study provides Supplementary Material on the association between the effectiveness of a medicinal plant and the synthesis of cytokines.

Data availability statement

The original contributions presented in the study are included in the article/Supplementary Material, further inquiries can be directed to the corresponding author.

Ethics statement

The animal studies were approved by the USU FMIPA Medan Health Research Ethics Committee (No. 0896/KEPH-FMIPA/2022). The studies were conducted in accordance with the local legislation and institutional requirements. Written informed consent was obtained from the owners for the participation of their animals in this study.

Author contributions

PS: Conceptualization, Investigation, Writing–original draft. SI: Data curation, Methodology, Writing–original draft. RS: Writing–original draft, Writing–review and editing, Data curation, Methodology, Supervision. AN: Data curation, Methodology, Writing–original draft, Writing–review and editing. MP: Formal Analysis, Methodology, Supervision, Writing–original draft, Writing–review and editing. CR: Formal Analysis, Project administration, Writing–original draft, Writing–review and editing.

Funding

The author(s) declare financial support was received for the research, authorship, and/or publication of this article. This research is supported by the World Class University (WCU) Fund with contract number: 38/UN5.2.3.1/PPM/KP-WCU/2022.

Conflict of interest

The authors declare that the research was conducted in the absence of any commercial or financial relationships that could be construed as a potential conflict of interest.

Publisher's note

All claims expressed in this article are solely those of the authors and do not necessarily represent those of their affiliated organizations, or those of the publisher, the editors and the reviewers. Any product that may be evaluated in this article, or claim that may be made by its manufacturer, is not guaranteed or endorsed by the publisher.

Supplementary material

The Supplementary Material for this article can be found online at: https://www.frontiersin.org/articles/10.3389/fphar.2024.1343936/full#supplementary-material

References

Abdulla Al-Mamun, M., Ataur Rahman, M., Habibur Rahman, M., Hoque, K. M. F., Ferdousi, Z., Matin, M. N., et al. (2017). Biochemical and histological alterations induced by the smoke of allethrin based mosquito coil on mice model. *BMC Clin. Pathol.* 17, 19. doi:10.1186/s12907-017-0057-9

Arif, A., Quds, R., and Mahmood, R. (2021). Bioallethrin enhances generation of ROS, damages DNA, impairs the redox system and causes mitochondrial dysfunction in human lymphocytes. *Sci. Rep.* 11 (1), 8300. doi:10.1038/s41598-021-87799-3

Borthwick, L. A. (2016). The IL-1 cytokine family and its role in inflammation and fibrosis in the lung. *Semin. Immunopathol.* 38 (4), 517–534. doi:10.1007/s00281-016-0559-z

Buyukokuroglu, M. E., Cemek, M., Yurumez, Y., Yavuz, Y., and Aslan, A. (2008). Antioxidative role of melatonin in organophosphate toxicity in rats. *Cell Biol. Toxicol.* 24 (2), 151–158. doi:10.1007/s10565-007-9024-z

Carr, A. C., and Maggini, S. (2017). Vitamin C and immune function. *Nutrients* 9 (11), 1211. doi:10.3390/nu9111211

Cesta, M. C., Zippoli, M., Marsiglia, C., Gavioli, E. M., Mantelli, F., Allegretti, M., et al. (2022). The role of interleukin-8 in lung inflammation and injury: implications for the management of COVID-19 and hyperinflammatory acute respiratory distress syndrome. *Front. Pharmacol.* 12, 808797. doi:10.3389/fphar.2021.808797

Chambial, S., Dwivedi, S., Shukla, K. K., John, P. J., and Sharma, P. (2013). Vitamin C in disease prevention and cure: an overview. *Ind. J. Clin. Biochem.* 28, 314–328. doi:10.1007/s12291-013-0375-3

Dennis, K. L., Blatner, N. R., Gounari, F., and Khazaie, K. (2013). Current status of interleukin-10 and regulatory T-cells in cancer. *Curr. Opin. Oncol.* 25 (6), 637–645. doi:10.1097/CCO.0000000000000006

Dinarello, C. A. (2018). Overview of the IL-1 family in innate inflammation and acquired immunity. *Immunol. Rev.* 281 (1), 8–27. doi:10.1111/imr.12621

Ellulu, M. S., Rahmat, A., Patimah, I., Khaza'ai, H., and Abed, Y. (2015). Effect of vitamin C on inflammation and metabolic markers in hypertensive and/or diabetic obese adults: a randomized controlled trial. *Drug Des. Devel Ther.* 9, 3405–3412. doi:10.2147/DDDT.S83144

Enayati, A. A., Hemingway, J., and Garner, P. (2007). Electronic mosquito repellents for preventing mosquito bites and malaria infection. *Cochrane Database Syst. Rev.* 2007 (2), CD005434. doi:10.1002/14651858.CD005434.pub2

Gargouri, B., Yousif, N. M., Bouchard, M., Fetoui, H., and Fiebich, B. L. (2018). Inflammatory and cytotoxic effects of bifenthrin in primary microglia and organotypic hippocampal slice cultures. *J. Neuroinflammation* 15 (1), 159. doi:10.1186/s12974-018-1198-1

Gonzalez-Aparicio, M., and Alfaro, C. (2020). Significance of the IL-8 pathway for immunotherapy. *Hum. Vaccin Immunother.* 16 (10), 2312–2317. doi:10.1080/21645515.2019.1696075

Hamid, A. H., Mutazah, R., Yusoff, M. M., Abd Karim, N. A., and Abdull Razis, A. F. (2017). Comparative analysis of antioxidant and antiproliferative activities of *Rhodomyrtus tomentosa* extracts prepared with various solvents. *Food Chem. Toxico* 108, 451–457. doi:10.1016/j.fct.2016.10.004

Hazarika, H., Krishnatreyya, H., Tyagi, V., Islam, J., Gogoi, N., Goyary, D., et al. (2022). The fabrication and assessment of mosquito repellent cream for outdoor protection. *Sci* Rep12 (1), 2180. doi:10.1038/s41598-022-06185-9

Hemilä, H., and Douglas, R. M. (1999). Vitamin C and acute respiratory infections. *Inter J Tuberc. Lung Dis.* 3 (9), 756–761.

Hernández, A. F., Parrón, T., and Alarcón, R. (2011). Pesticides and asthma. *Curr. Opin. Allergy Clin. Immunol.* 11 (2), 90–96. doi:10.1097/ACI.0b013e3283445939

Holford, P., Carr, A. C., Jovic, T. H., Ali, S. R., Whitaker, I. S., Marik, P. E., et al. (2020). Vitamin C—an adjunctive therapy for respiratory infection, sepsis and COVID-19. *Nutrients* 12 (12), 3760. doi:10.3390/nu12123760

Ibrahim, M. L., Lu, C., Klement, J. D., Redd, P. S., Yang, D., Smith, A. D., et al. (2020). Expression profiles and function of IL6 in polymorphonuclear myeloid-derived suppressor cells. *Cancer Immunol. Immunother.* 69 (11), 2233–2245. doi:10.1007/s00262-020-02620-w

Idris, M., Sukandar, E. R., Purnomo, A. S., Martak, F., and Fatmawati, S. (2022). Antidiabetic, cytotoxic and antioxidant activities of *Rhodomyrtus tomentosa* leaf extracts. *RSC Adv.* 12 (39), 25697–25710. doi:10.1039/d2ra03944c

Ihim, S. A., Abubakar, S. D., Zian, Z., Sasaki, T., Saffarioun, M., Maleknia, S., et al. (2022). Interleukin-18 cytokine in immunity, inflammation, and autoimmunity: biological role in induction, regulation, and treatment. *Front. Immunol.* 11 (13), 919973. doi:10.3389/fimmu.2022.919973

Ilyas, S., Hutahaean, S., Sinaga, R. S. H., and Situmorang, P. C. (2021). Apoptosis via cytochrome c in aortic tissue of diabetes mellitus after giving sikkam leaves (*Bischofia javanica* Blume). *J. Pharm. Pharmacogn. Res.* 9 (3), 313–323. doi:10.56499/jppres20.967_9.3.313

Ilyas, S., Hutahaean, S., Sinaga, R. S. H., and Situmorang, P. C. (2022). Effect of sikkam (*Bischofia javanica* Blume) ethanolic extract on the quality and quantity of hyperglycemic rat sperm. *J. Pharm. Pharmacogn. Res.* 10 (2), 270–278. doi:10.56499/jppres21.1204_10.2.270

Indalao, I. L., Sawabuchi, T., Takahashi, E., and Kido, H. (2017). IL-1β is a key cytokine that induces trypsin upregulation in the influenza virus-cytokine-trypsin cycle. *Arch. Virol.* 162 (1), 201–211. doi:10.1007/s00705-016-3093-3

Ipa, M., Widawati, M., Laksono, A. D., Kusrini, I., and Dhewantara, P. W. (2020). Variation of preventive practices and its association with malaria infection in eastern Indonesia: findings from community-based survey. *PLoS One* 15 (5), e0232909. doi:10.1371/journal.pone.0232909

Irianti, E., Ilyas, S., Hutahaean, S., Rosidah, R., and Situmorang, P. C. (2020). Placental histological on preeclamptic rats (*Rattus norvegicus*) after administration of nanoherbal haramonting (*Rhodomyrtus tomentosa*). *Res. J. Pharm Tech* 13 (8), 3879–3882. doi:10.5958/0974-360X.2020.00686.1

Iyer, S. S., and Cheng, G. (2012). Role of interleukin 10 transcriptional regulation in inflammation and autoimmune disease. *Crit. Rev. Immunol.* 32 (1), 23–63. doi:10.1615/critrevimmunol.v32.i1.30

Jalouli, M., Mofti, A., Elnakady, Y. A., Nahdi, S., Feriani, A., Alrezaki, A., et al. (2022). Allethrin promotes apoptosis and autophagy associated with the oxidative stress-related PI3K/AKT/mTOR signaling pathway in developing rat ovaries. *Int. J. Mol. Sci.* 23 (12), 6397. doi:10.3390/ijms23126397

Jiang, H., Guo, Z., Zeng, K., Tang, H., Tan, H., Min, R., et al. (2023). IL-1β knockdown inhibits cigarette smoke extract-induced inflammation and apoptosis in vascular smooth muscle cells. *PLoS One* 18 (2), e0277719. doi:10.1371/journal.pone.0277719

Kany, S., Vollrath, J. T., and Relja, B. (2019). Cytokines in inflammatory disease. *Int. J. Mol. Sci.* 20 (23), 6008. doi:10.3390/ijms20236008

Kasumba, J., Hettick, B., French, A., Wickliffe, J. K., Lichtveld, M. Y., Hawkins, W. B., et al. (2016). Analysis of pesticides and toxic heavy metals contained in mosquito coils. *Bull. Environ. Contam. Toxicol.* 97, 614–618. doi:10.1007/s00128-016-1938-9

Lai, T. N. H., André, C., Rogez, H., Mignolet, E., Nguyen, T. B. T., and Larondelle, Y. (2015). Nutritional composition and antioxidant properties of the sim fruit *(Rhodomyrtus tomentosa). Food Chem.* 168, 410–416. doi:10.1016/j.foodchem.2014.07.081

Lavanya, G., Voravuthikunchai, S. P., and Towatana, N. H. (2012). Acetone extract from *Rhodomyrtus tomentosa*: a potent natural antioxidant. *Evid. Based Complement. Altern. Med.* 2012, 535479. doi:10.1155/2012/535479

Lei, T., Lu, T., Yu, H., Su, X., Zhang, C., Zhu, L., et al. (2022). Efficacy of vitamin C supplementation on chronic obstructive pulmonary disease (COPD): a systematic review and meta-analysis. *Int. J. Chron. Obstruct Pulmon Dis.* 17, 2201–2216. doi:10.2147/COPD.S368645

Li, J., Chen, S., Xiao, X., Zhao, Y., Ding, W., and Li, X. C. (2017). IL-9 and Th9 cells in health and diseases-From tolerance to immunopathology. *Cytokine Growth Factor Rev.* 37, 47–55. doi:10.1016/j.cytogfr.2017.07.004

Li, Y., Lan, F., Yang, Y., Xu, Y., Chen, Y., Qin, X., et al. (2022). The absence of IL-9 reduces allergic airway inflammation by reducing ILC2, Th2 and mast cells in murine model of asthma. *BMC Pulm. Med.* 22 (1), 180. doi:10.1186/s12890-022-01976-2

Lobo, V., Patil, A., Phatak, A., and Chandra, N. (2010). Free radicals, antioxidants, and functional foods: impact on human health. *Pharmacogn. Rev.* 4 (8), 118–126. doi:10.4103/0973-7847.70902

Marreiro, D. D., Cruz, K. J., Morais, J. B., Beserra, J. B., Severo, J. S., and de Oliveira, A. R. (2017). Zinc and oxidative stress: current mechanisms. *Antioxidants (Basel)* 6 (2), 24. doi:10.3390/antiox6020024

Naz, M., Rehman, N., Nazam Ansari, M., Kamal, M., Ganaie, M. A., Awaad, A. S., et al. (2019). Comparative study of subchronic toxicities of mosquito repellents (coils, mats and liquids) on vital organs in Swiss albino mice. *Saudi Pharm. J.* 27 (3), 348–353. doi:10.1016/j.jsps.2018.12.002

Neves, J., Haider, T., Gassmann, M., and Muckenthaler, M. U. (2019). Iron homeostasis in the lungs-A balance between health and disease. *Pharm. (Basel)* 12 (1), 5. doi:10.3390/ph12010005

Pease, J. E., and Sabroe, I. (2002). The role of interleukin-8 and its receptors in inflammatory lung disease: implications for therapy. *Am. J. Respir. Med.* 1 (1), 19–25. doi:10.1007/BF03257159

Phaniendra, A., Jestad, D. B., and Periyasamy, L. (2015). Free radicals: properties, sources, targets, and their implication in various diseases. *Indian J. Clin. Biochem.* 30 (1), 11–26. doi:10.1007/s12291-014-0446-0

Qing, H., Desrouleaux, R., Israni-Winger, K., Mineur, Y. S., Fogelman, N., Zhang, C., et al. (2020). Origin and function of stress-induced IL-6 in murine models. *Cell* 182 (2), 1660–2387. doi:10.1016/j.cell.2020.08.044

Rojas, J. M., Avia, M., Martín, V., and Sevilla, N. (2017). IL-10: a multifunctional cytokine in viral infections. *J. Immunol. Res.* 2017, 6104054. doi:10.1155/2017/6104054

Simanullang, R. H., Situmorang, P. C., Herlina, M., Noradina, and Silalahi, B. (2022b). Cytochrome c expression by andaliman (*Zanthoxylum acanthopodium*) on cervical cancer histology. *Pak J. Biol. Sci.* 25 (1), 49–55. doi:10.3923/pjbs.2022.49.55

Simanullang, R. H., Situmorang, P. C., Herlina, M., Noradina, Silalahi, B., and Manurung, S. S. (2022a). Histological changes of cervical tumors following *Zanthoxylum acanthopodium* DC treatment, and its impact on cytokine expression. *Saudi J. Biol. Sci.* 29 (4), 2706–2718. doi:10.1016/j.sjbs.2021.12.065

Situmorang, P. C., Ilyas, S., Hutahaean, S., and Rosidah, R. (2021a). Histological changes in placental rat apoptosis via FasL and cytochrome c by the nano-herbal *Zanthoxylum acanthopodium*. *Saudi J. Bio Sci.* 28 (5), 3060–3068. doi:10.1016/j.sjbs.2021.02.047

Situmorang, P. C., Ilyas, S., Hutahaean, S., and Rosidah, R. (2021b). Components and acute toxicity of nanoherbal haramonting (*Rhodomyrtus tomentosa*). *J. Herbmed Pharmacol.* 10 (1), 139–148. doi:10.34172/jhp.2021.15

Situmorang, P. C., Ilyas, S., Siahaan, D. A. S., Restuati, M., Sari, E. R., Chairunisa, C., et al. (2022). Effect of *Rhodomyrtus tomentosa* Hassk. on HIF1α and VEGF expressions on hypertension placental. *J. Pharm. Pharmacogn. Res.* 10 (6), 1076–1086. doi:10.56499/jppres22.1517_10.6.1076

Situmorang, P. C., Simanullang, R. H., Syahputra, R. A., Hutahaean, M. M., Sembiring, H., Nisfa, L., et al. (2023). Histological analysis of TGFβ1 and VEGFR expression in cervical carcinoma treated with *Rhodomyrtus tomentosa*. *Pharmacia* 70 (1), 217–223. doi:10.3897/pharmacia.70.e96811

Sukweenadhi, J., Yunita, O., Setiawan, F., Kartini, Siagian, M. T., Danduru, A. P., et al. (2020). Antioxidant activity screening of seven Indonesian herbal extract. *Biodiversitas* 21 (5), 2062–2067. doi:10.13057/biodiv/d210532

Taherkhani, S., Suzuki, K., and Castell, L. (2020). A short overview of changes in inflammatory cytokines and oxidative stress in response to physical activity and antioxidant supplementation. *Antioxidants (Basel)* 9 (9), 886. doi:10.3390/antiox9090886

Tanaka, T., Narazaki, M., and Kishimoto, T. (2014). IL-6 in inflammation, immunity, and disease. *Cold Spring Harb. Perspect. Biol.* 6 (10), a016295. doi:10.1101/cshperspect.a016295

Vo, T. S., and Ngo, D. H. (2019). The health beneficial properties of *Rhodomyrtus tomentosa* as potential functional food. *Biomolecules* 9 (2), 76. doi:10.3390/biom9020076

Vorselaars, A. D. M., van den Berg, P. M., and Drent, M. (2021). Severe pulmonary toxicity associated with inhalation of pyrethroid-based domestic insecticides (Bop/Sapolio): a case series and literature review. *Curr. Opin. Pulm. Med.* 1 (4), 271–277. doi:10.1097/MCP.0000000000000779

Widowati, W., Jasaputra, D. K., Sumitro, S. B., Widodo, M. A., Mozef, T., Rizal, R., et al. (2020). Effect of interleukins (IL-2, IL-15, IL-18) on receptors activation and cytotoxic activity of natural killer cells in breast cancer cell. *Afr. Health Sci.* 20 (2), 822–832. doi:10.4314/ahs.v20i2.36

Wunnoo, S., Bilhman, S., Amnuaikit, T., Ontong, J. C., Singh, S., Auepemkiate, S., et al. (2021). Rhodomyrtone as a new natural antibiotic isolated from *Rhodomyrtus tomentosa* leaf extract: a clinical application in the management of acne vulgaris. *Antibiot. (Basel)* 10 (2), 108. doi:10.3390/antibiotics10020108

Zhang, Y. B., Li, W., Jiang, L., Yang, L., Chen, N. H., Wu, Z. N., et al. (2018). Cytotoxic and anti-inflammatory active phloroglucinol derivatives from *Rhodomyrtus tomentosa*. *Phytochemistry* 153, 111–119. doi:10.1016/j.phytochem.2018.05.018

frontiers | Frontiers in Pharmacology

TYPE Original Research
PUBLISHED 21 February 2024
DOI 10.3389/fphar.2024.1333715

OPEN ACCESS

EDITED BY
Boyang Ji,
BioInnovation Institute (BII), Denmark

REVIEWED BY
Zhigang Zhang,
Northeast Agricultural University, China
Samar A. Antar,
Virginia Tech, United States

*CORRESPONDENCE
Esam Mohamed Aboubakr,
esam_pharma@svu.edu.eg

RECEIVED 05 November 2023
ACCEPTED 25 January 2024
PUBLISHED 21 February 2024

CITATION
Abdulaal WH, Asfour HZ, Helmi N, Al Sadoun H, Eldakhakhny B, Alhakamy NA, Alqarni HM, Alzahrani SAM, El-Moselhy MA, Sharkawi SS and Aboubakr EM (2024), Capsaicin ameliorate pulmonary fibrosis via antioxidant Nrf-2/ PPAR-γ pathway activation and inflammatory TGF-β1/ NF-κB/COX II pathway inhibition.
Front. Pharmacol. 15:1333715.
doi: 10.3389/fphar.2024.1333715

Capsaicin ameliorate pulmonary fibrosis via antioxidant Nrf-2/ PPAR- γ pathway activation and inflammatory TGF-β1/ NF-κB/ COX II pathway inhibition

Wesam H. Abdulaal[1,2,3], Hani Z. Asfour[4], Nawal Helmi[5], Hadeel Al Sadoun[6], Basmah Eldakhakhny[7], Nabil A. Alhakamy[2,3,8], Hani Mohammed Alqarni[3], Saeed Ali Mohammed Alzahrani[3], Mohamed A. El-Moselhy[9,10], Sara S. Sharkawi[10] and Esam Mohamed Aboubakr[11]*

[1]Department of Biochemistry, King Fahd Medical Research Center, Faculty of Science, Cancer and Mutagenesis Unit, King Abdulaziz University, Jeddah, Saudi Arabia, [2]Mohamed Saeed Tamer Chair for Pharmaceutical Industries, Faculty of Pharmacy, King Abdulaziz University, Jeddah, Saudi Arabia, [3]Center of Excellence for Drug Research and Pharmaceutical Industries, King Abdulaziz University, Jeddah, Saudi Arabia, [4]Department of Medical Microbiology and Parasitology, Faculty of Medicine, King Abdulaziz University, Jeddah, Saudi Arabia, [5]Department of Biochemistry, College of Science, University of Jeddah, Jeddah, Saudi Arabia, [6]Department of Medical Laboratory Sciences, Faculty of Applied Medical Sciences, King Abdulaziz University, Jeddah, Saudi Arabia, [7]Department of Clinical Biochemistry, Faculty of Medicine, King Abdulaziz University, Jeddah, Saudi Arabia, [8]Department of Pharmaceutics, Faculty of Pharmacy, King Abdulaziz University, Jeddah, Saudi Arabia, [9]Clinical Pharmacy and Pharmacology Department, Ibn Sina National College for Medical Studies, Jeddah, Saudi Arabia, [10]Department of Pharmacology and Toxicology, Faculty of Pharmacy, Minia University, Minia, Egypt, [11]Department of Pharmacology and Toxicology, Faculty of Pharmacy, South Valley University, Qena, Egypt

Bleomycin is an effective antibiotic with a significant anticancer properties, but its use is limited due to its potential to induce dose-dependent pulmonary fibrosis. Therefore, this study aimed to assess the therapeutic potential of Capsaicin as an additional treatment to enhance patient tolerance to Bleomycin compared to the antifibrotic drug Pirfenidone. Pulmonary fibrosis was induced in rats through by a single intratracheal Bleomycin administration in day zero, followed by either Capsaicin or Pirfenidone treatment for 7 days. After the animals were sacrificed, their lungs were dissected and examined using various stains for macroscopic and histopathological evaluation. Additionally, the study assessed various antioxidant, anti-inflammatory, and antifibrotic parameters were assessed. Rats exposed to Bleomycin exhibited visible signs of fibrosis, histopathological alterations, increased collagen deposition, and elevated mucin content. Bleomycin also led to heightened increased inflammatory cells infiltration in the bronchoalveolar lavage, elevated fibrosis biomarkers such as hydroxyproline, alpha-smooth muscle actin (α-SMA) and transforming growth factor-beta (TGF-β1), increased inflammatory markers including tumor necrosis factor-alpha (TNF-α), interlukine-6 (Il-6), interlukine-1β (Il-1β) nuclear factor-kappa B (NF-κB), and Cyclooxygenase-2 (COX-2), and transforming growth factor-beta (TGF-β1),. Furthermore, it reduced the expression of peroxisome proliferator-activated receptor-gamma (PPAR-γ), increased oxidative stress biomarkers like nitric oxide (NO), malondialdehyde (MDA), myeloperoxidase (MPO) and protein carbonyl. Bleomycin also decreased the expression of nuclear factor erythroid

2–related factor 2 (Nrf-2), reduced glutathione (GSH), total antioxidant capacity, and the activities of catalase and superoxide dismutase (SOD). Treating the animals with Capsaicin and Pirfenidone following Bleomycin exposure resulted in improved lung macroscopic and microscopic characteristics, reduced collagen deposition (collagen I and collagen III) and mucin content, decreased inflammatory cell infiltration, lowered levels of hydroxyproline, α-SMA, and TGF-β1, decreased TNF-α, Il-6, Il-1β, NF-κB, and COX-2, increased PPAR-γ and Nrf-2 expression, and improvement improved in all oxidative stress biomarkers. In summary, Capsaicin demonstrates significant antifibrotic activity against Bleomycin-induced lung injury that may be attributed, at least in part, to the antioxidant and anti-inflammatory activities of Capsaicin mediated by upregulation of PPAR-γ and Nrf-2 expression and decreasing. TGF-β1, NF-κB and COX II proteins concentrations.

KEYWORDS

Capsaicin, bleomycin, Pirfenidone, pulmonary fibrosis, TGF-β1, PPAR-γ, TNF-α

1 Introduction

Bleomycin is a highly effective chemotherapy used extensively in the treatment of different types of cancer including; Hodgkin lymphoma and testicular germ-cell tumors. However, bleomycin has the potential to cause serious and life-threatening damage to the lungs (Ayilya et al., 2023). This can manifest as several conditions, including hypersensitivity pneumonitis, bronchiolitis obliterans organizing pneumonia (BOOP), acute interstitial pneumonia, and progressive pulmonary fibrosis (Demirkol et al., 2023). Pulmonary toxicity is a recognized adverse effect of anticancers, nevertheless, a mortality rate of 1%–4% from bleomycin is considered unacceptable for patients with treatable malignancies. The toxic effects of bleomycin are primarily caused by the generation of free radical and its lung specificity caused by bleomycin catalyzing hydrolase, which was not found in lung tissue, rendering this organ vulnerable to bleomycin toxicity (Usman et al., 2010; Ishida et al., 2023).

The development of lung fibrosis is mostly driven by acute inflammation; including significant upregulation of mononuclear macrophages, lymphocytes, and neutrophils. Bleomycin induces the release of inflammatory cytokines, TNF-α, IL-1, IL-18, IL-22, and IL-17a, from alveolar macrophages (Kadam and Schnitzer, 2023). It also stimulates endothelial cells to secrete IL-6. Cytokines stimulate lymphocytes and increase the expression of adhesion molecules on endothelial cells, which allows inflammatory cells to stick to the endothelium, enter the interstitium, and damage endothelial cells via the Fas-FasL pathway (Yoshizaki et al., 2010; Altintas et al., 2016). The activation of fibroblasts in pulmonary fibrosis occurs at early stage due to the stimulation of fibronectin. This stimulation might be caused by injured endothelial cells or by the presence of cytokines such as TNF-α, platelet derived growth factor (PDGF), and transforming growth factor-β (TGF-β) (Kabel et al., 2016; Chen et al., 2023). Prolonged exposure of the lungs to bleomycin can result in elevated production of collagen and the accumulation of different matrix proteins such as collagens, elastin, and proteoglycans. In addition, alveolar macrophages that have been stimulated by bleomycin promote the production of hyaluronan (Venkatesan et al., 2011; Wang et al., 2023). T cells also contribute to the lung damage caused by inflammation. Cytokines, such as IFN-γ and IL-13, are released during Th1 and Th2 inflammation, respectively (Lei et al., 2016).

Capsaicin, also known as trans-8-methyl-N-vanillyl-6-nonenamide, is the primary and most potent alkaloid in the capsaicinoid group, responsible for the characteristic chili flavor found in chili peppers (Ilie et al., 2019). Capsaicin offers substantial health benefits, including analgesic, anticancer, neuroprotective, and gastroprotective properties, which can largely be attributed to its antioxidant and anti-inflammatory characteristics. Furthermore, Capsaicin has been shown to modulate macrophage function and reduce the release of proinflammatory cytokines, reactive oxygen species (ROS), proteases, and lysosomal enzymes (Zimmer et al., 2012). Additionally, several studies highlighted the antifibrotic effect of Capsaicin through the inhibition of TGF-β1 signaling in various models of fibrosis such as kidney fibrosis (Liu et al., 2022).

Therefore, the present study aims to investigate the potential therapeutic effects of Capsaicin in mitigating Bleomycin-induced pulmonary toxicity in rats and elucidating the underlying mechanisms involved.

2 Materials and methods

2.1 Drugs and chemicals

Capsaicin, Bleomycin sulfate and Pirfenidone were procured from Sigma Aldrich (St. Louis, MO, United States) under the catalog numbers M2028, BP971, and P2116, respectively. All chemicals utilized in this study were of the highest quality available in the commercial market.

2.2 Animals

A total of 32 adult male Sprague Dawley rats, aged 10–12 weeks and weighing between 140 and 160 g, were sourced from the National Research Centre (NRC) in Giza, Egypt, for inclusion in this study. To allow the rats to adapt to the laboratory environment, they were acclimated for 1 week before the commencement of the experiment. Throughout the study, the animals were maintained under controlled conditions, with a temperature of 28 ± 2°C, humidity 55 ± 5% and a 12-h light/dark cycle. They were

provided with standard chow containing 20% protein, 8% fiber, 4% fat, 7% ash, and approximately 60% carbohydrates, along with *ad libitum* access to water. All procedures involving animals were carried out following approval from the ethical committee of the Faculty of Pharmacy at South Valley University, Egypt, under approval number (P.S.V.U 112/23), in accordance with international guidelines for the use of experimental animals (Animal Research: Reporting of *In vivo* Experiments) guidelines.

2.3 Experimental design

The animals were randomly divided into four groups, each consisting of 8 rats. They were assigned to different treatment groups: 1) Group one, serving as the control, received only the vehicle solutions for Capsaicin and Bleomycin. 2) Group two, the Bleomycin-only-treated group, received Bleomycin (5 U/kg body weight) (Razzaque et al., 1998) along with the vehicle solutions for Capsaicin and Pirfenidone (0.5% sodium carboxymethyl cellulose, CMC). 3) Group three received Bleomycin and Pirfenidone (50 mg/kg, administered orally) (Guo et al., 2019). 4) Group four received Bleomycin and Capsaicin (3 mg/kg, administered orally) (Lee et al., 2003). Anesthesia was administered to the animals, following which a single dose of Bleomycin (5 mg/kg) dissolved in saline was introduced via intratracheal instillation on day zero to induce pulmonary fibrosis. Conversely, the control rats were administered equivalent volumes of saline via the same route. Capsaicin and Pirfenidone were administered orally to the animals starting from day one and continued for 7 days. Upon concluding the experiment, the rats were anesthetized using thiopental sodium to collect bronchoalveolar lavage fluid. Subsequently, blood samples were collected from the retro-orbital venous plexus. These blood samples were maintained at room temperature until serum separation, accomplished by centrifugation at 3,000 rpm for 15 min. The sera were then collected and stored at −80°C for subsequent biochemical analyses. The lungs were removed, rinsed with ice-cold saline, and weighed to determine the lung/body weight index for macroscopic examination. The left lobe of each animal's lung was used to prepare lung tissue homogenate, while the right lobe was isolated for histopathological examination.

2.4 Collection of bronchoalveolar lavage fluid (BALF)

Under deep anesthesia, the thoracic cage was opened, revealing the rat tracheas, which were then exposed and cannulated. The lungs were subsequently flushed with 6 mL of 0.9% saline administered in 2 mL increments. Gentle chest compressions were performed to recover the saline. The bronchoalveolar lavage fluid (BALF) was collected and centrifugated at 2,000 rpm, maintained at 4°C for 10 min. The cells that settled were then resuspended in 500 µL of saline to assess the levels of inflammatory cells, including total and differential cell counts, following the method described by Henderson in 2005 (Henderson and Pathology, 2005).

2.5 Histopathological examination

The lung tissues of the rats were initially fixed in a 10% formaldehyde solution for 48 h. Subsequently, they underwent a dehydration process involving successive ethanol dilutions before being embedded in paraffin. The paraffin-embedded lung tissues were then sectioned into slices of 5 µm thickness using a sliding microtome. These tissue sections were subjected to staining procedures, including hematoxylin and Eosin (H and E), Masson trichrome stains (MTC), and periodic acid Schiff (PAS) stains, for histopathological examination. Examination of the slides was carried out employing a light microscope manufactured by Olympus Opticals in Tokyo, Japan, at a magnification of ×200. The degree of pulmonary fibrosis was assessed based on the MTC-stained tissue sections using the following grading system: Grade 0: Indicates normal lung tissue. Grade 1: Signifies minimal fibrous changes in alveoli or bronchial walls. Grade 2: Reflects moderate thickening of alveoli or bronchial walls without disruption of lung architecture. Grade 3: Represents tissue fibrosis accompanied by damage to lung architecture. Grade 4: Denotes severe distortion and architectural damage in addition to forming fibrous areas. Grade 5: Corresponds to total lung fibrosis. The fibrosis score was determined by analyzing ten fields within the lung sections. The quantitative evaluation of mucus production was expressed as the area filled with mucus relative to the total airway lumen area in the PAS-stained tissue sections.

2.6 The assessment of hydroxyproline content

The quantification of hydroxyproline content in lung homogenates was conducted by utilizing a kit acquired from Sigma Aldrich (St. Louis, MO, United States, Cat # MAK008), following the guidelines provided by the manufacturer. This assay relies on the oxidation of free hydroxyproline using chloramine-T, leading to the creation of a pyrrole compound that generates a chromophore when Ehrlich's reagent is introduced. The resulting product's absorbance can then be measured at 550 nm, as previously described (Cissell et al., 2017).

2.7 Colorimetric assessments of the oxidative stress biomarkers

We assessed various parameters, including lipid peroxidation, which was quantified using malondialdehyde (MDA), a major thiobarbituric acid reactive species. Additionally, we assessed carbonyl content, reduced glutathione (GSH), total antioxidant capacities (TAC), Myeloperoxidase (MPO) as well as catalase and superoxide dismutase (SOD) activities. These assessments were carried out in accordance with the manufacturer's instructions, employing commercially available kits as follows: MDA assay kit (Biodiagnostics, Egypt, Cat # MD2529), Protein Carbonyl Colorimetric Assay Kit (Cayman, Ann Arbor, Michigan, United States, Cat # 10005020), GSH assay kit (Biodiagnostics, Egypt, Cat # GR2511), TAC assay kit (Biodiagnostics, Egypt, Cat # TA2513), Myeloperoxidase (Abcam, Cambridge,

United Kingdom, Cat # ab105136), Catalase activity assay kit (Biodiagnostics, Egypt, Cat # SD2521), and SOD activity assay kit (Biodiagnostics, Egypt, Cat # CA2517).

2.8 The assessment of the nitrite content

We measured nitrite content, which is indicative of nitric oxide (NO), through a colorimetric method using the commercially available NO assay kit (Biodiagnostics, Egypt, Cat # NO2533). This assay relies on converting NO into nitrous acid, which subsequently reacts with sulfanilamide and N-(1-naphthyl) ethylenediamine to produce an azo dye. The absorbances of the samples were then determined colorimetrically at a wavelength of 540 nm (Archer, 1993).

2.9 Assessment of inflammatory biomarker

We quantified the lung tissue protein content of tumor necrosis factor-alpha (TNF-α) employing a solid-phase sandwich ELISA method. This assay utilized the Rat Tumor Necrosis Factor-α ELISA Kit (Sigma Aldrich, United States, Cat # RAB0480) and followed the manufacturer's instructions. Moreover, the level of the inflammatory mediators TNF- α, (Sigma Aldrich, United States, Cat # RAB0480), IL-1β (Sigma Aldrich, United States, Cat # RAB0273) and IL-6 (Sigma Aldrich, United States, Cat # RAB0311) were determined in the BALF, following the manufacturer instructions.

2.10 Immunohistochemical staining of α-SMA, Nrf-2, NF-Kβ, COX 2, TGF-β1, and PPAR-γ in the rats' lung tissue

The expression of various proteins, including alpha-smooth muscle actin (α-SMA), nuclear factor erythroid 2–related factor 2 (Nrf-2), nuclear factor-kappa B (NF-Kβ), cyclooxygenase-2 (COX-2), transforming growth factor-beta 1 (TGF-β1), and Peroxisome proliferator-activated receptor gamma (PPAR-γ), in the lung tissues was assessed through immunohistochemical staining. To perform this analysis, sections of lung tissue obtained from paraffin blocks were sliced into 5 μm thick sections. These sections then underwent deparaffinization and antigen retrieval by heating in steaming water at 80°C for 20 min. Washing steps, using 0.1 M PBS at pH 7.4, were carried out for 5 min between each stage of the process. Subsequently, the lung sections were incubated for 18 h with appropriately diluted rabbit polyclonal primary antibodies, namely, anti-α-SMA, anti-Nrf-2, anti-NF-Kβ, anti-COX 2, anti-TGF β1, and anti-PPAR-gamma (obtained from Abcam, Cambridge, United Kingdom, Cat # ab220164, ab31163, ab76302, ab179800, ab215715, and ab310323, respectively). Following incubation, the slides were washed and then incubated with a secondary antibody, HRP Anti-Rabbit IgG antibody (Abcam, Cambridge, United Kingdom, Cat # ab288151). To stain the target antigen, the tissue staining anti-rabbit kit (Abcam, Cambridge, United Kingdom, Cat # ab64261) was employed. Visual examination of the immune-stained lung tissues was conducted using a light microscope (Olympus Opticals, Tokyo, Japan). A total of five fields per slide were analyzed, scored, and quantified using Image-Pro Plus 5.0 image analysis software from the National Institutes of Health, located in Bethesda, MD, United States.

2.11 Western blot analysis

Tissue proteins were extracted using RIPA buffer (Beyotime) and their quantities were determined. Equal quantities of proteins were separated on 10% SDS-PAGE gel, proteins were transferred onto PVDF membranes (EMD Millipore, Billerica, MA, United States), treated with 5% BSA for 1 h at room temperature to stop further reactions. The membranes were subsequently placed at 4°C and treated overnight with primary antibodies; α-SMA (ab5694, Abcam), collagen I (ab260043, Abcam), and collagen III (ab7778, Abcam), membranes were washed using TBST solution and incubated with HRP-conjugated secondary antibodies for duration of 1 h at 36°C. The bands' intensity was determined by chemiluminescence technique, the obtained images were analyzed using ImageJ program.

2.12 Statistical analyses

For parametric data, we expressed the results as the mean ± standard deviation (SD), and we determined statistical significance using One-way ANOVA followed by Tukey's multiple comparison test. Nonparametric data were presented as the median along with the interquartile range, and we analyzed them using the Kruskal–Wallis test, followed by Dunn's *post hoc* test. The data analyses were conducted using GraphPad Prism software (Prism 8.1, GraphPad Software), with statistical significance defined as $p < 0.05$.

3 Results

3.1 The effects of Bleomycin, Pirfenidone, and Capsaicin on the white blood cell count in bronchoalveolar lavage fluid of the treated rats

Bleomycin administration resulted in a notable increase in both the total cell count and the proportions of macrophages, neutrophils, eosinophils, and lymphocytes in the bronchoalveolar lavage fluid (BALF) of the treated rats when compared to the control group. Conversely, treatment with Pirfenidone significantly reduced the total cell count and the proportions of neutrophils and eosinophils compared to the Bleomycin-only-treated rats. Of particular interest, Capsaicin treatment elicited a significant decrease in the total cell count and in the proportions of macrophages, neutrophils, and eosinophils compared to the Bleomycin-only-treated rats. Remarkably, these values in the Capsaicin-treated group nearly approached those of the control group, as illustrated in Table 1.

TABLE 1 The effect of Bleomycin, Pirfenidone, and Capsaicin on the white blood cell count in bronchoalveolar lavage fluid.

Groups	Total cells (x106/mL)	Macrophage (%)	Neutrophils (%)	Eosinophil (%)	Lymphocytes (%)
Control	0.49 ± 0.06	89.2 ± 7.6	4.1 ± 0.55	2.2 ± 0.3	4.1 ± 0.32
Bleomycin	1.3* ± 0.12	62.3* ± 5.5	28.1* ± 2.3	3.3* ± 0.41	8.8* ± 0.7
Bleomycin + Pirfenidone	1.1# ± 0.13	68.4 ± 7.1	25.6# ± 2.1	2.8# ± 0.19	9.68 ± 0.8
Bleomycin + Capsaicin	0.65#,$ ± 0.04	81.4#,$ ± 9.9	6.2#,$± 0.3	1.6#,$± 0.11	8.9 ± 1.15

Bleomycin (5 mg/kg) was administered via intratracheal instillation on day zero. Capsaicin (3 mg/kg) and Pirfenidone (50 mg/kg) were orally administered daily for 7 days. Results were analyzed by one-way ANOVA followed by Tukey's as a *post hoc* test ($n = 8$). *, #, and $ are considered statistically significant from the control, Bleomycin-only, and Bleomycin-plus Pirfenidone-treated group, respectively, at $p < 0.05$.

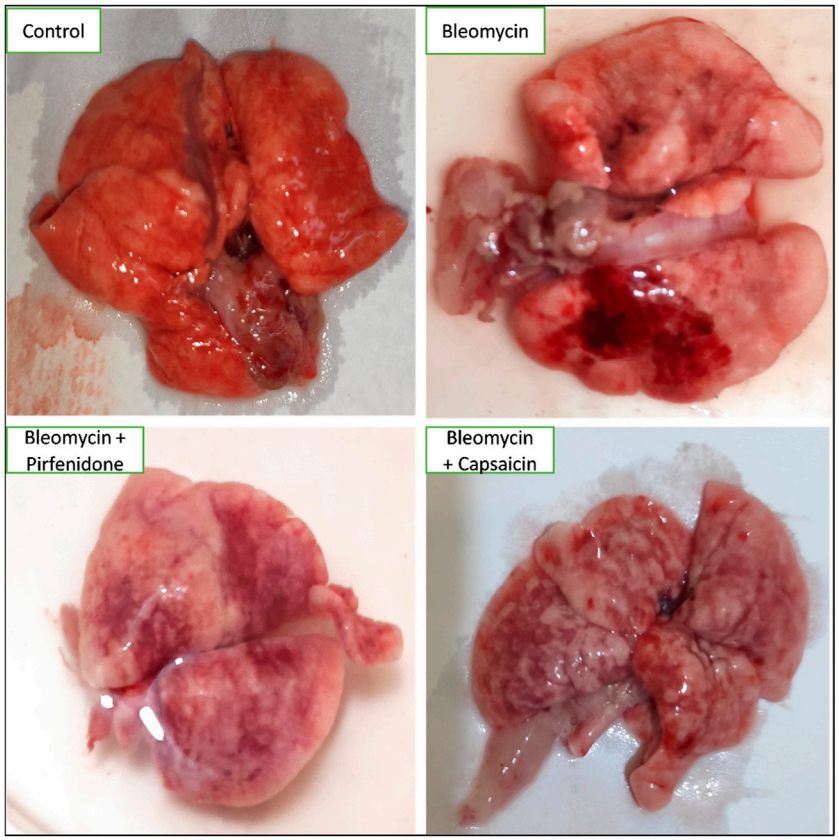

FIGURE 1
The effects of Bleomycin, Capsaicin, and Pirfenidone on the morphology of the rat lungs. Bleomycin (5 mg/kg) was administered via intratracheal instillation on day zero. Capsaicin (3 mg/kg) and Pirfenidone (50 mg/kg) were orally administered daily for 7 days.

3.2 The effects of Bleomycin, Pirfenidone, and Capsaicin on the macroscopic features of the lungs of the treated rats

In the control group, the lungs displayed a typical, healthy morphology characterized by a smooth and uniform surface. In contrast, the Bleomycin-treated group exhibited irregularities, coarseness, interstitial hemorrhagic lesions, atrophic alterations, tissue degeneration, notable tissue congestion, collapsed lung areas, and tissue consolidation, resulting in a loss of tissue elasticity. Treatment with Pirfenidone and Capsaicin was observed to enhance the macroscopic appearance of the lungs, leading to improved surface smoothness and elasticity. Additionally, there were decreased levels of congestion, hemorrhagic lesions, and tissue degeneration, as depicted in Figure 1.

3.3 The effects of Bleomycin, Pirfenidone, and Capsaicin on the histopathological features of the lung tissues of the treated rats

Staining with H and E (Figure 2A) highlighted that lung tissues from the control group displayed a normal architecture

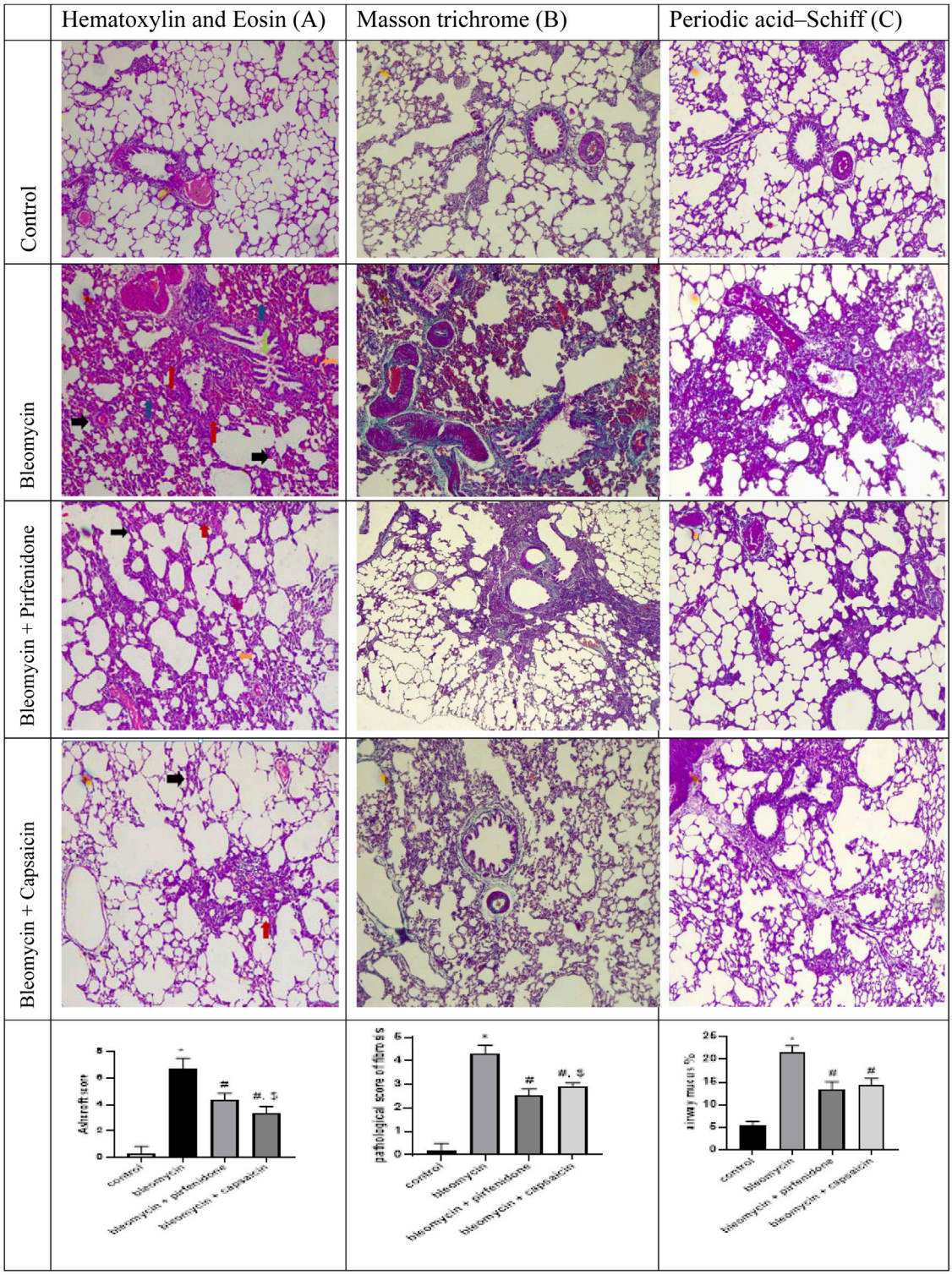

FIGURE 2
The effects of Bleomycin, Capsaicin, and Pirfenidone on the histopathological features of the rat lungs examined by hematoxylin and Eosin stain (Black arrow indicates degenerative alterations, blue arrows indicate predominantly collapsed alveoli, orange arrow indicates thickened inter-alveolar septa, red arrow indicates congested pulmonary blood vessels and green arrow indicates extensive cellular infiltration) **(A)**, Masson trichrome **(B)**, and Periodic acid–Schiff **(C)**. Bleomycin (5 mg/kg) was administered via intratracheal instillation on day zero. Capsaicin (3 mg/kg) and Pirfenidone (50 mg/kg) were administered orally for 7 days. Results were analyzed by one-way ANOVA followed by Tukey's as a *post hoc* test ($n = 8$). *, #, and $ are considered statistically significant from the control, Bleomycin-only, and Bleomycin-plus Pirfenidone-treated group, respectively, at $p < 0.05$.

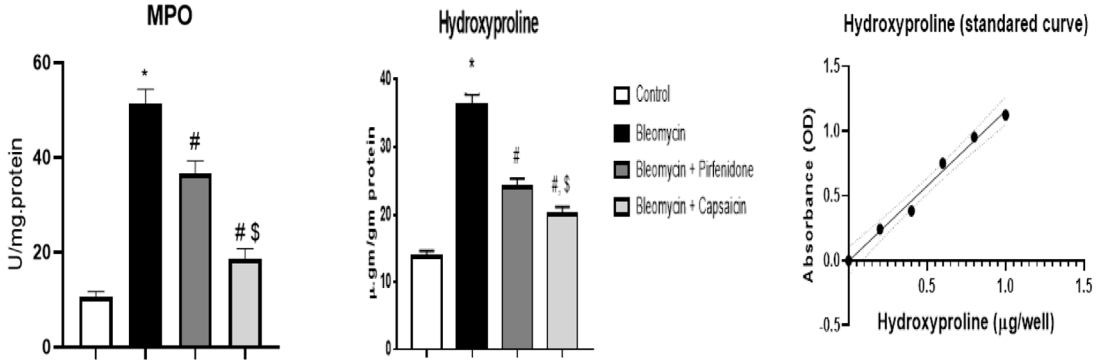

FIGURE 3
The effects of Bleomycin, Pirfenidone, and Capsaicin on the pulmonary hydroxyproline content. Bleomycin (5 mg/kg) was administered via intratracheal instillation on day zero. Capsaicin (3 mg/kg) and Pirfenidone (50 mg/kg) were orally administered daily for seven days. Results were analyzed by one-way ANOVA followed by Tukey's as a post-hoc test ($n = 8$). *, #, and $ are considered statistically significant from the control, Bleomycin-only, and Bleomycin- plus Pirfenidone-treated group, respectively, at $p < 0.05$.

characterized by thin inter-alveolar septa, patent alveoli, healthy pneumocytes of types I and II, normal nuclei, and unobstructed bronchioles lined with regular columnar epithelium. In contrast, the Bleomycin-treated group exhibited extensive tissue damage, degenerative alterations, and distortion of pulmonary structure. Alveoli were predominantly collapsed, inter-alveolar septa thickened significantly, and there was extensive cellular infiltration and blood congestion. The bronchioles displayed severe infiltration of lymphocytic cells, with noticeable shedding of bronchiolar epithelial cells into the lumen. The Pirfenidone-treated group demonstrated moderate lung tissue damage, notably congested pulmonary blood vessels, mild thickening of intra-alveolar septa, and profound infiltration of inflammatory cells. However, in the lung tissue of Capsaicin-treated rats, the degree of destruction was less pronounced than in the Bleomycin-only and Bleomycin-plus-Pirfenidone-treated groups.

Furthermore, mild inflammatory cell infiltration was observed. Blood vessels were not congested, and bronchiolar epithelium shedding was moderate. In some areas of lung tissue, inter-alveolar septa were slightly thickened. Subsequent staining with MTC to assess collagen deposition revealed that the control group exhibited minimal collagen accumulation in lung tissues, nearly devoid of tissue fibrosis. In contrast, the Bleomycin-treated rats displayed dense collagen deposition, extensive thickening of alveolar walls, and severe lung tissue fibrosis, particularly around blood vessels and in the peribronchiolar regions.

Conversely, Capsaicin treatment substantially reduced collagen deposition and accumulation when compared to the Bleomycin group. There was a notable reduction in observed fibrous tissue in the bronchiolar and alveolar regions as well as around blood vessels. This ameliorative effect was less pronounced in the Pirfenidone-treated group (Figure 2B). Staining with PAS to evaluate mucus secretion in the bronchiolar lumen revealed low mucus content in the control group. In contrast, the lung sections of Bleomycin-treated rats displayed a significant increase in mucus content. However, both Pirfenidone and Capsaicin administration reduced mucus content remarkably (Figure 2C).

3.4 The effects of Bleomycin, Pirfenidone, and Capsaicin on the pulmonary Myeloperoxidase (MPO) and hydroxyproline content of the treated rats

The data analysis revealed that Bleomycin administration resulted in a significant increase in the MPO and hydroxyproline content in the treated rats. Conversely, following the induction of lung fibrosis with Bleomycin, treatment with Pirfenidone and Capsaicin led to a significant reduction in both MPO and hydroxyproline contents compared to rats treated with Bleomycin alone. Capsaicin exhibited notably more promising results in this regard than Pirfenidone, as illustrated in Figure 3.

3.5 The effects of Bleomycin, Pirfenidone, and Capsaicin on the pulmonary oxidative stress biomarkers of the treated rats.

Data analyses revealed that a single intratracheal administration of Bleomycin induced oxidative stress, as evidenced by a significant increase in MDA levels and protein carbonyl content. Additionally, it led to a decrease in the levels of GSH, total antioxidant capacities, and the activities of both catalase and SOD when compared to the control group. However, when the Bleomycin-treated animals were challenged with either Pirfenidone or Capsaicin, these effects were significantly reversed. Notably, Capsaicin exhibited more potent antioxidant activity, with results comparable to those observed in the control animals, as depicted in Figure 4.

3.6 The effects of Bleomycin, Pirfenidone, and Capsaicin on the pulmonary NO levels

The administration of a single intratracheal dose of Bleomycin resulted in a notable increase in NO levels when

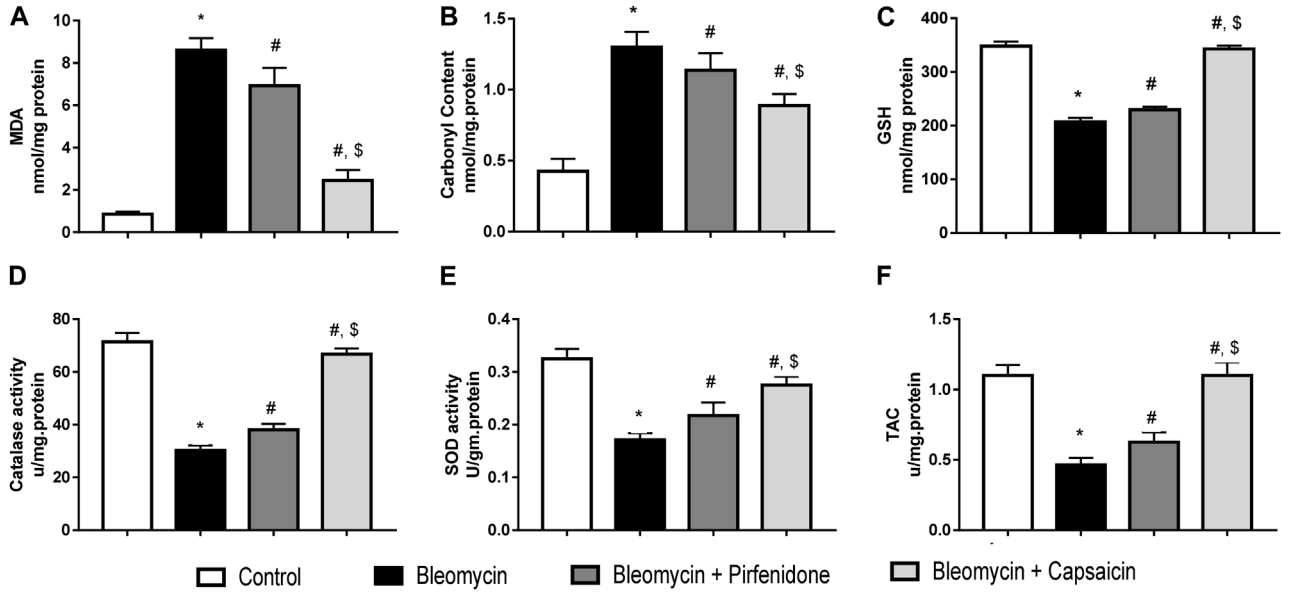

FIGURE 4
The effects of Bleomycin, Pirfenidone, and Capsaicin on the pulmonary malondialdehyde levels **(A)**, carbonyl content **(B)**, reduced glutathione levels **(C)**, catalase activity **(D)**, Superoxide dismutase activity **(E)**, and the total antioxidant capacity **(F)**. Bleomycin (5 mg/kg) was administered via intratracheal instillation on day zero. Capsaicin (3 mg/kg) and Pirfenidone (50 mg/kg) were orally administered daily for 7 days. Results were analyzed by one-way ANOVA followed by Tukey's as a *post hoc* test (n = 8). *, #, and $ are considered statistically significant from the control, Bleomycin-only, and Bleomycin-plus Pirfenidone-treated group, respectively, at $p < 0.05$.

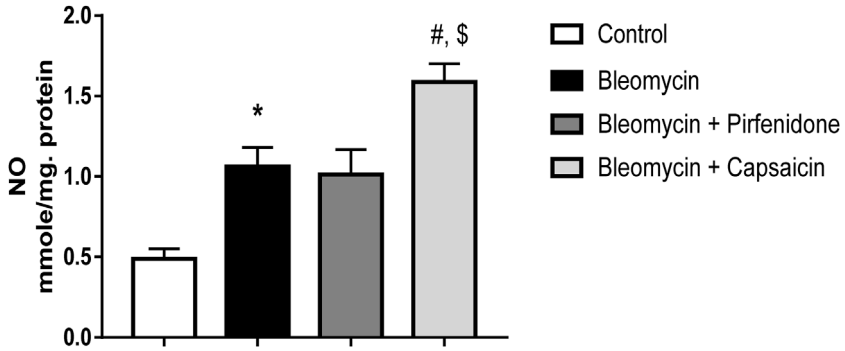

FIGURE 5
The effects of Bleomycin, Pirfenidone, and Capsaicin on the pulmonary nitric oxide (NO) levels. Bleomycin (5 mg/kg) was administered via intratracheal instillation on day zero. Capsaicin (3 mg/kg) and Pirfenidone (50 mg/kg) were orally administered daily for 7 days. Results were analyzed by one-way ANOVA followed by Tukey's as a *post hoc* test (n = 8). *, #, and $ are considered statistically significant from the control, Bleomycin-only, and Bleomycin-plus Pirfenidone-treated group, respectively, at $p < 0.05$.

compared to the intratracheal saline administration. Subsequent treatment of the Bleomycin-exposed animals with Pirfenidone did not lead to a significant decrease in NO levels. In contrast, the administration of Capsaicin significantly reduced the NO levels compared to the rats treated only with Bleomycin, as illustrated in Figure 5.

3.7 The effects of Bleomycin, Pirfenidone, and Capsaicin on the pulmonary TNF-α levels.

The administration of Bleomycin resulted in a significant elevation in the protein levels of the inflammatory biomarker,

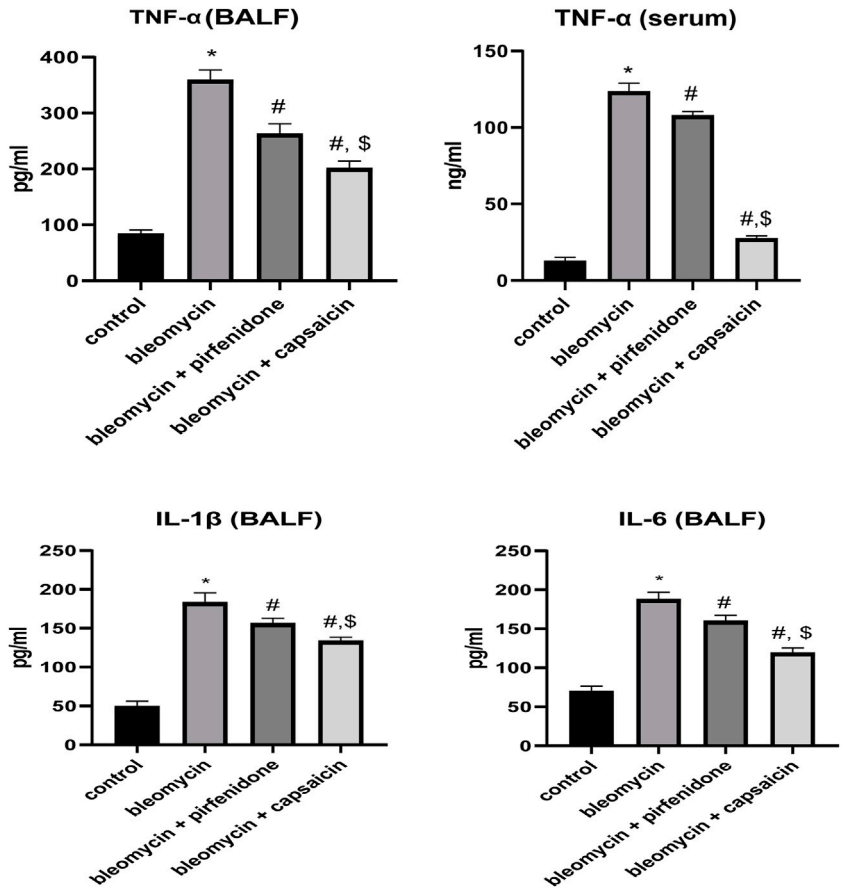

FIGURE 6
The effects of Bleomycin, Pirfenidone, and Capsaicin on the pulmonary tumor necrosis factor-alpha (TNF-α) levels in BALF and serum, IL-1β in BALF and IL-6 in BALF. Bleomycin (5 mg/kg) was administered via intratracheal instillation on day zero. Capsaicin (3 mg/kg) and Pirfenidone (50 mg/kg) were administered orally for 7 days. Results were analyzed by one-way ANOVA followed by Tukey's as a *post hoc* test (n = 8). *, #, and $ are considered statistically significant from the control, Bleomycin-only, and Bleomycin-plus Pirfenidone-treated group, respectively, at $p < 0.05$.

TNF-α, compared to the levels in the saline-treated animals. However, treatment with Pirfenidone and Capsaicin significantly mitigated the increase in TNF-α levels induced by Bleomycin. Notably, Capsaicin's effect in reducing the elevated TNF-α level was significantly more pronounced when compared to Pirfenidone, as depicted in Figure 6.

3.8 The effect of Bleomycin, Pirfenidone, and Capsaicin on the immunohistochemical reactivity of α-SMA, Nrf-2, NF-Kβ, COX 2, TGF-β1, and PPAR-γ in the rats' lung tissue.

Sections from rats treated solely with Bleomycin exhibited a significant increase in the immunoreactivity of α-SMA, NF-Kβ, COX 2, and TGF-β1. Furthermore, there was a significant decrease in the immunoreactivity of Nrf-2 and PPAR-γ compared to the control rats. Conversely, the administration of Pirfenidone significantly mitigated the impact of Bleomycin on α-SMA, Nrf-2, COX 2, TGF-β1, and PPAR-γ, although it did not significantly affect the immunoreactivity of NF-Kβ.Remarkably, Capsaicin administration substantially attenuated the effects of Bleomycin on the immunoreactivity of all the assessed parameters. Rats treated with Bleomycin and Capsaicin exhibited significantly reduced immunoreactivity of NF-Kβ and TGF-β1, along with increased immunoreactivity of PPAR-γ when compared to the rats treated with Bleomycin and Pirfenidone, as shown in Figure 7.

3.9 Western blot results

In the present study, western blot technique was used to determine the levels of α-SMA, Collagen I and Collagen III in the pulmonary tissue, and it was found that both capsaicin and perfinidone administration could significantly ameliorate the increased levels of α-SMA, Collagen I and Collagen III proteins due to bleomycin intratracheal administration and the ameliorative effect of capsaicin was significantly higher than pirfenidone effect as shown in Figure 8.

4 Discussion

Bleomycin, a highly effective antibiotic with anticancer properties, but its therapeutic applications is limited since it has

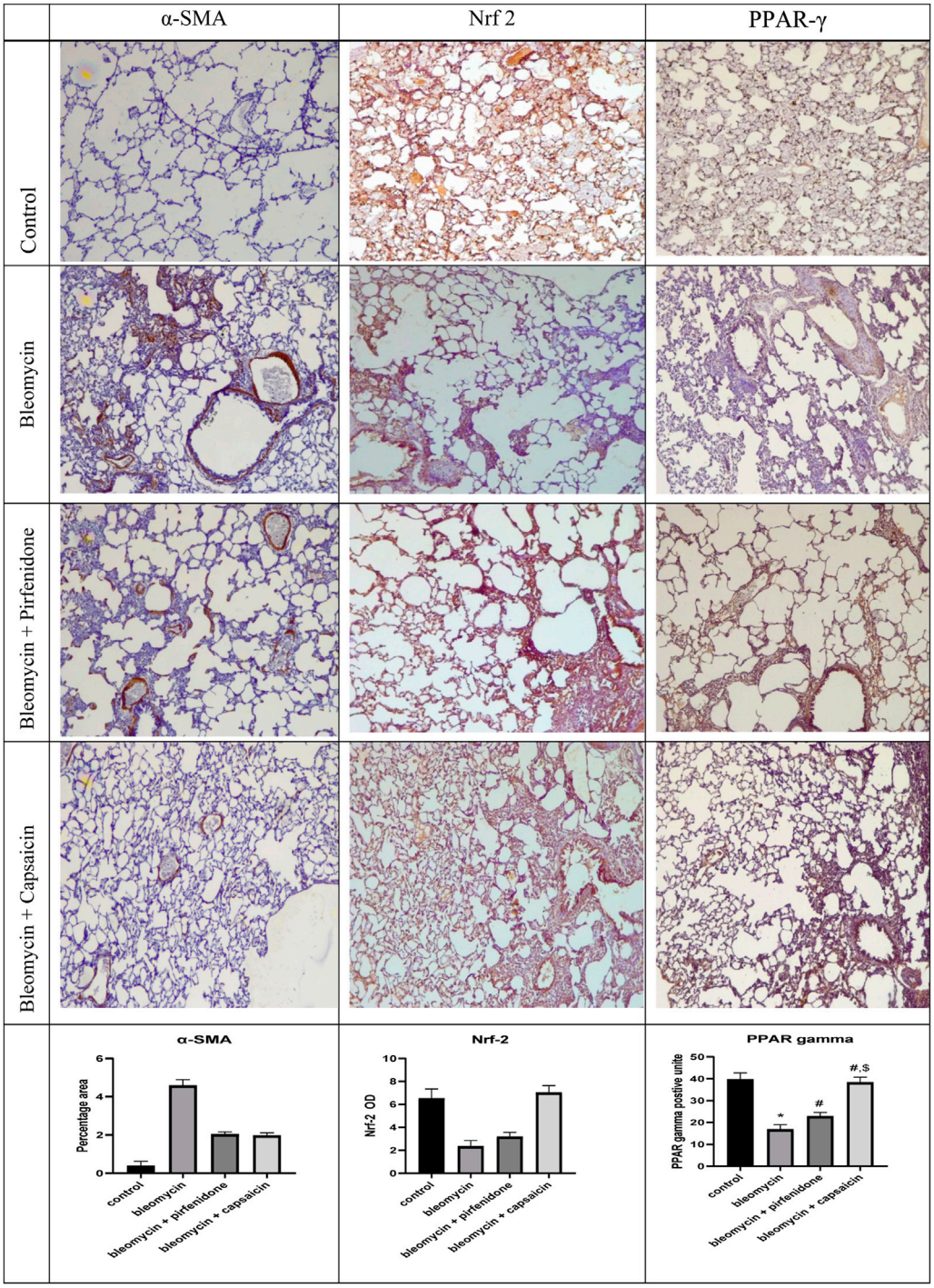

FIGURE 7
(Continued).

a tendency to induce lung fibrosis, which is depending on the dosage administered (Ezzie et al., 2011). Consequently, there has been a concerted effort to identify adjunct therapies that can mitigate this side effect. The present study represents the inaugural attempt to elucidate the therapeutic potential of Capsaicin in countering Bleomycin-induced pulmonary fibrosis.

The findings of this study underscore Bleomycin's capacity to induce marked morphological and histopathological alterations in lung tissue, indicative of its potent fibrogenic effect. Macroscopic examination of the lungs revealed distinct manifestations of Bleomycin's impact, including an irregular, coarse surface, interstitial hemorrhagic lesions, atrophic changes, tissue degeneration, significant tissue congestion, lung collapse, and tissue consolidation resulting in a loss of tissue elasticity. These observations align with prior research that has investigated the necroscopic effects of Bleomycin on lung tissues (Bahri et al.,

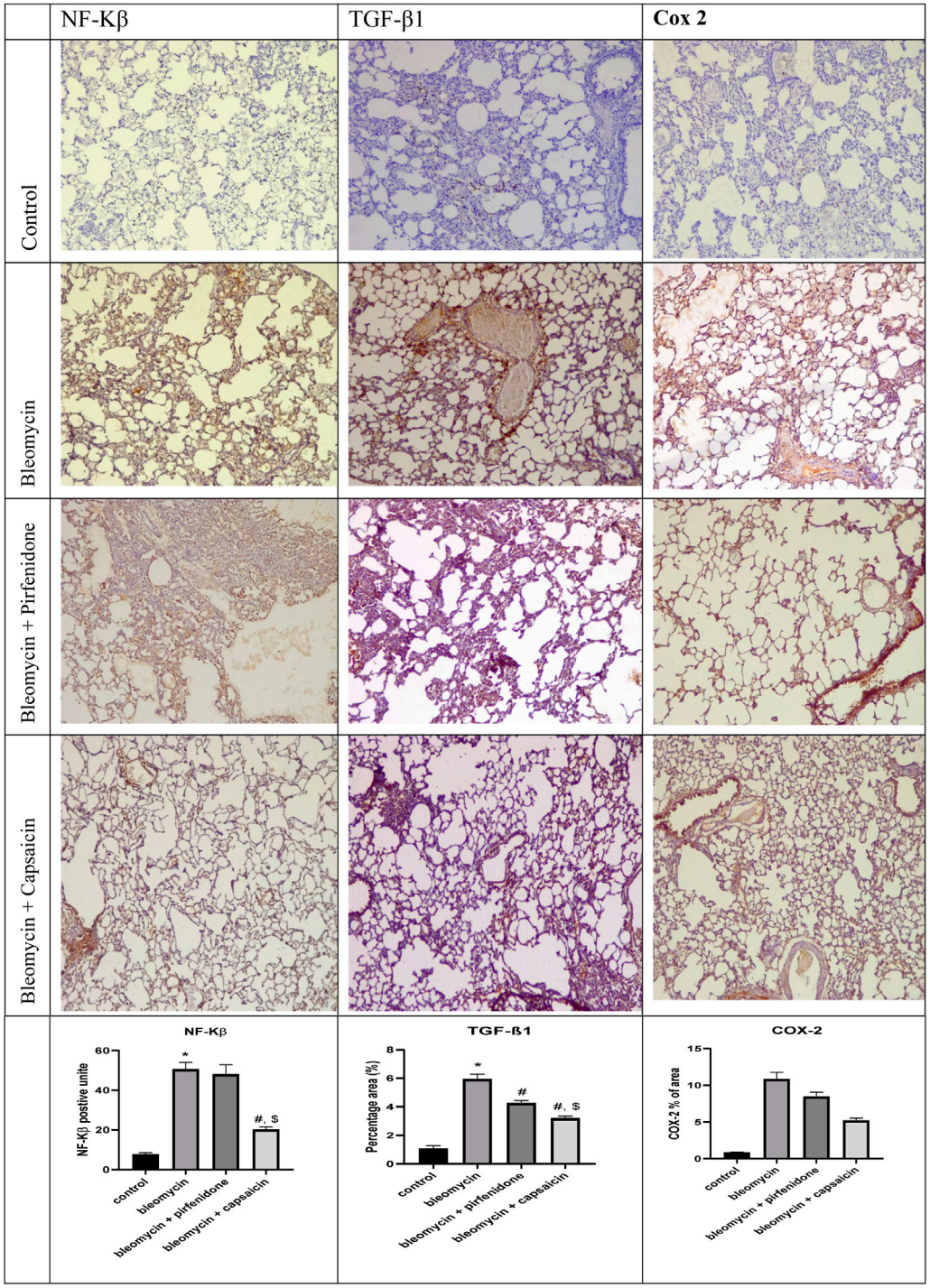

FIGURE 7
(Continued). The effects of Bleomycin, Pirfenidone, and Capsaicin on the pulmonary immunohistochemical reactivity of alpha-smooth muscle actin (α-SMA), nuclear factor erythroid 2–related factor 2 (Nrf-2), nuclear factor-kappa B (NF-Kβ), cyclooxygenase-2 (COX-2), transforming growth factor-beta 1 (TGF-β1), and Peroxisome proliferator-activated receptor gamma (PPAR-γ). Bleomycin (5 mg/kg) was administered via intratracheal instillation on day zero. Capsaicin (3 mg/kg) and Pirfenidone (50 mg/kg) were orally administered daily for 7 days. Results were analyzed by one-way ANOVA followed by Tukey's as a *post hoc* test ($n = 8$). *, #, and $ are considered statistically significant from the control, Bleomycin-only, and Bleomycin-plus Pirfenidone-treated group, respectively, at $p < 0.05$.

2020). Such changes can be attributed to the inflammation, epithelial injury, and excessive extracellular deposition induced by Bleomycin (Birnhuber et al., 2020). At the microscopic level, Bleomycin led to tissue degeneration, alveolar collapse, thickening of inter-alveolar septa, extensive cellular infiltration, congested blood vessels, infiltration of lymphocytic cells, and shedding of bronchiolar epithelial cells. Additionally, there was an increase in collagen and mucin content. These features of bleomycin-induced

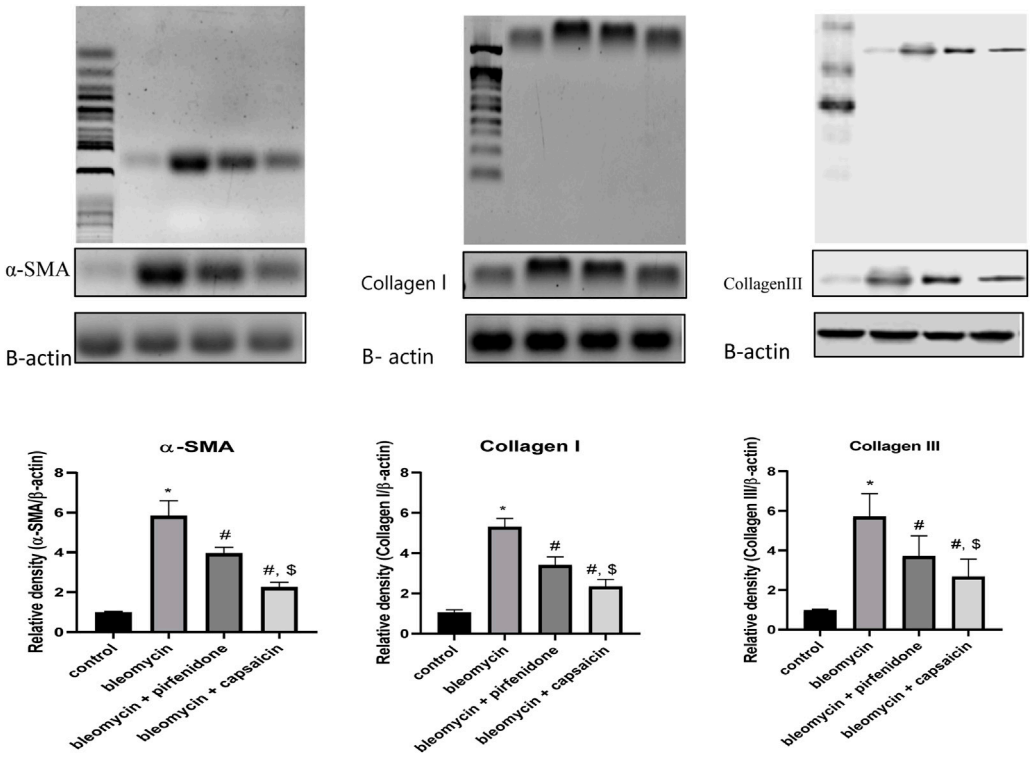

FIGURE 8
The effects of Bleomycin, Pirfenidone, and Capsaicin on the pulmonary protein expression of alpha-smooth muscle actin (α-SMA), CollagenI and CollagenIII. Results were analyzed by one-way ANOVA followed by Tukey's as a *post hoc* test (n = 8). *, #, and $ are considered statistically significant from the control, Bleomycin-only, and Bleomycin-plus Pirfenidone-treated group, respectively, at $p < 0.05$.

pulmonary fibrosis were also evident in the previous studies (Demirkol et al., 2023; Gul et al., 2023).

Significantly, the outcomes of this study underscore the effectiveness of Capsaicin treatment in improving the macroscopic lung characteristics as well as the histopathological distortions induced by Bleomycin in a comparable and even more substantial restorative effect when compared to the commercially available antifibrotic drug, Pirfenidone. These effects can be attributed to the anti-inflammatory and antifibrotic properties of Capsaicin (Huang et al., 2022; Mansouri et al., 2023), which were further highlighted through the assessment of fibrotic and inflammatory markers.

Pulmonary fibrosis is a characteristic condition observed in patients undergoing Bleomycin treatment. The disruption of alveolar epithelial cells and subsequent alveolar collapse trigger the activation of fibroblasts, which engulf the collapsed alveoli and deposit collagen and other fibrotic proteins (Carneiro et al., 2017). The excessive deposition of collagen enhances the tensile strength of the pulmonary interstitium, contributing to the restrictive nature of fibrotic lung diseases (Danaei et al., 2023). Hydroxyproline is a major component of the fibrillar collagen, and it is increased in case of increased collagen production and decreased turnover after injury (Yang et al., 2023). Mucins, the most common glycoprotein components of mucus, are secreted into the extracellular space. Mucus can capture, retain, and release biologically active molecules such as cytokines and growth factors. At the same time, the secreted mucins can regulate inflammatory and immune responses (Schultz and Stick, 2015).

α-SMA serves as a crucial marker of lung fibrosis, where significant polymerization of α-SMA occurs in proliferating fibroblastic cells within the alveolar interstitium (Song et al., 2013; Wang et al., 2019). Another key mediator of fibrosis is TGF-β, a profibrotic cytokine that plays a central role in the induction of fibrogenesis. It is upregulated and activated during lung fibrosis and promotes myofibroblast activation, proliferation and trans-differentiation and matrix preservation (Liu et al., 2019). TGF-β1 binding to its receptor induces α-SMA expression and subsequent myofibroblast differentiation, resulting in increased collagen deposition, as explained by (Abbas et al., 2023).

Similarly, in the current study, intratracheal administration of Bleomycin elicited an increase in the fibrosis score according to the Ashcroft scoring system. Additionally, there was an evident rise in CollagenI and CollagenIII proteins expression as determined by western blot technique in addition to collagen and mucin pulmonary content, as demonstrated by MTC and PAS staining, respectively. These effects were associated with a significant increase in pulmonary fibrotic markers such as hydroxyproline, TGF-β1 and α-SMA.

Interestingly, Capsaicin administration demonstrated promising antifibrotic activity in lung tissue evidenced by the significant reduction in the fibrosis score, CollagenI and CollagenIII proteins expression, collagen deposition, mucin

content, hydroxyproline content, and the immunohistochemical reactivity of α-SMA and TGF-β1, mirroring the effects of the approved antifibrotic Pirfenidone. Prior studies on Capsaicin have also substantiated its antifibrotic properties in various models, including its inhibition of TGF-β1 signaling to ameliorate kidney fibrosis (Liu et al., 2022).

To understand the mechanisms involved in the antifibrotic and ameliorative effects of Capsaicin in the Bleomycin-induced pulmonary fibrosis, we examined its impact on inflammatory cells besides some key mediators of inflammation and oxidative stress in the BAL and lung tissue.

Studies conducted on animal models involving intratracheal Bleomycin injection have revealed alterations in lavage fluid composition during fibrosis, characterized by a significant influx of inflammatory cells. Neutrophils are the first to appear, accompanied by increased percentages of lymphocytes and a transient influx of eosinophils, as documented by Fahey et al. (1982). Furthermore, Bleomycin-induced lung toxicity is marked by an augmentation in alveolar macrophages, as described by Kseibati et al. (2020). Protein molecules secreted by these inflammatory cells act as chemo-attractants and play a pivotal role in stimulating collagen synthesis by lung fibroblasts, contributing to lung fibrosis (Prasse et al., 2006).

The findings of the present study align with previous reports, wherein Bleomycin was found to increase both the total cell count and the percentages of macrophages, neutrophils, eosinophils, and lymphocytes. However, Capsaicin administration significantly mitigated the increase in the inflammatory cell count induced by Bleomycin. Capsaicin has previously demonstrated its ability to reduce inflammatory cell counts in BAL fluid in a model of lung ischemia-reperfusion injury in rabbits (Wang et al., 2019). These findings further underscore the anti-inflammatory effects elicited by Capsaicin.

The onset of pulmonary fibrosis is frequently preceded by acute inflammation of the lungs, triggered by viral and bacterial infections, radiation, chemotherapy, irritants, and pollutants. If left unresolved, this inflammation leads to the accumulation of fibrotic tissue in the lungs, causing respiratory dysfunction (Della Latta et al., 2015). Acute lung inflammation is characterized by the activation of inflammatory processes in response to lung injury, resulting in heightened permeability of lung capillary arteries and widespread destruction to the alveoli associated with fibrotic changes (Dorababu and Maraswami, 2023).

Upon lung injury, macrophages undergo a transformation into pro-inflammatory M1 phenotypes and start releasing pro-inflammatory cytokines (TNF-α, IL-6, IL-1β) and chemokines (IL-8, CCL7, CCL2). This results in an enhanced movement of monocytes and neutrophils towards the alveolar spaces, leading to their gradual accumulation (Brill et al., 2015; Frey et al., 2021). Neutrophils, in response, secrete a multitude of inflammatory mediators, reactive oxygen species, and proteinases, which cause damage to surfactant, basal membranes, and the epithelia-endothelial barrier, eventually leading to pulmonary fibrosis. Surfactant is a lipid-protein complex produced by alveolar epithelial type II cells (Dhooghe et al., 2014). It acts to reduce surface tension in the alveoli, preventing their collapse. During the development of acute lung injury, the loss of type II alveolar epithelial cells (AEC II) causes a notable reduction in surfactant production. Consequently, the collapse of alveoli occurs, allowing lung proteins to permeate into the alveolar space (Carignon et al., 2023; Ye et al., 2023).

The possible mechanisms of pulmonary tissue damage, fibrosis and cell death is disruption of tight-junction mediated cell-to-cell contacts, changes in extracellular matrix components and their interaction with epithelial cells, and disturbances in communication between epithelial and immune cells (Della Latta et al., 2015; Evangelista-Leite et al., 2023).

The current study revealed that Bleomycin increased the expression of inflammatory mediators such as TNF-α (BALF and lung tissue), NF-κB, TGF-β, IL-6 and Il-β along with elevated expression of the inducible COX-2 and increased NO production. Whereas, prostaglandins produced due to increased COX-2 expression have also been associated with the acceleration of pulmonary fibrosis (Oga et al., 2009).

Capsaicin administration effectively counteracted the inflammatory effects induced by Bleomycin by reducing the expression of TNF-α, NF-κB, TGF-β1 and COX-2, as well as decreasing NO production. These results align with previous studies demonstrating Capsaicin's anti-inflammatory effects against cyclophosphamide and acrylamide toxicities, as elucidated by Melekoglu et al. (2018); Abd Al Haleem et al. (2022).

Bleomycin was observed to decrease the immunoreactivity of PPAR-γ, a member of the nuclear hormone receptor family known for its role in modulating immune responses. PPAR-γ inhibits the expression of inflammatory mediators and influences immune cell differentiation toward anti-inflammatory phenotypes (Pascual et al., 2005). Additionally, PPAR-γ has been found to inhibit fibroblast proliferation, induce cell cycle arrest, and impede TGF-β1-induced myofibroblast differentiation and collagen secretion, hence effectively inhibit fibrosis (Milam et al., 2008). These findings suggest the potential of PPAR-γ agonists as therapeutic agents against pulmonary fibrosis. Interestingly, the present study demonstrated that capsaicin increased the expression of PPAR-γ in lung tissue, thereby we may postulate that the antifibrotic and anti-inflammatory properties of Capsaicin may be mediated in part through PPAR-γ activation.

The initial cellular injury accompanying lung fibrosis is mediated by reactive oxygen species (ROS) produced by infiltrating inflammatory cells. Activated macrophages, for instance, produce NO and peroxynitrite (Barnes and Belvisi, 1993). Moreover, inflammation and oxidative stress are interrelated, as NF-kB is activated in response to ROS production (Sen and Packer, 1996). Additionally, activated inflammatory cells produce ROS, which, in turn, recruit other inflammatory cells and amplifying the damage (Nathan, 2003). Nuclear factor erythroid 2–related factor 2 (Nrf-2) is a master regulator of cellular resistance to oxidative stress via modulation of the expression of genes encoding antioxidant enzymes and genes controlling immune and inflammatory responses, tissue remodeling and fibrosis (Hao et al., 2022). Alterations in the redox state activate Nrf2 which upregulates the production of antioxidant, xenobiotic-metabolizing, and cytoprotective enzymes, safeguarding cells against ROS (Chan and Kan, 1999). In the present study, Bleomycin significantly induced oxidative stress with increased ROS production, upregulated MPO pulmonary tissue concentration, elevated NO levels, elevated lipid

peroxidation and protein oxidation products (MDA and protein carbonyls respectively), decreased GSH levels, and total antioxidant capacity and reduced activity of antioxidant enzymes (catalase and SOD). This disturbance in the oxidative balance was associated with downregulation Nrf-2. Similar findings were reported by previous studies (Han et al., 2019), Capsaicin administration markedly alleviated oxidative stress by upregulating Nrf-2 expression, increasing antioxidant enzyme activities, GSH levels, and total antioxidant capacity, and reducing the products of oxidative stress, including MDA and protein carbonyls. Our results were in accordance with several studies highlighting the antioxidant effects of Capsaicin (Beltran et al., 2007; Nascimento et al., 2014; Thongin et al., 2022).

Collectively, Capsaicin exhibited promising antifibrotic activity against Bleomycin-induced pulmonary fibrosis and demonstrating efficacy comparable to the commercially available and approved antifibrotic drug, Pirfenidone. These antifibrotic effects may be attributed, at least in part, to the antioxidant and anti-inflammatory activities of Capsaicin mediated by upregulation of PPAR-γ and Nrf-2 expression.

5 Study limitations

Moving forward, there are several promising avenues for further research and clinical applications regarding Capsaicin's potential in treating pulmonary fibrosis. Firstly, deeper investigations into the precise molecular mechanisms underlying Capsaicin's antifibrotic and anti-inflammatory effects are warranted. Understanding how Capsaicin interacts with specific signaling pathways involved in fibrosis, such as TGF-β1, PPAR-γ, and NF-κB, can provide valuable insights and potential targets for drug development. Additionally, optimizing the dosage and administration regimen of Capsaicin is crucial. Future studies should explore various dosages and treatment durations to determine the most effective and safe therapeutic regimen. This will help establish standardized protocols for clinical applications. Combination therapies could hold great promise in enhancing treatment outcomes. Exploring the potential synergies between Capsaicin and existing medications like Pirfenidone or Nintedanib may lead to more potent treatment strategies for pulmonary fibrosis. Transitioning from preclinical studies to clinical trials is a critical step. Well-designed clinical trials are needed to evaluate the safety and efficacy of Capsaicin in patients with pulmonary fibrosis. These trials should assess parameters such as lung function, quality of life, and fibrosis progression. Identifying specific biomarkers associated with Capsaicin's therapeutic effects can aid in patient selection and monitoring of treatment responses, allowing for more personalized treatment approaches.

6 Conclusion

This study sheds light on the potential therapeutic efficacy of Capsaicin in mitigating the detrimental effects of Bleomycin which is an effective anticancer agent with high potential to cause dose-dependent pulmonary fibrosis. Our findings reveal that Capsaicin treatment exerts a considerable positive impact on both the macroscopic and microscopic aspects of lung tissue affected by Bleomycin. Intratracheal administration of bleomycin produced visible signs of fibrosis, histopathological alterations, increased collagen deposition, elevated mucin content, inflammatory cell infiltration and elevated fibrosis markers such as hydroxyproline, α-SMA and TGF-β1. Inflammatory markers such a TNF-α, IL-1β, IL-6, NF-κB and COX-2 as well as oxidative stress markers such as NO, MDA, and protein carbonyl were induced by bleomycin. Moreover, anti-inflammatory and antoioxidant mechanisms were compromised by bleomycin as evident by decreased the expression of PPAR-γ and Nrf-2, reduced GSH, total antioxidant capacity, and the activities of catalase and SOD.

On the other hand, treatment with Capsaicin following Bleomycin exposure improved lung macroscopic and microscopic characteristics and reversed the histopathological distortions induced by Bleomycin compared to the approved antifibrotic drug Pirfenidone. These effects were evidenced in the form of reduced collagen deposition, fibrosis score and mucin content, decreased inflammatory cell infiltration, lowered levels of fibrosis markers (hydroxyproline, α-SMA, and TGF-β1), downregulated inflammatory markers (TNF-α, IL-1β, IL-6, NF-κB, and COX-2) and oxidative stress markers (NO, MDA, and protein carbonyl). Parallel to these effects, Capsaicine enhanced the anti-inflammatory and antioxidant pathways (PPAR-γ, Nrf-2, GSH, total antioxidant capacity, and the activities of catalase and SOD.

In summary, Bleomycin-induced pulmonary fibrosis is closely associated with inflammatory responses and oxidative stress. Capsaicin emerges as a promising candidate for the treatment of Bleomycin-induced pulmonary fibrosis, with its multifaceted benefits encompassing anti-inflammatory, antifibrotic, and antioxidant activities. These findings pave the way for further research and clinical investigations and potentially offer new therapeutic avenues for managing pulmonary fibrosis and enhancing the quality of life for affected individuals.

Data availability statement

The original contributions presented in the study are included in the article/Supplementary Material, further inquiries can be directed to the corresponding author.

Ethics statement

The animal studies were approved by the ethical committee of the Faculty of Pharmacy at South Valley University, Egypt, under approval number (P.S.V.U 112/23). The studies were conducted in accordance with the local legislation and institutional requirements. Written informed consent was obtained from the owners for the participation of their animals in this study.

Author contributions

WA: Formal Analysis, Methodology, Resources, Writing–original draft. HZA: Software, Writing–original draft.

NH: Funding acquisition, Resources, Visualization, Writing–review and editing. HAS: Conceptualization, Data curation, Formal Analysis, Writing–review and editing. BE: Project administration, Validation, Writing–original draft. NA: Data curation, Formal Analysis, Writing–original draft. HMA: Investigation, Methodology, Writing–original draft. EA: Formal Analysis, Investigation, Methodology, Supervision, Writing–original draft, Writing–review and editing.

Funding

The author(s) declare financial support was received for the research, authorship, and/or publication of this article. This project was funded by the Deanship of Scientific Research (DSR) at King Abdulaziz University, Jeddah, under grant no. (RG-13-166-41).

Acknowledgments

The authors, therefore, acknowledge with thanks DSR for technical and financial support.

Conflict of interest

The authors declare that the research was conducted in the absence of any commercial or financial relationships that could be construed as a potential conflict of interest.

Publisher's note

Supplementary material

The Supplementary Material for this article can be found online at: https://www.frontiersin.org/articles/10.3389/fphar.2024.1333715/full#supplementary-material

References

Abbas, N. A. T., Nafea, O. E., Mohammed, H. O., Samy, W., Abdelmageed, A. F., Afifi, R., et al. (2023). Repurposing of carvedilol to alleviate bleomycin-induced lung fibrosis in rats: repressing of TGF-β1/α-SMA/Smad2/3 and STAT3 gene expressions. *Life Sci.* 324, 121692. doi:10.1016/j.lfs.2023.121692

Abd Al Haleem, E. N., Hasan, W. Y. S., and Arafa, H. M. M. (2022). Therapeutic effects of thymoquinone or capsaicin on acrylamide-induced reproductive toxicity in rats mediated by their effect on oxidative stress, inflammation, and tight junction integrity. *Drug Chem. Toxicol.* 45 (5), 2328–2340. doi:10.1080/01480545.2021.1942485

Altintas, N., Erboga, M., Aktas, C., Bilir, B., Aydin, M., Sengul, A., et al. (2016). Protective effect of infliximab, a tumor necrosis factor-alfa inhibitor, on bleomycin-induced lung fibrosis in rats. *Inflammation* 39 (1), 65–78. doi:10.1007/s10753-015-0224-z

Archer, S. (1993). Measurement of nitric oxide in biological models. *Faseb J.* 7 (2), 349–360. doi:10.1096/fasebj.7.2.8440411

Ayilya, B. L., Balde, A., Ramya, M., Benjakul, S., Kim, S. K., and Nazeer, R. A. (2023). Insights on the mechanism of bleomycin to induce lung injury and associated *in vivo* models: a review. *Int. Immunopharmacol.* 121, 110493. doi:10.1016/j.intimp.2023.110493

Bahri, S., Ben Ali, R., Nahdi, A., Mlika, M., Abdennabi, R., and Jameleddine, S. (2020). Salvia officinalis attenuates bleomycin-induced oxidative stress and lung fibrosis in rats. *Nutr. Cancer* 72 (7), 1135–1145. doi:10.1080/01635581.2019.1675724

Barnes, P. J., and Belvisi, M. J. T. (1993). Nitric oxide and lung disease. *Thorax* 48 (10), 1034–1043. doi:10.1136/thx.48.10.1034

Beltran, J., Ghosh, A. K., and Basu, S. (2007). Immunotherapy of tumors with neuroimmune ligand capsaicin. *J. Immunol.* 178 (5), 3260–3264. doi:10.4049/jimmunol.178.5.3260

Birnhuber, A., Egemnazarov, B., Biasin, V., Bonyadi Rad, E., Wygrecka, M., Olschewski, H., et al. (2020). CDK4/6 inhibition enhances pulmonary inflammatory infiltration in bleomycin-induced lung fibrosis. *Respir. Res.* 21 (1), 167. doi:10.1186/s12931-020-01433-w

Brill, S. E., Patel, A. R. C., Singh, R., Mackay, A. J., Brown, J. S., and Hurst, J. R. (2015). Lung function, symptoms and inflammation during exacerbations of non-cystic fibrosis bronchiectasis: a prospective observational cohort study. *Respir. Res.* 16 (1), 16. doi:10.1186/s12931-015-0167-9

Carignon, S., De Moura Rodrigues, D., Gosset, D., Culerier, E., Huot-Marchand, S., Savigny, F., et al. (2023). Lung inflammation and interstitial fibrosis by targeted alveolar epithelial type I cell death. *Front. Immunol.* 14, 1261483. doi:10.3389/fimmu.2023.1261483

Carneiro, P. J., Clevelario, A. L., Padilha, G. A., Silva, J. D., Kitoko, J. Z., Olsen, P. C., et al. (2017). Bosutinib therapy ameliorates lung inflammation and fibrosis in experimental silicosis. *Front. Physiol.* 8, 159. doi:10.3389/fphys.2017.00159

Chan, K., and Kan, Y. W. (1999). Nrf2 is essential for protection against acute pulmonary injury in mice. *Proc. Natl. Acad. Sci. U. S. A.* 96 (22), 12731–12736. doi:10.1073/pnas.96.22.12731

Chen, W., Pilling, D., and Gomer, R. H. (2023). The mRNA-binding protein DDX3 mediates TGF-β1 upregulation of translation and promotes pulmonary fibrosis. *JCI Insight* 8 (7), e167566. doi:10.1172/jci.insight.167566

Cissell, D. D., Link, J. M., Hu, J. C., and Athanasiou, K. A. (2017). A modified hydroxyproline assay based on hydrochloric acid in Ehrlich's solution accurately measures tissue collagen content. *Tissue Eng. Part C Methods* 23 (4), 243–250. doi:10.1089/ten.tec.2017.0018

Danaei, N., Sadeghi, H., Asfarm, A., Rostamzadeh, D., Panahi Kokhdan, E., Sadeghi, H., et al. (2023). Betulin-rich hydroalcoholic extract of Daphne oleoides attenuates bleomycin-induced pulmonary fibrosis in rat. *Heliyon* 9 (8), e19236. doi:10.1016/j.heliyon.2023.e19236

Della Latta, V., Cecchettini, A., Del Ry, S., and Morales, M. A. (2015). Bleomycin in the setting of lung fibrosis induction: from biological mechanisms to counteractions. *Pharmacol. Res.* 97, 122–130. doi:10.1016/j.phrs.2015.04.012

Demirkol, B., Gul, S., Cörtük, M., Akanıl Fener, N., Yavuzsan, E., Eren, R., et al. (2023). Protective efficacy of pirfenidone in rats with pulmonary fibrosis induced by bleomycin. *Sarcoidosis Vasc. Diffuse Lung Dis.* 40 (3), e2023036. doi:10.36141/svdld.v40i3.13847

Dhooghe, B., Noël, S., Huaux, F., and Leal, T. (2014). Lung inflammation in cystic fibrosis: pathogenesis and novel therapies. *Clin. Biochem.* 47 (7-8), 539–546. doi:10.1016/j.clinbiochem.2013.12.020

Dorababu, A., and Maraswami, M. (2023). Recent advances (2015-2020) in drug discovery for attenuation of pulmonary fibrosis and COPD. *Molecules* 28 (9), 3674. doi:10.3390/molecules28093674

Evangelista-Leite, D., Carreira, A. C. O., Nishiyama, M. Y., Gilpin, S. E., and Miglino, M. A. (2023). The molecular mechanisms of extracellular matrix-derived hydrogel therapy in idiopathic pulmonary fibrosis models. *Biomaterials* 302, 122338. doi:10.1016/j.biomaterials.2023.122338

Ezzie, M. E., Piper, M. G., Montague, C., Newland, C. A., Opalek, J. M., Baran, C., et al. (2011). Thrombospondin-1-deficient mice are not protected from bleomycin-induced pulmonary fibrosis. *Am. J. Respir. Cell Mol. Biol.* 44 (4), 556–561. doi:10.1165/rcmb.2009-0019OC

Fahey, P. J. (1982). Early diagnosis of bleomycin pulmonary toxicity using bronchoalveolar lavage in dogs. *Am. Rev. Respir. Dis.* 126 (1), 126–30.

Frey, D. L., Boutin, S., Dittrich, S. A., Graeber, S. Y., Stahl, M., Wege, S., et al. (2021). Relationship between airway dysbiosis, inflammation and lung function in adults with cystic fibrosis. *J. Cyst. Fibros.* 20 (5), 754–760. doi:10.1016/j.jcf.2020.12.022

Gul, A., Yang, F., Xie, C., Du, W., Mohammadtursun, N., Wang, B., et al. (2023). Pulmonary fibrosis model of mice induced by different administration methods of bleomycin. *BMC Pulm. Med.* 23 (1), 91. doi:10.1186/s12890-023-02349-z

Guo, J., Yang, Z., Jia, Q., Bo, C., Shao, H., and Zhang, Z. (2019). Pirfenidone inhibits epithelial-mesenchymal transition and pulmonary fibrosis in the rat silicosis model. *Toxicol. Lett.* 300, 59–66. doi:10.1016/j.toxlet.2018.10.019

Han, B., Li, S., Lv, Y., Yang, D., Li, J., Yang, Q., et al. (2019). Dietary melatonin attenuates chromium-induced lung injury via activating the Sirt1/Pgc-1α/Nrf2 pathway. *Food Funct.* 10 (9), 5555–5565. doi:10.1039/c9fo01152h

Hao, W., Li, M., Cai, Q., Wu, S., Li, X., He, Q., et al. (2022). Roles of NRF2 in fibrotic diseases: from mechanisms to therapeutic approaches. *Front. Physiol.* 13, 889792. doi:10.3389/fphys.2022.889792

Henderson, R. F. J. E., and Pathology, T. (2005). Use of bronchoalveolar lavage to detect respiratory tract toxicity of inhaled material. *Exp. Toxicol. Pathol.* 57, 155–159. doi:10.1016/j.etp.2005.05.004

Huang, Z., Sharma, M., Dave, A., Yang, Y., Chen, Z. S., and Radhakrishnan, R. (2022). The antifibrotic and the anticarcinogenic activity of capsaicin in hot chili pepper in relation to oral submucous fibrosis. *Front. Pharmacol.* 13, 888280. doi:10.3389/fphar.2022.888280

Ilie, M. A., Caruntu, C., Tampa, M., Georgescu, S. R., Matei, C., Negrei, C., et al. (2019). Capsaicin: physicochemical properties, cutaneous reactions and potential applications in painful and inflammatory conditions. *Exp. Ther. Med.* 18 (2), 916–925. doi:10.3892/etm.2019.7513

Ishida, Y., Mabuchi, Y., Naraoka, Y., Hisamatsu, D., and Akazawa, C. (2023). Conservation of markers and stemness in adipose stem and progenitor cells between cattle and other species. *Int. J. Mol. Sci.* 24 (4), 11908. doi:10.3390/ijms241511908

Kabel, A. M., Omar, M. S., and Elmaaboud, M. A. A. (2016). Amelioration of bleomycin-induced lung fibrosis in rats by valproic acid and butyrate: role of nuclear factor kappa-B, proinflammatory cytokines and oxidative stress. *Int. Immunopharmacol.* 39, 335–342. doi:10.1016/j.intimp.2016.08.008

Kadam, A. H., and Schnitzer, J. E. (2023). Characterization of acute lung injury in the bleomycin rat model. *Physiol. Rep.* 11 (5), e15618. doi:10.14814/phy2.15618

Kseibati, M. O., Shehatou, G. S. G., Sharawy, M. H., Eladl, A. E., and Salem, H. A. (2020). Nicorandil ameliorates bleomycin-induced pulmonary fibrosis in rats through modulating eNOS, iNOS, TXNIP and HIF-1α levels. *Life Sci.* 246, 117423. doi:10.1016/j.lfs.2020.117423

Lee, C. Y., Kim, M., and Yoon, S. W. (2003). Short-term control of capsaicin on blood and oxidative stress of rats *in vivo*. *Phytother. Res.* 17 (5), 454–458. doi:10.1002/ptr.1172

Lei, L., Zhao, C., Qin, F., He, Z. Y., Wang, X., and Zhong, X. N. (2016). Th17 cells and IL-17 promote the skin and lung inflammation and fibrosis process in a bleomycin-induced murine model of systemic sclerosis. *Clin. Exp. Rheumatol.* 34 (5), 14–22.

Liu, B., Bing, Q., Li, S., Han, B., Lu, J., Baiyun, R., et al. (2019). Role of A(2B) adenosine receptor-dependent adenosine signaling in multi-walled carbon nanotube-triggered lung fibrosis in mice. *J. Nanobiotechnology* 17 (1), 45. doi:10.1186/s12951-019-0478-y

Liu, Z., Wang, W., Li, X., Tang, S., Meng, D., Xia, W., et al. (2022). Capsaicin ameliorates renal fibrosis by inhibiting TGF-β1–Smad2/3 signaling. *Phytomedicine* 100, 154067. doi:10.1016/j.phymed.2022.154067

Mansouri, R. A., Ahmed, A. M., Alshaibi, H. F., and Aboubakr, E. M. (2023). Capsaicin ameliorates myocardial injury in diabetic rats via upregulating Nrf-2, HO-1 and iNOS tissue concentrations besides normalizing the distribution of structural proteins desmin and α-SMA. *Food Biosci.* 56, 103130. doi:10.1016/j.fbio.2023.103130

Melekoglu, R., Ciftci, O., Eraslan, S., Cetin, A., and Basak, N. (2018). Beneficial effects of curcumin and capsaicin on cyclophosphamide-induced premature ovarian failure in a rat model. *J. Ovarian Res.* 11 (1), 33–38. doi:10.1186/s13048-018-0409-9

Milam, J. E., Keshamouni, V. G., Phan, S. H., Hu, B., Gangireddy, S. R., Hogaboam, C. M., et al. (2008). PPAR-γ agonists inhibit profibrotic phenotypes in human lung fibroblasts and bleomycin-induced pulmonary fibrosis. *Am. J. Physiol. Lung Cell. Mol. Physiol.* 294 (5), L891–L901. doi:10.1152/ajplung.00333.2007

Nascimento, P. L., Nascimento, T. C. E. S., Ramos, N. S. M., Silva, G. R., Gomes, J. E. G., Falcão, R. E. A., et al. (2014). Quantification, antioxidant and antimicrobial activity of phenolics isolated from different extracts of Capsicum frutescens (Pimenta Malagueta). *Molecules* 19 (4), 5434–5447. doi:10.3390/molecules19045434

Nathan, C. (2003). Specificity of a third kind: reactive oxygen and nitrogen intermediates in cell signaling. *J. Clin. Invest.* 111 (6), 769–778. doi:10.1172/JCI18174

Oga, T., Matsuoka, T., Yao, C., Nonomura, K., Kitaoka, S., Sakata, D., et al. (2009). Prostaglandin F(2alpha) receptor signaling facilitates bleomycin-induced pulmonary fibrosis independently of transforming growth factor-beta. *Nat. Med.* 15 (12), 1426–1430. doi:10.1038/nm.2066

Pascual, G., Fong, A. L., Ogawa, S., Gamliel, A., Li, A. C., Perissi, V., et al. (2005). A SUMOylation-dependent pathway mediates transrepression of inflammatory response genes by PPAR-gamma. *Nature* 437 (7059), 759–763. doi:10.1038/nature03988

Prasse, A., Pechkovsky, D. V., Toews, G. B., Jungraithmayr, W., Kollert, F., Goldmann, T., et al. (2006). A vicious circle of alveolar macrophages and fibroblasts perpetuates pulmonary fibrosis via CCL18. *Am. J. Respir. Crit. Care Med.* 173 (7), 781–792. doi:10.1164/rccm.200509-1518OC

Razzaque, M. S., Hossain, M. A., Kohno, S., and Taguchi, T. (1998). Bleomycin-induced pulmonary fibrosis in rat is associated with increased expression of collagen-binding heat shock protein (HSP) 47. *Virchows Arch.* 432 (5), 455–460. doi:10.1007/s004280050191

Schultz, A., and Stick, S. (2015). Early pulmonary inflammation and lung damage in children with cystic fibrosis. *Respirology* 20 (4), 569–578. doi:10.1111/resp.12521

Sen, C. K., and Packer, L. J. (1996). Antioxidant and redox regulation of gene transcription. *FASEB J.* 10 (7), 709–720. doi:10.1096/fasebj.10.7.8635688

Song, X., Liu, W., Xie, S., Wang, M., Cao, G., Mao, C., et al. (2013). All-transretinoic acid ameliorates bleomycin-induced lung fibrosis by downregulating the TGF-β1/Smad3 signaling pathway in rats. *Lab. Invest.* 93 (11), 1219–1231. doi:10.1038/labinvest.2013.108

Thongin, S., Den-Udom, T., Uppakara, K., Sriwantana, T., Sibmooh, N., Laolob, T., et al. (2022). Beneficial effects of capsaicin and dihydrocapsaicin on endothelial inflammation, nitric oxide production and antioxidant activity. *Biomed. Pharmacother.* 154, 113521. doi:10.1016/j.biopha.2022.113521

Usman, M., Faruqui, Z. S., ud Din, N., and Zahid, K. F. (2010). Bleomycin induced pulmonary toxicity in patients with germ cell tumours. *J. Ayub Med. Coll. Abbottabad* 22 (3), 35–37.

Venkatesan, N., Ouzzine, M., Kolb, M., Netter, P., and Ludwig, M. S. (2011). Increased deposition of chondroitin/dermatan sulfate glycosaminoglycan and upregulation of β1,3-glucuronosyltransferase I in pulmonary fibrosis. *Am. J. Physiol. Lung Cell Mol. Physiol.* 300 (2), L191–L203. doi:10.1152/ajplung.00214.2010

Wang, H. H., Meng, Y. L., Yang, Z. M., Wang, X. X., Xu, H. X., and Wang, W. M. (2019). Effect of Dilong on expression of fibrogenic factors TGF-β1 and α-SMA in lung tissue of mice with pulmonary fibrosis. *Zhongguo Zhong Yao Za Zhi* 44 (24), 5473–5478. doi:10.19540/j.cnki.cjcmm.20190716.402

Wang, Q., Sundar, I. K., Lucas, J. H., Park, J. G., Nogales, A., Martinez-Sobrido, L., et al. (2023). Circadian clock molecule REV-ERBα regulates lung fibrotic progression through collagen stabilization. *Nat. Commun.* 14 (1), 1295. doi:10.1038/s41467-023-36896-0

Yang, X., Huang, X. J., Chen, Z., Xu, A. L., Zhou, H., Bi, X. L., et al. (2023). A novel quantification method of lung fibrosis based on Micro-CT images developed with the optimized pulmonary fibrosis mice model induced by bleomycin. *Heliyon* 9 (3), e13598. doi:10.1016/j.heliyon.2023.e13598

Ye, X., Zhang, M., Gu, H., Liu, M., Zhao, Y., Shi, Y., et al. (2023). Animal models of acute exacerbation of pulmonary fibrosis. *Respir. Res.* 24 (1), 296. doi:10.1186/s12931-023-02595-z

Yoshizaki, A., Yanaba, K., Iwata, Y., Komura, K., Ogawa, A., Akiyama, Y., et al. (2010). Cell adhesion molecules regulate fibrotic process via Th1/Th2/Th17 cell balance in a bleomycin-induced scleroderma model. *J. Immunol.* 185 (4), 2502–2515. doi:10.4049/jimmunol.0901778

Zimmer, A. R., Leonardi, B., Miron, D., Schapoval, E., Oliveira, J. R. D., and Gosmann, G. (2012). Antioxidant and anti-inflammatory properties of Capsicum baccatum: from traditional use to scientific approach. *J. Ethnopharmacol.* 139 (1), 228–233. doi:10.1016/j.jep.2011.11.005

frontiers | Frontiers in Pharmacology

TYPE Original Research
PUBLISHED 07 March 2024
DOI 10.3389/fphar.2024.1295356

OPEN ACCESS

EDITED BY
Sergio Fallone Andrade,
Lusofona University, Portugal

REVIEWED BY
Xianyu Li,
China Academy of Chinese Medical Sciences, China
Yi Wu,
Nanjing Agricultural University, China

*CORRESPONDENCE
Xuesong Yang,
yang_xuesong@126.com
Yong Ding,
dingyong641025@163.com
Guang Wang,
wangguang7453@126.com

†These authors have contributed equally to this work

RECEIVED 16 September 2023
ACCEPTED 22 February 2024
PUBLISHED 07 March 2024

CITATION
Lu J-Q, Luo Z-Y, Sun C, Wang S-M, Sun D, Huang R-J, Yang X, Ding Y and Wang G (2024), Baicalin administration could rescue high glucose-induced craniofacial skeleton malformation by regulating neural crest development.
Front. Pharmacol. 15:1295356.
doi: 10.3389/fphar.2024.1295356

Baicalin administration could rescue high glucose-induced craniofacial skeleton malformation by regulating neural crest development

Jia-Qi Lu[1,2†], Zhi-Yan Luo[1,2†], Chengyang Sun[2], Si-Miao Wang[2], Dixiang Sun[3], Ruo-Jing Huang[1], Xuesong Yang[2,4*], Yong Ding[1*] and Guang Wang[2,4*]

[1]The First Affiliated Hospital of Jinan University, Jinan University, Guangzhou, China, [2]Division of Histology and Embryology, International Joint Laboratory for Embryonic Development and Prenatal Medicine, School of Medicine, Jinan University, Guangzhou, China, [3]Department of Pathology, Mengyin County Hospital of Traditional Chinese Medicine, Linyi, China, [4]Key Laboratory for Regenerative Medicine of the Ministry of Education of China, Jinan University, Guangzhou, China

Hyperglycemia in pregnancy can increase the risk of congenital disorders, but little is known about craniofacial skeleton malformation and its corresponding medication. Our study first used meta-analysis to review the previous findings. Second, baicalin, an antioxidant, was chosen to counteract high glucose-induced craniofacial skeleton malformation. Its effectiveness was then tested by exposing chicken embryos to a combination of high glucose (HG, 50 mM) and 6 μM baicalin. Third, whole-mount immunofluorescence staining and *in situ* hybridization revealed that baicalin administration could reverse HG-inhibited neural crest cells (NCC) delamination and migration through upregulating the expression of Pax7 and Foxd3, and mitigate the disordered epithelial-mesenchymal transition (EMT) process by regulating corresponding adhesion molecules and transcription factors (i.e., E-cadherin, N-cadherin, Cadherin 6B, Slug and Msx1). Finally, through bioinformatic analysis and cellular thermal shift assay, we identified the AKR1B1 gene as a potential target. In summary, these findings suggest that baicalin could be used as a therapeutic agent for high glucose-induced craniofacial skeleton malformation.

KEYWORDS

baicalin, diabetes mellitus, hyperglycemia in pregnancy, NCC delamination and migration, craniofacial skeleton

Introduction

The generation of neural crest cells (NCCs) occurs when primary neurulation occurs, i.e., the process of dorsal fusion of the neural plate borders (Osório et al., 2004). Neurulation is defined as the morphogenetic process in which the neural plate transforms into a neural tube, and then the neural progenitor cells in the neural tube differentiate into the cellular components of the brain and the spinal cord (Colas and Schoenwolf, 2001). Failure of primary neurulation, i.e., defective formation of neural tube, will lead to malformations known as neural tube defects (NTDs), the second most prevalent congenital anomaly (Copp et al., 2003; Mitchell, 2005). It was reported that NTDs were closely associated with the

abnormal development of NCCs (Stevenson et al., 2004; Wang et al., 2016). During early vertebrate development, NCCs are derived from the dorsal-most aspect of the neural tube (Achilleos and Trainor, 2012). Thereafter, primitive NCCs undergo a succession of events in chronological order, including NCC induction, delamination, epithelial-mesenchymal transition (EMT), migration and differentiation, and eventually contribute a variety of NCC-derived cells (Zhang et al., 2017). Obviously, NCCs are endowed with the remarkable ability of migration and differentiation, thereby making up various cells and tissues of the neural crest (Takahashi et al., 2013; Simões-Costa and Bronner, 2015). The neural crest derivatives comprise the whole craniofacial skeleton, cerebral ganglions, enteric nervous system, and Schwann cells, while cranial NCCs contribute cranial bones, cartilage, smooth muscle, dentin, melanocytes, corneal endothelial cells, and neurons and glial cells in the peripheral nervous system (Cordero et al., 2011; Ishii et al., 2012). Regarding the regulation of NCC development, the interaction of transcription factors and cell signaling molecules has been suggested to involve the aforementioned morphogenetic formation, such as bone morphogenetic proteins (BMPs), Snai2 (Slug), Wnts, and fibroblast growth factors (FGFs), etc. (Barembaum and Bronner-Fraser, 2005). Given the close correlation between NCC development and NTDs (Takahashi et al., 2013; Reid et al., 2015), we investigated the treatment strategy for alleviating NCC malformation resulting from hyperglycemia in pregnancy (HIP) using chicken embryos, an early developmental vertebrate model.

HIP can cause very serious pregnancy-specific health problems (Negrato and Gomes, 2013). HIP is generally classified as either diabetes mellitus in pregnancy (DIP) or gestational diabetes mellitus (GDM), which is deemed damaged glucose tolerance during pregnancy. In other words, HIP could be regarded as a consequence of either preexisting diabetes or GDM (López Stewart, 2014; Hod et al., 2015). Approximately 80% of diabetic pregnancies are vested in GDM (Virjee et al., 2001). Noticeably, GDM is usually not diagnosed in the clinic until the 24th to 28th week of gestation, but then it is too late to implement treatment since the most important period for embryonic/fetal development is the early stage of embryo development. Thus, maternal HG could have already impacted the early development of the fetus. It was reported that maternal hyperglycemia greatly increased the risk of congenital abnormalities in the cardiovascular and nervous systems. For example, hyperglycemia could lead to NTDs, including exencephaly, anencephaly and rachischisis (Dheen et al., 2009; Sukanya et al., 2012). Up to 17% of neonates of diabetic mothers suffer from congenital heart diseases (e.g., atrioventricular septal defects (AVSDs) and tetralogy of Fallot) (Corrigan et al., 2009). Obviously, understanding and treating diabetes during pregnancy would help prevent or lower maternal and fetal complications (Negrato and Gomes, 2013).

As a flavone glycoside (i.e., glucuronide of baicalein), baicalin is produced from the combination of glucuronic acid and baicalein. In nature, baicalein exists in the roots of Scutellaria lateriflora and Cutellaria baicalensis, which have been used as herbal medicine to prevent miscarriage by improving the developmental competence of embryos (Abel, 1984; Qi et al., 2016; Preventive et al., 2023). Furthermore, in most Asian countries, baicalin is also largely used as an herbal supplement because of its broad scope of health benefits, such as anti-neuroinflammation (Wang et al., 2016), anticancer (Wang et al., 2015), anti-anxiety (Wang et al., 2008), and increased lung capability (Baek et al., 2014) as well as fertility (Zhang et al., 2015). Regarding its biological mechanism, baicalin is believed to perform effectively by suppressing oxidative stress (Yin et al., 2011). Our previous study showed that baicalin administration could attenuate HG-induced malformations of the cardiovascular and nervous systems during embryonic/fetal development (Wang et al., 2018a; Wang et al., 2020). However, whether baicalin can prevent or rescue the malformation of the neural crest-derived craniofacial skeleton under HG conditions remains elusive. Thus, this study focused on the beneficial effects of baicalin and its corresponding mechanism on challenging HG-induced damage to neural crest development using early chick embryos as an experimental model, which has been previously proven effective (Wang et al., 2015; Wang et al., 2018a).

Materials and methods

Meta-analysis

The meta-analysis was carried out using Stata version 13.1 (Stata Corp, College Station, TX, United States). The literature search was performed by querying PubMed, Embase, Cochrane Library and Web of Science for studies up to 1 January 2022, and the scientific question focused on the association between craniofacial anomalies and maternal diabetes. The flowchart of the search process is shown in Figure 1A. The inclusion criteria were as follows (Osório et al., 2004): articles reporting information on the association between gestational diabetes and craniofacial anomalies (Colas and Schoenwolf, 2001); articles in English or another European language; and (Copp et al., 2003) study design: cross-sectional studies, case–control studies, epidemiologic studies, population-based studies, observational studies, clinical trials or cohort studies. The articles were excluded if they (Osório et al., 2004) did not investigate the aims of the study (Colas and Schoenwolf, 2001); did not provide an explicit definition of gestational diabetes (Copp et al., 2003); lacked cranial and facial bone defect definitions; or (Mitchell, 2005) did not report original data (e.g., editorial, review or congress abstract).

A summary of the studies included in the meta-analysis is reported in Supplementary Table S1. For the risk of bias assessment, the quality of the studies was evaluated independently by the two assessors via the qualitative evaluation of observational studies, i.e., Newcastle Ottawa Scale (NOS). The Newcastle Ottawa Scale is shown in Supplementary Tables S2, S3. Any disagreement in quality assessment was resolved through consensus. Studies scoring >7 were considered at low risk of bias, scores between 5 and 7 indicated a moderate risk of bias, and scores below 5 indicated a high risk of bias. Heterogeneity among studies was assessed by using the Q and I^2 statistics. For the Q statistic, statistical significance was set at $p < 0.1$. Publication bias was evaluated using funnel plots and Egger's regression test, and the results are shown in Supplementary Figures S1A, B. $p < 0.1$ was considered to indicate statistical significance.

Avian embryos and treatment

Fertilized chick eggs were obtained from the Avian Farm of the South China Agriculture University. The eggs were incubated until the chick embryos reached the desired developmental HH stage

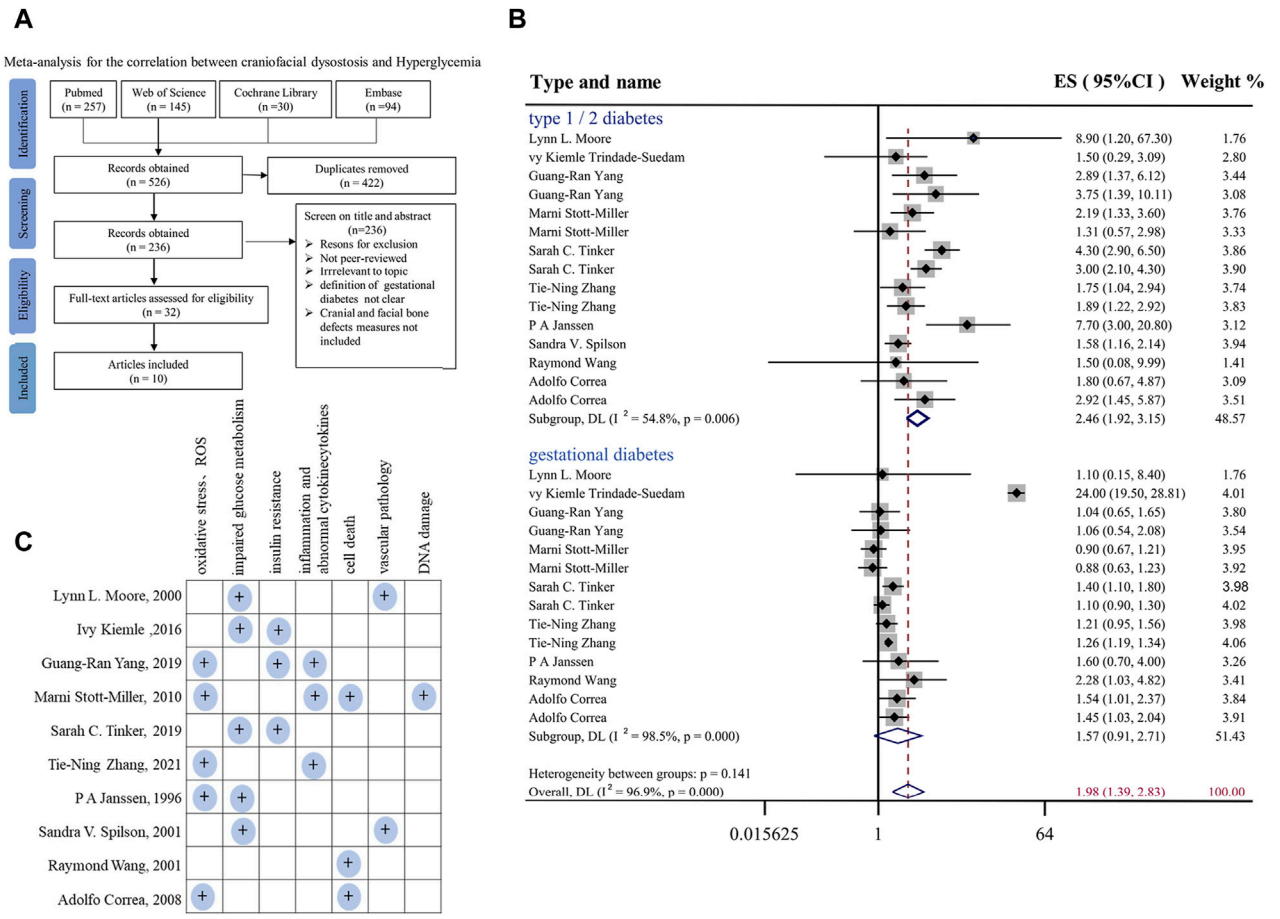

FIGURE 1
Meta-analysis for the correlation between hyperglycemia in pregnancy and craniofacial anomalies **(A)** Flow diagram of systematic literature search on hyperglycemia and craniofacial skeleton malformations. **(B)** Forest plot of effect sizes of studies examining the association of hyperglycemia in pregnancy and craniofacial anomalies included in the meta-analysis. Lowercase letters following the study year represent study arms within the same research. Effect size estimates (ES) are depicted by filled circles, with horizontal whiskers corresponding to 95% CIs. The length of the horizontal lines represents the 95% CIs for the effect size of hyperglycemia in pregnancy on craniofacial anomalies from each study. The weight of each study assigned to the meta-analysis expressed as a percentage is listed in the last column. The vertical solid line represents a mean difference of zero or no effect. I^2 is a measure of variation beyond chance among studies used in the meta-analysis. The hollow diamond indicates the overall mean effect size. **(C)** Summary and classification of potential mechanisms of craniofacial abnormalities caused by hyperglycemia during pregnancy mentioned in 10 included studies. Abbreviations: ES, effect size; CI, confidence interval.

(Hamburger and Hamilton, 1992) in a humidified incubator (Yiheng Instrument, Shanghai, China) at 38°C and 70% humidity. For the later stage chick embryos, 1.5-day preincubated chick embryos were exposed to either different concentrations of baicalin (Santa Cruz Biotechnology, Dallas, TX, United States), 50 mM glucose (Sigma, United States), or the same amount (approximately 200 μL) of 50 mM mannitol (osmotic control, Sigma, United States) through careful injection into windowed eggs *in vivo* (Figure 2A). For early gastrula embryos, HH0 (Hamburger and Hamilton, 1992) chick embryos were prepared and incubated with 50 mM mannitol, 6 μM baicalin, or/and 50 mM glucose (Wang et al., 2015) using early chick culture (EC culture) (Figure 3A) (Chapman et al., 2001).

Alizarin red staining of whole embryos

The craniofacial skeleton was visualized in 12-day (E12) chick embryos by staining with alizarin red dye (Solarbio, Beijing, China). Briefly, the embryos were fixed in 95% ethanol for 3 days, after which the skin and viscera were carefully removed before they were postfixed in 95% ethanol for 1 day. The embryos were then treated with 0.5% KOH (Jinan University, Guangzhou, China) for 48 h and stained with 0.001% alizarin red dye for 3 days. Finally, the embryos were cleared in a graded series of glycerol (diluted with water), and the craniofacial skeleton was photographed using a stereomicroscope (Olympus MVX10, Japan).

Immunofluorescence staining

Chick embryos were harvested after a given incubation time and fixed in 4% PFA overnight at 4°C. Immunofluorescence staining was performed on either whole-mount embryos or transverse sections using the following antibodies: Pax7 (1:200, DSHB, United States), E-cadherin (1:200, DSHB, United States), N-cadherin (1:200, DSHB, United States), and Cadherin6B (1:100, DSHB, United States), and HNK-1 (1:400, Sigma, United States). Briefly, the fixed embryos or transverse sections

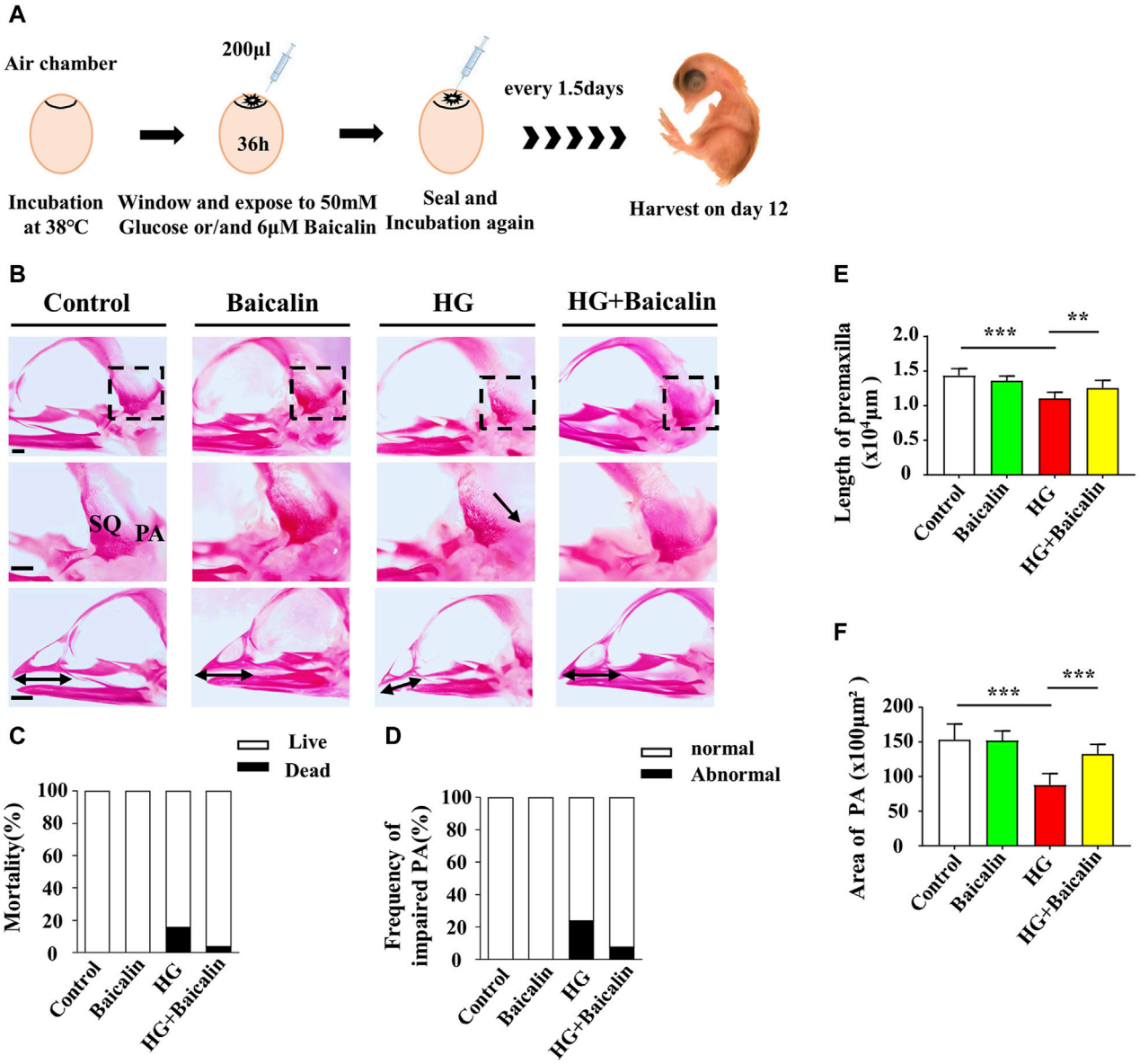

FIGURE 2
Assessing the development of the skulls of chicken embryos exposed to HG and/or baicalin **(A)** A schematic illustration showing that chicken embryos (preincubated for 1.5 days) were injected with an equal volume of mannitol (control, 50 mM HG, or/and 6 μM baicalin) every 3 days and then incubated at day 12. **(B)** Representative skull images of alizarin red-stained chicken embryos from the control, Baicalin, HG, and HG + Baicalin groups. **(C)** Bar charts showing the comparisons of the mortality of 12-day chick embryos among the control, Baicalin, HG, HG + Baicalin groups. **(D–F)** Comparisons of the frequency of PA defects **(D)**, length of the premaxilla **(E)** and area of the PA **(F)** in chicken embryos from the control, Baicalin, HG, and HG + Baicalin groups. Abbreviations: HG, high glucose; SQ, squamosal bone; PA, parietal bone. Scale bars = 1 mm in **(B)**.

were then incubated with these primary antibodies at 4°C overnight on a shaker. Following extensive washing, the embryos were incubated with an anti-rabbit IgG conjugated to Alexa Fluor 488 or Alexa Fluor 555 overnight at 4°C on a rocker. All the samples were later counterstained with DAPI (1:1000, Invitrogen, United States) at room temperature for 1 h.

In situ hybridization

Whole-mount *in situ* hybridization of chick embryos was performed according to a standard *in situ* hybridization protocol (Henrique et al., 1995). Digoxigenin-labeled probes were synthesized against Slug, Msx1, FoxD3, and FGF8 (Li et al., 2022). The stained whole-mount chick embryos were photographed by a stereomicroscope (Olympus MVX10, Tokyo, Japan) and then prepared for cryosectioning at a thickness of 16 μm on a cryostat microtome (Leica CM 1900).

RNA isolation and quantitative PCR

Total RNA was extracted from chick embryos using a TRIzol kit (Invitrogen, United States). PCR amplification of the cDNA was

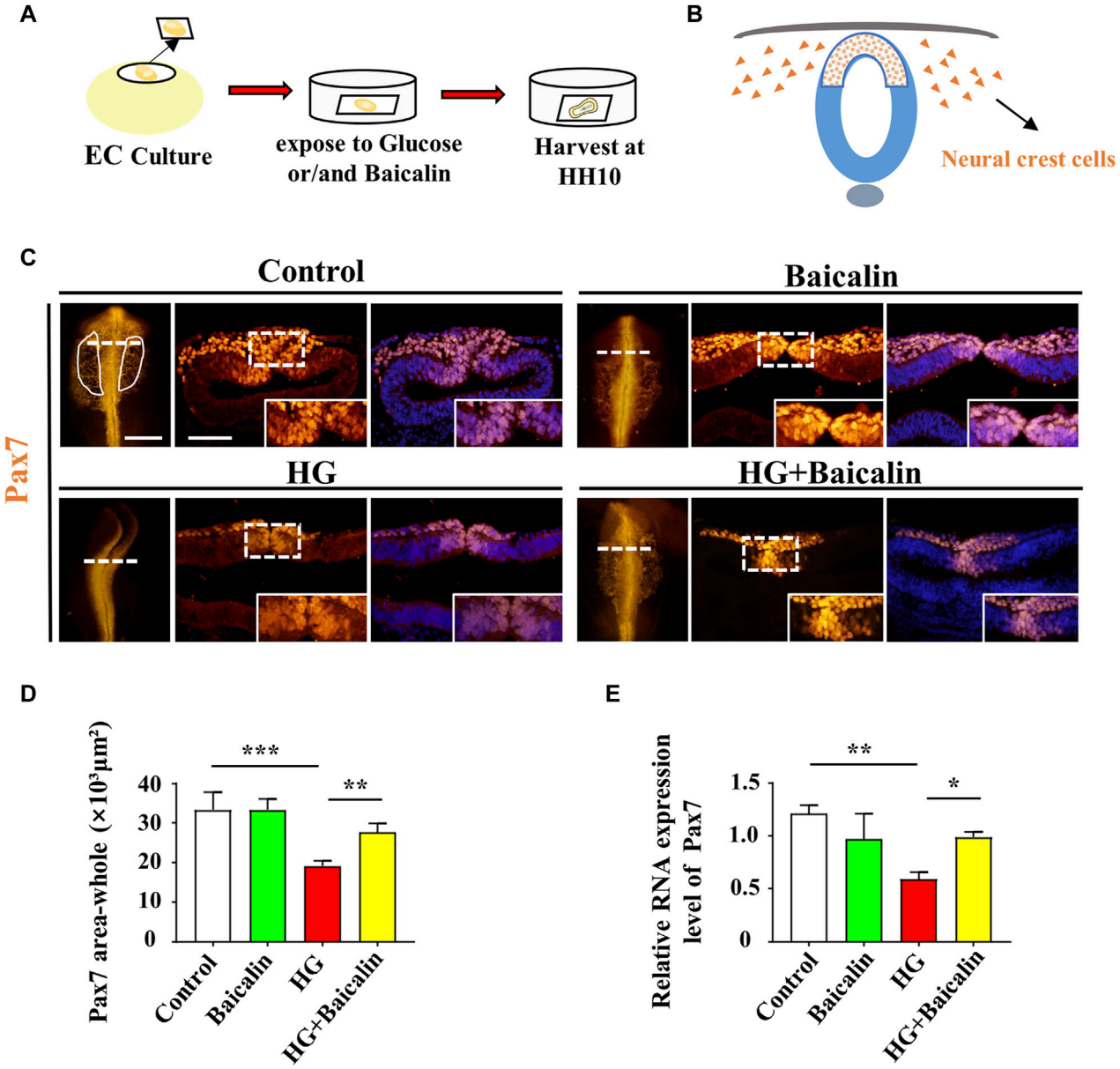

FIGURE 3
Assessing Pax7-labeled NCCs delaminated from chicken embryos exposed to HG and/or baicalin **(A)** A schematic illustration showing that gastrula chicken embryos were incubated with HG and/or baicalin from HH0 to HH10 in EC culture. **(B)** A schematic of the distribution of early NCCs on the neural tube. **(C)** Representative images of the cranial region of whole-mount Pax7 immunofluorescence, as well as the corresponding cross-sections at the levels indicated by dotted lines from the control, Baicalin, HG, and HG + Baicalin groups. **(D)** Comparisons of Pax7^{+} areas in whole-mount cranial regions of chick embryos from the control, Baicalin, HG, and HG + Baicalin groups. **(E)** Quantitative PCR data showing the mRNA expression of Pax7 in chicken embryos from the control, Baicalin, HG, and HG + Baicalin groups. Abbreviations: HG, high glucose. Scale bars = 200 μm in whole-mount; 100 μm in cross-section of **(C)**.

implemented using the corresponding specific primers (note: the sequences are provided in Supplementary Table S4). The PCRs were implemented in a Bio-Rad S1000TM Thermal cycler (Bio-Rad, United States).

Drug-target interaction prediction

For target prediction, the SMILES of baicalin from PubChem (https://pubchem.ncbi.nlm.nih.gov/) was employed to visualize the structure and predict the target on the Swiss Target Prediction website (http://www.swisstargetprediction.ch/).

Protein-protein interaction (PPI) network analysis

STRING (Search Tool for the Retrieval of Interacting Genes/Proteins, https://string-db.org) was used for protein-protein interaction (PPI) network analysis.

Molecular docking

The crystal structure of AKR1B1 (PDB: 1AZ1) was downloaded from the RSCB protein data bank (PDB) (http://www.rcsb.org/). Before molecular docking, open-source PyMOL (https://pymol.org) was employed to remove nonstandard amino acids, crystal water, and impurity chains from the initial structure of AKR1B1 and then hydrogenate and recalculate the charge. AutoDock Tools (ADT, version 4.2.6) was used to convert the protein into the PDBQT format. The structure of Baicalin (Molecule ID: MOL002776) was obtained from TCMSP and converted into mol2 format. Then, molecular docking studies were performed using AutoDock-Vina 1.1.2-. PyMOL 2.3.0 and Discovery Studio 2016 Client were used to visualize the best conformations and analyze the molecular interactions.

Cell culture and cellular thermal shift assay (CETSA)

The SH-Y5Y cell line (human neuroblastoma cells) was cultured in high glucose DMEM (Gibco, United States, 4.5 g/mL glucose), which contained 10% FBS (fetal bovine serum, ExCell, Shanghai, China) and 1% P/S (double antibody: penicillin 100 U/mL + streptomycin 100 μg/mL, Gibco, United States). Then, the flask was placed in an incubator at 37°C and 5% CO2. The cells were cultured *in vitro* and divided into two groups (control and baicalin). After baicalin treatment, the cells were lysed, supernatant was removed after centrifugation for gradient heating, and the proteins were denatured and precipitated by heating and removed by centrifugation. Western blotting was used to detect and quantify AKR1B1, and expression curves were drawn.

Western blot

The proteins were isolated from the cells via homogenates using a radio-immuno-precipitation assay (RIPA, Sigma, MO, United States). Western blotting was implemented based on the standard procedure as previously described (Wang et al., 2018b). Primary antibodies were used to detect the expression of AKR1B1 (1:1500, Proteintech, 15439-1-AP, Wuhan Sanying). The loading control was a β-actin antibody (1:1000, Abcam, ab32572, New Territories, HK). After incubation with secondary antibodies (HRP-conjugated goat anti-rabbit IgG 1:4000, EarthOx, 7074S, Millbrae, United States), the samples were developed with SuperSignalTM West Femto Chemiluminescent Substrate (ThermoFisher, Rockford, United States) and the Gel Doc™ XR + System (Bio-Rad, CA, United States).

Data analysis

The various markers' positive cell rates and relative mRNA expressions in the different experimental samples were analyzed using Image Pro-Plus 5.0 software (He et al., 2014). Statistical analysis was performed using the SPSS 13.0 statistical package program for Windows. The data are presented as the mean ± SE. Statistical significance was assessed by one-way ANOVA and Tukey's multiple comparisons test. $p < 0.05$ was considered to be statistically significant.

Results

Meta-analysis revealed the correlation between hyperglycemia in pregnancy and craniofacial malformation

First, to systemically assess the correlation between hyperglycemia in pregnancy and craniofacial malformation, we employed a meta-analysis (Gurevitch et al., 2018) at the four typical steps (identification, screening, eligibility, and inclusion) on the literature available in PubMed, Embase, Cochrane Library and Web of Science databases (Figure 1A). In the final included studies (Janssen et al., 1996; Moore et al., 2000; Åberg et al., 2001; Stott-Miller et al., 2010; Balsells et al., 2012; Trindade-Suedam et al., 2016; Yang et al., 2019; Tinker et al., 2020; Maniglio et al., 2022; Zhang et al., 2022), we selected all types of deformities involved in the development of head and facial bones, such as orofacial clefts, cleft lip and/or palate, and positional plagiocephaly. In the context of type I or II or gestational diabetes (Figure 1B). In the context of hyperglycemia in pregnancy, the effect size (ES) at the risk of fetal craniofacial abnormalities was 1.98 [95% confidence interval (CI): 1.39, 2.83] (Figure 1B). Publication bias was evaluated using funnel plots and Egger's regression test, and the results are shown in Supplementary Figure S1. Taken together, the results of the meta-analysis demonstrated that there are almost certainly associations between diabetes in pregnancy and craniofacial abnormalities, as shown here, but it is simultaneously suggested that there is still a lack of an effective therapeutic approach, which is at least partially due to the underlying biological mechanisms having not yet been completely elucidated. Therefore, we summarized and classified various potential mechanisms of craniofacial abnormalities caused by hyperglycemia during pregnancy mentioned in the 10 included studies, including impaired oxidative stress and glucose tolerance, as shown in Figure 1C.

Baicalin demonstrated its capacity to reverse the craniofacial malformation induced by high glucose

Our previous study not only revealed the antioxidant effects of baicalin but also confirmed its protective effect on embryonic development in a hyperglycemic environment (Wang et al., 2018a; Wang et al., 2020). To assess the impact of baicalin on countering craniofacial malformation induced by high glucose during pregnancy, we exposed chicken embryos to HG or HG + baicalin before harvesting them at 12 days of incubation (Figure 2A). Alizarin red staining was performed on chicken embryos treated with HG and/or baicalin, and then the skulls from the control, baicalin, HG, and HG + baicalin groups were photographed (Figure 2B). The results showed that HG increased the mortality of chick embryos and frequency of parietal bone (PA) defects, and additional application of baicalin reversed this tendency

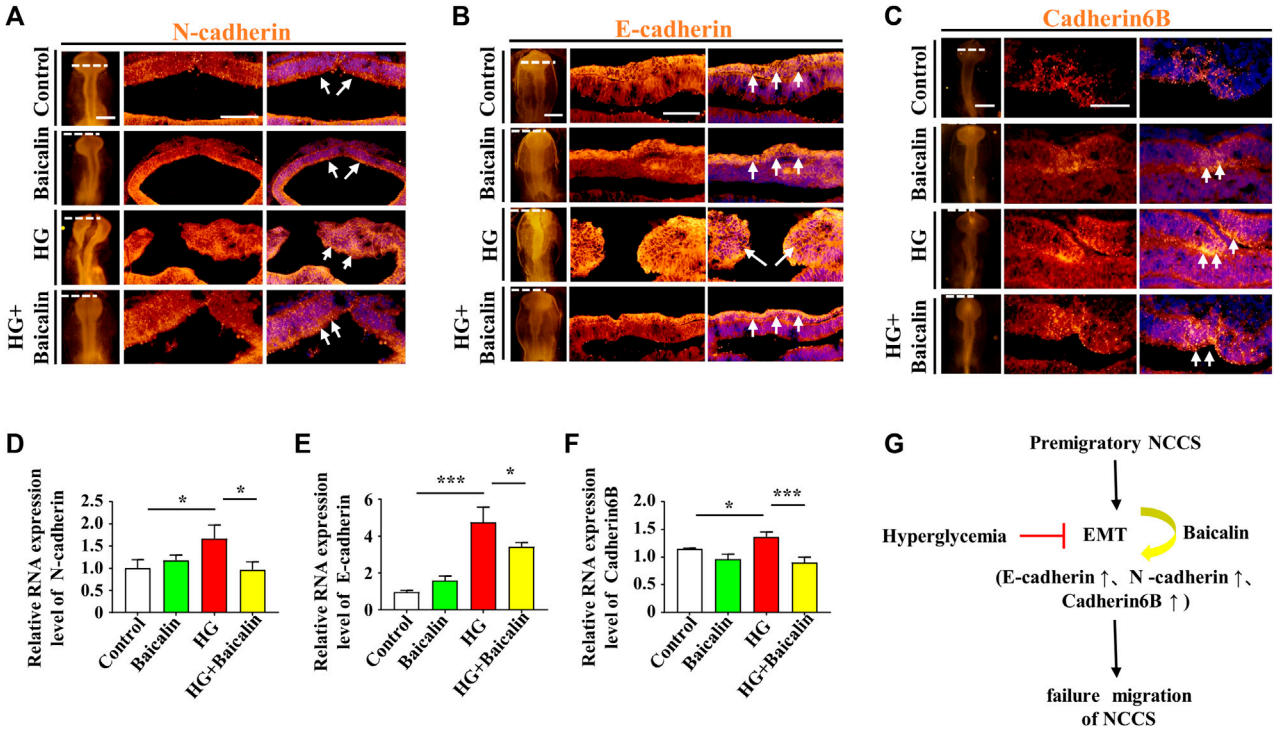

FIGURE 4
Assessing the expression of E-cadherin, N-cadherin, and cadherin 6B in the cranial regions of chicken embryos exposed to HG and/or baicalin **(A–C)** Representative images of the cranial region of whole-mount immunofluorescence of N-cadherin **(A)**, E-cadherin **(B)** and cadherin 6B **(C)**, as well as the corresponding cross-sections at the levels indicated by dotted lines from the control, Baicalin, HG, and HG + Baicalin groups. **(D–F)** Quantitative PCR data showing the mRNA expression of N-cadherin **(D)**, E-cadherin **(E)** and cadherin 6B **(F)** in chicken embryos from the control, Baicalin, HG, and HG + Baicalin groups. **(G)** The diagram indicates that baicalin rescues the early EMT process inhibited by a HG environment. Abbreviations: HG, high glucose. Scale bars = 200 μm in whole mounts of **(A–C)**; 100 μm in cross-sections of **(A–C)**.

(Figures 2C, D). The corresponding quantitative analysis showed that HG treatment significantly reduced the length of the premaxilla and area of the parietal bone (PA), but these effects were reversed by baicalin treatment (Figures 2E, F). This suggested that baicalin administration was indeed able to efficiently rescue the craniofacial malformation induced by high glucose concentrations during pregnancy.

Baicalin administration reversed HG-inhibited delamination of cranial NCCs on the dorsal side of the developing neural tube

To examine whether the aforementioned craniofacial malformation phenotype occurred in the early stage of neural crest development, we exposed gastrula chicken embryos to HG (50 mM) and/or baicalin (6 μM) in EC culture and then evaluated neural crest delamination after 42 h of incubation (Figure 3A). Whole-mount Pax7 immunofluorescence staining showed that baicalin did not only affect Pax7-labeled NCC delamination compared to the control, but it could significantly reverse the HG-induced reduction in Pax-7-labeled NCC delamination (Figures 3C, D), which was verified by quantitative PCR data (Figure 3E).

Loss of expression of EMT-related adhesion molecules is indispensable for EMT in NCC delamination (Gheldof and Berx, 2013). Whole-mount immunofluorescence staining against adhesion molecules, including N-cadherin, E-cadherin, and Cadherin 6B, was subsequently carried out (Figures 4A–C), and the results showed that the addition of baicalin could reverse the HG-increased expression of N-cadherin, which was confirmed by quantitative PCR data (Figure 4D), as well as E-cadherin and Cadherin 6B (Figures 4E, F). To examine whether the expression of EMT-related transcription factors (Duband et al., 1995) was affected, we implemented whole-mount *in situ* hybridization against Slug and Mxs1 in embryos exposed to HG or/and baicalin (Figures 5A, B). Baicalin significantly reversed the inhibition of HG-inhibited Slug (Figure 5C) and Msx1 (Figure 5E) expression on the dorsal side of neural tubes. The quantitative PCR data were generally the same as those from *in situ* hybridization (Figures 5D, F). This implied that baicalin could successfully rescue HG-inhibited NCC delamination by regulating the expression of EMT-related transcription factors and adhesion molecules.

Baicalin administration reversed HG-inhibited migration of cranial NCCs in cranial neural crest development

To determine whether the migration of NCCs in cranial neural crest development was affected, we implemented whole-

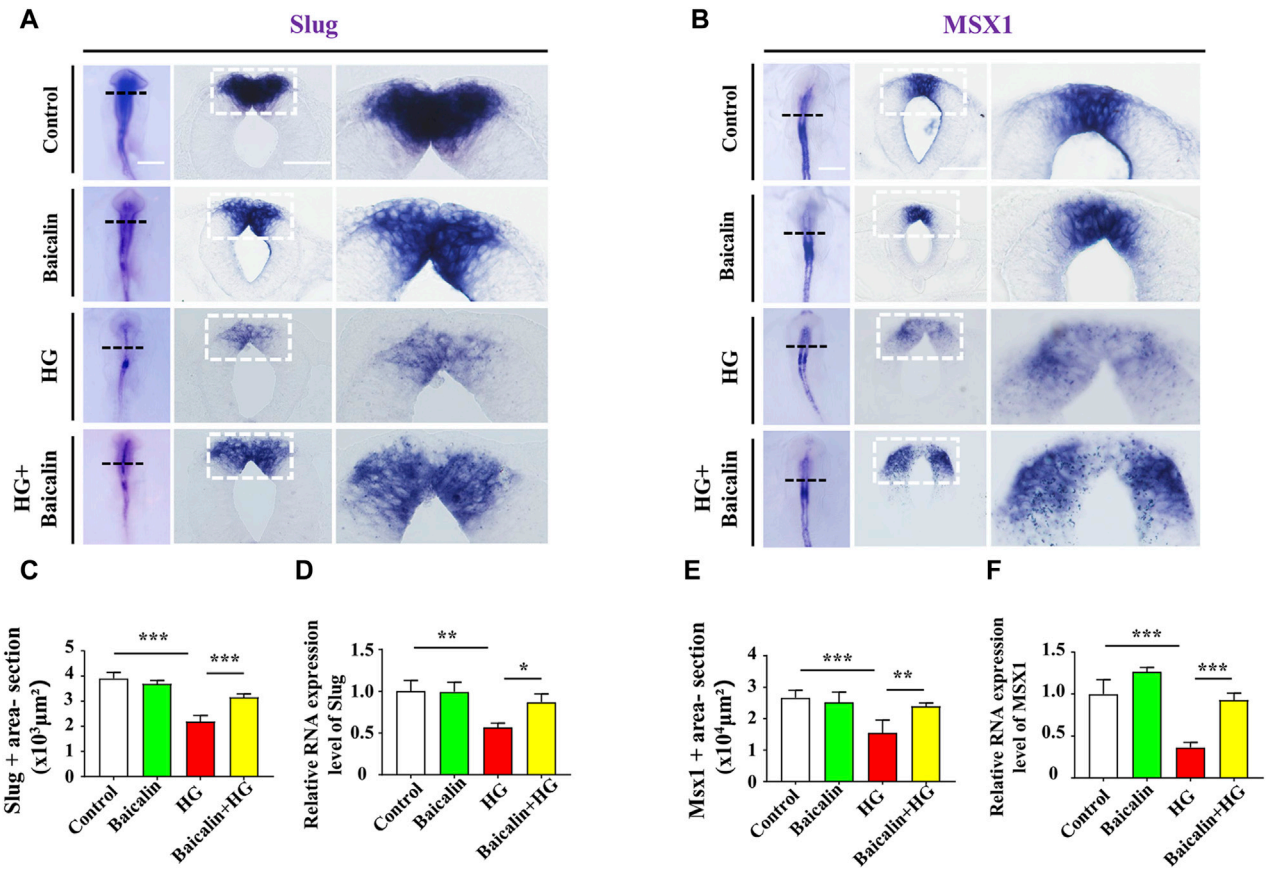

FIGURE 5
Assessing the expression of Slug and Msx1 in the cranial regions of chicken embryos exposed to HG and/or baicalin **(A)** Representative images of the cranial region of whole-mount Slug *in situ* hybridization, as well as the corresponding cross-sections at the levels indicated by dotted squares from the control, Baicalin, HG, and HG + Baicalin groups. **(B)** Representative images of the cranial region of whole-mount Msx1 *in situ* hybridization, as well as the corresponding cross-sections at the levels indicated by dotted squares from the control, Baicalin, HG, and HG + Baicalin groups. **(C)** Bar chart showing the comparisons of $Slug^+$ areas in the cranial regions of chicken embryos from the control, Baicalin, HG, and HG + Baicalin groups. **(D)** Quantitative PCR data showing the mRNA expression of Slug in chicken embryos from the control, Baicalin, HG, and HG + Baicalin groups. **(E)** Bar chart showing the comparisons of $Msx1^+$ areas in the cranial regions of chicken embryos from the control, Baicalin, HG, and HG + Baicalin groups. **(F)** Quantitative PCR data showing the mRNA expression of Msx1 in chicken embryos from the control, Baicalin, HG, and HG + Baicalin groups. Abbreviations: HG, high glucose. Scale bars = 200 μm in whole mounts of **(A,B)**; 100 μm in cross-sections of **(A,B)**.

mount immunofluorescence staining against HNK-1 (Bronner-Fraser, 1986) on chicken embryos treated with HG and/or baicalin. The results clearly indicated that combinational application of baicalin could resume HG-inhibited HNK-1-labeled NCC migration at both the whole-mount and section levels (Figures 6A–C).

Foxd3 and FGF8 are required for NCC migration (Stewart et al., 2006; Sato et al., 2011), so we carried out Foxd3 immunofluorescence staining after whole-mount Foxd3 *in situ* hybridization (Figure 7A; Supplementary Figure S2A). The combinational application of baicalin significantly reversed the HG-inhibited Foxd3 expression on the dorsal side of the neural tubes (Figure 7B), which was verified by subsequent quantitative PCR data (Figure 7C). However, in contrast to Foxd3 expression, the additional application of baicalin did not rescue HG-inhibited FGF8 expression (Supplementary Figure S2B). This suggests that baicalin administration could rescue HG-inhibited NCC migration through the involvement of Foxd3 gene expression regulation.

Baicalin may modulate NCC development by specifically binding to AKR1B1

To identify the potential targets of baicalin, we drew the chemical structure of baicalin (Figure 8A) and predicted its target proteins based on the Stitch website and Swiss Target Prediction (Figures 8B–D), which indicated that 28% of the top 15 targets were associated with the enzyme class. The potential target genes and proteins were enriched and analyzed for different biological pathways (Figure 8E), in which EGFR, PDGF, insulin pathways, TGF-beta, biological oxidations and cell adherins were involved. The most strongly correlated gene was AKR1B1 (Figure 8D). We performed a molecular docking analysis of baicalin and AKR1B1, and the results showed that the binding energy for baicalin and AKR1B1 was −8.4 kcal/mol. The three-dimensional diagram showed that baicalin bound to amino acid residues in the AKR1B1 pocket, where baicalin formed hydrogen bonds with Gln47, pi-sulfur with Tyr45 and an attractive charge with Asp102 (Figure 8F). To confirm the potential link between AKR1B1 and

10.3389/fphar.2024.1295356

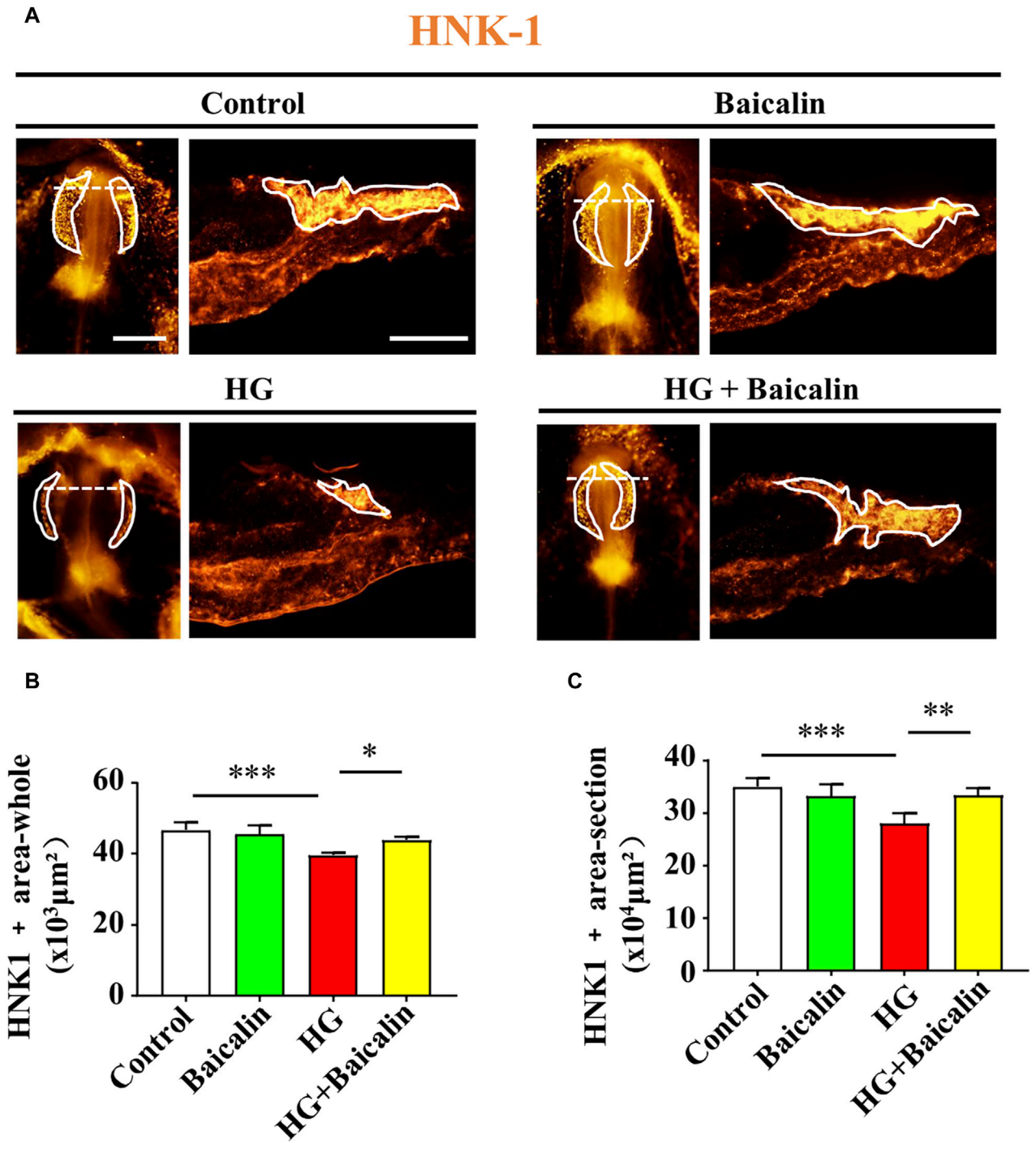

FIGURE 6
Assessing HNK-1-labeled migratory NCCs from chicken embryos exposed to HG and/or baicalin **(A)** Representative images of the cranial region of whole-mount HNK-1 immunofluorescence, as well as the corresponding cross-sections at the levels indicated by dotted lines from the control, Baicalin, HG, and HG + Baicalin groups. **(B,C)** Bar chart showing the comparisons of HNK-1^{+} areas in whole-mount **(B)** and histological sections **(C)** of chicken embryos from the control, Baicalin, HG, and HG + Baicalin groups. Scale bars = 200 μm in whole mount of **(A)**; 100 μm in cross-section of **(A)**.

NCC development, bioinformatics analysis was employed to construct a protein–protein interaction network. The results indicated that AKR1B1 may affect NCC-related genes through EGFR signaling. (Figure 8G). Finally, the direct binding of baicalin to AKR1B1 was further confirmed by an *in vitro* cellular thermal shift assay. With increasing temperature, the expression level of AKR1B1 in cells treated with baicalin was greater than that in the control (DMSO), especially at 54°C. AKR1B1 was verified to be the target of baicalin and to play a protective role intracellularly (Figures 9A–C).

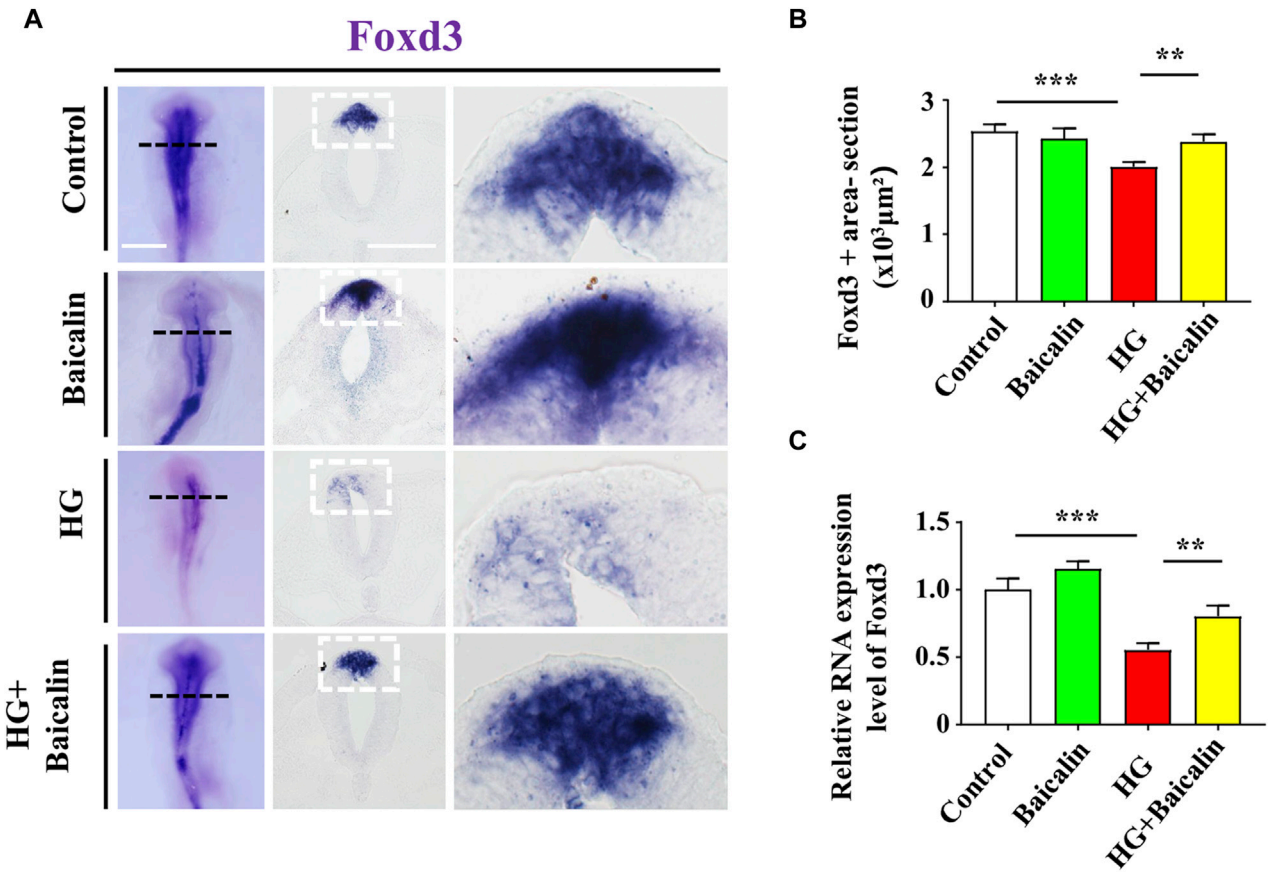

FIGURE 7
Assessing the expression of Foxd3 in the cranial regions of chicken embryos exposed to HG and/or baicalin **(A)** Representative images of the cranial region of whole-mount Foxd3 *in situ* hybridization, as well as the corresponding cross-sections at the levels indicated by dotted squares from the control, Baicalin, HG, and HG + Baicalin groups. **(B)** Bar chart showing the comparisons of Foxd3^{+} areas in the cranial regions of chicken embryos from the control, Baicalin, HG, and HG + Baicalin groups. **(C)** Quantitative PCR data showing the mRNA expression of Foxd3 in chicken embryos from the control, Baicalin, HG, and HG + Baicalin groups. Scale bars = 200 μm in whole mount of **(A)**; 50 μm in cross-sections of **(A)**.

Discussion

Growing evidence has shown that overt diabetes mellitus during pregnancy is closely associated with a dramatically increased risk of various perinatal disorders in nervous, cardiovascular and musculoskeletal system defects (Moore et al., 2000). In this study, we focused on craniofacial malformation in the presence of hyperglycemia in pregnancy, so a meta-analysis was first employed to comprehensively and systemically review the results of all previous studies in this area. From the view of the meta-analysis results, we could see that both preexisting diabetes before pregnancy and gestational diabetes could increase the risk of various craniofacial malformations but that this risk was worse in patients with preexisting diabetes than in those with gestational diabetes (Figure 1B). This definitely tamped down the previous observation that the exposure to hyperglycemia in pregnancy would adversely impact craniofacial skeleton development, thereby raising the possibility of having congenital and postnatal diseases (Mussatto et al., 2015). Meanwhile, there is no doubt that this highlights an obvious need to seek new medications to prevent or confront the developmental defects induced by diabetes in pregnancy.

As we know, chickens have not gained widespread use as an animal model in diabetes research primarily due to their nonmammalian nature, with their genetic makeup being approximately 70% homologous to that of humans (King, 2012; Shi et al., 2014). Among vertebrates, chicken embryos are favored models in developmental biology. They are easily accessible, have a short incubation period, and exhibit phenotypes similar to mammalian developmental abnormalities in a hyperglycemic environment (Datar and Bhonde, 2005; Datar and Bhonde, 2011; Bozkurt et al., 2021). Therefore, we chose chicken embryos as the model to proceed for our study.

From the literature included in the meta-analysis, we found that there are various mechanisms of craniofacial malformation caused by hyperglycemia, such as oxidative stress and ROS (Figure 1C). Baicalin, an extract of traditional Chinese medicine, has been extensively used as a traditional medicine to reduce inflammation in many East Asian countries for a long time (Ishimaru et al., 1995). In addition to anti-inflammation, baicalin also exhibits many other pharmacological properties, such as anticancer and anti-pruritic effects (Li-Weber, 2009; Trinh et al., 2010), which inspired us to employ it in this study. Another important factor in its favor is that baicalin could go

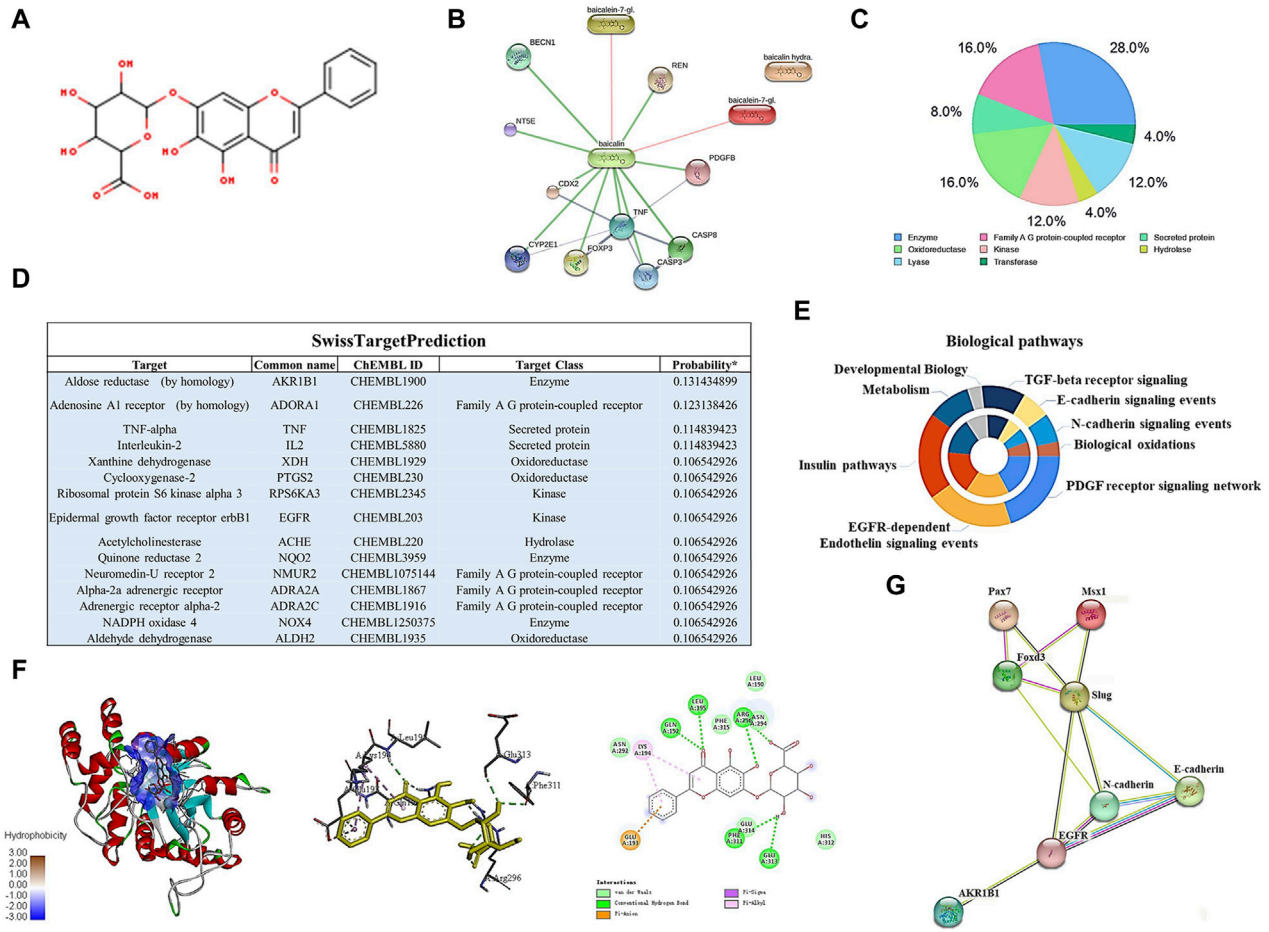

SwissTargetPrediction

Target	Common name	ChEMBL ID	Target Class	Probability*
Aldose reductase (by homology)	AKR1B1	CHEMBL1900	Enzyme	0.131434899
Adenosine A1 receptor (by homology)	ADORA1	CHEMBL226	Family A G protein-coupled receptor	0.123138426
TNF-alpha	TNF	CHEMBL1825	Secreted protein	0.114839423
Interleukin-2	IL2	CHEMBL5880	Secreted protein	0.114839423
Xanthine dehydrogenase	XDH	CHEMBL1929	Oxidoreductase	0.106542926
Cyclooxygenase-2	PTGS2	CHEMBL230	Oxidoreductase	0.106542926
Ribosomal protein S6 kinase alpha 3	RPS6KA3	CHEMBL2345	Kinase	0.106542926
Epidermal growth factor receptor erbB1	EGFR	CHEMBL203	Kinase	0.106542926
Acetylcholinesterase	ACHE	CHEMBL220	Hydrolase	0.106542926
Quinone reductase 2	NQO2	CHEMBL3959	Enzyme	0.106542926
Neuromedin-U receptor 2	NMUR2	CHEMBL1075144	Family A G protein-coupled receptor	0.106542926
Alpha-2a adrenergic receptor	ADRA2A	CHEMBL1867	Family A G protein-coupled receptor	0.106542926
Adrenergic receptor alpha-2	ADRA2C	CHEMBL1916	Family A G protein-coupled receptor	0.106542926
NADPH oxidase 4	NOX4	CHEMBL1250375	Enzyme	0.106542926
Aldehyde dehydrogenase	ALDH2	CHEMBL1935	Oxidoreductase	0.106542926

FIGURE 8
Bioinformatics analysis and target gene prediction of baicalin. **(A)** The two-dimensional structure of baicalin according to SwissTargetPrediction. **(B)** Prediction of the potential target protein of baicalin by using the Stitch website. **(C)** Pie chart shows the categories of baicalin-regulated targets based on SwissTargetPrediction. **(D)** The table shows the information about the predicted most likely targets for baicalin. **(E)** The enrichment and anlysis of potential target genes and proteins of baicalin from **(B,D)** for different biological pathways. **(F)** The proposed three- and two-dimensional binding models of the interaction between baicalin and AKR1B1 derived from Open-Source PyMOL and Discovery Studio 2016 Client software. In the three-dimensional interaction, baicalin is presented by carton, AKR1B1 is presented by ball-stick, and the binding residues are presented by sticks. **(G)** PPI analysis of AKR1B1 and NCC-related genes in this study using the Stitch website.

through the placental barrier at different gestational stages after being absorbed in the maternal intestine and entering maternal circulation (Song et al., 2010). Most of the abovementioned effects of baicalin result from its antioxidative and anti-inflammatory effects through upregulating antioxidant enzymes and suppressing NF-κB signaling pathways (Wu et al., 2018). Thus, baicalin is ideal for use in confronting diabetes in pregnancy since diabetes mellitus is regarded as an inflammatory disorder (Tsalamandris et al., 2019). Regarding the potential embryotoxicity of baicalin, our previous study showed that 6 μM baicalin itself did not have a significantly negative influence on embryo development (Wang et al., 2020). After deliberate choice (i.e., baicalin as the chosen compound) and exclusion of embryotoxicity, we first evaluated the effect of 6 μM baicalin on developing chicken embryos by observing the effect of the combined application of HG and baicalin on craniofacial skeleton development, and this *in vivo* experiment clearly showed that baicalin administration could successfully rescue high glucose-induced craniofacial skeleton malformation (Figure 2).

Embryos at an early stage of development are extremely vulnerable to environmentally harmful influences since their own immune system has not yet been well established (Hamdoun and Epel, 2007). Craniofacial bone is principally derived from the cranial neural crest at the early stage of embryo development, so we naturally started our study based on the spatiotemporal development of the neural crest at the initial stage, i.e., NCC delamination, EMT, migration, and differentiation, using a gastrula chicken embryo model. To determine the delamination of NCCs, we employed Pax7 as a marker for premigratory NCC generation (Basch et al., 2006) in gastrula chicken embryos exposed to HG or/and baicalin, mannitol was used as an osmotic control due to the HG. The results unmistakably demonstrated that baicalin administration indeed significantly rescued high glucose-restricted NCC production (Figure 3). In subsequent experiments to decipher the underlying mechanism, we found that baicalin could downregulate the HG-increased expression of adhesion molecules (N-cadherin, E-cadherin and cadherin 6B) in cranial neural tubes (Figure 4), indicating that the high glucose-restricted EMT process

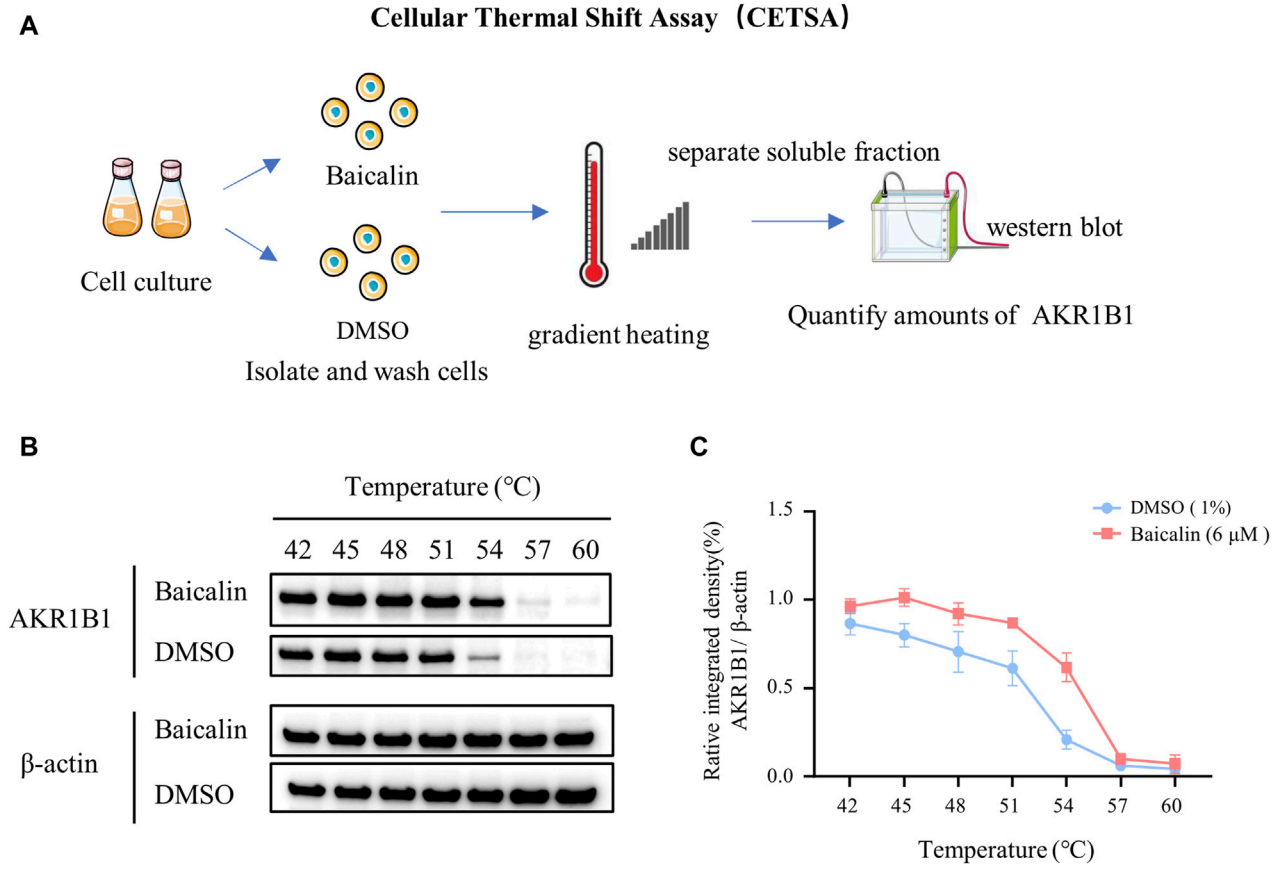

FIGURE 9
In vitro validation—cellular thermal shift assay. **(A)** A schematic illustration showing the process of cell culture *in vitro* and the cellular thermal shift assay. **(B)** Western blot data showing AKR1B1 expressions at the protein level in cells treated with baicalin or DMSO (control). **(C)** The curves quantified the changes in the expression of AKR1B1 with the increase of temperature.

and NCC delamination were lifted by baicalin administration. It is widely known that EMT is intensely associated with a reduction in cell–cell adhesion, i.e., the expression of these adhesion molecules must be downregulated, which is controlled by some EMT-related transcription factors, such as the zinc finger gene Slug (Duband et al., 1995). Likewise, we observed that the HG-suppressed expression of Slug and Msx1 on the dorsal side of neural tubes bounced back after baicalin administration (Figure 5), implying that baicalin administration is conducive to restoring the expression of these key EMT-related transcription factors, thereby promoting the process of neural crest EMT and delamination. After NCC delamination, NCCs migrate long distances to populate various peripheral sites. Immunofluorescence staining of HNK-1 was utilized to identify the influence of migratory NCCs by baicalin administration, and the results showed that the HG-inhibited HNK-1-labeled NCC migration was significantly rescued by baicalin administration (Figure 6). Therefore, what is the expression of genes controlling NCC migration in this scenario? For this purpose, we detected the expression of Foxd3 and FGF8 (Thomas and Erickson, 2009) in chicken embryos exposed to HG and/or baicalin, and the results showed that HG-inhibited Foxd3 expression increased again following baicalin administration (Figure 7), suggesting gene expression evidence underlying NCC migration improvement.

Finally, to further explore the mechanism of baicalin, we used the molecular informatics website to predict the potential target genes and proteins of baicalin and carried out enrichment analysis of these genes in biological pathways. The gene with the highest correlation was AKR1B1, which has been associated with multiple complications of diabetes and plays a role in ROS production and promoting EMT (Wu et al., 2017; Wu et al., 2020). We used molecular docking software to simulate docking with baicalin molecules and obtained ideal results. Molecular docking simulations also showed ideal results for the interaction between baicalin and AKR1B1. Therefore, we hypothesize that baicalin may target AKR1B1 to rescue craniofacial malformations in hyperglycemic pregnancy. However, AKR1B1 may influence the key genes involved in the epithelial-mesenchymal transition (EMT) process of neural crest cells through EGFR signaling (Zhang et al., 2021), a crucial pathway in NCC development (Gassmann et al., 1995; Golding et al., 2000). Additionally, Wu et al. (2020) suggested that the overexpression of AKR1B1 could suppress AMPK activation, thus promoting the EMT process in lens epithelial cells during diabetic cataract formation.

In recent years, the cell heat transfer assay (CETSA) has become widely used in drug discovery workflows. CETSA based on Western blot is mainly used to verify the target binding of a molecule to its target protein (Tolvanen, 2022). Therefore, we performed a CETSA of baicalin and AKR1B1 in our final research. Surprisingly, the thermal stability of AKR1B1 in cells treated with baicalin was significantly greater than that

in the control (DMSO), which was manifested as an increase in AKR1B1 expression, further confirming our speculation that baicalin can play a protective role in cells by targeting on AKR1B1 (Figure 9).

In summary, baicalin was chosen to confront high glucose condition was firstly verified in skull formation by exposing chicken embryos to the combined application of HG and baicalin. Based on the events in NCC development, baicalin administration was found to reverse HG-inhibited NCC delamination and EMT, as well as the expression of corresponding adhesion molecules and key EMT-related transcription factors. Additionally, HG-restricted NCC migration was significantly rescued by baicalin administration. Molecular docking and cell heat transfer assay revealed the possible target gene AKR1B1 of baicalin in confronting the craniofacial skeleton malformation caused by high glucose. The study suggests that baicalin's significant effect on confronting hyperglycemia-induced craniofacial skeleton malformation occurs mainly at the early stage of NCC development, although more comprehensive studies are needed to reveal the precise mechanism.

Data availability statement

The datasets presented in this study can be found in online repositories. The names of the repository/repositories and accession number(s) can be found in the article/Supplementary Material.

Ethics statement

The animal study was approved by the Committee for Animal Experimentation at Jinan University. The study was conducted in accordance with the local legislation and institutional requirements.

Author contributions

J-QL: Writing–original draft, Formal Analysis, Data curation, Writing–review and editing. Z-YL: Project administration, Writing–review and editing, Data curation. CS: Software, Investigation, Writing–review and editing, Data curation. S-MW: Methodology, Formal Analysis, Writing–review and editing, Investigation. DS: Writing–review and editing. R-JH: Visualization, Formal Analysis, Writing–review and editing. XY: Writing–review and editing. YD: Visualization, Formal Analysis, Writing–review and editing. GW: Methodology, Funding acquisition, Writing–review and editing.

Funding

The author(s) declare financial support was received for the research, authorship, and/or publication of this article. This study was supported by the National Natural Science Foundation of China (grant numbers 32170825 and 31971108); the Science and Technology Program of Guangzhou (202201020007 and 202201020089); the Guangdong Basic and Applied Basic Research Foundation (grant number 2023A1515010424); and the Guangdong Bureau of Traditional Chinese Medicine research Program (grant number 20221112).

Acknowledgments

We would like to thank Medical experimental center in Jinan University.

Conflict of interest

The authors declare that the research was conducted in the absence of any commercial or financial relationships that could be construed as a potential conflict of interest.

The reviewer XL is currently organizing a Research Topic with the author GW.

The author(s) declared that they were an editorial board member of Frontiers, at the time of submission. This had no impact on the peer review process and the final decision.

Publisher's note

Supplementary material

The Supplementary Material for this article can be found online at: https://www.frontiersin.org/articles/10.3389/fphar.2024.1295356/full#supplementary-material

References

Abel, E. L. (1984). Prenatal effects of alcohol. *Drug alcohol dependence* 14 (1), 1–10. doi:10.1016/0376-8716(84)90012-7

Åberg, A., Westbom, L., and Källén, B. (2001). Congenital malformations among infants whose mothers had gestational diabetes or preexisting diabetes. *Early Hum. Dev.* 61 (2), 85–95. doi:10.1016/s0378-3782(00)00125-0

Achilleos, A., and Trainor, P. A. (2012). Neural crest stem cells: discovery, properties and potential for therapy. *Cell Res.* 22 (2), 288–304. doi:10.1038/cr.2012.11

Baek, J.-S., Hwang, C.-J., Jung, H.-W., Park, Y.-K., Kim, Y.-H., Kang, J.-S., et al. (2014). Comparative pharmacokinetics of a marker compound, baicalin in KOB extract after oral administration to normal and allergic-induced rats. *Drug Deliv.* 21 (6), 453–458. doi:10.3109/10717544.2013.876561

Balsells, M., García-Patterson, A., Gich, I., and Corcoy, R. (2012). Major congenital malformations in women with gestational diabetes mellitus: a systematic review and meta-analysis. *Diabetes/metabolism Res. Rev.* 28 (3), 252–257. doi:10.1002/dmrr.1304

Barembaum, M., and Bronner-Fraser, M. (2005). "Early steps in neural crest specification," in *Seminars in cell & developmental biology* (Elsevier), 642–646.

Basch, M. L., Bronner-Fraser, M., and García-Castro, M. I. (2006). Specification of the neural crest occurs during gastrulation and requires Pax7. *Nature* 441 (7090), 218–222. doi:10.1038/nature04684

Bozkurt, E., Atay, E., Bilir, A., Ertekin, A., Buğra Koca, H., and Cem Sabaner, M. (2021). A novel model of early type 1 diabetes mellitus: the chick embryo air sack model. *Saudi J. Biol. Sci.* 28 (10), 5538–5546. doi:10.1016/j.sjbs.2021.08.074

Bronner-Fraser, M. (1986). Analysis of the early stages of trunk neural crest migration in avian embryos using monoclonal antibody HNK-1. *Dev. Biol.* 115 (1), 44–55. doi:10.1016/0012-1606(86)90226-5

Chapman, S. C., Collignon, J., Schoenwolf, G. C., and Lumsden, A. (2001). Improved method for chick whole-embryo culture using a filter paper carrier. *Dev. Dyn. official Publ. Am. Assoc. Anatomists* 220 (3), 284–289. doi:10.1002/1097-0177(20010301)220:3<284::AID-DVDY1102>3.0.CO;2-5

Colas, J. F., and Schoenwolf, G. C. (2001). Towards a cellular and molecular understanding of neurulation. *Dev. Dyn. official Publ. Am. Assoc. Anatomists* 221 (2), 117–145. doi:10.1002/dvdy.1144

Copp, A. J., Greene, N. D., and Murdoch, J. N. (2003). The genetic basis of mammalian neurulation. *Nat. Rev. Genet.* 4 (10), 784–793. doi:10.1038/nrg1181

Cordero, D. R., Brugmann, S., Chu, Y., Bajpai, R., Jame, M., and Helms, J. A. (2011). Cranial neural crest cells on the move: their roles in craniofacial development. *Am. J. Med. Genet. Part A* 155 (2), 270–279. doi:10.1002/ajmg.a.33702

Corrigan, N., Brazil, D. P., and McAuliffe, F. (2009). Fetal cardiac effects of maternal hyperglycemia during pregnancy. *Birth Defects Res. Part A Clin. Mol. Teratol.* 85 (6), 523–530. doi:10.1002/bdra.20567

Datar, S., and Bhonde, R. R. (2005). Shell-less chick embryo culture as an alternative *in vitro* model to investigate glucose-induced malformations in mammalian embryos. *Rev. Diabet. Stud. RDS* 2 (4), 221–227. doi:10.1900/RDS.2005.2.221

Datar, S. P., and Bhonde, R. R. (2011). Modeling chick to assess diabetes pathogenesis and treatment. *Rev. Diabet. Stud. RDS* 8 (2), 245–253. doi:10.1900/RDS.2011.8.245

Dheen, S. T., Tay, S. S., Boran, J., Ting, L. W., Kumar, S. D., Fu, J., et al. (2009). Recent studies on neural tube defects in embryos of diabetic pregnancy: an overview. *Curr. Med. Chem.* 16 (18), 2345–2354. doi:10.2174/092986709788453069

Duband, J., Monier, F., Delannet, M., and Newgreen, D. (1995). Epithelium-mesenchyme transition during neural crest development. *Cells Tissues Organs* 154 (1), 63–78. doi:10.1159/000147752

Gassmann, M., Casagranda, F., Orioli, D., Simon, H., Lai, C., Klein, R., et al. (1995). Aberrant neural and cardiac development in mice lacking the ErbB4 neuregulin receptor. *Nature* 378 (6555), 390–394. doi:10.1038/378390a0

Gheldof, A., and Berx, G. (2013). Cadherins and epithelial-to-mesenchymal transition. *Prog. Mol. Biol. Transl. Sci.* 116, 317–336. doi:10.1016/B978-0-12-394311-8.00014-5

Golding, J. P., Trainor, P., Krumlauf, R., and Gassmann, M. (2000). Defects in pathfinding by cranial neural crest cells in mice lacking the neuregulin receptor ErbB4. *Nat. Cell Biol.* 2 (2), 103–109. doi:10.1038/35000058

Gurevitch, J., Koricheva, J., Nakagawa, S., and Stewart, G. (2018). Meta-analysis and the science of research synthesis. *Nature* 555 (7695), 175–182. doi:10.1038/nature25753

Hamburger, V., and Hamilton, H. L. (1992). A series of normal stages in the development of the chick embryo. *Dev. Dyn.* 195 (4), 231–272. doi:10.1002/aja.1001950404

Hamdoun, A., and Epel, D. (2007). Embryo stability and vulnerability in an always changing world. *Proc. Natl. Acad. Sci.* 104 (6), 1745–1750. doi:10.1073/pnas.0610108104

He, Y.-q., Li, Y., Wang, X.-y., He, X.-d., Jun, L., Chuai, M., et al. (2014). Dimethyl phenyl piperazine iodide (DMPP) induces glioma regression by inhibiting angiogenesis. *Exp. Cell Res.* 320 (2), 354–364. doi:10.1016/j.yexcr.2013.10.009

Henrique, D., Adam, J., Myat, A., Chitnis, A., Lewis, J., and Ish-Horowicz, D. (1995). Expression of a Delta homologue in prospective neurons in the chick. *Nature* 375 (6534), 787–790. doi:10.1038/375787a0

Hod, M., Kapur, A., Sacks, D. A., Hadar, E., Agarwal, M., Di Renzo, G. C., et al. (2015). The International Federation of Gynecology and Obstetrics (FIGO) Initiative on gestational diabetes mellitus: a pragmatic guide for diagnosis, management, and care. *Int. J. Gynaecol. obstetrics official organ Int. Fed. Gynaecol. Obstetrics* 131, S173–S211. doi:10.1016/S0020-7292(15)30033-3

Ishii, M., Arias, A. C., Liu, L., Chen, Y.-B., Bronner, M. E., and Maxson, R. E. (2012). A stable cranial neural crest cell line from mouse. *Stem cells Dev.* 21 (17), 3069–3080. doi:10.1089/scd.2012.0155

Ishimaru, K., Nishikawa, K., Omoto, T., Asai, I., Yoshihira, K., and Shimomura, K. (1995). Two flavone 2′-glucosides from Scutellaria baicalensis. *Phytochemistry* 40 (1), 279–281. doi:10.1016/0031-9422(95)00200-q

Janssen, P. A., Rothman, I., and Schwartz, S. M. (1996). Congenital malformations in newborns of women with established and gestational diabetes in Washington State, 1984–91. *Paediatr. Perinat. Epidemiol.* 10 (1), 52–63. doi:10.1111/j.1365-3016.1996.tb00026.x

King, A. J. (2012). The use of animal models in diabetes research. *Br. J. Pharmacol.* 166 (3), 877–894. doi:10.1111/j.1476-5381.2012.01911.x

Li, H., Long, D., Lv, G., Cheng, X., Wang, G., and Yang, X. (2022). The double-edged sword role of TGF-β signaling pathway between intrauterine inflammation and cranial neural crest development. *FASEB J.* 36 (1), e22113. doi:10.1096/fj.202101343R

Li-Weber, M. (2009). New therapeutic aspects of flavones: the anticancer properties of Scutellaria and its main active constituents Wogonin, Baicalein and Baicalin. *Cancer Treat. Rev.* 35 (1), 57–68. doi:10.1016/j.ctrv.2008.09.005

López Stewart, G. (2014). *Diagnostic criteria and classification of hyperglycaemia first detected in pregnancy: a World Health Organization Guideline*.

Maniglio, P., Noventa, M., Tartaglia, S., Petracca, M., Bonito, M., Ricciardi, E., et al. (2022). The Obstetrician Gynecologist's role in the screening of infants at risk of severe plagiocephaly: Prevalence and risk factors. *Eur. J. Obstetrics Gynecol. Reproductive Biol.* 272, 37–42. doi:10.1016/j.ejogrb.2022.03.011

Mitchell, L. E. (2005). "Epidemiology of neural tube defects," in *American journal of medical genetics Part C: seminars in medical genetics* (Wiley Online Library), 88–94.

Moore, L. L., Singer, M. R., Bradlee, M. L., Rothman, K. J., and Milunsky, A. (2000). A prospective study of the risk of congenital defects associated with maternal obesity and diabetes mellitus. *Epidemiology* 11, 689–694. doi:10.1097/00001648-200011000-00013

Mussatto, K. A., Hoffmann, R., Hoffman, G., Tweddell, J. S., Bear, L., Cao, Y., et al. (2015). Risk factors for abnormal developmental trajectories in young children with congenital heart disease. *Circulation* 132 (8), 755–761. doi:10.1161/CIRCULATIONAHA.114.014521

Negrato, C. A., and Gomes, M. B. (2013). Historical facts of screening and diagnosing diabetes in pregnancy. *Diabetology Metabolic Syndrome* 5 (1), 22–28. doi:10.1186/1758-5996-5-22

Osório, L., Teillet, M.-A., Palmeirim, I., and Catala, M. (2004). Neural crest ontogeny during secondary neurulation: a gene expression pattern study in the chick embryo. *Int. J. Dev. Biol.* 53 (4), 641–648. doi:10.1387/ijdb.072517lo

Preventive, U., Vesco, K., Pedula, K., Beil, T., Whitlock, E., and Pettitt, D. (2023). *Screening for gestational diabetes during pregnancy: recommendation from the US preventive services task force*.

Qi, X., Li, H., Cong, X., Wang, X., Jiang, Z., Cao, R., et al. (2016). Baicalin increases developmental competence of mouse embryos *in vitro* by inhibiting cellular apoptosis and modulating HSP70 and DNMT expression. *J. Reproduction Dev.* 62, 561–569. doi:10.1262/jrd.2016-047

Reid, S. N., Ziermann, J. M., and Gondré-Lewis, M. C. (2015). Genetically induced abnormal cranial development in human trisomy 18 with holoprosencephaly: comparisons with the normal tempo of osteogenic–neural development. *J. Anat.* 227 (1), 21–33. doi:10.1111/joa.12326

Sato, A., Scholl, A. M., Kuhn, E., Stadt, H. A., Decker, J. R., Pegram, K., et al. (2011). FGF8 signaling is chemotactic for cardiac neural crest cells. *Dev. Biol.* 354 (1), 18–30. doi:10.1016/j.ydbio.2011.03.010

Shi, L., Ko, M. L., Huang, C. C., Park, S. Y., Hong, M. P., Wu, C., et al. (2014). Chicken embryos as a potential new model for early onset type I diabetes. *J. diabetes Res.* 2014, 354094. doi:10.1155/2014/354094

Simões-Costa, M., and Bronner, M. E. (2015). Establishing neural crest identity: a gene regulatory recipe. *Development* 142 (2), 242–257. doi:10.1242/dev.105445

Song, D., Guo, J., Wang, Y., Pan, G., Li, P., Zhang, W., et al. (2010). Ingredients of Shuanghuanglian injection powder permeation through placental barrier of rat in pregnancy. *Zhongguo Zhong yao za zhi= Zhongguo Zhongyao Zazhi= China J. Chin. Materia Medica* 35 (12), 1626–1629. doi:10.4268/cjcmm20101227

Stevenson, R. E., Seaver, L. H., Collins, J. S., and Dean, J. H. (2004). Neural tube defects and associated anomalies in South Carolina. *Birth Defects Res. Part A Clin. Mol. Teratol.* 70 (9), 554–558. doi:10.1002/bdra.20062

Stewart, R. A., Arduini, B. L., Berghmans, S., George, R. E., Kanki, J. P., Henion, P. D., et al. (2006). Zebrafish foxd3 is selectively required for neural crest specification, migration and survival. *Dev. Biol.* 292 (1), 174–188. doi:10.1016/j.ydbio.2005.12.035

Stott-Miller, M., Heike, C. L., Kratz, M., and Starr, J. R. (2010). Increased risk of orofacial clefts associated with maternal obesity: case–control study and Monte Carlo-based bias analysis. *Paediatr. Perinat. Epidemiol.* 24 (5), 502–512. doi:10.1111/j.1365-3016.2010.01142.x

Sukanya, S., Bay, B. H., Tay, S. S. W., and Dheen, S. T. (2012). Frontiers in research on maternal diabetes-induced neural tube defects: past, present and future. *World J. diabetes* 3 (12), 196–200. doi:10.4239/wjd.v3.i12.196

Takahashi, Y., Sipp, D., and Enomoto, H. (2013). Tissue interactions in neural crest cell development and disease. *Science* 341 (6148), 860–863. doi:10.1126/science.1230717

Thomas, A. J., and Erickson, C. A. (2009). *FOXD3 regulates the lineage switch between neural crest-derived glial cells and pigment cells by repressing MITF through a non-canonical mechanism*.

Tinker, S. C., Gilboa, S. M., Moore, C. A., Waller, D. K., Simeone, R. M., Kim, S. Y., et al. (2020). Specific birth defects in pregnancies of women with diabetes: national birth defects prevention study. *Am. J. obstetrics Gynecol.* 222 (2), 176.e1–176.e11. doi:10.1016/j.ajog.2019.08.028

Tolvanen, T. A. (2022). Current advances in CETSA. *Front. Mol. Biosci.* 9, 866764. doi:10.3389/fmolb.2022.866764

Trindade-Suedam, I. K., Lmv, K., Pimenta, L. A. F., Negrato, C. A., Franzolin, S. B., and Trindade Junior, A. S. (2016). Diabetes mellitus and drug abuse during pregnancy and the risk for orofacial clefts and related abnormalities. *Rev. latino-americana Enferm.* 24, e2701. doi:10.1590/1518-8345.0815.2701

Trinh, H.-t., Joh, E.-h., Kwak, H.-y., Baek, N.-i., and Kim, D.-h. (2010). Anti-pruritic effect of baicalin and its metabolites, baicalein and oroxylin A, in mice. *Acta Pharmacol. Sin.* 31 (6), 718–724. doi:10.1038/aps.2010.42

Tsalamandris, S., Antonopoulos, A. S., Oikonomou, E., Papamikroulis, G.-A., Vogiatzi, G., Papaioannou, S., et al. (2019). The role of inflammation in diabetes: current concepts and future perspectives. *Eur. Cardiol. Rev.* 14 (1), 50–59. doi:10.15420/ecr.2018.33.1

Virjee, S., Robinson, S., and Johnston, D. (2001). Screening for diabetes in pregnancy. *J. R. Soc. Med.* 94 (10), 502–509. doi:10.1177/014107680109401003

Wang, C.-J., Wang, G., Wang, X.-Y., Liu, M., Chuai, M., Lee, K. K. H., et al. (2016a). Imidacloprid exposure suppresses neural crest cells generation during early chick embryo development. *J. Agric. food Chem.* 64 (23), 4705–4715. doi:10.1021/acs.jafc.6b01478

Wang, C.-Z., Zhang, C.-F., Chen, L., Anderson, S., Lu, F., and Yuan, C.-S. (2015a). Colon cancer chemopreventive effects of baicalein, an active enteric microbiome metabolite from baicalin. *Int. J. Oncol.* 47 (5), 1749–1758. doi:10.3892/ijo.2015.3173

Wang, F., Xu, Z., Ren, L., Tsang, S. Y., and Xue, H. (2008). GABAA receptor subtype selectivity underlying selective anxiolytic effect of baicalin. *Neuropharmacology* 55 (7), 1231–1237. doi:10.1016/j.neuropharm.2008.07.040

Wang, G., Huang, W.-Q., Cui, S.-D., Li, S., Wang, X.-Y., Li, Y., et al. (2015b). Autophagy is involved in high glucose-induced heart tube malformation. *Cell cycle* 14 (5), 772–783. doi:10.1080/15384101.2014.1000170

Wang, G., Liang, J., Gao, L.-R., Si, Z.-P., Zhang, X.-T., Liang, G., et al. (2018a). Baicalin administration attenuates hyperglycemia-induced malformation of cardiovascular system. *Cell death Dis.* 9 (2), 234–317. doi:10.1038/s41419-018-0318-2

Wang, G., Lu, J.-Q., Ding, Y., Zhang, T., Song, J.-H., Long, D., et al. (2020). Baicalin rescues hyperglycemia-induced neural tube defects via targeting on retinoic acid signaling. *Am. J. Transl. Res.* 12 (7), 3311–3328.

Wang, G., Nie, J.-H., Bao, Y., Yang, X., and Chemistry, F. (2018b). Sulforaphane rescues ethanol-suppressed angiogenesis through oxidative and endoplasmic reticulum stress in chick embryos. *J. Agric. Food Chem.* 66 (36), 9522–9533. doi:10.1021/acs.jafc.8b02949

Wang, P., Cao, Y., Yu, J., Liu, R., Bai, B., Qi, H., et al. (2016b). Baicalin alleviates ischemia-induced memory impairment by inhibiting the phosphorylation of CaMKII in hippocampus. *Brain Res.* 1642, 95–103. doi:10.1016/j.brainres.2016.03.019

Wang, X.-Y., Li, S., Wang, G., Ma, Z.-L., Chuai, M., Cao, L., et al. (2015c). High glucose environment inhibits cranial neural crest survival by activating excessive autophagy in the chick embryo. *Sci. Rep.* 5 (1), 18321–18416. doi:10.1038/srep18321

Wu, T. T., Chen, Y. Y., Chang, H. Y., Kung, Y. H., Tseng, C. J., and Cheng, P. W. (2020). AKR1B1-Induced epithelial-mesenchymal transition mediated by RAGE-oxidative stress in diabetic cataract lens. *Antioxidants Basel, Switz.* 9 (4), 273. doi:10.3390/antiox9040273

Wu, X., Li, X., Fu, Q., Cao, Q., Chen, X., Wang, M., et al. (2017). AKR1B1 promotes basal-like breast cancer progression by a positive feedback loop that activates the EMT program. *J. Exp. Med.* 214 (4), 1065–1079. doi:10.1084/jem.20160903

Wu, Y., Wang, F., Fan, L., Zhang, W., Wang, T., Du, Y., et al. (2018). Baicalin alleviates atherosclerosis by relieving oxidative stress and inflammatory responses via inactivating the NF-κB and p38 MAPK signaling pathways. *Biomed. Pharmacother.* 97, 1673–1679. doi:10.1016/j.biopha.2017.12.024

Yang, G.-R., Dye, T. D., and Li, D. (2019). Effects of pre-gestational diabetes mellitus and gestational diabetes mellitus on macrosomia and birth defects in Upstate New York. *Diabetes Res. Clin. Pract.* 155, 107811. doi:10.1016/j.diabres.2019.107811

Yin, F., Liu, J., Ji, X., Wang, Y., Zidichouski, J., and Zhang, J. (2011). Baicalin prevents the production of hydrogen peroxide and oxidative stress induced by Aβ aggregation in SH-SY5Y cells. *Neurosci. Lett.* 492 (2), 76–79. doi:10.1016/j.neulet.2011.01.055

Zhang, K. R., Zhang, Y. F., Lei, H. M., Tang, Y. B., Ma, C. S., Lv, Q. M., et al. (2021). Targeting AKR1B1 inhibits glutathione *de novo* synthesis to overcome acquired resistance to EGFR-targeted therapy in lung cancer. *Sci. Transl. Med.* 13 (614), eabg6428. doi:10.1126/scitranslmed.abg6428

Zhang, P., Wang, G., Lin, Z., Wu, Y., Zhang, J., Liu, M., et al. (2017). Alcohol exposure induces chick craniofacial bone defects by negatively affecting cranial neural crest development. *Toxicol. Lett.* 281, 53–64. doi:10.1016/j.toxlet.2017.09.010

Zhang, T.-N., Huang, X.-M., Zhao, X.-Y., Wang, W., Wen, R., and Gao, S.-Y. (2022). Risks of specific congenital anomalies in offspring of women with diabetes: a systematic review and meta-analysis of population-based studies including over 80 million births. *PLoS Med.* 19 (2), e1003900. doi:10.1371/journal.pmed.1003900

Zhang, Y.-M., Zhang, Y.-Y., Bulbul, A., Shan, X., Wang, X.-Q., and Yan, Q. (2015). Baicalin promotes embryo adhesion and implantation by upregulating fucosyltransferase IV (FUT4) via Wnt/beta-catenin signaling pathway. *FEBS Lett.* 589 (11), 1225–1233. doi:10.1016/j.febslet.2015.04.011

frontiers | Frontiers in Pharmacology

TYPE Review
PUBLISHED 08 April 2024
DOI 10.3389/fphar.2024.1375585

OPEN ACCESS

EDITED BY
Xianyu Li,
China Academy of Chinese Medical Sciences, China

REVIEWED BY
Shengpeng Wang,
University of Macau, China
Nianrong Zhang,
China-Japan Friendship Hospital, China

*CORRESPONDENCE
Chuan Yang,
82392429@qq.com
Junzhi Lin,
linjunzhi@cdutcm.edu.cn
Chuan Zheng,
zhengchuan@cdutcm.edu.cn

†These authors have contributed equally to this work

RECEIVED 24 January 2024
ACCEPTED 21 March 2024
PUBLISHED 08 April 2024

CITATION
Zhang B, Cheng Y, Jian Q, Xiang S, Xu Q, Wang C, Yang C, Lin J and Zheng C (2024), Sishen Pill and its active phytochemicals in treating inflammatory bowel disease and colon cancer: an overview.
Front. Pharmacol. 15:1375585.
doi: 10.3389/fphar.2024.1375585

Sishen Pill and its active phytochemicals in treating inflammatory bowel disease and colon cancer: an overview

Boxun Zhang[1†], Yingying Cheng[2†], Qin Jian[3], Sirui Xiang[4], Qi Xu[4], Chuchu Wang[4], Chuan Yang[5*], Junzhi Lin[3*] and Chuan Zheng[3,6*]

[1]Department of Endocrinology, Hospital of Chengdu University of Traditional Chinese Medicine, Chengdu, China, [2]State Key Laboratory of Southwestern Chinese Medicine Resources, College of Pharmacy, Chengdu University of Traditional Chinese Medicine, Chengdu, China, [3]TCM Regulating Metabolic Diseases Key Laboratory of Sichuan Province, Hospital of Chengdu University of Traditional Chinese Medicine, Chengdu, China, [4]College of Basic Medicine, Chengdu University of Traditional Chinese Medicine, Chengdu, China, [5]Department of Dermatology, Hospital of Chengdu University of Traditional Chinese Medicine, Chengdu, China, [6]Sichuan Provincial Engineering Research Center of Innovative Re-development of Famous Classical Formulas, Tianfu TCM Innovation Harbour, Chengdu University of Traditional Chinese Medicine, Chengdu, China

The incidence of inflammatory bowel disease (IBD) and the associated risk of colon cancer are increasing globally. Traditional Chinese medicine (TCM) treatment has unique advantages. The Sishen Pill, a common Chinese patented drug used to treat abdominal pain and diarrhea, consists mainly of Psoraleae Fructus, Myristicae Semen, Euodiae Fructus, and Schisandra Chinensis. Modern research has confirmed that Sishen Pill and its active secondary metabolites, such as psoralen, myristicin, evodiamine, and schisandrin, can improve intestinal inflammation and exert antitumor pharmacological effects. Common mechanisms in treating IBD and colon cancer mainly include regulating inflammation-related signaling pathways such as nuclear factor-kappa B, mitogen-activated protein kinase, phosphatidylinositol 3-kinase, NOD-like receptor heat protein domain-related protein 3, and wingless-type MMTV integration site family; NF-E2-related factor 2 and hypoxia-inducible factor 1α to inhibit oxidative stress; mitochondrial autophagy and endoplasmic reticulum stress; intestinal immune cell differentiation and function through the Janus kinase/signal transducer and activator of transcription pathway; and improving the gut microbiota and intestinal barrier. Overall, existing evidence suggests the potential of the Sishen pill to improve IBD and suppress inflammation-to-cancer transformation. However, large-scale randomized controlled clinical studies and research on the safety of these clinical applications are urgently required.

KEYWORDS

inflammatory bowel disease, colon cancer, Sishen Pill, molecular mechanism, natural product

1 Introduction

Inflammatory bowel disease (IBD) is a chronic disease of the intestine that mainly includes ulcerative colitis (UC) and Crohn's disease (CD). Its incidence has shown an upward trend worldwide (Ng et al., 2017). UC, the most important type of IBD, progresses gradually from the rectum to the proximal segments of the colon, with its lesions often

localized to the mucosal epithelium. UC can occur in any part of the gastrointestinal tract and is commonly found in the terminal ileum and right colon. In addition to common discomfort symptoms, such as abdominal pain, diarrhea, and bloody stools, IBD is associated with an increased risk of various metabolic diseases, such as diabetes (Lu et al., 2020; Li et al., 2021b), acute coronary syndrome (D'Ascenzo et al., 2023; Zaka et al., 2023), nonalcoholic fatty liver disease (Chen et al., 2020c), and autoimmune skin diseases (Fu et al., 2018) such as rheumatoid arthritis and psoriasis. More importantly, IBD can increase the risk of various cancers, such as colon cancer (Gatenby et al., 2021; Piovani et al., 2022). A survey of patients with UC revealed that the estimated cumulative risk of UC-associated colorectal cancer was 0.7% within 10 years, but by 30 years, the risk rose to 33.2% (Kim et al., 2009). Treatment of IBD with 5-aminosalicylates can significantly reduce the incidence of colon cancer (Bonovas et al., 2017; Hsiao et al., 2022). In recent studies, targeted nutritional interventions (Cassotta et al., 2023), probiotics, and other intestinal microecological agents (Lee et al., 2022) were found to be effective in treating colitis-associated colon cancer (CACC). The process of IBD transformation into cancer involves complex molecular mechanisms, such as gene mutations, epigenetic alterations, persistent chronic inflammation, gut microbiota disorders, and others (Xue et al., 2018). Further exploration is warranted to limit intestinal inflammation and inhibit its transformation into colon tumors.

Natural botanical drugs have the therapeutic advantage of multiple pathways and multiple targets; numerous studies have confirmed that botanical drugs or their extracts could improve IBD, inhibit its progression to colon cancer, exerting an integrated pharmacological "anti-inflammatory + anti-cancer" effect (Yang et al., 2023b). Traditionally, the Sishen Pill is a Chinese patent drug commonly used to treat diarrhea and is mainly composed of Psoraleae Fructus, Myristicae Semen, Euodiae Fructus, and Schisandrae Chinensis at a dosage ratio of 4 : 2: 2 : 1. Jujubae Fructus and Zingiberis Rhizoma were also used as excipients in this formula. In traditional Chinese medicine (TCM), Sishen Pill is believed to "warm the kidneys to dispel cold and astringing the intestines to stop diarrhea." modern clinical studies showed that it could effectively treat IBD and other intestinal inflammatory injury (Li et al., 2018; Long and Cao, 2021b; Xu et al., 2022b). The main active metabolites in this formula, such as myristicin (Ismail Abo El-Fadl and Mohamed, 2022), psoralen (Zhou, 2020), deoxyschizandrin (Zhang et al., 2016), evodiamine (Ding et al., 2020), and others could improve the intestinal mucosal damage caused by IBD through various molecular mechanisms. Recent studies also found that the Sishen Pill can effectively treat colon cancer (Jiang et al., 2023) and prevent the progression of inflammatory cancer transformation (Cao et al., 2012; Cao, 2013; Cao et al., 2013); various metabolites in this formula could also suppress the growth of colonic tumor cells. This review comprehensively summarizes the experimental research on the treatment of IBD and colon cancer with Sishen Pill and its active phytochemicals, screens for core effective phytochemicals, clarifies key targets of action, generalizes the potential common molecular mechanism of Sishen Pill to treat IBD and colon cancer, and proposes a future research outlook based on the current research.

2 Metabolites investigation of Sishen Pill

The earliest records of the Sishen Pill can be traced back to the *Hua Tuo Shen Yi Mi Zhuan* during the Han Dynasty. The main disease it treats is "predawn diarrhea" (Wang et al., 2015). Modern research has found that this formula not only treats diarrhea but also has curative effects on multiple intestinal diseases such as UC (Long and Cao, 2021a), irritable bowel syndrome (Li et al., 2018a), colorectal cancer (Sun et al., 2021), and extraintestinal diseases such as depression (Luo et al., 2023) and breast cancer (Xu et al., 2022a). The multiple active metabolites contained in the Sishen Pill determine its multi-target therapeutic effects. Several studies have applied advanced technology to analyze qualitative or quantitative the metabolites in the Sishen Pill. Briefly, high performance liquid chromatography (HPLC) (Wei et al., 2021; Guo et al., 2023), HPLC-electrospray ionization-tandem mass spectrometry (HPLC-ESI-MS/MS) (Zhang et al., 2018), and flash evaporation-gas chromatography/mass spectrometry (FE-GC/MS) (Huang et al., 2019) have been used to identify effective metabolites in this formula. Sishen Pill contains various effective metabolites such as coumarins, lignin, alkaloids, terpenoids, and others (Guo et al., 2023). The main metabolites with potential therapeutic effects on IBD and/or colon cancer are shown in Figure 1.

Psoraleae Fructus is the dried ripe fruit of *Psoralea corylifolia* Linn. The Leguminosae family and its metabolites include coumarins, flavonoids, benzofurans, monoterpenes, and some trace elements (Mu et al., 2018). Other studies focused on psoralen, isopsoralen, and psoralidin in coumarins; bavachin, bavachinin, and neobavaisoflavone in flavonoids; and bakuchiol in monoterpenoids (Chopra et al., 2013). In addition to antibacterial, anti-inflammatory, antitumor, antiviral, and antioxidant effects, Psoraleae Fructus can regulate bone cell metabolism, enhance skin pigmentation, and act like estrogen, expanding its utility in orthopedics, dermatology, and gynecology (Ren et al., 2020; Sharifi-Rad et al., 2020). The coumarin content in Psoraleae Fructus is an important indicator that the Sishen Pill meets quality standards (Huang et al., 2019). Several studies have confirmed that intestinal bacteria play an important role in metabolic processes. Wang et al. developed a rapid, sensitive, and selective ultra-performance liquid chromatography-tandem mass spectrometry (UPLC-MS/MS) method and found that psoralenoside and isopsoralenoside could be metabolized to psoralen and isopsoralen by gut microbiota through de-glucosylation (Wang et al., 2014). Furthermore, Liu et al. investigated the metabolic profiles of psoralen and isopsoralen under intestinal conditions and confirmed that some metabolites, such as 6,7-furano-hydrocoumaric acid and 5,6-furano-hydrocoumaric acid, have stronger activities in antioxidant stress and as anti-inflammatories (Liu L. et al., 2019).

Myristica Semen, the dried seeds of *Myristica fragrans* Houtt. plants in the Myristiceae family are a common TCM medicinal and edible homologous that contains lignans such as dehydrodiisoeugenol and macelignan; phenylpropanoids such as myristicin, eugenol, isoeugenol, and elemicin; and terpene alcohols such as linalool, all found to have multiple pharmacological properties (Liu et al., 2023). In addition to the therapeutic effects on the digestive system, such as peptic ulcer and diarrhea, Myristicae Semen has also been shown to be active against Parkinson's disease and has anti-depressant, anti-epileptic, and anti-dementia effects (Liu et al., 2023). The combination of Myristicae Semen and Psoraleae Fructus, known as the traditional Ershen Pill

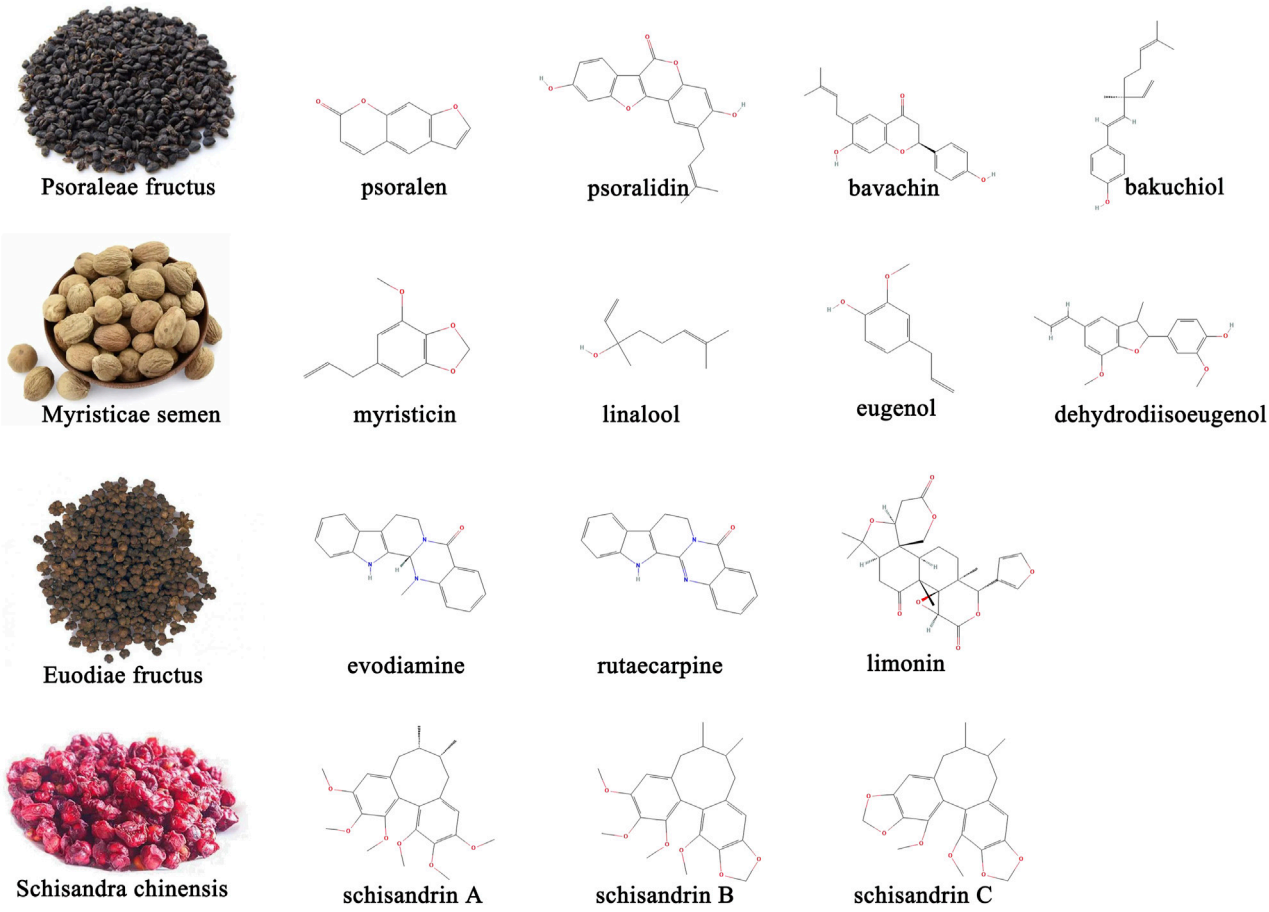

FIGURE 1
Representative active metabolites in Sishen Pill with potential therapeutic effects on IBD and/or colon cancer.

formula, is also used to treat intestinal diseases such as diarrhea and abdominal cold pain. Gao et al. (2017) used HPLC to "fingerprint" Ershen Pill-medicated serum and found that psoralen, isopsoralen, bakuchiol, corylin, and dehydrodiisoeugenol were the main metabolites absorbed into the blood.

Euodiae Fructus is a nearly ripe, dry fruit of the Rutaceae plant *Euodia rutaecarpa* (Juss.) Benth. or *E. rutaecarpa* (Juss.) var. *officinalis* (Dode) Huang, or *E. rutaecarpa* (Juss.) Benth. var. *bodinieri* (Dode) Huang; it contains mainly alkaloids, terpenoids, flavonoids, phenylpropanoids, anthraquinone, and sterols; research has now focused on metabolites such as evodiamine, rutaecarpine, rutaevine, and limonin (Kong et al., 2023). Euodiae Fructus is widely used in clinical practice and has multiple effects, including pain relief, anti-inflammatory effects, gastrointestinal protection, antitumor effects, central nervous system protection, cardiovascular protection, and glycolipid metabolism regulation. Recently, to solve the problems of low solubility and bioavailability of evodiamine, attempts have been made to develop novel phospholipid and nanocomplex drug carriers to deliver evodiamine, achieve better clinical efficacy and reduce side effects (Luo et al., 2021).

Schisandrae Chinensis originates from the dried and ripe fruits of the Magnoliaceae plant *Schisandra Chinensis* (Turcz.) Baill, or *Schisandra Sphenanthera* Rehd. et Wils; the former is called *Schisandrae Sphenantherae Fructus*, whereas the latter is called *Schisandrae Chinensis Fructus*. The effective metabolites of Schisandrae Chinensis contain lignans, volatile oils, polysaccharides, organic acids, terpenoids, and flavonoids. Among them, lignans are considered the primary active metabolites, including mainly schizandrin A, schizandrin B, schizandrin C, schizandrol A, schizandrol B, schistenherin A, and schistenherin B. Studies found that schisandrins could regulate the central nervous, cardiovascular, digestive, endocrine, and immune systems, and are often used for sleep promotion, regulation of glucose and lipid metabolism, and as anti-inflammatory and anti-diarrhea agents (Xing et al., 2021). Similar to evodiamine, schisandrins have relatively low bioavailability; new technologies such as self-emulsifying drug delivery systems and solubility have been improved to some extent (Shao et al., 2010).

3 Research progress on Sishen Pill in the treatment of IBD and colon cancer

3.1 Sishen Pill in the treatment of IBD

The clinical efficacy of the Sishen Pill in treating UC has been confirmed by multiple clinical studies. *Long* et al. conducted a meta-

TABLE 1 Pharmacological effects and molecular mechanisms of Si Shen Wan in the treatment of IBD.

Experimental model	Dosage form	Dosage	Pharmacological effect	Molecular mechanism	References
BALB/c mice	formula granules	2.5 g/kg/d	Regulating immune cells: Treg cell↑, Tfr cell↑, PD-1 and PD-L1 cells↓, Tfh9 and Tfh17 cells↓	Inhibiting STAT/SOCS signaling pathway: protein expression levels of p-STAT3, STAT3, p-STAT6 and STAT6 are decreased, and protein expression level of SOCS are increased	Huang et al. (2022), Kang et al. (2022)
BALB/c mice	volatile oil	0.075 g/kg/d	Regulating inflammatory factors: IL-10↑, IL-4↓, IL-17A↓, IL-21↓, IFN-γ↓	Inhibiting TLR/MyD88 signaling pathway: the levels of TLR2, MyD88, Rac1, IRAK4, IRAK1, TRAF6, TAB1, TAB2, MKK6, p38MAPK, and CREB proteins are downregulated	Huang et al. (2021)
Wistar rat	water decoction	2.5 g,5 g, 10 g/kg/d	Regulating oxidative stress and immune factors: lgE↓, MDA↓, IL-2↑, SOD↑, FT3↑, FT4↑	Regulating TLR4/IRAK-M signaling pathway: the protein expression level of TLR-4 is downregulated and IRAK-M protein is upregulated	Wang et al. (2019a)
Wistar rat	water pill	0.8 g,1.6 g and 3.2 g/kg/d	Regulating inflammatory factors: IL-1β↓, IL-10↑	Inhibiting PI3K/Akt/mTOR signaling pathway: the levels of p-PI3K, p-Akt, p-mTOR are decreased	Liu et al. (2021)
BALB/c mice	water pill	5 g/kg/d	Regulating the dendritic cell immunity: CD40↓, CD24↓, CD135↓, CD107b↓, CD115↓, CCR6↓, CD172a↑, F4/80↑	Inhibiting PI3K/Akt/mTOR signaling pathway: the level of PI3K, Akt, p-Akt, mTOR, p-mTOR, Raptor and Rictor are decreased	Liu et al. (2022)
SD rat	water pill	2.5 g/kg/d	Regulating T lymphocyte subsets: $CD4^+$T cell↓, $CD8^+$T cell↑, CD4/CD8↓, $CD4^+CD25^+$T cell↑, $CD4^+CD25^+Foxp3^+$T↑, Th17 cell↓, Treg/Th17↑	Regulating the expression of RORγt and STAT5a: the protein expression of RORγt is decreased and STAT5a is increased	Liu et al. (2016)
BALB/c mice	water pill	2.5 g/kg/d	Reduce inflammatory response: TLR-2↓, TLR-4↓	Regulating the gut microbiota disorders: the abundance of pathogenic bacteria such as *Eubacterium_fissicatena* was downregulated, and the abundance of beneficial strains for protecting the intestinal mucosa, such as *Lachnospiraceae_NK4A136*, *Muribaculaceae* and *Akkermansia* was upregulated	Jin et al. (2023)
C57BL/6	Ethanol extract	20 g/kg/d,40 g/kg/d	Regulating inflammation and oxidative stress factors: IL-6↓, TNF-α↓, MDA↓ ROS↓, T-AOC↑	Regulating the Nrf2/HO-1 signaling pathway: protein and mRNA expression levels of Nrf2, HO-1, NQO-1 upregulated	Zhang et al. (2021b)
SD rat	water decoction	6 g,12 g,24 g/kg/d	Regulating inflammation and immune factors: IL-6↓, IL-17↓, STAT3↓, IL-10↑, TGF-β1↑, PPARγ↑, the proportion of Th17 cells↓, the proportion of Treg cells↑	Regulating the gut microbiota disorders: the relative abundance of *Lactobacillus* and the concentration of butyric acid are increased	Wang et al. (2022b)
BALB/c mice	water pill	2.5 g/kg/d	Regulating inflammatory factors: $CD11c^+CD103^+$E-cadherin$^+$ cells↓, IL-1β↓, IL-4↓,IL-9↓, IL-17A↓	Regulating the gut microbiota disorders: the Simpson index and the relative abundance of *Akkermansia spp*. and *Corynebacterium spp*. are increased, and the relative abundance of the *Lachnospiraceae NK4A136* group are decreased	Chen et al. (2020b)
BALB/c mice	water pill	2.5 g/kg/d	Regulating inflammation and immune factors: Tcm cells↑, the balance of $CD4^+$ Tem and $CD8^+$ Tem cells is recovered; IL-2↓, IL-7↓, IL-12↓, IL-15↓, IL-10↑	Regulating the PI3K/Akt signaling pathway: the levels of PI3K, Akt, p-Akt, Id2, T-bet, FOXO3, Noxa, and C-myc proteins are decreased, and the levels of Rictor, Raptor, TSC1, TSC2, p-AMPKα, AMPKα, 4E-BP2, Kif2a and p70S6K are increased	Ge et al. (2020)

(Continued on following page)

TABLE 1 (*Continued*) Pharmacological effects and molecular mechanisms of Si Shen Wan in the treatment of IBD.

Experimental model	Dosage form	Dosage	Pharmacological effect	Molecular mechanism	References
SD rat	water decoction	6g, 12 g and 24 g/kg/d	Regulating inflammatory factors: IL-1β↓, TNF-α↓	Inhibiting the TLR-2/NF-κB signaling pathway: the expression levels of TLR2, MyD88, IRAK4, and NF-κB p65 in the colon tissue are decreased	Zhaohua et al. (2022)
BALB/c mice	water pill	2.5 g/kg/d	Regulating immune cells: $CD4^+$ Tcm↑, $CD4^+$ mTfh cells↑, and the percentages of $CD4^+$ and $CD8^+$ expressions on central memory T cells are enhanced	Regulating the JAK/STAT5 signaling pathway: the levels of JAK1, PIAS3, STAT5, p-STAT5, BIM, BAX, caspase-3, and β-casein are decreased, and the levels of JAK3, PISA1, Bcl-2, and caveolin-1 are decreased	Wang et al. (2022a)
SD rat	water pill	5 g/kg/d	Regulating inflammation and oxidative stress factors: IFN-γ↓, IL-1β↓, IL-17↓, IL-4↓, calprotectin↓, MPO↓, MDA↓, NO↓, iNOS↓, T-AOC↑, SOD↑, eNOS↑	Inhibiting the ubiquitination of NEMO/NLK signaling pathway: the expressions of NF-κBp65, NLK, ubiquitinated NEMO and downstream proteins TAK, CYLD, P38 are decreased	Wang et al. (2019d)
SD rat	water pill	5 g/kg/d	Regulating inflammatory factors and enzyme activity of ATPase: TNF-α↓, IL-2↓, IL-15↓, sICAM-1↓, SDH↑, LDH↓, Na+K + -ATPase↑, Ca2+Mg2+-ATPase↑	Regulating the expression of wnt/β-catenin pathway related proteins:β-catenin, ubiquitination of Ub-NARF and Ub-TCF, and expression of Wnt/β-catenin downstream proteins are downregulated	Zhao et al. (2019)
BALB/c mice	water pill	2.5 g/kg/d	Regulating inflammatory factors and the differentiation of inflammatory dendritic cells: TNF-α↓, IL-1β↓, IL-6↓, IL-12p70↓, IL-10↑, iNOS + DCs↓, TNF-α+DCs↓, E-cadherin + DCs↓, MHC-II + DCs↓, GM-CSFR + DCs↓	1. Inhibiting TLR-4/NF-κB signaling pathway: the activation of the TLR4, MyD88, TRAF6, TAB2, and NF-κBp65 proteins and activated IκB are inhibited 2. Regulating the gut microbiota disorders: the enrichment of *Aerococcus* is inhibited, and the relative abundance of *norank f Lachnospiraceae*, *Lachnospiraceae UCG-006*, *Parvibacter*, *Akkermansia*, and *Rhodococcus* is increased	Ge et al. (2022)
BALB/c mice	water pill	2.5 g/kg/d	Regulating the differentiation of Tfh: Tfh10↑, Tfr↑, Tfh17↓, BCL-6+T cells↓, PD-1+ T cells↓, Blimp-1+ T cells↑	Activating the BCL-6/Blimp-1 signaling pathway: the expression of Bcl-6, STAT3 and p-STAT3 are inhibited, and the level of Blimp-1 is increased	Liu et al. (2020)
SD rat	water pill	5 g/kg/d	Improved the intestinal barrier integrity: Claudin-5↑, JAM1↑, VE-cadherin↑, and Connexin↑	Regulating PI3K/Akt and Rho/ROCK signaling pathways: the proteins expression levels of p-RhoA, ROCK1, PI3K, Akt, Notch1 and p-Rac are decreased, and levels of p-AMPKαand PTEN are decreased	Zhang et al. (2021c)
SD rat	water decoction	3.4 g/kg/d	Regulating inflammatory factors: IL-1β↓, TNF-α↓	Activating autophagy and restoring the balance between autophagy and apoptosis: the levels of LC3II/I and Beclin-1 are upregulated, and the number of autophagosomes is increased	Yu et al. (2024)
C57/BL mice	Freeze-dried powder	5 g/kg	Regulating inflammatory and apoptotic factors: TNF-α↓, Bax↓, Bcl-2↑, Bcl-2/Bax↑	Inhibiting p38 MAPK signaling pathway: the mRNA expressions of p38 MAPK, p53, caspase-3, c-jun, c-fos are decreased	Zhao et al. (2013)

Abbreviations: Akt: protein kinase B, AMPK: AMP-activated kinase, BAX: BCL-2, associated X, Blimp-1: B lymphocyte-induced maturation protein-1, BIM: Bcl-2-like protein 11, CREB: cAMP-response element binding protein, 4E-BP2: eukaryotic translation initiation factor 4E-binding protein 2, eNOS:endothelial nitric oxide synthase, FOXO3: forkhead box O3a, FT3: free triiodothyronine, FT4: free thyroxin, IL: interleukin, IFN-γInterferon gamma, iNOS:inducible nitric oxide synthase, IRAK: human interleukin-1, receptor-associated kinase, JAK: janus kinase, JAM-1: Junctional Adhesion Molecule-1, Kif2a: kinesin family member 2a, LDH: layered double hydroxide, p38MAPK: phosphorylated form of P38 mitogen activated protein kinase, MDA: malondialdehyde, MKK6: Mitogen-activated Protein Kinase Kinase 6, mTOR: mammalian target of rapamycin, MyD88: Myeloid differentiation primary response gene 88, NEMO: NF-κB, essential modulator, PD-1: programmed death-1, PD-L1: programmed death-ligand 1, PI3K: phosphatidylinositol 3-kinase, PTEN: phosphatase and tensin homolog deleted on chromosome ten, Rac1: ras-related C3 botulinum toxin substrate 1, RORγt: retinoic acid-related orphan receptor gamma t, ROCK: rho kinase, PPAR:peroxisome proliferator-activated receptor, p70S6K: 70-kDa ribosomal protein S6 kinase, PIAS: Protein inhibitors of activated STATs, ROS: reactive oxygen species, STAT: SATA: signal transducer and activator of transcription, SOCS: suppressor of cytokine signaling, SOD: superoxide dismutase, sICAM-1: Soluble intercellular adhesion molecule-1, TAB: Transforming Growth Factor β-Activated Protein Kinase 1 binding Protein, TRAF6: TNF, receptor associated factor 6, TLR: toll like receptor, T-AOC: total antioxidant capacity, TGF-β1: transforming growth factor-beta 1, TSC: tuberous sclerosis complex, Tfh: follicular helper T cell, Tfr: follicular regulatory T cells, Ub-NARF: ubiquitinated Nemo-like-kinase-associated ring finger protein, Ub-TCF: ubiquitinated T-cell factor.

analysis of nine randomized controlled trials (RCTs) including 680 patients and found that, compared to sulfasalazine and mesalazine, the combined use of Sishen Pill could effectively improve the effectiveness of treatment, reduce C-reactive protein levels, and have a lower incidence of adverse reactions (Long and Cao, 2021b), however, among the original studies included in this meta-analysis, different studies adopted different forms of administration of Sishen Pills (oral or enema), and it remains to be further explored which administration route can achieve better therapeutic effects. *Zhang* et al. used network pharmacology and bioinformatics methods to screen 22 key targets of the Sishen Pill in treating UC (Zhang et al., 2019) and suggested that it could improve intestinal inflammatory state, repair intestinal mucosal injury, and inhibit disease progression by regulating multiple targets, however, further experimental research is needed to confirm the relevant conclusions based on bioinformatics analysis. Table 1 lists the relevant basic research progress on the Sishen Pill for the treatment of IBD. Briefly, several studies focused on the inhibitory effects of Sishen Pill on the toll-like receptor (TLR): *Huang* (Huang et al., 2021) and *Zhao* (Zhaohua et al., 2022) found that the formula could inhibit expression levels of myeloid differentiation factor 88 (MyD88), interleukin-1 receptor associated kinase 4 (Irak4), and nuclear factor-kappa B(NF-κB) by down-regulating the activation of TLR2. *Wang* (Wang et al., 2019a) and *Ge* (Ge et al., 2022) confirmed that TLR4 was the key target, and downregulating TLR4 could inhibit the occurrence of subsequent inflammatory responses through MyD88-dependent and MyD88-independent pathways. In addition, *Zhang* (Zhang et al., 2021c), *Wang* (Wang et al., 2022a) and *Zhao* (Zhao et al., 2013) explored the molecular mechanism of the Sishen Pill in inhibiting the inflammatory response and promoting intestinal mucosal repair via phosphatidylinositol 3-kinase (PI3K)/protein kinase B (PKB/Akt), Janus kinase (JAK)/signal transducer and activator of transcription 5 (STAT5), and mitogen activated protein kinase (MAPK) signal pathways. Moreover, the regulation of intestinal immune cells by Sishen Pill mainly manifests in different subsets of T lymphocytes and regulatory T cells (Treg) (Liu et al., 2016), helper T cells (Th) (Liu et al., 2016), follicular helper T cells (Tfh) (Liu et al., 2020), follicular regulatory T cells (Tfr) (Huang et al., 2022; Kang et al., 2022), memory T cells (TM) (Ge et al., 2020), and dendritic cells (Liu et al., 2022). For regulating the gut microbiota, Sishen Pill has been shown to increase the relative abundance of beneficial bacteria, such as *Lactobacillus* and *Akkermansia*, and to promote an increase in intestinal butyrate content (Chen et al., 2020b; Wang et al., 2022b; Ge et al., 2022). In summary, the above studies have elucidated the mechanism of action of Sishen Pill in treating IBD from different perspectives, but there is still a lack of deeper exploration on the key targets of action, and the application of molecular inhibitors/activators or gene knockout animal model and other experimental methods is necessary and anticipated in future research.

3.2 Sishen Pill in the treatment of colon cancer

The RCT carried out by *Sun* et al. confirmed that the additional application of Sishen Pill in chemotherapy could significantly improve the patient's discomfort symptoms, enhance the treatment effectiveness, reduce the probability of chemotherapy side effects (e.g., leukopenia, thrombocytopenia, liver and kidney function injury), and regulate immune cell levels ($CD8^+$ cells↓, $CD3^+$ and $CD4^+$ cells↑) (Sun et al., 2021). Another clinical study revealed the therapeutic mechanism of the Sishen Pill in treating colon cancer from the perspective of gut microbiota. Researchers found that the richness and diversity of fecal microbiota in postoperative colon cancer patients were lower compared to healthy individuals; the Sishen Pill could improve this trend (Tan et al., 2023). For patients undergoing radical resection of colorectal cancer, Sishen Pill could not only alleviate clinical symptoms such as abdominal distension, tiredness, knee pain, waist acid, and cold but also reduce the tumor marker CEA and immune function indexes $CD8^+$ and $CD8^+/CD4^+$ and increase the level of $CD4^+$ (Zhang Y. et al., 2021). It should be pointed out that all three clinical studies mentioned above exist some methodological flaws, for example, not using a double-blind study design, and lacking relevant descriptions about allocation concealment, which to some extent reduces the reliability of clinical trial results; besides, these studies have not adopted the core indicators of clinical research on colon cancer, such as whether it can improve the survival rate of patients? Longer follow-up periods are necessary in the further research. The cell experiment on the molecular mechanism of Sishen Pill treating colon cancer showed that serum medicated with 10% Sishen Pill could downregulate the viability of HCT116 cells and the expression level of glucose transporter 1 (GLUT-1) and promote the activation of enzymes related to aerobic glycolysis, such as hexokinase and fructose-6-phosphate kinase. It could also decrease the overexpression of methyltransferase-like 3 protein and inhibit m^6A RNA methylation, suggesting that Sishen Pill could regulate the glycolysis process by intervening in epigenetic modification, thereby inhibiting the proliferation of colon cancer cells (Jiang et al., 2023). In addition to the direct anticancer effect, *Cao* et al. also carried out research on the molecular mechanism of the Sishen Pill in inhibiting the transformation of colonic inflammatory lesions to colon cancer and found that the formula could downregulate the expression levels of nuclear factor e2-related factor 2 (Nrf2) and cyclooxygenase-2 (COX-2) in colon tissue, reducing the cancer formation rate of dextran sodium sulfate (DSS)-induced colitis mice; both oral and enema administrations had significant curative effects (Cao et al., 2012; Cao, 2013). In short, some studies also indicated the clinical effectiveness and molecular mechanism of Sishen Pill in the treatment of colon cancer; however, higher-quality clinical research and deeper mechanistic explorations are needed.

4 Research progress on metabolites of Sishen Pill in the treatment of IBD and colon cancer

4.1 Psoralea fructus

Zhou et al. studied the pharmacological effects and molecular mechanisms of psoralen, isopsoralen, and bakuchiol in treating IBD and confirmed that psoralen is the core pharmacodynamic substance and that the mechanism might be associated with the homeostasis of

bile acids regulated by farnesoid X receptor (FXR)-fibroblast growth factor 15 (FGF15) pathways (Zhou, 2020). *Ami* et al. applied network pharmacology to identify 13 metabolites with good bioavailability after the oral administration of Psoraleae Fructus; and 11 metabolites could significantly reduce the overproduction of nitric oxide (NO), tumor necrosis factor- α (TNF-α) and interleukin-6 (IL-6) in macrophages induced by lipopolysaccharide (LPS) (Lee et al., 2023). Besides, network pharmacology analysis has also been used to explore molecular mechanism of isobavachalcone, an active metabolite of Psoralea Fructus, in the treatment of IBD, and *Yang* et al. confirmed AKT1, matrix metalloprotein 9 (MMP9), epidermal growth factor receptor (EGFR), insulin-like growth factor 1(IGF1), and steroid receptor coactivator (SRC) were its core targets (Yang et al., 2023a). The identification of effective metabolites is a key focus of botanical drug research, and the above studies is mainly based on the drug concentration in the blood, or bioavailability as the main screening criterion, which may inevitably overlook the indispensable effects of some metabolites with poor bioavailability, and they may exer intestinal protective effect by regulating the gut microbiota or microbial metabolites, rather than entering the peripheral loop. In addition, bakuchiol (Lim et al., 2019) and bavachin (Hung et al., 2019) have been shown to have ideal anti-inflammatory activities, and can they effectively treat IBD? Further research is needed for confirmation.

In recent years, the anticancer activity of various metabolites contained in Psoraleae Fructus has received widespread attention. For example, psoralen can inhibit the invasion and metastasis of human colon cancer HCT-116 cells, and its mechanism may be related to the downregulation of β-catenin, TCF4 proteins, their downstream target genes, vascular endothelial growth factor (VEGF), and MMP-9. Similarly, psoralidin was confirmed to reduce cell viability and enhance cell apoptosis by inhibiting the NF-κB and Bcl-2/BCL-2 associated X (Bax) signaling pathways (Jin et al., 2016); concurrently, it could also trigger oxidative damage-mediated apoptosis via rapidly boosting reactive oxygen species (ROS) generation (Sun et al., 2022). Bakuchiol can activate c-Jun N-terminal kinase (JNK) phosphorylation, induce ROS generation, and regulate the expression of death receptors and various anti-apoptotic proteins (Park et al., 2016). In addition, bavacin and 8-methoxypsoralen activate caspases by suppressing the MAPK and PI3K/AKT pathways, thereby promoting cancer cell apoptosis (Bartnik et al., 2017; Wang et al., 2023a) (see Table 2 for further details).

4.2 Myristica semen

Studies found that myristicin and linalool, two main metabolites in Myristica Semen, could exert anti-inflammatory and antioxidant effects by regulating the expression levels of NF-κ B and Nrf-2 (Tekeli et al., 2018; Ismail Abo El-Fadl and Mohamed, 2022). Compared to using diclofenac alone, the composite formulation of diclofenac and eugenol could better inhibit the nuclear translocation of NF-κB by activating the Nrf2/heme oxygenase-1 (HO-1) signaling pathway, thereby demonstrating better therapeutic effects against UC (Wang et al., 2023c). *Zhang* et al. developed a new phospholipid nanovesicle containing the volatile oil medicine eugenol to treat UC and confirmed that it was more conducive to percutaneous absorption and had better clinical efficacy (Zhang et al., 2020c).

In investigating Myristica Semen in treating colon cancer, *Chen* et al. used a network pharmacology method to screen nine active metabolites including galbacin and 24 core targets (Chen et al., 2023). Piras et al. (2012) identified the anticancer activity of essential oils and myristicin extracted from Myristicae Semen, confirming that they had a significant inhibitory effect on the growth of a colon cancer cell line (undifferentiated Caco-2 cells). In addition, Duan et al. (2020) showed that myristicin could inhibit the proliferation, migration, and invasion of colon cancer cells and induce cellular apoptosis by regulating the mitogen-activated protein kinase (MAPKK/MEK)/extracellular regulated protein kinase (ERK) signaling pathway. In addition, the regulatory effect of linalool on the oxidative response was beneficial for the treatment of colon cancer; it was confirmed that cellular apoptosis was induced by promoting the production of hydroxyl radicals and 4-HNE (a marker of oxidative stress due to increased lipid peroxidation) (Iwasaki et al., 2016). Moreover, some studies focused on the inhibitory effects of eugenol, isoeugenol, and dihydrodiiisoeugenol on colon cancer cells, showing that their anti-cancer mechanisms involve the regulation of metabolic pathways, apoptosis/metastasis-related gene expression, and the activation of endoplasmic reticulum stress-induced inhibition of autophagy (Li et al., 2021a; Ghodousi-Dehnavi et al., 2021; Bilgin et al., 2023). In above studies, Iwasaki et al. (Iwasaki et al., 2016) and Li et al. (Li et al., 2021b) used the tumor xenograft model in their experiments, while evidence from other studies mainly came from cell experiments. Generally speaking, the anti-tumor effects of botanical drugs are not single target or single pathway, and there exist complex interactions between different molecular pathways. It is crucial to explore the overall effects in tumor xenograft animal models, which greatly increases the credibility of research results. Further details are presented in Table 3.

4.3 Euodiae fructus

Studies suggested that NF-κB was the key target of evodiamine in the treatment of IBD, and downregulating NF-κB pathway proteins and inhibiting NOD like receptor heat protein domain related protein 3 (NLRP3) expression could alleviate inflammation-induced cell damage and repair the intestinal mucosal barrier (Shen et al., 2019; Ding et al., 2020). Simultaneously, evodiamine could also promote the regulation of the gut microbiota, especially by increasing the relative abundance of the beneficial bacterium *Lactobacillus* and intestinal acetate content, inhibiting the proliferation of the pathogenic *Escherichia coli*, and reducing plasma LPS and various inflammatory factor levels (Shen et al., 2019; Wang et al., 2020c; Ding et al., 2020). Another study suggested that kelch-like ECH-associated protein 1 (KEAP1) is a key target of rutecarpine, inhibiting the interactions between KEAP1 and Nrf2 by binding to the KEAP1 kelch domain, thereby activating Nrf2, promoting its nuclear translocation, upregulating the Nrf2-mediated antioxidant response, and achieving the pharmacological effect of improving intestinal mucosal injury (Zhang et al., 2020b).

TABLE 2 Pharmacological effects and molecular mechanisms of the metabolites of Psoralea fructus in the treatment of IBD and colon cancer.

Disease	Category	Metabolites	Experimental model	Dosage	Pharmacological action	Molecular mechanism	References
IBD	coumarin	psoralen	C57BL/6	5,10,20 mg/kg	Regulating inflammatory factors: IL-6↓, IL-1β↓, TNF-α↓	Promoting he intestinal bile acid metabolism: the expression of Fxr, Fgf15 and some bile acid transporters are increased	Zhou (2020)
IBD	flavone	corylin	C57BL/6J	10,30,90 mg/kg	Regulating inflammatory factors: IL-6↓, TNF-α↓ Improving the intestinal barrier and blood-brain barrier: ZO-1↓, Occludin↓, Iba1↓(hippocampus)	Regulating the gut microbiota, tryptophan metabolism and 5-HT expression: 5-HT is reduced and 5-HTP is accumulated in the colon due to the binding of corylin and 5-HTDPC; besides, the concentration of tryptophan and the relative abundance of *Bacteroides*, *Escherichia-Shigella*, and *Turicibacter* is decreased and *Dubosiella*, *Enterorhabdus* and *Candidatus Stoquefichus* is increased	Wang et al. (2023f)
IBD	flavone	neobavaisoflavone	*In vivo*: C57BL/6J *In vitro*: T helper 9 (T_H9) cell	*In vivo*: 30 mg/kg *In vitro*: 1 μmol/L	Regulating immune cells: T_H9 cell differentiation↓	Decreasing IL-9 production of $CD4^+$ T cells by targeting PU.1: the expression of PU.1 (T_H9-related transcription factors) is decreased	Guo et al. (2021a)
colon cancer	coumarin	psoralen	HCT 116	20, 40 and 80 μg/mL	Inhibiting the cellular growth and metastasis: proliferation rate↓, migration rate↓, invasive ability↓	Inhibiting β-catenin/TCF4-MMP-9 signaling pathway: the levels of β-catenin, TCF4, VEGF and MMP-9 are decreased	Feng et al. (2021)
colon cancer	coumarin	psoralidin	SW480	5,10,20 μg/mL	Promoting the cellular apoptosis: cell viability↓, apoptosis rate↑, caspase-3 activity↑	Inhibiting the NF-κB and Bcl-2/Bax signaling pathways: the levels of NF-κB p65 and Bcl-2 protein expression are reduced, and Bax protein expression is increased	Jin et al. (2016)
colon cancer	coumarin	psoralidin	HT-29 and HCT-116	5,10,20 μg/mL	Promoting the cellular apoptosis: apoptosis cell rate↑, caspase 3/7 activity↑	Regulating the oxidative stress: the ROS generation is rapidly boosted and in turn triggering the DNA damage, mitochondria membrane potential decrease, and JUN 1/2 activation	Sun et al. (2022)

(Continued on following page)

TABLE 2 (*Continued*) Pharmacological effects and molecular mechanisms of the metabolites of Psoralea fructus in the treatment of IBD and colon cancer.

Disease	Category	Metabolites	Experimental model	Dosage	Pharmacological action	Molecular mechanism	References
colon cancer	flavone	bavachin	*In vitro*: HT-29 and HCT 116	*In vitro*: 20, 30, 40 μmol/L^{-1}	Promoting the cellular apoptosis: cell viability↓, apoptosis rate↑, cleaved PARP↑, cleaved Caspase-3↑	Up-regulating Gadd45a by activating the MAPK signaling pathway: the levels of Gadd45a and the phosphorylation levels of p38/ERK/JNK are upregulated	Wang et al. (2023a)
			In vivo: mouse xenograft model of human colorectal cancer	*In vivo*: 100 mg/kg/d			
colon cancer	monoterpene	bakuchiol	HCT116 and HT-29	1,5,10 μg/mL	Promoting the cellular apoptosis: DR4↑, DR5↑, cFLIP↓, Bcl2↓, XIAP↓, cleaved caspase-3, -8, -9 and PARP↑	Activating the ROS/JUN signaling pathway: the JNK phosphorylation is activated and the ROS generation is induced	Park et al. (2016)
colon cancer	coumarin	8-methoxypsoralen	SW 620	50, 100, 200 μg/mL	Promoting the cellular apoptosis: Bcl2↓, Bax↑, cleaved-3, -8, -9↑	Inhibiting the PI3K/AKT signalling pathway: the phosphorylation of AKT308 is decreased	Bartnik et al. (2017)

Abbreviations: Akt: protein kinase B, BAX: BCL-2, associated X, BCL: B-cell lymphoma, cFLIP: cellular fasassociated death domain-like interleukin-1β-converting enzyme-like inhibitory protein, DR: death receptor, ERK: extracellular regulated protein kinases, FXR: farnesoid X receptor, FGF15: fibroblast Growth Factor 15, 5-HTP: 5-hydroxytryptamine, Iba1:ionized calcium binding adaptor molecule 1, JUN: c-Jun N-terminal kinase, MAPK: mitogen activated protein kinase, MMP-9: Matrix metalloproteinase 9, NF-κB: nuclear factor-kappa B, PARP: Poly-ADP, ribose polymerase, PI3K: phosphatidylinositol 3-kinase, ROS: reactive oxygen species, TCF4: T cell factor 4, XIAP: X-linked inhibitor of apoptosis.

In parallel, Chien et al. found that evodiamine could activate the MAPK signaling pathway and induce cell apoptosis and G2/M arrest by upregulating the phosphorylation levels of ERK and JNK proteins (Chien et al., 2014). Other researchers (Huang et al., 2015), Zhu (Zhu et al., 2021), and Zhang (Zhang et al., 2022) suggested that the anti-inflammatory effects of evodiamine also involved PI3K, STAT3, and NF-κB signaling pathways. In addition, evodiamine can reverse the epithelial-mesenchymal transition of tumor-associated fibroblasts induced by promoting the phosphorylation of Smad2 and Smad3, thereby reducing the migration and invasion abilities of tumor cells (Yang et al., 2019). In addition, Woong et al.'s research confirmed that rutecarpine could also inhibit wingless-type MMTV integration site family (Wnt)/β-catenin-mediated signaling pathway, thereby downregulating the expression levels of epithelial mesenchymal transition biomarkers such as MMP-7, Snail, and N-cadherin (Byun et al., 2022). Li et al. developed an EGFR targeting evodiamine-encapsulated polyamino acid nanoparticles to resolve the issue of low solubility and bioavailability and compared it with the traditional evodiamine formulation. The new preparation significantly increased the cytotoxicity of colon cancer cells and inhibited cell adhesion, invasion, and migration (Li et al., 2019a). Others have designed new metabolites based on evodiamine that have shown promising antitumor activity (Wang et al., 2020a; Li et al., 2020b). It should be pointed out that the dosage of evodiamine is still controversial in different studies. The minimum dose is 1 mg/kg, while the maximum dose is 40 mg/kg. It can be seen that a more detailed dose-response and dose-toxicity relationships of evodiamine needs to be further determined, which is crucial for guiding the clinical application. Further details are presented in Table 4.

4.4 Schisandra chinensis

Multiple schisandrins have definite therapeutic effects in IBD. For example, schisandrin A (Wang et al., 2023b), schisandrin B (Liu et al., 2015), schisandrin C (Kim et al., 2022) and deoxyschizandrin (Yu and Qian, 2021) inhibited the NF-κB nuclear translocation and downstream pro-inflammatory signaling pathway activation; schisandrin B could also regulate AMPK/Nrf2, affect NLRP3 inflammasome, and then alleviate cell pyroptosis and intestinal epithelial damage caused by immune inflammation. In addition, Wang et al. conducted a pharmacokinetic analysis of seven different types of lignin in Schisandrae Chinensis and found that C_{max} and $AUC_{0-\infty}$ of schisandrin were significantly higher than those of other lignans; they also confirmed that it could treat UC by inhibiting the serum/glucocorticoid regulated kinase 1 (SGK1)/NLRP3 pathway and regulating the gut microbiota (Wang et al., 2023d).

Some studies focused on the therapeutic effects of metabolites in Schisandra Chinensis on colon cancer. Casarin et al. found that two types of lignins in Schisandrae Chinensis, (+)-deoxyschisandrin (1) and (−)-gomisin N, could induce the apoptosis of colon adenocarcinoma cells (LoVo); the mechanism was related to the downregulation of cyclin B protein expression, mediating G2/M phase arrest (Casarin et al., 2014). Schisandrin A has also been proven to have a regulatory effect on the cell cycle; it could downregulate the expression of HO-1 protein through the Nrf-2 signaling pathway, thereby reducing the production of reactive oxygen species and nitrogen oxides. However, it could also block NF-κB nuclear translocation and the activation of MAPKs to inhibit inflammatory response (Wan et al., 2019). Some studies focused on the therapeutic potential of Schisandrae Chinensis in inhibiting the

TABLE 3 Pharmacological effects and molecular mechanisms of the metabolites of Myristicae semen in the treatment of IBD and colon cancer.

Disease	Category	Metabolites	Experimental model	Dosage	Pharmacological action	Molecular mechanism	References
IBD	phenylpropanoid	myristicin	SD rat	150 mg/kg/d	Regulating inflammatory factors, oxidative stress and ERS: TNF-α↓, IL-1β↓, COX-2↓, IL-10↑, SOD↑, GPx↑, MDA↓, MPO↓, ERS markers GRP78 and CHOP↓	Regulating NF-κB and Nrf-2/HO-1 signalling pathway: the expression levels of NF-κB are decreased, and Nrf-2 and HO-1 are increased	Ismail Abo El-Fadl and Mohamed (2022)
IBD	phenylpropanoid	linalool	Wistar rat	200 mg/kg/d	Regulating inflammatory factors and oxidative stress: MDA↓, IL-1β↓, IL-6↓,TNF-α↓, COX-2↓, CAT↑	Regulating the NF-κB and Nrf-2: the expression levels of NF-κB and COX-2 are decreased and the expression level of Nrf-2 are increased	Tekeli et al. (2018)
colon cancer	phenylpropanoid	myristicin	HCT116 and LOVO	2 and 5 μg/mL	Promoting the cellular apoptosis: survival rate↓, migration ability↓, invasion rate↓, apoptosis rate↓	Regulating the MEK/ERK signaling pathway: the expression level of E-cad is increased, and p-MEK1/2、p-ERK1/2、CyclinD1、MMP-2、MMP-9 are decreased	Duan et al. (2020)
colon cancer	phenylpropanoids	linalool	*In vitro*: HCT 116	*In vitro*: 1, 10, 100,250, 500, 1,000 μmol L^{-1}	Promoting the cellular apoptosis: cell viability rate↓, cell apoptosis↑, tumor size and weight↓	Inducing the cancer-specific oxidative stress: the production of spontaneous hydroxyl radical is promoted, and 4-HNE, a marker of oxidative stress due to increased lipid peroxidation, is accumulated in the tumor tissue	Iwasaki et al. (2016)
			In vivo:SCID mice xenografted with human cancer cells	*In vivo*: 100 and 200 μg/kg^{-1}			
colon cancer	phenylpropanoids	eugenol	HT-29 cell	500 μg ml^{-1}	Inhibiting the gene expression related to cancer progression: APC and p53 genes↑, KRAS oncogene gene↓, cell survival percentage↓	Regulating metabolic pathways: (1) aminoacyl-tRNA biosynthesis; (2) valine, leucine, and isoleucine biosynthesis; (3)biotin metabolism; (4) steroid biosynthesis; (5) pantothenate and CoA biosynthesis; (6) glycerolipid metabolism; (7) galactose metabolism; and (8) glutamine and D-glutamate metabolism	Ghodousi-Dehnavi et al. (2021)
colon cancer	phenylpropanoids	isoeugenol	HT-29 cell	6.25,12.5,25,50,100 and 200 μg ml^{-1}	Promoting the cellular apoptosis: cell viability↓, migration ability↓, Bax↑, p53↑, caspase-3,7,8,9↑ and the ratio of Bax/Bcl-2↑	Downregulating the expression of cell metastasis related genes: the mRNA expressions of MMP2, MMP9, VEGF and HIF-1αdecreased	Bilgin et al. (2023)
colon cancer	lignan	dehydrodiisoeugenol	*In vitro*: HCT 116 and SW620 cells	*In vitro*: 20, 40, and 60 μmol L^{-1}	Inhibiting the cell growth: cell viability↓, cell inhibition rate↑, and the cell cycle arrest at the G1/S phase is induced	Activating endoplasmic reticulum stress-induced inhibition of autophagy via PERK/eIF2α and IRE1α/XBP-1s/CHOP pathways: protein expression levels of PERK,p-eIF2α, IRE1α, XBP-1s and CHOP are increased	Li et al. (2021a)
			In vivo:CDX and PDX tumor xenograft model	*In vivo*: 40mg/kg^{-1}			

Abbreviations: CAT: catalase activity, CHOP: CCAAT/enhancer-binding protein homologous protein, COX-2: cyclooxygenase-2, ERS: endoplasmic reticulum stress, eIF2α:eukaryotic translation initiation factor 2, ERK: extracellular regulated protein kinases, GPX: glutathione peroxidase, GRP78: glucose-related protein 78, HIF-1α: hypoxia-inducible factor 1α, HO-1: heme oxygenase, IRE1α: inositol-requiring enzyme 1α, IL:interleukin, MDA: malondialdehyde, MPO: myeloperoxidase, MEK: Ras/Raf/MAP, kinase-ERK, kinase, MMP: matrix metalloproteinase, NF-κB: nuclear factor-kappa B, Nrf-2: nuclear erythroid factor, SOD: superoxide dismutase, TNF-α: tumor necrosis factor-α, VEGF: vascular endothelial growth factor, XBP-1s: X Box Binding Protein-1.

10.3389/fphar.2024.1375585

"inflammation-cancer transformation." Li et al.'s experiment confirmed that schisandrin B could inhibit the occurrence of colitis-associated cancer by regulating the gut microbiota and activating the phosphorylation of focal adhesion kinase and its downstream kinase (Li et al., 2019b). Pu et al. (2021) found that the pharmacological effect of schisandrin B in inhibiting the proliferation and metastasis of colitis-related tumors was related to the downregulation of silencing regulatory protein 1(SIRT1) and inducing the expression of smad ubiquitination regulatory factor 2 (SMURF2) (Pu et al., 2021). The anti-tumor activity of some non-specific active substances of Schisandrae Chinensis, such as citral, cannot be ignored either; the experiment by Sheikh et al. confirmed that citral could inhibit the proliferation of HCT116 and HT29 cells in a dose-dependent and time-dependent manner; its mechanism was related to mediating the phosphorylation of p53 protein and promoting the mitochondrial release of apoptogenic factors (Sheikh et al., 2017). See Table 5 for more details.

5 Discussion on the common molecular mechanism of Sishen Pill in treating IBD and colon cancer

5.1 Regulating inflammation related signaling pathways

Chronic inflammation is not only an important feature of IBD but also a driver of the onset and development of colon cancer. Studies have found that chronic intestinal inflammation can cause DNA double chain breaks, oxidative stress damage, and epigenetic changes in intestinal epithelial cells, upregulate oncogenes, downregulate cancer suppressor genes, and promote the occurrence of dysplasia and cancer (Shah and Itzkowitz, 2022). Regulation of the inflammatory response is the core mechanism of Sishen Pill in treating IBD and inhibiting inflammation-cancer transformation, which involves multiple inflammation-related signaling pathways (Figure 2).

Many mechanistic studies on Sishen Pills focus on the regulatory effects of the NF-κB pathway (Wang et al., 2019d; Ge et al., 2022; Zhaohua et al., 2022). NF-κB is a classical key inflammatory modulator. LPS and other pro-inflammatory factors activate TLRs, induce NF-κB nuclear translocation, and regulate the gene expression of a variety of inflammatory mediators. In particular, LPS can promote the increase of TNF-α and multiple interleukins that act on macrophages to produce many inflammatory mediators and continuously induce NF-κB nuclear translocation to form a positive feedback cascade amplification effect. The basic activity of NF-κB is necessary for the normal proliferation and differentiation of cells to maintain the immune balance of epithelial tissue and inhibit the interference of inflammation on pithelial tissue homeostasis (Iacobazzi et al., 2023). Recently, a number of studies have focused on the role of NF-κB in promoting tumor cell apoptosis. As a landmark cell cycle protein, *cyclinD1* is also the target gene of NF-κB. The continuous activation of NF-κB can initiate cyclinD1 transcription, promote the G1/G0 phase-to-S phase transition, and lead to abnormal cell proliferation and cancer. Thus, inhibiting NF-κB activation or blocking its downstream key proteins is considered an important target for developing new antitumor drugs (Taniguchi and Karin, 2018; Deka and Li, 2023).

The pharmacological effects of the Sishen Pill in the treatment of IBD and colon cancer are also related to the regulation of the MAPK and PI3K/Akt signaling pathways. Extracellular regulated protein kinases (ERK)1/2, c-JNK, p38, and ERK5 are the main members of the MAPK family, and there is also extensive cross talk between different pathways: ERK mainly regulates cell growth and differentiation; JNK and p38 play more important roles in stress responses such as inflammation and cell apoptosis; and ERK5 can regulate pathological processes such as cell cycle acceleration and endothelial cell proliferation caused by growth factors and stress (Ronkina and Gaestel, 2022). In general, the MAPK signaling pathway can mediate the release of TNF-α, IL-1, IL-6, IL-8, and other inflammatory factors, cell apoptosis, and neutrophil activation, induce the expression of intracellular nitric oxide, improve the activity of intracellular inducible nitric oxide synthase, and induce the occurrence and development of IBD and colon cancer (Yong et al., 2009). In addition, PI3K is a key target that is closely related to inflammation and tumor development. In the inflammatory state, PI3K phosphorylates phosphatidylinositol 4,5-bisphosphate (PIP2) to generate phosphatidylinositol-3,4,5-triphosphate (PIP3), recruiting downstream proteins such as Akt. The activated AKT subsequently phosphorylates multiple downstream substrate proteins. PI3K can also promote the activation of NF-κB and regulate the inflammatory response by phosphorylating and inhibiting IκB kinase (IKK); it can also regulate biological processes such as cell proliferation, survival, apoptosis, and metabolism and then promote tumor progression. Briefly, it can 1) act on mammalian rapamycin target protein complex 1 (mTORC1) to promote protein synthesis and cell growth; 2) phosphorylate forkhead box O (FOXO) transcription factors, inhibit its transcriptional activity, and affect cell cycle, apoptosis, and metabolism; 3) inhibit the activity of glycogen synthase kinase 3 (GSK3) and regulate glycogen synthesis and cell cycle; 4) phosphorylate and activate the pro-apoptotic protein Bad, making it unable to bind to Bcl-2 or Bcl-XL, and thus reducing the occurrence of normal cell apoptosis (Mayer and Arteaga, 2016; Wang et al., 2023e). In the above study, Sishen Pill improved intestinal inflammatory factors, immune cell disorders, and a series of symptoms of IBD by downregulating the expression of key proteins in the MAPK (Zhao et al., 2013) and PI3K/Akt (Ge et al., 2020; Zhang et al., 2021c; Liu et al., 2021; Liu et al., 2022) signaling pathways, and its active metabolites bavachin (Wang et al., 2023a), myristicin (Duan et al., 2020), evodiamine (Chien et al., 2014), schisandrin B (Jiang et al., 2015), 8-methoxypsoralen (Bartnik et al., 2017), and schisandrin B (Dai et al., 2018). Consequently, the Sishen Pill could inhibit the progression of colon cancer by regulating the MAPK and PI3K pathways.

The NLRP3 inflammasome and Wnt signaling pathways affect pyroptosis and cell differentiation/apoptosis, respectively, and are potential targets for regulating colon inflammation-cancer transformation. NLRP3 inflammasome is composed of NLRP3, apoptosis-associated speck-like protein containing CARD (ASC) and effector pro-caspase-1, and can affect the occurrence and development of IBD and even cancer via regulating the maturation, secretion, and pyroptosis of IL-1β and IL-18. Studies

TABLE 4 Pharmacological effects and molecular mechanisms of the metabolites of Euodiae fructus in the treatment of IBD and colon cancer.

Disease	Category	Metabolites	Experimental model	Dosage	Pharmacological action	Molecular mechanism	References
IBD	alkaloid	evodiamine	C57BL/6 mice	20, 40 and 80 mg/kg	Regulating inflammatory factors and oxidative stress: IL-6↓, IL-1β↓, TNF-α↓, MPO↓	1. Regulating NF-κB signal and NLRP3 inflammasome: the levels of p-p65, p-IκB, NLRP3, ASC, Caspase-1 and IL-1βare decreased 2. Regulating the gut microbiota and intestinal barrier: the expression levels of ZO-1 and occludin are increased, the concentration of LPS is decreased, and the abundance of *Escherichia coli* and *Lactobacillus* is re-balanced	Shen et al. (2019)
IBD	alkaloid	evodiamine	*In vitro*: Human THP-1 cells *In vivo*: C57BL/6 mice	*In vitro*: 10 μmol/L *In vivo*: 20, 40 and 60 mg/kg	Regulating inflammatory factors: IL-1β↓, IL-18↓	Inducing autophagosome-mediated degradation of inflammasome via inhibiting NLRP3 and NF-κB pathways: the protein expression level of P62 is decreased, and LC3-II is increased; meanwhile, expression levels of key pathway proteins NLRP3, cleaved-caspase-1, ASC, NF-κBp65 and IκB are decreased	Ding et al. (2020)
IBD	alkaloid	evodiamine	SD rat	20 mg/kg	Regulating inflammatory factors: TNF-α↓, IL-6↓, IL-1β↓, IL-10↑	Regulating the gut microbiota, intestinal barrier and circulating metabolite levels: the abundance of *Lactobacillus acidophilus*, the concentration of protective acetate production and the expression level of colonic claudin-1 is increased, and the levels of branched chain amino acids and aromatic amino acids are regulated	Wang et al. (2020c)
IBD	alkaloid	rutaecarpine	*In vitro*: HCT 116 cell and primary intestinal epithelial cell *In vivo*: C57BL/6 mice	*In vitro*: HCT 116 cell: 2.5, 5 and 10 μmol/L; primary intestinal epithelial cell: 10 μmol/L and 20 μmol/L *In vivo*: 80 mg/kg	Regulating inflammatory factors: Cox2↓, Lcn2↓, TNF-α↓, IL-6↓	Inhibiting KEAP1-NRF2 interaction and upregulating NRF2-mediated antioxidant response: KEAP1 kelch domain is bound and NRF2 nuclear translocation is increased; meanwhile, H_2O_2-induced cytotoxicity and intracellular ROS accumulation are suppressed	Zhang et al. (2020b)
IBD	terpenoid	limonin	*In vitro*: RAW 264.7 *In vivo*: C57BL/6 mice	*In vitro*: 12.5, 25 and 50 pg/mL *In vivo*: 25,50,100 mg/kg	Regulating inflammatory factors: TNF-α↓, IL-1β↓, IL-6↓, COX-2↓, iNOS↓	Inhibiting PERK-ATF4-CHOP pathway of ER stress and NF-κB signaling: expression levels of BIP, p-PERK, p-eIF2α, ATF-4, CHOP are decreased, and the nuclear translocation of NF-κB is inhibited	Song et al. (2021)

(Continued on following page)

10.3389/fphar.2024.1375585

TABLE 4 (*Continued*) Pharmacological effects and molecular mechanisms of the metabolites of Euodiae fructus in the treatment of IBD and colon cancer.

Disease	Category	Metabolites	Experimental model	Dosage	Pharmacological action	Molecular mechanism	References
IBD	terpenoid	limonin	*In vitro*: NCM460	*In vitro*: 2.5, 5, 10, 20, 40, 80 and 160 μg/mL	Regulating inflammatory factors: TNF-α↓, IL-6↓, IL-10↑	Regulating STAT3/miR-214 signaling pathway: expression levels of pSTAT3 and miR-214 are reduced and the expression levels of PTEN and PDLIM2 are restored	Liu S. et al. (2019)
			In vivo: C57BL/6 mice	*In vivo*: 40, 80 and 160 mg/kg			
colon cancer	alkaloid	evodiamine	HCoEpiC and CCD-18Co cells	16,160 and 320 nmol/L	Inhibiting the epithelial mesenchymal transition of colon epithelial cells: the tumour-associated fibroblasts-induced tumour-associated fibroblasts-like phenotype is reversed and their migration is inhibited	Mediating the expression of phosphorylated Smad2/3: the expression of ZEB1/Snail is downregulated, and the expression of phosphorylated Smad2/3 is upregulated, meanwhile, the ratios of pSmad2/Smad2 and pSmad3/Smad3 are increased	Yang et al. (2019)
colon cancer	alkaloid	evodiamine	COLO205 and HT-29 cells	2.5,5 and 10 μmol/L	Promoting the cellular apoptosis and G2/M arrest: cleaved-3 and -PARP↑, cycB1↑, cdc25c↑	Promoting the activation of MAPK signaling pathway: the protein phosphorylation levels of ERK and JNK are increased	Chien et al. (2014)
colon cancer	alkaloid	evodiamine	C57BL/6 mice	40 mg/kg	Regulating inflammatory factors and inhibiting the tumor development: TNF-α↓, IL-10↑, IL-6↓, IL-1β↓, the number and size of tumors↓	Regulating the gut microbiota and their metabolites: SCFAs-producing bacteria is enriched, the levels of the pro-inflammatory bacteria is reduced, and some microbiota metabolites (especially the tryptophan related metabolites) are regulated	Wang et al. (2021)
						Improving the intestinal barrier via multiple pathways: expression levels of occludin, ZO-1 and E-cadherin are increased, and some gene expressions of Wnt signaling pathway, Hippo signaling pathway and IL-17 signaling pathway are regulated	
colon cancer	alkaloid	evodiamine	*In vitro*: LoVo cells	*In vitro*: 0.25,0.5,1,2,4 μg/mL	Inhibiting the cell proliferation and promoting the cellular apoptosis: PCNA↓, apoptosis rate↑, caspase-3↑	Decreasing HIF-1α expression though IGF-1/PI3K/Akt signaling: the phosphorylation of Akt1/2/3, HIF-1αand IGF-1 are downregulated	Huang et al. (2015)
			In vivo: athymic nude mice	*In vivo*: 5, 10 and 20 mg/kg			
colon cancer	alkaloid	evodiamine	*In vitro*: HCT116 cells	*In vitro*: 0.5, 1 and 2 μg/mL	Promoting the cellular apoptosis: Bcl-2↓, Bad↑, apoptosis rate↑	Regulating BMP9 and HIF-1α/p53 signaling pathway: the expression levels of BMP9 and HIF-1αare upregulated and the phosphorylation of p53 is increased	Li et al. (2020a)
			In vivo: athymic nude mice	*In vivo*: 10 mg/kg			

(Continued on following page)

10.3389/fphar.2024.1375585

TABLE 4 (*Continued*) Pharmacological effects and molecular mechanisms of the metabolites of Euodiae fructus in the treatment of IBD and colon cancer.

Disease	Category	Metabolites	Experimental model	Dosage	Pharmacological action	Molecular mechanism	References
colon cancer	alkaloid	evodiamine	HT29, HCT15 and SW480 cells	200 and 500 nmol/L	Inhibiting the cell proliferation and inducing G2/M arrest: number and volume of tumor ↓, G2/M accumulation↑	Suppressing the gene expression of controlling the proliferation of cancer stem cells: key genes of the Notch and Wnt signaling pathways are regulated	Kim et al. (2019)
colon cancer	alkaloid	evodiamine	SW 480 cells	5, 10 and 20 μg/mL	Promoting the cellular apoptosis: cell viability rate↓, cell apoptosis↑	Activating the autophagy: the protein expression levels of LC3 II and Beclin 1 are increased	Wang et al. (2019b)
colon cancer	alkaloid	evodiamine	*In vitro*: HCT116 cells	*In vitro*: 6 μmol/L	Inhibiting the tumor growth: survival ratio↓, number and volume of tumor↓	Regulating the gut microbiota: the relative abundance of *Campylobacter*, *Bifidobacterium* and *Lactobacillus* is increased, and *Enterococcus faecalis* and *Escherichia coli* are decreased	Zhu et al. (2021)
			In vivo: C57 mice	*In vivo*: 10 mg/kg		Downregulating the inflammatory IL6/STAT3/P65 signaling pathway: the expression of IL-6, p-STAT3, p-65 and the ratio of p-STAT3/STAT3 are decreased	
colon cancer	alkaloid	evodiamine	*In vitro*: HCT116 cells	*In vitro*: 0,1 and 5 μmol/L	Promoting the cellular apoptosis: cell viability↓, cleaved PARP↑, cleaved caspase-3↑	Targeting HSP70 and inactivating the HSP system: the N-terminal ATP-binding pocket of HSP70 is bound and causing its ubiquitin-mediated degradation	Hyun et al. (2021)
			In vivo: SCID mice xenografted with human cancer cells	*In vivo*: 20 mg/kg			
colon cancer	alkaloid	evodiamine	*In vitro*: SW480 cells	*In vitro*:100 and 200 μmol/L	Inhibiting inflammatory factors and inducing G2/M arrest: IL-1β↓, IL-2↓, IL-6↓, IL-17↓, IL-22↓, TNF-α↓, IL-15↑; G2/M accumulation↑	Inhibiting NF-κB signaling pathway: the phosphorylation levels of NF-κB, IKKα/β, IκBα and the expression level of S100a9 is decreased	Zhang et al. (2022)
			In vivo: C57BL/6	*In vivo*: 10 mg/kg			
colon cancer	alkaloid	evodiamine	*In vitro*: Lovo human colon cancer cells	*In vitro*: 7.5, 15, 30 and 60 μmol/L	Inducing the cellular apoptosis and S phase arrest: procaspase-3,8,9↓, caspase-3,8,9↑, Bax↑, Bcl-2/Bax ratio↓; cyclinA↓, cyclinB1↓, CDK1↓, CDK2↓,cdc25c↓	N/A	Zhang et al. (2010)
			In vivo: human colon carcinoma lovo xenograft mice	*In vivo*: 1 mg/kg			
colon cancer	alkaloid	evodiamine	*In vitro*: LoVo cells	*In vitro*:1,2,8 μg/mL	Inhibiting the cellular activity: cell viability, invasion and metastasis↓, tumor volume↓	Targeting EGFR protein to exert anti-tumor effects: protein expression levels of EGFR, VEGF, and MMP-2 are decreased	Li et al. (2019a)
			In vivo: BALB/c male athymic nude mice	*In vivo*: 4 mg/kg			
colon cancer	alkaloid	rutaecarpine	*In vitro*: RKO, SW480, HCT-15, HCT116, and Ls174T	*In vitro*: 5,10 and 20 μmol/L	Induced G0/G1 cell cycle arrest and apoptotic cell death: total cell death↓, migration rate↓, invasion rate↓, prolification rate↓, tumor volume and weight↓, G0/G1 accumulation↑	Inhibiting the Wnt/β-catenin-mediated signaling pathway: the expression levels of β-catenin and Wnt/β-catenin signaling pathway related proteins c-Myc, survivin, and cyclin D1 are downregulated; epithelial mesenchymal transition biomarkers such as MMP-7, Snail, and N-cadherin are downregulated	Byun et al. (2022)
			In vivo: xenograft nude mouse model	*In vivo*: 10 and 30 mg/kg			

(Continued on following page)

10.3389/fphar.2024.1375585

TABLE 4 (*Continued*) Pharmacological effects and molecular mechanisms of the metabolites of Euodiae fructus in the treatment of IBD and colon cancer.

Disease	Category	Metabolites	Experimental model	Dosage	Pharmacological action	Molecular mechanism	References
IBD	terpenoid	limonin	Balb/c mice	50 mg/kg	Inhibit the initiation of colitis-associated-cancer: TNF-α↓, prostaglandin E2↓, tumor incidence/number↓	Regulated Nrf2, SOD2 and the immunophenotyping of lymphocytes: the expression levels of Nrf2 and SOD 2 are increased; T cells (CD4 and CD8) and B cells (CD19) in spleen tissues are increased, and the CD335 (natural killer cells) is restored to normal level	Ishak et al. (2021)

Abbreviations: ATF2: activating transcription factor 2, Akt: protein kinase B, ASC: apoptosis-associated speck-like protein containing CARD, BMP9: bone morphogenetic protein-9, CHOP: CCAAT/enhancer-binding protein homologous protein, COX-2: cyclooxygenase-2, EGFR: epidermal growth factor receptor, ERK: extracellular regulated protein kinases, eIF2α:eukaryotic translation initiation factor 2, HIF-1α: hypoxia-inducible factor 1α, HSP: heat shock protein, IGF-1: insulin-like growth factor 1, iNOS:inducible nitric oxide synthase, IL: interleukin, IκB: inhibitor of NF-κB, JNK: c-Jun N-terminal kinase, Keap1: Kelch-like ECH-associated protein 1, LPS: lipopolysaccharide, LCN2: lipocalin-2, MAPK: mitogen activated protein kinase, MPO: myeloperoxidase, NF-κB: nuclear factor-kappa B, NLRP3: NOD, like receptor heat protein domain related protein 3, N/A: not applicable, Nrf2: NF-E2-related factor 2, PI3K: phosphatidylinositol 3-kinase, PCNA: proliferating cell nuclear antigen, PARP: poly ADP-ribose polymerase, PERK: Protein kinase R (PKR)-like endoplasmic reticulum kinase, PTEN: phosphatase and tensin homolog, SATA: signal transducer and activator of transcription, SCFA: short-chain fatty acid, SCID: severe combined immunodeficient, SOD: superoxide dismutase, STAT: signal transducer and activator of transcription, S100a9: S11 calcium binding protein A9, TNF-α: tumor necrosis factor-α, VEGF: vascular endothelial growth factor, ZO-1: zonulin-1.

found that for IBD patients during the active period, the production of IL-1β and IL-18 and the activity of caspase-1 increase, thereby mediating the occurrence of intestinal cell apoptosis (Qi et al., 2021). Cell apoptosis is an important pathological basis for the transformation from inflammation to cancer and can induce the release of pro-inflammatory cytokines and promote tumor infiltration into local tissues, thus increasing the risk of tumor occurrence and metastasis (He et al., 2024). In addition, the Wnt/β-catenin signaling pathway has been confirmed to influence the differentiation fate of cell development to a certain extent, affecting cancer cell proliferation, stemness, apoptosis, autophagy, and metabolism. The modification and degradation of β -catenin are key events in the occurrence and development of colon cancer (Zhao et al., 2022). The research indicates that Sishen Pills (Zhao et al., 2019) and their active metabolites, schisandrin B (Zhang et al., 2021a), schisandrin (Wang et al., 2023d), evodiamine (Kim et al., 2019; Shen et al., 2019; Ding et al., 2020), and rutaecarpine (Byun et al., 2022) could affect cell fate by regulating the NLRP3 and Wnt signaling pathways, thus offering a therapeutic role in IBD and colon cancer.

5.2 Inhibiting the oxidative stress

Research has shown that during chronic inflammation, innate immune cells such as macrophages produce large amounts of reactive oxygen species (ROS) and reactive nitrogen species (RNS), leading to the aggravation of oxidative stress. During the active phase of IBD, the expression of ROS in the intestinal mucosa increases, and the subsequent reaction of ROS with DNA can lead to chromosomal breakage, carcinogenesis, and tumor cell proliferation (Wu and Liu, 2022). Regulating the Nrf2/HO-1 pathway may be a way to treat IBD with Sishen Pills (Zhang et al., 2021b), involving their active metabolites such as myristicin (Ismail Abo El-Fadl and Mohamed, 2022), linalool (Tekeli et al., 2018), rutaecarpine (Zhang et al., 2020b) and schisandrin B (Zhang et al., 2021a). Under normal physiological conditions, the Nrf2 in cells binds to the kelch-like ECH-associated protein 1 (Keap1) in the cytoplasm and remains in a steady state; when Keap1 receives an oxidative stress signal, it can release Nrf2 and then transfer it to the nucleus and upregulate the expression of downstream antioxidant proteins, such as HO-1 (Ibrahim et al., 2023). At the same time, HO-1 can also block the NF-κB activation and downregulate the transcription of inflammatory factors and chemokines by inhibiting the production of cytokines and ROS (Wang and He, 2022); this may contribute to the treatment of IBD by inhibiting intestinal inflammation-cancer transformation (Lu et al., 2023).

As the α subunit of hypoxia inducible factor-1 (HIF-1), HIF-1α mediates the adaptive response of cells to a hypoxic environment. In general, HIF-1 is activated under cellular hypoxia; it can activate multiple target genes involved in regulating the cellular redox status to reduce ROS generation; it can also regulate the expression levels of mitochondria-specific genes to adapt to hypoxic environments and improve mitochondrial function. As the above studies showed, the anti-colon cancer effects of evodiamine (Huang et al., 2015; Li et al., 2020a) and isoeugenol may be mediated by HIF-1α. The activation of HIF-1α and its signaling pathway has bidirectional regulatory effects. Studies have confirmed that moderate activation can

promote cell survival and increase the protective effect against injury stimuli, whereas excessive activation can aggravate damage to intestinal cells (Taylor and Colgan, 2007). Due to the abnormal vascular microenvironment and inadequate local blood and oxygen supply to the tumor, hypoxia is a common feature of colon cancer; HIF-1α in the activated state can supply energy to tumor cells by upregulating glucose transporters and glycolysis related enzymes, helping cells adapt to the hypoxic environment. Previous studies confirmed that regulating aerobic glycolysis is an important factor for Sishen Pill to treat colon cancer (Zhang et al., 2021d; Jiang et al., 2023); whether it is related to HIF-1α remains to be determined. In addition, the activation of HIF-1α can also promote the tumor angiogenesis and metastasis by up regulating the expression of VEGF and MMP. As the above studies showed, several effective metabolites of Sishen Pill, such as psoralen, isoeugenol, and evodiamine, can downregulate the expression of VEGF and MMP proteins (Li et al., 2019a; Feng et al., 2021; Bilgin et al., 2023), thus promoting the apoptosis and having a therapeutic effect in colon cancer (Figure 3A).

5.3 Regulating the mitochondrial autophagy

Research has shown that impaired autophagy can disrupt the function of intestinal epithelial cells and affect innate and adaptive immune responses, ROS production, and endoplasmic reticulum stress (ERS), ultimately promoting the occurrence or progression of IBD (Alula and Theiss, 2023). Antimicrobial peptides secreted by intestinal Paneth cells are an important component of the intestinal mucus layer; however, owing to autophagy dysfunction, patients would experience decreased secretion of defensins and lysozymes by Paneth cells, leading to a weakened ability of the intestinal mucosa to resist the colonization of bacteria in the gut, hindering bacterial clearance, and damaging the intestinal mucosal barrier (Cray et al., 2021). At the same time, autophagy also participates in the mucus secretion and degradation metabolism of goblet cells, maintaining a stable balance of interactions between the intestinal mucosa and the gut microbiota (Naama et al., 2023). In the pathological environment of IBD, sustained inflammatory stimulation can lead to protein imbalance and abnormal folding in the lumen of the endoplasmic reticulum, exacerbating ERS. Autophagy can reduce the negative effects of ERS by clearing abnormal proteins and damaged organelles. Previous studies found that the Sishen Pill (Yu et al.) and its metabolites, myristicin (Ismail Abo El-Fadl and Mohamed, 2022) and evodiamine (Ding et al., 2020) promote autophagy and exert a positive influence on downregulating intestinal inflammatory responses.

Other studies have shown that dehydrodiisoeugenol (Li et al., 2021a) and evodiamine (Wang et al., 2019b) promote tumor cell apoptosis and exert anti-colon cancer effects by activating autophagy. Current research suggests that autophagy has a dual role in cancer occurrence. Autophagy is a surveillance system in normal cells that removes damaged organelles and aggregated proteins through lysosomes, consequently reducing DNA damage and protecting cells from malignant transformation (Yamazaki et al., 2021). Clinical studies have shown that a lack of autophagy-related proteins such as LC-3II, ATG5, and Beclin 1 can indicate poor prognosis in colon cancer patients (Choi et al., 2014). Autophagy can also provide key nutrients for tumor growth and metabolism and support tumor formation by inhibiting apoptosis (Galluzzi et al., 2015). Autophagy plays different roles in the different stages of malignant tumor development; a deeper exploration of the pharmacological mechanism of inflammation-cancer transformation as a whole is needed (Figure 3B).

5.4 Regulating intestinal immune cells

The regulatory effects of Sishen Pill on intestinal immune cells are also important for inhibiting the progression of IBD inflammation and its transformation into colon cancer. Taking Tregs as an example, the number of Tregs in the inflammatory mucosa of patients with IBD often shows a compensatory increasing trend, but the degree of increase is insufficient to control mucosal inflammation, leading to a relatively insufficient state (Hovhannisyan et al., 2011). Peripheral blood cell analysis has shown that the number of Tregs decreases, and the number of pro-inflammatory Th17 cells increases in IBD patients (Eastaff-Leung et al., 2010). Animal experiments have shown that the adoptive transfer of Tregs can alleviate enteritis by inhibiting Th1 and Th17 inflammatory responses, further confirming the regulatory effects of Tregs on intestinal inflammation (Boschetti et al., 2017). Multiple studies have shown that Sishen Pill can upregulate Tregs while downregulating the proportion of Th17 cells, thereby inhibiting the progression of IBD (Liu et al., 2016; Wang et al., 2022b; Huang et al., 2022). Schisandrin B upregulates the expression of forkhead box protein P3 (FoxP3) and promotes Treg proliferation and differentiation, regulating the intestinal immunity of IBD (Liu et al., 2015). The possible role of Tregs in treating intestinal tumors has also received widespread attention, but there is still debate over how Tregs affect the occurrence and progression of tumors. Some studies suggest that Tregs can lead to tumor growth and deterioration by inhibiting anti-tumor immune responses (Saito et al., 2016), associated with poor prognosis of the disease; however, further research is needed to investigate the effect of the Sishen Pill on Tregs in colon cancer models.

Memory T cells (Tms) are a crucial part of inflammatory immune responses. Tms can usually be divided into three main groups: central memory T cells (Tcm), effective memory T cells (Tem), and tissue-resident memory T cells (Trm). Zhao et al. found that the specific activation of Tm can prevent the recurrence of Crohn's disease (Zhao et al., 2020). Two studies found that Sishen Pills can increase the level of Tcm cells and inhibit intestinal inflammatory factors through the PI3K/Akt and JAK/STAT5 pathways (Ge et al., 2020; Wang et al., 2022a). In addition, Tcm has self-renewal and replication capabilities, can recognize tumor antigens, and exerts long-lasting anti-tumor effects (Wang et al., 2020d). However, there is currently no relevant report on the Sishen Pill and its active metabolites in treating colon cancer by regulating Tcm; a deeper understanding of the pharmacological mechanisms is urgently needed.

JAK/STAT is one of the central communication nodes of cell function and is essential for initiating innate immunity, coordinating adaptive immune mechanisms, and regulating

TABLE 5 Pharmacological effects and molecular mechanisms of the metabolites of Schisandra chinensis in the treatment of IBD and colon cancer.

Disease	Category	Metabolites	Experimental model	Dosage	Pharmacological action	Molecular mechanism	References
IBD	lignan	schisandrin A	SD rats	20, 40 and 80 mg/kg	Regulating the oxidative stress factors: GSH-P_X↑, SOD↑, eNOS↑, iNOS↑, T-AOC↑; NO↓, MPO↓	N/A	Zhang et al. (2020a)
IBD	lignan	schisandrin A	Kunming mice	20, 40 and 80 mg/kg	The symptoms of colitis and intestinal inflammation are improved	Inhibiting NF-κB/COX-2 pathway: the mRNA and protein expression of NF-κB and COX-2 are decreased	Wang et al. (2023b)
IBD	lignan	schisandrin B	SD rat	20, 40 and 80 mg/kg	The symptoms of colitis and intestinal inflammation are improved	Regulating the expression level of RORγt and FoxP3: the protein and gene expression levels of FoxP3 increased, and RORγ are reduced	Chen and Chen (2018)
IBD	lignan	schisandrin B	*In vitro*: HCT-116 cells	*In vitro*: 40 μmol/L	Regulating inflammatory factors: TNF-α↓, IL-6↓, IL-1β↓, IFN-γ↓	Inhibiting NF-κB and MAPKs signal pathways: the expression levels of pIκBα, NF-κBp65, MAPK, JUN and ERK are decreased	Liu et al. (2015)
			In vivo: C57BL/6 mice	*In vivo*: 10 mg/kg			
IBD	lignan	schisandrin B	C57BL/6 mice	10, 40 and 100 mg/kg	Regulating inflammatory factors: TNF-α↓, IL-6↓, IL-18↓, IL-1β↓	Regulating the pyroptosis via AMPK/Nrf2/NLRP3 inflammasome: the protein expression level of NLRP3, pro-caspased and ROS-induced mitochondrial damage are decreased, and pAMPK/AMPK and Nrf2 are increased	Zhang et al. (2021a)
IBD	lignan	schisandrin B	*In vitro*: CACO2 and HCT116 cells	*In vitro*: 6.25 μmol/L and 12.5 μmol/L	1. Regulating inflammatory factors: TNF-α↓, IL-1β↓, IL-6↓,IL-12↓, IL-23↓	1. Activating FAK and its downstream signal: the ratio of p-FAK/FAK, p-JUN/JUN, p-P38/P38, p-AKT/AKT and p-ERK/ERK are increased	Li et al. (2019b)
			In vivo: C57BL/6 mice	*In vivo*: 15 and 30 mg/kg	2. Protecting the intestinal epithelial barrier: FITC-dextran permeabilization↓, E-cadherin↑, Occludin↑	2. Regulating the gut microbiota: the relative abundance of *Rhodospirillaceae*, *Mollicutes*, *Gastranaerophilales* and *Lachnospiraceae* is decreased, and the relative abundance of *Bacteroide*, *Rikenellaceae RC9* gut group, *Odoribacter laneus* YIT 12061 and *coprostanoligenes* is increased	
					3. Inhibit the initiation and promotion of colitis-associated-cancer		
IBD	lignan	schisandrin	C57BL/6 mice	20, 40 and 80 mg/kg	Regulating inflammatory factors: TNF-α↓, IL-1β↓, IL-18↓, IL-6↓	1. Inhibiting the SGK1/NLRP3 signaling pathway: the protein expression level of NLRP3, Caspase-1, SGK1 are decreased	Wang et al. (2023d)
						2. Regulating the gut microbiota: the relative abundance of *Lactobacilli* spp is increased, the relative abundance of *Bacteroides* decreased, and the conversion of primary bile acids to secondary bile acids is promoted	

(Continued on following page)

TABLE 5 (*Continued*) Pharmacological effects and molecular mechanisms of the metabolites of Schisandra chinensis in the treatment of IBD and colon cancer.

Disease	Category	Metabolites	Experimental model	Dosage	Pharmacological action	Molecular mechanism	References
IBD	lignan	schisandrin C	HT-29 and Caco-2 cells, intestinal organoid, *C. elegans* wild-type N2 strain	*In vitro*: 5, 10 and 20 μmol/L *In vivo*: 10, 25, 50 and 100 μmol/L	Protecting the intestinal epithelial barrier: FITC-dextran permeabilization↓, MLCK and p-MLC↓, ZO-1↑, Occludin↑	Inhibiting NF-κB and p38MAPK/ ATF2 pathways: the phosphorylation of NF-κB, p38 MAPK, and ATF2 are decreased, and the nuclear localization of NF-κB and ATF2 are inhibited	Kim et al. (2022)
IBD	lignan	deoxyschizandrin	SD rat	20, 40 and 80 mg/kg	Regulating inflammatory factors and oxidative stress factors: TNF-α↓, IL-1β↓, IL-6↓, SOD↑, MDA↓, CAT↑ Inhibiting the apoptosis: Caspase-3↓, Bax↓, Bcl-2↑	Inhibiting the TLR4/NF-κB signaling pathway: the expression levels of TLR4, MyD88, and NF-κB are decreased	Yu and Qian (2021)
colon cancer	lignan	schisandrin A	CRC cell lines DLD1, RKO, SW480, SW620 and normal human colon epithelial cell line CCD 841 CoN	50, 75, 100, and 150 μmol/L	Inducing the cellular apoptosis and G0/G1 phase arrest: p-Rb (S807/811)↓, Cyclin D1↓, Cdk4↓, Cdk6↓, cleaved-PARP↑, cleaved-Caspase3↑, Bcl-2↓	Inhibiting heat shock factor 1: the induction of HSF1 target proteins such as HSP70 and HSP27 inhibited	Chen et al. (2020a)
colon cancer	lignan	schisandrin A	HT 29 cells	0.25, 0.5 and 1 μmol/L	Regulating oxidative stress factors, inflammatory factors and inducing S and G2/M phase arrest: ROS↓, nitrite production↓, CAT↓, SOD↓, GPx↓, IL-8↓, S-phase and G2/M phase cell cycle arrest	Inhibiting Nrf-2/HO-1 signalling pathway, the translocation of NF-κB and the activation of MAPKs: the expression levels of HO-1, p-p38, p-ERK and p-JNK are decreased, the nuclear transcription of Nrf2 is activated and NF-κB is inhibited	Wan et al. (2019)
colon cancer	lignan	schisandrin B	SW480	20,40 and 80 μmol/L	Promoting the cellular apoptosis: proliferation inhibition rate↑, cell apoptosis↑, invasion rate↓	Regulating the p38MAPK signaling pathway: the protein expression levels of p-p38 and p-p53 are increased	Jiang et al. (2015)
colon cancer	lignan	schisandrin B	SW620	0.1, 1 and 10 mg/L	Inhibiting the cellular proliferation and migration: cellular activity↓, migration ability↓	Regulating the VEGF/ PI3K/Akt signaling pathway: the expression levels of VEGFA、VEGF-R2、PI3K、Akt, p-Akt are decreased	Dai et al. (2018)
colon cancer	lignan	schisandrin B	*In vitro*: HCT 116 cells *In vivo*: C57BL/6 mice	*In vitro*: 3.125, 6.25, 12.5 and 25 μM *In vivo*: 3.75, 7.5, 15 and 30 mg/kg	Promoting the cellular apoptosis: LDH activity↑, caspase-3/9 levels↑, E-cadherin↑, p53↑, Bax↑, MMP-9↓, β-catenin↓, COX-2↓, COX-1↓	Attenuating colitis-associated colorectal cancer through SIRT1 linked SMURF2 signaling: SMURF2 protein expression ia upregulated and SIRT1 is inhibited	Pu et al. (2021)

Abbreviations: Akt: protein kinase B, ATF2: activating transcription factor 2, COX-2: cyclooxygenase-2, ERK: extracellular regulated protein kinases, eNOS:endothelial nitric oxide synthase, FAK: focal adhesion kinase, FoxP3: forkhead box protein P3, GSH-PX: glutathione peroxidase, HO-1: heme oxygenase, HSP: heat shock protein, IFN: interferon, IκB: inhibitor of NF-κB, iNOS: inducible nitric oxide synthase, JUN: c-Jun N-terminal kinase, MAPK: mitogen activated protein kinase, MPO: myeloperoxidase, MyD88: Myeloid differentiation primary response gene 88, MLCK: myosin light chain kinase, NF-κB: nuclear factor-kappa B, NO: nitric oxide, Nrf2: NF-E2-related factor 2, NLRP3: NOD, like receptor heat protein domain related protein 3, Nrf-2: nuclear erythroid factor, PI3K: phosphatidylinositol 3-kinase, RORγ: retinoic acid-related orphan receptor gamma t, ROS: reactive oxygen species, T-AOC: total antioxidant capacity, TLR4: toll-like receptor 4, SOD: superoxide dismutase,SGK1: serum/glucocorticoid regulated kinase 1, SIRT1: silencing regulatory protein 1, Smurf2: smad ubiquitination regulatory factor 2, VEGF: vascular endothelial growth factor.

inflammatory responses. In intestinal-associated lymphoid tissues, dendritic cells and other antigen-presenting cells initiate antigen-specific immune responses, determining the activation of B cells and the differentiation of initial T helper cells, driven by the cytokine-receptor interaction of JAK-STAT signaling. Furthermore, different subtypes of helper T cells (Th1, Th2, Th9, and Th17) regulate Tregs,

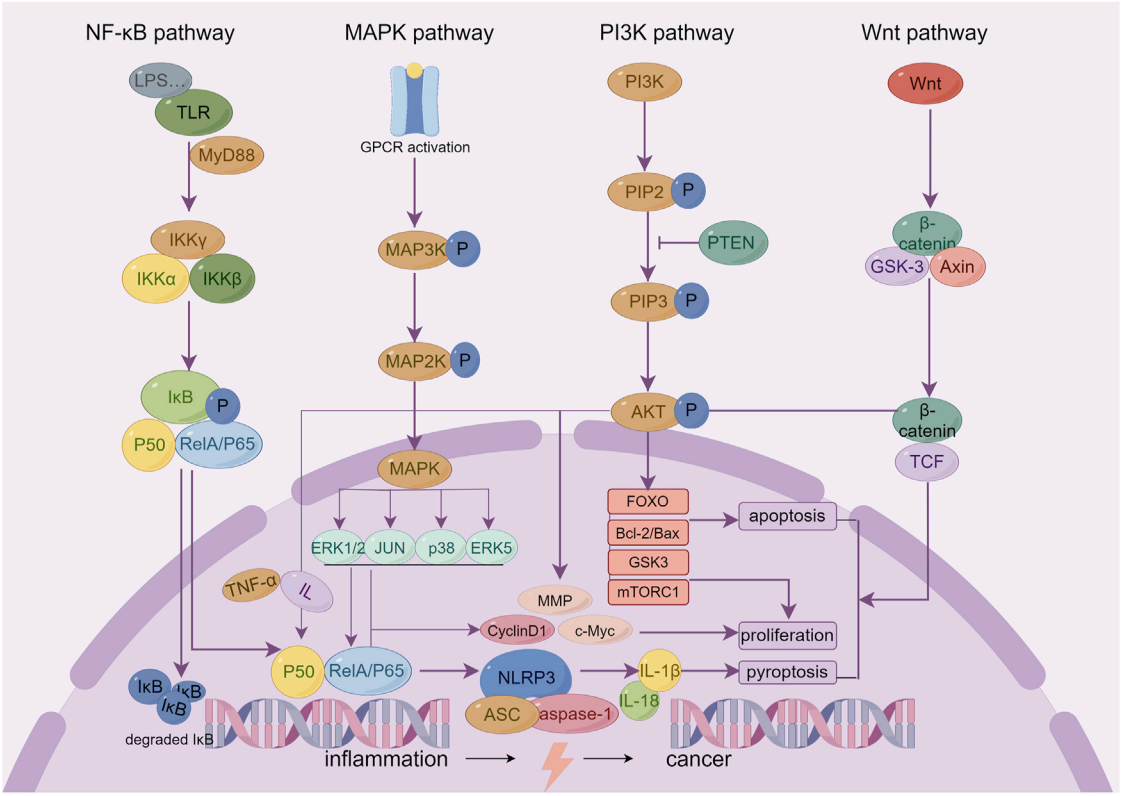

FIGURE 2
The key inflammatory related signaling pathways of Sishen Pill and its effective metabolites in treating IBD and colon cancer.

macrophages, and dendritic cells, among other immune cells, thereby regulating the intestinal inflammatory response and inhibiting tumor occurrence (Hu et al., 2021). JAK/STAT pathway inhibitors have been used to treat IBD, showing good therapeutic potential in preclinical studies (Salas et al., 2020). As mentioned above, multiple studies have confirmed that Sishen Pill can regulate intestinal cellular immunity by regulating JAK-STAT and the expression of its downstream protein suppressor of cytokine signaling (SOCS), one of the key signaling pathways by which the pill inhibits IBD immune inflammation and inflammation-cancer transformation (Liu et al., 2016; Liu et al., 2020; Wang et al., 2022a; Kang et al., 2022) (Figure 3C).

5.5 Regulating the gut microbiota and intestinal barrier

Research has shown widespread dysbiosis in the gut microbiota of both IBD and colon cancer patients and that Sishen Pill can affect the integrity of the intestinal barrier by regulating the gut microbiota and its metabolites. The decrease of *Akkermansia muciniphila* (AKK) and the increase of *Escherichia-Shigella* are significant characteristics of the gut microbiota in IBD population (Morgan et al., 2012; Alam et al., 2016); animal experiments have shown that *Akk* can promote the production of intestinal mucus, regulate the expression of tight junction proteins, and reduce the expression levels of inflammatory and chemotactic factors in the colon and serum (Bian et al., 2019). In addition, oral administration of inactivated *Akk* or the outer membrane protein of *Akk* (Amuc_1100) can also regulate $CD8^+$ T cells, improving IBD and preventing the occurrence of CACC (Wang et al., 2020b). Another study suggested that AKK bacteria could enrich M1-like tumor associated macrophages in the colon cancer microenvironment in NLRP3 dependent way, thereby inhibiting tumor formation and development (Fan et al., 2021a). On the contrary, certain types of *Escherichia-Shigella* can escape host immunity, adhere to and invade intestinal epithelium and macrophages in hosts with genetic susceptibility to IBD, and initiate IBD development (Zangara et al., 2023). Also, the genotoxin produced by *Escherichia-Shigella* can penetrate the colon cell membrane and migrate to the nucleus, causing DNA double strand breaks, cell cycle arrest, chromosomal aberrations, intestinal epithelial damage, and eventually leading to cancer (Fan et al., 2021b). The above studies show that Sishen Pill can increase the relative abundance of *AKK* in the intestine (Chen et al., 2020b; Ge et al., 2022; Jin et al., 2023) and its effective metabolites, evodiamine, and corylin, leading to significant inhibition of *Escherichia-Shigella* the proliferation (Zhu et al., 2021; Wang et al., 2023f) thereby exerting anti-inflammatory and anticancer pharmacological activities.

Some metabolites of the gut microbiota, such as short-chain fatty acids (SCFAs), are also important for developing colitis and tumors. Studies have shown a decreasing trend in intestinal SCFAs in both IBD and colon cancer populations (Wang et al., 2019c; Dalile et al., 2019). As the main source of energy for intestinal epithelial cells, SCFAs not only

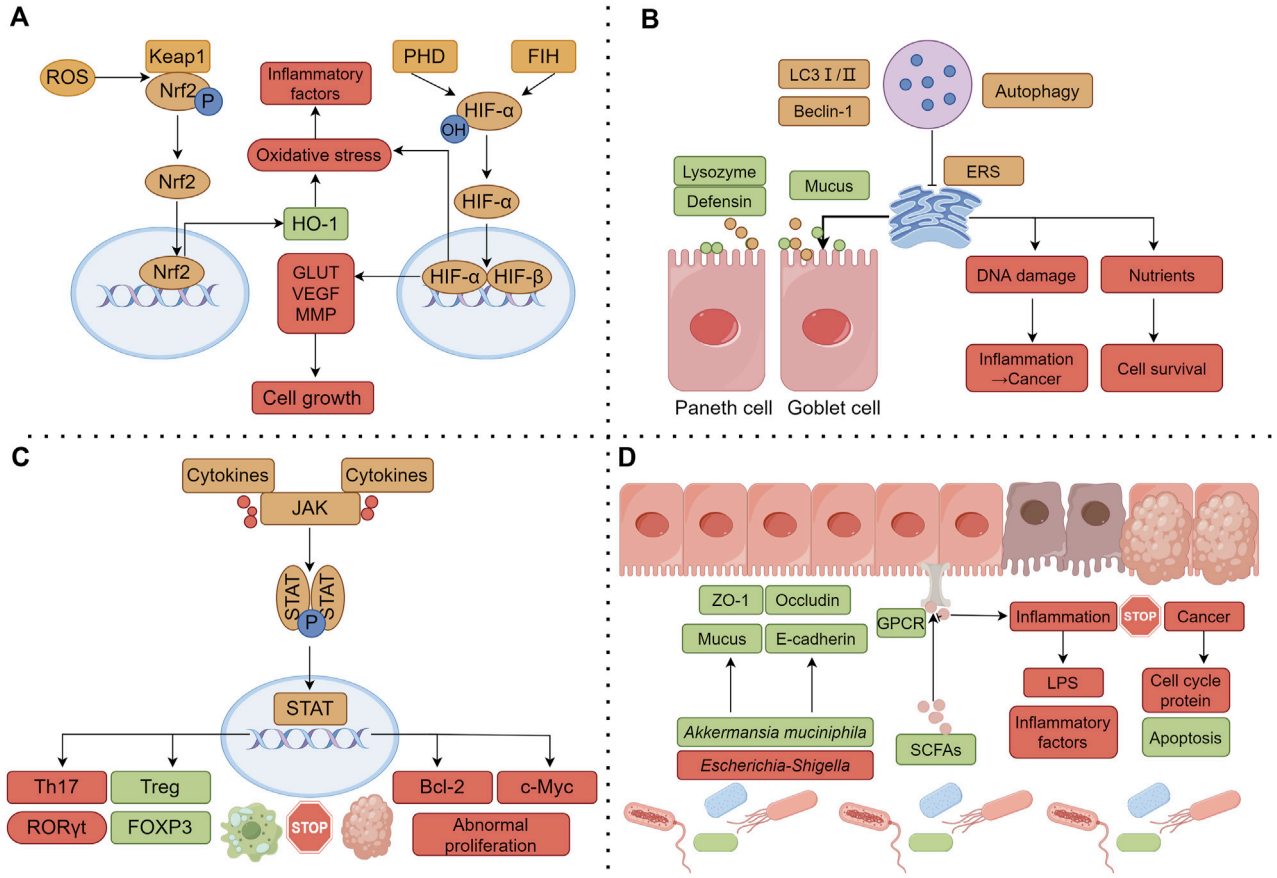

FIGURE 3
Common molecular mechanisms of Sishen Pill and its effective components in treating IBD and colon cancer. **(A)** Regulating the oxidative stress; **(B)** Regulating the mitochondrial autophagy; **(C)** Regulating intestinal immune cells; **(D)** Regulating the gut microbiota and internal barrier. Note: the green box represents the upregulated or promoted molecule, and the red box represents the downregulated or inhibited molecule.

promote the proliferation and differentiation of intestinal epithelial cells, reduce cell apoptosis, and maintain the mechanical barrier of the intestinal mucosa but also improve the secretion of intestinal mucoproteins, lubricate the intestine, block the adhesion of pathogens to the intestinal mucosa, and inhibit the occurrence of intestinal immune inflammation (Sun et al., 2017). In addition, butyrate in SCFAs has been proven to promote apoptosis and inhibit the proliferation of human colon cancer cells by activating G-protein coupled receptor 109A (GPR109A) (Moniri and Farah, 2021). The above research indicates that while regulating the gut microbiota, Sishen Pill can increase the contents of total SCFAs and butyrate in the intestine, thereby improving the inflammatory microenvironment of the intestine (Wang et al., 2022b).

Gut microbiota can affect the morphology and function of the intestinal barrier through various pathways; the integrity of the intestinal barrier is of great significance for the treatment of IBD and colon cancer. Post et al. detected 28 mucin proteins in the colonic mucosa of UC patients and found that seven mucin proteins, such as mucin 2 (MUC2), were significantly reduced; 30% of UC patients had abnormal permeability of the mucus layer, suggesting that abnormal colonic barrier function promotes the occurrence of UC (van der Post et al., 2019). Rath et al. showed that healing of the intestinal barrier has a high predictive value for the course of patients with remission-phase IBD; predictive ability of intestinal barrier healing might far exceed established or emerging parameters, such as endoscopic and histological remission (Rath et al., 2023). In addition, intestinal barrier damage and microbial translocation can activate chronic inflammation, further promoting the secretion of pro-inflammatory factors by immune cells and accelerating the process of colonic inflammation-cancer transformation (Shalapour and Karin, 2020). Another study found that when the intestinal vascular barrier is damaged, intestinal bacteria are more likely to spread to the liver, promoting the formation of a pre-metastatic niche for "colon-liver" metastasis, thereby promoting the recruitment of metastatic cells (Bertocchi et al., 2021). As mentioned earlier, Sishen Pills (Zhang et al., 2021c), schisandrin B (Li et al., 2019b), schisandrin C (Kim et al., 2022), and corylin (Wang et al., 2023f) can regulate the secretion of intestinal epithelial tight junction proteins and mucin, repair damaged intestinal mucosal barriers and inhibit the progression of IBD (Figure 3D).

6 Limitations and outlook

As a classic proprietary Chinese medicine for treating diarrhea, the curative effect of the Sishen Pill on IBD and colon cancer has

been widely studied. Briefly, TCM formulas can regulate multiple targets simultaneously and exert integrated pharmacological effects; they can not only regulate intestinal immune inflammation disorders and fight against tumors but can also improve various symptoms, such as abdominal pain and diarrhea, enhancing the patient's quality of life. In addition, preventive treatment of disease is a characteristic and an advantage of TCM; the application of the Sishen Pill in the early stage of IBD can effectively inhibit the transformation from inflammation to colon cancer. In summary, based on Western medical treatment, accumulating evidence suggests that the use of TCM represented by Sishen Pills can often bring more clinical benefits to patients. However, in terms of the current research on Sishen Pills, many limitations still need to be addressed.

Firstly, the above mentioned clinical studies and experimental studies have preliminarily confirmed the evidence that Sishen Pill can effectively treat IBD and colon cancer, however, the standardization of study design and reporting still needs further improvement. For example, 1) most studies do not provide quality testing reports and specific preparation methods of Sishen Pill; 2) there is a lack of description in the report regarding the experimental design methods and bias control strategies, such as specific measures for randomization of groups and baseline data of different groups before intervention; 3) there is a lack of description of animal or cell model selection criteria and modeling methods. In future studies, we recommend that: 1) design and report rigorously according to the requirements of the Cochrane Handbook (clinical study) (PT and Sally, 2024) and ARRIVE guidelines (animal experiments) (Kilkenny et al., 2012); 2) clinical studies should adopt internationally recognized major outcome measures, and basic experiments are necessary to observe the overall therapeutic effect of Sishen Pill on experimental animals, rather than just cell experimental evidence.

Second, there is still insufficient evidence on the safety of the Sishen Pill, posing a hidden danger in its clinical application. In recent years, liver damage caused by Psoraleae Fructus has become a focus of attention (Xu and Xiao, 2023). *Guo* et al. confirmed that the mechanism of liver injury could be associated with oxidative stress and mitochondrial damage-mediated apoptosis (Guo et al., 2021b) and that it may also be involved in liver regeneration, bile metabolism, energy metabolism, and other processes (Fan et al., 2024; Feng et al., 2024). Compared to bakuchiol, psoralen and isopsoralen have been confirmed to have stronger liver toxicity *in vivo*; their toxic effects are positively correlated with dosage (Mu et al., 2018). Similarly, Euodiae Fructus has also been shown to pose a potential risk of liver injury (Kong et al., 2023); its mechanism of action may be related to peroxidation injury, inflammatory factor mediation, mitochondrial damage, and drug– protein adduct formation (Wei et al., 2020). Other studies have reported that evodiamine exerts potential nephrotoxicity and cardiotoxicity (Yang et al., 2021). The impact of Myristicae Semen on the liver is two-sided; some studies confirmed that myristicin has a protective effect on drug-induced liver injury (Sohn et al., 2008; Yimam et al., 2016; Yang et al., 2018), while others found that Myristicae Semen extracts can also damage liver cells, increase serum transaminase levels and that the toxic effects are time- and dose-dependent (Cao et al., 2020). We believe that the "dose-effect-toxicity" relationship of the Sishen Pill should be further clarified through basic research to evaluate the clinical efficacy and safety. Further research should be conducted to enhance efficacy and detoxification using methods such as the processing and rational compatibility.

Third, although current research suggests that multiple metabolites in Sishen Pill have therapeutic effects on IBD and colon cancer, the active metabolites of this formula still need to be clarified. The currently elucidated molecular mechanisms may provide important links to its integrated pharmacological effects; however, the most critical target of action and differential pathways among different metabolites still require further exploration. We suggest using a more precise research approach as the next step in basic research. Luo and others (Luo et al., 2022) confirmed that MyD88 is the specific target for the anti-inflammatory effects of schisandrin B using target knockout models, carrying out target-metabolites binding assays, molecular docking, and experimental verification. In future research, high-throughput screening of the proteome and target-metabolites binding assays, vital for determining deeper pharmacological mechanisms of action and revealing the scientific connotations of TCM compatibility, should be widely used.

Fourth, clinical evidence of the Sishen Pill in treating colon cancer and inhibiting inflammation-cancer transformation is still lacking. As mentioned above, there are relatively few clinical and basic studies of Sishen Pill on treating colon cancer; more evidence is needed on its effective metabolites. However, there are complex interactions between different chemical metabolites, so the efficacy evaluation and mechanism exploration of Sishen Pill in treating colon cancer need to be further carried out. Besides, the transformation of colonic "inflammation-cancer" is a dynamic process; at present, only a few studies have focused on the effect of Sishen Pill and its metabolites on CACC. Specific clinical application strategies, including the best application nodes and treatment courses, are also urgently needed. In addition to the traditional dosage forms, the efficacy and safety of decoction enemas and volatile oils have also been preliminary confirmed; however, the differences in the indications of different dosage forms and how better market transformations can be performed need to be addressed stepwise through a series of studies. Large sample sizes, long-term follow-up RCTs, and real-world post-marketing reevaluations of formulas are necessary to better address the above issues.

7 Conclusion

Sishen Pills and its metabolites show great potential in the treatment of IBD, colon cancer and the inhibition of colonic inflammation-cancer transformation. Modern pharmacological research has confirmed that Sishen Pills molecular mechanisms mainly involve regulating inflammatory signaling pathways, inhibiting oxidative stress, improving mitochondrial mitophagy, regulating intestinal immune cells, and modulating the gut microbiota. Meanwhile, we should not overlook the limitations of current research. Due to the lack of rigorously designed large-sample RCTs, it is still difficult to answer questions about the long-term effectiveness and safety of the Sishen Pill in treating IBD and colon cancer. In future research, we recommend combining RCTs with real-world clinical studies to obtain stronger clinical evidence. At the same time, it is important to strengthen research on potential core metabolites of Sishen Pill, such as evodiamine and schisandrins, and clarify their key molecular targets, in order to lay the foundation for the new drug development.

Author contributions

BZ: Supervision, Writing–original draft, Writing–review and editing. YC: Writing–original draft, Writing–review and editing. QJ: Writing–original draft. SX: Writing–original draft. QX: Writing–original draft. CW: Writing–original draft. CY: Conceptualization, Supervision, Writing–original draft, Writing–review and editing. JL: Conceptualization, Supervision, Writing–original draft, Writing–review and editing. CZ: Conceptualization, Funding acquisition, Supervision, Writing–original draft, Writing–review and editing.

Funding

The author(s) declare financial support was received for the research, authorship, and/or publication of this article. This research was funded by the Sichuan Science and Technology Program (2023NSFSC1994) and China Postdoctoral Science Foundation (2022MD713683).

Acknowledgments

The figures in the article were drawn using FigDraw (www.figdraw.com).

Conflict of interest

The authors declare that the research was conducted in the absence of any commercial or financial relationships that could be construed as a potential conflict of interest.

Publisher's note

References

Alam, A., Leoni, G., Quiros, M., Wu, H., Desai, C., Nishio, H., et al. (2016). The microenvironment of injured murine gut elicits a local pro-restitutive microbiota. *Nat. Microbiol.* 1, 15021. doi:10.1038/nmicrobiol.2015.21

Alula, K. M., and Theiss, A. L. (2023). Autophagy in Crohn's disease: converging on dysfunctional innate immunity. *Cells* 12 (13), 1779. doi:10.3390/cells12131779

Bartnik, M., Sławińska-Brych, A., Żurek, A., Kandefer-Szerszeń, M., and Zdzisińska, B. (2017). 8-methoxypsoralen reduces AKT phosphorylation, induces intrinsic and extrinsic apoptotic pathways, and suppresses cell growth of SK-N-AS neuroblastoma and SW620 metastatic colon cancer cells. *J. Ethnopharmacol.* 207, 19–29. doi:10.1016/j.jep.2017.06.010

Bertocchi, A., Carloni, S., Ravenda, P. S., Bertalot, G., Spadoni, I., Lo Cascio, A., et al. (2021). Gut vascular barrier impairment leads to intestinal bacteria dissemination and colorectal cancer metastasis to liver. *Cancer Cell* 39 (5), 708–724.e11. doi:10.1016/j.ccell.2021.03.004

Bian, X., Wu, W., Yang, L., Lv, L., Wang, Q., Li, Y., et al. (2019). Administration of Akkermansia muciniphila ameliorates dextran sulfate sodium-induced ulcerative colitis in mice. *Front. Microbiol.* 10, 2259. doi:10.3389/fmicb.2019.02259

Bilgin, S., Erden Tayhan, S., Yıldırım, A., and Koç, E. (2023). Investigation of the effects of isoeugenol-based phenolic compounds on migration and proliferation of HT29 colon cancer cells at cellular and molecular level. *Bioorg Chem.* 130, 106230. doi:10.1016/j.bioorg.2022.106230

Bonovas, S., Fiorino, G., Lytras, T., Nikolopoulos, G., Peyrin-Biroulet, L., and Danese, S. (2017). Systematic review with meta-analysis: use of 5-aminosalicylates and risk of colorectal neoplasia in patients with inflammatory bowel disease. *Aliment. Pharmacol. Ther.* 45 (9), 1179–1192. doi:10.1111/apt.14023

Boschetti, G., Kanjarawi, R., Bardel, E., Collardeau-Frachon, S., Duclaux-Loras, R., Moro-Sibilot, L., et al. (2017). Gut inflammation in mice triggers proliferation and function of mucosal Foxp3+ regulatory T cells but impairs their conversion from CD4+ T cells. *J. Crohns Colitis* 11 (1), 105–117. doi:10.1093/ecco-jcc/jjw125

Byun, W. S., Bae, E. S., Kim, W. K., and Lee, S. K. (2022). Antitumor activity of rutaecarpine in human colorectal cancer cells by suppression of wnt/β-catenin signaling. *J. Nat. Prod.* 85 (5), 1407–1418. doi:10.1021/acs.jnatprod.2c00224

Cao, Y. (2013). Preventive effect of traditional Chinese medicine "Si-Shen bolus" on colitis associated cancer in mice. Doctor. master's thesis. Liaoning: Liaoning University of Traditional Chinese Medicine.

Cao, Y., Wang, Y.-J., Xie, X., and Tian, Z.-G. (2013). Effect of Sishen Pill on the expression of CD133 protein in colon cancer induced by colitis in mice. *Chin. Med. Mod. Distance Educ. China* 11 (08), 145–146.

Cao, Y., Zhao, D.-Y., Chai, J.-Y., and Tian, Z.-G. (2012). Chemopreventive effect of sishen pill on experimental colon cancer in rats. *J. Liaoning Univ. Traditional Chin. Med.* 14 (11), 127–129. doi:10.13194/j.jlunivtcm.2012.11.129.caoy.063

Cao, Z., Xia, W., Zhang, X., Yuan, H., Guan, D., and Gao, L. (2020). Hepatotoxicity of nutmeg: a pilot study based on metabolomics. *Biomed. Pharmacother.* 131, 110780. doi:10.1016/j.biopha.2020.110780

Casarin, E., Dall'Acqua, S., Smejkal, K., Slapetová, T., Innocenti, G., and Carrara, M. (2014). Molecular mechanisms of antiproliferative effects induced by Schisandra-derived dibenzocyclooctadiene lignans (+)-deoxyschisandrin and (-)-gomisin N in human tumour cell lines. *Fitoterapia* 98, 241–247. doi:10.1016/j.fitote.2014.08.001

Cassotta, M., Cianciosi, D., De Giuseppe, R., Navarro-Hortal, M. D., Armas Diaz, Y., Forbes-Hernández, T. Y., et al. (2023). Possible role of nutrition in the prevention of inflammatory bowel disease-related colorectal cancer: a focus on human studies. *Nutrition* 110, 111980. doi:10.1016/j.nut.2023.111980

Chen, B. C., Tu, S. L., Zheng, B. A., Dong, Q. J., Wan, Z. A., and Dai, Q. Q. (2020a). Schizandrin A exhibits potent anticancer activity in colorectal cancer cells by inhibiting heat shock factor 1. *Biosci. Rep.* 40 (3). doi:10.1042/bsr20200203

Chen, F., Yin, Y. T., Zhao, H. M., Wang, H. Y., Zhong, Y. B., Long, J., et al. (2020b). Sishen pill treatment of DSS-induced colitis via regulating interaction with inflammatory dendritic cells and gut microbiota. *Front. Physiol.* 11, 801. doi:10.3389/fphys.2020.00801

Chen, L.-L., and Chen, R.-J. (2018). Therapeutical effect of schizandrin B on ulcerative colitis in rats and underlying mechanism. *China Pharm.* 21 (11), 1941–1945.

Chen, X., Xu, H., Li, R.-N., Li, X.-L., Zhao, L.-N., and Xu, Z.-L. (2023). Mechanism of Myristica fragrans Houtt.Against colorectal carcinoma based on network pharmacology and molecular docking. *J. Med. Inf.* 36 (14), 16–21.

Chen, Y., Chen, L., Xing, C., Deng, G., Zeng, F., Xie, T., et al. (2020c). The risk of rheumatoid arthritis among patients with inflammatory bowel disease: a systematic review and meta-analysis. *BMC Gastroenterol.* 20 (1), 192. doi:10.1186/s12876-020-01339-3

Chien, C. C., Wu, M. S., Shen, S. C., Ko, C. H., Chen, C. H., Yang, L. L., et al. (2014). Activation of JNK contributes to evodiamine-induced apoptosis and G2/M arrest in human colorectal carcinoma cells: a structure-activity study of evodiamine. *PLoS One* 9 (6), e99729. doi:10.1371/journal.pone.0099729

Choi, J. H., Cho, Y. S., Ko, Y. H., Hong, S. U., Park, J. H., and Lee, M. A. (2014). Absence of autophagy-related proteins expression is associated with poor prognosis in patients with colorectal adenocarcinoma. *Gastroenterol. Res. Pract.* 2014, 179586. doi:10.1155/2014/179586

Chopra, B., Dhingra, A. K., and Dhar, K. L. (2013). Psoralea corylifolia L. (Buguchi) - folklore to modern evidence: review. *Fitoterapia* 90, 44–56. doi:10.1016/j.fitote.2013.06.016

Cray, P., Sheahan, B. J., and Dekaney, C. M. (2021). Secretory sorcery: Paneth cell control of intestinal repair and homeostasis. *Cell Mol. Gastroenterol. Hepatol.* 12 (4), 1239–1250. doi:10.1016/j.jcmgh.2021.06.006

Dai, G.-L., Gong, T., Li, Y., Ding, K., Wu, K.-L., Li, Z.-W., et al. (2018). Effect of schisandrin B on proliferation and migration of human SW620 colon cancer cell via VEGF/PI3K/Akt signaling pathway. *Chin. Pharm. J.* 53(14), 1186–1191.

Dalile, B., Van Oudenhove, L., Vervliet, B., and Verbeke, K. (2019). The role of short-chain fatty acids in microbiota-gut-brain communication. *Nat. Rev. Gastroenterol. Hepatol.* 16 (8), 461–478. doi:10.1038/s41575-019-0157-3

D'Ascenzo, F., Bruno, F., Iannaccone, M., Testa, G., De Filippo, O., Giannino, G., et al. (2023). Patients with inflammatory bowel disease are at increased risk of atherothrombotic disease: a systematic review with meta-analysis. *Int. J. Cardiol.* 378, 96–104. doi:10.1016/j.ijcard.2023.02.042

Deka, K., and Li, Y. (2023). Transcriptional regulation during aberrant activation of NF-κB signalling in cancer. *Cells* 12 (5), 788. doi:10.3390/cells12050788

Ding, W., Ding, Z., Wang, Y., Zhu, Y., Gao, Q., Cao, W., et al. (2020). Evodiamine attenuates experimental colitis injury via activating autophagy and inhibiting NLRP3 inflammasome assembly. *Front. Pharmacol.* 11, 573870. doi:10.3389/fphar.2020.573870

Duan, C.-Y., He, N.-N., Zhu, L., Fan, L., Yi, F., Wang, T., et al. (2020). The mechanism of myristicin lnhibiting proliferation, migration and invasion of colon cancer cell lines. *Mod. Traditional Chin. Med. Materia Medica-World Sci. Technol.* 22 (04), 907–913.

Eastaff-Leung, N., Mabarrack, N., Barbour, A., Cummins, A., and Barry, S. (2010). Foxp3+ regulatory T cells, Th17 effector cells, and cytokine environment in inflammatory bowel disease. *J. Clin. Immunol.* 30 (1), 80–89. doi:10.1007/s10875-009-9345-1

Fan, B.-B., Zhong, R.-Z., Ma, Z., Han, Y., and Shu, T. (2024). Progress in pharmacological studies of buguzhi (Psoralea). *Chin. Archives Traditional Chin. Med.*, 1–8.

Fan, L., Xu, C., Ge, Q., Lin, Y., Wong, C. C., Qi, Y., et al. (2021a). A. Muciniphila suppresses colorectal tumorigenesis by inducing TLR2/NLRP3-mediated M1-like TAMs. *Cancer Immunol. Res.* 9 (10), 1111–1124. doi:10.1158/2326-6066.Cir-20-1019

Fan, X., Jin, Y., Chen, G., Ma, X., and Zhang, L. (2021b). Gut microbiota dysbiosis drives the development of colorectal cancer. *Digestion* 102 (4), 508–515. doi:10.1159/000508328

Feng, K.-R., Wu, Y.-L., Li, W.-X., Wang, X.-Y., Zhang, H., Yang, L.-G., et al. (2024). Research progress on hepatotoxicity of Psoralea and its attenuation methods. *China J. Traditional Chin. Med. Pharm.* 1-8.

Feng, Y.-Y., Zhou, L.-H., Liu, N.-N., Sun, X.-T., Jia, R., and Li, Q. (2021). Effects of psoralen on invasion and metastasis of human colon cancer cells and β-catenin/TCF4-MMP-9 signaling pathway. *China J. Traditional Chin. Med. Pharm.* 36 (12), 7033–7037.

Fu, Y., Lee, C. H., and Chi, C. C. (2018). Association of psoriasis with inflammatory bowel disease: a systematic review and meta-analysis. *JAMA Dermatol* 154 (12), 1417–1423. doi:10.1001/jamadermatol.2018.3631

Galluzzi, L., Pietrocola, F., Bravo-San Pedro, J. M., Amaravadi, R. K., Baehrecke, E. H., Cecconi, F., et al. (2015). Autophagy in malignant transformation and cancer progression. *Embo J.* 34 (7), 856–880. doi:10.15252/embj.201490784

Gao, J.-R., Xu, S.-Z., Han, Y.-Q., Wei, L.-B., and Song, J.-M. (2017). Serum fingerprint of drug-couple Psoralea corylifolia-Myristica fragrants. *Chin. Traditional Herb. Drugs* 48 (12), 2401–2406.

Gatenby, G., Glyn, T., Pearson, J., Gearry, R., and Eglinton, T. (2021). The long-term incidence of dysplasia and colorectal cancer in a Crohn's colitis population-based cohort. *Colorectal Dis.* 23 (9), 2399–2406. doi:10.1111/codi.15756

Ge, W., Wang, H. Y., Zhao, H. M., Liu, X. K., Zhong, Y. B., Long, J., et al. (2020). Effect of sishen pill on memory T cells from experimental colitis induced by dextran sulfate sodium. *Front. Pharmacol.* 11, 908. doi:10.3389/fphar.2020.00908

Ge, W., Zhou, B. G., Zhong, Y. B., Liu, S. Q., Huang, J. Q., Yuan, W. Y., et al. (2022). Sishen pill ameliorates dextran sulfate sodium (DSS)-Induced colitis with spleen-kidney yang deficiency syndromes: role of gut microbiota, fecal metabolites, inflammatory dendritic cells, and TLR4/NF-κB pathway. *Evid. Based Complement. Altern. Med.* 2022, 6132289. doi:10.1155/2022/6132289

Ghodousi-Dehnavi, E., Hosseini, R. H., Arjmand, M., Nasri, S., and Zamani, Z. (2021). A metabolomic investigation of eugenol on colorectal cancer cell line HT-29 by modifying the expression of APC, p53, and KRAS genes. *Evid. Based Complement. Altern. Med.* 2021, 1448206. doi:10.1155/2021/1448206

Guo, J., Qiao, C., Zhou, J., Hu, S., Lin, X., Shen, Y., et al. (2021a). Neobavaisoflavone-mediated T(H)9 cell differentiation ameliorates bowel inflammation. *Int. Immunopharmacol.* 101 (Pt A), 108191. doi:10.1016/j.intimp.2021.108191

Guo, M., Liang, D.-Y., Huang, R., and Pan, X. (2023). The application of one test and multiple evaluation method in the content determinationand quality evaluation of 9 components in Sishen pills. *J. South-Central Univ. Natl. Sci. Ed.* 42 (02), 174–179. doi:10.20056/j.cnki.ZNMDZK.20230205

Guo, Z., Li, P., Wang, C., Kang, Q., Tu, C., Jiang, B., et al. (2021b). Five constituents contributed to the Psoraleae fructus-induced hepatotoxicity via mitochondrial dysfunction and apoptosis. *Front. Pharmacol.* 12, 682823. doi:10.3389/fphar.2021.682823

He, Z., Feng, D., Zhang, C., Chen, Z., Wang, H., Hou, J., et al. (2024). Recent strategies for evoking immunogenic Pyroptosis in antitumor immunotherapy. *J. Control Release* 366, 375–394. doi:10.1016/j.jconrel.2023.12.023

Hovhannisyan, Z., Treatman, J., Littman, D. R., and Mayer, L. (2011). Characterization of interleukin-17-producing regulatory T cells in inflamed intestinal mucosa from patients with inflammatory bowel diseases. *Gastroenterology* 140 (3), 957–965. doi:10.1053/j.gastro.2010.12.002

Hsiao, S. W., Yen, H. H., and Chen, Y. Y. (2022). Chemoprevention of colitis-associated dysplasia or cancer in inflammatory bowel disease. *Gut Liver* 16 (6), 840–848. doi:10.5009/gnl210479

Hu, X., Li, J., Fu, M., Zhao, X., and Wang, W. (2021). The JAK/STAT signaling pathway: from bench to clinic. *Signal Transduct. Target Ther.* 6 (1), 402. doi:10.1038/s41392-021-00791-1

Huang, J., Chen, Z. H., Ren, C. M., Wang, D. X., Yuan, S. X., Wu, Q. X., et al. (2015). Antiproliferation effect of evodiamine in human colon cancer cells is associated with IGF-1/HIF-1α downregulation. *Oncol. Rep.* 34 (6), 3203–3211. doi:10.3892/or.2015.4309

Huang, J., Jin, J., Kang, Z.-P., Liu, D.-Y., Cheng, S.-M., Zhong, Y.-B., et al. (2022). Effect of sisheng pill and its disassembly on expression of Treg cells and PD-1/PD-L1 in mice with colitis. *Lishizhen Med. Materia Medica Res.* 33 (06), 1284–1287.

Huang, J.-Q., Jiang, Q.-Q., Zhong, Y.-B., Wang, M.-X., Long, J., Zhao, H.-M., et al. (2021). Regulatory effect of volatile oil from sishenwan on TLR/MyD88 signaling pathway in mice with chronic ulcerative colitis. *Chin. J. Exp. Traditional Med. Formulae* 27 (23), 19–25. doi:10.13422/j.cnki.syfjx.20212301

Huang, Y.-L., Huang, Z.-P., and Wang, L.-L. (2019). Simultaneous determination of 8 active components in Sishen pills by flash evaporation-gas chromatography/mass spectrometry. *Chin. J. Pharm. Analysis* 39 (03), 510–517. doi:10.16155/j.0254-1793.2019.03.19

Hung, Y. L., Wang, S. C., Suzuki, K., Fang, S. H., Chen, C. S., Cheng, W. C., et al. (2019). Bavachin attenuates LPS-induced inflammatory response and inhibits the activation of NLRP3 inflammasome in macrophages. *Phytomedicine* 59, 152785. doi:10.1016/j.phymed.2018.12.008

Hyun, S. Y., Le, H. T., Min, H. Y., Pei, H., Lim, Y., Song, I., et al. (2021). Evodiamine inhibits both stem cell and non-stem-cell populations in human cancer cells by targeting heat shock protein 70. *Theranostics* 11 (6), 2932–2952. doi:10.7150/thno.49876

Iacobazzi, D., Convertini, P., Todisco, S., Santarsiero, A., Iacobazzi, V., and Infantino, V. (2023). New insights into NF-κB signaling in innate immunity: focus on immunometabolic crosstalks. *Biol. (Basel)* 12 (6), 776. doi:10.3390/biology12060776

Ibrahim, L., Stanton, C., Nutsch, K., Nguyen, T., Li-Ma, C., Ko, Y., et al. (2023). Succinylation of a KEAP1 sensor lysine promotes NRF2 activation. *Cell Chem. Biol.* 30 (10), 1295–1302.e4. doi:10.1016/j.chembiol.2023.07.014

Ishak, N. I. M., Mohamed, S., Madzuki, I. N., Mustapha, N. M., and Esa, N. M. (2021). Limonin modulated immune and inflammatory responses to suppress colorectal adenocarcinoma in mice model. *Naunyn Schmiedeb. Arch. Pharmacol.* 394 (9), 1907–1915. doi:10.1007/s00210-021-02101-6

Ismail Abo El-Fadl, H. M., and Mohamed, M. F. A. (2022). Targeting endoplasmic reticulum stress, Nrf-2/HO-1, and NF-κB by myristicin and its role in attenuation of ulcerative colitis in rats. *Life Sci.* 311 (Pt B), 121187. doi:10.1016/j.lfs.2022.121187

Iwasaki, K., Zheng, Y. W., Murata, S., Ito, H., Nakayama, K., Kurokawa, T., et al. (2016). Anticancer effect of linalool via cancer-specific hydroxyl radical generation in human colon cancer. *World J. Gastroenterol.* 22 (44), 9765–9774. doi:10.3748/wjg.v22.i44.9765

Jiang, E.-P., Li, H., Yu, C.-Y., and Zhu, W. (2015). Influence of schisandrin B in apoptosis and invasion of SW480 cells via p38MAPK signaling pathway. *J. Jilin Univ. Ed.* 41 (04), 675–679+885. doi:10.13481/j.1671-587x.20150401

Jiang, Y.-F., Huang, Y., Xiao, C., Zhou, S.-W., Zheng, L.-L., and You, F.-M. (2023). Inhibitory effect and mechanism of sishenwan-containing serum on aerobic glycolysis in human colon cancer cells. *Chin. J. Exp. Traditional Med. Formulae* 29 (19), 26–33. doi:10.13422/j.cnki.syfjx.20230130

Jin, J., Liu, D.-Y., Huang, J., Kang, Z.-P., Zhong, Y.-B., Long, J., et al. (2023). Regulation of sishen pills, ershen pills and wuweizi powder on intestinal microflora lmbalance in mice with colitis. *Chin. Archives Traditional Chin. Med.* 41 (04), 169–292. doi:10.13193/j.issn.1673-7717.2023.04.033

Jin, Z., Yan, W., Jin, H., Ge, C., and Xu, Y. (2016). Differential effect of psoralidin in enhancing apoptosis of colon cancer cells via nuclear factor-κB and B-cell lymphoma-2/B-cell lymphoma-2-associated X protein signaling pathways. *Oncol. Lett.* 11 (1), 267–272. doi:10.3892/ol.2015.3861

Kang, Z.-P., Jin, J., Jiang, Q.-Q., Zhao, H.-M., Cheng, S.-M., Zhong, Y.-B., et al. (2022). Effect of Sishen Pills and its split prescriptions on Tfr/Tfh9/Tfh17 cells in colitis mice. *China J. Chin. Materia Medica* 47 (05), 1300–1306. doi:10.19540/j.cnki.cjcmm.20211102.401

Kilkenny, C., Browne, W. J., Cuthill, I. C., Emerson, M., and Altman, D. G. (2012). Improving bioscience research reporting: the ARRIVE guidelines for reporting animal research. *Osteoarthr. Cartil.* 20 (4), 256–260. doi:10.1016/j.joca.2012.02.010

Kim, B. J., Yang, S. K., Kim, J. S., Jeen, Y. T., Choi, H., Han, D. S., et al. (2009). Trends of ulcerative colitis-associated colorectal cancer in Korea: a KASID study. *J. Gastroenterol. Hepatol.* 24 (4), 667–671. doi:10.1111/j.1440-1746.2008.05730.x

Kim, H., Yu, Y., Choi, S., Lee, H., Yu, J., Lee, J. H., et al. (2019). Evodiamine eliminates colon cancer stem cells via suppressing notch and wnt signaling. *Molecules* 24 (24), 4520. doi:10.3390/molecules24244520

Kim, M. R., Cho, S. Y., Lee, H. J., Kim, J. Y., Nguyen, U. T. T., Ha, N. M., et al. (2022). Schisandrin C improves leaky gut conditions in intestinal cell monolayer, organoid, and nematode models by increasing tight junction protein expression. *Phytomedicine* 103, 154209. doi:10.1016/j.phymed.2022.154209

Kong, Y.-D., Qi, Y., Cui, N., Zhang, Z.-H., Sun, Y.-P., Zeng, Y.-N., et al. (2023). Research progress on modern chemical constituents and pharmacological effects of evodia rutaecarpa. *Inf. Traditional Chin. Med.* 40 (05), 79–83+89. doi:10.19656/j.cnki.1002-2406.20230513

Lee, A., Chung, Y. C., Song, K. H., Ryuk, J. A., Ha, H., and Hwang, Y. H. (2023). Network pharmacology-based identification of bioavailable anti-inflammatory agents from Psoralea corylifolia L. in an experimental colitis model. *J. Ethnopharmacol.* 313, 116534. doi:10.1016/j.jep.2023.116534

Lee, S. Y., Lee, D. Y., Kang, J. H., Kim, J. H., Jeong, J. W., Kim, H. W., et al. (2022). Relationship between gut microbiota and colorectal cancer: probiotics as a potential strategy for prevention. *Food Res. Int.* 156, 111327. doi:10.1016/j.foodres.2022.111327

Li, C., Cai, G., Song, D., Gao, R., Teng, P., Zhou, L., et al. (2019a). Development of EGFR-targeted evodiamine nanoparticles for the treatment of colorectal cancer. *Biomater. Sci.* 7 (9), 3627–3639. doi:10.1039/c9bm00613c

Li, C., Zhang, K., Pan, G., Ji, H., Li, C., Wang, X., et al. (2021a). Dehydrodiisoeugenol inhibits colorectal cancer growth by endoplasmic reticulum stress-induced autophagic pathways. *J. Exp. Clin. Cancer Res.* 40 (1), 125. doi:10.1186/s13046-021-01915-9

Li, F. S., Huang, J., Cui, M. Z., Zeng, J. R., Li, P. P., Li, L., et al. (2020a). BMP9 mediates the anticancer activity of evodiamine through HIF-1α/p53 in human colon cancer cells. *Oncol. Rep.* 43 (2), 415–426. doi:10.3892/or.2019.7427

Li, J., Lu, Y., Wang, D., Quan, F., Chen, X., Sun, R., et al. (2019b). Schisandrin B prevents ulcerative colitis and colitis-associated-cancer by activating focal adhesion kinase and influence on gut microbiota in an *in vivo* and *in vitro* model. *Eur. J. Pharmacol.* 854, 9–21. doi:10.1016/j.ejphar.2019.03.059

Li, X., Wu, S., Dong, G., Chen, S., Ma, Z., Liu, D., et al. (2020b). Natural product evodiamine with borate trigger unit: discovery of potent antitumor agents against colon cancer. *ACS Med. Chem. Lett.* 11 (4), 439–444. doi:10.1021/acsmedchemlett.9b00513

Li, Y.-G., Deng, N., and Lin, X.-Y. (2018). Meta-analysis of sishen decoction on diarrhea-predominant lrritable bowel syndrome. *J. Emerg. Traditional Chin. Med.* 27 (02), 215–218.

Li, Z., Qiao, L., Yun, X., Du, F., Xing, S., and Yang, M. (2021b). Increased risk of ischemic heart disease and diabetes in inflammatory bowel disease. *Z Gastroenterol.* 59 (2), 117–124. doi:10.1055/a-1283-6966

Lim, H. S., Kim, Y. J., Kim, B. Y., and Jeong, S. J. (2019). Bakuchiol suppresses inflammatory responses via the downregulation of the p38 MAPK/ERK signaling pathway. *Int. J. Mol. Sci.* 20 (14), 3574. doi:10.3390/ijms20143574

Liu, D.-Y., Xu, R., Huang, M.-F., Wang, X., Zou, Y., Yue, H.-Y., et al. (2016). Mechanism of sishen wan in regulating balance of T lymphocyte subsets and Treg/Th17 in colitis rats. *Chin. J. Exp. Traditional Med. Formulae* 22 (03), 107–111. doi:10.13422/j.cnki.syfjx.2016030107

Liu, L., Zhang, L., Cui, Z. X., Liu, X. Y., Xu, W., and Yang, X. W. (2019). Transformation of psoralen and isopsoralen by human intestinal microbial *in vitro*, and the biological activities of its metabolites. *Molecules* 24 (22), 4080. doi:10.3390/molecules24224080

Liu, R., Wang, Y., Zhu, X.-D., Gao, Y.-K., Wang, H., and Zhong, X.-T. (2021). Effect of sishenwan on PI3K/Akt/mTOR signal pathway in colonic tissue of rats with ulcerative colitis model of spleen kidney yang deficiency. *Chin. J. Exp. Traditional Med. Formulae* 27 (04), 16–23. doi:10.13422/j.cnki.syfjx.20210437

Liu, R.-R., Sun, A.-Q., Yu, X.-J., He, M.-Y., Xie, H.-B., Gao, P., et al. (2023). Research progress on chemical composition and pharmacological effects of Myristicae Semen and predictive analysis on its quality marker. *Chin. Traditional Herb. Drugs* 54 (14), 4682–4700.

Liu, S., Zhang, S., Lv, X., Lu, J., Ren, C., Zeng, Z., et al. (2019). Limonin ameliorates ulcerative colitis by regulating STAT3/miR-214 signaling pathway. *Int. Immunopharmacol.* 75, 105768. doi:10.1016/j.intimp.2019.105768

Liu, S.-P., Ge, W., Cheng, S.-M., Yuan, W.-Y., Zhao, H.-M., Liu, D.-Y., et al. (2022). Regulation of Sishen Pill on the surface costimulatory molecules of dendritic cells in mice with spleen kidney yang deficiency colitis. *Lishizhen Med. Materia Medica Res.* 33 (12), 2878–2881.

Liu, W., Liu, Y., Wang, Z., Yu, T., Lu, Q., and Chen, H. (2015). Suppression of MAPK and NF-κ B pathways by schisandrin B contributes to attenuation of DSS-induced mice model of inflammatory bowel disease. *Pharmazie* 70 (9), 598–603.

Liu, X. K., Zhao, H. M., Wang, H. Y., Ge, W., Zhong, Y. B., Long, J., et al. (2020). Regulatory effect of sishen pill on Tfh cells in mice with experimental colitis. *Front. Physiol.* 11, 589. doi:10.3389/fphys.2020.00589

Long, C.-W., and Cao, H. (2021a). A meta-analysis on efficacy of modified sishen pill or combined with retention enema in treatment of ulcerative colitis compared with western medicine. *J. Pract. Traditional Chin. Intern. Med.* 35 (08), 147–148. doi:10.13729/j.issn.1671-7813.Z20201290

Long, C.-W., and Cao, H. (2021b). A meta-analysis on efficacy of modified sishen pill or combinedwith retention enema in treatment of ulcerative colitis compared with western medicine. *J. Pract. Traditional Chin. Intern. Med.* 35 (08), 147–148. doi:10.13729/j.issn.1671-7813.Z20201290

Lu, C., Xue, L., Luo, K., Liu, Y., Lai, J., Yao, X., et al. (2023). Colon-accumulated gold nanoclusters alleviate intestinal inflammation and prevent secondary colorectal carcinogenesis via nrf2-dependent macrophage reprogramming. *ACS Nano* 17 (18), 18421–18432. doi:10.1021/acsnano.3c06025

Lu, S., Gong, J., Tan, Y., and Liu, D. (2020). Epidemiologic association between inflammatory bowel diseases and type 1 diabetes mellitus: a meta-analysis. *J. Gastrointestin Liver Dis.* 29 (3), 407–413. doi:10.15403/jgld-798

Luo, C., Ai, J., Ren, E., Li, J., Feng, C., Li, X., et al. (2021). Research progress on evodiamine, a bioactive alkaloid of Evodiae fructus: focus on its anti-cancer activity and bioavailability (Review). *Exp. Ther. Med.* 22 (5), 1327. doi:10.3892/etm.2021.10762

Luo, W., Lin, K., Hua, J., Han, J., Zhang, Q., Chen, L., et al. (2022). Schisandrin B attenuates diabetic cardiomyopathy by targeting MyD88 and inhibiting MyD88-dependent inflammation. *Adv. Sci. (Weinh)* 9 (31), e2202590. doi:10.1002/advs.202202590

Luo, Y., Deng, Y., Shen, X.-M., Zhang, Y., Li, J.-C., Li, S., et al. (2023). Antidepressant effect of Sishen Wan and its effect on central monoamine nervous system. *Chin. J. Pharmacol. Toxicol.* 37 (02), 105–111.

Mayer, I. A., and Arteaga, C. L. (2016). The PI3K/AKT pathway as a target for cancer treatment. *Annu. Rev. Med.* 67, 11–28. doi:10.1146/annurev-med-062913-051343

Moniri, N. H., and Farah, Q. (2021). Short-chain free-fatty acid G protein-coupled receptors in colon cancer. *Biochem. Pharmacol.* 186, 114483. doi:10.1016/j.bcp.2021.114483

Morgan, X. C., Tickle, T. L., Sokol, H., Gevers, D., Devaney, K. L., Ward, D. V., et al. (2012). Dysfunction of the intestinal microbiome in inflammatory bowel disease and treatment. *Genome Biol.* 13 (9), R79. doi:10.1186/gb-2012-13-9-r79

Mu, G.-H., Shi, Y., Shen, M.-M., Wu, L.-T., Zhao, Q.-Z., and Liu, Y.-F. (2018). Overview and thoughts on on the main side effects of fructus Psoraleae. *World Chin. Med.* 13 (04), 1038–1042.

Naama, M., Telpaz, S., Awad, A., Ben-Simon, S., Harshuk-Shabso, S., Modilevsky, S., et al. (2023). Autophagy controls mucus secretion from intestinal goblet cells by alleviating ER stress. *Cell Host Microbe* 31 (3), 433–446.e4. doi:10.1016/j.chom.2023.01.006

Ng, S. C., Shi, H. Y., Hamidi, N., Underwood, F. E., Tang, W., Benchimol, E. I., et al. (2017). Worldwide incidence and prevalence of inflammatory bowel disease in the 21st century: a systematic review of population-based studies. *Lancet* 390 (10114), 2769–2778. doi:10.1016/s0140-6736(17)32448-0

Park, M. H., Kim, J. H., Chung, Y. H., and Lee, S. H. (2016). Bakuchiol sensitizes cancer cells to TRAIL through ROS- and JNK-mediated upregulation of death receptors and downregulation of survival proteins. *Biochem. Biophys. Res. Commun.* 473 (2), 586–592. doi:10.1016/j.bbrc.2016.03.127

Piovani, D., Hassan, C., Repici, A., Rimassa, L., Carlo-Stella, C., Nikolopoulos, G. K., et al. (2022). Risk of cancer in inflammatory bowel diseases: umbrella review and reanalysis of meta-analyses. *Gastroenterology* 163 (3), 671–684. doi:10.1053/j.gastro.2022.05.038

Piras, A., Rosa, A., Marongiu, B., Atzeri, A., Dessì, M. A., Falconieri, D., et al. (2012). Extraction and separation of volatile and fixed oils from seeds of Myristica fragrans by supercritical CO_2: chemical composition and cytotoxic activity on Caco-2 cancer cells. *J. Food Sci.* 77 (4), C448–C453. doi:10.1111/j.1750-3841.2012.02618.x

Pt, H. J., and Sally, G. (2024). *Cochrane Handbook for systematic reviews of interventions:cochrane book series*. John Wiley & Sons, Ltd.

Pu, Z., Zhang, W., Wang, M., Xu, M., Xie, H., and Zhao, J. (2021). Schisandrin B attenuates colitis-associated colorectal cancer through SIRT1 linked SMURF2 signaling. *Am. J. Chin. Med.* 49 (7), 1773–1789. doi:10.1142/s0192415x21500841

Qi, Y.-T., Zhang, F.-R., and Miao, Y.-L. (2021). Pyropotosis and inflammatory bowel disease. *Chin. J. Inflamm. Bowel Dis.* 05 (1), 92–95. doi:10.3760/cma.j.cn101480-20191022-00127

Rath, T., Atreya, R., Bodenschatz, J., Uter, W., Geppert, C. E., Vitali, F., et al. (2023). Intestinal barrier healing is superior to endoscopic and histologic remission for predicting major adverse outcomes in inflammatory bowel disease: the prospective ERIca trial. *Gastroenterology* 164 (2), 241–255. doi:10.1053/j.gastro.2022.10.014

Ren, Y., Song, X., Tan, L., Guo, C., Wang, M., Liu, H., et al. (2020). A review of the pharmacological properties of psoralen. *Front. Pharmacol.* 11, 571535. doi:10.3389/fphar.2020.571535

Ronkina, N., and Gaestel, M. (2022). MAPK-activated protein kinases: servant or partner? *Annu. Rev. Biochem.* 91, 505–540. doi:10.1146/annurev-biochem-081720-114505

Saito, T., Nishikawa, H., Wada, H., Nagano, Y., Sugiyama, D., Atarashi, K., et al. (2016). Two FOXP3(+)CD4(+) T cell subpopulations distinctly control the prognosis of colorectal cancers. *Nat. Med.* 22 (6), 679–684. doi:10.1038/nm.4086

Salas, A., Hernandez-Rocha, C., Duijvestein, M., Faubion, W., McGovern, D., Vermeire, S., et al. (2020). JAK-STAT pathway targeting for the treatment of inflammatory bowel disease. *Nat. Rev. Gastroenterol. Hepatol.* 17 (6), 323–337. doi:10.1038/s41575-020-0273-0

Shah, S. C., and Itzkowitz, S. H. (2022). Colorectal cancer in inflammatory bowel disease: mechanisms and management. *Gastroenterology* 162 (3), 715–730.e3. doi:10.1053/j.gastro.2021.10.035

Shalapour, S., and Karin, M. (2020). Cruel to Be kind: epithelial, microbial, and immune cell interactions in gastrointestinal cancers. *Annu. Rev. Immunol.* 38, 649–671. doi:10.1146/annurev-immunol-082019-081656

Shao, B., Tang, J., Ji, H., Liu, H., Liu, Y., Zhu, D., et al. (2010). Enhanced oral bioavailability of Wurenchun (Fructus Schisandrae Chinensis extracts) by self-emulsifying drug delivery systems. *Drug Dev. Ind. Pharm.* 36 (11), 1356–1363. doi:10.3109/03639045.2010.480975

Sharifi-Rad, J., Kamiloglu, S., Yeskaliyeva, B., Beyatli, A., Alfred, M. A., Salehi, B., et al. (2020). Pharmacological activities of psoralidin: a comprehensive review of the molecular mechanisms of action. *Front. Pharmacol.* 11, 571459. doi:10.3389/fphar.2020.571459

Sheikh, B. Y., Sarker, M. M. R., Kamarudin, M. N. A., and Mohan, G. (2017). Antiproliferative and apoptosis inducing effects of citral via p53 and ROS-induced mitochondrial-mediated apoptosis in human colorectal HCT116 and HT29 cell lines. *Biomed. Pharmacother.* 96, 834–846. doi:10.1016/j.biopha.2017.10.038

Shen, P., Zhang, Z., Zhu, K., Cao, H., Liu, J., Lu, X., et al. (2019). Evodiamine prevents dextran sulfate sodium-induced murine experimental colitis via the regulation of NF-κB and NLRP3 inflammasome. *Biomed. Pharmacother.* 110, 786–795. doi:10.1016/j.biopha.2018.12.033

Sohn, J. H., Han, K. L., Kim, J. H., Rukayadi, Y., and Hwang, J. K. (2008). Protective Effects of macelignan on cisplatin-induced hepatotoxicity is associated with JNK activation. *Biol. Pharm. Bull.* 31 (2), 273–277. doi:10.1248/bpb.31.273

Song, C., Chen, J., Li, X., Yang, R., Cao, X., Zhou, L., et al. (2021). Limonin ameliorates dextran sulfate sodium-induced chronic colitis in mice by inhibiting PERK-ATF4-CHOP pathway of ER stress and NF-κB signaling. *Int. Immunopharmacol.* 90, 107161. doi:10.1016/j.intimp.2020.107161

Sun, C., Zhao, L., Wang, X., Hou, Y., Guo, X., Lu, J. J., et al. (2022). Psoralidin, a natural compound from Psoralea corylifolia, induces oxidative damage mediated apoptosis in colon cancer cells. *J. Biochem. Mol. Toxicol.* 36 (7), e23051. doi:10.1002/jbt.23051

Sun, H.-H., Yang, J., and Wang, D.-J. (2021). Clinical study of Lizhong decoction and Sishen pill modified and subtractedcombined with FOLFIRl chemotherapy on elderly patients with advanced colon cancer with spleen and kidney Yang deficiency syndrome. *Chin. J. Integr. Traditional West. Med. Dig.* 29 (04), 276–279.

Sun, M., Wu, W., Liu, Z., and Cong, Y. (2017). Microbiota metabolite short chain fatty acids, GPCR, and inflammatory bowel diseases. *J. Gastroenterol.* 52 (1), 1–8. doi:10.1007/s00535-016-1242-9

Tan, Y.-B., Jiang, L.-J., Liao, Z.-J., and Zhou, Q. (2023). Clinical effect of Sishen pill combined with Lizhong decoction in the treatment of patients with spleen-kidney Yang deficiency syndrome after colorectal cancer surgery based on intestinal flora. *China Med.* 18 (07), 1054–1058.

Taniguchi, K., and Karin, M. (2018). NF-κB, inflammation, immunity and cancer: coming of age. *Nat. Rev. Immunol.* 18 (5), 309–324. doi:10.1038/nri.2017.142

Taylor, C. T., and Colgan, S. P. (2007). Hypoxia and gastrointestinal disease. *J. Mol. Med. Berl.* 85 (12), 1295–1300. doi:10.1007/s00109-007-0277-z

Tekeli, I. O., Ateşşahin, A., Sakin, F., Aslan, A., Çeribaşı, S., and Yipel, M. (2018). Protective effects of conventional and colon-targeted lycopene and linalool on ulcerative colitis induced by acetic acid in rats. *Inflammopharmacology* 27, 313–322. doi:10.1007/s10787-018-0485-x

van der Post, S., Jabbar, K. S., Birchenough, G., Arike, L., Akhtar, N., Sjovall, H., et al. (2019). Structural weakening of the colonic mucus barrier is an early event in ulcerative colitis pathogenesis. *Gut* 68 (12), 2142–2151. doi:10.1136/gutjnl-2018-317571

Wan, M. L. Y., Turner, P. C., Co, V. A., Wang, M. F., Amiri, K. M. A., and El-Nezami, H. (2019). Schisandrin A protects intestinal epithelial cells from deoxynivalenol-induced cytotoxicity, oxidative damage and inflammation. *Sci. Rep.* 9 (1), 19173. doi:10.1038/s41598-019-55821-4

Wang, A.-H., He, L.-J., and Zhu, X.-D. (2019a). Effect of sishenwan on toll-like receptor 4 and lRAK-M expression in colonic tissue of rats with ulcerative colitis of spleen-kidney yang deficiency type. *Chin. J. Exp. Traditional Med. Formulae* 25 (14), 70–76. doi:10.13422/j.cnki.syfjx.20191439

Wang, D., Ge, S., Chen, Z., and Song, Y. (2019b). Evodiamine exerts anticancer effects via induction of apoptosis and autophagy and suppresses the migration and invasion of human colon cancer cells. *J. buon* 24 (5), 1824–1829.

Wang, G., Yu, Y., Wang, Y. Z., Wang, J. J., Guan, R., Sun, Y., et al. (2019c). Role of SCFAs in gut microbiome and glycolysis for colorectal cancer therapy. *J. Cell Physiol.* 234 (10), 17023–17049. doi:10.1002/jcp.28436

Wang, H. Y., Zhao, H. M., Wang, Y., Liu, Y., Lu, X. Y., Liu, X. K., et al. (2019d). Sishen Wan® ameliorated trinitrobenzene-sulfonic-acid-induced chronic colitis via NEMO/NLK signaling pathway. *Front. Pharmacol.* 10, 170. doi:10.3389/fphar.2019.00170

Wang, L., Fang, K., Cheng, J., Li, Y., Huang, Y., Chen, S., et al. (2020a). Scaffold hopping of natural product evodiamine: discovery of a novel antitumor scaffold with excellent potency against colon cancer. *J. Med. Chem.* 63 (2), 696–713. doi:10.1021/acs.jmedchem.9b01626

Wang, L., and He, C. (2022). Nrf2-mediated anti-inflammatory polarization of macrophages as therapeutic targets for osteoarthritis. *Front. Immunol.* 13, 967193. doi:10.3389/fimmu.2022.967193

Wang, L., Tang, L., Feng, Y., Zhao, S., Han, M., Zhang, C., et al. (2020b). A purified membrane protein from Akkermansia muciniphila or the pasteurised bacterium blunts colitis associated tumourigenesis by modulation of CD8(+) T cells in mice. *Gut* 69 (11), 1988–1997. doi:10.1136/gutjnl-2019-320105

Wang, L.-H., Ma, D.-C., and Sun, L.-X. (2015). The origin and new exploration of SiShen pills. *West. J. Traditional Chin. Med.* 28 (03), 47–49.

Wang, M., Huang, X., Kang, Z., Huang, J., Wei, S., Zhao, H., et al. (2022a). Mechanism of sishen-pill-regulated special memory T and mTfh cell via involving JAK/STAT5 pathway in colitis mice. *Evid. Based Complement. Altern. Med.* 2022, 6446674. doi:10.1155/2022/6446674

Wang, M., Tian, B., Shen, J., Xu, S., Liu, C., Guan, L., et al. (2023a). Bavachin induces apoptosis in colorectal cancer cells through Gadd45a via the MAPK signaling pathway. *Chin. J. Nat. Med.* 21 (1), 36–46. doi:10.1016/s1875-5364(23)60383-8

Wang, M., Zhou, B., Cong, W., Zhang, M., Li, Z., Li, Y., et al. (2021). Amelioration of AOM/DSS-Induced murine colitis-associated cancer by evodiamine intervention is primarily associated with gut microbiota-metabolism-inflammatory signaling Axis. *Front. Pharmacol.* 12, 797605. doi:10.3389/fphar.2021.797605

Wang, M. X., Lin, L., Chen, Y. D., Zhong, Y. P., Lin, Y. X., Li, P., et al. (2020c). Evodiamine has therapeutic efficacy in ulcerative colitis by increasing Lactobacillus acidophilus levels and acetate production. *Pharmacol. Res.* 159, 104978. doi:10.1016/j.phrs.2020.104978

Wang, S.-J., Zhang, Y., Liang, H.-Y., Zhang, M.-B., and Xu, Z.-L. (2023b). Influence of deoxyschizandrin on NF KB/COX-2 signal pathway in colon of mice with inflammatory bowel disease. *West. J. Traditional Chin. Med.* 36 (09), 35–39.

Wang, T., Shen, Y., Luyten, S., Yang, Y., and Jiang, X. (2020d). Tissue-resident memory CD8(+) T cells in cancer immunology and immunotherapy. *Pharmacol. Res.* 159, 104876. doi:10.1016/j.phrs.2020.104876

Wang, W., Wang, S. K., Wang, Q., Zhang, Z., Li, B., Zhou, Z. D., et al. (2023c). Diclofenac and eugenol hybrid with enhanced anti-inflammatory activity through activating HO-1 and inhibiting NF-κB pathway *in vitro* and *in vivo*. *Eur. J. Med. Chem.* 259, 115669. doi:10.1016/j.ejmech.2023.115669

Wang, X., Shen, C., Wang, X., Tang, J., Wu, Z., Huang, Y., et al. (2023d). Schisandrin protects against ulcerative colitis by inhibiting the SGK1/NLRP3 signaling pathway and reshaping gut microbiota in mice. *Chin. Med.* 18 (1), 112. doi:10.1186/s13020-023-00815-8

Wang, Y., Zhang, T., and He, X. (2023e). Advances in the role of microRNAs associated with the PI3K/AKT signaling pathway in lung cancer. *Front. Oncol.* 13, 1279822. doi:10.3389/fonc.2023.1279822

Wang, Y., Zhu, X., Liang, Y., Li, X., Wang, Y., and Li, J. (2022b). Sishen wan treats ulcerative colitis in rats by regulating gut microbiota and restoring the Treg/Th17 balance. *Evid. Based Complement. Altern. Med.* 2022, 1432816. doi:10.1155/2022/1432816

Wang, Y. F., Liu, Y. N., Xiong, W., Yan, D. M., Zhu, Y., Gao, X. M., et al. (2014). A UPLC-MS/MS method for *in vivo* and *in vitro* pharmacokinetic studies of psoralenoside, isopsoralenoside, psoralen and isopsoralen from Psoralea corylifolia extract. *J. Ethnopharmacol.* 151 (1), 609–617. doi:10.1016/j.jep.2013.11.013

Wang, Z. J., Chen, L. H., Xu, J., Xu, Q. X., Xu, W., and Yang, X. W. (2023f). Corylin ameliorates chronic ulcerative colitis via regulating the gut-brain axis and promoting 5-hydroxytryptophan production in the colon. *Phytomedicine* 110, 154651. doi:10.1016/j.phymed.2023.154651

Wei, S.-T., Liu, Y.-Q., Huang, J., Sheng, Y.-H., and Tang, L.-M. (2020). Research progress of chemical component,Medicinal efficacy and liver toxicity of fructus evodiae. *World Chin. Med.* 15 (23), 3580–3585+3592.

Wei, W., Hou, J.-Z., Zhu, S.-J., Sheng, X.-Y., and Guo, H.-R. (2021). Study on quality control of multi-components in sishen pills based on fingerprints. *Chin. J. Inf. Traditional Chin. Med.* 28 (10).

Wu, W., and Liu, Z.-J. (2022). Mechanisms of the carcinogenesis of inflammatory bowel disease and current status of animal models researches. *Chin. J. Inflamm. Bowel Dis.* 06 (4), 281–286. doi:10.3760/cma.j.cn101480-20220913-00146

Xing, N.-N., Qu, H.-D., Ren, W.-C., and Ma, W. (2021). Main chemical constituents and modern pharmacological action of Schisandrae chinensis fructus:A review. *Chin. J. Exp. Traditional Med. Formulae* 27 (15), 210–218. doi:10.13422/j.cnki.syfjx.20211407

Xu, B., and Xiao, L.-B. (2023). Research Progress on hepatotoxicity and attenuation of Psoralea corylifolia. *Lishizhen Med. Materia Medica Res.* 34 (01), 159–161.

Xu, J., Zhang, Q., Wang, H., Zhang, Y., Cheng, P.-Y., and Gao, F. (2022a). Clinical observation on the efficacy and adverse reaction of modified sishen pill in combination with abemaciclib and endocrine therapy in patients with HR+/HER2-Advanced breast cancer. *Chin. J. Ration. Drug Use* 19 (12), 38–43.

Xu, Z.-L., Xu, H., Chen, X., Li, R.-N., Tao, X.-J., and Li, X.-L. (2022b). Meta-analysis of Sishen-pill alone or in combination in the treatment of inflammatory bowel disease. *China Mod. Dr.* 60 (29), 72–75+93.

Xue, M., Shi, L., Wang, W., Chen, S., and Wang, L. (2018). An overview of molecular profiles in ulcerative colitis-related cancer. *Inflamm. Bowel Dis.* 24 (9), 1883–1894. doi:10.1093/ibd/izy221

Yamazaki, T., Bravo-San Pedro, J. M., Galluzzi, L., Kroemer, G., and Pietrocola, F. (2021). Autophagy in the cancer-immunity dialogue. *Adv. Drug Deliv. Rev.* 169, 40–50. doi:10.1016/j.addr.2020.12.003

Yang, C.-Q., Lian, W.-Y., Wang, Y.-G., and Gao, Y. (2021). Research progress in pharmacology and toxicology of evodiamine. *China J. Chin. Materia Medica* 46 (20), 5218–5225. doi:10.19540/j.cnki.cjcmm.20210518.602

Yang, T., Li, S., and Deng, S.-Q. (2023a). Mechanism of isobavachalcone in treatment of ulcerative colitis. *J. Shanghai Univ. Sci. Ed.* 29 (02), 253–263.

Yang, W., Gong, X., Wang, X., and Huang, C. (2019). A mediator of phosphorylated Smad2/3, evodiamine, in the reversion of TAF-induced EMT in normal colonic epithelial cells. *Invest New Drugs* 37 (5), 865–875. doi:10.1007/s10637-018-0702-x

Yang, X. N., Liu, X. M., Fang, J. H., Zhu, X., Yang, X. W., Xiao, X. R., et al. (2018). PPARα mediates the hepatoprotective effects of nutmeg. *J. Proteome Res.* 17 (5), 1887–1897. doi:10.1021/acs.jproteome.7b00901

Yang, Y., Liu, Z., Lyu, H., Guo, X., Jiang, H., Liu, L., et al. (2023b). Traditional Chinese medicine-induced treatment in colitis-associated colorectal cancer. *Chin. Med. J. Engl.* 136 (10), 1249–1250. doi:10.1097/cm9.0000000000002667

Yimam, M., Jiao, P., Hong, M., and Jia, Q. (2016). Hepatoprotective activity of an herbal composition, MAP, a standardized blend comprising Myristica fragrans, Astragalus membranaceus, and poria cocos. *J. Med. Food* 19 (10), 952–960. doi:10.1089/jmf.2016.0048

Yong, H. Y., Koh, M. S., and Moon, A. (2009). The p38 MAPK inhibitors for the treatment of inflammatory diseases and cancer. *Expert Opin. Investig. Drugs* 18 (12), 1893–1905. doi:10.1517/13543780903321490

Yu, S., and Qian, H. (2021). Deoxyschizandrin treats mice with ulcerative colitis possibly via the TLR4/NF-κB signaling pathway. *Am. J. Transl. Res.* 13 (4), 3856–3863.

Yu, W.-L., Wang, Y., Cheng, J., Niu, L.-H., Chen, G.-Y., An, F.-L., et al. (2024). Effect of sishen pill and disassembling prescription on experimental ulcerative colitis in rats. *Pharmacol. Clin. Chin. Materia Medica*, 1–17. doi:10.13412/j.cnki.zyyl.20231020.001

Zaka, A., Mridha, N., Subhaharan, D., Jones, M., Niranjan, S., Mohsen, W., et al. (2023). Inflammatory bowel disease patients have an increased risk of acute coronary syndrome: a systematic review and meta-analysis. *Open Heart* 10 (2), e002483. doi:10.1136/openhrt-2023-002483

Zangara, M. T., Darwish, L., and Coombes, B. K. (2023). Characterizing the pathogenic potential of Crohn's disease-associated adherent-invasive *Escherichia coli*. *EcoSal Plus* 11, eesp00182022. doi:10.1128/ecosalplus.esp-0018-2022

Zhang, C., Fan, X., Xu, X., Yang, X., Wang, X., and Liang, H. P. (2010). Evodiamine induces caspase-dependent apoptosis and S phase arrest in human colon lovo cells. *Anticancer Drugs* 21 (8), 766–776. doi:10.1097/CAD.0b013e32833d26a9

Zhang, G., Yu, Y., Huang, H.-L., and Zhang, S.-C. (2019). Mechanism of sishenwan in treatment of ulcerative colitis based on network pharmacology and bioinformatics. *Chin. J. Exp. Traditional Med. Formulae* 25 (24), 142–149. doi:10.13422/j.cnki.syfjx.20192438

Zhang, W., Wang, W., Shen, C., Wang, X., Pu, Z., and Yin, Q. (2021a). Network pharmacology for systematic understanding of Schisandrin B reduces the epithelial cells injury of colitis through regulating pyroptosis by AMPK/Nrf2/NLRP3 inflammasome. *Aging (Albany NY)* 13 (19), 23193–23209. doi:10.18632/aging.203611

Zhang, W. F., Yang, Y., Su, X., Xu, D. Y., Yan, Y. L., Gao, Q., et al. (2016). Deoxyschizandrin suppresses dss-induced ulcerative colitis in mice. *Saudi J. Gastroenterol.* 22 (6), 448–455. doi:10.4103/1319-3767.195552

Zhang, X.-X., Jin, J.-W., Liu, C.-H., Zhou, M., He, Y.-X., Wang, F., et al. (2021b). Effect of Nrf2/HO-1 signaling pathway in intestinal protection by Sishen Pills against ulcerative colitis in mice. *China J. Chin. Materia Medica* 46 (16), 4187–4192. doi:10.19540/j.cnki.cjcmm.20210524.402

Zhang, X.-X., Li, X.-N., Hu, S., and Chang, R.-M. (2018). Simultaneous determination of nine bioactive components in Sishen Pills by HPLC-ESI-MS/MS. *Chin. Traditional Herb. Drugs* 49 (09), 2070–2075.

Zhang, X.-Y., Zhao, H.-M., Liu, Y., Liu, X.-K., Liu, F.-C., Chen, F., et al. (2020a). Regulation of schisandrin A on oxidative stress and ulcerative colitis in rats. *Chin. Archives Traditional Chin. Med.* 38 (02), 166–169+283. doi:10.13193/j.issn.1673-7717.2020.02.041

Zhang, X. Y., Zhao, H. M., Liu, Y., Lu, X. Y., Li, Y. Z., Pan, Q. H., et al. (2021c). Sishen pill maintained colonic mucosal barrier integrity to treat ulcerative colitis via Rho/ROCK signaling pathway. *Evid. Based Complement. Altern. Med.* 2021, 5536679. doi:10.1155/2021/5536679

Zhang, Y., Dai, H.-B., and Zhu, P.-F. (2021d). Observation on the curative effect of shenling baizhu powder and sishen Pill Combined with chemotherapy for radical resection of colorectal cancer. *Chin. J. Surg. Integr. Traditional West. Med.* 27 (04), 592–596.

Zhang, Y., Yan, T., Sun, D., Xie, C., Wang, T., Liu, X., et al. (2020b). Rutaecarpine inhibits KEAP1-NRF2 interaction to activate NRF2 and ameliorate dextran sulfate sodium-induced colitis. *Free Radic. Biol. Med.* 148, 33–41. doi:10.1016/j.freeradbiomed.2019.12.012

Zhang, Y., Zhang, H., Zhang, K., Li, Z., Guo, T., Wu, T., et al. (2020c). Co-hybridized composite nanovesicles for enhanced transdermal eugenol and cinnamaldehyde delivery and their potential efficacy in ulcerative colitis. *Nanomedicine* 28, 102212. doi:10.1016/j.nano.2020.102212

Zhang, Y., Zhang, Y., Zhao, Y., Wu, W., Meng, W., Zhou, Y., et al. (2022). Protection against ulcerative colitis and colorectal cancer by evodiamine via anti-inflammatory effects. *Mol. Med. Rep.* 25 (5), 188. doi:10.3892/mmr.2022.12704

Zhao, H., Ming, T., Tang, S., Ren, S., Yang, H., Liu, M., et al. (2022). Wnt signaling in colorectal cancer: pathogenic role and therapeutic target. *Mol. Cancer* 21 (1), 144. doi:10.1186/s12943-022-01616-7

Zhao, H. M., Huang, X. Y., Zhou, F., Tong, W. T., Wan, P. T., Huang, M. F., et al. (2013). Si shen wan inhibits mRNA expression of apoptosis-related molecules in p38 MAPK signal pathway in mice with colitis. *Evid. Based Complement. Altern. Med.* 2013, 432097. doi:10.1155/2013/432097

Zhao, H. M., Liu, Y., Huang, X. Y., Liu, X. K., Chen, F., Zhang, X. Y., et al. (2019). Pharmacological mechanism of Sishen Wan® attenuated experimental chronic colitis by inhibiting wnt/β-catenin pathway. *J. Ethnopharmacol.* 240, 111936. doi:10.1016/j.jep.2019.111936

Zhao, Q., Duck, L. W., Huang, F., Alexander, K. L., Maynard, C. L., Mannon, P. J., et al. (2020). CD4(+) T cell activation and concomitant mTOR metabolic inhibition can ablate microbiota-specific memory cells and prevent colitis. *Sci. Immunol.* 5 (54), eabc6373. doi:10.1126/sciimmunol.abc6373

Zhaohua, Z., Rong, L., Nana, D. U., and Xiangdong, Z. (2022). Efficacy of Sishen Wan on dinitrobenzene sulfonic acid-induced ulcerative colitis and its effect on toll-like receptor 2/interleukin-1 receptor-associated kinase-4/nuclear factor-κB signal pathway. *J. Tradit. Chin. Med.* 42 (4), 565–575. doi:10.19852/j.cnki.jtcm.20220608.001

Zhou, Z.-X. (2020). The screening of active ingredients and underlying mechanism in Psoraleae Fructus treatment of ulcerative colitis. doctor. doctor's thesis. Liaoning: Shenyang Pharmaceutical University.

Zhu, L. Q., Zhang, L., Zhang, J., Chang, G. L., Liu, G., Yu, D. D., et al. (2021). Evodiamine inhibits high-fat diet-induced colitis-associated cancer in mice through regulating the gut microbiota. *J. Integr. Med.* 19 (1), 56–65. doi:10.1016/j.joim.2020.11.001

frontiers | Frontiers in Pharmacology

TYPE Original Research
PUBLISHED 17 April 2024
DOI 10.3389/fphar.2024.1347970

OPEN ACCESS

EDITED BY
Xianyu Li,
China Academy of Chinese Medical Sciences, China

REVIEWED BY
Hong-he Xiao,
Liaoning University of Traditional Chinese Medicine, China
Li Luo,
Sichuan University, China

*CORRESPONDENCE
Shaozhuo Zhang,
zhangsz800@sina.com
Qilong Wang,
wangqilong_00@tjutcm.edu.cn

†These authors share first authorship

RECEIVED 01 December 2023
ACCEPTED 01 April 2024
PUBLISHED 17 April 2024

CITATION
Jia Z, Zhang J, Yang X, Chen H, Wang Y, Francis OB, Li Y, Liu Z, Zhang S and Wang Q (2024), Bioactive components and potential mechanisms of Biqi Capsule in the treatment of osteoarthritis: based on chondroprotective and anti-inflammatory activity.
Front. Pharmacol. 15:1347970.
doi: 10.3389/fphar.2024.1347970

Bioactive components and potential mechanisms of Biqi Capsule in the treatment of osteoarthritis: based on chondroprotective and anti-inflammatory activity

Ziyue Jia[1†], Jiale Zhang[2†], Xintong Yang[2†], Huiyou Chen[1†], Yuxing Wang[1], Opoku Bonsu Francis[2], Yuanchao Li[1], Zhanbiao Liu[2], Shaozhuo Zhang[1*] and Qilong Wang[2,3*]

[1]School of Chinese Materia Medica, Tianjin University of Traditional Chinese Medicine, Tianjin, China, [2]Institute of Traditional Chinese Medicine, Tianjin University of Traditional Chinese Medicine, Tianjin, China, [3]State Key Laboratory of Component-based Chinese Medicine, Tianjin University of Traditional Chinese Medicine, Tianjin, China

Cartilage damage and synovial inflammation are vital pathological changes in osteoarthritis (OA). Biqi Capsule, a traditional Chinese medicine formula used for the clinical treatment of arthritis in China, yields advantages in attenuating OA progression. The drawback here is that the bioactive components and pharmacological mechanisms by which Biqi Capsule exerts its anti-inflammatory and chondroprotective effects have yet to be fully clarified. For *in vivo* studies, a papain-induced OA rat model was established to explore the pharmacological effects and potential mechanisms of Biqi Capsule against OA. Biqi Capsule alleviated articular cartilage degeneration and chondrocyte damage in OA rats and inhibited the phosphorylation of NF-κB and the expression of pro-inflammatory cytokines in synovial tissue. Network pharmacology analysis suggested that the primary biological processes regulated by Biqi Capsule are inflammation and oxidative stress, and the critical pathway regulated is the PI3K/AKT signaling pathway. The result of this analysis was later verified on SW1353 cells. The *in vitro* studies demonstrated that Glycyrrhizic Acid and Liquiritin in Biqi Capsule attenuated H_2O_2-stimulated SW1353 chondrocyte damage via activation of PI3K/AKT/mTOR pathway. Moreover, Biqi Capsule alleviated inflammatory responses in LPS-stimulated RAW264.7 macrophages via the NF-κB/IL-6 pathway. These observations were suggested to have been facilitated by Brucine, Liquiritin, Salvianolic Acid B, Glycyrrhizic Acid, Cryptotanshinone, and Tanshinone IIA. Put together, this study partially clarifies the pharmacological mechanisms and the bioactive components of Biqi capsules against OA and suggests that it is a promising therapeutic option for the treatment of OA. Chemical compounds studied in this article. Strychnine (Pubchem CID:441071); Brucine (Pubchem CID:442021); Liquiritin (Pubchem

CID:503737); Salvianolic Acid B (Pubchem CID:6451084); Glycyrrhizic Acid (Pubchem CID:14982); Cryptotanshinone (Pubchem CID:160254); Tanshinone IIA (Pubchem CID:164676).

KEYWORDS

osteoarthritis, Biqi capsule, PI3K/Akt/mTOR pathway, NF-κB/IL-6 pathway, bioactive component

Highlights

- Biqi Capsule ameliorates papain-induced cartilage damage and inflammatory response.
- Biqi Capsule exerts its chondroprotective effect by activating the PI3K/AKT/mTOR pathway in chondrocytes and an anti-inflammatory effect by inhibiting the NF-κB/IL-6 pathway.
- Glycyrrhizic Acid and Liquiritin alleviate chondrocyte damage via the PI3K/AKT/mTOR pathway.

1 Introduction

Osteoarthritis is a complex disease characterized by pathological changes across all joint tissues, including cartilage, subchondral bone, ligaments, menisci, joint capsule, and synovium (Loeser et al., 2016). The incidence of OA is increasing globally, making it one of the primary diseases that reduce the quality of life and can even lead to disability in older adults (Allen et al., 2022). Currently, an estimated 240 million individuals worldwide have symptomatic OA. Low-grade chronic inflammation of the synovium plays a central role in the pathological progression of OA (Coaccioli et al., 2022). Pro-inflammatory mediators, such as cytokines, lipid mediators, and reactive oxygen species (ROS), produced by synoviocytes are responsible for the degradation of the extracellular matrix and cartilage loss (Zahan et al., 2020). In addition, the mediators that cause cartilage damage in OA (such as damage-associated molecular patterns and extracellular matrix components) can exude into the synovial fluid and recruit synovial macrophages, which further produce an excess of pro-inflammatory cytokines, accelerating cartilage degradation (Coaccioli et al., 2022). In summary, the triad of cartilage destruction, synovial inflammation, and macrophage activation contributes to an ongoing sterile wound-healing "vicious circle" resulting in joint tissue pathology. Modulating these cellular processes or intervening with factors that modify the phenotypic state of the cells may be a promising approach to slowing down OA development (Kulkarni et al., 2021). Biqi Capsule (NMPA approval number: Z10910026) is a Chinese traditional patent medicine used for the treatment of OA (SPGD, 2021). Biqi Capsule is composed of 10 Chinese herbs, including *Strychnos nux-vomica* L., *Pheretima aspergillum* (E. Perrier), *Codonopsis pilosula* (Franch.) Nannf., *Poria cocos* (Schw.) Wolf., *Atractylodes macrocephala* Koidz., *Ligusticum chuanxiong* Hort., *Salvia miltiorrhiza* Bunge, *Panax notoginseng* (Burk.) F. H. Chen ex C. Chow, *Achyranthes bidentata* BL., and *Glycyrrhiza uralensis* Fisch. Previous pharmacological studies have shown that Biqi Capsule alleviates local joint and systemic inflammation, synovial hyperplasia, and cartilage destruction caused by collagen-induced arthritis (CIA) (Wang et al., 2018), and its anti-inflammatory effect may be a result of inhibition of the NO-iNOS pathway and COX-2 pathway (Wang et al., 2011). The chemical components of Biqi Capsule have already been identified according to previous studies (Wang et al., 2011; Jing et al., 2018; Xing-Yan et al., 2021). However, the pharmacological mechanisms and bioactive components of Biqi Capsule which facilitate the treatment of OA remain largely unexplored.

In this study, we evaluate the anti-inflammatory and chondroprotective effects of Biqi Capsule using a papain-induced rat model of OA. Network pharmacology analysis and pathway-blocking experiments were used to explore the underlying mechanisms. Molecular docking and screening based on H_2O_2-stimulated SW1353 cells and LPS-stimulated RAW264.7 cells were performed to better assess the molecular dynamics and pharmacological activities of the bioactive components. Our results revealed the underlying mechanisms and bioactive components of Biqi Capsule in treating OA.

2 Materials and methods

2.1 Reagents and antibodies

Biqi Capsules were provided by Tianjin Darentang Pharmaceutical Jingwanhong Co. Ltd. (Tianjin, China) with the production batch number 31174066. The quality of Biqi Capsule is supervised by the National Medical Products Administration (NMPA) according to the Pharmacopoeia of the People's Republic of China 2020 Edition, Part I, Page 1808. Papain (76,220), poloxamer (P4894), Lipopolysaccharide (LPS, L2880), and Dimethyl sulfoxide (DMSO, D8418) were purchased from Sigma-Aldrich (Shanghai, China). LY294002 was purchased from MedChemExpress (NJ, USA). Strychnine, Brucine, Liquiritin, Salvianolic Acid B, Glycyrrhizic Acid, Cryptotanshinone, and Tanshinone IIA were purchased from Sichuan Vicky Biotechnology Co., Ltd. (Chengdu, China). The primary antibodies against PI3K p85 (#4257), Akt (#9272), p-Akt (#9275), NF-κB p65 (#8242), p-NF-κB p65 (#3033), PCNA (#13110), the second antibodies against rabbit (#7074) and mouse (#7076) IgG were purchased from Cell Signaling Technology (MA, USA). The primary antibodies against p-PI3K p85 (ab182651) and β-actin (ab8226) were purchased from Abcam (Cambridge, UK). The primary antibodies against mTOR (A11355) and p-mTOR (AP0978) were purchased from ABclonal Technology (Wuhan, China). Rat PGE2 Elisa Kit (LCSJZF30697) was purchased from LunChangShuo Biotech. (Xiamen, China); Rat IL-6 Elisa Kit (E04640r) was purchased from CUSABIO (Wuhan, China); Rat TNF-α Elisa Kit (KRC3011), Rat IL-1β Elisa Kit (BMS630) and

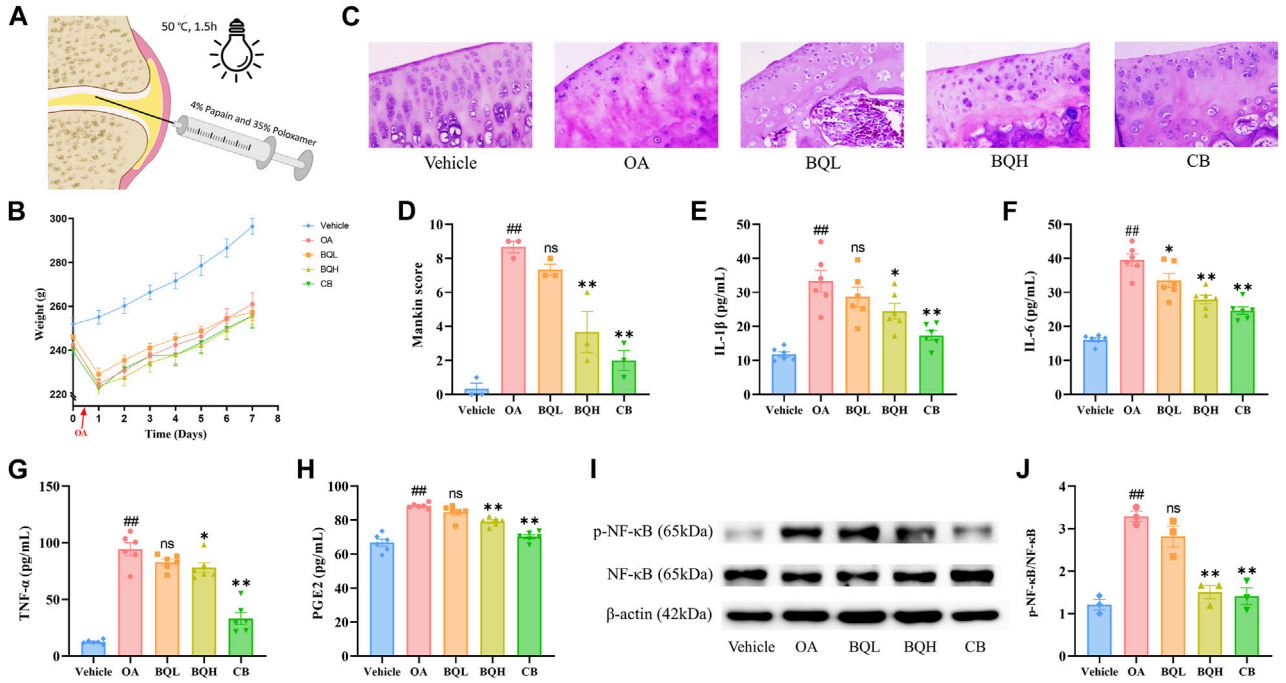

FIGURE 1
The efficacy of Biqi Capsule on papain-induced OA rats. The papain-induced OA rats were treated with Biqi Capsule for 7 days. **(A)** Construction of an OA rat model. **(B)** Weight of rats during the experiment. Data were present as mean ± SEM (n = 10). **(C)** Representative sections of HE staining knee joints from rats in different groups (400×). **(D)** HE staining sections of rat knee joints from each group were used for the assessment via Mankin score. Data were presented as mean ± SEM (n = 3, #$p < 0.05$, ##$p < 0.01$ compared with the Vehicle group; *$p < 0.05$, **$p < 0.01$ compared with the OA group). **(E–H)** After 7 days of treatment, the IL-1β, IL-6, TNF-α, and PGE2 levels in synovial tissue were examined by ELISA. Data were presented as mean ± SEM. (n = 6, #$p < 0.05$, ##$p < 0.01$ compared with the Vehicle group; *$p < 0.05$, **$p < 0.01$ compared with the OA group). **(I, J)** After 7 days of treatment, the phosphorylation of NF-κB (p65) in the synovial tissue was examined by Western Blot. The relative expression was quantified by ImageJ software. Data were presented as mean ± SEM. (n = 3, #$p < 0.05$, ##$p < 0.01$ compared with the Vehicle group; *$p < 0.05$, **$p < 0.01$ compared with the OA group).

mouse IL-6 ELISA Kit (88-7064-88) were purchased from Invitrogen (CA, USA).

2.2 Animals and models

Healthy male SD rats (n = 60, body weight: 160g–180 g) were purchased from SPF Biotechnology Co., Ltd. (Beijing, China). All experimental procedures were approved by the Animal Care and Use Committee of the Tianjin University of Traditional Chinese Medicine (Authorization number: TCM-LAEC2022129). All animals were kept at 22°C–26 °C and 55% ± 5% humidity with a 12 h light/dark cycle and allowed free access to food and water during the experiments. After a week of adjustment, all of the rats were randomly divided into five groups as follows: Vehicle group (equal normal saline solution, i. g.), OA group (equal normal saline solution, i. g.), BQL group (Biqi Capsule low dose, 0.648 g/kg·d, i. g., double clinical dose), BQH group (Biqi Capsule high dose, 1.296 g/kg·d, i. g.), Celecoxib group (CB, as a positive control, 24 mg/kg·d, i. g.). The rat model of OA was established using the invention patent method of the author's research group, which has been authorized by the China National Intellectual Property Administration (Approval number: CN102058877A). Previous studies have demonstrated that this model successfully simulates the pathophysiological processes of OA in humans and is suitable for pharmacological studies and efficacy evaluation of anti-osteoarthritic drugs (Zhanbiao et al., 2024). Briefly, the model of OA was induced by a sustained-release papain agent (4% papain and poloxamer). The sustained-release papain agent was injected into both knee joint compartments of rats anesthetized with pentobarbital and then monitored for 1.5 h at 50°C (Figure 1A).

2.3 Biqi Capsule experimental design

For the *in vivo* study, rats had undergone a single intra-articular injection with 50μL/knee joint sustained-release papain agent. The day after the establishment of the OA model, BQL and BQH administration groups received the indicated dosage of Biqi Capsule content powder (dissolved in double distilled water) by oral gavage daily for seven consecutive days. Meanwhile, rats in the OA and CB groups were administered water and celecoxib, respectively. The dose was administered as described above.

For the *in vitro* study, a solution from Biqi Capsule extract was prepared as follows (Wang et al., 2011): 10 g of Biqi Capsule content powder was mixed with 100 mL double-distilled water, extracted by ultrasonication twice at 37 °C for 1 h each. The extraction solution was centrifuged at 12,000rpm for 30 min and then freeze-dried to obtain the aqueous extract of Biqi Capsule. The extract was dissolved in a medium before use and filtered through a 0.22 μm pore size membrane filter (Millipore, USA).

2.4 Keen joint hematoxylin and eosin staining

Rats were euthanized on the eighth day to obtain the knee joints. The knee joints were fixed in 4% paraformaldehyde solution, decalcified with 1% nitric acid for 48h, dehydrated in gradient ethanol and xylene, and embedded in paraffin wax. Knee joint sections (4 μm) were stained with hematoxylin and eosin (HE) staining, and the cartilage abnormalities were evaluated by the modified Mankin score (Mankin and Lippiello, 1970; Mankin et al., 1971; Mankin et al., 1981; Takahashi et al., 2019; Sun et al., 2020).

2.5 Detection of inflammatory factors in tissue homogenate

Synovial tissues were rinsed with pre-chilled PBS, the blood was removed, and the tissues were dried with filter paper. The synovial tissues were weighed accurately and ground in a homogenizer (Servicebio, Wuhan, China) by adding 0.1 mg/μL PBS. The prepared tissue homogenate was centrifuged at 4 °C and 12,000 rpm for 15 min, and the supernatant was retained. The levels of PGE2, IL-6, IL-1β, and TNF-α were determined by ELISA according to the manufacturer's instructions.

2.6 Western blot analysis

Total protein from synovial tissue/cells was collected with RIPA lysis containing Phosphatase Inhibitor Cocktail and Protease Inhibitor Cocktail (Yeasen), then ground in a homogenizer. Concentrations of protein were determined by the BCA Protein Assay Reagent Kit. 10 μg protein was separated by SDS-PAGE electrophoresis and transferred to PVDF membranes (Merck, NJ, USA). After blocking with 5% fresh nonfat milk in tris-buffered saline containing 0.05% Tween-20, the membranes were incubated with primary antibody overnight at 4 °C, followed by HRP-conjugated secondary antibody incubation. The membranes were incubated with Chemiluminescent HRP Substrate (Merck) for 1 min, then images were developed through Amersham Imager 600 (GE, MA, USA). The relative expression was quantified by ImageJ software.

2.7 Network pharmacology analysis

2.7.1 Target prediction of compounds in Biqi Capsule

Quality markers also known as "Q-markers" of Traditional Chinese Medicine are efficacy-associated markers, identified by integrating multidiscipline-based strategies (including natural products chemistry, analytical chemistry, bionics, computer-aided design, pharmacology, system biology, and pharmacodynamics) (Yang et al., 2017). It is a parameter used to assess the functional properties that exist in the raw materials and products of TCM (including the decoction materials, decoctions, extractives, and Chinese patent medicines), which can be used as the indicators for quality control of TCM to embody the effectiveness. Based on the identification of chemical constituents and the analysis of Quality-markers, seven Quality-markers of Biqi Capsule are summarized in Figure 3A (Wang et al., 2011; Jing et al., 2018; Xing-Yan et al., 2021).

The structure files (Mol2 format) of the compounds were downloaded from PubChem (https://pubchem.ncbi.nlm.nih.gov/), and uploaded to the PharmMapper server (https://lilab-ecust.cn/pharmmapper/index.html). The species is restricted to "human" for virtual screening of target prediction based on reverse molecular docking. The target prediction results were used to select the top 50% of the Fit value as the critical targets for the compounds and were imported into the UniProt database for their corresponding gene names.

2.7.2 OA target gene prediction

OA-related targets were collected from three databases using "Osteoarthritis" as the keyword: the GeneCards database (https://www.genecards.org/), the Online Mendelian Inheritance in Man (OMIM) database (https://www.omim.org/) and the Therapeutic Target Database (TTD) (http://db.idrblab.net/ttd).

2.7.3 GO and KEGG analysis

The BQ targets identified in Section 2.7.1, along with the OA targets identified in Section 2.7.2, were both uploaded to the Draw Veen Diagram website (https://bioinformatics.psb.ugent.be/webtools/Venn/). Overlapping targets in the Veen diagram were taken into further consideration. Cytoscape 3.9.1 software (http://www.cytoscape.org/) was used to further analyze the overlapping targets. The compounds and overlapping targets were then exported into Cytoscape v3.9.1 to construct and analyze the network's topological structures using the MCODE plug-in with the "Degree value" setting. Targets with high degree values were considered essential targets for treating OA. Kyoto Encyclopedia of Genes and Genomics (KEGG) pathway enrichment analysis and gene ontology (GO) analysis in the DAVID database were performed to investigate gene function and pathway enrichment analysis. The official gene symbols of the common targets were entered with *H. sapiens* as the selected species. Analyses yielded the top 10 GO biological processes (BP), molecular functions (MF), cellular component (CC) terms, and the top 10 KEGG pathways. We sorted the desired data by applying filters on gene *p*-value. The analysis results were visualized via R-4.1.1. The top five entries in terms of *p*-value were selected to be displayed.

2.8 Cell culture

RAW264.7 and SW1353 cells were purchased from Procell Life Science and Technology Co., Ltd (Wuhan, China). Passage numbers of all cells for the experiment were 5–10. The RAW264.7 cells were cultured in high-glucose Dulbecco's Modified Eagle medium (DMEM; Gibco, MA, USA) containing 10% fetal bovine serum (FBS; Gibco), penicillin 100 U/mL (Gibco) and streptomycin 100 μg/mL (Gibco) at 37 °C in humidified conditions with 5% CO_2. SW1353 cells were cultured in Leibovitz's L-15 medium (Procell) containing 10% FBS, penicillin 100 U/mL, and streptomycin 100 μg/mL at 37°C in humidified conditions with no CO_2.

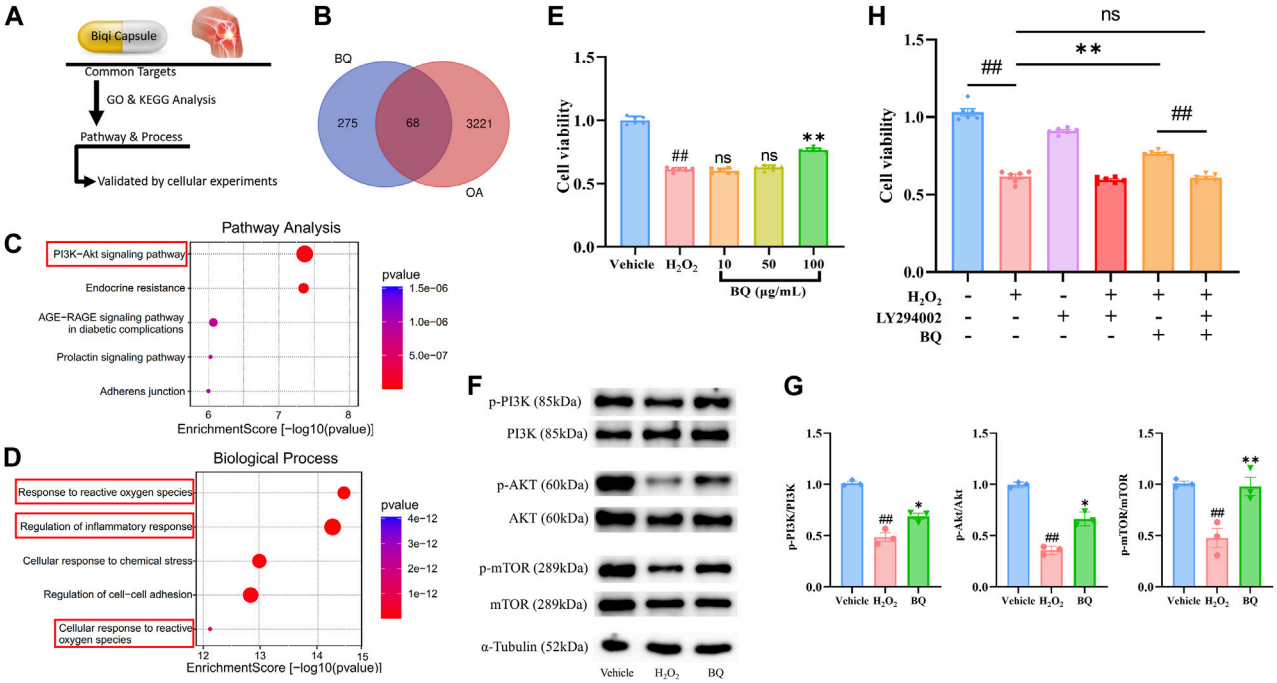

FIGURE 2
Network pharmacology analysis of Biqi Capsule for treating OA, and validated by H_2O_2-stimulated SW1353 cells. **(A)** Process of Network pharmacology prediction and cellular experiments validation. **(B)** Venn diagram showing overlap of OA genes and predicted compound targets. **(C)** Kyoto Encyclopedia of Genes and Genomes (KEGG) pathway enrichment analysis. **(D)** Gene Ontology (GO) analysis of biological processes. **(E)** SW1353 cells were incubated with H_2O_2 (260 μmol/L) and Biqi Capsule extract (BQ) for 12 h. Cell viability was determined by the CCK8 test. Data were presented as mean ± SEM. (n = 6, #$p < 0.05$, ##$p < 0.01$ compared with the Vehicle group; *$p < 0.05$, **$p < 0.01$ compared with the H_2O_2 group) **(F, G)** SW1353 cells were incubated with H_2O_2 (260 μmol/L) and Biqi Capsule extract (BQ) (100 μg/mL) for 12 h. The regulation effect of Biqi Capsule extract on phosphorylation of PI3K, AKT, and mTOR in SW1353 cells was measured by Western Blot analysis. The densitometric analyses of three independent experiments were shown. Data were presented as mean ± SEM. (n = 3, #$p < 0.05$, ##$p < 0.01$ compared with the Vehicle group; *$p < 0.05$, **$p < 0.01$ compared with the H_2O_2 group) **(H)** SW1353 cells were incubated with LY294002 (75 μmol/L) for 4 h and then co-incubated with H_2O_2 (260 μmol/L) and Biqi Capsule extract (100 μg/mL) for another 12 h. Cell viability was determined by the CCK8 test. Data were presented as mean ± SEM. (n = 6, #$p < 0.05$, ##$p < 0.01$ compared with the Vehicle group).

2.9 Screening drugs for effects of anti-chondrocyte damage

The human chondrosarcoma-derived cell line SW1353 is a promising substitute for a chondrocyte experimental model. It produces sufficient proliferative activity and presents a consistent response to the phenotype of primary human chondrocytes. H_2O_2 stimulation induced apoptosis and necrosis, decreased cell viability, and increased eight-isoprostane F2-α expression in SW1353 cells. It is often used as a model for osteoarthritis studies (Park et al., 2018; Pang et al., 2021). For *in vitro* studies, H_2O_2-stimulated SW1353 cells were used as the model for chondrocyte damage, and the reversal of cell damage by drugs of interest was investigated using the CCK8 kit (Yeasen, Shanghai, China). Specifically, SW1353 cells were cultured in a complete medium containing 260 μmol/L H_2O_2. H_2O_2 stimulation and drug administration were performed simultaneously. A total of Biqi Capsule extract (10, 50, 100 μg/mL) as well as seven compounds including Strychnine, Brucine, Liquiritin, Salvianolic Acid B, Glycyrrhizic Acid, Cryptotanshinone, Tanshinone IIA (all concentrations are 0.2, 1, 5 μmol/L) were examined in this study. SW1353 cells were seeded with the density of 5×10^3 cells per well in 96 well plates and incubated for 24 h before administration. The drugs were first dissolved in DMSO and then diluted with medium to the desired concentration while ensuring that the concentration of DMSO was less than 0.5‰. The DMSO was also supplemented in the Vehicle and H_2O_2 groups so that the DMSO concentration was the same in each group. The preparations were incubated for 12 h after administration and a CCK8 test was performed according to the manufacturer's instructions.

2.10 Screening drugs for anti-inflammatory effects

For *in vitro* studies, LPS-stimulated RAW264.7 cells were used as an inflammatory model for the screening of effective anti-inflammatory drugs. LPS stimulation and drug administration were performed simultaneously. RAW264.7 cells were seeded with the density of 1×10^4 cells per well in 96 well plates; after 24 h incubation, the culture medium was replaced with serum-free medium for another 12 h. According to the preliminary results from our pre-experiments, the cells were treated with LPS (500 ng/mL) and Biqi Capsule extract (10, 50, 100 μg/mL), Strychnine (0.1, 1, 10 μmol/L), Brucine (0.1, 1, 10 μmol/L), Liquiritin (0.1, 1, 10 μmol/

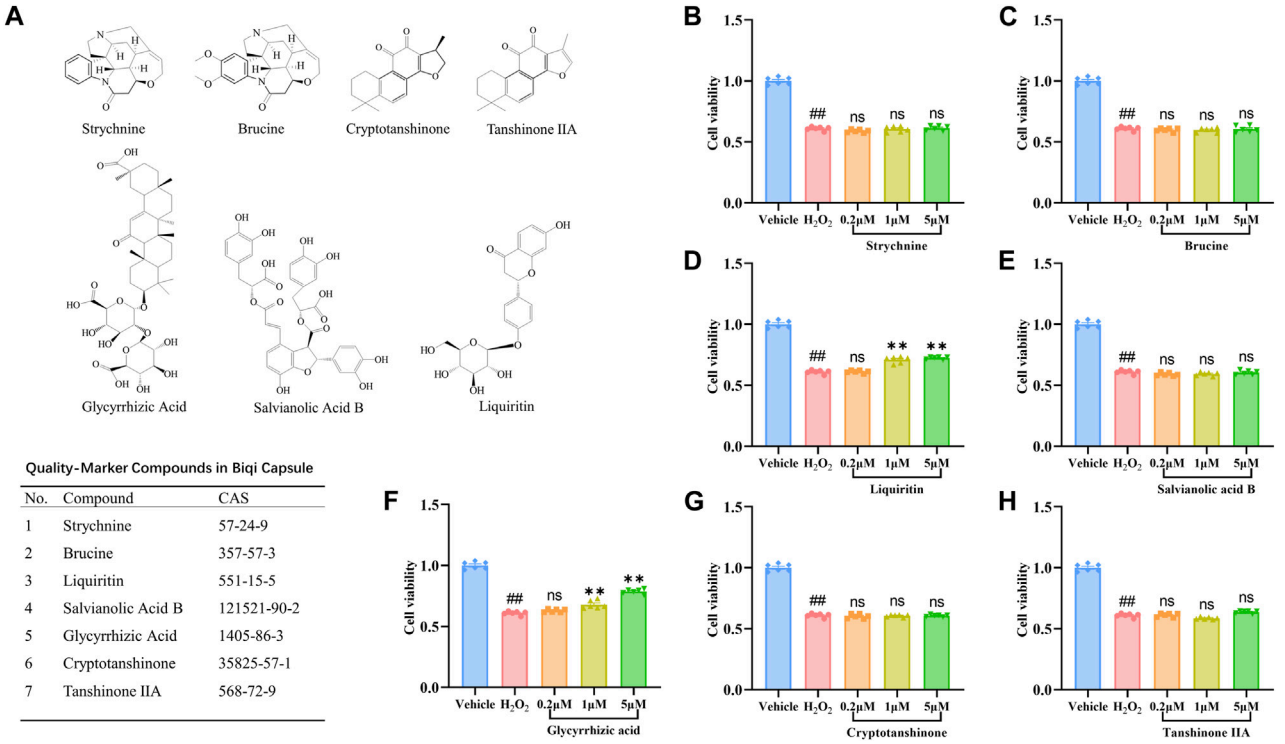

Quality-Marker Compounds in Biqi Capsule

No.	Compound	CAS
1	Strychnine	57-24-9
2	Brucine	357-57-3
3	Liquiritin	551-15-5
4	Salvianolic Acid B	121521-90-2
5	Glycyrrhizic Acid	1405-86-3
6	Cryptotanshinone	35825-57-1
7	Tanshinone IIA	568-72-9

FIGURE 3
Effect of seven compounds of Biqi Capsule on the viability of H_2O_2-stimulated SW1353 cells. **(A)** The chemical structures of seven Quality-markers of Biqi Capsule. **(B–H)** SW1353 cells were incubated with H_2O_2 (260 μmol/L) and Strychnine/Brucine/Liquiritin/Salvianolic Acid B/Glycyrrhizic Acid/Cryptotanshinone/Tanshinone IIA for 12h, respectively. Cell viability was determined by the CCK8 test. Data were presented as mean ± SEM. (n = 6, #p < 0.05, ##p < 0.01 compared with the Vehicle group; *p < 0.05, **p < 0.01 compared with the H_2O_2 group).

L), Salvianolic Acid B (0.1, 1, 10 μmol/L), Glycyrrhizic Acid (0.1, 1, 10 μmol/L), Cryptotanshinone (0.1, 1, 10 μmol/L), Tanshinone IIA (0.1, 1, 10 μmol/L) for 12 h. Next, the levels of IL-6 in the supernatant were determined by ELISA according to the manufacturer's instructions.

2.11 Molecular docking

The receptor is the crystal structure of RAC1, which is one of the critical targets according to the PPI network. The structure was obtained from the RCSB protein data bank, with the corresponding PDB code 1RYF. The ligands are Glycyrrhizic acid and Liquirtin, the structure files of which were obtained from PubChem.

Discovery Studio is a highly visual commercial software integrated by BIOVIA for life science research and used to perform molecular docking to investigate the interaction patterns between active compounds and critical targets. The receptor and ligands were processed by the prepare protein and prepare ligands modules, respectively, and then applied CHARMm force field on all ligands. The coordinates of the receptor active site were set to −1.23843, 73.5704, 38.9122, and a radius of 11. Parameters such as CDocker energy and CDocker interaction energy were used to evaluate the molecular docking results. The conformation with the highest CDocker interaction energy score value was selected as the most reliable binding conformation for further analysis.

2.12 Statistical analysis

Studies were designed to generate groups of equal size using randomization and blinded analysis. The data was presented as mean ± SEM of n measurements. N identifies the number of independent samples. Data were tested for normality using the Shapiro–Wilk test. Significant differences were assessed by either Student's t-test or one-way ANOVA, according to the number of groups compared. When significant variations were found by one-way ANOVA, the Tukey-Kramer post-hoc test for multiple comparisons was performed only if F achieved a p-value <0.05. All the statistical analyses were done using GraphPad Prism 9.5. Differences were considered significant at $p < 0.05$.

3 Results

3.1 Biqi Capsule attenuates papain-induced knee OA

We assessed the efficacy of Biqi Capsule on OA using a papain-induced OA model. Firstly, no changes were observed in the rate of body weight change in Biqi Capsule treated or OA rats when compared with the Vehicle group during the 7 days (Figure 1B), which partly indicated that the Biqi Capsule treatment exerted no apparent toxic effects on OA rats. HE staining of the tissues from the knee joint of papain-treated rats showed apparent cartilage damage,

mainly manifesting as localized greyish-white cartilage surface with no luster; the cartilage migration layer matrix was edematous with light red and uneven staining. Some chondrocytes showed degeneration of different sizes, clustering, and cellular disorganization; the chondrocytes in the mid and deep zones were dissolved and necrotic, with homogeneous red staining and loss of original structure, and in a few cases, there was mild hyperplasia and inflammatory cell infiltration in the synovium (Figure 1C, D). Administration of high-dose Biqi Capsule significantly ameliorated cartilage destruction and chondrocyte damage, showing similar results as celecoxib as a positive control.

Next, we measured inflammatory factors, including IL-1β, TNF-α, IL-6, and PGE2, in the synovium of rats. It was realized that Biqi Capsule significantly reduced IL-1β, IL-6, and TNF-α levels in the synovium of the OA rats (Figure 1E-G). Biqi Capsule also reduced PGE2 in the synovium, which led to hyperalgesia and allodynia (Figure 1H). Altogether, Biqi Capsule inhibited the expression and secretion of multi-cytokines, consequently inhibiting OA development.

NF-κB is a key signaling mediator of inflammation. Immunoblotting of synovial tissue showed a significant increase in the phosphorylation level of NF-κB in the OA group. These increased levels of phosphorylation were inhibited in a dose-dependent manner by Biqi Capsule (Figure 1I, J).

3.2 Network pharmacology analysis of Biqi Capsule

Network pharmacology analysis was performed to clarify the mechanisms of Biqi Capsule. Uploading seven components of Biqi Capsule to the PharmMapper server resulted in 275 candidate compound targets. By searching the OMIM, TTD, and GeneCards databases, 3221 OA-associated targets were retrieved. The 68 potential therapeutic targets of Biqi Capsule for OA were identified using Venn diagrams (Figure 2B). Furthermore, we conducted a KEGG and GO enrichment analysis on the 68 targets (Figures 2C, D). The significant and highest-scoring pathway was the PI3K/AKT pathway. Biological processes are mostly associated with inflammatory responses and oxidative stress. This suggests that the pharmacological mechanism of Biqi Capsule for the treatment of OA may be related to the inhibition of inflammatory response and oxidative stress, via PI3K/AKT signaling pathway.

3.3 Biqi Capsule extract reverses chondrosarcoma cell damage via PI3K/AKT/mTOR pathway

Network Pharmacology showed that the PI3K/AKT pathway is a critical pathway for Biqi Capsule in the treatment of OA. Activated PI3K/AKT/mTOR signaling has been found in many studies to promote chondrocyte proliferation and reduce cartilage damage (Sun et al., 2020). To confirm the anti-chondrocyte damage effect of Biqi Capsule, we examined the effect of Biqi Capsule extract on chondrosarcoma cell line SW1353 cell damage induced by H_2O_2 (Figure 2E). After H_2O_2 stimulation, the cell viability was significantly reduced, in association with the reduction of phosphorylation of PI3K, AKT, and mTOR. Biqi Capsule extract (100 μg/mL) increased the viability in H_2O_2-stimulated SW1353 cells. Mechanically, Biqi Capsule extract (100 μg/mL) upregulated the phosphorylation of PI3K, AKT, and mTOR in H_2O_2-stimulated SW1353 cells (Figure 2E~G). According to one study, PI3K inhibitor LY294002 could strongly inhibit the activation of PI3K in SW1353 cells both *in vivo* and *in vitro* (Huang et al., 2017; Xu et al., 2019; Zhu et al., 2019; Xu et al., 2020). In line with our current study, it was revealed that Biqi Capsule extract could not reverse the H_2O_2-stimulated damage in SW1353 cells that were treated with LY294002 (Figure 2H). Given these findings, we assumed that Biqi Capsule could ameliorate OA by stimulating, as well as enhancing the activity of the PI3K/AKT/mTOR pathway in knee joint cartilage.

3.4 Screening for bioactive components on H_2O_2-Stimulated SW1353 cells

To explore the active components of Biqi Capsule against chondrosarcoma cell damage, we screened for the effects of the seven components of Biqi Capsule, including Strychnine, Brucine, Liquiritin, Salvianolic Acid B, Glycyrrhizic Acid, Cryptotanshinone, Tanshinone IIA on the viability of H_2O_2-stimulated SW1353 cells. Among these components, Glycyrrhizic Acid and Liquiritin were found to increase cell viability. Moreover, the effects of Glycyrrhizic Acid and Liquiritin were also found to be dose-dependent (Figure 3).

3.5 Regulation of PI3K/AKT/mTOR pathway by Glycyrrhizic Acid and Liquiritin

The treatment with Glycyrrhizic Acid (5 μmol/L) and Liquiritin (5 μmol/L) resulted in a significant increase in cell viability (Figure 3D–F), so we investigated whether Glycyrrhizic Acid (5 μmol/L) and Liquiritin (5 μmol/L) could regulate the PI3K/AKT/mTOR pathway. Glycyrrhizic Acid and Liquiritin upregulated the phosphorylation of PI3K, AKT, and mTOR in H_2O_2-stimulated SW1353 cells (Figure 4A–D). Moreover, PI3K inhibitor blocks the protective effect of Glycyrrhizic Acid and Liquiritin on H_2O_2-induced SW1353 cells (Figure 4E).

3.6 Interaction of bioactive compounds with RAC1

In the PPI network, we obtained one key core target, RAC1, which is an upstream target of the PI3K/AKT/mTOR pathway. Glycyrrhizic Acid and Liquiritin treatment modulated the PI3K/AKT/mTOR pathway. Thus, we speculated that Glycyrrhizic Acid and Liquiritin actively target RAC1 to reduce chondrocyte damage via the RAC1/PI3K/AKT/mTOR pathway. To confirm this, we performed molecular docking studies to gain insight into the binding modes of Glycyrrhizic Acid and Liquiritin upon binding to vital regulatory sites on RAC1, respectively. A negative value of CDocker Energy indicates that the ligand-receptor has decent binding activity. We found that the CDocker

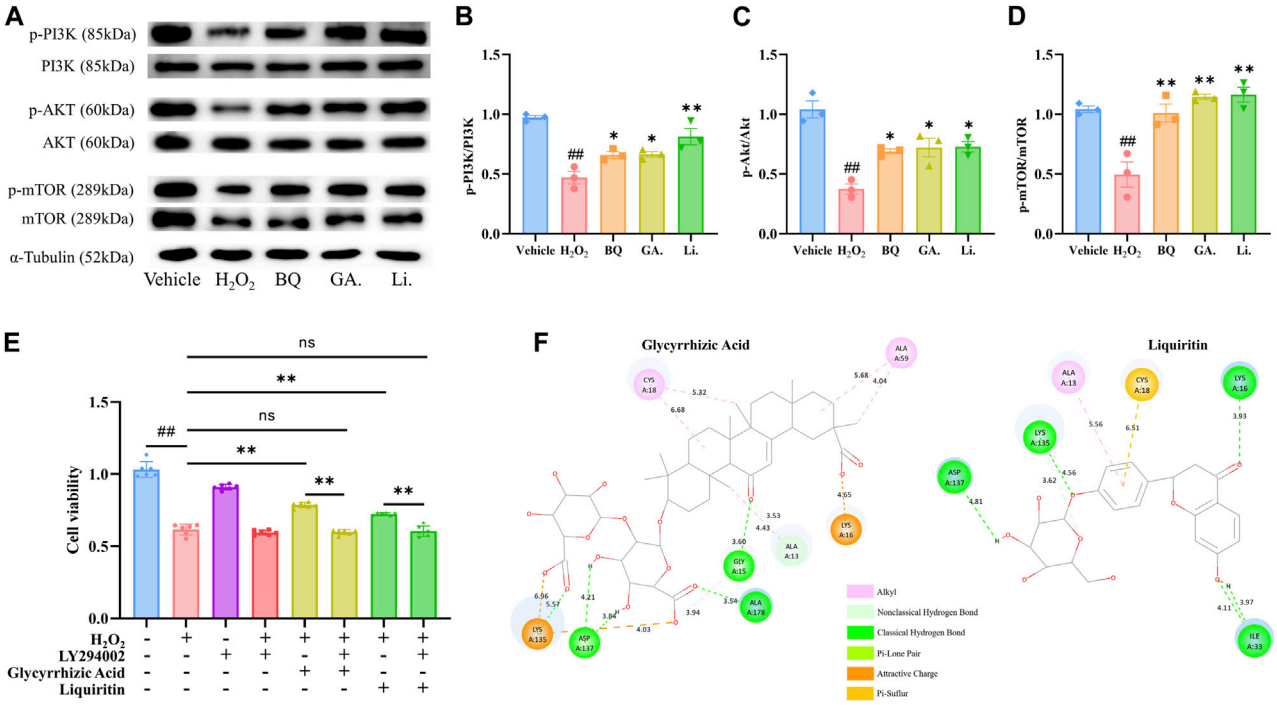

FIGURE 4
Effect of Glycyrrhizic Acid and Liquiritin on H_2O_2-stimulated SW1353 cells. **(A–D)** SW1353 cells were incubated with H_2O_2 (260 μmol/L) and Glycyrrhizic Acid (GA) (5 μmol/L)/Liquiritin (Li.) (5 μmol/L) for 12 h. The regulation effect of Biqi Capsule extract (BQ), Glycyrrhizic Acid, and Liquiritin on phosphorylation of PI3K, AKT, and mTOR in SW1353 cells was measured by western blot analysis. The densitometric analyses of three independent experiments were shown. Data were presented as mean ± SEM. (n = 3, #$p < 0.05$, ##$p < 0.01$ compared with the Vehicle group; *$p < 0.05$, **$p < 0.01$ compared with the H_2O_2 group) **(E)** SW1353 cells were incubated with LY294002 (75 μmol/L) for 4 h and then co-incubated with H_2O_2 (260 μmol/L) and Glycyrrhizic Acid (5 μmol/L)/Liquiritin (5 μmol/L) for another 12 h. Cell viability was determined by the CCK8 test. Data were presented as mean ± SEM. (n = 6, #$p < 0.05$, ##$p < 0.01$ compared with the Vehicle group) **(F)** Docking structure of active compounds with RAC1.

Energy of Glycyrrhizic Acid and Liquiritin with RAC1 were −91.3 and −53.9 respectively, which are all much less than zero, indicating that the docking structures of these compounds with RAC1 are considerably stable. We selected the docking structure with the lowest CDocker interaction energy after docking with RAC1 for further analysis. Figure 4F shows the chemical bonds and distances between the different atomic groups of each compound interacting separately with the different amino acids of the RAC1 protein. Glycyrrhizic Acid forms six hydrogen bonds with A13, A15, A137 and A178, Liquiritin forms six hydrogen bonds with A16, A33, A135 and A137. This finding indicates that the Glycyrrhizic Acid and Liquiritin may induce a conformational change in RAC1 that promotes binding to other downstream effectors.

3.7 Screening for active components on LPS-stimulated RAW264.7 cells

In vivo experiments and network pharmacology analysis showed the anti-inflammatory effect of Biqi Capsule. Thus, we examined the effects of Biqi Capsule extract and the seven compounds on the expression of IL-6 in LPS-stimulated RAW264.7 cells. The CCK8 test showed that none of the experimental concentrations of all drugs used were toxic to RAW264.7 cells (Figure 5A). After LPS stimulation, the IL-6 concentrations were significantly increased. Treatment with Biqi Capsule extract, Brucine, Liquiritin, Salvianolic acid B, Glycyrrhizic Acid, Cryptotanshinone, and Tanshinone IIA decreased IL-6 production (Figure 5B, D–I). In addition, the effect was found to be dose-dependent. Among these compounds, Glycyrrhizic Acid showed the most potent anti-inflammatory activity with EC_{50}: 2.25 μmol/L.

3.8 Biqi Capsule attenuates NF-κB activation *in vitro*

NF-κB signaling plays a central role in pro-inflammatory stress-related responses, which also mediates the expression of IL-6. To determine whether the anti-IL-6 effect of Biqi Capsule extract was related to NF-κB, we first detected the activation of NF-κB in RAW264.7 cells. Nuclear translocation and phosphorylation of NF-κB lead to the transcription of genes encoding proinflammatory mediators. Immunoblotting showed that the nuclear translocation and phosphorylation (Figure 5J–K) of NF-κB (p65) were all significantly increased after LPS stimulation. Notably, nuclear translocation and phosphorylation of NF-κB were inhibited by Biqi Capsule extract. In addition, the Biqi Capsule also inhibited the phosphorylation of NF-κB and the expression of IL-6 in OA rats. Taking these findings into consideration, we suggest that the therapeutic effect of Biqi

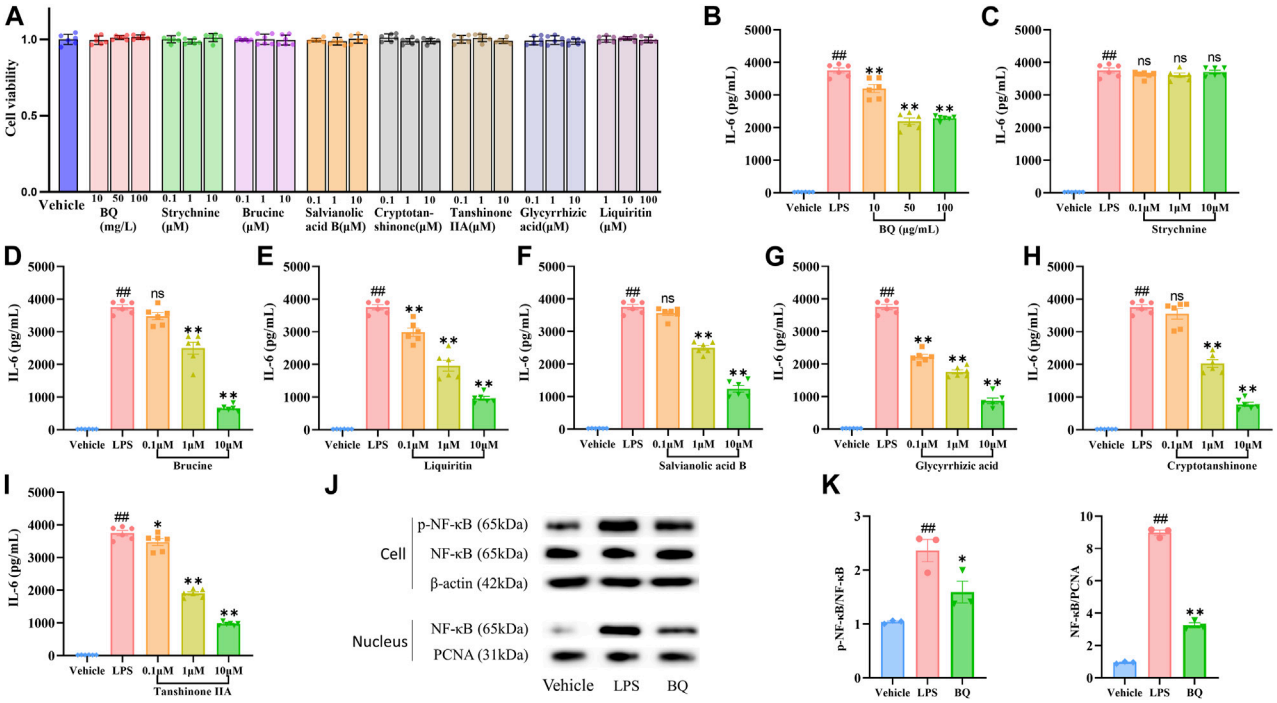

FIGURE 5
Effect of Biqi Capsule extract and seven compounds on the LPS-stimulated RAW264.7 cells. **(A)** RAW264.7 cells were incubated with drugs for 12h, respectively. Drug cytotoxicity was determined by the CCK-8 test. Data were presented as mean ± SEM. (n = 6) **(B–I)** RAW264.7 cells were incubated with LPS (500 ng/mL) and Biqi Capsule extract (BQ)/Strychnine/Brucine/Liquiritin/Salvianolic Acid B/Glycyrrhizic Acid/Cryptotanshinone/Tanshinone IIA for 12 h. IL-6 in the supernatant was examined by ELISA. Data were presented as mean ± SEM. (n = 6, #$p < 0.05$, ##$p < 0.01$ compared with the Vehicle group; *$p < 0.05$, **$p < 0.01$ compared with the LPS group) **(J, K)** RAW264.7 cells were incubated with LPS (500 ng/mL) and Biqi Capsule extract (BQ) (50 μg/mL) for 12 h. Nuclear and cytoplasm protein extractions of RAW264.7 cells were conducted according to the manual of the Nuclear Protein Extraction Kit (Solarbio, Beijing, China). The regulation effect of Biqi Capsule extract on phosphorylation and nuclear translocation of NF-κB (p65) in RAW264.7 cells was measured by western blot analysis. The purity of the nuclear protein was validated via western blotting with anti-β-actin. Data were presented as mean ± SEM. (n = 3, #$p < 0.05$, ##$p < 0.01$ compared with the Vehicle group; *$p < 0.05$, **$p < 0.01$ compared with the LPS group).

Capsule on the inflammatory response in OA is achieved via the NF-κB signaling pathway, and the bioactive components responsible for this observable effect are Brucine, Liquiritin, Salvianolic Acid B, Glycyrrhizic Acid, Cryptotanshinone, and Tanshinone IIA.

4 Discussion and conclusion

This study demonstrated the pharmacological mechanism and bioactive components of Biqi Capsule in the treatment of OA. The novel findings are as follows: 1. Biqi Capsule has chondroprotective and anti-synovitis effect in papain-induced OA rats. 2. Biqi Capsule exerts a chondroprotective effect by activating the PI3K/AKT/mTOR pathway in chondrocytes, and the relevant bioactive components are Glycyrrhizic Acid and Liquiritin. 3. Biqi Capsule exerts an anti-inflammatory effect by inhibiting the NF-κB/IL-6 pathway, and the relevant bioactive components are Brucine, Liquiritin, Salvianolic Acid B, Glycyrrhizic Acid, Cryptotanshinone, Tanshinone IIA. 4. Glycyrrhizic Acid and Liquiritin can be considered novel lead compounds for the treatment of osteoarthritis.

OA is a chronic progressive disease characterized by degenerative changes in the knee joint cartilage. Conventionally, the commonly used classes of drugs for the treatment of OA include NSAIDs, locally administered corticosteroids, analgesics, etc. The long-term use of these drugs gradually leads to obvious adverse effects that some patients cannot tolerate (Brophy and Fillingham, 2022). Biqi Capsules is used to treat many types of arthritis in Traditional Chinese medicine with proven efficacy and safety (Chen et al., 2018; Wang et al., 2020). A study investigated the effects of Biqi Capsule on CIA-induced rheumatoid arthritis in rats. The study revealed that Biqi Capsule alleviated local joint and systemic inflammation, synovial hyperplasia, and cartilage destruction caused by CIA (Wang et al., 2018). In this current study, we demonstrated that Biqi Capsule could resist the progression of papain-induced OA. Biqi Capsule improved joint function in rats, inhibited the expression of inflammatory factors in the synovium, and protected cartilaginous tissues from destruction.

PI3K/AKT signaling negatively modulates chondrocyte apoptosis under multiple pathological conditions, and the activated signaling can prevent OA by reducing chondrocyte apoptosis. Clinical studies have revealed that the PI3K/AKT pathway is downregulated in human cartilage tissues with OA when compared with normal cartilage (Rosa et al., 2011; Wang et al., 2020). Similarly, OA-like chondrocytes exposed to inflammation or oxidative stress showed downregulation of PI3K/AKT activity. It has been suggested that E2-mediated PI3K/AKT activation significantly promotes the proliferation and viability

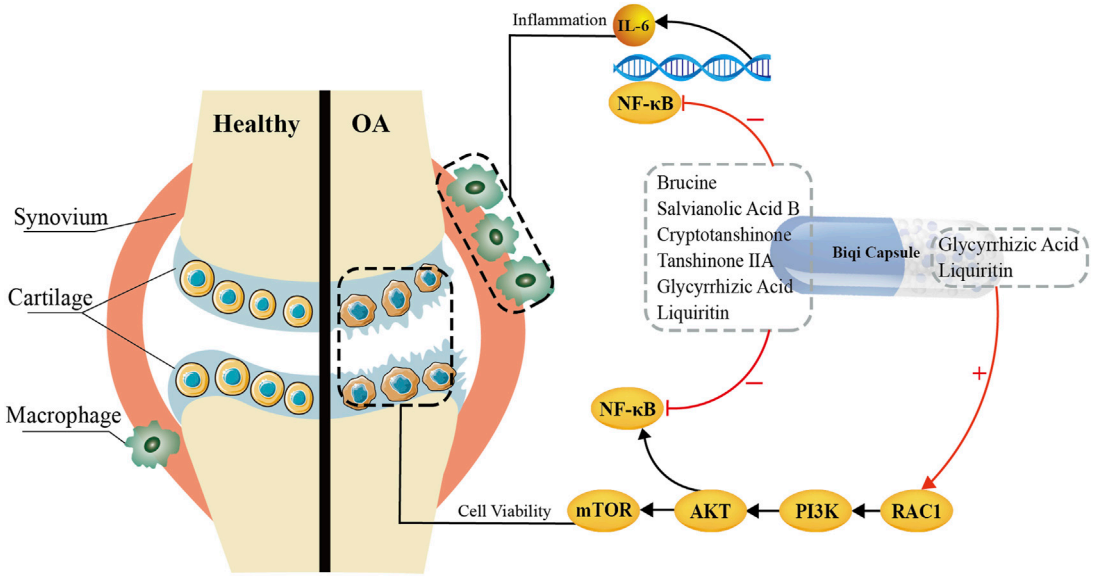

FIGURE 6
Bioactive Components and Potential Mechanisms of Biqi Capsule in the Treatment of Osteoarthritis.

of chondrocytes in OA rat model and ATDC5 chondrocytes (Huang et al., 2011; Fan et al., 2018). In this study, we first analyzed the possible mechanisms of Biqi Capsule for OA by employing network pharmacology. This revealed that PI3K/AKT might be the main target pathway of Biqi Capsule against cartilage damage. Consistent with the analysis, we validated that Biqi Capsule extract activates the PI3K/AKT and its downstream protein mTOR in H_2O_2-stimulated chondrocytes. Further, we performed PI3K/AKT/mTOR pathway inhibition experiments to highlight the chondroprotective mechanism of Biqi Capsule extract, which is mainly focused on the PI3K/AKT/mTOR axis. Furthermore, we screened seven compounds of Biqi Capsule. Firstly, we found that Glycyrrhizic Acid and Liquiritin activated the PI3K/AKT/mTOR pathway in H_2O_2-stimulated SW1353 cells and also inhibited cell death. Some studies have implied that both overactivation and inhibition of RAC1 in cartilage tissues lead to pathological effects, and regulation of RAC1 signaling is crucial for maintaining homeostasis in cartilaginous tissues (Woods et al., 2009; Suzuki et al., 2017). Meanwhile, the network pharmacology analysis (Supplementary Material S2) revealed that RAC1 is the key target protein responsible for the therapeutic effects observed in the treatment of osteoarthritis with Biqi Capsule; and is also intricately associated with the PI3K/AKT/mTOR pathway. Previous studies have suggested that PI3K is a direct target of activated RAC1: RAC1 interacts with the BCR homology domain of the PI3K regulatory subunit p8593, and this interaction is significantly enhanced when RAC1 is bound to GTP (Bokoch et al., 1996; Campa et al., 2015). Consequently, we performed molecular docking experiments on GTP-RAC1 binding site and two compounds that are known for their chondroprotective effects, Glycyrrhizic Acid and Liquiritin, to investigate their potential interactions with this binding site. The docking results demonstrated strong interactions of Glycyrrhizic Acid and Liquiritin with the site (−91.3 kcal/mol and −53.9 kcal/mol, respectively), with docking structures similar to that of GTP-RAC1 structure. Therefore, we suggest that Glycyrrhizic Acid and Liquiritin in Biqi Capsule exert their chondroprotective effects by activating RAC1 in chondrocytes, consequently activating the PI3K/AKT/mTOR pathway in these cells. Glycyrrhizic Acid and Liquiritin are both natural constituents derived from licorice. Both are known for their low toxicity and wide range of pharmacological activities. Glycyrrhizic acid, in particular exhibits favorable pharmacokinetic characteristics and has been extensively studied, leading to its development as a hepatoprotective drug in Japan and China for cases of chronic hepatitis. However, the development of Liquiritin as a drug has been faced with challenges due to its low bioavailability and limited absorption. Despite this, Liquiritin shows promise in preventing premature delivery caused by progesterone deficiency, as it acts as a strong selective inhibitor of AKR1C1, a key enzyme in progesterone metabolism (Ming and Yin, 2013; Qin et al., 2022). As far as we know, this is the first time that Glycyrrhizic Acid and Liquiritin are being suggested to exert chondroprotective effects via PI3K/AKT/mTOR pathway activation.

On the other hand, the inflammatory response that occurs in joints affected by osteoarthritis, synoviocytes are stimulated by cytokines and matrix fragments derived from cartilage degeneration and cellular stress products which activate the NF-κB signaling pathway via the TL-R and chemokine surface receptors (Midwood et al., 2009; Liu et al., 2012; Molnar et al., 2021). Afterward, the activated NF-κB mediates the synthesis of cytokines like IL-1β, IL-6, TNF-α, PGE2, MMPs1-13, ADAMTS4, ADAMTS5, chemokines like IL-8, CCL5, and angiogenic factors like VEGF and bFGF, which cause further cartilage degradation and inflammation of the synovium. Notably, NF-κB cooperates with activated AP-1 to mediate IL-1β-induced MMP1 and MMP3 expression as well as CTGF-triggered IL-6 production. Synovitis is then accompanied by a series of histological abnormalities that occur in the synovium, such as infiltration of

macrophages and lymphocytes, joint swelling, and stiffness. The definitive role of NF-κB in OA onset and progression provides evidence that interventions targeted at this signaling pathway might have beneficial therapeutic effects (Rigoglou and Papavassiliou, 2013; Burke et al., 2019; Molnar et al., 2021). The non-steroidal anti-inflammatory drugs (NSAIDs) and glucocorticoids are some of the pharmacologically active compounds that hinder the activation of NF-κB cascades. Inhibition of IL-6 activity reduces the severity of experimental OA (Latourte et al., 2017; Ansari et al., 2019). Regarding the anti-inflammatory effects of Biqi Capsule, a previous study indicated that Biqi Capsule could resist the inflammatory response of LPS-stimulated RAW264.7 cells via the NO-iNOS pathway and COX-2 pathway (Wang et al., 2011). Our study complements these previous findings by elucidating the regulatory role of Biqi Capsule on the NF-κB/IL-6 pathway in synovial tissue and macrophage. Per previous studies, the bioactive components of Biqi Capsule, Strychnine, Brucine, Cryptotanshinone, Glycyrrhizic Acid, and Liquiritin have been found to inhibit NO secretion on LPS-stimulated macrophages, while it was only cryptotanshinone that inhibited IL-6 expression (Qishuai et al., 2016). Our study supplemented the previous results by identifying the possible anti-inflammatory effect of Brucine, Liquiritin, Salvianolic Acid B, Glycyrrhizic Acid, Cryptotanshinone, Tanshinone ⅡA, which have already been proven to exert similar anti-inflammatory effects in a wide range of diseases (Yin et al., 2003; Gao et al., 2019; Zhai et al., 2019; Wu et al., 2020; Xiao et al., 2020; *Li* et al., 2021; Wang et al., 2022).

In addition, the PI3K/AKT signaling pathway, as the upstream pathway of NF-κB, is associated with inflammation in osteoarthritis to some extent. Previous studies have shown that some medicines (like the Huoxuezhitong capsule) can treat the inflammation by inhibiting the PI3K/AKT/NF-κB signaling pathway (Chen et al., 2013; Wang et al., 2016; Ju et al., 2020). This seems to be contrary to our current findings which suggest that Glycyrrhizic Acid and Liquiritin in Biqi Capsule treat osteoarthritis by activating PI3K/AKT. Both mTOR and NF-κB are downstream proteins of the PI3K/AKT signaling pathway. It appears that Glycyrrhizic Acid and Liquiritin, while activating mTOR via the PI3K/AKT pathway, would incidentally lead to the activation of NF-κB, resulting in an increased inflammatory response. However, our *in vivo* experiments showed that the chondroprotective effect of Biqi capsules did not exacerbate or even inhibit the inflammatory response. This may be due to the ability of active ingredients like Brucine in Biqi Capsule to inhibit the phosphorylation and nuclear translocation of NF-κB. This also demonstrates the characteristic "multi-component/multi-target/multi-pathway" of Traditional Chinese Medicines in the treatment of diseases. In conclusion, we have found that Glycyrrhizic Acid and Liquiritin in Biqi Capsule can activate the PI3K/AKT pathway, leading to the activation of the mTOR and the consequent treatment of cartilage damage. Additionally, components including Brucine can inhibit NF-κB activation, whether it is triggered by the activation of the PI3K/AKT pathway or by osteoarthritis itself (Figure 6).

There are several caveats in this study. Firstly, the pharmacological mechanism of the drugs *in vivo*, and whether components other than Glycyrrhizic Acid and Liquiritin have a chondroprotective effect, still need to be further explored considering the genetic differences between cell lines and natural cells or living organisms. Furthermore, although we discovered that Biqi Capsule extract, Glycyrrhizic Acid, and Liquiritin can activate the PI3K/AKT/mTOR pathway to resist H_2O_2-induced cell death (e.g., apoptosis, autophagy, etc.), yet it is unclear which mode of cell death is regulated by these drugs. Thus, further identification of signature proteins for a particular mode of cell death is warranted. What's more, no anti-inflammatory or chondroprotective effect of Strychnine was observed. In light of this, further investigation regarding Strychnine as an anti-inflammatory or chondroprotective agent is needed.

Overall, based on the anti-inflammatory and anti-cartilage damage effects of Biqi Capsule in OA rats, we suggest that Glycyrrhizic Acid and Liquiritin can exert chondroprotective effects by activating the PI3K/AKT/mTOR pathway; Brucine, Liquiritin, Salvianolic Acid B, Glycyrrhizic Acid, Cryptotanshinone, Tanshinone ⅡA can modulate the NF-κB/IL-6 pathway in macrophages and synovial tissues to exert anti-inflammatory effects. This may provide empirical evidence and a theoretical foundation for the clinical application of Biqi Capsule as well as the development of Glycyrrhizic Acid and Liquiritin as anti-OA lead compounds. Biqi Capsule is a promising therapeutic option for the treatment of OA.

Data availability statement

The original contributions presented in the study are included in the article/Supplementary Material, further inquiries can be directed to the corresponding authors.

Ethics statement

The animal study was approved by the all experimental procedures were approved by the Animal Care and Use Committee of the Tianjin University of Traditional Chinese Medicine (Authorization number: TCM-LAEC2022129). The study was conducted in accordance with the local legislation and institutional requirements.

Author contributions

ZJ: Formal Analysis, Investigation, Visualization, Writing–original draft, Writing–review and editing. JZ: Writing–review and editing. XY: Methodology, Software, Writing–original draft, Writing–review and editing. HC: Data curation, Writing–review and editing. YW: Data curation, Writing–review and editing. OP: Writing–review and editing. YL: Writing–review and editing. ZL: Writing–review and editing. SZ: Funding acquisition, Project administration, Supervision, Writing–review and editing. QW: Project administration, Supervision, Writing–review and editing.

Funding

The author(s) declare that financial support was received for the research, authorship, and/or publication of this article. This study was supported by the Scientific and Technological Innovation Project for Students of Tianjin University of Traditional Chinese Medicine (ZY2021-XZY33).

Conflict of interest

The authors declare that the research was conducted in the absence of any commercial or financial relationships that could be construed as a potential conflict of interest.

Publisher's note

All claims expressed in this article are solely those of the authors and do not necessarily represent those of their affiliated organizations, or those of the publisher, the editors and the reviewers. Any product that may be evaluated in this article, or claim that may be made by its manufacturer, is not guaranteed or endorsed by the publisher.

Supplementary material

The Supplementary Material for this article can be found online at: https://www.frontiersin.org/articles/10.3389/fphar.2024.1347970/full#supplementary-material

References

Allen, K. D., Thoma, L. M., and Golightly, Y. M. (2022). Epidemiology of osteoarthritis. *Osteoarthr. Cartil.* 30 (2), 184–195. doi:10.1016/j.joca.2021.04.020

Ansari, M. Y., Khan, N. M., Ahmad, N., Green, J., Novak, K., and Haqqi, T. M. (2019). Genetic inactivation of ZCCHC6 suppresses interleukin-6 expression and reduces the severity of experimental osteoarthritis in mice. *Arthritis Rheumatol.* 71 (4), 583–593. doi:10.1002/art.40751

Bokoch, G. M., Vlahos, C. J., Wang, Y., Knaus, U. G., and Traynor-Kaplan, A. E. (1996). Rac GTPase interacts specifically with phosphatidylinositol 3-kinase. *Biochem. J.* 315 (Pt 3), 775–779. doi:10.1042/bj3150775

Brophy, R. H., and Fillingham, Y. A. (2022). AAOS clinical practice guideline summary: management of osteoarthritis of the knee (nonarthroplasty), third edition. *J. Am. Acad. Orthop. Surg.* 30 (9), e721–e729. doi:10.5435/JAAOS-D-21-01233

Burke, C. J., Alizai, H., Beltran, L. S., and Regatte, R. R. (2019). MRI of synovitis and joint fluid. *J. Magn. Reson. Imaging.* 49 (6), 1512–1527. doi:10.1002/jmri.26618

Campa, C. C., Ciraolo, E., Ghigo, A., Germena, G., and Hirsch, E. (2015). Crossroads of PI3K and rac pathways. *Small GTPases* 6 (2), 71–80. doi:10.4161/21541248.2014.989789

Chen, J., Crawford, R., and Xiao, Y. (2013). Vertical inhibition of the PI3K/Akt/mTOR pathway for the treatment of osteoarthritis. *J. Cell. Biochem.* 114 (2), 245–249. doi:10.1002/jcb.24362

Chen, X. M., Wu, J. Q., Huang, Q. C., Zhang, J. Y., Pen, J. H., Huang, Z. S., et al. (2018). Systematic review and meta-analysis of the efficacy and safety of Biqi capsule in rheumatoid arthritis patients. *Exp. Ther. Med.* 15 (6), 5221–5230. doi:10.3892/etm.2018.6121

Coaccioli, S., Sarzi-Puttini, P., Zis, P., Rinonapoli, G., and Varrassi, G. (2022). Osteoarthritis: new insight on its pathophysiology. *J. Clin. Med.* 11 (20), 6013. doi:10.3390/jcm11206013

Fan, D. X., Yang, X. H., Li, Y. N., and Guo, L. (2018). 17β-Estradiol on the expression of G-protein coupled estrogen receptor (GPER/GPR30) mitophagy, and the PI3K/Akt signaling pathway in ATDC5 chondrocytes *in vitro*. *Med. Sci. Monit.* 24, 1936–1947. doi:10.12659/msm.909365

Gao, S., Wang, Y., Li, D., Guo, Y., Zhu, M., Xu, S., et al. (2019). TanshinoneIIA alleviates inflammatory response and directs macrophage polarization in lipopolysaccharide-stimulated RAW264.7 cells. *Inflammation* 42 (1), 264–275. doi:10.1007/s10753-018-0891-7

Huang, J. G., Xia, C., Zheng, X. P., Yi, T. T., Wang, X. Y., Song, G., et al. (2011). 17β-Estradiol promotes cell proliferation in rat osteoarthritis model chondrocytes via PI3K/Akt pathway. *Cell. Mol. Biol. Lett.* 16 (4), 564–575. doi:10.2478/s11658-011-0023-y

Huang, L., Cao, J., Cao, L., Gao, L., Yang, Y., and Xu, L. (2017). Puerarin induces cell apoptosis in human chondrosarcoma cell line SW1353 via inhibition of the PI3K/Akt signaling pathway. *Oncol. Lett.* 14 (5), 5585–5590. doi:10.3892/ol.2017.6901

Jing, Y., Jiang, Z., Liu, Y., and Wang, Y. (2018). Simultaneous determination of seven active compounds in Biqi Capsules by HPLC-UV-MS. *Chin. Tradit. Pat. Med.* 34 (8).

Ju, L., Hu, P., Chen, P., Xue, X., Li, Z., He, F., et al. (2020). Huoxuezhitong capsule ameliorates MIA-induced osteoarthritis of rats through suppressing PI3K/Akt/NF-κB pathway. *Biomed. Pharmacother.* 129, 110471. doi:10.1016/j.biopha.2020.110471

Kulkarni, P., Martson, A., Vidya, R., Chitnavis, S., and Harsulkar, A. (2021). Pathophysiological landscape of osteoarthritis. *Adv. Clin. Chem.* 100, 37–90. doi:10.1016/bs.acc.2020.04.002

Latourte, A., Cherifi, C., Maillet, J., Ea, H. K., Bouaziz, W., Funck-Brentano, T., et al. (2017). Systemic inhibition of IL-6/Stat3 signalling protects against experimental osteoarthritis. *Ann. Rheum. Dis.* 76 (4), 748–755. doi:10.1136/annrheumdis-2016-209757

Li, C., Li, L., and Lan, T. (2021). Co-treatment with disulfiram and glycyrrhizic acid suppresses the inflammatory response of chondrocytes. *J. Orthop. Surg. Res.* 16 (1), 132. doi:10.1186/s13018-021-02262-3

Liu, S. C., Hsu, C. J., Chen, H. T., Tsou, H. K., Chuang, S. M., and Tang, C. H. (2012). CTGF increases IL-6 expression in human synovial fibroblasts through integrin-dependent signaling pathway. *PLoS One* 7 (12), e51097. doi:10.1371/journal.pone.0051097

Loeser, R. F., Collins, J. A., and Diekman, B. O. (2016). Ageing and the pathogenesis of osteoarthritis. *Nat. Rev. Rheumatol.* 12 (7), 412–420. doi:10.1038/nrrheum.2016.65

Mankin, H. J., Dorfman, H., Lippiello, L., and Zarins, A. (1971). Biochemical and metabolic abnormalities in articular cartilage from osteoarthritic human hips. II. Correlation of morphology with biochemical and metabolic data. *J. Bone Jt. Surg. Am.* 53 (3), 523–537. doi:10.2106/00004623-197153030-00009

Mankin, H. J., Johnson, M. E., and Lippiello, L. (1981). Biochemical and metabolic abnormalities in articular cartilage from osteoarthritic human hips. III. Distribution and metabolism of amino sugar-containing macromolecules. *J. Bone Jt. Surg. Am.* 63 (1), 131–139. doi:10.2106/00004623-198163010-00017

Mankin, H. J., and Lippiello, L. (1970). Biochemical and metabolic abnormalities in articular cartilage from osteoarthritic human hips. *J. Bone Jt. Surg. Am.* 52 (3), 424–434. doi:10.2106/00004623-197052030-00002

Midwood, K., Sacre, S., Piccinini, A. M., Inglis, J., Trebaul, A., Chan, E., et al. (2009). Tenascin-C is an endogenous activator of Toll-like receptor 4 that is essential for maintaining inflammation in arthritic joint disease. *Nat. Med.* 15 (7), 774–780. doi:10.1038/nm.1987

Ming, L. J., and Yin, A. C. (2013). Therapeutic effects of glycyrrhizic acid. *Nat. Prod. Commun.* 8 (3), 1934578X1300800–8. doi:10.1177/1934578x1300800335

Molnar, V., Matisic, V., Kodvanj, I., Bjelica, R., Jelec, Z., Hudetz, D., et al. (2021). Cytokines and chemokines involved in osteoarthritis pathogenesis. *Int. J. Mol. Sci.* 22 (17), 9208. doi:10.3390/ijms22179208

Pang, K. L., Chow, Y. Y., Leong, L. M., Law, J. X., Ghafar, N. A., Soelaiman, I. N., et al. (2021). Establishing SW1353 chondrocytes as a cellular model of chondrolysis. *Life (Basel)* 11 (4), 272. doi:10.3390/life11040272

Park, C., Hong, S. H., Shin, S. S., Lee, D. S., Han, M. H., Cha, H. J., et al. (2018). Activation of the Nrf2/HO-1 signaling pathway contributes to the protective effects of sargassum serratifolium extract against oxidative stress-induced DNA damage and apoptosis in SW1353 human chondrocytes. *Int. J. Environ. Res. Public Health* 15 (6), 1173. doi:10.3390/ijerph15061173

Qin, J., Chen, J., Peng, F., Sun, C., Lei, Y., Chen, G., et al. (2022). Pharmacological activities and pharmacokinetics of liquiritin: a review. *J. Ethnopharmacol.* 293, 115257. doi:10.1016/j.jep.2022.115257

Qishuai, F., Guifang, W., Qiangson, W., Lina, G., and Yuanlu, C. (2016). Anti-inflammatory activity comparison of aqueous extract with monomer components of Biqi capsule. *Chin. J. Exp. Tradit. Med. Form.* 22 (03), 89–93.

Rigoglou, S., and Papavassiliou, A. G. (2013). The NF-κB signalling pathway in osteoarthritis. *Int. J. Biochem. Cell Biol.* 45 (11), 2580–2584. doi:10.1016/j.biocel.2013.08.018

Rosa, S. C., Rufino, A. T., Judas, F., Tenreiro, C., Lopes, M. C., and Mendes, A. F. (2011). Expression and function of the insulin receptor in normal and osteoarthritic human chondrocytes: modulation of anabolic gene expression, glucose transport and GLUT-1 content by insulin. *Osteoarthr. Cartil.* 19 (6), 719–727. doi:10.1016/j.joca.2011.02.004

SPGD (2021). *Guidelines for clinical application of Chinese patent medicines in the treatment of knee osteoarthritis (2020)*, 522–533.

Sun, C. M., Schwab, J. H., and Hornicek, F. J. (2020). Henry J. Mankin: a trailblazer in skeletal pathology research. *Spine (Phila Pa 1976)* 45 (6), 405–406. doi:10.1097/BRS.0000000000002730

Sun, K., Luo, J., Guo, J., Yao, X., Jing, X., and Guo, F. (2020). The PI3K/AKT/mTOR signaling pathway in osteoarthritis: a narrative review. *Osteoarthr. Cartil.* 28 (4), 400–409. doi:10.1016/j.joca.2020.02.027

Suzuki, D., Bush, J. R., Bryce, D. M., Kamijo, R., and Beier, F. (2017). Rac1 dosage is crucial for normal endochondral bone growth. *Endocrinology* 158 (10), 3386–3398. doi:10.1210/en.2016-1691

Takahashi, I., Matsuzaki, T., Kuroki, H., and Hoso, M. (2019). Joint unloading inhibits articular cartilage degeneration in knee joints of a monosodium iodoacetate-induced rat model of osteoarthritis. *Osteoarthr. Cartil.* 27 (7), 1084–1093. doi:10.1016/j.joca.2019.03.001

Wang, C., Zeng, L., Zhang, T., Liu, J., and Wang, W. (2016). Tenuigenin prevents IL-1β-induced inflammation in human osteoarthritis chondrocytes by suppressing PI3K/AKT/NF-κB signaling pathway. *Inflammation* 39 (2), 807–812. doi:10.1007/s10753-016-0309-3

Wang, K., Chu, M., Wang, F., Zhao, Y., Chen, H., and Dai, X. (2020). Putative functional variants of PI3K/AKT/mTOR pathway are associated with knee osteoarthritis susceptibility. *J. Clin. Lab. Anal.* 34 (6), e23240. doi:10.1002/jcla.23240

Wang, K., Zhang, D., Liu, Y., Wang, X., Zhao, J., Sun, T., et al. (2018). Traditional Chinese medicine formula Bi-Qi capsule alleviates rheumatoid arthritis-induced inflammation, synovial hyperplasia, and cartilage destruction in rats. *Arthritis Res. Ther.* 20 (1), 43. doi:10.1186/s13075-018-1547-6

Wang, Q. S., Cui, Y. L., Wang, Y. F., and Chi, W. (2011). Effects of compounds from bi-qi capsule on the expression of inflammatory mediators in lipopolysaccharide-stimulated RAW 264.7 macrophages. *J. Ethnopharmacol.* 136 (3), 480–487. doi:10.1016/j.jep.2010.06.008

Wang, Y., Wang, X., Li, Y., Xue, Z., Shao, R., Li, L., et al. (2022). Xuanfei Baidu Decoction reduces acute lung injury by regulating infiltration of neutrophils and macrophages via PD-1/IL17A pathway. *Pharmacol. Res.* 176, 106083. doi:10.1016/j.phrs.2022.106083

Wang, Z., Wu, J., Li, D., Tang, X., Zhao, Y., Cai, X., et al. (2020). Traditional Chinese medicine Biqi capsule compared with leflunomide in combination with methotrexate in patients with rheumatoid arthritis: a randomized controlled trial. *Chin. Med.* 15, 36. doi:10.1186/s13020-020-00319-9

Woods, A., Pala, D., Kennedy, L., Mclean, S., Rockel, J. S., Wang, G., et al. (2009). Rac1 signaling regulates CTGF/CCN2 gene expression via TGFbeta/Smad signaling in chondrocytes. *Osteoarthr. Cartil.* 17 (3), 406–413. doi:10.1016/j.joca.2008.07.002

Wu, Y. H., Wu, Y. R., Li, B., and Yan, Z. Y. (2020). Cryptotanshinone: a review of its pharmacology activities and molecular mechanisms. *Fitoterapia* 145, 104633. doi:10.1016/j.fitote.2020.104633

Xiao, Z., Liu, W., Mu, Y. P., Zhang, H., Wang, X. N., Zhao, C. Q., et al. (2020). Pharmacological effects of salvianolic acid B against oxidative damage. *Front. Pharmacol.* 11, 572373. doi:10.3389/fphar.2020.572373

Xing-Yan, Z., Hu-Ling, L., Xin, L., Yan-Yan, X., Jing, G., Yong, Z., et al. (2021). Research progress on Biqi Capsule and predictive analysis of its quality markers. *Chin. Tradit. Herb. Drugs.* 52 (09), 2746–2757.

Xu, X., Liu, X., Yang, Y., He, J., Gu, H., Jiang, M., et al. (2019). Resveratrol inhibits the development of obesity-related osteoarthritis via the TLR4 and PI3K/Akt signaling pathways. *Connect. Tissue Res.* 60 (6), 571–582. doi:10.1080/03008207.2019.1601187

Xu, X., Liu, X., Yang, Y., He, J., Jiang, M., Huang, Y., et al. (2020). Resveratrol exerts anti-osteoarthritic effect by inhibiting TLR4/NF-κB signaling pathway via the TLR4/akt/FoxO1 Axis in IL-1β-stimulated SW1353 cells. *Drug Des. Devel Ther.* 14, 2079–2090. doi:10.2147/DDDT.S244059

Yang, W., Zhang, Y., Wu, W., Huang, L., Guo, D., and Liu, C. (2017). Approaches to establish Q-markers for the quality standards of traditional Chinese medicines. *Acta Pharm. Sin. B* 7 (4), 439–446. doi:10.1016/j.apsb.2017.04.012

Yin, W., Wang, T. S., Yin, F. Z., and Cai, B. C. (2003). Analgesic and anti-inflammatory properties of brucine and brucine N-oxide extracted from seeds of Strychnos nux-vomica. *J. Ethnopharmacol.* 88 (2-3), 205–214. doi:10.1016/s0378-8741(03)00224-1

Zahan, O. M., Serban, O., Gherman, C., and Fodor, D. (2020). The evaluation of oxidative stress in osteoarthritis. *Med. Pharm. Rep.* 93 (1), 12–22. doi:10.15386/mpr-1422

Zhai, K. F., Duan, H., Cui, C. Y., Cao, Y. Y., Si, J. L., Yang, H. J., et al. (2019). Liquiritin from Glycyrrhiza uralensis attenuating rheumatoid arthritis via reducing inflammation, suppressing angiogenesis, and inhibiting MAPK signaling pathway. *J. Agric. Food Chem.* 67 (10), 2856–2864. doi:10.1021/acs.jafc.9b00185

Zhanbiao, L., Yuanlu, C., Limin, H., Xiumei, G., and Yongmei, S. (2024). *Pharmaceutical compositions for osteoarthritis moulding and methods of preparation and moulding(CN102058877A)*. Chinese Patent.

Zhu, M., Ying, J., Lin, C., Wang, Y., Huang, K., Zhou, Y., et al. (2019). Baicalin induces apoptotic death of human chondrosarcoma cells through mitochondrial dysfunction and downregulation of the PI3K/Akt/mTOR pathway. *Planta Med.* 85 (5), 360–369. doi:10.1055/a-0791-1049

frontiers | Frontiers in Pharmacology

TYPE Original Research
PUBLISHED 07 May 2024
DOI 10.3389/fphar.2024.1351538

OPEN ACCESS

EDITED BY
Xianyu Li,
China Academy of Chinese Medical Sciences, China

REVIEWED BY
Yin-Hu Wang,
New York University, United States
Zili Xie,
Icahn School of Medicine at Mount Sinai, United States
Maolin Wang,
China Academy of Chinese Medical Sciences, China

*CORRESPONDENCE
Heng Fan,
fanheng009@aliyun.com
Hui Wu,
2020xh0029@hust.edu.cn

†These authors have contributed equally to this work and share first authorship

RECEIVED 15 January 2024
ACCEPTED 16 April 2024
PUBLISHED 07 May 2024

CITATION
Gao F, Zhu F, Shuai B, Wu M, Wei C, Yuan Y, Gui Y, Tian Y, Fan H and Wu H (2024), Quercetin ameliorates ulcerative colitis by restoring the balance of M2/M1 and repairing the intestinal barrier via downregulating cGAS–STING pathway.
Front. Pharmacol. 15:1351538.
doi: 10.3389/fphar.2024.1351538

Quercetin ameliorates ulcerative colitis by restoring the balance of M2/M1 and repairing the intestinal barrier via downregulating cGAS–STING pathway

Fei Gao[1†], Feng Zhu[1†], Bo Shuai[1†], Meng Wu[2†], Chunzhu Wei[1], Yuyi Yuan[1], Yang Gui[1], Yushi Tian[1], Heng Fan[1*] and Hui Wu[1*]

[1]Department of Integrated Traditional Chinese and Western Medicine, Union Hospital, Tongji Medical College, Huazhong University of Science and Technology, Wuhan, China, [2]Department of Orthopedics, Union Hospital, Tongji Medical College, Huazhong University of Science and Technology, Wuhan, China

Macrophage polarization is closely associated with the pathogenesis of ulcerative colitis (UC). Quercetin, a flavonoid, has shown promise as a treatment for inflammatory diseases, but its specific mechanism of action remains unclear. This study investigates whether quercetin can regulate intestinal macrophage polarization and promote intestinal tissue repair via the cGAS-STING pathway for the treatment of UC. *In vivo*, mice with 3% DSS-induced UC were intraperitoneally injected with quercetin and RU.521 for 7 days, following which their general conditions and corresponding therapeutic effects were assessed. The impact of interferon-stimulated DNA (ISD) and quercetin on macrophage polarization and the cGAS-STING pathway was investigated using RAW264.7 cells and bone marrow-derived macrophages (BMDMs) *in vitro*. The results demonstrated that ISD induced M1 macrophage polarization and activated the cGAS-STING pathway *in vitro*, while quercetin reversed ISD's inflammatory effects. *In vivo*, quercetin suppressed the cGAS-STING pathway in the intestinal macrophages of DSS-induced UC mice, which reduced M1 macrophage polarization, increased M2 polarization, and facilitated intestinal barrier repair in UC. Taken together, these findings provide new insights into the mechanisms via which quercetin could be used to treat UC.

KEYWORDS

ulcerative colitis, macrophage polarization, quercetin, intestinal barrier, immunity

1 Introduction

Ulcerative colitis (UC), classified as an inflammatory bowel disease (IBD), presents with recurrent, prolonged and challenging-to-treat episodes. The intricate pathogenesis of UC increases the complexity of therapeutic approaches, which may lead to intestinal epithelial barrier disruption, immune response dysregulation, and disturbances in the gut microbiota (Costello et al., 2019; Li et al., 2022). Specifically, rectifying immune imbalances is a crucial aspect of UC treatment, with the restoration of the intestinal barrier representing a key therapeutic goal. Among the various immune cells within the intestinal environment, macrophages play a central role in innate immunity, engaging in functions such as cytokine secretion, pathogen elimination, modulation of inflammation, and tissue repair

(Subramanian Vignesh et al., 2013; Park et al., 2017; Hoeffel et al., 2021; Virga et al., 2021). Therefore, comprehending the polarization of intestinal macrophages and the preservation of intestinal barrier integrity holds significant relevance for advancing the treatment of UC.

Macrophage polarization refers to the dynamic process by which macrophages transition into activated states under specific conditions (Murray, 2017). In normal physiological circumstances, intestinal macrophages phagocytose microorganisms and initiate a controlled immune response as antigen-presenting cells (Zhang et al., 2023). However, persistent and excessive inflammatory stimuli can lead to macrophage overactivation, which may damage the intestinal mucosa. During active phases of UC, macrophages tend to polarize towards an inflammatory phenotype known as M1, which may degrade tight junction (TJ) proteins, causing damage to the intestinal epithelial barrier and triggering excessive inflammation (Lissner et al., 2015). Comparatively, M2-type macrophages possess anti-inflammatory properties and contribute to tissue repair by reducing inflammation and promoting the healing of damaged tissues (Kim et al., 2021). Thus, the ratio of M2 to M1 macrophages can serve as an indicator of UC progression, while the integrity of the intestinal barrier reflects the capacity of macrophages to facilitate tissue repair following polarization.

Studies have reported abnormal increases in double-stranded DNA (dsDNA) expression in the serum and damaged intestinal tissues of patients with IBD and mice model. Cyclic guanosine monophosphate-adenosine monophosphate synthase (cGAS) plays a crucial role in recognizing cytoplasmic dsDNA, which can effectively activate cGAS (Dalekos et al., 1993; Hopfner and Hornung, 2020; Zhao et al., 2021). Specifically, cGAS detects the anomalous presence of dsDNA in the cytosol, leading to the synthesis of 2′3′-cyclic GMP-AMP (2′3′-cGAMP), a secondary messenger molecule, which subsequently binds to stimulator of interferon genes (STING) located in the endoplasmic reticulum, inducing a conformational change in STING. This altered conformation recruits TANK-binding kinase 1 (TBK1), initiating a cascade of phosphorylation events. Among the key substrates, interferon regulatory factor 3 (IRF3) undergoes phosphorylation and translocates to the nucleus, resulting in the induction of the expression of type I interferon (IFN), chemokines, and several other inflammatory mediators and pro-apoptotic genes (Decout et al., 2021; Zhang et al., 2022). When introduced as an exogenous dsDNA stimulus in macrophages, interferon-stimulated DNA (ISD) specifically activate the cGAS-STING pathway, leading to the polarization of macrophages towards the M1 phenotype. Notably, microglia display a shift towards the M2 phenotype upon cGAS knockout (Cao et al., 2018; Jiang et al., 2021). Consequently, it is of significant interest to investigate whether the modulation of the cGAS-STING pathway can mediate macrophage polarization in UC.

UC imposes a substantial economic burden on patients and national healthcare systems due to its prolonged disease course and the high cost of medications. Common therapeutic drugs, such as aminosalicylic acid, steroids, and immunosuppressants, can lead to adverse effects, including gastrointestinal discomfort, osteoporosis and bone marrow suppression. Quercetin (Que), a widely occurring natural flavonoid found in various plants, possesses important pharmacological properties, including antioxidant, antibacterial, anti-tumor and immune-regulatory activities. Importantly, Que exhibits low toxicity and minimal side effects (Zhou Y. et al., 2023). Numerous studies have identified Que as a potential therapeutic agent for UC due to its potent anti-inflammatory properties. However, the specific mechanisms underlying its efficacy remain poorly understood (Dicarlo et al., 2019; Gravina et al., 2023; Wang et al., 2024). In our study, we investigate whether Que can ameliorate UC by modulating macrophage polarization and promoting the restoration of the intestinal barrier through the cGAS-STING pathway.

2 Materials and methods

2.1 Drugs and reagents

Que (Cat#R006828) with a purity of HPLC ≥97% was purchased from Shanghai Rawhn Chemical Technology Co., Ltd. (Shanghai, China). RU.521 (Cat#M9447), a cGAS inhibitor, from AbMole (Houston, United States), DSS (Cat#160110) from MP Biomedicals (San Diego, CA, United States), FITC-Dextran (Cat#HY-128868D) from MedChemExpress (Monmouth Junction, NJ, United States), M-CSF (Cat#315-02) from PeproTech (Rocky Hill, NJ, United States). CCK-8 (Cat#BS350A) from Biosharp (Hefei, China), Lipofectamine™ 3000 (Lip3000, Cat#L3000001) and APC CD206 antibody (REF#17-2061-82) from Invitrogen (Carlsbad, CA, United States). iNOS antibody (Cat#18985-1-AP), Arg1 antibody (Cat#16001-1-AP), α-Tublin (Cat#66031-1-lg), STING (Cat#19851-1-AP), IRF3 (Cat#11312-1-AP), p-IRF3 (Cat#29528-1-AP), ZO1 (Cat#21773-1-AP) and Occludin (Cat#27260-1-AP) from Proteintech (Wuhan, China). Additionally, TBK1 (Cat#3504T) and p-TBK1 (Cat#5483S) were purchased from Cell Signaling Technology (Danvers, MA, United States), cGAS (Cat#ZRB1406) from Merck Millipore (Billerica, MA, United States), ELISA kits for IL10, CCL17, CXCL10, TNF-α and IFN-β from Adsbio (Yancheng, China), β-actin (Cat#GB12001), RIPA lysis buffer (Cat#G2002-100ML) and Bicinchoninic Acid (BCA) protein assay kit (Cat# G2026-200T) from Servicebio (Wuhan, China), and the following antibodies BV510 anti-FVD (Cat# 564406) and APC-Cy7 anti-CD45 (Cat# 557659), PE F4/80 (Cat#565410), PC-CY5.5 CD11b (Cat#101227) and BV421 CD11C (Cat#117329) from BD Biosciences (Franklin Lakes, NJ, United States). Furthermore, Trizol was bought from TaKaRa (Tokyo, Japan), HiScript® III RT SuperMix for quantitative polymerase chain reaction (qPCR) (+gDNA wiper) and ChamQ SYBR qPCR Master Mix from Vazyme (Nanjing, China), blood urea nitrogen (BUN) assay kit (Cat#C013-2-1), creatinine (CRE) assay kit (Cat#C011-2-1), alanine aminotransferase (ALT) assay kit (Cat#C009-2-1) and aspartate aminotransferase (AST) assay kit (Cat# C010-2-1) from Jiancheng Bioengineering Institute (Nanjing, China).

ISD was generated by heating equimolar amounts of sense and antisense DNA oligonucleotides to 95°C for 5 min, followed by cooling to room temperature (Gui et al., 2019). Si-cGAS was synthesized by Paivi Biotechnology Co., Ltd. (Wuhan, China) and had the following sequences: si-cGAS (sense, 5′-CAGCUG AACACUGGCAGCUACUAUG-3′, antisense, 5′-CAUAGUAGC UGCCAGUGUUCAGCUG-3′). All oligonucleotides for ISD and

qPCR primers used in this study were provided by Beijing Tsingke Biotech Co., Ltd.

2.2 Mice

Male C57BL/6 J mice (weighing 20–22 g and aged 6–8 weeks) were purchased from SPF Biotechnology Co., LTD. (Beijing) (Quality certification: SCXK (jing) 2019-0010). All animal-related experiments were conducted in strict adherence to the guidelines of the Animal Research Institute Committee of HUST and were approved by the HUST Institutional Animal Care and Use Committee (IACUC).

The mice were provided unrestricted access to food and water and housed under specific pathogen-free (SPF) conditions, which included a 12-h light/dark cycle, a temperature maintained at 22 ± 1°C, and humidity levels ranging from 45% to 55%. They were allowed to acclimate for 5 days, after which they were divided into four groups (n = 8): the normal control group (Normal), the model group (DSS), the RU.521 group (RU.521, administered at a dosage of 10 mg/kg, serving as the positive control) (Ma et al., 2020), and the Que group (QUE, administered at a dosage of 30 mg/kg) (Yang et al., 2014). Except for the control group, acute colitis was induced by the administration of 3% DSS for 7 days. RU.521 and Que were administered via intraperitoneal injections over the same seven-day period, starting at the onset of colitis induction. Meanwhile, the model group received an equivalent volume of drinking water. On the eighth day, the mice were euthanized, and the tissues were collected for analysis.

2.3 Cells

RAW264.7 cells (Cat#SNL-112) were purchased from SUNNCELL (Wuhan, China) and cultured in Dulbecco's Modified Eagle's Medium (DMEM) with high glucose containing 5% fetal bovine serum (FBS). The culture was maintained in a humidified incubator with 5% CO2 and 95% air at 37°C. Bone marrow mesenchymal cells were isolated from the tibiofibula of mice and were stimulated with M-CSF at a concentration of 30 ng/mL in 5% FBS-1640 RPMI medium. The medium was replaced with fresh medium containing 20 ng/mL M-CSF on the third and fifth days. On the seventh day, the cell morphology was observed and confirmed through flow cytometry.

To determine the appropriate concentration of Que for intervention, the viability of both cell types was assessed after exposure to different concentrations of Que for 24 h, following the instructions provided with the CCK8 kit.

The cell experiment involved four distinct groups: the control group, the ISD (2 μg/mL) group, the si-cGAS + ISD group, and the Que (50 μmol/L) + ISD group. RAW264.7 cells and BMDMs were seeded in 9.6 cm^2 culture plates at a density of 5×10^5 cells per well and allowed to grow for 12 h in a humidified incubator. Subsequently, cells in all groups, except the control group, were transfected with ISD for 6 h. Following this transfection, the culture medium for all groups was replaced with 2 mL of fresh medium. Que was administered for an additional 24 h, and si-cGAS was transfected during the final 8 h of this period. To confirm the efficiency of si-cGAS transfection, quantitative real-time polymerase chain reaction analysis (qRT-PCR) and western blotting (WB) were performed. The transfection of ISD and si-cGAS was performed following the instructions provided for Lipofectamine™ 3000.

2.4 Evaluation of intestinal inflammation in mice

Throughout the experimental period, the weight of each mouse was consistently monitored. On the eighth day following drug intervention, the entire colon tissue was excised, photographed to record its length, and collected after mice were humanely euthanized via cervical dislocation under anesthesia induced by 1% pentobarbital sodium (50 mg/kg body weight). The intestines, specifically a segment approximately 0.5 cm proximal to the anus, were rinsed, circumferentially cut, and then preserved in 1 mL of 4% paraformaldehyde for the following experiments. To assess disease activity and calculate the disease activity index (DAI), weight loss, stool consistency and fecal occult blood were evaluated daily (Sann et al., 2013). Tissue sections were subjected to hematoxylin and eosin (H&E) staining for histological examination, while Alcian Blue/Phosphoric Acid Schiff (AB/PAS) staining was employed to visualize goblet cells, as previously described by Ma et al. (2020). Additionally, H&E staining was performed on the mice heart, liver, spleen, lung, and kidney tissues. The levels of blood urea nitrogen (BUN), creatinine (CRE), alanine aminotransferase (ALT) and aspartate aminotransferase (AST) in mouse serum were measured using assay kits to assess the safety of Que intervention in this study.

2.5 Preparation for single-cell suspension of mouse spleen, mesenteric lymph node

The procedure for obtaining a single-cell suspension from the mouse spleen and mesenteric lymph nodes was performed as previously described (Gao et al., 2022). Upon collection of the spleen and mesenteric lymph nodes, they were promptly immersed in pre-chilled 3% BSA in PBS. The tissues were finely chopped and softly homogenized. Following filtration through a 70 μm sieve, the cellular suspension was harvested. For spleen samples, erythrocytes were lysed prior to centrifugation and subsequent resuspension.

2.6 Flow cytometry

Flow cytometry was utilized to identify BMDMs and assess the M2/M1 cell ratio in the spleen, and MLNs post-intervention for macrophage polarization analysis. On the seventh day of M-CSF stimulation, bone marrow mesenchymal cells were collected and labeled with antibodies, including anti-FVD, APC-Cy7-conjugated anti-CD45, PE-conjugated F4/80, and PC-CY5.5-conjugated CD11b. For macrophage identification, cultured BMDMs received BV421-conjugated CD11C and APC-conjugated CD206 antibodies. Macrophages were

TABLE 1 Primers sequences.

Gene	Forward primer (5′–3′)	Reverse primer (5′–3′)
ISD	TACAGATCTACTAGTGATCTATG	ACTGATCTGTACATGATCTACA
cGAS	TTCCACGAGGAAATCCGCTGAG	CAGCAGGGCTTCCTGGTTTTTC
STING	GGTGGCCAGCCTGATGATCC	AGCCTTCCAGTAGCTGCCCT
iNOS	GAAGAAAACCCCTTGTGCTG	TCCAGGGATTCTGGAACATT
Arg1	CTTGGCTTGCTTCGGAACTC	GGAGAAGGCGTTTGCTTAGTTC
IFN-β	CTAACTGCAACCTTTCGAAGC	CTAGTGTCCTTTCATATGCAG
CCL17	CGAGAGTGCTGCCTGGATTACT	GGTCTGCACAGATGAGCTTGCC
IL10	GCTCTTACTGACTGGCATGAG	CGCAGCTCTAGGAGCATGTG
TNF-α	TACTGAACTTCGGGGTGATCG	TCCTCCACTTGGTGGTTTGC
CXCL10	CCAAGTGCTGCCGTCATTTTC	TCCCTATGGCCCTCATTCTCA
ZO1	CCAGCAACTTTCAGACCACC	TTGTGTACGGCTTTGGTGTG
Occludin	TAAGAGCTTACAGGCAGAACTAG	CTGTCATAATCTCCCACCATC

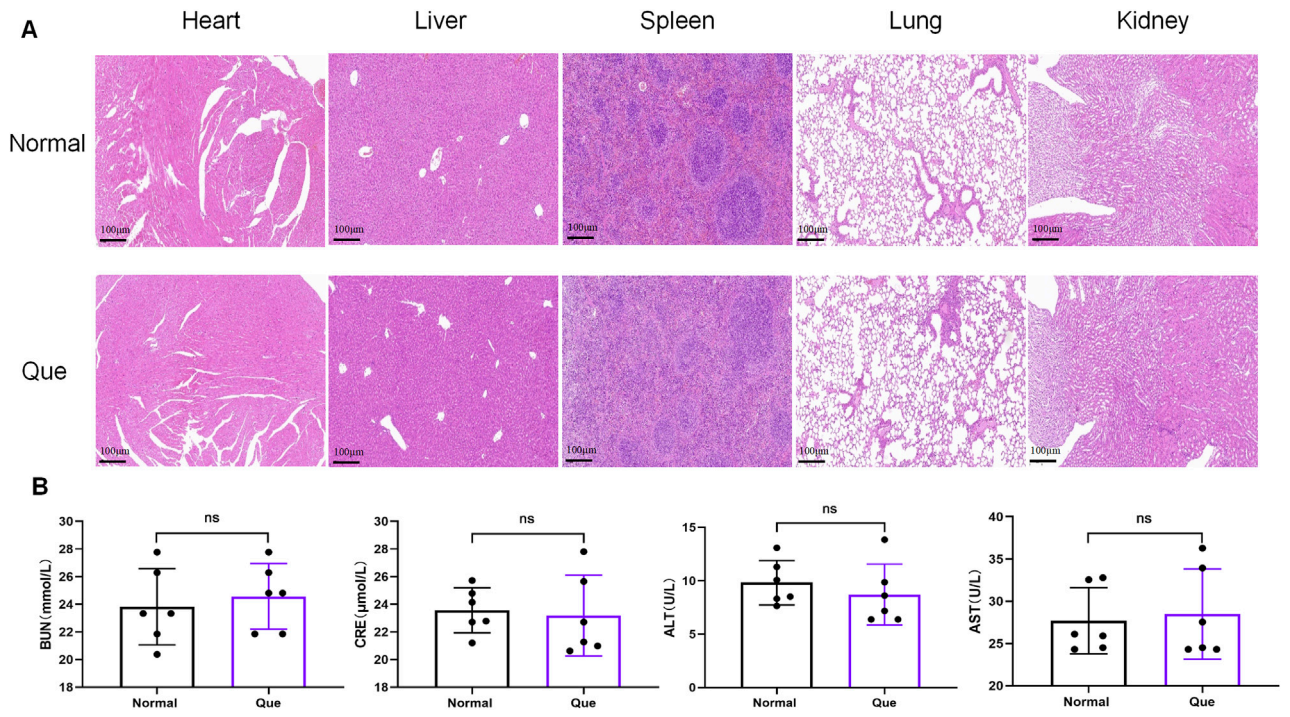

FIGURE 1
Quercetin is safe for mice. **(A)**. HE staining of heart, liver, spleen, lung, kidney tissues (Bar = 100 μm) (n = 6) **(B)** Statistical map of the levels of BUN, CRE, ALT and AST in mouse serum (n = 6). Data were shown as mean ± SD. ns (no significance) vs. normal group.

characterized as F4/80$^+$CD11b$^+$ cells, with M1 and M2 subsets defined as F4/80$^+$CD11b$^+$CD11C$^+$CD206$^-$ and F4/80$^+$CD11b$^+$CD11C$^-$CD206$^+$, respectively. The same flow cytometry protocol was applied to assess macrophage polarization in tissues (Ying et al., 2013; Ding et al., 2022). Cells and other tissues were analyzed using a BD LSR flow cytometer (BD Biosciences, San Jose, CA, United States), and the data were analyzed using the CytExpert software.

2.7 qRT-PCR

Total RNA was extracted from both clones and cells using Trizol. Subsequently, reverse transcription was carried out using HiScript® III RT SuperMix for qPCR (+gDNA wiper). Following reverse transcription, qPCR was conducted using ChamQ SYBR qPCR Master Mix. The procedures were conducted following the instructions of the respective reagents. The relative mRNA

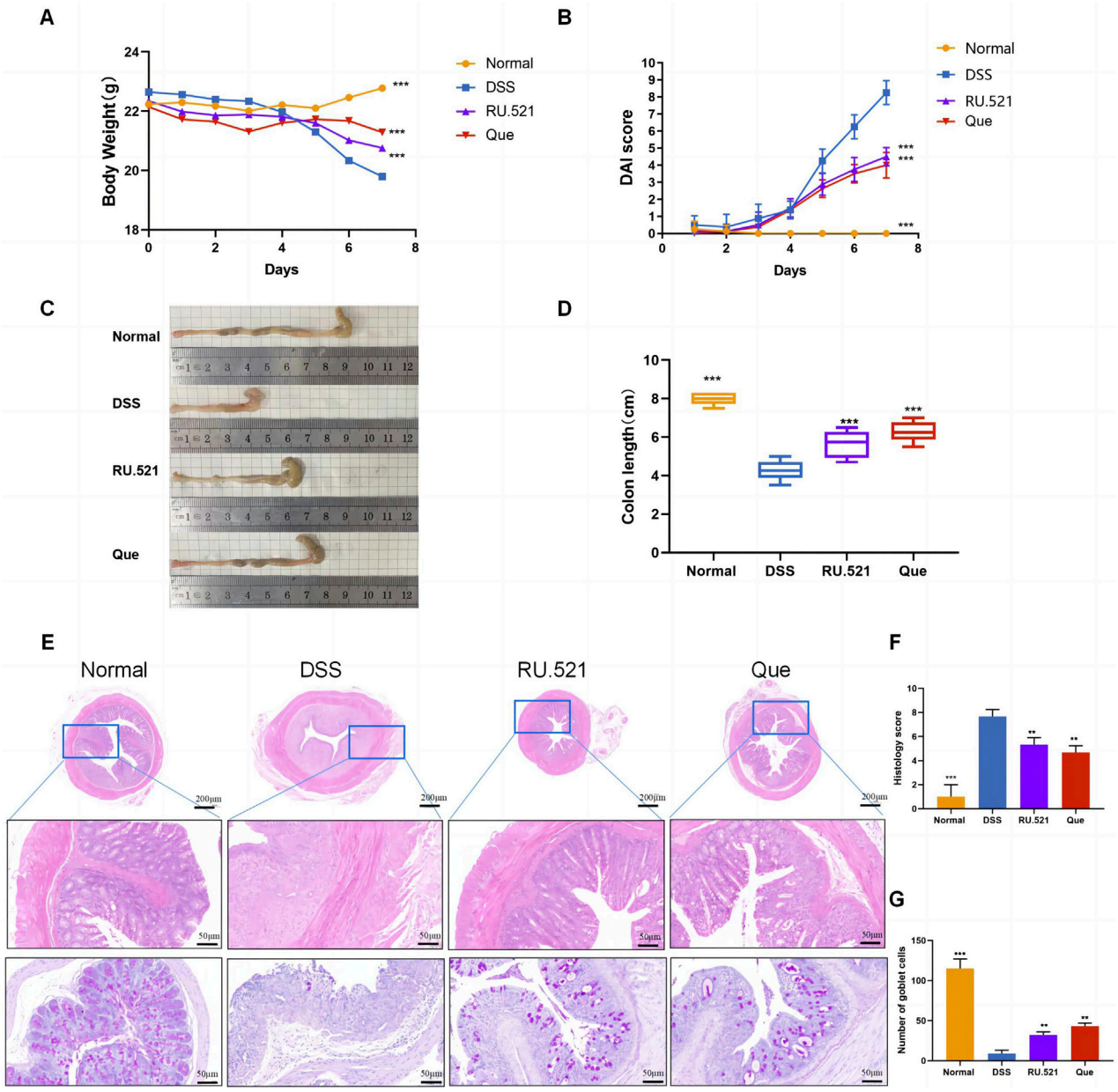

FIGURE 2
Quercetin alleviates DSS-induced UC. **(A)** Changes in body weight (n = 8). **(B)** DAI scores (n = 8). **(C)** Representative images of colon specimens from each group (n = 6). **(D)** Statistical analysis of colon length (n = 6). **(E)** Histological examination of colon tissues by HE and PAS staining (Bar = 200 μm, 50 μm) (n = 3). **(F)** Colonic histopathological scoring. **(G)** Number of goblet cells. Data are presented as mean ± SD. $^{**}p < 0.01$,$^{***}p < 0.001$.

expression levels were calculated using the $2^{-\Delta\Delta CT}$ method, with β-actin serving as the endogenous control. The primer sequences are provided in Table 1.

2.8 Western blotting

The cells or intestinal tissues were homogenized in RIPA lysis buffer using a grinder (50Hz, 120s, LUKA, Guangzhou). After centrifugation, the supernatant was collected, and protein concentrations were determined using a BCA protein assay kit. Subsequently, the samples were loaded onto either 8% or 10% sodium dodecyl sulfate–polyacrylamide gel electrophoresis (SDS-PAGE) gels with 15 wells and a thickness of 1.0 mm for rapid electrophoresis (200V, 30min). The target proteins were then transferred to a polyvinylidene (PVDF) membrane (Millipore, Billerica, MA, United States) (400mA, 30 min). Following a 20-min blocking step with a fast-blocking solution at room temperature, the protein bands were washed with 1 × TBST for 10 min and subsequently incubated with primary antibodies including cGAS, STING, TBK1, p-TBK1, iNOS, p-IRF3, β-actin, α-Tubulin (at a dilution of 1:1000), IRF3, and Arg1 (at a dilution of 1:5000) overnight at 4°C. The next day, the protein bands were washed three times with 1×TBST for 10 min each time and

10.3389/fphar.2024.1351538

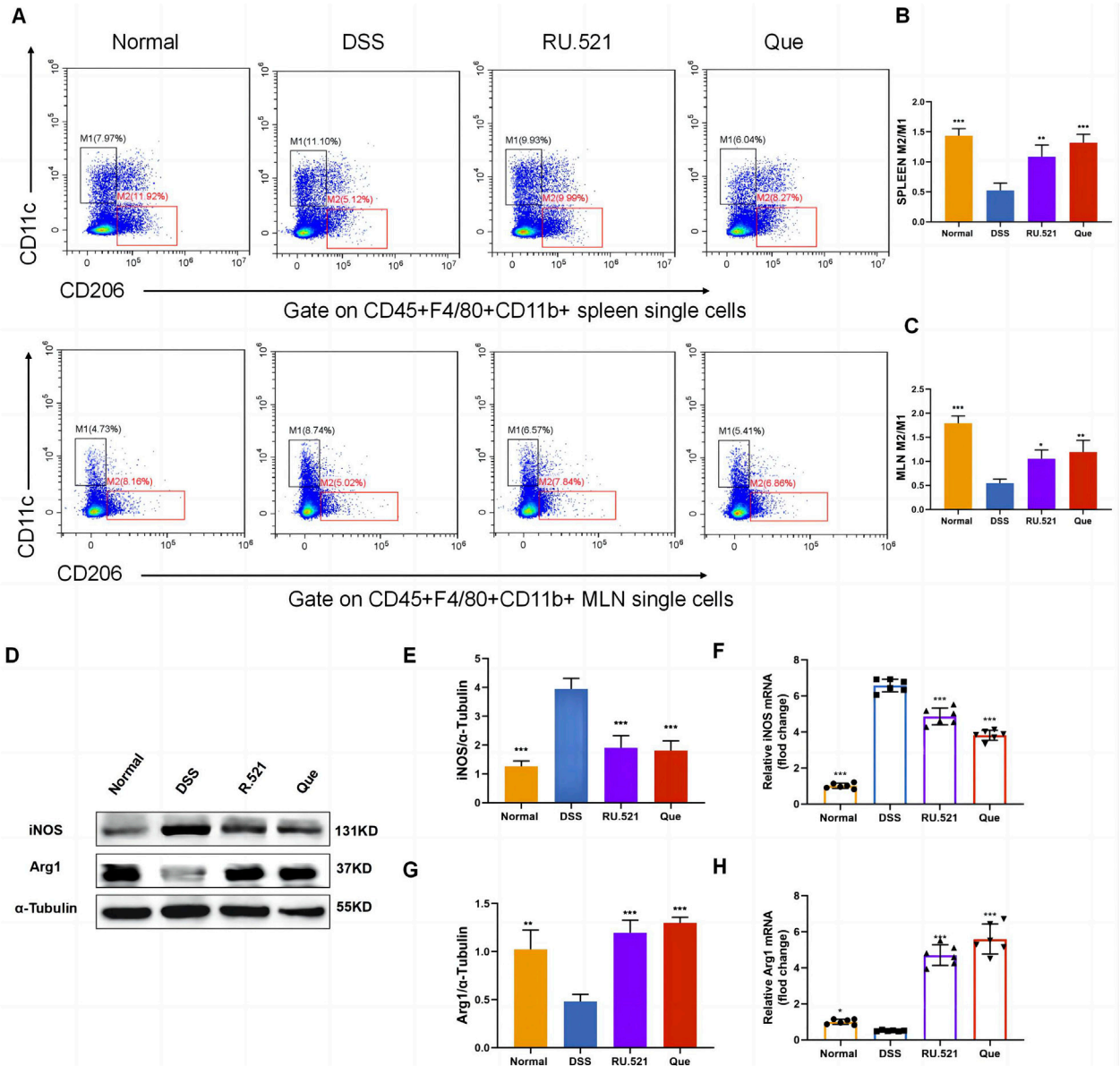

FIGURE 3
Quercetin restores M2/M1 ratio in mice. **(A)** Representative flow cytometry results and summarized percentages of $CD11c^{+}CD206^{-}$ cells (M1) and $CD11c^{-}CD206^{+}$ cells (M2) in the $CD45^{+}F4/80^{+}CD11b^{+}$ macrophages of spleen and mesenteric lymph nodes. **(B)** Statistical analysis of M2/M1 ratio in mice spleen ($n = 3$). **(C)** Statistical analysis of M2/M1 ratio in mice mesenteric lymph nodes ($n = 3$). **(D)** Representative western blot images of iNOS and Arg1 in mice colon tissues ($n = 3$). **(E,G)** Statistical analysis of iNOS and Arg1 protein abundance in mice colon ($n = 3$). **(F,H)** Statistical analysis of iNOS and Arg1 mRNA abundance in analysis colon ($n = 6$). Data are shown as mean ± SD. $^{*}p < 0.05$, $^{**}p < 0.01$, $^{***}p < 0.001$.

incubated with a secondary antibody (dilution, 1:5000) at room temperature for 1 h, followed by additional washing. Lastly, the bands were briefly immersed in an ECL exposure solution and placed in an exposure apparatus for visualization. Image analysis was performed using ImageJ software.

2.9 Enzyme-linked immunosorbent assay (ELISA)

The expression levels of IL10, CCL17, CXCL10, TNF-α and IFN-β in the colon homogenate supernatant were assessed using ELISA kits. Following the manufacturer's instructions, the standard product was initially diluted in a gradient, then both the samples and biotin-labeled antibodies were introduced to the enzyme labeling plate. Absorbance was measured at 450 nm using a microplate reader.

2.10 Immunofluorescent (IF)

Intestinal sections stained with H&E were deparaffinized, while RAW264.7 cells were fixed using 4% paraformaldehyde. After rehydration, both were washed with 1% TWEEN-PBS and

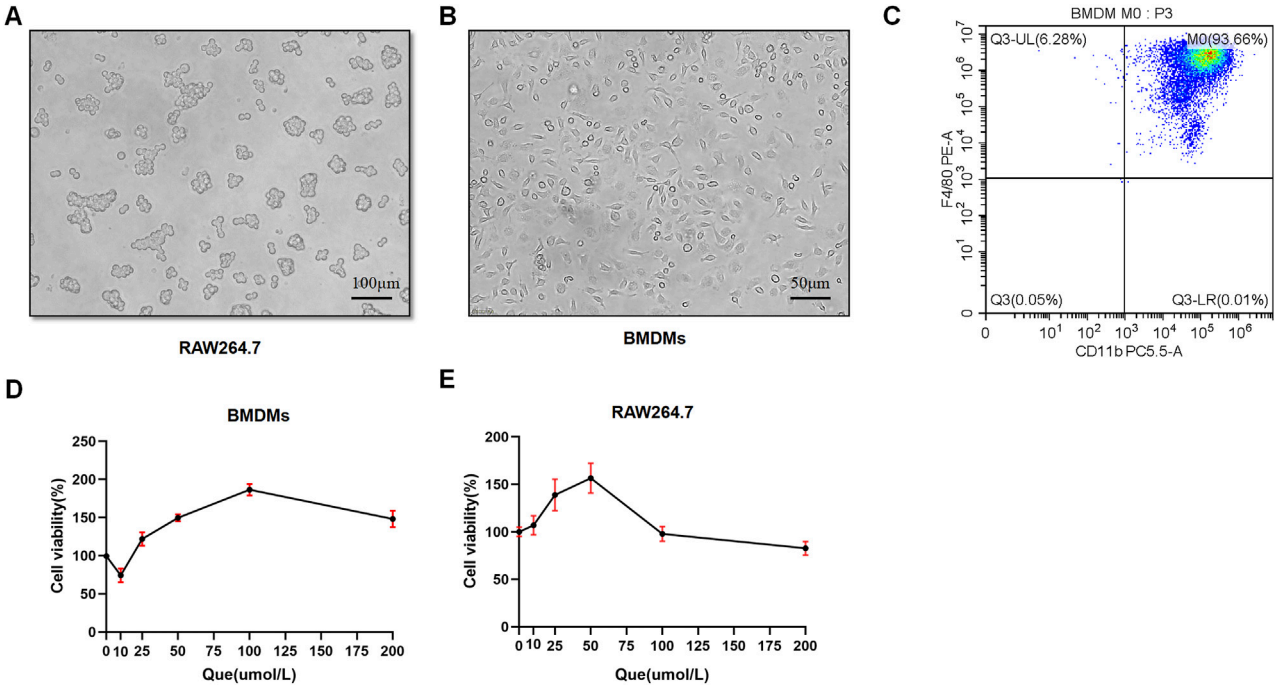

FIGURE 4
Successful induction of BMDMs and macrophage viability after 24-h quercetin (Que) intervention. **(A)** Morphology of RAW264.7 observed under a light microscope (Bar = 100 μm). **(B)** Morphology of BMDMs observed under a light microscope (Bar = 50 μm). **(C)** Flow cytometry results confirm the identification of BMDMs. **(D)** Viability of BMDMs. **(E)** Viability of RAW264.7 cells. Data are presented as mean ± SD.

blocked with 3% goat serum. For IF experiments, specific primary antibodies (anti-iNOS, anti-ZO1, anti-Occludin at 1:200 dilution, and anti-Arg1 at 1:500 dilution) were incubated overnight at 4°C after blocking. On the following day, the sections and cells were washed and subsequently incubated with secondary antibodies labeled with fluorescein isothiocyanate (FITC) or Cy3. Finally, they were counter-stained with 4′,6-diamidino-2-phenylindole (DAPI) for 5 min, and IF images were captured using a confocal laser scanning microscope (Olympus-FV1000).

2.11 FITC-dex assay

The abdominal hairs of the mice were removed, and they underwent a 24-h fasting. Next, they were orally administered with FITC-Dex (average molecular weight: 4000, 0.6 mg/g) while being kept away from light for 4 h. Prior to the assay, the mice were anesthetized using 1% pentobarbital. To measure fluorescence intensity (excitation 490 nm/emission 535 nm), serum samples were diluted 1:1 with a PBS solution. The quantification of Fluorescein isothiocyanate-dextran (FITC-Dex) in the serum was performed using a fluorescent enzyme label kit, following the manufacturer's instructions.

2.12 Statistical analysis

Statistical analysis was conducted using GraphPad Prism 8.0 (Graph Pad Software Inc., San Diego, CA, United States). Data are presented as mean ± standard deviation (SD). Two-tailed unpaired t-tests were employed to compare two groups, while a two-way analysis of variance (ANOVA) was utilized to analyze multiple groups. The significance levels were denoted as $^{*}p < 0.05$, $^{**}p < 0.01$, and $^{***}p < 0.001$.

3 Results

3.1 Quercetin ameliorates colitis symptoms and damage in colon tissues

The DSS-induced UC method in mice is well-established. First, we verified that Que at a concentration of 30 mg/kg was safe for mice after 7 days of intervention, The results of H&E staining showed that no obvious changes in the heart, liver, spleen, lung, or kidney tissues between the normal and Que-treated groups of mice. In addition, there were no significant deviations in serum levels of BUN, CRE, ALT and AST between groups (Figure 1). As shown in Figures 2A, B, mice treated with the cGAS inhibitor (RU.521) and Que exhibited significant improvements in weight loss, fecal characteristics and overall wellbeing compared to those receiving only DSS. Moreover, the interventions led to significant improvements in intestinal morphology and pathology, including reduced intestinal shortening, decreased infiltration of inflammatory cells, preserved crypts, and increased goblet cell counts in DSS-treated mice (Figures 2C–G). These results highlight the effectiveness of cGAS inhibition in reducing intestinal damage and improving UC and support the therapeutic potential of Que.

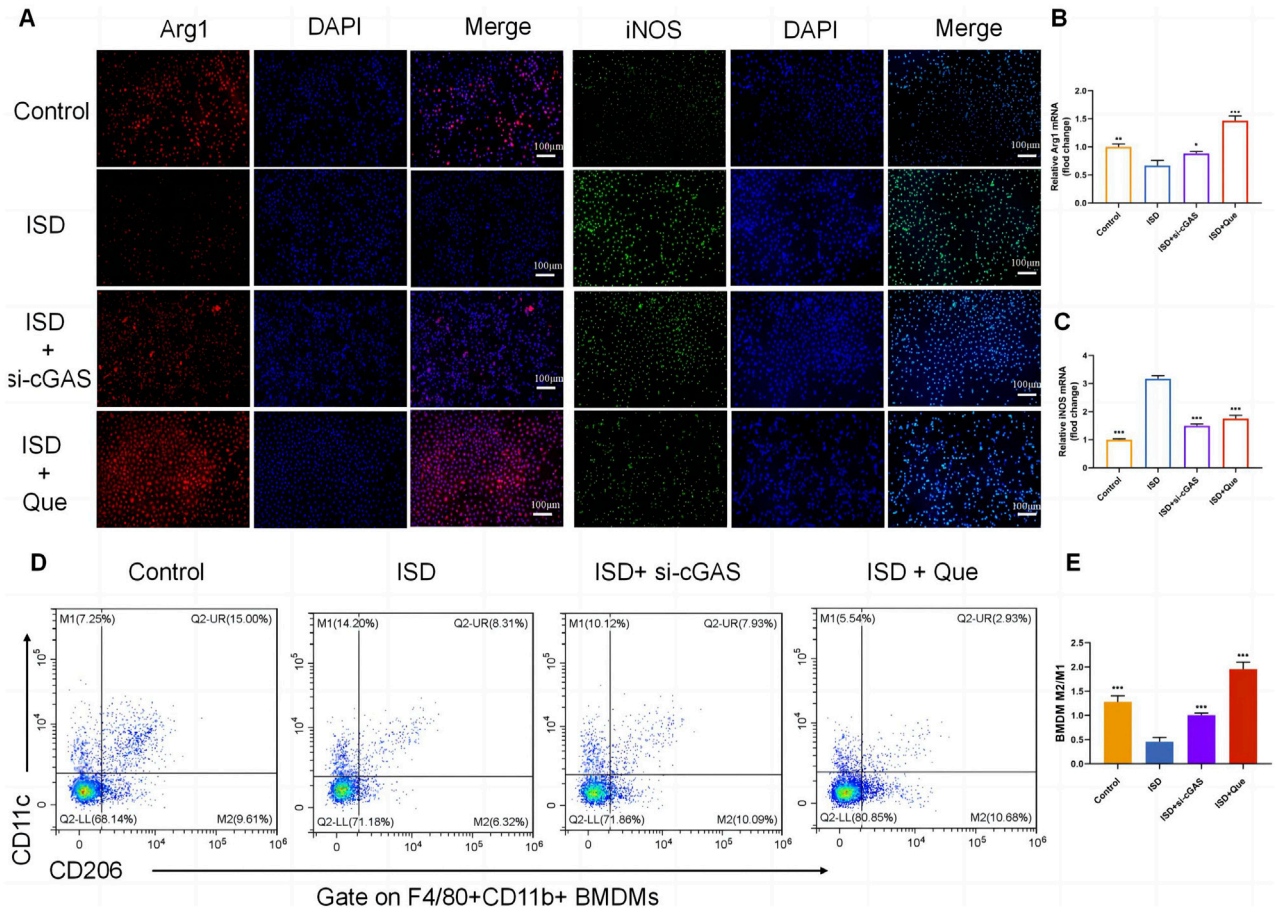

FIGURE 5
Quercetin restores the ratio of M2/M1 *in vitro*. **(A)** Immunofluorescence staining of Arg1 (red) and iNOS (green) expression in BMDMs (Bar = 100 μm); Nuclei were stained with DAPI (blue). **(B,C)** Quantification of iNOS and Arg1 mRNA levels in RAW264.7 cells (n = 3). **(D)** Flow cytometry results showing the percentages of M1 and M2 macrophages in BMDMs. **(E)** Statistical analysis of the M2/M1 ratio in BMDMs (n = 3). Data are presented as mean ± SD. $^{*}p < 0.05$, $^{**}p < 0.01$, $^{***}p < 0.001$ vs. ISD group.

3.2 Quercetin restores M2/M1 balance in mice

To investigate the changes in M2 and M1 subpopulations in mice following Que intervention and cGAS inhibition, we isolated the spleen and mesenteric lymph nodes for flow analysis. Compared to the model group, the intervention groups exhibited significant suppression of the M1 subpopulation and an increase in the M2 subpopulation (Figures 3A–C). Furthermore, the levels of Arg1 and iNOS in intestinal tissues were assessed using WB and qPCR. It was observed that iNOS levels increased while Arg1 levels decreased during colitis. However, these changes were reversed following intervention with RU.521 and Que (Figures 3D–H). Thus, these findings indicate that Que and cGAS inhibition contribute to the restoration of the M2/M1 ratio in mice.

3.3 Intervention concentration of quercetin for successfully inducing BMDMs

BMDMs and RAW264.7 cells were used to assess macrophage polarization *in vitro*. Initially, we observed the morphology of RAW264.7 cells with round shape, and the M-CSF-induced cells which displayed a flattened appearance with numerous protrusions (Figures 4A, B). Subsequently, flow cytometry analysis revealed that $F4/80^{+}CD11b^{+}$ cells constituted 93.66% of the total cells, confirming successful macrophage induction (Figure 4C). BMDMs and RAW264.7 cells were subjected to different concentrations of Que for 24 h, and 50 μmol/L was determined as the optimal intervention concentration for Que, as it did not affect the viability of both cell types (Figures 4D, E).

3.4 Quercetin regulates macrophage polarization *in vitro*

To investigate the impact of Que and cGAS inhibition on macrophage polarization *in vitro*, we used ISD, an exogenous stimulator known to activate cGAS expression, to intervene with macrophages. We assessed the state of macrophage polarization after inhibiting cGAS expression and administering Que. Following ISD intervention, there was a significant decrease in the fluorescence expression of Arg1 and an increase in iNOS in RAW264.7 cells. However, when compared to the ISD group, the

10.3389/fphar.2024.1351538

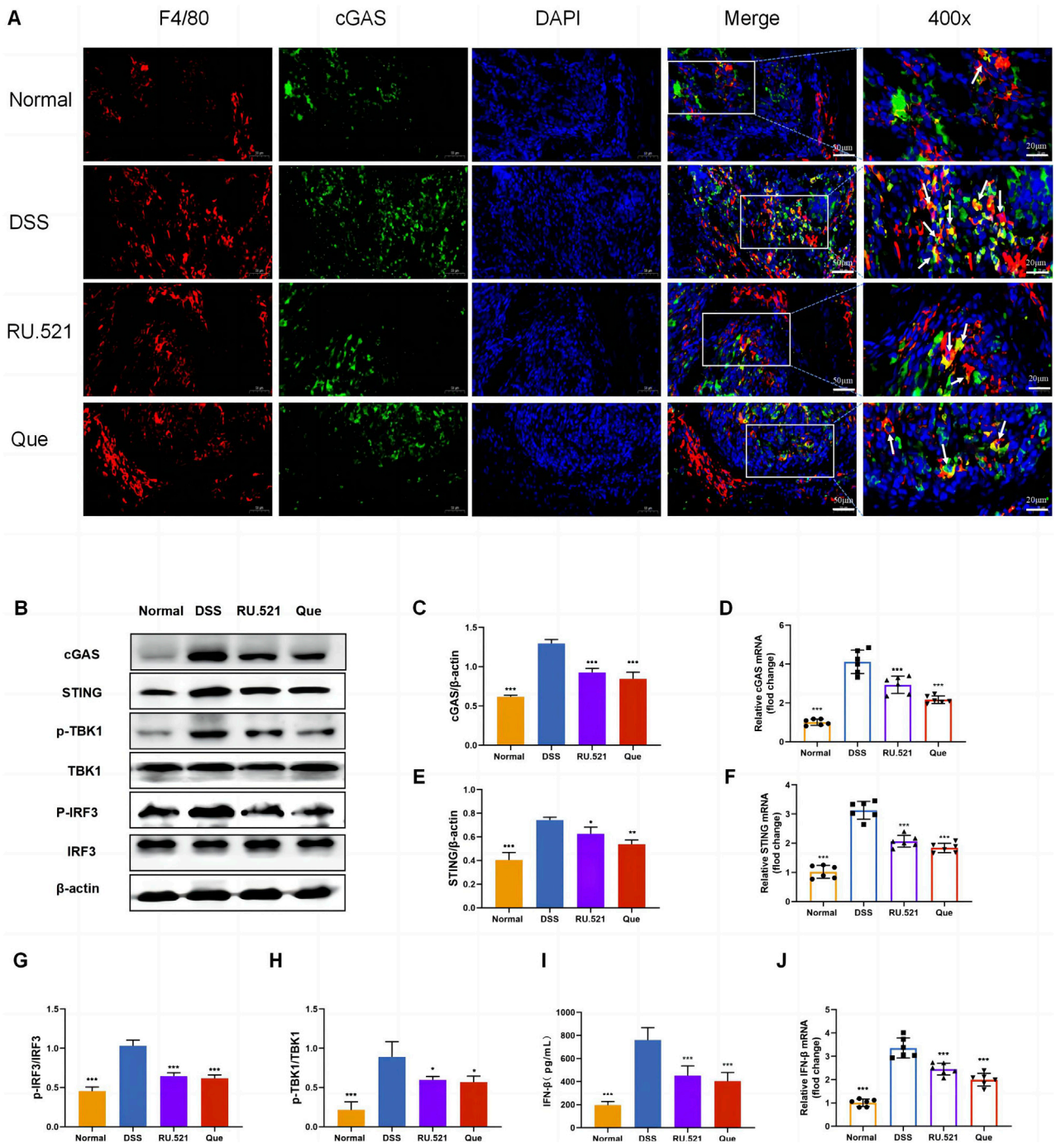

FIGURE 6
Quercetin inhibits the cGAS-STING pathway in intestinal macrophages. **(A)** Immunofluorescence staining of F4/80 (red) and cGAS (green) expression in colon tissues (Bar = 50 μm), with an enlarged view at 400× (Bar = 20 μm). Nuclei were stained with DAPI (blue). **(B)** Western blot analysis of the cGAS-STING pathway in colon tissues (n = 3). **(C,E,G,H,I)** Quantification of cGAS, STING, p-TBK1, p-IRF3 and IFN-β protein levels in colon tissues (n = 6). **(D,F,J)** Quantification of cGAS, STING, and IFN-β mRNA levels in colon (n = 6). Data are presented as mean ± SD. *p < 0.05, **p < 0.01, ***p < 0.001.

utilization of si-cGAS and Que led to a significant enhancement in Arg1 fluorescence expression, accompanied by a reduction in iNOS levels (Figure 5A). Similar changes were observed in the mRNA levels of Arg1 and iNOS in RAW264.7 cells (Figures 5B, C). Flow cytometry analysis provided further insights, demonstrating that ISD intervention resulted in an increased proportion of M1 cells and a reduced population of M2 cells. However, si-cGAS and Que effectively reversed this trend, redirecting macrophages away from the inflammatory phenotype (M1) towards M2 cells with anti-inflammatory properties (Figures 5D, E).

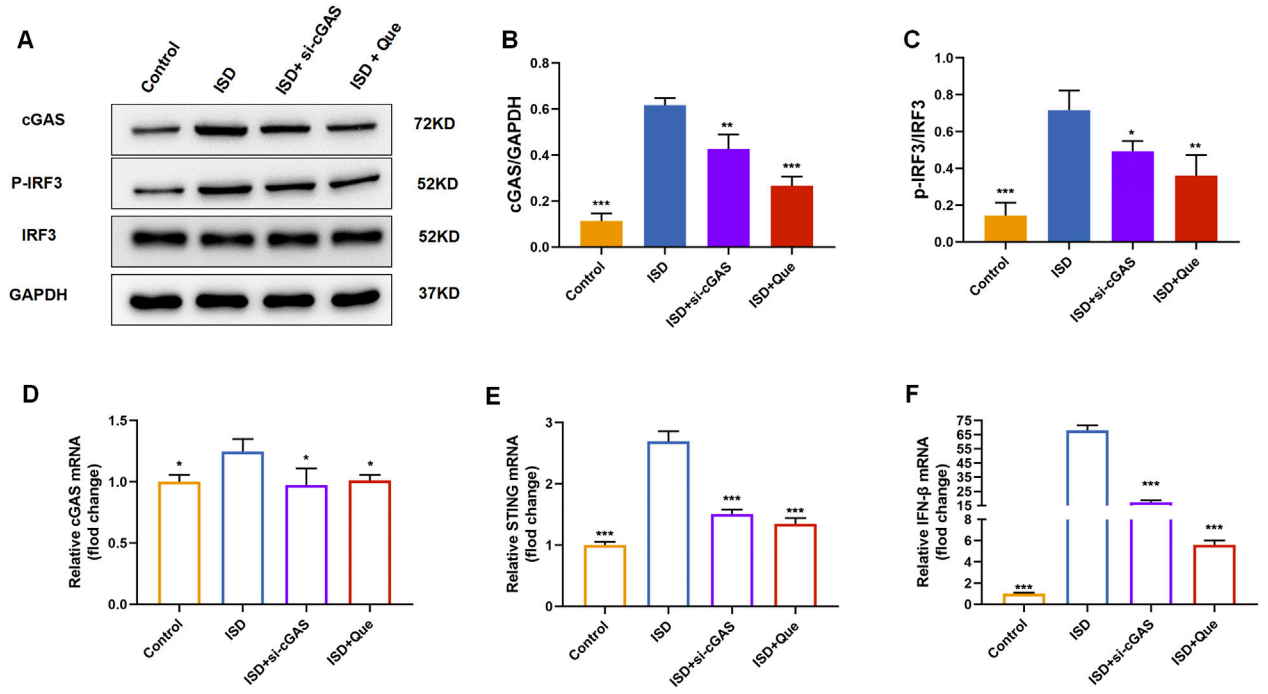

FIGURE 7
Quercetin inhibits the cGAS-STING pathway *in vitro*. **(A)** Western blot analysis of the cGAS、p-IRF3 in BMDMs (n = 3). **(B)** Quantification of cGAS protein levels in BMDMs. **(C)** Quantification of p-IRF3 protein levels in BMDMs. **(D–F)** Quantification of cGAS, STING, and IFN-β mRNA levels in RAW264.7 cells (n = 3). Data are presented as mean ± SD. *p < 0.05, **p < 0.01, ***p < 0.001.

3.5 Quercetin inhibits the cGAS-STING pathway during macrophage polarization

To investigate the role of the cGAS-STING pathway in the polarization of intestinal macrophages, we conducted double fluorescent labeling of intestinal F4/80 and cGAS proteins, which helped identify macrophages in the intestine. We observed that both Que and RU.521 reduced the fluorescence expression of F4/80 compared to the model group, indicating a decrease in intestinal macrophage infiltration. Under a 400-fold fluorescence microscope, we observed that the fluorescence expression of cGAS in intestinal macrophages was elevated in the intestinal tissues of mice in the model group. However, this expression was significantly reduced after the intervention of Que and RU.521, suggesting that both Que and RU.521 inhibited cGAS in intestinal macrophages (Figure 6A). Furthermore, we examined the changes in the cGAS-STING pathway in the colon and found that the expression of cGAS-STING pathway-related proteins (cGAS, STING, p-TBK, p-IRF3 and IFN-β) in mice significantly increased after modeling. Both Que and RU.521 reduced the levels of these proteins (Figures 6B, C, E, G–I). Additionally, mRNA levels of cGAS, STING, and IFN-β were detected by qPCR in both *in vitro* and *in vivo* experiments (Figures 6D, F, J). Based on findings regarding the regulation of macrophage polarization by Que and cGAS inhibition, it is evident that Que can inhibit the cGAS-STING pathway in gut macrophages, thereby influencing macrophage polarization.

We found that quercetin inhibited the ISD-activated cGAS-STING pathway in macrophages like RU.521 by detecting protein content and mRNA levels related to cGAS-STING pathway in BMDMs and raw264.7 cells (Figure 7). Combined with animal experiments' results, it was indicated that quercetin's regulation of macrophage polarization in UC mice was related to this pathway.

3.6 Quercetin reduces the levels of inflammation in macrophages, similar to cGAS inhibitor

To assess the impact of Que on intestinal inflammation through the inhibition of the cGAS-STING pathway, we measured the protein levels of anti-inflammatory factors CXCL10 and TNF-α, as well as the inflammatory factors CCL17 and IL10, using ELISA. Following DSS-induced enteritis, there was a significant increase in the protein levels of CXCL10 and TNF-α, coupled with a notable decrease in IL10 and CCL17. Both Que and RU.521 could significantly reduce the protein levels of CXCL10 and TNF-α while increasing the protein levels of IL10 and CCL17 following the induction of enteritis (Figures 8A–D). Consistent results were obtained when measuring mRNA levels in intestinal tissues and macrophages (Figures 8E–L). Thus, Que could mitigate intestinal inflammation by inhibiting the cGAS-STING pathway.

3.7 Quercetin improves intestinal structural integrity and permeability to restore intestinal barrier functions

ZO1 and Occludin are important components of TJs that are responsible for maintaining the integrity of intestinal epithelial and

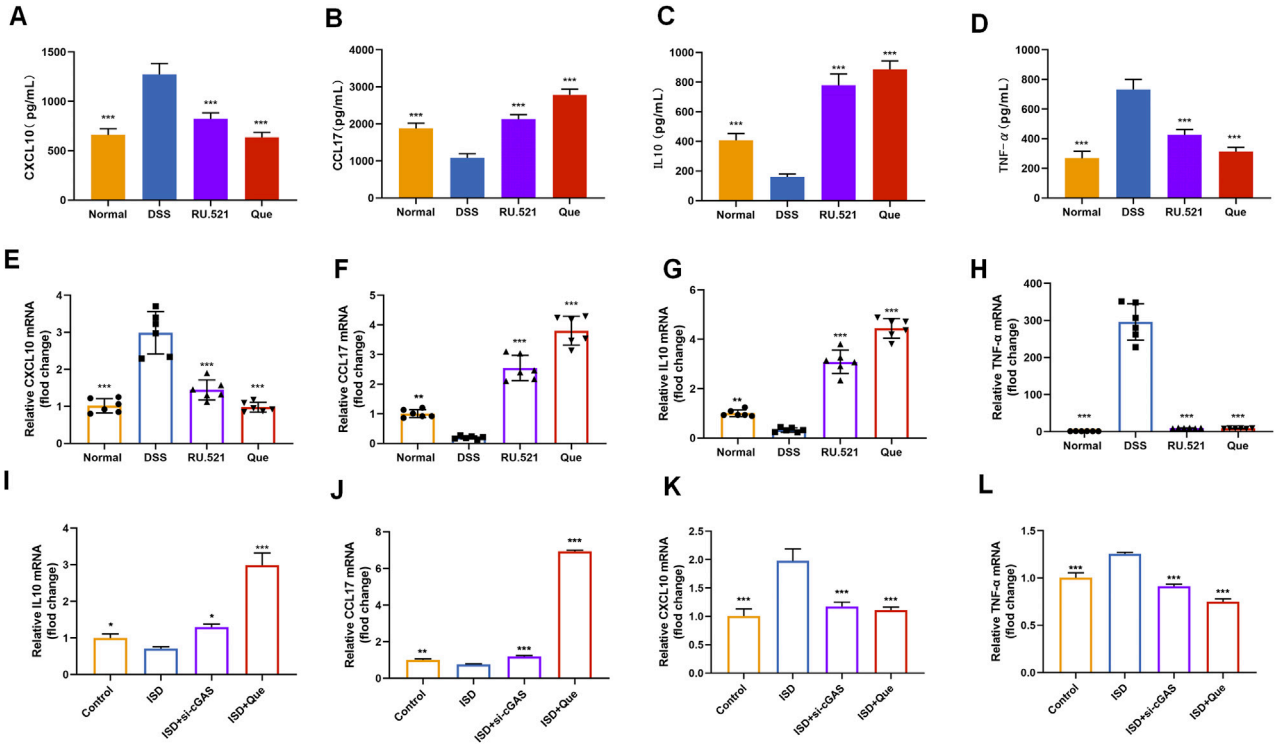

FIGURE 8
Quercetin and RU.521 reduce inflammatory factors and increase anti-inflammatory factors in colon and RAW264.7 cells. **(A–D)** Quantification of CXCL10, CCL17, IL10 and TNF-α protein levels in the colon (n = 6). **(E–H)** Quantification of CXCL10, CCL17, IL10 and TNF-α mRNA levels in the colon (n = 6). **(I–L)** Quantification of CXCL10, CCL17, IL10 and TNF-α levels in RAW264.7 cells (n = 3). Data are presented as mean ± SD. *p < 0.05, **p < 0.01, ***p < 0.001.

endothelial cells. The structural integrity of the intestine can be visually assessed through ultrastructure analysis. In DSS-induced mice, the fluorescence expression of ZO1 and Occludin in intestinal tissues was notably weakened. However, both Que and RU.521 significantly enhanced the fluorescence expression (Figure 9A). Consistent trends were observed in the mRNA levels of intestinal ZO1 and Occludin (Figures 9B, C). In the ultrastructure analysis, normal intestinal tissues exhibited long and well-arranged microvilli, with intact TJs located directly beneath them. In contrast, the model group displayed shorter, sparser or even shed microvilli, along with interrupted TJs. Both Que and RU.521 could repair the intestinal microvilli and TJs (Figure 10A). Intestinal permeability was assessed by tracking the distribution of FITC-labeled dextran, a macromolecular compound, in the intestine and its absorption into the bloodstream. After the induction of colitis, the fluorescence distribution of FITC-Dex significantly increased, as did the content of FITC-Dex in the serum. Treatment with Que and RU.521 alleviated this situation and improved intestinal permeability (Figures 10B, C). Collectively, Que demonstrated the ability to repair the damaged intestinal structure and enhance intestinal barrier function in UC mice by inhibiting cGAS.

4 Discussion

In recent years, there has been growing interest in the role of imbalanced intestinal macrophage polarization in the development of UC. Que, a natural compound found in various traditional Chinese medicines, has been shown to modulate macrophage polarization and is known for its effectiveness in treating inflammatory conditions, including UC (Huang et al., 2021; Wu et al., 2022; Zhou H. F. et al., 2023). While the activation of the cGAS-STING pathway has been linked to macrophage polarization imbalance and tissue damage in the heart, its role in macrophage polarization in UC has remained unclear (Cao et al., 2018; Decout et al., 2021; Tsai et al., 2021). Distinguished from the use of LPS combined with IFN-γ as stimulants for macrophage M1 polarization, this study employed synthetic dsDNA, namely, ISD, as the stimulant in the cellular part, confirming the promotive effect of ISD on macrophage inflammatory polarization. Furthermore, Que was found to inhibit the M1 polarization induced by ISD stimulation. Additionally, in intestinal tissues, Que reduced the expression of dsDNA and inhibited M1 polarization in UC mice, which was associated with the inhibition of the cGAS-STING pathway. In this study, we have provided evidence demonstrating that Que regulates macrophage polarization triggered by dsDNA through the cGAS-STING pathway. Furthermore, Que contributed to the restoration of the intestinal barrier, leading to the alleviation of UC (Figure 11).

In this study, we first demonstrated that Que effectively alleviated UC induced by DSS in mice based on significant improvements in various key parameters, including body weight, DAI, colon length, histopathological alterations and the preservation of goblet cells, which are all important for assessing the progression

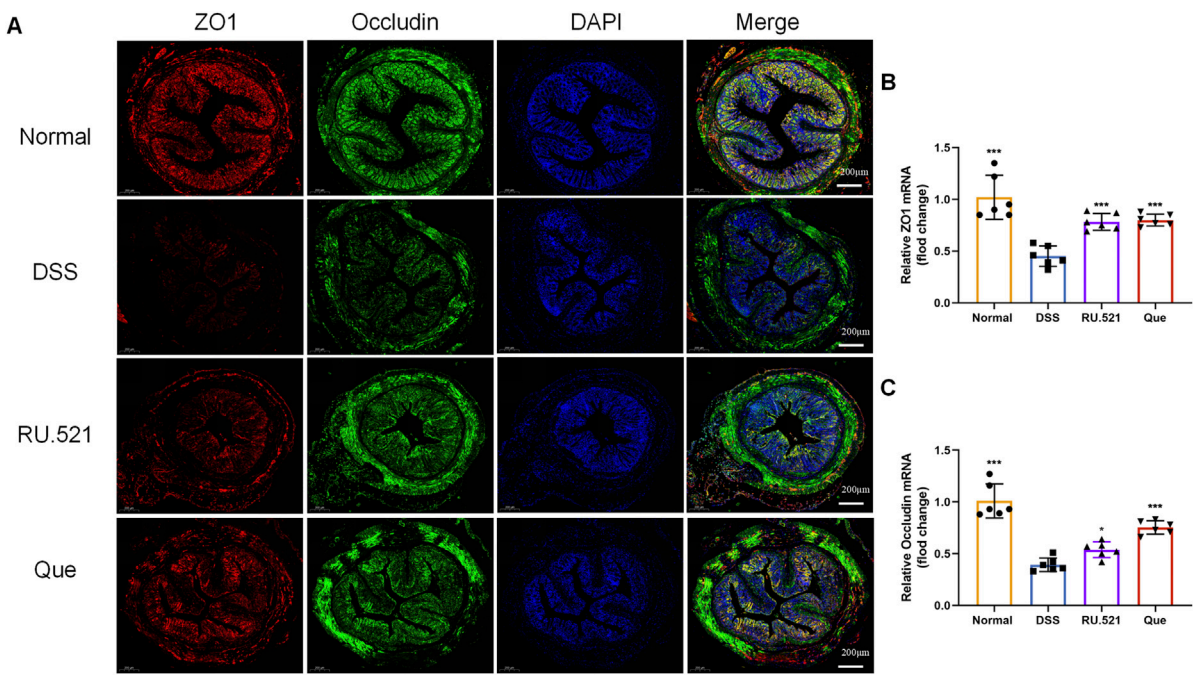

FIGURE 9
Quercetin promotes intestinal barrier function, similar to RU.521. **(A)** Representative images of ZO1 and Occludin expression examined by IF (Bar = 200 μm) in the colon. **(B,C)** Quantification of ZO1 and Occludin mRNA levels in mice colon (n = 6). Data are presented as mean ± SD. *p < 0.05, ***p < 0.001.

of enteritis-related diseases (Rhodes et al., 1985; Goyal et al., 2014). Furthermore, we employed the cGAS inhibitor RU.521 to suppress cGAS expression in the colon and observed that it could also mitigate the development of UC, suggesting that cGAS represents a potential therapeutic target for the treatment of UC and inhibiting cGAS could be a viable approach for UC therapy. However, further investigation is required to determine whether RU.521 treatment exerts a regulatory effect on macrophage polarization similar to Que.

Macrophages are a diverse group of immune cells present in various tissues, and among them, intestinal macrophages exhibit a high degree of plasticity and versatility. Macrophage polarization exists on a continuum, with M1 and M2 macrophages representing the two ends of this spectrum. M1 macrophages are classically activated and secrete pro-inflammatory cytokines such as TNF-α and IL-6, with the typical marker being iNOS, indicating their pro-inflammatory phenotype. Conversely, M2 macrophages are alternatively activated and secrete anti-inflammatory cytokines like IL-10 and TGF-β, with Arg1 serving as a characteristic marker, signifying their anti-inflammatory phenotype (Gordon et al., 2014; Zhao et al., 2017; Shapouri-Moghaddam et al., 2018). Our study revealed that both Que and RU.521 could inhibit the polarization of M1 macrophages and reduce the secretion of iNOS in the colon, spleen and mesenteric lymph nodes of mice with UC. Simultaneously, these interventions promoted the polarization of M2 macrophages and increased Arg1 expression. We further validated these findings *in vitro* using RAW264.7 cells and bone marrow-derived macrophages (BMDMs) that were successfully induced and cultured. Que, at a concentration of 50 μmol/L, was determined to be safe for BMDMs and RAW264.7 cells and effectively corrected the imbalance in macrophage polarization induced by ISD stimulation *in vitro*. The inhibition of cGAS in macrophages also led to a reduction in M1 polarization and an increase in M2 polarization, consistent with a prior study by Cao et al. (2018).

When pathogens invade the body, both pathogen DNA and host cell DNA, which may have been damaged by the pathogen, are released into the host cell's cytoplasm and accumulate, especially dsDNA, and represent one of the reasons for the observed abnormal increase in intestinal dsDNA levels observed in UC. At this point, cGAS, functioning as a cytoplasmic dsDNA sensor, becomes activated (Ou et al., 2021). In autoimmune and inflammatory diseases, the activation of the cGAS-STING pathway can lead to T cells differentiating into inflammatory phenotypes This results in the continual production of inflammatory factors, amplifying inflammatory responses. Furthermore, it induces macrophages to polarize towards the M1 phenotype (Martin et al., 2019; Shmuel-Galia et al., 2021). In this present study, we investigated how Que regulates the cGAS-STING pathway and found that similar to RU.521, Que could inhibit the activation of cGAS and STING, as well as the downstream phosphorylation of TBK1 and IRF3 in both intestinal macrophages and in vitro-cultured macrophages. Additionally, we observed a significant reduction in levels of IFN-β, TNF-α and CXCL10, which are associated with M1 macrophage polarization, in the colons of UC mice. Conversely, we observed an increase in levels of IL-10 and CCL17, which are associated with M2 macrophage polarization. Overall, Que can inhibit M1 macrophage polarization while promoting M2 macrophage polarization by suppressing the cGAS-STING pathway in UC.

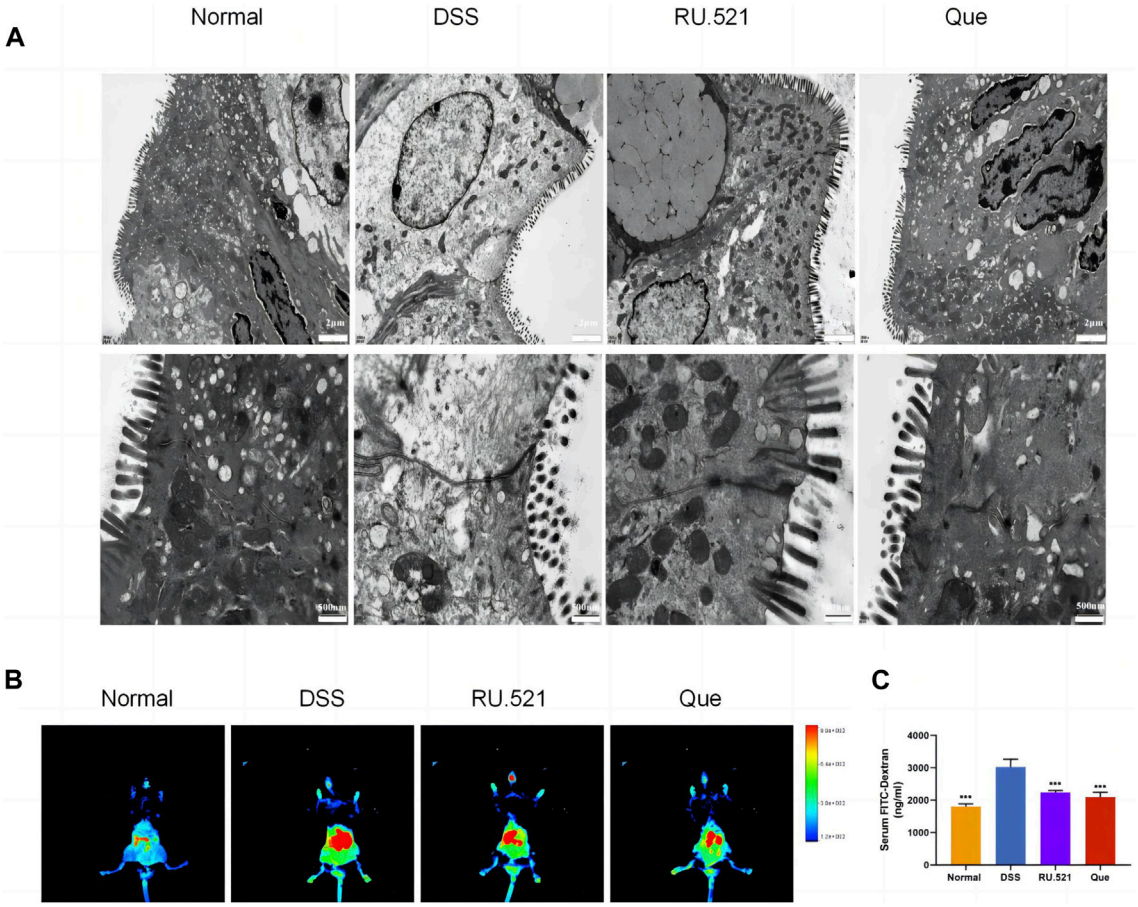

FIGURE 10
Quercetin improves intestinal structural integrity and permeability, similar to RU.521. **(A)** Representative images of intestinal ultrastructure (Bar = 2 μm, 500 nm). **(B)** Representative images of FITC-dextran distribution in mice colon. **(C)** Quantification of FITC-Dex content in mice serum (n = 3). Data are shown as mean ± SD. ***p < 0.001.

Intestinal macrophages play a pivotal role in the immune defense of the intestine. The complex interplay between macrophage polarization, interactions with other immune cells, and the restoration of the intestinal barrier contributes significantly to the complexities of UC. Notably, co-culturing intestinal epithelial cells (IECs) with M1-type macrophages leads to disruptions in epithelial barrier integrity, resulting in the disturbance of TJ proteins and increased apoptosis of IECs. Conversely, co-culturing IECs with M2 macrophages does not elicit such detrimental effects (Lissner et al., 2015). In co-culture experiments involving macrophages and goblet cells, M2 macrophages can boost the expression of mucin-2 (MUC2) and SPDEF (a goblet cell marker gene). This enhancement of goblet cell production and mucus recovery are beneficial for colon healing following injury induced by DSS (Liang et al., 2022). To assess whether Que's modulation of macrophage polarization impacts intestinal barrier restoration, further experiments were conducted. Our findings revealed that after Que and RU.521 interventions in DSS-induced UC mice, there was an upregulation in the expression of TJ proteins (Occludin and ZO1) in the gut. Additionally, the intestinal structure displayed enhanced integrity, including elongated villi and well-maintained TJs, along with reduced intestinal permeability. Occludin and ZO1 serve as predictive indicators of intestinal mucosal healing and the preservation of intestinal barrier function. Their levels decrease when intestinal mucosal damage occurs in UC (Shao et al., 2018). The disruption of intestinal structure and increased intestinal permeability are fundamental features of UC. These alterations result in the infiltration of pathogens, such as bacteria, into the intestinal lamina propria, subsequently triggering abnormal immune responses, including an imbalance in macrophage polarization (Na et al., 2019; Yao et al., 2019). Consequently, there exists a clear positive correlation between the equilibrium of intestinal barrier function and macrophage polarization. Que may inhibit the secretion of inflammatory factors by targeting the cGAS-STING signaling pathway to rectify imbalanced macrophage polarization, thereby contributing to the restoration of intestinal barrier function and ultimately ameliorating UC.

In summary, our study demonstrates that Que exerts its therapeutic effects in DSS-induced UC by modulating the cGAS-STING pathway to regulate macrophage polarization, resulting in an improvement in the structure and function of the intestinal barrier. These findings unveil a novel mechanism through which Que can be used to effectively treat patients suffering from UC.

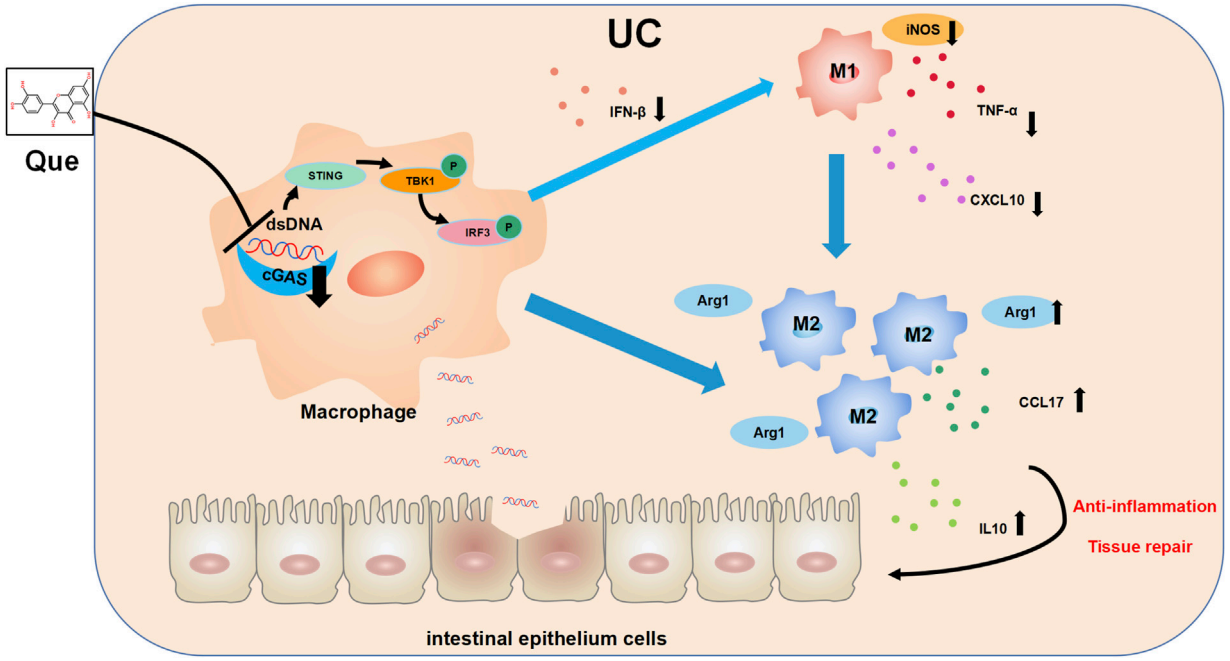

FIGURE 11
The mechanism diagram. Quercetin ameliorates ulcerative colitis by restoring the balance of M2/M1 and repairing the intestinal barrier via downregulating cGAS–STING pathway.

Data availability statement

The original contributions presented in the study are included in the article/Supplementary Material, further inquiries can be directed to the corresponding authors.

Ethics statement

The animal study was approved by the HUST Institution Animal Care and Use Committee (IACUC). The study was conducted in accordance with the local legislation and institutional requirements.

Author contributions

FG: Conceptualization, Funding acquisition, Software, Writing–original draft. FZ: Data curation, Methodology, Software, Writing–review and editing. BS: Data curation, Methodology, Software, Writing–review and editing. MW: Data curation, Methodology, Software, Writing–review and editing. CW: Investigation, Project administration, Validation, Writing–review and editing. YY: Investigation, Project administration, Validation, Writing–review and editing. YG: Investigation, Project administration, Validation, Writing–review and editing. YT: Project administration, Visualization, Writing–review and editing. HF: Conceptualization, Resources, Supervision, Writing–review and editing. HW: Conceptualization, Funding acquisition, Resources, Supervision, Writing–review and editing.

Funding

The author(s) declare that financial support was received for the research, authorship, and/or publication of this article. This work was supported by the National Natural Science Foundation of China (no. 82104637), and partially funded by the National Natural Science Foundation of China (no. 82174182).

Conflict of interest

The authors declare that the research was conducted in the absence of any commercial or financial relationships that could be construed as a potential conflict of interest.

Publisher's note

Supplementary material

The Supplementary Material for this article can be found online at: https://www.frontiersin.org/articles/10.3389/fphar.2024.1351538/full#supplementary-material

References

Cao, D. J., Schiattarella, G. G., Villalobos, E., Jiang, N., May, H. I., Li, T., et al. (2018). Cytosolic DNA sensing promotes macrophage transformation and governs myocardial ischemic injury. *Circulation* 137 (24), 2613–2634. doi:10.1161/CIRCULATIONAHA.117.031046

Costello, S. P., Hughes, P. A., Waters, O., Bryant, R. V., Vincent, A. D., Blatchford, P., et al. (2019). Effect of fecal microbiota transplantation on 8-week remission in patients with ulcerative colitis: a randomized clinical trial. *JAMA* 321 (2), 156–164. doi:10.1001/jama.2018.20046

Dalekos, G. N., Manoussakis, M. N., Goussia, A. C., Tsianos, E. V., and Moutsopoulos, H. M. (1993). Soluble interleukin-2 receptors, antineutrophil cytoplasmic antibodies, and other autoantibodies in patients with ulcerative colitis. *Gut* 34 (5), 658–664. doi:10.1136/gut.34.5.658

Decout, A., Katz, J. D., Venkatraman, S., and Ablasser, A. (2021). The cGAS-STING pathway as a therapeutic target in inflammatory diseases. *Nat. Rev. Immunol.* 21 (9), 548–569. doi:10.1038/s41577-021-00524-z

Dicarlo, M., Teti, G., Verna, G., Liso, M., Cavalcanti, E., Sila, A., et al. (2019). Quercetin exposure suppresses the inflammatory pathway in intestinal organoids from winnie mice. *Int. J. Mol. Sci.* 20 (22), 5771. doi:10.3390/ijms20225771

Ding, R., Li, H., Liu, Y., Ou, W., Zhang, X., Chai, H., et al. (2022). Activating cGAS-STING axis contributes to neuroinflammation in CVST mouse model and induces inflammasome activation and microglia pyroptosis. *J. neuroinflammation* 19 (1), 137. doi:10.1186/s12974-022-02511-0

Gao, F., Cui, D., Zuo, D., Shou, Z., Yang, J., Yu, T., et al. (2022). BMSCs improve TNBS-induced colitis in rats by inducing Treg differentiation by expressing PD-L1. *Biotechnol. Lett.* 44 (11), 1263–1275. doi:10.1007/s10529-022-03307-1

Gordon, S., Plüddemann, A., and Martinez Estrada, F. (2014). Macrophage heterogeneity in tissues: phenotypic diversity and functions. *Immunol. Rev.* 262 (1), 36–55. doi:10.1111/imr.12223

Goyal, N., Rana, A., Ahlawat, A., Bijjem, K. R., and Kumar, P. (2014). Animal models of inflammatory bowel disease: a review. *Inflammopharmacology* 22 (4), 219–233. doi:10.1007/s10787-014-0207-y

Gravina, A. G., Pellegrino, R., Palladino, G., Coppola, A., Brandimarte, G., Tuccillo, C., et al. (2023). Hericium erinaceus, in combination with natural flavonoid/alkaloid and B3/B8 vitamins, can improve inflammatory burden in Inflammatory bowel diseases tissue: an *ex vivo* study. *Front. Immunol.* 14, 1215329. doi:10.3389/fimmu.2023.1215329

Gui, X., Yang, H., Li, T., Tan, X., Shi, P., Li, M., et al. (2019). Autophagy induction via STING trafficking is a primordial function of the cGAS pathway. *Nature* 567 (7747), 262–266. doi:10.1038/s41586-019-1006-9

Hoeffel, G., Debroas, G., Roger, A., Rossignol, R., Gouilly, J., Laprie, C., et al. (2021). Sensory neuron-derived TAFA4 promotes macrophage tissue repair functions. *Nature* 594 (7861), 94–99. doi:10.1038/s41586-021-03563-7

Hopfner, K. P., and Hornung, V. (2020). Molecular mechanisms and cellular functions of cGAS-STING signalling. *Nat. Rev. Mol. Cell Biol.* 21 (9), 501–521. doi:10.1038/s41580-020-0244-x

Huang, J., Zheng, Y., Ma, J., Ma, J., Lu, M., Ma, X., et al. (2021). Exploration of the potential mechanisms of wumei pill for the treatment of ulcerative colitis by network Pharmacology. *Gastroenterology Res. Pract.* 2021, 4227668. doi:10.1155/2021/4227668

Jiang, G. L., Yang, X. L., Zhou, H. J., Long, J., Liu, B., Zhang, L. M., et al. (2021). cGAS knockdown promotes microglial M2 polarization to alleviate neuroinflammation by inhibiting cGAS-STING signaling pathway in cerebral ischemic stroke. *Brain Res. Bull.* 171, 183–195. doi:10.1016/j.brainresbull.2021.03.010

Kim, W., Jang, J. H., Zhong, X., Seo, H., and Surh, Y. J. (2021). 15-Deoxy-△12,14-Prostaglandin J2 promotes resolution of experimentally induced colitis. *Front. Immunol.* 12, 615803. doi:10.3389/fimmu.2021.615803

Li, X. V., Leonardi, I., Putzel, G. G., Semon, A., Fiers, W. D., Kusakabe, T., et al. (2022). Author Correction: immune regulation by fungal strain diversity in inflammatory bowel disease. *Nature* 608 (7922), E21. doi:10.1038/s41586-022-05102-4

Liang, L., Liu, L., Zhou, W., Yang, C., Mai, G., Li, H., et al. (2022). Gut microbiota-derived butyrate regulates gut mucus barrier repair by activating the macrophage/WNT/ERK signaling pathway. *Clin. Sci. Lond. Engl. 1979* 136 (4), 291–307. doi:10.1042/CS20210778

Lissner, D., Schumann, M., Batra, A., Kredel, L. I., Kühl, A. A., Erben, U., et al. (2015). Monocyte and M1 macrophage-induced barrier defect contributes to chronic intestinal inflammation in IBD. *Inflamm. bowel Dis.* 21 (6), 1297–1305. doi:10.1097/MIB.0000000000000384

Ma, C., Yang, D., Wang, B., Wu, C., Wu, Y., Li, S., et al. (2020). Gasdermin D in macrophages restrains colitis by controlling cGAS-mediated inflammation. *Sci. Adv.* 6 (21), eaaz6717. doi:10.1126/sciadv.aaz6717

Martin, G. R., Blomquist, C. M., Henare, K. L., and Jirik, F. R. (2019). Stimulator of interferon genes (STING) activation exacerbates experimental colitis in mice. *Sci. Rep.* 9 (1), 14281. doi:10.1038/s41598-019-50656-5

Murray, P. J. (2017). Macrophage polarization. *Annu. Rev. physiology* 79, 541–566. doi:10.1146/annurev-physiol-022516-034339

Na, Y. R., Stakenborg, M., Seok, S. H., and Matteoli, G. (2019). Macrophages in intestinal inflammation and resolution: a potential therapeutic target in IBD. *Nat. Rev. Gastroenterology hepatology* 16 (9), 531–543. doi:10.1038/s41575-019-0172-4

Ou, L., Zhang, A., Cheng, Y., and Chen, Y. (2021). The cGAS-STING pathway: a promising immunotherapy target. *Front. Immunol.* 12, 795048. doi:10.3389/fimmu.2021.795048

Park, S. H., Kang, K., Giannopoulou, E., Qiao, Y., Kang, K., Kim, G., et al. (2017). Type I interferons and the cytokine TNF cooperatively reprogram the macrophage epigenome to promote inflammatory activation. *Nat. Immunol.* 18 (10), 1104–1116. doi:10.1038/ni.3818

Rhodes, J. M., Black, R. R., Gallimore, R., and Savage, A. (1985). Histochemical demonstration of desialation and desulphation of normal and inflammatory bowel disease rectal mucus by faecal extracts. *Gut* 26 (12), 1312–1318. doi:10.1136/gut.26.12.1312

Sann, H., Erichsen, J., Hessmann, M., Pahl, A., and Hoffmeyer, A. (2013). Efficacy of drugs used in the treatment of IBD and combinations thereof in acute DSS-induced colitis in mice. *Life Sci.* 92 (12), 708–718. doi:10.1016/j.lfs.2013.01.028

Shao, T., Zhao, C., Li, F., Gu, Z., Liu, L., Zhang, L., et al. (2018). Intestinal HIF-1α deletion exacerbates alcoholic liver disease by inducing intestinal dysbiosis and barrier dysfunction. *J. hepatology* 69 (4), 886–895. doi:10.1016/j.jhep.2018.05.021

Shapouri-Moghaddam, A., Mohammadian, S., Vazini, H., Taghadosi, M., Esmaeili, S. A., Mardani, F., et al. (2018). Macrophage plasticity, polarization, and function in health and disease. *J. Cell. physiology* 233 (9), 6425–6440. doi:10.1002/jcp.26429

Shmuel-Galia, L., Humphries, F., Lei, X., Ceglia, S., Wilson, R., Jiang, Z., et al. (2021). Dysbiosis exacerbates colitis by promoting ubiquitination and accumulation of the innate immune adaptor STING in myeloid cells. *Immunity* 54 (6), 1137–1153.e8. doi:10.1016/j.immuni.2021.05.008

Subramanian Vignesh, K., Landero Figueroa, J. A., Porollo, A., Caruso, J. A., and Deepe, G. S., Jr (2013). Granulocyte macrophage-colony stimulating factor induced Zn sequestration enhances macrophage superoxide and limits intracellular pathogen survival. *Immunity* 39 (4), 697–710. doi:10.1016/j.immuni.2013.09.006

Tsai, C. F., Chen, G. W., Chen, Y. C., Shen, C. K., Lu, D. Y., Yang, L. Y., et al. (2021). Regulatory effects of quercetin on M1/M2 macrophage polarization and oxidative/antioxidative balance. *Nutrients* 14 (1), 67. doi:10.3390/nu14010067

Virga, F., Cappellesso, F., Stijlemans, B., Henze, A. T., Trotta, R., Van Audenaerde, J., et al. (2021). Macrophage miR-210 induction and metabolic reprogramming in response to pathogen interaction boost life-threatening inflammation. *Sci. Adv.* 7 (19), eabf0466. doi:10.1126/sciadv.abf0466

Wang, X., Xie, X., Li, Y., Xie, X., Huang, S., Pan, S., et al. (2024). Quercetin ameliorates ulcerative colitis by activating aryl hydrocarbon receptor to improve intestinal barrier integrity. *Phytotherapy Res. PTR* 38 (1), 253–264. doi:10.1002/ptr.8027

Wu, J., Luo, Y., Shen, Y., Hu, Y., Zhu, F., Wu, J., et al. (2022). Integrated metabonomics and network Pharmacology to reveal the action mechanism effect of shaoyao decoction on ulcerative colitis. *Drug Des. Dev. Ther.* 16, 3739–3776. doi:10.2147/DDDT.S375281

Yang, T., Kong, B., Gu, J. W., Kuang, Y. Q., Cheng, L., Yang, W. T., et al. (2014). Anti-apoptotic and anti-oxidative roles of quercetin after traumatic brain injury. *Cell. Mol. Neurobiol.* 34 (6), 797–804. doi:10.1007/s10571-014-0070-9

Yao, D., Dong, M., Dai, C., and Wu, S. (2019). Inflammation and inflammatory cytokine contribute to the initiation and development of ulcerative colitis and its associated cancer. *Inflamm. bowel Dis.* 25 (10), 1595–1602. doi:10.1093/ibd/izz149

Ying, W., Cheruku, P. S., Bazer, F. W., Safe, S. H., and Zhou, B. (2013). Investigation of macrophage polarization using bone marrow derived macrophages. *J. Vis. Exp.* 76, 50323. doi:10.3791/50323

Zhang, M., Li, X., Zhang, Q., Yang, J., and Liu, G. (2023). Roles of macrophages on ulcerative colitis and colitis-associated colorectal cancer. *Front. Immunol.* 14, 1103617. doi:10.3389/fimmu.2023.1103617

Zhang, Z., Zhou, H., Ouyang, X., Dong, Y., Sarapultsev, A., Luo, S., et al. (2022). Multifaceted functions of STING in human health and disease: from molecular mechanism to targeted strategy. *Signal Transduct. Target. Ther.* 7 (1), 394. doi:10.1038/s41392-022-01252-z

Zhao, F., Zheng, T., Gong, W., Wu, J., Xie, H., Li, W., et al. (2021). Extracellular vesicles package dsDNA to aggravate Crohn's disease by activating the STING pathway. *Cell death Dis.* 12 (9), 815. doi:10.1038/s41419-021-04101-z

Zhao, Q., Chu, Z., Zhu, L., Yang, T., Wang, P., Liu, F., et al. (2017). 2-Deoxy-d-Glucose treatment decreases anti-inflammatory M2 macrophage polarization in mice with tumor and allergic airway inflammation. *Front. Immunol.* 8, 637. doi:10.3389/fimmu.2017.00637

Zhou, H. F., Yang, C., Li, J. Y., He, Y. Y., Huang, Y., Qin, R. J., et al. (2023b). Quercetin serves as the major component of Xiang-lian Pill to ameliorate ulcerative colitis via tipping the balance of STAT1/PPARγ and dictating the alternative activation of macrophage. *J. Ethnopharmacol.* 313, 116557. doi:10.1016/j.jep.2023.116557

Zhou, Y., Qian, C., Tang, Y., Song, M., Zhang, T., Dong, G., et al. (2023a). Advance in the pharmacological effects of quercetin in modulating oxidative stress and inflammation related disorders. *Phytotherapy Res. PTR* 37 (11), 4999–5016. doi:10.1002/ptr.7966

frontiers | Frontiers in Pharmacology

TYPE Original Research
PUBLISHED 23 May 2024
DOI 10.3389/fphar.2024.1414675

OPEN ACCESS

EDITED BY
Guang Wang,
Jinan University, China

REVIEWED BY
Jun-sheng Tian,
Shanxi University, China
Rong Zhang,
Guangzhou University of Chinese Medicine, China
Hong-he Xiao,
Liaoning University of Traditional Chinese Medicine, China

*CORRESPONDENCE
Yanmiao Ma,
mymsxtcm@sxtcm.edu.cn
Tao Peng,
pengtao5197220@163.com

RECEIVED 09 April 2024
ACCEPTED 07 May 2024
PUBLISHED 23 May 2024

CITATION
Ma Y, Wei X, Peng J, Wei F, Wen Y, Liu M, Song B, Wang Y, Zhang Y and Peng T (2024), Ephedra sinica polysaccharide regulate the anti-inflammatory immunity of intestinal microecology and bacterial metabolites in rheumatoid arthritis.
Front. Pharmacol. 15:1414675.
doi: 10.3389/fphar.2024.1414675

Ephedra sinica polysaccharide regulate the anti-inflammatory immunity of intestinal microecology and bacterial metabolites in rheumatoid arthritis

Yanmiao Ma[1]*, Xiuhong Wei[1], Jiehao Peng[2], Fuxia Wei[2], Ya Wen[3], Mingran Liu[1], Bo Song[2], Yonghui Wang[1], Yumin Zhang[1] and Tao Peng[4,5]*

[1]Department of Basic Medical Sciences, Shanxi University of Chinese Medicine, Taiyuan, China, [2]Department of Third Clinical Medicine, Shanxi University of Chinese Medicine, Taiyuan, China, [3]Department of First Clinical Medicine, Shanxi University of Chinese Medicine, Taiyuan, China, [4]Famous Chinese Medicine Studio, Shanxi Hospital of Integrated Traditional Chinese and Western Medicine, Taiyuan, China, [5]Shanxi Provincial Key Laboratory of Classical Prescription Strengthening Yang, Shanxi Hospital of Integrated Traditional Chinese and Western Medicine Taiyuan, Taiyuan, China

Introduction: *Ephedra sinica* polysaccharide (ESP) exerts substantial therapeutic effects on rheumatoid arthritis (RA). However, the mechanism through which ESP intervenes in RA remains unclear. A close correlation has been observed between enzymes and derivatives in the gut microbiota and the inflammatory immune response in RA.

Methods: A type II collagen-induced arthritis (CIA) mice model was treated with Ephedra sinica polysaccharide. The therapeutic effect of ESP on collagen-induced arthritis mice was evaluated. The anti-inflammatory and cartilage-protective effects of ESP were also evaluated. Additionally, metagenomic sequencing was performed to identify changes in carbohydrate-active enzymes and resistance genes in the gut microbiota of the ESP-treated CIA mice. Liquid chromatography-mass spectrometry and gas chromatography-mass spectrometry were performed to observe the levels of serum metabolites and short-chain fatty acids in the gut. Spearman's correlational analysis revealed a correlation among the gut microbiota, antibiotic-resistance genes, and microbiota-derived metabolites.

Results: ESP treatment significantly reduced inflammation levels and cartilage damage in the CIA mice. It also decreased the levels of pro-inflammatory cytokines interleukin (IL)-6, and IL-1-β and protected the intestinal mucosal epithelial barrier, inhibiting inflammatory cell infiltration and mucosal damage. Here, ESP reduced the TLR4, MyD88, and TRAF6 levels in the synovium, inhibited the p65 expression and pp65 phosphorylation in the NF-κB signaling pathway, and blocked histone deacetylase (HDAC1 and HDAC2) signals. ESP influenced the gut microbiota structure, microbial carbohydrate-active enzymes, and microbial resistance related to resistance genes. ESP increased the serum levels of L-tyrosine, sn-glycero-3-phosphocholine, octadecanoic acid, N-oleoyl taurine, and decreased N-palmitoyl taurine in the CIA mice.

Conclusion: ESP exhibited an inhibitory effect on RA. Its action mechanism may be related to the ability of ESP to effectively reduce pro-inflammatory cytokines

levels, protect the intestinal barrier, and regulate the interaction between mucosal immune systems and abnormal local microbiota. Accordingly, immune homeostasis was maintained and the inhibition of fibroblast-like synoviocyte (FLS) proliferation through the HDAC/TLR4/NF-κB pathway was mediated, thereby contributing to its anti-inflammatory and immune-modulating effects.

KEYWORDS

rheumatoid arthritis, gut microbiota, systemic metabolism, TLR4/HDAC/NF-κB pathway, Ephedra sinica polysaccharide

1 Introduction

Rheumatoid arthritis (RA) is among the most common immune-mediated inflammatory diseases and is characterized by symmetrical joint pain, swelling, and stiffness. Chronic inflammation of the synovial membrane (synovium) can cause severe joint damage, disability, and work loss (Brown et al., 2024). Globally, approximately 1% of adults have RA. The exact cause of RA remains unclear. The intestine is composed of the body's largest population of innate and adaptive immune cells and is the largest immune organ in humans. Because of the interaction between the mucosal immune system and abnormal local microbiota, the disease starts at the mucosal site and affects synovial joints (Zaiss et al., 2021).

Ephedrae herba is the dried herbaceous stem of *Ephedra sinica* Stapf, *Ephedra intermedia* Schrenk et C. A. Mey., or *Ephedra equisetina* Bge. It has long been used as an herbal medicine in China relieving colds, edema, nasal congestion, and rheumatoid arthritis. *Ephedra* has anti-inflammatory properties (Cao et al., 2022). *Ephedra sinica* polysaccharide (ESP) exhibits a good therapeutic effect on RA (Zheng et al., 2023) by reducing the lipopolysaccharide stimulated nuclear translocation of the NF-κB p65 subunit, improving the levels of RA inflammatory markers, and reducing the release of inflammatory factors (TNF-α, IL-1β, and IL-6) and NO by inhibiting the TLR4 signaling pathway (Li et al., 2023). Arabinose and glucose contents in plant polysaccharides directly influence their immune activities (Wang et al., 2016).

The gut microbiota is a chief determinant of immune therapeutic responses. Bacterial metabolites are associated with human physiology and disease, thereby influencing the immune function. Dietary fibers undergo fermentation by the gut microbiota, resulting in the production of short-chain fatty acids (SCFAs), including acetic acid, propionic acid, and butyric acid. These SCFAs regulate the phenotype and/or function of macrophages, neutrophils, dendritic cells, and $CD4^+$ T cells (Wang et al., 2023a).

The gut microbiota can exert profound effects on the host's metabolism. The relationship between the gut microbiota, metabolites, and clinical features in the preclinical stage of RA remains unclear (Reinke et al., 2017). Toll-like receptors (TLRs) in intestinal epithelial cells can activate kinases, including interleukin-1 receptor-associated kinase and mitogen-activated protein kinase, thereby promoting the nuclear translocation of nuclear transcription factor-κB (NF-κB), stimulating the expression of inflammatory cytokines, and increasing the permeability of the small intestinal epithelial cell layer (Luo et al., 2023). Therefore, the impact of ESP on the gut microbiota must be better comprehended, along with a clear observation of ESP metabolites and an assessment of the downstream effects exerted by metabolites on RA.

The CIA mice model was used to simulate joint damage in RA and treated the mice with ESP for 21 days. At the end of the experiment, rectal feces, serum, and synovial tissue were collected from the mice to scrutinize the gut microbiota profile, joint damage, serum metabolites, and intestinal mucosal barrier of the CIA mice. We also investigated how the gut microbiota absorbs and uses macromolecular polysaccharides and how changes occur in its microbial-derived products. The goal explore the relationship between the gut microbiota, joint inflammation damage, and host immune dysregulation in RA pathogenesis.

2 Materials and methods

2.1 Reagents

Chromatographic column (ACQUITY BEH C18100 mm × 2.1 mm, 1.7 um); mass spectrometry-grade methanol (67-56-1, Thermo Fisher Scientific); mass spectrometry-grade acetonitrile (75-05-8, Thermo Fisher Scientific); bovine type II collagen (220195, SIGMA-ALDRICH); Freund's Complete Adjuvant (SLCL9648, SIGMA-ALDRICH); toll-like receptor 4 (A5258, ABclonal); NF-κB p65 (A2547, ABclonal); myeloid differentiation primary response 88 (67969-1-Ig, Proteintech); mouse IL-1β ELISA kit [JL18442, Sangon Biotech (Shanghai)]; mouse IL-6 ELISA kit [JL20268, Sangon Biotech (Shanghai); methotrexate [036210103, Sangon Biotech (Shanghai)]; PDTC (5108-96-3, MedChemExpress); TSA (58,880-19-6, MedChemExpress).

2.2 Animals

C57BL/6J mice were provided by Beijing Weitong Lihua Experimental Animal Technology Co., Ltd. (Beijing, China). The temperature was maintained at 15°C–25°C, relative humidity of 45%–55%, and a simulated natural light/dark cycle of 12 h each. All animals had free access to water and food.

2.3 Preparation and quality control of ESP

Ephedra sinica Stapf herba (401003136P) was decocted, and the filtrate obtained was concentrated to 0.5–1 g/mL. Ethanol (95%, anhydrous) was added at a 1:9 ratio to precipitate the extract for 30 min. The mixture was centrifuged at 4°C and 3,500 rpm for 10 min. This process was repeated 2–3 times. The resulting extract was filtered and subjected to rotary evaporation to obtain the ESP powder.

High-performance liquid chromatography (HPLC) was performed for the quality control of ESP. Experimental conditions for HPLC are detailed in the Supplementary Material S1.

2.4 Animals and treatments

After 1 week of acclimatization feeding, the mice were randomized into five groups: the natural control group (NC), collagen-induced arthritis group (CIA), methotrexate group (MTX), low ESP group (200 mg/kg), and high ESP group (400 mg/kg). Then, 1 mg/mL Type II collagen (220,195, Sigma-Aldrich) and Freund's complete adjuvant (SLCL9648, Sigma-Aldrich) were emulsified thoroughly on an ice bath at 1:1. Then, 0.1 mL of the emulsion was injected into the tail, back, and left hind paws of the mice, whereas 0.1 mL saline was injected at the same sites in mice from the blank group. After 1 week, immunization was reinforced by injecting 0.1 mL of the emulsion at the same sites.

Saline was orally administered to the NC and CIA groups daily. The MTX group received 9 mg/kg methotrexate tablets, and the ESP-L and ESP-H groups received the ESP suspension orally for 21 consecutive days.

2.5 Assessment of joint swelling and body weight changes in mice

To record the changes in the left hind paw volume and body weight of the mice, weekly measurements were conducted. The volume of the left hind paw joint was precisely measured using a specialized paw volume measurement device; the average value was obtained from three measurements.

2.6 MTT assay for cell proliferation

The mice fibroblast-like synoviocyte (FLS) cell line (CTCC-S004-MIC, Meisen) was cultured in DMEM medium containing 10% fetal bovine serum, 1% penicillin, and streptomycin at 37°C with 5% CO_2. FLS were seeded into 96-well plates at 8×10^3 cells/100 μL/well. The medium was changed after 24 h and different ESP concentrations were added to each well for continued culture for 24 or 48 h. Then, 10 μL of the MTT solution (M8180, Solarbio) was added to each well and incubated for 4 h in a CO_2 incubator. After 150 μL of DMSO was added to each well and crystals were allowed to completely dissolve, the optical density of each well was measured at 570 nm.

2.7 Scratch assay for the wound healing rate

The cells were vertically scratched using a 200 μL pipette tip and gently washed with PBS to remove detached cells. The medium was replaced with a 2% FBS-containing medium. The scratch width at 0 and 12 h was photographed under an inverted microscope (Nikon, Japan). The cell healing rate at 12 h was measured using ImageJ software.

2.8 Masson, Safranin O-fast green (S&F), and TRAP staining

Each joint tissue in every group was fixed with 4% paraformaldehyde, dehydrated with ethanol gradient, cleared with xylene, and 4μm sections. These slices were stained with Masson trichrome (G1340, Solarbio) to evaluate histopathological changes and collagen deposition. S&F staining (G1371, Solarbio) and TRAP Staining (G1492, Solarbio) were performed using a commercial kit. The modified Osteoarthritis International Study (OARSI) scoring system was used to evaluate the histological features of cartilage degeneration. The modified Mankin's scoring system is used for assessing the grades of the structure and tidemark intactness.

2.9 Enzyme-linked immunosorbent assay

Serum levels of IL-1β and IL-6 were quantitatively analyzed using the mice ELISA kit. Absorbance was read at 450 nm by using an ELISA reader. After a standard curve was constructed, the concentration of substances in the samples was calculated.

2.10 Cell culture and treatment

PDTC (1 mg, 5108-96-3, MedChemExpress) was dissolved in 6.09 mL of sterile water to prepare a 1 mM reserve solution. TSA (1 mg, 58,880-19-6, MedChemExpress) was dissolved in 3.3 mL of DMSO and stored as a 1mM reserve solution.

The cells were divided into five groups, namely, the Control group, Control + PDTC group, Control + PDTC group, ESP group, ESP group, ESP + PDTC group, and ESP + PDTC + TSA group. The cells were pretreated with 100 nM IL-1β and 100 nM TNF-α for 24 h.

2.11 Protein immunoblotting experiment

After the tissues or cells were collected, the proteinase inhibitor (PR20032, Proteintech) and phosphatase inhibitor cocktail (PR20015, Proteintech) were added to the RIPA lysis buffer (AR0102, Bosterbio). The protein concentration was quantified using the BCA assay kit (AR0146, Bosterbio). The proteins were separated through electrophoresis on denaturing SDS-PAGE gels (AR0138, Bosterbio). The proteins were transferred onto PVDF membranes (0000215179, Millipore), blocked with 5% non-fat milk in TBST, and incubated overnight with the following primary antibodies at 4°C: HDAC1 (1:10,000, Proteintech), HDAC2 (1: 10,000, Proteintech), TLR4 (1:1,000, ABclonal), MyD88 (1:1,000,

Proteintech), TRAF6 (1:2000, ABclonal), NF-κB p65 (1:4,000, Proteintech), pNF-κB p65 (1:1,000, Cell Signaling), ZO-1 (1:5000, Proteintech), and β-actin (1:5000, Bioworld Technology). The membranes were washed the next day, incubated with goat anti-rabbit IgG secondary antibody (1:5000, Proteintech) for 2 h, and then visualized using the Meilunbio® FG Super Sensitive ECL Luminescence Reagent (MA 0186, Meilunbio). ImageJ software was used for densitometry analysis.

2.12 Metagenomic analysis

DNA was extracted from the fecal samples, and its quality and purity were assessed. After the DNA was fragmented through ultrasonication, the fragments were purified and repaired. A base was added to the 3′end of the fragments and connected to an adapter required for the Illumina sequencing platform, thereby forming a complete sequencing template. Subsequently, the DNA fragment size was selected using methods such as agarose gel electrophoresis to remove unsuitable fragments and PCR amplification to increase the number of fragments in the library. The constructed sequencing library was subjected to quality control, and metagenomic sequencing was performed at the Illumina sequencing center.

2.13 Metabolomics analysis

The plasma metabolome was analyzed through gas chromatography-tandem mass spectrometry (GC-MS/MS; GC/MSD-7890B–5977B, Agilent Technologies, US) and liquid chromatography-tandem mass spectrometry (LC-MS/MS; UHPLC-Q-Exactive Orbitrap-MS, Agilent Technologies, US).

Blood was centrifuged for 10 min (4°C, 14,000 rpm). In total, 100 μL serum was mixed with 300 μL acetonitrile, vortexed for 1 min, and centrifuged for 10 min (4°C, 14,000 rpm). Then, 200 μL of the supernatant was collected. After drying the supernatant with nitrogen gas, 200 μL of acetonitrile was added to the dried sample for reconstitution, vortexed. The supernatant was used for injection analysis.

The raw data were processed using Compound Discoverer 3.3 software, and the metabolomics data were imported into SIMCA 14.1 software for multivariate data analysis. Differential metabolites were selected based on the basis of variable importance parameters (VIP >1) and t-tests ($p < 0.05$). Differential compounds were then identified and compared using the HMDB database (https://hmdb.ca/). Metabolic pathway analysis and screening were performed using MetaboAnalyst 5.0 (https://www.metaboanalyst.ca/).

0.2 g fecal sample was added to methanol to form a homogenate and centrifuged. The supernatant was collected, mixed with methanol, centrifuged again, and filtered. The final supernatant was collected and frozen.

Gas chromatography-mass spectrometry (GC/MS) analysis was conducted with an HP-5MS capillary column (30 m × 0.25 mm × 0.25 μm, Agilent J&W). 1-μL sample was automatically injected with a split ratio of 10:1, high-purity helium gas (<99.999%) being used as the carrier gas at a 1 mL/min flow rate and inlet temperature of 290°C. The temperature program: the column temperature: 40°C, 2 min; 300°C, 5 min. The mass spectrometry conditions included an EI ionization source and a scan range of m/z 40–400. Kovats retention indices were used to calculate compound retention times. The MassHunter quantification software was used for the automatic identification and integration of ion fragments. SCFA standards, including those for propionic acid (wkq20042911) and butyric acid (wkq20092401) were used for comparing retention times and corresponding MS spectra with the samples to confirm the SCFAs and calculate the concentrations.

2.14 Data processing

The raw data were processed using Compound Discoverer 3.3 to batch-extract compound peaks. After normalization, the data were imported into the SIMCA-P 13.0 statistical software package from Umetrics. The principal component analysis (PCA) and orthogonal partial least-squares discrimination analysis (OPLS-DA) were performed. Differential biomarkers were screened using t-tests. Differential metabolites were identified by combining them with the HMDB database (https://hmdb.ca/). GraphPad Prism 8.0.2 software was used to analyze the trend of changes in each metabolite. Metabolic pathways of the differential metabolites were analyzed using MetaboAnalyst 5.0 (https://www.metaboanalyst.ca/), and the involved metabolic pathways were visualized using KEGG (https://www.genome.jp/kegg/).

The Spearman rank correlation coefficient was employed to conduct the correlation analysis, to assess the strength of association between different taxonomic levels of microorganisms and resistance genes. We used $|R| > 0.3$ as the screening criterion, indicating that only correlations with an absolute correlation coefficient greater than 0.3 were considered to be of substantive significance. Furthermore, the *t*-test to compare the obtained correlation coefficients against this screening criterion to determine if there were significant differences. $p < 0.05$ was considered to be statistically significant in the correlation coefficient.

The data were presented as mean ± Standard error of the mean. One-way analysis of variance was used for multifactorial comparisons in this study. All data analysis was conducted with the SPSS 22.0 statistical software package (SPSS Inc, Chicago, IL, USA).

3 Results

3.1 Extraction and structural characterization of ESP

ESP was extracted from *E. sinica* Stapf, and the optimal extraction conditions for ESP were tested. Table 1 presents the monosaccharide composition of ESP.

3.2 ESP significantly improves the general condition of mice

To determine the preventive effect of ESP on RA occurrence, ESP was orally administered to the type II collagen-immunized C57BL/6J mice (Figure 1A). ESP dose-dependently inhibited the RA incidence, as evidenced by the significant increase in the thickness of the CIA left hind paw compared with the NC group (Figure 1B). Treatment of CIA mice with ESP (200, 400 mg/kg) and MTX gradually reduced the paw thickness (Figure 1C). After the mice were induced with collagen, their

TABLE 1 Composition of ESP.

No.	Name	Molecular formula	MW (g/mol)	Content (mg/kg)	Structure
1	D-Mannose	$C_6H_{12}O_6$	180.16	2828.57	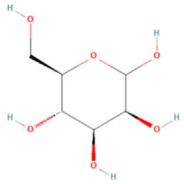
2	Glucosamine	$C_6H_{13}NO_5$	179.17	460.00	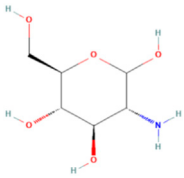
3	Ribose	$C_5H_{10}O_5$	150.13	1,057.14	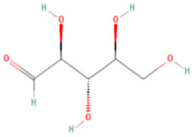
4	L-Rhamnose monohydrate	$C_6H_{14}O_6$	182.17	2674.29	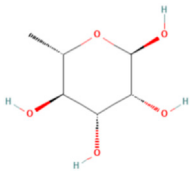
5	D-Glucuronic acid	$C_6H_{10}O_7$	194.14	3,334.29	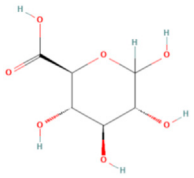
6	D-Galacturonic acid	$C_6H_{10}O_7$	194.14	11,214.29	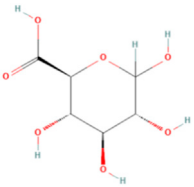
7	Glucose	$C_6H_{12}O_6$	180.16	33,622.86	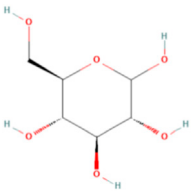
8	Galactose	$C_6H_{12}O_6$	180.16	5500.00	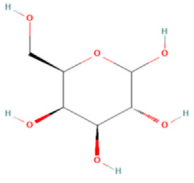

(Continued on following page)

TABLE 1 (*Continued*) Composition of ESP.

No.	Name	Molecular formula	MW (g/mol)	Content (mg/kg)	Structure
9	D-Xylose	$C_5H_{10}O_5$	150.13	651.43	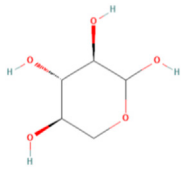
10	Arabinose	$C_5H_{10}O_5$	150.13	10,140.00	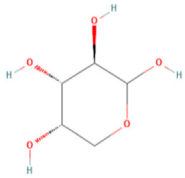
11	Fucose	$C_6H_{12}O_5$	164.16	102.86	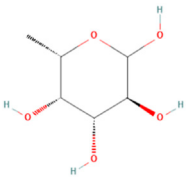

body weights exhibited a trend of stagnation or even decrease, and then gradually increased after 14 days. By contrast, the mice in the NC group displayed a continuous increase in body weight (Figure 1D). Importantly, no adverse reactions were observed in the ESP-treated mice, and high-dose ESP did not affect spleen and thymus weights (Supplementary Figure S1A). ESP-H treatment significantly suppressed cell proliferation (Figures 1E–G).

3.3 ESP prevents impairment of joint bone, cartilage, and intestinal barrier from RA

The impact of type II collagen on joint bone and cartilage damage was evaluated through histopathological staining. H&E staining of mice ankle joints revealed significant infiltration of inflammatory cells, fibroblast proliferation, and neovascularization in the CIA mice, with uneven surfaces noted on the articular cartilage and local vascular shading (Figure 2A). Masson staining unveiled damage to the joint cartilage surface in the CIA group, with a disordered arrangement of collagen fibers and unclear boundaries between the cartilage and subchondral tissues (Figures 2B,E). Safranin O/Fast Green staining demonstrated inflammatory changes in the cartilage tissues of the CIA group, loss of the normal structure, surface defects, synovial tissue proliferation, and intermittent tide lines. The staining results were evaluated based on the basis of the Mankin cartilage tissue score and OARSI joint pathology score (Figures 2C,F). TRAP staining unveiled numerous positively stained osteoclasts in the joints of the CIA mice (Figures 2D,G). The RA-affected cartilage injury in the joints can accelerate synovial inflammation by producing pro-inflammatory cytokines (Koepsell, 2020). ESP treatment alleviated synovial inflammation in type II collagen-treated mice and reduced joint damage. ESP dose-dependently reduced the serum levels of the pro-inflammatory factors IL-1β and IL-6 in the CIA mice (Figure 2H), consistent with the *in vitro* experimental results. These findings indicate that ESP has a strong anti-inflammatory effect.

Gut dysbiosis might trigger the breakdown of gut barrier integrity and the leakage of microbiota-derived metabolites into gut tissue and even venous or lymphatic circulation, enabling exposure of the immune cells to bacterial antigens leading to local and systemic inflammation, increased pro-inflammatory cytokines such as IL-1 and IL-6 (Romero-Figueroa et al., 2023) (Figure 3A). The H&E staining (Figure 3B) and AB-PAS (Figure 3C) results revealed severe epithelial damage, inflammatory cell infiltration, and mucosal injury in the CIA mice. These histopathological abnormalities were largely restored in the ESP-treated mice. The expression of the tight junction protein ZO-1 significantly decreased in the colon of the CIA mice. However, this expression markedly increased after ESP treatment (Figures 3D,E).

3.4 ESP exerts protective effects on synovial cells in CIA mice through the TLR4/HDAC/NF-κB signaling pathway

The expression levels of inflammatory proteins in the mice synovial tissue were evaluated through western blotting. Compared with the CIA group, the ESP treatment group exhibited significantly reduced TLR4, MyD88, and TRAF6 expression (Figure 4A). ESP inhibited p65 and phosphorylated p65 expression in the NF-κB signaling pathway (Figure 4B), thus blocking HDAC1 and HDAC2 signals (Figure 4C). As shown in cell experiments, the HDAC1/2 inhibitor TSA (100 nM) and NF-κB inhibitor PDTC (100 nM). TSA and PDTC partially inhibited the HDAC inflammatory expression in the synovium (Figures 4D,E).

3.5 ESP reverses gut dysbiosis in RA

The metagenomic sequencing analysis revealed a pro-inflammatory shift in the colonic microbiota of the CIA model, with an increase in the abundance of gram-negative bacteria

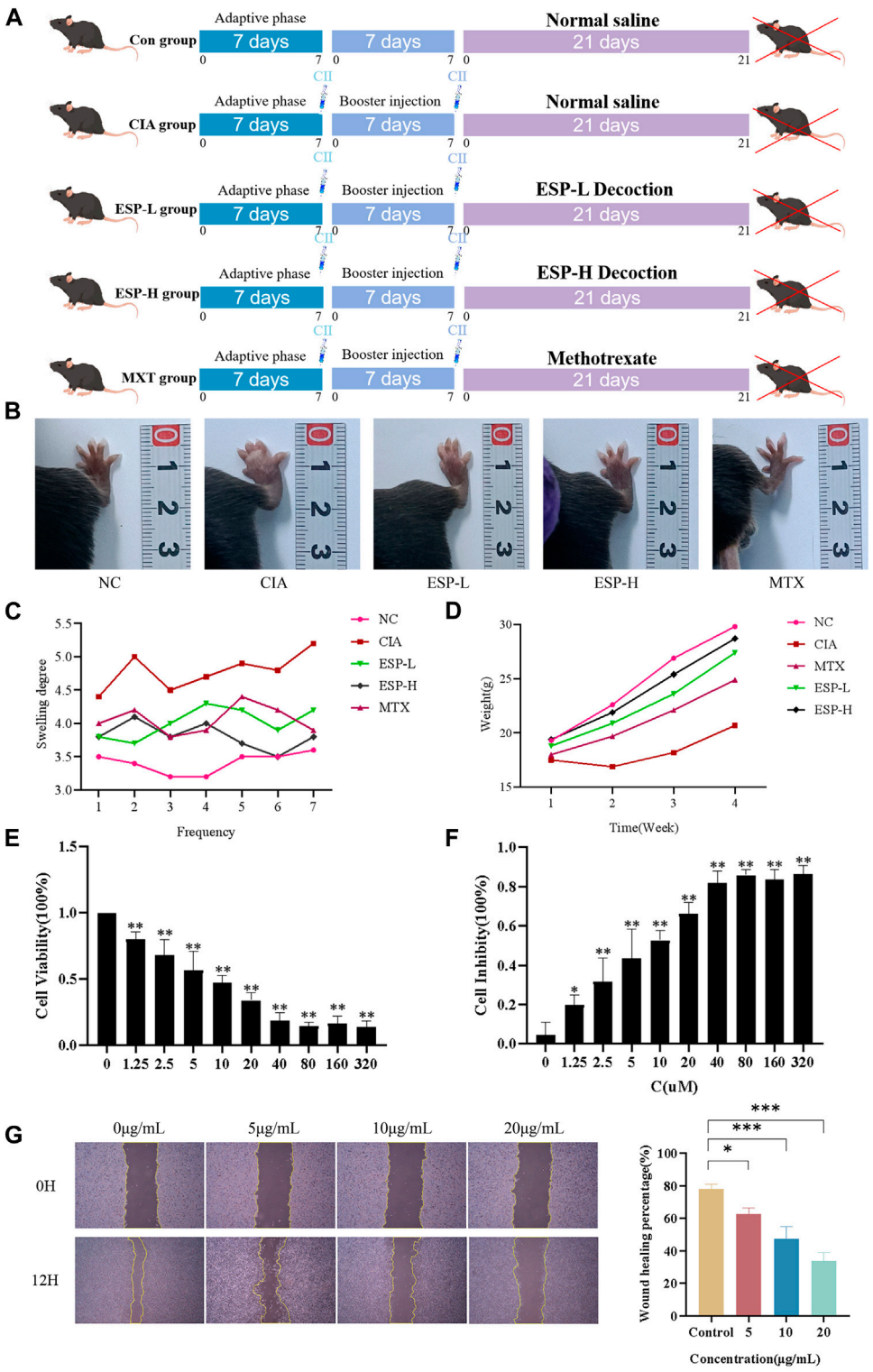

FIGURE 1
The role of ESP in the occurrence of rheumatoid arthritis. Timeline of animal experiments; **(B)** The effects of ESP on joint swelling in collagen-induced arthritis (CIA) rats; **(C–D)** Changes in the body weight and paw swelling in mice from each group; **(E–F)** Statistical analysis of MTT test results after treatment with different concentrations of ESP. **(G)** Statistical analysis of the impact of different concentraotins of ESP treatment on cell proliferatio(*p < 0.05; **p < 0.01 vs. 0 μM group).

containing immunogenic LPS in their cell walls (Deng et al., 2021). The abundance of bacteria with pro-inflammatory characteristics (*Alistipes*, *Enterococcus*, *Enterorhabdus*, *Odoribacter*, and *Escherichia*) was higher, whereas the ESP intervention caused the diversity of the intestinal microbiota in the CIA model improved (Supplementary Figure S1B–F), and an increase in the abundance of

10.3389/fphar.2024.1414675

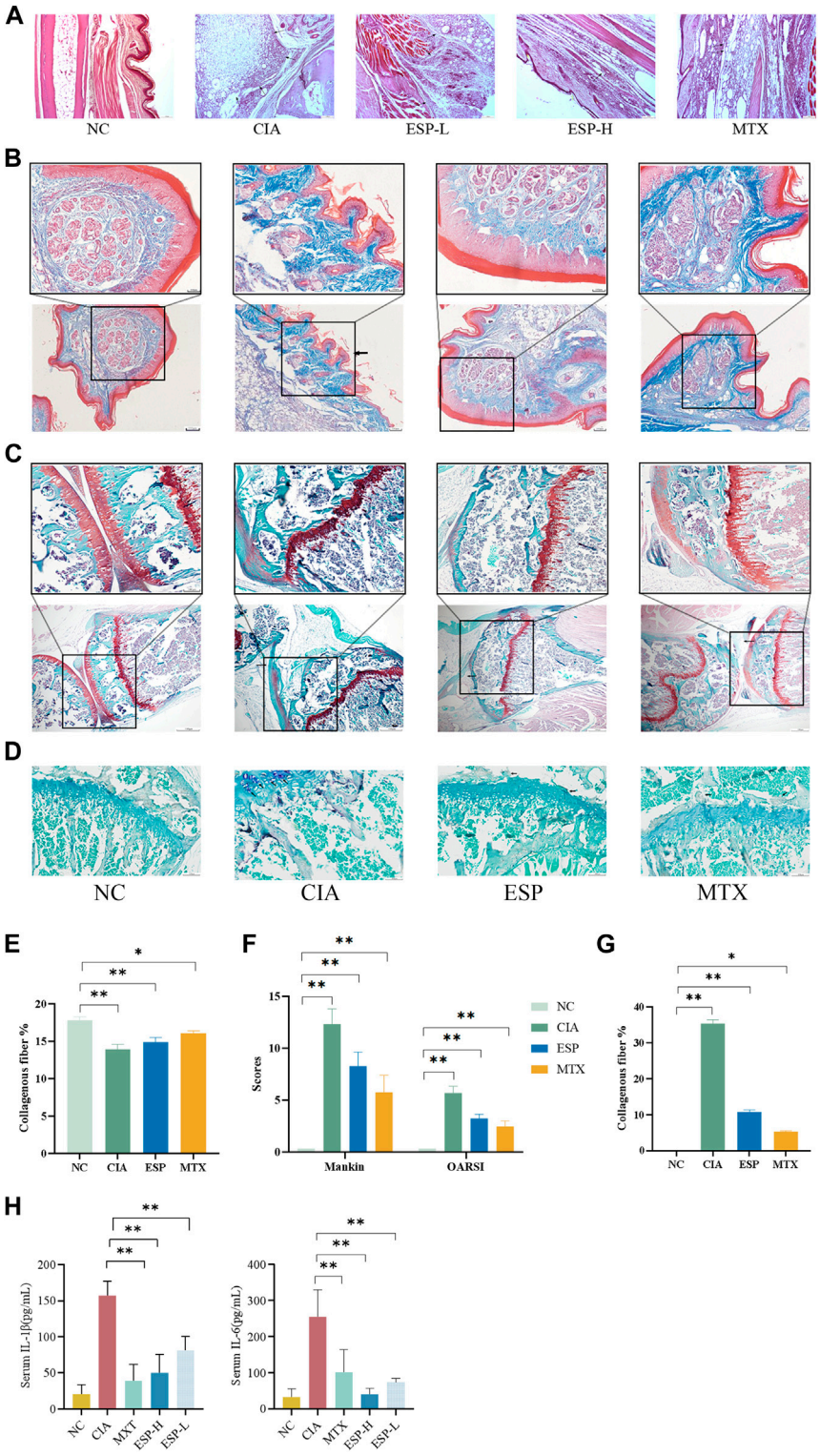

FIGURE 2
Effects of ESP on histopathology of joint tissues and immune organ indicators. **(A)** H&E staining of mice ankle joints; **(B.E)** Masson staining and statistical analysis; **(C,F)** Safranin O/Fast Green staining and Mankin cartilage tissue score, OARSI joint pathology score; **(D,G)** TRAP staining; **(H)** the IL-1β and IL-6 levels in the serum. (*$p < 0.05$; **$p < 0.01$)

anti-inflammatory bacteria (*Dubosiella*, *Roseburia*, *Bifidobacterium*, *Clostridium*, *Pseudoramibacter*, *Faecalibaculum*, and *Parabacteroides*).

The LEfSe analysis identified a higher abundance of *g_Enterococcus*, *g_Enterorhabdus*, *g_Alistipes*, *g_Odoribacter*, *s_Enterorhabdus caecimuris*, *s_Escherichia coli*, and *s_Enterococcus*

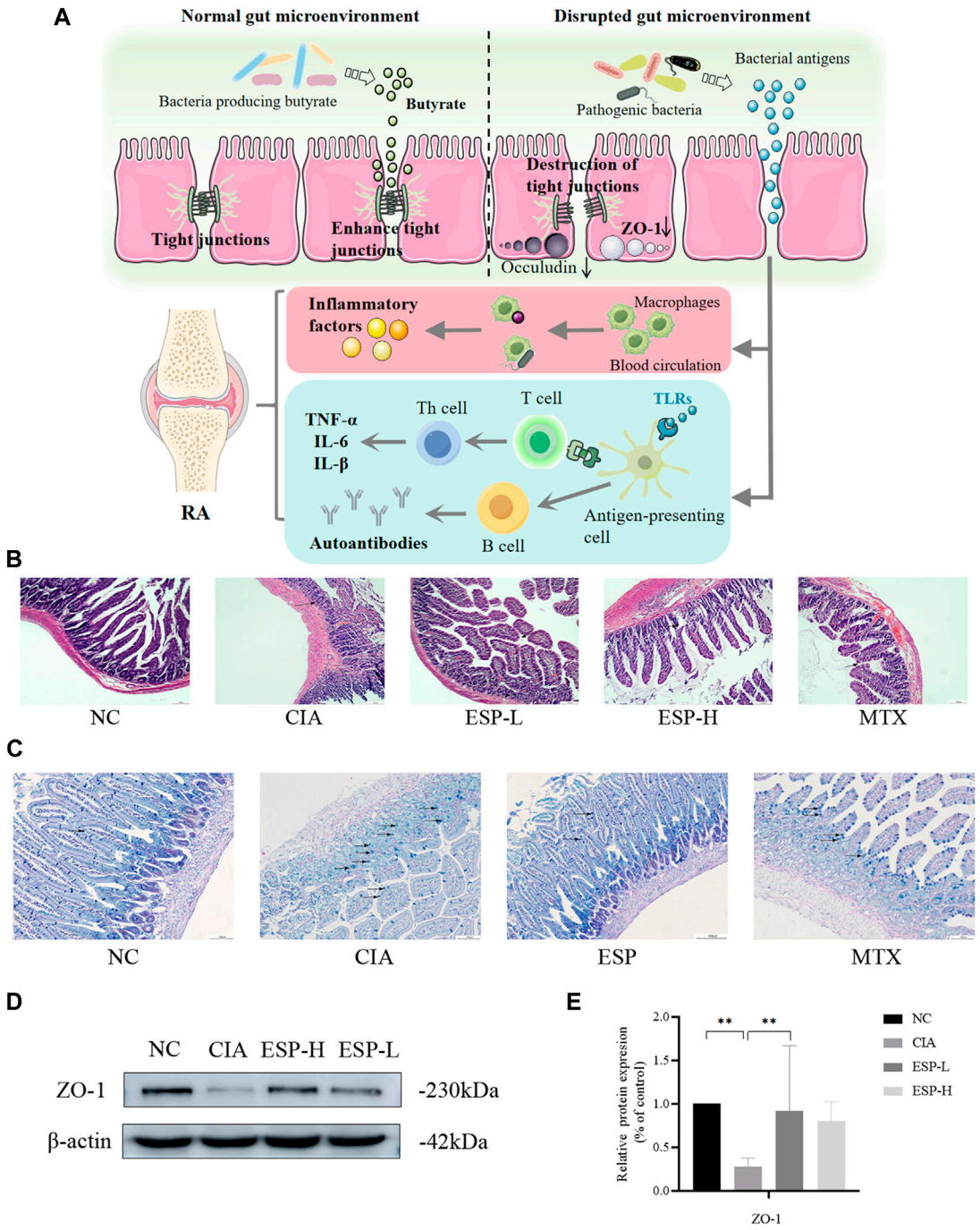

FIGURE 3
ESP restores intestinal barrier function in rheumatoid arthritis. **(A)** The link between the intestinal barrier and rheumatoid arthritis. After decreased secretion of ZO-1, the tight junctions are disrupted, leading to increased permeability. This allows the gut microbiota to enter the lamina propria through intestinal epithelial cells, leading to the production of inflammatory factors. Simultaneously, these microorganisms or their derived metabolites can enter the joints through the bloodstream; **(B)** H&E staining of mice intestinal tissues; **(C)** AB-PAS staining of mice intestinal tissues; **(D,E)** Immunoblotting detection of zonula occludens-1 (ZO-1) expression after ESP intervention. (*$p < 0.05$; **$p < 0.01$).

faecium in the CIA group. After the ESP treatment, the abundance of *g_Dubosiella*, *g_Pseudoramibacter*, *g_Bifidobacterium*, *g_Faecalibaculum*, *s_Dubosiella newyorkensis*, *s_Clostridium* sp. *26_22*, *s_Bifidobacterium pseudolongum*, and *s_Parabacteroides chinchillae* significantly increased in the gut microbiota of mice compared with the CIA group, consistent with the abundance in the NC group (Figures 5A,B; Supplementary Figure S1G,H).

Furthermore, an interaction ecological network constructed from the inter-group differential microbiota, thereby revealing the existence of mutual exclusion relationships between harmful and beneficial bacteria in the gut microbiota of the CIA mice (Figure 5D). Metagenomic sequencing revealed a relative increase in carbohydrate-active enzymes (CAZymes) CBM5, CBM36, and CBM58 in the CIA group (Figure 5E).

10.3389/fphar.2024.1414675

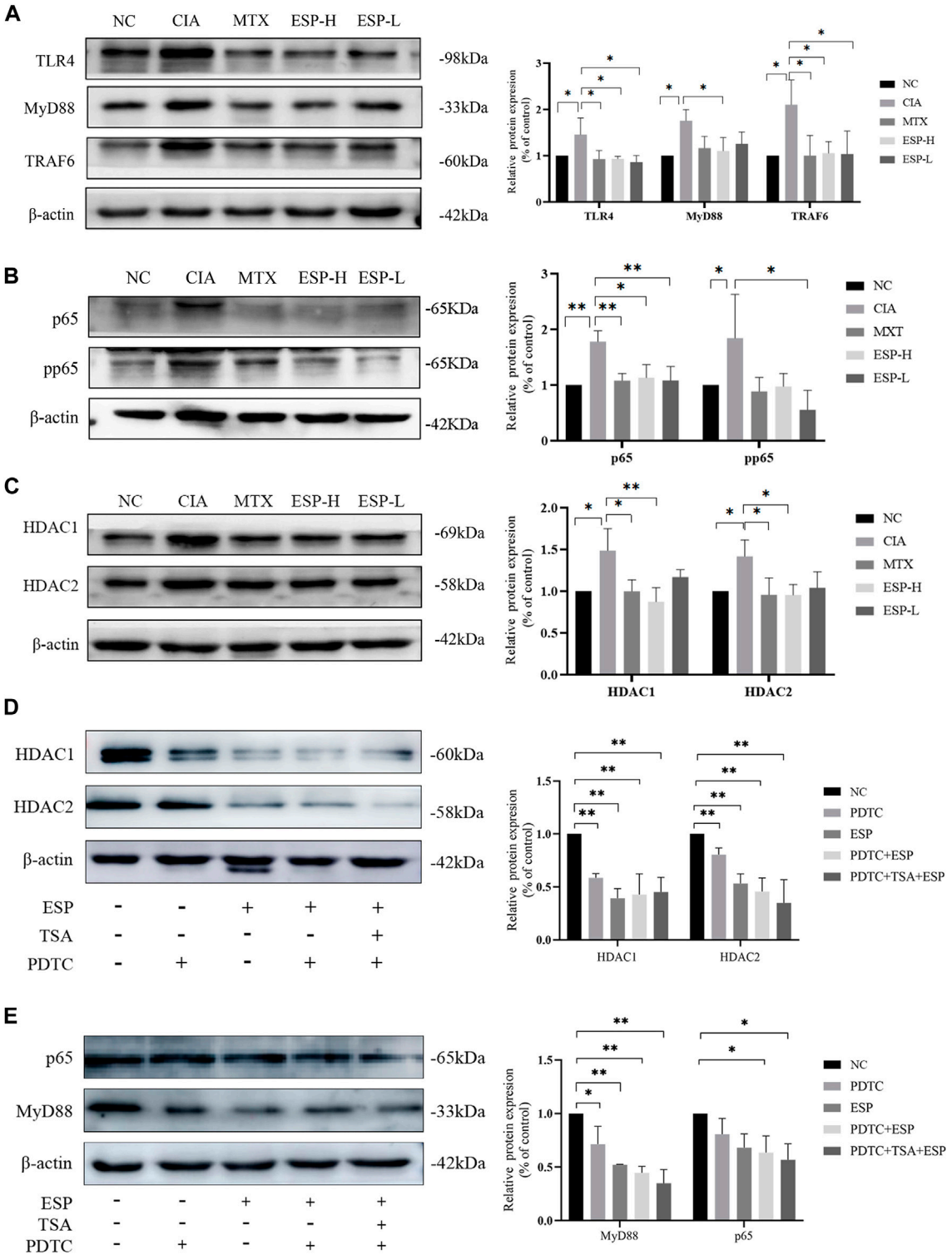

FIGURE 4
ESP exerts protective effects on CIA mice synovial cells through the TLR4/HDAC/NF-κB signaling pathway. **(A)** Immunoblotting detection of inflammatory proteins (TLR4, MyD88, TRAf6) expressions after ESP intervention; **(B,C)** Immunoblotting detection of the NF-κB signaling pathway proteins (p65, pp65, HDAC1, HDAC2) expressions after ESP intervention; **(D,E)** Immunoblotting detection of p65, MyD88, HDAC1, and HDAC2 protein expressions after ESP intervention and HDAC1/2 inhibitor TSA, NF-κB inhibitor PDTC intervention. (*$p < 0.05$; **$p < 0.01$).

10.3389/fphar.2024.1414675

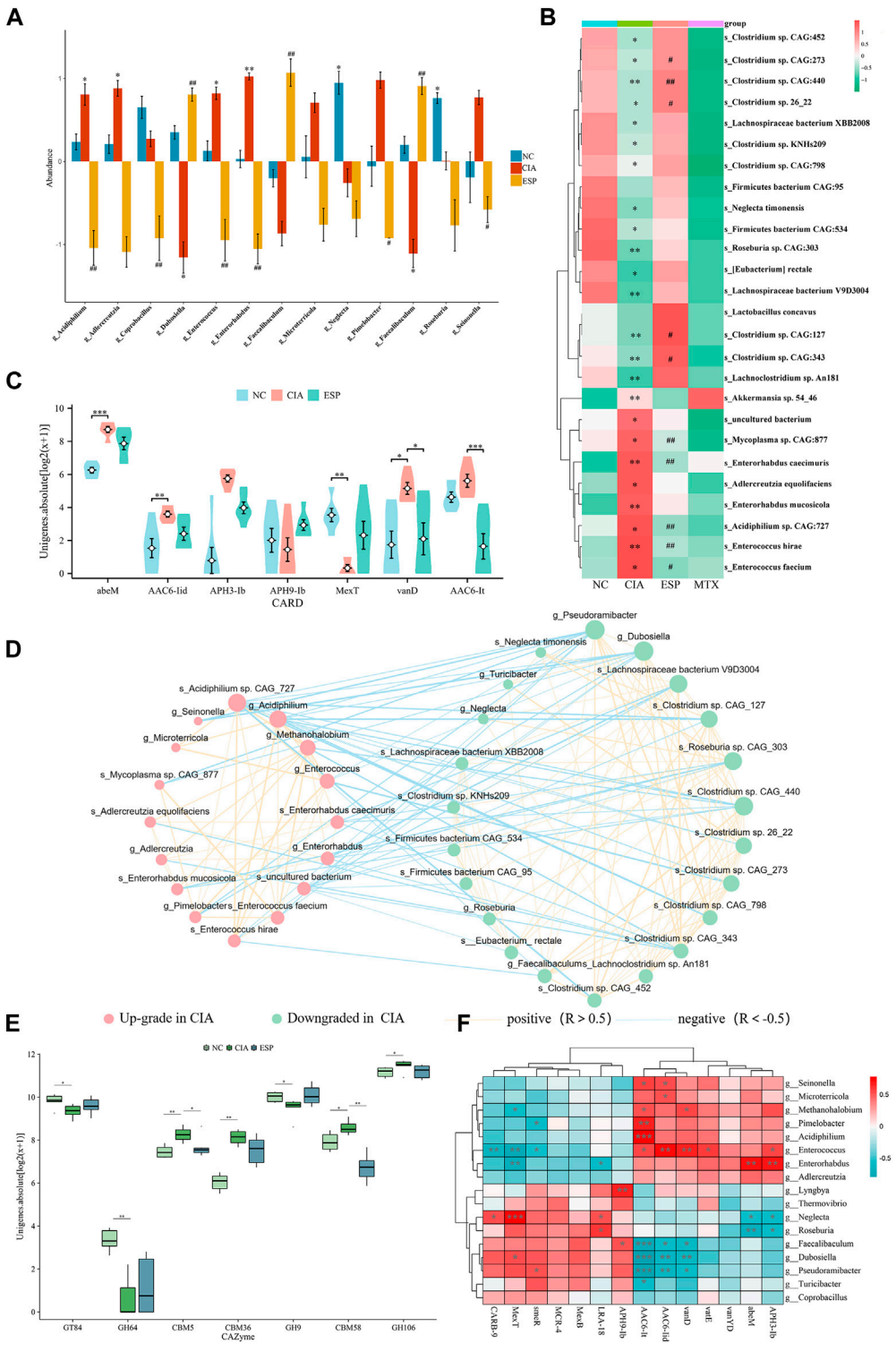

FIGURE 5
ESP regulates the gut microbiota in rheumatoid arthritis. **(A,B)** LEfSe analysis of changes in the gut microbiota abundance at the genus level **(A)** and species level; **(B)** between the groups of mice (*$p < 0.05$; **$p < 0.01$ vs NC group; $^{\#}p < 0.05$; $^{\#\#}p < 0.01$ vs CIA group); **(C)** statistical analysis of differences in resistance genes between the groups of mice; **(D)** ecological network of interactions between differentially abundant bacteria at the genus and species levels; **(E)** comparison of carbohydrate-active enzyme abundance in the mice between the groups; **(F)** Heatmap depicting the correlation between differentially abundant bacteria at the genus level and differentially resistant genes (*$p < 0.05$; **$p < 0.01$).

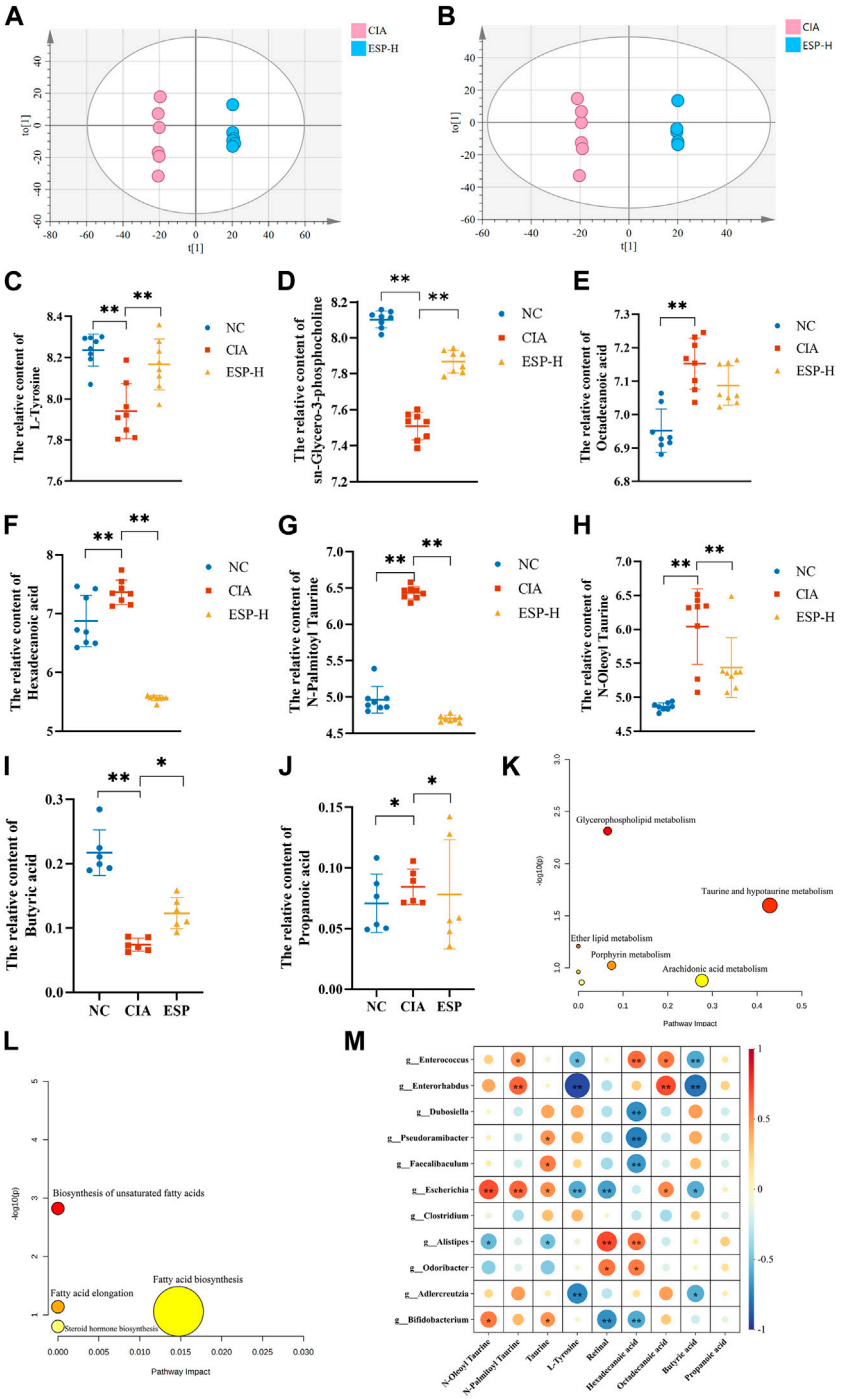

FIGURE 6
ESP regulates intestinal metabolites in rheumatoid arthritis. **(A,B)** Orthogonal partial least squares discriminant analysis (OPLS-DA) of the CIA group and ESP-H group under the positive ion mode **(A)** and negative ion mode **(B)**; **(C–H)** Changes in the content of different metabolites between the groups; **(I,J)** Changes in the content of different short-chain fatty acids between the study groups; **(K,L)** Pathway analysis of differential metabolites; **(M)** Heatmap depicting the correlation between differentially abundant bacteria at the genus level and differential metabolites (*$p < 0.05$; **$p < 0.01$).

By analyzing the microbial correlations of antibiotic resistance genes (ARGs) (Figures 5C,F), we found a negative correlation between APH3-lb, abeM, and *g_Roseburia*, and a positive correlation with *g_Enterorhabdus*. AAC6-lt was negatively correlated with *g_Dubosiella* and *g_Pseudoramibacter* and positively correlated with *g_Enterococcus*. These datas suggested that ESP counteracts pro-inflammatory bacteria such as *g_Enterococcus* and *s_Enterococcus hirae*, thereby improving RA-induced microbiota dysbiosis.

3.6 ESP modulates gut metabolites in RA

Given the major role of gut microbiota metabolites in regulating health and disease, a metabolomic analysis was conducted using the fecal samples from the mice (Supplementary Figure S2).

In the positive ion mode (Figure 6A), compared with the NC group, the levels of differential metabolites such as L-tyrosine and sn-glycero-3-phosphocholine decreased in the CIA group. In the negative ion mode (Figure 6B), the content of metabolites such as hexadecanoic acid, octadecanoic acid, N-oleoyl taurine, and N-palmitoyl taurine were reduced, and these trends were reversed after ESP administration (Figures 6C–H). The concentration of butyric acid in the fecal of mice induced by type II collagen decreased, while the concentration of propionic acid increased. Treatment with ESP was found to elevate the levels of butyric acid and reduce the levels of propionic acid (Figures 6I,J; Supplementary Figure S3).

The selected differential metabolites were inputted into the MetaboAnalyst 5.0 database for the pathway analysis. The pathways associated with the serum differential metabolites, including taurine and hypotaurine metabolism, porphyrin metabolism, arochidonic acid metabolism, and fatty acid biosynsis, exhibited a high correlation, which indicated their potential relevance to ESP therapy for RA. Figure 6K–L presents the metabolic pathway diagram (Detailed metabolites listed in Supplementary Material S2). It is found that butyric acid and L-Tyrosine are negatively correlated with *Enterococcus* and *Enterorhabdus*. Hexadecanoic acid is negatively correlated with *Dubosiella*, *Pseudoramibacter,* and *Bifidobacterium*, while positively correlated with *Enterococcus* (Figure 6M). It is speculated that the bacterial community may play a role through the action of secondary metabolites on the TLR4/HDAC/NF-κB signaling pathway.

4 Discussion

An interaction occurs among local inflammation, imbalanced gut microbiota, and host immune dysregulation in RA pathogenesis. (Eicher and Mohajeri, 2022). Microbiota-derived metabolites participate in signal transduction, maintenance of the mucosal barrier, and immune system regulation, thereby serving as key factors in the host-microbiota crosstalk in a pathogenic environment. Thus, they become a new participant in the mucosal immune function and inflammation, playing a crucial role in RA occurrence and development (Wolter et al., 2021). Traditional Chinese medicine comprises various monosaccharides, polysaccharides, and other carbohydrates, and so, a large amount of enzymes is required to facilitate their biological conversion. However, humans have a limited number of genes encoding CAZymes. The gut microbiota can encode a diverse and extensive CAZymes library. It thus breaks down and metabolizes a large amount of complex polysaccharides into SCFAs, regulates host immunity, and produces antioxidative substances.

Plant cell walls are composed of polysaccharides, and glycoside hydrolases (GHs) typically catalyze plant cell wall deconstruction (Hong et al., 2023). Medicinal plant fibers are often large-molecule polysaccharides promoting bacterial growth adept at fiber degradation (Ye et al., 2022).

Our monosaccharide mass spectrometry results revealed that ESP contains high levels of glucuronic acid, galactose, arabinose, and glucose. The immunomodulatory activity of polysaccharides depends on their molecular weight and monosaccharide composition. For example, arabinose and glucose contents in polysaccharides are related to significantly enhanced immunoreactivity (Wastyk et al., 2021). ESP alleviated synovial inflammation in the CIA mice and had a protective effect on type II collagen-induced joint damage, which manifested as significant improvements in body weight, paw swelling, and histological scores, and reduced IL-1β and IL-6 levels.

Polysaccharides exert a significant regulatory effect on the ecological imbalance of the gut microbiota. ESP greatly improved the CIA-induced gut microbiota imbalance in the mice. Activation of the NF-κB signaling pathway is associated with the *in vitro* immunomodulatory effects of polysaccharides (Wang et al., 2023a; Wang et al., 2023b). TLR4 expression activates the NF-κB pathway, thereby stimulating the release of inflammatory enzymes (Chang et al., 2024).

The mucosal barrier maintains the normal dynamic balance of the intestinal environment. This structure primarily includes the mucosal barrier, intestinal epithelial barrier, and immune barrier (Yang et al., 2023). The mucus layer protects intestinal epithelial cells and serves as a crucial medium for host-bacteria interactions. The colonic mucus barrier serves as the primary line of defense against intestinal pathogens. The reduced thickness and chemical composition of the mucus layer increases the ability of bacteria to penetrate the mucous barrier (Sang et al., 2023). ZO-1 is crucial for mucosal healing and epithelial barrier function, and its loss can induce defects in the repair process (Kuo et al., 2021). In the present study, ESP promoted intestinal barrier repair in the CIA mice, improved the permeability of the ileal and colonic mucosa, and inhibited intestinal inflammation.

In our study, the elevation of serum IL-1β and IL-6 levels in the CIA mice was restored after ESP treatment. This indicated that ESP could inhibit the entry of inflammatory factors from the intestine into the joints. Additionally, increased TLR4 expression in the CIA mice synovial inflammation activated the NF-κB pathway. This promotes the release of inflammatory enzymes and leads to joint and cartilage destruction, along with IL-1β- and IL-6-induced excessive osteoclast production. Furthermore, the analysis revealed that intestinal inflammation-induced elevation in HDAC1 and HDAC2 levels led to NF-κB phosphorylation, and TLR4 and MyD88 activation in the RA synovial tissue, which are critical factors in RA immune imbalance. Ultimately, ESP alleviates RA by suppressing inflammation in the intestine and synovium.

In the CIA model, the abundance of bacteria such as *Alistipes*, *Enterococcus*, and *Enterorhabdus* was higher, which led to or exacerbated infections. *Enterococcus* is a major cause of multidrug-resistant infections (Xiong et al., 2022). It can reshape the metabolic environment and serve as a source of fermented amino acids like *C. difficile*, which then promotes the persistence of infections (Smith et al., 2022). After ESP treatment was administered, the abundance of *Dubosiella, Bifidobacterium, Clostridium, Pseudoramibacter,* and other bacteria increased. *Clostridium* is a bacterium with strong butyrate-producing ability. It enhances the integrity of the epithelial barrier and inhibits

inflammation. *Dubosiella newyorkensis* plays a crucial role in enhancing mucosal barrier integrity and regulating Treg/Th17 balance. It also alleviates host mucosal and extraintestinal inflammation by producing SCFAs (especially propionate) (Zhang et al., 2024). Evidence from ESP intervention-involving experiments confirms an increase in butyrate. *Bifidobacterium* can reduce the incidence and severity of RA (Jiang et al., 2023). *B. pseudolongum* regulates enhanced immune therapeutic responses by producing the metabolite guanosine. *B. pseudolongum* induces Th1 differentiation, triggers IFN-γ production by $CD4^+$ and $CD8^+$ T cells (Mager et al., 2020), decomposes indigestible carbohydrates, and improves intestinal barrier integrity. Intestinal inflammation is associated with impaired lipid absorption, and an increase in *Bifidobacterium* abundance may help alleviate inflammation and increase lipid absorption (Weninger et al., 2023).

The carbohydrate-binding module (CBM) is a type of multi-module enzyme protein that responds to polysaccharide reactions and has a high affinity for tyrosine (Liu et al., 2022). CBMs typically attach to CAZymes to enhance their catalytic activity and are expressed on the surface of pathogenic proteins (Liberato et al., 2022). CAZymes include GHs, polysaccharide lyases, carbohydrate esterases, and lytic polysaccharide monooxygenases (Attia and Brumer, 2021). Infectious and inflammatory diseases are partially attributable to abnormal signal transduction involving various protease actions. The gut is rich in various proteases sourced from the host, microbes, and diet. Proteolytic activity must be strictly regulated to prevent tissue damag e (Crits-Christoph et al., 2022; Edwinson et al., 2022).

The gut microbiota also serves as a reservoir for ARGs (Crits-Christoph et al., 2022). Bacteria frequently exchange ARGs within the human microbiome, with the gut bacterial community being a hub for horizontal gene transfer (Carvalho et al., 2022). Chromosomally encoded efflux pumps are the major determinants of antibiotic resistance in *Pseudomonas aeruginosa*. MexT is a transcriptional activator of one such efflux pump in *P. aeruginosa*, which leads to increased antibiotic resistance (Kim et al., 2019). Bacteria can encode aminoglycoside-modifying enzymes such as acetyl-CoA-dependent aminoglycoside acetyltransferase and ATP/GTP-dependent phosphotransferase (APH). APH confers high levels of resistance to aminoglycoside antibiotics through enzymatic modification (Smith et al., 2019). The APH gene expression gradually increases with an increase in the arabitol concentration, and this increase is consistent with resistance phenotypes (Zhang et al., 2016). Aminoglycoside phosphotransferases can phosphorylate specific hydroxyl groups in aminoglycoside antibiotics (e.g., tobramycin and kanamycin), which are highly clinically relevant antibiotics, thereby rendering them very effective inactivators (Adam et al., 2024). AbeM was upregulated in imipenem-resistant *Acinetobacter baumannii* isolates (Choquet et al., 2021).

Metabolomics study showed that several metabolites displayed significant differences in enrichment between the CIA and ESP groups, including taurine, N-oleoyl taurine, and N-palmitoyl taurine. Taurine levels in the ESP group were significantly reduced. Taurine levels in the blood of patients with RA-related autoimmune diseases, such as systemic lupus erythematosus (Li et al., 2020) and primary Sjögren's syndrome (Herrala et al., 2020), increase, and their levels are positively correlated with disease activity. N-Oleoyl taurine increased and N-palmitoyl taurine levels decreased in the ESP group. Serum N-oleoyl taurine promotes proliferation, abnormal differentiation, and impaired cell apoptosis, with taurine being its core structure (Huang et al., 2019). N-palmitoyl taurine can induce cell migration and upregulate inflammatory metabolic pathways (Reinke et al., 2017). In our study, ESP upregulated butyrate levels in the CIA group. Butyrate is the most widely studied HDAC inhibitor that can promote Tconvs, inhibit Tregs and osteoclasts, suppress HDAC expression, and downregulate pro-inflammatory cytokine levels (He et al., 2022).

Our results demonstrated that ESP administered to the II collagen-induced mice significantly increased SCFA levels, whereas restored the anti-inflammatory cytokine levels and intestinal barrier function. Therefore, we speculated microbial metabolites regulate the balance and immune homeostasis of RA.

HDACs are crucial for various inflammatory diseases, with HDAC-1 capable of downregulating inflammatory signals to inhibit the expression of NF-κB-regulated genes. HDAC-2 does not directly participate in NF-κB signal transduction, but it regulates HDAC-1-associated NF-κB activity. HDAC-1 inhibition in intestinal epithelial cells induces increased phosphorylation and nuclear localization of p65 NF-κB. HDAC inhibitors maintain a balance between pro-inflammatory and anti-inflammatory gene expression (Pooladanda et al., 2019; He et al., 2022).

In conclusion, our study demonstrates that ESP can effectively reduce IL-1β and IL-6 levels, suppress inflammation in RA, inhibit tumor-like proliferation of synovial cells, counteract NF-κB phosphorylation, and protect against joint damage in the RA model. An integrated analysis of metagenomics and LC-MS/MS and GC-MS/MS metabolomics indicated that the potential mechanisms of ESP treatment in CIA are enriched in taurine and hypotaurine metabolism, porphyrin metabolism, and the enrichment of SCFA-producing bacteria such as *Dubosiella, Bifidobacterium, Clostridium*, and *Pseudoramibacter*. Furthermore, metabolites involved in metabolic pathways may contribute to the protective effects of ESP on CIA.

Data availability statement

The datasets presented in this study can be found in online repositories. The names of the repository/repositories and accession number(s) can be found in the article/Supplementary Material.

Ethics statement

The animal study was approved by The Ethics Committee of Shanxi University of Chinese Medicine. The study was conducted in accordance with the local legislation and institutional requirements.

Author contributions

YM: Writing–review and editing, Writing–original draft, Funding acquisition, Conceptualization. XW: Writing–original draft, Formal Analysis, Data curation. JP: Writing–original draft, Formal Analysis, Data curation. FW: Writing–original draft, Investigation. YW: Writing–review and editing, Data curation. ML: Writing–original draft, Investigation. BS: Writing–review and editing. YW: Writing–review and editing, Validation, Software, Resources. YZ: Writing–review and editing,

Supervision, Software. TP: Writing–review and editing, Methodology, Funding acquisition, Conceptualization.

Funding

The author(s) declare that financial support was received for the research, authorship, and/or publication of this article. The author(s) declare that financial support was received for the research, authorship, and/or publication of this article. This work was supported by the National Natural Science Foundation of China Youth Project (#82104731), the Innovation Team for Traditional Chinese Medicine of the Health Commission of Shanxi Province (#ZYYTD2024026), the Scientific and Technological Innovation Team of Shanxi University of Chinese Medicine (#2022TD 2005).

Acknowledgments

The authors thank the Laboratory of Experimental Formulae, the Laboratory Animal Research Platform, and the Cell Laboratory of the Experimental Management Center of the Shanxi University of Chinese Medicine for their support in all the experiments.

Conflict of interest

The authors declare that the research was conducted in the absence of any commercial or financial relationships that could be construed as a potential conflict of interest.

The reviewer J-ST declared a shared affiliation with the author(s) to the handling editor at the time of review.

Publisher's note

Supplementary material

The Supplementary Material for this article can be found online at: https://www.frontiersin.org/articles/10.3389/fphar.2024.1414675/full#supplementary-material

References

Adam, S., Fries, F., von Tesmar, A., Rasheed, S., Deckarm, S., Sousa, C. F., et al. (2024). The peptide antibiotic corramycin adopts a β-Hairpin-like structure and is inactivated by the kinase ComG. *J. Am. Chem. Soc.* 146, 8981–8990. doi:10.1021/jacs.3c13208

Attia, M. A., and Brumer, H. (2021). New family of carbohydrate-binding modules defined by a galactosyl-binding protein module from a cellvibrio japonicus endo-xyloglucanase. *Appl. Environ. Microbiol.* 87, e0263420. doi:10.1128/AEM.02634-20

Brown, P., Pratt, A. G., and Hyrich, K. L. (2024). Therapeutic advances in rheumatoid arthritis. *Bmj* 384, e070856. doi:10.1136/bmj-2022-070856

Cao, W., Liu, J., Dai, Y., Zhou, Y., Li, R., and Yu, P. (2022). Bibliometric analysis of marine traditional Chinese medicine in pharmacopoeia of the people's Republic of China: development, differences, and trends directions. *Evid. Based Complement. Altern. Med.* 2022, 3971967. doi:10.1155/2022/3971967

Carvalho, M. J., Sands, K., Thomson, K., Portal, E., Mathias, J., Milton, R., et al. (2022). Antibiotic resistance genes in the gut microbiota of mothers and linked neonates with or without sepsis from low- and middle-income countries. *Nat. Microbiol.* 7, 1337–1347. doi:10.1038/s41564-022-01184-y

Chang, L., Wang, C., Peng, J., Song, Y., Zhang, W., Chen, Y., et al. (2024). Rattan pepper polysaccharide regulates dss-induced intestinal inflammation and depressive behavior through microbiota-gut-brain axis. *J. Agric. Food Chem.* 72, 437–448. doi:10.1021/acs.jafc.3c08462

Choquet, M., Lohou, E., Pair, E., Sonnet, P., and Mullie, C. (2021). Efflux pump overexpression profiling in acinetobacter baumannii and study of new 1-(1-naphthylmethyl)-piperazine analogs as potential efflux inhibitors. *Antimicrob. Agents Chemother.* 65, e0071021. doi:10.1128/AAC.00710-21

Crits-Christoph, A., Hallowell, H. A., Koutouvalis, K., and Suez, J. (2022). Good microbes, bad genes? The dissemination of antimicrobial resistance in the human microbiome. *Gut Microbes* 14, 2055944. doi:10.1080/19490976.2022.2055944

Deng, C., Zhang, Q., He, P., Zhou, B., He, K., Sun, X., et al. (2021). Targeted apoptosis of macrophages and osteoclasts in arthritic joints is effective against advanced inflammatory arthritis. *Nat. Commun.* 12, 2174. doi:10.1038/s41467-021-22454-z

Edwinson, A. L., Yang, L., Peters, S., Hanning, N., Jeraldo, P., Jagtap, P., et al. (2022). Gut microbial β-glucuronidases regulate host luminal proteases and are depleted in irritable bowel syndrome. *Nat. Microbiol.* 7, 680–694. doi:10.1038/s41564-022-01103-1

Eicher, T. P., and Mohajeri, M. H. (2022). Overlapping mechanisms of action of brain-active bacteria and bacterial metabolites in the pathogenesis of common brain diseases. *Nutrients* 14, 2661. doi:10.3390/nu14132661

He, J., Chu, Y., Li, J., Meng, Q., Liu, Y., Jin, J., et al. (2022). Intestinal butyrate-metabolizing species contribute to autoantibody production and bone erosion in rheumatoid arthritis. *Sci. Adv.* 8, eabm1511. doi:10.1126/sciadv.abm1511

Herrala, M., Mikkonen, J., Pesonen, P., Lappalainen, R., Tjaderhane, L., Niemela, R. K., et al. (2020). Variability of salivary metabolite levels in patients with sjogren's syndrome. *J. Oral Sci.* 63, 22–26. doi:10.2334/josnusd.19-0504

Hong, M., Li, Z., Liu, H., Zheng, S., Zhang, F., Zhu, J., et al. (2023). Fusobacterium nucleatum aggravates rheumatoid arthritis through fada-containing outer membrane vesicles. *Cell Host Microbe* 31, 798–810.e7. doi:10.1016/j.chom.2023.03.018

Huang, J., Weinstein, S. J., Moore, S. C., Derkach, A., Hua, X., Mondul, A. M., et al. (2019). Pre-diagnostic serum metabolomic profiling of prostate cancer survival. *J. Gerontol. a Biol. Sci. Med. Sci.* 74, 853–859. doi:10.1093/gerona/gly128

Jiang, Z. M., Zeng, S. L., Huang, T. Q., Lin, Y., Wang, F. F., Gao, X. J., et al. (2023). Sinomenine ameliorates rheumatoid arthritis by modulating tryptophan metabolism and activating aryl hydrocarbon receptor via gut microbiota regulation. *Sci. Bull. (Beijing)* 68, 1540–1555. doi:10.1016/j.scib.2023.06.027

Kim, S., Kim, S. H., Ahn, J., Jo, I., Lee, Z. W., Choi, S. H., et al. (2019). Crystal structure of the regulatory domain of mext, a transcriptional activator of the mexefoprn efflux pump in pseudomonas aeruginosa. *Mol. Cells* 42, 850–857. doi:10.14348/molcells.2019.0168

Koepsell, H. (2020). Glucose transporters in the small intestine in health and disease. *Pflugers Arch.* 472, 1207–1248. doi:10.1007/s00424-020-02439-5

Kuo, W. T., Zuo, L., Odenwald, M. A., Madha, S., Singh, G., Gurniak, C. B., et al. (2021). The tight junction protein zo-1 is dispensable for barrier function but critical for effective mucosal repair. *Gastroenterology* 161, 1924–1939. doi:10.1053/j.gastro.2021.08.047

Li, H., Wang, Y., and Han, X. (2023). Esp-b4 promotes nasal epithelial cell-derived extracellular vesicles containing mir-146a-5p to modulate smad3/gata-3 thus relieving allergic rhinitis: esp-b4/mir-146a-5p in ar. *Phytomedicine* 108, 154516. doi:10.1016/j.phymed.2022.154516

Li, J., Ding, H., Meng, Y., Li, G., Fu, Q., Guo, Q., et al. (2020). Taurine metabolism aggravates the progression of lupus by promoting the function of plasmacytoid dendritic cells. *Arthritis Rheumatol.* 72, 2106–2117. doi:10.1002/art.41419

Liberato, M. V., Campos, B. M., Tomazetto, G., Crouch, L. I., Garcia, W., Zeri, A., et al. (2022). Unique properties of a dictyostelium discoideum carbohydrate-binding module expand our understanding of cbm-ligand interactions. *J. Biol. Chem.* 298, 101891. doi:10.1016/j.jbc.2022.101891

Liu, Y., Wang, P., Tian, J., Seidi, F., Guo, J., Zhu, W., et al. (2022). Carbohydrate-binding modules of potential resources: occurrence in nature, function, and application in fiber recognition and treatment. *Polym. (Basel)* 14, 1806. doi:10.3390/polym14091806

Luo, Y., Tong, Y., Wu, L., Niu, H., Li, Y., Su, L. C., et al. (2023). Alteration of gut microbiota in individuals at high-risk for rheumatoid arthritis associated with disturbed

metabolome and the initiation of arthritis through the triggering of mucosal immunity imbalance. *Arthritis Rheumatol.* 75, 1736–1748. doi:10.1002/art.42616

Mager, L. F., Burkhard, R., Pett, N., Cooke, N., Brown, K., Ramay, H., et al. (2020). Microbiome-derived inosine modulates response to checkpoint inhibitor immunotherapy. *Science* 369, 1481–1489. doi:10.1126/science.abc3421

Pooladanda, V., Thatikonda, S., Bale, S., Pattnaik, B., Sigalapalli, D. K., Bathini, N. B., et al. (2019). Nimbolide protects against endotoxin-induced acute respiratory distress syndrome by inhibiting TNF-α mediated NF-κB and HDAC-3 nuclear translocation. *Cell Death Dis.* 10, 81. doi:10.1038/s41419-018-1247-9

Reinke, S. N., Gallart-Ayala, H., Gomez, C., Checa, A., Fauland, A., Naz, S., et al. (2017). Metabolomics analysis identifies different metabotypes of asthma severity. *Eur. Respir. J.* 49, 1601740. doi:10.1183/13993003.01740-2016

Romero-Figueroa, M., Ramirez-Duran, N., Montiel-Jarquin, A. J., and Horta-Baas, G. (2023). Gut-joint axis: gut dysbiosis can contribute to the onset of rheumatoid arthritis via multiple pathways. *Front. Cell Infect. Microbiol.* 13, 1092118. doi:10.3389/fcimb.2023.1092118

Sang, X., Wang, Q., Ning, Y., Wang, H., Zhang, R., Li, Y., et al. (2023). Age-related mucus barrier dysfunction in mice is related to the changes in muc2 mucin in the colon. *Nutrients* 15, 1830. doi:10.3390/nu15081830

Smith, A. B., Jenior, M. L., Keenan, O., Hart, J. L., Specker, J., Abbas, A., et al. (2022). Enterococci enhance clostridioides difficile pathogenesis. *Nature* 611, 780–786. doi:10.1038/s41586-022-05438-x

Smith, C. A., Toth, M., Stewart, N. K., Maltz, L., and Vakulenko, S. B. (2019). Structural basis for the diversity of the mechanism of nucleotide hydrolysis by the aminoglycoside-2"-phosphotransferases. *Acta Crystallogr. D. Struct. Biol.* 75, 1129–1137. doi:10.1107/S2059798319015079

Wang, A., Liu, Y., Zeng, S., Liu, Y., Li, W., Wu, D., et al. (2023a). Dietary plant polysaccharides for cancer prevention: role of immune cells and gut microbiota, challenges and perspectives. *Nutrients* 15, 3019. doi:10.3390/nu15133019

Wang, A., Liu, Y., Zeng, S., Liu, Y., Li, W., Wu, D., et al. (2023b). Dietary plant polysaccharides for cancer prevention: role of immune cells and gut microbiota, challenges and perspectives. *Nutrients* 15, 3019. doi:10.3390/nu15133019

Wang, Q., Shu, Z., Xing, N., Xu, B., Wang, C., Sun, G., et al. (2016). A pure polysaccharide from ephedra sinica treating on arthritis and inhibiting cytokines expression. *Int. J. Biol. Macromol.* 86, 177–188. doi:10.1016/j.ijbiomac.2016.01.010

Wastyk, H. C., Fragiadakis, G. K., Perelman, D., Dahan, D., Merrill, B. D., Yu, F. B., et al. (2021). Gut-microbiota-targeted diets modulate human immune status. *Cell* 184, 4137–4153.e14. doi:10.1016/j.cell.2021.06.019

Weninger, S. N., Herman, C., Meyer, R. K., Beauchemin, E. T., Kangath, A., Lane, A. I., et al. (2023). Oligofructose improves small intestinal lipid-sensing mechanisms via alterations to the small intestinal microbiota. *Microbiome* 11, 169. doi:10.1186/s40168-023-01590-2

Wolter, M., Grant, E. T., Boudaud, M., Steimle, A., Pereira, G. V., Martens, E. C., et al. (2021). Leveraging diet to engineer the gut microbiome. *Nat. Rev. Gastroenterol. Hepatol.* 18, 885–902. doi:10.1038/s41575-021-00512-7

Xiong, X., Tian, S., Yang, P., Lebreton, F., Bao, H., Sheng, K., et al. (2022). Emerging enterococcus pore-forming toxins with mhc/hla-i as receptors. *Cell* 185, 1157–1171.e22. doi:10.1016/j.cell.2022.02.002

Yang, Y., Wang, Y., Zhao, L., Wang, F., Li, M., Wang, Q., et al. (2023). Chinese herbal medicines for treating ulcerative colitis via regulating gut microbiota-intestinal immunity axis. *Chin. Herb. Med.* 15, 181–200. doi:10.1016/j.chmed.2023.03.003

Ye, T. J., Huang, K. F., Ko, T. P., and Wu, S. H. (2022). Synergic action of an inserted carbohydrate-binding module in a glycoside hydrolase family 5 endoglucanase. *Acta Crystallogr. D. Struct. Biol.* 78, 633–646. doi:10.1107/S2059798322002601

Zaiss, M. M., Joyce, W. H., Mauro, D., Schett, G., and Ciccia, F. (2021). The gut-joint axis in rheumatoid arthritis. *Nat. Rev. Rheumatol.* 17, 224–237. doi:10.1038/s41584-021-00585-3

Zhang, G., Tian, J., Wang, C., Chen, J., and Feng, J. (2016). Identification of novel cryptic aminoglycoside phosphotransferases in pseudomonas aeruginosa. *Antimicrob. Agents Chemother.* 60, 6983–6985. doi:10.1128/AAC.01620-16

Zhang, Y., Tu, S., Ji, X., Wu, J., Meng, J., Gao, J., et al. (2024). Dubosiella newyorkensis modulates immune tolerance in colitis via the l-lysine-activated ahr-Ido1-kyn pathway. *Nat. Commun.* 15, 1333. doi:10.1038/s41467-024-45636-x

Zheng, Q., Mu, X., Pan, S., Luan, R., and Zhao, P. (2023). Ephedrae herba: a comprehensive review of its traditional uses, phytochemistry, pharmacology, and toxicology. *J. Ethnopharmacol.* 307, 116153. doi:10.1016/j.jep.2023.116153

frontiers | Frontiers in Pharmacology

TYPE Review
PUBLISHED 12 August 2024
DOI 10.3389/fphar.2024.1463140

OPEN ACCESS

EDITED BY
Xianyu Li,
China Academy of Chinese Medical Sciences, China

REVIEWED BY
Xiangwei Chang,
Anhui University of Chinese Medicine, China
Jianmei Zhang,
Sungkyunkwan University, Republic of Korea
Taoyun Wang,
Suzhou University of Science and Technology, China

*CORRESPONDENCE
Hanqing Pang,
hanqingpang@126.com

†These authors have contributed equally to this work and share first authorship

RECEIVED 11 July 2024
ACCEPTED 01 August 2024
PUBLISHED 12 August 2024

CITATION
Zhou Y, Gu C, Zhu Y, Zhu Y, Chen Y, Shi L, Yang Y, Lu X and Pang H (2024) Pharmacological effects and the related mechanism of scutellarin on inflammation-related diseases: a review.
Front. Pharmacol. 15:1463140.
doi: 10.3389/fphar.2024.1463140

Pharmacological effects and the related mechanism of scutellarin on inflammation-related diseases: a review

Yang Zhou[1,2†], Chenlin Gu[1,2†], Yan Zhu[1,2†], Yuting Zhu[1,2], Yutong Chen[1,2], Li Shi[1,2], Yang Yang[1,2], Xin Lu[1,2] and Hanqing Pang[1,2*]

[1]School of Medicine, Institute of Translational Medicine, Yangzhou University, Yangzhou, China, [2]Jiangsu Key Laboratory of Integrated Traditional Chinese and Western Medicine for Prevention and Treatment of Senile Diseases, Yangzhou University, Yangzhou, China

Inflammation is a biological response of multicellular organisms caused by injuries, pathogens or irritants. An excessive inflammatory response can lead to tissue damage and various chronic diseases. Chronic inflammation is a common feature of many diseases, making the search for drugs to treat inflammation-related diseases urgent. Scutellarin, a natural flavonoid metabolite, is widely used in the treatment of various inflammation-related diseases for its anti-inflammatory, anti-oxidant and anti-cancer activities. Scutellarin can inhibit key inflammatory pathways (PI3K/Akt, MAPK, and NF-κB, etc.) and activate the anti-oxidant related pathways (Nrf2, ARE, ect.), thereby protecting tissues from inflammation and oxidative stress. Modern extraction technologies, such as microwave-assisted, ultrasound assisted, and supercritical fluid extraction, have been utilized to extract scutellarin from Scutellaria and Erigeron genera. These technologies improve efficiency and retain biological activity, making scutellarin suitable for large-scale production. Scutellarin has significant therapeutic effects in treating osteoarthritis, pulmonary fibrosis, kidney injury, and cardiovascular diseases. However, due to its low bioavailability and short half-life, its clinical application is limited. Researchers are exploring innovative formulations (β-cyclodextrin polymers, triglyceride mimetic active ingredients, and liposome precursors, etc.) to improve stability and absorption rates. Despite these challenges, the potential of scutellarin in anti-inflammatory, anti-oxidant, and anti-cancer applications remains enormous. By optimizing formulations, exploring combination therapies, and conducting in-depth mechanistic research, scutellarin can play an important role in treating various inflammatory diseases, providing patients with more and effective treatment options.

KEYWORDS

scutellarin, inflammation, NF-κB, MAPK, PI3K/AKT, Nrf2/ARE

1 Introduction

Inflammation is a biological response of multicellular organism caused by sensitizing stimuli including damaged cells, pathogens or irritants. Moderate inflammatory response plays a crucial role in our long-term health through clearing infections and repairing tissue damage (Goodman et al., 2019; Henein et al., 2022;

Soliman and Barreda, 2022). While over-activation of inflammation could lead to tissue damage and various chronic diseases. Chronic inflammation is a well-recognized feature of most diseases, dramatically increasing global morbidity and mortality (Xia et al., 2023). Osteoarthritis (OA) is the most universal inflammatory disease of the joints (about 1 billion people), which brought an economic burden of nearly $140 billion (Wang et al., 2024). It is estimated that the majority of people suffer from OA by the age of 40–50 years and the incidence of OA is increasing due to the aging population and the high incidence rate of obesity (Jiang et al., 2024). Fibrosis, resulting from impaired tissue repair and remodeling, is a common long-term outcome of chronic inflammatory diseases (Massoud et al., 2024). Pulmonary fibrosis is characterized by fibroproliferation and abnormal tissue repair after injury, which could exacerbate the pathological process of pulmonary fibrosis through oxidative stress and inflammation-induced immune responses (Li Z. et al., 2024). In addition, inflammation is an important cause of excessive cardiovascular risk and progressive kidney injury. Chronic kidney disease accelerated dysregulation of the innate and adaptive immune systems, which would make the systemic inflammation and localized vascular inflammatory responses increase continuously, ultimately lead to atherosclerosis and microcirculatory dysfunction (Huck et al., 2024). That's why the research for drugs to treat inflammation-related diseases is so urgent.

Scutellarin, a natural flavonoid isolated from the root of *Scutellaria baicalensis* Georgi [Lamiaceae; Scutellaria], has been extensively used in the treatment of various diseases for its valuable biological activities, such as anti-oxidant, anti-inflammatory, and anti-cancer activities (Bian et al., 2020; Song et al., 2020). The mechanism by which scutellarin prevented and treated inflammation-related diseases included inhibiting the production of inflammatory mediators or oxidative stress responses. Cytokines and chemokines mediate the recruitment, activation, and proliferation of neutrophils, and promote the extravasation of monocytes and macrophages to the site of inflammation. These pro-inflammatory cytokines (IL-1, IL-6 and TNF-α, etc.) can activate the inflammatory cascades, thereby exacerbating organ and tissue injuries (Duan et al., 2024). Researches have shown that scutellarin can inhibit the production of these cytokines and reduce inflammatory responses (Cao et al., 2019; Aksit et al., 2023). For example, NF-κB is a key transcription factor that coordinates the expression of multiple genes associated with inflammatory responses (Mussbacher et al., 2023). Scutellarin can reduce the secretion of inflammatory mediators and significantly regulate the production of immune effector factors by mediating the NF-κB signaling pathway (Zhang et al., 2022). In addition, oxidative stress is another factor that exacerbates tissue damage caused by inflammatory reactions. The reactive oxygen species (ROS) produced during oxidative stress can activate various inflammatory signaling pathways, thereby promoting inflammation cascades. Scutellarin has been reported to have anti-oxidant properties, which can clear ROS, thereby reducing oxidative stress and reversing the trend towards inflammation (Zhang et al., 2022).

Scutellarin may have significant advantages in the treatment of inflammation-related diseases. Nevertheless, the low bioavailability and short half-life of flavonoids have limited the therapeutic efficacy of scutellarin in inflammation-related diseases. To solve the problem, researchers are committed to exploring new formulations of flavonoids including polymeric nanoparticles, liposomes, solid lipid microparticles, nanogels and nanocrystals (Sharma and Wairkar, 2024). However, whether the new formulations of scutellarin are economical, safe and effective is yet to be investigated, and the direction of specific drug dosage forms and delivery modalities of scutellarin still need to be explored in greater depth. Up to date, there has not been a systematic and complete review of the specific mechanisms of scutellarin against inflammation-related diseases, which has hindered its application and development as a good anti-inflammatory agent. This review is to provide valuable information for future applications of scutellarin in preventing and treating inflammation-related diseases.

2 Main sources and extraction methods of scutellarin

Scutellarin is a flavonoid glycoside mainly present in Scutellaria and Erigerontis genera (Chledzik et al., 2018). Scutellarin is frequently existed in *S. baicalensis* (Pei et al., 2022), and it was also identified in *Scutellaria lateriflora* L. [Lamiaceae; Scutellaria], *Scutellaria barbata* D.Don [Lamiaceae; Scutellaria], and *Oroxylum indicum* (L.) Kurz [Bignoniaceae; Oroxylum] as well. The Scutellaria genus is widely distributed in east Asia and north America (Irvin et al., 2019). The roots, stems and leaves of these plants contain large amounts of scutellarin. Breviscapine, the extract of *Erigeron breviscapus* (Vaniot) Hand.-Mazz. [Compositae; Erigeron] that is rich in scutellarin, has been reported to be effective for improving blood circulation. Studies revealed that the contents of scutellarin varied significantly depending on the plant species and parts (Georgieva et al., 2020). For example, the roots of *S. baicalensis* and the whole herb of *E. brevisacapus* are the main resources for extracting scutellarin (Nurul Islam et al., 2011; Georgieva et al., 2022). The sources of scutellarin and its available extraction methods were shown in Figure 1.

The extraction methods of scutellarin included traditional extraction techniques and modern extraction techniques (Hao et al., 2020). For traditional extraction methods (solvent extraction and hot reflux extraction), various solvents such as ethanol, methanol, or water can be used to extract scutellarin from plant materials (Yang et al., 2019b). Although these methods are easy to operate and have low equipment costs, they have disadvantages such as low efficiency and long-time consumption. With the development of science and technology, modern extraction techniques have greatly improved the extraction efficiency and purity of scutellarin (Xia et al., 2021). Ultrasound assisted extraction (UAE) utilizes the cavitation effect of ultrasound to accelerate the contact between solvents and plant materials, which could improve extraction efficiency, reduce solvent usage, and achieve an extraction rate of 50%–60% for scutellarin (Xiang and Wu, 2017). Microwave assisted extraction (MAE) utilizes microwave energy to rapidly heat solvents and plant materials, rapidly damaging cell walls and releasing scutellarin. The extraction rate of scutellarin is very high (about 70%–80%)

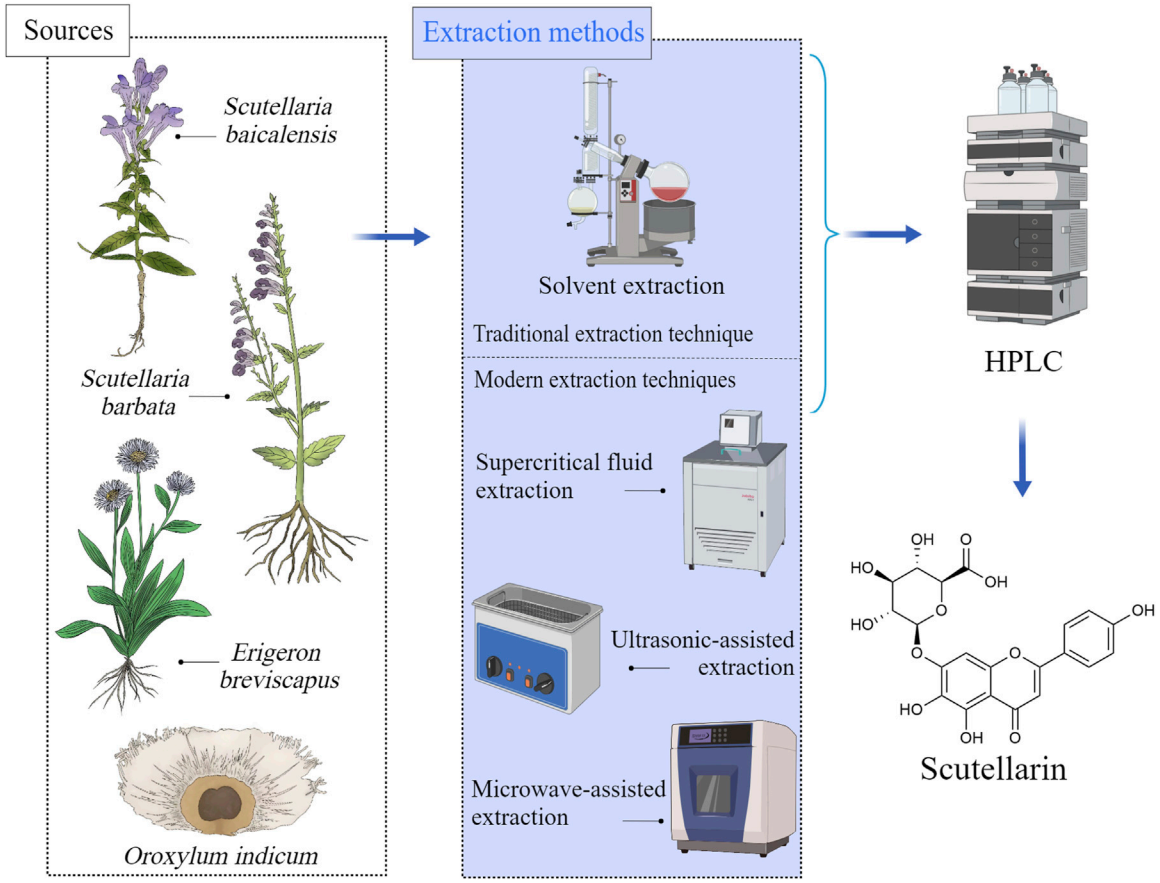

FIGURE 1
Sources of scutellarin and its available extraction methods, Created with MedPeer (medpeer.cn).

TABLE 1 Principles and advantages and disadvantages of scutellarin extraction methods.

Extraction	Methods Basic	Advantages	Disadvantages	Refs
Solvent Extraction	Solvent is used to dissolve scutellarin in the plant material and the active metabolite is extracted through an infusion process	Simple operation and low equipment requirement	Extraction efficiency is low and time consuming	Yang et al. (2019b)
Ultrasonic-assisted extraction	Utilizing the cavitation effect of ultrasonic waves to accelerate the contact between the plant material and the solvent and improve the extraction efficiency	Short time and high extraction efficiency	Specialized ultrasonic extraction equipment is required	Xiang and Wu (2017)
Microwave-assisted extraction	Utilizes microwave energy to heat the solvent and plant material to promote the release and dissolution of active metabolites	High extraction speed and low energy consumption	Requires specialized microwave extraction equipment	Li et al. (2015)
Supercritical fluid extraction	Extraction of Scutellarin from plant materials under high pressure using supercritical CO_2 as a solvent	Highly efficient and environmentally friendly, able to maintain the biological activity of Scutellarin	Expensive equipment and complicated operation	Yang and Wei (2018), Yang et al. (2019a)

(Li et al., 2015). Supercritical fluid extraction (SFE) uses supercritical carbon dioxide as a solvent under high pressure to preserve the biological activity of scutellarin, with an extraction rate of approximately 60%–70% (Yang and Wei, 2018; Yang et al., 2019a). These modern technologies not only have significant advantages in extraction efficiency, but also maintain the biological activity of scutellarin, making them suitable for large-scale industrial production and high-value extraction. The advantages and disadvantages of scutellarin extraction methods were summarized in Table 1.

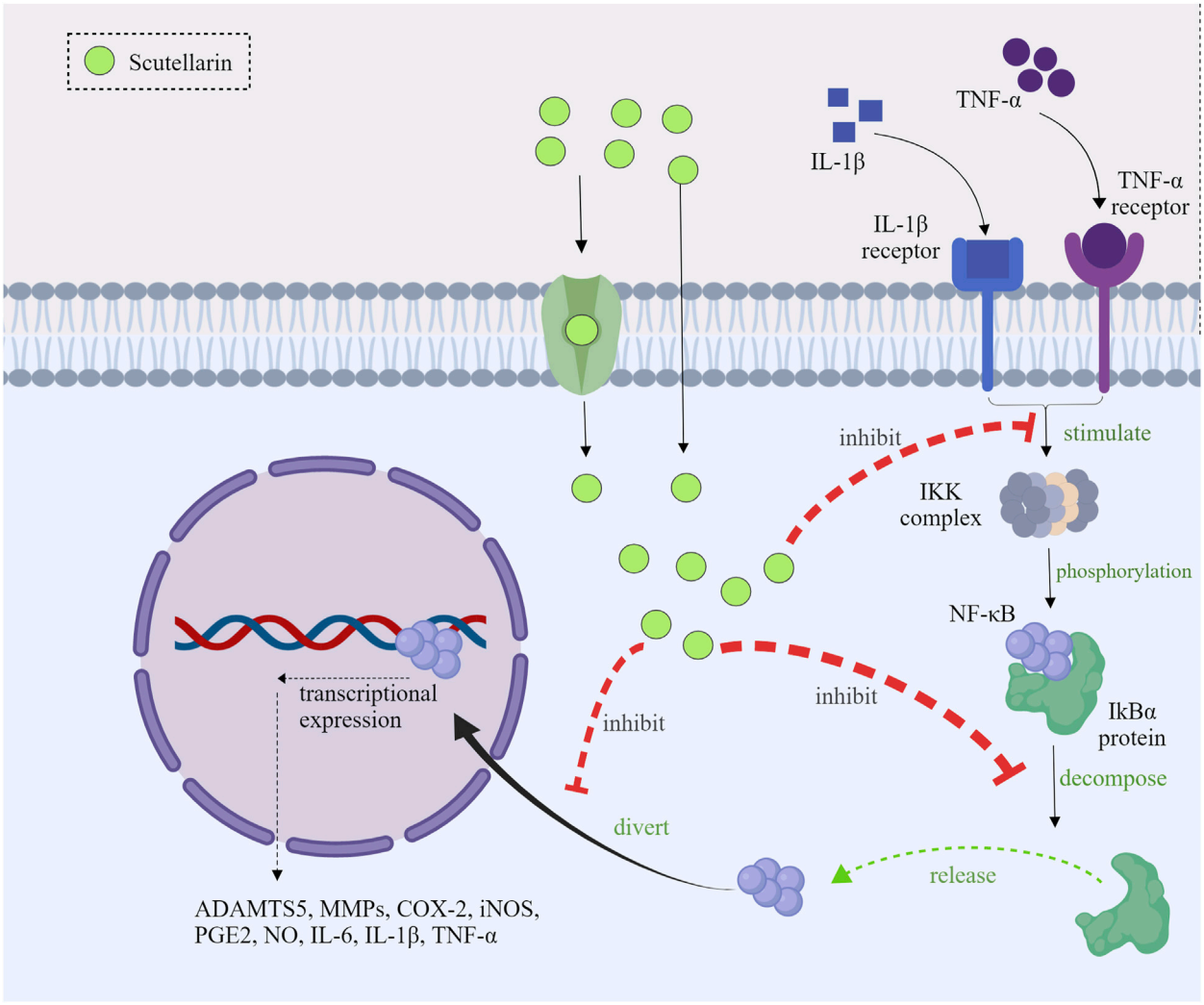

FIGURE 2
Mechanism diagram of scutellarin inhibiting the NF-κB pathways, Created with MedPeer (medpeer.cn).

3 Role of scutellarin on inflammatory signaling pathways

3.1 Inhibition of NF-κB pathways

3.1.1 Inhibition of IKK activation and IκBα phosphorylation

Under normal circumstances, nuclear factor-kappa B (NF-κB) was present in the cytoplasm as an inactive state, which was combined with the IκB proteins (Barnabei et al., 2021). When inflammatory response (such as LPS, cytokines, etc.) was initiated (Yang et al., 2021), the IκB kinase (IKK) complex would be activated (Moser et al., 2021), leading to IκBα phosphorylation, which could further promote the release of NF-κB and the degradation of the IκBα (Shen et al., 2019). Scutellarin could inhibit the activated IKK, thereby preventing the degradation and phosphorylation of IκBα (Peng et al., 2020; Park et al., 2022). As a consequence, scutellarin could make NF-κB binding to IκBα in the cytoplasm, and the inactivated NF-κB cannot exert its effects (Lu et al., 2021; Xu et al., 2021).

3.1.2 Prevention of NF-κB nuclear translocation

NF-κB translocation from the cytoplasm to the nucleus is necessary for inflammatory gene transcription. Scutellarin inhibited the nuclear translocation of the p65 subunit by stabilizing IκBα (Giridharan and Srinivasan, 2018). Studies indicated that the nuclear distribution of NF-κB p65 subunit was mainly present in the cytoplasm after scutellarin treatment (Wang et al., 2011; You et al., 2018). Scutellarin prevented nuclear translocation of NF-κB and thus inhibited its activity (Peng et al., 2020).

3.1.3 Reduction of NF-κB target gene expression

After entering into the nucleus, NF-κB activated transcription of a set of inflammatory genes (Alharbi et al., 2021). Scutellarin suppressed the expression of these inflammatory genes to attenuate inflammation. It has been shown that scutellarin significantly reduced LPS-induced mRNA and protein levels of IL-1β, IL-6, TNF-α, COX-2, and iNOS (Peng et al., 2020; Park et al., 2022; Aksit et al., 2023; Zhang et al., 2023; Duan et al., 2024). Scutellarin could alleviate the local and systemic inflammatory

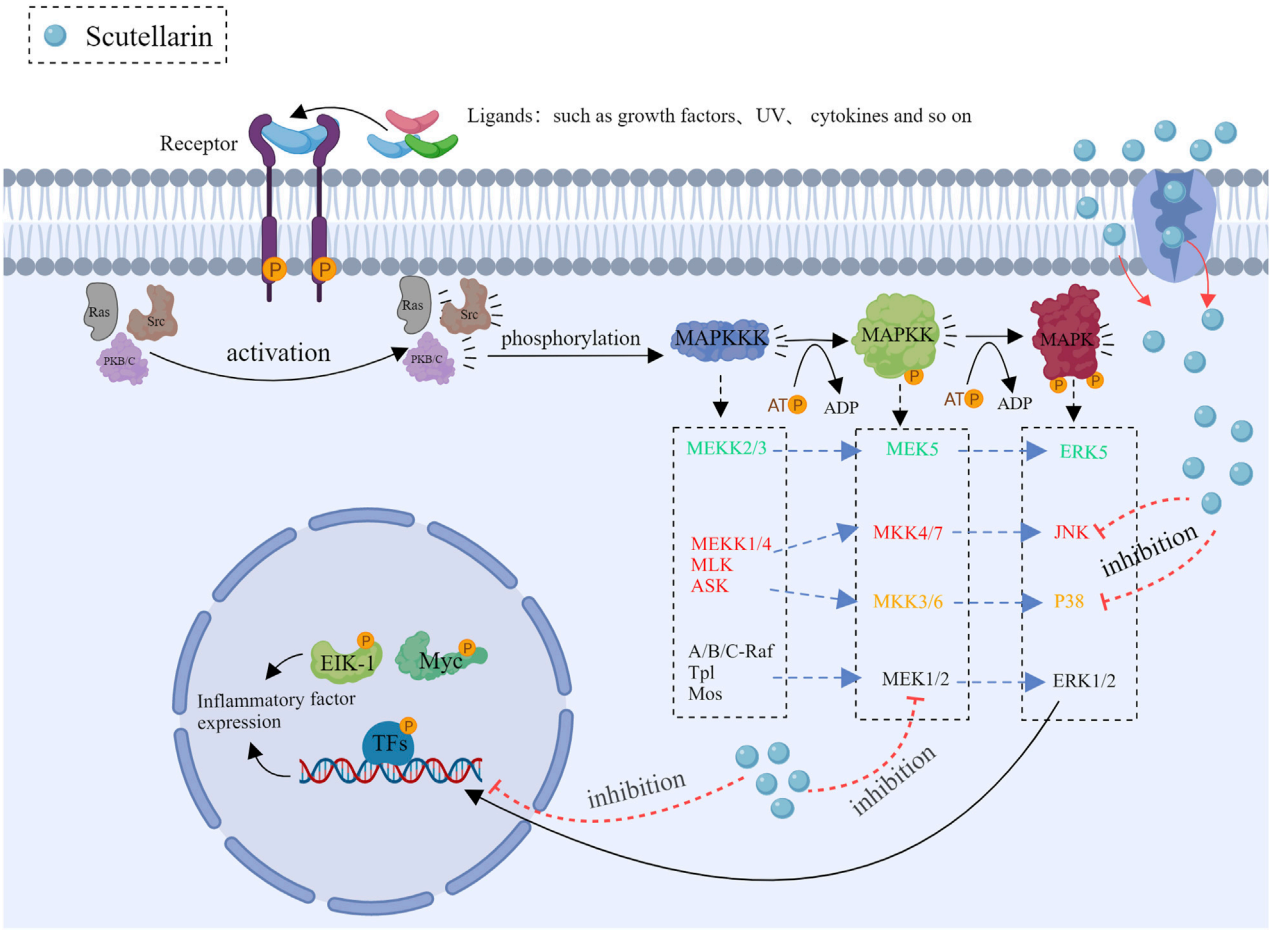

FIGURE 3
Mechanism diagram of scutellarin inhibiting the MAPK pathways, Created with MedPeer (medpeer.cn).

response through decreasing the expression of those pro-inflammatory mediators *in vivo* (Figure 2).

3.2 Inhibition of MAPK pathways

The major isozymes of the mitogen-activated protein kinase (MAPK) family included p38, JNK and ERK (Guo et al., 2020; Iroegbu et al., 2021; Van Gerrewey and Chung, 2024), the front two are closely related to inflammation. Scutellarin can be used as a therapeutic agent to inhibit inflammation by modulating the MAPK pathways.

3.2.1 Regulation of the JNK pathway

The JNK (c-Jun N-terminal kinase) signaling pathway is involved in cell stress response, apoptosis and inflammation. The JNK pathway is activated when cells are exposed to ultraviolet (UV) light, oxidative stress and cytokines (Liu B. et al., 2020). Upon activation, JNK can make the downstream transcription factor c-Jun phosphorylation, which plays a key role in gene expression associated with cell stress response or apoptosis. It has been demonstrated that dysregulated JNK signaling is closely related to numerous inflammatory diseases as well as cancers (Zhang et al., 2019). Scutellarin influenced the process of inflammation by regulating multiple factors of the JNK pathway. Scutellarin prevented JNK phosphorylation, thereby leading to the decrease in pro-inflammatory gene expression (You et al., 2018; Deng et al., 2024). Moreover, scutellarin also significantly reduced inflammation via inhibiting IL-1β and TNF-α production (You et al., 2018; Sun et al., 2019; Chen H. L. et al., 2020).

3.2.2 Regulation of the p38 pathway

The p38 pathway plays a key role in cellular stress response and inflammation (Yong et al., 2009). It is activated by stress kinases such as MKK3 and MKK6 (Rossa et al., 2006), which phosphorylate and activate downstream effector proteins, thereby affecting the production of inflammatory factors, cell proliferation, differentiation, and apoptosis. Scutellarin regulates the p38 pathway through various specific mechanisms, thereby exerting its anti-inflammatory effects (You et al., 2018). Scutellarin can also reduce the phosphorylation levels of transcription factors ATF2 and CHOP, causing the low expression of inflammatory genes (Wang Z. et al., 2022). Together, these results demonstrated that scutellarin could exert

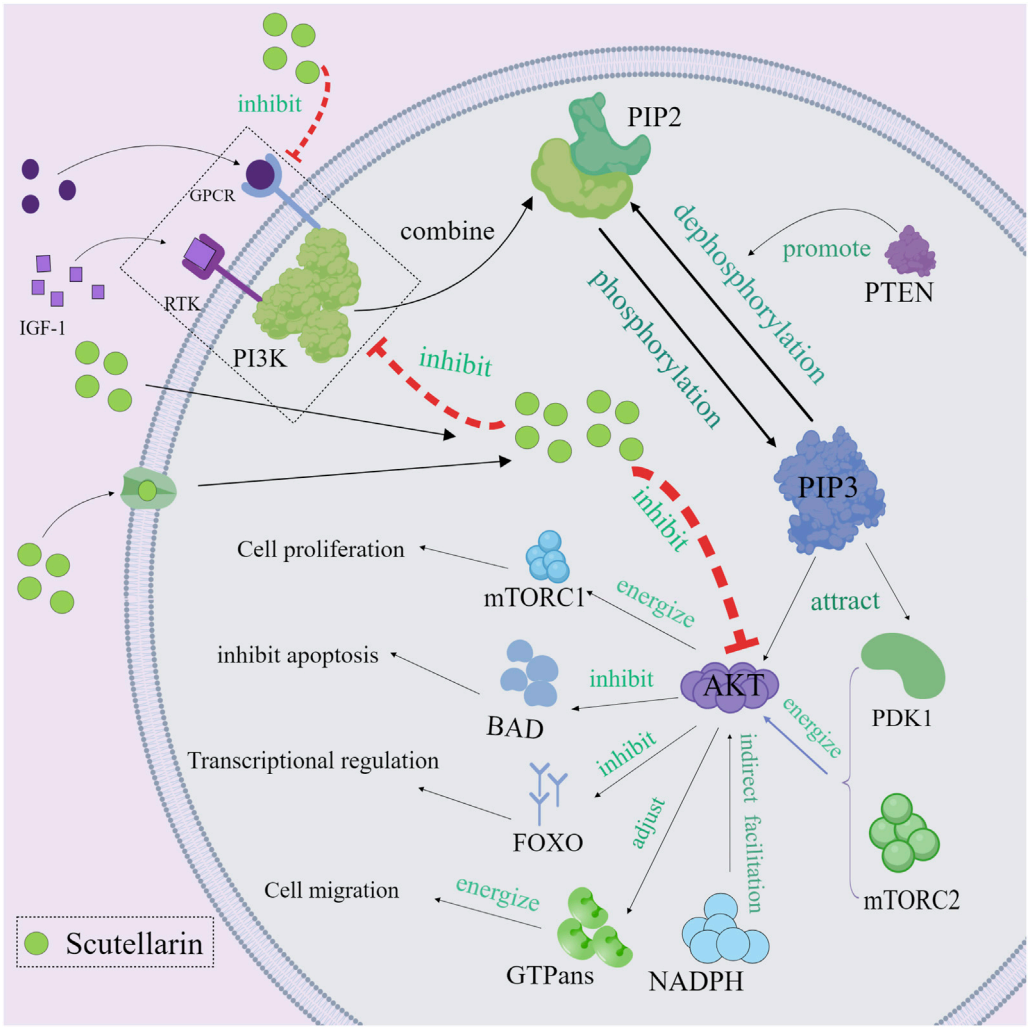

FIGURE 4
Mechanism diagram of scutellarin regulating of PI3K/Akt Pathway, Created with MedPeer (medpeer.cn).

the potent anti-inflammation effects through regulating p38 pathway (Figure 3).

3.3 Regulation of PI3K/Akt Pathway

The phosphatidylinositol 3-kinase/protein kinase B (PI3K/Akt) pathway plays a critical role in cell growth, survival, proliferation, and metabolism (Yong et al., 2009; Deng and Zhou, 2023). Aberrant activation of the PI3K/Akt pathway is strongly associated with cancer and inflammatory diseases (Alzahrani, 2019; Ghafouri-Fard et al., 2021). Scutellarin exerted the anti-inflammatory and anti-cancer effects through regulating the PI3K/Akt pathway (Wang et al., 2019; Hu et al., 2022). Mechanistically, receptor phosphorylation recruits and activates PI3K, which phosphorylates PIP2 to PIP3 (Carnero et al., 2008). The PH structural domain of Akt binds to PIP3, which recruits Akt to the cell membrane, thereby localizing Akt to the cell membrane and activating it. Akt is then phosphorylated and activated by pyruvate dehydrogenase kinase, isozyme 1 (PDK1) and mechanistic target of rapamycin complex 2 (mTORC2) (Xu et al., 2020). The fully activated Akt then enters the cytoplasm or nucleus to phosphorylate its downstream effector proteins. Scutellarin could inhibit PI3K activity, prevent phosphatidylinositol 4,5-bisphosphate 3 (PIP3) production, reduce Akt membrane localization, and directly inhibit Akt phosphorylation (Zhang et al., 2023). In this way, Akt could not be effectively phosphorylated, leading to the inactivated downstream effector proteins (mTOR, Bax, etc.) (Ju et al., 2021; Wang Z. et al., 2022). mTOR could promote the production of pro-inflammatory cytokines (such as IL-6 and TNF-α) by regulating translation factors 4E-BP1 and S6K. Therefore, inhibiting mTOR activity can reduce the expression of pro-inflammatory cytokines and alleviate the inflammatory response. Many current studies have discovered that scutellarin greatly reduced Akt-mediated pro-inflammatory cytokines such as TNF-α, IL-1β and IL-6, thereby attenuating the inflammatory response and tissue damage (Figure 4).

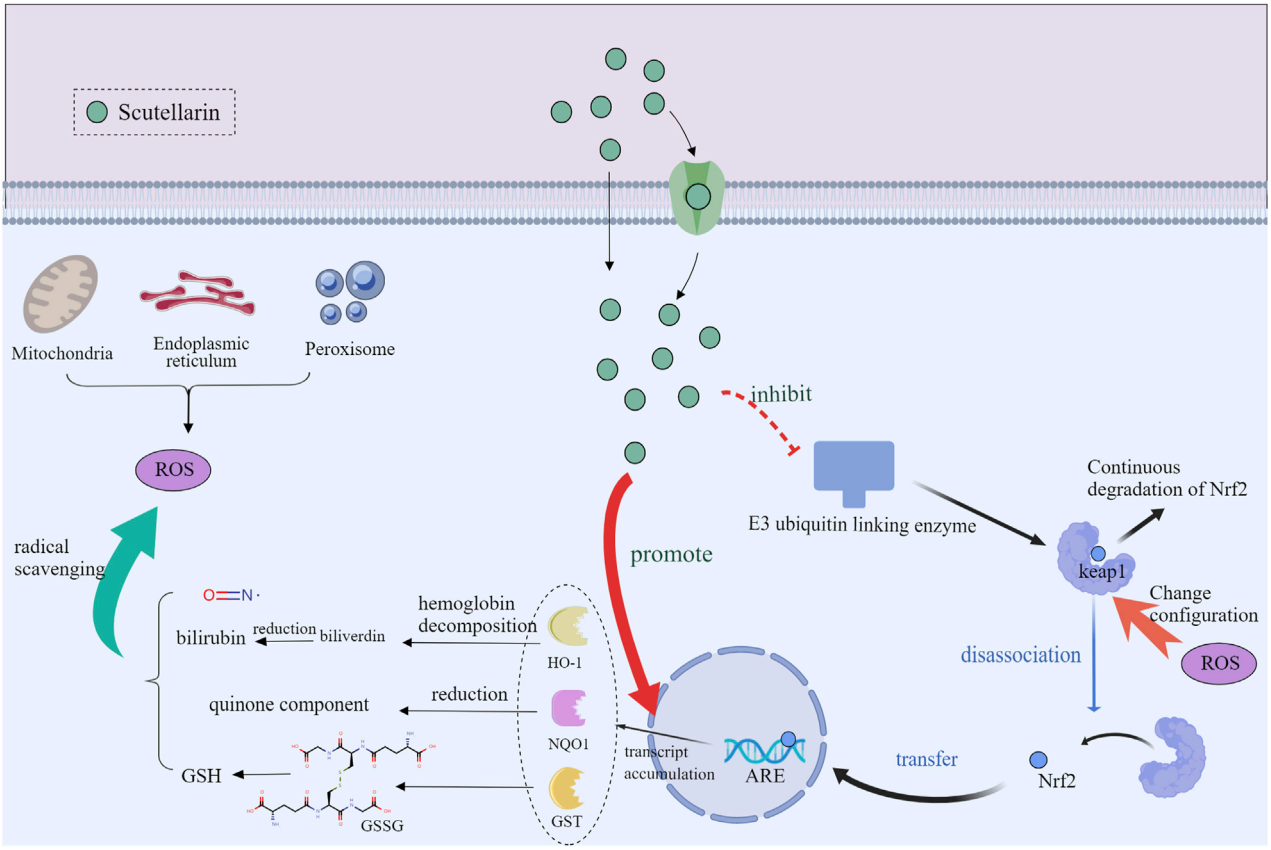

FIGURE 5
Mechanism diagram of scutellarin regulating of Nrf2/ARE Pathway, Created with MedPeer (medpeer.cn).

3.4 Activation of Nrf2/ARE pathway

The nuclear factor E2-associated factor 2/anti-oxidant response element (Nrf2/ARE) pathway is a key regulatory mechanism for cellular anti-oxidant and detoxification responses (Zgorzynska et al., 2021). Normally, Nrf2 is inhibited by kelch-like ECH-associated protein 1 (Keap1) protein and localized in the cytoplasm (Panieri and Saso, 2021; Song et al., 2021). Under oxidative stress or electrophilic conditions, Nrf2 is released from Keap1 and translocated to the nucleus. It has been shown that scutellarin promoted the nuclear translocation and release of Nrf2 by interfering with the interaction between Nrf2 and Keap1 (Li J. et al., 2023; Shahmohammadi et al., 2023). After entering the nucleus, Nrf2 initiates transcription of anti-oxidant genes through binding to ARE. Activated Nrf2 regulates the expression of a range of anti-oxidant, detoxification and anti-inflammation enzymes, such as heme oxygenase-1 (HO-1) (Zhang et al., 2023) and superoxide dismutase (SOD) (Shahmohammadi et al., 2023; Xie et al., 2023). By triggering the Nrf2/ARE pathway, scutellarin increases the expression levels of these anti-oxidant enzymes, which enhances cellular anti-oxidant capacity and protects cells from oxidative stress toxic damage and inflammation (Figure 5).

4 Specific role of scutellarin in inflammation-related diseases

Due to the obvious anti-inflammation and anti-oxidative effects, scutellarin has been used to treat osteoarthritis, pulmonary fibrosis, kidney injury and cardiovascular diseases (Table 2).

4.1 Osteoarthritis

Osteoarthritis (OA), an age-related degenerative joint disease (Panieri and Saso, 2021), is characterized by the subchondral bone remodeling, progressive degradation of cartilage, chronic pain and synovitis (Ruan et al., 2023). OA is a complex joint disorder, inflammation and oxidative stress are the main etiologies of this disease (Zahan et al., 2020). Several *in vivo* and *in vitro* studies have discovered that scutellarin was effective in inhibiting the progression of OA. For example, scutellarin significantly reduced cartilage tissue loss and lowered osteoarthritis research society international (OARSI) score in destabilization of medial meniscus (DMM) model mice, showing good therapeutic potential (Yi et al., 2021). Mechanistically, scutellarin reduced the expression of inflammatory cytokines and the nuclear translocation of β-catenin through regulating NF-κB, MAPK (Yang et al., 2022), and Wnt/β-catenin pathways (Liu F. et al., 2020), thereby protecting the cartilage matrix

TABLE 2 Mechanisms and modulation of scutellarin for the treatment of inflammation-related diseases.

Inflammation-related Diseases	Mechanism of action	Trends in action	Refs
Pulmonary fibrosis	NF-κB/NLRP3-mediated epithelial–mesenchymal transition and inflammation (−)	p-p65/p65, IκBα, NLRP3, CASP1, ASC, IL-1β, IL-18, GSDMDN, FN, VIM, CDH2, MMP-2, MMP-9↓	Peng et al. (2020)
Osteoarthritis (OA)	Reverse collagen II and aggrecan degradation; Nrf2 and NF-κB signaling pathways (−)	MMP-13, ADAMTS-5, COX-2, iNOS, IL-6, TNF-α, PGE2↓	Luo et al. (2020)
	MAPK and Wnt/β-catenin signaling pathways (−)	MMP1, MMP13, ADAMTS-5, Wnt3a↓; COL2A1, ACAN↑	Liu et al. (2020b)
	TLR4/NF-κB pathways (−)	IL-1β, TNF-α, IL-6, SOD, MDA, ICAM-1, MCP-1, CASP3, Bax/Bcl-2, TLR4↓	Zhang et al. (2017)
	NF-κB and PI3K/AKT signaling pathways (−)	IL-1β, iNOS, MMP13, ADAMTS-5, COX-2, IL-6↓	Wang et al. (2019)
	NF-κB/MAPK signaling pathways (−)	MMP3, MMP9, MMP13, ADAMTS4, ADAMTS5↓	Yang et al. (2022)
	PI3K/AKT/mTOR signaling pathways (−)	COL2A1, SOX9, IL-6 APOA1, ABCA1↑; MMP13, CH25H, CYP7B1, AKT, p-AKT, mTOR, p-mTOR↓	Ju et al. (2021)
Colitis	pro-inflammatory cytokines (−); apoptosis and oxidative stress (−)	MDA, NO, IL-6, TNF-α, Bax↓; SOD, TAS, Bcl-2↑	Aksit et al. (2023)
Colitis-associated colorectal cancer	Hedgehog signaling pathway (−)	proliferation, migration, colony formation↓	Zeng et al. (2022)
Rheumatoid arthritis (RA)	Regulate the Keap1/Nrf2/HO-1 pathways	IgG, IgE, TNF-α, IL-1β, IL-6, Th1/Th2, HO-1↓; Keap1, Nrf2↑	Li et al. (2023a)
Cerebral ischemia/reperfusion damage	Regulate MAPK signaling Pathway	TNF-α, IL-1β, p-JNK, p-p38, iNOS↓; p-ERK1/2↑	Chen et al. (2020a)
	PI3K/Akt pathway (+)	Nrf2, HO-1, SOD↑; ROS, NF-κB↓	Xie et al. (2023)
	Inflammatory responses and oxidative stress (−); MAPK/NF-κB pathways (−)	MDA, SOD, GSH, IL-6, IL-1β, NO, p65, p38↓	Zhang et al. (2022)
Renal ischemia–reperfusion injury	MAPK pathway (−); Pro-inflammatory macrophage polarization (−)	ERK, p38, JNK↓	Deng et al. (2024)
Myocardial ischemia–reperfusion injury	NLRP3 inflammasome activation (−); Akt/mTORC1/NLRP3 signaling pathways (−)	LDH, CK-MB, Myo, ALT, IL-1β, IL-18, cas1, IL-1β, NLRP3, TNF-α↓	Xu et al. (2020)
Cognitive deficits	Alleviate LPS-induced cognitive disturbances	AChE, TNF-α, IL-6, Nrf2, LC3 II, mTOR, P62↓	Baluchnejadmojarad et al. (2018)
Neuroinflammation-astrocyte	TLR4/NF-κB pathways (−)	TNF-α, IL-1β, IL-6, iNOS↓; IL-4, BDNF↑	Lu et al. (2021)
Neuroinflammation-Macrophages	NLRP3 Inflammasome Activation in Macrophages (−)	CASP1, IL-1β↓	Liu et al. (2017b)
Neuroinflammation-microglia	Mitigate microglia inflammation; mir-7036a-5p/MAPT/PRKCG/ERK signaling pathways (−)	Mir-7036a-5p, TNF-α, IL-1β, iNOS↓	Duan et al. (2024)
	Neuroinflammation and microglia activation (−)	NLRP3, CASP1, IL-1β↓	Bian et al. (2020)
	Neuroinflammation (−); AKT/NF-κB and p38/JNK pathways (−)	TNF-α, NO, IL-6, IL-1β, iNOS↓	You et al. (2018)
Neuroinflammation-microglia, astrocyte	Microglia inflammatory activation (−)	NO, TNF-α, IL-1, ROS, iNOS, NF-κB, JNK, ERK↓	Wang et al. (2011)
Kidney injury	Inflammation and oxidative stress (−); regulate Nrf2/PPAR-c/PGC-1a/NF-κB/TLR4 pathways	BUN, ROS, MDA, IL-10, TLR4, NF-κB, TNF-α↓; Nrf2, HO-1↑	Shahmohammadi et al. (2023)
	NLRP3 inflammasome activation (−)	BUN, SCr, Kim-1, IL-18, NGAL, Cys-C↓	Li et al. (2020)
Asthma	Smad/MAPK pathways (−)	CDH1↑, CDH2, α-SMA↓	Li et al. (2024a)
Foam cell	Autophagy (+); NLRP3 inflammasome activation (−)	Plin2, LC3B-II, Map1lc3b, Becn1↑	Gao et al. (2024)
Intervertebral disc degeneration	Regulate Rab8a *via* the PI3K/PTEN/Akt pathway	p62↓, Beclin-1, Rab8a, ATG5↑	Hu et al. (2022)
	NLRP3 inflammasome activation (−); NF-κB/MAPK signaling pathways (−)	p-p38, p-JNK↓; p-ERK1/2↑	Wang et al. (2022b)

Annotation "+": activate; "-": suppress; "↑": increase/upregulated; "↓": reduce/downregulate.

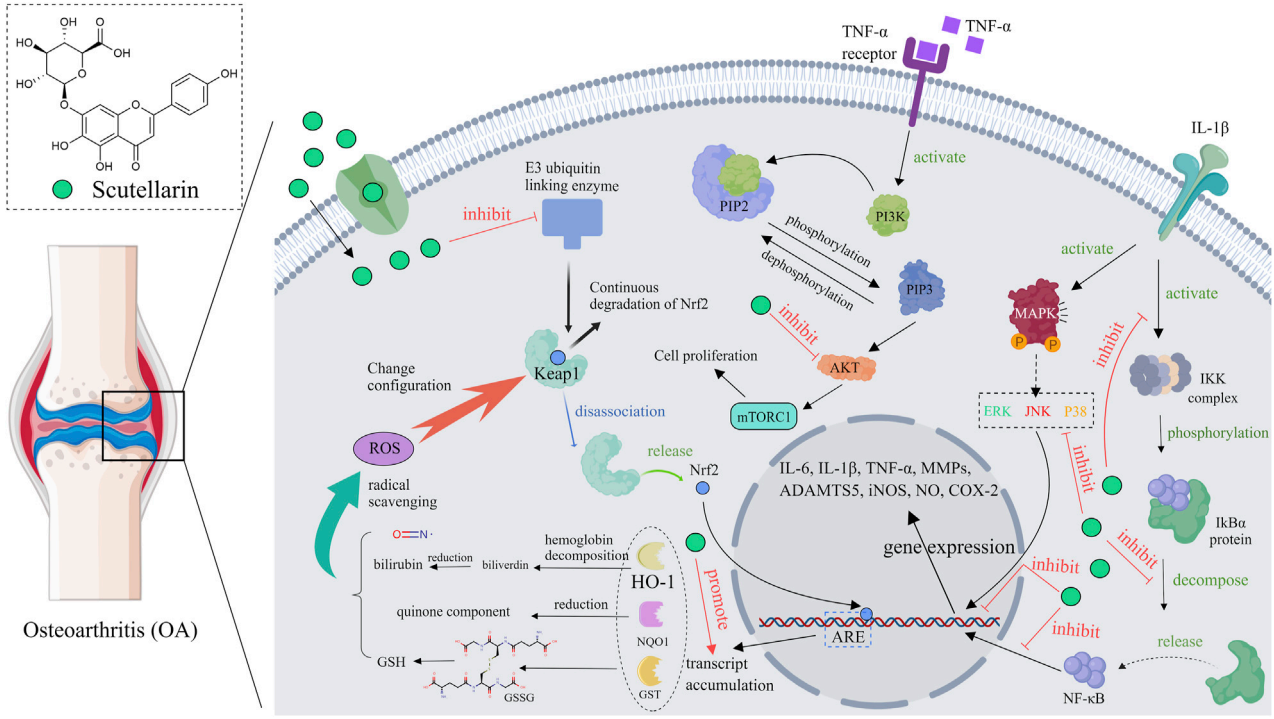

FIGURE 6
Diagram of the mechanism of action of scutellarin in the treatment of osteoarthritis, Created with MedPeer (medpeer.cn).

from degradation. Moreover, scutellarin can slow down the progression of osteoarthritis by reducing inflammation-related protein expression in chondrocytes, which may be attributed to its inhibitory effect on the PI3K/AKT/mTOR pathway (Ju et al., 2021). Scutellarin can also enhance the expression of Nrf2 dependent HO-1 by binding to Nrf2, thus reducing inflammation and matrix degradation (Luo et al., 2020). As high cholesterol levels are the high risks of OA, scutellarin can reduce the progression of OA through regulating cholesterol metabolism related proteins (CH25H, CYP7B1, ABCA1, and APOA-1) (Choi et al., 2019), In summary, scutellarin has potential therapeutic value in the treatment of OA by inhibiting the NF-κB, MAPK, PI3K/AKT/mTOR, and Wnt/β-catenin pathways, as well as regulating the expression of cholesterol metabolism related proteins (Figure 6).

4.2 Pulmonary fibrosis

Pulmonary fibrosis is an irreversible lung disease characterized by collagen deposition in the alveolar spaces. Inflammatory response and oxidative stress are closely related to the pathogenesis of pulmonary fibrosis (Liu M. H. et al., 2017). Research has shown that scutellarin can alleviate the inflammatory response of pulmonary fibrosis by inhibiting the production of various inflammatory factors (Peng et al., 2020). Scutellarin has significant anti-pulmonary fibrosis effects by acting on the TGF-β/Smad and NF-κB signaling pathways (Liu et al., 2019) Furthermore, scutellarin can directly inhibit the activation, proliferation, and production of collagen in fibroblasts (Luo et al., 2020), thus slowing down the pathological process of pulmonary fibrosis (Liu et al., 2019; Ma et al., 2020). Scutellarin can also alleviate lung tissue damage caused by oxidative stress *via* activating the Nrf2/ARE signaling pathway, and increasing the expression of anti-oxidant related enzymes (SOD, CAT, and HO-1, etc.) (Hao et al., 2023). Some studies have shown that scutellarin can reduce the expression levels of fibronectin, MMPs, and TIMP (Peng et al., 2020), thereupon then prevent extracellular matrix (ECM) deposition and maintain lung structure (Zhou et al., 2019). In summary, scutellarin reduces ECM deposition by blocking the production of inflammatory factors, reducing oxidative stress, and inhibiting fibroblast proliferation, thereby playing a therapeutic role in pulmonary fibrosis. These mechanisms reveal the broad prospects of scutellarin in the treatment of pulmonary fibrosis.

4.3 Kidney injury

Kidney injury is a common clinical syndrome characterized by decreased renal function resulting from the accumulation of metabolic waste and toxins in the body (Li et al., 2022). Inflammatory response and oxidative stress play key roles in the pathogenesis of kidney injury (Andrianova et al., 2020). Scutellarin inhibits the production of pro-inflammatory cytokines by suppressing the NF-κB signaling pathway, thereby alleviating inflammatory damage to renal tissue (Liu et al., 2022). Scutellarin can also increase the expression of anti-oxidant enzymes (SOD, CAT, HO-1, etc.) by activating the Nrf2/ARE signaling pathway, thereby protecting kidney tissue from oxidative stress damage (Shahmohammadi et al., 2023). In addition, scutellarin protects renal function by inhibiting the PI3K/Akt pathway and reducing

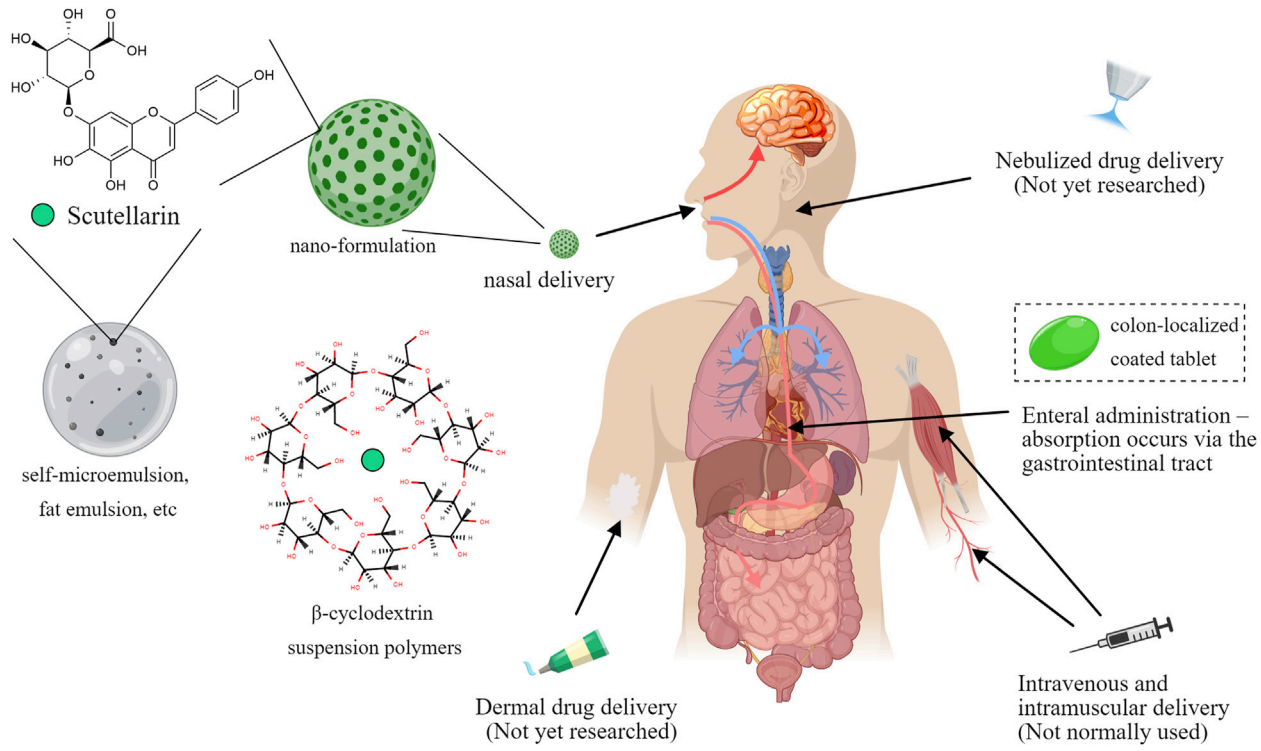

FIGURE 7
Forms and modes of administration of scutellarin, Created with MedPeer (medpeer.cn).

apoptosis of renal tubular epithelial cells (TECs) (Liu et al., 2022). TGF-β and Smad proteins can activate the production of fibrosis markers (collagen, fibronectin, etc.), while scutellarin can precisely inhibit the expression of TGF-β and Smad, and then reduced renal fibrosis (Wang H. et al., 2022). In summary, the effects of scutellarin on renal injury may be mediated through multiple pathways, such as inhibiting inflammation, oxidative stress, apoptosis of renal tubular epithelial cells, and renal fibrosis.

4.4 Cardiovascular diseases

Cardiovascular diseases (CVDs) are the leading cause of death and disability worldwide, closely associated with oxidative stress and inflammatory responses (Zhong et al., 2019). Scutellarin has anti-inflammatory and anti-oxidant properties, which can reduce the occurrence of CVDs. Scutellarin can inhibit the MAPK and NF-κB signaling pathways, thus reducing the inflammatory response caused by cardiovascular injury models (Zhang et al., 2022). Scutellarin can also reduce ROS production by activating the Nrf2/ARE signaling pathway, further alleviated oxidative stress-induced cardiovascular damage (Wang and Ma, 2018; Zhang et al., 2023). In addition, scutellarin can reduce the accumulation of lipids and the formation of foam cells (Gao et al., 2024), thereby reducing the generation of atherosclerosis. Remarkably, scutellarin can stabilize atherosclerotic plaque, reduce the risk of plaque rupture, and limit the occurrence of subsequent cardiovascular events (Xu et al., 2021). In summary, scutellarin has preventive and therapeutic effects on cardiovascular diseases by inhibiting the production of inflammatory factors, reducing oxidative stress levels, and stabilizing plaques.

5 Pharmacokinetic characterization of scutellarin and dosage form modification studies

Although scutellarin exerted strong anti-inflammatory activity in many cellular experiments, *in vivo* pharmacokinetic studies have indicated that scutellarin have some shortcomings for the treatment effects. The absolute oral bioavailability of scutellarin in Beagle dogs was reported to be 0.40% ± 0.19% (Ge et al., 2003), which was hardly absorbed. Scutellarin is also rapidly metabolized and excreted after intravenous injection, with a short elimination half-life of (52 ± 29) min (Jiang et al., 2003; Wu et al., 2021). Moreover, the chemical structure of scutellarin has phenolic hydroxyl group, it will be easy to produce precipitation in acidic solution. Studies have shown that flocculent precipitation could occur when scutellarin is dissolved in the infusion solution with pH < 3.8 (Xu et al., 2012), which implies that its absorption is reduced in gastrointestinal tract, partly explaining the low bioavailability.

To address the problem, more and more modern technologies have been gradually applied to improve the effectiveness of scutellarin. On the one hand, various special materials are used to improve the dosage form. For example, β-cyclodextrin suspension polymers are used as carriers to enhance the solubility of scutellarin (Liao et al., 2020); the triglyceride mimetic prodrug of scutellarin was designed to promote intestinal lymphatic transport and improve

oral bioavailability (Wang et al., 2021); liposome precursors of scutellarin were also prepared using liposome technology, which improved the stability of scutellarin *in vivo* and enhanced its bioavailability (Luo et al., 2019). Furthermore, other new dosage forms, such as encapsulation technology, self-microemulsion, and fat emulsion, have also been widely used in the study of scutellarin formulations, which have improved the bioavailability, solubility and safety of scutellarin (Tian et al., 2014). On the other hand, the drug targeting of scutellarin was also explored in various ways. For cerebrovascular diseases, the blood-brain barrier was a major pain point hindering drug action, for which administration *via* the nasal route has emerged (Liu and Ho, 2017). *In situ* gels based on nanosuspensions have been developed as intranasal delivery formulations of scutellarin and have been shown to improve its solubility and bioavailability, as well as prolong its retention time in the nasal cavity (Chen Y. et al., 2020). PLGA-PEG-AEAA nano-formulations of scutellarin have been developed to promote tumor delivery (Li L. et al., 2023). Besides, the traditional coating technology was also introduced to increase drug targeting. Scutellarin could be prepared as a colon-localized coated tablet, and the drug would be released on the colonic site at pH > 7.0, which significantly promoted the colon-targeted drug delivery (Li et al., 2013) (Figure 7).

6 Discussion

As a natural flavonoid, scutellarin possesses significant anti-inflammatory properties, and has been identified as a promising candidate drug for the treatment of multiple inflammation-related diseases. According to the existing publications, the anti-inflammatory effects of scutellarin could be attributed to acting on several key inflammation signaling pathways such as MAPK, NF-κB, and PI3K/Akt, which reduced the production of pro-inflammatory mediators and consequently attenuated inflammation (Chen H. L. et al., 2020; Liu F. et al., 2020). Scutellarin can inhibit the activation of NF-κB, thereby reducing the expression of TNF-α and IL-1β (Ju et al., 2021; Aksit et al., 2023; Li J. et al., 2023). In addition, scutellarin can exert anti-oxidant effects by triggering the Nrf2/ARE signaling pathway and increasing the expression of anti-oxidant enzymes, thus reducing cell damage caused by oxidative stress (Xie et al., 2023). These results indicated that scutellarin have potential application value in the prevention and treatment of various inflammation-related diseases, such as osteoarthritis (Wang et al., 2019; Liu F. et al., 2020; Zahan et al., 2020; Yang et al., 2022), pulmonary fibrosis (Hao et al., 2023), ischemia/reperfusion injury (Xie et al., 2023), cisplatin induced acute renal injury (Shahmohammadi et al., 2023), and diabetes induced cardiomyopathy (Xu et al., 2021).

According to the latest research results, the clinical application prospects of scutellarin are very broad. Scutellarin is a naturally extracted metabolite with good safety (Sun et al., 2019; Zhang et al., 2020), making it an ideal molecule for clinical applications. The multi-target ability of scutellarin makes it an anti-inflammatory drug with a wide range of pharmacological effects on complex inflammatory diseases (Peng et al., 2020). Researchers are currently researching new dosage form technologies to overcome the drawbacks caused by the properties of scutellarin, such as increasing the solubility and dissolution rate of scutellarin. These new dosage forms could not only increase the bioavailability, but also improve medication safety. However, there are still some problems in the dosage form studies, such as repetitive experiments, *in vivo* pharmacokinetics and drug release behavior studies. Hence, it is necessary to carry out in-depth studies on the *in vivo* pharmacokinetics and biopharmacy of the new dosage form. Moreover, the opening of new routes of drug delivery (transdermal, mucosal, nebulization, etc.) may bring new perspective to the drug development of scutellarin. Precision therapy should also be incorporated in the pre-clinical investigation of scutellarin using genomics and proteomics technologies.

In conclusion, scutellarin, as a typical flavonoid with multiple pharmacological effects and low toxicity, can be applied in anti-inflammatory, anti-oxidant and antitumor fields in the future. It is believed that scutellarin will play a prominent role in the treatment of various inflammatory diseases and provide new therapeutic options for patients through optimized formulations, combination therapies and in-depth studies on its mechanism.

Author contributions

YZh: Conceptualization, Data curation, Visualization, Writing–original draft, Writing–review and editing. CG: Conceptualization, Visualization, Software, Writing–original draft. YaZ: Software, Writing–original draft. YuZ: Writing–review and editing. YC: Writing–original draft. LS: Writing–original draft. YY: Writing–review and editing. XL: Writing–review and editing. HP: Conceptualization, Data curation, Funding acquisition, Visualization, Writing–original draft, Writing–review and editing.

Funding

The author(s) declare that financial support was received for the research, authorship, and/or publication of this article. This study is funded by the State Key Laboratory for Chemistry and Molecular Engineering of Medicinal Resources (Guangxi Normal University) (CMEMR2022-B11), the Natural Science Research of Jiangsu Higher education Institution of China (22KJB360018), and the China Postdoctoral Science Foundation (2024M752727).

Conflict of interest

The authors declare that the research was conducted in the absence of any commercial or financial relationships that could be construed as a potential conflict of interest.

Publisher's note

References

Aksit, H., Aksit, D., and Altun, E. (2023). Protective effects of scutellarin in experimental colitis in rats. *Biotech. Histochem* 98 (6), 432–444. doi:10.1080/10520295.2023.2224061

Alharbi, K. S., Fuloria, N. K., Fuloria, S., Rahman, S. B., Al-Malki, W. H., Javed Shaikh, M. A., et al. (2021). Nuclear factor-kappa B and its role in inflammatory lung disease. *Chem. Biol. Interact.* 345, 109568. doi:10.1016/j.cbi.2021.109568

Alzahrani, A. S. (2019). PI3K/Akt/mTOR inhibitors in cancer: at the bench and bedside. *Semin. Cancer Biol.* 59, 125–132. doi:10.1016/j.semcancer.2019.07.009

Andrianova, N. V., Zorov, D. B., and Plotnikov, E. Y. (2020). Targeting inflammation and oxidative stress as a therapy for ischemic kidney injury. *Biochem. (Mosc)* 85 (12), 1591–1602. doi:10.1134/s0006297920120111

Baluchnejadmojarad, T., Zeinali, H., and Roghani, M. (2018). Scutellarin alleviates lipopolysaccharide-induced cognitive deficits in the rat: insights into underlying mechanisms. *Int. Immunopharmacol.* 54, 311–319. doi:10.1016/j.intimp.2017.11.033

Barnabei, L., Laplantine, E., Mbongo, W., Rieux-Laucat, F., and Weil, R. (2021). NF-κB: at the borders of autoimmunity and inflammation. *Front. Immunol.* 12, 716469. doi:10.3389/fimmu.2021.716469

Bian, H. T., Wang, G. H., Huang, J. J., Liang, L., Xiao, L., and Wang, H. L. (2020). Scutellarin protects against lipopolysaccharide-induced behavioral deficits by inhibiting neuroinflammation and microglia activation in rats. *Int. Immunopharmacol.* 88, 106943. doi:10.1016/j.intimp.2020.106943

Cao, P., Liu, B., Du, F., Li, D., Wang, Y., Yan, X., et al. (2019). Scutellarin suppresses proliferation and promotes apoptosis in A549 lung adenocarcinoma cells via AKT/mTOR/4EBP1 and STAT3 pathways. *Thorac. Cancer* 10 (3), 492–500. doi:10.1111/1759-7714.12962

Carnero, A., Blanco-Aparicio, C., Renner, O., Link, W., and Leal, J. F. (2008). The PTEN/PI3K/AKT signalling pathway in cancer, therapeutic implications. *Curr. Cancer Drug Targets* 8 (3), 187–198. doi:10.2174/156800908784293659

Chen, H. L., Jia, W. J., Li, H. E., Han, H., Li, F., Zhang, X. L., et al. (2020a). Scutellarin exerts anti-inflammatory effects in activated microglia/brain macrophage in cerebral ischemia and in activated BV-2 microglia through regulation of MAPKs signaling pathway. *Neuromolecular Med.* 22 (2), 264–277. doi:10.1007/s12017-019-08582-2

Chen, Y., Liu, Y., Xie, J., Zheng, Q., Yue, P., Chen, L., et al. (2020b). Nose-to-Brain delivery by nanosuspensions-based *in situ* gel for breviscapine. *Int. J. Nanomedicine* 15, 10435–10451. doi:10.2147/ijn.S265659

Chledzik, S., Strawa, J., Matuszek, K., and Nazaruk, J. (2018). Pharmacological effects of scutellarin, an active component of genus Scutellaria and Erigeron: a systematic review. *Am. J. Chin. Med.* 46 (2), 319–337. doi:10.1142/s0192415x18500167

Choi, W. S., Lee, G., Song, W. H., Koh, J. T., Yang, J., Kwak, J. S., et al. (2019). The CH25H-CYP7B1-RORα axis of cholesterol metabolism regulates osteoarthritis. *Nature* 566 (7743), 254–258. doi:10.1038/s41586-019-0920-1

Deng, G., Zheng, B., Dou, M., Gao, Y., Zhang, X., Niu, Z., et al. (2024). Scutellarin alleviates renal ischemia-reperfusion injury by inhibiting the MAPK pathway and pro-inflammatory macrophage polarization. *Faseb J.* 38 (13), e23769. doi:10.1096/fj.202302243R

Deng, R. M., and Zhou, J. (2023). The role of PI3K/AKT signaling pathway in myocardial ischemia-reperfusion injury. *Int. Immunopharmacol.* 123, 110714. doi:10.1016/j.intimp.2023.110714

Duan, Z., Yang, L., Xu, D., Qi, Z., Jia, W., and Wu, C. (2024). Scutellarin attenuates microglia activation in LPS-induced BV-2 microglia via miRNA-7036a/MAPT/PRKCG/ERK Axis. *Adv. Biol. (Weinh)* 8, e2400123. doi:10.1002/adbi.202400123

Gao, W. C., Yang, T. H., Wang, B. B., Liu, Q., Li, Q., Zhou, X. H., et al. (2024). Scutellarin inhibits oleic acid induced vascular smooth muscle foam cell formation via activating autophagy and inhibiting NLRP3 inflammasome activation. *Clin. Exp. Pharmacol. Physiol.* 51 (4), e13845. doi:10.1111/1440-1681.13845

Ge, Q., Zhou, Z., Zhi, X., Ma, L., and Chen, X. (2003). Determination of sulfadiazine zinc by HPLC. *Chin. J. Pharm.* (12), 28–30.

Georgieva, Y., Katsarova, M., Stoyanov, P., Mladenov, R., Denev, P., Teneva, D., et al. (2020). Metabolite profile and anti-oxidant activity of some species of genus Scutellaria growing in Bulgaria. *Plants (Basel)* 10 (1), 45. doi:10.3390/plants10010045

Georgieva, Y. P., Gardjeva, P. A., Katsarova, M. N., Bozov, P. I., Gercheva, K. P., Murdjeva, M. A., et al. (2022). A study of flavonoid composition and antimicrobial activity of Scutellaria altissima L. from different floristic regions of Bulgaria. *Folia Med. Plovdiv.* 64 (4), 617–623. doi:10.3897/folmed.64.e64795

Ghafouri-Fard, S., Abak, A., Tondro Anamag, F., Shoorei, H., Majidpoor, J., and Taheri, M. (2021). The emerging role of non-coding RNAs in the regulation of PI3K/AKT pathway in the carcinogenesis process. *Biomed. Pharmacother.* 137, 111279. doi:10.1016/j.biopha.2021.111279

Giridharan, S., and Srinivasan, M. (2018). Mechanisms of NF-κB p65 and strategies for therapeutic manipulation. *J. Inflamm. Res.* 11, 407–419. doi:10.2147/jir.S140188

Goodman, S. B., Pajarinen, J., Yao, Z., and Lin, T. (2019). Inflammation and bone repair: from particle disease to tissue regeneration. *Front. Bioeng. Biotechnol.* 7, 230. doi:10.3389/fbioe.2019.00230

Guo, Y. J., Pan, W. W., Liu, S. B., Shen, Z. F., Xu, Y., and Hu, L. L. (2020). ERK/MAPK signalling pathway and tumorigenesis. *Exp. Ther. Med.* 19 (3), 1997–2007. doi:10.3892/etm.2020.8454

Hao, C., Chen, L., Dong, H., Xing, W., Xue, F., and Cheng, Y. (2020). Extraction of flavonoids from scutellariae radix using ultrasound-assisted deep eutectic solvents and evaluation of their anti-inflammatory activities. *ACS Omega* 5 (36), 23140–23147. doi:10.1021/acsomega.0c02898

Hao, W., Yu, T. T., Zuo, D. Z., Hu, H. Z., and Zhou, P. P. (2023). Stevioside attenuates bleomycin-induced pulmonary fibrosis by activating the Nrf2 pathway and inhibiting the NF-κB and TGF-β1/Smad2/3 pathways. *Exp. Lung Res.* 49 (1), 205–219. doi:10.1080/01902148.2023.2286465

Henein, M. Y., Vancheri, S., Longo, G., and Vancheri, F. (2022). The role of inflammation in cardiovascular disease. *Int. J. Mol. Sci.* 23 (21), 12906. doi:10.3390/ijms232112906

Hu, S., Zou, Y., Jiang, Y., Zhang, Q., Cheng, H., Wang, H., et al. (2022). Scutellarin-mediated autophagy activates exosome release of rat nucleus pulposus cells by positively regulating Rab8a via the PI3K/PTEN/Akt pathway. *Cell. Biol. Int.* 46 (10), 1588–1603. doi:10.1002/cbin.11838

Huck, D. M., Buckley, L. F., Chandraker, A., Blankstein, R., and Weber, B. (2024). Targeting pharmacotherapies for inflammatory and cardiorenal endpoints in kidney disease. *J. Cardiovasc Pharmacol.* 83 (6), 511–521. doi:10.1097/fjc.0000000000001482

Iroegbu, J. D., Ijomone, O. K., Femi-Akinlosotu, O. M., and Ijomone, O. M. (2021). ERK/MAPK signalling in the developing brain: perturbations and consequences. *Neurosci. Biobehav Rev.* 131, 792–805. doi:10.1016/j.neubiorev.2021.10.009

Irvin, L., Jackson, C., Hill, A. L., Bajaj, R., Mahmoudi, C., Vaidya, B. N., et al. (2019). Skullcaps (Scutellaria spp.): ethnobotany and current research. *Med. Plants Farm Pharm.*, 141–168. doi:10.1007/978-3-030-31269-5_7

Jiang, P., Hu, K., Jin, L., and Luo, Z. (2024). A brief review of current treatment options for osteoarthritis including disease-modifying osteoarthritis drugs (DMOADs) and novel therapeutics. *Ann. Med. Surg. (Lond)* 86 (7), 4042–4048. doi:10.1097/ms9.0000000000002214

Jiang, X., Li, S., Lan, K., Yang, J., and Zhou, J. (2003). Study on the pharmacokinetics of scutellarin in dogs. *Acta Pharm. Sin.* 38 (05), 371–373. doi:10.16438/j.0513-4870.2003.05.013

Ju, S., Tan, L., Liu, P., Tan, Y., Zhang, Y., Li, X., et al. (2021). Scutellarin regulates osteoarthritis *in vitro* by inhibiting the PI3K/AKT/mTOR signaling pathway. *Mol. Med. Rep.* 23 (1), 83. doi:10.3892/mmr.2020.11722

Li, G., Guan, C., Xu, L., Wang, L., Yang, C., Zhao, L., et al. (2020). Scutellarin ameliorates renal injury via increasing CCN1 expression and suppressing NLRP3 inflammasome activation in hyperuricemic mice. *Front. Pharmacol.* 11, 584942. doi:10.3389/fphar.2020.584942

Li, H., Luo, S., Su, J., Ke, H., Wang, W., and Yang, B. (2015). Optimization of extraction conditions for flavonoid composition and anti-oxidant activity of radix scutellariae. *Anal. Lett.* 48 (8), 1234–1244. doi:10.1080/00032719.2014.979360

Li, J., Wang, Q., and Zhang, X. (2023a). Scutellarin alleviates complete freund's adjuvant-induced rheumatoid arthritis in mice by regulating the Keap1/Nrf2/HO-1 pathway. *BIOCELL* 47 (6), 1307–1316. doi:10.32604/biocell.2023.028714

Li, L., Zou, Y., Wang, L., Yang, L., Li, Y., Liao, A., et al. (2023b). Nanodelivery of scutellarin induces immunogenic cell death for treating hepatocellular carcinoma. *Int. J. Pharm.* 642, 123114. doi:10.1016/j.ijpharm.2023.123114

Li, M., Jia, D., Li, J., Li, Y., Wang, Y., Wang, Y., et al. (2024a). Scutellarin alleviates ovalbumin-induced airway remodeling in mice and TGF-β-induced pro-fibrotic phenotype in human bronchial epithelial cells via MAPK and smad2/3 signaling pathways. *Inflammation* 47 (3), 853–873. doi:10.1007/s10753-023-01947-7

Li, S., Wang, R., Wang, Y., Liu, Y., Qiao, Y., Li, P., et al. (2022). Ferroptosis: a new insight for treatment of acute kidney injury. *Front. Pharmacol.* 13, 1065867. doi:10.3389/fphar.2022.1065867

Li, Y., Wang, J., Yang, D., Dong, M., and Gong, Y. (2013). Evaluation on preparation process of breviscapine colon-specific tables and its *in vitro* release. *Chin. J. Chin. Mater Med.* 38 (06), 817–820. doi:10.4268/cjcmm20130608

Li, Z., Yang, Y., and Gao, F. (2024b). Monomeric compounds from natural products for the treatment of pulmonary fibrosis: a review. *Inflammopharmacology*. doi:10.1007/s10787-024-01485-0

Liao, R., Liu, Y., Lv, P., Wu, D., Xu, M., and Zheng, X. (2020). Cyclodextrin pendant polymer as an efficient drug carrier for scutellarin. *Drug Deliv.* 27 (1), 1741–1749. doi:10.1080/10717544.2020.1856223

Liu, B., Hou, Q., Ma, Y., and Han, X. (2020a). HIPK3 mediates inflammatory cytokines and oxidative stress markers in monocytes in a rat model of sepsis through the JNK/c-Jun signaling pathway. *Inflammation* 43 (3), 1127–1142. doi:10.1007/s10753-020-01200-5

Liu, B., Rong, Y., Sun, D., Li, W., Chen, H., Cao, B., et al. (2019). Costunolide inhibits pulmonary fibrosis via regulating NF-kB and TGF-β_1/$Smad_2$/Nrf_2-NOX_4 signaling pathways. *Biochem. Biophys. Res. Commun.* 510 (2), 329–333. doi:10.1016/j.bbrc.2019.01.104

Liu, F., Li, L., Lu, W., Ding, Z., Huang, W., Li, Y. T., et al. (2020b). Scutellarin ameliorates cartilage degeneration in osteoarthritis by inhibiting the Wnt/β-catenin and MAPK signaling pathways. *Int. Immunopharmacol.* 78, 105954. doi:10.1016/j.intimp.2019.105954

Liu, M. H., Lin, A. H., Ko, H. K., Perng, D. W., Lee, T. S., and Kou, Y. R. (2017a). Prevention of bleomycin-induced pulmonary inflammation and fibrosis in mice by paeonol. *Front. Physiol.* 8, 193. doi:10.3389/fphys.2017.00193

Liu, S., and Ho, P. C. (2017). Intranasal administration of brain-targeted HP-β-CD/chitosan nanoparticles for delivery of scutellarin, a compound with protective effect in cerebral ischaemia. *J. Pharm. Pharmacol.* 69 (11), 1495–1501. doi:10.1111/jphp.12797

Liu, X., Qin, Z., Guan, C., Xu, L., Dai, J., Yang, C., et al. (2022). Scutellarin alleviates lipopolysaccharide-induced renal injury via mediating cysteine-rich protein 61-connective tissue growth factor-nephroblastoma overexpressed gene 1 expression to inhibit nuclear factor-κB signaling pathway. *Chin. Crit. Care Med.* 34 (4), 400–406. doi:10.3760/cma.j.cn121430-20210401-00767

Liu, Y., Jing, Y. Y., Zeng, C. Y., Li, C. G., Xu, L. H., Yan, L., et al. (2017b). Scutellarin suppresses NLRP3 inflammasome activation in macrophages and protects mice against bacterial sepsis. *Front. Pharmacol.* 8, 975. doi:10.3389/fphar.2017.00975

Lu, L., Yang, L. K., Yue, J., Wang, X. S., Qi, J. Y., Yang, F., et al. (2021). Scutellarin alleviates depression-like behaviors induced by LPS in mice partially through inhibition of astrocyte-mediated neuroinflammation. *Neurosci. Lett.* 765, 136284. doi:10.1016/j.neulet.2021.136284

Luo, S., Yang, Y., and Guo, Y. (2019). Determination of scutellarin plasma concentration and its pharmacokinetics in liposome by HighPerformance liquid chromatography. *Gui Chin. Med.* 17 (23), 18–19. doi:10.15912/j.cnki.gocm.2019.23.013

Luo, Z., Hu, Z., Bian, Y., Su, W., Li, X., Li, S., et al. (2020). Scutellarin attenuates the IL-1β-induced inflammation in mouse chondrocytes and prevents osteoarthritic progression. *Front. Pharmacol.* 11, 107. doi:10.3389/fphar.2020.00107

Ma, W. H., Li, M., Ma, H. F., Li, W., Liu, L., Yin, Y., et al. (2020). Protective effects of GHK-Cu in bleomycin-induced pulmonary fibrosis via anti-oxidative stress and anti-inflammation pathways. *Life Sci.* 241, 117139. doi:10.1016/j.lfs.2019.117139

Massoud, G., Parish, M., Hazimeh, D., Moukarzel, P., Singh, B., Cayton Vaught, K. C., et al. (2024). Unlocking the potential of tranilast: targeting fibrotic signaling pathways for therapeutic benefit. *Int. Immunopharmacol.* 137, 112423. doi:10.1016/j.intimp.2024.112423

Moser, B., Hochreiter, B., Basílio, J., Gleitsmann, V., Panhuber, A., Pardo-Garcia, A., et al. (2021). The inflammatory kinase IKKα phosphorylates and stabilizes c-Myc and enhances its activity. *Mol. Cancer* 20 (1), 16. doi:10.1186/s12943-021-01308-8

Mussbacher, M., Derler, M., Basílio, J., and Schmid, J. A. (2023). NF-κB in monocytes and macrophages - an inflammatory master regulator in multitalented immune cells. *Front. Immunol.* 14, 1134661. doi:10.3389/fimmu.2023.1134661

Nurul Islam, M., Downey, F., and Ng, C. K. Y. (2011). Comparative analysis of bioactive phytochemicals from Scutellaria baicalensis, Scutellaria lateriflora, Scutellaria racemosa, Scutellaria tomentosa and Scutellaria wrightii by LC-DAD-MS. *Metabolomics* 7 (3), 446–453. doi:10.1007/s11306-010-0269-9

Panieri, E., and Saso, L. (2021). Inhibition of the NRF2/KEAP1 Axis: a promising therapeutic strategy to alter redox balance of cancer cells. *Antioxid. Redox Signal* 34 (18), 1428–1483. doi:10.1089/ars.2020.8146

Park, M. Y., Ha, S. E., Kim, H. H., Bhosale, P. B., Abusaliya, A., Jeong, S. H., et al. (2022). Scutellarein inhibits LPS-induced inflammation through NF-κB/MAPKs signaling pathway in RAW264.7 cells. *Molecules* 27 (12), 3782. doi:10.3390/molecules27123782

Pei, T., Yan, M., Huang, Y., Wei, Y., Martin, C., and Zhao, Q. (2022). Specific flavonoids and their biosynthetic pathway in Scutellaria baicalensis. *Front. Plant Sci.* 13, 866282. doi:10.3389/fpls.2022.866282

Peng, L., Wen, L., Shi, Q. F., Gao, F., Huang, B., Meng, J., et al. (2020). Scutellarin ameliorates pulmonary fibrosis through inhibiting NF-κB/NLRP3-mediated epithelial-mesenchymal transition and inflammation. *Cell. Death Dis.* 11 (11), 978. doi:10.1038/s41419-020-03178-2

Rossa, C., Ehmann, K., Liu, M., Patil, C., and Kirkwood, K. L. (2006). MKK3/6-p38 MAPK signaling is required for IL-1beta and TNF-alpha-induced RANKL expression in bone marrow stromal cells. *J. Interferon Cytokine Res.* 26 (10), 719–729. doi:10.1089/jir.2006.26.719

Ruan, X., Gu, J., Chen, M., Zhao, F., Aili, M., and Zhang, D. (2023). Multiple roles of ALK3 in osteoarthritis. *Bone Jt. Res.* 12 (7), 397–411. doi:10.1302/2046-3758.127.Bjr-2022-0310.R1

Shahmohammadi, A., Golchoobian, R., Mirahmadi, S. M., Rousta, A. M., Ansari, F., Sharayeli, M., et al. (2023). Scutellarin alleviates lipopolysaccharide-provoked septic nephrotoxicity via attenuation of inflammatory and oxidative events and mitochondrial dysfunction. *Immunopharmacol. Immunotoxicol.* 45 (3), 295–303. doi:10.1080/08923973.2022.2141644

Sharma, A., and Wairkar, S. (2024). Flavonoids for treating pulmonary fibrosis: present status and future prospects. *Phytother. Res.* doi:10.1002/ptr.8285

Shen, J., Cheng, J., Zhu, S., Zhao, J., Ye, Q., Xu, Y., et al. (2019). Regulating effect of baicalin on IKK/IKB/NF-kB signaling pathway and apoptosis-related proteins in rats with ulcerative colitis. *Int. Immunopharmacol.* 73, 193–200. doi:10.1016/j.intimp.2019.04.052

Soliman, A. M., and Barreda, D. R. (2022). Acute inflammation in tissue healing. *Int. J. Mol. Sci.* 24 (1), 641. doi:10.3390/ijms24010641

Song, J. W., Long, J. Y., Xie, L., Zhang, L. L., Xie, Q. X., Chen, H. J., et al. (2020). Applications, phytochemistry, pharmacological effects, pharmacokinetics, toxicity of Scutellaria baicalensis Georgi. and its probably potential therapeutic effects on COVID-19: a review. *Chin. Med.* 15, 102. doi:10.1186/s13020-020-00384-0

Song, M. Y., Lee, D. Y., Chun, K. S., and Kim, E. H. (2021). The role of NRF2/KEAP1 signaling pathway in cancer metabolism. *Int. J. Mol. Sci.* 22 (9), 4376. doi:10.3390/ijms22094376

Sun, C. Y., Nie, J., Zheng, Z. L., Zhao, J., Wu, L. M., Zhu, Y., et al. (2019). Renoprotective effect of scutellarin on cisplatin-induced renal injury in mice: impact on inflammation, apoptosis, and autophagy. *Biomed. Pharmacother.* 112, 108647. doi:10.1016/j.biopha.2019.108647

Tian, L., Zhao, L., Gu, J., Cai, J., and Yu, L. (2014). Scutellarin listed on progress of new varieties and dosage form research. *Chin. J. Chin. Mater Med.* 39 (19), 3719–3722. doi:10.4268/cjcmm20141911

Van Gerrewey, T., and Chung, H. S. (2024). MAPK cascades in plant microbiota structure and functioning. *J. Microbiol.* 62 (3), 231–248. doi:10.1007/s12275-024-00114-3

Wang, H., Jiang, Q., and Zhang, L. (2022a). Baicalin protects against renal interstitial fibrosis in mice by inhibiting the TGF-β/Smad signalling pathway. *Pharm. Biol.* 60 (1), 1407–1416. doi:10.1080/13880209.2022.2097700

Wang, L., and Ma, Q. (2018). Clinical benefits and pharmacology of scutellarin: a comprehensive review. *Pharmacol. Ther.* 190, 105–127. doi:10.1016/j.pharmthera.2018.05.006

Wang, M. G., Seale, P., and Furman, D. (2024). The infrapatellar fat pad in inflammaging, knee joint health, and osteoarthritis. *NPJ Aging* 10 (1), 34. doi:10.1038/s41514-024-00159-z

Wang, S., Wang, H., Guo, H., Kang, L., Gao, X., and Hu, L. (2011). Neuroprotection of Scutellarin is mediated by inhibition of microglial inflammatory activation. *Neuroscience* 185, 150–160. doi:10.1016/j.neuroscience.2011.04.005

Wang, W., Li, J., Li, F., Peng, J., Xu, M., Shangguan, Y., et al. (2019). Scutellarin suppresses cartilage destruction in osteoarthritis mouse model by inhibiting the NF-κB and PI3K/AKT signaling pathways. *Int. Immunopharmacol.* 77, 105928. doi:10.1016/j.intimp.2019.105928

Wang, X., Zhang, C., Han, N., Luo, J., Zhang, S., Wang, C., et al. (2021). Triglyceride-mimetic prodrugs of scutellarin enhance oral bioavailability by promoting intestinal lymphatic transport and avoiding first-pass metabolism. *Drug Deliv.* 28 (1), 1664–1672. doi:10.1080/10717544.2021.1960928

Wang, Z., Zhang, P., Zhao, Y., Yu, F., Wang, S., Liu, K., et al. (2022b). Scutellarin protects against mitochondrial reactive oxygen species-dependent NLRP3 inflammasome activation to attenuate intervertebral disc degeneration. *Front. Bioeng. Biotechnol.* 10, 883118. doi:10.3389/fbioe.2022.883118

Wu, R., Liang, Y., Xu, M., Fu, K., Zhang, Y., Wu, L., et al. (2021). Advances in chemical constituents, clinical applications, pharmacology, pharmacokinetics and toxicology of Erigeron breviscapus. *Front. Pharmacol.* 12, 656335. doi:10.3389/fphar.2021.656335

Xia, J., Liu, C., Niu, H., Hou, W., and Li, S. (2021). Screening and isolation of potential lipoxidase and superoxide dismutase inhibitors from Scutellaria baicalensis Georgi using high-speed countercurrent chromatography target-guided by ultrafiltration-liquid chromatography-mass spectrometry. *J. Sep. Sci.* 44 (7), 1371–1382. doi:10.1002/jssc.202001072

Xia, Y., Xia, C., Wu, L., Li, Z., Li, H., and Zhang, J. (2023). Systemic immune inflammation index (SII), system inflammation response index (siri) and risk of all-cause mortality and cardiovascular mortality: a 20-year follow-up cohort study of 42,875 us adults. *J. Clin. Med.* 12 (3), 1128. doi:10.3390/jcm12031128

Xiang, Z., and Wu, X. (2017). Ultrasonic-microwave assisted extraction of total flavonoids from Scutellaria baicalensis using response surface methodology. *Pharm. Chem. J.* 51 (4), 318–323. doi:10.1007/s11094-017-1606-3

Xie, X., Wang, F., Ge, W., Meng, X., Fan, L., Zhang, W., et al. (2023). Scutellarin attenuates oxidative stress and neuroinflammation in cerebral ischemia/reperfusion injury through PI3K/Akt-mediated Nrf2 signaling pathways. *Eur. J. Pharmacol.* 957, 175979. doi:10.1016/j.ejphar.2023.175979

Xu, L., Chen, R., Zhang, X., Zhu, Y., Ma, X., Sun, G., et al. (2021). Scutellarin protects against diabetic cardiomyopathy via inhibiting oxidative stress and inflammatory response in mice. *Ann. Palliat. Med.* 10 (3), 2481–2493. doi:10.21037/apm-19-516

Xu, L. J., Chen, R. C., Ma, X. Y., Zhu, Y., Sun, G. B., and Sun, X. B. (2020). Scutellarin protects against myocardial ischemia-reperfusion injury by suppressing NLRP3 inflammasome activation. *Phytomedicine* 68, 153169. doi:10.1016/j.phymed.2020.153169

Xu, X., Yu, Y., Ni, X., and Song, J. (2012). Breviscapine injection's stability in different transfusions. *AMPJ* 16 (06), 843–846.

Yang, H., Wang, Z., Wang, L., Li, Y., Guo, J., Yang, X., et al. (2022). Scutellarin ameliorates osteoarthritis by protecting chondrocytes and subchondral bone microstructure by inactivating NF-κB/MAPK signal transduction. *Biomed. Pharmacother.* 155, 113781. doi:10.1016/j.biopha.2022.113781

Yang, X., Zhang, Q., Lu, H., Wang, C., and Xia, L. (2021). Suppression of lncRNA MALAT1 reduces LPS- or IL-17a-induced inflammatory response in human middle ear epithelial cells via the NF-κB signaling pathway. *Biomed. Res. Int.* 2021, 8844119. doi:10.1155/2021/8844119

Yang, Y., Wang, C., and Wei, M. (2019a). Kinetics and mass transfer considerations for an ultrasound-assisted supercritical CO2 procedure to produce extracts enriched in flavonoids from Scutellaria barbata. *J. CO2 Util.* 32, 219–231. doi:10.1016/j.jcou.2019.04.008

Yang, Y., Wang, C., and Wei, M. (2019b). Separation and quantification of bioactive flavonoids from Scutellaria barbata using a green procedure. *Food Bioprod. Process* 118, 77–90. doi:10.1016/j.fbp.2019.09.004

Yang, Y. C., and Wei, M. C. (2018). Development and characterization of a green procedure for apigenin extraction from Scutellaria barbata D. Don. *Food Chem.* 252, 381–389. doi:10.1016/j.foodchem.2017.12.086

Yi, N., Mi, Y., Xu, X., Li, N., Zeng, F., Yan, K., et al. (2021). Baicalein alleviates osteoarthritis progression in mice by protecting subchondral bone and suppressing chondrocyte apoptosis based on network pharmacology. *Front. Pharmacol.* 12, 788392. doi:10.3389/fphar.2021.788392

Yong, H. Y., Koh, M. S., and Moon, A. (2009). The p38 MAPK inhibitors for the treatment of inflammatory diseases and cancer. *Expert Opin. Investig. Drugs* 18 (12), 1893–1905. doi:10.1517/13543780903321490

You, P., Fu, S., Yu, K., Xia, Y., Wu, H., Yang, Y., et al. (2018). Scutellarin suppresses neuroinflammation via the inhibition of the AKT/NF-κB and p38/JNK pathway in LPS-induced BV-2 microglial cells. *N-S Arch. Pharmacol.* 391 (7), 743–751. doi:10.1007/s00210-018-1503-7

Zahan, O. M., Serban, O., Gherman, C., and Fodor, D. (2020). The evaluation of oxidative stress in osteoarthritis. *Med. Pharm. Rep.* 93 (1), 12–22. doi:10.15386/mpr-1422

Zeng, S., Tan, L., Sun, Q., Chen, L., Zhao, H., Liu, M., et al. (2022). Suppression of colitis-associated colorectal cancer by scutellarin through inhibiting Hedgehog signaling pathway activity. *Phytomedicine* 98, 153972. doi:10.1016/j.phymed.2022.153972

Zgorzynska, E., Dziedzic, B., and Walczewska, A. (2021). An overview of the Nrf2/ARE pathway and its role in neurodegenerative diseases. *Int. J. Mol. Sci.* 22 (17), 9592. doi:10.3390/ijms22179592

Zhang, L., Sun, S., Li, W., Zhang, W., Wang, X., and Yang, S. Y. (2017). Effect of Scutellarin inhibits collagen-induced arthritis through TLR4/NF-κB-mediated inflammation. *Mol. Med. Rep.* 16 (4), 5555–5560. doi:10.3892/mmr.2017.7292

Zhang, S., Zhang, J., Wei, D., An, H., Liu, W., Lai, Y., et al. (2020). Dengzhan Shengmai capsules and their active component scutellarin prevent cognitive decline in APP/PS1 mice by accelerating Aβ aggregation and reducing oligomers formation. *Biomed. Pharmacother.* 121, 109682. doi:10.1016/j.biopha.2019.109682

Zhang, X., Dong, Z., Fan, H., Yang, Q., Yu, G., Pan, E., et al. (2023). Scutellarin prevents acute alcohol-induced liver injury via inhibiting oxidative stress by regulating the Nrf2/HO-1 pathway and inhibiting inflammation by regulating the AKT, p38 MAPK/NF-κB pathways. *J. Zhejiang Univ. Sci. B* 24 (7), 617–631. doi:10.1631/jzus.B2200612

Zhang, Y., Zhang, Z., Wang, J., Zhang, X., Zhao, J., Bai, N., et al. (2022). Scutellarin alleviates cerebral ischemia/reperfusion by suppressing oxidative stress and inflammatory responses via MAPK/NF-κB pathways in rats. *Environ. Toxicol.* 37 (12), 2889–2896. doi:10.1002/tox.23645

Zhang, Z., Yi, P., Tu, C., Zhan, J., Jiang, L., and Zhang, F. (2019). Curcumin inhibits ERK/c-Jun expressions and phosphorylation against endometrial carcinoma. *Biomed. Res. Int.* 2019, 8912961. doi:10.1155/2019/8912961

Zhong, S., Li, L., Shen, X., Li, Q., Xu, W., Wang, X., et al. (2019). An update on lipid oxidation and inflammation in cardiovascular diseases. *Free Radic. Biol. Med.* 144, 266–278. doi:10.1016/j.freeradbiomed.2019.03.036

Zhou, Z., Kandhare, A. D., Kandhare, A. A., and Bodhankar, S. L. (2019). Hesperidin ameliorates bleomycin-induced experimental pulmonary fibrosis via inhibition of TGF-beta1/Smad3/AMPK and IkappaBalpha/NF-kappaB pathways. *Excli J.* 18, 723–745. doi:10.17179/excli2019-1094

Glossary

AChE activity	acetylcholinesterase
ADAMTS-5	a disintegrin and metalloproteinase with thrombospondin motifs 5
Akt	protein kinase B
ARE	anti-oxidant response element
Bax	Bcl-2 associated X protein
BUN	blood urea nitrogen
CAT	catalase
COX-2	cyclooxygenase-2
ERK	extracellular signal regulated kinase
HO-1	heme oxygenase-1
IKK	IκB kinase
iNOS	inducible nitric oxide synthase
IL-1	interleukin-1
IL-1β	interleukin-1β
IL-6	interleukin 6
JNK	Jun N-terminal kinase
Keap1	kelch-like ECH-associated protein 1
MAPK	mitogen-activated protein kinase
MAPKK	MAPK kinase
MAPKKK	MAPKK kinase
MDA	malondialdehyde
MMP-13	matrix metalloproteinase 13
MMP-2	matrix metalloproteinase 2
mTORC2	mechanistic target of rapamycin complex 2
NO	nitric oxide
Nrf2	nuclear factor erythroid 2-related factor 2
NF-κB	nuclear factor-kappa B
PDK1	pyruvate dehydrogenase kinase, isozyme 1
PGE2	prostaglandin E2
PI3K	phosphatidylinositol3 kinase
PIP2	phosphatidylinositol 4,5-bisphosphate
PTEN	phosphate and tension homology deleted on chromosome ten
ROS	reactive oxygen species
Smad	*drosophila* mothers against decapentaplegic protein
SOD	superoxide dismutase
TAS	total anti-oxidant status
TGF-β	transforming growth factor-β
TLR4	toll-like receptor 4
TNF-α	tumor necrosis factor-α

frontiers | Frontiers in Pharmacology

TYPE Original Research
PUBLISHED 30 October 2024
DOI 10.3389/fphar.2024.1451300

OPEN ACCESS

EDITED BY
Guang Wang,
Jinan University, China

REVIEWED BY
Xiangwei Chang,
Anhui University of Chinese Medicine, China
Amany Abdel-Rahman Mohamed,
Zagazig University, Egypt

*CORRESPONDENCE
Shan Xiang,
axiangshan@163.com
Fang Lian,
lianfangbangong@163.com

RECEIVED 19 June 2024
ACCEPTED 26 September 2024
PUBLISHED 30 October 2024

CITATION
Liu D, Wei C, Guan L, Ju W, Xiang S and Lian F (2024) Combining single-cell RNA sequencing and network pharmacology to explore the target of cangfu daotan decoction in the treatment of obese polycystic ovary syndrome from an immune perspective.
Front. Pharmacol. 15:1451300.
doi: 10.3389/fphar.2024.1451300

Combining single-cell RNA sequencing and network pharmacology to explore the target of cangfu daotan decoction in the treatment of obese polycystic ovary syndrome from an immune perspective

Danqi Liu[1,2], Chaofeng Wei[1], Lu Guan[1], Wenhan Ju[1], Shan Xiang[1,3]* and Fang Lian[1,3]*

[1]The First Clinical Medicine School, Shandong University of Traditional Chinese Medicine, Jinan, Shandong, China, [2]Department of Biomedical and Molecular Sciences, Queen's University, Kingston, ON, Canada, [3]Integrative Medicine Research Centre of Reproduction and Heredity, Affiliated Hospital, Shandong University of Traditional Chinese Medicine, Jinan, Shandong, China

Background: Polycystic ovary syndrome (PCOS) is a heterogeneous gynecological endocrine disorder linked to immunity. Cangfu Daotan Decoction (CFDT), a classic Chinese medicine prescription, is particularly effective in treating PCOS, specifically in patients with obesity; however, its specific mechanism remains unclear.

Methods: Part 1: Peripheral blood mononuclear cells were collected on egg retrieval day from obese and normal-weight patients with PCOS and healthy women undergoing *in vitro* fertilization (IVF)-embryo transfer. Next, scRNA-seq was performed to screen the key genes of bese patients with PCOS. Part 2: Active ingredients of CFDT and obesity-related PCOS targets were identified based on public databases, and the binding ability between the active ingredients and targets was analyzed. Part 3: This part was a monocentric, randomized controlled trial. The obese women with PCOS were randomized to CFDT (6 packets/day) or placebo, and the healthy women were included in the blank control group (43 cases per group). The clinical manifestations and laboratory outcomes among the three groups were compared.

Results: Based on the scRNA-seq data from Part 1, CYLD, ARPC3, CXCR4, RORA, JUN, FGL2, ZEB2, GNLY, FTL, SMAD3, IL7R, KIR2DL1, CTSD, BTG2, CCL5, HLA, RETN, CTSZ, and NCF2 were potential key genes associated with obese PCOS were identified. The proportions of T, B, and natural killer cells were higher in patients with PCOS compared to healthy women, with even higher proportions observed in obese patients with PCOS. Gene ontology and the Kyoto encyclopedia of genes and genomes analysis depicted that the differentially expressed genes were related to immune regulation pathways. Network pharmacology analysis identified that the key active components in CFDT were quercetin, carvacrol, β-sitosterol, cholesterol, and nobiletin, and TP53, AKT1, STAT3, JUN, SRC, etc. were the core targets. The core targets and their enrichment pathways overlapped with those in Part 1. Clinical trials in Part 3 found

that CFDT reduced the dosage of gonadotropins use in patients with PCOS, increased the number of high-quality embryos, and improved the ongoing pregnancy rate.

Conclusion: CFDT can improve the immune microenvironment of patients to some extent, reduce their economic burden, and enhance IVF outcomes. The improvement in the immune microenvironment in obese patients with PCOS may be linked to targets such as JUN and AKT.

KEYWORDS

polycystic ovary syndrome, immune abnormalities, obesity, single-cell RNA sequencing, network pharmacology, cangfu daotan decoction

1 Introduction

Polycystic ovary syndrome (PCOS) is among the most common gynecological endocrine diseases affecting the health of women of childbearing age. Globally, the prevalence of PCOS ranges from 4% to 21% (Bozdag et al., 2016). Clinical symptoms of PCOS include menstrual irregularities, infertility, hirsutism, acne, obesity, acanthosis nigricans, and mood disorders (Legro et al., 2013). Clinically, combined oral contraceptives are the first-line treatment for PCOS menstrual abnormalities (Mohamed et al., 2018), hirsutism, and acne (Frey and Aakvaag, 1981). Clomiphene is used as a first-line drug for the treatment of PCOS infertility (Misso et al., 2012). However, its efficacy is often limited and associated with many side effects (Hughes et al., 2010). As PCOS is a heterogeneous disease with different complexities and individual patient manifestations, the clinical treatment and comprehensive management of PCOS are extremely challenging (Christ and Cedars, 2023).

Moreover, most patients with PCOS seek medical treatment in adolescence or early childbearing age for irregular menstruation, acne, and infertility (Witchel et al., 2020). Most treatments focus on treating

TABLE 1 Composition and action of CFDT.

Pinyin name	Full species name	Pharmacological effects	Toxicity	Doses (g)
Cangzhu	*Atractylodes lancea (Thunb.) DC.* [*Asteraceae; Atractylodis Rhizoma*]	Cangzhu has anti-inflammatory, stimulates intestinal peristalsis, regulates gut microbiota, and improves cholesterol metabolism (Koonrungsesomboon et al., 2014; Qu et al., 2022).	NA (Liu et al., 2008)	15
Xiangfu	*Cyperus rotundus L.* [*Cyperaceae; Cyperi Rhizoma*]	Xiangfu has anti-androgenic, anti-diabetic, anti-inflammatory, lipid-lowering, and anti-obesity effects, and it improves lipid and glucose metabolism (Kanagali et al., 2022; Pirzada et al., 2015; Xue et al., 2023).	NA (Abo-El-Yazid et al., 2022)	10
Banxia	*Pinellia ternata (Thunb.) Breit.* [*Araceae; Pinelliae Rhizoma*]	Banxia has anti-inflammatory, anti-tumor, antitussive, and antiasthmatic properties (Tao et al., 2023).	Irritant toxicity, cardiotoxicity, hepatotoxicity and embryotoxicity, but the toxicity is weakened after processing (Zou et al., 2023)	9
Chenpi	*Citrus reticulata Blanco* [*Rutaceae; Citri Reticulatae Pericarpium*]	Chenpi can improve hepatic steatosis, oxidative stress, and inflammation (Ke et al., 2020).	NA (Nakajima et al., 2020)	10
Fuling	*Wolfiporia cocos (Schwein.) Ryvarden and Gilb.* [*Polyporaceae; Poria*]	Fuling has antibacterial, antioxidant, anti-inflammatory, immunomodulatory, and hepatoprotective and renoprotective effects (Nie et al., 2020).	NA (Li et al., 2022)	15
Zhiqiao	*Citrus aurantium L.* [*Rutaceae; Aurantii Fructus Immaturus*]	Zhiqiao has anxiolytic, anti-obesity, antibacterial, antioxidant, insecticidal, and anti-diabetic activities (Suntar et al., 2018).	NA (Lamichhane et al., 2022)	12
Chuanxiong	*Ligusticum chuanxiong Hort.* [*Apiaceae; Chuanxiong Rhizoma*]	Chuanxiong has anti-inflammatory, antioxidant, neuroprotective, and antifibrotic effects (Ran et al., 2011).	NA (Long et al., 2023)	6
Dannanxing	*Arisaema erubescens (Wall.) Schott* [*Araceae; Arisaematis Rhizoma Praeparatum*]	Dannanxing can dry dampness, resolve phlegm, dispel wind, relieve pain, and reduce swelling (Wang et al., 2023b).	Nephrotoxicity, toxicity is reduced after processing (Wang et al., 2023b)	6
Huashi	*Talc*	Huashi has antibacterial and adsorptive effects (Addala et al., 2022).	Inhalation toxicity (Johnson, 2021)	6
Shenqu	*Massa Medicata Fermentata*	Shenqu can improve intestinal flora and fight inflammation (Zhang et al., 2020).	NA (Liu et al., 2022)	8

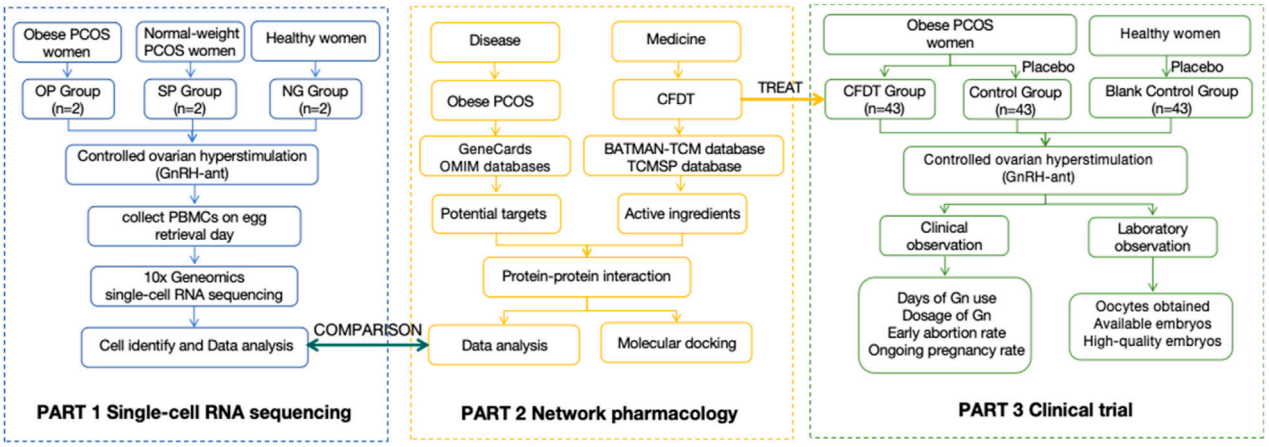

FIGURE 1
Flow chart of the study.

current clinical symptoms while ignoring the long-term health risks associated with PCOS. Therefore, developing a more complete treatment plan for PCOS is crucial. Recently, several studies have exhibited that traditional Chinese medicine can improve PCOS with fewer adverse reactions (Moini Jazani et al., 2019).

Single-cell RNA sequencing (scRNA-seq) is used to directly analyze gene expression, intracellular population heterogeneity, and cell status at the single-cell level. This can help us better understand transcriptional dynamics and gene regulatory relationships (Azizi et al., 2018). The Cangfu Daotan Decoction (CFDT) is an herbal formula consisting of ten medicinal herbs (the main components of CFDT are displayed in Table 1). It exhibits a significant effect in treating obesity infertility; however, its potential targets and mechanisms of action remain unclear. Network pharmacology is an emerging discipline that comprehensively uses multidisciplinary knowledge (Alam et al., 2022), such as systems biology, multi-omics, pharmacology, and computer network analysis, to study the global, systematic, and network nature of drug effects (Zhao et al., 2023). Recently, network pharmacology has provided new research methods to reveal the complex mechanisms of traditional Chinese medicine. Our study used scRNA-seq technology to identify differentially expressed genes in immune cells in the peripheral blood of patients with PCOS, we systematically analyzed the characteristics of the immune microenvironment. We used network pharmacology and molecular docking technology to systematically analyze the possible active ingredients and potential molecular interaction mechanisms of CFDT in treating PCOS to provide a scientific basis for the pharmacological research and clinical treatment of CFDT in PCOS treatment. Furthermore, we explored the clinical efficacy of CFDT in treating PCOS, particularly in patients with obesity.

2 Materials and methods

This study was divided into three parts. In part 1, we used scRNA-seq to analyze the immune microenvironment status of patients with PCOS. In part 2, we used network pharmacology to analyze the targets of CFDT. In part 3, we explored the clinical effect of CFDT based on a double-blind clinical trial. This process is illustrated in Figure 1.

2.1 Diagnostic criteria

The diagnostic criteria for PCOS were formulated following Rotterdam criteria in 2003 (2 out of 3) (Rotterdam, 2004):

1) Oligo- or anovulation,
2) Clinical and biochemical signs of hyperandrogenism,
3) Polycystic ovaries.

2.2 Inclusion criteria

Patients with PCOS met the diagnostic criteria for PCOS and the following conditions:

1) Age: 22–40 years,
2) Cohabitation for more than 1 year after marriage, normal sexual life, no contraception, and no pregnancy,
3) The husbands' semen analysis results were generally normal.

Obese patients with PCOS have a body mass index (BMI) > 30 kg/m^2; normal-weight patients with PCOS have a BMI <23 kg/m^2 (Caballero, 2019).

The following conditions were met for healthy women:

1) Age: 22–40 years old,
2) Cohabitation for more than 1 year after marriage, normal sexual life, no contraception, and no pregnancy.

2.3 Exclusion criteria

1) Those who could not get pregnant due to reproductive system malformation or severe systemic diseases,

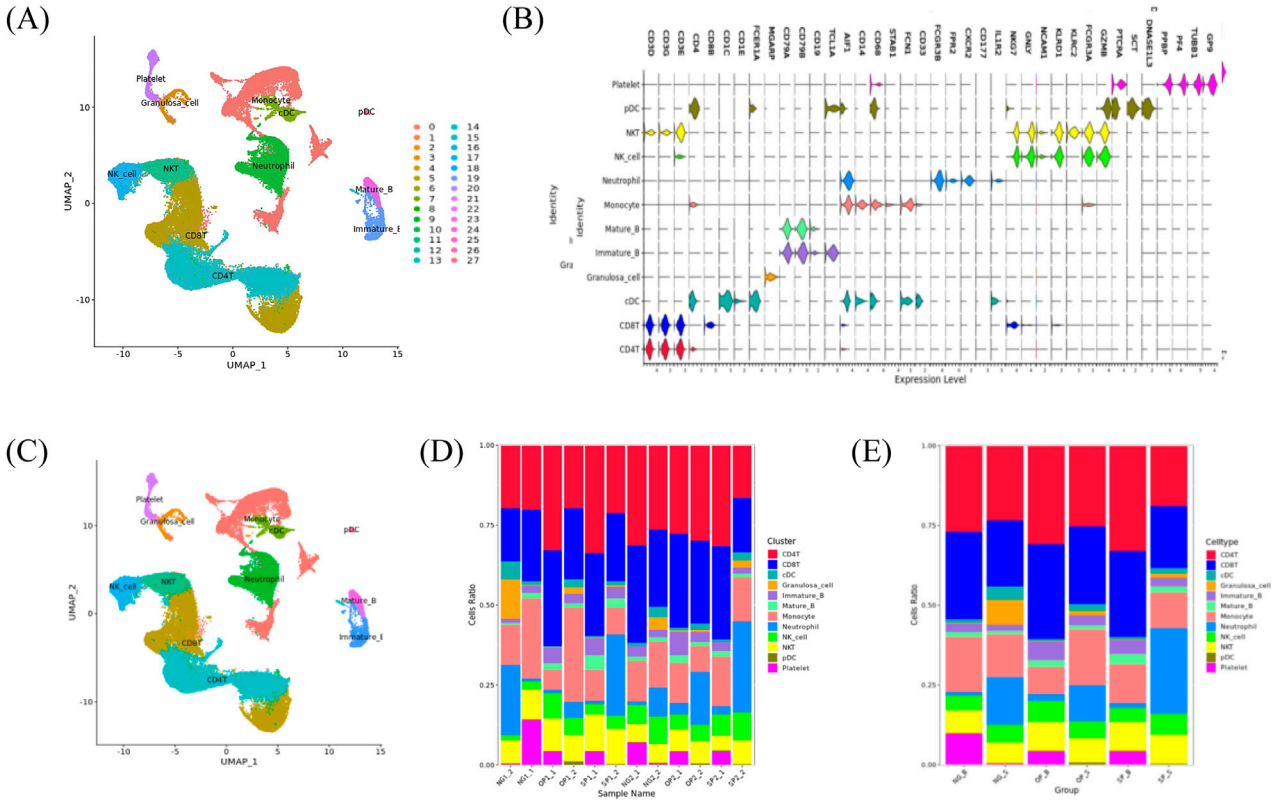

FIGURE 2
ScRNA-seq cell definition results. **(A)** Cell clustering UMAP visualization clustering results. **(B)** Violin plot of marker gene expression in each cluster. **(C)** UMAP plot of the cell subpopulation distribution. **(D)** Histogram of the cell proportion in each sample. **(E)** Histogram of the cell proportion in each sample.

2) Those with pelvic inflammation, tubal adhesion, obstruction, and adrenal cortical insufficiency,
3) Those with autoimmune diseases such as systemic lupus erythematosus, rheumatoid arthritis, and inflammatory bowel disease,
4) Those with infertility caused by other diseases, such as endometriosis and hyperprolactinemia,
5) Those who did not meet the inclusion criteria did not take medication as prescribed or had poor compliance.

2.4 scRNA-seq

In part 1, obese patients with PCOS (OP group), non-obese patients with PCOS (SP group), and women with simple male factor infertility (NG group) who underwent *in vitro* fertilization-embryo transfer (IVF-ET) at the Reproductive and Genetic Center of our hospital and met the inclusion criteria were selected. Peripheral blood was collected from each subject on the day of egg retrieval. All patients were subjected to controlled ovarian hyperstimulation with antagonist protocol. When there were more than three follicles with a diameter ≥18 mm, 8,000–10000 IU of human chorionic gonadotropin (hCG) was injected intramuscularly to induce follicle maturation, and transvaginal oocyte retrieval was performed 36 h later (Reichman et al., 2011). Peripheral blood mononuclear cells (PBMCs) were separated by density gradient centrifugation (Golke et al., 2022). High-throughput sequencing was performed using the 10x Geneomics sequencing platform to obtain sequencing data for subsequent data analysis. CellRanger software was used to control the data quality. Barcode sequence markers in the sequence and UMI markers of different mRNA molecules in each cell were identified for quantification to obtain quality control statistical information, such as the number of high-quality cells and gene median. Principal component analysis was performed using gene expression, and uniform manifold approximation and projection (UMAP) dimensionality reduction technology was used for visual clustering in two-dimensional images (Yang et al., 2021).

2.5 Cell definition and differential gene analysis

The SingleR package was used to calculate the Spearman's correlation between the cell expression profile to be identified, and the reference dataset based on the single-cell reference expression quantification public dataset, and the cell type that had the greatest correlation with the sample cells was selected as the final cell type to be identified (Figure 2). According to $P < 0.05$ and the difference fold $|\log_2 FC|>0.25$, the significantly different genes in obese patients with PCOS were screened out, and the gene ontology (GO) analysis of the differential genes and the

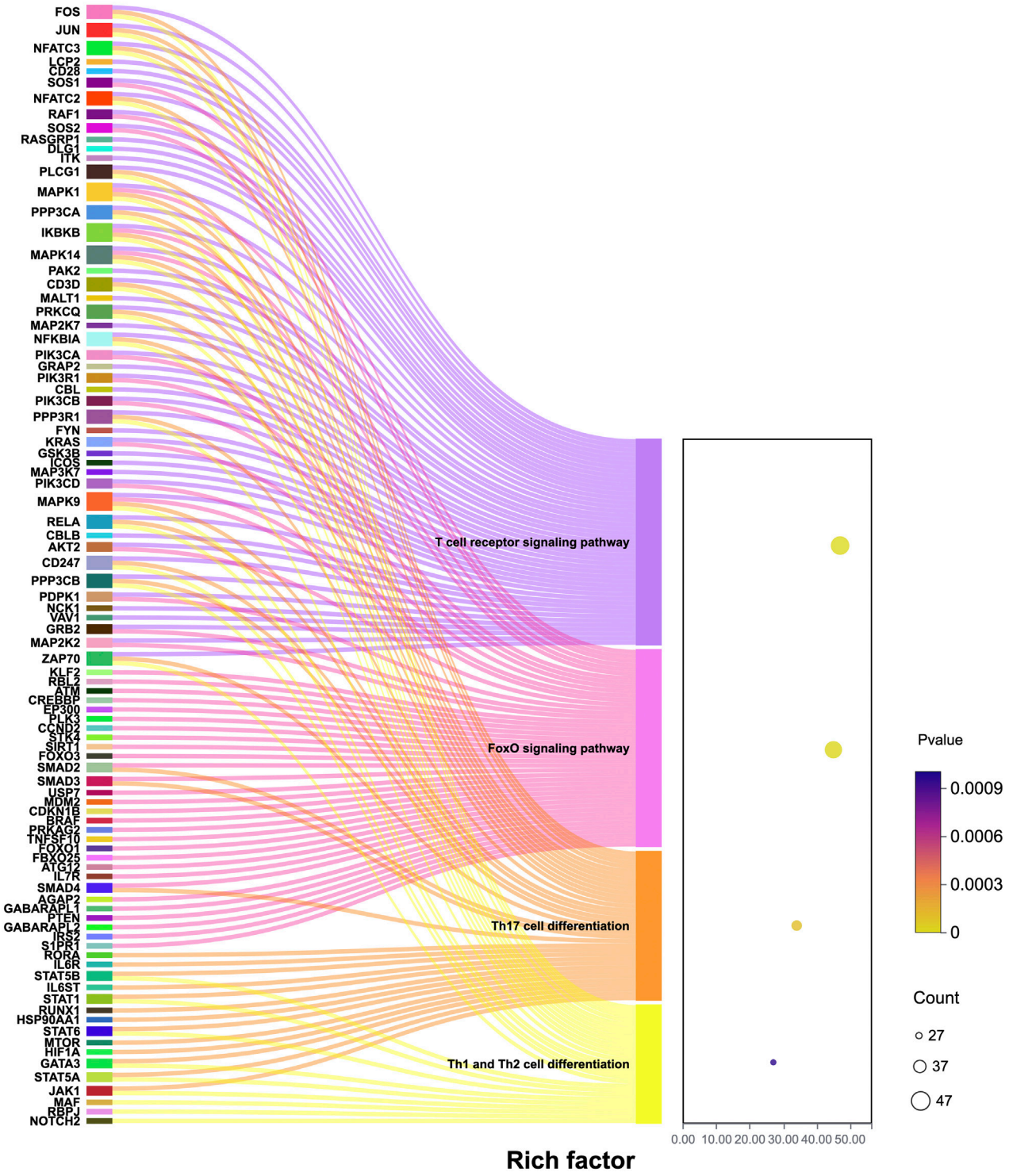

FIGURE 3
Differential gene enrichment mulberry bubble chart.

Kyoto encyclopedia of genes and genomes (KEGG) were performed through the hypergeometric distribution test. KEGG and Reactome analyses were used to identify GO functional items with significantly enriched differential genes and the main metabolic and signal transduction pathways involved.

2.6 Collection of chemical components and target prediction of CFDT

In part 2, the traditional Chinese medicine database and analysis platform (TCMSP, https://tcmsp-e.com/) was used to retrieve the

classic prescriptions used in this study and the constituent Chinese medicines of CFDT. The BATMAN-TCM database (http://bionet.ncpsb.org.cn/batman-tcm/) was used for Chinese medicines that could not be retrieved by the TCMSP database. The TCMSP database was used to retrieve the active ingredients of *Atractylodes lancea*, *Cyperus rotundus*, *Pinellia ternata (Thunb.) Breit.*, *Citrus reticulata Blanco*, *Poria*, *Citrus aurantium*, and *Ligusticum chuanxiong*. Oral bioavailability ≥30% and drug-likeness (DL) ≥ 0.18 were used as screening conditions to obtain the possible active ingredients of the compound. By logging into the BATMAN-TCM database (http://bionet.ncpsb.org.cn/batman-tcm/), the effective ingredients of *Arisaema consanguineum*, *Talc*, and *Massa Medicata Fermentata* and proteins with high credibility were obtained as candidate genes. The targets obtained were calibrated using data from the UniProt database (https://www.uniprot.org/), non-human genes were eliminated, invalid duplicate targets were deleted, and standardized gene names were obtained. Using "obese polycystic ovary syndrome" as the keyword, GeneCards (https://www.genecards.org/) and OMIM (https://www.omim.org/) databases were used to search to obtain possible targets related to the disease. All targets in the database were integrated into a table, duplicate genes were eliminated, and the UniProt database was used for correction to obtain disease-target gene information. To further study the protein-protein interaction of CFDT in the treatment of obese PCOS, the drug-intersection genes were uploaded to the interaction database String (https://string-db.org/) was used to construct the protein-protein interaction network (PPI), and the core targets were selected to make the protein interaction network diagram. Cytoscape is an information visualization software primarily used to visually analyze biological information and social networks. Cytoscape (version 3.7.2) was used to draw the CFDT network diagrams and a common target PPI network diagram. The network was topologically analyzed, with the node size and color reflecting the degree value. The larger the node, the greater the degree value. The thickness of the edge was used to reflect the size of the combined score. The thicker the edge, the greater the combined score. The higher the degree value of a node, the higher its degree of centrality, which means that the node is more important in the network (Udrescu et al., 2020). The clusterProfiler package of Rstudio was used to perform GO enrichment and KEGG pathway analyses on the target genes (Chen et al., 2022). The structure files of the key active ingredients of CFDT were retrieved through the PubChem database (https://pubchem.ncbi.nlm.nih.gov/). The receptor proteins were retrieved from the Protein Data Bank (http://www.rcsb.org/pdb) database. The receptor proteins were molecularly docked with ligand small molecules using AutoDock Vina software (version 1.1.2). The affinity was evaluated and visualized according to the spatial effect, repulsion, and hydrogen bond of the receptor-ligand complex.

2.7 Trial drugs and schemes

The cases included in part 3 were from the Integrative Medicine Research Center of Reproduction and Heredity in Affiliated Hospital of Shandong University of Traditional Chinese Medicine (from June 2021 to June 2023). In part 3, all obese patients with PCOS who underwent IVF treatment were selected and divided into the CFDT and control groups using the random number table method (43 cases in each group). Forty-three normal women whose husbands were infertile were selected as the blank control group. Serum luteinizing hormone, follicle-stimulating hormone, and estradiol levels were measured on the third day of the menstrual cycle before entering the cycle, and antral follicle count was measured by transvaginal ultrasound. The subjects were administered CFDT or placebo (both provided by the Preparation Room of the Affiliated Hospital of Shandong University of Traditional Chinese Medicine, mainly composed of dextrin, 3 g/packet) for intervention according to the groups, three packets at a time, twice a day, starting from the sixth day of menstruation (two cycles before IVF cycles), stopping during menstruation until the hCG administration day of the IVF cycle. Peripheral blood serum was collected on the day of egg retrieval.

The decoction was prepared as follows: 1) Talcum (8 g) and Massa Medicata Fermentata (15 g) were wrapped separately in gauze and steeped together with the other eight herbs in cold water for 30 min 2) The mixture was boiled and simmered for 30 min before pouring the liquid. 3) Cold water was added again, and the mixture was boiled for another 20 min, after which the liquid was poured out. 4) The decoctions from both the boiling sessions were combined. Strain out the residue. The resulting decoction was divided into two doses to be administered daily, with each dose of 150 mL.

2.8 Statistical analysis

The original database was established using Excel, and the data were statistically analyzed using the Statistical Package for the Social Sciences software (version 23.0). If the data met normality, variance analysis was used to compare the three groups, and $P < 0.05$ indicated that the difference was statistically significant. The measurement data are expressed as the mean ± standard deviation ($\bar{x} \pm s$). The comparison of the rates between the two groups was performed using the Fisher exact probability method of the four-cell table data using the χ^2 test, and $P < 0.05$ indicated that the difference was statistically significant.

3 Results

3.1 Identification of cell clusters and dimension reduction analysis

The scRNA-seq analysis identified 27 cell clusters and seven cell types. Marker gene expression in the eight-cell types differed between cell types. The proportions of T cells, B cells, and natural killer (NK) cells in patients with PCOS were higher than those in normal women, with even higher proportions observed in obese patients with PCOS. The proportion of DC and monocytes in patients with PCOS was lower than in normal women. There was a non-significant difference in the proportion of DC cells between OP and SP groups. Compared with the SP group, the OP group had a more significant decrease in monocytes.

Pairwise comparisons were made between NG and OP, NG and SP, and SP and OP groups, and the differences related to obesity and

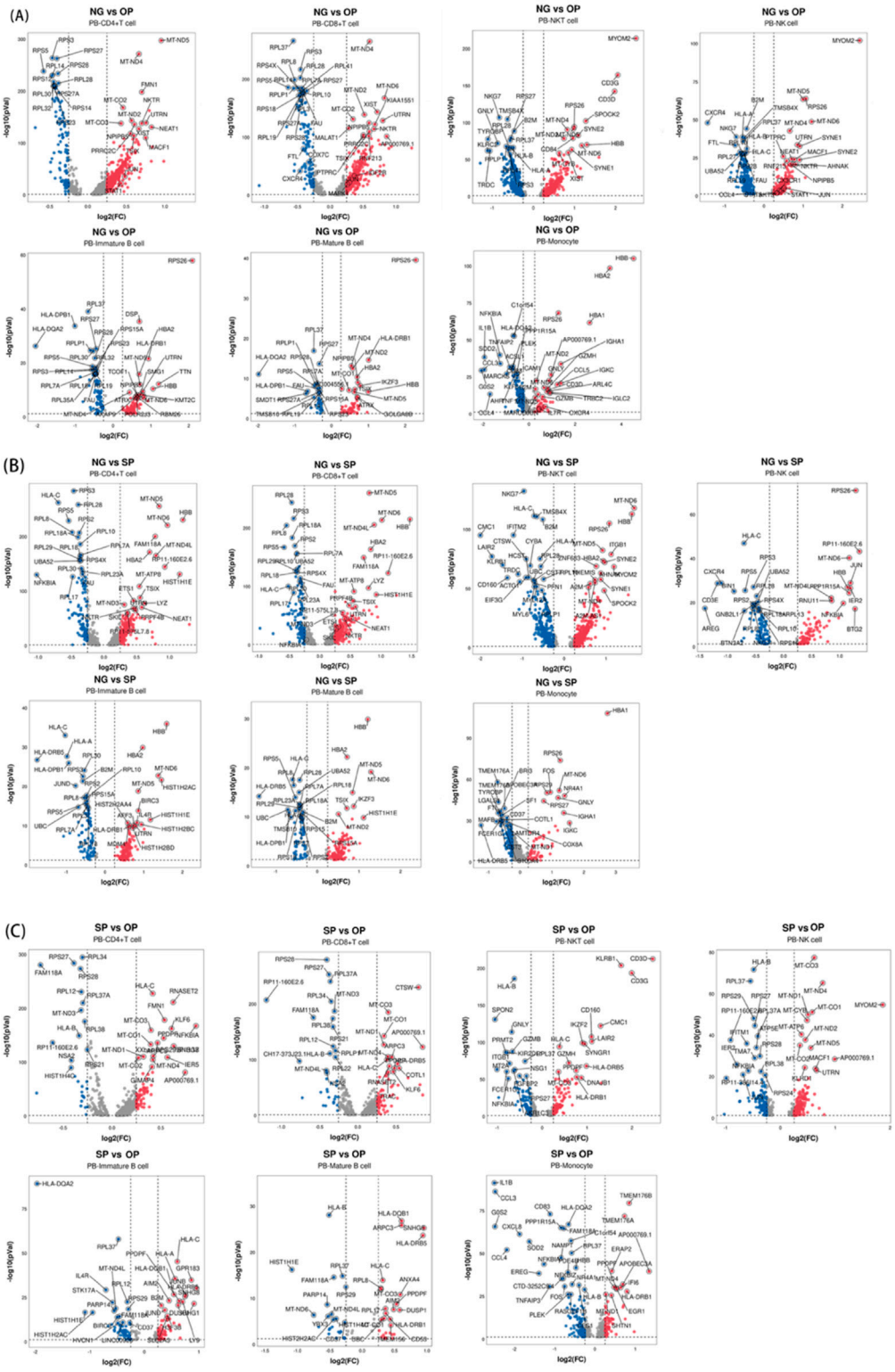

FIGURE 4
Volcano plot of differentially expressed genes in PBMCs between each group. **(A)** Differential genes between NG and OP. **(B)** Differential genes between NG and SP. **(C)** Differential genes between SP and OP.

PCOS were screened ($P < 0.05$, $|\log_2 FC|>0.25$). The clusterProfiler package was used to perform GO and KEGG enrichment analyses on the differentially expressed genes of each cell group in NG_B and OP_B groups. The B cell KEGG enrichment results were non-significant; therefore, we used reactome enrichment analysis instead.

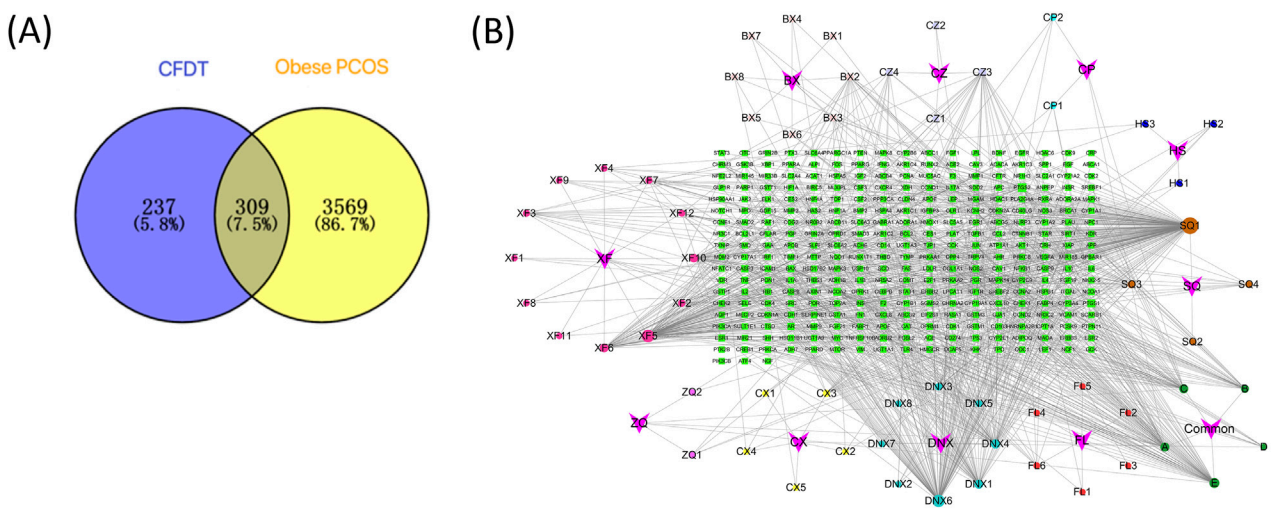

FIGURE 5
(A) Venn diagram of CFDT ingredients and potential targets of obese PCOS. **(B)** CFDT active ingredient-target network.

3.2 CD4$^+$ T cell activation in obese PCOS

Compared with normal women, the CD4$^+$ T cell activation-related genes JUN, NFATC2, SOS1, AKT, and MAPK9 in patients with PCOS and obesity were upregulated and enriched in the T cell receptor (TCR) signaling pathway, FoxO signaling pathway, Th17 cell differentiation signaling pathway, and Th1 and Th2 cell differentiation pathways, as depicted in Figure 3. The TCR signaling pathway is a critical part of the immune system (Shah et al., 2021), is mainly responsible for the activation and functional regulation of T cells, and is essential for T cells to recognize antigens, produce immune responses, and maintain the balance of the immune system (Rellahan et al., 1997). JUN is at the "crossroads" of the TCR signaling pathway and is a key gene in the TCR signaling pathway (Ono, 2020).

In this study, we analyzed the differentially expressed genes between NG and OP and NG and SP groups ($P > 0.05$, $|\log_2 FC| \geq 0.25$) (Figure 4). A total of 19 genes were screened, including CYLD, ARPC3, CXCR4, RORA, JUN, FGL2, ZEB2, GNLY, FTL, SMAD3, interleukin (IL)7R, KIR2DL1, CTSD, BTG2, CCL5, HLA, RETN, CTSZ, and NCF2. These potential target genes are related to Th1, Th2, Th17 differentiation, FγR-mediated phagocytosis pathway, NOD-like receptor signaling pathway, NF-κB signaling pathway, FoxO signaling pathway, and tumor necrosis factor (TNF) signaling pathways, MHC protein complex binding, antigen presentation function, ferroptosis, and oxidative phosphorylation.

3.3 Prediction of candidate bioactive ingredients for CFDT treatment of obese PCOS

According to the TCMSP and BATMAN-TCM databases, screening by OB ≥ 30% and DL ≥ 0.18, 56 candidate bioactive ingredients were identified (Table 1). Furthermore, using the GeneCards and OMIM databases, 3,308 and 646 small molecules were obtained, respectively. After deduplication, 3,878 targets related to obese PCOS were identified and the obtained genes were corrected using the UniProt database. The intersection of active ingredients and disease targets is depicted in a Venn diagram (Figure 5A). Finally, the direct active ingredient-target interaction network of CFDT was constructed using Cytoscape (Figure 5B). These genes may act as interactive target genes for treating obese PCOS. The top five candidate bioactive ingredients (with high degree value) are quercetin, apigenin, β-sitosterol, cholesterol, and nobiletin.

All 309 genes in the gene set for CFDT treatment of obese PCOS were imported into STRING, and the PPI network of genes for CFDT treatment of obese PCOS was constructed using Cytoscape (version 3.7.2), as revealed in Figure 6. The key targets in PPI network were tumor protein 53 (TP53), the serine/threonine kinase AKT1 (AKT1), signal transducer and activator of transcription 3 (STAT3), JUN (Jun proto-oncogene, Jun), sarcoma gene (SRC), estrogen receptor 1, interleukin 6, heat shock protein 90 alpha family class a member 1, TNF, and catenin beta 1.

According to the GO analysis with the lowest *P* value, the top five biological processes are steroid metabolic process, response to drug, response to nutrient levels, regulation of small molecule metabolic process, and regulation of lipid metabolic process. The top five cellular components are membrane raft, membrane microdomain, membrane region, caveola, and plasma membrane raft. The top five molecular functions are steroid binding, DNA-binding transcription factor binding, RNA polymerase II-specific DNA-binding transcription factor binding, nuclear receptor activity, and ligand-activated transcription factor activity (the bar graph of the top 10 is displayed in Figure 7A). The results of KEGG functional enrichment analysis revealed that the active components of CFDT affected obese PCOS mainly through the PI3K-AKT, TNF, HIF-1, and IL-17 signaling pathways, and EGFR tyrosine kinase inhibitor resistance (the bubble chart of the top 20 is exhibited in Figure 7B).

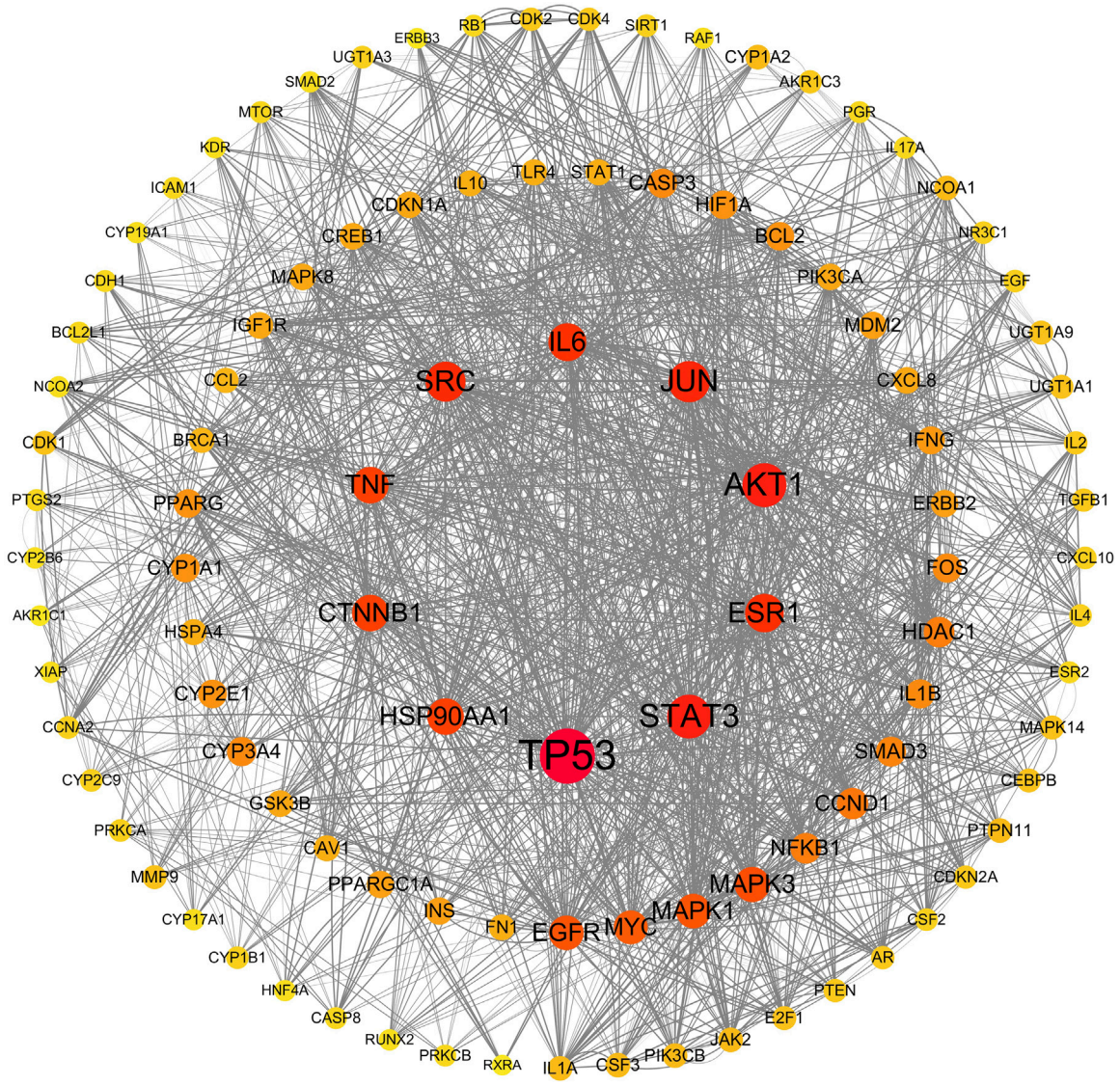

FIGURE 6
PPI network of genes for CFDT treatment of obese PCOS.

3.4 Molecular docking of the active components of CFDT with core targets

Molecular docking was used to assess the efficacy of the screened active drugs and targets to validate the outcomes of network pharmacology. The five compounds with the highest degree values in the herb-compound-target network analysis and the key targets (TP53, AKT1, STAT3, JUN, and SRC) based on the degrees of common targets in the PPI network were selected for molecular docking by PPI network screening using AutoDock Vina (version 1.1.2). The results depicted that all five critical active ingredients exhibited good binding activity with all five core targets (Figure 8). JUN and AKT1 have relatively lower binding energies with the five vital active ingredients; therefore, the effect is the best, as depicted in Figure 8 and Table 2.

3.5 Comparison of clinical manifestations and laboratory outcomes

In part 3, the gonadotropin (Gn) dosage, Gn medication days, early abortion rate, ongoing pregnancy rate (Table 3), number of oocytes obtained, number of available embryos, and number of high-quality embryos were compared among the three groups of patients (Table 4).

4 Discussion

The symptoms of PCOS usually start with puberty and are characterized by excessive androgen, irregular ovulation, and polycystic ovarian changes. It usually coexists with insulin resistance, dyslipidemia, and obesity (Luan et al., 2022). It also

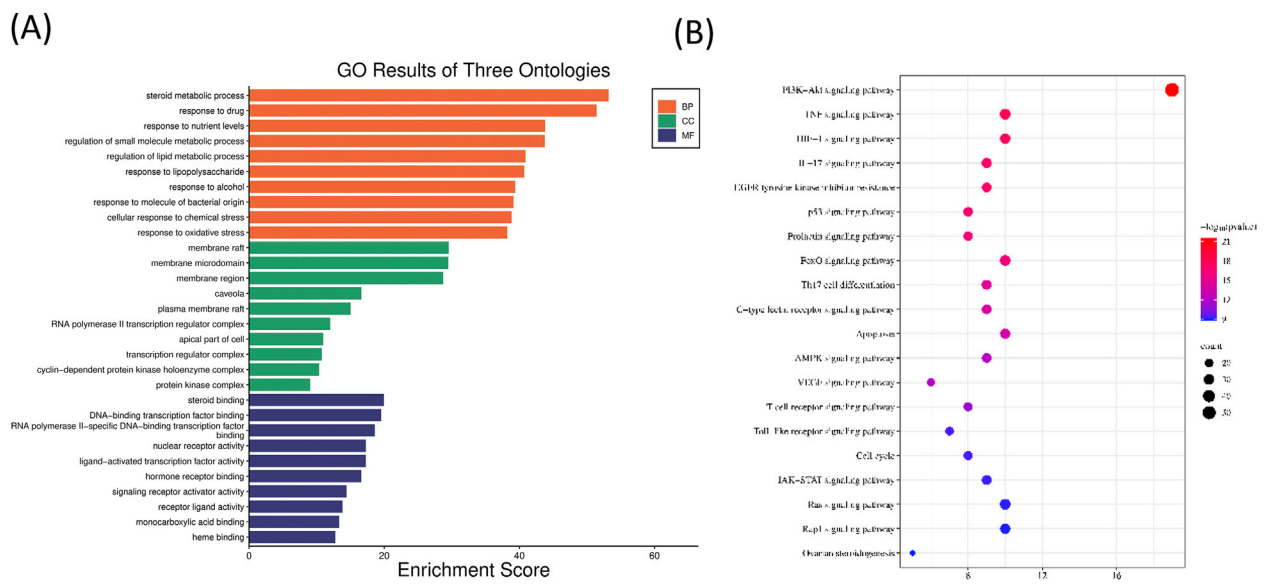

FIGURE 7
(A) GO analysis of the CFDT treatment of obese PCOS. **(B)** KEGG analysis for CFDT treatment of obese PCOS.

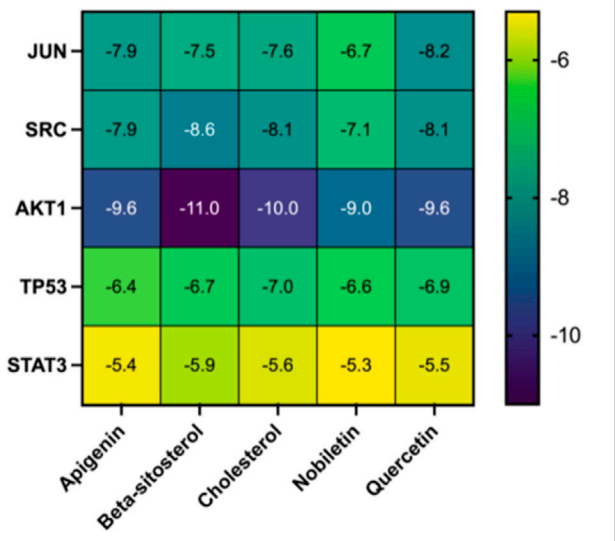

FIGURE 8
Heatmap of the molecular docking score. Binding energy (kcal/mol) of active compounds of herbs and key target molecules.

has a significant risk of cardiovascular and metabolic sequelae (including diabetes and metabolic syndrome). It is among the most common gynecological endocrine diseases that affect the health of women of childbearing age (Meier, 2018; Sadeghi et al., 2022). It is now generally believed that PCOS is closely linked to immune dysregulation and chronic low-level inflammation (Wang J. et al., 2023). Therefore, treatment from an immune perspective may become a new approach to treat PCOS. Traditional Chinese medicine has exhibited certain advantages in clinical practice, but there is a lack of high-quality research evidence. Consequently, we focused on an immunological perspective, using scRNA-seq and network pharmacology technology to explore the possible mechanism of traditional Chinese medicine in treating PCOS, specifically obese PCOS (Moini Jazani et al., 2019).

Changes in the proportion of immune cells are a key sign indicating a change in the immune microenvironment. In our study, the T cell proportion in peripheral blood samples of obese patients with PCOS increased. From the perspective of cell cluster gene set expression, the T cell function of obese patients with PCOS was in a relatively stimulated state compared with that of the NG group. The differential gene enrichment results of T cells in obese patients with PCOS were mainly concentrated in biological processes, such as protein localization, immune defense, viral infection, cell adhesion, and immune regulation, which are closely associated with the immune response. KEGG enrichment analysis mainly focused on the TCR signaling pathway, antigen processing and presentation, Th-17 signaling pathway, NF-κB signaling pathway, FoxO signaling pathway, B-cell receptor signaling pathway, Th17 cell differentiation pathway, and Th1 and Th2 cell differentiation pathways. These signaling pathways are closely correlated with T-cell activation, differentiation, and cytokine release (Shah et al., 2021). The TCR signaling pathway is crucial for T cell activation and is an important signaling pathway in the immune response (Alcover et al., 2018). It is also involved in antigen recognition, cytokine production, immune responses, and other processes. Furthermore, the potential target genes CYLD (Reiley et al., 2007) and CXCR4 in the T cells of obese patients with PCOS are crucial for maintaining T cell homeostasis.

In this study, we used network pharmacology to construct the intersection target network diagram of CFDT and GO and KEGG enrichment analysis to reveal the core targets and signaling pathways of CFDT in treating obese PCOS. Fifty-six effective active ingredients of CFDT were obtained, 3,878 genes related to

TABLE 2 Docking patterns of active compounds and key targets.

	AKT1	JUN
Nobiletin	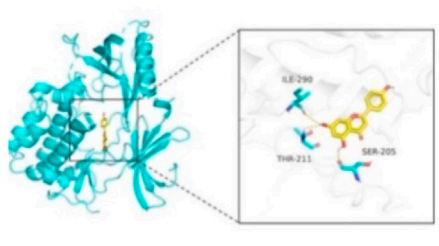	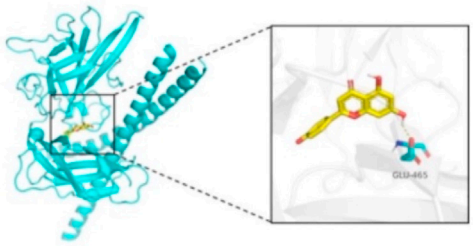
Quercetin	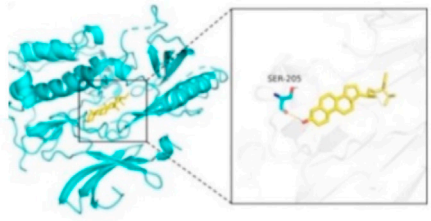	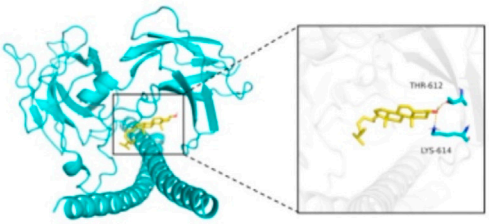
Cholesterol	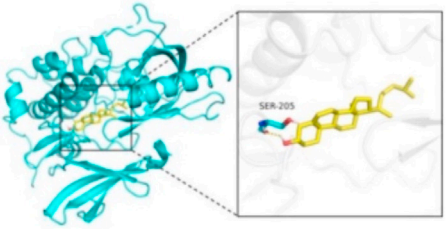	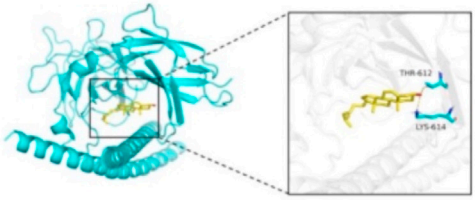
Nobiletin	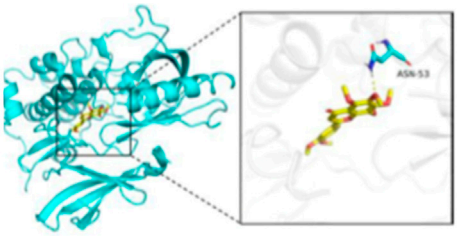	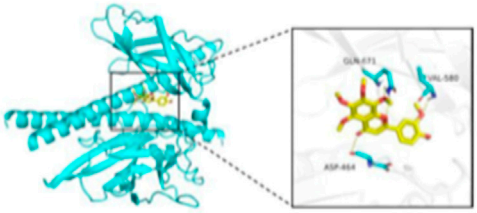
Quercetin	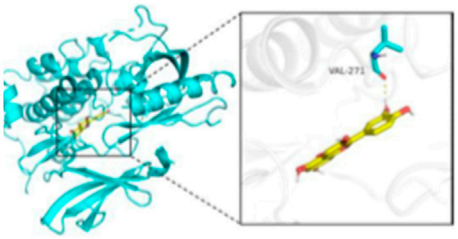	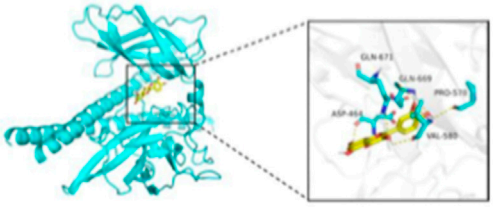

obese PCOS were obtained, and 309 potential drug targets were obtained, of which TP53, AKT1, STAT3, JUN, and SRC were the top five targets. These potential target genes are vital for immune and inflammatory processes. They participate in regulating immune and inflammatory responses through different mechanisms and pathways.

TP53 is a tumor suppressor gene that encodes the p53 protein, which plays a key role in cell cycle regulation, DNA repair, cell apoptosis, and tumor inhibition. p53-mediated GHRH antagonists have a positive effect on inflammation (Barabutis et al., 2018). AKT1 is a member of the AKT family. The AKT signaling pathway regulates the survival, differentiation, and activation of

TABLE 3 Comparison of clinical manifestations among three groups of patients.

Group	Gn medication days	Gn dosage (IU)	Early abortion rate	Ongoing pregnancy rate
blank control group (n = 41)	8.98 ± 2.21	1786.89 ± 406.28	2/41 (9.76%)	19/41 (46.3%)
CFDT group (n = 40)	8.75 ± 1.43	1896.56 ± 336.90$^{\#}$	6/40 (15%)	16/40 (40.0%)$^{\#}$
control group (n = 38)	9.82 ± 1.67	2260.53 ± 586.67*	5/38 (13.2%)	6/38 (15.8%)*

*$P < 0.05$ compared with blank control group.
$^{\#}P < 0.05$ compared with control group.

TABLE 4 Comparison of laboratory outcomes among three groups of patients.

Group	Oocytes obtained	Available embryos	High-quality embryos
blank control group (n = 41)	9.27 ± 4.25$^{\#}$	8.39 ± 4.19$^{\#}$	3.71 ± 1.47
CFDT group (n = 40)	21.03 ± 6.61*	17.33 ± 2.61*$^{\#}$	3.83 ± 1.38$^{\#}$
control group (n = 38)	23.79 ± 5.82*	20.00 ± 4.56*	2.76 ± 1.30*

*$P < 0.05$ compared with blank control group.
$^{\#}P < 0.05$ compared with control group.

immune cells while affecting the inflammatory response. AKT activation can promote the survival and function of T and B cells and produce inflammatory factors (Santinon et al., 2022; Szydlowski et al., 2014; Zhao et al., 2019). STAT3 is a key factor in the JAK-STAT signaling pathway and is involved in cell growth, differentiation, survival, and immune regulation (Hillmer et al., 2016). Studies have found that STAT3 can inhibit autocrine IFN signaling in mouse DC and regulate Th17/Treg cell homeostasis (Zhao et al., 2021). The gene JUN which overlaps with the results of Part 1 is a major component of the AP-1 transcription factor complex and can directly participate in inflammatory responses and immune regulation by regulating the expression of inflammatory factors and cytokines (Hata et al., 2023). When T cells recognize and bind to antigenic peptides of the major histocompatibility complex through their T cell receptors, the TCR signaling pathway is activated. In the TCR signaling pathway, AP-1 is regulated by multiple upstream signals, including a series of phosphorylation events triggered by Src family kinases, Syk family kinases ZAP-70, and intrachain kinases such as Lck and Fyn. These events promote signal transduction and activation pathways, such as the Ras/MAPK pathway, leading to the activation of AP-1. AP-1 activation is essential for T cell function. It is directly involved in regulating the expression of multiple immune response-related genes, including cytokines, cell surface molecules, and factors that promote cell cycle progression. Thus, AP-1 plays a regulatory role in T cell proliferation, differentiation (such as differentiation of helper T cells Th1 and Th2), and cell death. SRC encodes a non-receptor tyrosine kinase. SRC kinases play a role in various cell types. SRC kinases regulate various key processes in the immune system, including cell activation, proliferation, differentiation, and cell-to-cell communication (Brian and Freedman, 2021). KEGG pathway enrichment analysis revealed that the potential targets of CFDT for obese PCOS were mainly immune regulation and inflammation-related signaling pathways, such as the IL-17 signaling pathway, FoxO signaling pathway, Th17 cell differentiation, TCR signaling pathway, PI3K-Akt signaling pathway, and Toll-like receptor signaling pathway. The immune system is a defense system composed of many biological structures that protect the host from diseases. If the human immune system is out of balance, it can lead to various diseases. Patients with PCOS were found to be in a chronic low-grade inflammatory state, including high white blood cell levels, endothelial dysfunction, and proinflammatory cytokine disorders (Gonzalez et al., 2014; Petrikova et al., 2010). It can be inferred that CFDT, a traditional Chinese decoction, may affect obese PCOS through mechanisms related to immune regulation and inflammatory responses.

In the clinical trial described in part 3, CFDT exhibited good clinical efficacy. Women of childbearing age usually release one egg during each menstrual cycle. To improve the success rate and reduce medical expenses, IVF patients will be treated using an ovarian stimulation superovulation protocol to obtain more eggs in a single cycle, thereby increasing the possibility of pregnancy. Studies have found that high doses of Gn during IVF-ET will affect the endocrine environment during egg growth and embryo transfer, which may affect embryo implantation and later development. Exogenous gonadotropins may also interfere with trophoblast growth and invasion, thereby affecting pregnancy outcomes (Liu et al., 2021). This study revealed that the doses of Gn used in the CFDT group (1896.56 ± 336.90 IU) were statistically lower than those in the control group (2260.53 ± 586.67 IU). The day of using Gn was also reduced. The dosage and duration of Gn use can reduce the economic and psychological burden on patients. The laboratory results indicated a statistically non-significant difference in the number of eggs retrieved between the CFDT (21.03 ± 6.61) and control groups (23.79 ± 5.82). However, the number of high-quality embryos in the CFDT group (3.83 ± 1.38) was statistically higher than in the control group (2.76 ± 1.30). This suggests that the CFDT group can obtain a more satisfactory number of eggs retrieved by reducing the dosage of Gn and improving D3 embryo quality. Clinical data revealed that the continuous pregnancy rate in the CFDT group (40%) was significantly higher than that in the control group (15.8%), indicating that CFDT can improve the treatment outcome of patients with obese PCOS.

Our study has some limitations. First, the sample size in part 1 was relatively small, which might have caused deviations in the results. In the future, more samples can be included in the scRNA-seq database for comprehensive analysis. Second, the study only focused on scRNA-seq, network pharmacology, and clinical manifestations and did not verify the sequencing results directly. In the future, T cells can be separated for cell culture, CFDT-containing serum can be used for intervention, and potential target gene detection can be performed on different cell subsets.

5 Conclusion

To summarize, this study combines scRNA-seq, network pharmacology, and clinical observation for the first time. It innovatively explores the effects of traditional Chinese medicine on obese PCOS from an immune perspective. Bioinformatics analysis and clinical observation results depicted that patients with PCOS, particularly obese patients with PCOS, have changes in the immune microenvironment. Quercetin, carvacrol, β-sitosterol, cholesterol, and nobiletin are the main active ingredients of CFDT. These ingredients may improve the immune microenvironment of obese patients with PCOS through targets such as TP53, AKT1, STAT3, JUN, and SRC and are based on pathways such as TRC signaling pathways, thereby improving clinical outcomes. These findings are expected to guide the application and further development of CFDT for treating PCOS.

Data availability statement

The data on human single-cell RNA sequencing are not readily available because of patient privacy or ethical restrictions. Reasonable requests to access the datasets should be directed to corresponding author.

Ethics statement

The studies involving humans were approved by Ethics Committee of the Affiliated Hospital of Shandong University of Traditional Chinese Medicine. The studies were conducted in accordance with the local legislation and institutional requirements. The participants provided their written informed consent to participate in this study. Written informed consent was obtained from the individual(s) for the publication of any potentially identifiable images or data included in this article.

Author contributions

DL: Formal Analysis, Methodology, Writing–original draft. CW: Data curation, Investigation, Writing–review and editing. LG: Formal Analysis, Writing–review and editing. WJ: Writing–review and editing. SX: Methodology, Resources, Supervision, Writing–review and editing. FL: Funding acquisition, Methodology, Project administration, Resources, Supervision, Writing–review and editing.

Funding

The author(s) declare that financial support was received for the research, authorship, and/or publication of this article. This research was supported by the Natural Science Foundation of China (grant number: 82174429), Natural Science Foundation of China (grant number: 81774355).

Conflict of interest

The authors declare that the research was conducted in the absence of any commercial or financial relationships that could be construed as a potential conflict of interest.

Publisher's note

References

Abo-El-Yazid, Z. H., Ahmed, O. K., El-Tholoth, M., and Ali, M. A. (2022). Green synthesized silver nanoparticles using Cyperus rotundus L. extract as a potential antiviral agent against infectious laryngotracheitis and infectious bronchitis viruses in chickens. *Chem. Biol. Technol. Agric.* 9 (1), 55. doi:10.1186/s40538-022-00325-z

Addala, D. N., Kanellakis, N. I., Bedawi, E. O., Dong, T., and Rahman, N. M. (2022). Malignant pleural effusion: updates in diagnosis, management and current challenges. *Front. Oncol.* 12, 1053574. doi:10.3389/fonc.2022.1053574

Alam, N., Banu, N., Alam, N. U., Ruman, U., Khan, Z., Ibn Aziz, M. A., et al. (2022). Deciphering the pharmacological potentials of methanol extract of sterculia foetida seeds using experimental and computational approaches. *Evid. Based Complement. Altern. Med.* 2022, 3403086. doi:10.1155/2022/3403086

Alcover, A., Alarcon, B., and Di Bartolo, V. (2018). Cell biology of T cell receptor expression and regulation. *Annu. Rev. Immunol.* 36, 103–125. doi:10.1146/annurev-immunol-042617-053429

Azizi, E., Carr, A. J., Plitas, G., Cornish, A. E., Konopacki, C., Prabhakaran, S., et al. (2018). Single-cell map of diverse immune phenotypes in the breast tumor microenvironment. *Cell* 174 (5), 1293–1308. doi:10.1016/j.cell.2018.05.060

Barabutis, N., Schally, A. V., and Siejka, A. (2018). P53, GHRH, inflammation and cancer. *EBioMedicine* 37, 557–562. doi:10.1016/j.ebiom.2018.10.034

Bozdag, G., Mumusoglu, S., Zengin, D., Karabulut, E., and Yildiz, B. O. (2016). The prevalence and phenotypic features of polycystic ovary syndrome: a systematic review and meta-analysis. *Hum. Reprod.* 31 (12), 2841–2855. doi:10.1093/humrep/dew218

Brian, B. F. T., and Freedman, T. S. (2021). The src-family kinase lyn in immunoreceptor signaling. *Endocrinology* 162 (10), bqab152. doi:10.1210/endocr/bqab152

Caballero, B. (2019). Humans against obesity: who will win? *Adv. Nutr.* 10 (Suppl. l_1), S4–S9. doi:10.1093/advances/nmy055

Chen, S., Zhang, Y., Ding, X., and Li, W. (2022). Identification of lncRNA/circRNA-miRNA-mRNA ceRNA network as biomarkers for hepatocellular carcinoma. *Front. Genet.* 13, 838869. doi:10.3389/fgene.2022.838869

Christ, J. P., and Cedars, M. I. (2023). Current guidelines for diagnosing PCOS. *Diagn. (Basel)* 13 (6), 1113. doi:10.3390/diagnostics13061113

Frey, H., and Aakvaag, A. (1981). The treatment of essential hirsutism in women with cyproterone acetate and ethinyl estradiol. Clinical and endocrine effects in 10 cases. *Acta Obstet. Gynecol. Scand.* 60 (3), 295–300. doi:10.3109/00016348109158134

Golke, T., Mucher, P., Schmidt, P., Radakovics, A., Repl, M., Hofer, P., et al. (2022). Delays during PBMC isolation have a moderate effect on yield, but severly compromise cell viability. *Clin. Chem. Lab. Med.* 60 (5), 701–706. doi:10.1515/cclm-2022-0003

Gonzalez, F., Kirwan, J. P., Rote, N. S., Minium, J., and O'Leary, V. B. (2014). Glucose and lipopolysaccharide regulate proatherogenic cytokine release from mononuclear cells in polycystic ovary syndrome. *J. Reprod. Immunol.* 103, 38–44. doi:10.1016/j.jri.2014.01.001

Hata, M., Andriessen, E., Hata, M., Diaz-Marin, R., Fournier, F., Crespo-Garcia, S., et al. (2023). Past history of obesity triggers persistent epigenetic changes in innate immunity and exacerbates neuroinflammation. *Science* 379 (6627), 45–62. doi:10.1126/science.abj8894

Hillmer, E. J., Zhang, H., Li, H. S., and Watowich, S. S. (2016). STAT3 signaling in immunity. *Cytokine Growth Factor Rev.* 31, 1–15. doi:10.1016/j.cytogfr.2016.05.001

Hughes, E., Brown, J., Collins, J. J., and Vanderkerchove, P. (2010). Clomiphene citrate for unexplained subfertility in women. *Cochrane Database Syst. Rev.* 2010 (1), CD000057. doi:10.1002/14651858.CD000057.pub2

Johnson, N. F. (2021). Inhalation toxicity of Talc. *J. Aerosol Med. Pulm. Drug Deliv.* 34 (2), 79–107. doi:10.1089/jamp.2020.1609

Kanagali, S. N., Patil, B. M., Khanal, P., and Unger, B. S. (2022). Cyperus rotundus L. reverses the olanzapine-induced weight gain and metabolic changes-outcomes from network and experimental pharmacology. *Comput. Biol. Med.* 141, 105035. doi:10.1016/j.compbiomed.2021.105035

Ke, Z., Zhao, Y., Tan, S., Chen, H., Li, Y., Zhou, Z., et al. (2020). Citrus reticulata Blanco peel extract ameliorates hepatic steatosis, oxidative stress and inflammation in HF and MCD diet-induced NASH C57BL/6 J mice. *J. Nutr. Biochem.* 83, 108426. doi:10.1016/j.jnutbio.2020.108426

Koonrungsesomboon, N., Na-Bangchang, K., and Karbwang, J. (2014). Therapeutic potential and pharmacological activities of Atractylodes lancea (Thunb.) DC. *Asian Pac J. Trop. Med.* 7 (6), 421–428. doi:10.1016/S1995-7645(14)60069-9

Lamichhane, G., Pandey, J., and Devkota, H. P. (2022). Bioactive chemical constituents and pharmacological activities of ponciri fructus. *Molecules* 28 (1), 255. doi:10.3390/molecules28010255

Legro, R. S., Arslanian, S. A., Ehrmann, D. A., Hoeger, K. M., Murad, M. H., Pasquali, R., et al. (2013). Diagnosis and treatment of polycystic ovary syndrome: an Endocrine Society clinical practice guideline. *J. Clin. Endocrinol. Metab.* 98 (12), 4565–4592. doi:10.1210/jc.2013-2350

Li, L., Zuo, Z. T., and Wang, Y. Z. (2022). The traditional usages, chemical components and pharmacological activities of wolfiporia cocos: a review. *Am. J. Chin. Med.* 50 (2), 389–440. doi:10.1142/S0192415X22500161

Liu, S., Chen, L., Duan, W., Meng, Z., Dong, H., and Wang, X. (2022). Comparison of physicochemical and bioactive properties of polysaccharides from Massa Medicata Fermentata and its processed products. *ACS Omega* 7 (50), 46833–46842. doi:10.1021/acsomega.2c05932

Liu, S., Hong, L., Mo, M., Xiao, S., Chen, C., Li, Y., et al. (2021). Evaluation of endometrial immune status of polycystic ovary syndrome. *J. Reprod. Immunol.* 144, 103282. doi:10.1016/j.jri.2021.103282

Liu, Y., Jia, Z., Dong, L., Wang, R., and Qiu, G. (2008). A randomized pilot study of atractylenolide I on gastric cancer cachexia patients. *Evid. Based Complement. Altern. Med.* 5 (3), 337–344. doi:10.1093/ecam/nem031

Long, Y., Yu, S., Li, D., Shi, A., Ma, Y., Deng, J., et al. (2023). Preparation, characterization and safety evaluation of Ligusticum chuanxiong essential oils liposomes for treatment of cerebral ischemia-reperfusion injury. *Food Chem. Toxicol.* 175, 113723. doi:10.1016/j.fct.2023.113723

Luan, Y. Y., Zhang, L., Peng, Y. Q., Li, Y. Y., Liu, R. X., and Yin, C. H. (2022). Immune regulation in polycystic ovary syndrome. *Clin. Chim. Acta* 531, 265–272. doi:10.1016/j.cca.2022.04.234

Meier, R. K. (2018). Polycystic ovary syndrome. *Nurs. Clin. North Am.* 53 (3), 407–420. doi:10.1016/j.cnur.2018.04.008

Misso, M. L., Teede, H. J., Hart, R., Wong, J., Rombauts, L., Melder, A. M., et al. (2012). Status of clomiphene citrate and metformin for infertility in PCOS. *Trends Endocrinol. Metab.* 23 (10), 533–543. doi:10.1016/j.tem.2012.07.001

Mohamed, A. A., Ahmed, M. M., Gomaa, M., and Ebraheim, L. L. M. (2018). Bone health consequence of adjuvant Anastrozole in monotherapy or associated with biochanin-A in ovariectomized rat model. *Life Sci.* 212, 159–167. doi:10.1016/j.lfs.2018.09.059

Moini Jazani, A., Nasimi Doost Azgomi, H., Nasimi Doost Azgomi, A., and Nasimi Doost Azgomi, R. (2019). A comprehensive review of clinical studies with herbal medicine on polycystic ovary syndrome (PCOS). *Daru* 27 (2), 863–877. doi:10.1007/s40199-019-00312-0

Nakajima, A., Nemoto, K., and Ohizumi, Y. (2020). An evaluation of the genotoxicity and subchronic toxicity of the peel extract of Ponkan cultivar 'Ohta ponkan' (Citrus reticulata Blanco) that is rich in nobiletin and tangeretin with anti-dementia activity. *Regul. Toxicol. Pharmacol.* 114, 104670. doi:10.1016/j.yrtph.2020.104670

Nie, A., Chao, Y., Zhang, X., Jia, W., Zhou, Z., and Zhu, C. (2020). Phytochemistry and pharmacological activities of wolfiporia cocos (F.A. Wolf) ryvarden and gilb. *Front. Pharmacol.* 11, 505249. doi:10.3389/fphar.2020.505249

Ono, M. (2020). Control of regulatory T-cell differentiation and function by T-cell receptor signalling and Foxp3 transcription factor complexes. *Immunology* 160 (1), 24–37. doi:10.1111/imm.13178

Petrikova, J., Lazurova, I., and Yehuda, S. (2010). Polycystic ovary syndrome and autoimmunity. *Eur. J. Intern Med.* 21 (5), 369–371. doi:10.1016/j.ejim.2010.06.008

Pirzada, A. M., Ali, H. H., Naeem, M., Latif, M., Bukhari, A. H., and Tanveer, A. (2015). Cyperus rotundus L.: traditional uses, phytochemistry, and pharmacological activities. *J. Ethnopharmacol.* 174, 540–560. doi:10.1016/j.jep.2015.08.012

Qu, L., Liu, C., Ke, C., Zhan, X., Li, L., Xu, H., et al. (2022). Atractylodes lancea rhizoma attenuates DSS-induced colitis by regulating intestinal flora and metabolites. *Am. J. Chin. Med.* 50 (2), 525–552. doi:10.1142/S0192415X22500203

Ran, X., Ma, L., Peng, C., Zhang, H., and Qin, L. P. (2011). Ligusticum chuanxiong Hort: a review of chemistry and pharmacology. *Pharm. Biol.* 49 (11), 1180–1189. doi:10.3109/13880209.2011.576346

Reichman, D. E., Missmer, S. A., Berry, K. F., Ginsburg, E. S., and Racowsky, C. (2011). Effect of time between human chorionic gonadotropin injection and egg retrieval is age dependent. *Fertil. Steril.* 95 (6), 1990–1995. doi:10.1016/j.fertnstert.2011.02.043

Reiley, W. W., Jin, W., Lee, A. J., Wright, A., Wu, X., Tewalt, E. F., et al. (2007). Deubiquitinating enzyme CYLD negatively regulates the ubiquitin-dependent kinase Tak1 and prevents abnormal T cell responses. *J. Exp. Med.* 204 (6), 1475–1485. doi:10.1084/jem.20062694

Rellahan, B. L., Graham, L. J., Stoica, B., DeBell, K. E., and Bonvini, E. (1997). Cbl-mediated regulation of T cell receptor-induced AP1 activation. Implications for activation via the Ras signaling pathway. *J. Biol. Chem.* 272 (49), 30806–30811. doi:10.1074/jbc.272.49.30806

Rotterdam, E. A.-S. P. C. W. G. (2004). Revised 2003 consensus on diagnostic criteria and long-term health risks related to polycystic ovary syndrome (PCOS). *Hum. Reprod.* 19 (1), 41–47. doi:10.1093/humrep/deh098

Sadeghi, H. M., Adeli, I., Calina, D., Docea, A. O., Mousavi, T., Daniali, M., et al. (2022). Polycystic ovary syndrome: a comprehensive review of pathogenesis, management, and drug repurposing. *Int. J. Mol. Sci.* 23 (2), 583. doi:10.3390/ijms23020583

Santinon, F., Ezzahra, B. F., Bachais, M., Sarabia Pacis, A., and Rudd, C. E. (2022). Direct AKT activation in tumor-infiltrating lymphocytes markedly increases interferon-gamma (IFN-gamma) for the regression of tumors resistant to PD-1 checkpoint blockade. *Sci. Rep.* 12 (1), 18509. doi:10.1038/s41598-022-23016-z

Shah, K., Al-Haidari, A., Sun, J., and Kazi, J. U. (2021). T cell receptor (TCR) signaling in health and disease. *Signal Transduct. Target Ther.* 6 (1), 412. doi:10.1038/s41392-021-00823-w

Suntar, I., Khan, H., Patel, S., Celano, R., and Rastrelli, L. (2018). An overview on Citrus aurantium L.: its functions as food ingredient and therapeutic agent. *Oxid. Med. Cell Longev.* 2018, 7864269. doi:10.1155/2018/7864269

Szydlowski, M., Jablonska, E., and Juszczynski, P. (2014). FOXO1 transcription factor: a critical effector of the PI3K-AKT axis in B-cell development. *Int. Rev. Immunol.* 33 (2), 146–157. doi:10.3109/08830185.2014.885022

Tao, X., Li, J., He, J., Jiang, Y., Liu, C., Cao, W., et al. (2023). Pinellia ternata (Thunb.) Breit. attenuates the allergic airway inflammation of cold asthma via inhibiting the activation of TLR4-medicated NF-kB and NLRP3 signaling pathway. *J. Ethnopharmacol.* 315, 116720. doi:10.1016/j.jep.2023.116720

Udrescu, L., Bogdan, P., Chis, A., Sirbu, I. O., Topirceanu, A., Varut, R. M., et al. (2020). Uncovering new drug properties in target-based drug-drug similarity networks. *Pharmaceutics* 12 (9), 879. doi:10.3390/pharmaceutics12090879

Wang, J., Yin, T., and Liu, S. (2023a). Dysregulation of immune response in PCOS organ system. *Front. Immunol.* 14, 1169232. doi:10.3389/fimmu.2023.1169232

Wang, M., Yang, N., Wu, X., Zou, T., Zheng, J., Zhu, H., et al. (2023b). Insight into nephrotoxicity and processing mechanism of Arisaema erubescens (wall.) schott by metabolomics and network analysis. *Drug Des. Devel Ther.* 17, 1831–1846. doi:10.2147/DDDT.S406551

Witchel, S. F., Teede, H. J., and Pena, A. S. (2020). Curtailing PCOS. *Pediatr. Res.* 87 (2), 353–361. doi:10.1038/s41390-019-0615-1

Xue, B. X., He, R. S., Lai, J. X., Mireku-Gyimah, N. A., Zhang, L. H., and Wu, H. H. (2023). Phytochemistry, data mining, pharmacology, toxicology and the analytical methods of Cyperus rotundus L. (Cyperaceae): a comprehensive review. *Phytochem. Rev.* 22, 1353–1398. doi:10.1007/s11101-023-09870-3

Yang, Y., Sun, H., Zhang, Y., Zhang, T., Gong, J., Wei, Y., et al. (2021). Dimensionality reduction by UMAP reinforces sample heterogeneity analysis in bulk transcriptomic data. *Cell Rep*. 36 (4), 109442. doi:10.1016/j.celrep.2021.109442

Zhang, X., Zhang, H., Huang, Q., Sun, J., Yao, R., and Wang, J. (2020). Effect of Massa Medicata Fermentata on the gut microbiota of dyspepsia mice based on 16S rRNA technique. *Evid. Based Complement. Altern. Med.* 2020, 7643528. doi:10.1155/2020/7643528

Zhao, L., Zhang, H., Li, N., Chen, J., Xu, H., Wang, Y., et al. (2023). Network pharmacology, a promising approach to reveal the pharmacology mechanism of Chinese medicine formula. *J. Ethnopharmacol.* 309, 116306. doi:10.1016/j.jep.2023.116306

Zhao, Y., Han, P., Liu, L., Wang, X., Xu, P., Wang, H., et al. (2019). Indirubin modulates CD4(+) T-cell homeostasis via PD1/PTEN/AKT signalling pathway in immune thrombocytopenia. *J. Cell Mol. Med.* 23 (3), 1885–1898. doi:10.1111/jcmm.14089

Zhao, Y., Luan, H., Jiang, H., Xu, Y., Wu, X., Zhang, Y., et al. (2021). Gegen Qinlian decoction relieved DSS-induced ulcerative colitis in mice by modulating Th17/Treg cell homeostasis via suppressing IL-6/JAK2/STAT3 signaling. *Phytomedicine* 84, 153519. doi:10.1016/j.phymed.2021.153519

Zou, T., Wang, J., Wu, X., Yang, K., Zhang, Q., Wang, C., et al. (2023). A review of the research progress on Pinellia ternata (Thunb.) Breit.: botany, traditional uses, phytochemistry, pharmacology, toxicity and quality control. *Heliyon* 9 (11), e22153. doi:10.1016/j.heliyon.2023.e22153

frontiers | Frontiers in Pharmacology

TYPE Original Research
PUBLISHED 19 November 2024
DOI 10.3389/fphar.2024.1483518

OPEN ACCESS

EDITED BY
Michael Heinrich,
University College London, United Kingdom

REVIEWED BY
Fei Lin,
The First Affiliated Hospital of Xinjiang Medical University, China
Bing You Yang,
Heilongjiang University of Chinese Medicine, China

*CORRESPONDENCE
Hengwen Chen,
chenhengwen@163.com
Xuanhui He,
hexuanzi1646@sina.com

†These authors have contributed equally to this work and share first authorship

RECEIVED 20 August 2024
ACCEPTED 07 November 2024
PUBLISHED 19 November 2024

CITATION
Yao B, Ma J, Ran Q, Chen H and He X (2024) Mechanism of *Valeriana officinalis L.* extract improving atherosclerosis by regulating PGC-1α/Sirt3/Epac1 pathway.
Front. Pharmacol. 15:1483518.
doi: 10.3389/fphar.2024.1483518

Mechanism of *Valeriana officinalis L.* extract improving atherosclerosis by regulating PGC-1α/Sirt3/Epac1 pathway

Bo Yao[1,2†], Jingzhuo Ma[1†], Qingzhi Ran[1], Hengwen Chen[1*] and Xuanhui He[1*]

[1]Guang'anmen Hospital, China Academy of Chinese Medical Sciences, Beijing, China, [2]School of Pharmaceutical Sciences, Changchun University of Chinese Medicine, Changchun, China

Objective: To investigate the protective effect of the of *Valeriana officinalis L.* extract on mitochondrial injury in AS mice and the underlying mechanism.

Methods: Firstly, Ultra-High performance liquid chromatography-quadrupole time-of-flight mass spectrometer (UPLC / Q-TOF-MS) was proposed to explore the chemical composition of *Valeriana officinalis L.* extract. ApoE-/- mice were employed for in vivo experiments. The efficacy of *Valeriana officinalis L.* extract was detected by B-ultrasound, Biochemical, Oil Red O staining, HE staining and Masson staining analysis. The molecular mechanism of *Valeriana officinalis L.* extract in regulating mitochondrial energy metabolism for the treatment of atherosclerosis was elucidated after Monitoring System of Vascular Microcirculation *in Vivo* and transmission electron microscopy. Use the corresponding reagent kit to detect ACTH level, CHRNα1 level and ATP level, and measure the expression levels of PGC-1α, Sirt3, Epac1, Caspase-3, and Caspase-9 through real-time qPCR, and Western blot.

Results: A total of 29 metabolites were newly discovered from KYXC using UPLC-MS. The drug had a significant positive effect on the growth of atherosclerotic plaque in mice. It also improved the microcirculation of the heart and mesentery, reduced the levels of CHOL, TG, and VLDL in the serum, and increased the levels of HDL-C to maintain normal lipid metabolism in the body. Additionally, it increased the levels of ATP, improved the ultrastructure of mitochondria to maintain mitochondrial energy metabolism, and increased the levels of T-SOD to combat oxidative stress of the organism. Furthermore, the drug significantly increased the mRNA and protein expression of PGC-1α and Sirt3 in aortic tissue, while decreasing the mRNA and protein expression of Epac1, Caspase-3, and Caspase-9.

Conclusion: This study has verified that the extract of *Valeriana officinalis L.* is highly effective in enhancing atherosclerosis disease. The mechanism is suggested through the PGC-1α/Sirt3/Epac1 signaling pathway, which improves mitochondrial energy metabolism.

KEYWORDS

***Valeriana officinalis L.* extract, atherosclerosis, PGC-1α/Sirt3/Epac1 pathway, mitochondrial damage, traditional Chinese medicine**

1 Introduction

Cardiovascular disease (CVD) is the leading cause of morbidity and mortality, affecting over 523 million people globally, and CVD mortality rates are predominated by atherosclerotic diseases (Nedkoff et al., 2023). Atherosclerosis (AS), a cardiovascular disease with a significant global mortality rate, has been a prominent focus of research in related fields for many years (Arnett et al., 2019). While medication treatment and surgical intervention can partially impede the progression of AS in clinical, cardiovascular and cerebrovascular diseases resulting from AS remain a significant global cause of mortality and disability (Marchio et al., 2019). Atherosclerosis is an essential clinical pathophysiological process characterized by endothelial damage and dysfunction leading to lipid deposition in the vascular wall. It involves various structural alterations in the vascular walls of large and medium-sized arteries, followed with the development of atherosclerotic plaques (Libby, 2021). This condition is typically manifested by the excessive accumulation of ox-LDL and intravascular hyperplasia (Jaganjac et al., 2020). Under microscopic examination, various pathological changes can be observed, including lipid deposition, smooth muscle cell proliferation, monocyte infiltration, and increased external matrix (Falk, 2006). These changes are strongly associated with the mechanisms of lipid metabolism disorder, inflammatory reaction, vascular endothelial cell dysfunction, and other mechanisms (Zhou and Wu, 2023). Thus, the occurrence and development of atherosclerosis can be effectively inhibited. By controlling lipid metabolism, reducing inflammatory reaction, and improving the function of vascular endothelial cells.

The ApoE$^{-/-}$ mice is currently a widely used model for studying atherosclerosis. This is due to its ability to develop atherosclerotic lesions spontaneously, as well as its close resemblance to humans in terms of pathology and histology (Manea et al., 2020). Additionally, research has demonstrated that the progression of atherosclerosis in ApoE$^{-/-}$ mice closely resembles type II hyperlipidemia in humans. These mice readily develop atherosclerotic plaques at specific locations, including the aortic root, lesser curvature of the aortic arch, major branches of the aorta, as well as branches of the pulmonary and carotid arteries (Haofei Han et al., 2019). The study included a group of ApoE$^{-/-}$ mice who were fed a standard diet. ApoE$^{-/-}$ mice that were given a typical diet experienced challenges in initiating AS lesions and developing AS plaques. The introduction of a diet high in fat expedited the onset and progression of AS, aligning with existing literature findings.

Peroxisome proliferator-activated receptor-γ coactivator (PGC-1α) is a transcription co activator in regulating metabolic processes in the body (Rius-Pérez et al., 2020). It does so by influencing the activity of various transcription factors involved in metabolic signal transduction, mitochondrial function, inflammation, oxidative stress, etc. (Pérez et al., 2019) Sirtuin 3 (Sirt3) is a type III histone deacetylase that relies on nicotinamide adenine dinucleotide (NAD^+) for its function. It has a crucial role in regulating mitochondrial respiration, ROS clearance, lipid metabolism, fatty acid oxidation, and antioxidant activity (Lv et al., 2017). Epac, as an effector of cAMP, has been shown to protect myocardial cells from ischemic damage in the heart due to the absence of Epac1. Additionally, inhibiting the expression of Epac1 gene can suppress mitochondrial fission and ROS generation in vascular smooth muscle cells (Musheshe et al., 2022). Research has identified Sirt3 as the target gene of PGC-1α, and PGC-1α can greatly influence mitochondrial generation with inducing Sirt3 expression, and Giralt's experiment suggests that an Epac1 signalosome may exist at the mitochondria (Giralt et al., 2011; Fazal et al., 2017). Previous research conducted using a high-fat diet mouse model found that PGC-1α can promote lipid metabolism and fatty acid oxidation (Weerawatanakorn et al., 2023). Thus, enhancing the expression of PGC-1α/Sirt3/Epac1 signaling pathway to improve lipid deposition and thus regulate mitochondrial energy metabolism is a promising method to promote the regression of atherosclerotic plaque.

Valeriana officinalis L. (Caprifoliaceae; *Valeriana officinalis L.* radix et rhizoma) is a perennial herbaceous plant belonging to the Caprifoliaceae family and the Valeriana genus. The "Quality Standards for Chinese and Ethnic Medicinal Materials in Guizhou Province" (2003 edition) includes it, and it is widely used as a traditional medicinal material in Jiangsu Province, Zhejiang Province, Hubei Province, Sichuan Province, Guizhou Province and other places in China. It often grows under forests, along ravines, and on high mountain slopes (Hao Zhang and Keyi, 2023). Its nature is spicy, sweet, and warm, and it is associated with the heart and liver meridians. It has functions such as clearing heat and stopping diarrhea, calming the heart and mind, regulating qi and relieving pain, and dispelling wind and dampness (Zhang, 2021). The investigation into the therapeutic application of the traditional Chinese medicinal *Valeriana officinalis L.* for cardiovascular diseases commenced in 1994. Our group isolated 65 metabolites from the roots and stems of *Valeriana officinalis L.* in the previous study (Chen et al., 2016; Chen et al., 2015). We subsequently carried out animal and cellular studies to confirm that certain metabolites have the ability to enhance myocardial ischemia. Clinically, it has been proved that the volatile oil of *Valeriana officinalis L.* has notable therapeutic properties in relieving angina symptoms and improving myocardial ischemia. Furthermore, it has been found to be more effective than metabolite salvia miltiorrhiza in improving angina symptoms, reducing the frequency of angina, shortening the duration of angina attacks, and no toxicity to liver, kidney, and hematopoietic tissues (Yang and Wang, 1994). Moreover, Zhu et al. (2016), discovered that the iridoids in valerian can significantly reduce the lipid biochemical indicators in the serum of hyperlipidemic rats, enhance the ability of lipid metabolism in rats, and thus reduce the incidence of atherosclerosis. However, the mechanism of *Valeriana officinalis L.* on atherosclerosis is not yet fully understood.

This work aimed to explore the potential of *Valeriana officinalis L.* extract (KYXC) in improving AS plaque formation, and to uncover its precise molecular mechanism. The molecular mechanism is shown in Figure 1. After establishing an AS model in ApoE$^{-/-}$ mice, it was found that KYXC can inhibit lipid production and aggregation, enhance ATP synthesis, and improve mitochondrial function. Regarding the mechanism, it is noteworthy that KYXC can activate the expression of PGC-1α and Sirt3, while reducing the expression levels of Epac1 and apoptotic proteins such Caspase-3 and Caspase-9. This leads to an enhancement in mitochondrial energy metabolism. The study has discovered and proven the effectiveness of utilizing *Valeriana officinalis L.* extract as a treatment for AS, which could potentially establish a novel approach for a new treatment method, providing innovative research ideas for better clinical treatment of AS.

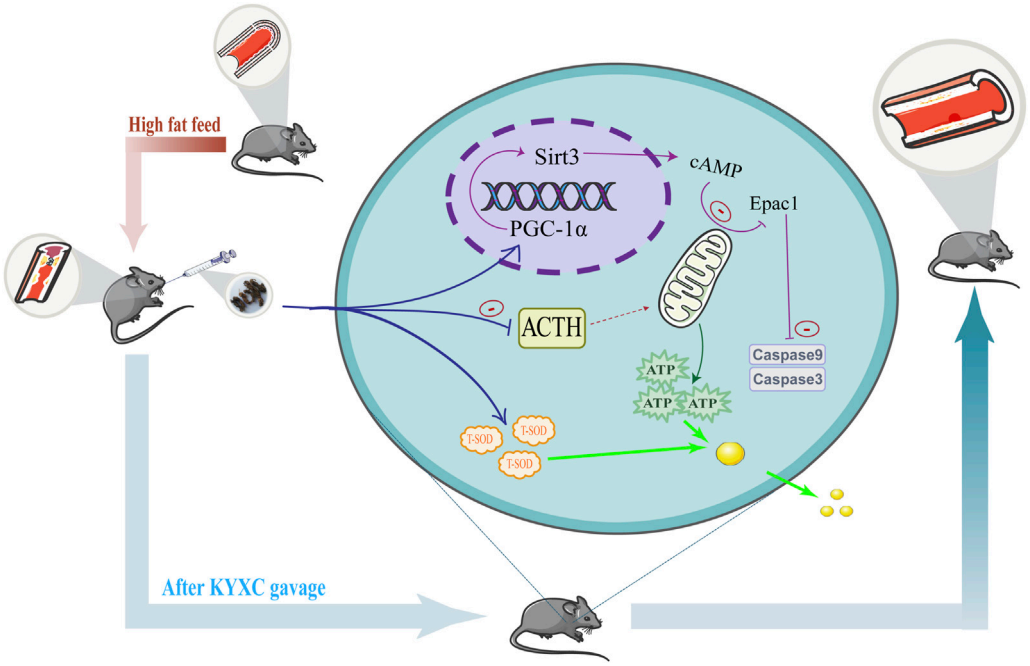

FIGURE 1
Mechanism diagram of the mechanism corresponding to KYXC improving plaque formation in AS mice.

2 Materials and methods

2.1 Preparation of KYXC

Valeriana officinalis L. (No. 01670385) sample has been deposited in the Specimen Museum of the School of Pharmacy, Guiyang University of Traditional Chinese Medicine (No. 55 Shidong Road, Guiyang City, Guizhou Province 550009, China). Medicinal herb information can be accessed through the Chinese Virtual Herbarium, a digital herbarium in China (https://www.cvh.ac.cn/index.php) Search. The *Valeriana officinalis L.* extract was obtained from Shaanxi Haiyisi Biotechnology Co., Ltd., with batch number HYS20221025. According to the identification of Deputy Chief Pharmacist Yang Hui and Chief Pharmacist Rong Lixin, it is *Valeriana officinalis L.*

The dried radix et rhizoma of *Valeriana officinalis L.* are weighed at 10 kg. The medicinal herbs of *Valeriana officinalis L.* were extracted by 10 times of water through heating reflux for twice, each time for 1.0 h. The extracts were mixed and concentrated under reduced pressure. Ethanol was added to bring the ethanol content to 70%. After 24 h, the extracts were dried in vacuum at 60°C. Finally, 1.8 kg of KYXC extract were obtained. The dry extract yielding rate of KYXC was 18.00%.

In addition, we conducted physical and chemical quality testing on the extract of *Valeriana officinalis L.*, confirming that it is a brown powder with a special odor and a fine powder that can pass 100% through 80 mesh. Among them, its ash content is 3.18%, heavy metal content ≤10 ppm, arsenic (As) content ≤2 ppm, lead (Pb) content ≤2 ppm, cadmium (Cd) content ≤0.2 ppm, mercury (Hg) content ≤0.1 ppm, all of which conform the Traditional Chinese Medicine--Determination of heavy metals in herbal medicines used in Traditional Chinese Medicine (ISO 18664:2015).

2.2 Drugs

The Rosuvastatin calcium tablets were purchased from AstraZeneca Pharmaceuticals (China) Co., Ltd., with the national drug approval number HJ20160545 and batch number 503778. All of the aforementioned drugs have undergone inspection and are now being utilized.

2.3 Main reagents and antibodies

Mass spectrometry grade solvents (including methanol, acetonitrile, and formic acid) were purchased from Thermo Fisher Scientific Co., Ltd. Proteintech provided PGC-1α antibody mouse clonal antibody, Sirt3 antibody rabbit clonal antibody, Caspase-9 antibody mouse clonal antibody, and Caspase-3 antibody mouse clonal antibody. Gene Tex Company supplied Sirt3 antibody rabbit clonal antibody. Jackson supplied Epac1 HRP × Polyclonal Goat Anti-Rabbit IgG and HRP × Polyclonal Goat Anti-Mouse IgG.

2.4 Animal model and treatment

A cohort of 70 SPF grade C57BL/6J mice and ApoE$^{-/-}$ mice, aged 8–10 weeks, male, weighing 22–26 g, were provided from Beijing Weitong Lihua Experimental Animal Technology Co., Ltd., with license number SCXK (Beijing) 2021-0006. They were raised in the

SPF level animal laboratory of Guang' anmen Hospital, Chinese Academy of Traditional Chinese Medicine, under license number SYXK (Beijing) 2014-0041. The optimal temperature for breeding is between 22°C–25°C, while the relative humidity should be maintained at 55%–70%. It is recommended to provide a 12-hour light-dark cycle and ensure that the animals have unrestricted access to food and water. The high-fat feed was purchased from Beijing Huafukang Biotechnology Co., Ltd., with certificate number SCXK (Beijing) 2019-0008. The high fat feed is composed of 78.85% basic feed, 21% fat, and 0.15% cholesterol, all of which have undergone sterilization using cobalt-60 beam irradiation. Finally, mice were euthanized at the end of the assay.

The mice were categorized into several groups: a control group (CG), a model group (MG), a blank group (BG), a rosuvastatin group (RG), a low-dose KYXC group (KG-L), a medium dose KYXC group (KG-M), and a high-dose KYXC group (KG-H). Each group consisted of 10 mice. The CG group utilized C57BL/6J normal mice, while the other groups employed ApoE$^{-/-}$ mice of the same strain. With the exception of the CG group and the BG group, the remaining groups were administered a high-fat diet for a duration of 24 weeks in order to induce the development of an atherosclerosis model in mice. During the modeling period, a total of 3 mice were randomly selected from each group to undergo testing for the formation of aortic plaque every 4 weeks. A substantial difference ($P < 0.05$) suggested the successful establishment of the atherosclerosis mouse model. Following successful modeling, all groups were administered normal feed. The RG group received a dose of 0.05 g kg^{-1} d^{-1} via gavage, while the KYXC group received doses of 0.10, 0.21, and 0.43 g kg^{-1} d^{-1} via gavage. The CG, MG, and BG groups were given an equivalent volume of distilled water. This treatment regimen was maintained for a duration of 6 weeks.

2.5 UPLC/Q-TOF-MS analysis

A chemical composition analysis of the extract obtained from *Valeriana officinalis L.* using UPLC/Q-TOF-MS technique was carried out as below. The chromatographic settings included the use of acetonitrile (B) mixed with 0.1% formic acid water (A) as the mobile phase. The flow rate was set at 0.4 mL·min^{-1}. The sampler temperature was maintained at 10°C. The sample size used was 2 μL. The temperature of the column is 40°C, and the range of wavelengths detected by the UV is from 190 nm to 500 nm. The MS conditions comprise of the electric spray ion source (ESI), both positive and negative ion detection modes, full scan scanning mode, and a scanning range of 50–1500 Da. Parameters of the ion source include a temperature of 120°C, nitrogen gas used as both the carrier gas and desolvent gas, a cone hole gas flow rate of 50 L/h, a desolvent gas temperature of 450°C, a desolvent gas flow rate of 800 L/h, and a cone hole voltage of 40 V. The capillary voltage is set at +3.0 KV in the positive ion mode and −2.5 KV in the negative ion mode. The gas used for collision induced dissociation is argon with a purity of 99.95%. The collision energy is 6 eV for low collisions and ranges from 12 to 45 eV for high collisions. The samples underwent testing using the 2,998 ultra-high performance liquid chromatography and Xevo G2-S Q-TOF high-resolution time-of-flight mass spectrometer, manufactured by Waters in the United States. The chromatographic column used is a Waters column with dimensions of 250 mm × 4.6 mm and a particle size of 5 μm. The extraction solvent consists of 50% methanol, and the recommended extraction duration is 30 min.

2.6 B-ultrasound analysis

Monitor the development of plaques in AS mice according on the timeline specified in the experimental design. The mouse's front chest was shaved for skin preparation, and put into the small animal anesthesia machine for anesthesia. Following effective administration of anesthesia, it was fixed on the operating platform in a supine position. Aortic ultrasound and cardiac ultrasound were then conducted to examine the development of atherosclerotic plaque.

2.7 Biochemical analysis

Following a 6-week period of administration, blood samples were collected from the eyeball of mice. The levels of blood lipid indicators in the serum of mice, including CHOL, TG, LDL-C, and HDL-C, were then measured using a fully automated biochemical analyzer.

2.8 Microvascular analysis

Following a 6-week period of treatment, a single mice was randomly chosen from each group to undergo anesthesia. Subsequently, the heart and mesenteric microvasculature were observed by Monitoring System of Vascular Microcirculation *in Vivo* (OCTA). The OCTA algorithm is used for the extraction of three-dimensional microvascular signals. The acquired data is then extracted using vResolve software for vascular signal extraction, then picture synthesis is performed using Reconstruction UI software.

2.9 Oil red O staining analysis

Following a 6-week period of medication intervention, samples were collected after a 12-hour fasting period. Separate and remove the blood vessels in the general aortic region, fix them for a duration of 24 h, and subsequently dissect them open. Begin by immersing them in a 60% isopropanol solution for a duration of 3 s. Next, proceed to stain them using an oil red O staining solution at a temperature of 37°C in a dark environment for 60 min. Finally, remove them after the staining process is complete. Submerge them in a solution of 60% isopropanol to distinguish red adipose plaques in the inner space and colorless in other regions. Then, eliminate the blood vessels and use filter paper to eliminate any remaining water. Examine the entirety of the plaque formation in the aorta using a microscope, collect images and analyze the percentage of gross oil red fat area using Image Pro plus 6.0 software.

Obtain a specimen of aorta tissue, encase it in OCT, and slice it using a frozen sectioning machine with a thickness of 20 μm. The process involves staining, sealing, and observing the lipid staining in Aortic endothelial cells using Oil Red O staining method under the microscope.

TABLE 1 Primer sequence.

Gene name	Forward primers (5′-3′)	Reverse primer (5′-3′)
PGC-1α	AACTGCAGATTTGATGGAGCTAC	CATGTAGAATTGGCAGGTGGA
Sirt3	CTGGATGGACAGGACAGATAAGA	GTTGTGGTCTGGTTCATGTTTGT
caspase-9	GCCCCTCACAGTTCAGAATGG	GCCCACAACTGCATGTGTAGA
caspase-3	GCTTCCTTGTTGCACAAAGAA	CATCACATGCTGCATTCACTTAG
Epac1	CGGTGGTCTCAGAGGAGTTGTA	GAGATAGATGGTGGGTGTCTGCT
GAPDH	CAAGCTCATTTCCTGGTATGACA	TCTCTTGCTCAGTGTCCTTGCT

2.10 HE and masson staining analysis

After a duration of 6 weeks, samples were collected and then embedded in paraffin to preserve the heart tissue specimen. Subsequently, the tissue was sectioned. The tissue was sliced into sequential sections measuring 4 μm in thickness. These sections were then submitted to HE and Masson staining in order to observe any pathological and morphological alterations associated with the heart. Images were acquired for analysis.

2.11 Mitochondrial functional analysis

Following a 6-week period of delivery, a sample of aorta tissue measuring roughly 1 mm^3 was collected and subjected to a series of procedures including fixation, dehydration, infiltration, embedding, slicing, and staining. The prepared sample was then examined under a transmission electron microscope for observation. Collected images were subjected to analysis.

2.12 Serum index assay

After a duration of 6 weeks, adhere to the directions provided by the reagent kit to measure the concentrations of ACTH, CHRNα1, and ATP in the serum of mice.

2.13 Analysis of antioxidant levels

Perform a dissection on the cardiac tissue of mice on a platform made of ice. Subsequently, store the dissected tissue in a freezer set to a temperature of −80°C. Weigh the heart tissue and add corresponding reagents, grind it into tissue homogenate, centrifuge at 12,000 rpm for 15 min, and take the supernatant. Perform T-SOD activity detection in tissue supernatant following the directions provided with the reagent kit.

2.14 RT-qPCR analysis

Mice aorta and cardiac tissues were subjected to RNA extraction using Trizol reagent. Following reverse transcription of RNA into complementary DNA (cDNA) using a reverse transcription kit, a real-time quantitative PCR (qPCR) kit was employed to identify the presence of PGC-1α, Sirt3, Epac1, Caspase-9, and Caspase-3 mRNA in the aorta and heart tissue using a real-time quantitative PCR apparatus. Each reaction is replicated three times. The RT-qPCR primers are listed in Table 1.

2.15 Western-blot analysis

Solidify To prepare the aortic tissue, first grind it. Then, take a portion of the ground tissue and add cold protease inhibitors and lysate. Next, break and grind the tissue using a tissue grinder. After that, centrifuge the mixture and collect the supernatant. Measure the protein concentration using the BCA protein quantification kit's instructions. Finally, adjust the protein concentration using RIPA. Conduct Western Blot studies following the denaturation of the protein solution. Prepare the separation gel and concentration gel according to the molecular weight of the target protein. Employing the wet transfer technique for film transfer. Once the membrane transfer is finished, proceed to seal it for a duration of 30 min. Dilute the primary antibodies PGC-1α, Sirt3, Caspase-9, Caspase-3, and Epac1 in the respective ratios of 1:10000, 1:2000, 1:10000, 1:2000, and 1:1000. Incubate the diluted antibodies overnight at a temperature of 4°C. The secondary antibody chosen was goat anti-mouse IgG (H + L) HRP 1:10000. It was incubated at room temperature, in the absence of light, and on a shaking bed for a duration of 2 h. Position the chemiluminescence apparatus for automated exposure and conduct quantitative analysis utilizing ImageJ.

2.16 Statistical analysis

The grade data were analyzed using SPSS 27.0 software. The statistical analysis was conducted using GraphPad software version 6. The results were reported as the mean plus or minus the standard deviation. Comparisons involving more than two groups were conducted using one-way analysis of variance (ANOVA) with Bonferroni *post hoc* testing to evaluate the differences among the groups. A *p*-value of less than 0.05 was used to determine statistical significance.

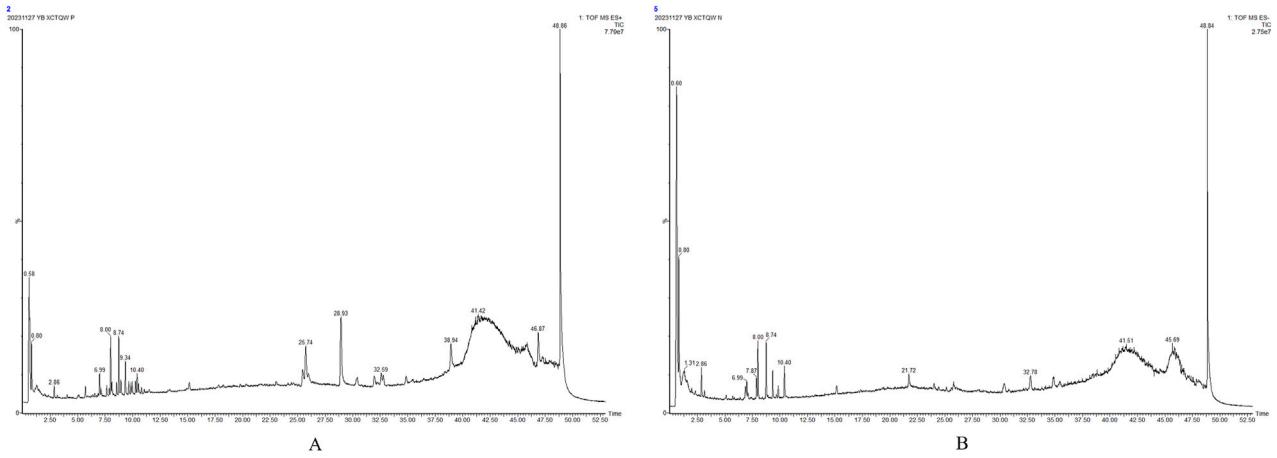

FIGURE 2
BPC of KYXC in positive ion mode. **(A)** BPC of KYXC in negative ion mode **(B)**.

3 Results

3.1 KYXC chemical metabolites analyzed by UPLC/Q-TOF-MS

This study initially organized the pertinent material on the chemical makeup of KYXC using literature and related databases. The chemical composition information of the traditional Chinese medication KYXC was compiled by conducting a comprehensive search of domestic and international literature, as well as relevant chemical databases like Scifinder, Pubmed, ChemicalBook, CNKI, etc. By utilizing chromatographic peak separation as a measure, the elution parameters were fine-tuned, and the ultimate analytical conditions were established. Under these circumstances, excellent chromatographic separation and a significant mass spectrometry response were achieved. Figures 2A, B depict the Basic Peak Graph (BPC) of positive and negative ions, respectively. The metabolites can be found in Table 2, 3. It is evident that a total of 29 substances were identified. Volvalerenic A is the primary metabolite among them.

3.2 KYXC reduces the formation of aortic plaques in mice

Figures 3A, B demonstrate that mice in the MG group, after being fed a high-fat diet, developed many atherosclerotic plaques in both the aortic arch and abdominal aorta. This indicates that the modeling process was successful. When comparing the CG group to the MG group, the mice in the MG group exhibited noticeable plaque and an irregular aortic wall, with a significant distinction ($P < 0.01$). Additionally, when comparing the MG group to each treatment group, the atherosclerotic plaques were decreased to varying extents, and the difference was substantial ($P < 0.001$).

Cardiac remodeling and alterations in heart function are strongly associated with modifications in left ventricular volume (LVVs), interventricular septal thickness (IVSd), left ventricular posterior wall thickness (LVPWd), ejection fraction (EF), and other markers. Thus, these markers are frequently employed to assess heart function and can precisely depict cardiac function. According to Figures 3C–F, the LVVs of the MG group increased significantly compared to the CG group ($P < 0.01$). Additionally, the LVVs of the KG-M group were significantly reduced compared to the MG group ($P < 0.05$). Furthermore, the statistical analysis revealed that there was no significant impact on the markers of IVSd, LVPWd, EF, and other parameters. This suggests that the current condition of AS has not resulted in substantial alterations in the functioning of the heart.

3.3 KYXC improves blood lipid abnormalities in mice

The serum lipid levels in each group of mice were detected and the findings are presented in Figure 4. The MG group exhibited a considerable increase in the levels of CHOL, TG, VLDL, and LDL-C compared to the CG group ($P < 0.001$). Conversely, the HDL-C levels dramatically dropped ($P < 0.001$). Similarly, the BG group also showed a significant increase in all indicators ($P < 0.001$). The CHOL content in the KG-M, KG-H, and RG groups was dramatically decreased compared to the MG group ($P< 0.001$). Additionally, the TG and VLDL content in the RG, KG-L, and KG-M groups were reduced to varying degrees ($P < 0.01$). The HDL-C levels in the RG and KG-L groups showed a substantial rise ($P < 0.01$). The LDL-C levels in each treatment group declined to different extents, although there was no statistically significant difference.

3.4 KYXC promotes the formation of microvessels in mice

The Micro VCC (Optoprobe, United Kingdom) vascular microcirculation monitoring equipment can be utilized along with OCTA (optical coherence tomography angiography) mode

TABLE 2 List of Constituent Analysis Metabolites for KYXC positive Ion Mode, including Chemical Abstracts Service Registry Numbers (CAS No.) and molecular weights (MW). Sorted alphabetically by acronym.

Number	metabolite name	Formula	CAS	Adducts	Extraction Mass(Da)	Found At Mass (Da)	Mass error (mDa)	Observed RT (min)	Response	type
1	1-hydroxy-1,11,11-decahydrocyclopropaneazulene-10-one	C14H22O2	—	+K	261	261.127	1.8	2.62	2,007	Magnolianes
2	3-caffeoylquinic acid methyl ester	C17H20O9	123483-19-2	+Na	368.34	391.0954	−4.5	5.75	1,834	Phenylacrylic acids
3	3β-Hydroxy-5α,8α- epidioxyergosta-6,22-diene	C29H50O2	—	+K	—	469.3429	−1.3	37.39	8,633	Triterpenes
4	8-Hydroxypinoresinol_1	C20H18O7	81426-17-7	+NH4	374.38	388.1345	−4.6	9.19	708	Lignan class
5	Benzoic acid	C7H6O2	65-85-0	+Na	122.12	145.0225	−3.5	3.15	1,058	Aromatic derivatives
6	lariciresinol-4-O-β-D-glucopyranoside	C26H34O11	143663-00-7	+H	522.54	523.2165	−0.8	9.57	777	Lignan class
7	oleanolic acid	C30H48O3	508-02-1	+Na	456.7	479.3446	−4.9	34.13	911	Triterpenes
8	olivil-4-O-β-D-glucopyranoside	C26H34O12	56440-73-4	+Na	538.55	561.1921	−2.2	4.2	1,521	Lignan class
9	Protocatechualdehyde	C7H6O3	139-85-5	+H	138.12	139.0433	4.3	0.82	1,060	Aromatic derivatives
10	Stearic acid	C18H36O2	57-11-4	+H	284.48	285.2743	−4.5	41.13	5,695	Carboxylic acids
11	Stigmastere-3,7-dione	C29H48O2	—	+H	—	429.3692	−3.5	42.9	1,2526	Triterpenes
12	stigmasterol	C29H48O	83-48-7	+H	412.7	413.373	−4.8	36.75	1,887	Triterpenes
13	Valtrate	C22H30O8	18296-44-1	+H	422.47	423.1973	−4	32.15	2,104	Cycloene ether terpenes
14	Volvalerenal K	C20H34O4	—	+Na	—	361.2317	−3.2	32.6	2,419	Magnolianes
15	Volvalerenl B	C15H20O3	—	+H	—	249.1439	−4.7	15.09	4,617	Gemaranes

10.3389/fphar.2024.1483518

TABLE 3 List of Constituent Analysis Metabolites for KYXC negative Ion Mode, including Chemical Abstracts Service Registry Numbers (CAS No.) and molecular weights (MW). Sorted alphabetically by acronym.

Number	metabolite name	Formula	CAS	Adducts	Extraction Mass(Da)	Found At Mass (Da)	Mass error (mDa)	Observed RT (min)	Response	type
1	(+)-Piresil-4-O-beta-D-glucopyraside	C26H32O11	69251-96-3	-H, +HCOO	520.53	519.1864	−0.8	7.33	4,233	Lignan class
2	4-Hydroxybenzoic acid	C7H6O3	99-96-7	-H	138.12	137.0254	1	2.5	692	Aromatic derivatives
3	4-Hydroxycinnamic acid	C9H8O3	7400-08-0	-H	164.16	163.0399	−0.1	4.59	854	Aromatic derivatives
4	Acacetin	C16H12O5	480-44-4	-H	284.26	283.0608	−0.4	10.41	24235	Flavonoids
5	caffeic acid	C9H8O4	331-39-5	-H	180.16	179.0351	0.1	3.28	1375	Aromatic derivatives
6	Ferulic Acid	C10H10O4	1135-24-6	+HCOO	194.18	239.0565	0.4	3.15	708	Aromatic derivatives
7	Pinorespiol	C20H18O8	4263-88-1	+Cl	358.39	421.0745	4.9	2.87	6,659	Lignan class
8	quercetin	C15H10O7	117-39-5	+HCOO	302.24	347.0426	1.7	15.16	5,533	Flavonoids
9	Rutin	C27H30O16	153-18-4	-H	610.52	609.145	−1.1	5.91	1528	Flavonoids
10	Sucrose	C12H22O11	57-50-1	-H	342.3	341.1084	−0.5	0.89	3,517	Carbohydrates
11	ursolic acid	C30H48O3	77-52-1	-H, +HCOO	456.71	455.3524	−0.7	30.36	116232	Triterpenes
12	Volvalerenal D	C15H22O4	—	-H	—	265.1473	2.8	42.52	33387	Gemaranes
13	Volvalerenic A	C15H22O2	—	-H	—	233.1542	−0.5	23.07	9,828	Gemaranes
14	Volvalerenl C	C16H22O4	—	-H	—	277.1439	−0.7	25.48	12780	Gemaranes

10.3389/fphar.2024.1483518

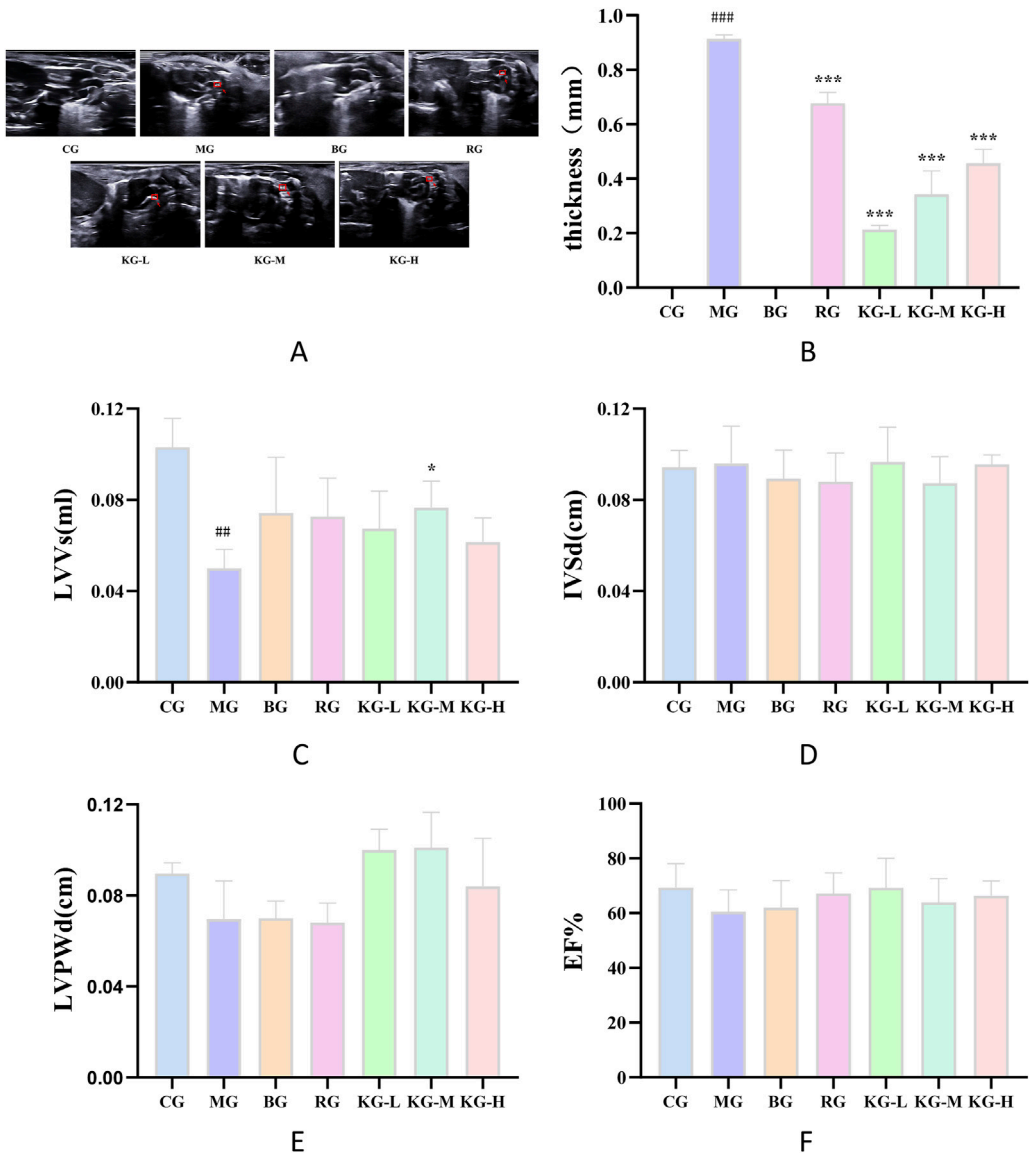

FIGURE 3
The effect of KYXC on mouse aortic plaques (The position indicated by the arrow in the figure is atherosclerotic plaque) **(A)** Effect of KYXC on Atherosclerotic Plaque in mice. **(B)** The Effect of KYXC on Mouse Cardiac Function. **(C–F)** (Compared with the CG group, #$P < 0.05$, ## $P < 0.01$, ### $P < 0.001$; Compared with the MG group, * $P < 0.05$, ** $P < 0.01$, *** $P < 0.001$).

scanning in the OPTO-III scanning program to acquire three-dimensional vascular data of the sample. The analysis software can be utilized to analyze the enhancement of microcirculation in the sample with greater intuitiveness and precision. The picture displays the following values from left to right: Vessel Perimeter Index (VPI), Vessel Diameter Index (VDI), Vessel Skeleton Density (VSD), Vessel Area Density (VAD), and Vessel Complexity Index (VCI). The color corresponds to the magnitude of blood flow, with red indicating the highest and blue indicating the lowest. VPI is a measure of the relationship between the circumference of blood vessels and the total area of an image. VDI is a measure of the relationship between the area of blood vessels and their length. VSD is a measure of the relationship between the length of blood vessels in an image and the total area of the image. VAD is calculated by comparing the area of blood vessels to the total area of the image. The formula for calculating VCI is VCI = P2/(4π*A), where *P* represents the circumference of the blood vessel and A represents the area of the blood vessel. Figure 5A depicts the microcirculation of the heart. The results indicate that the MG group exhibits varied degrees of reduction in VPI, VDI, VSD, VAD, and VCI compared to the CG group. Following KYXC therapy, the microcirculation coefficients of each group exhibited varied degrees of improvement, with KG-M and KG-H showing particularly notable enhancements. Figure 5B illustrates the microcirculation of the mesentery, which indirectly reflects the intestinal absorption of mice. The results indicate that the MG group shows a reduction in VP I, VDI, VSD, VAD, and VCI compared to the CG group. Following KYXC treatment, the microcirculation must be enhanced to different extents, particularly in the KG-L and KG-H groups.

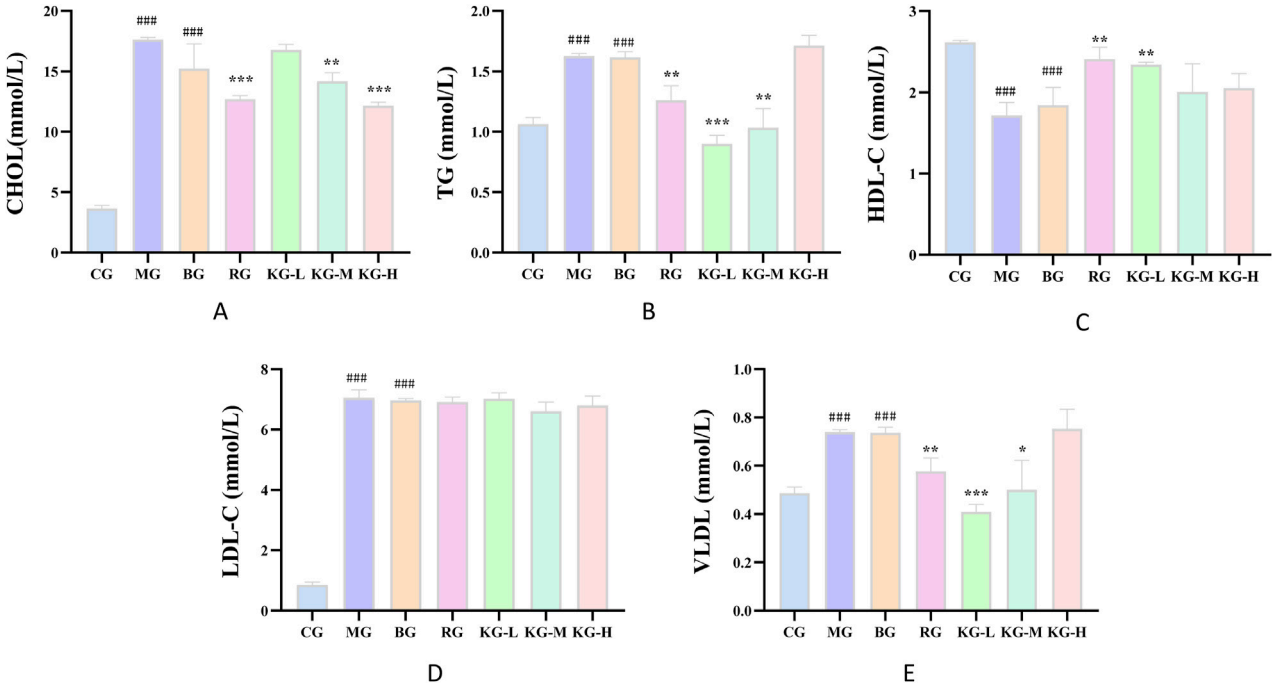

FIGURE 4
The effect of KYXC on blood lipids in AS mice **(A-E)**. (Compared with the CG group, # $P < 0.05$, ## $P < 0.01$, ### $P < 0.001$; Compared with the MG group, * $P < 0.05$, ** $P < 0.01$, *** $P < 0.001$).

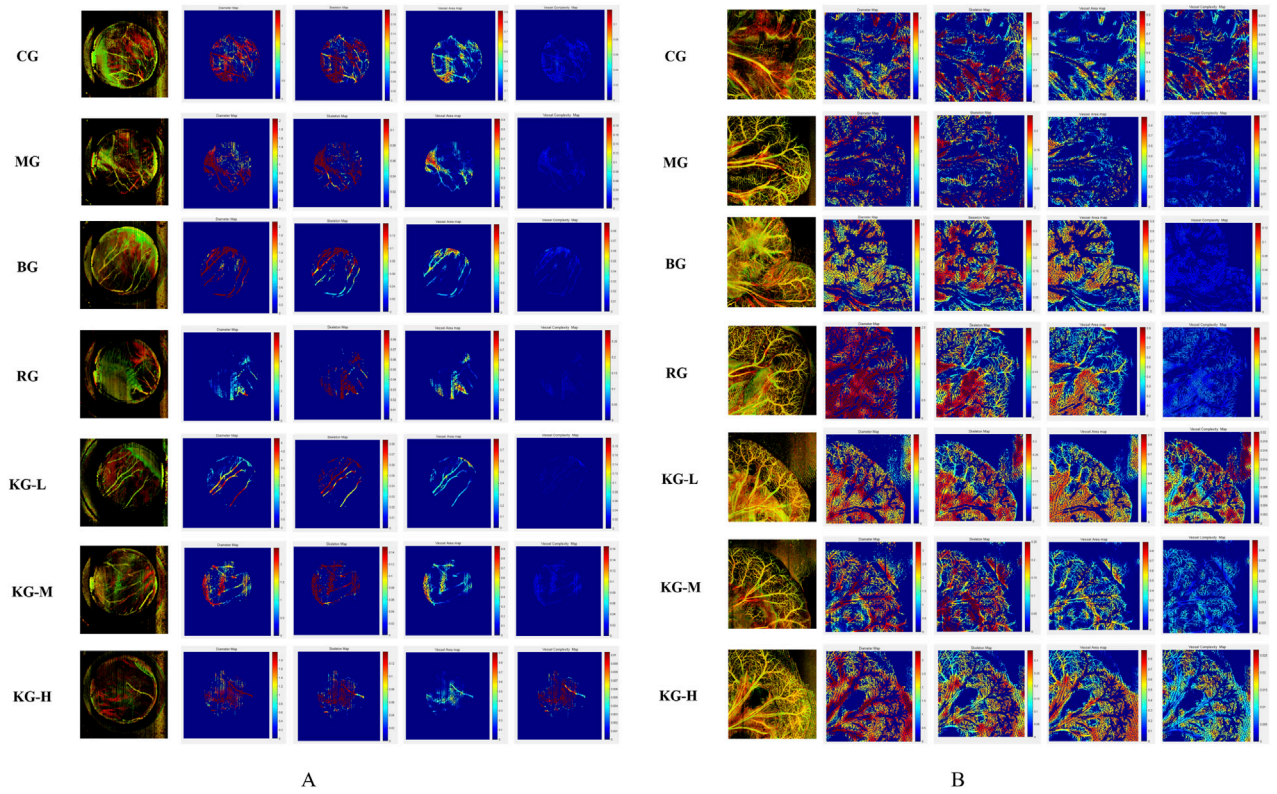

FIGURE 5
The effect of KYXC on Mouse Cardiac Microcirculation. **(A)** (Scanning Range 0.6 cm* 0.6 cm; Image Pixels 800 * 800) The effect of KYXC on intestinal and mesenteric microcirculation in mice. **(B)** (scanning range 1 cm * 1 cm; image pixels 900 * 900).

10.3389/fphar.2024.1483518

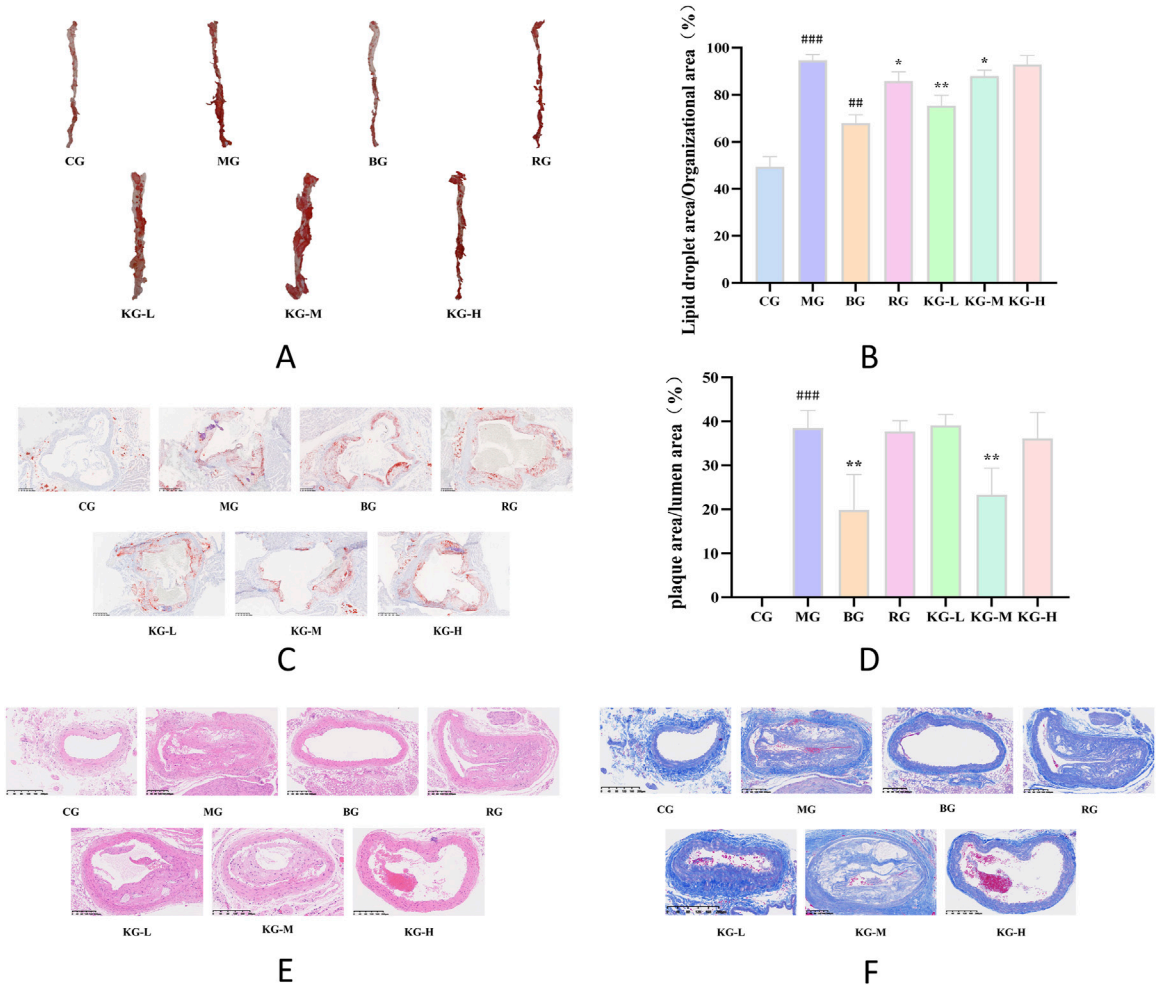

FIGURE 6
Oil Red O staining of the aorta of mice in each group. **(A)** The effect of KYXC on the ratio of aortic lipid droplet area to total tissue area in mice. **(B)** Red oil O staining of aortic roots in each group of mice. **(C)** (Scale bar: 200 μm) The effect of KYXC on the ratio of aortic plaque area to luminal area in AS mice. **(D)** HE staining of aortic roots in each group of mice. **(E)** Masson staining of aortic roots in each group of mice. **(F)** (Compared with the CG group, # $P < 0.05$, ## $P < 0.01$, ### $P < 0.001$; Compared with the MG group, * $P < 0.05$, ** $P < 0.01$, *** $P < 0.001$).

3.5 KYXC reduces lipid droplet formation on the aortic wall

Figures 6A, B demonstrate that the red color observed on the aorta of mice, following staining with oil red O, corresponds to the area occupied by AS plaques. The aorta wall of mice in the CG group is translucent and has a smooth texture, without any noticeable accumulation of red lipid plaques. The study found no notable disparity in the inner lining of the aorta between the BG group and the CG group. This suggests that a regular diet did not have a substantial impact on the development of aortic plaques in ApoE$^{-/-}$ mice (Figure 6C). In comparison to the CG group, the MG group had a significant accumulation of elevated red lipid deposits on the primary aortic vessel wall. These deposits were clearly demarcated from the vessel wall. In addition, the MG group had a significantly higher percentage of AS plaque area compared to the CG group ($P < 0.001$). After administering a low-dose KYXC, the plaque burden was significantly reduced, and the percentage of plaque area to total vascular area was significantly lower in the MG group ($P < 0.01$). Furthermore, the treatment effect was superior to that in the RG group (Figure 6B). As depicted in Figure 6D, the area of the aortic inner wall plate in the MG group expanded significantly ($P < 0.001$) compared to the CG group, and there was a substantial accumulation of lipids on the inner wall of the lumen. In each treatment group, lipid deposition was reduced to varying extents compared to the MG group, with the KG-M group showing particularly noticeable reduction.

3.6 KYXC improves pathological status of mice aortic tissue

Figures 6E, F display the results of HE and Masson staining of mice aortic tissue. The HE staining resulted in blue staining of the nuclei on the aorta wall, while the cytoplasm, muscle fibers, collagen fibers, and red blood cells were stained in different shades of red. On the other hand, Masson staining specifically dyed the collagen fibers in the aortic wall blue. The histological architecture of the inner wall of the aorta in the CG group is characterized by normalcy, integrity,

and orderly arrangement. The inner, middle, and exterior membrane layers are distinctly observable, exhibiting well-defined borders and multiple layers of flexible membranes. Collagen deposition is negligible and there is no apparent formation of plaques. In the aorta of the MG group, the arrangement of smooth muscle cells is disorganized, with a notable thickening of the innermost layer, widespread lipid plaques, and considerable infiltration of inflammatory cells. There is a notable accumulation of collagen fibers in the connective tissue of the heart muscle, characterized by a disorganized pattern of strips or networks; The RG, KG-L, KG-M, and KG-H groups had a considerably improved pathological structure compared to the MG group. Additionally, there was a varied degree of reduction in AS plaques. There was a decrease in the severity of aortic intimal hyperplasia, as well as a significant reduction in the number of inflammatory cells. Simultaneously, the process of collagen deposition among the cells of the aorta wall was also enhanced to different extents, with KG-H showing the most notable improvement.

3.7 KYXC improves mitochondrial structure and function in mice

In order to further investigate the impact of KYXC on the aorta of AS mice, transmission electron microscopy was used to examine the mitochondrial ultrastructure of endothelial cells in each group of aorta. Figure 7A displays the findings from transmission electron microscopy. The mitochondria in the aortic endothelial cells of mice in the CG group displayed normal morphology, clear numbers, neat arrangement, and complete structure. In contrast, the endothelial cells of mice in the MG group exhibited a reduction or absence of mitochondrial cristae, severe damage to the membrane structure, and a significant presence of fat particles in their vicinity. The morphology of mitochondria in the RG, KG-L, KG-M, and KG-H groups of endothelial cells appeared to resemble the normal structure, with faintly visible mitochondrial cristae.

3.8 KYXC improves serum antioxidant levels in mice

According to the data presented in Figures 7B–E, the levels of ACTH and CHRNα1 were considerably higher in the MG group compared to the CG group ($P < 0.01$). After treatment, the RG, KG-L, KG-M, and KG-H groups all showed varied degrees of reduction in these levels ($P < 0.05$). In comparison to the CG group, the levels of ATP and T-SOD in the mice from the MG group were dramatically decreased ($P < 0.05$). Each treatment group exhibited a significant rise in these levels when compared to the MG group ($P < 0.05$). Furthermore, following the administration of different doses of KYXC, the ATP levels in the mice were shown to be higher compared to those in the RG group.

3.9 KYXC improves gene expression related to PGC-1α/Sirt3/Epac1pathway

According to Figures 8A–E, the expression levels of PGC-1α and Sirt3 mRNA in the aortic tissue of mice in the MG group were significantly lower compared to the CG group. On the other hand, the expression levels of Epac1, caspase-9, and caspase-3 were significantly higher in the MG group ($P < 0.01$). When comparing the MG group to each treatment group, the expression levels of PGC-1α and Sirt3 mRNA in the aortic tissue were significantly higher, while the expression levels of Epac1, caspase-9, and caspase-3 mRNA showed varying degrees of improvement ($P < 0.05$). In the heart tissue, the expression level of caspase-3 mRNA was significantly higher in the MG group compared to the CG group ($P < 0.01$). However, in each treatment group, the expression level of caspase-3 mRNA in the heart tissue was reduced to varying degrees ($P < 0.05$), with no significant difference observed in other indicators. Refer to Figure 8F.

3.10 KYXC improves the expression of PGC-1α/Sirt3/Epac1 pathway related proteins and related apoptotic proteins

Figure 9 displays the protein expression of mouse aortic tissue. In comparison to the CG group, the MG group showed a significant decrease in the expression levels of PGC-1α and Sirt3 proteins, while there was a significant increase in the expression levels of Epac1, caspase-9, and caspase-3 ($P < 0.05$). Furthermore, when comparing the MG group to each treatment group of mice, there was a significant increase in the protein expression levels of PGC-1α and Sirt3, while the protein expression levels of Epac1, caspase-9, and caspase-3 showed varying degrees of improvement ($P < 0.05$).

4 Discussion

As civilization has progressed and living conditions have improved, the prevalence of AS has steadily risen. Cardiovascular and cerebrovascular disorders resulting from atherosclerosis have emerged as the primary cause of mortality worldwide, garnering increasing attention from scholars (Roth et al., 2020). Atherosclerosis is strongly associated with dysregulation of lipid metabolism, inflammatory response, malfunction of vascular endothelial cells, and other underlying processes (Zhou and Wu, 2023). Researchers and academics have undertaken studies on frequently prescribed clinical medications that lower cholesterol levels, reduce inflammation, and prevent blood clotting (Wang et al., 2024). Although there has been notable advancement in drug-based treatment approaches, there are still persistent difficulties like drug resistance, adverse effects, and high rates of recurrence. Thus, it is crucial to strengthen treatment strategies in order to improve clinical efficacy.

Traditional Chinese medicine possesses the benefits of having various targets and routes as a result of its active substances that cause irritation. Consequently, it has demonstrated promise therapeutic efficacy in the treatment of cardiovascular illnesses. Several investigations have demonstrated that traditional Chinese medicine is capable of efficiently reducing the development of atherosclerotic plaque with few adverse effects. It has been widely employed in the management of cardiovascular disorders (Xing et al., 2020). Prior research has shown that valerian terpenes can enhance myocardial damage by suppressing the creation and

10.3389/fphar.2024.1483518

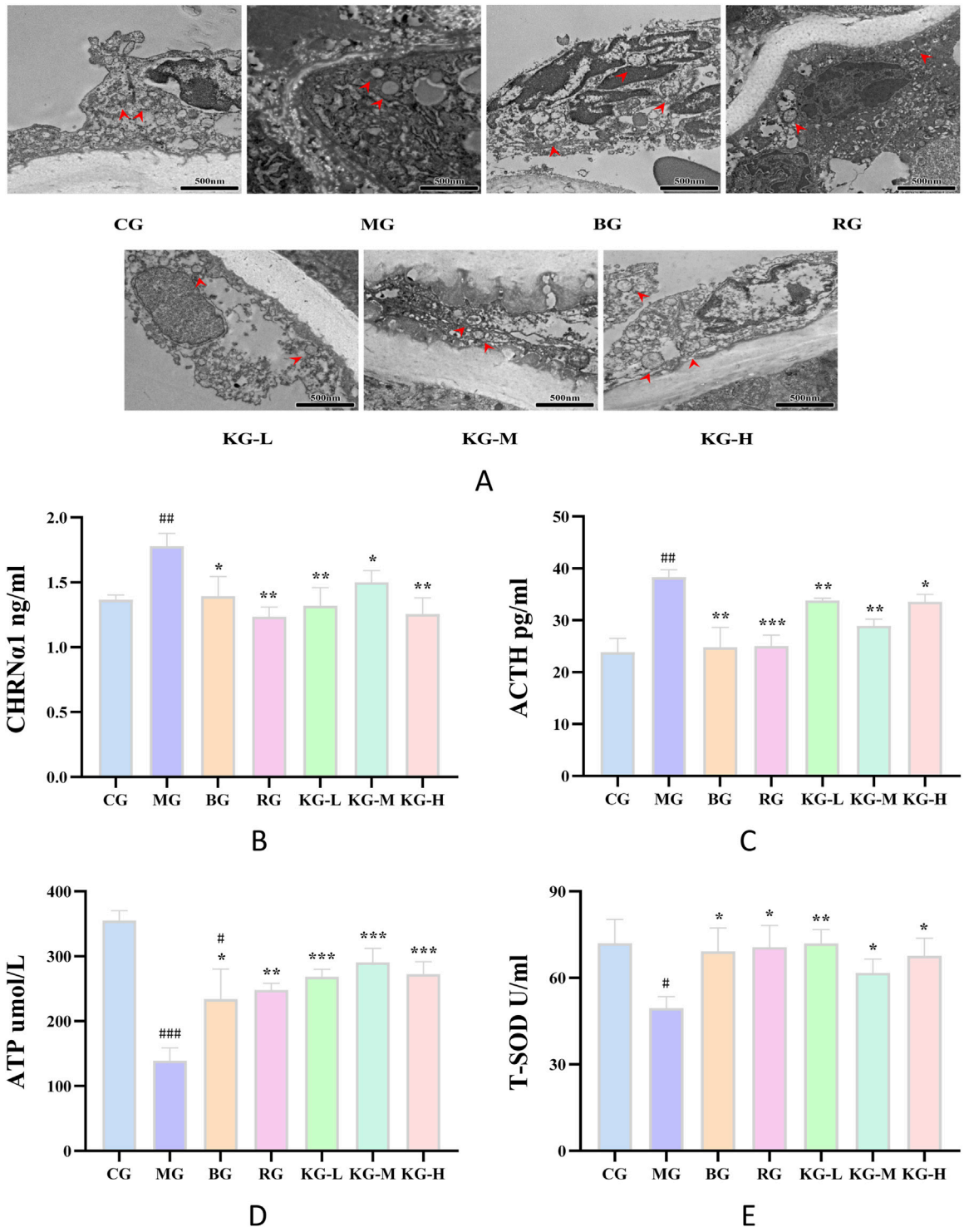

FIGURE 7
The effect of KYXC on the ultrastructure of mitochondria in AS mice. Scale bar: 500 nm **(A)** (The position indicated by the arrow in the figure is mitochondria) (Scale bar: 200 μm). The effect of KYXC on serum indicators of AS mice **(B–E)**. (Compared with the CG group, # $P < 0.05$, ## $P < 0.01$, ### $P < 0.001$; Compared with the MG group, * $P < 0.05$, ** $P < 0.01$, *** $P < 0.001$).

function of xanthine oxidase, diminishing the synthesis of free radicals, mitigating the peroxidation of cell membrane lipids, limiting the aggregation of platelets, and enhancing microcirculation. Furthermore Nawrot et al. (2022), discovered through human pharmacology research that extracts derived from Valerian roots have the ability to significantly reduce heart rate in patients, providing protection to the heart and so enhancing the prevention and progression of cardiovascular diseases.

Nevertheless, there is currently a lack of complete study into the effects of KYXC on AS mice generated by a high-fat diet, and

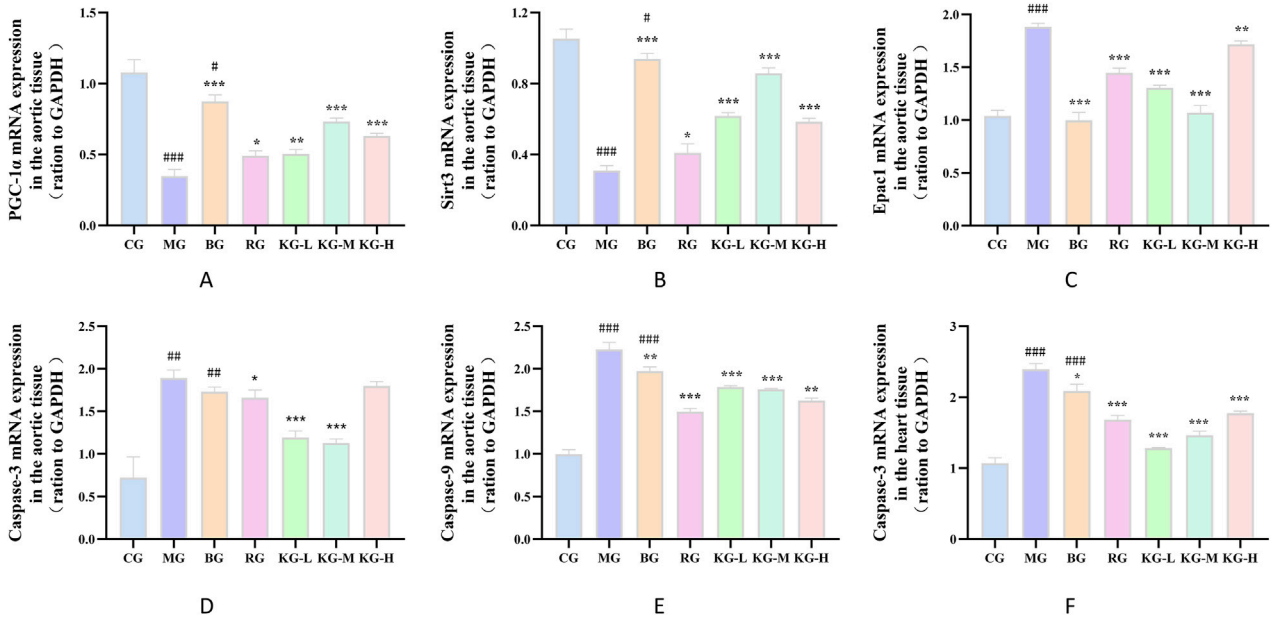

FIGURE 8
The effect of KYXC on the mRNA expression of PGC-1α, Sirt3, Epac1, caspase-9, and caspase-3 in the aortic tissue of AS mice **(A–E)**. The effect of KYXC on the mRNA expression of caspase-3 in the heart tissue of AS mice **(F)**. (Compared with the CG group, # $P < 0.05$, ## $P < 0.01$, ### $P < 0.001$; Compared with the MG group, * $P < 0.05$, ** $P < 0.01$, *** $P < 0.001$).

the precise mechanism by which it improves the AS effect remains unknown. This work effectively created AS model in ApoE$^{-/-}$ mice by a high-fat diet. The objective was to examine the potential anti-atherosclerosis impact of KYXC and its underlying mechanism. The findings suggest that Volvalerenic A, the primary metabolite in KYXC, can enhance the accumulation of lipids, mitigate the inflammatory milieu, alleviate mitochondrial damage, and eventually impede the progression of atherosclerosis by activating the PGC-1α/Sirt3/Epac1 signaling pathway. Furthermore, this study utilized the cutting-edge technique of dynamic visualization of vascular microcirculation for real-time monitoring to visually assess the positive impact of KYXC on heart and mesenteric microcirculation. Following KYXC treatment, various parameters related to the vascular system, such as the vascular perimeter index, vascular diameter index, vascular skeleton density, vascular area density, and vascular complexity index, were found to have improved in both the heart and mesentery of mice. This suggests that KYXC has the potential to enhance arterial stiffness in these organs. The impact on membrane microcirculation more clearly demonstrates the significance of KYXC in enhancing microcirculation and cardiovascular function.

The presence of a lipid metabolism issue is regarded as the primary cause of AS and one of the most perilous elements contributing to the development of AS disorders (Manickam et al., 2022). This disorder is defined by abnormally high levels of cholesterol (CHOL) and triglycerides (TG) in the bloodstream (Kemal et al., 2020). Hence, assessing plasma CHOL and TG levels is a dependable method for evaluating lipid disorders. CHOL is an essential building block of cell membranes and is also a crucial metabolite of certain hormones, like steroid hormones. It plays a significant role in the transportation, metabolism, and storage of lipids (Lu et al., 2022). Thermogenesis is the primary energy source for the organism and also serves as a reservoir for surplus heat. Typically, the liver produces TG which is then carried by VLDL to peripheral tissues for lipid metabolism (Borén et al., 2022). However, elevated amounts of TG have a notable impact on the structural stability and thermal remodeling of VLDL and LDL (Jayaraman et al., 2019), resulting in the development of unstable plaques. As dyslipidemia progresses, the body's ability to perform normal lipid metabolism and produce plaque is impaired, resulting in persistently elevated levels of CHOL and TG. The continuous buildup of lipids in atherosclerotic plaque speeds up the development of atherosclerosis. LDL is the main contributor to cholesterol and fat buildup on the artery wall (Malekmohammad et al., 2017). Following oxidative modification, LDL transforms into oxidized LDL (ox-LDL), which is the primary inflammatory metabolite of atherosclerotic plaque (Díaz-García et al., 2023). Subsequently, monocytes underwent a transformation into macrophages, which then engulfed ox-LDL through various mechanisms. This process resulted in the formation of foam cells, which led to the thickening of the inner layer of blood vessels (intima) and narrowing of the vascular lumen. These changes further exacerbated the development of atherosclerosis, ultimately resulting in the blockage of blood vessels and the formation of blood clots (thrombosis), along with other negative outcomes (Lu et al., 2022). VLDL, or very low-density lipoprotein, serves as the primary transporter of triacylglycerol in the bloodstream. Its levels tend to rise in certain medical disorders such diabetes, metabolic syndrome, obesity, and dyslipidemia (Jayaraman et al., 2019). Elevated triacylglycerol levels decrease the structural integrity of VLDL and its derivative LDL, hence initiating AS. The results obtained from the oil red O staining, HE staining, Masson staining, and biochemical analysis clearly demonstrate that KYXC effectively decreased the levels of CHOL,

10.3389/fphar.2024.1483518

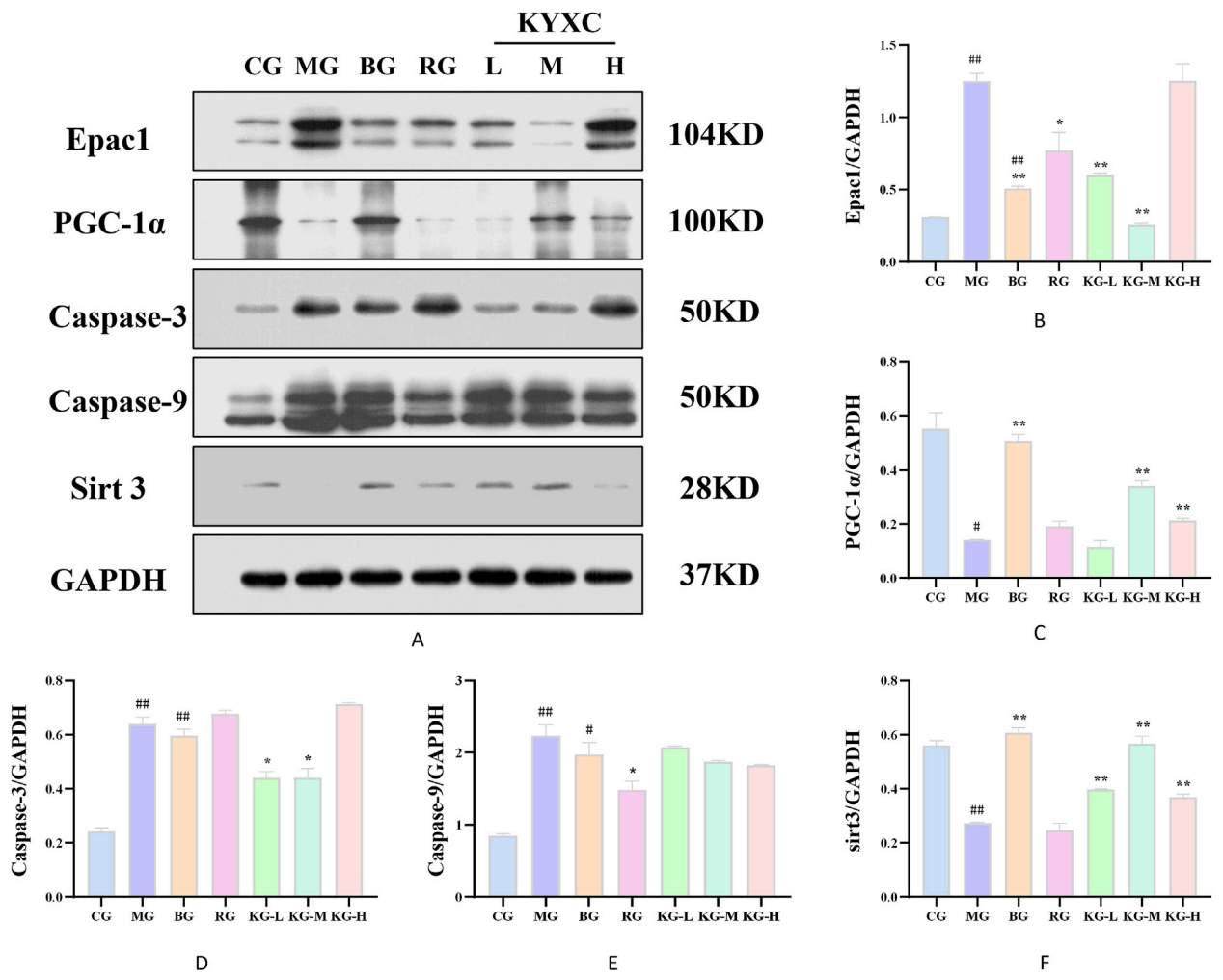

FIGURE 9
The effect of KYXC on the expression of PGC-1α, Sirt3, Epac1, caspase-9 and caspase-3 proteins in the aorta of AS mice **(A-F)**. (Compared with the CG group, # $P < 0.05$, ## $P < 0.01$, ### $P < 0.001$; Compared with the MG group, * $P < 0.05$, ** $P < 0.01$, *** $P < 0.001$).

TG, and VLDL in the serum ($P < 0.05$). Additionally, KYXC reduced lipid deposition, inflammatory cell infiltration, and collagen fiber attachment in the aortic wall, thereby mitigating the development of vascular stenosis and unstable plaque, ultimately delaying the progression of atherosclerosis.

Mitochondria are organelles responsible for generating energy within eukaryotic cells. They are commonly referred to as the "power plants" of intracellular living activities and have significant involvement in lipid metabolism and energy metabolism (Liu et al., 2020). A primary role of mitochondria is to generate ATP, which serves as the energy source for numerous physiological processes in the body (Kim et al., 2016). Damage to the mitochondria can cause an imbalance in energy metabolism throughout the body, particularly in organs that have a high metabolic rate and require a lot of energy. Furthermore, mitochondria contribute to the regulation of cellular redox status by managing the generation and removal of reactive oxygen species (ROS) within the antioxidant defense system (Chen et al., 2024). According to Shuhong Yang et al. (2012), Valerian extract has been shown to dramatically decrease the levels of lactate dehydrogenase (LDH), creatine kinase (CK), and malondialdehyde (MDA), while significantly increasing the levels of superoxide dismutase (SOD), glutathione peroxidase (GSHPx), and ATPase. According to Wu and Zhang (2022), ACTH plays a role in lipid metabolism via controlling the mobility of mitochondria. Furthermore, during periods of bodily stress, there is a substantial rise in ACTH levels. This increase triggers the opening of mitochondrial membrane channel pores, resulting in a significant alteration of mitochondrial permeability. Consequently, the mitochondria experience swelling of the mitochondrial matrix and a loss of polarization in the mitochondrial membrane potential (Ran et al., 2024). These changes ultimately lead to the rupture of the outer membrane of the mitochondria, a decrease in ATP production, abnormal mitochondrial energy metabolism, and ultimately an impact on cellular function. Our research findings indicate that lipid metabolism irregularities lead to a substantial increase in the amount of ACTH ($P < 0.01$) and a significant drop in the level of ATP ($P < 0.01$). Additionally, these abnormalities disturb the structure of mitochondria and cause the disappearance of cristae. Following KYXC therapy, there was a reduction in ACTH levels and an improvement in ATP levels to different extents. This suggests that KYXC has the ability

to enhance ACTH and ATP levels in the body, promoting homeostasis. The plasma membrane contains the entire amount of superoxide dismutase (T-SOD), which serves as an important indicator of oxidative stress in the body (Zheng et al., 2022). This study aimed to assess the degree of oxidative stress in the body by measuring the expression of T-SOD. As depicted in Figure 7E, the T-SOD content exhibited varying degrees of increase ($P < 0.05$) following KYXC treatment, suggesting a notable enhancement in the body's oxidative stress level post-treatment.

Multiple studies have shown that the PGC-1α/Sirt3/Epac1 pathway is linked to cellular death. PGC-1α is a transcription regulatory factor that controls the body's response to oxidative stress and mitochondrial metabolism (Zhang et al., 2020). Sirt3, the first deacetylase in the sirtuins family, is mostly present in the mitochondrial matrix and has a powerful protective effect on mitochondria (Li et al., 2020). Research has indicated that PGC-1α has a role in mitochondrial oxidative metabolism, cell apoptosis, and signal modulation by raising the expression of Sirt3 and enhancing deacetylase activity (Zu et al., 2021). Jia You et al. (2016) discovered that by over-expressing PGC-1α and reducing Sirt3 gene expression, they were able to demonstrate that PGC-1α can effectively enhance the expression of Sirt3, boost Sirt3's deacetylase activity, and contribute to the regulation of myocardial hypertrophy, mitochondrial function, reactive oxygen species clearance, energy metabolism, and other related factors. Cyclic adenosine monophosphate (cAMP) is a ubiquitous second messenger found in cells that activates many proteins to control mitochondrial function. Epac1, a protein that is directly activated by cAMP, has demonstrated more effectiveness in controlling important factors such as MMP, ATP synthesis rate, and respiratory chain activity in mouse mitochondria (Li et al., 2024). Furthermore, the research conducted by Laudette et al. (2021) indicates that Epac1 has the ability to enhance the generation of mitochondrial ROS following extended lipid excess, while simultaneously decreasing mitochondrial respiration and ATP synthesis. Our study also showed that as the expression level of Epac1 protein decreased, the CHOL and TG contents in mice blood lipids significantly decreased, while the ATP and T-SOD contents in mitochondria significantly increased, which is consistent with previous research reports. The initiation of cellular apoptosis is marked or accompanied by an elevation in the concentration of apoptotic proteins. Stimulation of cells leads to the release of pro-apoptotic proteins, including cytochrome C. This release activates the caspase-9 and caspase-3 systems, with caspase-9 acting as an upstream promoter and caspase-3 as a downstream effector (Park, 2024; Peng et al., 2024). This work conducted RT-qPCR studies to examine the mRNA expression of PGC-1α, Sirt3 and Epac1 proteins, as well as their linked apoptotic proteins, before and after administration. The results revealed that KYXC can increase the expression of PGC-1α in AS mice. The mRNA expression levels of Sirt3, Epac1, Caspase-3, and Caspase-9 were decreased significantly ($P < 0.05$), which aligns with prior experimental findings. Thus, we posit that maintaining the proper functioning of the PGC-1α/Sirt3/Epac1 signaling pathway could be a crucial approach to treating AS.

However, our study exclusively examined the potential protective effects of *Valeriana officinalis L.* extract and its underlying molecular mechanisms using an animal model, rather than a cellular model of depression, which introduces certain limitations to the research. To determine whether *Valeriana officinalis L.* extract possesses potential for development as an anti-atherosclerosis drug, *in vitro* experiments are also imperative. Despite these limitations, our research provides valuable reference points for future studies.

5 Conclusion

The aforementioned findings suggest that *Valeriana officinalis L.* extract shows great potential as a Chinese herbal medicine for the management of atherosclerosis. The visualization of vascular microcirculation *in vivo* monitoring system and advanced bioinformatics technology are applied to validate the efficacy and mechanism of *Valeriana officinalis L.* extract in improving dyslipidemia in atherosclerotic mice. This was achieved by modulating the PGC-1α/Sirt3/Epac1 signaling pathway. Our findings aim to offer novel insights for the clinical management of atherosclerosis using modernized traditional Chinese medicine. This study has initially identified valtrate as the primary metabolite in the extract of *Valeriana officinalis L.* However, further investigation is required to establish whether Volvalerenic A is responsible for improving AS plaques and to identify any more potent metabolites. And the related study is going on in our lab.

Data availability statement

The original contributions presented in the study are included in the article/Supplementary Material, further inquiries can be directed to the corresponding authors.

Ethics statement

The animal study was approved by the Experimental Animal Ethics and Welfare Committee of Guang'anmen Hospital, Chinese Academy of Traditional Chinese Medicine (IACUC-GAMH-2024-001). The study was conducted in accordance with the local legislation and institutional requirements.

Author contributions

BY: Software, Writing–original draft, Writing–review and editing. JM: Software, Writing–review and editing. QR: Resources, Writing–review and editing. HC: Writing–review and editing. XH: Writing–review and editing.

Funding

The author(s) declare that financial support was received for the research and/or publication of this article. This study was supported by the National Natural Science Foundation of China (No. 82205091 and No. 82074396), the Clinical Research Funds for the Centralized High level Chinese Medicine Hospitals (HLCMHPP2023077), Scientific and Technological Innovation Project of China Academy of Chinese Medical Sciences (CI2023CO22YL and CI2021A04619).

Conflict of interest

The authors declare that the research was conducted in the absence of any commercial or financial relationships that could be construed as a potential conflict of interest.

Publisher's note

All claims expressed in this article are solely those of the authors and do not necessarily represent those of their affiliated organizations, or those of the publisher, the editors and the reviewers. Any product that may be evaluated in this article, or claim that may be made by its manufacturer, is not guaranteed or endorsed by the publisher.

Supplementary material

The Supplementary Material for this article can be found online at: https://www.frontiersin.org/articles/10.3389/fphar.2024.1483518/full#supplementary-material

References

Arnett, D. K., Khera, A., and Blumenthal, R. S. (2019). 2019 ACC/AHA guideline on the primary prevention of cardiovascular disease: Part 1, lifestyle and behavioral factors. *JAMA Cardiol.* 4, 1043–1044. doi:10.1001/jamacardio.2019.2604

Boré, J., Taskinen, M. R., Björnson, E., and Packard, C. J. (2022). Metabolism of triglyceride-rich lipoproteins in health and dyslipidaemia. *Nat. Rev. Cardiol.* 19, 577–592. doi:10.1038/s41569-022-00676-y

Chen, H. W., He, X. H., Yuan, R., Wei, B. J., Chen, Z., Dong, J. X., et al. (2016). Sesquiterpenes and a monoterpenoid with acetylcholinesterase (AchE) inhibitory activity from Valeriana officinalis var. latiofolia *in vitro* and *in vivo*. *Fitoterapia* 110, 142–149. doi:10.1016/j.fitote.2016.03.011

Chen, H. W., Wei, B. J., He, X. H., Liu, Y., and Wang, J. (2015). Chemical components and cardiovascular activities of Valeriana spp. *Evid. Based Complement. Altern. Med.*, 947619. doi:10.1155/2015/947619

Chen, P., Yao, L., Yuan, M., Wang, Z., Zhang, Q., Jiang, Y., et al. (2024). Mitochondrial dysfunction: a promising therapeutic target for liver diseases. *Genes Dis.* 11, 101115. doi:10.1016/j.gendis.2023.101115

Díaz-García, E., Sanz-Rubio, D., GarcíA-Tovar, S., Alfaro, E., Cubero, P., Gil, A. V., et al. (2023). Inflammasome activation mediated by oxidised low-density lipoprotein in patients with sleep apnoea and early subclinical atherosclerosis. *Eur. Respir. J.* 61, 2201401. doi:10.1183/13993003.01401-2022

Falk, E. (2006). Pathogenesis of atherosclerosis. *J. Am. Coll. Cardiol.* 47, C7–C12. doi:10.1016/j.jacc.2005.09.068

Fazal, L., Laudette, M., Paula-Gomes, S., Pons, S., Conte, C., Tortosa, F., et al. (2017). Multifunctional mitochondrial Epac1 controls myocardial cell death. *Circ. Res.* 120, 645–657. doi:10.1161/circresaha.116.309859

Giralt, A., Hondares, E., Villena, J. A., Ribas, F., DíAZ-DelfíN, J., Giralt, M., et al. (2011). Peroxisome proliferator-activated receptor-gamma coactivator-1alpha controls transcription of the Sirt3 gene, an essential component of the thermogenic brown adipocyte phenotype. *J. Biol. Chem.* 286, 16958–16966. doi:10.1074/jbc.M110.202390

Haofei Han, Y. Z., Qiang, L. I. U., Hao, J. I. A., and Qibing, L. I. U. (2019). Advances in transgenic mouse model of atherosclerosis. *Chin. J. Pharmacol. Toxicol.* 33, 138–146. doi:10.3867/j.issn.1000-3002.2019.02.008

Hao Zhang, L. Z., and Keyi, H. U. O. (2023). High gamma-aminobutyric acid (GABA) oolong tea alleviates high-fat diet-induced metabolic disorders in mice. *ACS Omega. Contemp. Hortic.* 46, 79–81. doi:10.14051/j.cnki.xdyy.2023.15.007

Jaganjac, M., Milkovic, L., Gegotek, A., Cindric, M., Zarkovic, K., Skrzydlewska, E., et al. (2020). The relevance of pathophysiological alterations in redox signaling of 4-hydroxynonenal for pharmacological therapies of major stress-associated diseases. *Free Radic. Biol. Med.* 157, 128–153. doi:10.1016/j.freeradbiomed.2019.11.023

Jayaraman, S., Baveghems, C., Chavez, O. R., Rivas-Urbina, A., SáNCHEZ-Quesada, J. L., and Gursky, O. (2019). Effects of triacylglycerol on the structural remodeling of human plasma very low- and low-density lipoproteins. *Biochim. Biophys. Acta Mol. Cell. Biol. Lipids* 1864, 1061–1071. doi:10.1016/j.bbalip.2019.03.001

Jia You, Z. Y., Chen, S., Zhuoming, L. I., and Peiqing, L. I. U. (2016). Upregulation of SIRT3 contributes to myocardial protective effect of PGC1α. *J. Sun Yat-sen Univ. Sci.* 37, 343–350. doi:10.13471/j.cnki.j.sun.yat-sen.univ(med.sci).2016.0061

Kemal, A., Teshome, M. S., Ahmed, M., Molla, M., Malik, T., Mohammed, J., et al. (2020). Dyslipidemia and associated factors among adult patients on antiretroviral therapy in armed force comprehensive and specialized hospital, addis ababa, Ethiopia. *HIV AIDS (Auckl)* 12, 221–231. doi:10.2147/hiv.S252391

Kim, Y., Mcgee, S., Czeczor, J. K., Walker, A. J., Kale, R. P., Kouzani, A. Z., et al. (2016). Nucleus accumbens deep-brain stimulation efficacy in ACTH-pretreated rats: alterations in mitochondrial function relate to antidepressant-like effects. *Transl. Psychiatry* 6, e842. doi:10.1038/tp.2016.84

Laudette, M., Sainte-Marie, Y., Cousin, G., Bergonnier, D., Belhabib, I., Brun, S., et al. (2021). Cyclic AMP-binding protein Epac1 acts as a metabolic sensor to promote cardiomyocyte lipotoxicity. *Cell. Death Dis.* 12, 824. doi:10.1038/s41419-021-04113-9

Li, X. S. R., Liu, W., Jiang, G., Lian, J., Zhong, Y., Zhou, J., et al. (2024). Celastrol ameliorates neuronal mitochondrial dysfunction induced by intracerebral hemorrhage via targeting cAMP-activated exchange protein-1. *Adv. Sci. (Weinh)* 11, e2307556. doi:10.1002/advs.202307556

Libby, P. (2021). The changing landscape of atherosclerosis. *Nature* 592, 524–533. doi:10.1038/s41586-021-03392-8

Li, M., Li, C. M., Ye, Z. C., Huang, J., Li, Y., Lai, W., et al. (2020). Sirt3 modulates fatty acid oxidation and attenuates cisplatin-induced AKI in mice. *J. Cell. Mol. Med.* 24, 5109–5121. doi:10.1111/jcmm.15148

Liu, S., Guo, R., Liu, F., Yuan, Q., Yu, Y., and Ren, F. (2020). Gut microbiota regulates depression-like behavior in rats through the neuroendocrine-immune-mitochondrial pathway. *Neuropsychiatr. Dis. Treat.* 16, 859–869. doi:10.2147/ndt.S243551

Lu, Y., Cui, X., Zhang, L., Wang, X., Xu, Y., Qin, Z., et al. (2022). The functional role of lipoproteins in atherosclerosis: novel directions for diagnosis and targeting therapy. *Aging Dis.* 13, 491–520. doi:10.14336/ad.2021.0929

Lv, P. 2017. *New mechanism in regulating adult mouse myocardial ischemia/reperfusion injury: NR-SIRT3-p53/PGC-1α improve mitophagy and mitochondrial biogenesis*. Fourth Military Medical University.

Malekmohammad, K., Bezsonov, E. E., and Rafieian-Kopaei, M. (2017). Role of lipid accumulation and inflammation in atherosclerosis: focus on molecular and cellular mechanisms. *Front. Cardiovasc Med.* 8, 707529. doi:10.3389/fcvm.2021.707529

Manea, S. A., Vlad, M. L., Fenyo, I. M., Lazar, A. G., Raicu, M., Muresian, H., et al. (2020). Pharmacological inhibition of histone deacetylase reduces NADPH oxidase expression, oxidative stress and the progression of atherosclerotic lesions in hypercholesterolemic apolipoprotein E-deficient mice; potential implications for human atherosclerosis. *Redox Biol.* 28, 101338. doi:10.1016/j.redox.2019.101338

Manickam, V., Dhawan, U. K., Singh, D., Gupta, M., and Subramanian, M. (2022). Pomegranate peel extract decreases plaque necrosis and advanced atherosclerosis progression in *apoe*$^{-/-}$ mice. *Front. Pharmacol.* 13, 888300. doi:10.3389/fphar.2022.888300

Marchio, P., Guerra-Ojeda, S., Vila, J. M., Aldasoro, M., Victor, V. M., and Mauricio, M. D. (2019). Targeting early atherosclerosis: a focus on oxidative stress and inflammation. *Oxid. Med. Cell. Longev.* 2019, 8563845. doi:10.1155/2019/8563845

Musheshe, N., Oun, A., Sabogal-GuáQUETA, A. M., Trombetta-Lima, M., Mitchel, S. C., Adzemovic, A., et al. (2022). Pharmacological inhibition of Epac1 averts ferroptosis cell death by preserving mitochondrial integrity. *Antioxidants (Basel)* 11, 314. doi:10.3390/antiox11020314

Nawrot, J., Gornowicz-Porowska, J., Budzianowski, J., Nowak, G., Schroeder, G., and Kurczewska, J. (2022). Medicinal herbs in the relief of neurological, cardiovascular, and respiratory symptoms after COVID-19 infection A literature review. *Cells* 11, 1897. doi:10.3390/cells11121897

Nedkoff, L., Briffa, T., Zemedikun, D., Herrington, S., and Wright, F. L. (2023). Global trends in atherosclerotic cardiovascular disease. *Clin. Ther.* 45, 1087–1091. doi:10.1016/j.clinthera.2023.09.020

Park, W. H. (2024). Propyl gallate induces human pulmonary fibroblast cell death through the regulation of Bax and caspase-3. *Ann. Med.* 56, 2319853. doi:10.1080/07853890.2024.2319853

Peng, L., Zhu, X., Wang, C., Jiang, Q., Yu, S., Song, G., et al. (2024). Indole-3-carbinol (I3C) reduces apoptosis and improves neurological function after cerebral ischemia-reperfusion injury by modulating microglia inflammation. *Sci. Rep.* 14, 3145. doi:10.1038/s41598-024-53636-6

Pérez, S., Rius-Pérez, S., Finamor, I., Martí-Andrés, P., Prieto, I., García, R., et al. (2019). Obesity causes PGC-1α deficiency in the pancreas leading to marked IL-6 upregulation via NF-κB in acute pancreatitis. *J. Pathol.* 247, 48–59. doi:10.1002/path.5166

Ran, Q., Li, A., Tan, Y., Zhang, Y., Zhang, Y., and Chen, H. (2024). Action and therapeutic targets of myosin light chain kinase, an important cardiovascular signaling mechanism. *Pharmacol. Res.* 206, 107276. doi:10.1016/j.phrs.2024.107276

Rius-PéREZ, S., Torres-Cuevas, I., MilláN, I., Ortega Á, L., and PéREZ, S. (2020). PGC-1α, inflammation, and oxidative stress: an integrative view in metabolism. *Oxid. Med. Cell. Longev.* 2020, 1452696. doi:10.1155/2020/1452696

Roth, G. A., Mensah, G. A., Johnson, C. O., Addolorato, G., Ammirati, E., Baddour, L. M., et al. (2020). Global burden of cardiovascular diseases and risk factors, 1990-2019: update from the GBD 2019 study. *J. Am. Coll. Cardiol.* 76, 2982–3021. doi:10.1016/j.jacc.2020.11.010

Shuhong Yang, F. C., Hongmei, M. A., and Wang, T. (2012). Protection of Valeriana officinalis L extract preconditioning on ischmia-reperfusion injury in rat hearts *in vitro*. *Med. J. Wuhan Univ.* 33, 639–643. doi:10.14188/j.1671-8852.2012.05.003

Wang, S. Q., Xiang, J., Zhang, G. Q., Fu, L. Y., Xu, Y. N., Chen, Y., et al. (2024). Essential oil from Fructus Alpinia zerumbet ameliorates atherosclerosis by activating PPARγ-LXRα-ABCA1/G1 signaling pathway. *Phytomedicine* 123, 155227. doi:10.1016/j.phymed.2023.155227

Weerawatanakorn, M., He, S., Chang, C. H., Koh, Y. C., Yang, M. J., and Pan, M. H. (2023). High gamma-aminobutyric acid (GABA) oolong tea alleviates high-fat diet-induced metabolic disorders in mice. *ACS Omega* 8, 33997–34007. doi:10.1021/acsomega.3c04874

Wu, Z., and Zhang, C. (2022). Role of the cytoskeleton in steroidogenesis. *Endocr. Metab. Immune Disord. Drug Targets* 22, 549–557. doi:10.2174/1871530321666211119143653

Xing, Q., Fu, L., Yu, Z., and Zhou, X. (2020). Efficacy and safety of integrated traditional Chinese medicine and western medicine on the treatment of rheumatoid arthritis: a meta-analysis. *Evid. Based Complement. Altern. Med.* 2020, 4348709. doi:10.1155/2020/4348709

Yang, G. Y., and Wang, W. (1994). Clinical studies on the treatment of coronary heart disease with Valeriana officinalis var latifolia. *Zhongguo Zhong Xi Yi Jie He Za Zhi* 9, 540–542.

Zhang, J. (2021). Research status and prospects of tongren broad leaved valerian. *Guangdong Chem. Ind.* 48, 107+147.

Zhang, K., Cheng, H., Song, L., and Wei, W. (2020). Inhibition of the peroxisome proliferator-activated receptor gamma coactivator 1-alpha (PGC-1α)/Sirtuin 3 (SIRT3) pathway aggravates oxidative stress after experimental subarachnoid hemorrhage. *Med. Sci. Monit.* 26, e923688. doi:10.12659/msm.923688

Zheng, H., Huang, S., Wei, G., Sun, Y., Li, C., Si, X., et al. (2022). CircRNA Samd4 induces cardiac repair after myocardial infarction by blocking mitochondria-derived ROS output. *Mol. Ther.* 30, 3477–3498. doi:10.1016/j.ymthe.2022.06.016

Zhou, Y., and Wu, Q. (2023). Spotlight on HOX cluster-embedded antisense lncRNAs in cardiovascular diseases (Review). *Int. J. Mol. Med.* 52, 114. doi:10.3892/ijmm.2023.5317

Zhu, J., Xu, K., Zhang, X., Cao, J., Jia, Z., Yang, R., et al. (2016). Studies on the regulation of lipid metabolism and its mechanism of the iridoids rich fraction in Valeriana jatamansi Jones. *Biomed. Pharmacother.* 84, 1891–1898. doi:10.1016/j.biopha.2016.10.099

Zu, Y., Chen, X. F., Li, Q., Zhang, S. T., and Si, L. N. (2021). PGC-1α activates SIRT3 to modulate cell proliferation and glycolytic metabolism in breast cancer. *Neoplasma* 68, 352–361. doi:10.4149/neo_2020_200530N584

frontiers | Frontiers in Pharmacology

TYPE Original Research
PUBLISHED 04 December 2024
DOI 10.3389/fphar.2024.1449994

OPEN ACCESS

EDITED BY
Xianyu Li,
China Academy of Chinese Medical Sciences, China

REVIEWED BY
Swati Haldar,
Albert Einstein College of Medicine, United States
Xianjun Xiao,
Chengdu University of Traditional Chinese Medicine, China

*CORRESPONDENCE
Xi-Lin Ouyang,
oyxl-xg@163.com
Jing-Jing Zhong,
zhongjingjing2011@126.com

RECEIVED 16 June 2024
ACCEPTED 18 November 2024
PUBLISHED 04 December 2024

CITATION
Ouyang X-L, Yuan Z-L, Chen X-B, Gan H-W, Guo S-H, Cai J and Zhong J-J (2024) Can aged *Camellia oleifera* Abel oil truly be used to treat atopic dermatitis?
Front. Pharmacol. 15:1449994.
doi: 10.3389/fphar.2024.1449994

Can aged *Camellia oleifera* Abel oil truly be used to treat atopic dermatitis?

Xi-Lin Ouyang[1]*, Zhang-Lin Yuan[1], Xiao-Bing Chen[1], Hong-Wan Gan[2], Sen-Hui Guo[1], Juan Cai[1] and Jing-Jing Zhong[2]*

[1]Department of Pharmacy, Gannan Healthcare Vocational College, Ganzhou, China, [2]Department of Dermatology, Ganzhou People's Hospital, Ganzhou, China

Atopic dermatitis is an inflammatory skin condition characterized by erythema, eruption, lichenification, and pruritus. Aged *Camellia oleifera* Abel oil, an effective empirical plant oil utilized by the Gannan Hakka people in China to alleviate the symptoms of atopic dermatitis. However, no scientific studies have been reported to prove whether this oil is truly effective. We conducted this study to confirm whether aged *C. oleifera* oil could alleviate the symptoms of 2,4-dinitrochlorobenzene (DNCB)-induced atopic dermatitis in mice. Differences in the thickness and weight of the right and left ears were measured. ELISA was used to determine the serum levels of the inflammatory factors IL-4, IgE, IFN-γ, and TNF-α. HE staining was performed to observe inflammatory cell infiltration in the mouse skin lesions. In addition, the metabolites of aged *C. oleifera* oils were analyzed, and molecular docking was used to assess the binding affinity of the major metabolites to filaggrin, a protein involved in skin barrier function. Animal studies showed that aged *C. oleifera* oil significantly improved the symptoms of atopic dermatitis. HE staining and measurement of inflammatory factor levels revealed similar results. A total of 41 metabolites were tentatively identified in the oil, with fatty acids emerging as the major metabolites. Molecular docking confirmed that the three most abundant fatty acids, i.e., oleic acid, *n*-hexadecanoic acid, and octadecanoic acid, bind well to filaggrin. Our results suggest that aged *C. oleifera* oils can be used to ameliorate the symptoms of atopic dermatitis. Fatty acids may be the major active metabolites responsible for the observed therapeutic effects by reducing transdermal water loss, increasing skin hydration, alleviating DNCB-induced skin barrier alterations, and eliminating itchy scratching caused by dry skin.

KEYWORDS

***Camellia oleifera* Abel oil, GC/Q-TOF MS, atopic dermatitis, fatty acids, molecular docking, major metabolites**

Abbreviations: AD, Atopic dermatitis; COO, *Camellia oleifera* Abel oil; DNCB, 2,4-dinitrochlorobenzene; ELISA, enzyme-linked immunosorbent assay; GC/Q–TOF MS, gas chromatography/quadrupole time-of-flight mass spectrometry; HE, hematoxylin-eosin; IFN-γ, interferon gamma; IL-4, interleukin 4; IgE, immunoglobulin E; TNF-α, tumor necrosis factor alpha.

1 Introduction

Atopic dermatitis (AD), also known as eczema, is a common skin condition characterized by reddening, swelling, itching, blistering, and erosion of the skin (Clebak et al., 2023). The intense itching associated with AD can disrupt sleep, and scratching often exacerbates the condition, leading to infection and inflammation, which increases the difficulty of treatment (Garmhausen et al., 2013). There are various direct causes of AD, including genetic and environmental factors, skin barrier dysfunction, microbiological imbalances, immune dysregulation, skin inflammation, and environmental interactions; as a result, the prevalence of AD is increasing worldwide (Suaini et al., 2021). In addition to avoiding exposure to allergens, people with AD had to be treated with topical medications. These topical medications include topical steroid creams, antihistamines, topical immunomodulators, and ultraviolet light. However, long-term or excessive use of medications can cause obvious side effects such as skin atrophy, hyperpigmentation, abnormal hair growth, skin dryness, hormone dependency, and suppression of immune function (Leung et al., 2004). Therefore, it is important to treat AD not only to ensure that the drugs are safe and effective, but also to minimize side effects. It is worthwhile searching for anti-AD drugs from natural medicinal plants with low toxicity and significant efficacy.

People in many regions have traditionally used plant oils to treat AD (Linnamaa et al., 2010). Several natural plant oils, such as coconut oil, lavender oil, grapeseed oil, olive oil, and sunflower oil, have long been used as natural remedies for the treatment of various topical skin diseases (Foster et al., 2010; Simon et al., 2014; El-Salamouni et al., 2020). *Camellia oleifera* Abel oil (COO), an edible oil widely used in China, is also known as "Oriental olive oil". The "Compendium of Materia Medica" (本草纲目, compiled by Shizhen Li, a pharmacologist in the Ming Dynasty), a pharmacological work that mainly introduces the basic theories of materia medica and traditional Chinese medicine, states that "COO is cool in nature, cools the blood, stops bleeding, clears heat, and removes toxins". When fresh COO is stored for a long time, it becomes aged COO. It is generally believed by the Gannan Hakka people of China that the edible value of aged COO is decreased compared to fresh COO, while the medicinal effect is enhanced. The longer COO is stored, the better its medicinal effect. Modern pharmacological studies have shown that the active metabolites of COO that confer its anti-inflammatory properties may be total saponins (Zhang F. et al., 2022), and polyphenolic extracts have also been proposed to confer these properties (Chang et al., 2020). Unfortunately, polyphenolic compounds that are purified from active extracts have been shown to have low anti-inflammatory activity (Zhang et al., 2021).

In addition to the metabolites mentioned above, COO is rich in saturated and unsaturated fatty acids, including oleic acid, palmitic acid, palmitoleic acid, stearic acid, linoleic acid, linolenic acid, and eicosenoic acid (Yang et al., 2016; Zhang F. et al., 2022; Gao et al., 2024). Fatty acids are also the major metabolites of plant oils and may contribute to promoting wound healing and protecting skin barrier homeostasis through antioxidant and anti-inflammatory mechanisms (Lin et al., 2018). Therefore, to investigate whether aged COO can be used in the treatment of AD and whether fatty acids are the active metabolites with anti-AD activity, we established an animal model of AD to validate the therapeutic effects, determined metabolites of aged COO by GC/Q–TOF MS, and evaluated the possibility that the major metabolites exert anti-AD effects.

2 Materials and methods

2.1 Instruments and reagents

Cellular inflammatory factor levels were determined using a fully automatic microplate absorbance reader (WD-2102B, Beijing Liuyi). Compositional analysis was performed with an Agilent 7250 GC/Q–TOF MS system.

2,4-dinitrochlorobenzene (DNCB) was purchased from Sigma–Aldrich, St. Louis, MO, United States of America, and prednisone acetate (PA) was obtained from Shanghai Macklin Biochemical Co., Ltd. Shanghai, China. A mouse interferon gamma (IFN-γ) assay kit, mouse tumor necrosis factor alpha (TNF-α) assay kit, mouse immunoglobulin E (IgE) assay kit, and mouse interleukin 4 (IL-4) assay kit were purchased from Wuhan Elabscience Biotechnology Co., Ltd. Xylene, anhydrous ethanol, and 95% ethanol were purchased from Xilong Scientific Co., Ltd., China. Hematoxylin staining solution was purchased from Zhongshui Jinqiao Co., Ltd., China. Eosin staining solution was purchased from Solarbio Co., Ltd., Beijing, China. Hematoxylin was obtained from Servicebio (G1040 Servicebio, Wuhan, China).

2.2 Samples

The seeds of *C. oleifera* were collected from Xingguo County, Ganzhou, China, in November 2020. The flowchart of the seeds processed and extracted was as follows: *C. oleifera* seeds → Removing impurities → Sun drying → Hulling and separating → Further drying → Crushing → Steaming → Machine pressing → Filtering → *C. oleifera* oil. The COO was stored in a sealed container at room temperature.

2.3 Animals

Twenty 6-week-old male BALB/c mice were purchased from Spearfish (Beijing) Biotechnology Co. Ltd., license No. SCXK (Beijing) 2019–0010. The feeding conditions were as follows: temperature, 20°C–26°C; humidity, 40%–70%; and free access to drinking water. The mice were allowed to acclimate and were fed for 7 days, and then the mice were randomly divided into four groups (n = 5/group): a vehicle (acetone:olive oil = 34:1)-treated control group, a DNCB-treated group, a PA/DNCB-treated group, and a COO/DNCB-treated group. All the animal studies were conducted in accordance with a protocol that was approved by the Animal Ethics Committee of Gannan Healthcare Vocational College (approval number: 20220106).

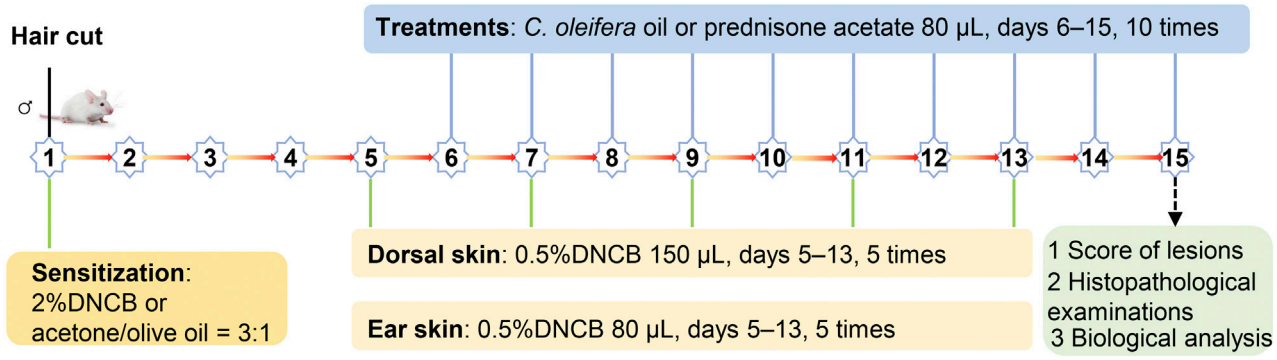

FIGURE 1
DNCB-induced AD model experimental design and treatment schedule.

2.4 Establishment of the AD model and treatment

The AD model was established as described in the literature (Kim et al., 2021). Briefly, the hair was removed from a 2-cm × 2-cm area on the back of BALB/c mice using electric clippers, and then the skin was sensitized with DNCB solution. In all groups except for the vehicle-treated control group, the skin on the back of mice was sensitized with 150 μL of 2% DNCB acetone-olive oil solution, while 10 μL of 2% DNCB acetone-olive oil solution was applied to the right ear on day 1. Subsequently, the mice in the COO/DNCB-treated group were stimulated with an acetone-olive oil mixture containing 0.5% DNCB on days 5, 7, 9, 11, and 13, while these mice were treated with corresponding amounts of aged COO on the skin of the backs and right ears from day 5 to day 14. As a control, the mice in the DNCB-treated group were treated with corresponding volumes of acetone-olive oil solution on the skin of the back and right ear, and the PA/DNCB-treated group was treated with prednisone acetate (Figure 1).

2.5 Measurement of indicators

2.5.1 Observation of skin tissue appearance

The severity of erythema/hemorrhage, edema, abrasion/erosion, and dryness/scarring/inflammation on the back skin of mice in each group was observed and scored after the last treatment on day 15. The scoring criteria were as follows: 0, none; 1, mild; 2, moderate; 3, severe; and 4, very severe, with scores ranging from 0 to four for desquamation (dryness), edema (papules), erythema (hemorrhage), and epidermal peeling (scratches) (Wang et al., 2021).

2.5.2 Weight and thickness differences between left and right ear

Animals were killed 24 h after the last treatment, and serum was collected for subsequent measurements of the IL-4, TNF-α, IgE, and TFN-γ levels. The mouse ears were carefully cleaned, and round ear slices were collected from the same position in the middle of the left and right ears using an 8-mm diameter metal punch. Each tissue sample was weighed using an electronic balance to calculate the difference in weight between the left and right ears, and the right ear sample was embedded in paraffin for the HE staining. In each group, the center thickness of the right and left ears was measured with calipers at the end of drug treatment, and the difference in thickness between the right and left ears was calculated.

2.5.3 HE staining

Inflammatory cell infiltration into the skin lesions of mice was observed by HE staining to evaluate whether aged COOs can be used to treat AD. Right ear tissue from the mice was embedded in paraffin and sectioned at a thickness of 5 μm. The sections were incubated and dried in an oven at a constant temperature of 60°C for 2–4 h. After deparaffinization, the tissue sections were immersed in gradient ethanol solutions (75%, 85%, 95%Ⅰ, 95%Ⅱ, 100%Ⅰ, and 100%Ⅱ) for 60 min each for dehydration and hydrated in distilled water for a few minutes. Finally, the sections were stained with hematoxylin and eosin for 3–5 min each. After dehydration, the tissue sections were sealed with xylene, and inflammatory cell infiltration was observed under a microscope.

2.5.4 Measurement of the serum IL-4, TNF-α, IgE, and TFN-γ concentrations

The levels of the inflammatory factors IL-4, IgE, IFN-γ, and TNF-α in the serum of mice were determined by ELISA. Whole-blood samples were collected in serum separator tubes and incubated at room temperature for 2 h. The samples were then centrifuged at 1000 *g* for 20 min. The serum was removed and transferred to microcentrifuge tubes and stored at 4°C in a refrigerator. IL-4, TNF-α, IgE, and TFN-γ levels in the mouse serum samples were measured as described in the ELISA kit instructions.

2.6 Metabolite analysis

2.6.1 Pre-treatment of samples

Metabolite analysis of aged COO was performed according to the ConPhyMP guidelines (Heinrich et al., 2022). One hundred milligrams of COO sample were added to a 15-mL centrifuge tube,

n-hexane was added to a final volume of 10 mL, and the mixture was vortexed for 1 min. Then, 1 mL of sample was transferred to a 1.5-mL centrifuge tube and centrifuged at 10,000 rpm for 5 min, after which the supernatant was transferred to an injection vial for measurement; *n*-hexane was used as the blank.

2.6.2 Chromatographic conditions

The metabolites of the COO were analyzed via GC/Q–TOF MS. The chromatographic procedure involved an HP-5 MS UI column (30 m × 0.25 mm × 0.25 μm) with a shunt injection of carrier gas (He), an injection volume of 1.0 μL, and a column flow rate of 1 mL·min^{-1}. The starting temperature was 40°C, and the temperature was increased from 40°C to 310°C at a rate of 10°C·min^{-1}. The mass spectrometry conditions were as follows: full-scan mode, ionization source EI, ionization energy of 70 eV, transmission line temperature of 310°C, ion source temperature of 200°C, quadrupole temperature of 150°C, solvent delay time of 4 min, and scanning mass range of 20–550 amu.

2.7 Molecular docking

Three major fatty acids, namely, *n*-hexadecanoic acid, oleic acid, and octadecanoic acid, were used as small molecules for docking studies with filaggrin of the stratum corneum, which is closely related to AD (Earlia et al., 2019). In this docking study, the crystal structure files of filaggrin were obtained from the PDB database (www.rcsb.org), saved in pdb format, and then preprocessed as follows: removal of water of crystallization and non-standard peptide chains, merging of nonpolar hydrogens, merging of lone pairs of electrons, removal of solvent molecules, addition of all hydrogen atoms, recalculation of Gasteiger charge, and modification to Autodock four atom types. Then, the files were converted to pdbqt format using Autodock Tools 4.2.6 for backup (Morris et al., 2009). Using the CAS number of the small molecule of the ligand, the 3D structure file (.sdf format) of the ligand was obtained from the PubChem database (https://pubchem.ncbi.nlm.nih.gov/). The small molecules in the PubChem database have been optimized in terms of their preliminary structure and are in the ideal initial conformation for docking. The ligands were correctly protonated at pH = 7.4 (reference human pH: 7.35–7.45) and then converted to pdbqt format using OpenBabel 3.1.1 (O'Boyle et al., 2011). Docking was performed using the latest version of AutoDock vina 1.2.3 with the following parameters: algorithm exhaustiveness of 16, candidate docking results (num_modes) of 9, and energy threshold (energy_range) of ±3 kcal/mol.

2.8 Statistical analysis

All the experimental data were statistically analyzed using GraphPad Prism nine software. The results are expressed as the mean ± standard deviation (SD). Analysis of variance (ANOVA) was used to determine the statistical significance of differences between groups, with $p < 0.05$ considered to indicate statistical significance and $p < 0.01$ considered to indicate high statistical significance.

3 Results

3.1 Evaluation of the use of COO to improve skin appearance in AD model mice

To investigate whether COO exerts anti-AD effects, we successfully established an AD model using a previously described method (Kim et al., 2021). DNCB-stimulated mice developed hemorrhages, edema, vesicles, scaling, and dryness, which caused constant itching, while the skin of all mice in the vehicle-treated control group began to regrow new hair. After the COO and PA were applied, the mice exhibited a similar skin appearance: the skin of the mice in the two groups improved in terms of hemorrhage and vesiculation, and the hair of some mice in the COO/DNCB-treated group began to regrow (Figure 2A). The PA/DNCB-treated group scored the highest, and the COO/DNCB-treated group had the second highest score, while the DNCB-treated group was the lowest. This result confirmed the ameliorative effect of COO on ameliorating the development of AD mice symptoms, but not as effective as the PA/DNCB-treated group (Figure 2B).

3.2 Effects of COO on the thickness and weight of the right and left ears of AD model mice

To determine the degree of skin swelling in AD model mice, differences in thickness of the right and left ears of the same mice were analyzed. Compared with those of mice in the vehicle-treated control group, the right ears of mice in other groups were swollen, and the differences in thickness of the left and right ears in each group were significant. Compared with those in the DNCB-treated group, the differences in the PA/DNCB-treated and COO/DNCB-treated groups were not significant. The thickness difference between the right and left ears of mice in the COO/DNCB-treated group was greater after the use of tea oil. The results showed that the right ear swelling did not seem to improve in the COO/DNCB-treated group of mice, and the severity of AD appeared to increase (Figure 3A).

Similar results were observed for differences in the weight of the right and left ears. The difference in skin weight between the right and left ears was greatest in mice treated with COO, but the difference was not statistically significant compared to mice in other groups. Moreover, the difference between the right and left ear weights of mice in all groups was not statistically significant (Figure 3B).

3.3 HE staining analysis of right ear tissue

HE staining was used to determine the efficacy of aged COO in the treatment of mice with AD. As shown in Figure 4A, normal mouse skin histology was observed under a light microscope; the epidermal thickness and numbers of mast cells in the right ears were maintained at low levels, and no obvious lesions were observed. However, abnormal histological changes were observed in the dorsal skin and ears of DNCB-treated mice. Histopathology revealed that the ear tissues of mice in the DNCB-treated group were covered with

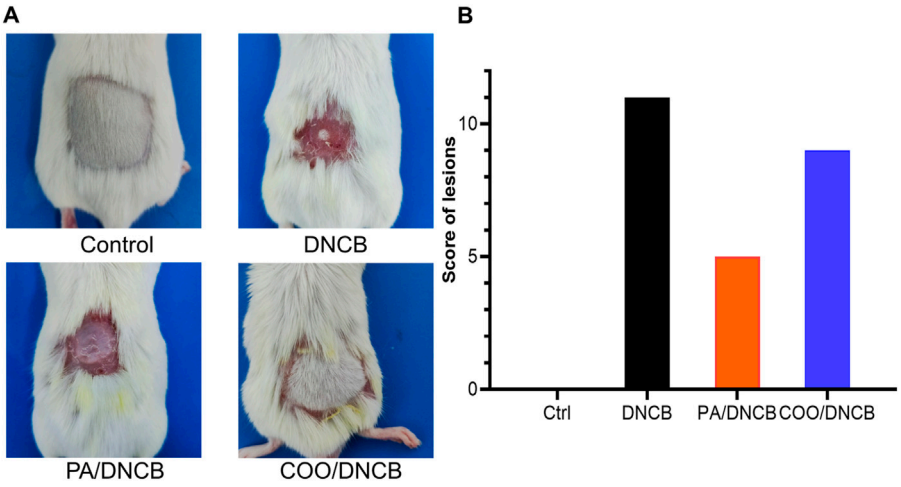

FIGURE 2
Typical appearance of mice in each group. **(A)** Effect of aged COO on the severity of DNCB-induced AD-like skin. Representative images of the vehicle-treated control group, DNCB-treated group, PA/DNCB-treated group, and COO/DNCB-treated group. **(B)** Scores of each group.

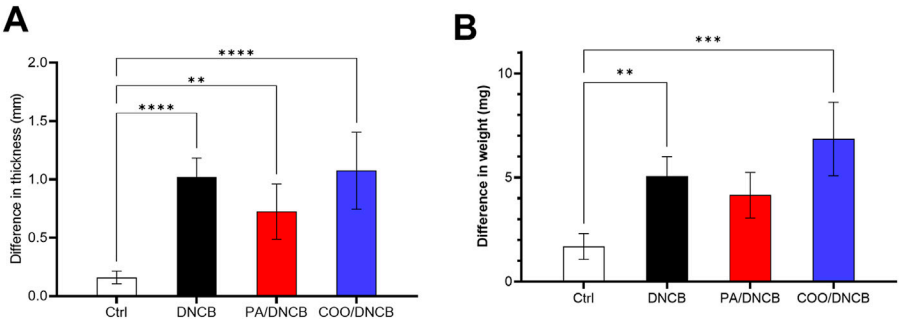

FIGURE 3
Differences in thickness and weight on the left and right ears of mice. **(A)** Difference in thickness between left and right ears **(B)** Difference in weight between left and right ears.

squamous epithelium, with thickening of the epidermal layer, surface hyperkeratosis, hyperplasia of spindle cells, and dilation of blood vessels in the dermal layer, and the infiltration of inflammatory cells, such as lymphocytes and plasma cells, was observed. Compared with the vehicle-treated control group, the DNCB-treated group exhibited the dense infiltration of inflammatory cells. In addition, the mean thickness of the epidermal layer in the right ear in the DNCB-treated group was increased by 3.7-fold compared to the vehicle-treated control group (Figure 4B).

Mice treated with PA showed a significant improvement in inflammatory infiltration, amelioration of pathological changes, and improved therapeutic results, with the average thickness of the epidermal layer in the ear being 55% of that of the DNCB-treated group. The COO/DNCB-treated group showed similar results to those of the PA/DNCB-treated group after treatment. In the COO/DNCB-treated group, inflammatory cell infiltration was reduced in most areas, and pathological changes were ameliorated. However, focal vasodilatation and lymphocyte and plasma cell infiltration were still observed. The inflammatory cell infiltration was improved, and the epidermal layer was thinner compared to the DNCB-treated group. The epidermal thickening of the ear skin in the COO/DNCB-treated group was 48% of that in the DNCB-treated group.

3.4 Effect of COO on expression of cytokines in the ear

As shown in Figure 5, repeated application of DNCB significantly increased the serum levels of inflammatory cytokines in mice in the DNCB-treated group compared with those in the vehicle-treated control group, as indicated by a 4.2-fold increase in IL-4 levels, a 3.4-fold increase in IgE levels, a 3.6-fold increase in TNF-α levels, and a 2.3-fold increase in IFN-γ levels. These results indicate that the dermatitis model has been successfully established.

The results showed that the IL-4 level in the COO/DNCB-treated group was 97.12 ± 19.62 pg·mL^{-1}. Compared with the

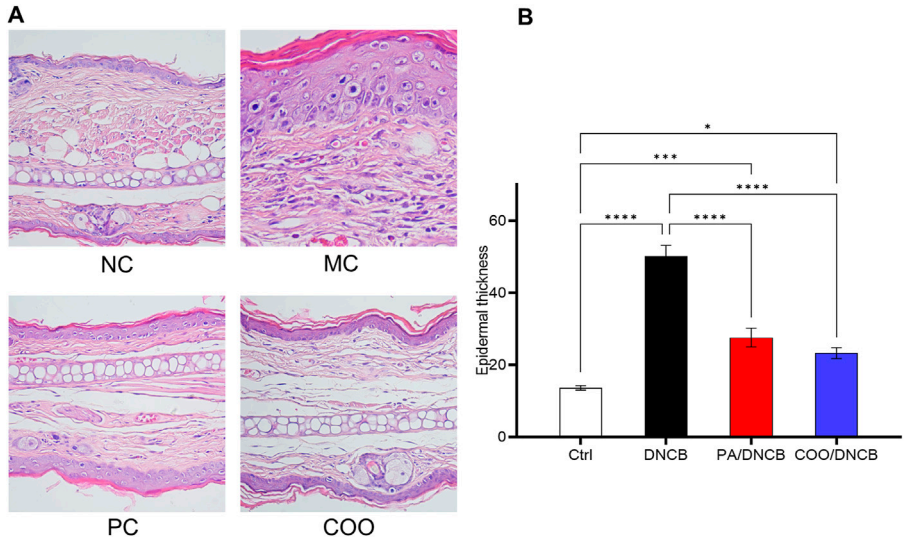

FIGURE 4
Histopathology of mouse ear skin after treatment with aged COO. **(A)** Results of HE staining on mouse skin tissues. **(B)** Comparison of epidermal layer thickness of ear skin between the vehicle-treated control group, DNCB-treated group, PA/DNCB-treated group, and COO/DNCB-treated group.

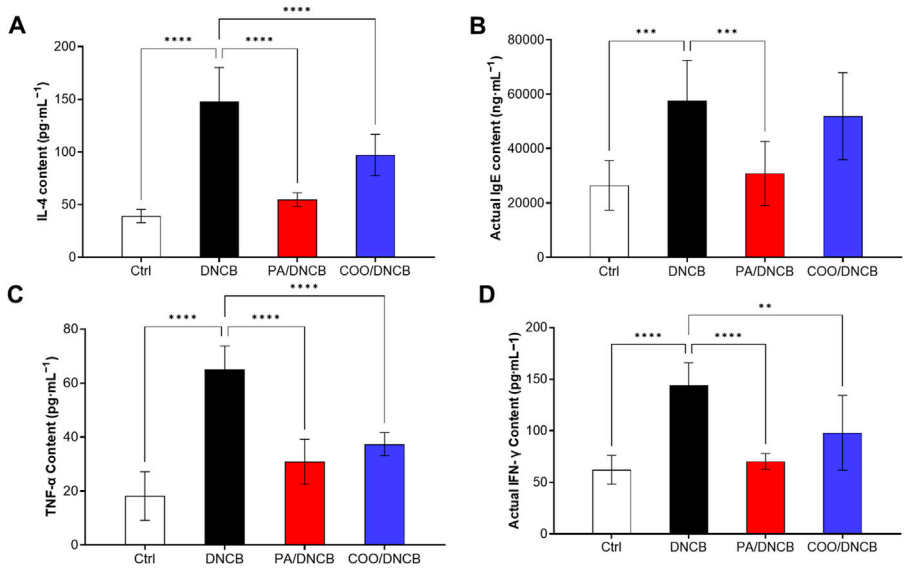

FIGURE 5
Effect of aged COO on serum levels of IFN-γ **(A)**, IL-4 **(B)**, IgE **(C)**, and TNF-α **(D)** in DNCB-induced mice.

DNCB-treated group, the serum IL-4 level in the COO/DNCB-treated group was 40.6% lower than that of the DNCB-treated group but higher than that of the PA/DNCB-treated group, which had a serum IL-4 level of 54.67 ± 6.585 pg·mL^{-1} (Figure 5A).

IgE is an immunoglobulin and mediator of mast cell activation that plays a central role in type 1 hypersensitivity reactions and chronic allergic diseases (Wollenberg et al., 2021). When antigens cross-link with specifically bound IgE, mast cell degranulation is induced, followed by the secretion of histamine, leukotrienes, and chemokine-activated mediators, leading to itching and skin inflammation. The results showed that IgE levels were significantly reduced by 46.4% in the PA/DNCB-treated group compared to the DNCB-treated group (Figure 5B). The IgE level in the COO/DNCB-treated group decreased by about 9.9% compared with the DNCB-treated group, indicating that COO tended to reduce the inflammatory response in AD.

The analysis of TNF-α showed similar results. In response to inflammatory factors, TNF-α levels increase rapidly (Luo et al., 2022). The results showed that the level of TNF-α in the PA/DNCB-treated group was 30.86 ± 8.322 pg·mL^{-1}, which was reduced by 52.5% compared with the DNCB-treated group (Figure 5C). The level of TNF-α in the COO/DNCB-treated group was 37.38 ±

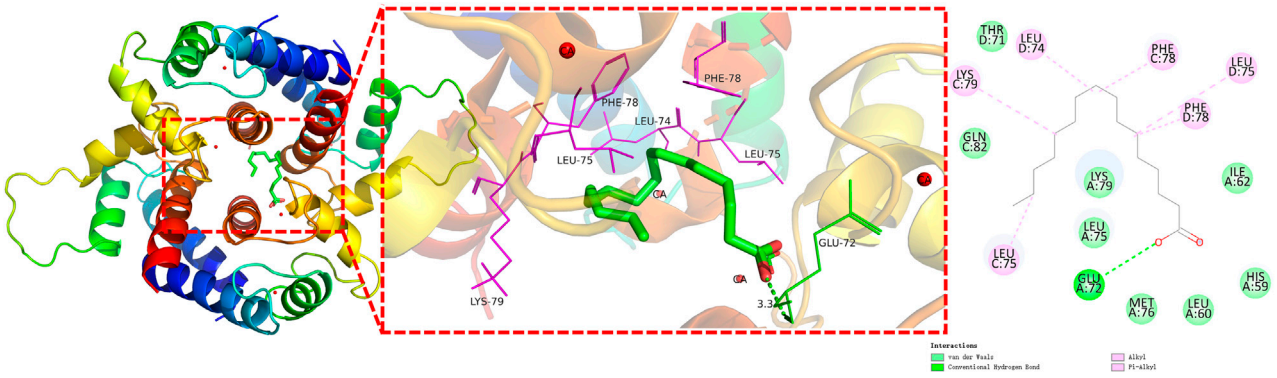

FIGURE 6
Interaction analysis of filaggrin with *n*-hexadecanoic acid docking results (π-bonds are shown as purple dashed lines; hydrogen bonds are shown as green dashed lines).

4.281 pg·mL^{-1}, which decreased by 42.5% compared with the DNCB-treated group.

IFN-γ is secreted mainly by activated T cells and is also known as an immune interferon (Fagundes et al., 2023). IFN-γ promotes the expression of MHC class II molecules, activates macrophages, and inhibits viral replication. The results showed that the level of IFN-γ in the PA/DNCB-treated group was 70.32 ± 7.597 pg·mL^{-1}, which decreased by 51.2% (Figure 5D) compared with the DNCB-treated group. The IFN-γ level in the COO/DNCB-treated group was 97.94 ± 36.29 pg·mL^{-1}, which decreased by 32.0% compared with the DNCB-treated group.

3.5 Metabolite analysis of COO

The compositions of COO were analyzed using Agilent MassHunter Unknowns Analysis software. As shown in Supplementary Table S1, forty-one metabolites were detected in COO, and the three major peaks (approximately 69.38%) were identified as oleic acid (112–80-1), *n*-hexadecanoic acid (57–10-3), and (*E*,*E*)-2,4-decadienal (CAS: 25,152–84-5). These results clearly indicate aged COO contains a considerable proportion of unsaturated fatty acids, among which oleic acid is the main metabolite (Zhang X.-L. et al., 2022). Supplementary Table S2 shows that the compositions of COO contain fatty acids (66.96%), esters (1.38%), alkanes (4.52%), aldehydes or ketones (25.67%). In addition, small amounts of nitrogen-containing metabolites (1.48%) were detected.

3.6 Molecular docking

The molecular docking results revealed that *n*-hexadecanoic acid, oleic acid, and octadecanoic acid had the good binding affinity, docking with filaggrin with the binding affinity at −6.979, −6.855, and −6.909 kcal·mol^{-1}, respectively. All values are higher than that of the two eutectic ligands present in filaggrin 4pcw (−4.190 kcal·mol^{-1} and −4.144 kcal·mol^{-1}, respectively). In general, the lower the resulting affinity is, the more stable the binding conformation is; in the absence of a positive control, binding affinities less than −6 kcal·mol^{-1} are generally considered to indicate more stable ligand-receptor interactions (Shityakov and Förster, 2014). Thus, the results confirm that the ability of the fatty acid ligands to bind to filaggrin is better than that of the eutectic ligands, indicating the good binding potential of each fatty acid to filaggrin.

The surface binding pocket pattern diagram of *n*-hexadecanoic acid, which had the best effect (Figure 6), shows that the ligand bound within the pocket-like region inside the protein, and the two had good complementary shapes that were suitable for producing a specific binding effect. Figure 6 shows that the *n*-hexadecanoic acid ligand formed a hydrogen bond with the amino acid residue GLU A72 and six π/alkyl interactions or π-π stacking interactions with other amino acid residues (LEU C75, LYS C79, LEU D74, PHE C78, LEU D75, and PHE D78). We also observed that the binding sites of *n*-hexadecanoic acid and one of the proto-cocrystalline ligands were almost identical, which indicates that the two were well bound and confirms that the two had good affinity.

4 Discussion

In this study, we investigated the effect of aged COO on DNCB-induced AD-like skin damage in BALB/c mice. Typical AD symptoms such as erythema, papules, and severe itching could be clearly observed in the skin of mice after repeated alternating applications of DNCB. Analysis of the degree of ear skin thickness and weight swelling in the mice showed that the ears of the DNCB-treated group were more swollen than those of the vehicle-treated control group, and the thickness of the left and right ears was significantly different between the groups. When treated with PA or COO, the difference in thickness between the DNCB-treated and COO/DNCB-treated groups was significant compared with the vehicle-treated control group. The epidermis of ear specimens from the DNCB-treated group is hyperkeratotic and thickened, and the dermis is predominantly infiltrated by inflammatory cells and shows vasodilation, as shown by HE staining. We hypothesized that this thickening, in addition to

hyperkeratosis, was associated with echinocyte proliferation and visible dermal vasodilation.

The monocyte/macrophage system that is stimulated by inflammation is activated by the release of many inflammatory factors, such as IL-6, IL-1β, TNF-α, and IFN-γ. To determine the changes of inflammatory markers in COO-treated AD mice, serum levels of IL-4, TNF-α, IgE, and TFN-γ were further analyzed. It is well known that IgE is an immunoglobulin and a mediator of mast cell activation that plays a central role in type 1 hypersensitivity reactions and chronic allergic diseases (Wollenberg et al., 2021). When antigen cross-links with specifically bound IgE, mast cell degranulation is induced, followed by secretion of histamine, leukotrienes, and chemokine-activating mediators, leading to itching and skin inflammation (Galli et al., 2008). As shown in this study, repeated treatment of the right ear of mice with DNCB resulted in infiltration of inflammatory cells into the dermis and increased serum levels of IgE. Topical application of COO reduced serum levels of IgE and significantly suppressed the number of inflammatory cells infiltrating the skin injury in AD mice.

Overexpression of IL-4 has been implicated as a key factor in inflammatory diseases such as AD (Elbe-Bürger et al., 2002). IL-4 induces the differentiation of initial $CD4^+$ T cells into Th2 cells, which in turn produce more cytokines and initiate a type 2 inflammatory response (Cernescu et al., 2021). In addition, IL-4 and IL-13 together induce the conversion of immunoglobulins to IgE in B cells and stimulation of afferent neurons via the IL-4 receptor subunit-α (IL-4Rα) to promote pruritus (Bitton et al., 2020). In our results, serum levels of IL-4 were reduced in the COO/DNCB-treated group, suggesting that COO inhibits Th2 cell production by reducing serum levels of IL-4 and may play a bridging role in reducing serum levels of IgE.

TNF-α produced during the initiation phase of AD induces the production of various chemokines and adhesion molecules, leading to the recruitment and proliferation of inflammatory cells within the skin. In response to inflammatory factors, TNF-α levels increase rapidly (Luo et al., 2022). COO has been shown to have anti-inflammatory activity (Zhang et al., 2021; Zhou et al., 2024). Our experiments also showed that serum TNF-α levels were reduced in DNCB-induced BALB/c mice coated with COO, suggesting that the development of AD-like symptoms could be inhibited. COO has also previously been shown to inhibit TNF-α expression in activated human inflammatory cells (Zhang et al., 2021). Therefore, we hypothesized that the inhibitory effect of COO on inflammatory cell infiltration in the AD model may be mediated by blocking TNF-α expression and downstream chemokine/adhesion molecules.

In addition, IFN-γ is mainly secreted by activated T cells, also known as immune interferons (Fagundes et al., 2023). IFN-γ promotes the expression of MHC class II molecules, activates macrophages, and inhibits viral replication. In our experiments, serum levels of IFN-γ were reduced in mice coated with COO, suggesting that COO may have potential anti-AD effects.

Therefore, the experimental results showed that topical application of aged COO downregulated the expression of IgE, IL-4, IFN-γ, and TNF-α, and alleviated the development of AD-like symptoms in DNCB-induced BALB/c mice. Moreover, although aged COO had beneficial effects in ameliorating AD symptoms, they were weaker than those of prednisone acetate.

Based on the metabolite analysis of COO by GC/Q-TOF MS method and molecular docking analysis of three fatty acids with filaggrin binding capacity results, we conclude that fatty acids, which are the major chemical metabolites in COO, may have antipruritic and anti-inflammatory activities, and are potent active metabolites in the treatment of AD (Chang et al., 2020). In fact, many plant oils rich in polyunsaturated fatty acids play an important role as immunomodulators (Kildaci et al., 2021). These plant oils can be used to improve skin barrier function and reduce inflammation, and they are considered potential anti-wrinkle agents (Jung et al., 2007), but the saturation, concentration, and *cis-trans* structure of the double carbon bonds in these fatty acids of plant oils may influence the amelioration of AD symptoms (Venter et al., 2019; Olejnik et al., 2023). In addition, oral and topical oils for AD may have different mechanisms of action. Oral administration of COO may activate free fatty acid receptor 4 (FFA4) to increase regulatory T cells to ameliorate AD (Son et al., 2020). Topical application of aged COO may be the result of fatty acids in COO stably binding to the filaggrin of the epidermis, protecting the unique barrier structure of the cuticular surface layer, and preventing water loss, which may be the mechanism by which COO plays a role in the treatment of AD (Jung et al., 2007).

Filaggrin is not only a key component of epidermal keratin but also dissociates from keratin fiber bundles, transforming and degrading to form mixtures of water-absorbing amino acids that trap moisture in the skin through hydration (Cabanillas and Novak, 2016). Application of aged COO reduced transdermal water loss, increased skin hydration, alleviated DNCB-induced skin barrier alterations, and eliminated itchy scratching caused by dry skin. Meanwhile, aged COO inhibited matrix metalloproteinase (MMP)-1 activity and induced human type I procollagen synthesis (Zhang et al., 2024). Furthermore, in inflammatory skin, plant oils high in oleic acid or deficient or low in linoleic acid may cause additional structural damage to the stratum corneum, whereas plant oils rich in linoleic acid and saturated fatty acids may have beneficial effects (Poljšak and Kočevar Glavač, 2022). Therefore, we conclude that *n*-hexadecanoic acid, oleic acid, and octadecanoic acid have the best potential to be used as drug candidates for the treatment of AD, and filaggrin may be the drug target of the anti-AD effect (Earlia et al., 2019). These fatty acids play an important role in the anti-AD effect through coordinated action.

This study has some obvious limitations. During the experiment, the bare skin of the mice was wrapped in gauze or fed individually to prevent them from sucking on each other, but scratches on skin are still unavoidable. In addition, we only studied COO stored for 3 years, whether COO stored for longer periods has therapeutic effects needs to be determined. In addition, further cell experiments are needed to verify the effect.

5 Conclusion

In conclusion, administration of COO that was stored for 3 years attenuated the development of DNCB-induced AD symptoms in BALB/c mice and effectively ameliorated DNCB-induced AD symptoms. Infants and young children are susceptible to AD. However, due to the underdeveloped skin structure of infants and young children, the stratum corneum and epidermis of their

skin are significantly thinner than those of adults, and the structure of the epidermis and dermis, as well as the skin appendages, are significantly different from those of adults, so the safety of the drug is preferred. Considering that COO has medicinal and edible values, we believe that aged COO is a promising anti-inflammatory and anti-allergic agent with significant efficacy, especially for infants and children. In the traditional use of aged COO, it is often believed that the longer aged COO is stored, the more effective it is. However, aged COO, especially oil that was stored for more than 5 years, tended to suffer from rancidity due to influences such as container, light, and storage time, which had significantly changed in the content of organic acids and advanced fatty acid esters. Not only did this oil have an unpleasant odor, but it could also affect the efficacy of treating AD. Therefore, our future focus is to investigate whether fresh COO is effective and how long COO should be stored to be effective, and to conduct further cell experiments to explore the mechanism.

Data availability statement

The original contributions presented in the study are included in the article/Supplementary Material, further inquiries can be directed to the corresponding authors.

Ethics statement

All the animal studies were conducted in accordance with a protocol that was approved by the Animal Ethics Committee of Gannan Healthcare Vocational College (approval number: 20220106). The study was conducted in accordance with the local legislation and institutional requirements.

Author contributions

X-LO: Writing–review and editing, Writing–original draft, Methodology, Investigation, Funding acquisition, Data curation, Conceptualization. Z-LY: Writing–review and editing, Validation, Methodology, Funding acquisition, Formal Analysis. X-BC: Writing–review and editing, Resources, Investigation, Formal Analysis. H-WG: Writing–review and editing, Validation, Methodology, Conceptualization. S-HG: Writing–review and editing, Visualization, Formal Analysis, Data curation. JC: Writing–review and editing, Formal Analysis, Data curation. J-JZ: Writing–review and editing, Visualization, Validation, Project administration, Methodology, Investigation, Data curation.

Funding

The author(s) declare that financial support was received for the research, authorship, and/or publication of this article. The work was supported by the Science and Technology Planning Project of the Jiangxi Provincial Health Commission (No: 202210095), the Science and Technology Planning Project of the Jiangxi Provincial Education Department (Nos GJJ217101 and GJJ2209712), and the Science and Technology Planning Project of the Jiangxi Provincial Administration of Traditional Chinese Medicine (No: 2021A332).

Conflict of interest

The authors declare that the research was conducted in the absence of any commercial or financial relationships that could be construed as a potential conflict of interest.

Publisher's note

All claims expressed in this article are solely those of the authors and do not necessarily represent those of their affiliated organizations, or those of the publisher, the editors and the reviewers. Any product that may be evaluated in this article, or claim that may be made by its manufacturer, is not guaranteed or endorsed by the publisher.

Supplementary material

The Supplementary Material for this article can be found online at: https://www.frontiersin.org/articles/10.3389/fphar.2024.1449994/full#supplementary-material

References

Bitton, A., Avlas, S., Reichman, H., Itan, M., Karo-Atar, D., Azouz, N. P., et al. (2020). A key role for IL-13 signaling via the type 2 IL-4 receptor in experimental atopic dermatitis. *Sci. Immunol.* 5 (44), eaaw2938. doi:10.1126/sciimmunol.aaw2938

Cabanillas, B., and Novak, N. (2016). Atopic dermatitis and filaggrin. *Curr. Opin. Immunol.* 42, 1–8. doi:10.1016/j.coi.2016.05.002

Cernescu, L. D., Haidar, L., and Panaitescu, C. (2021). Dendritic cell-CD4$^+$ T cell interaction: the differential role of IL-4/IL-13 in serum IgE levels in house dust mite allergic patients. *Exp. Ther. Med.* 21 (1), 95. doi:10.3892/etm.2020.9527

Chang, M., Qiu, F.-C., Lan, N.-N., Zhang, T., Guo, X., Jin, Q.-Z., et al. (2020). Analysis of phytochemical composition of *Camellia oleifera* oil and evaluation of its anti-inflammatory effect in lipopolysaccharide-stimulated RAW 264.7 macrophages. *Lipids* 55 (4), 353–363. doi:10.1002/lipd.12241

Clebak, K. T., Helm, L., Uppal, P., Davis, C. R., and Helm, M. F. (2023). Atopic dermatitis. *Prim. Care Clin. Office Pract.* 50 (2), 191–203. doi:10.1016/j.pop.2022.12.004

Earlia, N., Muslem, Suhendra, R., Amin, M., Prakoeswa, C. R. S., Khairan, et al. (2019). GC/MS analysis of fatty acids on pliek u oil and its pharmacological study by molecular docking to filaggrin as a drug candidate in atopic dermatitis treatment. *Sci. World J.* 2019, 8605743. doi:10.1155/2019/8605743

Elbe-Bürger, A., Olt, S., Stingl, G., Egyed, A., Klubal, R., Mann, U., et al. (2002). Overexpression of IL-4 alters the homeostasis in the skin. *J. Invest. Dermatol.* 118 (5), 767–778. doi:10.1046/j.1523-1747.2002.01753.x

El-Salamouni, N. S., Ali, M. M., Abdelhady, S. A., Kandil, L. S., Elbatouti, G. A., and Farid, R. M. (2020). Evaluation of chamomile oil and nanoemulgels as a promising treatment option for atopic dermatitis induced in rats. *Expert Opin. Drug Deliv.* 17 (1), 111–122. doi:10.1080/17425247.2020.1699054

Fagundes, B. O., de-Sousa, T. R., and Victor, J. R. (2023). Gamma-delta (γδ) T cell-derived cytokines (IL-4, IL-17, IFN-γ and IL-10) and their possible implications for atopic dermatitis development. *Int. J. Dermatol.* 62 (4), 443–448. doi:10.1111/ijd.16364

Foster, R. H., Hardy, G., and Alany, R. G. (2010). Borage oil in the treatment of atopic dermatitis. *Nutrition* 26 (7), 708–718. doi:10.1016/j.nut.2009.10.014

Galli, S. J., Tsai, M., and Piliponsky, A. M. (2008). The development of allergic inflammation. *Nature* 454 (7203), 445–454. doi:10.1038/nature07204

Gao, L., Jin, L.-H., Liu, Q.-N., Zhao, K.-X., Lin, L.-K., Zheng, J.-Y., et al. (2024). Recent advances in the extraction, composition analysis and bioactivity of *Camellia* (*Camellia oleifera* Abel.) oil. *Trends Food Sci. Technol.* 143, 104211. doi:10.1016/j.tifs.2023.104211

Garmhausen, D., Hagemann, T., Bieber, T., Dimitriou, I., Fimmers, R., Diepgen, T., et al. (2013). Characterization of different courses of atopic dermatitis in adolescent and adult patients. *Allergy* 68 (4), 498–506. doi:10.1111/all.12112

Heinrich, M., Jalil, B., Abdel-Tawab, M., Echeverria, J., Kulić, Ž., McGaw, L. J., et al. (2022). Best Practice in the chemical characterisation of extracts used in pharmacological and toxicological research-The ConPhyMP-Guidelines. *Front. Pharm.* 13, 953205. doi:10.3389/fphar.2022.953205

Jung, E., Lee, J., Baek, J., Jung, K., Lee, J., Huh, S., et al. (2007). Effect of *Camellia japonica* oil on human type I procollagen production and skin barrier function. *J. Ethnopharmacol.* 112 (1), 127–131. doi:10.1016/j.jep.2007.02.012

Kildaci, I., Budama-Kilinc, Y., Kecel-Gunduz, S., and Altuntas, E. (2021). Linseed oil nanoemulsions for treatment of atopic dermatitis disease: formulation, characterization, *in vitro* and *in silico* evaluations. *J. Drug Deliv. Sci. Tec.* 64, 102652. doi:10.1016/j.jddst.2021.102652

Kim, T. Y., Kim, Y. J., Jegal, J., Jo, B. G., Choi, H. S., and Yang, M. H. (2021). Haplopine ameliorates 2,4-dinitrochlorobenzene-induced atopic dermatitis-like skin lesions in mice and TNF-α/IFN-γ-Induced inflammation in human keratinocyte. *Antioxidants* 10, 806. doi:10.3390/antiox10050806

Leung, D. Y. M., Boguniewicz, M., Howell, M. D., Nomura, I., and Hamid, Q. A. (2004). New insights into atopic dermatitis. *J. Clin. Invest.* 113 (5), 651–657. doi:10.1172/jci21060

Lin, T.-K., Zhong, L., and Santiago, J. L. (2018). Anti-inflammatory and skin barrier repair effects of topical application of some plant oils. *Int. J. Mol. Sci.* 19 (1), 70. doi:10.3390/ijms19010070

Linnamaa, P., Savolainen, J., Koulu, L., Tuomasjukka, S., Kallio, H., Yang, B., et al. (2010). Blackcurrant seed oil for prevention of atopic dermatitis in newborns: a randomized, double-blind, placebo-controlled trial. *Clin. Exp. Allergy* 40 (8), 1247–1255. doi:10.1111/j.1365-2222.2010.03540.x

Luo, J.-L., Li, Y., Zhai, Y.-M., Liu, Y., Zeng, J.-X., Wang, D., et al. (2022). D-Mannose ameliorates DNCB-induced atopic dermatitis in mice and TNF-α-induced inflammation in human keratinocytes via mTOR/NF-κB pathway. *Int. Immunopharmacol.* 113, 109378. doi:10.1016/j.intimp.2022.109378

Morris, G. M., Huey, R., Lindstrom, W., Sanner, M. F., Belew, R. K., Goodsell, D. S., et al. (2009). AutoDock4 and AutoDockTools4: automated docking with selective receptor flexibility. *J. Comput. Chem.* 30 (16), 2785–2791. doi:10.1002/jcc.21256

O'Boyle, N. M., Banck, M., James, C. A., Morley, C., Vandermeersch, T., and Hutchison, G. R. (2011). Open Babel: an open chemical toolbox. *J. Cheminformatics* 3 (1), 1–14. doi:10.1186/1758-2946-3-33

Olejnik, A., Gornowicz-Porowska, J., Jenerowicz, D., Polańska, A., Dobrzyńska, M., Przysławski, J., et al. (2023). Fatty acids profile and the relevance of membranes as the target of nutrition-based strategies in atopic dermatitis: a narrative review. *Nutrients* 15 (17), 3857. doi:10.3390/nu15173857

Poljšak, N., and Kočevar Glavač, N. (2022). Vegetable butters and oils as therapeutically and cosmetically active ingredients for dermal use: a review of clinical studies. *Front. Pharm.* 13, 868461. doi:10.3389/fphar.2022.868461

Shityakov, S., and Förster, C. (2014). *In silico* predictive model to determine vector-mediated transport properties for the blood–brain barrier choline transporter. *Adv. Appl. Bioinforma. Chem.* 7 (null), 23–36. doi:10.2147/AABC.S63749

Simon, D., Eng, P. A., Borelli, S., Kagi, R., Zimmermann, C., Zahner, C., et al. (2014). Gamma-linolenic acid levels correlate with clinical efficacy of evening primrose oil in patients with atopic dermatitis. *Adv. Ther.* 31 (2), 180–188. doi:10.1007/s12325-014-0093-0

Son, S. E., Park, S. J., Koh, J. M., and Im, D. S. (2020). Free fatty acid receptor 4 (FFA4) activation ameliorates 2,4-dinitrochlorobenzene-induced atopic dermatitis by increasing regulatory T cells in mice. *Acta Pharmacol. Sin.* 41 (10), 1337–1347. doi:10.1038/s41401-020-0435-1

Suaini, N. H. A., Tan, C. P. T., Loo, E. X. L., and Tham, E. H. (2021). Global differences in atopic dermatitis. *Pediatr. Allergy Immunol.* 32 (1), 23–33. doi:10.1111/pai.13335

Venter, C., Meyer, R. W., Nwaru, B. I., Roduit, C., Untersmayr, E., Adel-Patient, K., et al. (2019). EAACI position paper: influence of dietary fatty acids on asthma, food allergy, and atopic dermatitis. *Allergy* 74, 1429–1444. doi:10.1111/all.13764

Wang, L., Xian, Y.-F., Hu, Z., Loo, S. K. F., Ip, S. P., Chan, W. Y., et al. (2021). Efficacy and action mechanisms of a Chinese herbal formula on experimental models of atopic dermatitis. *J. Ethnopharmacol.* 274, 114021. doi:10.1016/j.jep.2021.114021

Wollenberg, A., Thomsen, S. F., Lacour, J.-P., Jaumont, X., and Lazarewicz, S. (2021). Targeting immunoglobulin E in atopic dermatitis: a review of the existing evidence. *World Allergy Organ. J.* 14 (3), 100519. doi:10.1016/j.waojou.2021.100519

Yang, C.-Y., Liu, X.-M., Chen, Z.-Y., Lin, Y.-S., and Wang, S.-Y. (2016). Comparison of oil content and fatty acid profile of ten new *Camellia oleifera* cultivars. *J. Lipids* 2016, 3982486. doi:10.1155/2016/3982486

Zhang, F., Zhu, F., Chen, B.-L., Su, E.-Z., Chen, Y.-Z., and Cao, F.-L. (2022a). Composition, bioactive substances, extraction technologies and the influences on characteristics of *Camellia oleifera* oil: a review. *Food Res. Int.* 156, 111159. doi:10.1016/j.foodres.2022.111159

Zhang, T., Qiu, F.-C., Chen, L., Liu, R.-J., Chang, M., and Wang, X.-G. (2021). Identification and *in vitro* anti-inflammatory activity of different forms of phenolic compounds in *Camellia oleifera* oil. *Food Chem.* 344, 128660. doi:10.1016/j.foodchem.2020.128660

Zhang, X.-L., Ma, H.-L., Quaisie, J., Gu, C., Guo, L.-N., Liu, D.-D., et al. (2022b). Tea saponin extracted from seed pomace of *Camellia oleifera* Abel ameliorates DNCB-induced atopic dermatitis-like symptoms in BALB/c mice. *J. Func. Foods* 91, 105001. doi:10.1016/j.jff.2022.105001

Zhang, Y., Zhao, W., Liao, J., Zhang, Y., Wang, L., Li, P., et al. (2024). Evaluation of the therapeutic effect of Sacha inchi oil in atopic dermatitis mice. *Int. Immunopharmacol.* 138, 112552. doi:10.1016/j.intimp.2024.112552

Zhou, L.-J., Peng, Y.-L., Xu, Z., Chen, J.-Y., Zhang, N.-B., Liang, T., et al. (2024). The antioxidant, anti-inflammatory and moisturizing effects of *Camellia oleifera* oil and its potential applications. *Molecules* 29 (8), 1864. doi:10.3390/molecules29081864

frontiers | Frontiers in Pharmacology

TYPE Original Research
PUBLISHED 23 December 2024
DOI 10.3389/fphar.2024.1481273

OPEN ACCESS

EDITED BY
Xianyu Li,
China Academy of Chinese Medical Sciences, China

REVIEWED BY
Juan Wang,
Guilin Medical University, China
Wei-Ting Kuo,
National Taiwan University, Taiwan

*CORRESPONDENCE
Yingtian Jia,
shimutianhero@126.com
Tao Yang,
yangtao901212@163.com

†These authors have contributed equally to this work and share first authorship

RECEIVED 15 August 2024
ACCEPTED 02 December 2024
PUBLISHED 23 December 2024

CITATION
Tan T, Chen Q, Chen P, Li S, Hu W, Yang T and Jia Y (2024) Zhili decoction ameliorates ulcerative colitis by modulating gut microbiota and related metabolite, and inhibiting the TLR4/NF-κB/NLRP3 pathway.
Front. Pharmacol. 15:1481273.
doi: 10.3389/fphar.2024.1481273

Zhili decoction ameliorates ulcerative colitis by modulating gut microbiota and related metabolite, and inhibiting the TLR4/NF-κB/NLRP3 pathway

Tianying Tan[1†], Qin Chen[2†], Ping Chen[3], Shuangshuang Li[1,4], Wenting Hu[1,5], Tao Yang[5*] and Yingtian Jia[4*]

[1]College of Clinical Medicine, Guizhou University of Traditional Chinese Medicine, Guiyang, China, [2]Department of Anorectal, Kunming Municipal Hospital of Traditional Chinese Medicine, The Third Affiliated Hospital of Yunnan University of Chinese Medicine, Kunming, China, [3]Colorectal and Anal Surgery, Chongqing Jiangbei District Hospital of Traditional Chinese Medicine, Chongqing, China, [4]Colorectal and Anal Surgery, The Affiliated Traditional Chinese Medicine Hospital of Southwest Medical University, Luzhou, China, [5]Colorectal and Anal Surgery, The First Affiliated Hospital of Guizhou University of Traditional Chinese Medicine, Guiyang, China

Ethnopharmacological Importance: Zhili decoction (ZLD) is a traditional Chinese medicine prescription for ulcerative colitis (UC). However, the mechanism by which ZLD exerts its therapeutic effects in the context of UC remains unclear.

Aim of study: The aim of this study was to investigate the effects of ZLD on the gut microbiota and related fecal metabolite levels using a mouse model of UC. In addition, we examined the underlying molecular mechanisms responsible for these effects.

Materials and methods: The major components of ZLD were detected by ultra-performance liquid chromatography-mass spectrometry (UPLC-MS). An integrated approach employing 16S rRNA and fecal metabolomics was employed to assess the potential impacts of ZLD on gut flora abundance and diversity, fecal metabolite levels, and various metabolic pathways. To further investigate the potential mechanisms of ZLD in treating UC, the expression of genes and proteins were examined by RT-qPCR, immunohistochemical staining and Western blotting.

Results: ZLD markedly alleviated symptoms and inflammatory injury in mice with UC. DSS induced notable alterations in the gut microbiome, and ZLD enhanced gut microbial diversity in UC mice by augmenting the abundance of Bacteroidota, Christensenella, *Lactobacillus*, etc., while reducing the *Firmicutes*/*Bacteroidota* ratio. ZLD treatment significantly modified the metabolic profile of mice with UC. It significantly suppressed the arachidonic acid metabolic pathway and promoted the butyrate acid metabolic pathway. ZLD reduced inflammatory factors and inhibited TLR4/NF-κB/NLRP3 pathway expression. In addition, correlation analysis demonstrated a close relationship between gut microbes, fecal metabolites, and inflammatory factors.

Conclusion: ZLD alleviated UC by regulating gut flora, modulating related metabolite levels, and inhibiting TLR4/NF-κB/NLRP3 pathway.

KEYWORDS

ulcerative colitis, Zhili decoction, gut microbiome, metabolism, TLR4/NF-κB/NLRP3 pathway

1 Introduction

Ulcerative colitis (UC) is persistent inflammation that extends from the mucosal end of the rectum toward the colonic end, often progressing over time (Eisenstein, 2018; Ng et al., 2017). Symptoms include bloody diarrhea, pus, and abdominal pain. The global incidence of UC is on the rise, particularly among younger individuals, possibly due to lifestyle and dietary changes, as well as environmental factors (Molodecky et al., 2012). This increasing prevalence makes UC a major global public health concern,

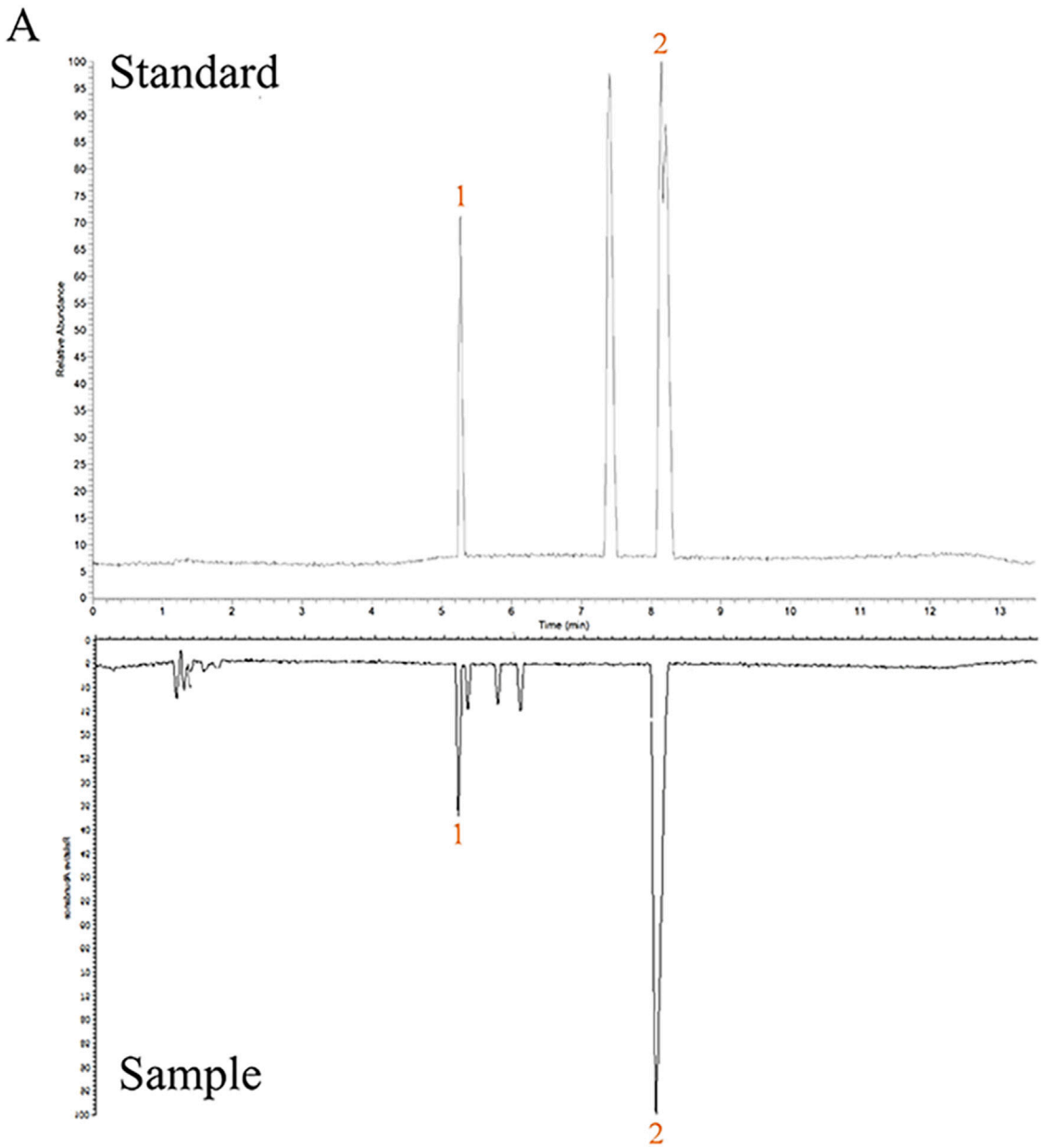

FIGURE 1
(Continued).

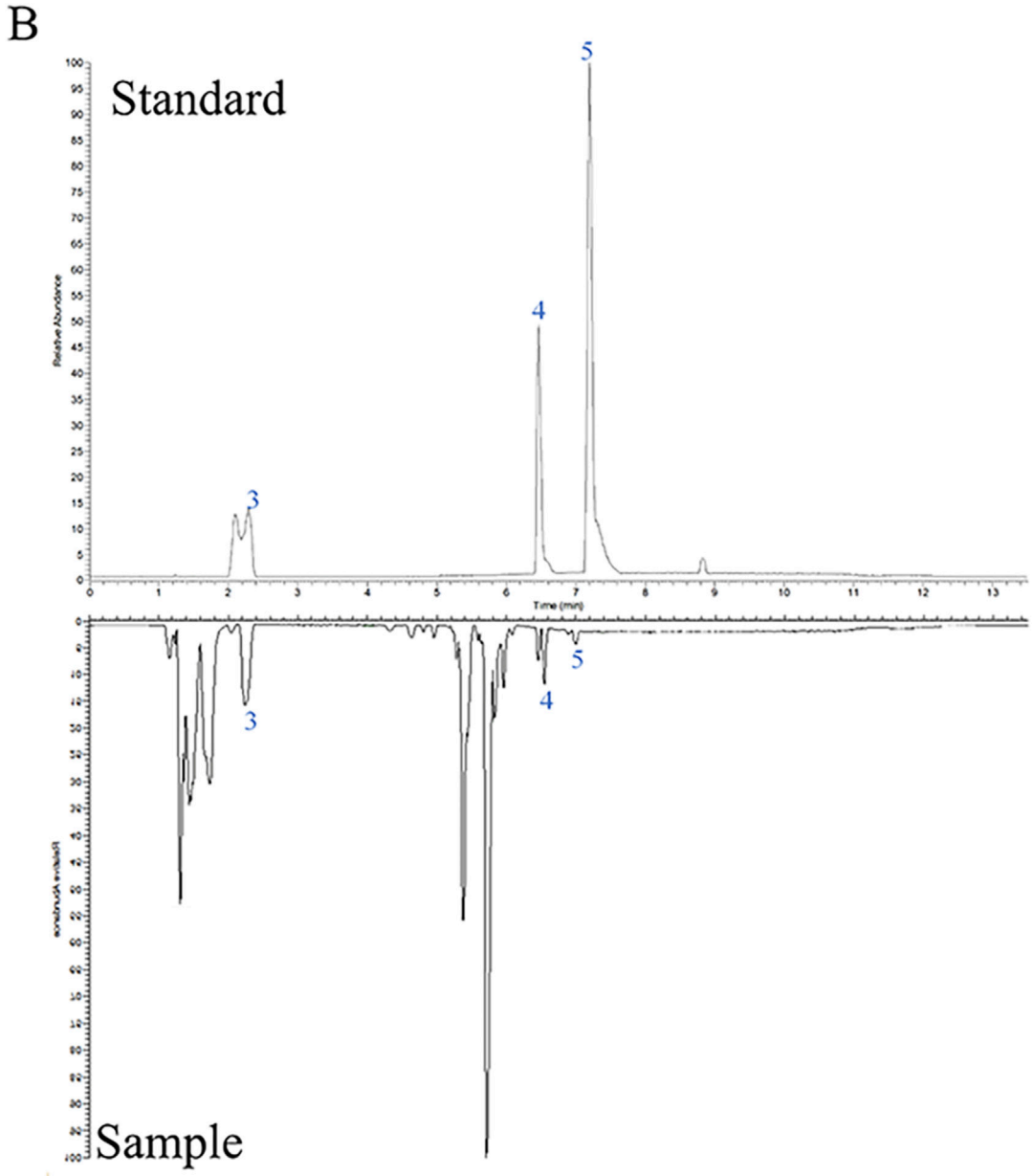

FIGURE 1
(Continued). Chemical analysis of ZLD extract under positive **(A)** and negative **(B)** modes. 1, phellodendrine; 2, berberine; 3, gallic acid; 4, quercetin; 5, galangin.

impacting the wellbeing of individuals worldwide. While current treatment options like anti-inflammatory medications and anti-tumor necrosis factor (TNF) targeted therapies can be used to manage moderate to severe symptoms (Nakase et al., 2021; Salice et al., 2019), they often induce severe adverse effects, including liver and kidney impairment or an increased risk of infections (Ford and Peyrin-Biroulet, 2013; Luthra et al., 2015). Thus, advancing safe and economical therapeutic approaches for UC remains a critical priority in medical research.

The intestinal microbiota constitutes a pivotal element of the intestinal barrier, influencing various physiological functions. It facilitates nutrient absorption and metabolism, and regulates the immune system (Round and Mazmanian, 2009). Beneficial microbiota actively counteract potential pathogens, preserving mucosal integrity and immune homeostasis (Honda and Littman, 2016; Mu et al., 2017). Nevertheless, research indicates a close association between intestinal microbiota and UC development (Frank et al., 2007). Patients with UC exhibit reduced microbial diversity, with a decline in beneficial species and an increase in harmful microorganisms (Ni et al., 2017). This imbalance affects related-metabolite production, decreasing the levels of short-chain fatty acids (SCFAs) (Parada Venegas et al., 2019). SCFAs, encompassing acetic, propionic, and butyrate acids, represent metabolic byproducts of beneficial bacteria generated through the intestinal fermentation of dietary fiber. They exhibit anti-inflammatory and antioxidant effects by activating G protein-

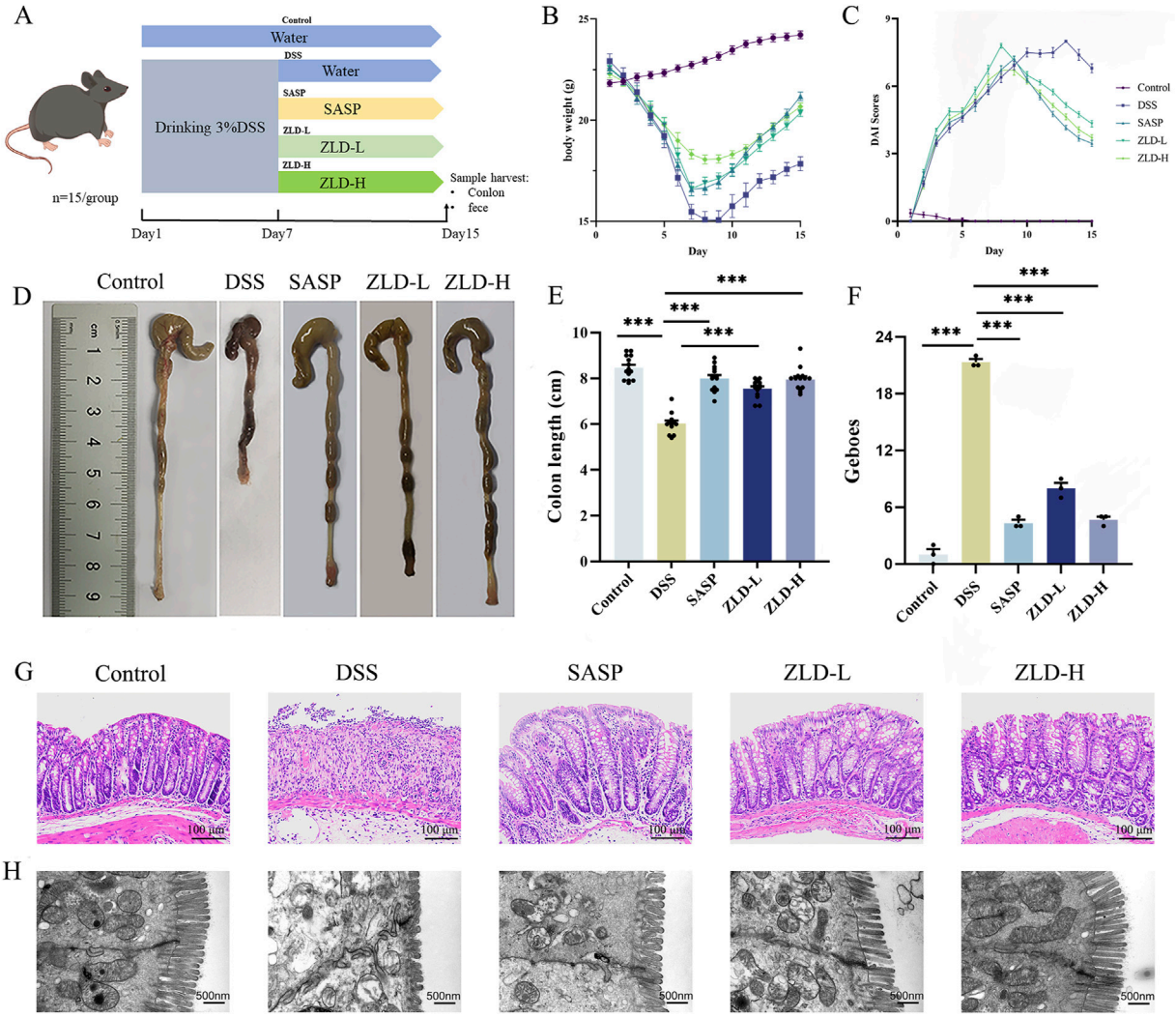

FIGURE 2
(A) Schematics of the experimental design. **(B, C)** Changes in body weight and DAI for mice. **(D, E)** Colon length measurements and comparisons across different groups. **(F, G)** Histopathologic picture of mouse colon and histological scores of colonic tissues (magnification × 200). **(H)** Representative images of colon tissues obtained using transmission electron microscopy (scale bars = 500 nm). ZLD-L: low dose ZLD; ZLD-H: high dose ZLD; all groups: n = 15; $^{*}p < 0.05$, $^{**}p < 0.01$, $^{***}p < 0.001$, $^{ns}p > 0.05$.

coupled receptors on colonic epithelial cells, inhibiting the level of pro-inflammatory factors, and controlling immune responses. This promotes the intestinal mucosal barrier to repair and maintain its integrity (Morrison and Preston, 2016). Thus, disruptions in microbial communities alter metabolite levels, affecting host metabolism and triggering UC(Zhou et al., 2020). Targeting gut flora alterations may provide an avenue for UC management.

Zhili Decoction (ZLD) is a traditional compound formula documented in the Color Atlas of Hmong Medicines in Traditional Chinese Medicine, comprising *Acalypha australis* L. (AAL) (known as Tie Xian Cai in Chinese) and *Phellodendron chinense* var. *glabriusculum C.K. Schneid.* (Huang Pi Shu or Chuan Huang Bai in Chinese), is a traditional remedy known for treating diarrhea and dysentery. AAL exhibits anti-inflammatory properties and promotes apoptosis (Kim et al., 2020). It has been used to treat dysentery and diarrhea. Additionally, AAL reduces the production of interleukin (IL)-6 and tumor necrosis factor (TNF)-α by inhibiting the activation of NF-κB (Chen et al., 2023). In contrast, Phellodendron chinense var. glabriusculum C.K. Schneid. has anti-inflammatory, analgesic, and uric acid-lowering properties, and helps regulate intestinal flora (Chan et al., 2008; Chen et al., 2010). Both herbal components demonstrate therapeutic effects on ulcerative colitis (UC) by reducing nitric oxide (NO), IL-1, and IL-1β levels (Park et al., 2007). However, its underlying mechanism of action against UC remains unclear. This study aims to explore the efficacy and potential mechanisms of ZLD in UC.

2 Materials and methods

2.1 Reagents

The details regarding the reagents utilized in this investigation can be found in Supplementary Table S1.

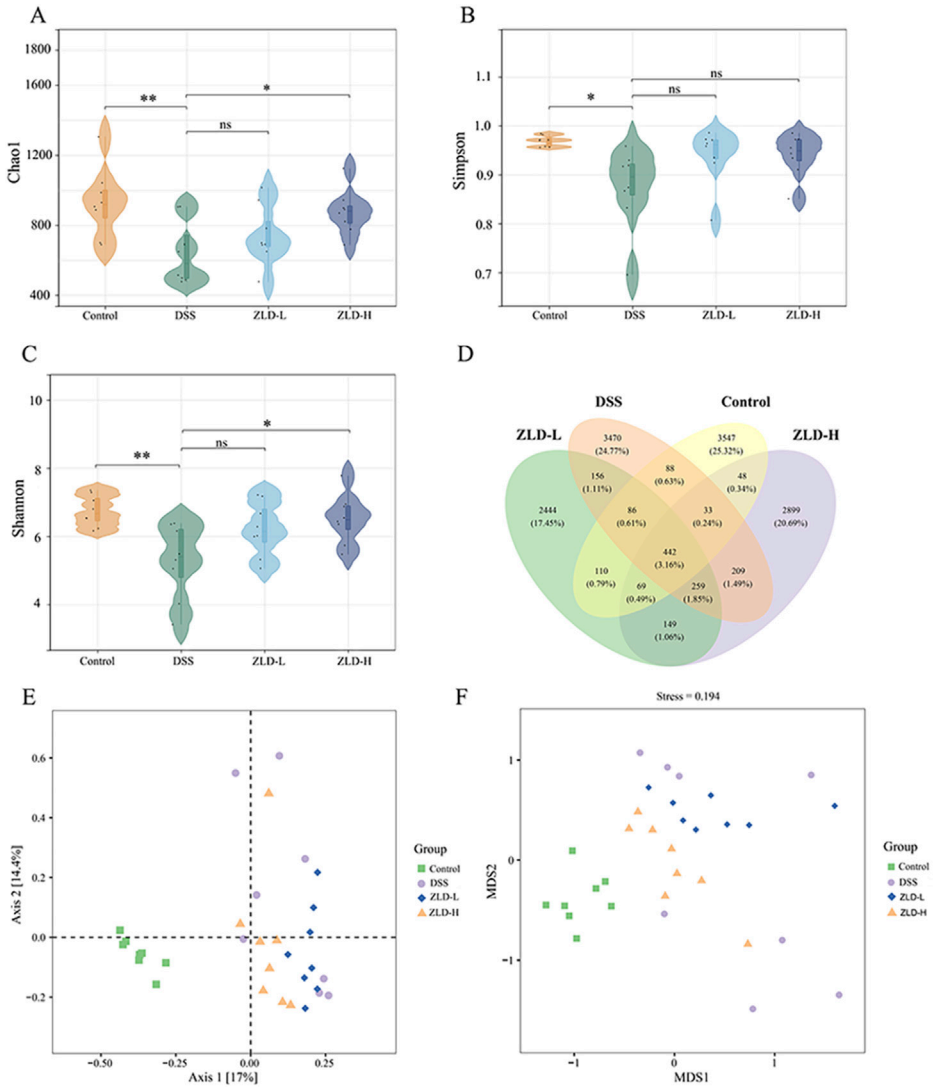

FIGURE 3
Gut microbiome diversity (n = 8 per group). α diversity compared by Chao1 **(A)** Simpson **(B)** and Shannon **(C)** index. **(D)** Venn plot of the out numbers in each group; **(E)** PCoA plots; **(F)** NMDS plots; *$p < 0.05$, *$p < 0.01$, ***$p < 0.001$, ^{ns} $p > 0.05$.

2.2 Preparation of ZLD

The fresh bark of *Phellodendron chinense* var. *glabriusculum C.K.Schneid.* and *Acalypha australis* L. (Dechangxiang, Guizhou) was crushed and blended in a 1:1 ratio. Subsequently, 1000 g of ZLD was soaked in 10 L of water for 1 h, refluxed at 100°C for 2 h, filtered and extracted with 8000 mL of water at the same temperature for another 1.5 h. The resulting filtrates were combined, condensed, and subjected to vacuum freeze-drying to yield a powdered extract. Finally, a 58.2g ZLD was obtained for the follow-up experiment.

2.3 ZLD chemical analysis

0.5g ZLD powder was dissolved with 10 mL distilled water and extracted with 50% methanol. After vibration and centrifugation at 12,000 rpm for 30 min, the supernatant was transferred and evaporated to dryness at a temperature under vacuum. The residue was dissolved in 1 mL of ddH2O and centrifugated at 12,000 rpm for 15 min twice prior to analysis. The standard substances were dissolved in methanol. The chemical analyses were performed using Thermo Fisher Q Exactive coupled with a Vanquish UPLC system. The mobile phase in positive mode included H2O with 0.1% FA (A) and methanol (B). The gradient conditions included: 0–2 min at 10% B; 2–3 min at 10%–35% B; 3–10 min at 35%–45% B; 10–11 min at 45%–90% B; 11–12 min at 90% B; and 12–12.5 min at 90%–10% B. The mobile phase also consisted of 0.1% FA (C) and methanol (D) under negative mode. The negative mode gradient conditions are: 0–2 min at 10% D; 2–3 min at 10%–35% D; 3–5 min at 35%–90% D; 5–7 min at 90%–95% D; 7–9 min at 95% D; 9–11 min at 95%–10% D. The experimental conditions included a flow rate of

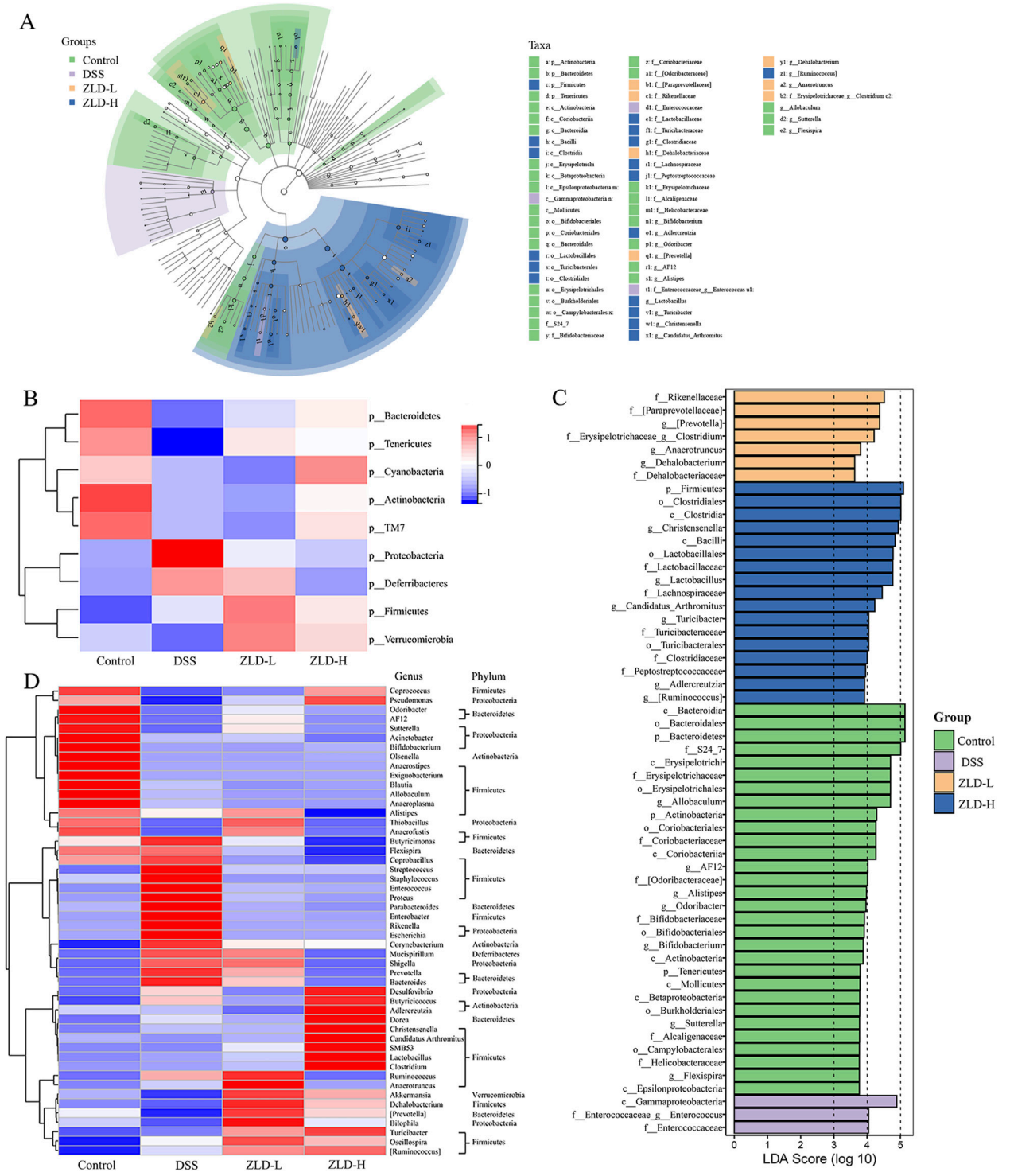

FIGURE 4
Gut microbiome composition (n = 8 per group). **(A)** Cladogramrepresenting the results of LEfSe analysis. **(B)** Heatmap of the different fecal microbiota in each group at the phylum level. Different colors indicate different metabolite expressions. **(C)** LDA scores; **(D)** The heatmap illustrates the 50 distinct genera of fecal microbiota. Different colors indicate different metabolite levels.

200 μL/min and a constant temperature of 40°C. The mass conditions were: spray voltage: +3.4KV/-3 KV; sheath gas pressure: 40 arb; aux gas pressure: 10 arb; capillary temp: 300°C; heater temp: 320°C.

2.4 Animals and ethical approval

Eight-week-old specific pathogen-free (SPF) C57BL/6J mice, weighing 20 ± 2 g, were obtained from Beijing

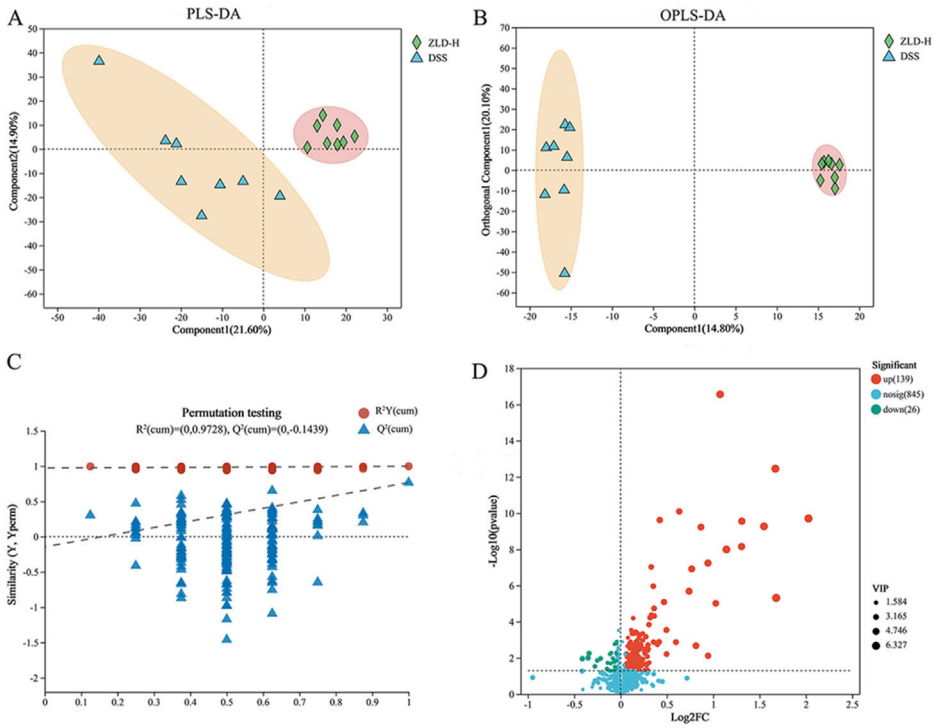

FIGURE 5
Metabolite differences between the dextran sulfate sodium and Zhili decoction high-dose treated groups in a positive model. **(A)** PLS-DA; **(B)** OPLS-DA; **(C)** OPLS-DA permutation test; **(D)** Volcano plots.

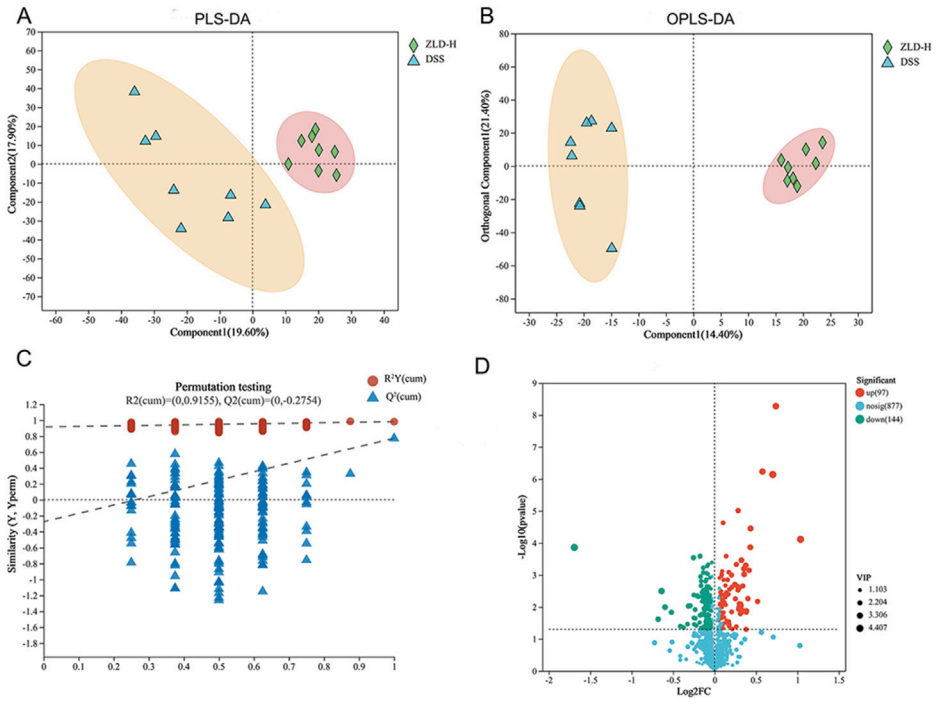

FIGURE 6
Analysis of metabolites showed differences between DSS and high-dose ZLD groups in the negative mode. **(A)** PLS-DA; **(B)** OPLS-DA; **(C)** OPLS-DA permutation test. **(D)** Volcano plots.

10.3389/fphar.2024.1481273

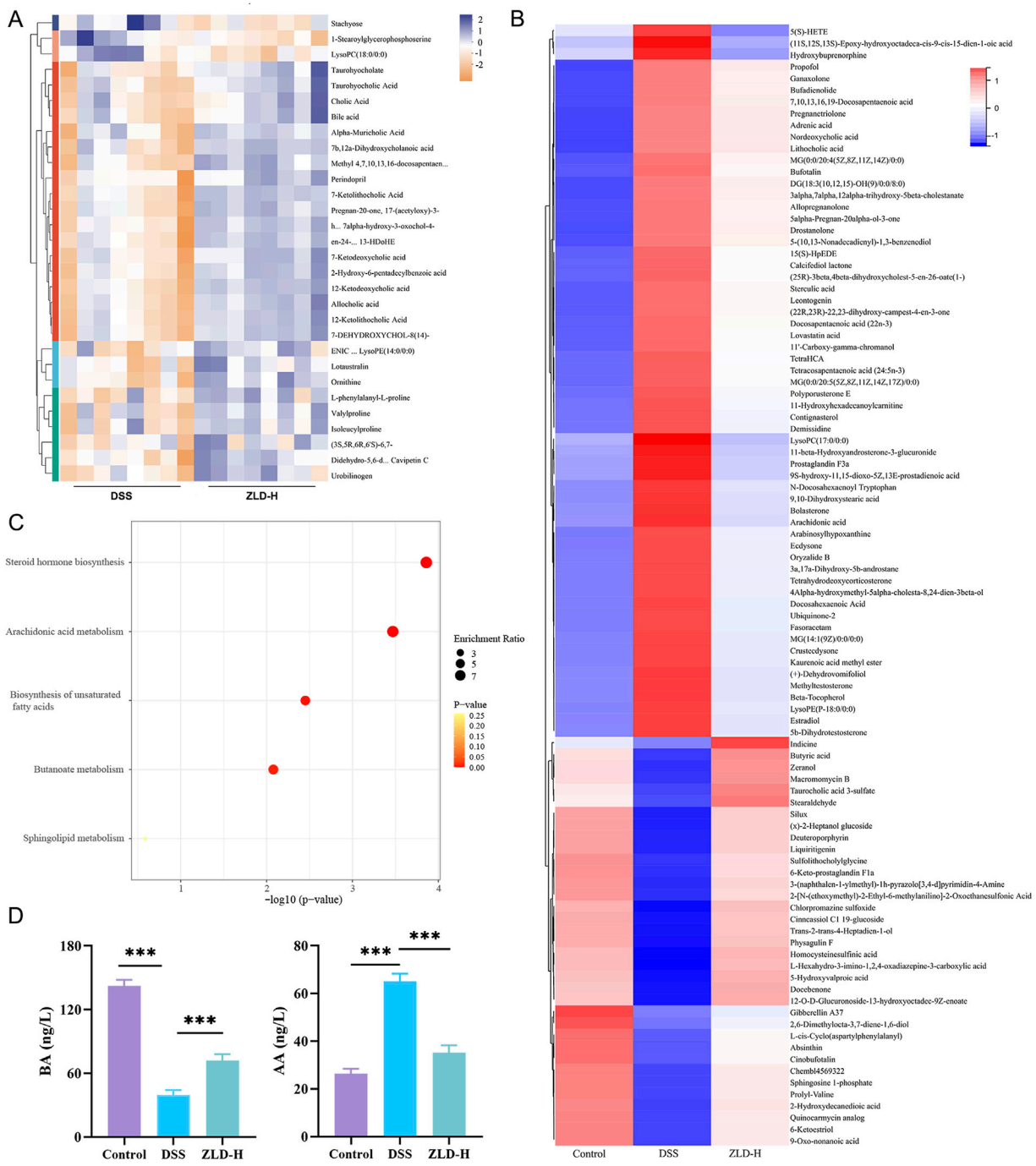

FIGURE 7
Fecal metabolite composition (n = 8 per group). **(A)** Heatmap displaying the top 30 fecal metabolites differently expressed between the DSS and ZLD-H groups in the positive ion mode. Different colors indicate different metabolite expressions; **(B)** Heatmap analysis depicting the relative levels of 96 potential biomarkers through cluster analysis; **(C)** Metabolic pathway analysis; **(D)** Expression of butyrate acid and arachidonic acid.

Huafukang Animal Breeding Center (License No. SCXK-[jing]-2019–0008). Mice were adapted and fed for 1 week, and experimental phase keeping was performed under standard laboratory conditions. The experimental procedures received approval from Guizhou University of Traditional Chinese Medicine Animal Research Institute (approval number 20230047).

2.5 UC model and drug administration

UC induction with dextran sulfate sodium (DSS) was performed as previously reported. Mice were kept in a controlled space under SPF conditions and received sterile diet and water. Experimental mice were divided randomly into control, DSS, sulfasalazine (SASP), ZLD low-dose (ZLD-L), and ZLD high-dose (ZLD-H) groups (n = 15 per group).

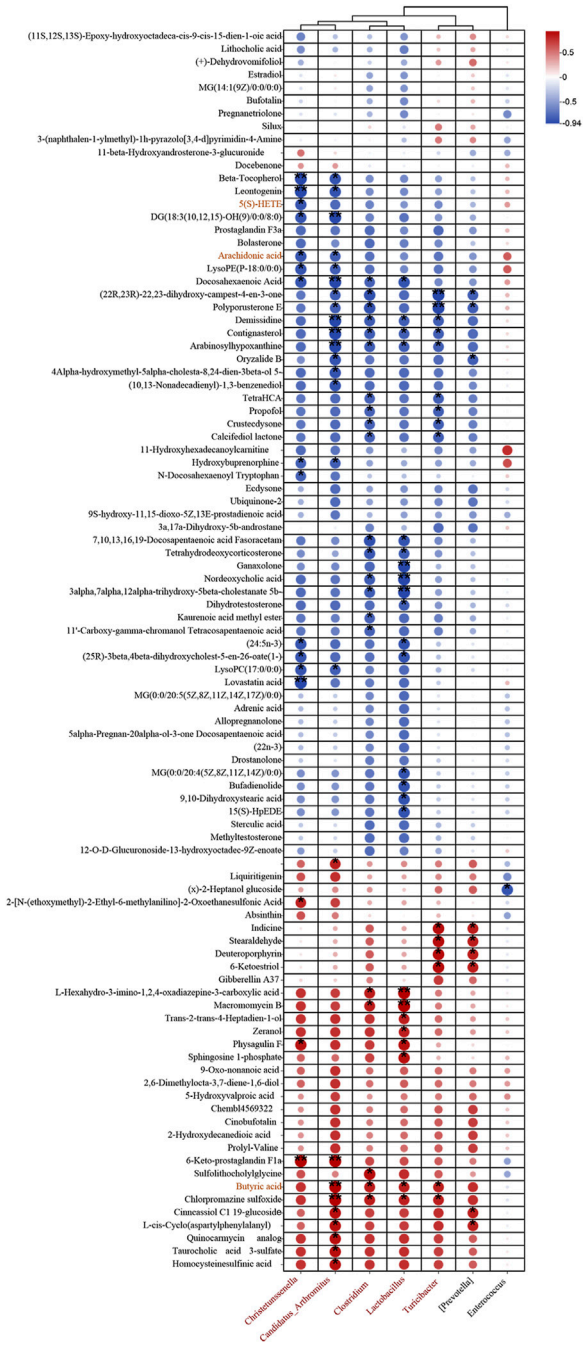

FIGURE 8
Association between markedly distinct gut microbiome (at genus) and significantly modified fecal metabolites. Fecal metabolites associated with major metabolic pathways are highlighted in red. (*p < 0.05, **p < 0.01, ***p < 0.001).

UC was induced in groups DSS, SASP, ZLD-L, and ZLD-H by administering 3% DSS (w/v) over a period of 7 consecutive days. Mice in the control group were provided with deionized drinking water for a period of 14 days. Following UC induction, the reference group mice were administered 125 mg/kg/d SASP. Mice in the ZLD-L and ZLD-H groups were fed 291.25 mg/kg/d and 873.75 mg/kg/d ZLD, respectively. SASP and ZLD were administered orally once daily for 7 days. All treated mice were euthanized on the 14th day.

The severity of the disease was assessed daily basis by monitoring body weight, dietary intake, fecal occult blood, and consistency of stool. The Disease Activity Index (DAI) was computed based on established criteria (Li et al., 2021) (Supplementary Table S2). DAI scores were calculated by summing the weight change, defecation, and occult blood scores, and then dividing it by three. On day 13, fresh feces were harvested from each mouse and frozen at −80°C in sterile EP tubes. The following day, colon tissues were obtained also stored at −80°C.

2.6 Histopathologic analysis

Colon tissues from the mice were fixed in a 4% paraformaldehyde solution, then embedded in paraffin and subsequently sectioned at a thickness of 5 μM. The sections were processed for hematoxylin and eosin (HE) staining, followed by visualization and photography under a light microscope (Nikon Fi3, Japan). Pathological scoring of colonic injury was conducted using the Geboes score (Supplementary Table S3) (Shi et al., 2017).

2.7 Staining by transmission electron microscopy (TEM)

Colon tissues (<1 mm^3) were fixed in 2.5% glutaraldehyde and phosphate buffer solution. Following fixation, gradual dehydration was performed using progressive ethanol concentrations. After embedding and solidification, sections of 70 nm were cut using an ultramicrotome (Leica UC7). These sections were stained with electron microscopy dyes to enhance contrast for cellular organelles and structures. Subsequently, the samples were observed for their ultrastructure using 80 kV transmission electron microscopy (HT7800/HT7700), and images were captured.

2.8 ELISA assay

Add 10 mg of tissue to 500 μL of extract (containing protease inhibitor and Ripa lysate) and homogenize using a homogenizer. The homogenate was subjected to centrifugation at a speed of 12,000 revolutions per minute for a duration of 10 min at a temperature of 4°C. Following this, the supernatant was carefully extracted for use in the ELISA assay. Pro-inflammatory cytokine levels, including TNF-α, IL-6, IL-1β, and IL-18, were assessed using an ELISA kit (Sevier, China) as per the manufacturer's guidelines.

Fecal samples were selected and subjected to three freeze-thaw cycles at −20°C. They were then filtered and extracted using a butanol: methanol: water (5:25:70, v/v/v) solution. The specific metabolites were quantified following the instructions provided with the ELISA kits.

2.9 Immunohistochemical (IHC) assay

Paraffin sections of colon tissue were stained using rabbit polyclonal antibodies against Toll-like receptor 4 (TLR4, dilution 1:400) and NLR family pyrin domain containing 3 (NLRP3, dilution

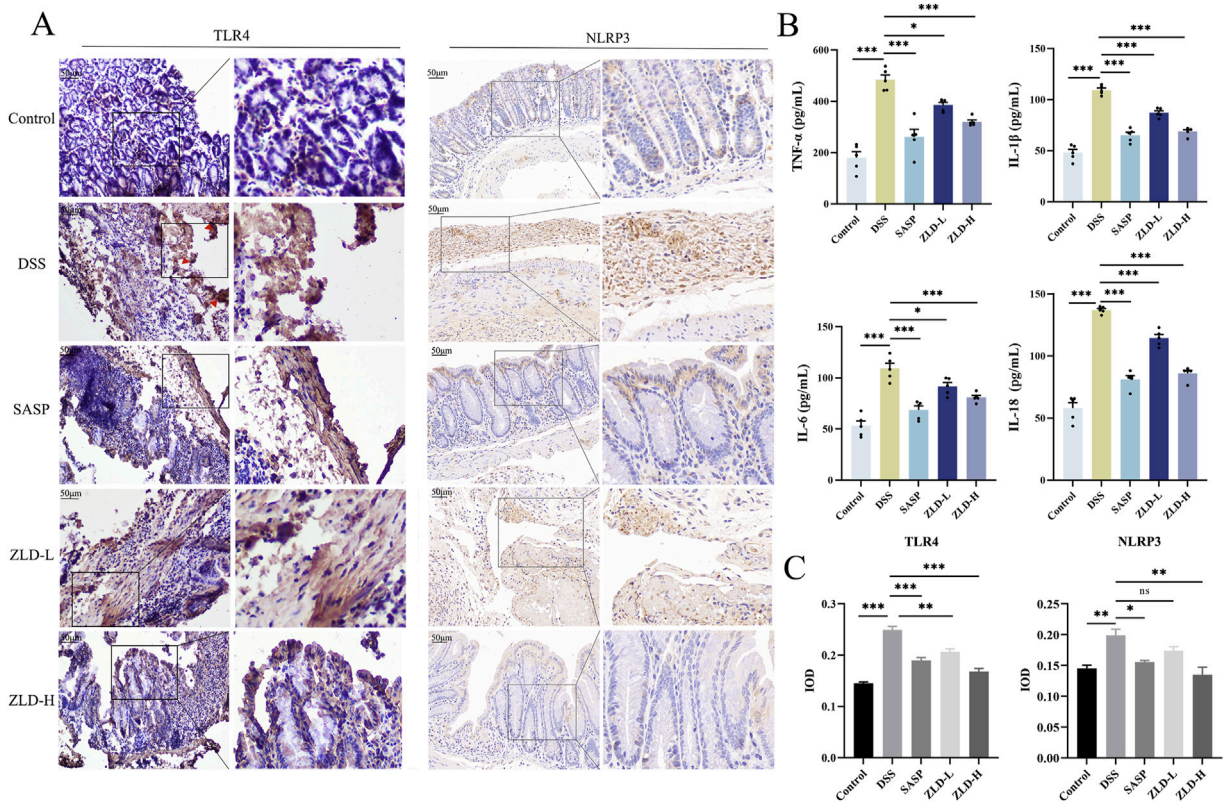

FIGURE 9
Expression of inflammatory factors, TLR4, NLRP3 in colonic tissues. **(A, C)** TLR4 and NLRP3 protein levels for colon tissues (scale bars = 500 μm); **(B)** TNF-α, IL-1β, IL-6, IL-8 levels of colon tissues; $^{*}p < 0.05$, $^{**}p < 0.01$, $^{***}p < 0.001$, $^{ns}p > 0.05$.

1:50), along with polyclonal anti-rat IgG (1:200) antibodies. Section images were taken with NIS Elements Imaging Software Version 4.0.

2.10 Real-time quantitative (RT-q) PCR analysis

Total RNA was extracted using the Tissue RNA Purification kit (EZBioscience, China), following the manufacturer's guidelines. Quantify RNA using the kit (refer to Supplementary Table S1 for details). RT-qPCR analysis was conducted using the CFX96 Real-Time System (BIO-RAD, United States). Supplementary Table S4 contains the primer sequences used in this study.

2.11 Western blotting (WB) analysis

FastPrep-24TM5G (MP Biomedicals, United States) for extraction of total proteins from PBS-washed colon tissues. The specific experimental procedures of the Western blot have been cited in previous studies (Yang et al., 2024). Used the following antibodies at the indicated dilutions: β-actin (dilution 1:100,000), NF-κB (dilution 1:1,000), Phospho-inhibitor of NF-κB alpha (p-IKBα, dilution 1:1,000), cleaved caspase-1 (dilution 1:3,000), apoptosis-associated speck-like protein containing a CARD (ASC; dilution 1: 1,000), NLRP3 (dilution 1:500), and HRP-conjugated (dilution 1: 10,000). Bands were visualized and quantified utilizing the ChemiDocTM Imaging System (BIO-RAD, United States) and Image Lab software.

2.12 16S rRNA sequencing analysis for intestinal flora

Genomic DNA of feces collected from control, DSS, ZLD-L, and ZLD-H groups was extracted using the DNA kit (Omega Bio-Tek, China) according to the instructions. The V3-V4 hypervariable regions of the bacterial 16S rRNA gene were amplified from genomic DNA using specific primers (338F 5′-ACTCCTACGGGAGGCAGCA-3′ and 806R 5′-GGACTACHVGGGTWTCTAAT-3′). Samples were individually labeled with unique barcodes during PCR amplification, utilizing Tks Gflex DNA Polymerase. The quantity and quality of the amplified products were assessed with the gel electrophoresis. Following this, a purification of the PCR product was conducted using VAHTSTM DNA Clean Beads and AMPure XP Beads, respectively. The purified PCR products were characterized with the Quant-iT PicoGreen dsDNA Assay Kit. Libraries were constructed and sequenced using the MiSeq Reagent Kit v3 (Illumina, United States). Raw data were generated in FASTQ format. Microbiome biological information was analyzed using QIIME2 to obtain Operational Taxonomic Units (OTU). The

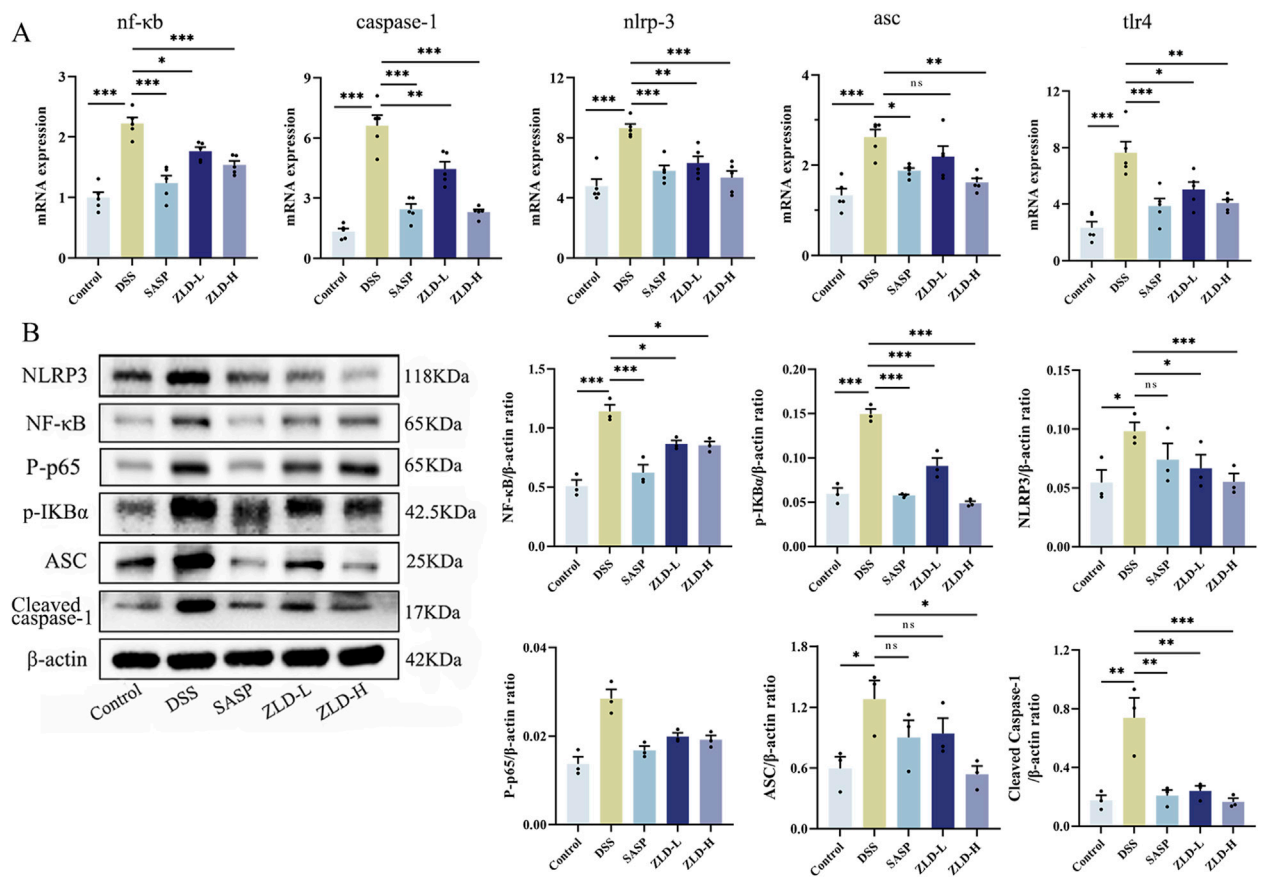

FIGURE 10
ZLD modulates inflammatory pathway **(A)** Effects on mRNA levels of nf-κb, caspase-1, nlpr3, asc and tlr4; **(B)** Effects on protein levels of p-IKBα, NF-κB p65, P-p65, cleaved caspase-1, NLRP3, and ASC; *$p < 0.05$, **$p < 0.01$, ***$p < 0.001$, ^{ns} $p > 0.05$).

index of Chao1, Shannon, and Simpson, as well as principal coordinates analysis (PCoA) and non-metric multidimensional scaling (NMDS) plots, were generated using R software and QIIME2 software. To detect taxonomic units that differ significantly between groups, we used the Least Discriminant Analysis Effect Size (LEfSe) method.

2.13 Fecal metabolomic data analysis

Referring to previous studies described (Lu et al., 2021), to implement the operation, metabolite extraction involved adding 50 mg of fecal sample to 400 μL of extraction solution (methanol: water = 4:1) containing 0.02 mg/mL of the internal standard (L-2-chlorophenylalanine) in an EP tube. The supernatant obtained after sample grinding was pipetted into an analytical vial. The UPLC-Q Exactive system (Thermo Fisher Scientific) with an HSS T3 column (100 mm × 2.1 mm, 1.8 μm) and Q Exactive mass spectrometry were used for detection. The mobile phases were composed of a solution of 0.1% formic acid in water and acetonitrile (95:5, v/v) (referred to as solvent A), as well as a solution of 0.1% formic acid in acetonitrile, isopropanol, and water (47.5:47.5:5, v/v) (referred to as solvent B) (Zhang et al., 2023). The automatic injector was set to 4°C and programmed to dispense a volume of 3 μL. Information Dependent Acquisition (IDA) controlled by Xcalibur software (Thermo-Fisher) was used to collect mass spectrometry data. The mass spectra were continuously assessed in positive and negative status for further analysis in the subsequent stage.

2.14 Statistical analysis

Data were subjected to analysis using GraphPad Prism 9.0 software. The student's test and one-way ANOVA were used, and all data were expressed as mean ± standard error of the mean (SEM). The co-occurrence among intestinal flora and metabolites was calculated based on the relative abundance by Spearman's rank correlation coefficient ($P< 0.05$) using R package Hmisc. Visualization of results was achieved using R 4.03. Differences were considered statistically significant for P-values < 0.05.

3 Results

3.1 Chemical analysis of ZLD extract

The chemical analysis showed that 108 compounds were contained in ZLD (Supplementary Table S5). Among them,

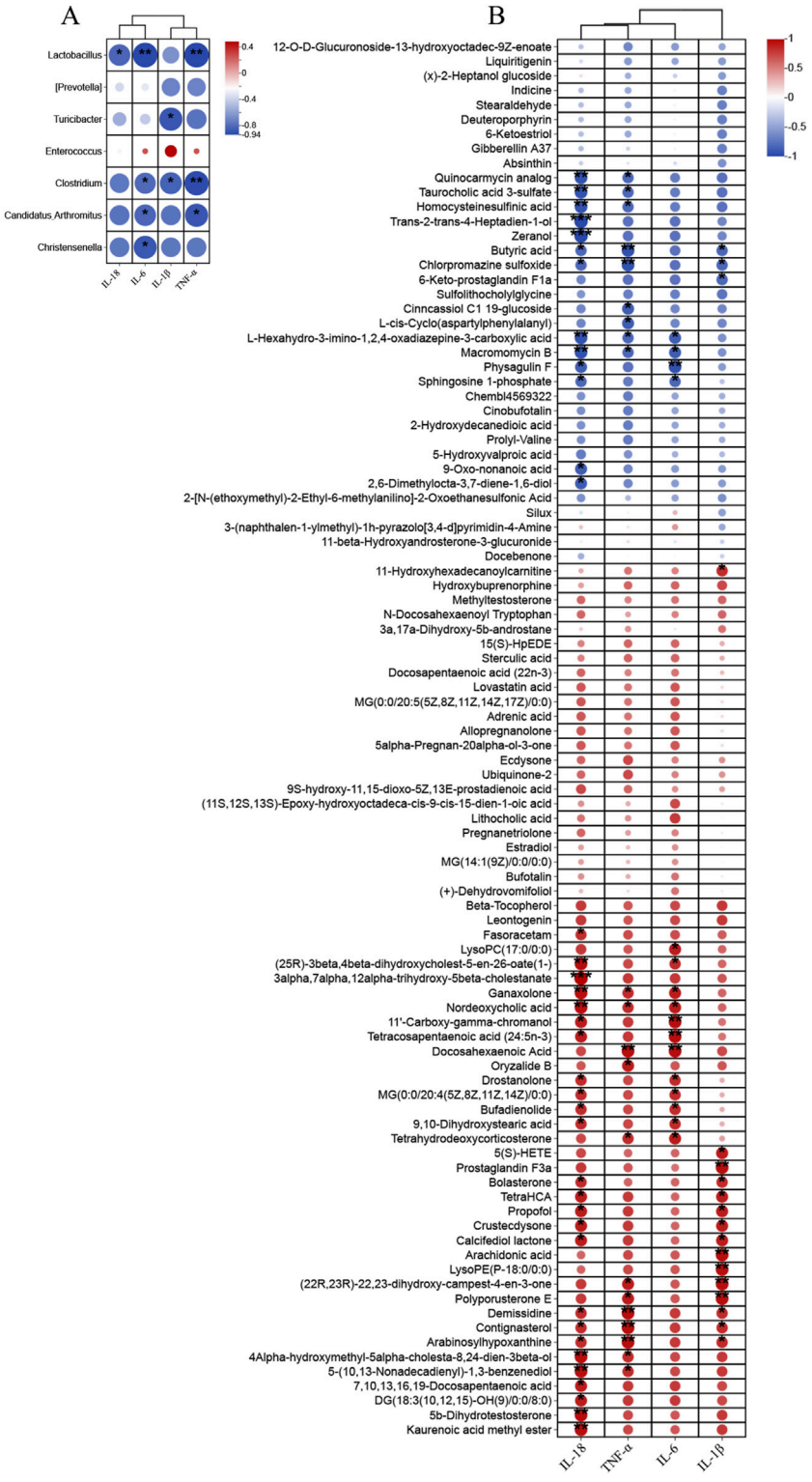

FIGURE 11
Correlation analysis was performed to examine **(A)** the relationship between differential gut microbiota (at the genus) and inflammatory factors, **(B)** the association between significantly altered fecal metabolites and inflammatory factors.

hellodendrine and berberine were identified under the positive mode, according to the standard substances (Figure 1A). The three chemicals in the ZLD extract were identified as gallic acid, quercetin, and galanin (Figure 1B).

3.2 The evolution of DSS-induced UC in mice

Protocol design is illustrated in Figure 2A. In contrast to the control mice, the DSS group exhibited a reduction in body weight

(Figure 2B), elevated DAI score (Figure 2C), and shortened colon length (Figures 2D, E). Histopathological examination revealed extensive inflammatory cell infiltration and ulceration in the colon mucosa of the DSS group compared with the other experimental groups, with significantly higher Geboes values (Figures 2F, G). Treatment with SASP, ZLD-L, and ZLD-H significantly ameliorated the pathological alterations of the colon tissue and reduced the Geboes values (Supplementary Table S3). In addition, TEM results showed that the intestinal barrier and tight junctions were disrupted in the DSS group (Figure 2H). Nevertheless, the ZLD-L and ZLD-H groups exhibited significantly improved intestinal barrier structures as compared to the model group, while the SASP group did not show a significant improvement.

3.3 ZLD altered the diversity and composition of the gut microbiome

Mouse fecal samples were subjected to high-throughput 16S rRNA sequencing in order to evaluate the impact of ZLD on gut flora. We utilized sparse curves, as well as α and β diversity indices, to assess the microbial species diversity present in the samples. These curves were relatively flat for each group (Supplementary Figure S1). A Venn diagram unveiled a combined total of 442 OTUs across the four groups, as illustrated in Figure 3D. To assess alpha diversity in the gut microbiota, Chao1, Simpson, and Shannon indices were utilized at the OTU level. Compared to other groups, the DSS group exhibited reduced.

Chao1, Simpson, and Shannon indices, indicating decreased microbiota richness and diversity (Figures 3A–C). Treatment with ZLD-L and ZLD-H significantly raised Chao1, Simpson, and Shannon indices values (Chao1 and Shannon: $P< 0.05$) versus the DSS group. However, differences in those three indices for the ZLD-L group and in the Simpson index for the ZLD-H were not significant. PCoA and NMDS were conducted to evaluate the β diversity across groups. Microbial community analysis using PCoA and NMDS revealed distinct clustering patterns between groups. The DSS group displayed a broader distribution than the control group, while the ZLD-L and ZLD-H groups demonstrated distributions similar to the control group (Figures 3E, F). Thus, ZLD could comprehensively elevate the α and β diversity of microbiota in mice with UC.

The gut microbiota in the DSS group was predominantly predominantly composed of the phylum level *Bacteroidota*, *Firmicutes*, and *Proteobacteria* (see Supplementary Figure S2). The relative abundance of *Bacteroidota* decreased, while that of *Firmicutes*, *Proteobacteria* increased in DSS group (Figure 4B). Additionally, the DSS group exhibited a higher *Firmicutes*/*Bacteroidota* (F/B) ratio was elevated in the DSS group than in the control group (Supplementary Figure S3). *Bacteroidota*, *Firmicutes*, *Proteobacteria,* and *Verrucomicrobia* were the main components of the intestinal flora in the ZLD-L and ZLD-H groups (Supplementary Figure S2).

Compared to the DSS group, the relative abundance of *Firmicutes* and *Bacteroidetes* increased in the ZLD-L and ZLD-H groups (Figure 4B). The F/B ratio decreased in the ZLD-H group and increased in the ZLD-L group compared to the DSS group (Supplementary Figure S3). However, neither difference was statistically significant. Additionally, ZLD treatment elevated the abundance of *Verrucomicrobia* and depressed *Proteobacteria*. The taxonomic composition by group at various levels is illustrated in Supplementary Figures S4–7 to provide further elucidation.

Lactobacillus, *Akkermansia*, and *Prevotella* were the predominant genera in all four groups, as illustrated in Figure 4A. LEfSe analysis was conducted to determine distinctive bacteria across the groups. In contrast to the DSS group, at the genus level, the ZLD-H exhibited an enhanced relative abundance of *Coprococcus*, [*Prevotella*], *Clostridium*, *Christensenella*, *Lactobacillus*, *Candidatus_Arthromitus*, *Turicibacter*, and degraded relative abundance of 13 other microorganisms, including *Prevotella*, *Enterococcus, Bacteroides*, *Parabacteroides*, *Ruminococcus*, *Enterococcus*, *Streptococcus*, *Staphylococcus*, *Proteus*, *Enterobacter*, *Shigella*, *Rikenella*, *Escherichia*, and *Mucispirillum*. The relative abundance of *Turicibacter* and *Anaerofustis* was elevated, yet that of *Streptococcus*, *Staphylococcus*, *Enterococcus*, *Proteus*, *Enterobacter*, *Parabacteroides*, *Rikenella*, *Escherichia*, *Desulfovibrio*, and *Butyricicoccus* was reduced for the ZLD-L group than for the DSS group. The findings suggest that ZLD treatment induces changes in the composition and diversity of gut microbiota, as depicted in Figure 4D.

We identified 50 critical microbial species with linear discriminant analysis (LDA) scores >4 (Figure 4C). 21 key differential gut microbes species were identified utilizing LDA >4 as a criterion, with 7 signature differential gut microbes at the genus level: [*Prevotella*], *Clostridium*, *Christensenella*, *Lactobacillus*, *Candidatus_Arthromitus*, *Turicibacter*, *Enterococcus*.

3.4 The impact of ZLD on metabolites

Our previous results indicated that, among the tested compounds, ZLD-H treatment was the most effective in managing UC. Furthermore, it significantly promoted specific beneficial flora. Subsequently, we analyzed the effect of ZLD-H on fecal metabolism using liquid chromatography-tandem mass spectrometry. Mice metabolic profiling carried out using Partial Least Squares Discriminant Analysis (PLS-DA) and Orthogonal Partial Least Squares Discriminant Analysis (OPLS-DA) (Figures 5, 6), revealed significant differences in metabolite profiles between the DSS and ZLD-H groups (Supplementary Figures S8, S9), with samples in the ZLD-H group resembling those from the control group. The DSS group formed distinct metabolic clusters compared to the ZLD-H group (cationic model: $R^2Y = 0.9728$, $Q^2 = -0.1439$; anionic model: $R^2Y = 0.91555$, $Q^2 = -0.2754$).

The top 30 metabolites, identified in both positive and negative ion modes, that exhibited differentially expressed between the DSS and ZLD-H groups, as well as between the control and DSS groups are shown in Figure 7A, Supplementary Figures S10–S12. Metabolites with VIP (Variable importance for the projection) scores> 1 and *P*-values < 0.05 were selected. This metabolite screen yielded 96 metabolites, as illustrated in Supplementary Table S6 and Figure 7B. The DSS and ZLD-H groups exhibited differential metabolites totaling 58. ZLD-H significantly enhanced the levels of 29 metabolites, including butyrate acid (BA), zeranol,

macromomycin B, and taurocholic acid 3-sulfate, while significantly reducing the levels of other 29 metabolites including 5(S)-HETE, arachidonic acid (AA), tetrahydrodeoxycorticosterone, docosahexaenoic acid, estradiol, and 5b-dihydrotestosterone.

Metabolic pathway enrichment analysis using MetaboAnalyst 6.0 indicated significant alterations in five major pathways (Figure 7C). Four pathways, including steroid hormone biosynthesis, AA metabolism, unsaturated fatty acid biosynthesis, and BA metabolism, were the main enriched in these differential metabolites. Thus, ZLD treatment significantly reduced the abundance of AA, 5(S)-HETE, while increasing that of BA. Furthermore, AA metabolism was shown to be hyperactivated in UC (Wu et al., 2022), whereas the butanoate metabolism pathway was shown to be inhibited (Jia et al., 2023).

Quantitative analysis by ELISA further revealed that ZLD significantly increased the levels of BA while reducing the levels of AA (Figure 7D).

3.5 Association between intestinal flora and fecal metabolites

To delve deeper into the interplay between specific microbes and differential metabolites, we performed correlation analyses to reveal the coordinated changes between ZLD treatment metabolites and 7 specific microbiomes.

Based on the criteria of $|r|>0.57$ and $P< 0.05$, the correlation identified 111 pairs of significantly correlated differential flora-metabolites ($P< 0.05$), with 19 pairs of correlations being more significant ($P< 0.01$). *Christensenella*, *Clostridium*, *Candidatus_Arthromitus*, *Lactobacillus* abundance was negatively correlated with most of the elevated differential metabolites and positively correlated with most of the reduced differential metabolites in the DSS group. The ZLD-induced specific enterobacterial genera *Christensenella*, *Candidatus_Arthromitus* with AA, and *Christensenella* were negatively correlated with 5(S)-HETE; whereas *Clostridium*, *Candidatus_Arthromitus*, *Lactobacillus*, and *Turicibacter* were all positively correlated with BA (Figure 8). In accordance with these results, we hypothesized that the modulation of key metabolite levels by specific gut flora influences corresponding metabolic pathways, thereby potentially explaining the therapeutic mechanism of ZLD for UC. This involves downregulation of the levels of AA, 5(S)-HETE to inhibit the over-activity of the AA metabolic pathway in its participation, and upregulation by BA to promote the BA metabolic pathway.

3.6 Effect of ZLD on levels of inflammatory factors and the TLR4/NF-κB/NLRP3 signaling pathway

In Figure 9B, levels of IL-6, IL-1β, IL-18, and TNF-α were markedly increased in the DSS group compared to the control group. However, the levels of these pro-inflammatory factors were reduced in the SASP, ZLD-L, and ZLD-H groups than the DSS group. This demonstrated a significant mitigates the inflammatory response by ZLD. Previous studies have highlighted a positive feedback loop between NF-κB and NLRP3 in gut inflammation (Zhang et al., 2022). IHC staining showed than the control group, that the expression of TLR4 and NLRP3 was significantly increased in the UC group (Figure 9A). However, their expression was notably reduced by SASP and ZLD-H treatment. To further elucidate the involvement of the TLR4/NF-κB/NLRP3 pathway in UC, analysis of mRNA and protein expression levels of key targets in the colons of experimental animals. RT-qPCR analysis revealed significant upregulation of genes encoding tlr4, nf-κb, caspase-1, nlrp3 and asc in the DSS group, as illustrated in Figure 10A. Treatments with SASP and ZLD mitigated this upregulation. WB analysis (Figure 10B) confirmed these findings, showing significantly increased protein concentrations of Cleaved caspase-1, NF-κB p65, P-p65, p-IKBα, NLRP3, and ASC by DSS. These changes markedly were inhibited by the SASP, ZLD-L, and ZLD-H groups.

3.7 Correlative analysis of inflammatory factors with differential microbiology and metabolites

As Figure 11A showed, TNF-α was significantly negatively correlated with *Clostridium*, *Lactobacillus*, *Candidatus_Arthromitus*, IL-6 was significantly negatively correlated with *Clostridium*, *Christensenella*, *Lactobacillus*, *Candidatus_Arthromitus*. As well as IL-18 was significantly negatively correlated with *Lactobacillus* and IL-1β with *Clostridium*, *Turicibacter*. Changes in the levels of inflammatory factors were closely related to metabolites in addition to gut microbes as well. TNF-α, IL-1β, and IL-18 exhibited a negative correlation with BA, and IL-1β was positively correlated with 5(S)-HETE and AA. And TNF-α, IL-1β, IL-6 and IL-18 were associated with 22, 16, 16 and 37 metabolites, respectively (Figure 11B).

4 Discussion

This study highlights the therapeutic potential of ZLD in the treatment of UC, focusing on its ability to modulate gut microbiota, microbial metabolites, and inflammatory pathways. Mice treated with ZLD showed a significant improvement in disease activity with increases in body weight, reductions in colon shortening, and lower DAI scores. Histopathological improvements, including reduced colonic inflammation and enhanced intestinal barrier integrity, were evident following ZLD treatment, as observed through histological and transmission electron microscopy (TEM) analyses. Collectively, these findings indicate that ZLD effectively ameliorates disease symptoms, prevents colonic damage, and promotes intestinal barrier repair in the DSS-induced UC mouse model.

Dysbiosis of the gut microbiota has emerged as a key contributor to UC pathogenesis (Haneishi et al., 2023; Nishida et al., 2018). Mice with UC were shown to exhibit a lower abundance and number of gut microbial species than their healthy counterparts, while high microbial diversity benefits health (Jialing et al., 2020; Peng et al., 2020). Moreover, the F/B ratio is commonly used to assess gut microbiota imbalance, with studies showing alterations in this ratio in UC mice (Kabeerdoss et al., 2015; Liu Y-J et al., 2020b). One of the

key findings of the present study is the modulatory effect of ZLD on gut microbiota composition. ZLD reversed the dysregulation of the F/B ratio in UC mice, reduced the abundance of pathogenic bacteria (e.g., *Enterococcus*, *Shigella, Escherichia*), and promoted the growth of beneficial bacteria, including *Lactobacillus*, *Christensenella*, and butyrate-producing *Clostridium* species. Notably, *Lactobacillus* has been shown to mitigate intestinal injury by inhibiting the release of inflammatory mediators including IL-6, IL-1β, and TNF-α, thereby alleviating intestinal inflammation (Li et al., 2023). Similarly, *Christensenella* has been reported to reduce the expression of TLR4 and NF-κB, as well as inflammatory cytokines such as IL-1β, IL-6, and TNF-α in both the liver and colon, further modulating the inflammatory response (Pan et al., 2022). These results support the well-established link between gut microbiota dysbiosis and various intestinal diseases, including UC (Cheng et al., 2023; Li et al., 2021). Collectively, these findings suggest that ZLD may exert therapeutic effects in UC by regulating gut microbiota, inhibiting the growth of pathogenic bacteria, promoting beneficial bacterial proliferation, improving intestinal microecology, and reducing the inflammatory response.

Dysbiosis of the intestinal flora not only affects the gut environment but is also closely associated with metabolic alterations. In our study, UC mice exhibited significant metabolic disruptions, and treatment with ZLD modulated gut flora metabolites, particularly by promoting butyrate acid (BA) production and inhibiting the accumulation of arachidonic acid (AA) and its metabolite 5(S)-HETE. BA, a key short-chain fatty acid, BA, a key short-chain fatty acid, has potent anti-inflammatory properties, primarily by inhibiting NF-κB activation and reducing interferon-γ production, thus mitigating inflammation (Salvi and Cowles, 2021). Additionally, BA enhances mucin production, strengthens tight junctions, and promotes epithelial cell repair and intestinal barrier restoration (Hamer et al., 2008). AA is a key precursor of inflammatory mediators and can be metabolized into leukotrienes and prostaglandins, both of which play critical roles in inflammation and immune responses. In UC, the AA pathway is activated, converting AA into the inflammatory mediator leukotriene A4 (LTA4) (Gür et al., 2018; Kim et al., 2021; Tjonneland et al., 2009). This activation triggers signaling pathways like NF-κB, promoting the expression and release of inflammatory factors, which establish a positive feedback loop that exacerbates inflammation (Serhan and Savill, 2005). Consequently, inhibiting AA metabolic pathways and their inflammatory products presents a promising therapeutic strategy for UC. Our findings demonstrate that ZLD promoted BA production and inhibited the accumulation of AA and its metabolite 5(S)-HETE, further highlighting its potential in reducing inflammation and protecting the intestinal barrier.

In this study, ZLD significantly reduced inflammatory responses by lowering the levels of TNF-α, IL-1β, IL-6, and IL-8, as well as the expression of TLR4, p-IκBα, NF-κB, caspase-1, NLRP3, and ASC proteins and genes in UC mice. These findings are consistent with previous studies, which demonstrate that the activation of NF-κB and the NLRP3 inflammasome results in elevated levels of caspase-1, IL-1β, and IL-18 (Wang et al., 2018). We propose that ZLD exerts its therapeutic effect in UC by inhibiting the TLR4/NF-κB/NLRP3 signaling pathway. The efficacy of ZLD is closely linked to its ability to block the positive feedback loop of inflammation in UC by modulating this key inflammatory cascade. Previous research has shown that intestinal epithelial cells recognize TLRs, which are critical for detecting microbial signals from the gut microbiota (Burgueño and Abreu, 2020). Specifically, intestinal microbes (e.g., *Escherichia*, *Bacteroides*, and *Enterococcus*) release LPS, which activates the TLR4/NF-κB/NLRP3 inflammasome pathway, leading to the release of pro-inflammatory cytokines, including IL-1β, TNF-α, and IL-6, thereby contributing to the pathogenesis of UC(Kawai and Akira, 2011; Afonina et al., 2017; Liu et al., 2023). Moreover, the correlations between gut microbiota composition, microbial metabolites, and inflammatory cytokines suggest that ZLD's therapeutic effects may be mediated via the gut microbiota.

Research has highlighted the association between dysbiosis of gut microbiota, host metabolic functions, and diverse intestinal disorders such as UC(Cheng et al., 2023; Li et al., 2021). In the study, a tight association between gut microbiota and fecal metabolites was found by correlation analysis, which suggests that an imbalance of gut microbes may influence metabolic pathways. *Christensenella* was found to be associated with reduced levels of the metabolites AA, 5(S)-HETE, and *Candidatus_Arthromitus*, *Clostridium*, *Lactobacillus*, and *Turicibacter* were associated with increased levels of the metabolite BA. In this study, ZLD reduced AA and 5(S)-HETE levels and increased BA levels. AA and 5(S)-HETE were positively correlated with inflammatory factors and BA showed a correlation with inflammatory factors.

This study explored the therapeutic mechanisms of ZLD in treating UC. n conclusion, ZLD regulated UC through modulation of gut bacteria, gut bacteria-metabolite interactions, and the TLR4/NF-κB/NLRP3 signaling pathway. Correlation analysis further indicated that several significantly altered gut microbes were closely associated with changes in fecal metabolites and inflammatory factors. These findings suggest that ZLD exerts its therapeutic effects in UC via multiple pathways, including gut microbiota, metabolites, and inflammatory pathways.

Data availability statement

The original contributions presented in the study are included in the article/Supplementary Material, further inquiries can be directed to the corresponding authors.

Ethics statement

The animal study was approved by Guizhou University of Traditional Chinese Medicine Animal Research Institute. The study was conducted in accordance with the local legislation and institutional requirements.

Author contributions

TT: Funding acquisition, Writing–original draft, Data curation, Software, Writing–review and editing. QC: Funding acquisition,

Writing–review and editing, Data curation, Formal Analysis, Project administration. PC: Formal Analysis, Writing–original draft, Methodology, Validation. SL: Methodology, Writing–original draft, Formal Analysis, Software. WH: Formal Analysis, Methodology, Writing–review and editing. TY: Funding acquisition, Writing–review and editing, Project administration, Supervision. YJ: Writing–review and editing, Project administration, Supervision.

Funding

The author(s) declare that financial support was received for the research, authorship, and/or publication of this article. The financial support of this study is the National Natural Science Foundation of China (82260936); Science and Technology Program of Guizhou Province (QiankeHe-ZK [2024] General 399); Science and Technology Innovation Team Building Projectof Guizhou University ofTCM (No. TD [2022]005); Yunnan Provincial Science and Technology Department-Applied Basic Research Joint Special Funds of Chinese Medicine (202101AZ070001-268, 202301AZ070001-089); Health Research Project of Kunming Health and Health Commission (2022-04-01-009); Kunming Health Science and Technology Talent Cultivation Project and "Ten Hundred Thousand" talent project (2022-SW (Reserve Personnel)-60); Natural Science Project of Guizhou University of Traditional Chinese Medicine Graduate Education Innovation Program (YCXZRS202202).

Acknowledgments

Our greatest acknowledgment is to all the reviewers who participated in the review work and all our colleagues in this study for their hard work.

Conflict of interest

The authors declare that the research was conducted in the absence of any commercial or financial relationships that could be construed as a potential conflict of interest.

Publisher's note

Supplementary material

The Supplementary Material for this article can be found online at: https://www.frontiersin.org/articles/10.3389/fphar.2024.1481273/full#supplementary-material

References

Afonina, I. S., Zhong, Z., Karin, M., and Beyaert, R. (2017). Limiting inflammation-the negative regulation of NF-κB and the NLRP3 inflammasome. *Nat. Immunol.* 18 (8), 861–869. doi:10.1038/ni.3772

Burgueño, J. F., and Abreu, M. T. (2020). Epithelial Toll-like receptors and their role in gut homeostasis and disease. *Nat. Rev. Gastroenterol. Hepatol.* 17 (5), 263–278. doi:10.1038/s41575-019-0261-4

Chan, B. C. L., Hon, K. L. E., Leung, P. C., Sam, S. W., Fung, K. P., Lee, M. Y. H., et al. (2008). Traditional Chinese medicine for atopic eczema: PentaHerbs formula suppresses inflammatory mediators release from mast cells. *J. Ethnopharmacol.* 120 (1), 85–91. doi:10.1016/j.jep.2008.07.034

Chassaing, B., Aitken, J. D., Malleshappa, M., and Vijay-Kumar, M. (2014). Dextran sulfate sodium (DSS)-induced colitis in mice. *Curr. Protoc. Immunol.* 104, 1–15. doi:10.1002/0471142735.im1525s104

Chen, B., Wang, Y., Niu, Y., and Li, S. (2023). Acalypha australis L. Extract attenuates DSS-induced ulcerative colitis in mice by regulating inflammatory factor release and blocking NF-κB activation. *J. Med. Food* 26 (9), 663–671. doi:10.1089/jmf.2023.K.0037

Chen, M.-L., Xian, Y.-F., Ip, S.-P., Tsai, S.-H., Yang, J.-Y., and Che, C.-T. (2010). Chemical and biological differentiation of cortex phellodendri chinensis and cortex phellodendri amurensis. *Planta Med.* 76 (14), 1530–1535. doi:10.1055/s-0030-1249774

Cheng, H., Zhang, D., Wu, J., Liu, J., Zhou, Y., Tan, Y., et al. (2023). Interactions between gut microbiota and polyphenols: a mechanistic and metabolomic review. *Phytomedicine* 119, 154979. doi:10.1016/j.phymed.2023.154979

Eisenstein, M. (2018). Ulcerative colitis: towards remission. *Nature* 563 (7730), S33. doi:10.1038/d41586-018-07276-2

Ford, A. C., and Peyrin-Biroulet, L. (2013). Opportunistic infections with anti-tumor necrosis factor-α therapy in inflammatory bowel disease: meta-analysis of randomized controlled trials. *Am. J. Gastroenterol.* 108 (8), 1268–1276. doi:10.1038/ajg.2013.138

Frank, D. N., St Amand, A. L., Feldman, R. A., Boedeker, E. C., Harpaz, N., and Pace, N. R. (2007). Molecular-phylogenetic characterization of microbial community imbalances in human inflammatory bowel diseases. *Proc. Natl. Acad. Sci. U. S. A.* 104 (34), 13780–13785. doi:10.1073/pnas.0706625104

Gür, Z. T., Çalışkan, B., and Banoglu, E. (2018). Drug discovery approaches targeting 5-lipoxygenase-activating protein (FLAP) for inhibition of cellular leukotriene biosynthesis. *Eur. J. Med. Chem.* 153, 34–48. doi:10.1016/j.ejmech.2017.07.019

Hamer, H. M., Jonkers, D., Venema, K., Vanhoutvin, S., Troost, F. J., and Brummer, R. J. (2008). Review article: the role of butyrate on colonic function. *Aliment. Pharmacol. Ther.* 27 (2), 104–119. doi:10.1111/j.1365-2036.2007.03562.x

Haneishi, Y., Furuya, Y., Hasegawa, M., Picarelli, A., Rossi, M., and Miyamoto, J. (2023). Inflammatory bowel diseases and gut microbiota. *Int. J. Mol. Sci.* 24 (4), 3817. doi:10.3390/ijms24043817

Honda, K., and Littman, D. R. (2016). The microbiota in adaptive immune homeostasis and disease. *Nature* 535 (7610), 75–84. doi:10.1038/nature18848

Jia, J., Zheng, W., Tang, S., Song, S., and Ai, C. (2023). Scytosiphon lomentaria fucoidan ameliorates DSS-induced colitis in dietary fiber-deficient mice via modulating the gut microbiota and inhibiting the TLR4/NF-κB/MLCK pathway. *Int. J. Biol. Macromol.* 253 (Pt 8), 127337. doi:10.1016/j.ijbiomac.2023.127337

Jialing, L., Yangyang, G., Jing, Z., Xiaoyi, T., Ping, W., Liwei, S., et al. (2020). Changes in serum inflammatory cytokine levels and intestinal flora in a self-healing dextran sodium sulfate-induced ulcerative colitis murine model. *Life Sci.* 263, 118587. doi:10.1016/j.lfs.2020.118587

Kabeerdoss, J., Jayakanthan, P., Pugazhendhi, S., and Ramakrishna, B. S. (2015). Alterations of mucosal microbiota in the colon of patients with inflammatory bowel disease revealed by real time polymerase chain reaction amplification of 16S ribosomal ribonucleic acid. *Indian J. Med. Res.* 142 (1), 23–32. doi:10.4103/0971-5916.162091

Kawai, T., and Akira, S. (2011). Toll-like receptors and their crosstalk with other innate receptors in infection and immunity. *Immunity* 34 (5), 637–650. doi:10.1016/j.immuni.2011.05.006

Kim, H.-J., Joe, H.-I., Zhang, Z., Woo Lee, S., Lee, K.-Y., Kook, Y.-B., et al. (2020). Anti-inflammatory effect of Acalypha australis L. via suppression of NF-κB signaling in LPS-stimulated RAW 264.7 macrophages and LPS-induced septic mice. *Mol. Immunol.* 119, 123–131. doi:10.1016/j.molimm.2020.01.010

Kim, W., Jang, J.-H., Zhong, X., Seo, H., and Surh, Y.-J. (2021). 15-Deoxy-△12,14-Prostaglandin J2 promotes resolution of experimentally induced colitis. *Front. Immunol.* 12, 615803. doi:10.3389/fimmu.2021.615803

Li, C., Peng, K., Xiao, S., Long, Y., and Yu, Q. (2023). The role of Lactobacillus in inflammatory bowel disease: from actualities to prospects. *Cell Death Discov.* 9 (1), 361. doi:10.1038/s41420-023-01666-w

Li, Q., Cui, Y., Xu, B., Wang, Y., Lv, F., Li, Z., et al. (2021). Main active components of Jiawei Gegen Qinlian decoction protects against ulcerative colitis under different dietary environments in a gut microbiota-dependent manner. *Pharmacol. Res.* 170, 105694. doi:10.1016/j.phrs.2021.105694

Liu, H., Chen, R., Wen, S., Li, Q., Lai, X., Zhang, Z., et al. (2023). Tea (Camellia sinensis) ameliorates DSS-induced colitis and liver injury by inhibiting TLR4/NF-κB/NLRP3 inflammasome in mice. *Biomed. Pharmacother.* 158, 114136. doi:10.1016/j.biopha.2022.114136

Liu P, P., Bian, Y., Liu, T., Zhong, J., Zhong, Y., Zhuang, S., et al. (2020). Huai hua san alleviates dextran sulphate sodium-induced colitis and modulates colonic microbiota. *J. Ethnopharmacol.* 259, 112944. doi:10.1016/j.jep.2020.112944

Liu Y-J, Y.-J., Tang, B., Wang, F.-C., Tang, L., Lei, Y.-Y., Luo, Y., et al. (2020). Parthenolide ameliorates colon inflammation through regulating Treg/Th17 balance in a gut microbiota-dependent manner. *Theranostics* 10 (12), 5225–5241. doi:10.7150/thno.43716

Lu, L., Tang, M., Li, J., Xie, Y., Li, Y., Xie, J., et al. (2021). Gut microbiota and serum metabolic signatures of high-fat-induced bone loss in mice. *Front. Cell Infect. Microbiol.* 11, 788576. doi:10.3389/fcimb.2021.788576

Luthra, P., Peyrin-Biroulet, L., and Ford, A. C. (2015). Systematic review and meta-analysis: opportunistic infections and malignancies during treatment with anti-integrin antibodies in inflammatory bowel disease. *Aliment. Pharmacol. Ther.* 41 (12), 1227–1236. doi:10.1111/apt.13215

Molodecky, N. A., Soon, I. S., Rabi, D. M., Ghali, W. A., Ferris, M., Chernoff, G., et al. (2012). Increasing incidence and prevalence of the inflammatory bowel diseases with time, based on systematic review. *Gastroenterology* 142 (1), 46–54. doi:10.1053/j.gastro.2011.10.001

Morrison, D. J., and Preston, T. (2016). Formation of short chain fatty acids by the gut microbiota and their impact on human metabolism. *Gut Microbes* 7 (3), 189–200. doi:10.1080/19490976.2015.1134082

Mu, Q., Kirby, J., Reilly, C. M., and Luo, X. M. (2017). Leaky gut as a danger signal for autoimmune diseases. *Front. Immunol.* 8, 598. doi:10.3389/fimmu.2017.00598

Nakase, H., Uchino, M., Shinzaki, S., Matsuura, M., Matsuoka, K., Kobayashi, T., et al. (2021). Evidence-based clinical practice guidelines for inflammatory bowel disease 2020. *J. Gastroenterol.* 56 (6), 489–526. doi:10.1007/s00535-021-01784-1

Ng, S. C., Shi, H. Y., Hamidi, N., Underwood, F. E., Tang, W., Benchimol, E. I., et al. (2017). Worldwide incidence and prevalence of inflammatory bowel disease in the 21st century: a systematic review of population-based studies. *Lancet* 390 (10114), 2769–2778. doi:10.1016/S0140-6736(17)32448-0

Ni, J., Wu, G. D., Albenberg, L., and Tomov, V. T. (2017). Gut microbiota and IBD: causation or correlation? *Nat. Rev. Gastroenterol. Hepatol.* 14 (10), 573–584. doi:10.1038/nrgastro.2017.88

Nishida, A., Inoue, R., Inatomi, O., Bamba, S., Naito, Y., and Andoh, A. (2018). Gut microbiota in the pathogenesis of inflammatory bowel disease. *Clin. J. Gastroenterol.* 11 (1), 1–10. doi:10.1007/s12328-017-0813-5

Pan, T., Zheng, S., Zheng, W., Shi, C., Ning, K., Zhang, Q., et al. (2022). Christensenella regulated by Huang-Qi-Ling-Hua-San is a key factor by which to improve type 2 diabetes. *Front. Microbiol.* 13, 1022403. doi:10.3389/fmicb.2022.1022403

Parada Venegas, D., De la Fuente, M. K., Landskron, G., González, M. J., Quera, R., Dijkstra, G., et al. (2019). Short chain fatty acids (SCFAs)-Mediated gut epithelial and immune regulation and its relevance for inflammatory bowel diseases. *Front. Immunol.* 10, 277. doi:10.3389/fimmu.2019.00277

Park, E.-K., Rhee, H. I., Jung, H.-S., Ju, S. M., Lee, Y.-A., Lee, S.-H., et al. (2007). Antiinflammatory effects of a combined herbal preparation (RAH13) of Phellodendron amurense and Coptis chinensis in animal models of inflammation. *Phytother. Res.* 21 (8), 746–750. doi:10.1002/ptr.2156

Peng, L., Gao, X., Nie, L., Xie, J., Dai, T., Shi, C., et al. (2020). Astragalin attenuates dextran sulfate sodium (DSS)-Induced acute experimental colitis by alleviating gut microbiota dysbiosis and inhibiting NF-κB activation in mice. *Front. Immunol.* 11, 2058. doi:10.3389/fimmu.2020.02058

Round, J. L., and Mazmanian, S. K. (2009). The gut microbiota shapes intestinal immune responses during health and disease. *Nat. Rev. Immunol.* 9 (5), 313–323. doi:10.1038/nri2515

Salice, M., Rizzello, F., Calabrese, C., Calandrini, L., and Gionchetti, P. (2019). A current overview of corticosteroid use in active ulcerative colitis. *Expert Rev. Gastroenterol. Hepatol.* 13 (6), 557–561. doi:10.1080/17474124.2019.1604219

Salvi, P. S., and Cowles, R. A. (2021). Butyrate and the intestinal epithelium: modulation of proliferation and inflammation in homeostasis and disease. *Cells* 10 (7), 1775. doi:10.3390/cells10071775

Serhan, C. N., and Savill, J. (2005). Resolution of inflammation: the beginning programs the end. *Nat. Immunol.* 6 (12), 1191–1197. doi:10.1038/ni1276

Shi, H. Y., Chan, F. K. L., Chan, A. W. H., Higashimori, A., Kyaw, M., Ching, J. Y. L., et al. (2017). Accuracy of faecal immunochemical test to predict endoscopic and histological healing in ulcerative colitis: a prospective study based on validated histological scores. *J. Crohns Colitis* 11 (9), 1071–1077. doi:10.1093/ecco-jcc/jjx088

Tjonneland, A., Overvad, K., Bergmann, M. M., Nagel, G., Linseisen, J., Hallmans, G., et al. (2009). Linoleic acid, a dietary n-6 polyunsaturated fatty acid, and the aetiology of ulcerative colitis: a nested case-control study within a European prospective cohort study. *Gut* 58 (12), 1606–1611. doi:10.1136/gut.2008.169078

Wang, S., Lin, Y., Yuan, X., Li, F., Guo, L., and Wu, B. (2018). REV-ERBα integrates colon clock with experimental colitis through regulation of NF-κB/NLRP3 axis. *Nat. Commun.* 9 (1), 4246. doi:10.1038/s41467-018-06568-5

Wu, J., Luo, Y., Shen, Y., Hu, Y., Zhu, F., Wu, J., et al. (2022). Integrated metabonomics and network pharmacology to reveal the action mechanism effect of shaoyao decoction on ulcerative colitis. *Drug Des. Devel Ther.* 16, 3739–3776. doi:10.2147/DDDT.S375281

Yang, T., Qin, N., Liu, F., Zhao, Y., Liu, W., and Fan, D. (2024). Berberine regulates intestinal microbiome and metabolism homeostasis to treat ulcerative colitis. *Life Sci.* 338, 122385. doi:10.1016/j.lfs.2023.122385

Zhang, H.-X., Li, Y.-Y., Liu, Z.-J., and Wang, J.-F. (2022). Quercetin effectively improves LPS-induced intestinal inflammation, pyroptosis, and disruption of the barrier function through the TLR4/NF-κB/NLRP3 signaling pathway *in vivo* and *in vitro*. *Food Nutr. Res.* 66. doi:10.29219/fnr.v66.8948

Zhang, S., Shang, Z., Liu, Z., Hu, X., and Yi, J. (2023). Flavor production in fermented chayote inoculated with lactic acid bacteria strains: genomics and metabolomics based analysis. *Food Res. Int.* 163, 112224. doi:10.1016/j.foodres.2022.112224

Zhou, X., Wang, J., Lu, Y., Chen, C., Hu, Y., Liu, P., et al. (2020). Anti-depressive effects of Kai-Xin-San on lipid metabolism in depressed patients and CUMS rats using metabolomic analysis. *J. Ethnopharmacol.* 252, 112615. doi:10.1016/j.jep.2020.112615

frontiers | Frontiers in Pharmacology

TYPE Original Research
PUBLISHED 24 December 2024
DOI 10.3389/fphar.2024.1510380

OPEN ACCESS

EDITED BY
Boyang Ji,
BioInnovation Institute (BII), Denmark

REVIEWED BY
Hong-he Xiao,
Liaoning University of Traditional Chinese Medicine, China
Yang Ke,
China Jiliang University, China
Weicheng Hu,
Yangzhou University, China

*CORRESPONDENCE
Zhongqiang Sang,
sangzhongqiang2024@163.com

RECEIVED 12 October 2024
ACCEPTED 12 December 2024
PUBLISHED 24 December 2024

CITATION
Sang Y, Du J, Zulikala D and Sang Z (2024) Mechanistic analysis of Tanshinone IIA's regulation of the ATM/GADD45/ORC signaling pathway to reduce myocardial ischemia-reperfusion injury.
Front. Pharmacol. 15:1510380.
doi: 10.3389/fphar.2024.1510380

Mechanistic analysis of Tanshinone IIA's regulation of the ATM/GADD45/ORC signaling pathway to reduce myocardial ischemia-reperfusion injury

Yiwei Sang[1], Jiangnan Du[1], Dilimulati Zulikala[1] and Zhongqiang Sang[2]*

[1]Nature Drug Discovery Group, School of Pharmacy, Queen's University Belfast, Belfast, United Kingdom, [2]Dermatology Department, Shanghai Zhongye Hospital, Shanghai, China

Background: By far, one of the best treatments for myocardial ischemia is reperfusion therapy. The primary liposoluble component of Danshen, a traditional Chinese herbal remedy, Tanshinone IIA, has been shown to have cardiac healing properties. The purpose of this work is to investigate the processes by which Tanshinone IIA influences myocardial ischemia-reperfusion injury (MIRI) in the H9C2 cardiac myoblast cell line, as well as the association between Tanshinone IIA and MIRI.

Methods and results: The cardiac cells were divided into a normal group, a model group and Tanshinone IIA treatment groups. After 4 h of culture with the deprivation of oxygen and glucose, the cells were incubated normally for 2 h. The success of the model and the capacity of Tanshinone IIA to heal cardiac damage were validated by the outcomes of cell viability, morphology, and proliferation. The efficacy of Tanshinone IIA in treating MIRI was further confirmed by the scratch assay and biomarker measurement. The differentially expressed genes were examined using transcriptome sequencing. The Ataxia-Telangiectasia Mutated (ATM)/Growth Arrest and DNA Damage (GADD45)/Origin Recognition Complex (ORC) signaling pathway was identified as being crucial to this process by KEGG pathway analysis and GO enrichment. Molecular docking and RT-qPCR were used to confirm our results. The crucial function of the ATM/GADD45/ORC pathway was further confirmed by the addition of an ATM inhibitor, which inhibited the expression of ATM.

Conclusion: Tanshinone IIA can relieve the myocardial ischemia-reperfusion injury in cardiac cells by activating the ATM/GADD45/ORC pathway.

KEYWORDS

myocardial ischemia-reperfusion injury, H9C2, ATM, GADD45, ORC

1 Introduction

Acute myocardial infarction (AMI) is an ischaemic heart disease caused by myocardial ischaemia and necrosis due to acute coronary artery congestion. It has become one of the greatest causes of mortality worldwide. Reperfusion, one of the most effective treatments for AMI, can help patients restore their coronary artery blood flow. However, increasing

evidence shows that reperfusion treatment can cause myocardial ischemia-reperfusion injury (MIRI). MIRI has a complex pathomechanism involving metabolic disorders (Salameh et al., 2020), mitochondrial dysfunction (Tian et al., 2023), inflammation (Salameh et al., 2020; Tian et al., 2023), autophagy disorders and the release of high levels of reactive oxygen species (ROS) caused by oxidative stress (Yu et al., 2006). These injuries lead to myocardial damage and then aggravate heart failure or even lead to sudden cardiac death.

Among them, the excess ROS can attack DNA directly, causing base oxidation, glycation damage and DNA strand breaks. Massive release of inflammatory factors not only can increase oxidative stress but promote the expression of genes related to DNA damage. Furthermore, metabolic disorders can lead to a plunge in intracellular ATP levels, affecting the activity of DNA repair enzymes, exacerbating the consequences of DNA damage.

The ATM signaling pathway is a crucial signal transduction pathway that cells utilize to respond to DNA damage, particularly DNA double-strand breaks. Studies have shown that ATM activation can lead to Murine Double Minute 2 (MDM2) E3 phosphorylation and activity inhibition, which causes rapid accumulation of p53 (Chen, 2012). P53 activation can inhibit cell cycle progression (Chen, 2016). The cells arrest in the G2/M phase, and checkpoints are activated (St Clair et al., 2004). This arrest helps repair DNA damage, especially fatal double-strand breaks (Gatz and Wiesmüller, 2006).

Danshen is a traditional Chinese herb derived from the root and rhizome of Salvia miltiorrhiza, a Labiatae plant (Yuan et al., 2024). It promotes blood circulation to prevent blood stasis (Yuan et al., 2024; Cao et al., 2017). Danshen is frequently utilized in the clinical management of cardiovascular and cerebrovascular conditions (Qin et al., 2023). It can effectively relieve the clinical symptoms of ischemic cardiovascular and cerebrovascular diseases and reduce complications and sequelae.

Tanshinone ⅡA, the main liposoluble constituent of Danshen (Yang et al., 2020), has garnered widespread attention for its efficacy in treating AMI. Studies have shown that Tanshinone ⅡA possesses significant anti-inflammatory, antioxidant, and anti-fibrotic effects in cardiovascular protection. Ren et al. (2010) found that Tanshinone IIA effectively suppresses the release of inflammatory factors following myocardial infarction by reducing the expression of monocyte chemoattractant protein-1 (MCP-1), thereby decreasing the infiltration of inflammatory cells. This anti-inflammatory property is also crucial in the treatment of MIRI, as post-reperfusion inflammation often leads to secondary myocardial damage.

In addition to its anti-inflammatory effects, Tanshinone IIA demonstrates robust antioxidant potential. In AMI models, Tanshinone IIA enhances the activity of antioxidant enzymes such as superoxide dismutase (SOD) and glutathione peroxidase (GSH-Px) and reduces the production of oxidative stress marker malondialdehyde (MDA), thereby alleviating oxidative stress-induced myocardial damage (Chen et al., 2021). During MIRI, the sudden increase in ROS directly damages myocardial cells activates inflammatory signaling pathways, such as the NF-κB pathway, promoting the release of inflammatory factors (Hu et al., 2015). Therefore, Tanshinone IIA may effectively interrupt the vicious cycle of MIRI injury by inhibiting both oxidative stress and inflammatory signaling pathways.

Myocardial fibrosis is a core manifestation of myocardial remodelling after AMI and MIRI and is a primary pathological mechanism leading to heart failure. During fibrosis, myocardial tissue gradually hardens due to the deposition of type I and III collagen, which impairs normal cardiac function. Gao et al. (2019) indicated that TIIA also has significant anti-fibrotic effects, inhibiting myocardial fibrosis by reducing the expression of TGF-β and α-smooth muscle actin (α-SMA). This effect has potential application value in MIRI models, helping to prevent the progression of myocardial fibrosis and protecting cardiac function after myocardial infarction.

Previous studies have sufficiently demonstrated the therapeutic effects of Tanshinone IIA on AMI and MIRI. Therefore, we aim to investigate the regulatory role of Tanshinone on the ATM signaling pathway from the perspective of DNA damage, as well as the therapeutic mechanism in H9C2 cell ischemia-reperfusion injury. It provides experimental evidence supporting the usage of Tanshinone IIA in the prevention and treatment of ischemic cardiovascular diseases.

2 Materials and methods

2.1 Materials

The rat-myocardium-derived cardiac myoblast cell line H9C2 was purchased from the Union Medical University Cell Experiment Center (lot No. SCSP-5211).

Tanshinone ⅡA was purchased from the National Institutes for Food and Drug Control (lot No. WVH2-4LD1).

2.2 Cell culture and treatment

The rat cardiomyocytes, H9C2 cell line was cultivated in high-glucose DMEM (Gibco™, lot No. 8122512) supplemented with 10% (v/v) FBS (Invitrogen™, lot No. 10099-141). The culture was then incubated at 37°C with 5% CO_2. Several groups were created out of these cells: normal group, model group and Tanshinone ⅡA treatment groups.

For the normal group, the cells were cultured and incubated as normal. For the model group, the cells were first treated as described for the normal group. PBS was used to wash the cells once the density reached 80%. The glucose-free DMEM (Gibco™, lot No.2323012) without serum was introduced. For 4 h, the cells were incubated at 37°C with 85% N_2, 10% H_2, and 5% CO_2. Then, the medium was replaced with high-glucose DMEM, and the cells were incubated with 5% CO_2 at 37°C for 2 h.

For the treatment groups, the cells were treated as the model group. Different doses of Tanshinone ⅡA were added to the serum and glucose-free DMEM to final concentrations of 1, 5, 10, 20, 40, 80, 160, 320, and 640 μmol/L.

For the inhibitor group, the ATM kinase inhibitor KU-55933 (Selleck, lot No. S1092) was added to the serum and glucose-free media together with Tanshinone ⅡA to a final concentration of 10 μmol/L.

2.3 CCK-8 assay

Approximately 10^4 cells were added to each well of a 96-well plate. After they reached 80%–90% confluence, the cells were cultured as described in Section 2.2. Each well received 10 μL of CCK-8 solution (DOJINDO, lot No. TR689), and the plate was incubated for an hour with 5% CO_2 at 37°C. The absorbance was measured following incubation at a wavelength of 450 nm.

2.4 Cellular morphology

The morphology of the cultivated cells was observed using an inverted microscope (Olympus Corporation, TH4-200).

2.5 Fluorescence staining

In a 6-well plate, about 2×10^5 cells were put into each well. Following the outline described in Section 2.2, the cells were grown until they reached 80%–90% confluence. Culture media was used to dilute the EdU. The medium was supplemented with prewarmed EdU solution until the final concentration of EdU was 10 μmol/L. The cells underwent incubation in a CO_2 environment at a temperature of 37°C for 2 h. Subsequently, the medium was substituted with a stationary medium, and the cells were cultured at room temperature for 15 min. Subsequently, the cells underwent a gentle wash with PBS, followed by the addition of 0.3% Triton X-100 to the cell suspension. The cells were cultivated for 10 min at room temperature, followed by a PBS wash and a further 20 min at room temperature with the blocking solution. Following washing, the cells were grown for 30 min at room temperature in the dark with 500 μL of Click solution added. Following a PBS wash, the cells were incubated for an additional 30 min at room temperature using 200 μL of streptavidin-HRP working solution. 200 μL of DAB colouring solution was applied after washing. After 10 min of RT culture, the cells were cleaned with PBS. DAPI was employed as the counterstain. A fluorescence microscope was used to observe and record the data. ImageJ was used to analyse the results.

2.6 Scratch assay

The 6-well plate was filled with about 10^5 H9C2 cells per well, and the cells were cultivated until they achieved 80%–90% confluence. The cells were subsequently incubated as described in Section 2.2. A vertical line scratch was made in the centre of each well using a sterile 200 μL pipette tip. The wells were washed gently with PBS to remove detached cells and debris. Images of the scratches were captured with an inverted microscope. The cells were subsequently incubated with serum-free medium in 5% CO_2 at 37°C. Images were captured every 12 h. ImageJ was used to analyse these images.

2.7 Determination of cellular supernatant biomarkers

The cellular supernatant was isolated to measure the levels of Aspartate transaminase (AST), Creatine kinase (CK) and Lactate dehydrogenase (LDH) via ELISA (Jianglai, lot No. JL21297-96T, JL46377-96T, JL46377-96T). The cells were subsequently centrifuged at 2,500 rpm and 4°C for 10 min, after which the supernatant was collected according to the kit instructions.

2.8 Transcriptomic sequencing

The cells underwent a washing procedure using pre-cold PBS, followed by total RNA extraction utilizing TRIzol. Oligo (dT) Dynabeads were employed for the isolation of mRNA. A reverse transcription kit was employed to synthesize the first-strand cDNA. Polymerase Chain Reaction (PCR) was subsequently used for cDNA amplification and cDNA library establishment. The Illumina sequencing platform was used to perform second-generation double-terminal sequencing.

2.9 RT–qPCR

TRIzol was employed to extract the total RNA from the cells. The extracted RNA was utilized for the synthesis of cDNA through the process of reverse transcription. Then, the PCR solution system was prepared, split into microcentrifuge tube and amplified in a real-time quantitative PCR instrument.

The PCR solution system employed consisted of the following components: Hieff qPCR SYBR Green Master Mix (10 μL), forward primer (0.4 μL), reverse primer (0.4 μL), cDNA (2 μL), and ddH_2O (7.2 μL). The sequences of the forward primer and reverse primer are presented in Table 1. GAPDH served as the reference gene. The $2^{-\Delta\Delta CT}$ method was employed to determine the relative expression levels of mRNAs.

The reaction conditions were established as follows: an initial denaturation phase at 95°C for a duration of 10 min, followed by denaturation at 95°C for 10 s, and an annealing phase at 60°C for 30 s. Denaturation and annealing were regarded as one cycle. Forty cycles were performed in this reaction.

2.10 Molecular docking

The three-dimensional structural files of the target proteins were acquired from the Protein Data Bank (https://www.rcsb.org/) and UniProt (https://www.uniprot.org/) databases. The molecular structures of the ligands were obtained from the PubChem database (https://pubchem.ncbi.nlm.nih.gov/). Coordinate files for the receptor and ligand were generated utilizing AutoDock Tools software. The receptor underwent the removal of water molecules, followed by the separation of the ligand from the receptor. Following the incorporation of nonpolar hydrogens, molecular docking was performed (Cao et al., 2023).

2.11 Western blot

The cells were harvested and subjected to lysis with a suitable lysis buffer that included protease inhibitors, followed by the assessment of protein concentration utilizing a BCA kit. Equal

TABLE 1 PCR primer sequences.

Gene	Primer sequence (5′~3′)	Product length/bp
ATM	F: CGAGGCGTACAATGGTGAAGGAC	118
	R: TGGTTGGCTGGAATGCTGATGC	
GADD45	F: CCGCAGAGCAGAAGATCGAAAGG	104
	R: CTCGTACACGCCGACAGTTATGG	
ORC	F: GGAGCACAGCAGAACAAGAGGTC	119
	R: ACCACCACATTCCAGAGACTTCATTG	
GADPH	F: TCTGAGCCTCCTCCAACCCAAC	108
	R: CGTTCACACCGACCTTCACCATC	

volumes of protein were combined with loading buffer, subjected to boiling at 95°C for 5 min, subsequently loaded into 8% SDS-PAGE gels, and then electrophoresed to achieve separation of proteins according to their molecular weight. The proteins were subsequently transferred onto a PVDF membrane utilizing wet transfer techniques. The membrane underwent a blocking procedure using a blocking buffer composed of 5% non-fat milk in TBST for a duration of 90 min at room temperature, aimed at minimizing non-specific binding. The samples were incubated overnight at 4°C with primary antibodies targeting ATM, GADD45, ORC, and β-actin (Cell Signalling, 2,873, 4,632, 4,731, 4,967), which served as the internal control, all diluted in blocking buffer at the concentration of 0.5 μL/mL. Following the washing procedure, the membrane underwent incubation with HRP-conjugated secondary antibodies, which were diluted in blocking buffer for 1 h at room temperature. The membrane underwent a subsequent washing, followed by the application of enhanced chemiluminescence (ECL) substrate, and the detection of protein bands was accomplished utilizing a chemiluminescence imaging system. The analysis of band intensities was conducted utilizing ImageJ for quantification.

2.12 Statistical analysis

For data analysis, GraphPad Prism 10.1.2 was utilised. The results were presented as mean ± standard deviation (mean ± sd). One-way ANOVA was employed to examine the differences between the two groups. When $p < 0.05$, the differences were considered statistically significant.

3 Results

3.1 Effect of Tanshinone IIA on MIRI in the H9C2

Cells in Tanshinone IIA treatment groups were treated as shown in Figure 1A. The model group exhibited a significant reduction in cell viability when compared to the normal group ($p < 0.01$). In contrast, the treatment groups receiving Tanshinone IIA exhibited a notable increase in cell viability at concentrations of 10 and 20 μmol/L ($p < 0.01$) and 40 μmol/L ($p < 0.05$) in comparison to the model group (Figure 1B).

Based on these cell viability results, concentrations of 10, 20, and 40 μmol/L were selected for further experiments. Figure 1C illustrates that the levels of CK, AST, and LDH were markedly elevated in the model group compared to the normal group ($p < 0.01$). In comparison to the model group, the levels of CK and AST were markedly reduced in the Tan-L (10 μmol/L), Tan-M (20 μmol/L), and Tan-H (40 μmol/L) groups ($p < 0.01$). Comparably, the levels of LDH exhibited a significant decrease in the Tan-L group ($p < 0.05$), Tan-M group ($p < 0.01$), and Tan-H group ($p < 0.01$) when contrasted with the model group.

Figure 1D shows that cells in the normal group were neatly arranged with regular shapes and small intercellular spaces. In contrast, cells in the model group varied in size, were loosely arranged with large intercellular spaces, and exhibited numerous pieces of cell debris. The Tan-L and Tan-M groups displayed more closely arranged cells with relatively regular shapes, though some irregular areas remained. Cells in the Tan-H group were tightly arranged with regular shapes and showed only mild signs of damage.

According to the DAPI and EdU staining results presented in Figure 1E, Tanshinone IIA treatment effectively alleviated the decrease in cell viability and abnormal proliferation caused by the model.

As indicated in Table 2, the relative wound density in the model group was significantly lower than that of the normal group ($p < 0.01$). Compared to the model group, the relative wound density significantly decreased at 60 h in both the medium-dose and high-dose Tanshinone IIA treatment groups ($p < 0.01$).

3.2 Gene differential expression analysis via transcriptomic sequencing

A correlation heatmap (Figure 2A) was used to visualize gene correlations between the groups. It revealed that all Pearson coefficients were greater than 0.9, indicative of strong positive correlations.

The gene with a p-value threshold of less than 0.05 and a $\log_2$(FC) threshold less than or more than 0 was identified as a differentially expressed gene. Differentially expressed genes are illustrated in volcano plots (Figures 2B, C). In comparison to the

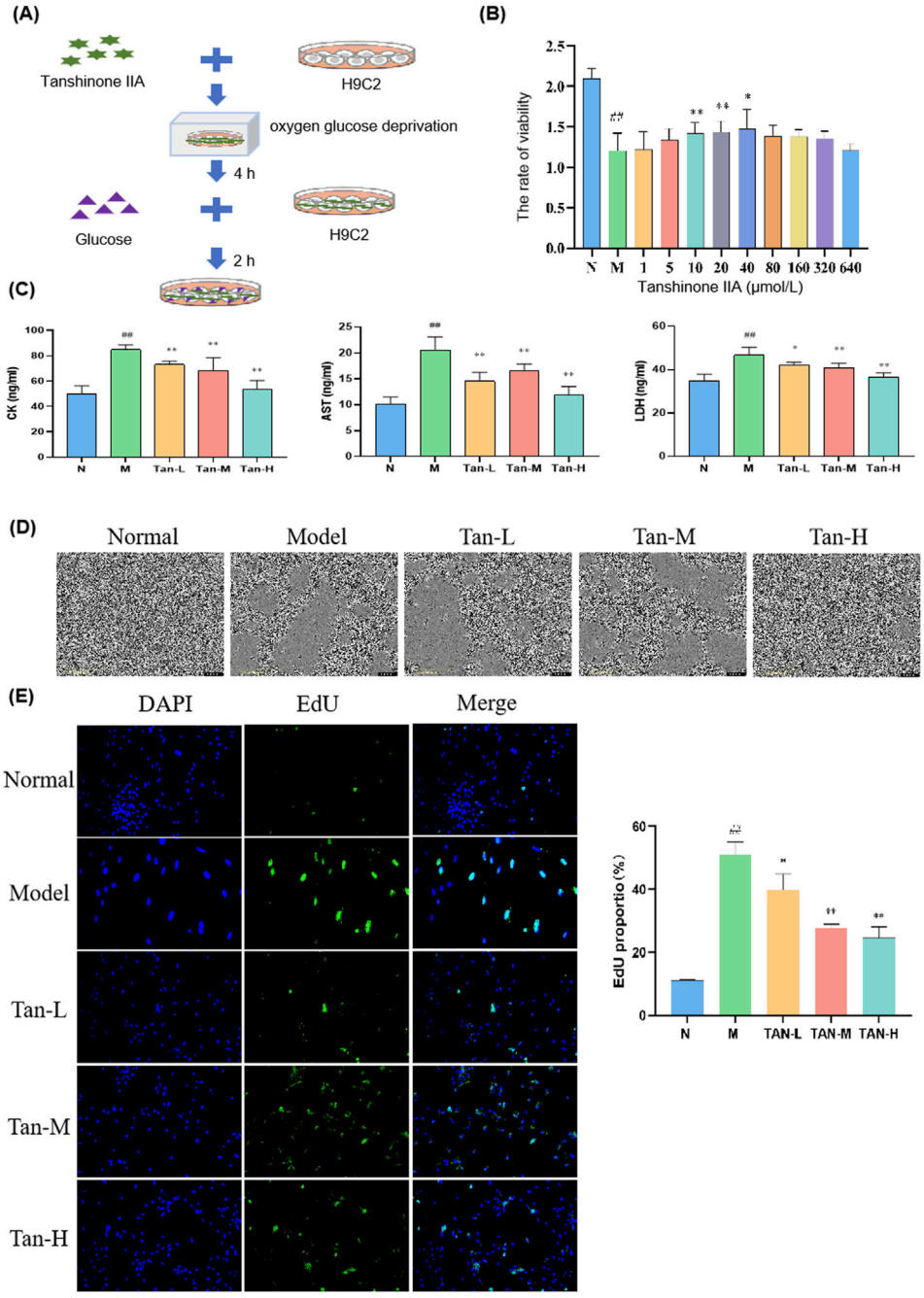

FIGURE 1
Effect of Tanshinone IIA on myocardial ischemia-reperfusion injury in the H9C2. Notes: **(A)** Cell culture and treatment; **(B)** viability rate of H9C2; **(C)** changes in the level of CK, AST and LDH in H9C2; **(D)** morphology of H9C2 cells; **(E)** fluorescence staining of H9C2 cells. $^{\#\#}p < 0.01$ vs. the normal group, $^{*}p < 0.05$ vs. the model group, $^{**}p < 0.01$ vs. the model group (n = 6, Mean ± sd).

control group, the experimental group demonstrated 4,603 differentially expressed genes, comprising 2,482 genes that were upregulated and 2,121 genes that were downregulated (Figure 2B). In the analysis of the Tanshinone IIA treatment group versus the model group, a total of 1,717 differentially expressed genes were identified, comprising 942 that were upregulated and 775 that were downregulated (Figure 2C).

A Venn diagram (Figure 2D) visualizes the distribution and overlap of the differentially expressed genes. Of the 4,603 genes differentially expressed between the normal and model groups and the 1,717 genes between the model and Tanshinone IIA treatment groups, 623 genes were commonly differentially expressed.

As shown in Figure 2F, the differentially expressed genes were enriched in Gene Ontology categories encompassing biological processes (BP), cellular components (CC), and molecular functions (MF). The main biological processes involved protein folding, peptide synthesis, and translation. The cellular components primarily included the ribosome, mitochondrial parts, and nucleus.

TABLE 2 Relative wound density (mean ± sd).

Group	Dose (μmol/L)	n	12 h (%)	24 h (%)	36 h (%)	48 h (%)	60 h (%)
Normal	—	5	42.06 ± 1.82	59.26 ± 2.29	71.83 ± 1.83	77.94 ± 1.99	85.21 ± 1.44
Model	—	5	5.97 ± 1.05##	6.89 ± 1.39##	9.75 ± 1.52##	13.31 ± 1.59##	16.62 ± 1.66##
Tan-L	10	5	8.20 ± 0.68	9.42 ± 0.96	12.65 ± 1.57	15.83 ± 1.58	19.16 ± 1.67
Tan-M	20	5	7.46 ± 1.02	8.21 ± 0.92	10.14 ± 1.10	14.93 ± 1.71	21.70 ± 3.29**
Tan-H	40	5	11.18 ± 2.08**	14.11 ± 3.16**	17.96 ± 3.91**	21.17 ± 4.43**	28.27 ± 4.27**

Note: ##$p < 0.01$ vs. the normal group, **$p < 0.01$ vs. the model group.

Key molecular functions were unfolded protein binding, RNA binding, and structural molecule activity. The KEGG pathway analysis (Figure 2G) revealed that these genes were predominantly enriched in pathways associated with the cell cycle, Huntington's disease, oxidative phosphorylation, Parkinson's disease, the FoxO signaling pathway, and protein processing in the endoplasmic reticulum.

3.3 Tanshinone IIA relieves myocardial ischemia-reperfusion injury through ATM/GADD45/ORC pathway activation

Based on the KEGG pathway analysis and literature review, the cell cycle has been identified as a key pathway through which Tanshinone IIA alleviates myocardial ischemia-reperfusion injury. As a result, the pathway genes in the cell cycle were imported into Cytoscpe. The core genes were screened using CytoHubba, and the top three genes, ATM,GADD45 and ORC, were selected for RT-qPCR analysis according to the Degree value. To verify the effectiveness of ATM/GADD45/ORC pathway (Figure 3A), follow-up experiments were conducted.

Figure 3B illustrates that the model group exhibited a notable reduction in ATM expression relative to the normal group ($p < 0.05$), alongside significant decreases in GADD45 and ORC expressions ($p < 0.01$). Moreover, the Tan-H group demonstrated significantly reduced expression levels of ATM, GADD45, and ORC compared to the model group ($p < 0.01$).

Figure 3C presents the molecular structure of Tanshinone IIA alongside the 3D structures of GADD45, ORC, and ATM. The docking results in Figure 3D indicate that Tanshinone IIA can interact with GADD45, ORC, and ATM. Specifically, it binds to ATM and ORC via hydrogen bonds with GLY-95 and GLN-399, respectively, and forms three hydrogen bonds with GADD45 involving VAL-40, TYR-41, and PRO-120.

To further validate the involvement of the ATM/GADD45/ORC pathway, the ATM inhibitor KU-55933 was introduced into the model system (Figure 4A).

Figure 4B illustrates that the model group demonstrated markedly elevated levels of CK, AST, and LDH in comparison to the normal group ($p < 0.01$). Conversely, the Tan-H group exhibited markedly lower levels of these enzymes in comparison to the model group ($p < 0.01$). In comparison to the Tan-H group, the inhibitor group exhibited a statistically significant elevation in CK levels ($p < 0.05$) and notably higher concentrations of AST and LDH ($p < 0.01$).

Figure 4C demonstrates that the model group exhibited markedly reduced expression levels of ATM, GADD45, and ORC1 in comparison to the normal group ($p < 0.05$). The Tan-H group demonstrated a notable enhancement in the expression of these genes in comparison to the model group ($p < 0.05$). Nonetheless, the inhibitor group exhibited markedly lower expression levels of ATM, GADD45, and ORC1 in comparison to the Tan-H group ($p < 0.05$).

4 Discussion

Acute myocardial infarction is a global ischemic cardiovascular disease with high mortality and morbidity (Li et al., 2023). As of 2020, approximately 1.72% of the global population was plagued with AMI (Khan et al., 2020). Reperfusion therapy is an effective treatment for ischemic diseases. However, ischemia-reperfusion injury after reperfusion is also fatal (Verma et al., 2002). As a result, prevention and treatment of MIRI have become a key procedure during AMI treatment. It always causes myocardial necrosis, endothelial dysfunction, inflammation and oxidative stress (Yao et al., 2023).

Pharmacological studies have shown that Danshen promotes coronary artery expansion, improves myocardial ischemia and repairs myocardial damage. It can also increase the hypoxia tolerance of myocardial cells, thereby protecting the anoxic myocardium (Feng et al., 2022). The effective constituent Tanshinone ⅡA has the effects of heart protection, coronary dilation, anti-atherosclerosis, anti-platelet, anticoagulant, anti-thrombosis and inhibition of myocardial hypertrophy (Cao et al., 2017; Feng et al., 2022).

According to the previous research, Tanshinone ⅡA has a great therapeutic effect to MIRI. Hu et al. used rat cardiomyocytes, H9C2, to establish MIRI cell model (Hu et al., 2023) and found that Tanshinone ⅡA effectively attenuated H9c2 cardiomyocyte damage through inhibiting ferroptosis in the MIRI injury model. Li et al. used SD rats to establish MIRI rat model (Li et al., 2016) and found that Tanshinone IIA could activate the PI3K/Akt/mTOR signaling pathway to relieve MIRI in rats. Pan et al. used C57BL/6 mice to establish MIRI mouse model (Zhai et al., 2024) and found that Tanshinone IIA contributed to the improvement of the area of myocardial infarction, reducing myocardial enzyme levels, and promoting myocardial contractility recovery. Liu et al. used Japanese white rabbits to establish MIRI rabbit model (Liu et al., 2017) and found that Tanshinone IIA can significantly enhance the secretion of VEGF and the activity of oxygen free radical scavenging

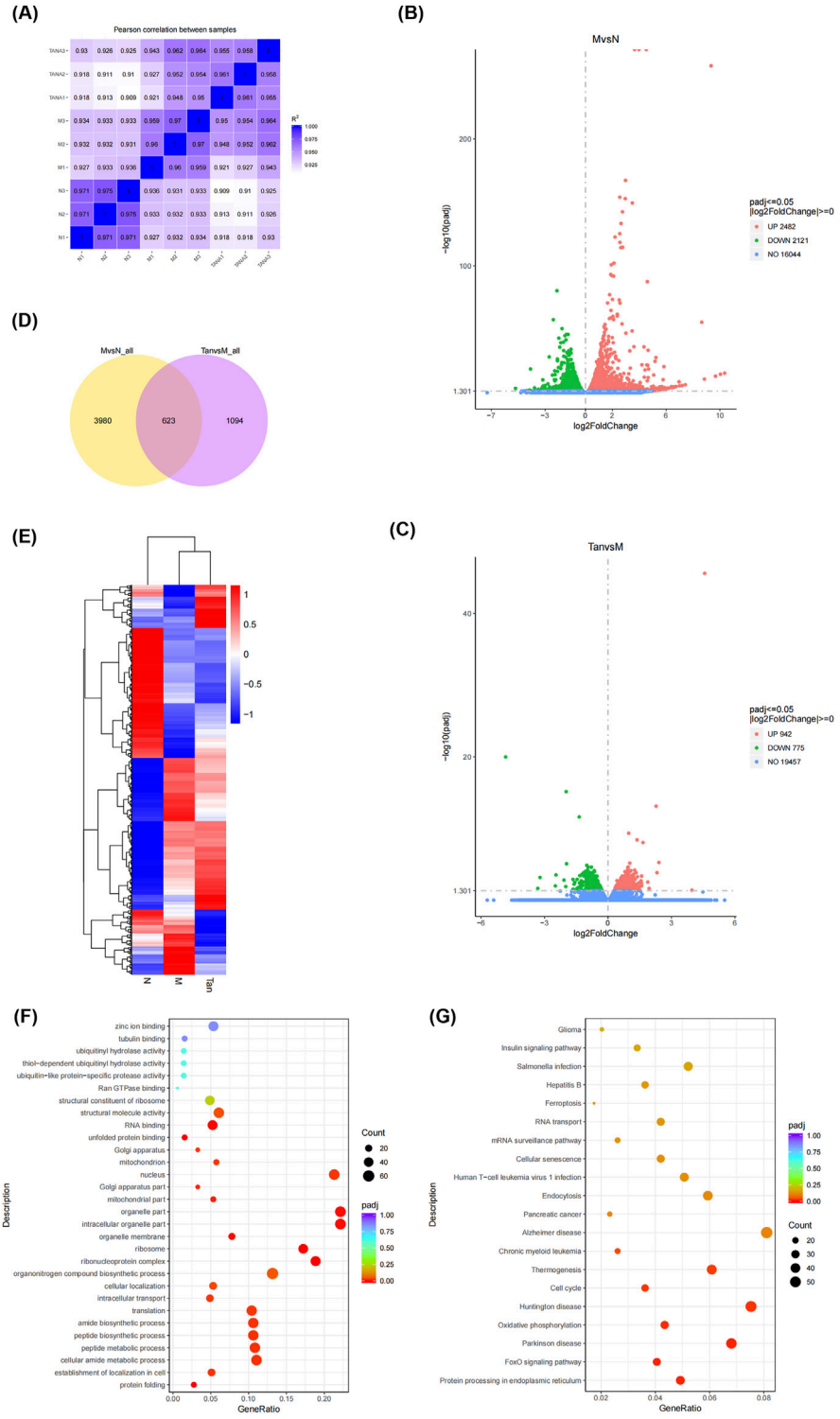

FIGURE 2
Gene differential expression analysis. Notes: **(A)** Gene correlation analysis between groups; **(B)** volcano plot of differentially expressed genes in the model group and normal group; **(C)** volcano plot of differentially expressed genes in the Tanshinone IIA treatment group and model group; **(D)** venn diagram of differentially expressed genes in the groups; **(E)** clustering heatmap of differentially expressed genes; **(F)** GO enrichment analysis; **(G)** KEGG pathway analysis.

enzymes, accelerate the neovascularization of vascular endothelium in ischemic myocardium, promote angiogenesis, inhibit lipid peroxidation reactions during MIRI and alleviate the inflammatory response of myocardial vascular endothelium. Thus, it improves the function of damaged vascular endothelium after I/R injury and has a definite protective effect on acute MIRI in

10.3389/fphar.2024.1510380

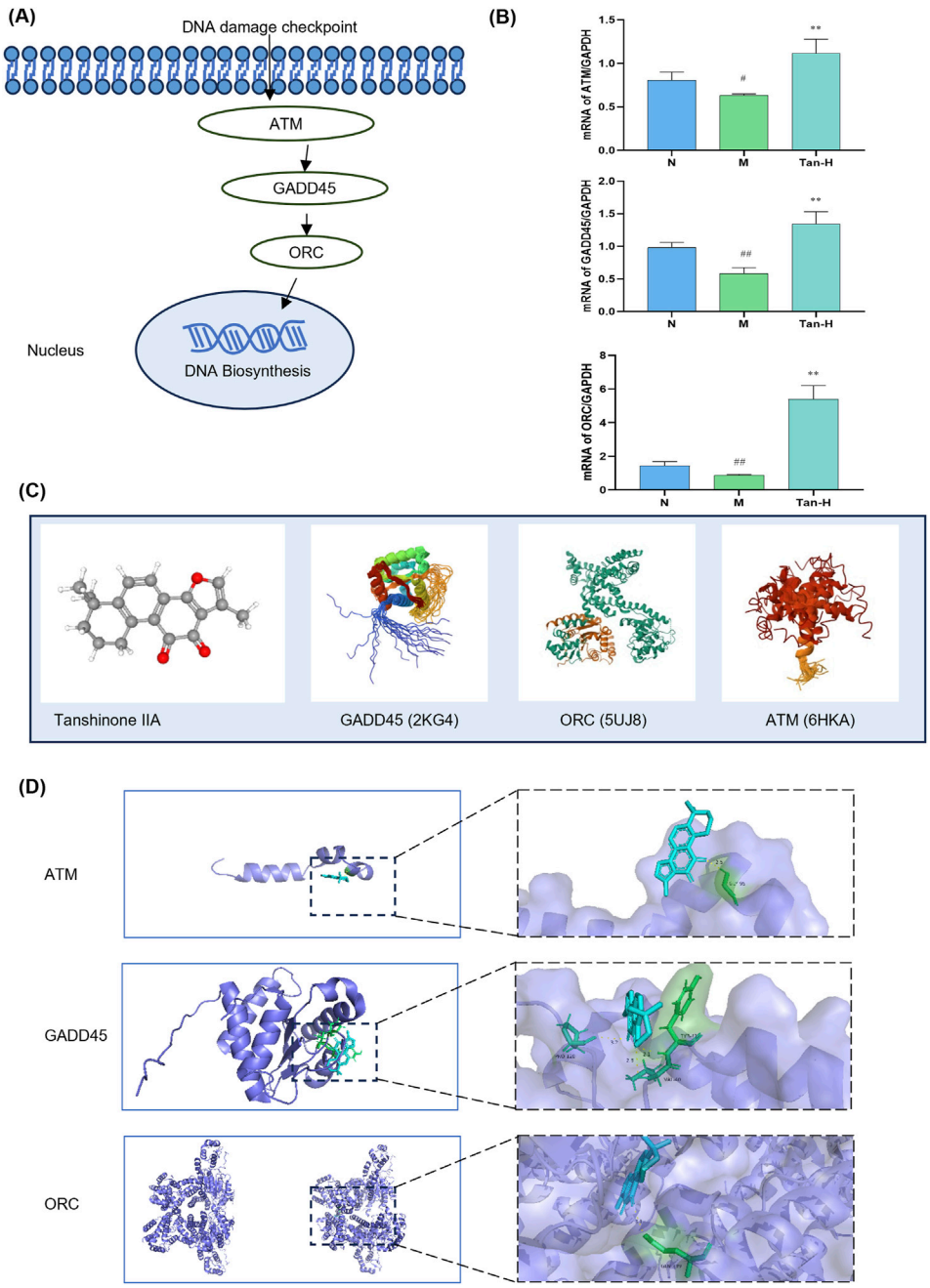

FIGURE 3
Pathway validation. Notes: **(A)** ATM/GADD45/ORC pathway; **(B)** mRNA expression of ATM, GADD45 and ORC in H9C2; **(C)** molecular structure of Tanshinone IIA and pathway-related proteins; **(D)** molecular docking image of Tanshinone IIA and pathway-related protein. $^{\#}p < 0.05$ vs. the normal group, $^{\#\#}p < 0.01$ vs. the normal group, $^{**}p < 0.01$ vs. the model group (n = 6, mean ± sd).

rabbits. Researchers have used various cells and experimental animals to establish different models of MIRI, and all have shown that Tanshinone IIA has a preventive and therapeutic effect on MIRI. It is considered that the effect of Tanshinone IIA to this disease model has been proved and there is no need to add a positive drug to certify its therapeutic effect. Besides, the mechanisms of commonly used positive drugs in ischemic cardiovascular disease are not accordant with the mechanism studied in the research. As a result, the positive control was not mentioned in the whole study.

In this study, the myoblast cell line H9C2 was deprived of oxygen and glucose to establish an MIRI model *in vitro*. Tanshinone IIA was added at the same time to simulate MIRI. In terms of cell viability, morphology and migration, significant differences were detected between the normal group and the model group, indicating the success of the cell model. A statistically significant difference existed between the model group and the Tanshinone IIA treatment groups. These findings suggest that Tanshinone IIA can reduce myocardial apoptosis caused by MIRI. In addition, the EdU staining results revealed that Tanshinone IIA treatment relieved

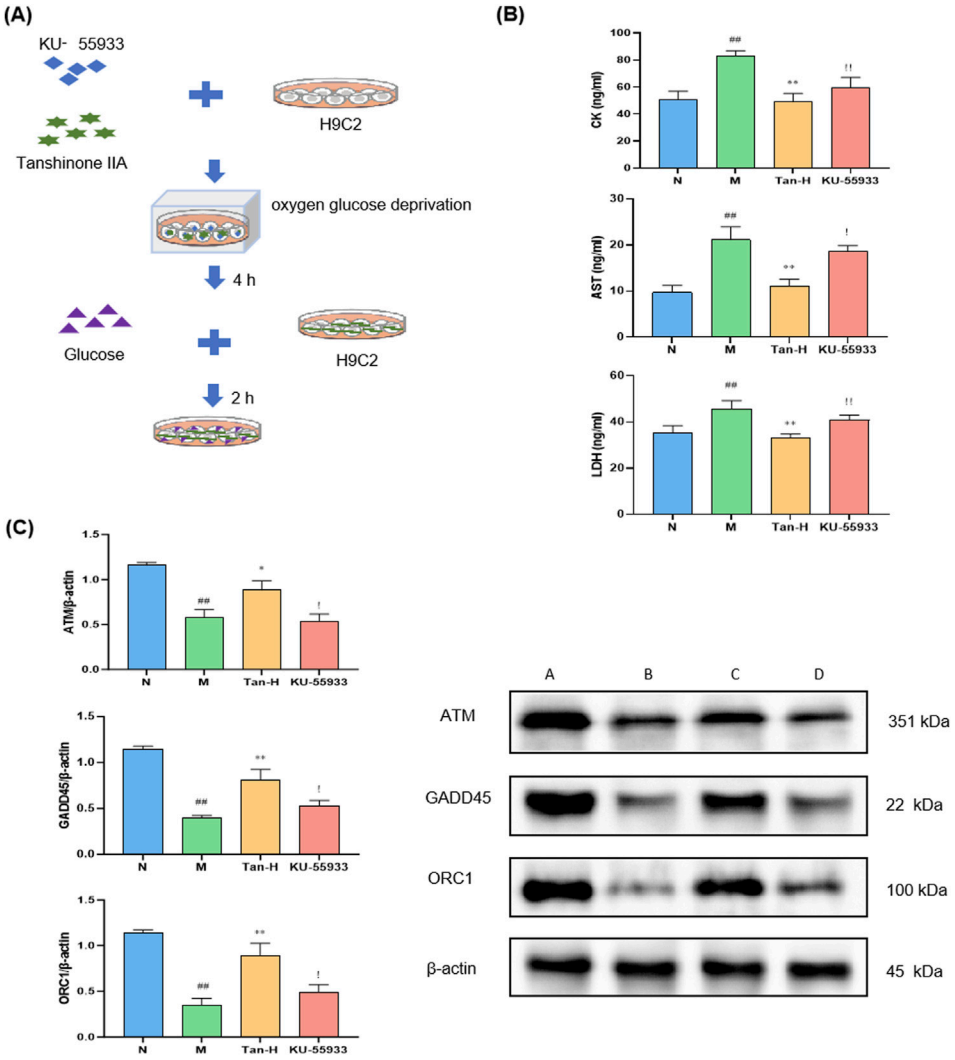

FIGURE 4
Pathway validation through ATM inhibitor. Notes: **(A)** Cell culture and treatment; **(B)** changes in the level of CK, AST and LDH in H9C2; **(C)** expression of ATM, GADD45 and ORC in H9C2. $^{\#}p < 0.05$ vs. the normal group, $^{\#\#}p < 0.01$ vs. the normal group; $^{*}p < 0.05$ vs. the model group, $^{**}p < 0.01$ vs. the model group; $^{!}p < 0.05$ vs. the Tanshinone IIA treatment group, $^{!!}p < 0.01$ vs. the Tanshinone IIA treatment group (n = 6, mean ± sd).

the decrease in myocardial cell viability and abnormal proliferation caused by MIRI.

After modelling, cardiac biomarkers were measured to verify the effect of Tanshinone IIA on myocardial protection from MIRI. CK, AST and LDH are cardiac markers commonly used in the clinic. The expression levels can be used to quantify the extent of MIRI (Toldo et al., 2018). In this study, the levels of CK, AST and LDH decreased, and the cell viability increased significantly after treatment. These findings suggest that Tanshinone IIA may reduce inflammation, improve myocardial cell apoptosis and thereby protect against MIRI.

Then, transcriptomic sequencing was performed to analyse the differences in gene expression between the groups. According to the transcriptomic sequencing results, many genes exhibited differences among the groups. Many genes were enriched in the cell cycle pathway. ATM, GADD45 and ORC are key genes in the cell cycle pathway, and their transcriptomic sequencing results also differ greatly.

The RT–qPCR results revealed that Tanshinone IIA can increase the mRNA expression of ATM, GADD45 and ORC in cardiomyocytes damaged by MIRI. On the basis of the gene differential analysis and RT–qPCR results, we can speculate that Tanshinone IIA can repair DNA damage and promote DNA biosynthesis by stimulating key factors involved in the ATM/GADD45/ORC pathway (Figure 5). The molecular docking results revealed the combination of Tanshinone IIA with these three proteins, which may provide additional evidence supporting the above conjecture.

ATM, GADD45 and ORC are key proteins involved in ATM signaling pathway. ATM is a serine–threonine protein kinase. It is the key factor in the DNA damage response. It can phosphorylate p53 and Chk2 (Li and Stern, 2005; Meulmeester et al., 2005). Therefore, the interaction between MDM2 and p53 is inhibited, which can increase p53 levels, inhibit the cell cycle, and trigger checkpoint and DNA repair activation (Kastan and Lim, 2000). P53 can bind with GADD45 in the promoter region and transcriptionally activate it (Kim et al., 2013). GADD45 is also a crucial protein in DNA repair. It can stimulate p38-JNK mitogen-

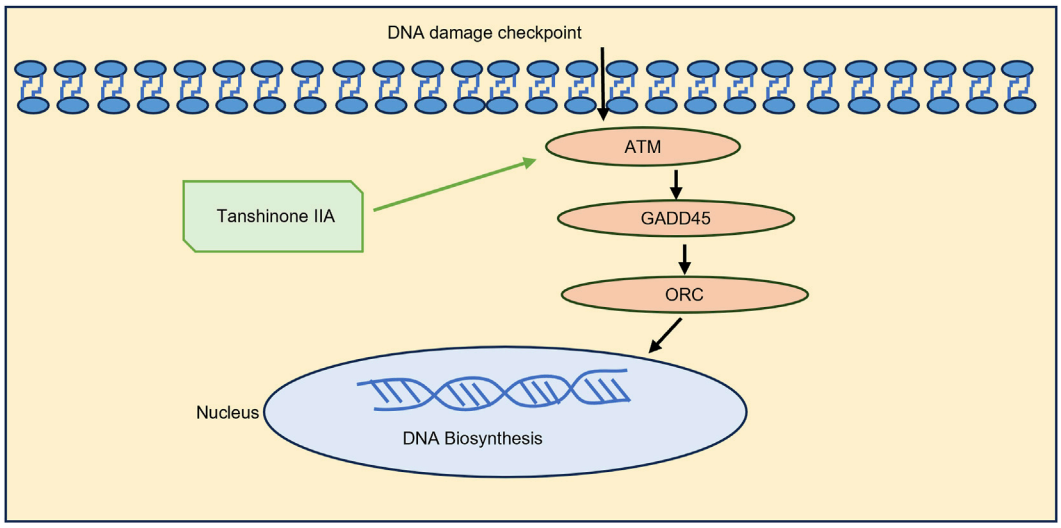

FIGURE 5
Mechanism by which Tanshinone IIA improves myocardial damage caused by MIRI.

activated protein kinase (MAPK), mediating the immune response (Rodríguez-Jiménez et al., 2021). GADD45 expression is related to ROS production and the activation of NADPH oxidase, which potentially promotes the counter-regulation of oxidative damage (Wan et al., 2000; De La Fuente et al., 2009). On the other hand, active Chk2 can amplify DNA damage signals (Li and Stern, 2005). Its key substrate, CDC25A, can activate CDK2 (Ditano et al., 2021), thereby activating ORC. The ORC is the origin of DNA replication and can regulate the cell cycle (Ohta et al., 2003). The increased expression of these three genes can improve DNA repair and new DNA biosynthesis. To verify the above findings, an ATM inhibitor was used for cell treatment. KU-55933 was used in cell culture together with Tanshinone IIA to inhibit the expression of ATM. The levels of CK, AST, and LDH in the cell supernatant of the inhibitor group were markedly elevated compared to those observed in the Tan-H group. Furthermore, the Western blot analysis demonstrated that Tanshinone IIA markedly enhanced the protein expression levels of ATM, GADD45, and ORC1 through ATM activating.

The experimental findings indicate that Tanshinone IIA mitigates myocardial ischemia-reperfusion injury in cardiac cells. The mechanism could be linked to the activation of the ATM/GADD45/ORC pathway.

Data availability statement

The data presented in the study are deposited in Zenodo, accession DOI: 10.5281/zenodo.14284052. It can be accessed through the URL: https://zenodo.org/records/14284052.

Ethics statement

Ethical approval was not required for the studies on animals in accordance with the local legislation and institutional requirements because only commercially available established cell lines were used.

Author contributions

YS: Conceptualization, Methodology, Writing–original draft, Writing–review and editing. JD: Data curation, Formal Analysis, Methodology, Writing–review and editing. DZ: Data curation, Formal Analysis, Methodology, Writing–review and editing. ZS: Conceptualization, Investigation, Methodology, Supervision, Writing–review and editing.

Funding

The author(s) declare that no financial support was received for the research, authorship, and/or publication of this article.

Conflict of interest

The authors declare that the research was conducted in the absence of any commercial or financial relationships that could be construed as a potential conflict of interest.

Generative AI statement

The author(s) declare that no Generative AI was used in the creation of this manuscript.

Publisher's note

All claims expressed in this article are solely those of the authors and do not necessarily represent those of their affiliated organizations, or those of the publisher, the editors and the reviewers. Any product that may be evaluated in this article, or claim that may be made by its manufacturer, is not guaranteed or endorsed by the publisher.

References

Cao, C., Qi, Y. T., Wang, A. A., Wang, Z. Y., Liu, Z. X., Meng, H. X., et al. (2023). Huoxin pill reduces myocardial ischemia reperfusion injury in rats via TLR4/NFκB/NLRP3 signaling pathway. *Chin. J. Integr. Med.* 29 (12), 1066–1076. doi:10.1007/s11655-023-3640-1

Cao, H., Wu, J., Jia, L., and Yang, G. (2017). Progress in study of tanshinone IIA'S pharmacological effects on cardiovascular system. *World J. traditional Chin. Med.* 12 (07), 1718–1722. doi:10.3969/j.issn.1673-7202.2017.07.059

Chen, J. (2012). The roles of MDM2 and MDMX phosphorylation in stress signaling to p53. *Genes and Cancer* 3 (3-4), 274–282. doi:10.1177/1947601912454733

Chen, J. (2016). The cell-cycle arrest and apoptotic functions of p53 in tumor initiation and progression. *Cold Spring Harb. Perspect. Med.* 6 (3), a026104. doi:10.1101/cshperspect.a026104

Chen, R., Chen, W., Huang, X., and Rui, Q. (2021). Tanshinone IIA attenuates heart failure via inhibiting oxidative stress in myocardial infarction rats. *Mol. Med. Rep.* 23 (6), 404. doi:10.3892/mmr.2021.12043

De La Fuente, H., Lamana, A., Mittelbrunn, M., Perez-Gala, S., Gonzalez, S., García-Diez, A., et al. (2009). Identification of genes responsive to solar simulated UV radiation in human monocyte-derived dendritic cells. *PLoS ONE* 4 (8), e6735. doi:10.1371/journal.pone.0006735

Ditano, J. P., Sakurikar, N., and Eastman, A. (2021). Activation of CDC25A phosphatase is limited by CDK2/cyclin A-mediated feedback inhibition. *Cell Cycle* 20 (13), 1308–1319. doi:10.1080/15384101.2021.1938813

Feng, K., Li, W., Wang, X., Wu, Y., Zhang, H., Liu, X., et al. (2022). Chemical components and pharmacological action for Salviae Miltiorrhizae Radix et Rhizoma and predictive analysis on quality markers. *Chin. Traditional Herb. Drugs* 53 (02), 609–618. doi:10.7501/j.issn.0253-2670.2022.02.031

Gao, S., Li, L., Li, L., Ni, J., Guo, R., Mao, J., et al. (2019). Effects of the combination of tanshinone IIA and puerarin on cardiac function and inflammatory response in myocardial ischemia mice. *J. Mol. Cell. Cardiol.* 137, 59–70. doi:10.1016/j.yjmcc.2019.09.012

Gatz, S. A., and Wiesmüller, L. (2006). p53 in recombination and repair. *Cell Death Differ.* 13 (6), 1003–1016. doi:10.1038/sj.cdd.4401903

Hu, H., Zhai, C., Qian, G., Gu, A., Liu, J., Ying, F., et al. (2015). Protective effects of tanshinone IIA on myocardial ischemia reperfusion injury by reducing oxidative stress, HMGB1 expression, and inflammatory reaction. *Pharm. Biol.* 53 (12), 1752–1758. doi:10.3109/13880209.2015.1005753

Hu, T., Zou, H. X., Le, S. Y., Wang, Y. R., Qiao, Y. M., Yuan, Y., et al. (2023). Tanshinone IIA confers protection against myocardial ischemia/reperfusion injury by inhibiting ferroptosis and apoptosis via VDAC1. *Int. J. Mol. Med.* 52 (5), 109. doi:10.3892/ijmm.2023.5312

Kastan, M. B., and Lim, D. S. (2000). The many substrates and functions of ATM. *Nat. Rev. Mol. Cell Biol.* 1 (3), 179–186. doi:10.1038/35043058

Khan, M. A., Hashim, M. J., Mustafa, H., Baniyas, M. Y., Al Suwaidi, S. K. B. M., AlKatheeri, R., et al. (2020). Global epidemiology of ischemic heart disease: results from the global burden of disease study. *Cureus* 12 (7), e9349. doi:10.7759/cureus.9349

Kim, Y.-A., Kim, M. Y., Yu, H. Y., Mishra, S. K., Lee, J. H., Choi, K. S., et al. (2013). Gadd45β is transcriptionally activated by p53 via p38α-mediated phosphorylation during myocardial ischemic injury. *J. Mol. Med.* 91 (11), 1303–1313. doi:10.1007/s00109-013-1070-9

Li, J., and Stern, D. F. (2005). DNA damage regulates Chk2 association with chromatin. *J. Biol. Chem.* 280 (45), 37948–37956. doi:10.1074/jbc.M509299200

Li, Q., Shen, L., Wang, Z., Jiang, H. P., and Liu, L. X. (2016). Tanshinone IIA protects against myocardial ischemia reperfusion injury by activating the PI3K/Akt/mTOR signaling pathway. *Biomed. and Pharmacother. = Biomedecine and Pharmacother.* 84, 106–114. doi:10.1016/j.biopha.2016.09.014

Li, X., Ou, W., Xie, M., Yang, J., Li, Q., and Li, T. (2023). Nanomedicine-based therapeutics for myocardial ischemic/reperfusion injury. *Adv. Healthc. Mater.* 12 (20), e2300161. doi:10.1002/adhm.202300161

Liu, J., Wu, S., Li, L., and Ao, J. (2017). Protective effect of danshen A sodium sulfonate injection on vascular endothelial injury after ischemic preconditioning in rabbits with myocardial ischemia preconditioning. *WORLD Chin. Med.* 12 (03), 618–622. doi:10.3969/j.issn.1673-7202.2017.03.036

Meulmeester, E., Pereg, Y., Shiloh, Y., and Jochemsen, A. G. (2005). ATM-mediated phosphorylations inhibit Mdmx/Mdm2 stabilization by HAUSP in favor of p53 activation. *Cell CycleGeorget. Tex.* 4 (9), 1166–1170. doi:10.4161/cc.4.9.1981

Ohta, S., Tatsumi, Y., Fujita, M., Tsurimoto, T., and Obuse, C. (2003). The ORC1 cycle in human cells: II. Dynamic changes in the human ORC complex during the cell cycle. *J. Biol. Chem.* 278 (42), 41535–41540. doi:10.1074/jbc.M307535200

Qin, W., Xu, J., Yang, T., and Wang, P. (2023). Research progress of tanshinone IIA signaling pathway in the treatment of nerve injury after ischemic stroke. *Chin. Clin. Pharmacol. Ther.* 28 (06), 705–713. doi:10.12092/j.issn.1009-2501.2023.06.014

Ren, Z. H., Tong, Y. H., Xu, W., Ma, J., and Chen, Y. (2010). Tanshinone II A attenuates inflammatory responses of rats with myocardial infarction by reducing MCP-1 expression. *Phytomedicine Int. J. Phytotherapy Phytopharm.* 17 (3-4), 212–218. doi:10.1016/j.phymed.2009.08.010

Rodríguez-Jiménez, P., Fernández-Messina, L., Ovejero-Benito, M. C., Chicharro, P., Vera-Tomé, P., Vara, A., et al. (2021). Growth arrest and DNA damage-inducible proteins (GADD45) in psoriasis. *Sci. Rep.* 11 (1), 14579. doi:10.1038/s41598-021-93780-x

Salameh, A., Dhein, S., Mewes, M., Sigusch, S., Kiefer, P., Vollroth, M., et al. (2020). Anti-oxidative or anti-inflammatory additives reduce ischemia/reperfusions injury in an animal model of cardiopulmonary bypass. *Saudi J. Biol. Sci.* 27 (1), 18–29. doi:10.1016/j.sjbs.2019.04.003

St Clair, S., Giono, L., Varmeh-Ziaie, S., Resnick-Silverman, L., Liu, W. J., Padi, A., et al. (2004). DNA damage-induced downregulation of Cdc25C is mediated by p53 via two independent mechanisms: one involves direct binding to the cdc25C promoter. *Mol. Cell* 16 (5), 725–736. doi:10.1016/j.molcel.2004.11.002

Tian, J., Zheng, Y., Mou, T., Yun, M., Tian, Y., Lu, Y., et al. (2023). Metformin confers longitudinal cardiac protection by preserving mitochondrial homeostasis following myocardial ischemia/reperfusion injury. *Eur. J. Nucl. Med. Mol. Imaging* 50 (3), 825–838. doi:10.1007/s00259-022-06008-z

Toldo, S., Mauro, A. G., Cutter, Z., and Abbate, A. (2018). Inflammasome, pyroptosis, and cytokines in myocardial ischemia-reperfusion injury. *Am. J. Physiology. Heart Circulatory Physiology* 315 (6), H1553–H1568. doi:10.1152/ajpheart.00158.2018

Verma, S., Fedak, P. W. M., Weisel, R. D., Butany, J., Rao, V., Maitland, A., et al. (2002). Fundamentals of reperfusion injury for the clinical cardiologist. *Circulation* 105 (20), 2332–2336. doi:10.1161/01.cir.0000016602.96363.36

Wan, Y., Wang, Z., Shao, Y., Xu, Y., Voorhees, J., and Fisher, G. (2000). UV-induced expression of GADD45 is mediated by an oxidant sensitive pathway in cultured human keratinocytes and in human skin *in vivo*. *Int. J. Mol. Med.* 6 (6), 683–688. doi:10.3892/ijmm.6.6.683

Yang, Y., Wei, Y., and Fang, F. (2020). *Advances in the mechanism of Salvia miltiorrhiza against cardiovascular diseas. Clin. J. Chin. Med.* 12 (21), 37–40+56.

Yao, L., He, F., Zhao, Q., Li, D., Fu, S., Zhang, M., et al. (2023). Spatial multiplexed protein profiling of cardiac ischemia-reperfusion injury. *Circulation Res.* 133 (1), 86–103. doi:10.1161/CIRCRESAHA.123.322620

Yu, S.-W., Andrabi, S. A., Wang, H., Kim, N. S., Poirier, G. G., Dawson, T. M., et al. (2006). Apoptosis-inducing factor mediates poly(ADP-ribose) (PAR) polymer-induced cell death. *Proc. Natl. Acad. Sci. U. S. A.* 103 (48), 18314–18319. doi:10.1073/pnas.0606528103

Yuan, Q., Wang, T., Fu, H., Li, X., and Lei, P. (2024). Research progress on the active ingredients and pharmacological effects of Salvia miltiorrhiza. *Journal of Liaoning University of Traditional Chinese Medicine* 26 (09), 172–179. doi:10.13194/j.issn.1673-842x.2024.09.033

Zhai, P., Chen, Q., Wang, X., Ouyang, X., Yang, M., Dong, Y., et al. (2024). The combination of Tanshinone IIA and Astragaloside IV attenuates myocardial ischemia-reperfusion injury by inhibiting the STING pathway. *Chin. Med.* 19 (1), 34. doi:10.1186/s13020-024-00908-y

frontiers | Frontiers in Pharmacology

TYPE Review
PUBLISHED 14 January 2025
DOI 10.3389/fphar.2024.1467193

OPEN ACCESS

EDITED BY
Xianyu Li,
China Academy of Chinese Medical Sciences, China

REVIEWED BY
Li Yu,
Nanjing University of Chinese Medicine, China
Denglang Zou,
Qinghai Normal University, China

*CORRESPONDENCE
Xu Chen,
chenxu@glmc.edu.cn
Juan Wang,
juanlovelife@163.com,
407271431@qq.com

‡These authors have contributed equally to this work

RECEIVED 19 July 2024
ACCEPTED 18 December 2024
PUBLISHED 14 January 2025

CITATION
Zhao Y, Wu J, Liu X, Chen X and Wang J (2025) Decoding nature: multi-target anti-inflammatory mechanisms of natural products in the TLR4/NF-κB pathway.
Front. Pharmacol. 15:1467193.
doi: 10.3389/fphar.2024.1467193

Decoding nature: multi-target anti-inflammatory mechanisms of natural products in the TLR4/NF-κB pathway

Yue Zhao[1,2], Jiacai Wu[3‡], Xiaolan Liu[1,2‡], Xu Chen [1,2*] and Juan Wang [2,4*]

[1]College of Pharmacy, Guilin Medical University, Guilin, China, [2]Key Laboratory of Pharmacognosy, College of Pharmacy, Guilin Medical University, Guilin, China, [3]College of Intelligent Medicine and Biotechnology, Guilin Medical University, Guilin, China, [4]Guangxi Key Laboratory of Molecular Medicine in Liver Injury and Repair, Guilin Medical University, Guilin, China

Natural products are valuable medicinal resources in the field of anti-inflammation due to their significant bioactivity and low antibiotic resistance. Research has demonstrated that many natural products exert notable anti-inflammatory effects by modulating the Toll-like receptor 4 (TLR4) and nuclear factor kappa B (NF-κB) signaling pathways. The research on related signal transduction mechanisms and pharmacological mechanisms is increasingly being discovered and validated. However, there is currently a lack of comprehensive reviews focusing on the pharmacological mechanisms of natural products targeting the TLR4/NF-κB pathway for anti-inflammatory effects. In light of these considerations, this review comprehensively synthesizes recent research findings concerning the TLR4/NF-κB signaling pathway, including the translocation of TLR4 activation to lysosomes within the cytoplasm, the assembly of protein complexes mediated by ubiquitin chains K63 and K48, and the deacetylation modification of p65. These discoveries are integrated into the classical TLR4/NF-κB pathway to systematically elucidate the latest mechanisms among various targets. Additionally, we summarize the pharmacological mechanisms by which natural products exert anti-inflammatory effects through the TLR4/NF-κB pathway. This aims to elucidate the multitarget advantages of natural products in the treatment of inflammation and their potential applications, thereby providing theoretical support for molecular pharmacology research on inflammation and the development of novel natural anti-inflammatory drugs.

KEYWORDS

natural products, NF-κB pathway, TLR4 pathway, inflammation, molecular pharmacology

1 Introduction

Inflammation represents a nonspecific immune response of the body to pathogenic microorganisms, injurious substances, or other stimulating factors, serving as a fundamental component of the body's immune defense mechanisms (Kotas and Medzhitov, 2015). Though self-limiting inflammation is a physiological response necessary for pathogen clearance, persistent inflammation is detrimental to the organs experiencing inflammation and can trigger systemic reactions in other organs. In particular

chronic inflammatory diseases are considered as one leading cause of mortality worldwide, with over 50% of deaths attributed to inflammation-related diseases (Furman et al., 2019). For instance, sustained inflammation accelerates the progression of atherosclerosis and endothelial dysfunction and then results in joint deformities and loss of function in rheumatoid arthritis (RA) (Aletaha and Smolen, 2018).

Acute and chronic inflammatory reactions often necessitate pharmacological interventions to halt further progression. However, the side effects associated with general chemical anti-inflammatory drugs and antibiotic resistance cannot be ignored, such as weight gain, elevated blood pressure, an increased risk of cataracts and glaucoma, and gastrointestinal disorders (Kavanaugh and Wells, 2014). Furthermore, the issue of antibiotic resistance stemming from certain antibiotic-based anti-inflammatory drugs is a critical concern, with the World Health Organization (WHO) designating bacterial resistance as a major public health crisis (Leung et al., 2011) Underscoring the urgent need to identify anti-inflammatory medications with low adverse reactions and reduced resistance (Wagenlehner and Dittmar, 2022).

Over the past 3 decades, Natural products have emerged as a significant source of novel therapeutics for treating diseases (Newman and Cragg, 2007). In comparison to chemically synthesized drugs, natural product-based medications offer distinct advantages in terms of structural novelty, biocompatibility, and functional diversity, attributes that have been evolutied through extensive natural selection during evolution. Statistics reveal that more than 50% of drugs approved by the United States Food and Drug Administration (FDA) for market authorization from 1939 to 2016 have originated from natural products (Rodrigues et al., 2016). Natural products exhibit superior characteristics of multi-target modulation, broad adaptability, and high safety, showcasing immense potential in the realm of anti-inflammatory properties (HUANG et al., 2018).

With the continuous advancement of life science technologies, research on the pathways of action mechanisms of natural products has become indispensable, given the diverse structures and complex mechanisms of action of plant-based medicines. The NF-κB protein, a transcription factor that regulates the expression of numerous immune-related genes, is present in almost all animal cells (Cai et al., 2022). The TLR4/NF-κB pathway it is involved in plays a crucial role in mediating inflammatory responses, immune reactions, antimicrobial defense, and immune homeostasis. Upon exposure to inflammatory stimuli, such as IL-1, TNF-α or lipopolysaccharide (LPS), the NF-κB signaling pathway is activated. This activation leads to an increase in the expression of key proteins including MyD88, NF-κB inhibitory protein (IκB), and p65, resulting in the translocation of NF-κB to the nucleus where it binds to DNA and promotes the release of pro-inflammatory factors (Doyle and O'Neill, 2006; Gray et al., 2016; O'Neill and Bowie, 2007).

As mentioned earlier, the TLR4/NF-κB pathway plays a significant role in regulating inflammatory signaling. With the rapid development of life science technology, it is necessary to timely summarize the latest research on TLR4/NF-κB, to quickly understand the research status and development trends in this field. Therefore, this review systematically explores the interactions between key targets in the upstream and downstream pathways of TLR4/NF-κB, while also supplementing and incorporating the latest research findings. Such as the membrane translocation after TLR4 activation,the assembly of protein complexes mediated by ubiquitin chains K63 and K48 and the deacetylation of p65 inhibits NF-κB activity. In addition, given the limitations of current chemical anti-inflammatory drugs in clinical applications, this review systematically summarizes the molecular pharmacological mechanisms by which natural products exert anti-inflammatory effects through the TLR4/NF-κB pathway. This will provide an important theoretical basis for the development of natural anti-inflammatory drugs, deepen the understanding of drug mechanisms, guide future research directions, and promote advances in pharmacology.

2 Method

This comprehensive review was performed by searching PubMed, using a time-based filter to capture all potential studies from 2000 to 15 June 2024, and selecting 58 unique, representative, and innovative natural product articles for review, covering as comprehensively as possible various drug doses, modeling methods, and pharmacological mechanisms. We used two types of search strategies, the first type was applied in "TLR4/NF - κ B signaling pathway in inflammation", the search included both "All Field" (TLR4/NF-κB, signal transduction) and "title/abstract" (inflammation, immunity).

The second type was applied in "Anti-inflammatory mechanism of Natural products in the TLR4/NF/κ B pathway", the search included both "All Field" (TLR4/NF-κB, Natural products) and title/abstract (herb, plant compounds, mechanism, signaling pathway, inflammation). Use the logical conjunction 'AND' between the search term 'All Field' and 'Title/Abstract'. All Fields and Title/Abstract were reasonably matched according to the actual search results. In addition, a supplementary search was conducted on the reference list of the included studies.

The botanical names mentioned in this review were cross-checked using the International Plant Names Index (IPNI 2023; www.ipni. org) and The Plant List (TPL 2013; www.theplantlist. org) databases, and the plant names used were "Accepted" in TPL.

3 The application of natural products in inflammation

In the field of inflammatory diseases, especially chronic inflammatory diseases, natural products not only exhibit similar therapeutic effects as steroidal anti-inflammatory drugs, but also have advantages such as low side effects, low drug resistance, and diverse biological activities. Consequently, an increasing number of advanced and innovative mechanisms are being explored by researchers. For instance, some natural products have been developed as immunosuppressants, offering unique targeting capabilities to inhibit immune responses and prevent organ rejection. One example is resveratrol, which activates SIRT1 (a deacetylase) to suppress the transcriptional activity of NF-κB, thereby reducing the production of pro-inflammatory cytokines (Jhou et al., 2017; Mendes et al., 2017). In addition, the establishment of the InflamNat database, in conjunction with

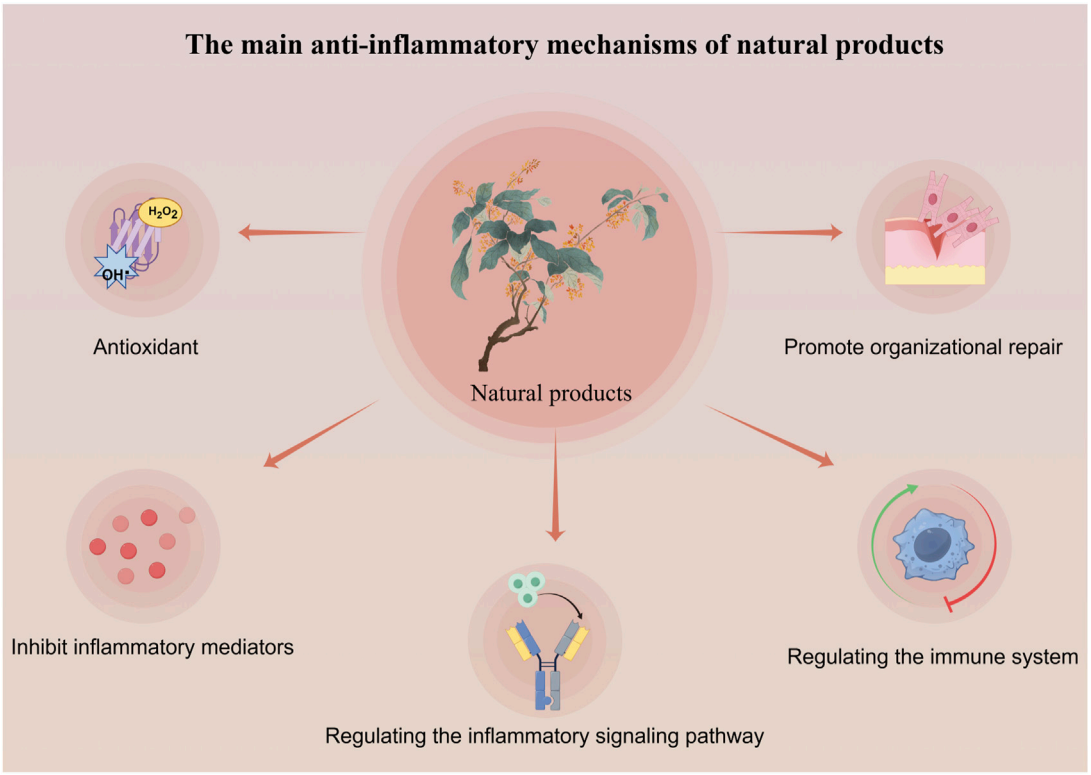

FIGURE 1
The main anti-inflammatory mechanisms of natural product.

network pharmacology, enables researchers to rapidly screen natural products with potential anti-inflammatory activity and predict their mechanisms of action (Zhang et al., 2022; Guo et al., 2024). On this basis, the structural characteristics of natural products also provide new insights for drug design. By studying the structure-activity relationships of these compounds, scientists can identify key structural features to optimize their pharmacological activity (Itoh and Inoue, 2019; Tew et al., 2020). At the same time, innovations in biotechnology such as single-cell multi omics applications, mass spectrometry imaging techniques, and the development of COX-1 and COX-2 inhibitors mimicking nonsteroidal anti-inflammatory drugs have highlighted the potential of natural products in regulating immune responses and inflammation (Nielsen and McNulty, 2019; Hou et al., 2022; Zhu et al., 2022).

Natural products exert anti-inflammatory effects through multi-target and multi-level effects. They can not only regulate common inflammatory signal transduction, but also work synergistically through antioxidant, tissue repair, and immune enhancement pathways (Zhang et al., 2010; Fang et al., 2024; Álvarez-Martínez et al., 2020) (As seen in Figure 1). For example, resveratrol activates SIRT1 to regulate the NF-κB signaling pathway, inhibiting the expression of pro-inflammatory cytokines. It also activates the Nrf2 signaling pathway, promoting the expression of antioxidant enzymes, enhancing cellular resistance to oxidative stress, and reducing oxidative damage associated with inflammation. Additionally, resveratrol promotes the expression of vascular endothelial growth factor (VEGF), facilitating angiogenesis and tissue repair (Baur and Sinclair, 2006). In contrast, conventional anti-inflammatory nonsteroidal drugs like aspirin primarily inhibit cyclooxygenase (COX) to exert their effects, while corticosteroids such as prednisone target a single protein, S6 kinase (S6K), to suppress the mTOR signaling pathway and diminish cellular responses to inflammatory stimuli (Mathiesen et al., 2014; Ng and Yeomans, 2018). Although these conventional therapies may offer more potent anti-inflammatory effects, their long-term use in chronic conditions such as rheumatoid arthritis and ulcerative colitis can lead to adverse reactions that are intolerable for patients. (Natural products in different anti-inflammatory mechanisms of TLR4/NF-κB pathway in Table 1).

With the in-depth research on the pathogenesis of inflammation by molecular biology, various signaling pathways triggering inflammation have attracted widespread attention. We conducted searches through the Web of Science, PubMed, and PubMed Central electronic databases, using terms ranging from subject headings (inflammation) to keywords (inflammation, signaling, mechanism), to retrieve research articles spanning 20 years from 2004 to 2024. Among the 15,000 articles screened, we found that among numerous anti-inflammatory signals, the NF-κB pathway appeared most frequently, accounting for 48.39%. This highlights the crucial role of the NF-κB signaling pathway plays in inflammatory signal transduction (Figure 2).

In conclusion, the TLR4/NF-κB pathway is essential in inflammation regulation. The screening and development of natural products with targeted anti-inflammatory effects represent a novel direction and strategy for treating inflammatory

TABLE 1 Natural products in different anti-inflammatory mechanisms of TLR4/NF-κB pathway.

Main mechanism	Botanical name Compound name	Ref.
Inhibiting TLR4 activated	*Scutellaria baicalensis* Georgi Baicalin	Fu et al. (2020)
	— Ferulic acid	Rehman et al. (2018)
Inhibition of TLR4 expression	*Lycium ruthenicum* Murray Polysaccharide	Peng et al. (2014)
	Sophora flavescens Aiton Oxymatrine	Lu et al. (2017a)
	Glycyrrhiza uralensis Fisch Glycyrrhetinic acid	Shi et al. (2020)
	Glycine max (L.) Merr Genistein	Jeong et al. (2014)
	— Quercetin	Zhao et al. (2021)
Inhibition of MyD88 Expression	*Forsythia suspensa* (Thunb.) Vahl Phillygenin	Hu et al. (2020)
	Echinacea purpurea (L.) Moench Echinacea polysaccharide	Zhang et al. (2020)
	Anemarrhena asphodeloides Bunge Timosaponin B-II	Zhang et al. (2015b)
Inhibition of TAK1 and IRAK1/4 Complex Activation	*Reynoutria japonica* Houtt Polydatin	Jiang et al. (2015)
	Euphorbia pekinensis Rupr Euphorbia Factor L2	Tang et al. (2021)
	Panax ginseng C. A. Mey Ginsenoside Rg5	Kim et al. (2012)
	Cullen corylifolium (L.) Medik Psoralen	Li et al. (2021)
	Paris polyphylla Sm Polyphyllin I	Wang et al. (2018a)
Inhibition of IKK Complex Activation	*Lycoris radiata* (L'Hér.) Herb Narciclasine	Shen et al. (2019)
	Panax notoginseng (Burkill) F.H.Chen Notoginsenoside R1	Jiao et al. (2021)
	— Genistein-3′-sodium sulfonate	Liu et al. (2021)
Inhibition of TRAF6 Expression and Ubiquitination	*Angelica gigas* Nakai Nodakenin	Rim et al. (2012)
	Catharanthus roseus (L.) G. Don Tabersonine	Zhang et al. (2018)
Inhibition of IκBα Degradation and Ubiquitination	*Myristica fragrans* Houtt Myrislignan	Jin et al. (2012)
	Epimedium brevicornu Maxim Icariside II	Zhou et al. (2019)
	Waltheria indica L Antidesmone	Lu et al. (2017b)
Deacetylation of p65	*Coptis chinensis* Franch Berberine	Zhang et al. (2023)

(Continued on following page)

TABLE 1 (*Continued*) Natural products in different anti-inflammatory mechanisms of TLR4/NF-κB pathway.

Main mechanism	Botanical name Compound name	Ref.
	— Resveratrol	Jhou et al. (2017)
Inhibition of p65 phosphorylation and nuclear translocation	*Rabdosia rubescens* (Hemsl.) H. Hara Oridonin	Li et al. (2018)
	Panax notoginseng (Burkill) F. H. Chen Ginsenoside B	Ran et al. (2018)
	Siraitia grosvenorii (Swingle) C. Jeffrey ex A. M. Lu and Zhi Y. Zhang Mogroside V	Han et al. (2024)
	Lindera aggregate (Sims) Kosterm Evodiamine	Fan et al. (2017)

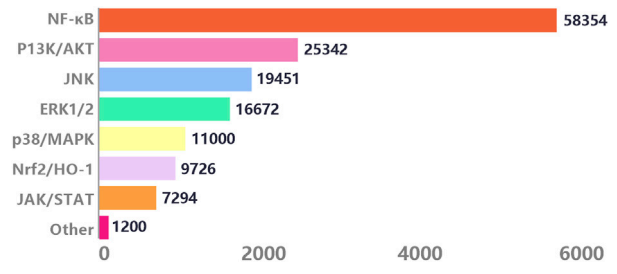

FIGURE 2
Journal analysis of inflammatory signaling pathways from 2019 to 2014.

diseases, while also advancing the modernization and clinical application of natural products.

4 TLR4/NF-κB signaling pathway in inflammation

4.1 The structure and activation of TLR4

4.1.1 TLR4 structure

TLR4, a member of the Toll-like receptor family, is a type I transmembrane protein discovered by Poltorak in 1998 (Fitzgerald and Kagan, 2020). Encoded by the TLR4 gene, it is expressed in various tissue cells, including monocytes and macrophages. TLR4 is mainly activated by LPS, a crucial immunoactivating factor derived from the surface of various bacteria (*Escherichia coli*, *Salmonella* spp.,*Pseudomonas aeruginosa*, *Vibrio cholerae*, *Enterobacter* spp. et al.). It is a characteristic component of the outer membrane of Gram-negative bacteria, playing a vital role in bacterial structure while also being recognized by the host immune system, thereby triggering a cascade of immune responses (Fitzgerald and Kagan, 2020).

The extracellular domain of TLR4 is a member of the leucine-rich repeat (LRR) family, playing a crucial role in ligand recognition and receptor dimerization. TLR4 exhibits a characteristic curved solenoid structure, with the myeloid differentiation protein 2 (MD2) intricately embedded within it (Kim et al., 2005; Kelley et al., 2013). When LPS binds to MD2, the LRR specifically recognizes the pattern recognition of related molecules (PAMP) and sends a signal to MD2, leading to TLR4 dimerization (Akashi et al., 2000). The intracellular domain of TLR4 is characterized by a conserved TIR domain that exhibits significant homology to the IL-1 receptor. Upon stimulation by extracellular MD2, the intracellular TIR domain is capable of initiating downstream NF-κB signaling transduction (Liu et al., 2014).

4.1.2 Activation of TLR4 signaling pathway

Upon invasion of the body by bacteria, the LPS present in the bacterial outer membrane is selectively identified and bound by TLR4, subsequently initiating the TLR4 signaling cascade. Lipid A, the hydrophobic component of LPS, initially attaches near the cell membrane as an endotoxin, and subsequently associates with a cluster of differentiation 14 (CD14) to form a complex. CD14, as the activation site of TLR4, can disassemble the LPS aggregates into monomeric molecules (Alarcón-Vila et al., 2020; Fitzgerald and Kagan, 2020; Alarcón-Vila et al., 2020). Subsequently, individual LPS molecules bind to MD-2, then cause the activation of TLR4 (Figure 3). After activation, the external structure and conformation of TLR4 is changed, leading to dimerization of the intracellular TIR domain. The dimerized TIR domain is recognized by TIR through TIR-TIR interactions. After recognition, it will lead to the occurrence of so-called "Myddosome" and "Triffosome" phenomena on the cell surface. The downstream signaling of the "Myddosome" involves the participation of MyD88 and MyD88 adapter-like (Haftcheshmeh et al.) proteins, along with the transitional role of TIR domain-containing adaptor protein (TIRAP) (Bonham et al., 2014; Akira, 2003). On the contrary, the "Triffosome" pathway is composed of TIR domain-containing adaptor-inducing interferon-β (TRIF) and TRIF-related adaptor molecule (TRAM) (Kagan et al., 2008). The different assembly complexes initiate different immune responses, thereby activating MyD88-dependent and the TRIF-dependent two TLR4-NF-κB pathways within the cells (Anderberg et al., 2017).

In the MyD88-dependent signaling pathway, the TIR domain carries a positive charge and binds to Mal protein with a negative charge through electrostatic forces. Upon binding, MyD88 is recruited to the activated TLR4 complex, initiating the MyD88-dependent signaling pathway. Activated interleukin receptor-associated kinases (IRAKs), such as IRAK1, IRAK2, and IRAK4,

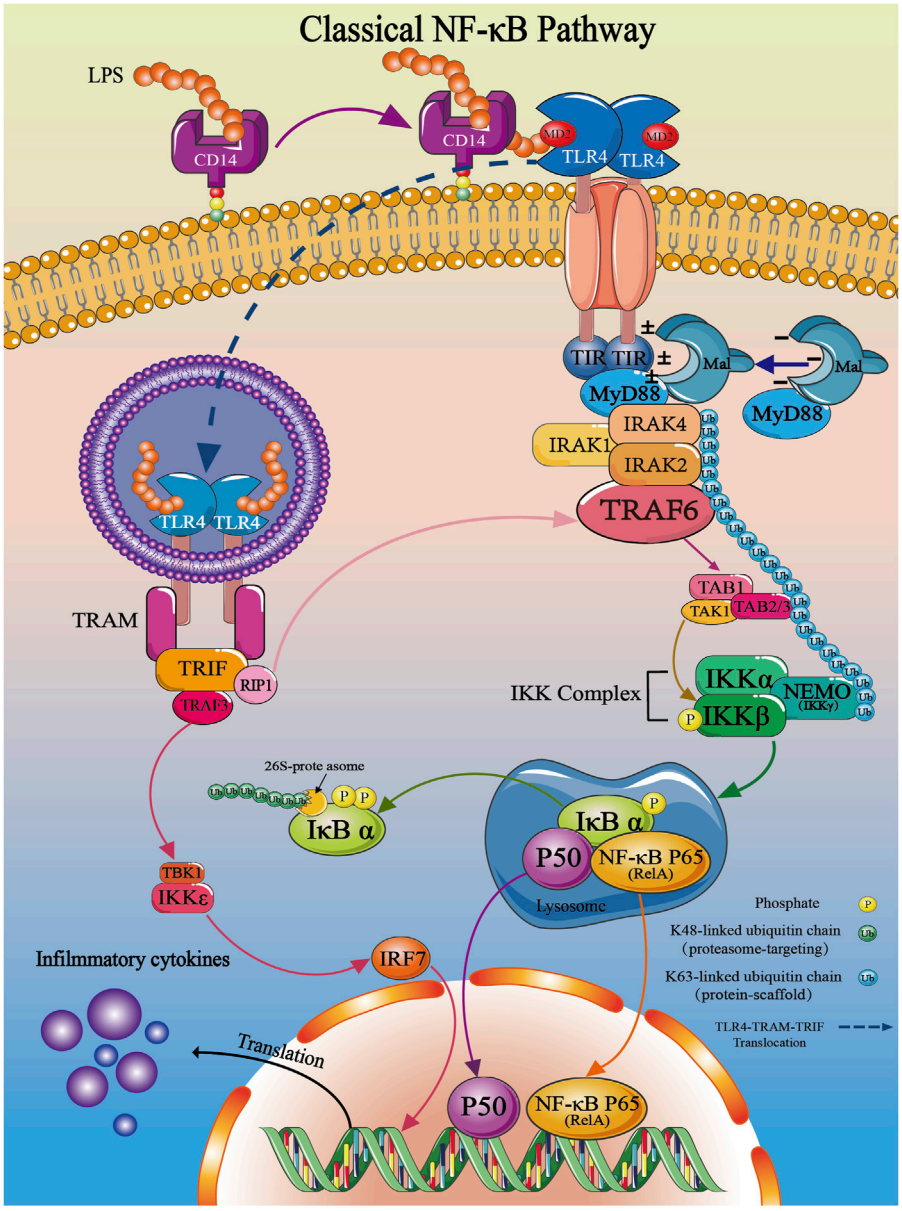

FIGURE 3
Overview of the TLR4/NF-κB classical signal pathway.

then activate tumor necrosis factor receptor-associated factor 6 (TRAF6), ultimately resulting in the activation of NF-κB (Figure 3) (Park and Lee, 2013; Tanimura et al., 2008). In another TRIF-dependent signaling pathway, TLR4 recruits TRIF and TRAM, which contains a TIR domain. As a substrate of protein kinase Cε (PKCε), TRAM allows it to target to the plasma membrane through its N-terminal myristoylation. Upon LPS stimulation, within 120 min, TRAM and TRIF translocate together with TLR4 into the endosome (Kobayashi et al., 2006; Rowe et al., 2006; Tanimura et al., 2008). During this stage, TRIF initiates the recruitment of tumor necrosis factor receptor-associated factor 3 (TRAF3) and receptor-interacting protein-1 (RIP1), resulting in TRAF3 self-ubiquitination and the formation of a complex with Tbk1 and IKKε. Subsequent phosphorylation of Tbk1 and IKKε leads to the activation of interferon regulatory factor 3 (IRF3) (Zanoni et al., 2011). IRF3 then forms homodimers and heterodimers with IRF7, binds to specific DNA sequences in the cell nucleus, and transcribes interferons (IFNs) and IFN-induced genes. Additionally, TRIF is capable of activating NF-κB by recruiting TRAF6 (late activation) (Figure 3) (Weiss and Barker, 2018). Through transient transfection experiments, Xiaoqin Su demonstrated the association between TRIF and TRAF6 (Sato et al., 2003; Jiang et al., 2004). Additionally, three TRAF6 binding motifs were found in TRIF, indicating the specific interaction between TRIF and TRAF6, resulting in the activation of NF-κB signaling pathways downstream (Ye et al., 2002). Hence, TIRAP and TRAM can be seen as 'sorting adaptors' that are involved in determining the subcellular

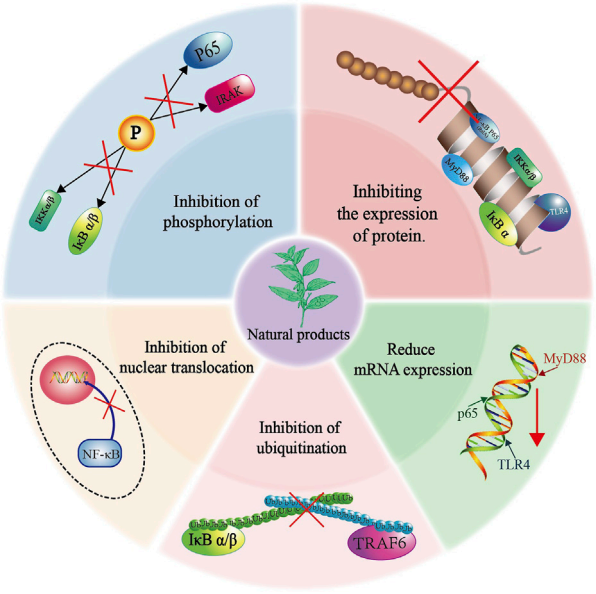

FIGURE 4
Mechanisms of Natural products' anti-inflammatory effects based on the NF-κB pathway.

placement of TLR signaling or the particular pathways that are triggered (Kagan, 2012; Di Lorenzo et al., 2022).

After activation of TRAF6, it exerts ubiquitination effects to activate IκB kinase (IKK) signaling: TRAF6, functioning as an E3 ubiquitin ligase, forms a ubiquitin ligase complex with the E2 conjugating enzyme complex UBC13-Uev1a, generating free K63-linked polyubiquitin chains (K63) to exert multiple ubiquitin effects (Deng et al., 2000; Wooff et al., 2004; Newton et al., 2008; Skaug et al., 2009; Xu et al., 2009). The formed K63 sequentially links IRAK1/2/4-TAK1-TAB1/2/3-NEMO (IKKγ) in the order of signal transduction, facilitating signal transduction among these proteins. Among them, transforming growth factor-β-activated kinase 1 (TAK1), upon receiving signals from free K63 polyubiquitin chains, activates TAK1-binding protein 1/2/3 (TAB1/2/3) signals to form a complex, leading to IKKβ phosphorylation, degradation of IKKβ, and initiation of NF-κB nuclear translocation (Figure 3) (Adhikari et al., 2007). Therefore, it is evident that unanchored free K63 chains play a pivotal role in the activation of IKK (Xia et al., 2009). Until now, four distinct types of ubiquitin chains-K11, K48, K63, and M1 chains have been implicated in the canonical NF-κB activation pathway (Figure 3) (Adhikari et al., 2007). Nevertheless, the precise mechanisms underlying the roles of K11 and M1 chains remain ambiguous, necessitating additional research in subsequent studies (Jin et al., 2008; Xu et al., 2009; Iwai, 2012).

4.2 The structure and activation of classic NF-κB

4.2.1 The structure and inflammation of NF-κB

In mammals, five proteins, namely, p65 (RelA), RelB, c-Rel, p50 (NF-κB 1; and its precursor p105), and p52 (NF-κB 2; and its precursor p100) are classified as members of the NF-κB family. NF-κB protein family is a multifunctional transcription factor. Upon stimulation by LPS, oxidative stress, inflammatory cytokines, free radicals, or bacteria, the NF-κB protein family can specifically bind to κB sites in the promoter regions of various genes, promoting the transcription and translation of target genes, and it serves as an upstream regulatory protein for various downstream effector factors. Through the regulation of inflammatory cytokines, adhesion molecules, chemokines, and surface receptors, it participates in the regulation of immune responses, cell apoptosis, and tumorigenesis (Chen et al., 2011). NF-κB has classical and non-classical pathways two distinct signaling pathways, each pathway owns specific activation mechanisms (Sun, 2011; Cildir et al., 2016; Sun, 2017). The activation of the NF-κB pathway is initiated by diverse external stimuli that trigger the production and secretion of pro-inflammatory cytokines such as TNF-α, IL-1, IL-6, and so on (Zhang K. et al., 2015). In a state of homeostasis, the proteins p65 and p50 are confined to the cytoplasm by the IκB, resulting in the masking of their nuclear localization sequences and hindering their movement into the nucleus for DNA binding. The κB proteins possess a Rel-homology-domain (RHD) which facilitates their ability to bind to DNA, form dimers, and translocate into the nucleus. Among the five NF-κB family proteins, only p65, RelB, and c-Rel contain a transcriptional activation domain (TAD) that is responsible for activating target genes (Sehnert et al., 2020). The IKK complex consists of two homologous catalytic subunits, IKKα (IKK1) and IKKβ (IKK2), as well as a regulatory subunit, IKKγ (NF-κB essential modulator, NEMO) (Häcker and Karin, 2006). IKKβ plays a crucial role in initiating the classical NF-κB signaling pathway in response to pro-inflammatory cytokines and microbial stimuli, whereas IKKα predominantly governs the activation of the non-canonical NF-κB pathway (Israël, 2010; Ruland, 2011).

During homeostasis, the IκB confines the proteins p65 and p50 to the cytoplasm, thereby masking their nuclear localization sequences and preventing their entry into the nucleus to bind DNA. The κB proteins possess a Rel-homology-domain (RHD) which facilitates they binding to DNA, form dimers, and translocate into the nucleus. Within the NF-κB protein family, only p65, RelB, and c-Rel possess a transcriptional activation domain (TAD) that is accountable for triggering target genes. The IKK complex is made up of two similar catalytic components, IKKα (also named IKK1) and IKKβ (also referred to as IKK2), along with a regulatory subunit called IKKγ (also called NF-κB essential modulator or NEMO) (Häcker and Karin, 2006). IKKβ is essential for starting the traditional NF-κB signaling pathway when pro-inflammatory cytokines and microbial stimuli are present, while IKKα mainly controls the non-canonical NF-κB pathway activation.

4.2.2 Activation of NF-κB signaling pathway

TAK1 phosphorylation leads to the binding of IKKs to the N-terminus of NEMO. Following this, IKKα/β/γ goes through oligomerization and phosphorylation, leading to the activation of IKKβ (Häcker and Karin, 2006; Ghosh and Hayden, 2008). When activated, IKKβ starts the process of phosphorylating IκB-α proteins, which then leads to their degradation through K48-linked ubiquitination by the 26S-proteasome (Gallo et al., 2017). The breakdown of IκB-α reveals the nuclear localization sequence (NLS) of cytoplasmic p65, which helps the p50/p65 dimer move

into the nucleus (Hayden and Ghosh, 2008; Wertz and Dixit, 2010). In the nucleus, the NF-κB dimer (p50/p65) interacts with promoter regions of chromosomal loci, facilitating the transcription of target genes (Figure 3) (Hoffmann et al., 2006; Hayden and Ghosh, 2008).

5 Anti-inflammatory mechanism of natural products in the TLR4/NF/κB pathway

The potential of Natural products in modulating the TLR4/NF-κB signaling pathway for the treatment of inflammation has garnered widespread attention among researchers. In inflammatory responses, Natural products effectively inhibit the expression of TLR4, thereby interrupting its recognition of pathogen-released LPS from bacteria, viruses, and other pathogens, thus preventing the activation of the NF-κB signaling pathway. Furthermore, Natural products can reduce the protein expression of pro-inflammatory factors, and inhibit IκB's phosphorylation and ubiquitination processes, thereby influencing the signal transmission of the NF-κB pathway. Some Natural products even prevent NF-κB from entering the cell nucleus, hinder its binding with DNA, and consequently reduce the expression of pro-inflammatory factors, ultimately exerting anti-inflammatory effects (Figure 3). Based on the TLR4/NF-κB signaling pathway described earlier, we will categorize the mechanisms of action of Natural products at various targets and systematically summarize the molecular mechanisms by which Natural products exert anti-inflammatory effects in the TLR4/NF-κB pathway.

5.1 Inhibiting TLR4 activated by LPS

Fu et al. (2020) confirmed that baicalin extracted from Rhizoma Scutellaria baicalensis Georgi. [Lamiaceae] can reduce CD14 protein and mRNA expression through a CD14-dependent mechanism, inhibiting TLR4 activation and alleviating LPS-induced inflammatory responses. Furthermore, in a RAW264.7 cell model with CD14 knockout, the inhibition effect of baicalin on the inflammatory response induced by LPS was reversed. Additionally, Shafiq Ur Rehman et al. (2018) showed that ferulic acid (FA) can disrupt the binding site of the TLR4/MD2 complex, inhibiting TLR4 activation by LPS, which is crucial for triggering neuroinflammation through microglial cell activation.

5.2 Inhibition of TLR4 expression

Peng et al. (2014) found that the fruit of *Lycium ruthenicum* Murray. [Solanaceae] polysaccharide LRGP3 reduced the protein and mRNA expression of TLR4, leading to decreased levels of pro-inflammatory cytokines IL-1, IL-6, and TNF-α in the macrophages. Oxymatrine (OM), extracted from Root of *Sophora flavescens* Aiton. [Fabaceae], was shown to inhibit TLR4 levels in LPS-stimulated MS1 cells and the translocation of p65 to the cell nucleus, thereby reducing the release of IL-1β and alleviating the inflammatory response (Lu M. et al., 2017). Shi et al. (2020) found that glycyrrhetinic acid (GL) from the Rhizome of *Glycyrrhiza uralensis* Fisch. [Fabaceae] could inhibit TLR4 expression in the hepatitis virus (MHV) infection mouse, affect the HMGB1-TLR4 immune regulatory axis, and serve as a hepatoprotective factor in hepatic infectious diseases. Jeong et al. (2014) Jeong demonstrated that genistein attenuated the pro-inflammatory response of BV2 microglial cells stimulated by LPS, inhibited the binding of LPS to TLR4 in BV2 microglial cells and then weakened the downstream NF-κB signaling transduction. Le et al. (2020) found that quercetin exerted neuroprotective effects on HIBI mice by inhibiting TLR4 activation, thereby reducing oxidative stress and inflammatory responses in activated microglial cells.

5.3 Inhibition of MyD88 expression

Phillygenin (PhI) from Fruit of *Forsythia suspensa* (Thunb.) Vahl. [Oleaceae] is a lignan compound that can inhibit the expression of MyD88 protein, and then suppress LPS-induced pro-inflammatory responses and LX2 cell activation, thereby inhibiting liver fibrosis (Hu et al., 2020). Zhang et al. (2020) investigated that *Echinacea* polysaccharide (EP) from the Root of *Echinacea purpurea* (L.) Moench. [Asteraceae] alleviated LPS-induced lung injury by inhibiting MyD88 expression and downregulating the TLR4/NF-κB signaling pathway. Zhang T. et al. (2015) discovered that timosaponin B-II (TB) from the Rhizome of *Anemarrhena asphodeloides* Bunge. [Asparagaceae], a major bioactive component in *anemarrhena asphodeloides*, inhibited MyD88 expression in LPS-induced ALI mice.

5.4 Inhibition of TAK1 and IRAK1/4 complex activation

Jiang et al. (2015) found polydatin (PD) from the Root of *Polygonum Reynoutria japonica* Houtt. [Polygonaceae] inhibit the activation of IRAK1 and IRAK4, regulate NF-κB signal transduction, and alleviate acute lung injury in mice. Tang et al. (2021) demonstrated that *Euphorbia* factor L2 (EFL2) extracted from the Seed of *Euphorbia pekinensis* Rupr. [Euphorbiaceae] inhibited IRAK4 activation and IKK phosphorylation, significantly downregulating the IRAK4-IKKβ-IRF5 and NF-κB signaling pathways to treat rheumatoid arthritis. Kim et al. (2012) found that ginsenoside Rg5 from the Root of Panax ginseng C.A.Mey. [Araliaceae], inhibited IRAK-1 phosphorylation induced by LPS, and promoted the degradation of IRAK1 and IRAK4, thereby blocking NF-κB signal transduction and improving lung inflammation. Psoralen, from the Fruit of *Cullen corylifolium* (L.) Medik. Psoralen [Leguminosae], was found to downregulate IRAK4 protein expression in an inflammation model of human periodontal ligament cells induced by Porphyromonas gingivalis LPS (P. gingivalis LPS), and then downregulate proteins in the TLR4 and NF-κB signaling pathways to treatment and prevention of periodontitis (Li et al., 2021). Polyphyllin I (PPI), a major component of the classic anti-inflammatory herb Rhizome *Paris polyphylla* Sm. [Melanthiaceae], was studied by Wang Q. et al. (2018). They found that when PPI inhibited the overexpression of IRAK1, TRAF6 and Tak1, it suppressed NF-κB transcription, inhibiting the production of

pro-inflammatory mediators mediated by NF-κB in activated macrophages and improving synovial inflammation in CIA mice.

5.5 Inhibition of IKK complex activation

Shen et al. (2019) isolated narciclasine (NCS) from the aerial and bulb of Lycoris radiata (L'Hér.) Herb. [Amaryllidaceae], which can inhibit IKK/β phosphorylation in LPS-induced macrophages, thereby preventing the activation of the IKK complex. Similarly, *notoginsenoside* R1 (NG-R1) from the rhizome and root of *Panax notoginseng* (Burkill) F.H.Chen. [Araliaceae] inhibits the inflammatory cytokine production by improving the phosphorylation of IKKα/β and P65, as well as the nuclear translocation of P65, thus exerting anti-rheumatoid arthritis effect in TNF-Tg mice (Jiao et al., 2021). Liu et al. (2021) revealed that genistein-3′-sodium sulfonate (GSS) reduces IKK expression, and inhibits IκB degradation and P65 phosphorylation, which demonstrates that a neuroprotective effect of GSS on ischemic stroke rats.

5.6 Inhibition of TRAF6 expression and ubiquitination

Nodakenin is a coumarin isolated from the root of *Angelica gigas* Nakai. [Apiaceae], was discovered to inhibit the ubiquitination of TRAF6. This caused an obvious reduction in the binding of p-TAK1 and TRAF6 induced by LPS, thereby inhibiting the degradation of IκBα and the transcriptional activity of NF-κB (Rim et al., 2012). Eupatolide, a novel active component from the dry head inflorescence of *Inula britannica* L. [Asteraceae], can induce the proteasomal degradation of TRAF6. By inducing the polyubiquitination of TRAF6 through Lys48 linkage, thereby suppressing the release of inflammatory factors and mitigating the inflammatory process (Lee J. et al., 2010). Likewise, Tabersonine (TAB), an alkaloid from the herb of *Catharanthus roseus* (L.) G. Don [Apocynaceae], has shown inhibitory effects on TRAF6 ubiquitination. Depeng et al. (Zhang et al., 2018) initially observed through luciferase assays that TAB treatment significantly inhibits NF-κB luciferase activity driven by TRAF6. Subsequently, immunoprecipitation experiments confirmed that TAB can reduce the K63-linked polyubiquitination of TRAF6.

5.7 Inhibition of IκBα degradation and ubiquitination

Myrislignan, isolated from the seed of *Myristica fragrans* Houtt. [Myristicaceae], was reported can inhibit the ubiquitination degradation of IκBα and nuclear translocation (Jin et al., 2012). Zhou et al. (2019) found that icariside II (ICS II) from the leaf of *Epimedium brevicornu* Maxim. [Berberidaceae] inhibits IκB degradation, and modulates the TLR4/MyD88/NF-κB pathway to attenuate endotoxin-induced neuroinflammation. Lu X. et al. (2017) found that treatment with Antidesmone from the root and stem of *Waltheria indica* L. [Malvaceae] could inhibit the degradation of IκBα in lung tissue nuclear extracts, reduce p65 protein levels, can inhibit inflammation on stimulated macrophages and thereby prevent acute lung injury by regulating NF-κB signaling pathways.

5.8 Deacetylation of p65

Natural products, through deacetylation of NF-κB p65, inhibition of p65 transcriptional activity and have anti-inflammatory effects. *Coptis chinensis* Franch. [Ranunculaceae] is a classic anti-inflammatory traditional Chinese medicine, and berberine isolated from it has been found to have significant anti-inflammatory activity in recent years (Zhang et al., 2017; Li et al., 2020; Tew et al., 2020; Haftcheshmeh et al., 2022). Shuchen Zhang et al. show that berberine reduces the acetylation of NF-κB subunit p65 at site Lys310 (p65 Lys310), leading to the inhibition of NF-κB translocation and transcriptional activity to suppress the expressions of inflammatory factors (Zhang et al., 2023). Jyun Pei Jhou et al. found that resveratrol-mediated transcriptional enhancement of the Fcγ RIIB gene resulted in reduced binding of acetylated p65 NF-κB (K310) and P-p65 NF - κ B (S468) to the −480 promoter region of Fcgr2b gene, improving lupus erythematosus (Jhou et al., 2017).

5.9 Inhibition of p65 phosphorylation and nuclear translocation

Oridonin (Ori), a diterpenoid compound isolated from the dry aboveground parts of Rabdosia rubescens (Hemsl.) H. Hara. [Lamiaceae], exhibits diverse biological activities (Dong et al., 2014; Wang et al., 2016; Liu et al., 2016), besides the inhibition of the phosphorylation of IκBα and p65, it also suppressing NF-κB DNA binding activity (Li et al., 2018). Zhao et al. (2016) demonstrated that oridonin dose-dependently inhibits p65 nuclear translocation, alleviating sepsis-induced renal injury. Similarly, Ran et al. (2018) showed through immunofluorescence analysis that pretreatment with ginsenoside B significantly blocks p65 nuclear translocation in rat chondrocytes. Han et al. (2024) demonstrated that after treatment with mogroside V from the fruit of *Siraitia grosvenorii* (Swingle) C. Jeffrey ex A.M.Lu & Zhi Y. Zhang. [Cucurbitaceae], the levels of P-p65 in mouse lung tissues were reduced, indicating the therapeutic efficacy of MV in alleviating lung inflammation induced by asthma. Evodiamine (EVO), is a natural alkaloid from the root tuber of *Lindera aggregate* (Sims) Kosterm. [Lauraceae], improves abnormal states of lung and intestinal tissues by inhibiting NF-κB expression *in vivo*, significantly reducing mortality induced by yeast polysaccharides. The mechanism may involve the inhibition of IκBα phosphorylation and p65 nuclear translocation, attenuating yeast polysaccharide-induced p65 DNA binding activity (Fan et al., 2017).

There are many other Natural products with anti-inflammatory effects. The anti-inflammatory pharmacological mechanisms of various Natural products are summarized in Table 2.

6 Discussion

The TLR4/NF-κB pathway plays a crucial regulatory role in the field of inflammation. As a member of the nuclear transcription factor family, NF-κB protein can regulate the transcription of various genes, inducing the transcription of genes encoding inflammatory mediators such as cytokines, chemokines, and adhesion molecules. Activation of the TLR4/NF-κB signaling

TABLE 2 Anti-inflammatory pharmacology of Natural products in TLR4/NFκB pathway.

Family	Botanical name/ Compound name	Application	Doses/ Duration	*In vitro*/*In vivo* models	Mechanisms	Ref.
Solanaceae	*Lycium ruthenicum Murray* polysaccharide	*In vitro*	10–80 μg/mL for 24 h	LPS-induced RAW264.7 inflammatory model	Reduces TLR4 protein expression; Inhibits IκBα degradation	Peng et al. (2014)
Solanaceae	*Lycium barbarum* L polysaccharides	*In vivo*	400, 800, 1,600 mg/kg, i.g., daily, for 8 weeks	The Wistar rats mode of liver fibrosis was established by gavage olive oil with 40 v/v% CCl4	Reduces TLR4 protein expression; Inhibits p65 phosphorylation	Gan et al. (2018)
Polyporaceae	*Ganoderma lucidum* (Leyss. ex Fr.) Polysaccharide peptide	*In vivo*	100, 200 mg/kg, i.g., daily, for 35 days	The Wistar rats were intradermally injected with bovine type II collagen in the tail base to establish the collagen-induced arthritis (CIA) model	Reduces p65 protein expression; Inhibits IκBα, p65 phosphorylation; Inhibits IκBα degradation	Meng et al. (2023)
Apiaceae	*Angelica sinensis (Oliv.) Diels* Aboveground part polysaccharide	*In vivo* *In vitro*	50, 100, 150 mg/kg, i.p., daily, for 14 days 5, 10, 20 μg/mL for 12 h	The C57BL/N mice model of colonic inflammation was established by intraperitoneal injection of DSS. LPS-induced IPEC-J2 cells inflammatory model	Reduces TLR4 protein expression; Inhibits p65 Phosphorylation	Zou et al. (2023)
Asteraceae	Echinacea purpurea (L.) Moench Echinacea polysaccharide	*In vivo* *In vitro*	5, 10 mg/kg, i.p., for 24 h 100 μg/mL for 1 h	The C57BL/6 mice mode of acute lung injury was established by intraperitoneal injection of LPS. LPS-induced RAW264.7 inflammatory model	Reduces TLR4, MyD88, p65 protein expression; Increases IκBα protein expression; Inhibits IκBα and p65 phosphorylation	Zhang et al. (2020)
Lamiaceae	Rabdosia rubescens (Hemsl.) H. Hara Oridonin	*In vivo* *In vitro*	10 mg/kg, i.p., daily, for 12 weeks 2.5, 5, 10, 20 μM for 12, 24, 48 h	The SD rats model of insulin resistance was established by fed a high-fat diet; The insulin resistance model rats were converted into DM rats by a single intraperitoneal injection of STZ. A rat mesangial cell line (HBZY-1)	Reduces TLR4 protein expression; Inhibits IκB-α, p65 phosphorylation; Prevents p65 nuclear translocation	Li et al. (2018)
Betulaceae	*Betula platyphylla Sukaczev* Betulin	*In vivo* *In vitro*	4, 8 mg/kg, i.p., for 24 h 2, 4, 8 μg/mL for 1 h	Sepsis-induced acute lung injury in SD rats was established by CLP. LPS-induced rat HBZY-1 mesangial cell line inflammatory model	Reduces TLR4 mRNA expression; Inhibits IκB-α, IKK-α/β and p65 phosphorylation; Prevents p65 nuclear translocation	Zhao et al. (2016)
Berberidaceae	Epimedium brevicornu Maxim. Icariside II	*In vivo*	3, 10 mg/kg, i.g., for 14 days	The SD rats model of acute neuroinflammation was established by intraventricular injection of LPS.	Reduces TLR4、MyD88 and TRAF6 protein expression; Inhibits IκB degradation	Zhou et al. (2019)
Paeoniaceae	Paeonia suffruticosa var. papaveracea (Andrews) A. Kern. Paeoniflorin-6′-O-benzene sulfonate (CP-25)	*In vivo*	35 mg/kg, i.g., daily, for 40 days	The DBA/1 mice model of CIA was established by intradermal injection of the chicken CII mixture was then emulsified with Freund's complete adjuvant into the back and base of the tail	Reduces TRAF2 protein expression; Inhibits p65 phosphorylation	Shu et al. (2019)
Melanthiaceae	Paris polyphylla Sm. Polyphyllin I	*In vivo* *In vitro*	1 mg/kg, i.g., daily, for 7 weeks; 0.25, 0.5, 1 μM for 3 h	The CIA model of C57BL/6 and DBA/1J mice LPS and IFN- γ Stimulate primary bone marrow-derived macrophages (BMMs) and peritoneal macrophages (PEMs)	Reduces p65, MyD88, IRAK1, TRAF6 and TAK1 protein expression; Inhibits IKK-α/β and p65 phosphorylation; Prevents p65 nuclear translocation	Wang et al. (2018a)

(Continued on following page)

TABLE 2 (*Continued*) Anti-inflammatory pharmacology of Natural products in TLR4/NFκB pathway.

Family	Botanical name/ Compound name	Application	Doses/ Duration	*In vitro*/*In vivo* models	Mechanisms	Ref.
Polygonaceae	*Reynoutria japonica* Houtt Polydatin	*In vivo* *In vitro*	20, 80 mg/kg, i.p., for 1 h 2, 4, 8 μM for 2 h	The Balb/c mice mode of acute lung injury was established by intraperitoneal injection of LPS. LPS-induced human bronchial epithelial BEAS-2B cells	Reduces TLR4, MyD88 and IRAK-1 protein expression; Inhibits IKKα/β, IκB-α and p65 phosphorylation	Jiang et al. (2015)
Euphorbiaceae	*Euphorbia pekinensis* Rupr. Euphorbia Factor L2	*In vivo* *In vitro*	15, 40 mg/kg, i.p., for 8 days 0.1–100 μM for 20 h	The K/BxN mice model of K/BxN serum metastatic arthritis (STA) was established by intraperitoneal injection of K/BxN mouse serum RAW264.7 cells Bone marrow cells were harvested from the tibias and femurs of C57BL/6 mice	Reduces p65, IKK-α/β, IκB-α, IRAK4, and IKK-β protein expression; Inhibits IKK-α/β, IκB-α, IKKβ and p65 phosphorylation; Prevents p65 nuclear translocation	Tang et al. (2021)
Zingiberaceae	*Curcuma longa* L Curcumin salicylate monoester	*In vivo*	0.1, 0.2 mmol/kg, i.p., daily, for 14 days	The SD rats with Freund's complete adjuvant (FCA)-induced arthritis (Ye et al.).	Inhibits IκB-α, IKKs and p65 phosphorylation	Zhang et al. (2019)
Lamiaceae	Scutellaria baicalensis Georgi Baicalin	*In vivo* *In vitro*	100 mg/kg, i.p., for 3 days 6.25–200 μM for 24 h	The male Balb/c and C57BL/6 mice model of ulcerative colitis (UC) was established by intraperitoneal injection of DSS or LPS. LPS-induced RAW264.7 inflammatory model	Reduces CD14, MyD88 protein expression; Inhibits p65 phosphorylation	Fu et al. (2020)
—	— Quercetin	*In vivo*	30, 60 mg/kg, i.g., daily, for 6 Weeks	The SD rats of diabetes were established by intravenous streptozotocin	Reduces TLR4, MyD88 and p65 protein expression	Zhao et al. (2021)
—	— Quercetin	*In vivo* *In vitro*	50 mg/kg, i.p., for 0, 24, 48 h 0–50 μM for12 h	Establishment of neonatal hypoxic-ischemic brain injury (HIBI) mice model The mouse BV2 microglial cells were incubated in a hypoxic chamber containing 1% O_2/5% CO_2/94% N_2 for 3 h	Reduces TLR4, MyD88 and p65 protein expression	Le et al. (2020)
Leguminosae	*Cullen corylifolium* (L.) Medik Psoralen	*In vitro*	3.125, 6.25, 12.5, 25 μg/mL for 24 h	Primary hPDLCs were obtained and cultured from the ligament tissues in the middle of the premolar roots using a tissue explant method	Reduces TLR4, IRAK4 and P-p65 protein expression	Li et al. (2021)
Fabaceae	Glycine max (L.) Merr. Genistein	*In vitro*	25, 50 μM for 24 h	LPS-induced BV2 microglia inflammatory model	Reduces TLR4, MyD88 and p65 protein expression; Inhibits IκB-α degradation	Jeong et al. (2014)
—	— Genistein-3′-sodium sulfonate	*In vivo* *In vitro*	1 mg/kg, sublingual vein injection for 110min 10 μM for 24 h	The SD rats of transient middle cerebral artery occlusion and reperfusion (tMCAO) were established LPS-induced BV2 microglial cells as *in vitro* model	Reduces IKK and p65 protein expression; Inhibits IκB-α ubiquitination; InhibitsIKK and p65 phosphorylation	Liu et al. (2021)
—	— Hesperetin	*In vivo* *In vitro*	50 mg/kg, i.g., daily, for 5 Weeks 50 μM for 24 h	The C57BL/6 N mice mode of oxidative brain damage was established by intraperitoneal injection of LPS. LPS-induced mouse hippocampal (HT-22) and murine microglia (BV2) cell (*In vitro* model)	Reduces TLR4 protein expression; Inhibits p65 phosphorylation	Muhammad et al. (2019)
Rutaceae	Citrus × aurantium L. Naringenin	*In vivo*	10–50 mg/kg, p.o., daily, for 21 days	The Wistar rats mode of cerebral ischemia was established by MCAO.	Reduces p65 protein expression	Raza et al. (2013)

(Continued on following page)

TABLE 2 (*Continued*) Anti-inflammatory pharmacology of Natural products in TLR4/NFκB pathway.

Family	Botanical name/ Compound name	Application	Doses/ Duration	*In vitro*/*In vivo* models	Mechanisms	Ref.
Piperaceae	*Piper nigrum* L Alkaloids	*In vivo* *In vitro*	50 mg/kg, i.g., for 5 h 0–8 μM for 24 h	The ICR mice mode of acute paw edema was established by injected into the right hind paw of carrageenan suspension (100 μL per mouse) LPS-induced RAW264.7 inflammatory model	Reduces IKKα/β protein expression; Inhibits IKKα/β, IκB-α and p65 phosphorylation; Inhibits IκB-α degradation	Pei et al. (2020)
Rubiaceae	Nauclea officinalis Pierre ex Pit. Strictosamide	*In vitro*	0–200 μM for 24 h	LPS-induced RAW264.7 inflammatory model	Inhibits IKKα, IκB-α, p65 phosphorylation	Li et al. (2017)
Lauraceae	*Lindera aggregate* (Sims) Kosterm Evodiamine	*In vivo* *In vitro*	10, 15 mg/kg, i.p., for 30 h 25, 50, 100 μM for 7 h	The C57BL/6J mice model of non-septic shock was established by intraperitoneal injection of zymosan Collect peritoneal macrophages from C57BL/6J mouse injected intraperitoneally with mercapto acetate broth	Inhibits IκB-α, p65 phosphorylation; Inhibits IκB-α degradation; Prevents p65 nuclear translocation	Fan et al. (2017)
Apocynaceae	Catharanthus roseus (L.) G.Don Tabersonine	*In vivo* *In vitro*	10–40 mg/kg, i.p., for 6 h 1–10 μM for 24 h	The C57BL/6 mice mode of acute lung injury was established by tracheal instillation of LPS Collect peritoneal macrophages induced by thioglycollate broth in the abdominal cavity of C57BL/6J mice	Inhibits TRAF6 ubiquitination; Prevents p65 nuclear translocation	Zhang et al. (2018)
Nitrariaceae	Peganum harmala L. Harmine	*In vivo* *In vitro*	30 mg/kg, i.p., for 1 day 2–50 μM for 24 h	The ICR mice model of inflammation by intraperitoneal injection of LPS. LPS-induced RAW264.7 inflammatory model	Prevents p65 nuclear translocation	Liu et al. (2017)
Malvaceae	*Waltheria indica L* Antidesmone	*In vivo* *In vitro*	2–8 mg/kg, i.p., for 12 h 0–200 μg/mL for 24 h	The Balb/c mice mode of acute lung injury was established by tracheal instillation of LPS. LPS-induced RAW264.7 inflammatory model	Inhibits IκB-α degradation; Prevents p65 nuclear translocation	Lu et al. (2017b)
Amaryllidaceae	*Lycoris radiata* (L'Hér.) Herb narciclasine	*In vitro*	0.001–0.016 μM for 24 h	LPS-induced RAW264.7 inflammatory model	Inhibits IκB-α degradation; Inhibits IκB-α, IKKα/β, p65 phosphorylation; Prevents p65 nuclear translocation	Shen et al. (2019)
Papaveraceae	Chelidonium majus L. Chelidonine	*In vivo* *In vitro*	1–9 mg/kg, i.g., daily, for 12 days 0–100 μM for 24 h	The Balb/c mice mode of inflammation was established by intraperitoneal injection of LPS. LPS-induced RAW264.7 inflammatory model	Reduces TLR4 protein expression; Inhibits of p65 nuclear translocation; Blocking IκB-α Phosphorylation and degradation	Liao et al. (2018)
Zingiberaceae	Curcuma longa L. Curcumin	*In vivo*	1–9 mg/kg, intestinal perfusion for 2 h	Lung lesion-induced Wistar rats mode was established by intestinal ischemia-reperfusion injury	Reduces TLR4 and MyD88 protein expression	Fan et al. (2015)
Zingiberaceae	Curcuma longa L. Curcumin	*In vivo*	5–20 μM for 24 h	The Wistar rats model of cerebral I/R injury was established by middle cerebral artery occlusion (MCAO, 1-h occlusion, and 24-h reperfusion)	Inhibits of p65 protein expression	Jin et al. (2007)

(Continued on following page)

TABLE 2 (*Continued*) Anti-inflammatory pharmacology of Natural products in TLR4/NFκB pathway.

Family	Botanical name/ Compound name	Application	Doses/ Duration	*In vitro*/*In vivo* models	Mechanisms	Ref.
Ranunculaceae	*Aconitum carmichaelii* Debeaux Fuzi lipid-soluble alkaloids	*In vitro*	0–500 ng/mL for 24 h	IL-1β-induced human fibroblast-like synoviocytes-rheumatoid arthritis	Increases IκBα protein expression; Inhibits IκBα Phosphorylation; Inhibits of p65 nuclear translocation	Guo et al. (2022)
Fabaceae	Sophora flavescens Aiton Oxymatrine	*In vitro*	0–5 mg/mL for 24 h	Pancreatic microvascular endothelial cells and LPS induced inflammation to establish the cell model of microcirculation disturbances of acute pancreatitis	Reduces TLR4、MyD88 and p65 mRNA expression; Inhibits of p65 nuclear translocation	Lu et al. (2017a)
Fabaceae	Sophora flavescens Aiton Matrine	*In vivo* *In vitro*	100 mg/kg, i.g., daily, for 6 weeks 25 μM for 24 h	The SD rat model of RA was established by injected intra-dermally with 30 μg bovine type II collagen Using either mice splenic T cells stimulated with PMA/ionomycin or rat splenic T cells	Reduces p65and IκBα protein expression; Inhibits IκBα phosphorylation	Niu et al. (2017)
Convolvulaceae	Erycibe obtusifolia Benth. Scopoletin	*In vivo* *In vitro*	50–200 mg/kg, i.p., for 6 h 30–300 μM for 20 h	The acute inflammatory model resembling gout in ICR mice was induced by injecting MSU crystals into the pouch cavity MSU-induced RAW264.7 inflammatory model	Inhibits IκB-α,IKKα, p65 phosphorylation; Inhibits IκB-α degradation	Yao et al. (2012)
Apiaceae	Angelica gigas Nakai Nodakenin	*In vivo* *In vitro*	10, 20 mg/kg, i.p., for 1 h 25–100 μM for 24 h	The C57BL/6 mouse model of sepsis was established by intraperitoneal injection of LPS. LPS-induced RAW264.7 inflammatory mode	Reduces IRAK1 protein expression; Inhibits IκB-α Protein degradation; Inhibits TAK1、IKKα/β and IκB-α/β phosphorylation; Inhibits TRAF6 ubiquitination	Rim et al. (2012)
Schisandraceae	Schisandra chinensis (Turcz.) Baill. Schisandrin B	*In vivo* *In vitro*	50 μM, intra-articular injection., for 4 weeks 25–150 μM for 24 or 48 h	The SD rats were used to develop osteoarthritis by surgical resection of medial meniscus in knee joints Collecting chondrocytes from knee and hip cartilage collected from SD rats	Prevents p65 nuclear translocation	Ran et al. (2018)
—	— Ferulic acid	*In vivo* *In vitro*	20 mg/kg, i.g., for 7 days 10, 100 μM for 24 h	The C57BL/6 mice model of neuroinflammation was established by intraperitoneal injection of LPS. LPS-induced BV2 cells inflammatory model	Reduces TLR4 protein expression; Inhibits IKK and p65 phosphorylation	Rehman et al. (2018)
Phyllanthaceae	Phyllanthus amarus Schumach. & Thonn. Phyllanthin	*In vitro*	1.56–25 μM for 24 h	The human myeloid leukemia cells (U937) were induced to differentiate to obtain macrophage-like phenotype by the addition of PMA to the cells	Reduces TLR4, MyD88, IKK-α/β, p65 protein expression; Inhibits IKK-α/β, p65 phosphorylation; Inhibits IκB-α degradation	Harikrishnan et al. (2018)
Cucurbitaceae	Cucurbita moschata Duchesne Dehydrodiconiferyl alcohol	*In vivo* *In vitro*	100, 300 mg/kg, i.p., daily, for 7 days 10–80 μM for 24 h	Colitis was induced in C57BL/6 mice by the administration of 3.5% DSS dissolved in drinking water Bone marrow cells were prepared and differentiated into macrophages using M-CSF (*In vitro* model)	Reduces IKK-β protein expression; Inhibits IKK-β phosphorylation; Inhibits IκB-α degradation	Lee et al. (2015)

(Continued on following page)

TABLE 2 (*Continued*) Anti-inflammatory pharmacology of Natural products in TLR4/NFκB pathway.

Family	Botanical name/ Compound name	Application	Doses/ Duration	*In vitro*/*In vivo* models	Mechanisms	Ref.
Oleaceae	Forsythia suspensa (Thunb.) Vahl Phillygenin	*In vitro*	6.25–200 μg/mL for 24 h	LPS-induced LX2 cells (hepatic stellate cells from the human liver that have been immobilized) inflammatory mode	Reduces TLR4, MyD88, TAK1, IKK-β, p65 protein expression; Inhibits IκB-α and p65 phosphorylation; Inhibits IκB-α degradation	Hu et al. (2020)
Myristicaceae	Myristica fragrans Houtt. Myrislignan	*In vitro*	6.25–50 μg/mL for 24 h	LPS-induced RAW264.7 inflammatory mode	Inhibits IκB-α ubiquitination; Inhibits p65 phosphorylation	Jin et al. (2012)
Cucurbitaceae	*Siraitia grosvenorii* (Swingle) C.Jeffrey ex A.M.Lu and Zhi Y.Zhang Mogroside V	*In vivo* *In vitro*	50 mg/kg, i.g., daily, for 32 days 100 μg/mL for 2 h	The Balb/c mice model of asthmatic was established by intraperitoneal injection of OVA. LPS-induced RAW264.7 inflammatory model	Reduces p65 protein expression; Inhibits p65 phosphorylation	Han et al. (2024)
Fabaceae	Glycyrrhiza uralensis Fisch. Glycyrrhetinic acid	*In vivo* *In vitro*	20 mg/kg, i.p., for 6 days 10–1,000 μg/mL for 6 h	The C57BL/6 mice model of MHV infection was established by intraperitoneal injection of plaque forming unit (PFU) of MHV-A59 Murine hepatitis virus (MHV) infection model	Reduces TLR4 expression	Shi et al. (2020)
Asparagaceae	*Anemarrhena asphodeloides* Bunge Timosaponin B-II	*In vivo*	20, 40 mg/kg, i.p., for 15 min	The Balb/C mice mode of acute lung injury was established by intratracheal injection of LPS.	Reduces TLR4, MyD88, p65 protein expression	Zhang et al. (2015b)
Araliaceae	Kalopanax pictus (Thunb.) Nakai Kalopanaxsaponin A	*In vivo* *In vitro*	10, 20 mg/kg, i.g., daily, for 3 days 50 ng/mL for 1 h	The ICR mice mode of Colitis was established by intrarectal administration of TNBS. Peritoneal macrophages from male ICR mice were stimulated with LPS or peptidoglycan	Reduces IRAK1, IκB-β protein expression; Inhibits IKK-β, p65 phosphorylation; Inhibits IκB-α degradation	Joh and Kim (2011)
Fabaceae	Glycine max (L.) Merr. Soyasaponin I	*In vivo* *In vitro*	10, 20 mg/kg, i.g., daily, for 5 days 2–20 μM for 20 h	The ICR mice mode of Colitis was established by intrarectal administration of TNBS. LPS-stimulated peritoneal macrophages from male C57BL/6 mice	Inhibits IκB-α phosphorylation; Prevents p65 nuclear translocation; Inhibits IκB-α degradation	Lee et al. (2010a)
Asparagaceae	Terauchia anemarrhenifolia Nakai Timosaponin AIII	*In vivo* *In vitro*	5, 10 mg/kg, i.g., daily, for 3 days 2–10 μM for 20 h	The C57BL/6 mice mode of Colitis was established by intrarectal administration of TNBS. LPS-stimulated peritoneal macrophages from male C57BL/6 mice	Reduces IRAK1, TAK1 potein expression; Inhibits IRAK1,TAK 1, IκB-α and p65 phosphorylation; Inhibits IκB-α degradation	Lim et al. (2015)
Araliaceae	Panax notoginseng (Burkill) F.H.Chen Notoginsenoside R1	*In vivo* *In vitro*	20 mg/kg, i.p., daily, for 8 weeks 5–200 μM for 24 h	The TNF-Tg mice established the RA model and were bred as heterozygotes on a C57BL/6 background, then Near infrared-indocyanine green (NIR-ICG) was injected into footpads Mouse Primary Lymphatic Endothelial Cells/C57-6,092 were stimulated by TNF-α and NG-R1	Reduces p65、 IKKα/β phosphorylation	Jiao et al. (2021)
Araliaceae	Panax ginseng C.A.Mey. Ginsenoside Rg5	*In vivo* *In vitro*	2.5, 5 mg/kg, i.p., for 1 h 5, 10 μM for 20 h	The C57BL/6 mice model of acute lung injury was established by intratracheal injection of LPS.	Reduces IRAK1/4 protein expression; Inhibits IRAK1, IKK-β, p65 phosphorylation	Kim et al. (2012)

(Continued on following page)

TABLE 2 (*Continued*) Anti-inflammatory pharmacology of Natural products in TLR4/NFκB pathway.

Family	Botanical name/ Compound name	Application	Doses/ Duration	*In vitro*/*In vivo* models	Mechanisms	Ref.
				Isolation of alveolar macrophages from alveolar lavage fluid		
Theaceae	Camellia sinensis (L.) Kuntze Catechins	*In vitro*	10 μg/L for 12, 24, 48 h	Human dental pulp cells were isolated from healthy permanent teeth	Inhibits p65 phosphorylation; Prevents p65 nuclear translocation	Wang et al. (2020)
—	— Resveratrol	*In vivo* *In vitro*	50, 100 mg/kg, i.g., daily, for 6 days 12.5–50 μM for 36 h	The Balb/c mice model of acute T. gondii infection was established by intraperitoneally (i.p.) injected with tachyzoites of T. gondii RH Strain NCTC 1469 cells were infected with T. gondii at the ratio of tachyzoite: cells = 5 : 1 for 4 h	Reduces TLR4 MyD88 protein expression; Prevents p65 nuclear translocation; Inhibits IκB-α degradation	Lu et al. (2021)
Asphodelaceae	*Aloe vera* (L.) Burm.f Aloin	*In vivo*	30 mg/kg, i.g., for 8 weeks	The C57BL/B6 mice model of neurodegenerative diseases was established by subcutaneous injection D-gal	Reduces p65 protein expression	Zhong et al. (2019)
Asteraceae	Inula britannica L. Eupatolide	*In vitro*	0.1–10 μM for 0.5 h	LPS-induced RAW264.7 inflammatory model	Reduces IκB-α and p65 protein expression; Inhibits IκB-α、IKK-α/β and p65 phosphorylation; Inhibits TRAF6 ubiquitination	Lee et al. (2010b)
Ranunculaceae	*Coptis chinensis* Franch. coptisine	*In vivo*	150 mg/kg, i.g., daily, for 12 weeks	The C57BL/6J mice model of atherosclerosis (AS) was established by gavage of 1.25% cholesterol and 21% fat orally daily for 12 weeks	Reduces p65 mRNA expression; Reduces IκB-α and p65 protein expression; Prevents p65 nuclear translocation;	Feng et al. (2017)
Gentianaceae	Gentiana cruciata *L* Gentiopicroside	*In vivo* *In vitro*	50 mg/kg, i.p., for 30 min 1,000 μg/mL	The C57BL/6 mice model of sepsis was established by intraperitoneally injected of LPS. LPS and IFN-γinduced primary bone marrow-derived macrophages (BMMs) or peritoneal macrophages (PEMs) inflammatory model	Inhibits IKK-α/β and p65 phosphorylation; Prevents p65 nuclear translocation; Inhibits IκB-α degradation	Wang et al. (2019)
Brassicaceae	*Isatis tinctoria* L Isatidis folium water extract (WIF)	*In vivo* *In vitro*	100, 200 mg/kg, i.g 50, 100, and 200 μg/mL for 1 h	The Balb/c mice model of atopic dermatitis was established by intraperitoneally injected of 2,4-dinitrochlorobenzene (DNCB) TNF-α/IFN-γinduced HaCaT cells inflammatory model	Prevents p65 nuclear translocation	Min et al. (2023)
Caprifoliaceae	*Lonicera japonica* Thunb *Lonicera japonica* Thunb extrate (LTE) and luteolin	*In vivo* *In vitro*	LTE 1.75 g/kg or Lut 18, 35, 70 μmol/kg, i.g., for 7 days LTE 10 ug/mLor Lut 10 μM for 24 h	The C57BL/6 mice model of ALI was established by intraperitoneal injection of LPS. LPS-induced BEAS-2B cells inflammatory model	Reduces MyD88 and IκB-α protein expression; Inhibits p65 phosphorylation	Jia et al. (2023)
Ranunculaceae	*Coptis chinensis* Franch Berberine	*In vivo* *In vitro*	40 mg/kg i.g., daily, for 1 or 4 weeks 5 μM for 24 h	The C57BL/6 mice model of acute inflammation was established by intraperitoneally injected of LPS. The C57BL/6 mice model of chronic inflammation was established by fed a high fat diet (20 kcal% carbohy-drates,	Reduce p65 acetylation; Prevents p65 nuclear translocation	Zhang et al. (2023)

(Continued on following page)

TABLE 2 (*Continued*) Anti-inflammatory pharmacology of Natural products in TLR4/NFκB pathway.

Family	Botanical name/ Compound name	Application	Doses/ Duration	*In vitro*/*In vivo* models	Mechanisms	Ref.
				20 kcal% protein and 60 kcal% fat) LPS-induced RAW264.7 and BMDM cells inflamma-tory model		
—	— Resveratrol	*In vivo* *In vitro*	20 mg/kg i.p., daily, for 6 weeks 0, 2.5, 5, 7.5, 10 μM for 2 and 6 h	MRL/lpr mice (Spontaneous lupus erythematosus like mouse model) —	Reduce p65 acetylation; Prevents p65 nuclear translocation	Jhou et al. (2017)

pathway is primarily initiated by TLR4 recognizing pathogen molecules like LPS as ligands, through two signaling pathways dependent on MyD88 and TRIF, activating the downstream TRAF6 as an E3 ubiquitin ligase to form free K63 ubiquitin chains. Upon receiving the K63 ubiquitin chain signal, the downstream IKK complex promotes IκB phosphorylation and degradation, releasing NF-κB p65, initiating the nuclear translocation of NF-κB, where it exerts its role as a transcription factor, regulating the transcription of various genes such as TNF-α, IL-1, IL-6. The release of these inflammation-related factors triggers inflammatory responses, leading to processes like vasodilation, leukocyte infiltration, and tissue damage in inflammatory pathologies.

Natural product compounds demonstrate significant biological activities and functional diversity by influencing multiple targets within the TLR4/NF-κB pathway. They effectively inhibit the expression of proteins and mRNA, suppress the phosphorylation and ubiquitination of key proteins, and hinder the translocation of p65 into the nucleus, thereby exhibiting anti-inflammatory properties (Figure 4). In most current studies, it has been shown that Natural products can interact with multiple protein targets, but it has become difficult to identify the most biologically active true target (Rix and Superti-Furga, 2009; Klessig et al., 2016). With the advancement of molecular biology and the arrival of the post-genomic era, more and more research on Natural products mechanisms is being combined with chemical proteomics techniques. This comprehensive method of searching and identifying multiple protein targets in active small molecules can effectively identify the true targets. Subsequent validation of the screened targets in omics through molecular biology and pharmacological experiments can greatly improve the scientific validity and credibility of the research (Wang S. et al., 2018).

In addition, compared to traditional chemically synthesized drugs, the efficacy of Natural products may be affected by factors such as plant origin, growth environment, and collection time, resulting in unstable efficacy and difficulty in ensuring consistency with each use. Therefore, by modifying the chemical structure, the bioavailability, metabolic pathways, and targeting of compounds can be altered to enhance their pharmacological effects. And develop drug delivery systems targeting natural products, such as microspheres, nanoparticles, liposomes, etc., which can improve their release rate and bioavailability *in vivo*, and enhance the stability of drug efficacy. Therefore, it is essential to focus on interdisciplinary collaboration, integrating disciplines such as pharmacology, pharmacy, and molecular materials science, which can contribute to the significant development of research on Natural products.

Collectively, NF-κB, as a central regulatory factor in the treatment and intervention of inflammatory diseases, will provide valuable insights for the development of new anti-inflammatory natural plant-based drugs with better efficacy and safety by introducing high-throughput omics techniques and emphasizing interdisciplinary collaboration to deeply study the activation mechanism of the NF-κB pathway by natural products.

Author contributions

YZ: Conceptualization, Data curation, Formal Analysis, Investigation, Methodology, Project administration, Resources, Software, Validation, Visualization, Writing–original draft, Writing–review and editing. XL: Data curation, Visualization, Writing–review and editing. JW: Supervision, Writing–review and editing. XC: Funding acquisition, Supervision, Writing–review and editing. JW: Methodology, Supervision, Writing–review and editing.

Funding

The author(s) declare that financial support was received for the research, authorship, and/or publication of this article. This work was supported by the Innovation Project of Guangxi Graduate Education (YCSW2024439), the Special Fund of the Central Government Guiding Local Scientific and Technological Development by Guangxi Science and Technology Department (GuikeZY21195024), the National Natural Science Foundation of China (82460798), the Guangxi Science and Technology Major Program (GuikeAA23023035-7), Natural Science Foundation of Guangxi (2022GXNSFAA103029), the third batch of Lijiang Scholar Award in Guilin (2022-5-07).

Conflict of interest

The authors declare that the research was conducted in the absence of any commercial or financial relationships that could be construed as a potential conflict of interest.

Publisher's note

References

Adhikari, A., Xu, M., and Chen, Z. J. (2007). Ubiquitin-mediated activation of TAK1 and IKK. *Oncogene* 26, 3214–3226. doi:10.1038/sj.onc.1210413

Akashi, S., Shimazu, R., Ogata, H., Nagai, Y., Takeda, K., Kimoto, M., et al. (2000). Cutting edge: cell surface expression and lipopolysaccharide signaling via the toll-like receptor 4-MD-2 complex on mouse peritoneal macrophages. *J. Immunol.* 164, 3471–3475. doi:10.4049/jimmunol.164.7.3471

Akira, S. (2003). Toll-like receptor signaling. *J. Biol. Chem.* 278, 38105–38108. doi:10.1074/jbc.R300028200

Alarcón-Vila, C., Baroja-Mazo, A., De Torre-Minguela, C., Martínez, C. M., Martínez-García, J. J., Martínez-Banaclocha, H., et al. (2020). CD14 release induced by P2X7 receptor restricts inflammation and increases survival during sepsis. *Elife* 9, e60849. doi:10.7554/eLife.60849

Aletaha, D., and Smolen, J. S. (2018). Diagnosis and management of rheumatoid arthritis: a review. *JAMA* 320, 1360.1360–1372. doi:10.1001/jama.2018.13103

Álvarez-Martínez, F. J., Barrajón-Catalán, E., and Micol, V. (2020). Tackling antibiotic resistance with compounds of natural origin: a comprehensive review. *Biomedicines* 8, 405. doi:10.3390/biomedicines8100405

Anderberg, S. B., Luther, T., and Frithiof, R. (2017). Physiological aspects of Toll-like receptor 4 activation in sepsis-induced acute kidney injury. *Acta Physiol. (Oxf)* 219, 573–588. doi:10.1111/apha.12798

Baur, J. A., and Sinclair, D. A. (2006). Therapeutic potential of resveratrol: the *in vivo* evidence. *Nat. Rev. Drug Discov.* 5, 493–506. doi:10.1038/nrd2060

Bonham, K. S., Orzalli, M. H., Hayashi, K., Wolf, A. I., Glanemann, C., Weninger, W., et al. (2014). A promiscuous lipid-binding protein diversifies the subcellular sites of toll-like receptor signal transduction. *Cell* 156, 705–716. doi:10.1016/j.cell.2014.01.019

Cai, C., Tang, Y.-D., Zhai, J., and Zheng, C. (2022). The RING finger protein family in health and disease. *Signal Transduct. Target. Ther.* 7, 300. doi:10.1038/s41392-022-01152-2

Chen, W., Li, Z., Bai, L., and Lin, Y. (2011). NF-kappaB in lung cancer, a carcinogenesis mediator and a prevention and therapy target. *FBL* 16, 1172–1185. doi:10.2741/3782

Cildir, G., Low, K. C., and Tergaonkar, V. (2016). Noncanonical NF-κB signaling in health and disease. *Trends Mol. Med.* 22, 414–429. doi:10.1016/j.molmed.2016.03.002

Deng, L., Wang, C., Spencer, E., Yang, L., Braun, A., You, J., et al. (2000). Activation of the IkappaB kinase complex by TRAF6 requires a dimeric ubiquitin-conjugating enzyme complex and a unique polyubiquitin chain. *Cell* 103, 351–361. doi:10.1016/s0092-8674(00)00126-4

Di Lorenzo, F., Duda, K. A., Lanzetta, R., Silipo, A., De Castro, C., and Molinaro, A. (2022). A journey from structure to function of bacterial lipopolysaccharides. *Chem. Rev.* 122, 15767–15821. doi:10.1021/acs.chemrev.0c01321

Dong, Y., Zhang, T., Li, J., Deng, H., Song, Y., Zhai, D., et al. (2014). Oridonin inhibits tumor growth and metastasis through anti-angiogenesis by blocking the Notch signaling. *PLoS One* 9, e113830. doi:10.1371/journal.pone.0113830

Doyle, S. L., and O'neill, L. A. (2006). Toll-like receptors: from the discovery of NFkappaB to new insights into transcriptional regulations in innate immunity. *Biochem. Pharmacol.* 72, 1102–1113. doi:10.1016/j.bcp.2006.07.010

Fan, X., Zhu, J.-Y., Sun, Y., Luo, L., Yan, J., Yang, X., et al. (2017). Evodiamine inhibits zymosan-induced inflammation *in vitro* and *in vivo*: inactivation of NF-κB by inhibiting IκBα phosphorylation. *Inflammation* 40, 1012–1027. doi:10.1007/s10753-017-0546-0

Fan, Z., Yao, J., Li, Y., Hu, X., Shao, H., and Tian, X. (2015). Anti-inflammatory and antioxidant effects of curcumin on acute lung injury in a rodent model of intestinal ischemia reperfusion by inhibiting the pathway of NF-Kb. *Int. J. Clin. Exp. Pathol.* 8, 3451–3459.

Fang, S., Zhang, B., Xiang, W., Zheng, L., Wang, X., Li, S., et al. (2024). Natural products in osteoarthritis treatment: bridging basic research to clinical applications. *Chin. Med.* 19, 25. doi:10.1186/s13020-024-00899-w

Feng, M., Kong, S. Z., Wang, Z. X., He, K., Zou, Z. Y., Hu, Y. R., et al. (2017). The protective effect of coptisine on experimental atherosclerosis ApoE(-/-) mice is mediated by MAPK/NF-κB-dependent pathway. *Biomed. Pharmacother.* 93, 721–729. doi:10.1016/j.biopha.2017.07.002

Fitzgerald, K. A., and Kagan, J. C. (2020). Toll-like receptors and the control of immunity. *Cell* 180, 1044–1066. doi:10.1016/j.cell.2020.02.041

Fu, Y.-J., Xu, B., Huang, S.-W., Luo, X., Deng, X.-L., Luo, S., et al. (2020). Baicalin prevents LPS-induced activation of TLR4/NF-κB p65 pathway and inflammation in mice via inhibiting the expression of CD14. *Acta Pharmacol. Sin.* 42, 88–96. doi:10.1038/s41401-020-0411-9

Furman, D., Campisi, J., Verdin, E., Carrera-Bastos, P., Targ, S., Franceschi, C., et al. (2019). Chronic inflammation in the etiology of disease across the life span. *Nat. Med.* 25, 1822–1832. doi:10.1038/s41591-019-0675-0

Gallo, L. H., Ko, J., and Donoghue, D. J. (2017). The importance of regulatory ubiquitination in cancer and metastasis. *Cell Cycle* 16, 634–648. doi:10.1080/15384101.2017.1288326

Gan, F., Liu, Q., Liu, Y., Huang, D., Pan, C., Song, S., et al. (2018). Lycium barbarum polysaccharides improve CCl(4)-induced liver fibrosis, inflammatory response and TLRs/NF-kB signaling pathway expression in wistar rats. *Life Sci.* 192, 205–212. doi:10.1016/j.lfs.2017.11.047

Ghosh, S., and Hayden, M. S. (2008). New regulators of NF-kappaB in inflammation. *Nat. Rev. Immunol.* 8, 837–848. doi:10.1038/nri2423

Gray, P., Dunne, A., Brikos, C., Jefferies, C. A., Doyle, S. L., and La, O. N. (2016). MyD88 adapter-like (Mal) is phosphorylated by Bruton's tyrosine kinase during TLR2 and TLR4 signal transduction. *J. Biol. Chem.* 291, 26240. doi:10.1074/jbc.A116.508892

Guo, C., He, L., Hu, N., Zhao, X., Gong, L., Wang, C., et al. (2022). Aconiti Lateralis Radix Praeparata lipid-soluble alkaloids alleviates IL-1β-induced inflammation of human fibroblast-like synoviocytes in rheumatoid arthritis by inhibiting NF-κB and MAPKs signaling pathways and inducing apoptosis. *Cytokine* 151, 155809. doi:10.1016/j.cyto.2022.155809

Guo, Y., Peng, X., Liu, F., Zhang, Q., Ding, L., Li, G., et al. (2024). Potential of natural products in inflammation: biological activities, structure-activity relationships, and mechanistic targets. *Arch. Pharm. Res.* 47, 377–409. doi:10.1007/s12272-024-01496-z

Häcker, H., and Karin, M. (2006). Regulation and function of IKK and IKK-related kinases. *Sci. STKE* 2006, re13. doi:10.1126/stke.3572006re13

Haftcheshmeh, S. M., Abedi, M., Mashayekhi, K., Mousavi, M. J., Navashenaq, J. G., Mohammadi, A., et al. (2022). Berberine as a natural modulator of inflammatory signaling pathways in the immune system: focus on NF-κB, JAK/STAT, and MAPK signaling pathways. *Phytotherapy Res.* 36, 1216–1230. doi:10.1002/ptr.7407

Han, M., Liu, H., Liu, G., Li, X., Zhou, L., Liu, Y., et al. (2024). Mogroside V alleviates inflammation response by modulating miR-21-5P/SPRY1 axis. *Food Funct.* 15, 1909–1922. doi:10.1039/d3fo01901b

Harikrishnan, H., Jantan, I., Haque, M. A., and Kumolosasi, E. (2018). Phyllanthin from Phyllanthus amarus inhibits LPS-induced proinflammatory responses in U937 macrophages via downregulation of NF-κB/MAPK/PI3K-Akt signaling pathways. *Phytotherapy Res.* 32, 2510–2519. doi:10.1002/ptr.6190

Hayden, M. S., and Ghosh, S. (2008). Shared principles in NF-kappaB signaling. *Cell* 132, 344–362. doi:10.1016/j.cell.2008.01.020

Hoffmann, A., Natoli, G., and Ghosh, G. (2006). Transcriptional regulation via the NF-kappaB signaling module. *Oncogene* 25, 6706–6716. doi:10.1038/sj.onc.1209933

Hou, J. J., Zhang, Z. J., Wu, W. Y., He, Q. Q., Zhang, T. Q., Liu, Y. W., et al. (2022). Mass spectrometry imaging: new eyes on natural products for drug research and development. *Acta Pharmacol. Sin.* 43, 3096–3111. doi:10.1038/s41401-022-00990-8

Hu, N., Wang, C., Dai, X., Zhou, M., Gong, L., Yu, L., et al. (2020). Phillygenin inhibits LPS-induced activation and inflammation of LX2 cells by TLR4/MyD88/NF-κB signaling pathway. *J. Ethnopharmacol.* 248, 112361. doi:10.1016/j.jep.2019.112361

Huang, M., Tan, Y.-Q., Luo, J., and Shen, J.-Y. (2018). Antimicrobial resistance of Chinese herbal medicine. *Chin. J. Exp. Traditional Med. Formulae* 24, 218–224. doi:10.13422/j.cnki.syfjx.20182336

Israël, A. (2010). The IKK complex, a central regulator of NF-kappaB activation. *Cold Spring Harb. Perspect. Biol.* 2, a000158. doi:10.1101/cshperspect.a000158

Itoh, H., and Inoue, M. (2019). Comprehensive structure-activity relationship studies of macrocyclic natural products enabled by their total syntheses. *Chem. Rev.* 119, 10002–10031. doi:10.1021/acs.chemrev.9b00063

Iwai, K. (2012). Diverse ubiquitin signaling in NF-κB activation. *Trends Cell Biol.* 22, 355–364. doi:10.1016/j.tcb.2012.04.001

Jeong, J.-W., Lee, H. H., Han, M. H., Kim, G.-Y., Kim, W.-J., and Choi, Y. H. (2014). Anti-inflammatory effects of genistein via suppression of the toll-like receptor 4-mediated signaling pathway in lipopolysaccharide-stimulated BV2 microglia. *Chemico-biological Interact.* 212, 30–39. doi:10.1016/j.cbi.2014.01.012

Jhou, J. P., Chen, S. J., Huang, H. Y., Lin, W. W., Huang, D. Y., and Tzeng, S. J. (2017). Upregulation of FcγRIIB by resveratrol via NF-κB activation reduces B-cell numbers and ameliorates lupus. *Exp. Mol. Med.* 49, e381. doi:10.1038/emm.2017.144

Jia, Q., Wen, J., Yang, Q., Liu, S., Zhang, J., Wang, T., et al. (2023). Lonicera japonica Thunb extract ameliorates lipopolysaccharide-induced acute lung injury associated with luteolin-mediated suppression of NF-κB signaling pathway. *J. Inflamm. (Lond)* 20, 44. doi:10.1186/s12950-023-00372-9

Jiang, Q., Yi, M., Guo, Q., Wang, C., Wang, H., Meng, S., et al. (2015). Protective effects of polydatin on lipopolysaccharide-induced acute lung injury through TLR4-MyD88-NF-κB pathway. *Int. Immunopharmacol.* 29, 370–376. doi:10.1016/j.intimp.2015.10.027

Jiang, Z., Mak, T. W., Sen, G., and Li, X. (2004). Toll-like receptor 3-mediated activation of NF-kappaB and IRF3 diverges at Toll-IL-1 receptor domain-containing adapter inducing IFN-beta. *Proc. Natl. Acad. Sci. U. S. A.* 101, 3533–3538. doi:10.1073/pnas.0308496101

Jiao, D., Liu, Y., Hou, T., Xu, H., Wang, X., Shi, Q., et al. (2021). Notoginsenoside R1 (NG-R1) promoted lymphatic drainage function to ameliorating rheumatoid arthritis in TNF-tg mice by suppressing NF-κB signaling pathway. *Front. Pharmacol.* 12, 730579. doi:10.3389/fphar.2021.730579

Jin, C.-Y., Lee, J.-D., Park, C., Choi, Y. H., and Kim, G.-Y. (2007). Curcumin attenuates the release of pro-inflammatory cytokines in lipopolysaccharide-stimulated BV2 microglia. *Acta Pharmacol. Sin.* 28, 1645–1651. doi:10.1111/j.1745-7254.2007.00651.x

Jin, H., Zhu, Z.-G., Yu, P.-J., Wang, G.-F., Zhang, J.-Y., Li, J.-R., et al. (2012). Myrislignan attenuates lipopolysaccharide-induced inflammation reaction in murine macrophage cells through inhibition of NF-κB signalling pathway activation. *Phytotherapy Res.* 26, 1320–1326. doi:10.1002/ptr.3707

Jin, L., Williamson, A., Banerjee, S., Philipp, I., and Rape, M. (2008). Mechanism of ubiquitin-chain formation by the human anaphase-promoting complex. *Cell* 133, 653–665. doi:10.1016/j.cell.2008.04.012

Joh, E.-H., and Kim, D.-H. (2011). Kalopanaxsaponin A ameliorates experimental colitis in mice by inhibiting IRAK-1 activation in the NF-κB and MAPK pathways. *Br. J. Pharmacol.* 162 (0), 1731–1742. doi:10.1111/j.1476-5381.2010.01195.x

Kagan, J. C. (2012). Signaling organelles of the innate immune system. *Cell* 151, 1168–1178. doi:10.1016/j.cell.2012.11.011

Kagan, J. C., Su, T., Horng, T., Chow, A., Akira, S., and Medzhitov, R. (2008). TRAM couples endocytosis of Toll-like receptor 4 to the induction of interferon-beta. *Nat. Immunol.* 9, 361–368. doi:10.1038/ni1569

Kavanaugh, A., and Wells, A. F. (2014). Benefits and risks of low-dose glucocorticoid treatment in the patient with rheumatoid arthritis. *Rheumatology* 53, 1742–1751. doi:10.1093/rheumatology/keu135

Kelley, S. L., Lukk, T., Nair, S. K., and Tapping, R. I. (2013). The crystal structure of human soluble CD14 reveals a bent solenoid with a hydrophobic amino-terminal pocket. *J. Immunol.* 190, 1304–1311. doi:10.4049/jimmunol.1202446

Kim, J. I., Lee, C. J., Jin, M. S., Lee, C. H., Paik, S. G., Lee, H., et al. (2005). Crystal structure of CD14 and its implications for lipopolysaccharide signaling. *J. Biol. Chem.* 280, 11347–11351. doi:10.1074/jbc.M414607200

Kim, T. W., Joh, E. H., Kim, B., and Kim, D. H. (2012). Ginsenoside Rg5 ameliorates lung inflammation in mice by inhibiting the binding of LPS to toll-like receptor-4 on macrophages. *Int. Immunopharmacol.* 12, 110–116. doi:10.1016/j.intimp.2011.10.023

Klessig, D. F., Tian, M., and Choi, H. W. (2016). Multiple targets of salicylic acid and its derivatives in plants and animals. *Front. Immunol.* 7, 206. doi:10.3389/fimmu.2016.00206

Kobayashi, M., Saitoh, S., Tanimura, N., Takahashi, K., Kawasaki, K., Nishijima, M., et al. (2006). Regulatory roles for MD-2 and TLR4 in ligand-induced receptor clustering. *J. Immunol.* 176, 6211–6218. doi:10.4049/jimmunol.176.10.6211

Kotas, M. E., and Medzhitov, R. (2015). Homeostasis, inflammation, and disease susceptibility. *Cell* 160, 816–827. doi:10.1016/j.cell.2015.02.010

Le, K., Song, Z., Deng, J., Peng, X., Zhang, J., Wang, L., et al. (2020). Quercetin alleviates neonatal hypoxic-ischemic brain injury by inhibiting microglia-derived oxidative stress and TLR4-mediated inflammation. *Inflamm. Res.* 69, 1201–1213. doi:10.1007/s00011-020-01402-5

Lee, I.-A., Park, Y.-J., Yeo, H.-K., Han, M. J., and Kim, D.-H. (2010a). Soyasaponin I attenuates TNBS-Induced colitis in mice by inhibiting NF-κB pathway. *J. Agric. Food Chem.* 58, 10929–10934. doi:10.1021/jf102296y

Lee, J., Choi, J., and Kim, S. (2015). Effective suppression of pro-inflammatory molecules by DHCA via IKK-NF-κB pathway, *in vitro* and *in vivo*. *Br. J. Pharmacol.* 172 (0), 3353–3369. doi:10.1111/bph.13137

Lee, J., Tae, N., Lee, J. J., Kim, T., and Lee, J. H. (2010b). Eupatolide inhibits lipopolysaccharide-induced COX-2 and iNOS expression in RAW264.7 cells by inducing proteasomal degradation of TRAF6. *Eur. J. Pharmacol.* 636, 173–180. doi:10.1016/j.ejphar.2010.03.021

Leung, E., Weil, D. E., Raviglione, M., Nakatani, H., and World Health Organization World Health Day Antimicrobial Resistance Technical Working, G (2011). The WHO policy package to combat antimicrobial resistance. *Bull. World Health Organ* 89, 390–392. doi:10.2471/BLT.11.088435

Li, D., Chen, J., Ye, J., Zhai, X., Song, J., Jiang, C., et al. (2017). Anti-inflammatory effect of the six compounds isolated from Nauclea officinalis Pierrc ex Pitard, and molecular mechanism of strictosamide via suppressing the NF-κB and MAPK signaling pathway in LPS-induced RAW 264.7 macrophages. *J. Ethnopharmacol.* 196, 66–74. doi:10.1016/j.jep.2016.12.007

Li, H., Fan, C., Lu, H., Feng, C., He, P., Yang, X., et al. (2020). Protective role of berberine on ulcerative colitis through modulating enteric glial cells-intestinal epithelial cells-immune cells interactions. *Acta Pharm. Sin. B* 10, 447–461. doi:10.1016/j.apsb.2019.08.006

Li, H., Xu, J., Li, X., Hu, Y., Liao, Y., Zhou, W., et al. (2021). Anti-inflammatory activity of psoralen in human periodontal ligament cells via estrogen receptor signaling pathway. *Sci. Rep.* 11, 8754. doi:10.1038/s41598-021-85145-1

Li, J., Bao, L., Zha, D., Zhang, L., Gao, P., Zhang, J., et al. (2018). Oridonin protects against the inflammatory response in diabetic nephropathy by inhibiting the TLR4/p38-MAPK and TLR4/NF-κB signaling pathways. *Int. Immunopharmacol.* 55, 9–19. doi:10.1016/j.intimp.2017.11.040

Liao, W., He, X., Yi, Z., Xiang, W., and Ding, Y. (2018). Chelidonine suppresses LPS-Induced production of inflammatory mediators through the inhibitory of the TLR4/NF-κB signaling pathway in RAW264.7 macrophages. *Biomed. and Pharmacother.* 107, 1151–1159. doi:10.1016/j.biopha.2018.08.094

Lim, S. M., Jeong, J. J., Kang, G. D., Kim, K. A., Choi, H. S., and Kim, D. H. (2015). Timosaponin AIII and its metabolite sarsasapogenin ameliorate colitis in mice by inhibiting NF-κB and MAPK activation and restoring Th17/Treg cell balance. *Int. Immunopharmacol.* 25, 493–503. doi:10.1016/j.intimp.2015.02.016

Liu, C., Liu, S., Xiong, L., Zhang, L., Li, X., Cao, X., et al. (2021). Genistein-3'-sodium sulfonate attenuates neuroinflammation in stroke rats by down-regulating microglial M1 polarization through α7nAChR-NF-κB signaling pathway. *Int. J. Biol. Sci.* 17, 1088–1100. doi:10.7150/ijbs.56800

Liu, Q., Ma, Y., Alhussein, M., Zhang, Y., and Peng, L. (2016). Green data center with IoT sensing and cloud-assisted smart temperature control system. *Comput. Netw.* 101, 104–112. doi:10.1016/j.comnet.2015.11.024

Liu, X., Li, M., Tan, S., Wang, C., Fan, S., and Huang, C. (2017). Harmine is an inflammatory inhibitor through the suppression of NF-κB signaling. *Biochem. biophysical Res. Commun.* 489, 332–338. doi:10.1016/j.bbrc.2017.05.126

Liu, Y., Yin, H., Zhao, M., and Lu, Q. (2014). TLR2 and TLR4 in autoimmune diseases: a comprehensive review. *Clin. Rev. Allergy and Immunol.* 47, 136–147. doi:10.1007/s12016-013-8402-y

Lu, J.-M., Jin, G.-N., Lu, Y.-N., Zhao, X.-D., Lan, H.-W., Mu, S.-R., et al. (2021). Resveratrol modulates Toxoplasma gondii infection induced liver injury by intervening in the HMGB1/TLR4/NF-κB signaling pathway. *Eur. J. Pharmacol.* 910, 174497. doi:10.1016/j.ejphar.2021.174497

Lu, M., Zhang, Q., Chen, K., Xu, W., Xiang, X., and Xia, S. (2017a). The regulatory effect of oxymatrine on the TLR4/MyD88/NF-κB signaling pathway in lipopolysaccharide-induced MS1 cells. *Phytomedicine* 36, 153–159. doi:10.1016/j.phymed.2017.10.001

Lu, X., Pu, Y., Kong, W., Tang, X., Zhou, J., Gou, H., et al. (2017b). Antidesmone, a unique tetrahydroquinoline alkaloid, prevents acute lung injury via regulating MAPK and NF-κB activities. *Int. Immunopharmacol.* 45, 34–42. doi:10.1016/j.intimp.2017.01.026

Mathiesen, O., Wetterslev, J., Kontinen, V. K., Pommergaard, H. C., Nikolajsen, L., Rosenberg, J., et al. (2014). Adverse effects of perioperative paracetamol, NSAIDs, glucocorticoids, gabapentinoids and their combinations: a topical review. *Acta Anaesthesiol. Scand.* 58, 1182–1198. doi:10.1111/aas.12380

Mendes, K. L., Lelis, D. F., and Santos, S. H. S. (2017). Nuclear sirtuins and inflammatory signaling pathways. *Cytokine Growth Factor Rev.* 38, 98–105. doi:10.1016/j.cytogfr.2017.11.001

Meng, M., Wang, L., Yao, Y., Lin, D., Wang, C., Yao, J., et al. (2023). Ganoderma lucidum polysaccharide peptide (GLPP) attenuates rheumatic arthritis in rats through inactivating NF-κB and MAPK signaling pathways. *Phytomedicine* 119, 155010. doi:10.1016/j.phymed.2023.155010

Min, G. Y., Kim, T. I., Kim, J. H., Cho, W. K., Yang, J. H., and Ma, J. Y. (2023). Anti-atopic effect of isatidis folium water extract in TNF-α/IFN-γ-Induced HaCaT cells and DNCB-induced atopic dermatitis mouse model. *Molecules* 28, 3960. doi:10.3390/molecules28093960

Muhammad, T., Ikram, M., Ullah, R., Rehman, S. U., and Kim, M. O. (2019). Hesperetin, a citrus flavonoid, attenuates LPS-induced neuroinflammation, apoptosis and memory impairments by modulating TLR4/NF-κB signaling. *Nutrients* 11, 648. doi:10.3390/nu11030648

Newman, D. J., and Cragg, G. M. (2007). Natural products as sources of new drugs over the last 25 years. *J. Nat. Prod.* 70, 461–477. doi:10.1021/np068054v

Newton, K., Matsumoto, M. L., Wertz, I. E., Kirkpatrick, D. S., Lill, J. R., Tan, J., et al. (2008). Ubiquitin chain editing revealed by polyubiquitin linkage-specific antibodies. *Cell* 134, 668–678. doi:10.1016/j.cell.2008.07.039

Ng, J. C., and Yeomans, N. D. (2018). Helicobacter pylori infection and the risk of upper gastrointestinal bleeding in low dose aspirin users: systematic review and meta-analysis. *Med. J. Aust.* 209, 306–311. doi:10.5694/mja17.01274

Nielsen, A. J., and Mcnulty, J. (2019). Polyphenolic natural products and natural product-inspired steroidal mimics as aromatase inhibitors. *Med. Res. Rev.* 39, 1274–1293. doi:10.1002/med.21536

Niu, Y., Dong, Q., and Li, R. (2017). Matrine regulates Th1/Th2 cytokine responses in rheumatoid arthritis by attenuating the NF-κB signaling. *Cell Biol. Int.* 41, 611–621. doi:10.1002/cbin.10763

O'neill, L. A., and Bowie, A. G. (2007). The family of five: TIR-domain-containing adaptors in Toll-like receptor signalling. *Nat. Rev. Immunol.* 7, 353–364. doi:10.1038/nri2079

Park, B. S., and Lee, J. O. (2013). Recognition of lipopolysaccharide pattern by TLR4 complexes. *Exp. Mol. Med.* 45, e66. doi:10.1038/emm.2013.97

Pei, H., Xue, L., Tang, M., Tang, H., Kuang, S., Wang, L., et al. (2020). Alkaloids from black pepper (Piper nigrum L.) exhibit anti-inflammatory activity in murine macrophages by inhibiting activation of NF-κB pathway. *J. Agric. Food Chem.* 68, 2406–2417. doi:10.1021/acs.jafc.9b07754

Peng, Q., Liu, H., Shi, S., and Li, M. (2014). Lycium ruthenicum polysaccharide attenuates inflammation through inhibiting TLR4/NF-κB signaling pathway. *Int. J. Biol. Macromol.* 67, 330–335. doi:10.1016/j.ijbiomac.2014.03.023

Ran, J., Ma, C., Xu, K., Xu, L., He, Y., Moqbel, S. a.A., et al. (2018). Schisandrin B ameliorated chondrocytes inflammation and osteoarthritis via suppression of NF-κB and MAPK signal pathways. *Drug Des. Dev. Ther.* 12, 1195–1204. doi:10.2147/dddt.S162014

Raza, S. S., Khan, M. M., Ahmad, A., Ashafaq, M., Islam, F., Wagner, A. P., et al. (2013). Neuroprotective effect of naringenin is mediated through suppression of NF-κB signaling pathway in experimental stroke. *Neuroscience* 230, 157–171. doi:10.1016/j.neuroscience.2012.10.041

Rehman, S. U., Ali, T., Alam, S. I., Ullah, R., Zeb, A., Lee, K. W., et al. (2018). Ferulic acid rescues LPS-induced neurotoxicity via modulation of the TLR4 receptor in the mouse Hippocampus. *Mol. Neurobiol.* 56, 2774–2790. doi:10.1007/s12035-018-1280-9

Rim, H. K., Cho, W., Sung, S. H., and Lee, K. T. (2012). Nodakenin suppresses lipopolysaccharide-induced inflammatory responses in macrophage cells by inhibiting tumor necrosis factor receptor-associated factor 6 and nuclear factor-κB pathways and protects mice from lethal endotoxin shock. *J. Pharmacol. Exp. Ther.* 342, 654–664. doi:10.1124/jpet.112.194613

Rix, U., and Superti-Furga, G. (2009). Target profiling of small molecules by chemical proteomics. *Nat. Chem. Biol.* 5, 616–624. doi:10.1038/nchembio.216

Rodrigues, T., Reker, D., Schneider, P., and Schneider, G. (2016). Counting on natural products for drug design. *Nat. Chem.* 8, 531–541. doi:10.1038/nchem.2479

Rowe, D. C., Mcgettrick, A. F., Latz, E., Monks, B. G., Gay, N. J., Yamamoto, M., et al. (2006). The myristoylation of TRIF-related adaptor molecule is essential for Toll-like receptor 4 signal transduction. *Proc. Natl. Acad. Sci. U. S. A.* 103, 6299–6304. doi:10.1073/pnas.0510041103

Ruland, J. (2011). Return to homeostasis: downregulation of NF-κB responses. *Nat. Immunol.* 12, 709–714. doi:10.1038/ni.2055

Sato, S., Sugiyama, M., Yamamoto, M., Watanabe, Y., Kawai, T., Takeda, K., et al. (2003). Toll/IL-1 receptor domain-containing adaptor inducing IFN-beta (TRIF) associates with TNF receptor-associated factor 6 and TANK-binding kinase 1, and activates two distinct transcription factors, NF-kappa B and IFN-regulatory factor-3, in the Toll-like receptor signaling. *J. Immunol.* 171, 4304–4310. doi:10.4049/jimmunol.171.8.4304

Sehnert, B., Burkhardt, H., Dubel, S., and Voll, R. E. (2020). Cell-type targeted NF-kappaB inhibition for the treatment of inflammatory diseases. *Cells* 9, 1627. doi:10.3390/cells9071627

Shen, C.-Y., Xu, X.-L., Yang, L.-J., and Jiang, J.-G. (2019). Identification of narciclasine from Lycoris radiata (L'Her.) Herb. and its inhibitory effect on LPS-induced inflammatory responses in macrophages. *Food Chem. Toxicol.* 125, 605–613. doi:10.1016/j.fct.2019.02.003

Shi, X., Yu, L., Zhang, Y., Liu, Z., Zhang, H., Zhang, Y., et al. (2020). Glycyrrhetinic acid alleviates hepatic inflammation injury in viral hepatitis disease via a HMGB1-TLR4 signaling pathway. *Int. Immunopharmacol.* 84, 106578. doi:10.1016/j.intimp.2020.106578

Shu, J. L., Zhang, X. Z., Han, L., Zhang, F., Wu, Y. J., Tang, X. Y., et al. (2019). Paeoniflorin-6'-O-benzene sulfonate alleviates collagen-induced arthritis in mice by downregulating BAFF-TRAF2-NF-κB signaling: comparison with biological agents. *Acta Pharmacol. Sin.* 40, 801–813. doi:10.1038/s41401-018-0169-5

Skaug, B., Jiang, X., and Chen, Z. J. (2009). The role of ubiquitin in NF-kappaB regulatory pathways. *Annu. Rev. Biochem.* 78, 769–796. doi:10.1146/annurev.biochem.78.070907.102750

Sun, S. C. (2011). Non-canonical NF-κB signaling pathway. *Cell Res.* 21, 71–85. doi:10.1038/cr.2010.177

Sun, S. C. (2017). The non-canonical NF-κB pathway in immunity and inflammation. *Nat. Rev. Immunol.* 17, 545–558. doi:10.1038/nri.2017.52

Tang, J., Cheng, X., Yi, S., Zhang, Y., Tang, Z., Zhong, Y., et al. (2021). Euphorbia factor L2 ameliorates the progression of K/BxN serum-induced arthritis by blocking TLR7 mediated IRAK4/IKKβ/IRF5 and NF-kB signaling pathways. *Front. Pharmacol.* 12, 773592. doi:10.3389/fphar.2021.773592

Tanimura, N., Saitoh, S., Matsumoto, F., Akashi-Takamura, S., and Miyake, K. (2008). Roles for LPS-dependent interaction and relocation of TLR4 and TRAM in TRIF-signaling. *Biochem. Biophys. Res. Commun.* 368, 94–99. doi:10.1016/j.bbrc.2008.01.061

Tew, X. N., Lau, N. J. X., Chellappan, D. K., Madheswaran, T., Zeeshan, F., Tambuwala, M. M., et al. (2020). Immunological axis of berberine in managing inflammation underlying chronic respiratory inflammatory diseases. *Chemico-biological Interact.* 317, 108947. doi:10.1016/j.cbi.2020.108947

Wagenlehner, F. M. E., and Dittmar, F. (2022). Re: global burden of bacterial antimicrobial resistance in 2019: a systematic analysis. *Eur. Urol.* 82, 658. doi:10.1016/j.eururo.2022.08.023

Wang, F., Han, Y., Xi, S., and Lu, Y. (2020). Catechins reduce inflammation in lipopolysaccharide-stimulated dental pulp cells by inhibiting activation of the NF-κB pathway. *Oral Dis.* 26 (0), 815–821. doi:10.1111/odi.13290

Wang, J., Li, F., Ding, J., Tian, G., Jiang, M., Gao, Z., et al. (2016). Investigation of the anti-asthmatic activity of Oridonin on a mouse model of asthma. *Mol. Med. Rep.* 14, 2000–2006. doi:10.3892/mmr.2016.5485

Wang, Q., Zhou, X., Yang, L., Luo, M., Han, L., Lu, Y., et al. (2019). Gentiopicroside (GENT) protects against sepsis induced by lipopolysaccharide (LPS) through the NF-κB signaling pathway. *Ann. Transl. Med.* 7, 731. doi:10.21037/atm.2019.11.126

Wang, Q., Zhou, X., Zhao, Y., Xiao, J., Lu, Y., Shi, Q., et al. (2018a). Polyphyllin I ameliorates collagen-induced arthritis by suppressing the inflammation response in macrophages through the NF-κB pathway. *Front. Immunol.* 9, 2091. doi:10.3389/fimmu.2018.02091

Wang, S., Tian, Y., Wang, M., Wang, M., Sun, G. B., and Sun, X. B. (2018b). Advanced activity-based protein profiling application strategies for drug development. *Front. Pharmacol.* 9, 353. doi:10.3389/fphar.2018.00353

Weiss, J., and Barker, J. H. (2018). Diverse pro-inflammatory endotoxin recognition systems of mammalian innate immunity. *F1000Research* 7, doi:10.12688/f1000research.13977.1

Wertz, I. E., and Dixit, V. M. (2010). Signaling to NF-kappaB: regulation by ubiquitination. *Cold Spring Harb. Perspect. Biol.* 2, a003350. doi:10.1101/cshperspect.a003350

Wooff, J., Pastushok, L., Hanna, M., Fu, Y., and Xiao, W. (2004). The TRAF6 RING finger domain mediates physical interaction with Ubc13. *FEBS Lett.* 566, 229–233. doi:10.1016/j.febslet.2004.04.038

Xia, Z. P., Sun, L., Chen, X., Pineda, G., Jiang, X., Adhikari, A., et al. (2009). Direct activation of protein kinases by unanchored polyubiquitin chains. *Nature* 461, 114–119. doi:10.1038/nature08247

Xu, M., Skaug, B., Zeng, W., and Chen, Z. J. (2009). A ubiquitin replacement strategy in human cells reveals distinct mechanisms of IKK activation by TNFalpha and IL-1beta. *Mol. Cell* 36, 302–314. doi:10.1016/j.molcel.2009.10.002

Yao, X., Ding, Z., Xia, Y., Wei, Z., Luo, Y., Feleder, C., et al. (2012). Inhibition of monosodium urate crystal-induced inflammation by scopoletin and underlying mechanisms. *Int. Immunopharmacol.* 14, 454–462. doi:10.1016/j.intimp.2012.07.024

Ye, H., Arron, J. R., Lamothe, B., Cirilli, M., Kobayashi, T., Shevde, N. K., et al. (2002). Distinct molecular mechanism for initiating TRAF6 signalling. *Nature* 418, 443–447. doi:10.1038/nature00888

Zanoni, I., Ostuni, R., Marek, L. R., Barresi, S., Barbalat, R., Barton, G. M., et al. (2011). CD14 controls the LPS-induced endocytosis of Toll-like receptor 4. *Cell* 147, 868–880. doi:10.1016/j.cell.2011.09.051

Zhang, D., Li, X., Hu, Y., Jiang, H., Wu, Y., Ding, Y., et al. (2018). Tabersonine attenuates lipopolysaccharide-induced acute lung injury via suppressing TRAF6 ubiquitination. *Biochem. Pharmacol.* 154, 183–192. doi:10.1016/j.bcp.2018.05.004

Zhang, H., Lang, W., Wang, S., Li, B., Li, G., and Shi, Q. (2020). Echinacea polysaccharide alleviates LPS-induced lung injury via inhibiting inflammation, apoptosis and activation of the TLR4/NF-κB signal pathway. *Int. Immunopharmacol.* 88, 106974. doi:10.1016/j.intimp.2020.106974

Zhang, H., Shan, Y., Wu, Y., Xu, C., Yu, X., Zhao, J., et al. (2017). Berberine suppresses LPS-induced inflammation through modulating Sirt1/NF-κB signaling pathway in RAW264.7 cells. *Int. Immunopharmacol.* 52, 93–100. doi:10.1016/j.intimp.2017.08.032

Zhang, K., Jiao, X. F., Li, J. X., and Wang, X. W. (2015a). Rhein inhibits lipopolysaccharide-induced intestinal injury during sepsis by blocking the toll-like receptor 4 nuclear factor-κB pathway. *Mol. Med. Rep.* 12, 4415–4421. doi:10.3892/mmr.2015.3925

Zhang, L., Wang, G., Hou, W., Li, P., Dulin, A., and Bonkovsky, H. L. (2010). Contemporary clinical research of traditional Chinese medicines for chronic hepatitis B in China: an analytical review. *Hepatology* 51, 690–698. doi:10.1002/hep.23384

Zhang, N., Liu, Z., Luo, H., Wu, W., Nie, K., Cai, L., et al. (2019). FM0807 decelerates experimental arthritis progression by inhibiting inflammatory responses and joint destruction via modulating NF-κB and MAPK pathways. *Biosci. Rep.* 39. doi:10.1042/bsr20182263

Zhang, R., Ren, S., Dai, Q., Shen, T., Li, X., Li, J., et al. (2022). InflamNat: web-based database and predictor of anti-inflammatory natural products. *J. Cheminform* 14, 30. doi:10.1186/s13321-022-00608-5

Zhang, S., Xu, P., Zhu, Z., Zhou, L., Li, J., Zhou, R., et al. (2023). Acetylation of P65lys310 by P300 in macrophages mediates anti-inflammatory property of berberine. *Redox Biol.* 62, 102704. doi:10.1016/j.redox.2023.102704

Zhang, T., Wang, J., Wang, S., and Ma, C. (2015b). Timosaponin B-II inhibits lipopolysaccharide-induced acute lung toxicity via TLR/NF-κB pathway. *Toxicol. Mech. Methods* 25, 665–671. doi:10.3109/15376516.2015.1045652

Zhao, B., Zhang, Q., Liang, X., Xie, J., and Sun, Q. (2021). Quercetin reduces inflammation in a rat model of diabetic peripheral neuropathy by regulating the TLR4/MyD88/NF-κB signalling pathway. *Eur. J. Pharmacol.* 912, 174607. doi:10.1016/j.ejphar.2021.174607

Zhao, H., Zheng, Q., Hu, X., Shen, H., and Li, F. (2016). Betulin attenuates kidney injury in septic rats through inhibiting TLR4/NF-κB signaling pathway. *Life Sci.* 144, 185–193. doi:10.1016/j.lfs.2015.12.003

Zhong, J., Wang, F., Wang, Z., Shen, C., Zheng, Y., Ma, F., et al. (2019). Aloin attenuates cognitive impairment and inflammation induced by d-galactose via down-regulating ERK, p38 and NF-κB signaling pathway. *Int. Immunopharmacol.* 72, 48–54. doi:10.1016/j.intimp.2019.03.050

Zhou, J., Deng, Y., Li, F., Yin, C., Shi, J., and Gong, Q. (2019). Icariside II attenuates lipopolysaccharide-induced neuroinflammation through inhibiting TLR4/MyD88/NF-κB pathway in rats. *Biomed. Pharmacother.* 111, 315–324. doi:10.1016/j.biopha.2018.10.201

Zhu, Y., Ouyang, Z., Du, H., Wang, M., Wang, J., Sun, H., et al. (2022). New opportunities and challenges of natural products research: when target identification meets single-cell multiomics. *Acta Pharm. Sin. B* 12, 4011–4039. doi:10.1016/j.apsb.2022.08.022

Zou, Y. F., Li, C. Y., Fu, Y. P., Jize, X. P., Zhao, Y. Z., Peng, X., et al. (2023). Angelica sinensis aboveground part polysaccharide and its metabolite 5-MT ameliorate colitis via modulating gut microbiota and TLR4/MyD88/NF-κB pathway. *Int. J. Biol. Macromol.* 242, 124689. doi:10.1016/j.ijbiomac.2023.124689

frontiers | Frontiers in Pharmacology

TYPE Original Research
PUBLISHED 03 March 2025
DOI 10.3389/fphar.2025.1515485

OPEN ACCESS

EDITED BY
Weicheng Hu,
Yangzhou University, China

REVIEWED BY
Imran Khan,
Abdul Wali Khan University Mardan, Pakistan
Shichao Lv,
First Teaching Hospital of Tianjin University of Traditional Chinese Medicine, China
Wenrui Xia,
Chengdu University of Traditional Chinese Medicine, China

*CORRESPONDENCE
Longtao Liu,
liulongtao1976@126.com
Min Wu,
wumin@gamyy.cn

†These authors have contributed equally to this work

RECEIVED 23 October 2024
ACCEPTED 10 February 2025
PUBLISHED 03 March 2025

CITATION
Li D, Li Y, Yang S, Zhang X, Cao Y, Zhao R, Zhao Y, Jin X, Lu J, Wang X, Wang Q, Liu L and Wu M (2025) Polydatin combined with hawthorn flavonoids alleviate high fat diet induced atherosclerosis by remodeling the gut microbiota and glycolipid metabolism. *Front. Pharmacol.* 16:1515485. doi: 10.3389/fphar.2025.1515485

Polydatin combined with hawthorn flavonoids alleviate high fat diet induced atherosclerosis by remodeling the gut microbiota and glycolipid metabolism

Dan Li[1,2†], Yujuan Li[1†], Shengjie Yang[1†], Xiaonan Zhang[3], Yu Cao[3], Ran Zhao[1,4], Yixi Zhao[1,5], Xiao Jin[1], Jing Lu[1,5], Xinyue Wang[1], Qiutao Wang[1], Longtao Liu[3]* and Min Wu[1]*

[1]Guang'an Men Hospital, China Academy of Chinese Medical Sciences, Beijing, China, [2]The Dongfang Hospital of Beijing University of Chinese Medicine, Beijing, China, [3]Xiyuan Hospital, China Academy of Chinese Medical Sciences, Beijing, China, [4]Aerospace Center Hospital, Beijing, China, [5]Graduate School, Beijing University of Chinese Medicine, Beijing, China

Background: Atherosclerosis is a widely studied pathophysiological foundation of cardiovascular diseases. Inflammation and dyslipidemia are risk factors that promote the formation of atherosclerotic plaques. The gut microbiota and their metabolites are considered independent risk factors for atherosclerosis. Polydatin combined with hawthorn flavonoids, as the extracts of *Polygonum cuspidatum Sieb. et Zucc*. and *Crataegus pinnatifida Bunge*, have shown excellent cardiovascular protective effects. However, the underlying mechanism requires further investigation. Our study aimed to explore the anti-atherosclerotic mechanism through gut microbiota and their metabolites.

Methods: ApoE$^{-/-}$ mice were fed either a normal-chow diet or a high-fat diet. The polydatin combined with hawthorn flavonoids group received varied doses of polydatin and hawthorn flavonoids: a high dose (polydatin 200 mg/kg daily; hawthorn flavonoids 100 mg/kg daily), a medium dose (polydatin 100 mg/kg daily; hawthorn flavonoids 50 mg/kg daily), and a low dose (polydatin 50 mg/kg daily; hawthorn flavonoids 25 mg/kg daily). The control and model groups were administered distilled water (0.2 mL daily). The experiment lasted for 24 weeks.

Results: Polydatin combined with hawthorn flavonoids administration significantly reduced lipid and inflammatory cytokine levels, meanwhile, the atherosclerotic lesions in a high-fat diet-induced ApoE$^{-/-}$ mice were significantly decreased. Additionally, polydatin combined with hawthorn flavonoids also inhibited the enhancement of trimethylamine N-oxide (TMAO), trimethylamine (TMA) levels of HFD-induced ApoE$^{-/-}$ mice by regulating the expression of hepatic flavin-containing enzyme monooxygenase 3 (FMO3). 16S rRNA sequencing results demonstrated that high-dose polydatin combined with hawthorn flavonoids treatment increased the abundance of *Actinobacteriota*, *Atopobiaceae* and *Coriobacteriaea_UCG-002*, and decreased the abundance of *Desulfobacterota*. *Norank_f_Muribaculaceae* was enriched in the medium-dose polydatin combined with hawthorn flavonoids and simvastatin groups, and *Lactobacillus* was mainly increased in the simvastatin and the low-dose

polydatin combined with hawthorn flavonoids groups. According to the metagenetic results, functional annotations also suggested that the biological processes of each group mainly focused on metabolism-related processes. Specifically, polydatin combined with hawthorn flavonoids may regulate the abundance of TMA-producing bacteria (Coriobacteriaceae, *Desulfovibrio*, *Muribaculum*, and *Clostridium*) and related enzymes in glycolipid metabolic pathways to exert an important effect on the prevention of atherosclerosis.

Conclusion: Our results suggested that polydatin combined with hawthorn flavonoids could regulate the glucolipid metabolism-related pathway, attenuate inflammatory cytokine levels, and reduce atherosclerotic plaques by remodeling gut microbiota.

KEYWORDS

atherosclerosis, gut microbiota, TMAO, polydatin, hawthorn flavonoids

1 Introduction

Cardiovascular diseases (CVDs) are the leading cause of mortality worldwide (Bansilal et al., 2015). Atherosclerosis is one of the pathological basis of CVDs and is characterized by chronic inflammatory artery disease accompanied by disturbances in glucose and lipid metabolism (Joris and Gloor, 2019). Inflammation spreads throughout the process of atherosclerosis, and in combination with lipid deposition, aggravates the progression of atherosclerotic plaques (Blagov et al., 2023). Risk factors, including dyslipidemia and diabetes, promote atherosclerosis progression (Vaccarezza and Galassi, 2023). There has been increasing evidence that gut microbiota can regulate gut microbial homeostasis in the human body (Zhou et al., 2020). The gut microbiota is responsible for converting different complex substances into bioactive metabolites (Lau et al., 2017) and is considered an indicator of host pathology, including CVDs (Wang and Zhao, 2018). Thus, on one hand, gut microbiota may indirectly affect atherosclerosis by increasing the risk of glucose and lipid metabolism disorders, such as obesity and diabetes (Traughber et al., 2023); on the other hand, gut microbiota influences atherosclerosis by enhancing the direct risk factors of atherosclerotic lesions through its metabolites (Ma and Li, 2018).

Trimethylamine-N-oxide (TMAO) is generated from dietary sources, which are widely present in high-protein diets and dairy products (Koeth et al., 2019). Intriguingly, trimethylamine (TMA)-producing bacteria, a type of specific gut bacteria (Rath et al., 2019), may be involved in the metabolism of these foods by producing TMA-lyse [mainly choline-TMA lyase (CutC/D)] (Simó and García-Cañas, 2020), and the oxidation of the hepatic flavin-containing enzyme monooxygenase 3 (FMO3) also participates in the microbial pathways involved in TMA/TMAO formation (Schugar and Brown, 2015). Recent studies have reported that choline utilization (cut) gene clusters, such as *Lachnoclostridium*, *Desulfovibrio*, and *Clostridium*, promote the conversion of choline to TMA, which is associated with elevated TMAO levels (Cai et al., 2022). The gut microbial alterations by TMA-producing bacteria are often accompanied by elevated TMAO levels, plaque lipid deposition, high lipid levels, and damaged cholesterol transport (Luo et al., 2022). In addition, inflammatory cytokines have been highlighted as a central driving force that is triggered by TMAO (Singh et al., 2017) and aggravate genes related to gluconeogenesis and glucose transport (Gao et al., 2015), thus indicating the microbial mechanism of atherosclerosis (Saaoud et al., 2023). Collectively, the gut microbiota, acting as a virtual endocrine organ (Qi et al., 2021), accompanied by TMAO, contribute to the pathologic processes of atherosclerosis through various mechanisms, mainly via inflammation (Bolte et al., 2021) and glycolipid metabolism disorders (Massey and Brown, 2021). These effects occur when there is an imbalance occurs in the host's gut microbiota.

It is widely known that statins may prevent the progression of atherosclerosis to a certain extent. However, myopathy, renal disease, rhabdomyolysis, and other muscle-related adverse diseases associated with statins should not be overlooked. It has been shown that natural compounds may confer protection against atherosclerotic cardiovascular disease (ASCVD) through various mechanisms (Arauna et al., 2019). Especially, many plant compound are beneficial for metabolic diseases, such as CVD, obesity, and diabetes, which are caused by the metabolic disorder of fat, sugar, and protein (Wang et al., 2022). emerging evidence has indicated that paeonol prevents the development of atherosclerosis by suppressing the release of inflammatory cytokines (Li et al., 2009).

Modern pharmacological studies (Qu et al., 2021) and clinical trials (Zifu et al., 2022) have confirmed that specific Chinese herbs or extracts have shown excellent potential therapeutic effects in ASCVD owing to their prominent detoxifying and blood-activating effects (Xue et al., 2013). *Polygonum cuspidatum Sieb. et Zucc.* (*P. cuspidatum*) and *Crataegus pinnatifida Bunge* (*C. pinnatifida*) as representative detoxifying and blood-activating herbs (Qin et al., 2022), are known for their efficacy in blood activation and resolving stasis, clearing heat, and detoxification (Zhu et al., 2018a). "Stasis" and "poison" in traditional Chinese medicine are not only pathogenic factors, but also pathological products of zang-fu dysfunction. "Stasis poison" consists of two elements including "stasis" and "poison," which interact and influence each other. Toxic heat obstructed in the blood vessels is easy to become blood stasis. The application of activating blood and detoxification in AS has become increasingly extensive. In the Qing Dynasty, Wang Qingren summarized the theory of stasis and established detoxification and blood-activating decoction. *P. cuspidatum* as one of the representative Chinese herbs for promoting blood circulation, clearing heat, removing dampness and relieving pain, was first recorded in "Mingyi Bielu". *P. cuspidatum* is often used in TCM to clear dampness and heat,

and detoxifying, promoting blood circulation, and removing blood stasis (Wu et al., 2020). It was mentioned first for"treating dysentery" in *Tang Materia Medica* (*Tang Ben Cao*) dating back to 659 AD, the first known official pharmacopeia in the world (Liu et al., 2011). Moreover, it acts on tonifying the spleen to promote digestion and activate blood circulation to dissipate blood stasis.

Extensive evidence has shown that polydatin (Zhao et al., 2022) or hawthorn flavonoids (Hu et al., 2022) could exert cardioprotective effects and alleviate metabolic disorders, partially via the gut microbiota. Previously, our team combined hawthorn to promote blood circulation and resolving blood stasis with *P. cuspidatum* to clear heat and detoxify (Feng et al., 2011), applied it to the treatment of acute coronary syndrome, and achieved great clinical efficacy (Wu et al., 2021). In addition, our previous clinical trial also confirmed the remarkable anti-atherosclerotic efficacy of polydatin (the extract of *P. cuspidatum*) combined with hawthorn flavonoids (the extract of hawthorn) (Liu et al., 2014). However, the intimate associations and mechanisms were unknown. Therefore, we hypothesized that the anti-atherosclerotic mechanism of polydatin combined with hawthorn flavonoids (PH), compatibility of traditional Chinese medicines, is linked with the inhibition of TMAO (Li and Tang, 2017), related pathways, and the regulation of gut microbiota disorders (Trøseid et al., 2020). Taking these factors into consideration, we evaluated the indicators of lipids, inflammation, and plaque area, provided an integrated metagenomic sequencing (Zhulin, 2016), and targeted metabolomics (Fiehn, 2016) analysis of the metabolite TMAO to further explore the specific therapeutic mechanism of PH.

2 Materials and methods

2.1 Drugs and diets

Polydatin (purity ≥98%, 140 g, PO210425, Xi'an Guanjie BioTech Co. Ltd., Xi'an, China) and hawthorn flavonoids (purity ≥90%, no. AKH15-2; Linyi Aikang Pharmaceutical Co., Ltd., Shandong, China) were mixed to prepare a solution. simvastatin was purchased from Hangzhou MSD Pharmaceutical Co. Ltd. (20 mg, U010049; Zhangzhou, China). All the natural products using from a single manufacturing batch. The drug dosage standard for this experiment was in accordance with the First edition of Chinese Pharmacopoeia 2015. The clinical recommended daily oral doses for adults were 15 g knotcane and 12 g hawthorn. The dosage for mice was converted according to the equivalent dose ratio of adult (adult weight calculated by 60 kg) to the body surface area of mice and the content percentage of Chinese medicine components in Chinese medicinal materials. The high-fat diet (HFD) containing 21% saturated fat, 0.15% cholesterol and 1% choline was purchased from Keao Xieli Feed Co., Ltd. [SCXK (Beijing) 2019–0003].

2.2 Animal experiments

Specific pathogen-free (SPF) male C57BL/6J mice (8-week-old, 19–21 g) and male apolipoprotein E knockout ($ApoE^{-/-}$) mice of the same age and genetic background were obtained from Vital River Laboratory Animals (Beijing, China). The mice were bred in a SPF laboratory and had free access to food and water. After 13 weeks, aortic atherosclerotic plaque formation was confirmed by microscopic observation after dissection, indicating that the atherosclerotic model was successfully prepared. Subsequently, all mice were randomly assigned to six groups (n = 10 in each group): (Bansilal et al., 2015): control: C57BL/6J mice received normal diet; (Joris and Gloor, 2019); model: $ApoE^{-/-}$ mice received HFD; (Blagov et al., 2023); low dose of PH group (PHL): HFD supplemented with polydatin (50 mg/kg daily) and hawthorn flavonoids (25 mg/kg daily); (Vaccarezza and Galassi, 2023); medium dose of PH group (PHM): HFD supplemented with polydatin (100 mg/kg daily) and hawthorn flavonoids (50 mg/kg daily); (Zhou et al., 2020); high dose of PH group (PHH): HFD supplemented with polydatin (200 mg/kg daily) and hawthorn flavonoids (100 mg/kg daily); (Lau et al., 2017); simvastatin: HFD supplemented with simvastatin (5 mg/kg daily). The control and model groups received distilled water (0.2 mL daily). The experiment lasted for 24 weeks, and all mice were fasted overnight and euthanized using isoflurane inhalation at the end of the experiment. The experimental protocol was approved by Institutional Animal Care and Use Committee (IACUC), Guang'an men Hospital, China Academy of Chinese Medical Sciences. The protocol for *in vivo* studies was approved by the Ethics Committee of Guang'anmen Hospital, China Academy of Chinese Medical Sciences (IACUC-GAMH-2021-013).

2.3 Histology

After collection of blood samples, the circulatory system was rinsed with normal saline. The thoracic aorta was isolated, and adherent fat was removed. The heart and aorta were perfused with phosphate-buffered saline for 10 min and then with 3.5% paraformaldehyde for 5 min. The heart was then rapidly removed, fixed in 10% buffered neutral formalin for 24 h, and washed in tap water to remove the formalin. For enface staining of the plaque areas in the mice, the whole aorta was soaked with Oil Red O (ORO) solution and photographed against a black background. The aortic sinus specimens were fixed with 4% paraformaldehyde, dehydrated in layers, and embedded in paraffin wax. Continuous sections (5 μm) were taken from the aortic sinus to the aortic arch at intervals of 40 mm, and atherosclerotic aortic sinus lesions were evaluated using hematoxylin-eosin (H&E) staining. The remaining aortic sinus samples were buried at the optimal cutting temperature, and frozen sections were used for ORO staining to evaluate lipid deposition areas. The ratio used to make a working dilution of the red O dye was 3:2 (red O dye:distilled water). The ratio of isopropanol to distilled water was 3:2, which formed a 60% isopropanol solution. Subsequently, the aorta was removed from the 10% formalin solution, rinsed for 1–2 min with distilled water, dipped in 60% isopropanol for 1 min, stained with the oil red O working dilution for 10 min, and then the aorta was placed in 60% isopropanol. Aortas were differentiated until the vascular wall of the aortas was transparent, and the difference between the color and the plaque was clear. Finally, the aortas were stored in 10% formalin, after staining and taking photos. Three lesion areas were compared by using computer-supported morphometry (ImageJ software) at 30-μm intervals, and the average lesion size was estimated. The percentage of plaque in total vascular area represented the relative severity of AS.

2.4 Lipid measurements

The plasma concentrations of cholesterol (TC), triglycerides (TG), low-density lipoprotein cholesterol (LDL-C), very low-density lipoprotein cholesterol (VLDL-C), and high-density lipoprotein cholesterol (HDL-C) were measured using an automatic bioinformatic instrument (BackmanAU5821, United States).

2.5 AimPlex multiplex immunoassays of inflammatory cytokines

Serum levels of interleukin-1-beta (IL-1β), interleukin-2 (IL-2), interleukin-6(IL-6), interleukin-17A (IL-17A), tumor necrosis factor alpha (TNF-α) and hs-CRP were measured using the Aimplex Mice Custom Premixed Analyte kit (Beijing Quantobio, China).

2.6 Immunological biomarkers analysis

Paraffin-embedded fixed aortic arch tissues were sliced into approximately 10 μm sections. These sections were incubated with nuclear factor-κB (NF-κB) p65 Rabbit PolyClonal antibody (Proteintech; 10745-1-AP, 1:500); tumor necrosis factor alpha (TNF-α) antibody (Proteintech; 60291-1-Ig, 1:1,000); and Anti-FMO3 Antibody (abcam; ab126711, 1:5000) for overnight at 4°C. After being washed, slices were incubated with horseradish peroxidase (HRP)-conjugated anti-rabbit secondary antibody (Proteintech; SA00001-2, 1:300) for 1 h at 37°C. Hematoxylin was added to the slices for 30 s and the slices were counterstained after washing with PBS. The area of positive staining represented the levels of NF-κB and TNF-α in the aortic arch tissue, which was calculated and evaluated using the ImageJ software.

2.7 Western blot

Protein concentrations in the aorta and liver tissues were quantified using a BCA kit (Thermo Scientific). Proteins were separated by 5% or 10% sodium dodecyl sulfate-polyacrylamide gel electrophoresis and transferred onto polyvinylidene fluoride membranes (Millipore, Burlington, MA). The membrane was blocked with 5% skimmed milk, for 1 h, and then incubated with primary antibody overnight at 4°C: TNF-α, NF-κB p65 and Anti-FMO3 antibody were same as the above (as shown in 2.6); β-actin (ABclonal, AC026, 1:1,000). The blots were incubated with HRP-conjugated anti-rabbit IgG for 1 h. After washing, the membranes were analyzed using chemiluminescence detection kit.

2.8 Quantitative RT-PCR

Total RNA was extracted from liver tissues using TRIzol reagent. The cDNA was synthesized using SuperScript II (TaKaRa Bio). RT-PCR for mRNA amplification was performed using a SYBR Green Master Mix kit. Details of the real-time PCR conditions are shown in Supplementary Table S1. The target mRNA level was normalized to the β-actin level. All primer sequences were designed using the PrimerBank software and are listed in Supplementary Table S2.

2.9 TMA and TMAO detected by HPLC-MS/MS

Serum TMAO and TMA levels were measured using the Waters ACQUITY ultra-high-performance liquid chromatography system (Waters Corporation, Milford, MA, United States). Samples were separated using a mobile phase gradient consisting of a mixture of 5 mM ammonium formate as solvent A and acetonitrile as solvent B. The analytes were eluted using the following gradient profile: 90% B, 10% A for 1 min; 3.5 min, 50% A, 50% B; and reconditioning at 90% B, 10% A for 8.6 min. The detailed contents of the mobile phase gradient and mass spectrometry conditions are shown in Supplementary Tables S3, S4. Data processing was completed using the TargetLynx software.

2.10 DNA extraction and 16S rRNA sequencing

Bacterial DNA was extracted from 0.5 g fecal samples utilizing the FastDNA® Spin Kit for SoilDNA (Qiagen, Limburg). DNA integrity was detected using 1% agarose gel electrophoresis, and the concentration and purity of DNA were detected using a NanoDrop 2000 microspectrophotometer (Thermo Fisher Scientific, United States). The forward primer 338F (5′-ACTCCT ACGGGAGGCAGCAG-3′) and reverse primer 806R (5′-GGACTACHVGGGTWTCTAAT-3′) were used to amplify the V3-V4 variable region of the bacterial 16S rRNA gene. Amplification was performed according to the standard protocols. PCR products were detected by 2% agarose gel electrophoresis and purified using an AxyPrep DNA Gel Extraction Kit (Invitrogen, Carlsbad, CA, United States). A NEXTFLEX Rapid DNA-Seq Kit (Bioo Scientific, United States) was used to prepare the sequencing library. The amplified products were collected and sequenced on an Illumina MiSeq PE300/NovaSeq PE250 platform (Illumina, San Diego, United States). All raw sequences have been submitted to the Sequences Read Archive database at the NCBI under accession number PRJNA1122934.

2.11 Biochemical analyses

The quality control and splicing process of the raw sequencing sequences were based on the fastp software that was merged with FLASH. The UPARSE software was used to cluster operational taxonomic units (OTUs) with a 97% similarity cutoff. Each sequence was classified using the RDP classifier and compared to the Silva 16S rRNA database (V128) at a threshold of 70%. Alpha diversity and beta diversity analysis was used to show the distribution and similarity using principal coordinate analysis (PCoA). The differences at different taxonomic levels were evaluated using linear discriminant analysis effect size (LEfSe). A correlation heatmap was utilized to visualize the relationships between the different species and other parameters.

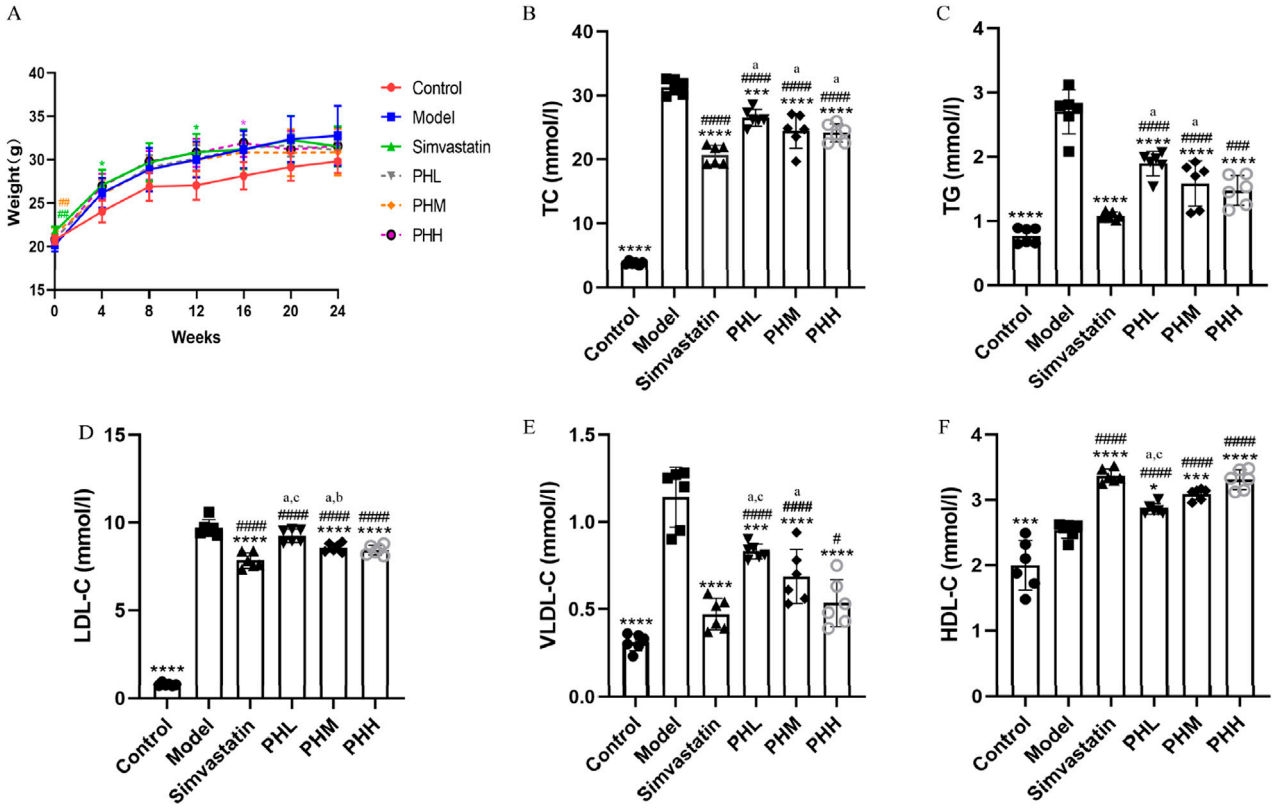

FIGURE 1
PH alleviated serum lipid levels in ApoE$^{-/-}$ mice. **(A)** Body weight. **(B)** TC. **(C)** TG. **(D)** LDL-C. **(E)** VLDL-C. **(F)** HDL-C. All data are shown as the mean ± SD (n = 6). $^{*}P < 0.05$, $^{**}P < 0.01$, $^{***}P < 0.001$, $^{****}P < 0.0001$, vs. Model; $^{\#}P < 0.05$, $^{\#\#}P < 0.01$, $^{\#\#\#}P < 0.001$, $^{\#\#\#\#}P < 0.0001$, vs. Control; $^{a}P < 0.05$ vs. simvastatin; $^{b}P < 0.05$ vs. PHL; $^{c}P < 0.05$ vs. PHH.

2.12 Metagenome sequence and taxonomic annotation

Quality control and optimization were performed using software fastp, and filtered reads were assembled (contigs ≥300 bp). In addition, open reading frames (ORFs) prediction and translation of contigs were performed using MetaGene to obtain the corresponding amino acid sequences. CD-HIT was used to cluster the predicted genetic sequences, and the non-redundant gene set was constructed. Diamond was used to align the amino acid sequences with the GENES database using BLASTP (version 2.2.28) and annotate the kyoto encyclopedia of genes and genomes (KEGG) databases (version 94.2). The amino acid sequences were aligned to the carbohydrate-active enzymes (CAZymes) database using HMMER (version 3.1b2). The abundance and differences in the corresponding species, CAZy, and KEGG functional categories were estimated using normalized RPKM values.

2.13 Statistical analyses

Statistical analyses were performed using GraphPad Prism 9.0. All data were presented as the mean ± standard deviation (SD), and multiple comparisons were analyzed using ANOVA. Statistical significance was set at $P < 0.05$.

3 Results

3.1 Polydatin and hawthorn flavonoids (PH) reduced body weight and lipid levels in HFD-fed ApoE$^{-/-}$ mice

Throughout the experiment, an obvious increase in body weight was observed in HFD-fed mice. After 11-week of intervention, the PH and simvastatin groups may have experienced a lower gain in body weight than that of the model group (Figure 1A). In addition to the possible anorexic effect that may be induced by HFD, supplementation with PH or simvastatin may also have exerted certain effects on the body weight and metabolic function of mice. Compared to the control group, a remarkably increasing trend of TC, TG, LDL-C, and VLDL-C was observed in HFD-fed mice ($P < 0.001$). Whereas mice supplemented with PH or simvastatin exhibited low levels of TC, TG, LDL-C, and VLDL-C, accompanied by high levels of HDL-C, reflecting the hyperlipidemia caused by the HFD; these levels were reversed by PH or simvastatin administration (Figures 1B–F). These results,

10.3389/fphar.2025.1515485

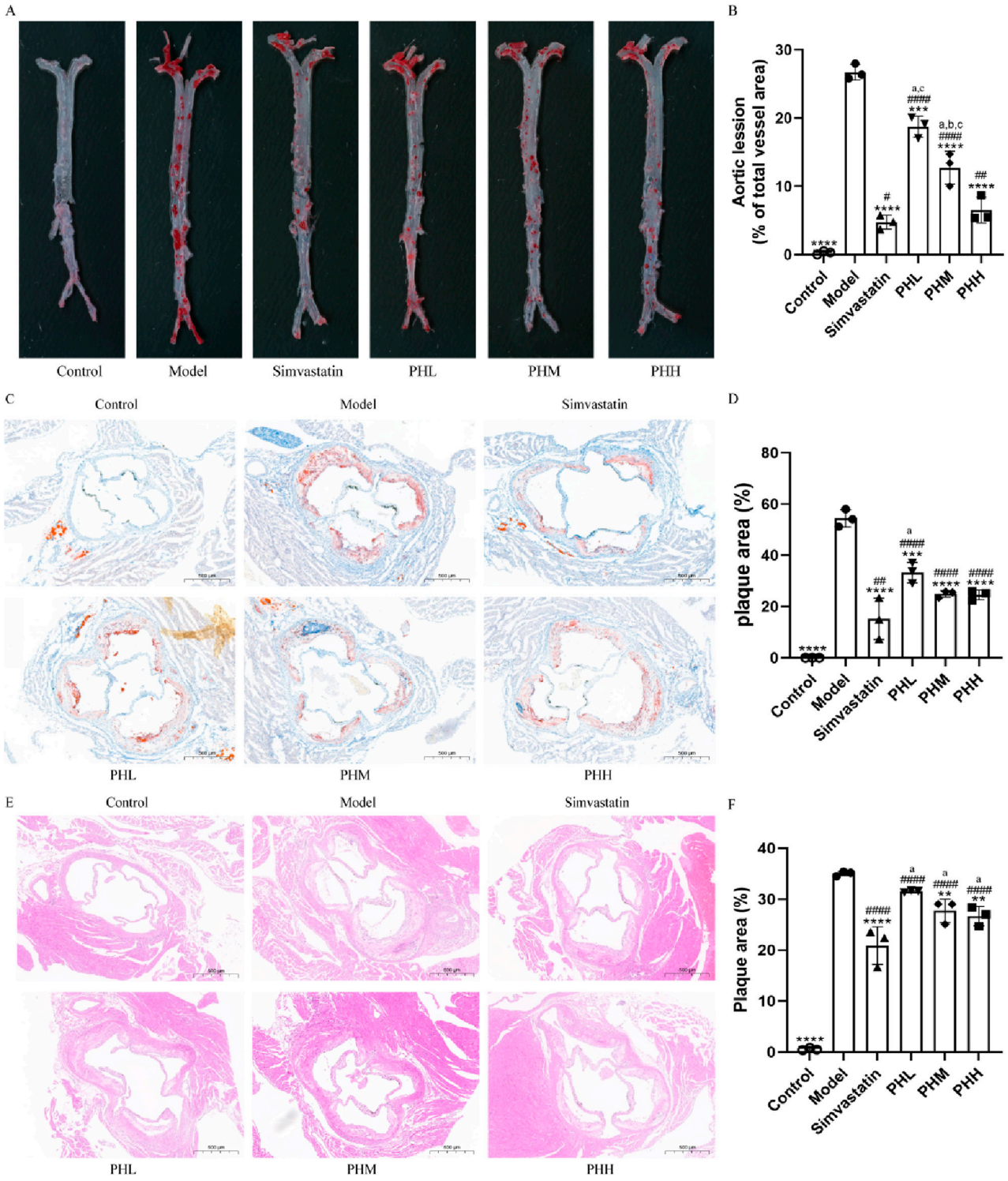

FIGURE 2
PH attenuated atherosclerosis injury in HFD-fed ApoE$^{-/-}$ mice. **(A, B)** Image of enface aortas stained with ORO, and quantitative analysis of the aortic lesion ratio. **(C, D)** Image of aortic roots sections stained with ORO, and quantitative analysis of the aortic roots cross-sectional lesions ratio. **(E, F)** Image and quantitative analysis of aortic roots sections stained with H&E, illustrating the proportion of the cross-sectional lesions in the aortic roots. All data are shown as the mean ± SD (n = 3). $^{**}P < 0.01$, $^{***}P < 0.001$, $^{****}P < 0.0001$, vs. Model; $^{\#}P < 0.05$, $^{\#\#}P < 0.01$, $^{\#\#\#\#}P < 0.0001$, vs. Control; $^{a}P < 0.05$ vs. Simvastatin; $^{b}P < 0.05$ vs. PHL; $^{c}P < 0.05$ vs. PHH.

10.3389/fphar.2025.1515485

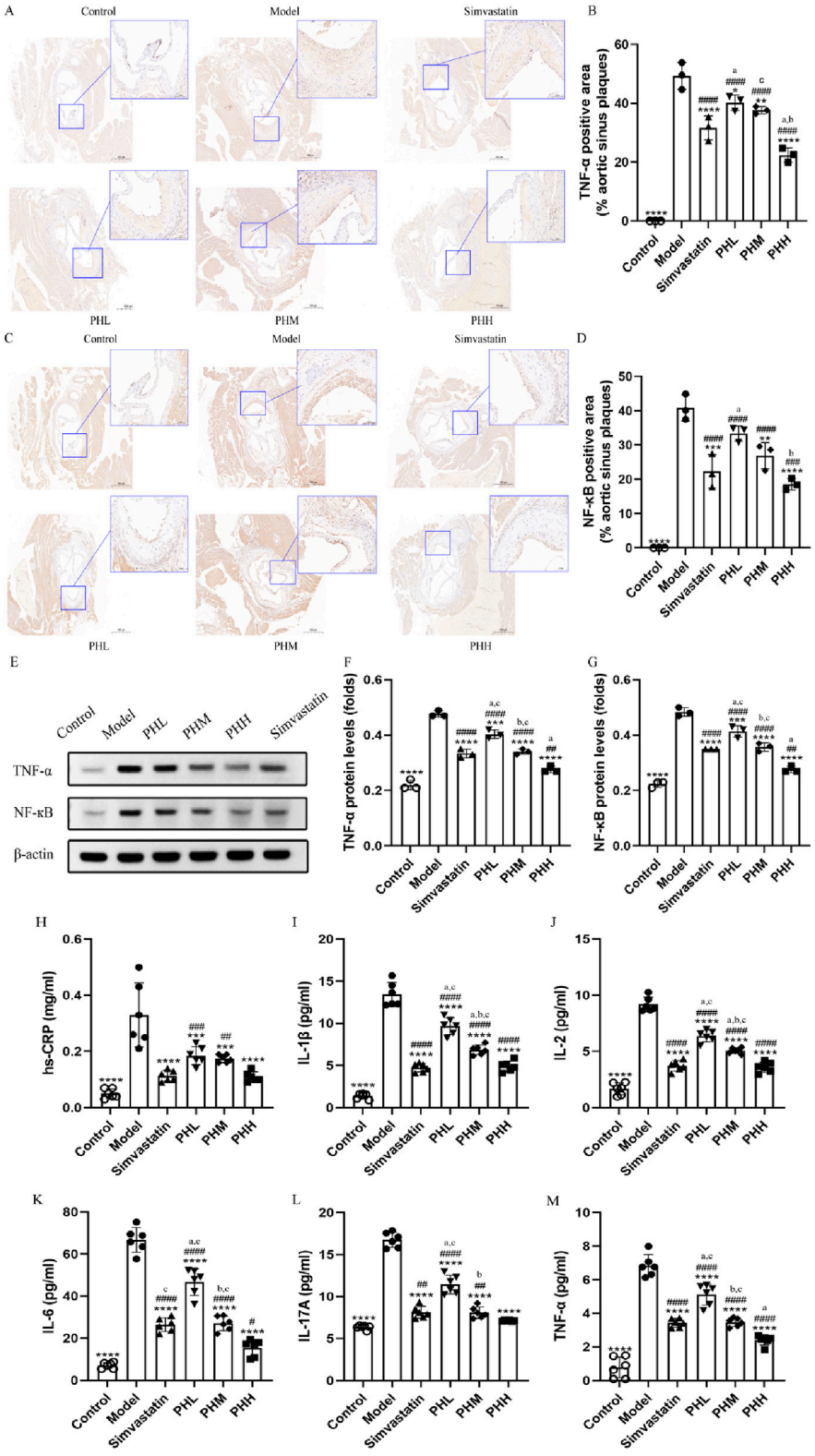

FIGURE 3
PH inhibited the activation of serum inflammatory cytokine in HFD-fed ApoE$^{-/-}$ mice. **(A)** and **(B)** Image and quantitative analysis of immunohistochemical staining of the aortic sinus and the proportion of the TNF-α positive area to the aortic sinus plaques (n = 3). **(C, D)** Image and quantitative analysis of immunohistochemical staining of the aortic sinus and the proportion of the NF-κB positive area to the aortic sinus plaques (n = 3). **(E)** Protein expression of TNF-α and NF-κB. **(F, G)** Quantitative analysis of TNF-α and NF-κB protein levels in the aortic sinus plaques (n = 3). **(H–M)** Serum hs-CRP, IL-1β, IL-2, IL-6, IL-17A, and TNF-α levels (n = 6). $^{*}P < 0.05$, $^{**}P < 0.01$, $^{***}P < 0.001$, $^{****}P < 0.0001$, vs. Model; $^{\#}P < 0.05$, $^{\#\#}P < 0.01$, $^{\#\#\#}P < 0.001$, $^{\#\#\#\#}P < 0.0001$, vs. Control; $^{a}P < 0.05$ vs. Simvastatin; $^{b}P < 0.05$ vs. PHL; $^{c}P < 0.05$ vs. PHH.

together with the increase in body weight, highlight the synergistic effect of lipid metabolism as a potential modulator of atherosclerosis and the important role of PH on the treatment of dyslipidemia.

3.2 PH attenuates HFD-induced atherosclerosis in HFD-fed ApoE$^{-/-}$ mice

Atherosclerotic plaque size was measured to assess the pathological changes in atherosclerosis. The ratio of the plaque area to the entire aorta or aortic root in the model group increased after HFD feeding. The results of ORO staining revealed that the rising trend in atherosclerotic plaque area was inhibited, and even reduced in different doses of the PH or simvastatin groups as compared with the model group (Figures 2A, C). The aorta inner wall was smooth without any evidence of obvious plaques attached in the control group, whereas lipid deposition was more prominent with an amount of foam cells within the plaque and aortic vessel stenosis in the model group (Figures 2A, C). Specifically, quantitative analysis revealed that the proportion of aortic lesions to the total aortic vessel area in the PH group showed a descending trend compared to that of the model group ($P < 0.0001$) (Figure 2B). The therapeutic effects of PHM and PHH on atherosclerosis were significant. Consistently, the proportion of cross-sectional lesions of the aortic roots reduced in the PHM and PHH groups, compared to the model group ($P < 0.01$) (Figure 2D). The results of H&E staining also suggested that the atherosclerotic plaques and lesions in the Model group were higher than those in the Control group (Figure 2E). The lesion area in the aortas in the PH and simvastatin groups mice was significantly reduced ($P < 0.001$) (Figure 2F). In summary, PHM, PHH, and simvastatin had exerted significant effects on atherosclerosis and delayed plaque deterioration.

3.3 PH improved inflammatory cytokine levels in HFD-fed ApoE$^{-/-}$ mice

Besides lipid abnormalities, the progression of atherosclerosis is also influenced by systemic inflammation to a certain extent. Given that inflammatory cytokines have been recognized as an index of atherosclerosis in epidemiological studies, immunohistochemical staining of aortic root plaques was conducted. We observed that the expression of TNF-α and NF-κB was more prominent in mice fed an HFD than in mice fed a chow diet. Nevertheless, dietary supplementation with PH and simvastatin diminished the intensity of the staining, implying that a strong antagonistic action was exerted against the inflammatory reaction during the process of atherosclerotic plaque formation (Figures 3A, C). Quantitative analysis was utilized to assess the specific efficacy of PH and simvastatin. As shown in Figures 3B, D, the ratio of TNF-α and NF-κB positive area to the aortic sinus plaques in PH and simvastatin groups were dramatically decreased ($P < 0.0001$), especially obvious in PHH group. Thus, the therapeutic effect of PHH in down-regulating TNF-α and improving inflammation factor levels is superior to that of simvastatin (Figure 3B). Consistently, we observed that the downregulation of NF-κB protein in aortic plaque in PHM, PHH, and simvastatin group was more significant than that in model group ($P < 0.0001$) (Figure 3E), with the lowest protein expression in the PHH group (Figures 3F, G).

Furthermore, we measured the levels of other important inflammatory mediators to confirm the effects of PH on atherosclerosis. The results were consistent with the previously reported changes, demonstrating that the serum levels of hs-CRP, TNF-α, IL-1β, IL-2, IL-6, and IL-17A in model group mice dramatically increased in mice fed an HFD (Figures 3H–M). After PH and simvastatin administration, a dose-dependent decrease in the inflammatory cytokine levels was observed, with the lowest level in PHH group ($P < 0.05$) (Figure 3M). This suggested that inflammatory cytokines, represented by TNF-α and NF-κB, are closely related to the progression of atherosclerotic plaques. PH reduces inflammatory factor levels, thereby improving atherosclerotic plaque formation, with the most pronounced effects found in the PHH group.

3.4 PH inhibited the enhancement of TMA and TMAO level in HFD-fed ApoE$^{-/-}$ mice

To investigate the underlying mechanism of PH on atherosclerosis, atherosclerotic markers TMAO, and the TMAO metabolic pathway-related proteins were assessed. We observed that the HFD containing 1% choline induced an elevation of TMA and TMAO levels in the model group mice. Similar to the findings of previous studies (Li et al., 2021), choline accelerated atherosclerotic progression in the present study. We observed the attenuation of TMA and TMAO in the PHH group, compared to the model group ($P < 0.001$). Notably, TMA and TMAO levels were reversed by PH supplementation at high doses, indicating that the therapeutic effect of PHH was more prominent than that of the others (Figures 4A, B).

Hepatic FMO3 is a crucial enzyme involved in the conversion of TMA to TMAO. Thus, we focused on assessing the dynamic changes in FMO3 expression and activity. In line with previous findings, the results demonstrated that compared to the control group, the protein and mRNA levels of FMO3 in mice were upregulated in the model group ($P < 0.01$). PH downregulated the protein and mRNA expression of FMO3, which was more evident in terms of protein expression of FMO3. Similarly, a high dose of PH exhibited an unexpected effect on TMA/TMAO metabolism (Figures 4C–E). In conclusion, we speculated that activation of the TMA/FMO3/TMAO pathway is an important incentive for atherosclerosis, and PH inhibits TMAO generation through the involvement of hepatic FMO3.

3.5 The effect of PH on microbial diversity and distribution during the process of atherosclerosis

To explore the microbial mechanism, 16S rRNA gene sequencing with a 97% similarity criterion for operational taxa was acquired from 36 samples. After sequence quality control and splicing, 3375 operational taxonomic units (OTUs) were identified. The rank-abundance curve declined smoothly and eventually flattened (Supplementary Figure S1A). The species

10.3389/fphar.2025.1515485

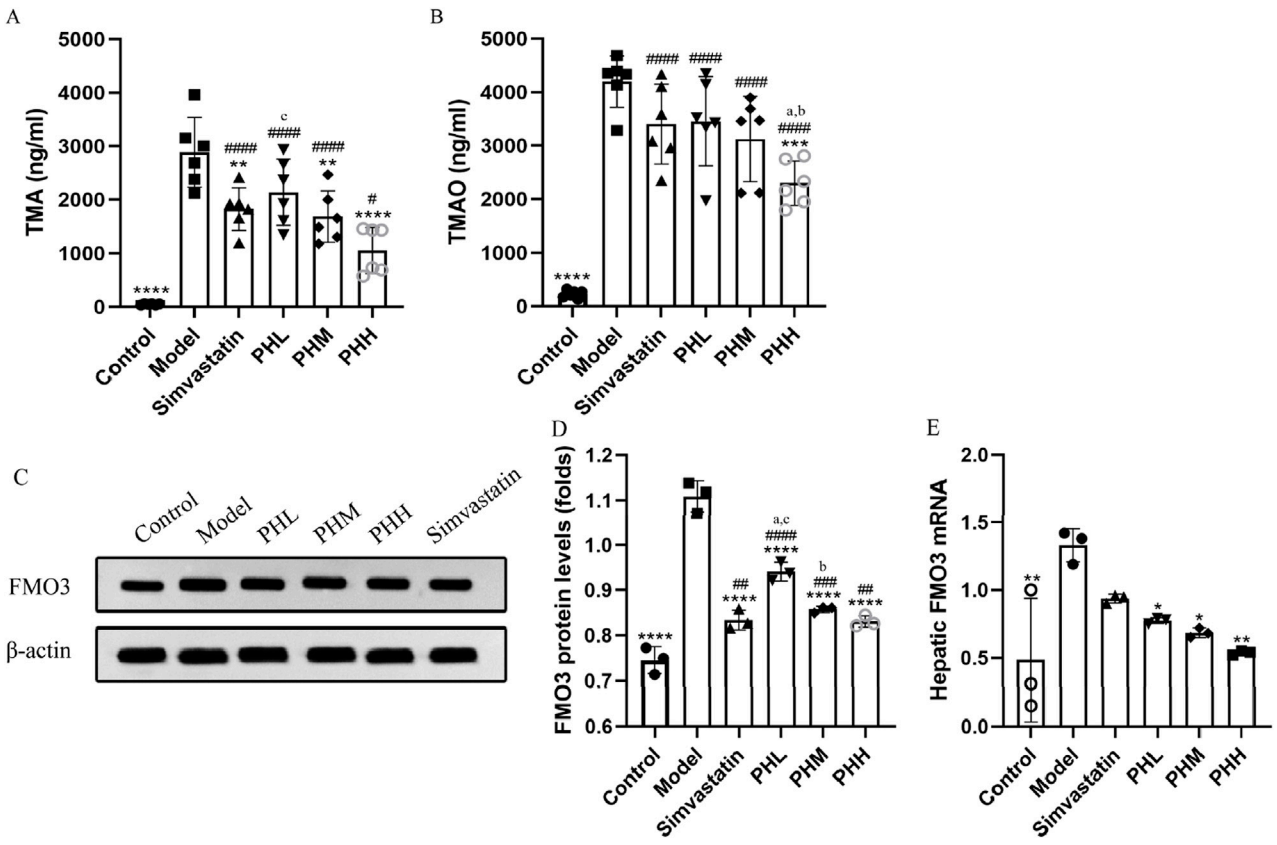

FIGURE 4
PH regulated TMA/TMAO metabolism involving hepatic FMO3 in HFD-fed ApoE$^{-/-}$ mice. **(A, B)** Serum TMA and TMAO levels (n = 6). **(C, D)** Western blot detection and quantitative analysis of FMO3 protein in liver tissues expression (n = 3). **(E)** mRNA levels of FMO3 in liver tissues quantified by qPCR (n = 3). All data are shown as the mean ± SD. $^{*}P < 0.05$, $^{**}P < 0.01$, $^{***}P < 0.001$, $^{****}P < 0.0001$, vs. Model; $^{\#}P < 0.05$, $^{\#\#}P < 0.01$, $^{\#\#\#}P < 0.001$, $^{\#\#\#\#}P < 0.0001$, vs. Control; $^{a}P < 0.05$ vs. Simvastatin; $^{b}P < 0.05$ vs. PHL; $^{c}P < 0.05$ vs. PHH.

cumulative and rarefaction curve revealed that the sequences per sample were sufficient and the sequencing depth was qualified for analysis later (Supplementary Figures S1B, C). Alpha (α) diversity analysis revealed that microbial diversity and abundance were reduced after an HFD intervention (Supplementary Figures S2, S3; Supplementary Tables S5, S6; Figures 5A–C); however, this trend was reversed or attenuated after PH administration (Figures 5D, E; Supplementary Figure S7). The gut microbiota characteristics were explored and analyzed at different levels, and 11 phyla, 14 classes, 32 orders, 50 families, 116 genera, and 201 species were identified. Moreover, the detail of distribution of different species were shown in Supplementary Figures S4–S6. At the phylum level, the proportion of *Desulfobacterota* markedly increased in the model group, while decreased in the PHM, PHH and simvastatin groups (Figure 5E).

3.6 The improvement of HFD-fed induced atherosclerosis by PH may be related to the alteration of gut microbiota

Diversity analysis was performed to identify the alterations of gut microbial structure. The PCoA plot showed a remarkable separation among the four groups (control, model, PHH, and simvastatin) along the PC2 axis, which explained 13.96% of the variation in the microbial structure (Figure 6A). The segregated microbial structure among the three groups (control, PHH, and simvastatin) was consistently visualized using non-metric multidimensional scaling (NMDS) analysis (Figure 6B). The microbiota composition was clustered by partitioning around the medoids, and three enterotypes were identified. We identified that the proportion of *Lactobacillus* increased with the administration in PH or simvastatin (Figure 6C). Notably, the enterotypes in the PHH and simvastatin groups were mainly clustered into *g_Lactobacillus* and *g_norank_f_Muribaculaceae_1 group*, indicating that PHH and simvastatin reversed the HFD-induced enterotype switch (Supplementary Figure S8). Presumably, PHH and simvastatin protected the atherosclerotic mice against microbes. Accumulating evidence indicates that the HFD-induced decrease in gut microbial diversity can be restored to some extent by PH treatment. *Bacteroidetes* and *Bacteroides* were enriched in the control group, whereas *Alistipes*, *f_*Clostridiaceae, and *f_*Defluviitaleaceae were the predominant genera in the model group. PH administration significantly improved the proportion of *p_ Actinobacteria*, *f_Atopobiaceae*, and *g_*Coriobacteriaceae_*UCG-002*, whereas it decreased the proportions of *f_*Clostridiaceae and *f_*Defluviitaleaceae in the model group mice (Supplementary Figure S9). Finally, the multigroup difference

10.3389/fphar.2025.1515485

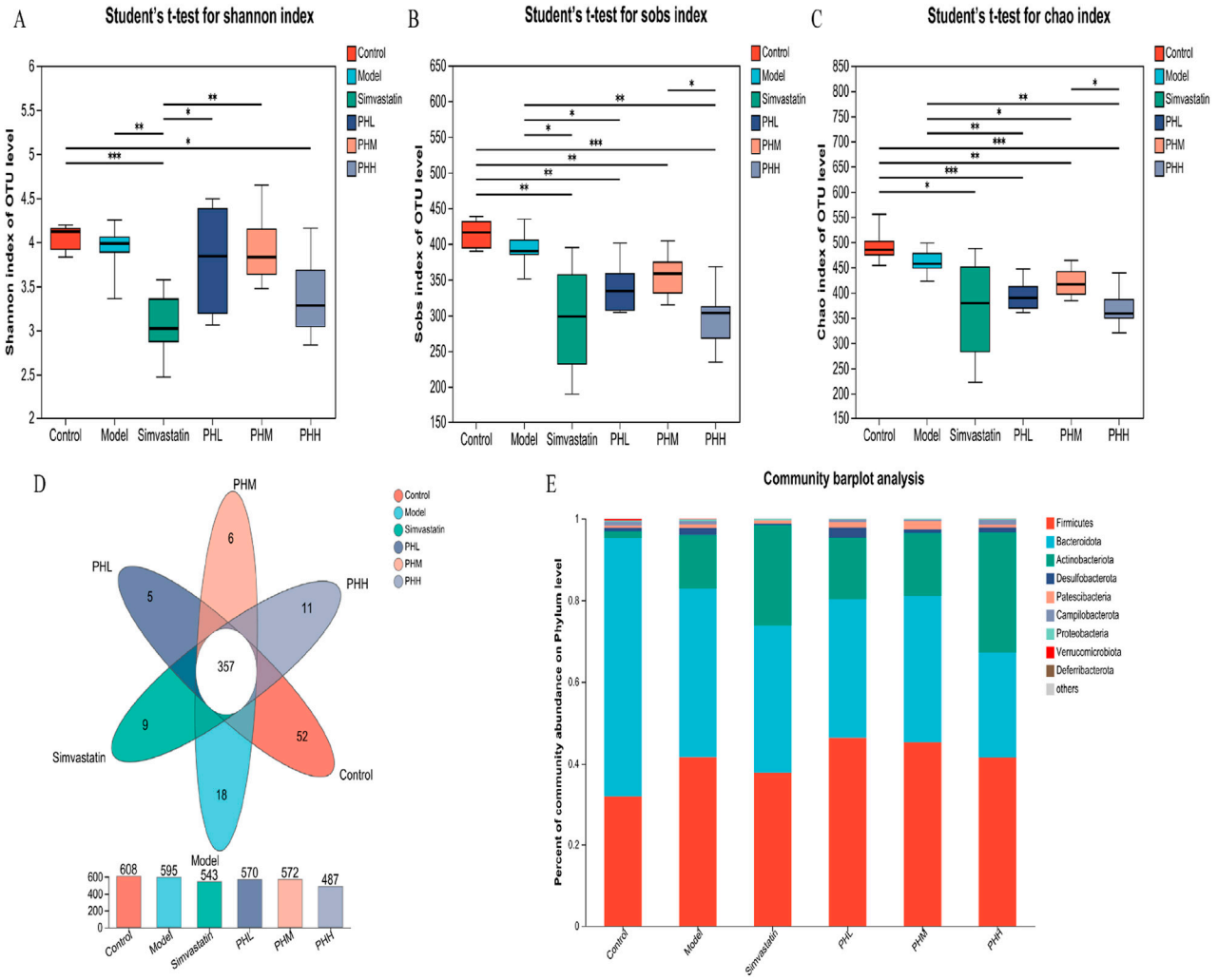

FIGURE 5
(A–C) Alpha diversity was analyzed by the Shannon, Sobs, Chao index; **(D)** Venn diagrams of OTUs; **(E)** Taxonomic composition/microbial compositions at the phylum level. *$P < 0.05$, **$P < 0.01$, ***$P < 0.001$, ****$P < 0.0001$.

analysis suggested that HFD increased the abundance of *Antinobacteriota*, *Desulfobacterota*, and Coriobacteriaceae_*UCG-002* in the model group and reduced the abundance of *Bacteroidetes*, *Bacteroides*, and *norank_f_Mribaculaceae*, whereas PH treatment reversed these changes (Figures 6D–J).

3.7 Uncovering the anti-atherosclerotic mechanism of PH: targeting the functional capacity of gut microbiota

We further conducted the metagenomic sequencing analysis to investigate the core functional capacity of different genes. Based on the LEfSe analysis, we observed that 37 differential KEGG pathways were identified in PHL and PHH groups, and ribosome, protein export, and RNA polymerase pathways were enriched in the model group. Most of the 37 differentially expressed functional pathways were highly enriched in the carbohydrate metabolism and membrane transport-related pathways. Among these, ABC transporters, carbon metabolism, glycerolipid metabolism, and glucagon signaling pathways were identified in the PHL group, and the biosynthesis of amino acids, starch, and sucrose metabolism were increased in the PHH group (Supplementary Figure S10A). Additionally, fatty acid metabolism, fatty acid and lipopolysaccharide biosynthesis were enriched in the control group, whereas the enrichment was reduced in the PHH group. A similar trend was observed in the multi-group comparison analysis (Figures 7B–I). Based on these results, we investigated the enrichment of CAZymes by LEfSe analysis. At the class level, glycosyl transferases (GTs) and carbohydrate esterases (CEs) were highly enriched in the PHL and PHH groups, whereas glycoside hydrolases (GHs) were mainly present in the simvastatin group (Figure 7A). The HFD-induced abundance of CAZymes was restored by PH administration, at the family level. Several CAZymes, including GT2_Glyco_tranf_2_3 and CE1, were enriched in the PHH group (Supplementary Figure S10B).

10.3389/fphar.2025.1515485

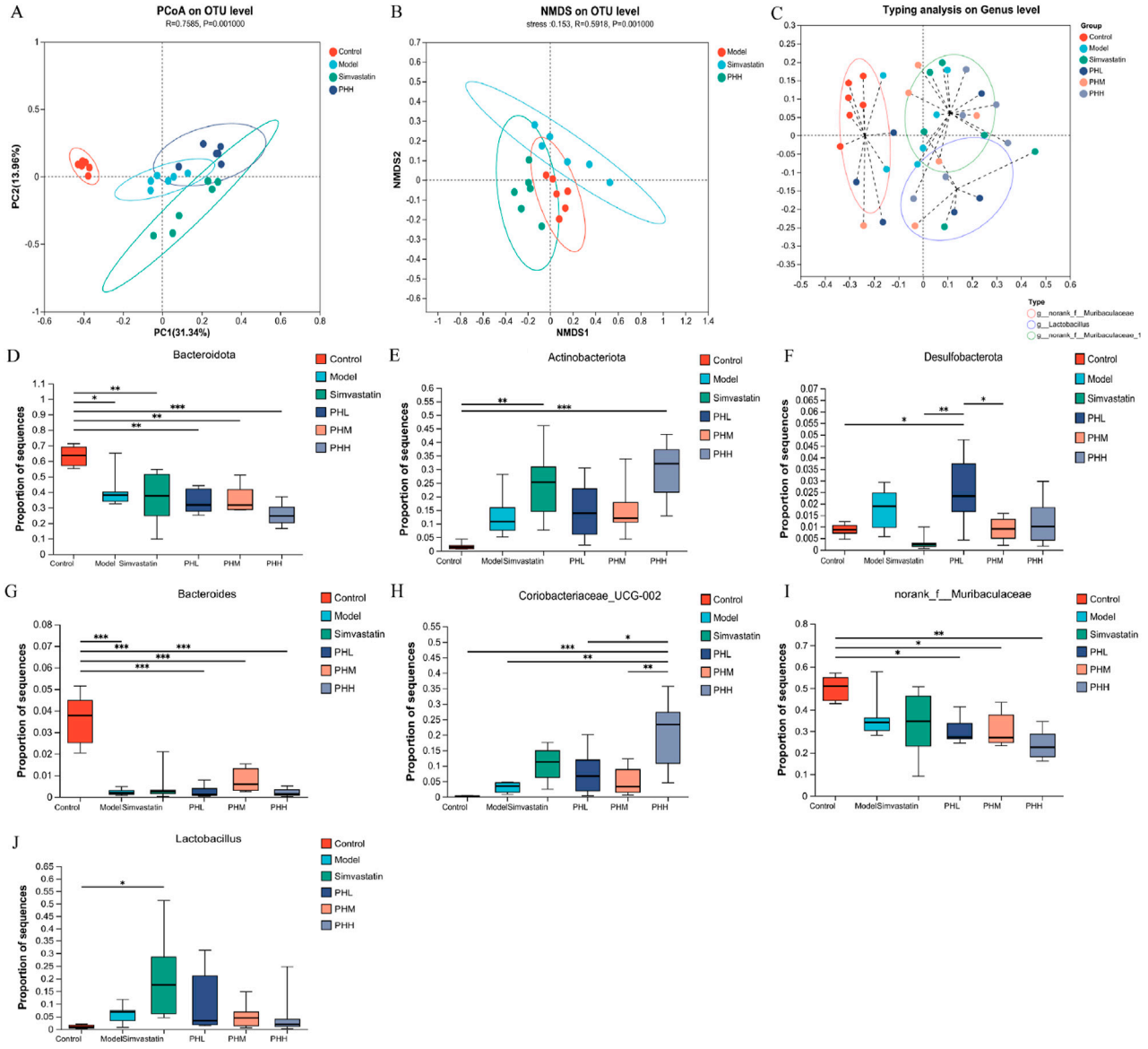

FIGURE 6
(A) PCoA plot; **(B)** NMDS analysis; **(C)** Effects of PH or simvastatin on enterotype of mice; **(D–F)** Multigroup difference analysis at the phylum level; **(G–J)** Multigroup difference analysis at the genus level; n = 6. *P < 0.05, **P < 0.01, ***P < 0.001.

3.8 Association analysis among atherosclerotic parameters, microbiota species, and microbial functions

We constructed a heatmap to visualize the associations between the gut microbiota and bioinformatic parameters. *Desulfobacterota* demonstrated a significant positive correlation with lipid levels (TG, TC, and LDL-C) and inflammatory cytokines (hs-CRP, IL-2, IL-1β, and IL-17A). Additionally, *Firmicutes* displayed a similar trend with TG, LDL-C, IL-2, and IL-1β (Figure 8A). Notably, *Firmicutes*, *Lachnoclostridium* and *Turicibacter* demonstrated significant positive correlations with TMA, TMAO, lipid, and inflammatory cytokine levels. *Desulfovibrio*, *Muribaculum*, and *Allobaculum* also correlated with lipid levels and inflammatory cytokines. *Bacteroides*, Prevotellaceae_*Ga6A1_group*, and *Eubacterium_fissicatena_group* negatively correlated with TMA, TMAO, lipid levels, and inflammatory cytokines (Supplementary Figure S11A), thereby indicating that these microbial biomarkers may be involved in the development of atherosclerosis.

Associations between atherosclerotic variables, the KEGG functional pathways, and gut microbiota were analyzed. At Level 3, ABC transporters demonstrated positive correlations with lipid levels (TG, TC, LDL-C, and VLDL-C) and inflammatory cytokines (IL-2, IL-6, IL-17A, IL-1β, hs-CRP, and TNF-β). In particular, LDL-C demonstrated a positive correlation with the metabolic pathways, including carbon, starch, and sucrose metabolism (Figure 8B). At level 2, ko00520, ko00030, and ko00550 demonstrated similar associations with the lipid and inflammatory cytokine levels (Figure 8C). At module level, M00001 (Glycolysis), M00016 (Lysine biosynthesis), and M00051 (*De novo* pyrimidine

10.3389/fphar.2025.1515485

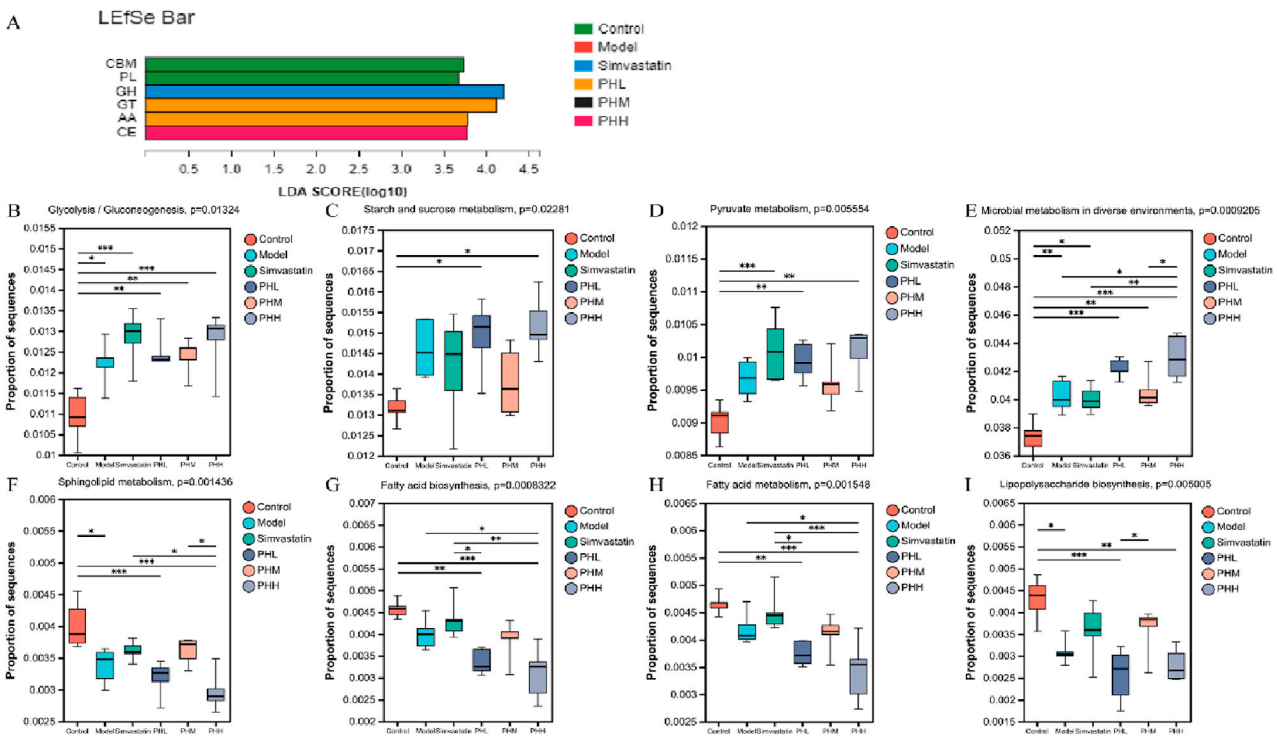

FIGURE 7
(A) LEfSe analysis of the differential enrichment of CAZymes at the family level (LDA>3); **(B–I)** Multigroup comparison analysis of KEGG pathways; $^{*}P < 0.05$, $^{**}P < 0.01$, $^{***}P < 0.001$.

biosynthesis) demonstrated positive correlations with lipid and IL-1β levels (Figure 8D). *Uncultured_bacterium_g_Turicibacter*, and *uncultured_bacterium_g_Desulfovibrio* exhibited positive correlations with TMAO, lipids, and inflammatory cytokine levels, whereas *Bacteroides_acidifaciens* exhibited negative correlations with TMAO, lipid, and inflammatory cytokine levels (Supplementary Figure S10B). In addition, we observed that metabolic pathways, including starch and sucrose metabolism, and ABC transporters, including M00001, M00051, and M00003, exhibited a positive correlation with *s_Desulfovibrio_fairfieldensis* and *s_Allobaculum_stercoricanis*, but a negative correlation with *Bacteroides* spp. and *s_Lactobacillus_murinus* (Supplementary Figures S12A, B).

3.9 PH regulated the glycolipid metabolic pathways via TMA-producing bacteria related to atherosclerosis

Considering the pathways involved in the choline metabolism, TMAO, and associated gut microbiota, TMA-producing bacteria were selected for gene set construction. The gene set included CutC-related bacteria, which may have contributed to the therapeutic effects of PH. Critical KEGG pathways among different groups were identified using linear discriminant analysis. Glycolysis/gluconeogenesis, fluid shear stress, atherosclerosis, drug metabolism, and the HIF-1signaling pathway were highly enriched in the PHH group (Figure 9F; Supplementary Figure S13). Further multigroup comparison analysis revealed that the abundance of glycolysis/gluconeogenesis and HIF-1signaling pathway markedly increased after PHH treatment (Figures 9B–E). Thus, an analysis of intergroup differences in metabolic pathways was conducted based on these findings. The abundance of 6-phospho-beta-glucosidase [EC:3.2.1.86], which is involved in the glycolysis/gluconeogenesis metabolic pathway. The abundance of phosphoglycerate mutase [EC:5.4.2.11] and fructose-bisphosphate aldolase [EC:4.1.2.13] were increased in the model group. In addition, other related enzymes, such as 6-phosphofructokinase [EC:2.7.1.90] and fructose-bisphosphatase [EC:3.1.3.11], may also exerted an important effect (Figure 9G). We hypothesized that phosphoglycerate mutase and fructose-bisphosphate aldolase were the main contributors of glycolysis/gluconeogenesis pathway. Moreover, the gene ontology (GO) functional annotation results suggested that the biological processes (BP) of each group were mainly enriched in metabolic and biosynthetic processes (Figure 9A).

Correlation analyses between metabolic pathways and TMA/TMAO revealed that ko00240, ABC transporters, and auxiliary activities positively correlated with TMA, suggesting that TMA-producing bacteria were mainly involved in the progression of atherosclerosis via metabolic pathways and related enzymes (Figures 9H–J). Moreover, we identified the top 20 species that contributed to the differences in pathways at level 3. Metabolic functions are involved in different pathways, including glycolysis/gluconeogenesis, microbial metabolism, biosynthesis of secondary metabolites, and carbon metabolism. *Desulfovibrio*, *Prevotella*, *Muribaculum*, *Clostridium*, *unclassified_f_*Lachnospiraceae, *unclassified_o_Bacteroidales*, *unclassified_f_Muribaculaceae*, and

10.3389/fphar.2025.1515485

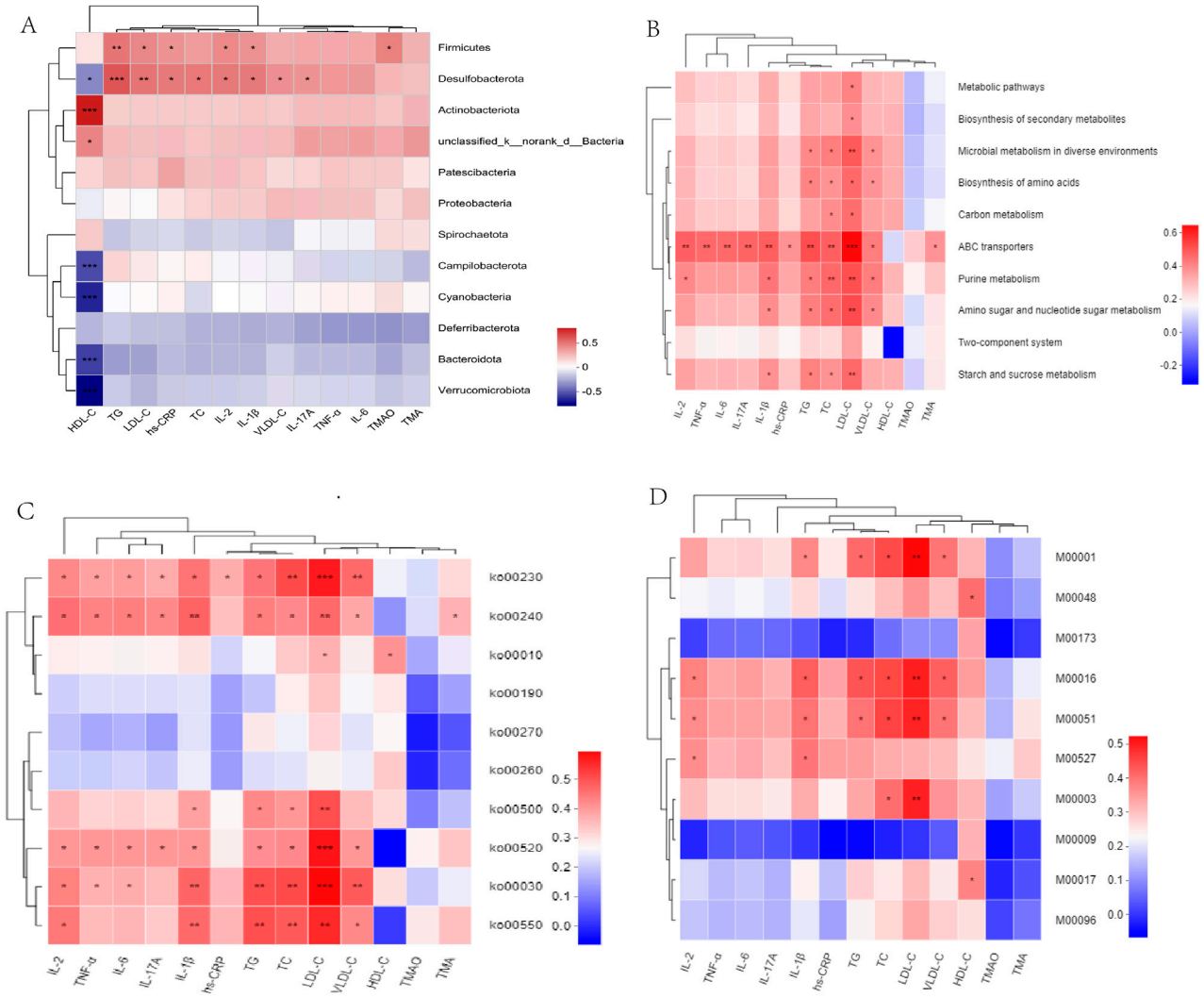

FIGURE 8
(A) Correlation heatmaps of gut microbiota and atherosclerotic parameters at the phylum levels. **(B–D)** Correlation between atherosclerotic parameters and KEGG functional pathways at level 3, level 2, and modules. *$P < 0.05$, **$P < 0.01$, ***$P < 0.001$.

*unclassified_f_*Coriobacteriaceae were contributed to these metabolic pathways (Figures 9K, L).

Finally, we further investigated the association between the TMA-producing bacteria and TMA/TMAO levels. Interestingly, Lachnospiraceae_*bacterium*, *Muribaculaceae_bacterium*_Isolate-104_(HZI), *Clostridiales_bacterium*, bacterium_0.1xD8-71, *Helicobacter_ganmani*, *Desulfovibrio*_sp., *Clostridium*_sp._CAG:417, and *Clostridium*_sp._CAG:451 exhibited positive correlations with TMA and TMAO. However, Coriobacteriaceae_*bacterium*, *Ileibacterium_valens*, *Dubosiella_newyorkensis*, *Olsenella*_sp._KGMB02461, *unclassified_g_Parabacteroides*, and *Lachnoclostridium*_sp. An181 expression exhibited negative correlations with TMA and TMAO (Figures 10M, N). Specifically, the abundance of *s_Clostridium*_sp._CAG:557, *s_Clostridium_cuniculi*, and *s_Clostridium_disporicum* increased in the model group, while the HFD-induced increase in the abundance of *Clostridium* spp. Was partially restored by PH administration. In addition, similar changes were observed in certain gut microbial species, such as *s_Lachnoclostridium*_sp._An118, *s_Muribaculaceae_bacterium*_Isolate-104_(HZI), and *s_unclassidied_g_Desulfobibrio* (Figures 10A–L). We speculated that CutC-related bacteria, such as Lachnospiraceae, *Muribaculaceae*, *Clostridium*, and *Desulfovibrio* prompted the progression of atherosclerosis via glycolipid metabolic pathways.

4 Discussion

In this study, we uncovered the anti-atherosclerotic mechanism of PH through gut microbiota and metabolites. Our results suggested that PH could regulate the glucolipid metabolism-related pathway, attenuate inflammatory cytokine levels, and reduce atherosclerotic plaques by remodeling gut microbiota. Modern pharmacological studies have shown that polydatin is extensively used for the treatment of atherosclerosis and systemic metabolic disorders owing to its medicinal properties, including anti-inflammatory (Tang et al., 2018), antioxidant (Lv et al., 2019), and lipid metabolism modulation (Huang et al., 2018). Furthermore,

10.3389/fphar.2025.1515485

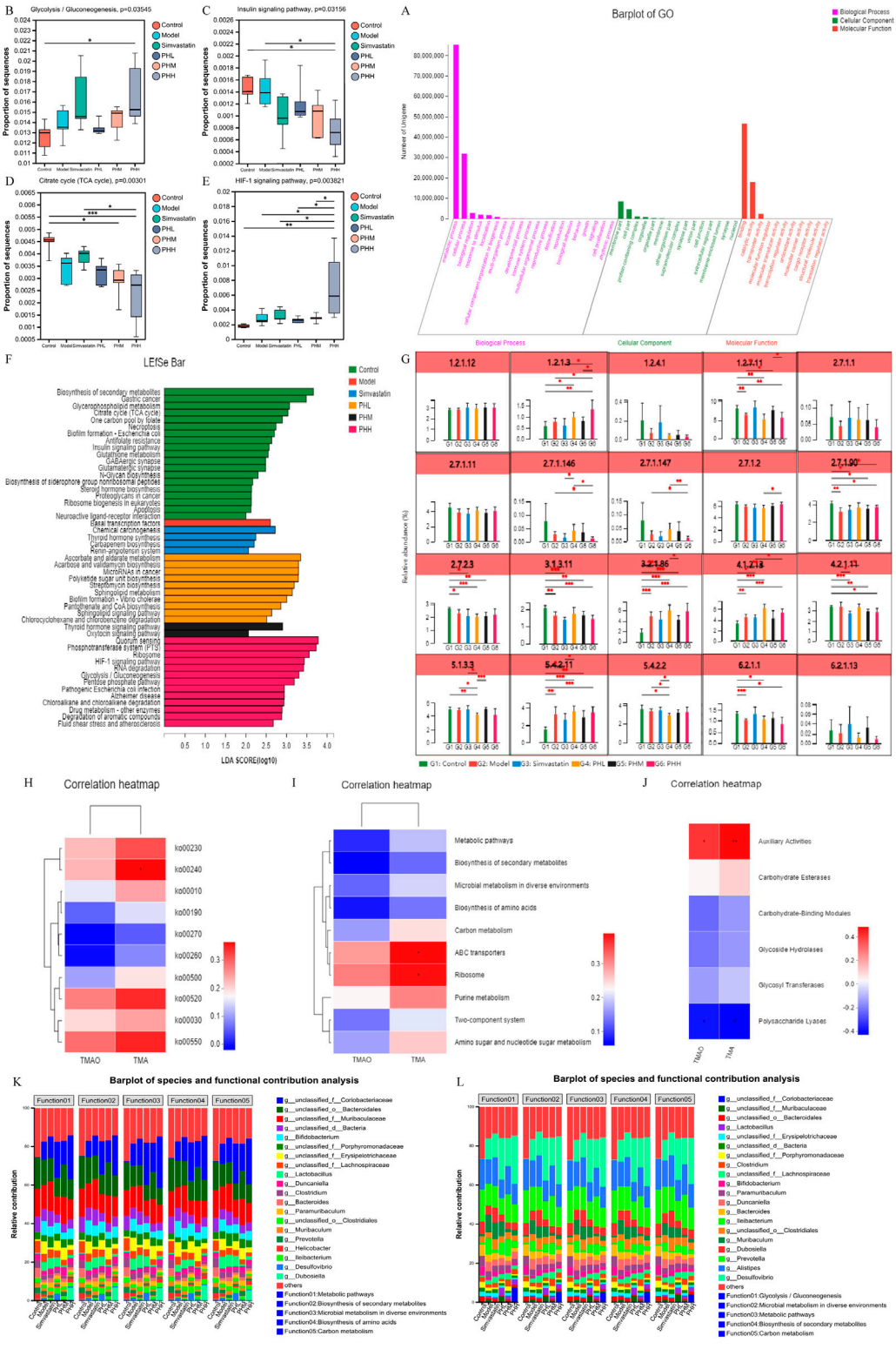

FIGURE 9
(A) GO function annotation analysis; **(B–E)** Multigroup variance analysis of KEGG pathways based on TMA-producing bacteria gene set; **(F)** Linear discriminant analysis of TMA-producing bacteria gene set; **(G)** Analysis of intergroup difference in metabolic pathways; **(H–J)** Spearman's correlation analysis between metabolic pathways and TMA/TMAO; **(K, L)** Analysis of species function contribution. *$P < 0.05$, **$P < 0.01$, ***$P < 0.001$.

10.3389/fphar.2025.1515485

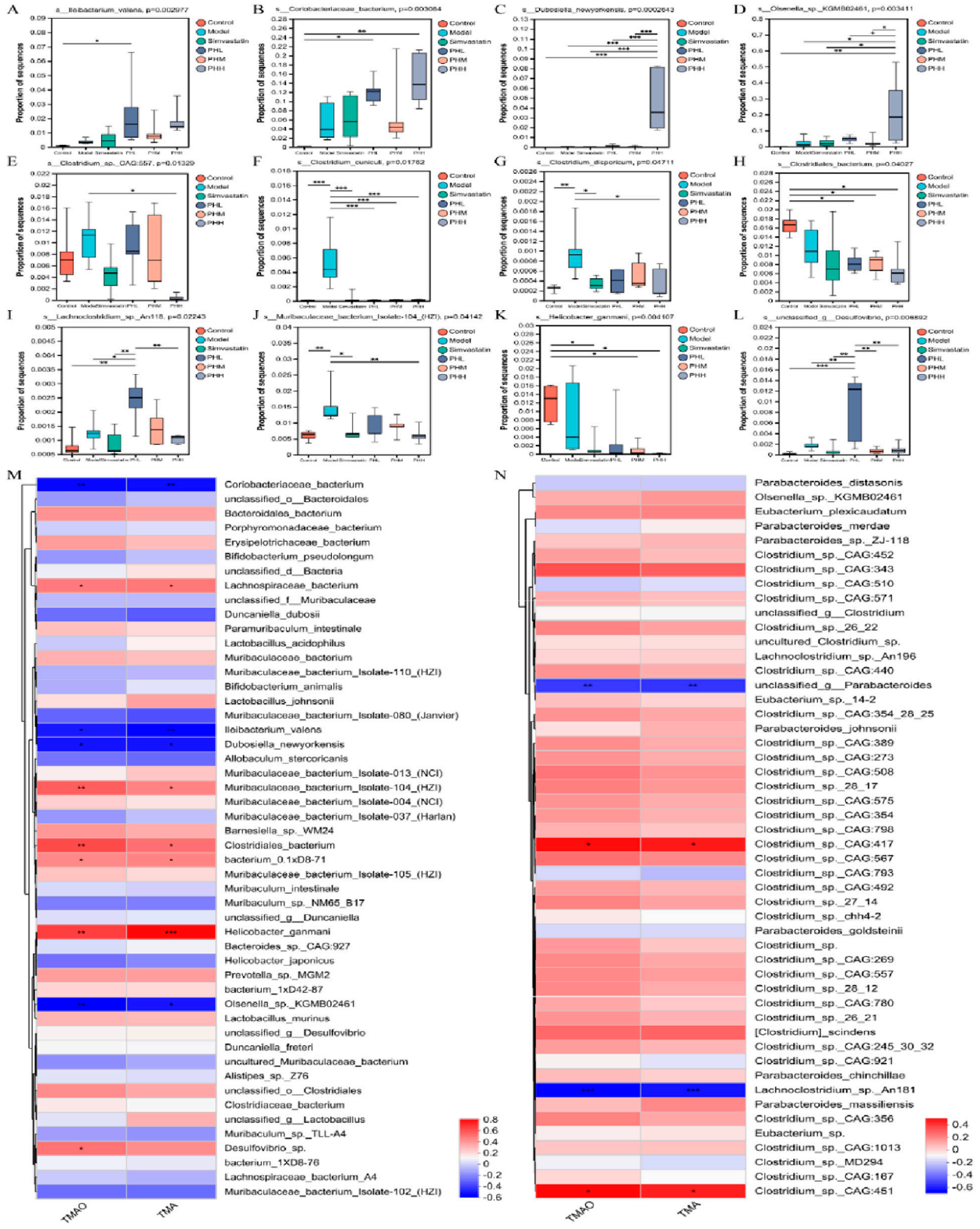

FIGURE 10
(A–L) Multigroup variance analysis of TMA-producing bacteria gene set; **(M, N)** Spearman's correlation analysis between TMA-producing bacteria and TMA/TMAO. *$P < 0.05$, **$P < 0.01$, ***$P < 0.001$.

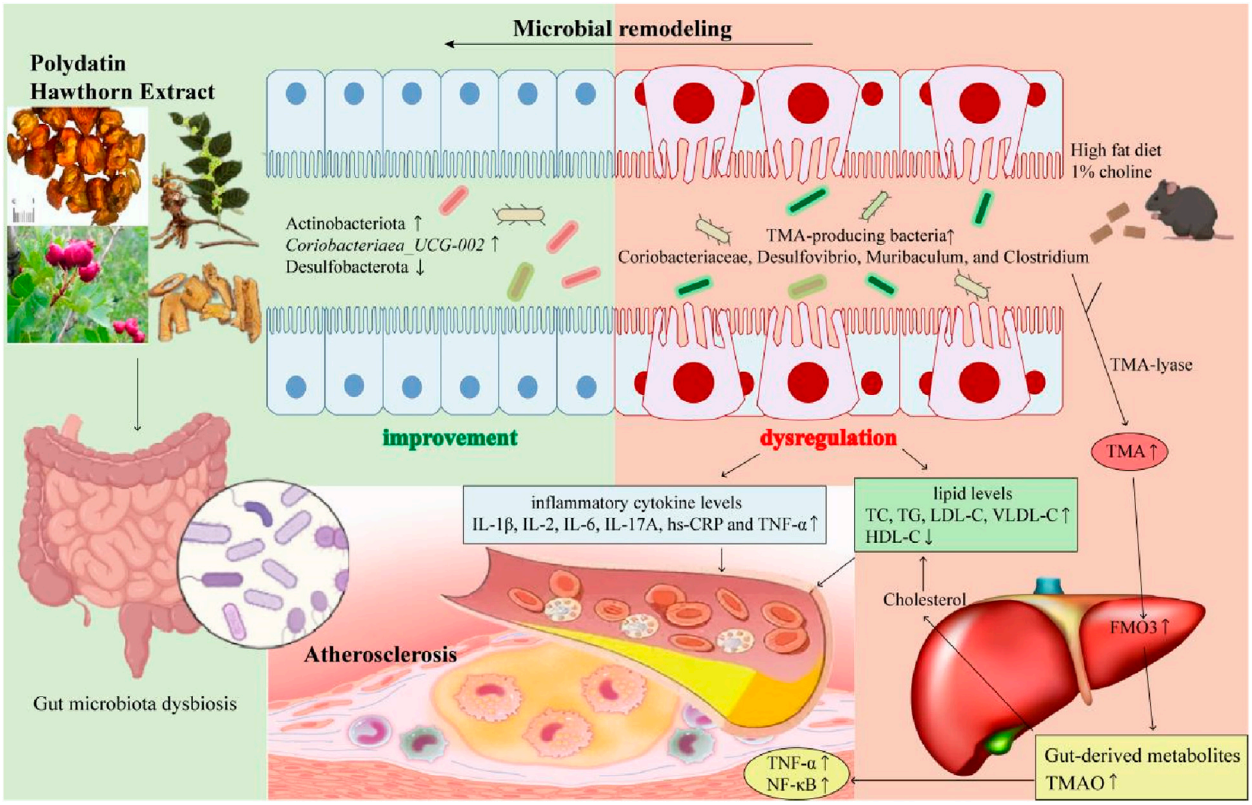

FIGURE 11
The gut microbial mechanism of polydatin combined with hawthorn flavonoids against AS. Polydatin combined with hawthorn flavonoids protects against atherosclerosis by microbial remodeling *in vivo*: 1) PH administration could increase the abundance of Actinobacteriota and *Coriobacteriaea_UCG-002*, decrease the abundance of *Desulfobacterota*; 2) HFD-induced changes in TMA-producing bacteria (Coriobacteriaceae, *Desulfovibrio*, *Muribaculum*, and *Clostridium*) increased TMA levels by TMA-lyase, upregulated the expression of FMO3, increased the gut-derived metabolites TMAO levels, which was accompanied by an increase in lipid levels and inflammatory cytokines levels. 3) PH alleviate atherosclerotic plagues by moderating gut microbiota dysbiosis to regulate the TMA/FMO3/TMAO pathway.

hawthorn flavonoids alleviate metabolic hyperlipidemia by altering bacterial and gut-derived metabolites related to cholesterol homeostasis (Hu et al., 2022). Dyslipidemia plays an important role in the development of ASCVD (Ballard-Hernandez and Sall, 2023). Statins reduce LDL cholesterol levels and prevent ASCVD by inhibiting 3-hydroxy-3-methylglutaryl-CoA reductase (HMGCR) and increasing the expression of low density lipoprotein receptor (LDLR) (Grundy et al., 2018). Proprotein convertase subtilisin/kexin type 9 (PCSK9) is a serine protease that homologous binds with epidermal growth factor precursors to the LDLR domain A (EGF-A) in the liver and initiates degradation of LDLR via the lysosomal pathway, resulting in elevated plasma LDL-C levels (Hao et al., 2022). Blocking the direct interaction between PCSK9 and LDLR may be the key point to ameliorating hyperlipidemia and ASCVD (Wang et al., 2024).

Our clinical trial confirmed that polydatin combined with hawthorn flavonoids can exert anti-atherosclerotic effect on patients with carotid atherosclerosis by promoting plaque stability and decreasing the inflammatory factors levels (Liu et al., 2014), which suggested that the combination of polydatin and hawthorn flavonoids could exhibit an amazing anti-atherosclerotic effect. Our previous research confirmed that the mice in the model group may have experienced an increase in the serum TC, TG, and LDL-C levels; however, hawthorn flavonoids and simvastatin reversed these changes and increased HDL-C levels (Wang et al., 2019). Furthermore, polydatin moderates the lipid metabolism via inhibiting the formation of peritoneal macrophage-derived foam cells in ApoE$^{-/-}$mice (Wu et al., 2015). It is reasonable to speculate that polydatin combined with hawthorn flavonoids may have excellent lipid-regulating effects. Our data revealed that PH could reverse dyslipidemia by reducing lipid levels (TC, TG, LDL-C, and VLDL-C) and body weight and increasing HDL-C levels.

Our previous results demonstrated that polydatin could reduce TNF-α and IL-1β levels in the peritoneal macrophages of ApoE$^{-/-}$mice (Wu et al., 2015), and hawthorn flavonoids could inhibit the elevation of hs-CRP and IL-1β (Wang et al., 2019). Additionally, our clinical trial data confirmed that 15 g of *P. cuspidatum* combined with 10 g of hawthorn granule formula exerted cardioprotective effects by reducing hs-CRP, TNF-α, and IL-6 levels. We also observed that the plaque score decreased, and the level of plaque stability was strongly enhanced in patients with carotid atherosclerosis (Wu et al., 2021). Furthermore, our previous research revealed that hawthorn flavonoids (Wang et al., 2019) and polydatin (Zhang et al., 2023) could individually improve atherosclerotic plaques in ApoE$^{-/-}$mice. Consistent with these findings, we observed that PH could reduce serum inflammatory

factors (IL-1β, IL-2, IL-6, IL-17A, hs-CRP and TNF-α) levels and improve atherosclerotic plaques.

In our study, the alpha diversity analysis revealed that *Firmicutes*, *Bacteroidetes*, *Actinobacteria*, and *Desulfobacterota* accounted for the majority of species in our study, and the microbial diversity and abundance were reduced after the HFD intervention. *Firmicutes* and *Bacteroidetes*, as dominant bacteria in a healthy body, are involved in lipid regulation and BAs metabolism. *Firmicutes* may increase the formation of lipopolysaccharides and other metabolic endotoxins leading to chronic inflammation, while *Bacteroidota*, as a Gram-negative anaerobic bacterium, plays an important role in maintaining immune homeostasis and regulating immunity (The Human Microbiome Project Consortium, 2012). Our result was similar to previous studies, with *Bacteroidetes* and *Firmicutes* constituting more than other species, with *Actinobacteria*, *Desulfobacterota* followed them. Although the species abundance or number of the microbiota varied between individuals, the gut microbiota was semblable among individuals at higher taxonomic levels, such as the phylum level. In particular, we observed that the proportion of *Desulfobacterota* was increased in the model group, however, it was decreased in the PHM, PHH and simvastatin groups. *Desulfovibrio*, a Gram-negative bacterium, is involved in lipid metabolism and inflammation by producing lipopolysaccharide to trigger the release of IL-1β, IL-6, and TNF-β and alter intestinal permeability and microbial composition (Zhang et al., 2018). Previous research revealed that HFD-induced gut microbial alterations in atherosclerotic mice are mainly reflected in the enrichment of *Desulfovibrio* (Zhu et al., 2018b). *Muribaculaceae* (S24-7) can inhibit the inflammation (Luo et al., 2021), gut microbial dysbiosis, and intestinal dysfunction by degrading mucin (Lee et al., 2019). Simvastatin attenuates HFD-induced hyperlipidemia by increasing the abundance of *Lactobacillus* and reducing the level of TG and TC (Zhang et al., 2020). Most studies have confirmed that *Lactobacillus* spp. can moderate lipid metabolism (Yoo et al., 2013) and reduce cholesterol availability (Pereira and Gibson, 2002). Our findings revealed that *norank_f_Muribaculaceae* was enriched in the PHM and simvastatin groups. Additionally, *Lactobacillus* was mainly increased in the simvastatin and PHL groups. Furthermore, PHH and simvastatin administration also switched the enterotype to *g_Lactobacillus* and *g_norank_f_Muribaculaceae_1* to optimize the gut microbiota composition (Watanabe et al., 2021). *In vivo* studies have revealed that the inhibition of C-C chemokine motif ligands can reduce TMAO levels and the abundance of *Muribaculaceae* to improve glucose and lipid metabolism disorders (Chang and Chen, 2021). Coriobacteriaceae_*UCG-002* belongs to the *Coribacteriaceae* family, which accelerates cholesterol absorption and exhibits a positive correlation with the levels of TG (Han et al., 2022). However, a recent report had suggested that *Coriobacteriaea*_UCG-002 can improve obesity (Jiao et al., 2023). The β-diversity analysis in our study revealed that PHH and simvastatin improved the abundance of *Actinobacteria* and *Coriobacteriaea*_UCG-002. Furthermore, harmful bacteria such as *Alistipes*, *f*_Clostridiaceae, and *f*_Defluviitaleaceae were the predominant genera in the model group. *Alistipes* have been recognized as an inflammatory indicator in most studies (Dong et al., 2019). The class *Clostridia*, which includes *f*_Clostridiaceae and *f*_Defluviitaleaceae, has often been reported to prompt the progression of colitis in mice (Zha et al., 2020), which is consistent with our observations. In our study, *Desulfobacterota*, *Firmicutes*, *Desulfovibrio*, and *Muribaculum* have strong correlations with lipid and inflammatory cytokine levels.

The KEGG functional analysis revealed increased enrichment of glycerolipid metabolism and glucagon signaling pathways in the PHL group; additionally, biosynthesis of amino acids, starch, and sucrose metabolism demonstrated increased enrichment in the PHH group. Accordingly, ko00520, ko00030, and ko00550 were positively associated with lipid and inflammatory cytokine levels at Level 2 while *s_Desulfovibrio_fairfieldensis*, *s_Allobaculum_stercoricanis* exhibited positive correlation with the metabolic pathways and starch and sucrose metabolism. A decrease in *Desulfovibrio* may contribute to the improvement of glycolipid metabolism (Huang et al., 2022) and inflammation (Shenghua et al., 2020). Thus, the microbial therapeutic effects of PH administration may be attributed to glycerolipid metabolism. Accumulating evidences reveal that gut microbiota and the metabolite TMAO may mechanistically participated in the pathogenesis of atherosclerosis (Díez-Ricote et al., 2022), although the specific mechanism has not yet been fully elucidated. Consistent with previous reports, our results confirmed that an HFD containing 1% choline increased TMA and TMAO levels in the model group mice (Thomas and Fernandez, 2021). Interestingly, we observed that PH moderated the TMA/FMO3/TMAO pathway by downregulating the protein and mRNA expression of FMO3, which is consistent with previous findings. Accumulating evidence has documented that (Lu et al., 2023), cholesterol homeostasis serves as a crucial mediator of metabolic disorders. TMAO promotes the transformation of macrophages into foam cells via cholesterol accumulation involved in the scavenger receptors SR-AI and CD36 (Wang et al., 2011). Furthermore, HFD may cause changes in BAs signaling by affecting the microbiota. BAs binds to receptors such as FXR and TGR5 and regulates host metabolism either by directly binding to promoter regions or by releasing potent regulatory factors such as fibroblast growth factor 15/19 (FGF19) in humans or pigs and glucagon-like peptide-1 (GLP-1) (Perino and Schoonjans, 2022). Previous studies have shown that the intake of a high-fat diet may cause liver damage while altering BAs and gut microbiota (Huang et al., 2024). Consistent with this mechanism, our correlation analysis revealed a positive correlation between TMA and ko00240, ABC transporters, and auxiliary activities Expression of hepatic Abcg5/g8 expression have been suggested to increase TMAO levels (Chen et al., 2019). In addition, our data suggested that the abundance of *Firmicutes*, *Turicibacter*, and *Lachnoclostridium* might participate in the process of accelerating the TMAO levels. Consistently, *Turicibacter* and *Lachnoclostridium* have been associated with butyric acid, which may promote imbalanced lipid metabolism and elevation of TMAO levels (Li et al., 2019). At the species level, we observed positive correlations of *uncultured_bacterium_g_Desulfovibrio*; *s_Desulfovibrio_fairfieldensis*; metabolic pathways, including starch and sucrose metabolism; ABC transporters, including M00001, M00051, and M00003, with *s_Allobaculum_stercoricanis*, but a negative correlation with beneficial bacteria, including *Bacteroides* spp., *s_Lactobacillus_murinus* and *s_Muribaculaceae_bacterium*. In line with previous findings, the observed alterations in the abundance of *Alloprevotella*, and *norank_f*_Desulfovibrionaceae could have contributed to an immunoprotective effect on ABC transporters,

carbohydrate digestion and absorption, and glycerophospholipid metabolism pathways (Sun et al., 2022).

Since TMA-producing bacteria are the main contributors to the production of TMAO and atherosclerosis, they were identified for gene set construction to further investigate the relationship between TMAO and atherosclerosis. Glycolysis/gluconeogenesis, drug metabolism, and HIF-1signaling pathway were highly enriched in the PHH group, suggesting that a high dose of PH could change the abundance of TMA-producing bacteria and regulate the above functional pathways to attenuate the pathological process of atherosclerosis. In addition, we observed that phosphoglycerate mutase [EC:5.4.2.11] and fructose-bisphosphate aldolase [EC: 4.1.2.13] were increased in mice fed an HFD, whereas PH administration could reverse these changes. Consistent with previous research, aloe polysaccharides may produce health benefits by upregulating the gene expression of fructose-bisphosphate aldolase (Liu et al., 2021). The cell-free extract of *Clostridium sporogenes* exhibited a high fructose-bisphosphate aldolase activity (Golovchenko et al., 1983). GO functional annotation also suggested that the BP of each group were mainly focused on metabolism-related processes. According to the results of the species contribution analysis, *Clostridium* was among the top five contributors to metabolic pathways, and *Desulfovibrio*, *Prevotella*, *Muribaculum*, *unclassified_f_*Lachnospiraceae, *unclassified_o_Bacteroidales* were other important species involved in metabolic processes. The genera *Clostridium* (Clostridiaceae) and *Collinsella* (Coriobacteriaceae) possess TMA lyase activity and influence the level of TMAO (Cho et al., 2017). *Clostridium*, *Desulfovibrio*, and *Collinsella* participate widely in the synthesis of TMA, which is generated from choline in dairy diets (Onyszkiewicz et al., 2020). In addition, Lachnospiraceae_*bacterium*, *Muribaculaceae_bacterium_Isolate-104_(HZI)*, *Clostridiales_bacterium*, *Desulfovibrio_*sp., *Clostridium_*sp._CAG: 417, and *Clostridium_*sp._CAG:451 exhibited positive correlations with TMA and TMAO levels. The abundance of *s_Clostridium_*sp._CAG:557, *s_Clostridium_cuniculi*, and *s_Clostridium_disporicum* increased in the model group, and the PH administration partially restored the HFD-induced abundance of these *Clostridium_*spp.

5 Conclusion

In conclusion, our results suggested that PH administration could reduce inflammatory factors and lipid levels, thereby attenuating the development of atherosclerotic plaques in HFD-induced mice. In addition, PH exerts its beneficial effects by remodeling the gut microbiota and regulating its derived metabolite, TMAO. In particular, PH-induced changes in TMA-producing bacteria and enzymes involved in the glycolipid metabolic pathways have important effects on atherosclerosis therapy. In this study, we found that of all treatment groups, PHH group was the most effective in improving gut microbial diversity, anti-inflammatory effects, antioxidant capacity, and lipid metabolism in a dose-dependent manner. Simvastatin group may play an anti-atherosclerosis role mainly by increasing the abundance of *Lactobacillus* and *norank_f_Muribaculaceae*. PHL and PHM may exert therapeutic effects by increasing the abundance of *Lactobacillus* and *norank_f_Muribaculaceae*, respectively. PHH and simvastatin improved the abundance of *Actinobacteria* and *Coriobacteriaea_UCG-002*. Furthermore, PHH could change the abundance of TMA-producing bacteria and regulate the Glycolysis/gluconeogenesis, drug metabolism, and HIF-1signaling functional pathways to attenuate the pathological process of atherosclerosis. To summarize, PH has the potential to regulate the abundance of TMA-producing bacteria (Coriobacteriaceae, *Desulfovibrio*, *Muribaculum*, and *Clostridium*), moderate the TMA-FMO3-TMAO pathway, and influence the related enzymes in glycolipid metabolic pathways, thereby exerting an important effect on the expression of TMAO, lipids, and inflammation, ultimately alleviating the progression of atherosclerosis (Figure 11). Nevertheless, the underlying mechanisms and new targets of gut microbial biomarkers require further investigation.

Data availability statement

The data presented in the study are deposited in the NCBI Sequence Read Archive (SRA) repository, accession number PRJNA1122934.

Ethics statement

The animal study was approved by the Ethics Committee of Guang'anmen Hospital, China Academy of Chinese Medical Sciences. The study was conducted in accordance with the local legislation and institutional requirements.

Author contributions

DL: Data curation, Formal Analysis, Investigation, Supervision, Validation, Visualization, Writing–original draft, Writing–review and editing. YL: Data curation, Investigation, Software, Supervision, Validation, Visualization, Writing–review and editing. SY: Formal Analysis, Investigation, Supervision, Validation, Visualization, Writing–review and editing. XZ: Investigation, Supervision, Validation, Visualization, Writing–review and editing. YC: Software, Supervision, Validation, Visualization, Writing–review and editing. RZ: Investigation, Software, Validation, Visualization, Writing–review and editing. YZ: Software, Validation, Writing–review and editing. XJ: Software, Validation, Visualization, Writing–review and editing. JL: Investigation, Supervision, Validation, Writing–review and editing. XW: Investigation, Supervision, Validation, Visualization, Writing–review and editing. QW: Software, Supervision, Validation, Visualization, Writing–review and editing. LL: Conceptualization, Formal Analysis, Funding acquisition, Investigation, Project administration, Software, Visualization, Writing–review and editing. MW: Conceptualization, Data curation, Funding acquisition, Investigation, Project administration, Supervision, Validation, Visualization, Writing–review and editing.

Funding

The author(s) declare that financial support was received for the research, authorship, and/or publication of this article. This study was supported by the National Natural Science Foundation of China (http://www.nsfc.gov.cn; grant numbers 82074254 and 82374281), the Beijing Natural Science Foundation (grant numbers 7172185), Science and Technology Innovation Project of China Academy of Chinese Medical Sciences (No. CI2021A01413), The fifth batch of TCM clinical Excellent Talents Training Project National TCM Talent Letter (2022)] No. 1, Beijing TCM Science and Technology Development Fund Project (BJZYYB-2023-73) and Beijing Municipal Health Commission, Independent Innovation of the Capital Health Development Scientific Research Special Project (2024-2-4154).

Conflict of interest

The authors declare that the research was conducted in the absence of any commercial or financial relationships that could be construed as a potential conflict of interest.

Generative AI statement

The author(s) declare that no Generative AI was used in the creation of this manuscript.

Publisher's note

All claims expressed in this article are solely those of the authors and do not necessarily represent those of their affiliated organizations, or those of the publisher, the editors and the reviewers. Any product that may be evaluated in this article, or claim that may be made by its manufacturer, is not guaranteed or endorsed by the publisher.

Supplementary material

The Supplementary Material for this article can be found online at: https://www.frontiersin.org/articles/10.3389/fphar.2025.1515485/full#supplementary-material

References

Arauna, D., Furrianca, M., Espinosa-Parrilla, Y., Fuentes, E., Alarcón, M., and Palomo, I. (2019). Natural bioactive compounds as protectors of mitochondrial dysfunction in cardiovascular diseases and aging. *Mol. Basel, Switz.* 24 (23), 4259. doi:10.3390/molecules24234259

Ballard-Hernandez, J., and Sall, J. (2023). Dyslipidemia update. *Nurs. Clin. N. Am.* 58 (3), 295–308. doi:10.1016/j.cnur.2023.05.002

Bansilal, S., Castellano, J. M., and Fuster, V. (2015). Global burden of CVD: focus on secondary prevention of cardiovascular disease. *Int. J. Cardiol.* 201 (Suppl. 1), S1–S7. doi:10.1016/s0167-5273(15)31026-3

Blagov, A. V., Markin, A. M., Bogatyreva, A. I., Tolstik, T. V., Sukhorukov, V. N., and Orekhov, A. N. (2023). The role of macrophages in the pathogenesis of atherosclerosis. *Cells* 12 (4), 522. doi:10.3390/cells12040522

Bolte, L. A., Vich Vila, A., Imhann, F., Collij, V., Gacesa, R., Peters, V., et al. (2021). Long-term dietary patterns are associated with pro-inflammatory and anti-inflammatory features of the gut microbiome. *Gut* 70 (7), 1287–1298. doi:10.1136/gutjnl-2020-322670

Cai, Y. Y., Huang, F. Q., Lao, X., Lu, Y., Gao, X., Alolga, R. N., et al. (2022). Integrated metagenomics identifies a crucial role for trimethylamine-producing Lachnoclostridium in promoting atherosclerosis. *NPJ biofilms microbiomes* 8 (1), 11. doi:10.1038/s41522-022-00273-4

Chang, T. T., and Chen, J. W. (2021). Direct CCL4 inhibition modulates gut microbiota, reduces circulating trimethylamine N-oxide, and improves glucose and lipid metabolism in high-fat-diet-induced diabetes mellitus. *J. Inflamm. Res.* 14, 6237–6250. doi:10.2147/jir.S343491

Chen, Y., Weng, Z., Liu, Q., Shao, W., Guo, W., Chen, C., et al. (2019). FMO3 and its metabolite TMAO contribute to the formation of gallstones. *Biochimica biophysica acta Mol. basis Dis.* 1865 (10), 2576–2585. doi:10.1016/j.bbadis.2019.06.016

Cho, C. E., Taesuwan, S., Malysheva, O. V., Bender, E., Tulchinsky, N. F., Yan, J., et al. (2017). Trimethylamine-N-oxide (TMAO) response to animal source foods varies among healthy young men and is influenced by their gut microbiota composition: a randomized controlled trial. *Mol. Nutr. and food Res.* 61 (1). doi:10.1002/mnfr.201600324

Díez-Ricote, L., Ruiz-Valderrey, P., Micó, V., Blanco, R., Tomé-Carneiro, J., Dávalos, A., et al. (2022). TMAO upregulates members of the miR-17/92 cluster and impacts targets associated with atherosclerosis. *Int. J. Mol. Sci.* 23 (20), 12107. doi:10.3390/ijms232012107

Dong, Y., Cheng, H., Liu, Y., Xue, M., and Liang, H. (2019). Red yeast rice ameliorates high-fat diet-induced atherosclerosis in Apoe(-/-) mice in association with improved inflammation and altered gut microbiota composition. *Food and Funct.* 10 (7), 3880–3889. doi:10.1039/c9fo00583h

Feng, Y., Xu, H., Qu, D., Zheng, F., Shi, D. Z., and Chen, K. J. (2011). Study on the tongue manifestations for the blood-stasis and toxin syndrome in the stable patients of coronary heart disease. *Chin. J. Integr. Med.* 17 (5), 333–338. doi:10.1007/s11655-011-0615-4

Fiehn, O. (2016). Metabolomics by gas chromatography-mass spectrometry: combined targeted and untargeted profiling. *Curr. Protoc. Mol. Biol.* 114 (4.1-.4.2), 1–30. doi:10.1002/0471142727.mb3004s114

Gao, X., Xu, J., Jiang, C., Zhang, Y., Xue, Y., Li, Z., et al. (2015). Fish oil ameliorates trimethylamine N-oxide-exacerbated glucose intolerance in high-fat diet-fed mice. *Food and Funct.* 6 (4), 1117–1125. doi:10.1039/c5fo00007f

Golovchenko, N. P., Belokopytov, B. F., and Akimenko, V. K. (1983). Glucose metabolism in Clostridium sporogenes and Clostridium sticklandii bacteria. *Mikrobiologiia* 52 (6), 869–874.

Grundy, S. M., Stone, N. J., Bailey, A. L., Beam, C., Birtcher, K. K., Blumenthal, R. S., et al. (2018). 2018 AHA/ACC/AACVPR/AAPA/ABC/ACPM/ADA/AGS/APhA/ASPC/NLA/PCNA guideline on the management of blood cholesterol: executive summary: a report of the American college of cardiology/American heart association Task Force on Clinical practice guidelines. *J. Am. Coll. Cardiol.* 73 (24), 3168–3209. doi:10.1016/j.jacc.2018.11.002

Han, H., Wang, M., Zhong, R., Yi, B., Schroyen, M., and Zhang, H. (2022). Depletion of gut microbiota inhibits hepatic lipid accumulation in high-fat diet-fed mice. *Int. J. Mol. Sci.* 23 (16), 9350. doi:10.3390/ijms23169350

Hao, Q., Aertgeerts, B., Guyatt, G., Bekkering, G. E., Vandvik, P. O., Khan, S. U., et al. (2022). PCSK9 inhibitors and ezetimibe for the reduction of cardiovascular events: a clinical practice guideline with risk-stratified recommendations. *BMJ Clin. Res. ed* 377, e069066. doi:10.1136/bmj-2021-069066

Hu, H., Weng, J., Cui, C., Tang, F., Yu, M., Zhou, Y., et al. (2022). The hypolipidemic effect of hawthorn leaf flavonoids through modulating lipid metabolism and gut microbiota in hyperlipidemic rats. *Evidence-based complementary Altern. Med. eCAM* 2022, 3033311. doi:10.1155/2022/3033311

Huang, L., Li, Y., Tang, R., Yang, P., Zhuo, Y., Jiang, X., et al. (2024). Bile acids metabolism in the gut-liver axis mediates liver injury during lactation. *Life Sci.* 338, 122380. doi:10.1016/j.lfs.2023.122380

Huang, Z., Tian, G., Cheng, S., Zhao, D., Zhang, Y., Jia, Y., et al. (2018). Polydatin attenuates atherosclerosis in ApoE ⁄- mice through PBEF mediated reduction of cholesterol deposition. *Am. J. Chin. Med.* 46 (8), 1841–1859. doi:10.1142/s0192415x18500921

Huang, Z. R., Zhao, L. Y., Zhu, F. R., Liu, Y., Xiao, J. Y., Chen, Z. C., et al. (2022). Anti-Diabetic effects of ethanol extract from sanghuangporous vaninii in high-fat/sucrose diet and streptozotocin-induced diabetic mice by modulating gut microbiota. *Foods Basel, Switz.* 11 (7), 974. doi:10.3390/foods11070974

Jiao, W., Sang, Y., Wang, X., and Wang, S. (2023). Metabonomics and the gut microbiome analysis of the effect of 6-shogaol on improving obesity. *Food Chem.* 404 (Pt B), 134734. doi:10.1016/j.foodchem.2022.134734

Joris, B. R., and Gloor, G. B. (2019). Unaccounted risk of cardiovascular disease: the role of the microbiome in lipid metabolism. *Curr. Opin. Lipidol.* 30 (2), 125–133. doi:10.1097/mol.0000000000000582

Koeth, R. A., Lam-Galvez, B. R., Kirsop, J., Wang, Z., Levison, B. S., Gu, X., et al. (2019). l-Carnitine in omnivorous diets induces an atherogenic gut microbial pathway in humans. *J. Clin. investigation* 129 (1), 373–387. doi:10.1172/jci94601

Lau, K., Srivatsav, V., Rizwan, A., Nashed, A., Liu, R., Shen, R., et al. (2017). Bridging the gap between gut microbial dysbiosis and cardiovascular diseases. *Nutrients* 9 (8), 859. doi:10.3390/nu9080859

Lee, K. S., Palatinszky, M., Pereira, F. C., Nguyen, J., Fernandez, V. I., Mueller, A. J., et al. (2019). An automated Raman-based platform for the sorting of live cells by functional properties. *Nat. Microbiol.* 4 (6), 1035–1048. doi:10.1038/s41564-019-0394-9

Li, D. Y., and Tang, W. H. W. (2017). Gut microbiota and atherosclerosis. *Curr. Atheroscler. Rep.* 19 (10), 39. doi:10.1007/s11883-017-0675-9

Li, H., Dai, M., and Jia, W. (2009). Paeonol attenuates high-fat-diet-induced atherosclerosis in rabbits by anti-inflammatory activity. *Planta medica*. 75 (1), 7–11. doi:10.1055/s-0028-1088332

Li, L., Guo, W. L., Zhang, W., Xu, J. X., Qian, M., Bai, W. D., et al. (2019). Grifola frondosa polysaccharides ameliorate lipid metabolic disorders and gut microbiota dysbiosis in high-fat diet fed rats. *Food and Funct.* 10 (5), 2560–2572. doi:10.1039/c9fo00075e

Li, X., Su, C., Jiang, Z., Yang, Y., Zhang, Y., Yang, M., et al. (2021). Berberine attenuates choline-induced atherosclerosis by inhibiting trimethylamine and trimethylamine-N-oxide production via manipulating the gut microbiome. *NPJ biofilms microbiomes* 7 (1), 36. doi:10.1038/s41522-021-00205-8

Liu, C., Du, P., Guo, Y., Xie, Y., Yu, H., Yao, W., et al. (2021). Extraction, characterization of aloe polysaccharides and the in-depth analysis of its prebiotic effects on mice gut microbiota. *Carbohydr. Polym.* 261, 117874. doi:10.1016/j.carbpol.2021.117874

Liu, L. T., Zheng, G. J., Zhang, W. G., Guo, G., and Wu, M. (2014). Clinical study on treatment of carotid atherosclerosis with extraction of polygoni cuspidati rhizoma et radix and crataegi fructus: a randomized controlled trial. *Zhongguo Zhong yao za zhi = Zhongguo zhongyao zazhi = China J. Chin. materia medica* 39 (6), 1115–1119.

Liu, P., Kallio, H., Lü, D., Zhou, C., and Yang, B. (2011). Quantitative analysis of phenolic compounds in Chinese hawthorn (Crataegus spp.) fruits by high performance liquid chromatography-electrospray ionisation mass spectrometry. *Food Chem.* 127 (3), 1370–1377. doi:10.1016/j.foodchem.2011.01.103

Lu, J., Shang, X., Yao, B., Sun, D., Liu, J., Zhang, Y., et al. (2023). The role of CYP1A1/2 in cholesterol ester accumulation provides a new perspective for the treatment of hypercholesterolemia. *Acta Pharm. Sin. B* 13 (2), 648–661. doi:10.1016/j.apsb.2022.08.005

Luo, J., Wang, Z., Fan, B., Wang, L., Liu, M., An, Z., et al. (2021). A comparative study of the effects of different fucoidans on cefoperazone-induced gut microbiota disturbance and intestinal inflammation. *Food and Funct.* 12 (19), 9087–9097. doi:10.1039/d1fo00782c

Luo, T., Guo, Z., Liu, D., Guo, Z., Wu, Q., Li, Q., et al. (2022). Deficiency of PSRC1 accelerates atherosclerosis by increasing TMAO production via manipulating gut microbiota and flavin monooxygenase 3. *Gut microbes* 14 (1), 2077602. doi:10.1080/19490976.2022.2077602

Lv, R., Du, L., Zhang, L., and Zhang, Z. (2019). Polydatin attenuates spinal cord injury in rats by inhibiting oxidative stress and microglia apoptosis via Nrf2/HO-1 pathway. *Life Sci.* 217, 119–127. doi:10.1016/j.lfs.2018.11.053

Ma, J., and Li, H. (2018). The role of gut microbiota in atherosclerosis and hypertension. *Front. Pharmacol.* 9, 1082. doi:10.3389/fphar.2018.01082

Massey, W., and Brown, J. M. (2021). The gut microbial endocrine organ in type 2 diabetes. *Endocrinology* 162 (2), bqaa235. doi:10.1210/endocr/bqaa235

Onyszkiewicz, M., Jaworska, K., and Ufnal, M. (2020). Short chain fatty acids and methylamines produced by gut microbiota as mediators and markers in the circulatory system. *Exp. Biol. Med. (Maywood, NJ)* 245 (2), 166–175. doi:10.1177/1535370219900898

Pereira, D. I., and Gibson, G. R. (2002). Cholesterol assimilation by lactic acid bacteria and bifidobacteria isolated from the human gut. *Appl. Environ. Microbiol.* 68 (9), 4689–4693. doi:10.1128/aem.68.9.4689-4693.2002

Perino, A., and Schoonjans, K. (2022). Metabolic Messengers: bile acids. *Nat. Metab.* 4 (4), 416–423. doi:10.1038/s42255-022-00559-z

Qi, X., Yun, C., Pang, Y., and Qiao, J. (2021). The impact of the gut microbiota on the reproductive and metabolic endocrine system. *Gut microbes* 13 (1), 1–21. doi:10.1080/19490976.2021.1894070

Qin, C., Yang, G., Wu, S., Zhang, H., and Zhu, C. (2022). Synthesis, physicochemical characterization, antibacterial activity, and biocompatibility of quaternized hawthorn pectin. *Int. J. Biol. Macromol.* 213, 1047–1056. doi:10.1016/j.ijbiomac.2022.06.028

Qu, S., Li, K., Yang, T., Yang, Y., Zheng, Z., Liu, H., et al. (2021). Shenlian extract protects against ultrafine particulate matter-aggravated myocardial ischemic injury by inhibiting inflammation response via the activation of NLRP3 inflammasomes. *Environ. Toxicol.* 36 (7), 1349–1361. doi:10.1002/tox.23131

Rath, S., Rud, T., Pieper, D. H., and Vital, M. (2019). Potential TMA-producing bacteria are ubiquitously found in mammalia. *Front. Microbiol.* 10, 2966. doi:10.3389/fmicb.2019.02966

Saaoud, F., Liu, L., Xu, K., Cueto, R., Shao, Y., Lu, Y., et al. (2023). Aorta- and liver-generated TMAO enhances trained immunity for increased inflammation via ER stress/mitochondrial ROS/glycolysis pathways. *JCI insight* 8 (1), e158183. doi:10.1172/jci.insight.158183

Schugar, R. C., and Brown, J. M. (2015). Emerging roles of flavin monooxygenase 3 in cholesterol metabolism and atherosclerosis. *Curr. Opin. Lipidol.* 26 (5), 426–431. doi:10.1097/mol.0000000000000215

Shenghua, P., Ziqin, Z., Shuyu, T., Huixia, Z., Xianglu, R., and Jiao, G. (2020). An integrated fecal microbiome and metabolome in the aged mice reveal anti-aging effects from the intestines and biochemical mechanism of FuFang zhenshu TiaoZhi(FTZ). *Biomed. Pharmacother.* 121, 109421. doi:10.1016/j.biopha.2019.109421

Simó, C., and García-Cañas, V. (2020). Dietary bioactive ingredients to modulate the gut microbiota-derived metabolite TMAO. New opportunities for functional food development. *Food and Funct.* 11 (8), 6745–6776. doi:10.1039/d0fo01237h

Singh, R. K., Chang, H. W., Yan, D., Lee, K. M., Ucmak, D., Wong, K., et al. (2017). Influence of diet on the gut microbiome and implications for human health. *J. Transl. Med.* 15 (1), 73. doi:10.1186/s12967-017-1175-y

Sun, Y., Wang, F., Liu, Y., Liu, S., An, Y., Xue, H., et al. (2022). Microbiome-metabolome responses of Fuzhuan brick tea crude polysaccharides with immune-protective benefit in cyclophosphamide-induced immunosuppressive mice. *Food Res. Int. Ott. Ont* 157, 111370. doi:10.1016/j.foodres.2022.111370

Tang, S., Tang, Q., Jin, J., Zheng, G., Xu, J., Huang, W., et al. (2018). Polydatin inhibits the IL-1β-induced inflammatory response in human osteoarthritic chondrocytes by activating the Nrf2 signaling pathway and ameliorates murine osteoarthritis. *Food and Funct.* 9 (3), 1701–1712. doi:10.1039/c7fo01555k

Thomas, M. S., and Fernandez, M. L. (2021). Trimethylamine N-oxide (TMAO), diet and cardiovascular disease. *Curr. Atheroscler. Rep.* 23 (4), 12. doi:10.1007/s11883-021-00910-x

Traughber, C. A., Iacano, A. J., Neupane, K., Khan, M. R., Opoku, E., Nunn, T., et al. (2023). Impavido attenuates inflammation, reduces atherosclerosis, and alters gut microbiota in hyperlipidemic mice. *iScience* 26 (4), 106453. doi:10.1016/j.isci.2023.106453

Trøseid, M., Andersen, G., Broch, K., and Hov, J. R. (2020). The gut microbiome in coronary artery disease and heart failure: current knowledge and future directions. *EBioMedicine* 52, 102649. doi:10.1016/j.ebiom.2020.102649

The Human Microbiome Project Consortium (2012). Structure, function and diversity of the healthy human microbiome. *Nature* 486 (7402), 207–214. doi:10.1038/nature11234

Vaccarezza, M., and Galassi, F. M. (2023). Inflammation beats cholesterol: a comment on the unequivocal driver of cardiovascular disease risk. *J. Clin. Med.* 12 (7), 2519. doi:10.3390/jcm12072519

Wang, S. Z., Wu, M., Chen, K. J., Liu, Y., Sun, J., Sun, Z., et al. (2019). Hawthorn extract alleviates atherosclerosis through regulating inflammation and apoptosis related factors: an experimental study. *Chin. J. Integr. Med.* 25 (2), 108–115. doi:10.1007/s11655-018-3020-4

Wang, W. Z., Liu, C., Luo, J. Q., Lei, L. J., Chen, M. H., Zhang, Y. Y., et al. (2024). A novel small-molecule PCSK9 inhibitor E28362 ameliorates hyperlipidemia and atherosclerosis. *Acta Pharmacol. Sin.* 45 (10), 2119–2133. doi:10.1038/s41401-024-01305-9

Wang, X. F., Chen, X., Tang, Y., Wu, J. M., Qin, D. L., Yu, L., et al. (2022). The therapeutic potential of plant polysaccharides in metabolic diseases. *Pharm. Basel, Switz.* 15 (11), 1329. doi:10.3390/ph15111329

Wang, Z., Klipfell, E., Bennett, B. J., Koeth, R., Levison, B. S., Dugar, B., et al. (2011). Gut flora metabolism of phosphatidylcholine promotes cardiovascular disease. *Nature* 472 (7341), 57–63. doi:10.1038/nature09922

Wang, Z., and Zhao, Y. (2018). Gut microbiota derived metabolites in cardiovascular health and disease. *Protein and cell* 9 (5), 416–431. doi:10.1007/s13238-018-0549-0

Watanabe, Y., Takeuchi, N., Yang, J., Obana, N., Morinaga, K., Kusada, H., et al. (2021). Complete genome sequence of Atopobiaceae bacterium strain P1, isolated from mouse feces. *Microbiol. Resour. Announc.* 10 (28), e0062721. doi:10.1128/mra.00627-21

Wu, M., Li, X., Wang, S., Yang, S., Zhao, R., Xing, Y., et al. (2020). Polydatin for treating atherosclerotic diseases: a functional and mechanistic overview. *Biomed. Pharmacother.* 128, 110308. doi:10.1016/j.biopha.2020.110308

Wu, M., Liu, M., Guo, G., Zhang, W., and Liu, L. (2015). Polydatin inhibits formation of macrophage-derived foam cells. *Evidence-based complementary Altern. Med. eCAM* 2015, 729017. doi:10.1155/2015/729017

Wu, M., Yang, S., Liu, G., Gu, C., Ren, P., Zhao, R., et al. (2021). Treating unstable angina with detoxifying and blood-activating formulae: a randomized controlled trial. *J. Ethnopharmacol.* 281, 114530. doi:10.1016/j.jep.2021.114530

Xue, M., Yin, H. J., Wu, C. F., Ma, X. J., Guo, C. Y., Huang, Y., et al. (2013). Effect of Chinese drugs for activating blood circulation and detoxifying on indices of thrombosis,

inflammatory reaction, and tissue damage in a rabbit model of toxin-heat and blood stasis syndrome. *Chin. J. Integr. Med.* 19 (1), 42–47. doi:10.1007/s11655-011-0604-7

Yoo, S. R., Kim, Y. J., Park, D. Y., Jung, U. J., Jeon, S. M., Ahn, Y. T., et al. (2013). Probiotics L. plantarum and L. curvatus in combination alter hepatic lipid metabolism and suppress diet-induced obesity. *Obes. (Silver Spring, Md)* 21 (12), 2571–2578. doi:10.1002/oby.20428

Zha, Z., Lv, Y., Tang, H., Li, T., Miao, Y., Cheng, J., et al. (2020). An orally administered butyrate-releasing xylan derivative reduces inflammation in dextran sulphate sodium-induced murine colitis. *Int. J. Biol. Macromol.* 156, 1217–1233. doi:10.1016/j.ijbiomac.2019.11.159

Zhang, Q., Fan, X., Ye, R., Hu, Y., Zheng, T., Shi, R., et al. (2020). The effect of simvastatin on gut microbiota and lipid metabolism in hyperlipidemic rats induced by a high-fat diet. *Front. Pharmacol.* 11, 522. doi:10.3389/fphar.2020.00522

Zhang, Q., Yu, H., Xiao, X., Hu, L., Xin, F., and Yu, X. (2018). Inulin-type fructan improves diabetic phenotype and gut microbiota profiles in rats. *PeerJ* 6, e4446. doi:10.7717/peerj.4446

Zhang, X., Wang, Z., Li, X., Chen, J., Yu, Z., Li, X., et al. (2023). Polydatin protects against atherosclerosis by activating autophagy and inhibiting pyroptosis mediated by the NLRP3 inflammasome. *J. Ethnopharmacol.* 309, 116304. doi:10.1016/j.jep.2023.116304

Zhao, G., Yang, L., Zhong, W., Hu, Y., Tan, Y., Ren, Z., et al. (2022). Polydatin, A glycoside of resveratrol, is better than resveratrol in alleviating non-alcoholic fatty liver disease in mice fed a high-fructose diet. *Front. Nutr.* 9, 857879. doi:10.3389/fnut.2022.857879

Zhou, W., Cheng, Y., Zhu, P., Nasser, M. I., Zhang, X., and Zhao, M. (2020). Implication of gut microbiota in cardiovascular diseases. *Oxidative Med. Cell. Longev.* 2020, 5394096. doi:10.1155/2020/5394096

Zhu, L., Zhang, D., Zhu, H., Zhu, J., Weng, S., Dong, L., et al. (2018b). Berberine treatment increases Akkermansia in the gut and improves high-fat diet-induced atherosclerosis in Ape(-/-) mice. *Atherosclerosis* 268, 117–126. doi:10.1016/j.atherosclerosis.2017.11.023

Zhu, W., Buffa, J. A., Wang, Z., Warrier, M., Schugar, R., Shih, D. M., et al. (2018a). Flavin monooxygenase 3, the host hepatic enzyme in the metaorganismal trimethylamine N-oxide-generating pathway, modulates platelet responsiveness and thrombosis risk. *J. thrombosis haemostasis JTH* 16 (9), 1857–1872. doi:10.1111/jth.14234

Zhulin, I. B. (2016). Classic spotlight: 16S rRNA redefines microbiology. *J. Bacteriol.* 198 (20), 2764–2765. doi:10.1128/jb.00616-16

Zifu, T., Jiaquan, L., and Juan, Z. (2022). Effect of Qinghe Jiedu Huoxue Huayu Recipe on blood stasis and toxin syndrome in patients with non-ST segment elevation acute coronary syndrome, serum Lp-PLA2, TNF- α, and PIGF expression level. *Cell. Mol. Biol. (Noisy-le-Grand, France)* 67 (4), 121–129. doi:10.14715/cmb/2021.67.4.14

Glossary

PH	polydatin and hawthorn leaf flavonoids
P. cuspidatum	*Polygonum cuspidatum Sieb. et Zucc*
C. pinnatifida	*Crataegus pinnatifida Bunge*
CVDs	Cardiovascular diseases
TMAO	Trimethylamine N-oxide
TMA	trimethylamine
FMO3	flavin-containing enzyme monooxygenase 3
HFD	high-fat diet
H&E	hematoxylin-eosin
TC	cholesterol
TG	triglyceride
LDL-C	low-density lipoprotein cholesterol
VLDL-C	very low density lipoprotein cholesterol
HDL-C	high-density lipoprotein cholesterol
NF-κB	nuclear factor-κB
TNF-α	tumor necrosis factor alpha
IL-1β	interleukin-1-beta
IL-2	interleukin-2
IL-6	interleukin-6
IL-17A	interleukin-17
OTUs	operational taxonomic units
ORFs	open reading frames
PCoA	principle coordinate analysis
NMDS	non-metric multidimensional scaling
LDA	linear discriminant analysis
LEfSe	linear discriminant analysis effect size
CAZymes	carbohydrate-active enzymes
GTs	glycosyl transferases
CEs	carbohydrate esterases
GHs	glycoside hydrolases
BP	biological processes.

frontiers | Frontiers in Pharmacology

TYPE Review
PUBLISHED 02 May 2025
DOI 10.3389/fphar.2025.1523272

OPEN ACCESS

EDITED BY
Weicheng Hu,
Yangzhou University, China

REVIEWED BY
Gina Stella Garcia-Romo,
National Autonomous University of Mexico, Mexico
Shokoh Parham,
University of Technology Malaysia, Malaysia

*CORRESPONDENCE
Yongsheng Fan,
fyszjtcm@163.com
Ting Zhao,
zhaoting@zcmu.edu.cn

†PRESENT ADDRESS
Zhiyan Huang,
The Second Affiliated Hospital of Zhejiang Chinese Medical University, Hangzhou, China

‡These authors have contributed equally to this work

RECEIVED 05 November 2024
ACCEPTED 14 April 2025
PUBLISHED 02 May 2025

CITATION
Huang Z, Li X, Zhu Q, Zhu M, Fan Y and Zhao T (2025) Traditional Chinese medicine for lupus nephritis: modulation of autoimmune pathogenesis.
Front. Pharmacol. 16:1523272.
doi: 10.3389/fphar.2025.1523272

Traditional Chinese medicine for lupus nephritis: modulation of autoimmune pathogenesis

Zhiyan Huang[1†‡], Xiaolong Li[2‡], Qingmiao Zhu[2], Mengyu Zhu[2], Yongsheng Fan[3*] and Ting Zhao[4*]

[1]The First Affiliated Hospital of Zhejiang Chinese Medical University, Hangzhou, China, [2]School of Basic Medical Sciences, Zhejiang Chinese Medical University, Hangzhou, China, [3]The Second Affiliated Hospital of Zhejiang Chinese Medical University, Hangzhou, China, [4]Key Laboratory of Chinese Medicine Rheumatology of Zhejiang Province, Research Institute of Chinese Medical Clinical Foundation and Immunology, School of Basic Medical Sciences, Zhejiang Chinese Medical University, Hangzhou, China, [5]Research Institute of Chinese Medical Clinical Foundation and Immunology, Hangzhou, China

Ethnopharmacological relevance: Lupus nephritis (LN) is an immune complex glomerulonephritis commonly associated with systemic lupus erythematosus. Traditional Chinese medicine (TCM) has emerged as a promising adjuvant therapy for LN, due to its low toxicity and diverse therapeutic effects for long-term management.

Materials and methods: A comprehensive search of PubMed and Web of Science was conducted up to 7 June 2024, using keywords related to lupus nephritis, traditional Chinese medicine, immune cells, and kidney resident cells. Study quality were assessed based on Good Automated Manufacturing Practice guidelines, with evaluations jointly conducted by two authors.

Results: This review includes 31 research papers and summarizes seven herbal formulas and 18 phytochemicals that modulate the autoimmune pathogenesis of LN. Their mechanisms involve regulating immune cells activation, differentiation, apoptosis, as well as influencing resident kidney cells to support renal protection and immune homeostasis. Since TCM exhibit bidirectional regulation, they activate regulatory immune cells while suppress pathogenic factors. Inconsistent or inconclusive findings are discussed.

Conclusion: This review summarizes current research on herbal formulas and phytochemicals in immune cells and kidney resident cells in LN, highlighting the potential and significance of TCM treatment. It also addresses the limitations of existing studies and suggests that future research should focus on exploring the immunosuppressive and kidney-protective effects of herbal formulas and phytochemicals, as well as enhancing the clinical translation and standardization of TCM.

KEYWORDS

lupus nephritis, plant extracts, herbal formula, Chinese herbal, immune system, systemic lupus erythematosus

1 Introduction

Lupus nephritis (LN) is a type of glomerulonephritis that represents one of the most severe organ manifestations, affecting approximately 50% of the systemic lupus erythematosus (SLE) cases and posing a significant risk for morbidity and mortality (Anders et al., 2020; Parikh et al., 2020). The pathophysiology of LN is heterogeneous, including the deposition of autoantibodies and immune complexes (ICs), the activation and/or proliferation of infiltrating immune cells and kidney resident cells, and the presence of various pathogenic molecules at the site of injury (Davidson, 2016; Lech and Anders, 2013; Mohan et al., 2023).

Conventional treatments encompass steroid therapy, cyclophosphamide (CYC), and mycophenolate mofetil (MMF), while alternative therapies, including anti-BLYS agents, novel calcineurin inhibitors, CD20 blockade, and anti-interferon agents have also been explored (Askanase et al., 2023; Desai et al., 2024). These advancements have enhanced life expectancy and quality, but there has not been significant progress in improving renal failure and mortality rates (Nossent et al., 2024; Parikh et al., 2020). Besides, evidences proved that these drugs can induce cytotoxicity through immunosuppressive and pharmacologic effects, resulting in side effects such as amenorrhea/ovarian failure, cytopenia, and serious infections (Singh et al., 2016a; Singh et al., 2016b). This highlights the urgent need for multi-target therapy and the development of better long-term treatment options or strategies for LN.

The quest for novel therapies, as well as the fact that LN being more common and severe in East Asians than in African-Americans (Petri et al., 2023), have spurred the exploration of TCM. TCMs exhibit diverse and integrated pharmacological effects that help mitigate the progression of LN. Moreover, their ability of reducing adverse side effects makes them a valuable option of long-term adjuvant therapy (Dou et al., 2023). Evidence indicates that combining herbal formulas and phytochemicals such as Shenqi Dihuang decoction, Liuwei Dihuang pill, and Astragalus injection with conventional treatments like cyclophosphamide (CTX) and glucocorticoids (GC) enhances clinical efficacy and reduces SLE disease activity scores more effectively than CTX and GC alone. Moreover, this combined treatment approach has been associated with a lower risk of adverse reactions such as infection, gastrointestinal discomfort, and insomnia (Li et al., 2024), as well as a slightly higher likelihood of reducing or discontinuing glucocorticoid dosage (Li et al., 2014). Additionally, botanical drugs like Cordyceps and artemisinin may help prevent the recurrence of LN and protect kidney function (Lu, 2002).

This review uniquely integrates immune metabolic regulation with the therapeutic potential of TCM in LN, providing a comprehensive analysis of recent advances in preclinical studies. By systematically summarizing the molecular mechanisms and therapeutic implications, this review offers new insights into TCM's role in LN treatment and identifies key directions for future research. All the herbal formulas and phytochemicals discussed in this review are within the domain of traditional Chinese medicine.

2 Methods

In this review, experimental research (*in vitro* and *in vivo* studies) published or available for early access up to 7 June 2024, were retrieved from databases such as PubMed and Web of Science. The search terms included *lupus nephritis*, *traditional Chinese medicine* (e.g., herbal prescriptions, Chinese herbal drugs, plant extracts, herbal extracts), *immune cells* (e.g., T lymphocytes, B lymphocytes), and *kidney-resident cells* (e.g., Podocytes, Mesangial cells).

The inclusion criteria were as follows: (1) studies related to the specified keywords, either individually or in combination, focusing on the therapeutic effects or mechanisms of TCM in LN; (2) studies providing experimental data from *in vitro* or *in vivo* research with detailed methodologies; and (3) full-text articles published in English.

The exclusion criteria were: (1) duplicate search results; (2) studies deemed irrelevant based on title and abstract screening; (3) records lacking mechanistic insights or providing insufficient information; and (4) purely theoretical or review articles.

Based on these criteria, a total of 31 studies investigating the mechanisms of Traditional Chinese Medicine in the treatment of LN were included in this review. The quality and methodological rigor of these studies were assessed using the criteria outlined by the Good Automated Manufacturing Practice (GAMP) best practice guidelines (https://ga-online.org/best-practice/). The evaluation was jointly conducted by authors HZY and LXL. The detailed evaluation results are provided in the supplementary materials.

3 Cellular pathogenesis of lupus nephritis

3.1 T cells

3.1.1 T cells activation

T cells constitute the majority of kidney-infiltrating immune cells in patients with LN and in lupus-prone mice, and are implicated in the development of progressive kidney failure (Linke et al., 2022; Mohan et al., 2023). T cells can either cause direct cytotoxicity or recruit other inflammatory cells, such as monocytes/macrophages, playing a crucial role in the pathogenesis of experimental and human LN. Studies have revealed that Triptolide, a diterpenoid triepoxide derived from the botanical drug Tripterygium wilfordii Hook. f., inhibits lymphocyte activation and T-cell expression of interleukin-2 at the transcriptional level, positioning it as one of the few immunosuppressants acting at the early stage of T-cell activation signaling (Qiu and Kao, 2003). This characteristic classifies triptolide as operating within a category of immunosuppressants similar to CYC and tacrolimus (Qiu et al., 1999). Furthermore, unlike CYC and tacrolimus, triptolide inhibits both Ca^{2+}-dependent and Ca^{2+}-independent pathways, thereby affecting T-cell activation through CD28 co-stimulation, indicating that triptolide has broader immunosuppressive effects in the treatment of conditions involving CYC-resistant T-cell activation (Gu et al., 2016; Song et al., 2023). Although there is a lack of studies on other botanical drugs, this example suffices to illustrate the broad potential of TCM in the treatment of LN, particularly as a supplement to targeted therapy.

3.1.2 T cells differentiation

In LN, dysregulated $CD4^+$ T cell subsets include Th1, Th17, Tfh, and Treg cells. Th1 and Treg cells are decreased, while Th2, Th17,

Tfh17, and Tfh cells are increased. A strong correlation between Th17 and Treg cells with renal involvement was observed (Yuan et al., 2022). These immunological mechanisms are central to TCM-related research and will be discussed further.

3.1.2.1 CD4⁺ Th1 T cells

Numerous clinical and experimental findings have demonstrated a pathogenic role of imbalance towards Th1 cell-mediated immune responses in LN (Chan et al., 2006; Fakhfakh et al., 2022; Linke et al., 2022), which is partly attributed to high glomerular expression of interleukin-12 (IL-12) and interleukin-18 (IL-18) (Liu et al., 2012; Tucci et al., 2010). However, TCM has demonstrated the ability to alter this cellular population imbalance. Hachimi-jio-gan (Ba-Wei-Di-Huang-Wan, HMG) modulated an imbalance toward Th1 predominance in MRL/lpr mice by inhibiting IL-12 production and ameliorating autoimmune disorders (Furuya et al., 2001). Additionally, the Th1 axis was suppressed and the Th2 axis became predominant in Sairei-to-treated MRL/lpr mice, possibly due to an increase in IL-4-producing cells and suppression of IFN-γ expression (Ito et al., 2002). Furthermore, Antroquinonol (Tsai et al., 2012) and DCB-SLE1 (Tsai et al., 2011) have been shown, in mouse models, to reduce renal production of IL-18, thereby facilitating the differential regulation of T cells in treatment. They also exhibit the ability to inhibit local renal inflammation by suppressing NF-κB activation.

3.1.2.2 CD4⁺ Th17 T cells

The level of Th17 cells was found to be higher in LN patients (Fakhfakh et al., 2022). Several reports indicate that interleukin-17 (IL-17) and Th17 cells play important roles in the pathogenesis of LN, with PP2A, ROCK, CREM, and CaMK4 pathways shown to facilitate IL-17 production in SLE (Koga et al., 2017). Celastrol inhibited phospho-STAT3 expression in cultured Th17 cells and upregulated phospho-STAT5 expression in induced regulatory T (iTreg) cells, thereby suppressing Th17 cell induction and promoting iTreg cell generation. It also reduced IL-17 expression in Th17 cells compared with untreated cells (Astry et al., 2015; Zhang et al., 2018). Furthermore, studies have shown that menthone could serve as a potential antirheumatic phytochemical, as its effect on regulating the number of Th1 and Th17 cells and inhibiting the release of pro-inflammatory cytokines, including TNF-α, IL-1β, and IL-6, has been confirmed (Chen X. et al., 2022). DCB-SLE1 has been shown to suppress IL-6 and IL-17 production in an accelerated severe LN model (Tsai et al., 2011), thereby regulating the number of Th17 cells. Administration of lipopolysaccharide resulted in a mixed Th1, Th2, and Th17 response in normal mice, and this effect was inhibited by *in vivo* Tetrandrine (Zou et al., 2019).

Interestingly, Jakiela et al. claimed that Th17 expansion was not related to LN activity, renal histology, or blood and urine inflammatory biomarkers, but was associated with a higher cumulative dose of CYC (Jakiela et al., 2018). This suggests that the use of TCM may help reduce the occurrence of side effects from chronic immunosuppressive therapy and improve treatment efficiency.

3.1.2.3 CD4⁺ Treg cells

Except for the germinal center-Tfr/Tfh imbalance mentioned above, it has been more commonly observed in the pathogenesis of LN that there are fewer Treg cells in LN patients' peripheral blood than healthy individuals', with a considerable increase in Th17 cell-to-Treg cell ratios (Li et al., 2022b).

Several have been shown to influence Treg cells in LN. Astragaloside IV (AST IV) has the ability to markedly increase the Foxp3 expression as well as IL-10 and TGF-β secretion levels in Treg in a dose-dependent manner (Li et al., 2016). Antroquinonol can enhance Treg cell suppression in accelerated severe LN (Tsai et al., 2012). Baicalin induces Foxp3 protein expression in cultured T cells, promotes Treg cell differentiation and regulatory activity. It also restores Foxp3 expression following its initial IL-6-mediated inhibition (Yang et al., 2012).

Apart from LN, the abnormal Treg/Th17 ratio is involved in the pathogenesis of many immune-mediated inflammatory diseases. Xu, etc., reviewed that there were nine active ingredients (including Oxymatrine, Baicalin, Triptolide, Paeoniflorin, Sinomenine, Celastrol, Emodin, Diosgenin and Chlorogenic acid) originating from TCM reported to have an immunological regulatory effect on the Th17/Treg axis in IMID treatment (Xu et al., 2020). The mechanism of action of these botanical drugs need to be further explored. The immune-modulating mechanisms on Th17/Treg axis by TCM might provide a broader insight into the treatment of IMID.

3.1.2.4 CD4⁺ Tfh cells

Follicular helper CD4 T (Tfh) cells play a significant role in germinal center formation, B-cell development, affinity maturation, and immunoglobulin class switching (Crotty, 2011; Fazilleau et al., 2009; Zhu et al., 2016). IL-21, a critical cytokine produced by Tfh cells, potently stimulates the differentiation of B cells (King et al., 2008). Tfh cells have been found to increase in LN patients and are associated with B cell activation as well as *in situ* inflammation (Arazi et al., 2019; Liarski et al., 2014; Yuan et al., 2022).

Follicular regulatory T (Tfr) cells, also located in the germinal center and sharing phenotypic characteristics with Tfh cells and Treg cells, inhibit Tfh cells mediated B cell responses (Xu et al., 2017; Zhu et al., 2016). Tfr cells are reported to be reduced in patients with SLE compared with healthy individuals, but this reduction is corrected after standard-of-care treatment (Liu et al., 2018; Xu et al., 2017). Additionally, a progressive reduction in Tfr cells and decreased Tfr/Tfh ratio despite increased Tregs in the renal lymph nodes of NZBWF1/j mice were repored (Kumar et al., 2022).

Artesunate (ART) has shown therapeutic effects by reducing the number of Tfh cells and maintenance of the ratio of Tfr to Tfh in the spleen of MRL/lpr mice (Dang et al., 2019). Baicalin has the ability of inhibiting Tfh cell differentiation and IL-21 production by mTOR activation inhibition, and it can promote Foxp3⁺ regulatory T cell differentiation, including Tfr cells (Yang et al., 2019). Although studies of the balance of Tfr and Tfh cells have been sparse, TCM has shown great therapeutic potential in this regard. (Figure 1 illustrates the differentiation and interaction of the T cell family and the effect of TCM on these processes.).

3.2 B cells

3.2.1 B cells and plasma cells

SLE is characterized by the loss of B-cell tolerance and presence of autoantibodies. Anti-dsDNA antibodies cross-react with several renal cell types and are thought to be central to the nephritis process

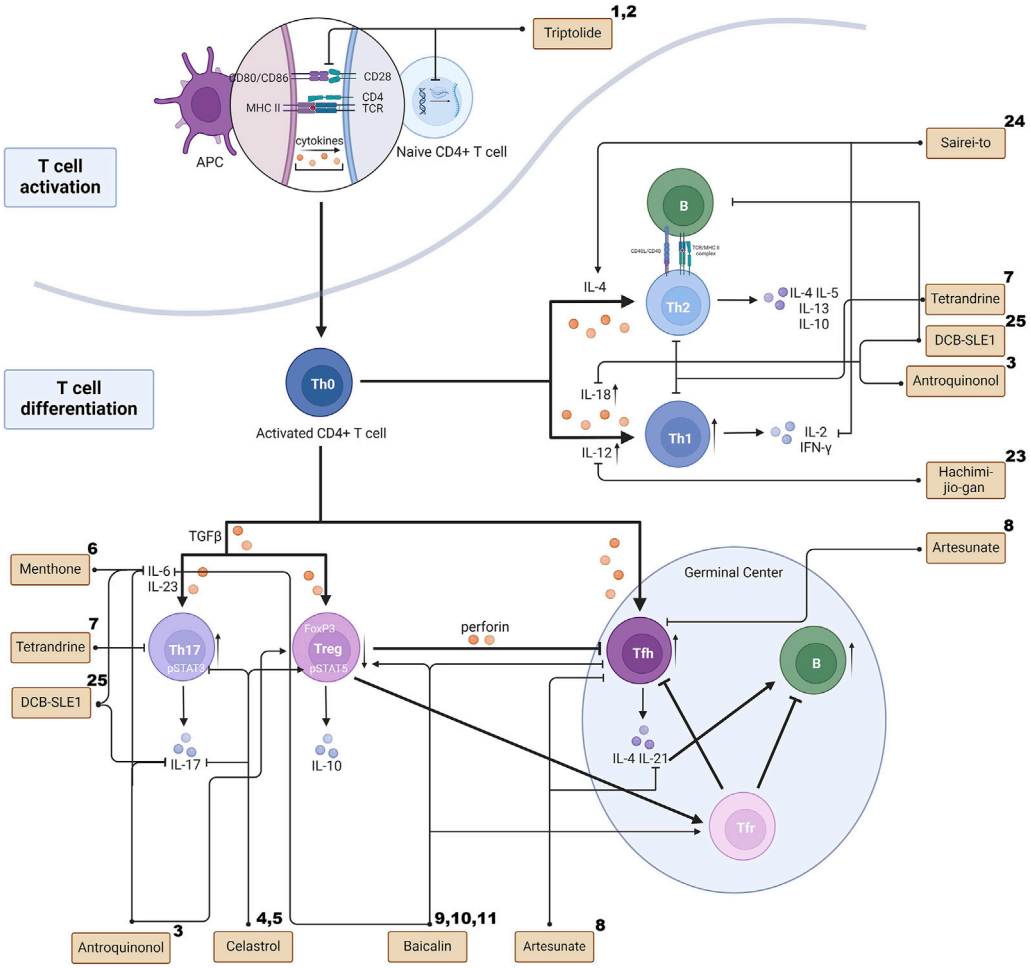

FIGURE 1
The effects of TCM on T cell activation, differentiation and interaction. The superscript numbers of the herbal formulas/phytochemicals correspond to the reference numbers in Tables 1, 2. Created with BioRender.com.

(Tsokos et al., 2016). Researches has focused on the ability of TCM to reduce of autoreactive B cells. Tripterygium wilfordii Hook F (TWHF) regulates the functions of 24 differentially expressed genes (including HMOX1, ALB, and CASP1) through hydrogen bonding, mainly concentrated in the B-cell signaling pathway (Cai et al., 2023). Sairei-to downregulates the proportion of CD19 and the serum levels of IgG1 in MRL/lpr mice, thereby suppressing B cell function (Ito et al., 2002).

Additionally, the upstream regulation of B cells and the role of B cell subsets in the pathogenesis of LN have been further studied. B-cell activating factor (BAFF) and a proliferation-inducing ligand (APRIL) are the most important factors involved in the maturation and activation of B cells (Samy et al., 2017). A study shows that Langchuangping Granule (LG) could attenuate the renal injury via suppressing sBAFF level and BAFF mRNA expressions (Li et al., 2012). Jieduquyuzishen prescription (JP) can downregulate the BAFF/BAFF-R signaling pathway as effectively as GC and suppress proliferation and survival of lymphocytes activated by mBAFF(Wu et al., 2015). BAFF and APRIL are ideal targets for LN treatment, and the value of TCM in this area requires further exploration.

B cell subsets that play a role in the pathogenesis of LN include age-associated B cells (ABCs) and kidney-infiltrated plasma cells (Espeli et al., 2011; Mohan et al., 2023; Rubtsova et al., 2017). Peripheral blood ABCs are increased compared with healthy controls in patients with SLE and strongly correlate with anti-chromatin antibody levels and track with disease activity (Ramsköld et al., 2019; Wang et al., 2018). Infiltrated plasma cells are often present in the renal medulla in LN patients, especially proliferative and membranous types. These cells had the phenotypic characteristics of fully differentiated plasma cells and, similar to long-lived bone marrow plasma cells, they are not in cell cycle (Espeli et al., 2011). However, there is a lack of research on the relationship between TCM and these B cell subsets. More detailed and in-depth researches are needed.

3.2.2 Bregs

Evidences has shown that the percentages of Bregs and their secretion of IL-35 and IL-10 are significantly decreased in LN patients (Heinemann et al., 2016; Watanabe et al., 2010; Xiong et al., 2022). A decrease has been observed in CD72, a regulatory receptor on B cells, while the addition of soluble semaphorin 3A can

TABLE 1 The effects of phytochemicals on LN treatment.

Phytochemical	Origin	Immunocyte/ kidney resident cell	Cytokine	Signaling pathway	References
Triptolide	Tripterygium wilfordii Hook.f. [Celastraceae; Tripterygii wilfordii radix]	Inhibit T cells activation	Inhibit T-cell expression of interleukin-2 at the level of transcription	Inhibit both Ca (2+)-dependent and Ca (2+)-independent pathways, therefore affecting T-cell activation through CD28 co-stimulation	1 (Qiu et al., 1999)
		Downregulate monocytes	Downregulate monocyte chemoattractant protein-1 (MCP-1)	Not mentioned	2 (Tao et al., 2008)
Antroquinonol	Antrodia camphorata [Polyporaceae; Antrodiae camphoratae fructus]	Inhibit local renal inflammation Suppress T cell proliferation/activation Modulate Th1/Th2 cells cytokines balance Upregulate Treg cells Suppress Th17 cells induction	Inhibit IL-18 production	Suppress NF-κB activation	3 (Tsai et al., 2012)
			Suppress IL-6 expression and IL-17 production	Activate Nrf2 pathway	
		Ameliorated development of severe renal lesions, especially cellular crescent formation, neutrophil infiltration, fibrinoid necrosis	Not mentioned		
Celastrol	Celastrus aculeatus Merr. [Celastraceae; Celastri aculeati herba]	Suppress Th17 cells induction	Lower IL-17 expression in Th17	Inhibit phospho-STAT3 expression in Th17 cells	4 (Astry et al., 2015)
		Promote Treg cells generation	Not mentioned	Upregulate phospho-STAT5 expression in Treg cells	5 (Zhang et al., 2018)
Menthone	Mentha × piperita L. [Lamiaceae; Menthae piperitae folium et aetheroleum]	Regulate the number of Th1 and Th17 cells	Inhibit the release of pro-inflammatory cytokines including TNF-α, IL-1β, and IL-6	Not mentioned	6 (Chen X. et al., 2022)
Tetrandrine (TET)	Stephania tetrandra S. Moore [Menispermaceae; Stephaniae tetrandrae radix]	Inhibit the differentiation of proinflammatory Th1, Th2 and Th17 cells Spare the generation of Tregs	Not mentioned	Inhibit master transcription factors, namely, T-bet, Gata3 and RORγt	7 (Zou et al., 2019)
Artesunate (ART)	Artemisia annua L. [Asteraceae; Artemisiae annuae herba]	Reduce the number of Tfh cells Maintain the ratio of Tfr to Tfh cells	Decrease the levels of pathogenic cytokines (IL-6, IFN-γ and IL-21)	Activate JAK2-STAT3 signaling pathway	8 (Dang et al., 2019)
Baicalin	Scutellaria baicalensis Georgi [Lamiaceae; Scutellariae baicalensis radix]	Inhibit Tfh cells differentiation	Inhibit IL-21 production in Tfh	inhibit mTOR activation	9 (Yang et al., 2019)
		Promote Treg cells differentiation and function including part of Tfr cells	Induce Foxp3 protein expression in T cells	Not mentioned	10 (Yang et al., 2012)
		Reconstruct B cells' regulatory functions by upregulating IL-10 expression	Induce semaphorin 3 A expression	Upregulate CD72-semaphorin3A axis	11 (Yoshioka, 2021)
Astragaloside IV (AST IV)	Astragalus mongholicus Bunge [Fabaceae; Astragali radix]	Promote Treg cells function	Increase the Foxp3 expression as well as IL-10 and TGF-β secretion levels in Treg	Not mentioned	12 (Li et al., 2016)

(Continued on following page)

TABLE 1 (*Continued*) The effects of phytochemicals on LN treatment.

Phytochemical	Origin	Immunocyte/ kidney resident cell	Cytokine	Signaling pathway	References
Wogonin	Scutellaria baicalensis Georgi [Lamiaceae; Scutellariae baicalensis radix]	Suppress B cells function	Suppresses IL-10 production	Inhibit the STAT3 and ERK signaling pathway inhibit mRNA and protein levels of Hif-1α	13 (Fan et al., 2020)
Depigmented-polymerized (DPG-POL-Phl p)	Phleum pratense L. [Poaceae; Phlei pratensis herba]	Induce IL-10 (+)CD19 (+) CD5 (hi) and IL-10 (+) CD19 (+)CD5 (hi)CD38 (int)CD24 (int) regulatory B cells	Increase in IL-10 expression	Not mentioned	14 (Layhadi et al., 2023)
Active metabolites in Hedyotis diffusa Willd (HDW): asiatic acid, neoandrographolide, glycyrrhetinic acid, oleanolic acid, ursolic acid, and wilforlide A		Ameliorate neutrophil NETosis	Ameliorate the expression of STAT3, IL-17, Ly6G, and MPO in the kidney	Inhibit the IL-6 and STAT3/IL-17 signaling pathways	15 (Li et al., 2022a)
Citral	Litsea cubeba (Lour.) Pers. [Lauraceae; Litseae cubebae fructus]	Ameliorate intrinsic cell proliferation, cellular crescents, neutrophil influx, fibrinoid necrosis in the glomerulus, and peri-glomerular infiltration of mononuclear leukocytes			16 (Ka et al., 2015)
		Inhibit macrophages	Reducing ATP-induced IL-1β secretion and caspase-1 activation	Not mentioned	
Demethylzeylasteral (T-96)	Tripterygium wilfordii Hook.f. [Celastraceae; Tripterygii wilfordii radix]	Restrict macrophage infiltration	Reduce the downstream pro-inflammatory mediators such as TNF-α, COX-2 and ICAM-1	Inhibit the activation of NF-κB	17 (Hu et al., 2015)
M1	Panax ginseng C.A.Mey. [Araliaceae; Ginseng radix]	Modulate Th cell activation	Decrease the secretion of pro IL-1β and p-IκB in BMDC	Not mentioned	18 (Lin et al., 2019)
		Induce Treg cell differentiation	Inhibit NLRP3 inflammasome associated with autophagy induction		
		Inhibit $CD4^+$ T cell proliferation			
		Protect podocytes	Reduce the ATP-mediated production of ROS	Not mentioned	
			Inhibit the activation of NLRP3 inflammasome by enhancing the induction of autophagy		
Fisetin	Producted widely from botanical drugs	Suppress the endocytic activity of dendritic cells	Suppress the expression of CD80 and CD86	Not mentioned	19 (Liu et al., 2010)
			Suppress the production of IL-12, IL-6, and TNF-α		
Petroleum ether extract of Bidens pilosa L. [Asteraceae; Bidens pilosa herba]		Induce a semi-mature status in DCs Induce M2 polarization or a hybrid M1/M2 phenotype in MØs	Immature or semi-mature DCs expressing IL-10 facilitated the immune tolerance through inducing Tregs	Not mentioned	20 (Rodríguez Mesa et al., 2023)
Eucarbwenstols A-H	Eucalyptus robusta Sm. [Myrtaceae; Eucalypti robustae folium]	Prevents the podocyte cells' injury	Modulate ROS and regulate mitochondrial membrane potentia	Not mentioned	21 (Chen T. et al., 2022)
Stragalin	Astragalus mongholicus Bunge [Fabaceae; Astragali mongholici radix]	Protect mesangial cells Inhibit leukocyte recruitment	Decrease the distribution intensity of ICAM-1, immunoglobulins and C3	Not mentioned	22 (Chen et al., 1995)

improve its expression (Vadasz et al., 2014). Although there are no direct studies on the effects of TCM on Breg cells in LN, related research has demonstrated the role of TCM in this context. Depigmented-polymerized phleum pratense (DPG-POL-Phl p) was prominent at inducing IL-10^{+}CD19^{+}CD5^{hi} and IL-10^{+}CD19^{+}CD5^{hi}CD38^{int}CD24^{int} Breg cell subsets (Layhadi et al., 2023). Additionally, administration of Yupinfeng San, a traditional Chinese medical formula, can induce propionic acid production by intestinal bacteria to stabilize IL-10 expression in Breg cells (Zhou et al., 2021) or restore the immune suppressor function of Bregs by inhibiting the expression of Bcl2L12 (Zhou et al., 2019). S. baicalensis extract and its metabolites, baicalin and baicalein, can induce semaphorin 3A expression (Yoshioka et al., 2021), thereby potentially restoring B cells' regulatory functions by upregulating IL-10 expression (Eiza et al., 2023).

Although IL-10 is known as a potent anti-inflammatory cytokine (Mollazadeh et al., 2019; Saraiva and O'Garra, 2010) and has been emphasized in Breg cell-related therapy, excessive IL-10 levels may lead to immune disorders and increase the risk of autoimmune diseases by disrupting the immune balance and regulating the activation of immune cells. For example, research has showen that IL-10 can increase CD8^{+} T cell infiltration in tissue, induce IFN-γ production, and favor effective T cell memory responses (Saraiva et al., 2020). Recent evidence indicates that IL-10 plays dual roles in SLE: it may inhibit pro-inflammatory effector functions but also seems to be a main driver of the extrafollicular antibody response, promoting direct differentiation of activated B cells into plasma cells (Biswas et al., 2022). Despite the emphasis on promoting Breg cells and IL-10, there are also studies on inhibiting IL-10 using TCM. For example, Wogonin suppresses IL-10 production in B cells via inhibition of the STAT3 and ERK signaling pathways and reduce mRNA and protein levels of the transcription factor Hif-1α(Fan et al., 2020).

The aforementioned studies have indicated that TCM may play a role in inducing Bregs and their regulatory factors in LN treatment. On the other hand, due to the pleiotropic effects of cytokines, herbal formulas particularly, offers a more comprehensive regulatory effect owing to its ambiguous targeting, which may reduce side effects and promote positive regulation. Therefore, the therapeutic role of TCM warrants more attention and further exploration. (Figure 2 illustrates the differentiation and interaction of the B cell family and the effect of TCM on these processes.).

3.3 NK cells and NKT cells

In SLE patients, circulating levels of Natural Killer (NK) cells were diminished and their cytotoxicities were impaired (Park et al., 2009). Active nephritis in SLE is substantially associated with ILT2^{+} NKT cell and Ki67^{+} NK cell frequencies (Chen et al., 2023; Hudspeth et al., 2019). Additionally, an elevated ratio of CD56^{bright}CD16^{-} to CD57^{+}CD56^{dim}CD16^{+} NK cell distinguishes renal involvement in SLE (Li et al., 2023). The defective functions of NK cells may be due to changes in apoptosis-related protein expressions, such as reduced expression of TRAIL, Bcl-2, and TNFR1(Liphaus et al., 2024). The decline in NK cells may be related to increased consumption due to autoimmunity, as suggested by the fact that the high expression of MCP-1, a chemokine that induces NK cell migration and activation, thereby facilitating kidney disease-related inflammation in LN (Liu et al., 2023).

Although NK cells are one of the most important lymphocytes, their pathogenic role in LN has not received much attention, and the reason for their reduced quantity and weakened pathogenicity in LN have not been clearly studied. Herbal formulas like DCB-SLE1 have been found to suppress NK cell activity (Tsai et al., 2011). However, studies on the effects of TCM on NK cells in the context of treatment are still lacking.

3.4 Neutrophils

Neutrophils accumulate in the kidneys of patients with proliferative LN, and their products and ability to induce other immune cells may contribute to pathogenesis of the disease (Nishi and Mayadas, 2019). The herbal formulas and phytochemicals, such as the DCB-SLE1, Antroquinonol, and Citral, have been shown to reduce neutrophil infiltration in the kidney (Tsai et al., 2011; Tsai et al., 2012; Ka et al., 2015). However, some also provide protective effect on neutrophils. For example, JP can reduce the apoptosis and increase the survival of polymorphonuclear neutrophils (Wu et al., 2015).

Neutrophil extracellular traps (NETs) are fibrous networks that protrude from the membranes of activated neutrophils. Excess NETs damage normal tissues and induce inflammation and immune injury to kidneys (Lee et al., 2017). NETs are elevated in the circulation of patients with SLE, particularly in those with LN, and their abundance correlates with circulating levels of anti-double-stranded DNA (dsDNA), C3 and C4, and proteinuria (Hakkim et al., 2010; van der Linden et al., 2018). Hedyotis diffusa Willd (HDW) treatment has been proven to ameliorate the expression of STAT3, IL-17, Ly6G, and MPO in the kidney and neutrophil Extracellular Trap formation (NETosis), thereby relieving LN (Li et al., 2022a). However, the view that reduced degradation of NETs contributes to LN progression is challenged by experimental data in lupus-prone mice that genetically fail to produce NETs but still suffer from the disease (Kienhöfer et al., 2017; Nishi and Mayadas, 2019). Overall, the role of neutrophils in the pathogenesis of LN and the application of TCM in this field require further study. (Figure 3 illustrates the infiltration, apoptosis and NETosis of the neutrophil family, as well as the effect of TCM on these processes.).

3.5 Monocytes and macrophages

Pathogenic macrophages in LN are classified according to source and function. Along with infiltrating monocyte-derived (MoMac) macrophages, the kidneys also have a network of tissue-resident macrophages (TrMac) located around the glomeruli and tubulointerstitium (Mohan et al., 2023). TrMacs orchestrate leukocyte recruitment and are major responders to ICs, while MoMacs take up and present IC antigen (Richoz et al., 2022). Additionally, subpopulations called classically activated macrophages (M1) and alternative activated macrophages (M2)

TABLE 2 The effects of herbal formulas on LN treatment.

Herbal formula	Ingredient	Immunocyte/kidney resident cell	Cytokine	Signaling pathway	References
Hachimi-jio-gan (Ba-Wei-Di-Huang-Wan, HMG)	Rehmannia glutinosa (Gaertn.) Libosch. ex DC. [Orobanchaceae; Rehmanniae glutinosae rhizoma], Cornus officinalis Siebold & Zucc. [Cornaceae; Cornus officinalis sarcocarpium], Dioscorea oppositifolia L. [Dioscoreaceae; Dioscoreae oppositifoliae rhizoma], Alisma plantago-aquatica subsp. Orientale (Sam.) Sam. [Alismataceae; Alismatis plantago-aquaticae tuber], Poria cocos (Schw.) Wolf [Polyporaceae; Poria], Paeonia × suffruticosa Andrews [Paeoniaceae; Paeoniae suffruticosae cortex], Cinnamomum verum J.Presl [Lauraceae; Cinnamomi verum cortex] and Aconitum carmichaelii Debeaux [Ranunculaceae; Aconiti carmichaelii radix]	Modulate Th1/Th2 cytokines balance	Inhibit IL-12 production	Not mentioned	23 (Furuya et al., 2001)
Sairei-to	Bupleurum chinense DC. [Apiaceae; Bupleuri chinensis radix], Glycyrrhiza uralensis Fisch. [Fabaceae; Glycyrrhizae radix], Cinnamomum cassia (L.) J.Presl [Lauraceae; Cinnamomi cortex], Scutellaria baicalensis Georgi [Lamiaceae; Scutellariae radix], Alisma plantago-aquatica subsp. orientale (Sam.) Sam. [Alismataceae; Alismatis rhizoma], Pinellia ternata (Thunb.) Breit. [Araceae; Pinelliae rhizoma], Polyporus umbellatus (Pers.) Fries [Polyporaceae; Polypori sclerotium], Poria cocos (Schw.) F.A.Wolf [Polyporaceae; Poriae sclerotium], Atractylodes lancea (Thunb.) DC. [Asteraceae; Atractylodis rhizoma], Ziziphus jujuba Mill. [Rhamnaceae; Zizyphi fructus], Panax ginseng C.A.Mey. [Araliaceae; Ginseng radix] and Zingiber officinale Roscoe [Zingiberaceae; Zingiberis rhizoma]	Modulate Th1/Th2 cytokines balance	Enhance IL-4 production Suppress the IFN-γexpression	Not mentioned	24 (Ito et al., 2002)
		Suppress B cells function	Downregulates CD19 and the serum levels of IgG1		
DCB-SLE1	Atractylodes macrocephala Koidz. [Asteraceae; Atractylodis macrocephalae rhizoma], Eucommia ulmoides Oliv. [Eucommiaceae; Eucommiae cortex], *Lonicera japonica* Thunb. [Caprifoliaceae; Lonicerae caulis], and Hedyotis diffusa Willd. [Rubiaceae; Hedyotidis diffusae herba]	Modulate Th1/Th2 cytokines balance	Inhibit IL-18 production	Inhibit Renal NF-B activation	25 (Tsai et al., 2011)
		regulate the number of Th17 cells	suppress IL-6 and IL-17 production		
		Suppress B cell activation Decrease autoantibody production	Not mentioned		
		Inhibits Renal Infiltration of T Cells, Monocytes/ Macrophages, and Neutrophils	Not mentioned		
		suppress NK cell activity	Not mentioned		
Langchuangping Granule (LG)	Sophora tonkinensis Gagnep. [Fabaceae; Sophorae tonkinensis radix], Panax notoginseng (Burkill) F.H.Chen	Suppress B cells function	Suppress sBAFF level and BAFF mRNA expressions	Not mentioned	26 (Li et al., 2012)
		Downregulate monocytes			

(Continued on following page)

TABLE 2 (*Continued*) The effects of herbal formulas on LN treatment.

Herbal formula	Ingredient	Immunocyte/kidney resident cell	Cytokine	Signaling pathway	References
	[Araliaceae; Notoginseng radix], Ligustrum lucidum Ait. [Oleaceae; Ligustri lucidi fructus], Gentiana macrophylla Pall. [Gentianaceae; Gentianae macrophyllae radix], Arnebia euchroma (Royle) Johnst. [Boraginaceae; Arnebiae radix], herba Radix Saposhnikovia divaricata (Turcz.) Schischk. [Apiaceae; Saposhnikoviae radix], etc.		Downregulate monocyte chemoattractant protein-1 (MCP-1)	Inhibit NF-κB signaling pathway	27 (Li et al., 2011)
Jieduquyuzishen prescription	Artemisia annua L. [Asteraceae; Artemisiae annuae herba], Cimicifuga heracleifolia Kom. [Ranunculaceae; Cimicifugae heracleifoliae rhizoma], Hedyotis diffusa Willd. [Rubiaceae; Hedyotis diffusae herba], Paeonia veitchii Lynch [Paeoniaceae; Paeoniae veitchii radix], Trionyx sinensis Wiegmann [Trionychidae; Trionycis sinensis carapax], *Centella asiatica* (Linn.) Urban [Apiaceae; Centellae asiaticae herba], Citrus medica Linn. var. sarcodactylis (Noot.) Swingle [Rutaceae; Citri medicae var. sarcodactylis fructus], Glycyrrhiza uralensis Fisch. [Fabaceae; Glycyrrhizae uralensis rhizoma], Coix lacryma-jobi L. var. Mayuen (Roman.) Stapf [Poaceae; Coicis semen], Rehmannia glutinosa (Gaert.) Libosch. [Orobanchaceae; Rehmanniae radix preparata]	Suppress proliferation and survival of lymphocytes (B cells included) activated by mBAFF Reduce the apoptosis and raise the survival of polymorphonuclear neutrophils	Not mentioned	Downregulate the BAFF/BAFF-R signaling pathway	28 (Wu et al., 2015)
Yupinfeng San	Astragalus membranaceus (Fisch.) Bunge [Fabaceae; Astragli radix], Atractylodes macrocephala Koidz. [Asteraceae; Atractylodis macrocephalae rhizoma] and Saposhnikovia divaricata (Turcz. ex Ledeb.) Schischk. [Apiaceae; Saposhnikoviae radix]	Restore the immune suppressor function of Breg cells	Stabilize the IL-10 expression in B cells Inhibit the expression of Bcl2L12	Induce propionic acid production by intestinal bacteria, which counteracts the effects of Tristetraprolin on inducing IL-10 mRNA decay in B cells through the AKT/T-bet/granzyme B pathway	29 (Zhou et al., 2021) 30 (Zhou et al., 2019)
Langchuangjing Granule (LCJ)	Rehmannia glutinosa (Gaertn.) Libosch. ex DC. [Orobanchaceae; Rehmanniae radix], Leonurus japonicus Houtt. [Lamiaceae; Leonuri herba], Hedyotis diffusa Willd. [Rubiaceae; Hedyotis diffusae herba], Cornus officinalis Siebold & Zucc. [Cornaceae; Corni fructus], Paeonia × suffruticosa Andrews [Paeoniaceae; Moutan cortex], etc.	Suppress the proliferation of mesangial cell	Inhibit the increase of serum ICAM-1 content	Not mentioned	31 (Zhu et al., 2004)

are often discussed in the context of LN mechanism (Chávez-Galán et al., 2015). While it is commonly agreed that kidney macrophages in MRL/lpr mice with spontaneous LN are skewed towards the M1 phenotype rather than the M2 phenotype (Iwata et al., 2012), research has confirmed that M2-phenotype macrophages ($CD163^+$) are the dominant subpopulation in human LN. A significant association has been observed among $CD163^+$ macrophages, crescents, complement activation, kidney fibrosis and progression to kidney failure (Olmes et al., 2016; Sciascia et al., 2022; Tao et al., 2021).

Macrophage depletion ameliorates nephritis induced by antibodies against the glomerular basement membrane. Demethylzeylasteral (T-96) exhibits reno-protective effects in LN by inhibiting the activation of NF-κB, reducing downstream pro-inflammatory mediators such as TNF-α, COX-2 and ICAM-1, and thus restricting macrophage infiltration (Hu et al., 2015). Similarly, LG downregulates monocyte chemoattractant protein-1 (MCP-1) in BXSB LN mice though the NF-κB signaling pathway (Li et al., 2011). Production of MCP-1 by spleen cells in (NZB x NZW) F1 mice also decreased after triptolide or tripdiolide therapy (Tao et al., 2008).

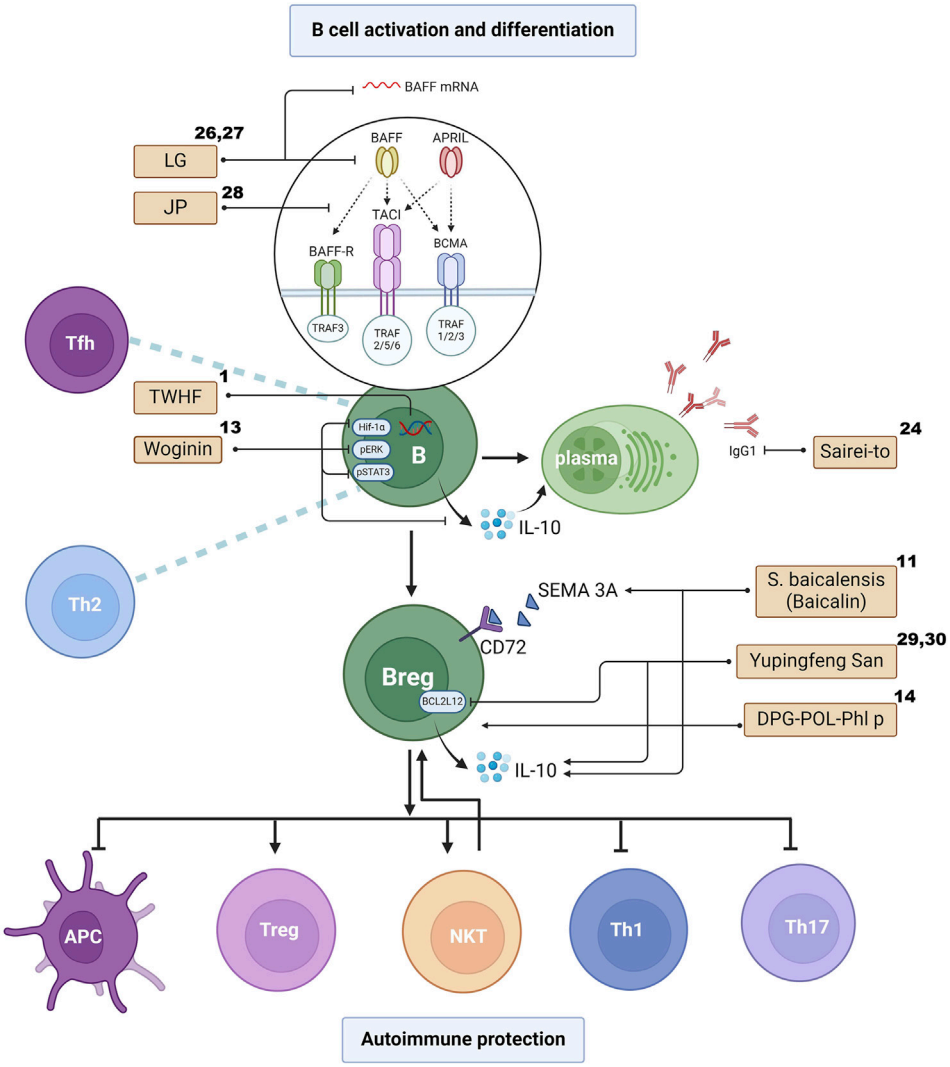

FIGURE 2
The effects of TCM on B cell activation, differentiation and interaction. The superscript numbers of the herbal formulas/phytochemicals correspond to the reference numbers in Tables 1, 2. Created with BioRender.com.

Additionally, Citral alleviates the mouse ASLN model by reducing ATP-induced IL-1β secretion and caspase-1 activation in LPS-primed macrophages (Ka et al., 2015). In the studies related to the treatment of monocyte-macrophages with TCM in LN, many showed that TCM can effectively inhibit the autoimmune response of macrophages, but none have distinguished between macrophage types. As mentioned above, the anti-inflammatory or pro-inflammatory effects and the states in the autoimmune response of different types of macrophages in the development of LN are not consistent, so the therapeutic targets of drugs should be further clarified.

3.6 Dendritic cells

In LN, dendritic cells (DC) infiltrate the kidneys, function to present antigens, and organize tertiary lymphoid structures that amplify inflammation (Kurts et al., 2020; Maria and Davidson, 2017), thus playing a critical role in the evolution of LN. when treated with M1, an active metabolite of ginsenoside, the LPS-primed bone marrow-derived dendritic cells (BMDCs) significantly reduced the expression levels of NLRP3, decreased the secretion of pro-IL-1β and p-IκB, and inhibited $CD4^+$ T cell proliferation (Lin et al., 2019). Fisetin at non-toxic concentrations suppressed the expression of costimulatory molecules CD80 and CD86, the production of cytokines IL-12, IL-6, and TNF-α, and the endocytic activity of DC during LPS-induced DC maturation (Liu et al., 2010). Bidens pilosa L. petroleum ether extract induced a semi-mature status in DCs, regardless of exposure to a maturation stimulus (Rodríguez Mesa et al., 2023). Additionally, phytochemicals such as Coumarins, Triptolide, Flavonoids from Astragalus membranaceus (Fisch.) Bunge, and Flavonoid luteolin have been confirmed to inhibit the maturation and function of DCs. However, these studies were not performed in specific LN models.

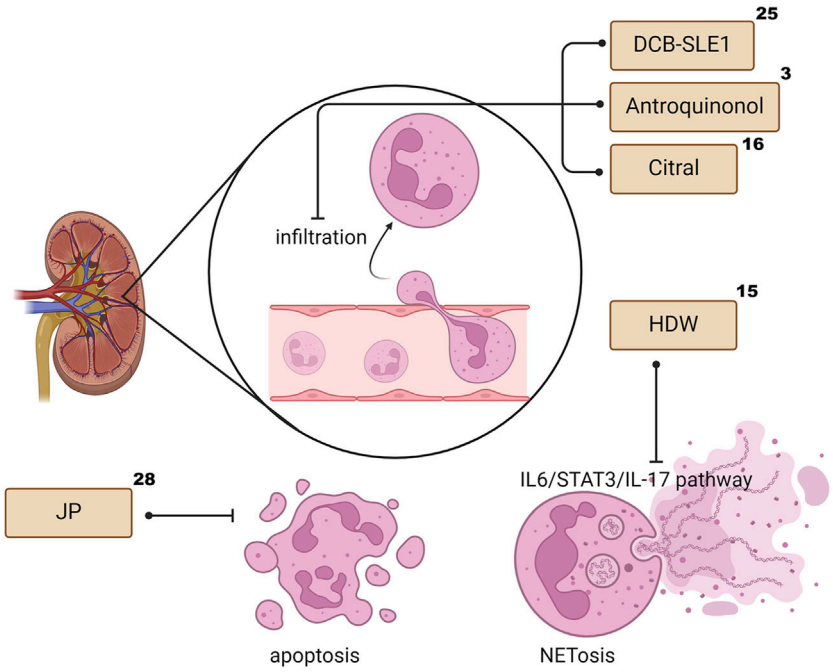

FIGURE 3
The effects of TCM on Neutrophil infiltration, apoptosis and NETosis. The superscript numbers of the herbal formulas/phytochemicals correspond to the reference numbers in Tables 1, 2. Created with BioRender.com.

Since DCs are the key link between innate immunity and adaptive immunity and play crucial roles in both promoting immune defense and maintaining immune tolerance (Liu et al., 2021), they are attractive therapeutic targets for autoimmune disease, including LN. For example, evidence reveals that tolerance is observed when partial- or semi-maturation of DCs occurs, and the semi-mature DC phenotype seems to continuously tolerize lymph node T cells against tissue-derived self-antigens or apoptotic cells (Lutz and Schuler, 2002). Hopefully, the therapeutic potential of DCs may bring inspiration for LN treatment with traditional Chinese medicine.

3.7 Resident kidney cells

Resident kidney cells, including podocytes, mesangial cells, and tubular epithelial cells have always been considered essential factors in LN. On one hand, damage to these resident kidney cells leads to varying degrees of kidney function loss (Bhargava et al., 2023; Kwok and Tsokos, 2018). On the other hand, inflammatory stimuli to resident cells cause them to produce pro-inflammatory cytokines and present antigen, further aggravating kidney injury (Bhargava et al., 2023; Jamaly et al., 2021; Kwok and Tsokos, 2018; Sakhi et al., 2019).

3.7.1 Podocytes

Reactive oxygen species (ROS) generation can affect the integrity of the podocyte cytoskeleton, resulting in subsequent podocyte detachment from the glomerular basement membrane and onset of proteinuria (Bruno et al., 2023; Guo et al., 2024). Eucarbwenstols A-H could prevent podocyte injury through ROS modulation and regulation of mitochondrial membrane potential (Chen T. et al., 2022), thus potentially having a renoprotective effect.

Aberrant activation of the NLRP3 inflammasome, which might be partly caused by autophagy dysfunction (Biasizzo and Kopitar-Jerala, 2020), plays a significant role in the pathogenesis of LN. Inhibition of NLRP3 has been shown to ameliorate proteinuria, renal histologic lesions, and podocyte foot process effacement (Fu et al., 2017; Ummarino, 2017; Wu et al., 2021). The forementioned M1 can not only reduce ATP mediated ROS production but also inhibit the activation of NLRP3 inflammasome by enhancing autophagy induction in LPS-primed and ATP-activated podocyte (Lin et al., 2019).

Recent findings suggest that podocytes share many elements of the innate and adaptive immune systems (Bhargava and Tsokos, 2019). They produce and express complement components and receptors, as well as major histocompatibility complex and co-stimulatory molecules, which may be involved in local immune events (Moll et al., 2006; Appay et al., 1990). However, the study of TCM in these related fields has not yet been explored.

3.7.2 Mesangial cells

As the mesangium is one of the primary sites for IC deposition, mesangial cells (MCs) constantly undergo severe damage, resulting in excessive proliferation and increased extracellular matrix production (Liu M. et al., 2022). ICAM-1, a cell surface

glycoprotein and an adhesion receptor that regulate leukocyte recruitment from circulation to sites of inflammation (Bui et al., 2020), was found in the mesangial area and deposited along the glomerular capillary walls in MRL/lpr mice. The distribution intensity of ICAM-1, immunoglobulins and C3 significantly decreased after treatment with stragalin in form of decoction (Chen et al., 1995). Langchuangjing Granule (LCJ) can also inhibit the increase of serum ICAM-1 content and partially improve plasma distribution, as well as suppress the atrophy of renal corpuscles and the proliferation of mesangial cells (Zhu et al., 2004).

The role of resident kidney cells in the development of LN is becoming more defined and distinct. However, there is a huge gap in the field of TCM treatment for resident kidney cells. Research on cells that play an equally important role in the pathogenesis of LN, such as tubular epithelial cells, has not been conducted. Additionally, the pathogenic capacities of resident kidney cells, such as podocytes' abilities to present antigens and participate in the formation of crescents, have not been studied in the area of TCM. More recent studies have pointed to the restoration of kidney resident cell function using cell-targeted approaches to prevent and treat LN, and TCM should play a role in this effort. (Tables 1, 2, the plant name has been checked with http://mpns.kew.org/mpns-portal/).

4 Discussion

The pathogenesis of LN involves abnormal autoimmune responses, including autoantibody and immune complex deposition, activation of infiltrating immune cells, and damage to kidney resident cells. Traditional Chinese Medicine (TCM) treatments, primarily in the form of herbal formulas and phytochemicals, exhibit distinct therapeutic effects in LN by suppressing autoimmune activity, promoting regulatory functions, and protecting kidney cells. This review explores the role of TCM in modulating immunity and mitigating LN pathogenesis, highlighting its potential value in LN treatment.

Previous reviews on TCM treatment for LN have primarily categorized therapeutic effects based on specific drugs, detailing the mechanisms of herbal formulas and phytochemicals (Dou et al., 2023; Liu L. et al., 2022; Wang et al., 2022). In contrast, this review not only acknowledges previous research findings but also adopts an innovative approach by focusing on LN immunopathogenesis, systematically delineating TCM applications within immune mechanisms. This perspective enhances clarity, provides deeper insights into specific pathways, and offers greater research value for future studies.

However, this review has several limitations:

1. Limited coverage of certain immune cells. While this section provides a comprehensive review of T cells, B cells, neutrophils, monocytes, and dendritic cells, the discussion of others (e.g., NK cells, macrophage subtypes) remains limited due to the lack of relevant research.
2. Lack of mechanistic detail in some areas. Although various immune pathways are mentioned, some mechanisms are only briefly introduced. For example, while the relationship between resident kidney cells and immune responses is acknowledged, the specific ways in which TCM influences kidney cell-mediated immune modulation remain unexplored.
3. Absence of standardized evaluation of TCM effects. This review highlights the potential immunomodulatory effects of several herbal formulas and phytochemicals; however, there is no standardized comparison of their efficacy. Additionally, discussions on dosage, bioavailability, and pharmacokinetics of TCM compounds in LN treatment remain limited, despite their crucial role in clinical translation.
4. Insufficient discussion of clinical relevance. The review predominantly focuses on preclinical (*in vitro* and *in vivo*) studies, while clinical evidence for TCM interventions is scarcely addressed due to the diversity of herbal formulas and phytochemicals.

Therefore, the following directions for future research are proposed:

1. Expanding the study of immune cell subtypes and kidney resident cells. The autoimmune mechanisms underlying LN remain unclear, and research on TCM in LN is still incomplete and often idealized. Further investigation is needed into the roles of NK cells, specific macrophage subtypes, dendritic cells, and various kidney resident cells in LN pathogenesis, as well as their modulation by TCM.
2. Mechanistic exploration of TCM effects. Future studies should elucidate the precise molecular pathways through which TCM regulates immune responses in LN, particularly in relation to cytokine signaling, metabolic regulation, and epigenetic modifications.
3. Integration of TCM with conventional LN therapies. Research should explore the synergistic effects of TCM with standard immunosuppressive treatments (e.g., corticosteroids, MMF, anti-BAFF therapy) to assess whether TCM can enhance efficacy or mitigate side effects.
4. Clinical translation and standardization. More clinical trials are required to validate the efficacy and safety of TCM formulations. Establishing standardized dosages and assessing the bioavailability of TCM monomers will facilitate their clinical application.

5 Conclusion

This review offers insights into the cellular mechanisms of LN while primarily clarifying the immunological basis for selecting herbal formulas and phytochemicals of TCM origin in LN therapy. However, future research should address gaps in immune cell coverage, mechanistic insights, clinical applicability, and pharmacological standardization to improve the translational potential of TCM in LN treatment. With continued in-depth investigation, the development of more efficient, effective, and low-toxicity herbal formulas and phytochemicals for LN treatment is achievable.

Author contributions

ZH: Conceptualization, Data curation, Methodology, Visualization, Writing – original draft, Writing – review and editing. XL: Investigation, Visualization, Writing – review and editing. QZ: Conceptualization, Investigation, Methodology,

Writing – original draft. MZ: Conceptualization, Investigation, Methodology, Writing – original draft. YF: Funding acquisition, Project administration, Supervision, Writing – review and editing. TZ: Funding acquisition, Project administration, Supervision, Writing – review and editing.

Funding

The author(s) declare that financial support was received for the research and/or publication of this article. This work was supported by the National Natural Science Foundation of China [grant number 82104798], Zhejiang Chinese Medical University school-level research fund project-natural Science Youth Exploration Project [grant number 2024JKZKTS20].

Conflict of interest

The authors declare that the research was conducted in the absence of any commercial or financial relationships that could be construed as a potential conflict of interest.

Generative AI statement

The author(s) declare that no Generative AI was used in the creation of this manuscript.

Publisher's note

Supplementary material

The Supplementary Material for this article can be found online at: https://www.frontiersin.org/articles/10.3389/fphar.2025.1523272/full#supplementary-material

References

Anders, H.-J., Saxena, R., Zhao, M.-h., Parodis, I., Salmon, J. E., and Mohan, C. (2020). Lupus nephritis. *Nat. Rev. Dis. Prim.* 6 (1), 7. doi:10.1038/s41572-019-0141-9

Appay, M. D., Kazatchkine, M. D., Levi-Strauss, M., Hinglais, N., and Bariety, J. (1990). Expression of CR1 (CD35) mRNA in podocytes from adult and fetal human kidneys. *Kidney Int.* 38 (2), 289–293. doi:10.1038/ki.1990.198

Arazi, A., Rao, D. A., Berthier, C. C., Davidson, A., Liu, Y., Hoover, P. J., et al. (2019). The immune cell landscape in kidneys of patients with lupus nephritis. *Nat. Immunol.* 20 (7), 902–914. doi:10.1038/s41590-019-0398-x

Askanase, A., Khalili, L., Tang, W., Mertz, P., Scherlinger, M., Sebbag, E., et al. (2023). New and future therapies: changes in the therapeutic armamentarium for SLE. *Best. Pract. Res. Clin. Rheumatol.* 37, 101865. doi:10.1016/j.berh.2023.101865

Astry, B., Venkatesha, S. H., Laurence, A., Christensen-Quick, A., Garzino-Demo, A., Frieman, M. B., et al. (2015). Celastrol, a Chinese herbal compound, controls autoimmune inflammation by altering the balance of pathogenic and regulatory T cells in the target organ. *Clin. Immunol.* 157 (2), 228–238. doi:10.1016/j.clim.2015.01.011

Bhargava, R., Li, H., and Tsokos, G. C. (2023). Pathogenesis of lupus nephritis: the contribution of immune and kidney resident cells. *Curr. Opin. Rheumatol.* 35 (2), 107–116. doi:10.1097/bor.0000000000000887

Bhargava, R., and Tsokos, G. C. (2019). The immune podocyte. *Curr. Opin. Rheumatol.* 31 (2), 167–174. doi:10.1097/bor.0000000000000578

Biasizzo, M., and Kopitar-Jerala, N. (2020). Interplay between NLRP3 inflammasome and autophagy. *Front. Immunol.* 11, 591803. doi:10.3389/fimmu.2020.591803

Biswas, S., Bieber, K., and Manz, R. A. (2022). IL-10 revisited in systemic lupus erythematosus. *Front. Immunol.* 13, 970906. doi:10.3389/fimmu.2022.970906

Bruno, V., Mühlig, A. K., Oh, J., and Licht, C. (2023). New insights into the immune functions of podocytes: the role of complement. *Mol. Cell Pediatr.* 10 (1), 3. doi:10.1186/s40348-023-00157-3

Bui, T. M., Wiesolek, H. L., and Sumagin, R. (2020). ICAM-1: a master regulator of cellular responses in inflammation, injury resolution, and tumorigenesis. *J. Leukoc. Biol.* 108 (3), 787–799. doi:10.1002/jlb.2mr0220-549r

Cai, B., Lu, H., Ye, Q., Xiao, Q., Wu, X., and Xu, H. (2023). Identification of potent target and its mechanism of action of Tripterygium wilfordii Hook F in the treatment of lupus nephritis. *Int. J. Rheum. Dis.* 26 (8), 1529–1539. doi:10.1111/1756-185x.14780

Chan, R. W., Lai, F. M., Li, E. K., Tam, L. S., Chow, K. M., Li, P. K., et al. (2006). Imbalance of Th1/Th2 transcription factors in patients with lupus nephritis. *Rheumatol. Oxf.* 45 (8), 951–957. doi:10.1093/rheumatology/kel029

Chávez-Galán, L., Olleros, M. L., Vesin, D., and Garcia, I. (2015). Much more than M1 and M2 macrophages, there are also CD169(+) and TCR(+) macrophages. *Front. Immunol.* 6, 263. doi:10.3389/fimmu.2015.00263

Chen, N., Dai, Y., Li, H., Long, X., Ke, J., Zhang, J., et al. (2023). Increased ILT2(+) natural killer T cells correlate with disease activity in systemic lupus erythematosus. *Clin. Rheumatol.* 42 (11), 3113–3121. doi:10.1007/s10067-023-06750-1

Chen, T., Ruan, D. D., Zhang, J. H., Wang, H. L., Wu, M., Wu, Q. Y., et al. (2022). Eucarbwenstols A-H, eight novel compounds from Eucalyptus robusta prevents MPC-5 injury via ROS modulation and regulation of mitochondrial membrane potential. *Bioorg Chem.* 129, 106159. doi:10.1016/j.bioorg.2022.106159

Chen, X., Wu, Q., Gong, Z., Ren, T., Du, Q., Yuan, Y., et al. (2022). A natural plant ingredient, menthone, regulates T cell subtypes and lowers pro-inflammatory cytokines of rheumatoid arthritis. *J. Nat. Prod.* 85 (4), 1109–1117. doi:10.1021/acs.jnatprod.1c01231

Chen, X., Yu, L., and Lu, Y. (1995). Image analysis for intercellular adhesion molecule-1 expression in MRI/lpr mice: effects of Chinese herb medicine. *Zhonghua Yi Xue Za Zhi* 75 (4), 204–206.

Crotty, S. (2011). Follicular helper CD4 T cells (TFH). *Annu. Rev. Immunol.* 29, 621–663. doi:10.1146/annurev-immunol-031210-101400

Dang, W. Z., Li, H., Jiang, B., Nandakumar, K. S., Liu, K. F., Liu, L. X., et al. (2019). Therapeutic effects of artesunate on lupus-prone MRL/lpr mice are dependent on T follicular helper cell differentiation and activation of JAK2-STAT3 signaling pathway. *Phytomedicine* 62, 152965. doi:10.1016/j.phymed.2019.152965

Davidson, A. (2016). What is damaging the kidney in lupus nephritis? *Nat. Rev. Rheumatol.* 12 (3), 143–153. doi:10.1038/nrrheum.2015.159

Desai, S. B., Ahdoot, R., Malik, F., Obert, M., and Hanna, R. (2024). New guidelines and therapeutic updates for the management of lupus nephritis. *Curr. Opin. Nephrol. Hypertens.* 33, 344–353. doi:10.1097/mnh.0000000000000969

Dou, L. L., Zhang, X. Y., Liu, D., and Liu, D. (2023). Role of traditional Chinese medicine for the treatment of lupus nephritis: mechanisms and applications. *Altern. Ther. Health Med.* 30, 154–165.

Eiza, N., Sabag, A. D., Kessler, O., Neufeld, G., and Vadasz, Z. (2023). CD72-semaphorin3A axis: a new regulatory pathway in systemic lupus erythematosus. *J. Autoimmun.* 134, 102960. doi:10.1016/j.jaut.2022.102960

Espeli, M., Bökers, S., Giannico, G., Dickinson, H. A., Bardsley, V., Fogo, A. B., et al. (2011). Local renal autoantibody production in lupus nephritis. *J. Am. Soc. Nephrol.* 22 (2), 296–305. doi:10.1681/asn.2010050515

Fakhfakh, R., Zian, Z., Elloumi, N., Abida, O., Bouallegui, E., Houssaini, H., et al. (2022). Th17 and Th1 cells in systemic lupus erythematosus with focus on lupus nephritis. *Immunol. Res.* 70 (5), 644–653. doi:10.1007/s12026-022-09296-7

Fan, L., Qiu, D., Huang, G., Chen, J., Wu, Q., Xiong, S., et al. (2020). Wogonin suppresses IL-10 production in B cells via STAT3 and ERK signaling pathway. *J. Immunol. Res.* 2020, 3032425. doi:10.1155/2020/3032425

Fazilleau, N., Mark, L., McHeyzer-Williams, L. J., and McHeyzer-Williams, M. G. (2009). Follicular helper T cells: lineage and location. *Immunity* 30 (3), 324–335. doi:10.1016/j.immuni.2009.03.003

Fu, R., Guo, C., Wang, S., Huang, Y., Jin, O., Hu, H., et al. (2017). Podocyte activation of NLRP3 inflammasomes contributes to the development of proteinuria in lupus nephritis. *Arthritis Rheumatol.* 69 (8), 1636–1646. doi:10.1002/art.40155

Furuya, Y., Kawakita, T., and Nomoto, K. (2001). Immunomodulating effect of a traditional Japanese medicine, hachimi-jio-gan (ba-wei-di-huang-wan), on Th1 predominance in autoimmune MRL/MP-lpr/lpr mice. *Int. Immunopharmacol.* 1 (3), 551–559. doi:10.1016/s1567-5769(00)00024-2

Gu, C., Liu, F., Luo, X., Zhou, X., Yang, J., and Levin, L. S. (2016). Triptolide reduces the required dose of tacrolimus by attenuating inflammation, enhancing immunosuppression, and increasing donor chimerism in a heterotopic hindlimb transplantation model. *Plastic and reconstructive surgery*, 138 (6), 1243–1253. doi:10.1097/PRS.0000000000002770

Guo, Z., Guo, Q., Li, X., Gao, X., Zhang, L., and Xu, K. (2024). Urinary biomarkers associated with podocyte injury in lupus nephritis. *Front. Pharmacol.* 15, 1324540. doi:10.3389/fphar.2024.1324540

Hakkim, A., Fürnrohr, B. G., Amann, K., Laube, B., Abed, U. A., Brinkmann, V., et al. (2010). Impairment of neutrophil extracellular trap degradation is associated with lupus nephritis. *Proc. Natl. Acad. Sci. U. S. A.* 107 (21), 9813–9818. doi:10.1073/pnas.0909927107

Heinemann, K., Wilde, B., Hoerning, A., Tebbe, B., Kribben, A., Witzke, O., et al. (2016). Decreased IL-10(+) regulatory B cells (Bregs) in lupus nephritis patients. *Scand. J. Rheumatol.* 45 (4), 312–316. doi:10.3109/03009742.2015.1126346

Hu, Q., Yang, C., Wang, Q., Zeng, H., and Qin, W. (2015). Demethylzeylasteral (T-96) treatment ameliorates mice lupus nephritis accompanied by inhibiting activation of NF-κB pathway. *PLoS One* 10 (7), e0133724. doi:10.1371/journal.pone.0133724

Hudspeth, K., Wang, S., Wang, J., Rahman, S., Smith, M. A., Casey, K. A., et al. (2019). Natural killer cell expression of Ki67 is associated with elevated serum IL-15, disease activity and nephritis in systemic lupus erythematosus. *Clin. Exp. Immunol.* 196 (2), 226–236. doi:10.1111/cei.13263

Ito, T., Seo, N., Yagi, H., Ohtani, T., Tokura, Y., Takigawa, M., et al. (2002). Unique therapeutic effects of the Japanese-Chinese herbal medicine, Sairei-to, on Th1/Th2 cytokines balance of the autoimmunity of MRL/lpr mice. *J. Dermatol Sci.* 28 (3), 198–210. doi:10.1016/s0923-1811(01)00161-x

Iwata, Y., Boström, E. A., Menke, J., Rabacal, W. A., Morel, L., Wada, T., et al. (2012). Aberrant macrophages mediate defective kidney repair that triggers nephritis in lupus-susceptible mice. *J. Immunol.* 188 (9), 4568–4580. doi:10.4049/jimmunol.1102154

Jakiela, B., Kosałka, J., Plutecka, H., Bazan-Socha, S., Sanak, M., and Musiał, J. (2018). Facilitated expansion of Th17 cells in lupus nephritis patients. *Clin. Exp. Immunol.* 194 (3), 283–294. doi:10.1111/cei.13196

Jamaly, S., Rakaee, M., Abdi, R., Tsokos, G. C., and Fenton, K. A. (2021). Interplay of immune and kidney resident cells in the formation of tertiary lymphoid structures in lupus nephritis. *Autoimmun. Rev.* 20 (12), 102980. doi:10.1016/j.autrev.2021.102980

Ka, S. M., Lin, J. C., Lin, T. J., Liu, F. C., Chao, L. K., Ho, C. L., et al. (2015). Citral alleviates an accelerated and severe lupus nephritis model by inhibiting the activation signal of NLRP3 inflammasome and enhancing Nrf2 activation. *Arthritis Res. Ther.* 17, 331. doi:10.1186/s13075-015-0844-6

Kienhöfer, D., Hahn, J., Stoof, J., Csepregi, J. Z., Reinwald, C., Urbonaviciute, V., et al. (2017). Experimental lupus is aggravated in mouse strains with impaired induction of neutrophil extracellular traps. *JCI Insight* 2 (10), e92920. doi:10.1172/jci.insight.92920

King, C., Tangye, S. G., and Mackay, C. R. (2008). T follicular helper (TFH) cells in normal and dysregulated immune responses. *Annu. Rev. Immunol.* 26, 741–766. doi:10.1146/annurev.immunol.26.021607.090344

Koga, T., Ichinose, K., and Tsokos, G. C. (2017). T cells and IL-17 in lupus nephritis. *Clin. Immunol.* 185, 95–99. doi:10.1016/j.clim.2016.04.010

Kumar, P., Balakrishnan, S., Surendra Lele, S., Setty, S., Dhingra, S., Epstein, A. L., et al. (2022). Restoration of follicular T regulatory/helper cell balance by ox40l-JAG1 cotreatment suppresses lupus nephritis in NZBWF1/j mice. *J. Immunol.* 208 (11), 2467–2481. doi:10.4049/jimmunol.2200057

Kurts, C., Ginhoux, F., and Panzer, U. (2020). Kidney dendritic cells: fundamental biology and functional roles in health and disease. *Nat. Rev. Nephrol.* 16 (7), 391–407. doi:10.1038/s41581-020-0272-y

Kwok, S. K., and Tsokos, G. C. (2018). New insights into the role of renal resident cells in the pathogenesis of lupus nephritis. *Korean J. Intern Med.* 33 (2), 284–289. doi:10.3904/kjim.2017.383

Layhadi, J. A., Moya, R., Tan, T. J., Lenormand, M. M., Sharif, H., Parkin, R. V., et al. (2023). Single-cell RNA sequencing identifies precise tolerogenic cellular and molecular pathways induced by depigmented-polymerized grass pollen allergen extract. *J. Allergy Clin. Immunol.* 151 (5), 1357–1370.e9. doi:10.1016/j.jaci.2022.11.030

Lech, M., and Anders, H.-J. (2013). The pathogenesis of lupus nephritis. *J. Am. Soc. Nephrol.* 24 (9), 1357–1366. doi:10.1681/asn.2013010026

Lee, K. H., Kronbichler, A., Park, D. D., Park, Y., Moon, H., Kim, H., et al. (2017). Neutrophil extracellular traps (NETs) in autoimmune diseases: a comprehensive review. *Autoimmun. Rev.* 16 (11), 1160–1173. doi:10.1016/j.autrev.2017.09.012

Li, D., Pan, B., Ma, N., Wang, X., Deng, X., Lai, H., et al. (2024). Efficacy and safety of Shenqi Dihuang decoction for lupus nephritis: a systematic review and meta-analysis. *J. Ethnopharmacol.* 323, 117602. doi:10.1016/j.jep.2023.117602

Li, G. Y., Liu, S. X., and Lu, X. Q. (2012). Effects of langchuangping granule on the expression of B lymphocyte activating factor in the peripheral blood B cells of BXSB lupus nephritis mice. *Zhongguo Zhong Xi Yi Jie He Za Zhi* 32 (3), 367–370.

Li, G. Y., Lu, X. Q., and Liu, S. X. (2011). Langohuangping granule down-regulated monocyte chemoattractant protein-1 via suppressing nuclear factor kappa B signaling pathway in BXSB lupus nephritis mice. *Zhongguo Zhong Xi Yi Jie He Za Zhi* 31 (12), 1685–1689.

Li, H., Geng, L., Cao, Z., Jin, Z., Yan, Q., Long, X., et al. (2023). CD56brightCD16-to CD57+CD56dimCD16+ NK cell ratio discriminates disease activity and renal involvement in patients with systemic lupus erythematosus. *Clin. Exp. Rheumatol.* 41 (9), 1768–1776. doi:10.55563/clinexprheumatol/o6bjl8

Li, J., Huang, L., Wang, S., Yao, Y., and Zhang, Z. (2016). Astragaloside IV attenuates inflammatory reaction via activating immune function of regulatory T-cells inhibited by HMGB1 in mice. *Pharm. Biol.* 54 (12), 3217–3225. doi:10.1080/13880209.2016.1216133

Li, M., Ma, J. J., Zhao, X. L., and Zhu, Y. (2014). Treating lupus nephritis by a drug pair of radix astragali and rehmanniae radix combined with glucocorticoid: a preliminary clinical study. *Zhongguo Zhong Xi Yi Jie He Za Zhi* 34 (8), 956–959.

Li, Y., Ding, T., Chen, J., Ji, J., Wang, W., Ding, B., et al. (2022a). The protective capability of Hedyotis diffusa Willd on lupus nephritis by attenuating the IL-17 expression in MRL/lpr mice. *Front. Immunol.* 13, 943827. doi:10.3389/fimmu.2022.943827

Li, Y., Tang, D., Yin, L., and Dai, Y. (2022b). New insights for regulatory T cell in lupus nephritis. *Autoimmun. Rev.* 21 (8), 103134. doi:10.1016/j.autrev.2022.103134

Liarski, V. M., Kaverina, N., Chang, A., Brandt, D., Yanez, D., Talasnik, L., et al. (2014). Cell distance mapping identifies functional T follicular helper cells in inflamed human renal tissue. *Sci. Transl. Med.* 6 (230), 230ra46. doi:10.1126/scitranslmed.3008146

Lin, T. J., Wu, C. Y., Tsai, P. Y., Hsu, W. H., Hua, K. F., Chu, C. L., et al. (2019). Accelerated and severe lupus nephritis benefits from M1, an active metabolite of ginsenoside, by regulating NLRP3 inflammasome and T cell functions in mice. *Front. Immunol.* 10, 1951. doi:10.3389/fimmu.2019.01951

Linke, A., Tiegs, G., and Neumann, K. (2022). Pathogenic T-cell responses in immune-mediated glomerulonephritis. *Cells* 11 (10), 1625. doi:10.3390/cells11101625

Liphaus, B. L., Silva, S. C., Palmeira, P., Silva, C. A., Goldenstein-Schainberg, C., and Carneiro-Sampaio, M. (2024). Reduced expressions of apoptosis-related proteins TRAIL, Bcl-2, and TNFR1 in NK cells of juvenile-onset systemic lupus erythematosus patients: relations with disease activity, nephritis, and neuropsychiatric involvement. *Front. Immunol.* 15, 1327255. doi:10.3389/fimmu.2024.1327255

Liu, C., Wang, D., Song, Y., Lu, S., Zhao, J., and Wang, H. (2018). Increased circulating CD4(+)CXCR5(+)FoxP3(+) follicular regulatory T cells correlated with severity of systemic lupus erythematosus patients. *Int. Immunopharmacol.* 56, 261–268. doi:10.1016/j.intimp.2018.01.038

Liu, J., Zhang, X., Cheng, Y., and Cao, X. (2021). Dendritic cell migration in inflammation and immunity. *Cell Mol. Immunol.* 18 (11), 2461–2471. doi:10.1038/s41423-021-00726-4

Liu, L., Zhang, L., and Li, M. (2022). Application of herbal traditional Chinese medicine in the treatment of lupus nephritis. *Front. Pharmacol.* 13, 981063. doi:10.3389/fphar.2022.981063

Liu, M., Zhang, L., Wang, Y., Hu, W., Wang, C., and Wen, Z. (2022). Mesangial cell: a hub in lupus nephritis. *Front. Immunol.* 13, 1063497. doi:10.3389/fimmu.2022.1063497

Liu, S. H., Lin, C. H., Hung, S. K., Chou, J. H., Chi, C. W., and Fu, S. L. (2010). Fisetin inhibits lipopolysaccharide-induced macrophage activation and dendritic cell maturation. *J. Agric. Food Chem.* 58 (20), 10831–10839. doi:10.1021/jf1017093

Liu, X., Bao, C., and Hu, D. (2012). Elevated interleukin-18 and skewed Th1: Th2 immune response in lupus nephritis. *Rheumatol. Int.* 32 (1), 223–229. doi:10.1007/s00296-010-1609-9

Liu, Y., Xu, K., Xiang, Y., Ma, B., Li, H., Li, Y., et al. (2023). Role of MCP-1 as an inflammatory biomarker in nephropathy. *Front. Immunol.* 14, 1303076. doi:10.3389/fimmu.2023.1303076

Lu, L. (2002). Study on effect of Cordyceps sinensis and artemisinin in preventing recurrence of lupus nephritis. *Zhongguo Zhong Xi Yi Jie He Za Zhi* 22 (3), 169–171.

Lutz, M. B., and Schuler, G. (2002). Immature, semi-mature and fully mature dendritic cells: which signals induce tolerance or immunity? *Trends Immunol.* 23 (9), 445–449. doi:10.1016/s1471-4906(02)02281-0

Maria, N. I., and Davidson, A. (2017). Renal macrophages and dendritic cells in SLE nephritis. *Curr. Rheumatol. Rep.* 19 (12), 81. doi:10.1007/s11926-017-0708-y

Mohan, C., Zhang, T., and Putterman, C. (2023). Pathogenic cellular and molecular mediators in lupus nephritis. *Nat. Rev. Nephrol.* 19 (8), 491–508. doi:10.1038/s41581-023-00722-z

Moll, S., Lange, S., Mihatsch, M. J., Dragic, Z., Schifferli, J. A., and Inal, J. M. (2006). CRIT is expressed on podocytes in normal human kidney and upregulated in membranous nephropathy. *Kidney Int.* 69 (11), 1961–1968. doi:10.1038/sj.ki.5000379

Mollazadeh, H., Cicero, A. F. G., Blesso, C. N., Pirro, M., Majeed, M., and Sahebkar, A. (2019). Immune modulation by curcumin: the role of interleukin-10. *Crit. Rev. Food Sci. Nutr.* 59 (1), 89–101. doi:10.1080/10408398.2017.1358139

Nishi, H., and Mayadas, T. N. (2019). Neutrophils in lupus nephritis. *Curr. Opin. Rheumatol.* 31 (2), 193–200. doi:10.1097/bor.0000000000000577

Nossent, J. C., Keen, H. I., Preen, D. B., and Inderjeeth, C. A. (2024). Population-wide long-term study of incidence, renal failure, and mortality rates for lupus nephritis. *Int. J. Rheum. Dis.* 27 (2), e15079. doi:10.1111/1756-185x.15079

Olmes, G., Büttner-Herold, M., Ferrazzi, F., Distel, L., Amann, K., and Daniel, C. (2016). CD163+ M2c-like macrophages predominate in renal biopsies from patients with lupus nephritis. *Arthritis Res. Ther.* 18, 90. doi:10.1186/s13075-016-0989-y

Parikh, S. V., Almaani, S., Brodsky, S., and Rovin, B. H. (2020). Update on lupus nephritis: core curriculum 2020. *Am. J. Kidney Dis.* 76 (2), 265–281. doi:10.1053/j.ajkd.2019.10.017

Park, Y. W., Kee, S. J., Cho, Y. N., Lee, E. H., Lee, H. Y., Kim, E. M., et al. (2009). Impaired differentiation and cytotoxicity of natural killer cells in systemic lupus erythematosus. *Arthritis Rheum.* 60 (6), 1753–1763. doi:10.1002/art.24556

Petri, M., Fang, C., and Goldman, D. W. (2023). East-asian lupus nephritis in the hopkins lupus cohort. *Rheumatol. Immunol. Res.* 4 (3), 157–161. doi:10.2478/rir-2023-0022

Qiu, D., and Kao, P. N. (2003). Immunosuppressive and anti-inflammatory mechanisms of triptolide, the principal active diterpenoid from the Chinese medicinal herb Tripterygium wilfordii Hook. f. *Drugs R. D.* 4 (1), 1–18. doi:10.2165/00126839-200304010-00001

Qiu, D., Zhao, G., Aoki, Y., Shi, L., Uyei, A., Nazarian, S., et al. (1999). Immunosuppressant PG490 (triptolide) inhibits T-cell interleukin-2 expression at the level of purine-box/nuclear factor of activated T-cells and NF-kappaB transcriptional activation. *J. Biol. Chem.* 274 (19), 13443–13450. doi:10.1074/jbc.274.19.13443

Ramsköld, D., Parodis, I., Lakshmikanth, T., Sippl, N., Khademi, M., Chen, Y., et al. (2019). B cell alterations during BAFF inhibition with belimumab in SLE. *EBioMedicine* 40, 517–527. doi:10.1016/j.ebiom.2018.12.035

Richoz, N., Tuong, Z. K., Loudon, K. W., Patiño-Martínez, E., Ferdinand, J. R., Portet, A., et al. (2022). Distinct pathogenic roles for resident and monocyte-derived macrophages in lupus nephritis. *JCI Insight* 7 (21), e159751. doi:10.1172/jci.insight.159751

Rodríguez Mesa, X. M., Contreras Bolaños, L. A., Modesti Costa, G., Mejia, A. L., and Santander González, S. P. (2023). A bidens pilosa L. Non-polar extract modulates the polarization of human macrophages and dendritic cells into an anti-inflammatory phenotype. *Molecules* 28 (20), 7094. doi:10.3390/molecules28207094

Rubtsova, K., Rubtsov, A. V., Thurman, J. M., Mennona, J. M., Kappler, J. W., and Marrack, P. (2017). B cells expressing the transcription factor T-bet drive lupus-like autoimmunity. *J. Clin. Invest.* 127 (4), 1392–1404. doi:10.1172/jci91250

Sakhi, H., Moktefi, A., Bouachi, K., Audard, V., Hénique, C., Remy, P., et al. (2019). Podocyte injury in lupus nephritis. *J. Clin. Med.* 8 (9), 1340. doi:10.3390/jcm8091340

Samy, E., Wax, S., Huard, B., Hess, H., and Schneider, P. (2017). Targeting BAFF and APRIL in systemic lupus erythematosus and other antibody-associated diseases. *Int. Rev. Immunol.* 36 (1), 3–19. doi:10.1080/08830185.2016.1276903

Saraiva, M., and O'Garra, A. (2010). The regulation of IL-10 production by immune cells. *Nat. Rev. Immunol.* 10 (3), 170–181. doi:10.1038/nri2711

Saraiva, M., Vieira, P., and O'Garra, A. (2020). Biology and therapeutic potential of interleukin-10. *J. Exp. Med.* 217 (1), e20190418. doi:10.1084/jem.20190418

Sciascia, S., Cozzi, M., Barinotti, A., Radin, M., Cecchi, I., Fenoglio, R., et al. (2022). Renal fibrosis in lupus nephritis. *Int. J. Mol. Sci.* 23 (22), 14317. doi:10.3390/ijms232214317

Singh, J. A., Hossain, A., Kotb, A., and Wells, G. (2016a). Risk of serious infections with immunosuppressive drugs and glucocorticoids for lupus nephritis: a systematic review and network meta-analysis. *BMC Med.* 14 (1), 137. doi:10.1186/s12916-016-0673-8

Singh, J. A., Hossain, A., Kotb, A., and Wells, G. A. (2016b). Comparative effectiveness of immunosuppressive drugs and corticosteroids for lupus nephritis: a systematic review and network meta-analysis. *Syst. Rev.* 5 (1), 155. doi:10.1186/s13643-016-0328-z

Song, J., He, G. N., and Dai, L. (2023). A comprehensive review on celastrol, triptolide and triptonide: Insights on their pharmacological activity, toxicity, combination therapy, new dosage form and novel drug delivery routes. *Biomedicine and pharmacotherapy*, 162, 114705. doi:10.1016/j.biopha.2023.114705

Tao, J., Zhao, J., Qi, X. M., and Wu, Y. G. (2021). Complement-mediated M2/M1 macrophage polarization may be involved in crescent formation in lupus nephritis. *Int. Immunopharmacol.* 101 (Pt A), 108278. doi:10.1016/j.intimp.2021.108278

Tao, X., Fan, F., Hoffmann, V., Gao, C. Y., Longo, N. S., Zerfas, P., et al. (2008). Effective therapy for nephritis in (NZB x NZW)F1 mice with triptolide and tripdiolide, the principal active components of the Chinese herbal remedy Tripterygium wilfordii Hook F. *Arthritis Rheum.* 58 (6), 1774–1783. doi:10.1002/art.23513

Tsai, P. Y., Ka, S. M., Chang, J. M., Chang, W. L., Huang, Y. J., Hung, L. M., et al. (2011). Therapeutic potential of DCB-SLE1, an extract of a mixture of Chinese medicinal herbs, for severe lupus nephritis. *Am. J. Physiol. Ren. Physiol.* 301 (4), F751–F764. doi:10.1152/ajprenal.00706.2010

Tsai, P. Y., Ka, S. M., Chang, J. M., Lai, J. H., Dai, M. S., Jheng, H. L., et al. (2012). Antroquinonol differentially modulates T cell activity and reduces interleukin-18 production, but enhances Nrf2 activation, in murine accelerated severe lupus nephritis. *Arthritis Rheum.* 64 (1), 232–242. doi:10.1002/art.33328

Tsokos, G. C., Lo, M. S., Costa Reis, P., and Sullivan, K. E. (2016). New insights into the immunopathogenesis of systemic lupus erythematosus. *Nat. Rev. Rheumatol.* 12 (12), 716–730. doi:10.1038/nrrheum.2016.186

Tucci, M., Stucci, S., Strippoli, S., and Silvestris, F. (2010). Cytokine overproduction, T-cell activation, and defective T-regulatory functions promote nephritis in systemic lupus erythematosus. *J. Biomed. Biotechnol.* 2010, 457146. doi:10.1155/2010/457146

Ummarino, D. (2017). Lupus nephritis: NLRP3 inflammasome ignites podocyte dysfunction. *Nat. Rev. Rheumatol.* 13 (8), 451. doi:10.1038/nrrheum.2017.97

Vadasz, Z., Haj, T., Balbir, A., Peri, R., Rosner, I., Slobodin, G., et al. (2014). A regulatory role for CD72 expression on B cells in systemic lupus erythematosus. *Semin. Arthritis Rheum.* 43 (6), 767–771. doi:10.1016/j.semarthrit.2013.11.010

van der Linden, M., van den Hoogen, L. L., Westerlaken, G. H. A., Fritsch-Stork, R. D. E., van Roon, J. A. G., Radstake, T., et al. (2018). Neutrophil extracellular trap release is associated with antinuclear antibodies in systemic lupus erythematosus and anti-phospholipid syndrome. *Rheumatol. Oxf.* 57 (7), 1228–1234. doi:10.1093/rheumatology/key067

Wang, S., Wang, J., Kumar, V., Karnell, J. L., Naiman, B., Gross, P. S., et al. (2018). IL-21 drives expansion and plasma cell differentiation of autoreactive CD11c(hi)T-bet(+) B cells in SLE. *Nat. Commun.* 9 (1), 1758. doi:10.1038/s41467-018-03750-7

Wang, Y.-J., Li, Y.-X., Li, S., He, W., Wang, Z.-R., Zhan, T.-P., et al. (2022). Progress in traditional Chinese medicine and natural extracts for the treatment of lupus nephritis. *Biomed. and Pharmacother.* 149, 112799. doi:10.1016/j.biopha.2022.112799

Watanabe, R., Ishiura, N., Nakashima, H., Kuwano, Y., Okochi, H., Tamaki, K., et al. (2010). Regulatory B cells (B10 cells) have a suppressive role in murine lupus: CD19 and B10 cell deficiency exacerbates systemic autoimmunity. *J. Immunol.* 184 (9), 4801–4809. doi:10.4049/jimmunol.0902385

Wu, D., Ai, L., Sun, Y., Yang, B., Chen, S., Wang, Q., et al. (2021). Role of NLRP3 inflammasome in lupus nephritis and therapeutic targeting by phytochemicals. *Front. Pharmacol.* 12, 621300. doi:10.3389/fphar.2021.621300

Wu, D. H., Xu, L., Wen, C. P., Xie, G. Q., Ji, J. J., Pan, J. L., et al. (2015). The effects of Jieduquyuzishen prescription-treated rat serum on the BAFF/BAFF-R signal pathway. *PLoS One* 10 (2), e0118462. doi:10.1371/journal.pone.0118462

Xiong, H., Tang, Z., Xu, Y., Shi, Z., Guo, Z., Liu, X., et al. (2022). CD19(+)CD24(high)CD27(+) B cell and interleukin 35 as potential biomarkers of disease activity in systemic lupus erythematosus patients. *Adv. Rheumatol.* 62 (1), 48. doi:10.1186/s42358-022-00279-8

Xu, B., Wang, S., Zhou, M., Huang, Y., Fu, R., Guo, C., et al. (2017). The ratio of circulating follicular T helper cell to follicular T regulatory cell is correlated with disease activity in systemic lupus erythematosus. *Clin. Immunol.* 183, 46–53. doi:10.1016/j.clim.2017.07.004

Xu, Y. Y., Wang, D. M., Liang, H. S., Liu, Z. H., Li, J. X., Wang, M. J., et al. (2020). The role of Th17/treg Axis in the traditional Chinese medicine intervention on immune-

mediated inflammatory diseases: a systematic review. *Am. J. Chin. Med.* 48 (3), 535–558. doi:10.1142/s0192415x20500275

Yang, J., Yang, X., and Li, M. (2012). Baicalin, a natural compound, promotes regulatory T cell differentiation. *BMC Complement. Altern. Med.* 12, 64. doi:10.1186/1472-6882-12-64

Yang, J., Yang, X., Yang, J., and Li, M. (2019). Baicalin ameliorates lupus autoimmunity by inhibiting differentiation of Tfh cells and inducing expansion of Tfr cells. *Cell Death Dis.* 10 (2), 140. doi:10.1038/s41419-019-1315-9

Yoshioka, Y., Kamata, Y., Tominaga, M., Umehara, Y., Yoshida, I., Matsuoka, N., et al. (2021). Extract of Scutellaria baicalensis induces semaphorin 3A production in human epidermal keratinocytes. *PLoS One* 16 (4), e0250663. doi:10.1371/journal.pone.0250663

Yuan, S., Zeng, Y., Li, J., Wang, C., Li, W., He, Z., et al. (2022). Phenotypical changes and clinical significance of CD4(+)/CD8(+) T cells in SLE. *Lupus Sci. Med.* 9 (1), e000660. doi:10.1136/lupus-2022-000660

Zhang, J., Shan, J., Chen, X., Li, S., Long, D., and Li, Y. (2018). Celastrol mediates Th17 and Treg cell generation via metabolic signaling. *Biochem. Biophys. Res. Commun.* 497 (3), 883–889. doi:10.1016/j.bbrc.2018.02.163

Zhou, C. J., Ma, F., Liao, W. J., Song, L. J., Yu, D., Song, Y. N., et al. (2019). Restoration of immune suppressor function of regulatory B cells collected from patients with allergic rhinitis with Chinese medical formula Yupingfeng San. *Am. J. Transl. Res.* 11 (3), 1635–1643.

Zhou, C. J., Xie, B. L., Han, H. Y., Wang, Y., Wang, Y. H., Hong, J. Y., et al. (2021). Short-chain fatty acids promote immunotherapy by modulating immune regulatory property in B cells. *J. Immunol. Res.* 2021, 2684361. doi:10.1155/2021/2684361

Zhu, F. S., Jin, S., and Wang, Y. (2004). Experimental study on inhibitory effect of langchuangjing granule on lupoid change of kidney in lupus-prone mice. *Zhongguo Zhong Xi Yi Jie He Za Zhi* 24 (4), 343–347.

Zhu, Y., Zou, L., and Liu, Y. C. (2016). T follicular helper cells, T follicular regulatory cells and autoimmunity. *Int. Immunol.* 28 (4), 173–179. doi:10.1093/intimm/dxv079

Zou, H., He, T., and Chen, X. (2019). Tetrandrine inhibits differentiation of proinflammatory subsets of T helper cells but spares *de novo* differentiation of iTreg cells. *Int. Immunopharmacol.* 69, 307–312. doi:10.1016/j.intimp.2019.01.040

Glossary

LN	lupus nephritis
SLE	systemic lupus erythematosus
TCM	traditional Chinese medicine
CYC	cyclophosphamide
MMF	mycophenolate mofetil
GC	glucocorticoids
Th1 cell	T helper 1
Th17 cell	T helper 17
Tfh cell	T follicular helper
Treg cell	T regulatory
iTreg cell	induced regulatory T
ABCs	age-associated B cells
MoMac	monocyte-derived macrophages
TrMac	tissue-resident macrophages
M1	classically activated macrophages
M2	alternative activated macrophages
NK cell	Natural Killer
DC	dendritic cells
BMDC	bone marrow-derived dendritic cell
MC	mesangial cell
IL-17	interleukin-17
IL-21	interleukin-21
IL-4	interleukin-4
IL-12	interleukin-12
IL-18	interleukin-18
IL-1	interleukin-1
IL-6	interleukin-6
IL-10	interleukin-10
IL-35	interleukin-35
IL-17	interleukin-17
NETs	Neutrophil extracellular traps
NETosis	Neutrophil Extracellular Trap formation
AST IV	Astragaloside IV
BAFF	B-cell activating factor
APRIL	a proliferation-inducing ligand
ROS	Reactive oxygen species
MCP-1	monocyte chemoattractant protein-1
TWHF	Tripterygium wilfordii Hook F
LG	Langchuangping Granule
JP	Jieduquyuzishen prescription
DPG-POL-Phl p	Depigmented-polymerized phleum pratense
T-96	Demethylzeylasteral
LCJ	Langchuangjing Granule.

Frontiers in Pharmacology

Explores the interactions between chemicals and living beings

The most cited journal in its field, which advances access to pharmacological discoveries to prevent and treat human disease.

Discover the latest Research Topics

See more →

Frontiers

Avenue du Tribunal-Fédéral 34
1005 Lausanne, Switzerland
frontiersin.org

Contact us

+41 (0)21 510 17 00
frontiersin.org/about/contact